Number 1 Volume 19 1955

BULLETIN

of the

ACADEMY OF SCIENCES OF THE USSR

— PHYSICAL SERIES —

(Izvestiya Akademii Nauk SSSR)
(Seriya fizicheskaya)

Reproduction rights reserved
by
Columbia Technical Translations
5 Vermont Avenue
White Plains, New York

Single Issues
$20

Reprinted
1960

THE ROLE OF CASCADE TRANSITIONS IN THE EXCITATION OF SPECTRAL LINES

- S. E. Frish and I. P. Zapesochnyi

In the simplest case of excitation of spectral lines, when reabsorption and quenching collisions can be neglected, the intensity I of the line is proportional to the number of excitation events ΔN_k at the initial level. Assuming, also, that stepwise excitations do not occur,

$$I \sim N_e(V)\, N_0 Q_{0k}(V) + \sum_{i=k+1}^{\infty} \Delta N_i,$$

where $N_e(V)$ is the number of electrons having the given velocity V, N_0 is the number of atoms in the ground state, $Q_{0k}(V)$ is the excitation function for the k^{th} level and ΔN_i is the number of transitions to this level from higher levels. In the absence of quenching collisions $\Delta N_i = N_i A_{ik}$, where N_i is the number of atoms in the i^{th} state and A_{ik} is the spontaneous transition probability. If the relative value of A_{ik} (as regards all possible transitions $i \to 1$) is small, ΔN_i will be of the same order as the number of excitations of the i^{th} level. Since, in general, there is no reason to consider the excitation collision cross sections of the atoms to be smaller for higher levels than for deeper lying levels, it follows that the second term in the above equation cannot be considered negligible relative to the first. Investigators have so far failed to give due weight to this circumstance in interpreting the results of experimental studies of the excitation of atoms by electronic collisions. It has generally been assumed that cascade transitions play a negligible role in the excitation of most lines and that the optical excitation function is identical with the excitation function for the initial energy level involved. Actually, however, cascade transitions cannot be ignored. Specifically, in the case of the excitation of the visible triplet of mercury (5461, 4358 and 4047 A) one cannot neglect the cascade transitions from the 7^3P_J levels; with the exception of the unlikely $7^3P_J \to 7^1S_0$ transition, the only possible transitions from these to lower levels are transitions to 7^3S_1. The fact that the role of these transitions has not been clarified hitherto must be attributed to the limitations of earlier experiments.

In order to clarify the role of cascade transitions, we carried out a series of experiments to determine the variation of the intensities of the mercury lines with the energy of the exciting electrons. The intensities were measured by photoelectric methods and special attention was given to insuring a monoenergetic exciting electron beam[1]. The observed optical excitation function for the 5461, 4358 and 4047 A mercury lines is shown in the accompanying figure. It will be noted that the curve has several sharp peaks, located at somewhat higher (1-4 volts) potentials than the corresponding excitation potentials. The dash-lines represent excitation functions for different energy levels into which the experimental curve can be resolved. The first low peak in the experimental curve (at 8.2 v) is associated with excitation of the 7^3S_1 level; the next three peaks correspond to excitations of the 7^3P_J, 8^3P_J and 9^3P_J levels having excitation potentials of 8.6, 9.4 and 9.8 ev, respectively. The next peak is connected with excitation of the unresolved group of levels n^3P_J, with $n \geqslant 10$. The diffuse peak at about 12.4 ev is probably related to the recombination of mercury ions. As may be seen the role of cascade transitions - particularly from the 7^3P_J level - is very important.

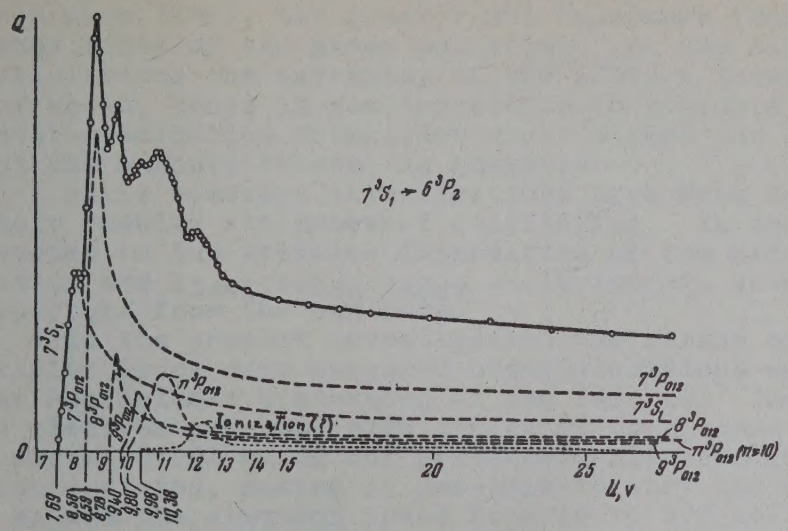

Experimentally determined excitation function of the 5461 A mercury line and the components into which it can be resolved.

The presence of cascade transitions can readily be verified. Excitation of the 7^3P_J level should be accompanied by emission of the infrared triplet = 11282, 13673 and 13950 A; while excitation of the 8^3P_J level should result in emission of the triplet = 6907, 7082 and 7092 A. The photoelectric photometer used in the experiments did not have the sensitivity in the red and infrared region requisite for recording these lines. However, the latter triplet was detected and recorded by conventional photographic methods. The optical function for the excitation of the 6907 A line was determined and its peak value compared with that of the peak in the figure. The ratio of the maxima proved to be about 0.1. Thus the role of cascade transitions was directly confirmed.

"A. A. Zhdanov" Physical Institute
of Leningrad State University

References

1. S. E. Frish and I. P. Zapesochnyi, Doklady AN SSSR, 95, 971 (2954); I. P. Zapesochnyi, Vestnik (Review) Leningrad State University, 11, 67 (1954).

* * * * *

RATIO OF LINE INTENSITIES IN THE VISIBLE TRIPLET OF MERCURY

- V. V. Lebedeva and V. A. Fabrikant

In studying discharges in mercury vapor the probabilities of the transitions associated with the 5461, 4358 and 4047 A lines of the visible triplet of mercury are particularly important. These probabilities have been computed earlier by one of the present authors[1] on the basis of experimental determinations of the lifetime of the higher state (7^3S_1). In the calculations we made use of the ratios of the intensities of the triplet lines, obtained by means of the sum rule: $I_{5461}:I_{4358}:I_{4047} = 67:100:45$.

The fact that inter-combination lines are present in the spectrum of mercury indicates that the normal coupling in the atom is disturbed.

It is known[2] that the brighter the inter-combination line originating from some level, the greater the departure from the sum rule for the other lines of the given multiplet. At the time of the above-mentioned calculations the intensity of the 12070 A inter-combination line was not known, hence it was impossible to evaluate how the presence of the inter-combination transition might affect the operation of the sum rule for the mercury triplet in question.

While numerous investigations have been devoted to the problem, their results are somewhat conflicting. In one of the latest studies[3] devoted to the relative intensities of the triplet lines the reported ratios are $I_{5461}:I_{4358}:I_{4047}$ = 110:100:41, which indicates a radical departure from the sum rule.

In the present investigation the ratios of the intensities of the triplet lines were measured under conditions which virtually exclude any appreciable distortion of the results. The source utilized was an electron-gun tube with a flat oxide cathode, containing mercury vapor at 0.001 mm Hg col pressure. Electron guns of different design were employed, making it possible to vary the current between 0.5 and 6 ma and the electron speed from 10 to 300 volts. The intensity ratios were measured by the photographic method of heterochromic photometry on an ISP-51 spectrograph.

Particular attention was given to the different factors which could lead to errors in the experimental results: the influence of variations of the sensitivity of the photographic plates and the slope of the blackening curve with changes in the exposure time in photographing the standard sources and the investigated spectra, interference effects in the collimator of the spectrograph, possible vignetting of the light beams in the spectrograph, the effect of possible inaccuracies in plotting the density (blackening) curves, and the influence of polarization of the lines incident to excitation by the electron beam. Control measurements showed that the effect of reabsorption was neglible or absent under our conditions and that the ratios of the intensities of the triplet lines were independent of the electron speed in the beam.

The final value of the intensity ratios was obtained by averaging over 15 series of measurements (15 plates), taking into account the relative accuracy of each series. Each series comprised on the average of 20 measurements for $I_{5461}:I_{4358}$ and 14 measurements for $I_{4047}:I_{4358}$. The final result $I_{5461}:I_{4358}:I_{4047}$ = 69:100:47 is accurate within about ±2% and is within ~4% of the theoretical ratios based on the sum rule.

A theoretical evaluation of the intensity of the triplet lines and the 12070 A line was carried out by the approximate quantum mechanical method developed by Iavorski[4] and based on describing the atomic state by means of semi-empirical functions. Spin-orbital coupling was taken into account. The following transition probabilities were obtained: $A_{12070} = 0.007 \cdot 10^8$ sec^{-1}, $A_{5461} = 2.4 \cdot 10^8$ sec^{-1}, $A_{4358} = 2.7 \cdot 10^8$ sec^{-1}, and $A_{4047} = 1.1 \cdot 10^8$ sec^{-1}. The corresponding intensity ratios are $I_{12070}:I_{5461}:I_{4358}:I_{4047}$ = 0.09; 69;100;46.

On the basis of the computed transition probability values we calculated the lifetime of the 7^3S_1 state to be $0.2 \cdot 10^{-8}$ sec, which is of the same order of magnitude as the reported experimental value of $0.7 \cdot 10^{-8}$ sec (Ref. 5). As might be expected the approximate method of calculation leads to an overly high value of the probabilities and, consequently, to an underestimated lifetime.

Computation of the oscillator strengths (f-numbers) for the resonance lines of mercury yielded $f_{1850} = 2.0$ and $f_{2537} = 0.09$; the

experimental values[6] are $f_{1850} = 0.98$ and $f_{2537} = 0.025$. The agreement as regards order of magnitude for the 2537 A line indicates that the theoretical evaluation of the intensity of the 12070 A line may be considered fairly reliable. The low theoretical value found for the intensity of the 12070 A line is in agreement with the experimentally established fact that the sum rule holds for the visible triplet of mercury.

"V. M. Molotov" Moscow Power Institute
and the
Physics Department of Moscow State University

References

1. V. A. Fabrikant, Izv. (Bulletin) AN SSSR, Ser. fiz., 3, 441 (1936).
2. I. L. Fabelinski, Zhur. eksp. i teor. fiz., 7, 741 (1937).
3. J. W. Schouten and J. A. Smit, Physica, 10, 661 (1934).
4. L. A. Vainshtein and B. M. Iavorski, Doklady AN SSSR, 87, 919 (1952).
5. A. Mitchelland G. M. Murphy, Phys. Rev., 46, 531 (1934).
6. A Mitchell and M. Zemansky, Rezonansnoe izluchenie i vozbuzhdennye atomy M.-L. 1937. [(Resonance radiation and excited atoms), Cambridge 1934.]

DETERMINING THE OSCILLATOR STRENGTHS (f-NUMBERS) IN THE SPECTRA OF IRON AND NICKEL

- G. F. Parchevski and N. P. Penkin

The f-numbers in the spectra of elements of the iron group can be determined using emission or absorption methods or by the method of Rozhdestvenski "hooks." The last is devoid of the shortcomings inherent in the emission and absorption methods and is more accurate, particularly at high values of the optical density of the investigated vapor column.

The values of the f-numbers for the lines of iron and nickel obtained by the method of emission and that of absorption differ markedly. In some cases the results obtained by the same investigator show surprising variation. Measurement of the f-numbers in the spectra of iron and nickel by the Rozhdestvenski method of "hooks" should a) yield reliable data and b) through comparison of such data with data obtained by other methods permit evaluating the applicability of the other available methods to multiple-line spectra.

In the present investigation we determined the relative values of the strengths of the oscillators in the spectra of iron and nickel by Rozhdestvenski's method of "hooks."

The experimental set-up consisted of a continuum source (SVD type krypton tube), a large Rozhdestvenski interferometer and a suitable spectroscopic instrument (we used an E-1 quartz spectrograph and an autocollimating diffraction grating spectrograph). The vapor column of the investigated element was maintained in a high-temperature vacuum furnace with a graphite tube heater. Temperatures of about

2000-2500°K could be attained in the tube by passing a heavy current (1500 amperes) through it. The furnace was mounted in one branch of the interferometer and a compensator in the other. With a plane-parallel transparent plate in the spectrograph crossed with the interferometer, the "hooks" near the absorption lines could readily be observed. The values of the strength of the oscillators of the corresponding transitions were determined from measurements of the distances between the "hook" peaks.

Spectrograms comprising photographs of the "hooks" at the absorption lines of 14 multiplets of iron were obtained and measured. These lines are located in the interval between 2900 and 4400 A and are associated with transitions from the a^5D, a^5F and a^3F levels of the iron atom. The relative values of the f-numbers were determined for 56 lines.

Similarly, spectrograms containing photographs of the hooks near the absorption lines of 20 multiplets of nickel were obtained and measured. These lines lie in the 3100 to 3900 A range and are associated with transitions from the a^3F, a^3D and a^1D levels of the nickel atom. The relative f-number values were determined for 48 nickel lines.

The error in the determination of the relative f-numbers for the lines of any single multiplet amounts to 3-8%; for lines of different multiplets the error may attain 10-20%.

The values of the f-numbers for the lines of iron and nickel obtained by the method of "hooks" and those determined by the methods of emission and absorption were carefully compared. The comparison showed that

a) the f-numbers obtained by the methods of anomalous dispersion and of emission are in poor agreement; the noted divergence may be attributed to the influence of reabsorption and self-reversal in determinations by the emission method;

b) the f-numbers for the lines of one multiplet, obtained by the methods of anomalous dispersion and of absorption, do not differ by more than 40% as a rule (there are exceptional greater divergences).

For lines associated with transitions to different lower levels the divergence between the results obtained by the last two methods amounts to an order of magnitude on the average. This divergence may be attributed to errors in determining the concentrations of atoms at the initial levels.

Analysis of our results and comparison of these with the data in literature justifies the assertion that where lines associated with transitions to lower and ground levels of the atoms are concerned the f-number values determined by the method of "hooks" are more trustworthy than the values determined by other methods.

To obtain complete information on the f-numbers of extensive, many-line spectra it would appear advisable to employ the method of "hooks" in conjunction with other methods: for lines of medium intensity the absorption method yields reliable results, while for weak lines associated with transitions from high levels the emission method is preferable.

Physical Institute of
"A. A. Zhdanov" Leningrad State University

DIAGRAM OF PERIODIC SYSTEM OF ATOMIC IONIZATION POTENTIALS

- A. A. Dibrova

The purpose of the present report is to acquaint a wider circle of spectroscopists with the graphic diagram of atomic ionization potentials based on a new and simple relationship discovered by the writer. It should be noted that any other spectral terms can be systematized through the construction of diagrams similar to the one pictured below.

I have shown in earlier communications[1 & 2] that the ionization potentials in isoelectronic series of atoms or molecules are fairly closely characterized by the following expressions:

$$J_{(z)} = Az(Z - a), \qquad (1)$$

or

$$\overline{J}_{(z)} = \frac{J_{(z)}}{z} = A(Z - a), \qquad (2)$$

where $J_{(z)}$ is the ionization potential of the z^{th} order, for example, of LiI, BeII . . ., $\overline{J}_{(z)}$ is the mean or "specific" ionization potential referred to a unit charge on the obtained ion, A is a constant which is a function of the principal quantum number for the level, Z is the ordinal number of the element and a is a shielding constant which has the same value for 1, 2, or 3 isoelectronic series of the same sublevel.

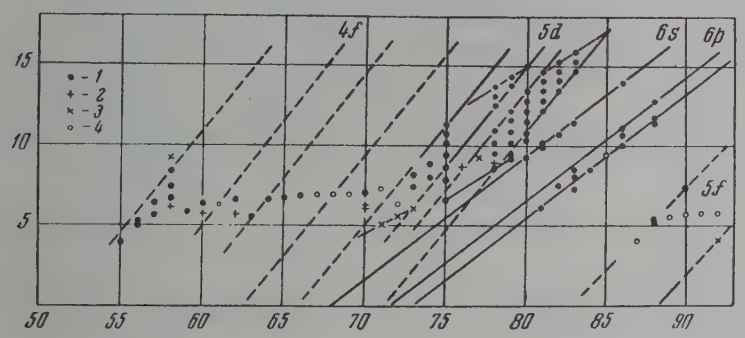

Part of the complete diagram of the periodic system of atomic ionization potentials (isoelectronic series of period VI and the beginning of VII) constructed on the basis of data in the literature: 1) Refs. 3 and 4, 2) Ref. 5, 3) Ref. 6, 4) Ref. 7.

The part of the complete periodic system of atomic ionization potentials diagram shown in the accompanying figure comprises the isoelectronic series of period VI and the beginning of period VII. Its interest stems from the fact that there is very little experimental information available for these series; however, what few data there are and the regularities noted for the preceding periods make it possible to sketch in the scheme of ionization potentials for the isoelectronic series of sublevels 4f and 5f.

The reproduced diagram is constructed according to equation (2) on the basis of data published since the war (Refs. 3 through 7).

A number of interesting deductions may be made from the complete diagram of mean ionization potentials. Among the more important are the following:

1. The mean values of the ionization potentials of both s-electrons at all atomic levels except the first are virtually equivalent; this facilitates identifying s-electrons in many doubtful cases (for example, in transition elements).

2. The p-sublevels in all atomic levels are clearly resolved into two groups each, with three states per group; only at the second level (period II) do all the electrons of each group have appreciably different values of mean ionization potential. In all other periods of each set of three p-states the mean potential values are close; in the case of complex shells, they are virtually identical.

3. The d- and f-sublevels, containing 10 and 14 states respectively, readily divide into two groups of states, comprising 5 and 7 states per group; the electrons entering into each group have different mean ionization potentials. Within each group we note a regular variation of the mean potential values over the isovalent series.

4. Inasmuch as the values of the mean ionization potential increase in the order $np < ns < (n-1)d < (n-2)f < \ldots$, the sequence of the filling of successive atomic levels can be characterized by the following single, general scheme:

ns, [(n - 3)g and ns; (n - 2)f and ns; (n - 1)d and ns], np.

L'vov Polytechnical Institute.

References

1. A.A.Diborova, Zhur. eksp. i teor. fiz., 8, 7,805 (1938).
2. A.A.Diborova, Naukovi zapiski (Scientific Notes) of Lvov State University, Chemical series, 1, 19 (1949).
3. Spravochnik khimika (Chemist's Handbook), Vol. I, L.-M. 1951.
4. Kaye & Laby, Spravochnik fizika ekspermentatora ("Experimental Physicist's Handbook") M. 1949. [Prob. Tables of Physical & Chemical Constants.]
5. D.K.Bois, Usp. fiz. nauk, 30, 3-4, 245 (1946).
6. A.I.Zaidel' & others, Tablitsy spektral'nikh linii (Tables of spectrum lines), p. 538, GTTI, M. 1952.
7. W.Finkelnburg, ZS. f. Naturforschung, 2a, 16 (1947).

* * * * *

ON CONDITIONS UNDER WHICH KIRCHHOFF'S LAW IS APPLICABLE TO THE RADIATION OF THE PLASMA OF A GAS DISCHARGE

- S. L. Mandel'shtam and N. K. Sukhodrev

1. When optical methods are used to investigate the properties of the plasma of a gas discharge - for example, to determine the plasma temperature, the relative concentrations of excited and non-excited atoms and ions , etc. - it is often essential to know the relation between the emitting and absorbing capacity as well as between the emission and absorption of a luminous layer of finite thickness in a region where the plasma is not in a state of thermodynamic equilibrium. Below we will examine the conditions under which the emission-absorption relation is characterized by Kirchhoff's law both where spectrum lines and continuous spectra due to free-bound and free-free electron transitions are concerned. Our analysis is essentially an inversion of Milne's examination of the relation between the probabilities of direct and reverse elementary processes[1].

2. We turn first to the case of a spectrum line. Let us assume that the atom passes from state i to state k, emitting a quantum $h\nu = E_i - E_k$. Let us consider a layer of luminous gas of finite thickness l. The change in the intensity of radiation of frequency ν over an interval dl in the direction normal to the layer boundary will be given by

$$dI_\nu\, d\nu = a_{ik}N_i h\nu\, d\nu\, dl - b_{ki}N_k h\nu I_\nu\, d\nu\, dl + b_{ik}N_i h\nu I_\nu\, d\nu\, dl, \tag{1}$$

where I_ν is the intensity of the radiation per unit frequency interval, $a_{ik}N_i$ is the number of emissions, $b_{ki}N_k I_\nu$ is the number of absorptions and $b_{ik}N_i I_\nu$ is the number of forced emissions at the frequency ν; the Einstein coefficients a_{ik}, b_{ik} and b_{ki} satisfy the following relationships*:

$$\frac{a_{ik}}{b_{ik}} = \frac{2h\nu^3}{c^2}, \quad \frac{b_{ik}}{b_{ki}} = \frac{g_k}{g_i}. \tag{2}$$

Integrating (1), we obtain

$$I_\nu\, d\nu = \frac{\frac{a_{ik}}{b_{ik}}}{\frac{b_{ki}N_k}{b_{ik}N_i} - 1} d\nu \left(1 - e^{-h\nu(b_{ki}N_k - b_{ik}N_i)\,l}\right) = J_{1\nu}\, d\nu \left(1 - e^{-k_\nu l}\right), \tag{3}$$

where

$$J_{1\nu} = \frac{\frac{a_{ik}}{b_{ik}}}{\frac{b_{ki}N_k}{b_{ik}N_i} - 1}. \tag{4}$$

Obviously $(1 - e^{-k_\nu l})\, d\nu = A_\nu\, d\nu$ is the absorption of radiation of frequency ν by the layer l. Then equation (3) assumes the form

$$\frac{I_\nu}{A_\nu} = J_{1\nu}. \tag{5}$$

Going over to an infinitely thin layer, we obtain from (3) at the limit:

$$\frac{I_\nu}{k_\nu l} = J_{1\nu}, \tag{6}$$

i.e., we see that $J_{1\nu}$ is also the ratio of the emitting to the absorbing capacity of the plasma.

In the case of a Boltzmann distribution of the atoms over the excited levels, with $T = T_{EL}$ we have

$$N_i = \frac{g_i}{g_0} N_0 e^{-\frac{E_i}{kT_{EL}}} \quad \text{and} \quad N_k = \frac{g_k}{g_0} N_0 e^{-\frac{E_k}{kT_{EL}}}.$$

Substituting these values in (4) and invoking the relationships (2), we obtain

$$J_{1\nu} = \frac{2h\nu^3}{c^2} \cdot \frac{1}{e^{\frac{h\nu}{kT_{EL}}} - 1}. \tag{7}$$

---

* Here we are using Einstein coefficients for monochromatic radiation (computed for a unit frequency interval) rather than the usually employed values for the entire line as a whole.

3. The case of a continuous spectrum due to free-free transitions can be analyzed in an analogous fashion. Emission at the frequency ν is associated with a change in the kinetic energy of the electron in the ion field: $h\nu = \varepsilon - \varepsilon'$. The basic equation in this case has the form

$$dI_\nu\, d\nu = N_e(\varepsilon)\, N_j F_1(\varepsilon\varepsilon')\, v\, h\nu\, d\varepsilon\, dl - N_e(\varepsilon')\, N_j F_2(\varepsilon'\varepsilon)\, v' h\nu I_\nu\, d\varepsilon'\, dl + \\ + N_e(\varepsilon)\, N_j F_3(\varepsilon\varepsilon')\, v h\nu I_\nu\, d\varepsilon\, dl, \qquad (8)$$

where $N_e(\varepsilon)$ and $N_e(\varepsilon')$ are the concentrations of electrons of energies ε and ε', N_j is the ion concentration and F_1, F_2 and F_3 are the effective cross sections of the processes accompanied by emission or absorption and satisfy the following relationships[2]:

$$\frac{F_1}{F_3} = \frac{2h\nu^3}{c^2} \quad \text{and} \quad \frac{F_2}{F_3} = \frac{\varepsilon}{\varepsilon'}. \qquad (9)$$

Integrating (5) yields

$$I_\nu\, d\nu = \frac{\frac{F_1}{F_3}}{\frac{F_2 N_e(\varepsilon')\, v'}{F_3 N_e(\varepsilon)\, v} - 1}\, d\nu\,(1 - e^{-h\nu_\nu l}) = J_{2\nu}\, d\nu\,(1 - e^{-h\nu_\nu l}). \qquad (10)$$

In the case of a Maxwellian distribution of electron velocities, with $T = T_{EL}$ we get

$$N_e(\varepsilon) = N_e \frac{2\pi\varepsilon^{1/2}}{(\pi k T_{EL})^{3/2}}\, e^{-\frac{\varepsilon}{kT_{EL}}} \quad \text{and} \quad N_e(\varepsilon') = N_e \frac{2\pi\varepsilon'^{1/2}}{(\pi k T_{EL})^{3/2}}\, e^{-\frac{\varepsilon'}{kT_{EL}}}.$$

Substituting and invoking (9) we obtain

$$J_{2\nu} = \frac{2h\nu^3}{c^2} \cdot \frac{1}{e^{\frac{h\nu}{kT_{EL}}} - 1}. \qquad (11)$$

4. In the case of a continuum due to free-bound transitions, radiation of frequency ν is emitted when an electron of energy ε collides with an ion in the energy state E_i. As a result of recombination an atom in the energy state E_k is formed; the emitted quantum

$$h\nu = \varepsilon + E_i + E_j - E_k,$$

where E_j is the ionization energy.

Here the basic equation has the form

$$dI_\nu\, d\nu = N_e(\varepsilon)\, N_j(E_i)\, G_1(\varepsilon)\, v h\nu\, d\varepsilon\, dl - N_0(E_k)\, G_2(\nu)\, h\nu I_\nu\, d\nu\, dl + \\ + N_e(\varepsilon)\, N_j(E_i)\, G_3(\varepsilon)\, v h\nu I_\nu\, d\varepsilon\, dl, \qquad (12)$$

The coefficients G satisfy the following relationships[2]

$$\frac{G_1}{G_3} = \frac{2h\nu^3}{c^2} \quad \text{and} \quad \frac{G_2}{G_3} = \frac{2g_i}{g_k} \cdot \frac{8\pi m\varepsilon}{h^2}. \qquad (13)$$

Integrating (12), we obtain

$$I_\nu\, d\nu = J_{3\nu}\, d\nu\,(1 - e^{-h\nu_\nu l}), \qquad (14)$$

where

$$J_{3\nu} = \frac{G_1 / G_3}{\frac{G_2 N_0(E_k)}{G_3 N_e(\varepsilon) N_j(E_i)\, v} - 1}. \qquad (15)$$

If the distribution of electron velocities is characterized by Maxwell's law, the distribution of atoms and ions among energy levels by Boltzmann's law and the ionization by Saha's formula, i.e., if

$$\left.\begin{aligned} N_e(\varepsilon) &= N_e \frac{2\pi\varepsilon^{1/2}}{(\pi k T_{EL})^{3/2}} e^{-\frac{\varepsilon}{kT_{EL}}}, & N_j(E_i) &= \frac{g_i}{g_j} N_j e^{-\frac{E_i}{kT_{EL}}}, \\ N_0(E_h) &= \frac{g_h}{g_0} N_0 e^{-\frac{E_h}{kT_{EL}}}, & \frac{N_j}{N_0} N_e &= \frac{2g_i}{g_0} \cdot \frac{(2\pi m k T_{EL})^{3/2}}{h^3} e^{-\frac{E_j}{kT_{EL}}}, \end{aligned}\right\} \quad (16)$$

equation (15), taking into account (12) and (16) assumes the form

$$J_{3\nu} = \frac{2h\nu^3}{c^2} \cdot \frac{1}{e^{\frac{h\nu}{kT_{EL}}} - 1}. \quad (17)$$

5. Thus it will be seen that the ratio of the emitting capacity to the absorbing capacity of plasma not in a state of thermodynamic equilibrium, as well as the ratio of emission to the absorption of a layer of finite thickness, is equal to the intensity of radiation of a black body at $T = T_{EL}$ for the given frequency when the following conditions are satisfied:

a) in the case of a spectrum line, the distribution of atoms among excited levels conforms to Boltzmann's law, with $T = T_{EL}$;

b) in the case of a continuous spectrum due to free-free electron transitions, the electron velocity distribution is Maxwellian, with $T = T_{EL}$;

c) in the case of a continuous spectrum due to free-bound transitions, in addition to a) and b), Saha's ionization formula holds.

All these conditions are normally realized in the plasma of electric arcs and sparks and in some types of low-pressure gas discharges.

"P. N. Lebedev" Physical Institute of the
Academy of Sciences of the USSR

References

1. E.A.Milne, Phil. Mag., 47, 209 (1924).
2. R.H.Fowler, Statistical Mechanics. Cambridge, 1936.

* * * *

OPTICAL DETERMINATION OF CHANGES IN THE DENSITY AND COMPOSITION OF VAPOR MIXTURES IN A DISCHARGE GAP

- A. M. Shukhtin

Observations of anomalous dispersion, carried out by the method of Rozhdestvenski, showed that initiation of the discharge current is accompanied by an appreciable reduction of dispersion in the vapor. At the same time the distance between the peaks of the "hooks" is reduced. In view of this we advanced the hypothesis that the concentration of normal atoms in the gap may decrease under the influence of

the discharge current. The decrease in vapor density, computed on the basis of the change in dispersion, proved to be very considerable. In order to verify the results we employed a modification of the method of anomalous dispersion. A discharge tube containing caesium vapor was introduced into one branch of a Rozhdestvenski interferometer and a cell filled with caesium vapor was mounted in the other branch. The tube and cell were warmed by heaters with independent temperature controls. The temperature controls were adjusted so that the effective optical length of the vapor column of the discharge tube wouldexceed the optical length of the vapor column of the cell a known number of times (for example, five times). With this arrangement dispersion curves characterized by a certain slope appear in the spectrogram near the absorption line. The slope of the dispersion curves decreases when the discharge current is turned on and as it is increased in strength. At a certain current value the dispersion curves straighten out over the entire length of the spectrum. Further increase in the current strength causes the dispersion curves to deflect in the direction opposite to their initial slope. The straightening of the bands indicates that the optical lengths of the vapor columns of the cell and discharge tube are equal. The straightening of the bands occurs at the same discharge current strength near the lines of both the first and second doublets of the principal series, This means that under the given experimental conditions the discharge current does not produce an appreciable change in the f-numbers of the doublet components.

The results of determinations of the variation of vapor density obtained by the method of straightening of the interference bands are in agreement with the results of independent measurements by the method of Rozhdestvenski "hooks" within the limits of the experimental error.

Where the vapor column consists of a mixture of atoms or molecules of different kinds, the straightening of the bands method can be used to determine changes in the concentration of particles of each kind separately. Thus the method can be used for investigating the influence of the discharge current on the composition of a vapor mixture.

Quantitative data on the variation of the composition of a vapor mixture can be obtained by the method of "hooks," using the conventional procedure. The method of "hooks" allows of measuring the relative change in the concentration of the normal atoms of each of the elements of a mixture separately. An alteration of the composition of the mixture under the influence of the discharge current will occur when the decrease in vapor density produced by the current is different for the different elements comprising the mixture. Measurements made on mixtures of caesium and sodium vapors and later on a mixture of caesium, rubidium and sodium showed that the variation of the vapor density does differ for different elements. The differences in the variation for different elements become quite appreciable at relatively heavy currents. In one of the experiments, for example, with a discharge current of 8 amperes the vapor density ofcaesium was reduced by a factor of 6.6, whereas that of sodium decreased by a factor of only 3.3

Physical Institute of
Leningrad State University

ON DETERMINING THE CONCENTRATION OF EXCITED MERCURY ATOMS IN DISCHARGES IN A MIXTURE OF MERCURY VAPOR WITH INERT GASES

- N. P. Penkin and M. N. Palladin

Excited atoms play an important part in the plasma of a gas discharge. They largely determine the optical properties of the discharge and participate actively in the processes of step-excitation, ionization and second order collisions.

Experiments have shown that the most reliable and accurate data on the concentration of excited atoms in a discharge is obtainable by means of the Rozhdestvenski method of "hooks"[1].

Discharge tubes containing a mixture of mercury vapor with argon are widely used in practice. Measurements of the resonance radiation yield of mercury in discharges through such mixtures indicate that $6^3P_{0,2} \rightarrow 6^3P_1$ transitions play an important role[2]. Hence, investigation of the dependence of the populations of the $6^3P_{0,1,2}$ levels on the discharge conditions is of practical as well as theoretical interest. Panevkin[3] and Kenty[4] have measured the concentration of atoms at these levels. However, the data obtained by these investigators for the 6^3P_2 level, for example, differ by an appreciable factor.

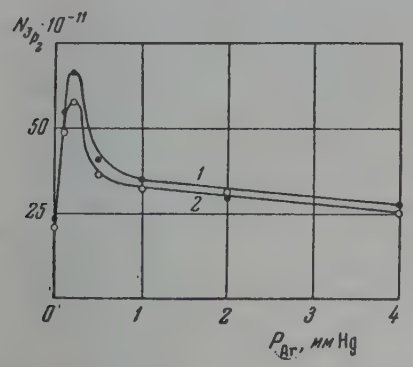

Variation of population of the 6^3P_2 level of Hg with the pressure of Ar in the vapor mixture (p_{Hg} = 6.5·10^{-3} mm) and the discharge current: 1) I = 0.5 amperes; 2) I = 0.2 amperes.

We measured the populations of the $6^3P_{0,1,2}$ levels of mercury atoms by the Rozhdestvenski method both in pure mercury vapor and in mixtures of the vapor with inert gases (argon, neon and xenon). Most of the measurements were made with discharges in a mixture of mercury and argon under the following conditions: discharge current - 0.2 or 0.5 amperes, mercury vapor pressure - 6.5·10^{-3}, 2·10^{-3}, 3·10^{-2} mm Hg col. The partial pressure of the inert gas was varied between 0 and 4 mm Hg col.

At a mercury vapor pressure of 6.5·10^{-3} mm Hg col only the "hooks" in the vicinity of the 5461 A line could be photographed and measured; at higher vapor pressures we were able to record and measure the "hooks" near all the lines of the visible triplet of mercury.

The curves of the variation of the populations of the $6^3P_{0,1,2}$ levels of mercury with the pressure of the admixed inert gas exhibit a pronounced peak at about 0.2 mm Hg col. As the pressure of the inert gas is increased the curves fall off, at first sharply and then more gradually (see accompanying figure).

The concentrations of excited atoms as measured by the method of "hooks" proved to be at least an order of magnitude higher than the concentrations measured by Panevkin and several-fold greater than the concentrations determined by Kenty.

The type of inert gas appears to have little effect on the population of atomic levels. The inert gas acts primarily to change the electron concentration and the electron-gas temperature and to retard diffusion of metastable atoms to the walls of the discharge tube.

The greatest population of the 6^3P_2 level is observed when the admixed gas is argon; the lowest, when the gas is xenon.

In addition to the above mentioned optical measurements we also used probes to determine the electron concentration (n_e) and the electron temperature (T_e) under the experimental conditions. The addition of an inert gas to the mercury vapor lowers the electron temperature and reduces the electron concentration. It is noteworthy that at first, with the introduction of a minute quantity of inert gas (a few tenths of a millimeter pressure) n_e and T_e fall off sharply; further increase in the partial pressure of the inert gas results in a further but much slower decrease in these quantities.

Using the results of our probe measurements and Fabrikant's equations[5], we calculated the number of collisions resulting in excitation to the 6^3P_2 level for a discharge current of 0.5 amperes, a mercury vapor pressure of $6.5 \cdot 10^{-3}$ mm Hg and different argon and xenon pressures (0 to 4 mm Hg). The curve for the number of collisions parallels the curve for the population of the 6^3P_2 level (i.e., coincides with it if the values are multiplied by the appropriate constant factor). It follows, therefore, that the lifetime of the excited mercury atoms in the 6^3P_2 state remains constant and that step-processes and cascade transitions have no appreciable effect on the population of this level.

We also computed the values of the equilibrium concentrations of the mercury atoms at the 6^3P_0, 6^3P_1 and 6^3P_2 levels using Boltzmann's equation (with the electron temperature in the exponent). It was found that as the discharge current and the mercury vapor and inert gas pressures are increased the populations of the metastable levels approach the equilibrium values; these values are virtually attained at a mercury vapor pressure exceeding $2 \cdot 10^{-2}$ mm Hg col, a current of 0.5 amperes and an argon pressure of a few millimeters of Hg col. In contrast the population of the emitting 6^3P_1 level did not exceed 60% of the equilibrium value at any of the experimental conditions.

The proximity of the values of the concentration of excited atoms as measured by the "hooks" method to the values given by Boltzmann's equation indicates that dissociation of the metastable atoms occurs as a result of collisions with electrons.

The results of our photoelectric measurements of the variations of the intensity of the lines of the visible triplet of mercury with the discharge conditions show that $6^3P_{0,2} \rightarrow 6^3P_1$ transitions begin to play a significant role in the emission at electron concentrations of the order of 10^{12} cm^{-3}; this is in agreement with the results of measurements by the method of "hooks."

Physical Institute of
Leningrad State University

References

1. Iu.M.Kagan & N.P.Penkin, Izv. AN SSSR, Ser. fiz., 14, 721 (1950).
2. F.Butaeva & V.Fabrikant, Ibid., 9, 3, 230 (1945).
3. K.Panevkin, Doklady AN SSSR, 59, 683 (1948).
4. K.Kenty, J. Appl. Phys., 21, 1309 (1950).
5. V.Fabrikant, Doklady AN SSSR, 15, 451 (1937).

SPECTROSCOPIC INVESTIGATION OF HIGH-FREQUENCY DISCHARGES IN GASES AND IN A FLAME AT ATMOSPHERIC PRESSURE

- V. S. Rossikhin and I. L. Tsikora

The present study was devoted to an investigation of the spectra of high-frequency discharges in air, carbon dioxide, acetylene and in an air-acetylene flame at atmospheric pressure.

The purpose of the work was to investigate the nature of the elementary processes taking place in such discharges and specifically to elucidate the mechanism of the formation of such radicals as C_2 and CH, which play an important part in the combustion process.

Two different generators were used to obtain the high-frequency discharges: a Tesla coil generator of damped oscillations, having a frequency of $1.6 \cdot 10^6$ cps and a Hartley vacuum tube generator, having a frequency of $2.85 \cdot 10^7$ cps. The oscillating circuit of the tube generator was inductively coupled to the discharge chamber by means of a suitable coil.

The high-frequency discharges in CO_2, C_2H_2 and air were investigated in a special ebonite chamber with quartz windows. The investigated gas was supplied to the chamber by the pressure due to a difference in water level in two communicating vessels, one of which contained the gas. A specially designed burner was used for obtaining the spectra of high-frequency discharges in different parts of the flame.

The spectra were photographed with an ISP-22 spectrograph on Type 3 NIKFI and isochrom plates.

The investigation of the spectra of high-frequency discharges in carbon dioxide and acetylene at atmospheric pressure has yielded new information on the mechanism of the formation of C_2 and CN. The formation of these radicals in a discharge in CO_2 is possible only when there is complete dissociation of the CO_2 or CO molecules. Under our conditions, the resultant free atoms combined with nitrogen to form CN or polymerized to produce the C_2 radical. The latter formed in discharges in acetylene only as the result of rupture of the C-H bond in the H-C≡C-H molecule.

Various, possibly competing mechanisms lead to the formation of the C_2 radical and solid carbon in an acetylene-air flame. Up to a 12% acetylene content in the mixture, processes leading to the formation of free radicals (C_2, CH and OH) predominate; with further enrichment of the mixture the processes resulting in the formation of particles of solid carbon begin to predominate.

The formation of C_2 radicals and solid carbon particles both in discharges in C_2H_2 and in the acetylene-air flame comprises two simultaneous independent processes. The C_2 radicals are formed in a flame by virtue of splitting off of the hydrogen atoms from the C_2H_2 molecules.

The more probable mechanism of the formation of CH in a flame is $C_2 + OH = CH + CO$.

Dnepropetrovsk State University

INVESTIGATION OF THE DISTRIBUTION OF MOLECULES OVER THE VIBRATIONAL STATES IN A GLOW DISCHARGE

- T. N. Popova and N. A. Prilezhaeva

The relative intensity of the bands in a molecular emission spectrum is determined by the probability of the corresponding transition W_{ik} and the population n_i of the higher level:

$$I_{ik} = CW_{ik}n_i \qquad (1)$$

where C is a coefficient which remains virtually constant for all the bands of a given system. The values of n_i (i.e., the distributions of the molecules over the vibrational levels of the higher state) have not been investigated until now.

The purpose of the present investigation was to study the factors affecting the population of the upper vibrational states. The relative intensity I_{ik} of the bands was determined experimentally while the values of W_{ik} were taken from the literature or, where necessary, calculated. Having this data one can use (1) to find the ratios: $n_o:n_1:n_2:$ . . ., i.e., the relative population values of the upper levels.

We investigated the second positive system of the bands of N_2, the violet system of CN bands and the first negative system of the bands of CO^+. The spectrum excitation sources were 1) the positive column of a glow discharge with a current density on the order of 70 ma/cm^2 and 2) a condensed discharge with V = 10,000 volts and C = 0.01 μf. The pressure was varied between 0.1 and 8 mm. The relative intensities were determined from spectrograms by photographic photometry.

The transition probability for the second positive system of N_2 was determined graphically by the method of Gaydon and Pearse[1]; that for the first negative system of CO^+ was found by the method proposed by Manneback[2], while the transition probability for the CN system was taken from the report of Ornstein and Brinkman[3].

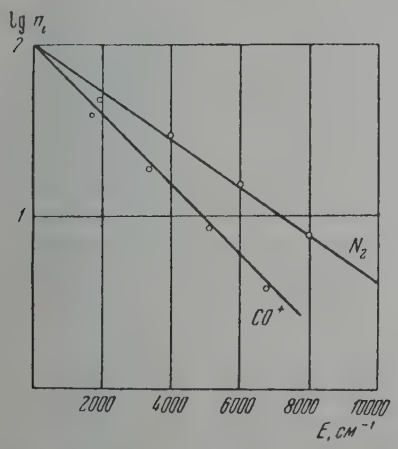

Dependence of the population of the higher levels of N_2 and CO^+ molecules on the vibrational energy.

The results showed that the populations of the higher levels decrease exponentially with increasing vibrational energy E_i of the levels (see accompanying figure). If the distribution is represented in the form

$$n_i = n_o e^{-E_i/kT},$$

we arrive at the temperature values listed in the accompanying table.

It will be seen that the temperature characterizing the distribution is appreciably higher than the actual temperature of the gas and much lower than the electron temperature, which under our experimental conditions should lie between 20,000 and 30,000°K.

From our data it may tentatively be concluded that the probability of excitation of successive vibrational states by electronic collisions falls off according to the exponential law. This may serve to explain why the higher vibrational states are generally weakly represented in the spectra of discharges at low pressures.

Temperatures (K^o) characterizing the distribution of N_2, CN and CO molecules among the vibrational levels of the upper state

Discharge conditions	N_2, second positive system	CN, violet system	CO^+, first negative system
P = 0.1 mm, glow disch.	--	--	7000°
P = 1 mm, glow disch.	4500	5100	6000
P = 8 mm, glow disch.	4400	5000	--
P = 0.1 mm, condensed spark discharge	5800	6000	8700

Siberian Physico-Technical Institute of
"V. V. Kuibyshev" Tomsk State University

References

1. A.Gaydon & R.Pearse, Proc. Roy. Soc., 173, 37 (1939).
2. C.Manneback, Physica, 17, 1001 (1952).
3. L.S.Ornstein & H.Brinkman, Proc.Amst.Soc., 34, 33 (1931).

* * * *

DETERMINING THE DISSOCIATION ENERGY OF SrO, CaO AND MgO FROM THE INTENSITY OF THE RESONANCE LINES OF THE METAL ATOMS IN FLAME SPECTRA

- I. V. Veits, L. V. Gurvich and V. V. Korobov

The dissociation energy of the metallic oxides, SrO, CaO and MgO, was determined on the basis of measurements of the equilibrium dissociation constants of the oxides in C_2H_2 + air and C_2H_2 + O_2 flames. To this end solutions of known concentration of the chlorous salts of the metals were introduced into the flame, maintained by a mixture of known composition, by means of a Lundegardt atomizer. The partial pressure p_M of the metal atoms was determined on the basis of the absolute intensity of the resonance line of the metal atoms in the flame at a distance of 1-2 mm above the internal cone. The following lines were chosen for the purposes of the investigation: Sr: λ = 4607 A, A_{mn} = $= 1.25 \cdot 10^8$ sec^{-1}; Ca: λ = 4227 A, $A_{mn} = 1.48 \cdot 10^8$ sec^{-1}; Mg: λ = 4571 A, $A_{mn} = 2.5 \cdot 10^2$ sec^{-1}.

The flame temperature T and the partial pressure of atomic oxygen p_O were computed theoretically from the composition of the fuel mixture. The partial pressure of the metal oxide p_{MO} was calculated on the basis of the known concentration of the salt solution, the composition of the fuel mixture and the value of p_M, on the assumption that the metal was present in the flame only in the form of oxide vapor and single atoms. Supplementary calculations indicated that this assumption is justified.

The dissociation energy was calculated by means of the following equation:

$$D_0(\mathrm{OM}) = T(\Delta\Phi^* - R \ln K_p), \qquad (1)$$

where T is the absolute temperatureof the flame, $\Delta\Phi^* = \Phi^*_M + \Phi^*_0 - \Phi^*_{OM}$, and $K_p = p_O p_M / p_{OM}$ is the equilibrium constant of the dissociation reaction.

The values of Φ^* - the potentials of the vapors of the metals, atomic oxygen and the metallic oxides - were calculated by the methods of statistical thermodynamics[1,2], using the constants recommended by Moore[3] for the single atoms and the values of the constants determined by Lagerqvist and his co-workers[4-6] for the oxides. Determinations of the dissociation energy of each of the oxides were carried out in a series of several flames, fed by mixtures of different compositions and having different temperatures; this procedure insured the elimination of accidental errors. The dissociation energy of magnesium oxide was also determined from the variation of the relative intensity of the Mg lines in flames having different temperatures by means of the following equation:

$$\frac{p'_M}{p''_M} = \frac{J'_{rel}}{J''_{rel}} \cdot \frac{T'}{T''} \cdot \frac{Q(T')}{Q(T'')} e^{\frac{C_2}{\lambda}\left(\frac{1}{T'} - \frac{1}{T''}\right)} = \frac{\Sigma p'_M \left[e^{\Delta\Phi^*/R} + p''_0 e^{D_0/RT''}\right]}{\Sigma p''_M \left[e^{\Delta\Phi^*/R} + p'_0 e^{D_0/RT'}\right]}. \qquad (2)$$

All the quantities in this equation (except the sought D_0) can be measured or computed; hence a numerical solution yields the value of D_0. Separate determinations of the relative intensities of the 4571 A Mg line in C_2H_2 + air flames and of the 2852 A Mg line in C_2H_2 + O_2 flames gave values for the dissociation energy, D_0, of magnesium oxide which were in close agreement with the value determined on the basis of the measured absolute intensity of the 4571 A line of Mg.

The following dissociation energy values, allowing for the possible experimental errors, were obtained

$D_0(MgO) = 100.0 \pm 3.0$ Kcal/mol,
$D_0(CaO) = 114.3 \pm 3.0$ Kcal/mol,
$D_0(SrO) = 110.8 \pm 3.0$ Kcal/mol.

Investigation of K_p in the dissociation of SrO over a wide temperature range (2450 to 3210°K) made it possible to determine $D_T(SrO)$ from the variation of ln K_p with 1/T. By comparing the corresponding value of $D_0(SrO) = 116.0 \pm 4.0$ Kcal/mol with the value of $D_0(SrO)$ computed according to equation (1) for the different possible ground states of SrO ($^1\Sigma, ^3\Sigma, ^3\Pi$) we were able to resolve the current controversy regarding the identity of the ground electronic state of alkali-metal oxide molecules by showing that it is the $^1\Sigma$ state.

Institute of Mineral Fuels of the
Academy of Sciences of the USSR

References

1. J.Mayer & M.Mayer, Statisticheskaia mekhanika. M.1952. [Statistical Mechanics. London-N.Y. 1940.]
2. A.Gordon & C.Barnes, J.Chem. Phys. 1, 297 (1933).
3. C.Moore, Atomic Energy Levels, Vols. I & II, Wash. 1949 & 1951.
4. A.Lagerqvist & U.Uhler, Ark. f. fysik, 1, 459 (1949).
5. G.Almqvist & A.Lagerqvist, Ark. f. fysik, 1, 477 (1949).
6. A.Lagerqvist, Nature, 170, 885 (1952).

SPECTROMETRY OF SOME EARLY-STAGE STARS

- M. V. Dolidze

Systematic investigation of the spectra of stars of the P. Cygni, Wolf-Rayet and Be types is of particular interest in view of the fact that these stars are not stationary. One of the principal results obtained from photometry of their continuous spectra is the exceptionally low temperature T_c of these stars, much below the temperature T_{st} normally characteristic of their spectral class. Various reasons for this anomaly have been advanced in astronomic literature.

In 1951-1952 at the Abastuman Astrophysical Observatory of the Academy of Sciences of the Georgian SSR we recorded spectrograms of 14 stars of the above-mentioned types: nine of the P Cygni type, three Wolf-Rayet and two Be stars. We also obtained spectrograms of 28 reference stars, some of which are comprised in the Greenwich gradients program. The spectrograms were recorded with a prism camera having a 20 cm diameter lens, a relative aperture of 1:5 and a refraction angle of the prism of $15^{\circ}\ 30'$. The dispersion of the instrument is 140 A mm^{-1} at H_γ. Clear images of sections of the spectrum from 3780 A to H_β were obtained on Agfa "Astro" and Ilford "Zenith" plates; the spectrum between 5110 and 6300 A was photographed on Agfa panchromatic plates. The recorded spectra were processed on a Moll microdensitometer at magnifications of 50 and 25 times and partially on a microphotometer.

Relative spectrophotometric gradients were determined for all 14 stars. A change in the value of the gradient with time was noted for AG Pegasi and P Cygni. In the case of P Cygni the change is similar to the change in the brilliance of this star over the same period.

A decrement of the Balmer series and of the temperature was established for AG Pegasi and P Cygni from the hydrogen, helium and "nebulum" lines by the method of Zanstr.

It has been suggested that the above-mentioned disparity between T_c and T_{st} is caused by reddening of the stars due to selective interstellar absorption. To check this hypothesis we selected two groups of 3-5 stars each around P Cygni, situated at the two values of the distance to P Cygni reported in astronomical literature (1000 and 300 parasec). The stars of the far group were chosen so that the distortion of their interstellar absorption would be the same in each case.

Comparing the energy distribution in the photographic region of the spectrum of P Cygni with the average distribution for each of the groups it may be said that P Cygni shows the same degree of reddening as the "far" group of stars. Hence in the photographic region, T_c proves to be normal for the given spectral class. However, in comparing the energy distribution of P Cygni with that of the "near" group of stars only half the reddening can be attributed to the effect of selective interstellar absorption; the remaining half of the reddening can be explained as being due to the presence of a shell about the star, as suggested by V. V. Sobolev, or by recourse to the theory of extended photospheres, advanced by Kozyrev. Supplementary calculations were carried out on the basis of the latter theory, taking into account the variation of the continuous absorption coefficient with the frequency.

Similar verification measurements, but with reference to only one group of surrounding stars, were made for Wolf-Rayet type stars and for two stars of the P Cygni type. In the cases of four stars the anomalously low value of T_c can be almost wholly explained by the effect of selective interstellar absorption.

Abastuman Astrophysical Observatory of the
Georgian SSR Academy of Sciences

ON THE APPLICABILITY OF STATISTICAL THEORY TO PRESSURE AND DOPPLER BROADENING OF SPECTRUM LINES*

- I. I. Sobel'man

Historically, two concepts have developed in connection with the theory of the broadening of spectrum lines: the statistical and the impact concept. In the statistical treatment it is assumed that the intensity distribution in lines $I(\omega)d\omega$ is proportional to the probability of the instantaneous frequency ω_p of the oscillator assuming a value within the interval ω to $\omega + d\omega$[1-4]. The impact theory treatment is based on Fourier analysis of the process:

$$f(t) = \exp\left\{i \int_{-\infty}^{t} \omega_p(t')\, dt'\right\},$$

where $\omega_p = \omega_0 + \Delta(t)$; $\Delta(t) = C_n R^{-n}$ is the shift of the oscillator frequency due to the interaction. In computing the Fourier component

$$f_\omega \backsim \lim_{T\to\infty} \frac{1}{(2\pi T)^{1/2}} \int_{-T/2}^{T/2} \exp\{i[\varphi(t) - (\omega - \omega_0)t]\}\, dt, \qquad (1)$$

where $\varphi(t) = \int_{-\infty}^{t} \omega_p(t')\, dt'$; it is assumed that most important factor is the sudden perturbation experienced by the emitting atom in a sufficiently close approach to (i.e. collision with) another particle, in consequence of which the radiation is broken up into a series of independent, incoherent wave trains. In (1) it is assumed that $\varphi(t) = \omega_0 t + \bar{\alpha}_k$ during the interval τ_k and that the phase $\bar{\alpha}_k$ changes abruptly at the instant of collision[1,2]. It can be shown[5] that the two treatments represent two limiting cases of the general expression (1). Thus, at large values of $\omega - \omega_0$ for the edges of the line, with

$$\omega - \omega_0 \gg \frac{v^{n/(n-1)}}{C_n^{1/(n-1)}} = \Omega, \qquad (2)$$

where v is the relative velocity and C_n and n are determined by the type of interaction obtaining, the statistical expression for $I(\omega)d\omega$ is valid. And, on the other hand, when $\omega - \omega_0 \ll \Omega$ the impact distribution will obtain. This result can readily be understood from the point of view of general spectral regularities for frequency modulation[6]. Let us consider two examples:

1) $\Delta = a \cos \mu t$; $\varphi(t) = (a/\mu) \sin \mu t$. The character of the spectrum is wholly determined by the magnitude of the modulation index a/μ. In the general case the spectrum will comprise a series of components having frequencies that are multiples of μ; in the limiting case, when $a/\mu \gg 1$, $I(\omega)d\omega$ will coincide with the statistical distribution and the width of the spectrum will equal the full width of the fluctuation band $2a$.

2) Rectangular frequency modulation: $\Delta = a_n$ with $t_n \leq t \leq t_n + \tau_n$; here a_n and τ_n are random independent variables. The band produced by the wave train will have a width $2/\tau_n$ and be symmetrical relative to $\omega_o + a_n$. It can readily be seen that this train will contribute to the intensity in the low frequency interval about $\omega_o + a_n$, as statistical theory requires, if only $1/\tau_n \ll a_n$. Here $a_n\tau_n$ plays the part of the modulation index.

In both examples the governing factor is the value of the ratio of the "depth of modulation" (a in the first case; a_n in the second) to the "rate of modulation" (μ in the first case; $1/\tau_n$ in the second).

---

* A complete text of the report appears in Doklady AN SSR 98,43 (1954)

In our problem the maximum shift C_n/ρ^n (ρ is the "sighting" range) and the reciprocal of the collision time v/ρ are analogues of a and μ and of a_n and $1/\tau_n$, respectively. Ω has the meaning of a modulation index. Ω does not depend on the density N of the perturbing particles. The distribution of intensity, however, between the regions $(\omega-\omega_0)>\Omega$ and $(\omega-\omega_0)<\Omega$ does depend on N. At low and moderate pressures, when $(3/4\pi N)^{1/3}$ is much larger than the effective collision radius ρ_0 the major part of the intensity falls into the region of impact broadening.

We encounter a fully analogous situation in examining Doppler broadening of spectrum lines. The frequency of the radiation of an atom moving towards the observer with a velocity v is shifted $\Delta\omega = -\omega_0 v/c$; here v retains a constant value v_n over a period τ_n (the free-path time). Inasmuch as τ_n and v_n are random and independent variables, we have here an analogue of the rectangular frequency modulation example discussed above. The usually employed[1] statistical expression for Doppler broadening is valid only when $v_n\omega_0/c\tau_n \gg 1$ or $L \gg \lambda$, where L is the free path ($L = \overline{\tau}_n\overline{v}_n$) and λ is the wave length. When $L \lesssim 1$, the loss of coherence with changes in v (and, consequently of $v\omega_0/c$) begins to predominate.

In this case we can readily obtain a dispersion distribution for $I(\omega)d\omega$, similar to the impact distribution, with a width $2/\tau_0$, where τ_0 is the gas-kinetic free-path time.

This result may be important for the lines of a Raman spectrum in a gas, associated with semi-symmetrical vibrations of molecules not having a dipole moment, for which the effective broadening cross section may be smaller than the gas-kinetic one[7-9].

The above analysis indicates that the breadth of such lines at pressures on the order of the atmospheric will be equal to $2/\tau_0$ even if the impact mechanism of Weisskopf is relatively ineffective.

References

1. V.F.Weisskopf, Usp. fiz. nauk, 13, 596 (1933).
2. A.Unzol'd in Symposium "Sovremennye problemy astrofiziki i fiziki Solntsa" (Modern problems of astrophysics and physics of the Sun). M. 1951.
3. H.Margenau, Phys. Rev., 48, 755 (1935).
4. H.Margenau, Phys. Rev., 82, 156 (1951).
5. I.Sobel'man, Doklady AN SSSR, 98, 1, 43 (1954).
6. S.Rytov, Thesis, Trudy FIAN SSSR, 2, 1, 41 (1940).
7. Kh.Sterin, Thesis, FIAN SSSR, 1949.
8. Kh.Sterin, Izv. AN SSSR, Ser. fiz., 14, 411 (1950).
9. I.Sobel'man, Izv. AN SSSR , Ser. fiz., 17, 554 (1953).

* * * *

CALIBRATION CURVES AND THE BREADTH OF SPECTRUM LINES IN AN AC ARC DISCHARGE

- I. M. Nagibina

1. The present investigation was devoted to measurement of the breadth of the spectrum lines of certain elements at different concentrations in an AC arc. Appropriate calibration curves were plotted. The analysis was carried out with aqueous solutions of salts of the

investigated elements; the material was introduced into the arc by placing drops of the solution on the carbon electrodes.

At first, i.e., at low concentrations of the elements, the Mn II 2949 A, Pn I 2873 A and Cd I 3261 A lines are characterized by a linear dependence between the logarithm of the relative intensity and the logarithm of the concentration (we used "converted" concentrations: the gravimetric ratio of the analytic to the reference element). At higher concentrations a "bend" appears in the calibration curve. The breadth of the spectrum lines remains constant in the rectilinear region of the "growth curve"; broadening of the spectrum lines begins at about the concentration values at which the calibration curve starts to deviate from a straight line.

For the Mn II 2563 A line the calibration curve is rectilinear in the range of concentrations from 0.5 to 100%; the breadth of the line remains constant and equals 0.065 A on the average.

2. To obtain the true line breadth one must take into account the apparatus intensity distribution function. When Doppler broadening was allowed for, the line shapes proved to be dispersional in character.

Taking account of the apparatus function could thus be reduced to evaluation of an integral equation of the form

$$I(u) = \int_{-\infty}^{+\infty} \frac{\delta^2}{\mu^2 + \delta^2} \cdot \frac{\varepsilon^2}{\varepsilon^2 + r\,[4\pi t\,(\nu + \mu)\cos i - 2k\pi]^2}\, d\mu,$$

where $\mu = \nu - \nu_0$, δ is the true breadth, $u \equiv 4\pi t\nu \cos i - 2k\pi$, $\varepsilon = 1 - r$ (here r is reflection coefficient for semitransparent mirrors) and t is the etalon constant.

Solution of the equation $I(u) = \frac{1}{2} I(0)$, with r = 0.83-0.87, gives

$$\gamma = 0{,}87\delta + 1{,}6\alpha,$$

where γ is the measured breadth and α is the instrument breadth.

3. Viatskin has advanced the hypothesis that quenching collisions between excited atoms or ions and similar atoms or ions in the region of the discharge play an important part in the broadening of spectrum lines in an arc discharge. If such is the case, the line breadth should be proportional to the density of the luminous gas*. Our experiments have shown that for the investigated lines, in the range of concentrations where line broadening does occur, the variation in line breadth with concentration is linear. Self-reversal was observed at the highest concentrations.

4. The breadth of the Mn II 2949 A line was measured at different values of the discharge current (3, 6 and 9 amperes). Calibration curves were plotted for these excitation conditions.

The results showed that the "bend" in the calibration curve appears earlier (i.e. at lower concentrations) with heavier currents. The beginning of broadening of the 2949 A line is also displaced accordingly. The dependence of the line breadth on the concentration remains linear however.

5. In order to determine the effect of extraneous atoms on the line breadth we measured the breadth of the Mn II 2949 A line in the case of ternary and more complex solutions.

The analytic solutions were prepared by adding sulfates of Zn, Al, Cd, Mg, Ni and Na (in concentrations of 15, 50 and 100% relative to the internal standard) to binary Mn-Cu solutions. The measurements

---

* The present author carried out the experimental part of the investigation of Ref. 1.

indicated that the presence of a third component has no effect (within the limits of the measurement error) on the breadth of the Mn II 2949 A line.

6. It may be concluded, therefore, that the physical breadth of the spectrum can uniquely characterize the concentration of the emitting atoms in the cloud of the arc discharge when the analytic material is introduced into the discharge in the described manner. The linear dependence noted above can be utilized for quantitative spectrum analysis of solutions and powders. The range of determinable concentrations can be set by appropriate selection of the discharge current strength.

In conclusion the writer wishes to thank V. K. Prokof'ev and A. I. Viatskin for their interest and helpful advice.

Leningrad Institute of Precision
Mechanics and Optics

Reference

1. A. Ia. Viatskin and I. M. Nagibina, Doklady AN SSSR, 98, 1, 59 (9 (1954).

* * * *

INVESTIGATION OF THE SHAPE AND BREADTH OF SPECTRUM LINES IN DC ARCS

- V. F. Kitaeva

In view of the high degree of ionization obtaining in electric arcs, the electric fields of the charged particles (electrons and ions) comprising the plasma have an appreciable influence on the shape and breadth of the spectrum lines.

In the case of lines with a linear stark effect this influence may be regarded as a stistical process; in the case of lines with a quadratic Stark effect, as an impact process[1]. Hitherto experimental studies have been concerned mainly with lines subject to a linear Stark effect[2-4].

The primary purpose of the present investigation was to study the shape of spectrum lines with a quadratic Stark effect, produced by a DC arc. We studied the following sodium lines: 6160.7, 5153.6, 4752 (sharp series), 5890 (resonance line, principal series) and 4982.8 A (diffuse series). Thus we investigated the shape and breadth of Na lines both along a series and for different series. In addition we also investigated the Tl 5330 A line.

As a result of the investigation it was established that the shape of the Na 5890 A line, which has a small quadratic Stark effect (Stark constant 10^{-6} A $cm^2 kv^{-2}$), in a DC arc is determined wholly by Lorentz collisions and the Doppler effect; as might be expected[1] broadening due to interaction with the ions and electrons of the arc plasma is small compared to Doppler and Lorentz broadening.

An analogous situation obtains for the Tl 5350 A line. The optical collision radius in an arc for the Na 5890 A and Tl 5350 A lines is approximately (within 10%) equal to the collision radius for these lines as measured in an air-acetylene flame. It has been established that the breadth of the lines of the sharp series of Na increases with their number in the series. This is consonant with the theory which predicts that the higher the Stark constant the broader the line. The Stark constants for the Na 6160.7, 5153.6 and 4752 A lines are $0.7 \cdot 10^{-5}$, $2.5 \cdot 10^{-5}$ and $7.3 \cdot 10^{-5}$ respectively (the first two were computed by the author; the last value is taken from Ref. 1). The half-breadths of these lines are 0.147, 0.172 and 0.32 A, respectively.

The Na 5153.6 and 4752 A lines are asymmetric: the slope of the line contours is steeper on the short wave than on the long wave side. The asymmetry of the lines increases with their number in the series: thus, the asymmetry so small as to be undetectable (under our experimental conditions) for the 6160.7 A line and greatest for the 4752 A line. We also made a comparison of the theoretical and experimental data for these lines. The theoretical contours were computed taking into account only Lorentz and Doppler broadening. The agreement for the 6160.7 A line is satisfactory. In the case of the 5153.6 and 4752 A lines, there is agreement only for half the line; the other half of the experimental line deviates from the theoretical contour.

The broadest of the measured Na lines proved to be the 4982.8 A line of the diffuse series whose half-breadth is about 0.50 A.

Our data show that the spectrum lines in a DC arc differ markedly in half-breadth: the lines of the diffuse series are broadest, the resonance line is the sharpest. The breadths of the lines in any one series increase with the number of the line in the series.

The shape of the narrowest lines is determined by the Doppler effect and Lorentz collisions with neutral particles. The shape of the wide lines apparently depends to an appreciable degree on interaction between the excited atoms and charged particles in the arc plasma.

"P. N. Lebedev" Physical Institute of the
Academy of Sciences of the USSR

References

1. S.L.Mandel'shtam & N.N.Sobolev, Zhur. eksp. i teor. fiz.,21,350 (1951).
2. G.Reman, Lijnverbreeding in de lichtboog. Utrecht 1937.
3. V.I.Danilova, Izv. AN SSSR, Ser. fiz., 11, 252 (1947).
4. J.Holtsmark & B.Trumpy, ZS. f. Phys., 31, 803 (1925).

THE EFFECT OF SELF-ABSORPTION ON THE INTENSITY OF SPECTRUM LINES IN A DC ARC

- V. S. Mel'chenko

The experimental data reported by many investigators show that the absorption of light in the source itself (i.e., self-absorption) has a considerable effect on the intensity of the spectrum lines. Where discharges at atmospheric pressures are concerned not only is there no suitable method for allowing for the possible effect of self-absorption, there is no reliable way of determining whether self-absorption is present or not.

The experimental part of our investigation consisted of determining the variation of the spectrum lines of sodium with the concentration of emitting atoms. We varied the concentration of emitting atoms in the discharge gap by using samples having different concentrations of NaCl. The absolute concentrations were measured by a method developed earlier[1]. The degree of ionization was evaluated from the Ba I 4726 A and Ba II 4900 A lines. The Cu I 5106 and 5218-5220 A lines were used to gage and check the temperature of the arc.

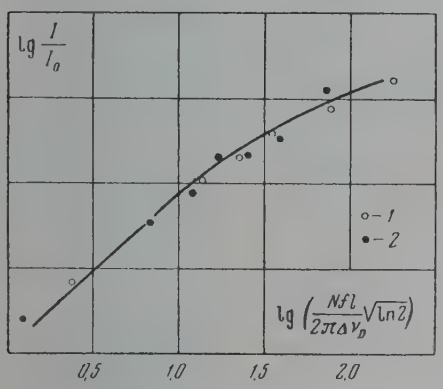

Variation of line intensity with the concentration of Na atoms in the arc gap. Curve: theoretical; points: experimental values: 1) 6161 A; 2) 6154 A.

Our measurements showed that the concentration of sodium atoms in the discharge gap increases linearly from $2.5 \cdot 10^{15}$ cm^{-3} for a 1% NaCl content in the sample to $25 \cdot 10^{15}$ cm^{-3} for a 30% NaCl content. The degree of ionization of the easily ionized component of the arc vapor decreases in proportion to the increase in the sodium concentration from 0.9 for the 1% NaCl sample to 0.41 with the 30% NaCl sample.

Thus it will be seen that the concentration of neutral sodium atoms participating in the emission and absorption of the investigated atomic lines varies non-linearly in the range from $2.5 \cdot 10^{14}$ to $1.5 \cdot 10^{16}$ cm^{-3} as the NaCl concentration in the sample is varied between 1 and 30%. The theoretical concentration dependence of the line intensities was subsequently computed for this range of concentrations. The mean value of the vapor temperature was found to be 5600°K.

We determined the variation of the intensity of the sodium lines with the concentration of Na atoms in the gap by comparison of their intensities with those of the homologous lines of barium. The width of the spectrograph slit was adjusted so that the measurement would comprise the full integral intensity of the lines. The measurements were made for the lines of the second and third doublets of the principal series and two doublets of the sharp and diffuse series of sodium: λ = 3303, 2853, 6161, 6155, 5688 and 5683 A, using conventional photographic photometry procedure.

We used the following equation for computing the intensity of the arc spectrum lines:

$$I = I_0 \int_0^\infty (1 - e^{-k_\nu l}) \, d\nu, \qquad (1)$$

where I_o is the intensity of black body radiation for the frequency of the given line at the temperature of the source, k_ν is the absorption coefficient for the line and l is the thickness of the emitting layer (under our conditions the diameter of the arc, equal to 3 mm). We assumed that the value of k_ν is affected by both collision and Doppler broadening. We calculated the values of k_ν accordingly; further computations based on (1) were carried out graphically.

Satisfactory agreement of the experimental and theoretical data was obtained (see accompanying figure).

The plotted intensity increment curves for the investigated lines show that the departure from linearity of the variation of intensity with the concentration of atoms becomes noticeable at the point where

$$\lg\left(\frac{Nfl}{\pi\Delta\nu_D}\sqrt{\ln 2}\right)=1{,}2, \qquad (2)$$

where N the concentration of atoms at the lower level associated with the given line, f is the oscillator strength (f-value) and $\Delta\nu_D$ is the Doppler breadth of the line (by way of illustration the theoretical curve and the experimental points for the lines of the 6161 - 6154 A doublet -- lower levels $3^2P_{3/2}$ and $3^2P_{1/2}$ -- are shown in the accompanying figure).

From equation (2) one can find the critical concentration N_{crit} at which self-absorption begins to have a pronounced effect on the intensity of the line. Since we determined the variation of the concentration of atoms in the luminous cloud (discharge gap) with the concentration of sodium in the sample, we could readily calculate the critical concentrations of Na in the sample for the different lines.

Equation (2) can, of course, be used for determining the critical concentrations not only of sodium but of other elements as well.

On the basis of certain tentative assumptions regarding the rate of transfer of different elements from the sample into the discharge, we calculated the probably critical concentrations for a number of lines of 16 elements. The results indicate that for most resonance lines self-absorption begins to play an important role from concentrations appreciable under 1% by weight in the sample; for particularly intense lines the critical concentration may be on the order of 10^{-4}%. To obtain more reliable data one must determine the actual relationship between the concentration of the various elements in the discharge and their concentration in the sample.

Siberian Physico-Technical Institute at
"V. V. Kuibyshev" Tomsk State University

Reference

1. N.A.Prilezhaeva and V.N.Goriachev, Izv. AN SSSR, Ser. fiz., 14, 742 (1950).

HYPERFINE STRUCTURE OF THE SPECTRUM LINES AND THE NUCLEAR SPINS OF U^{233} AND Pu^{239}*

- L. A. Korostyleva, A. R. Striganov and N. M. Iashin

Early in 1953 the present authors and independently Frishen, Kalitievski and Chaika made spectroscopic determinations of the spins of U^{233} and Pu^{239} nuclei. Subsequently we carried out more detailed investigations of the hyperfine structure of the spectrum lines of these isotopes, the results of which are summarized below.

The high resolving power instrument employed consisted of a glass plate Fabry-Perot etalon (IZS-9) crossed with a three-prism, glass optics Steinheil spectrograph. The source was a water-cooled, hollow-cathode, argon filled discharge tube which was connected to a suitable vacuum installation incorporating a circulating system.

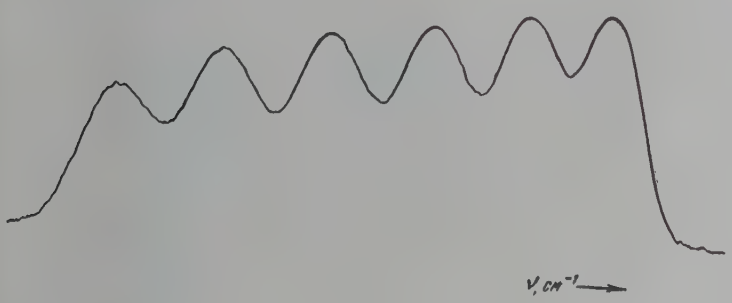

Fig. 1. Microphotogram of the hyperfine structure of the U I 5915.4 A line.

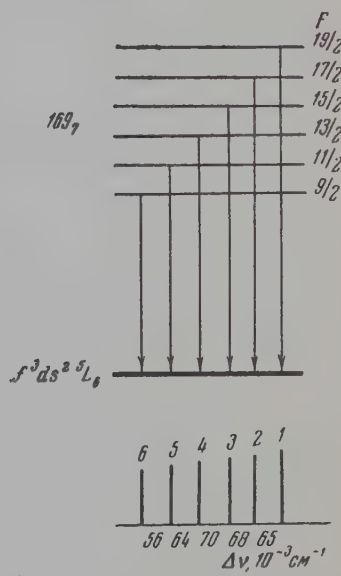

Fig. 2. Transition scheme and the hyperfine structure of the U I 5915.4 A line.

In investigating the hyperfine structure of the spectrum lines we used pure isotopes in the form of U_3O_8 and PuO_2. Samples of 3.5 to 8 mg were loaded into the tube. The oxides were reduced to the metal in the tube by atomic hydrogen under the conditions of the electric discharge. The DC voltage for the tube was supplied by a high-voltage rectifier. The optimum excitation conditions for uranium and plutonium were found to be: argon pressure in tube - 2 mm Hg col and current - 0.2 amperes. Several spectrograms showing the hyperfine structure of uranium and plutonium lines in the 4100 to 6500 A region were obtained, using 6, 10 and 15 mm etalon spacers and exposure times of 20-30 minutes.

Careful examination of the U^{233} spectrograms disclosed 12 lines with a distinct hyperfine structure. For four of these - 6826.93, 5976.32, 5915.40 and 4515.28 A - we detected a fully resolved six-component structure. On the basis of this six-component structure it can readily be deduced that the nuclear spin of U^{233}, I = 5/2.

We made the most detailed study of the hyperfine structure of the 5915.40 A arc line of U^{233}. A microphotogram of this line showing the six components, characterized by decreasing intensities for lower wave

---

* The complete report is printed in Zhur. eksp. i teor., fiz., 28, 471 (1955). [Translation in Soviet Physics - JETP, 1, 310 (1955).]

numbers, is reproduced in Fig. 1. The transition scheme is given in the upper part of Fig. 2, while in the lower part of the figure the hyperfine structure of the 5915.40 line is represented schematically. The transition scheme was plotted on the basis of the experimentally determined falling off of the intensity of the components, taking into account the intensity rule and assuming that only the upper term undergoes splitting. This assumption is borne out by the fact that the 6828.93 A line, which has the same lower term, has half the splitting width and an inverse order in the intensity of the hyperfine structure components. The relative intensities of the hyperfine components proved to be

$$i_1:i_2:i_3:i_4:i_5:i_6 = 34:30:28:25:21:19$$

whence it follows that within the limits of the measurement error the intensity law is observed. The intervals between successive components, starting with the longest wavelength one were found to be 0.056, 0.064, 0.070, 0.068 and 0.065 cm^{-1}. Comparison of the experimental and theoretical values shows that the measured component distances do not conform with the normal interval rule. This indicates that the U^{233} nucleus has a large quadrupole moment. Since according to Anderson and White[1] the overall width of the 5915.4 A line in the case of U^{235} equals 0.21 cm^{-1}, we can roughly evaluate the ratio of the nuclear magnetic moments of U^{233} and U^{235} as

$$\mu_{233}/\mu_{235} = 0.323/0.21 \approx 1.5$$

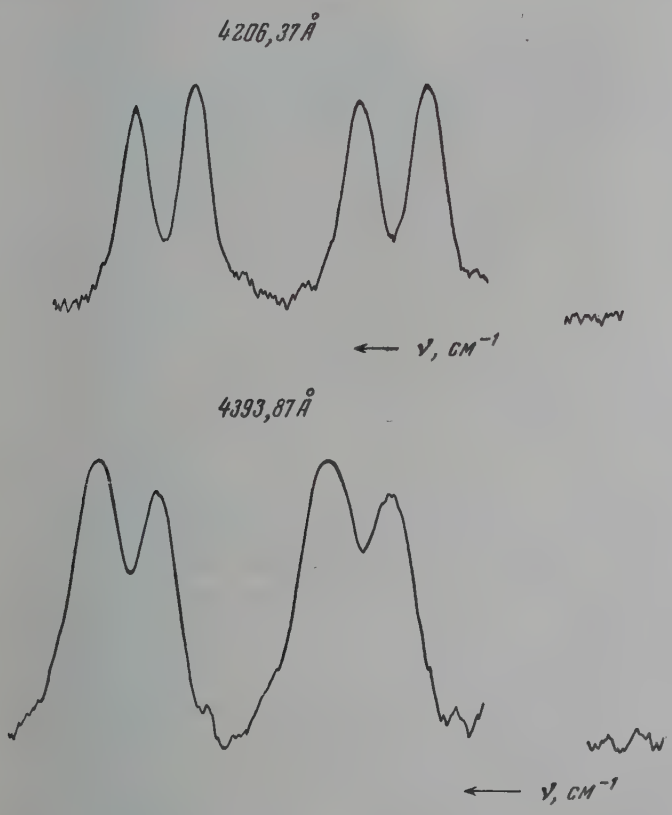

Fig. 3. Microphotograms of the hyperfine structure of two plutonium lines.

Inasmuch as the magnetic moment of U^{235} is negative[2], it follows from the splitting of the 5915.40 A line of U^{233} that the magnetic moment of the U^{233} nucleus must be positive.

Analysis of the spectrograms recorded for plutonium showed that about 70 lines split into two components; the most intense of these are the following: 4196.16, 4206.37, 4298.14, 4293.87, 4406.73, 4441.57, 4456.61, 4468.48, 4472.70, 4504.80, 4535.95, 4630.82 and 4664.10 A. It follows from the dobblet structure of the spectrum lines of P^{239} that the nuclear spin of this isotope equals 1/2.

The full hyperfine structure width of the plutonium lines varies between 0.04 and 0.2 cm^{-1}. The greatest spread was observed for the 4097.51, 4468.48, 4472.70 and 4504.80 A lines. Most of the split lines of plutonium have components of approximately equal intensity. A number, however, have components differing markedly in intensity; in some

the higher wavelength component is brighter; in others the short wave one. By way of illustration microphotograms of the hyperfine structure of the 4206.37 and 4393.87 A lines in two orders of the spectrum are reproduced in Fig. 3. The fact that in some cases the long wave component is more intense while in others the short wave component is stronger must be attributed to the splitting of different levels (upper and lower). The variation may also be connected with reversal of some sublevels of the hyperfine structure.

From the determined value for the nuclear spin of Pu^{239} it follows that according to theory the quadrupole moment of this nucleus equals zero.

In conclusion we might note that about a year after our investigation our data on the nuclear spins of U^{233} and Pu^{239} were confirmed by findings of Sluis and McNally[2] and Van den Berg, Klinkenberg and Regnault[3].

References

1. O.E.Anderson & H.K.White, Phys. Rev., 71, 911 (1947).
2. K.L.V.Sluis & J.R.McNally, J. Opt. Soc. Am., 44, 87 (1954).
3. M. Van den Berg & P.F.A.Klinkenberg & P.Regnault, Physica, 20, 37 (1954).

* * * *

ISOTOPE SHIFT IN THE SPECTRUM OF PLUTONIUM*

- A. R. Striganov, L. A. Korostyleva and Iu. P. Dontsov

The purpose of the present investigation, which was carried out in mid-1953, was to detect and measure the isotope shift in the spectrum lines of plutonium. The work was done on the same set-up as was used in the study of the splitting of the spectrum lines of U^{233} and Pu^{239} (see preceding article)[1]. The sample consisted of a mixture of Pu^{239} and Pu^{240} in the form of dioxides. Eight milligrams of the material were placed into the discharge tube. As in the previous experiments the plutonium oxide was reduced to the metal by atomic hydrogen under the discharge conditions. Excitation was effected at a pressure of 1-2 mm Hg col of argon, using a current of 0.2 amperes. Two spectra, using a 10 and a 15 mm spacer in the Fabry-Perot etalon, were photographed in the 4100-6500 A region with an exposure time of 60 min.

Approximately twenty lines with indications of isotopic structure were found in the spectrograms. Some of these comprised two components, others consisted of three. Visual comparison of the structure of these lines in the spectrograms of the Pu^{239} - Pu^{240} sample with the structure of the same lines in spectrograms obtained for pure Pu^{239} showed that one of the components in each group is due to Pu^{240}. By way of illustration the structure of the 4493.67 and 4206.37 A lines is shown schematically in the accompanying figure; as may be seen the former has two components, the latter three. We measured the intensities of

---

* The full report appears in Zhur. eksp. i teor. fiz., 28, 240 (1955). [Translation in Soviet Physics - JETP, 1, 354 (1955).]

the components of a series of spectrum lines exhibiting isotopic structure; the results confirmed the presence of isotope shift in the spectrum of plutonium.

In the investigated spectral region we detected 13 lines of plutonium with a clear isotopic structure: 4140.10, 4151.38, 4159.87, 4478.63, 4986.72, 5044.53, 5590.51 and 5630.48 A and 6 lines with isotopic and hyperfine structure: 4206.37, 4396.31, 4468.48, 4472.70, 4676.18 and 6192.63 A. In the case of all except the 6192.63 A line the shift is "negative," i.e., the Pu^{240} component is shifted to the side of lower wave numbers. The magnitude of the isotope shift lies between 0.08 and 0.29 cm^{-1}; it will be noted that the mass number difference $\Delta A = 1$. The greatest shift is exhibited by the 4159.87, 4396.31, 4468.48, 4484.20 and 4986.72 A lines. The isotope shift in the plutonium spectrum is approximately of the same magnitude as the shift observed in the spectra of uranium[2] and thorium[3]. Comparing the isotope shift in the spectra of the elements of the actinium series with the shift in the spectrum of the preceding heavy elements (Hg, Tl, Pb) we note a jump to higher values in the actinium series. Such "jumps" have already been detected in the case of Ce, Nd, Sm, and Eu as well as for Pb. It has recently been established that in these elements the "jumps" are connected with great changes in the shape of the nucleus. Presumably the relatively large isotope shift in the spectra of the actinium series elements can be attributed to the same cause.

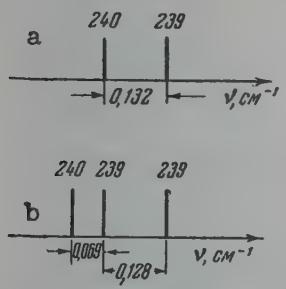

Structure of two plutonium lines: a - 4493.67 A; b - 4206.37 A.

References

1. L.A.Korostyleva, A.R.Striganov & N.M.Iashin - preceding article in this issue of the Bulletin (Trans. p. 26; Orig. p. 31).
2. J.R.McNally, J. Opt. Soc. Am., 39, 271 (1949).
3. G.L.Stukenbrocker & J.R.McNally, J.Opt.Soc.Am., 43, 36 (1953).

* * * *

THE EFFECT OF LIGHT FROM A MERCURY ARC ON THE EMISSION OF A FLAME

- S. M. Kishko and V. S. Miliianchuk

The purpose of the present investigation was to study the possible scattering of light from molecules in an excited state; to this end we irradiated an illuminating gas flame, which contains a considerable concentration of excited C_2, CH and OH groups, with the full spectrum of a mercury arc. A comparison of the spectrum of the flame irradiated with mercury arc light (Spectrum b, see page 31) with the spectrum obtained under the same conditions and with the same exposure (120 hours)but without irradiation (Spectrum a) shows that some new bands appear under the influence of irradiation. These bands correspond to transitions between the same electronic levels as those associated with the bands in the spectrum of the non-irradiated flame. Under the action of the mercury arc light there also appear new lines, corresponding to

forbidden transitions between rotational levels. From an analysis of the rotational structure of the Swan lines of C_2 (0, 0 and 2, 3) it follows that under the influence of irradiation there appear in the flame spectrum forbidden branches corresponding to transitions with $|\Delta J| = 2$ and $|\Delta J| = 3$ (J is the rotational quantum number). The intensity of the usual bands of the flame spectrum is also increased by irradiation with light from a mercury arc.

It can be shown by applying the principle of correspondence that in the case of quantum processes of the second order, except where resonance fluorescence is concerned, the frequency of the emitted light depends on the frequency of the incident light. In the exceptional case of resonance fluorescence, while the emitted frequency is independent of the incident frequency, the emitted frequency is equal to a frequency associated with an allowed transition. Consequently, the effect observed in our case cannot be explained as due to a process of the second order.

It follows from the principle of correspondence that there may occur processes of the third order in which the frequency of the emitted light does not depend on the frequency of the incident radiation. The possibility of such third order processes is also indicated by the change of three units in the value of J. From expressions derived by means of quantum electrodynamics for the probability of processes of the third order in which one photon having a momentum $\hbar\mathbf{k}$ ($\mathbf{k}$ is the wave vector) is absorbed and two photons having momenta $\hbar\mathbf{k}$ and $\hbar\mathbf{k}'$ are emitted it follows 1) that in such processes $J \rightarrow J$, $J \rightarrow J \pm 1$, $J \rightarrow J \pm 2$ and $J \rightarrow J \pm 3$ transitions are possible, 2) that the selection rule for the vibrational quantum number υ may be violated, 3) that the selections rules relating to parity, symmetry and sign of the initial and final states are not violated, and 4) that the frequency emitted in such processes is $\omega' = (E_a - E_b)/\hbar$ (E_a and E_b are the energies in the initial and final states of the molecule, respectively), i.e. is independent of the frequency of the incident light.

Hence, normally forbidden lines, such as those we observed, can appear in the case of third order processes of the type discussed. The forbidden lines produced as a result of such processes of the third order can have an appreciable intensity only when $\hbar c|\mathbf{k}| \backsim E_a - E_i$ (E_i being the energy of the molecule in the intermediate state), ie., only in the case of resonance. Thus, the observed phenomenon can be explained as a resonance fluorescence of the third order.

Physical Institute of
L'vov State University

Spectrum of illuminating gas flame (propane & butane): a) not irradiated; b) irradiated with light from mercury arc.

(See page 29.)

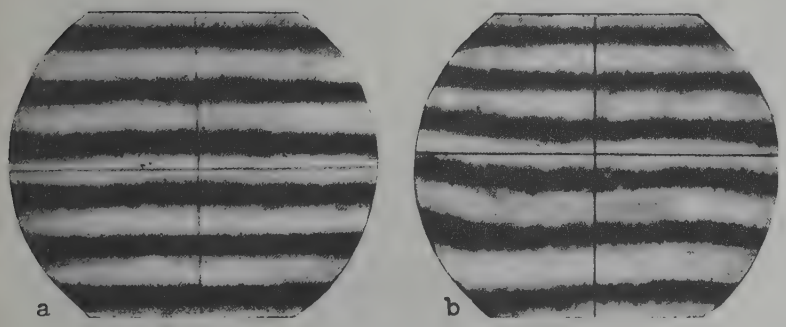

Interferograms produced by grating replica (from original ruled on aluminum on glass): a)in the zero order; b) in the first order of the spectrum.

(See page 32.)

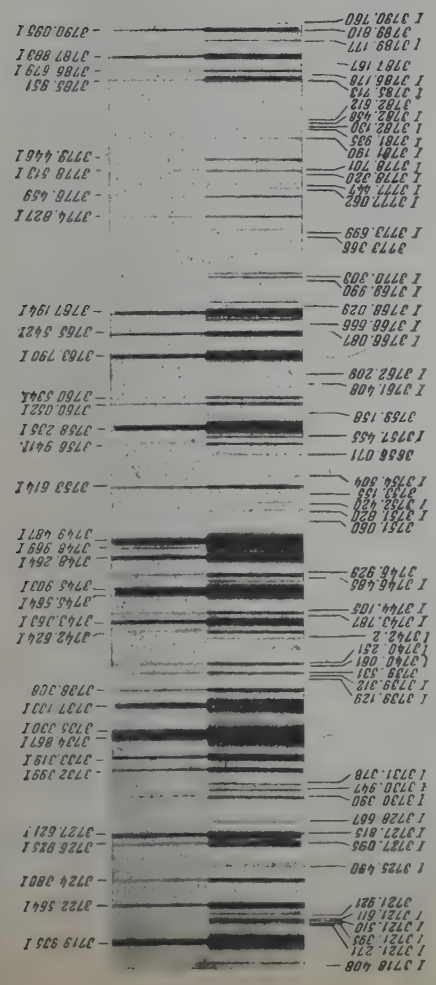

Fig. 1. One of charts from atlas of iron spectra (First arc chart -- see page 32).

Fig. 2. Twenty fifth chart from the second part of the atlas, showing appearance of iron arc spectrum as viewed in spectrum projector (see page 33).

DIFFRACTION GRATING REPLICAS

- A. A. Nizhin and F. Z. Pedos

The availability of diffraction gratings has a direct bearing on the further development of the spectroscopic instrument industry. The use of gratings has been limited by the difficulties of production and the high cost of quality gratings.

Copies or replicas of diffraction gratings can be successfully used in many spectroscopic instruments with a short focal length (up to one meter). Various methods of preparing grating replicas are described in the literature[1-5]. Most of these methods, while of undoubted interest, have a series of shortcomings as the result of which they fail to assure exact replicas of the parent grating.

The method of producing replicas based on the use of thin polymer films mounted on a rigid base merits particular attention.

Having introduced certain improvements in the known methods of making replicas and developed certain new procedures for the basic operation of transferring the microrelief of the parent grating to a gelatin layer[5], we have succeeded in obtaining satisfactory reflection replicas from diffraction gratings ruled on aluminum coated on glass. Specifically we made good replicas from a grating ruled with 600 lines/mm and having a ruled area of 50 x 60 mm which reflects 74% of the light into the first order at a wavelength of 5893 A and has a resolving power of 36,000.

The spectral purity of the lines produced by our replicas and their resolving power were evaluated visually on a spectroscope having a focal length of one meter using a slit width of 0.015 mm and a 20 X magnifier lens. A good proportion of the replicas gave good resolution in the first order of the 4957.61 and 4957.31 A arc lines of iron, which indicates a resolving power of 16,000. A further check using a 3-meter focal length instrument showed that the best replicas have a resolving power in the first order of up to 30,000.

Inspection with an interferometer showed that deviations from the plane of the ruled area of the replicas do not exceed 0.13 μ. The wave front error in the first order of the spectrum for replicas having a resolving power of 16,000 or more also does not exceed 0.13 μ over an area of 45 x 45 mm. The interferograms produced by one of these replicas in the zero and first orders of the spectrum are reproduced on page 31.

Tests on the replicas have also shown that their characteristics do not change with time and vary little with temperature. As regards their ability to concentrate light they are fully comparable to the parent grating.

The described diffraction gratings are fully suitable for use in low and medium dispersion spectroscopic instruments.

References

1. R.J.Wallace, Astr. Journ., 22, 123 (1905).
2. R.W.Wood, Nature, 140, 723 (1937).
3. R.A.Sawyer, Eksperimental'naia spektroskopiia, M. 1953. Experimental Spectroscopy, N.Y. 1944.
4. S.T.Merton, Proc. Roy. Soc., 201, 187 (1950); G.D.Dew & L.A.Sayce, Proc. Roy. Soc., 207, 278 (1951).

ATLAS OF SPECTRUM LINES FOR GLASS PRISM SPECTROGRAPHS

- S. K. Kalinin

In connection with the great development of spectroscopic methods of analysis Soviet science and industry is making ever more extensive use of various types of high-quality spectroscopic instruments, including the ISP-51 three-prism glass spectrograph.

Until recently investigations with this instrument have been hampered by the lack of suitable atlases and tables of spectrum lines. The need for such aids has been acutely felt by workers in both scientific research and industrial laboratories.

To fill the lacuna the personnel of the Physico-Technical Institute of the Academy of Sciences of the Kazakh SSR compiled an atlas of spectrum lines containing the basic data needed for the analysis of spectra in the 3700-9100 A region[1,2]. The most important spectrum lines of the elements used for purposes of practical analysis are concentrated in this region. Extension of the charts into the region of shorter wavelengths was limited by the transmission characteristics of the instrument's optical system, which cuts off at about 3700 A, while the long-wave boundary was imposed by the sensitivity range of the photographic materials available to us.

For convenience in use, the atlas has been divided into two parts:

The first contains 38 photographs of the arc and spark spectra of iron obtained by means of an ISP-51 spectrograph equipped with a UF-84 camera. The instrument has a high dispersion and a high resolving power and produces a good quality image over the entire plate.

The source used for the arc series of charts was an activated AC arc (220 v, 6 amp); the condensed spark for the spark spectra was produced by an IG-2 generator (C = 0.01 μf, L = 0.01 microhenries).

The iron spectrum was photographed in sections, the successive sections being brought to the center of the plate. Two photographs with different exposures were obtained for each section; the exposure times were selected so to obtain the most intense lines without overexposure on the short-exposure photograph and to bring out the maximum amount of detail in the long-exposure photograph. The 3700-5700 A region was photographed on "Isoortho" plates, the 5700-7500 A region on "Paninfra" plates and the 7500-9100 A region on "Infra" plates.

The recorded spectra were enlarged 20 times and assembled in the form of 21 charts for the arc spectrum and 17 charts for the spark spectrum. The wavelengths of 1808 iron lines are marked on the charts. The wavelength values are taken from the tables of Zaidel, Prokof'ev and Raiski, supplemented by data from other investigators. Where possible the lines are identified as belonging to neutral (I) or ionized (II) atoms. In addition the lines of nitrogen and oxygen are marked on the spark spectrum. A reproduction of one of the arc charts, considerably reduced in size, is shown in Fig. 1 (p. 31). The atlas is supplemented by a description of the charts and a full table of the wavelengths of iron lines.

The second part of the atlas consists of 26 charts showing individual sections of the iron spectrum as it appears when the spectrograms are viewed in a spectrum projector (Fig. 2, p. 31). A wavelength scale is drawn under the spectrum to facilitate location and identification of the lines and in addition the positions of 1130 lines of 76 other elements, with the symbol for the element, the wavelength of the line to the nearest 0.1 A and the intensity in relative units are marked on the charts.

The line intensities were evaluated in the 10-point scale from spectrograms obtained by photographing the spectra of the pure elements and standards containing 10, 1, 0.1, 0.01, 0.001 and 0.0001% of the element in question. The standards were prepared using a granite type silica mineral since this material approximates the composition of many ores. Samples of 15-20 mg weight were burned in an activated AC arc (8-10 amp) between carbon electrodes (for some elements between copper electrodes). From successive spectrograms it was established at what concentration of the element each of the characteristic lines appeared. Lines which appeared in the spectrum of the standard samples with a content of the element of 10% and higher were assigned the intensity value of 1; lines appearing at a concentration of under 0.001% were assigned a value of 10 on the scale.

The spectrograms so obtained served as the basis for the selection of lines to be marked on the atlas charts. Of the great number (over 60,000) of lines in this region of the spectrum only the most intense were chosen for inclusion in the charts. More full representation is given to lines of the alkali and alkali-earth elements. Some of the spark lines of Si, P, etc., commonly used in analytic practice and the positions of the more intense heads of the bands associated with CN, CaF, AlO, LaO and other molecules, observed in arc spectra, are also indicated in the charts.

The descriptive and reference material in the atlas is arranged in the same order as in our preceding publication[3].

The atlas should greatly facilitate carrying qualitative and semi-quantitative analyses for Li, Na, K, Rb, Cs, Ca, Sr and Ba as well as for Al, Tl, Cr, Pb, Nb and other elements, that have sensitive lines in the visible and infrared ranges of the spectrum. The atlas may also prove useful in astrophysical investigations.

**Physico-Technical Institute of the
Academy of Sciences of the Kazakh SSR**

1. S.K.Kalinin & V.L.Marzuvanov, Atlas dugovogo i iskrovogo spektrov zheleza ot 3718 do 9739 A (Atlas of iron arc and spark spectra, 2718-9739 A)Alma-Alta 1954.

2. S.K.Kalinin, L.E.Naimark, V.L.Marzuvanov & K.I.Ismagulova, Atlas spektral'nykh linii elementov - Oblast' 3718-9130 A (Atlas of spectrum lines of the elements - Range 3718-9130 A) Alma-Alta 1955.

3. S.K.Kalinin, Iavnel', Alekseeva & Naimark, Atlas spektral'nykh linii dlia kvartsevogo spektografa (Atlas of spectrum lines for a quartz spectrog.)M.-L. 1952.

* * * * * * *

SOME CHARACTERISTICS OF LOW-VOLTAGE PULSED DISCHARGES

- D.B.Gurevich, R.A.Esin & V.K.Prokof'ev

Low-voltage pulsed discharges are finding increasingly wide use in spectroscopic analysis. The present report is devoted to the results of our investigation of the process of ejection of the luminous jet in such discharges, the duration of the ejection process and of the emission of the spectrum lines of individual elements in the zone of the jet.

1. For investigating the ejection process we assembled a special circuit designed to fire a single pulse, supplied from a battery of capacitors having a

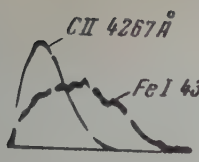

Emission of spectrum lines in the zone of the jet of a low-voltage pulsed discharge. The excitation potential of the Fe I 4325 A line is 4.5 ev; that of the Cu II 4267 A line is 20.9 ev.

maximum capicatance of 6000 μf and charged to 300 v. The discharge pulse was localized by an insulating bushing with a 1 mm opening. The upper electrode was located slightly off to the side to allow the jet to develop to its full length. We employed a mirror scanning system to observe the individual stages of the jet ejection process and measure the variation of its luminosity with time. In addition the individual stages in the development of the jet were photographed with an exposure time of $1.5 \cdot 10^{-5}$ sec.

Our investigations showed that the luminous (incandescent) material is discharged from the opening in the insulating bushing at a very high velocity: 800 m/sec or higher. The jet is distinctly striated. At the very first instant there is a maximal ejection of material which forms a luminous cloud at an appreciable distance from the electrode; the luminescence of the cloud dies down in some 0.003 sec. Ion lines predominate in the emission from the ejected stream while neutral atom lines predominate in the spectrum of the cloud. The cross section of the jet varies little with time.

2. The character of the spectrum lines in the pulse discharge was investigated using a circuit in which the capacitance could be varied between 200 and 5000 μf (at 300 v). The emission from the pulse discharge was projected on a diaphragm, separating out the emission from individual sections of the flame. The spectrum line of interest was then separated from the restricted beam by means of a plane grating spectroscope (dispersion - 7 A/mm) and detected by a FEU-17 photomultiplier, the output of which was amplified by an electronic amplifier with a 1 mc pass-band. The amplified signal was fed into a cathode-ray tube, the sweep of which was adjusted to obtain a trace of the line-emission intensity with a resolution in time of $2 \cdot 10^{-5}$ sec. The pattern on the tube screen was photographed with a fast camera.

In this manner we investigated the emission of spectrum lines of H, Cu, Zn, Fe, C and Sn with diverse excitation potentials. The results may be summarized thus:

1) Ion lines appear first, show a steep leading edge (on the screen) and are extinguished earlier than the lines of neutral atoms; the emission of neutral atom lines reaches a peak later and persists longer (see above figure). There is a definite connection between the duration of emission and the excitation potential of the upper level of the line. Spectrum lines with low excitation potentials (4-5 ev) persist for some time after the discharge current ceases. Thus, where the discharge current flows for $3.4 \cdot 10^{-4}$ sec, the emission of such low-potential lines is discernable to $4.4 \cdot 10^{-4}$ sec from the zero instant.

2) The discharge temperature at different instants was evaluated from the relative intensity of the 5105 and 5133 A lines of copper. It was found that the temperature falls off rapidly from 11,000°K at the $3.6 \cdot 10^{-4}$ instant to 7000°K at $3.6 \cdot 10^{-4}$ sec. Measurements of the relative intensity of the N II 5045 and 5179 A lines were used to determine the temperature in the vicinity of the electrode. In the first stage of ejection the temperature of the jet in the immediate vicinity of the electrode rises to 33,000°K; by $1.3 \cdot 10^{-4}$ sec after the initial instant it falls off to 22,000°K.

3) Records of the current and voltage variations in time made it possible to evaluate the energy released in the pulse discharge. It was found that about 50% of the energy stored in the capacitors is liberated in the discharge.

4) The contour of the H line was investigated oscillographically at different stages of the discharge. The breadth of this line is about 20A and does not vary with time (at least in the case of time intervals exceeding $5 \cdot 10^{-5}$ sec).

THE DFS-2 AND DFS-3 DIFFRACTION GRATING SPECTROGRAPHS

- R. I. Tveriankina

In 1953 the optical instrument industry of the Soviet Union started producing two types of grating spectrographs intended for qualitative and quantitative emission analysis of metals, alloys, ores and minerals and other spectroscopic investigations in the 2000 to 10,000 A region of the spectrum.

1. The DFS-2 spectrograph uses a Paschen-Runge type mounting and consists of two independent optical systems with two-meter radius concave gratings having 600 and 1200 lines/mm. The two systems are mounted one above the other inside a cylindrical metal housing 2 meters in diameter (see Fig. 11, p.336 , Trans. No. 6, Vol. 18 of the Bulletin, i.e., the preceding issue). The two systems have separate entry slits and cassette holders. The spectrum from 2000 to 10,000 A has a length of 1000 and 2000 mm, the dispersion is 8.3 and 4.2 A/mm, the resolving power 42,000 and 84,000 with the 600 and 1200 lines/mm gratings, resp. The aperture ratio is 1:30. The cassettes take a 500 mm length of film and can be shifted laterally to photograph any desired section of the spectrum.

The great astigmatism of concave diffraction grating systems precludes the use of step weakeners or diaphragms in front of the slit to limit the slit height. Hence the DFS-2 spectrograph has provision for mounting step weakeners or special filters in the cassette, immediately in front of the film in order to reduce the intensity of only the desired lines. The spectrum is limited in height by means of special slit diaphragms which are also located at the film. The cassettes can be shifted up and down which allows of photographing several spectra under each other.

2. The DSF-3 spectrograph employs autocollimation with reflection in the vertical plane; it has a 4-meter focal length mirror and is equipped with interchangeable 600 or 1200 lines/mm plane gratings. The body of the instrument is a long welded tube (see Fig. 12, p.336, No. 6, Vol. 18 of the Bulletin). The reflecting mirror is mounted at one end of the tube, while the entry slit, the cassette holder and the grating mount are located at the other end. The grating mount rotates on a vertical axis. Whereas in the DFS-2 instrument the entire spectrum is formed at one time, in the DFS-3 individual sections of the spectrum are brought to the plate by rotating the grating. A portion of the spectrum 1000 or 500 A in extent (dispersion 4 or 2 A/mm) is received by the 24 cm photographic plate, depending on which of the two gratings is in place. The corresponding resolving powers are 72,000 and 144,000. The relative aperture of the system is 1:42.

One may judge of the superior resolving power and spectral qualities of the DFS-2 and DFS-3 instruments by comparing their spectra with those obtained with prism instruments having approximately the same dispersion and relative aperture. Thus in the iron spectrum obtained with the DFS-2 using the 1200 lines/mm grating (reciprocal dispersion 4.2 A/mm in the 3100 A region) one can see fully resolved lines only 0.093 and 0.077 A apart. No such resolution is obtained with the KS-55 prism spectrograph which has a dispersion of 4.6 A/mm in this region.

Juxtaposing the spectra of iron in the vicinity of 2350 A recorded by means of the DFS-2 with the 600 lines/mm grating (dispersion 8.3 A/mm) and by means of the ISP-22 spectrograph (dispersion 6.5 A/mm) we note that the 2348.303 and 2348.099 lines are equally well resolved in both despite the difference in plate factors. Comparing the spectrum in the vicinity of 4200 A obtained with the UF-85 instrument having a dispersion of 3 A/mm with the spectrum photographed with the DFS-2 with the 1200 lines/mm grating (dispersion 4.2/mm) we observe that the DFS-2 separates lines 0.12 A distant and yields clearer lines.

The spectrum of the 3883.4-3871.4 A band of cyanogen obtained in the first and second orders on the DFS-3 spectrograph shows the superior quality and high resolving power of the instrument: lines at a distance of 0.05 A are fully and clearly separated. In photographing the fine structure of mercury lines with the DFS-3 and the 1200 lines/mm grating, particularly clear pictures were obtained of the lines near 4358 and 3655 A; all the components can be clearly distinguished.

The diffraction gratings with 1200 lines/mm regularly mounted in the DFS-2 and DFS-3 spectrographs throw a maximum concentration of energy into the first order in the 2800 A region; they can be used for work in the short ultraviolet (1976 A) without noticeable weakening of the spectrum.

* * * * * * *

A PHOTOELECTRIC SPECTROGRAPH FOR QUANTITATIVE SPECTRUM ANALYSIS

- I.V.Podmoshenski & L.D.Kondrasheva

Of the various extant methods of emission analysis the one having the greatest potentialities as regards worthwhile improvement in speed and accuracy is the photoelectric method. During the last decade there have been published many descriptions of photoelectric set-ups, in most of which photomultiplier tubes are employed as radiation receivers. (The spectrograph described by Averbukh et al in Zavod. labr. [The Factory Laboratory] 20, 1 (1954), is an outstanding exception.)

Photomultipliers with an antimony-cesium cathode have an inferior sensitivity stability and a lower (about one order of magnitude) signal to dark current ratio as compared with cesium-antimony photocells equipped with shielding and insulation rings. However the absence of dependable electronic circuits for measuring weak photocurrents restricts the use of photocells.

In the photoelectric set-up described herein antimony-cesium photocells with uviol (ultraviolet-transmitting) glass envelopes were employed for recording the intensity of the spectrum lines.

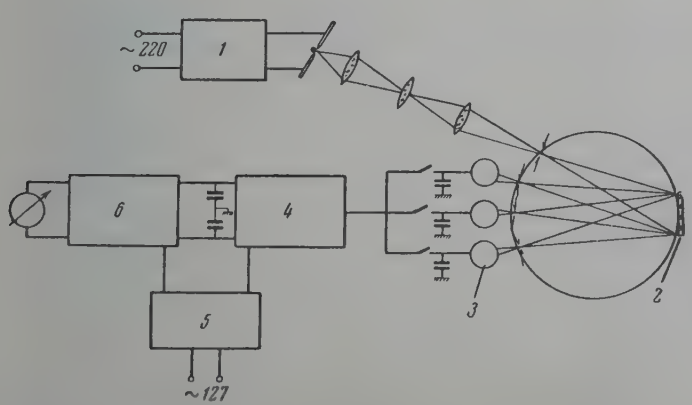

Block diagram of the photoelectric set-up:
1) source, 2) grating, 3) photocells, 4) vacuum tube electrometer, 5) voltage stabilizer, 6) vacuum tube voltmeter

The dispersing element employed to form the spectrum in the 2000-5000 A region is a concave 1200 lines/mm grating with a radius of curvature of 2 meters and a dispersion of 4 A/mm in the first order.

The set-up has a system of movable exit slits permitting simultaneous separate measurement of the intensities of eight spectrum lines. In designing the set-up special provisions were made to maintain a constant temperature and reduce vibration.

The photocurrent is recorded by the accumulation of charge method. The charge is amplified by a specially developed electrometer [sic].

Commonly vacuum tube electrometers with an electrometric output and a time constant on the order of 10^{-4} sec are used in such recording circuits. In this set-up a pulsed circuit is used. In measurement the storage capacitor is discharged through the input resistance of a vacuum tube electrometer, the discharge time being $5 \cdot 10^{-3}$ sec. The discharge current is amplified by an AC amplifier and then limited. Thus at the amplifier-limiter output there is formed a rectangular pulse which charges a high-capacity capacitor. The charge on this capacitor is proportional to the logarithm of the charge built up in the first storage capacitor.

A differential vacuum tube voltmeter measures the difference between the charges on the output capacitors; consequently the indications of the voltmeter are proportional to the logarithm of the relative intensity of the spectrum lines. This same voltmeter is also used in setting the exit slits to the desired spectrum lines. Use of the described circuit makes it feasible to reduce the input resistance of the electrometer by about six orders of magnitude compared to the value common to convential circuits which results in greater freedom from interference effects and makes for less exacting requirements where the electrometric characteristics of the input tube are concerned.

The measurement process is fully automatic. The circuits are powered from the regular AC line, the voltage being controlled by an electronic stabilizer. The spectrum is excited by means of the arc and spark generator with electronic control described below in this issue. The electronic measuring circuits are thoroughly shielded so that the operation of the arc and spark generator or other generators in the vicinity of the set-up does not affect the recorded results.

The measurement error in extensive electric and photometric tests did not exceed 1%. Trial analyses of low-alloy steels showed that the accuracy of determination is at least equal to that attained with photographic recording.

* * * * * * *

USE OF AN ELECTROMETER WITH A DYNAMIC CAPACITOR FOR RECORDING SPECTRA

- L.P.Maliavkin & I.S.Abramson

The systems for photoelectric recording of spectra commonly employed can be divided into two classes according to the type of amplifier used: those with DC amplifiers and those with AC amplifiers. Each class has certain advantages and disadvantages peculiar to it[1,2]. The desirability of developing a system which would reunite the advantages of both classes is obvious. We developed and tested one promising system employing an electrometer with a dynamic capacitor[3,4], based on the method of parametric modulation of Mandel'shtam and Papaleksi. Attainment of the highest degree of sensitivity of which the dynamic capacitor circuit is theoretically capable is hampered by drift of the capacitor modulation factor and of the difference in contact potentials. The effect of the first drift can be minimized by the use of negative feedback. In the case of the actual light fluxes from indi-

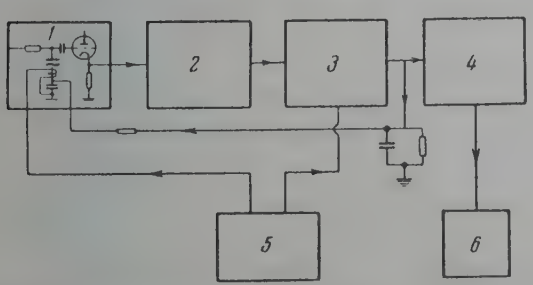

Block diagram of set-up:
1) Coupling unit, 2) three-stage narrow-band amplifier, 3) synchronous detector, 4) differential cathode follower, 5) modulator unit, 6) recording instrument.

vidual emission spectrum lines the second drift proves to be negligibly small compared to the potential built up on the storage capacitor. In practice, therefore, the sensitivity threshold of the circuit in measuring light fluxes is determined not by the above-mentioned factors but by the dark current of the radiation receiver and the leakage current or, more precisely, by the fluctuation or drift in the values of these two currents inasmuch as the currents themselves can be compensated for.

The set-up consisted of the units pictured in the accompanying block diagram. The coupling unit 1 comprises the dynamic capacitor and a one tube amplifier. This is a separate unit and is mounted adjacent to the radiation receiver. In order to minimize the effects of external interference (electric noise from the light source, the input circuit and static in general) on the electrometer it is essential to use a narrow pass-band amplifier. In the described set-up we employed a three-stage narrow-band amplifier (2 in the diagram) with a twin-T network RC filter in conjunction with a synchronous ring detector having a time constant of 1 sec (3 in diagram). It should be noted that proper selection of the time constant is important where stable operation of the whole system is concerned. If the detector time constant is not correlated with the time constant of the input circuit, oscillatory effects may appear and the circuit may develop a tendency toward self-excitation.

By way of recording instrument (6 in diagram) we used an EPP-09 type electronic potentiometer having a sensitivity of 10 mv per scale deflection and an indicating time of 2.5 sec.

A differential cathode follower (4 in diagram) was used to match the resistance of the detector with that of the recording instrument. DC feedback was accomplished by applying the full rectified output voltage on the input of the stage connected to the dynamic capacitor; thus the whole system with the exception of the cathode follower was comprised in the feedback circuit. Modulation of the dynamic capacitor was effected at a frequency of 170 cps from the special oscillator (5) which also supplied the commutating voltage for the synchronous detector.

The set-up was investigated in two stages: first, we tested the effectiveness of the electrometer circuit for measuring small currents and second, we made a systematic study of the applicability of the electrometer circuit for the purposes of spectrum analysis.

Tests of the electrometer showed that the circuit attains the normal operating state about 8 minutes after being turned on; most of this interval is accounted for by the warm-up time of the cathode follower. The linearity of the system was checked over the range from 0.05 to 20 volts; no departure from linearity was observed. This range of voltages with a 500 $\mu\mu$f capacitor and a charging time of 100 sec corresponds to a light flux measurement range of $2.5 \cdot 10^{-9}$ - 10^{-6} lumens (given a photocell response of 100 microamp/lumen).

The tests also showed that the circuit is relatively insensitive to supply voltage variations: fluctuations of the nominally 220 v supply between 140 and 250 v had no noticeable effect on the indications of the instrument. The circuit is also little sensitive to variations of the amplification factor; thus the readings remained constant despite a five-fold variation (from 1500 to 7500) of the gain.

The instrument error, determined by repeated measurement over a period of many days of the same input voltage (1.5 v) amounted to ± 0.28%.

The applicability of the electrometer circuit to recording spectra was investigated using the optical portion of the photoelectric set-up described in an earlier communication[2].

For this part of the investigation a STsV-4 (cesium-antimony) photocell and a styroflex insulation storage capacitor were mounted in each of the measurement channels. A special switching mechanism was introduced into the EPP-09 recording instrument to actuate the group of relays, triggered when the voltage on the

comparison channel capacitor reached a certain value. The measurement procedure employed was the same as with the earlier set-up[2]: during the exposure interval the electrometer indicated the voltage on the storage capacitor of the comparison (internal standard) channel; when this voltage reached a set level the special switching mechanism in the EPP-09 automatically cut-off the light source and switched the electrometer to the channel of the investigated spectrum line. The exposure time (i.e., the time to build up the triggering charge) was usually about 30-40 sec.

Tests using stable light sources (a mercury tube and an incandescent lamp) showed that the measurement error in this case, as determined on the basis of a large number of measurements over a period of many days, is 0.52%. When an activated AC arc produced by the generator with electronic control was used as the source, the error in determining the Cr content in steels amounted to 0.6-1.8% (Cr concentrations ranging from 0.04 to 4.5%).

Operational tests of the electrometer set-up showed that it has the following meritorious features: 1) the circuit does not consume any appreciable amount of energy from the measured voltage source (i.e., has a negligible internal loss); 2) the results of measurement are not affected by variations in the supply voltage, the parameters of the circuit components, the emission characteristics of the source and so on within the limits likely to be encountered; 3) the circuit does not require any special selection or matching of tubes and components with the exception of the dividing capacitor in the grid circuit of the input tube; 4) the circuit can be coupled to any, even the lowest internal resistance recording instrument; 5) by virtue of the use of a storage capacitor at the input and a narrow pass-band amplifier and proper selection of the operating frequency (one which is not a multiple of the supply line frequency), the circuit is insensitive to external interference in general and specifically to interference from the light source and source generator.

Commission on Spectroscopy at the
Academy of Sciences of the USSR
and the
"P.N.Lebedev" Physical Institute of the
Academy of Sciences of the USSR

References

1. Sbornik "Problemy sovremennoi fiziki" (Symposium "Problems in modern physics") Series III, Issue 16, M. 1951.

2. I.S.Abramson, KH.E.Sterin & A.N.Mogilevski, Izv. (Bulletin) AN SSR, Ser. fiz., 18, 264 (1954).

3. I.Shintel'meister, Elektronnaia lampa kak pribor dlia fizicheskikh izmerenii (The electron tube as a tool for physical measurements).M.-L. 1949.

4. A.M.Bonch-Bruevich, Primenenie elektronnykh lamp v eksperimental'noi fiziki (The application of electron tubes in experimental physics).M.-L. 1954.

* * * * * * *

THE USE OF A HIGH FLUX MONOCHROMATOR IN CONJUNCTION WITH PHOTOELECTRIC RECORDING IN RAMAN SPECTROSCOPY

- Ia.S.Bobovich & D.B.Gurevich

An effective means of improving the sensitivity threshold and resolving power of photoelectric spectrum recorders is the use of a monochromator having a high flux transmission. We assembled a high radiant power monochromator and tested it thoroughly in a photoelectric recording set-up. The high flux value obtained with the monochromator is due to the use of a large effective aperture (180 mm dia) and high slits (50 mm). The design employs a simple autocollimating system. The objective consists of two cemented lenses 180 mm in diameter and has a focal length of about 1200 mm. Both outer surfaces are coated. The dispersing element is a 600 lines/mm plane grating with a 150 x 150 mm ruled surface, capable of concentrating over 50% of the light on one side in the second order in the blue region.

The radiation receiver used for testing the monochromator was a FEU-17 photomultiplier which was coupled to a DC amplifier employing a bridge circuit assembled about a 6Zh1Zh tube. The spectrum was recorded by a light spot on photographic paper.

The operating stability, sensitivity threshold and resolving power of the set-up were tested by recording the Raman spectra of several different substances. Repeated recordings of the spectrum of toluene showed that even in the absence of voltage stabilization of the power supply for the mercury tubes the very weak 843 cm^{-1} line can be recorded with an average error not exceeding 4.6%. The error in measuring the intensity of stronger lines varies from a fraction of a percent to 3%. The degree of accuracy attained surpasses that possible with photographic photometry. The principal source of error is the instability of the emission of the high-pressure mercury tubes, which is appreciable even when the power supply voltage is stabilized.

The sensitivity threshold was evaluated from the record of the Raman spectrum of a mixture consisting of 95% CCl_4 and 5% of 2,2,3-trimethylbutane. This material was chosen to permit direct comparison of the results with the data obtained earlier by Sushchinski by photographic methods. It was found that when the 2,2,3-trimethylbutane content in the mixture is only 1% the characteristic analytic line still comes through well and the relative accuracy of determination is within about 15%, which is acceptable in many cases. Yet in photographing the spectrum the component in question cannot be detected when present in concentrations under 5%.

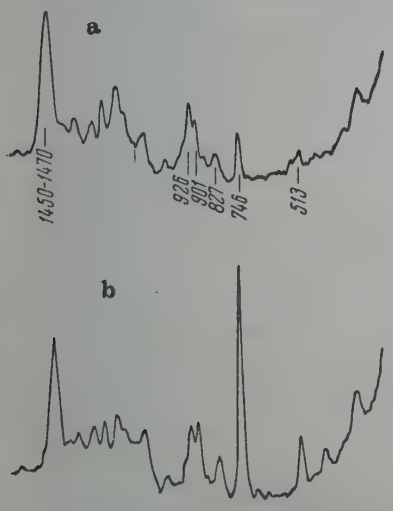

Record of the polarization spectrum of 2,2,4-trimethylpentane obtained at the full aperture of the monochromator: a) weak component; b) strong component.

The resolution attained allows distinguishing lines 10-12 cm^{-1} apart. This is not sufficient to permit the analysis of many mixtures containing components characterized by lines differing little in frequency. It may be possible to increase the resolving power of the set-up further by introducing a better slit to compensate for the curvature of the line images and making more complete use of the reserve sensitivity of the set-up.

We carried out quantitative and qualitative analyses of a number of synthetic mixtures containing alkene, alkane and aromatic compounds on the described set-up. The data obtained were compared with the results of analyses of the same mixtures

by photographic spectroscopy. We found that even when only small samples are available (2 cm^3) the error in intensity measurements in most cases does not exceed 6% and in some cases remains under 2%. The low sensitivity-threshold of the set-up allowed making determinations which could not be effected by the photographic method.

We also investigated the applicability of the photoelectric recording set-up to polarization measurements in the spectra of weakly scattering substances (saturated hydrocarbons). The average error in such measurements was found to be within 4-8% which is better than can be achieved by photographic photometry.

The record of the polarization spectrum of 2,2,4-trimethylpentane obtained on the set-up is shown in the accompanying figure.

* * * * * * *

THE ST-7 STEELOMETER*

- E.L.Berman

The ST-7 Steeloscope is a specialized instrument intended for rapid quantitative analysis of metals and alloys, using either an arc or spark source. It has a constant deflection three-prism dispersing system; transition from one spectrum region to another is effected by rotation of the prism assembly.

The characteristics of the instrument - dispersion, transmission, resolving power and magnification of the eyepiece - provide for ready observation of the necessary analytic lines in the spectra of ferrous and non-ferrous alloys. The steeloscope is equipped with two interchangeable condensers - one with a short, the other with a long focal length - for illumination of the slit. The use of one or the other is determined by the relative positions of the electrode stand and the instrument proper. Photographic wedges instead of polarizing prisms are used in the ST-7 for photometric purposes. The incident light is first split into two beams of approximately equal intensity by the dividing prism which is located immediately behind the focal plane of the viewing telescope. After passing through the photometric wedges which attenuate the beams as necessary, the two divided beams are reunited by a special combining prism and directed into the field of view of the eyepiece. One of the beams forms a spectrum with a narrow vertical window in the middle; the spectrum of the second beam appears in this window. Thus the observer sees a vertical dividing cross-line flanked by the two analytic lines. The requisite analytic lines are brought to the dividing cross-line by rotating the prism assembly and displacement of part of the optical system of the photometer section. The photometer permits close juxtaposition of the spectrum lines over their whole length, so that sections of lines corresponding to the <u>same</u> part of the entry slit can be compared directly.

---

*Translator's note: In the translation of the article on New Spectroscopic Instruments in No. 6, Vol. 18 of the BULLETIN the designation of spectrometers in this class was erroneously transliterated as "stylo-". From the more detailed description in the present article it would appear that the name is borrowed from the Twyman designed Vickers "Steeloscope" without regard for the fact that this visual comparator is intended for the analysis of non-ferrous as well as ferrous alloys. C.T.T.

It may be noted that one of the great shortcomings of the polarizing photometers formerly available was in that the upper portion of one line was compared with the lower portion of the other line, i.e., the comparison was effected for sections corresponding to the upper and lower sections of the slit. The ST-7 instrument is free of this shortcoming.

A general view of the ST-7 steelometer with the separate stand mounting the sample and the counter-electrode is shown in the photograph on page 44. The photometric wedges are displaced to equalize the line intensities by means of the handwheels 3. The wedges are provided with suitably graduated scales which are projected on screen 4 when the lamp 5 is lit by pressing button 1. The spectrum image is focused by turning knob 2 which moves the collimator lens. Another knob, located on the other side of the instrument (not visible in the photograph) rotates the dispersing prism assembly.

The stand assembly consists of an adjustable stand and electrode and reference holders. The stand can be rotated in the horizontal plane by turning knob 7 and raised and lowered by means of knob 8 (just visible behind the main bracket in the photograph). The stand can also be tipped to the desired angle by turning the handwheel 9 and rotated together with the sample about the optical axis of the instrument by means of handwheel 10. The sample is mounted on the stand by means of a screw clamp. The electrode holder can be rotated in the horizontal plane. The steelometer is regularly supplied with an IG-2 spark generator. The unit equipment also includes a silencer-shield for the generator which serves to deaden the sound and protect the operator against the danger of shocks.

In plants and factories the steelometer is generally installed in foundry and similar rapid-analysis laboratories and is used for on-the-spot analytic control of production. Analysis of a sample for 3-4 components requires only 8-10 minutes, which makes it possible to carry out several check analyses during the course of a melt. The accompanying table shows the alloys successfully analyzed by means of the ST-7 instrument, the elements determined, the limiting concentrations and the analytic line pairs used. The average relative error in analyses is 4-7%.

Alloy	Elements determ.	Concent. range	Line pairs, Å	
Silumin AL-2	Silicon	10÷13	Si 6371,3	Fe 6400
	Iron	0,8÷1,5	Fe 5269,5	Cu 5292,5
	Copper	до 0,8	Cu 5105,5	Fe 5110,4
Brass silicide LKS-65-1,5,3	Silicon	1,3÷1,6	Si 6346,6	Fe 6400
	Zinc	28,5÷31,5	Zn 6362,3	Fe 6400
	Lead	2,5÷3,5	Pb 5608,8	Fe 5615,6
Brass L-62	Zinc	36,5÷39,5	Zn 6362,3	Fe 6400
Brass silicide LK-80-3	Silicon	2,5÷4	Si 6346,6	Fe 6400
	Zinc	15÷18,5	Zn 6362,3	Fe 6400
Al alloy AL8	Magnesium	9,5÷11,5	Mg 5183,6	Cu 5153,24
Zn alloy TsA4M3	Aluminum	3,5÷4,5	Al 5696,5	N 5666,6
	Copper	2,5÷3,5	Cu 5105,5	Fe 5110,4
Cast iron	Silicon	2÷2,7	Si 6346,6	Fe 6400
	Manganese	0,8÷1,0	Mn 4823	Fe 4859,8
Steel L-36 and precision cstgs	Silicon	0,17÷0,37	Si 6346,6	Fe 6301.5
	Manganese	0,50÷0,8	Mn 4323	Fe 4859,8

* * * * * * *

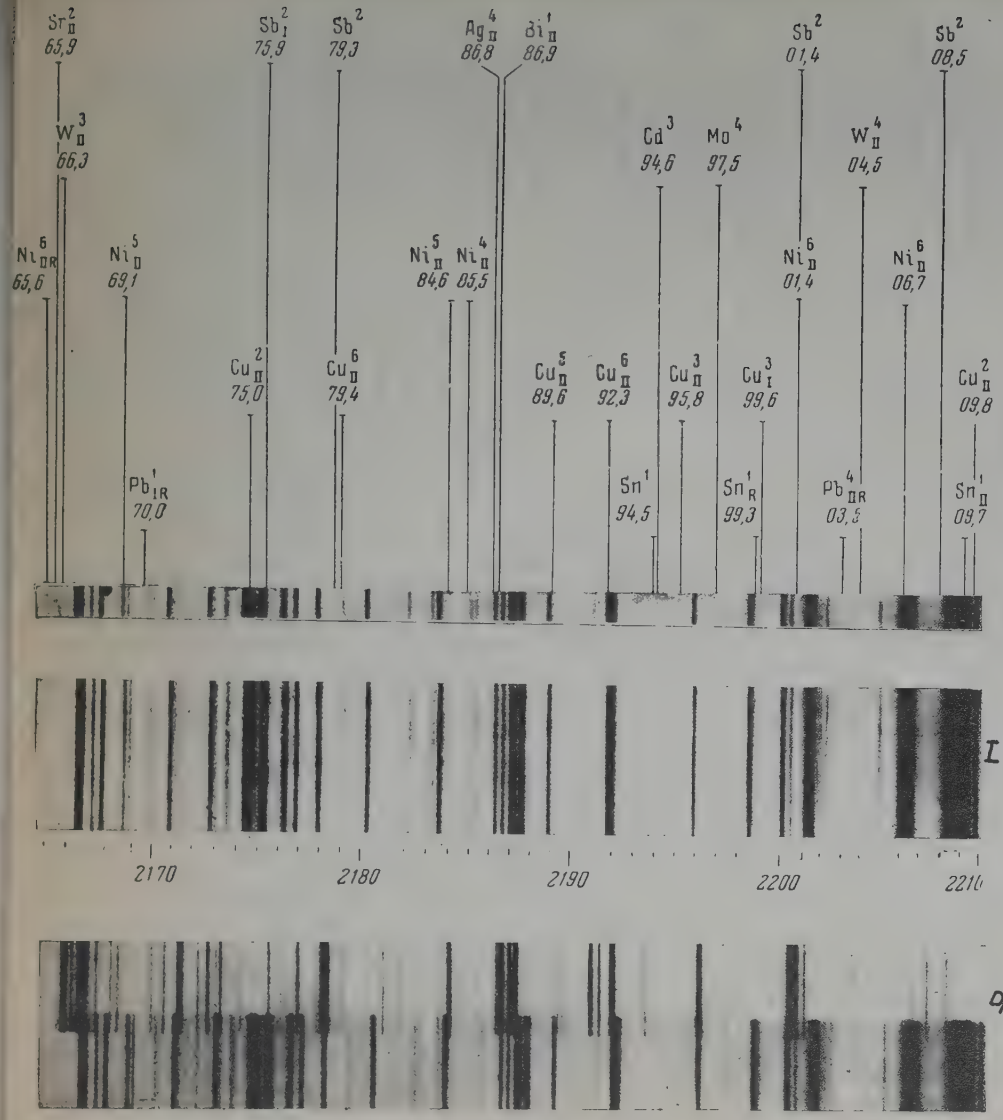

Third chart from spark section of the Atlas of Arc and Spark Spectra of the Elements (see p. 45).

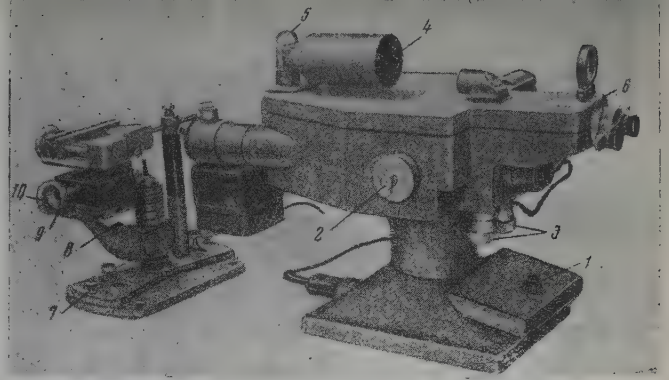

ST-7 Steelometer (see page 42).

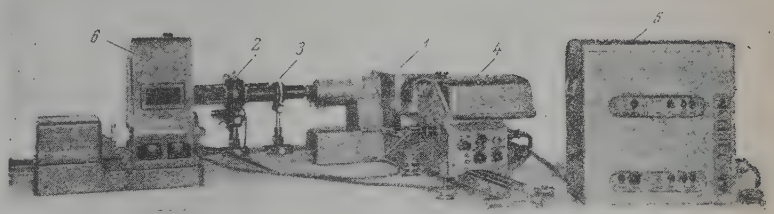

IKS-11 Infrared spectrometer: 1) monochromator, 2) source, 3) housing, 4) micrometer screw, 5) drum, 6) telescoping cell, 7) liquid cell, 8) gas cell, 9) mounting slide, 10 & 11) connecting fittings.

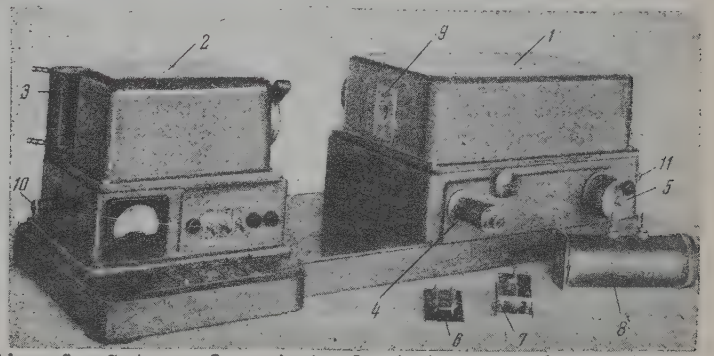

Fig. 1. Set-up for photoelectric recording of Raman spectra: 1) ISP-51 Spectrograph without camera, 2) source, 3) condenser, 4) unit comprising exit collimator, electronic circuit & motor with reduction gear, 5) stabilized power supply, 6) recording unit. The PS-381 set comprises units 4, 5 and 6. (see p. 46)

ATLAS OF ARC AND SPARK SPECTRA OF THE ELEMENTS (2100-6600 A)

- A.K.Rusanov, E.V.Gusiatskaia & N.V.Il'iasova

Spectroscopic analysis is now widely used in science and industry and consequently there is a great need for various aids designed to facilitate the interpretation of spectrograms, identification of lines, etc. Not least in importance among such aids are charts showing the positions of the characteristic lines of various elements with reference to the familiar spectrum of iron[1-3].

Until now there has been no atlas designed specifically for use in the rapid interpretation of spark spectra despite the fact that spark sources are finding increasing application not only in the analysis of metals and alloys but also in the investigation of many non-conducting powdered substances (ores, slags, etc). To meet this need we have compiled an atlas of arc and spark spectra of the elements in the 2100 to 6700 A range obtained by means of an ISP-22 medium dispersion quartz spectrograph.

The spark-spectrum section of the atlas comprises 23 charts. As may be seen from the reproduction of one chart on p. 44 , the appropriate sections of the spark and arc spectra, photographed contiguously, are printed at the bottom of the sheet; some distance above this double strip we have the spark spectrum of iron with reference to which the positions of the more intense lines in the spark spectra of 66 elements are marked. The lines associated with neutral atoms are identified by I, those due to ions by II and the tendency to self-reversal is indicated. The intensities of the linesare given in the 10-point scale; the intensities were evaluated on the basis of the appearance of the lines in the spectra of standard ammonium nitrate powders containing 0.001, 0.01, 0.1, 1 and 10% of the element. In this way the influence of self-absorption and self-reversal on the line intensities was minimized. An intensity value of 1 means that the line will ordinarily appear in the spectrum when the concentration of the element in the standard powder is over 10%; 2 and 3 means the line appears in the spectrum of the powder with 10% concentration of the element; 4 and 5 correspond to 1%, etc. Lines with an intensity value of 10 can be detected when the concentration is 0.001% or less. The test powders were introduced into the region of the spark discharge under standard conditions by means of a powder atomizer.

The spectra were excited by an IG-2 spark generator in a Raiski circuit. The use of a 0.01 μf capacitor with L = 0.01 microhenries in the spark circuit insured adequate "hardness" of the discharges.

The arc section of the atlas gives the more intense lines of 64 elements and is arranged similarly to the spark section. The line intensities listed were established on the basis of the appearance of the spectra of carbon base powders containing 0.001, 0.01 etc. % of the elements. In each case a 20 mg sample of the powder was vaporized at the anode of the DC carbon arc (220 v, 10 amp).

In using the spark section of the atlas it should be borne in mind that the appearance of the spectra differs somewhat for different discharge regimes. The contiguous iron arc and spark spectra reproduced at the bottom of the charts make it possible to compare the two and form some idea of the probable appearance of spectra intermediate between the arc and the "hard" spark.

The charts reproduced in the atlas were all enlarged 20 times by means of a PS-18 spectrum projector. Hence for interpretation purposes the investigated spectrum can be projected for viewing directly on to the atlas charts; when the spectrogram includes an iron spectrum, the lines of this can be brought into coincidence with the corresponding iron lines in the chart.

The text section of the atlas contains a table of wavelengths of the analytic lines, with mention of the interfering lines of other elements, as well as a table of the wavelengths of the arc and spark lines of iron.

All-Union Institute of Mineral Raw Materials

References

1. A.K.Rusanov, Spektral'nyi analiz rud i mineralov, s prilozheniem atlasa dugovykh spektrov elementov (Spectroscopic analysis of ores and minerals supplemented by an atlas of arc spectra of the elements) (2500-3500 A). M. 1948.
2. S.K.Kalinin, A.A.Iavnel', A.I.Alekseeva & L.E.Naimark, Atlas spektral'nykh linii (Atlas of spectrum lines). M.-L. 1952.
3. L.N.Indichenko, Rasshifrovka spektrogramm rud i mineralov (Interpretation of the spectrograms of ores and minerals). M. 1951.

* * * * * * *

PHOTOELECTRIC RECORDING INSTRUMENTS*

- T. K. Fal'k

The use of photoelectric methods for recording weak light fluxes reduces the time required for making analyses and greatly simplifies determination of the frequencies and relative intensities of spectrum lines.

Three different instruments for measuring and recording weak spectra were brought out in 1953 in the Soviet Union. All three operate on the same principle and differ only as regards operating range and the design of the dispersing system. Each assembly consists of a monochromator with an adjustable dispersing unit, a photomultiplier located behind a fixed exit slit, an amplifying and recording section and a power supply unit.

The same basic electric circuit is employed in all three instruments. In every case the photomultiplier receives the monochromatic pulse and transforms it into an electric signal which then goes to a DC amplifier employing a bridge circuit. The amplified current (amplification factor = 10^4) is recorded by a sensitive galvanometer whose deflection is proportional to the strength of the electric signal. The record is made by a light spot on photographic paper mounted on a revolving drum. The voltage supply to the photomultiplier and amplifier is kept constant to within 0.1% by electronic stabilizers.

The PS-381 recorder (see Fig. 1, p.44) is designed as an attachment to the ISP-51 spectrograph. The monochromator is formed by the entrance collimator and prism assembly of the spectrograph together with the exit collimator supplied with the PS-381. This exit collimator has a focal length of 300 mm and produces a linear dispersion of 25 A/mm at 4500 A. The useful range of the instrument is 4000 to 5400 A. The radiation receiver is an antimony-cesium photomultiplier tube.

The unit is equipped with an electric motor driving a reduction gear for rotating the prism assembly; a gear selector allows setting three different speeds, related in the proportion of 1:3:9. The different regions of the spectrum are focused on the slit automatically.

The unit was designed primarily for recording Raman spectra; the instrument was tested by recording the spectrum of toluene (Fig. 2, a). All the principal lines of toluene are discernible in the record which was traced in approximately 20 minutes. The sensitivity of the system permits registering the 842 cm^{-1} line which has an intensity of 5 units. It will be seen that the 1004 and 1031 cm^{-1} lines ($\Delta\nu$ = 27 cm^{-1}) are clearly resolved and that there is indication of separation of the 1605 and 1586 cm^{-1} lines ($\Delta\nu$ = 19 cm^{-1}). The reproducibility of the record is within 5%; the linearity, within 2-3%.

---

*The full report appears in Zhur. eksp. i teor. fiz., 27, 318 (1954).

The PS-382 instrument differs from the preceding in that it has two exit slits and is equipped with entry and exit collimators having a longer focal length (800 mm). An antimony-cesium photomultiplier is located behind one slit and an oxygen-cesium tube behind the other. The overall operating range of the instrument is 3600 to 10,000 A; the focusing of the spectrum lines on the slits is automatic in this range. The dispersion is 11 A/mm at 4400 A and 50 A/mm at 7000 A.

The antimony-cesium photomultiplier can be used for recording Raman spectra as well as absorption and fluorescence spectra in the near ultraviolet and visible regions. The oxygen-cesium cell can be used for recording absorption spectra in the visible and near infrared regions, the spectra of various light sources and fluorescence spectra. The instrument was successfully used to record the third and fourth overtones of the absorption band of benzene, the emission spectrum of molecular nitrogen, the spectrum of argon to 10,600 A, etc.

The DFS-4 spectrometer with interchangeable 600 and 1200 lines/mm gratings can be used either for photographing spectra on plates or photoelectric recording in the region from 3600 to 7000 A. The dispersion of the instrument is 6.5 A/mm and the relative aperture 7.3 with the 600 lines/mm grating in place and 13.5 A/mm and 10.4 with the 1200 lines/mm grating. The focal length of the reflecting mirror is 1200 mm. The height of the slit is 40 mm. The grating is rotated by means of a precision worm pair. The rate of displacement of the spectrum relative to the slit can be varied between 1.6 and 27 cm^{-1} sec^{-1}. The radiation receiver in the DFS-4 is an antimony-cesium photomultiplier.

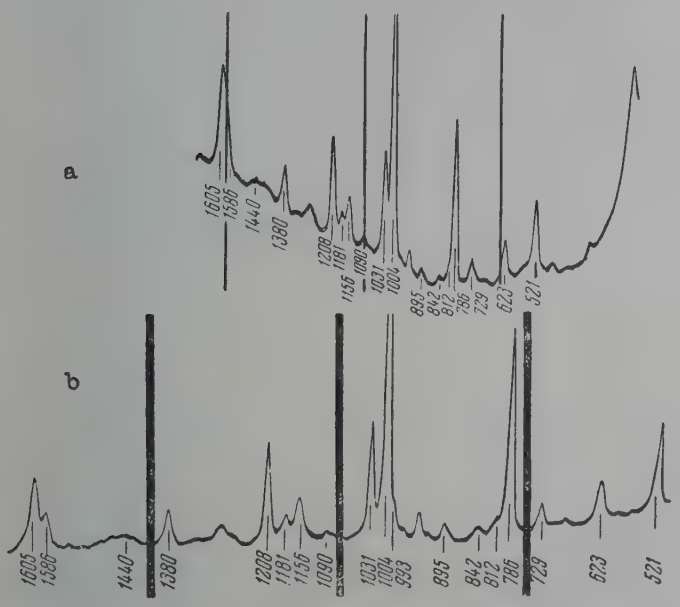

Fig. 2. Recorded spectra of toluene: a) with the PS-381 attachment; b) with the DFS-4.

From a comparison of the records of the spectrum of toluene made with the PS-381 (Fig. 2 a) and the DFS-4 (Fig. 2 b) instruments under analogous conditions, it will be seen that the DFS-4 has higher dispersion and resolving power. In Fig. 2 b the resolution of the 1004 and 1031 cm^{-1} lines amounts to 80% of the height of the 1031 cm^{-1} line; the 1605 and 1568 cm^{-1} lines are well separated and there is indication of resolution of the 1004 and 993 cm^{-1} lines ($\Delta\nu$ = 11 cm^{-1}). In practice the resolution of the instrument is limited by the sensitivity threshold of the photomultiplier, because of which it is necessary to use a relatively wide slit. The spectrometer itself is capable of resolving lines 5-6 cm^{-1} apart. The spectra of heptane and isooctane were also recorded with the instrument; the principal lines of heptane are clearly discernible in the recorded spectrum of a 20% solution of heptane in isooctane.

* * * * * * *

THE IKS-11 AND IKS-6 INFRARED SPECTROMETERS

- L.V.Smirnova

The IKS-11 and IKS-6 infrared spectrometers are intended for automatic recording of absorption and emission spectra in the region from 0.75 to 20 μ. Both instruments employ an autocollimating mounting. The relative aperture of the IKS-11 is 4.5; that of the IKS-6 is 5.5. The IKS-6 has a higher resolving power than the IKS-11 (limits of resolution 1.4 cm^{-1} and 3 cm^{-1}).

The IKS-11 instrument (see figure p.44) consists of a monochromator 1 and an illumination unit 2. The radiation source, an IKR-1 rod, is enclosed in a metal housing 3 cooled by circulating water. The widths of the entrance and exit slits are adjusted by rotating the micrometer screw 4. The wavelength is set by drum 5 which is graduated with reference to known emission and absorption lines. The unit is supplied with three different absorption cells: a telescoping cell 6, a constant thickness cell 7 and a gas cell 8. For analysis the cells are mounted on slide 9 in front of the monochromator. The instrument units are filled with dry air or nitrogen through connecting sleeves 10 and 11.

The IKS-6 instrument (see Fig. 22, p. 339, trans. Bulletin No. 6, Vol. 18 - the preceding issue) consists of a monochromator and two interchangeable illumination units. Both lighting units are used when working with the long gas cell (see Fig. 23, same reference); only one is needed in working with the cells 6, 7 and 8 mentioned above. The light source is enclosed in a metal shield. The monochromator slits are normally adjusted in width manually by means of a micrometer screw, but the instrument has provision for the installation of cams for automatic opening of the slits. As in the IKS-11 the wavelength is set by means of a suitably graduated drum. Also, as in the IKS-11 the radiation source is an IKR-1 rod which attains a temperature of 1600-1800° when drawing 0.6 amp at 80-100 volts.

To permit working over the entire 0.75-20 μ range the instrument is equipped with interchangeable prisms of F-1 glass, lithium fluoride, rock salt, sylvine and potassium bromide. The radiation receiver is a vacuum thermocouple with a sensitivity of 1-2 v/w. The emf of the thermocouple is amplified by an FEOU-15 amplifier and recorded on photographic paper. The time required to record the spectrum over the entire operating range of the instrument varies between 1.5 minutes and 3 hours.

* * * * * * *

CERTAIN OPERATING CHARACTERISTICS OF PHOTOELECTRIC SPECTRUM SCANNING EQUIPMENT

- I.S.Abramson & A.N.Mogilevski

Certain difficulties are encountered in using spectrum scanning equipment for photoelectric recording of Raman spectra. These difficulties stem from the low level of the light flux and are manifested in loss of resolving power of the entire photoelectric set-up (including the optical as well as the electrical parts), an increase in recording time and a decrease in accuracy of measurement.

The reduced resolving power of the optical part of the system results from the necessity of increasing the width of the entrance and exit slits of the spectroscopic instrument in order to bring the flux from the lines to a measurable level. Assuming that the contour of the spectrum line is characterized by the usual dispersion curve, the broadening of the line contour due to the width of the entrance slit can be readily computed. The breadth of the contour at half-height equals $\sqrt{s_1^2 + s_2^2}$, where s_1 is the intrinsic breadth of the line at half-

height and s_2 is the slit width. When the spectrum is displaced relative to an exit slit of width s_3, the light signal behind the slit and consequently the resultant electric signal produced by the radiation receiver will have an even greater width. With sufficient accuracy for purposes of comparative evaluation this resultant width is given by $\sqrt{s_1^2 + s_2^2 + s_3^2}$. It may be noted that the calculated contours of the output signals can be approximated by a wave of the form $\cos^2 \Omega t$ or in case the line breadth is commensurate with the width of the slits by a probability curve. When the spectrum line is narrow compared to the slits the output signal is approximated by a triangular waveform (when the entrance and exit slits are of equal width).

The electric circuit of the scanning-recording system, or, specifically, the time constant of the system filters introduces an additional distortion of the signal shape. The character of the distortion depends on the ratio of the filter time constant to the duration of the signal. The influence of the ratio in the case of triangular waveform signals is shown in Fig. 1.

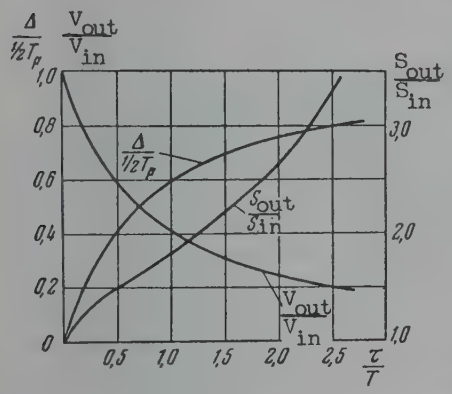

Fig. 1. Variation of the relative amplitude V_{out}/V_{in}, relative shift $\Delta/\frac{1}{2}T_p$ and the relative width S_{out}/S_{in} of a triangular pulse with the ratio of the time constant $\tau = CR$ of a single section filter to the duration of the signal. V_{out} and V_{in} are the peak amplitudes of the output and input signals; Δ is the shift of the peak; S_{out} and S_{in} are the widths at half-height of the output and input pulses.

Whereas the broadening of the lines due to increased slit width is symmetric, the distortion introduced by the filter is asymmetric, i.e., the line (signal) contours are extended in the direction of scanning. Hence it is of interest to analyze how two signals of equal duration separated by a distance commensurate with their width will be recorded. Calculations indicate that the recorded amplitudes will differ appreciably from the true amplitudes. For example, in the case of two triangular signals whose peaks are 1.5 times their width apart and whose durations are equal to each other and to the time constant of the filter, the recorded amplitude ratio will differ by 17% from the true ratio when the amplitude of the first is half that of the second. On the other hand, when the amplitude of the first is twice that of the second, the recorded difference will be 73%. When the amplitude of the second signal drops to one tenth that of the first, it becomes virtually undistinguishable. It follows, therefore, that whether two neighboring lines are resolved depends both on the ratio of their peak intensities and (where this ratio is not equal to unity) on the direction of scanning. Hence it is more expedient to evaluate the resolving power of a photoelectric recording set-up on the basis of the observed distortion of the contour of a single line. From the shape of the trailing edge of the signal produced by a single spectrum line one can readily estimate the minimal separation and intensities of lines for which effective resolution will be obtained. Lines having an amplitude at the peak below the amplitude of the corresponding point on the trailing edge of the investigated single line will not be resolved since in view of the characteristics of the scanning system they will result merely in a retardation or extension of the trailing edge and will not produce even a horizontal plateau, which might be taken as the criterion for resolution.

We also investigated the matter of using multiple section filters, having a steeper characteristic curve near the cut-off region than single section filters.

To this end we analyzed a multiple section RC-filter of the audio-frequency type.

Having calculated the transient characteristics[2] of filters with different numbers of sections, we determined the relative values of the "time to steady state" (time constant) for filters consisting of two and three sections in terms of the time constant for a single section filter. We also determined the equivalent noise pass-band of such filters[3]. From the practical point of view comparison of the time constants of filters with different numbers of sections but equal noise pass-bands is of interest. The computed data are summarized in the table below.

Characteristics of filters with 1, 2 and 3 sections

Number of sections	1	2	3
Relative time constant	1	2.41	4.57
Equivalent noise band (in 1/RC)	1	0.33	0.17
Relative time constant with equal noise pass-band	1	0.80	0.78

It will be seen from the table that the optimum number of sections is two. further increase in the number of sections gives negligable improvement while the transmission factor goes down appreciably with each section added (making it necessary to increase the amplification factor accordingly).

Analysis of a low-frequency RC-filter with sections separated by tubes showed that in this case as well the optimum number of sections is two. The time constant of such a filter circuit with a noise pass-band equal to that of a single section filter equals 0.765 the time constant of a single section. It may be noted that the typical photoelectric recording circuit with a single stage DC amplifier and an inertia indicator is essentially such a two-section filter circuit. The first section in these circuits is an RC-filter, connected into the control grid circuit of the amplifier tube (i.e. the tube between the two sections), while the second section is formed by the inertia indicator. It is assumed that the time constant of the indicator is chosen in the usual manner.

Thus the use of complex (multiple section) filters makes it possible to reduce the noise band by 20-30% and consequently increase the noise to signal ratio by 10-15% without prolonging the time to steady state. This applies to systems with DC as well as AC amplifiers.

When a recording potentiometer is used as the indicating element in a spectrometric set-up it is important to take into account certain operating characteristics of these instruments under the conditions where the travel time of the pen carriage is commensurate with the duration of the recorded pulse. The distortions introduced under such conditions by an inertialess pen instrument differ from those produced by an inertia instrument (for example, a galvanometer with a large time constant) in that their character depends not only on the shape and duration of the recorded pulse but also on its amplitude. The difference is due to the fact that as the amplitude decreases, the steepness of the pulse waveform is reduced at every point and hence the recording process is facilitated and the relative distortion is reduced. An inertia indicator on the other hand distorts pulses of all amplitudes (but of the same analytic form and equal duration) to an equal degree.

Thus in recording with a pen potentiometer when the travel time of the carriage is commensurate with the pulse duration, the ratio of the amplitudes of two neighboring pulses is distorted: the apparent ratio is shifted in the direction of unity since lower pulses are cut down less than higher ones. This distortion of the true amplitude ratio leads also to a deterioration of the signal-to-noise ratio. Thus where inertialess recording instruments are concerned it may be said that with decreasing amplitude of the recorded signal its duration can be reduced

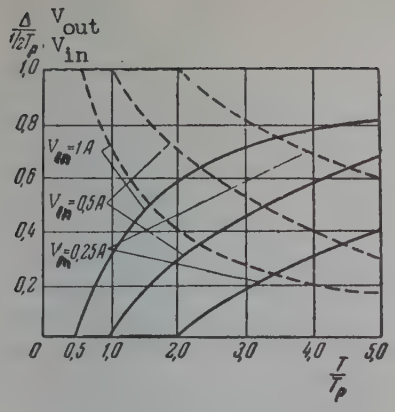

Fig. 2. Variation of the relative amplitude V_{out}/V_{in} (dash lines) and relative shift $\Delta/\frac{1}{2}T_p$ (solid lines) of a triangular pulse with the ratio of the travel time of the pen carriage T to the pulse duration T_p for three values of V_{in} expressed in terms of A, the full scale scale of the instrument. For the meaning of the other letters see Fig. 1.

in proportion without altering the degree of distortion. In other words, the pass band of the instrument is wider in recording weaker signals. Consequently the pass band for noises is wider than the signal pass band if the amplitude of the signal is greater than the amplitude of the noise. The distortions introduced by a recording pen potentiometer are shown in Fig. 2.

An inertialess recording potentiometer will not distort the shape or relative amplitudes of the signals if the maximum of the first derivative with respect to time of the strongest signal is equal to or less than the speed of the pen carriage, expressed in the same units. For example, an undistorted record of a triangular pulse having an amplitude equal to the full scale deflection of the potentiometer will be obtained only if the duration of the pulse equals at least 2T, where T is the travel time of the carriage over the full scale. The minimal duration (for undistorted recording) of a $\cos^2 \Omega t$ form pulse is 3.14 T; that for an $e^{-\beta x^2}$ pulse is 2.6 T (in the last case the duration was computed for the o.1 height level). If the above condition is satisfied, the signal-to-noise ratio will remain constant since in this case the potentiometer does not affect the overall frequency characteristic of the system as a whole.

It follows from what has been stated above, that unlike a galvanometer with a large time constant, a recording potentiometer cannot be used as an auxiliary selective element in spectrum recording systems.

Commission of Spectroscopy at the
OFMN of the USSR Academy of Sciences

References

1. I.S.Abramson, KH.E.Sterin & A.N.Mogilevski, Izv. (Bulletin) AN SSSR, Ser. fiz., 18, 264 (1953).
2. K.M.Polivanov & B.I.Iakhinson, Elektrichestvo, 4, 57 (1948).
3. A.A.Kolosov, Rezonansnye sistemy i rezonansnye usiliteli (Resonance systems and resonant amplifiers), M. 1949.

* * * * * * *

A METHOD OF RECORDING RAPIDLY VARYING PROCESSES BY MEANS OF INERTIA RECEIVERS

- A.M.Bonch-Bruevich & Ia.A.Imas

1. The solution of many spectroscopic problems involves the rapid recording of infrared radiation. Such recording is often rendered difficult by the inertia of the receiving component (thermocouple, bolometer, photoresistance, etc.) which slows the response of the entire measuring system. We suggest here a method which makes it possible to observe processes taking place in an interval much shorter than the time constant (response time) of the receiver. It is based on the use of correcting electric circuit which permits designing a measuring instrument incorporating a receiver with a time constant τ and yet having a response time τ/a. In other words, introducing the correcting circuit has the effect of reducing the time constant of the radiation receiver by a factor of $1/a$.

2. The characteristics of the correcting circuit must be such that when the voltage at its input varies according to the $\left(1-e^{-\frac{t}{\tau}}\right)$ law its output voltage will vary as $\left(1-e^{-\frac{at}{\tau}}\right)$. This corresponds to a transition from a signal which a receiver with a time constant τ would emit (upon an instantaneous change in the incident radiation by a constant value) to a signal that would be emitted by a receiver with the time constant τ/a under the same circumstances. The requisite frequency characteristic of the circuit will have the form

$$M_k(\omega)=\frac{a\sqrt{1+\omega^2\tau^2}}{\sqrt{a^2+\omega^2\tau^2}}, \qquad (1)$$

where $M_k(\omega)$ is the ratio of the output to the input voltage. A frequency response of this kind can readily be realized for a limited frequency range by the introduction of simple RC network into the amplifier coupled to the radiation receiver.

3. The correction is accompanied by an increase in the fluctuation voltage at the output of the circuit. A correcting network having a frequency characteristic described by (1) accentuates the high-frequency components of noise spectrum of the receiver. Analysis shows that reduction of the effective time constant of the system by a factor a leads to an increase in the noise signal (voltage) at the output by a factor

$$\varkappa=\sqrt{a^2-\frac{a(a^2-1)}{\omega_{rp}\tau}\operatorname{arc\,tg}\frac{\omega_{rp}\tau}{a}}; \qquad (2)$$

where ω_{rp} is the upper limit of the amplifier passband without the correcting network.

Inasmuch as for correct reproduction of the signal the condition $\frac{\omega_{rp}\tau}{a}\gg 1$ must be satisfied, we have

$$\varkappa\approx a. \qquad (3)$$

Hence the fluctuation voltage increases by approximately the same factor as the effective time constant is reduced by.

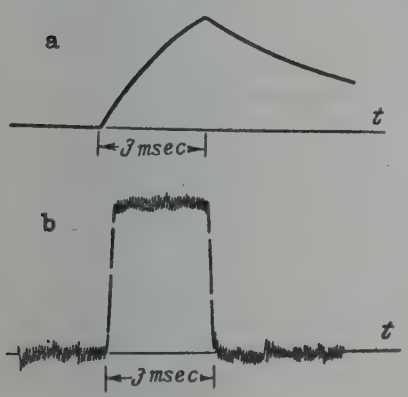

Oscillograms of radiation pulses received by a bolometer: a) without correction, b) with correction. The breaks in the pulse waveform correspond to intervals of 100 microsec.

4. The accompanying figure shows at a) the oscillogram of a 3 msec radiation pulse recorded by a bolometer with a time constant of 0.03 sec and at b) the oscillogram of a similar pulse obtained after the introduction of a correcting network ($a = 150$) into the recording system. It will be seen that introduction of the correcting network made it possible to record a true picture of a process having a duration of 0.01τ but at the same time raised the fluctuation voltage level appreciably.

* * * * * * *

THE SF-2m RECORDING SPECTROPHOTOMETER

- V.N.Osipova

The SF-2m spectrophotometer is designed to record photoelectrically continuous curves of the coefficients of transmission or of the density of transparent substances as well as the reflection coefficients of light scattering surfaces over the entire range of the visible spectrum from 4000 to 7500 A. The results of measurement are automatically recorded on a special paper chart. The recording time for the full range may be varied between 3 and 10 minutes depending on the intricacy of the curves recorded.

The dispersing element is a double monochromator, selected with a view to eliminating scattered light. The width of the emerging spectrum can be varied between 2 and 5 mμ and once set remains constant over the entire spectrum. The beam from the monochromator enters the photometric section which is designed about a polarizing photometer.

Two beams of light, polarized perpendicularly to each other, enter the photometric sphere. Any inequality of the beams, due, for example, to absorption in the investigated specimen, produces periodic variation of the illumination incident on the photocell and, consequently, a like fluctuation of the photocurrent which in turn gives rise to a signal on the amplifier output. The signal is further amplified and the resultant voltage is applied to the armature winding of a reversible electric motor, causing it to rotate in the appropriate direction. By means of a suitable reduction gear and special cam arrangement the motor turns the analyzer prism of the photometer to restore photometric equilibrium, i.e., returns the signal at the amplifier output to "zero". The rotation of the analyzer prism is transmitted through another reduction gear to the pen recording the coefficient of transmission (or reflection) on the special chart. All the while the wavelength motor, operating a cam through a reduction gear, moves the middle slit of the instrument over the spectrum, steadily changing the wavelength of the light emerging from the monochromator. The drum carrying the record chart rotates in unison. Thus the spectral transmission or reflection curve is recorded on the instrument chart.

A photograph of the instrument is reproduced in Prokof'ev's report in No. 6, Vol. 18 of the Bulletin (see Fig. 20, p. 339).

The indications of the instrument received by our laboratory were checked by recording the transmission and density of a series of standard neutral filters and comparing the record with the data in the log of the instrument. Highly satisfactory results were obtained: the error in transmission measurements did not exceed 0.5%; that in density determinations remained under ±0.0125. The reproducibility of the record for transmission was within 0.2%; that for density, within 0.005. [The density values are presumably fractional values rather than percentages. Translator]

* * * * * * *

THE MF-4 RECORDING MICROPHOTOMETER

- G.Ia.Kossov

The MF-4 recording microphotometer (see Fig. 26, p. 343 trans. Bulletin, No. 6, Vol. 18 - the preceding issue) is intended for continuous photoelectric recording as well as individual measurement of the coefficient of transmission or the degree of blackening of plates and films.

The light flux passing through the investigated area of the film or plate is measured by a selenium photocell and a mirror galvanometer. As the mirror deflects, different sections of the galvanometer scale are projected on the indicator screen and at the same time the reflection of the light beam producing the record on a photographic plate is deflected accordingly. Thus the MF-4 provides both a direct reading of the blackening or density of the spectrogram and a trace of the variation in blackening.

The recording instrument incorporates a complete MF-2 microphotometer, i.e., is designed about this comparator. The transmission record is made on a 13 x 18 cm photographic plate having a speed of 0.5 to 20 GOST (State Standards rating). The scanning rate can be varied between 4 and 60 mm/min by regulating the reduction gear motor. The adjustable scaling mechanism provides for object-to-record ratios from 1:1 to 1:∞.

The instrument is powered from the regular AC supply line through a current stabilizer.

The receiving-recording system of the MF-4 has considerable inertia, so that the scanning rate (rate of displacement of the spectrogram) has to be correlated with the structure of the spectrogram. According to calculations based on the data in the instrument log and the results of tests the full response time is somewhat in excess of 0.7 sec. In a series of tests the scanning rate for spectrograms having different structures were set in accord with the calculated response time. It was found that the instrument will correctly record the transmission of spectrograms with lines down to 0.002 in width if the scanning rate and scale ratio are properly selected.

Repeated measurements of the transmission of the same "object" with the same setting as well as with different adjustments of the instrument show a deviation of up to 0.1 mm from the average value, which corresponds approximately to the accuracy of measurement of the trace on the photographic record plate. When the "object" is moved or re-inserted between recordings the deviation of the "throws" on the photographic plate from the mean value amounts to 0.25-0.30 mm and may attain up to 1.5 mm from individual points; this must be attributed in part at least to non-uniformity of the density of the lines in the spectrograms.

The accuracy of the instrument as regards reproduction of distances was checked by making a record of a high-precision graduated scale; the tests showed that the error in distance indications does not exceed 0.02 mm (on the object).

The operation of the lamp voltage stabilizer was checked by careful examination of a uniform trace on a photographic plate. It was found that the variations of the light flux from the mean value do not exceed 0.2%.

As compared with similar instruments the MF-4 has a number of advantageous features making for easier and more dependable operation: the receiving-recording system is simple and reliable; the instrument is powered from the regular electric supply line; it is relatively insensitive to vibration; it uses either plates or film and , in addition, can be used for direct measurement of individual lines. Thus the MF-4 is both more convenient to use and more dependable in operation than comparable foreign-made microphotometers and should find wide application in our spectroscopic laboratories.

* * * * * * *

VAPORIZATION OF METAL ELECTRODES IN A DC ARC

- G.P.Skorniakov

The present report summarizes the results of an investigation of the vaporization of metal electrodes in a DC arc. Specifically the information on vaporization was gained by recording the luminescence distribution in the discharge cloud composed of the vapor of the electrode material. The distribution was recorded by means of a slitless spectrograph.

We studied the vaporization of copper electrodes used in conjunction with counter electrodes of different substances: Al, Mg, Zn, Si, Sn, Pb, C, Mo, W, Cr, Mn, Fe, Co and Ni. In our investigation we evaluated the influence on the vaporization of the polarity and of the following attributes of the electrode material: 1) thermal conductivity, 2) melting and boiling points of the metal, 3) oxidizability of the electrode material and the melting or sublimation temperature of the oxides, and 4) the ionization potential of the vapor and the plasma temperature.

Part of the experimental data in the form of enlarged photographs of the arc are reproduced in Figs. I through IV. Analysis of the experimental data in the light of the physical characteristics of the elements shows that none of the above enumerated properties affects the vaporization in a consistent or progressive manner. Only in particular cases, when manifest to an exceptional degree, does one or another of these properties assume a predominant and determining role (for example, a very low fusion temperature obviously inhibits vaporization of a metal oxide).

We did, however, note a consistent connection between the vaporization and the polarity. Here the elements fall into two groups, which we designate A and C. Group A comprises Cu, Mg, Zn, Al, Si, Sn, Pb, C, Mo and W. Group C includes Fe, Co, Ni, Mn and Cr.

The elements of Group A are characterized by more intense vaporization at the anode; in the case of some of the elements the vaporization is much faster than when the element forms the cathode. The elements of Group C volatilize as readily or even more strongly when forming the cathode.

The importance of polarity where the intensity of vaporization is concerned would appear to indicate that favorable vaporization conditions at the anode are due not so much to the greater liberation of energy at the anode as to the continuous "freshening" of the region surrounding the anode by the field acting on the ionized vapor: the reduction of the vapor density in the vicinity of the anode under the influence of the electric field facilitates entry of new additional vapor into the arc cloud.

In contrast, at the cathode, the field acts to hinder movement of the ionized vapor into the gap; consequently the vapor density near the cathode builds up and the high concentration slows evaporation from the cathode.

The above reasoning does not explain the behavior of the elements in Group C. Further experiments were obviously needed to clarify the situation. To this end we measured the potential drop in the arc, for the voltage drop furnishes a clue to some of the properties of the vapor in the gap and an indication of the degree to which the vapor participates in carrying the current.

The measurements showed that the elements of Group C produce a greater change in the voltage than elements of Group A. The influence of the properties of the electrode should be manifested mainly through the ionic component of the current. And, in fact, juxtaposition of photographs of the arcs and the voltage drop data shows that an increase in the influence of the electrode on the voltage is always accompanied by an increase in the amount of the vapor of the electrode material present in the arc gap.

Here we must note the exceptional nature of the influence of elements of the iron group on the voltage drop: experiments showed that in the case of these elements there is not only faster vaporization at the cathode, there is also observed

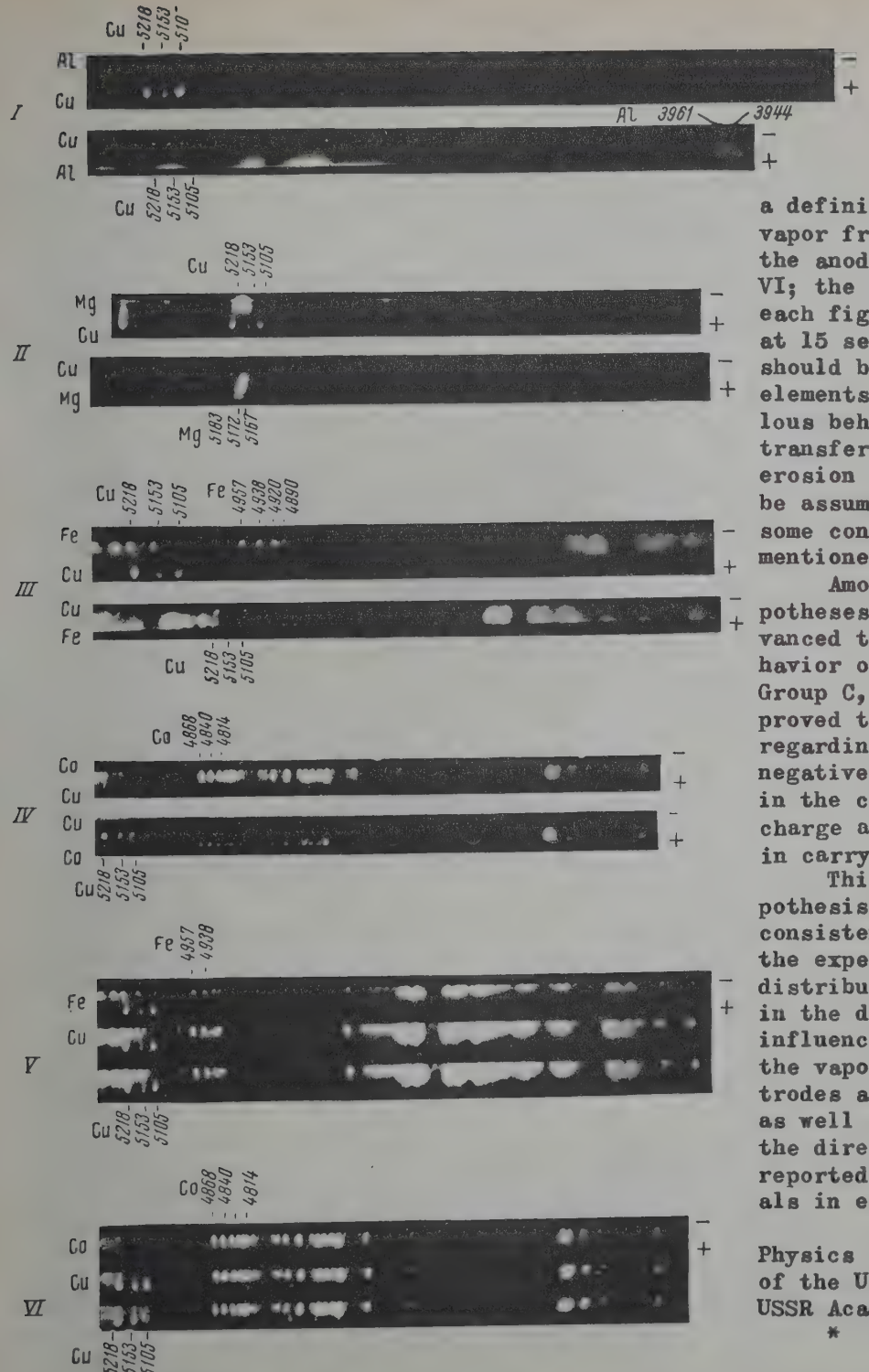

a definite movement of the vapor from the cathode to the anode (see Figs. V and VI; the three spectra in each figure were photographed at 15 sec intervals). It should be noted that these elements exhibit an anomalous behaviour in material transfer and electroerosion processes. It may be assumed that there is some connection between the mentioned phenomena.

Among the various hypotheses which might be advanced to explain the behavior of the elements of Group C, the most fruitful proved to be the hypothesis regarding the formation of negative Fe, Co and Ni ions in the cloud of the discharge and their active role in carrying the current.

This is the only hypothesis which provides a consistent explanation for the experimentally observed distribution of luminescence in the discharge cloud, the influence of polarity on the vaporization of electrodes and voltage asymmetry as well as the anomaly in the direction of transfer reported for certain materials in electric arcs.

Physics of Metals Institute
of the Ural Branch of the
USSR Academy of Sciences

* * * *

Spectra of DC arcs between a copper electrode and electrodes of other elements with alternate polarities. The upper edges of each spectrum correspond to the cathode; the lower edges, to the anode. I - Cu & Al; II - Cu & Mg; III Cu & Fe; IV - Cu & Co. V- Cu and Fe, VI - Cu and Co; the last two show the movement of vapor of elements of the iron group from the cathode to the anode. The three spectra in each group were photographed at intervals of 15 sec with the same polarity.

FURTHER RESULTS OF PHOTOELECTRIC INVESTIGATION OF SPARK SPECTRA

- S. L. Mandel'shtam and I. P. Tindo

The purpose of the present investigation was to determine experimentally the influence of the composition and pressure of the gas and of the length of the gap on the temperature and other characteristics of the gas spectrum excited in the channel of a spark discharge.

We employed the set-up described earlier[1] by means of which we could obtain oscillograms of the photocurrent produced by the investigated spectrum line during an individual discharge pulse. We studied spectrum lines attributed to neutral hydrogen and nitrogen atoms and to singly and doubly ionized nitrogen atoms.

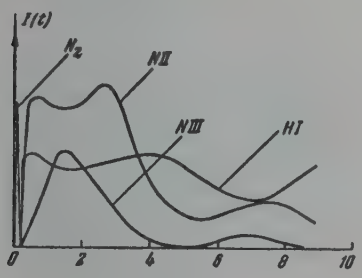

Fig. 1. Variation in the intensity of spectrum lines and bands during development of a spark discharge in industrial grade nitrogen at low pressure. L = 10 μH, C = 0.25 μf, U_0 = 14 kv, d = 13 mm, P = 20 mm Hg; N_2 - 4059 A band, H I - H_α line (6562 A), N II - 5045 A line, N III - 4097 A line.

The first part of the investigation was devoted to studying the emission during the early stages of development of the spark discharge. It was established that in discharges in industrial grade nitrogen and argon at reduced pressures (100 mm Hg col and lower) the emission during the initial fraction of a microsecond comprises the molecular bands of nitrogen, belonging to the second positive system of the nitrogen molecule, as well as weak neutral atom lines.

As the discharge develops further the N_2 bands fade and the intense emission of the N II and then of the N III lines, characteristic of spark spectra, begins (Fig. 1).

The duration of the initial, molecular spectrum increases as the pressure of the gas is reduced. Increasing the length of the gap (with voltage kept constant) has a similar effect.

The cited data show that at reduced gas pressures a spark discharge passes through a typical glow discharge stage. These spectroscopic observations confirm the results of Rogowski's[2] measurements of the electric characteristics of a spark discharge.

In the second part of the investigation we studied the influence of the discharge parameters on the discharge temperature. The temperatures were determined by the usual method from the relative intensities of the 5045, 5179, 5495 and 5535 A N II lines with known transition probabilities[3]. We established that the pressure exerts a very strong effect on the nature of the temperature variation during the discharge pulse. At reduced pressures the rate of temperature increase during the initial stage of the discharge is relatively low; the maximum temperature is attained after a longer interval as the pressure is decreased (Fig. 2).

Increasing the gap at reduced pressures results in an analogous shift of the temperature maximum.

The results of temperature measurements help explain the observed variations of the spectrum incident to changes in the gas pressure and the gap length in general and, in particular, the presence of the

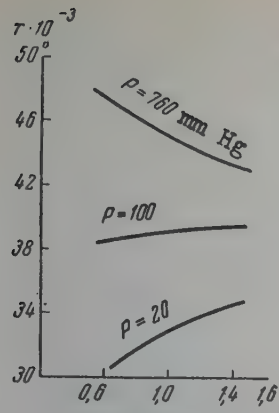

Fig. 2. Temperature variation during development of a discharge in industrial grade nitrogen at different pressures. L, C and U_o same as in Fig. 1.

two intensity peaks in the N II and H I line curves appearing during the first half-cycle of the oscillatory discharge (Fig. 1).

We also measured the temperature in the spark channel at atmospheric pressure in hydrogen and argon. For argon we obtained approximately the same value as in air: $40 \cdot 10^3$ °K. The discharge temperature in hydrogen is appreciably higher — $45 \cdot 10^3$ °K; moreover, in contrast to the case in air, the discharge temperature in hydrogen remains virtually constant during the first microsecond.

In the cases of discharges in nitrogen we established that the length of the spark gap has a noticeable effect on the discharge temperature at atmospheric pressures as well.

The third part of our investigation was devoted to determining whether the Boltzmann distribution of atoms over the excited levels persists under the conditions of a discharge at low pressures. An earlier approximate analysis[3] indicated that at pressures under 100 mm Hg, one might expect the equilibrium between first and second order atom-electron collisions to be disturbed, i.e., a departure from the Boltzmann equilibrium. The experiments confirmed this expectation.

"P. N. Lebedev" Physical Institute of
the Academy of Sciences of the USSR

References

1. L.A.Vainshtein, M.A.Leontovich, L.P.Maliavkin & S.L.Mandel'shtam, Zhur. eksp. i teor. fiz., 24, 326 (1953).
2. W.Rogowski, Phys. ZS., 33, 797 (1932).
3. S.L.Mandel'shtam & N.K.Sukhodrev, Zhur. eksp.i teor.fiz., 24, 701 (1953).

* * * * * *

INVESTIGATION OF THE INSTANTANEOUS BRIGHTNESS OF PULSE DISCHARGES IN INERT GASES

- K. S. Vul'fson, I. Sh. Libin and F. A. Charnia

We investigated the variation with time of the brightness of pulse discharges in argon, krypton and xenon at different pressures and with pulses of different power, using a mirror scanning procedure.

The pulse discharge tube was connected directly to the terminals of the storage capacitor, thus reducing the inductance and resistance of the discharge circuit to a minimum. The period of the oscillatory discharge current was 10^{-5} sec. The discharge gap measured 10 mm. The instantaneous brightness values were found by photometry of the

scan photographs on a MF-2 non-recording microphotometer. The resolving power of the scanning set-up was $4 \cdot 10^6$ sec^{-1}. The spectral region covered in the investigation was 380 to 580 mμ.

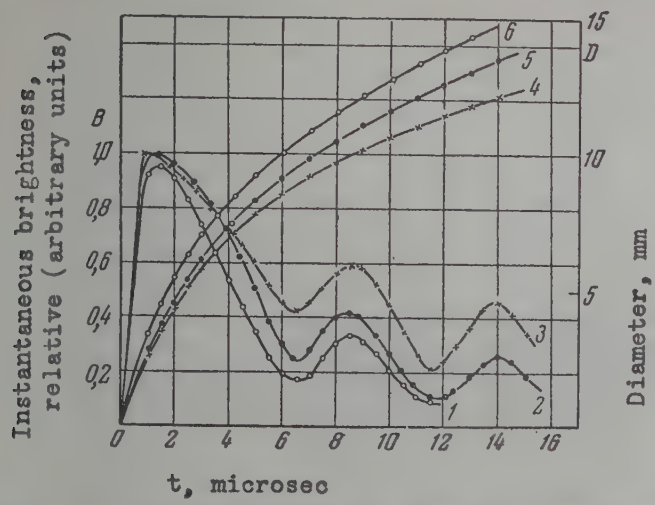

Fig. 1. Variation with time of the instantaneous brightness and diameter of pulse discharges in argon, krypton and xenon at p = 2 atmos. U = 8 kv and C = 4 μf. Curves 1-3: instantaneous brightness; 4-6: diameter. 1 and 6: Ar, 2 and 5: Kr, 3 and 4: Xe.

Photometric processing of the central portions of the scan series yielded the data for the curves for the instantaneous brightness of discharges in argon, krypton and xenon shown in Fig. 1. Curves giving the variation of the discharge diameter are plotted in the same figure. As may be seen from the figure, peak instantaneous brightness values for argon, krypton and xenon under the experimental conditions (p = 2 atmospheres, U = 8 kv and C = 4 μf) proved to be virtually identical. The peak brightness is attained most rapidly in xenon, next in krypton and last in argon. The decay in light emission is fastest in argon and slowest in xenon. The diameter of the discharge channel and its rate of expansion decreases with increasing molecular weight of the gas which is in conformity with the data of Ref. 1.

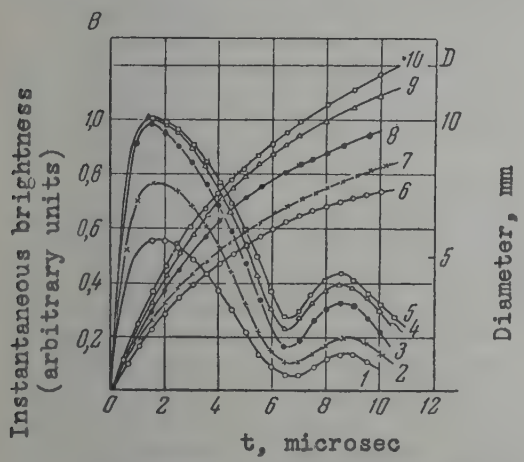

Fig. 2. Variation with time of the instantaneous brightness and diameter of pulse discharges in krypton at p = 2 atmos., C = 4 μf and different capacitor voltages: 1 and 6: 3 kv, 2 and 7: 4 kv, 3 and 8: 6 kv, 4 and 9: 8 kv, 5 and 10: 10 kv. Curves 1-5 - brightness; 6-10 - diameter.

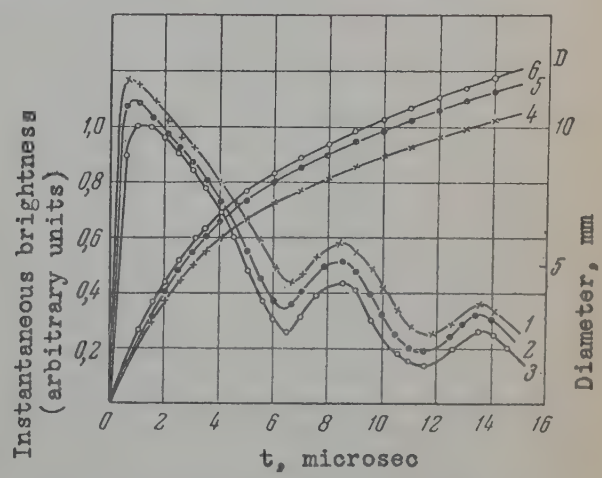

Fig. 3. Variation with time of the instantaneous brightness and diameter of pulse discharges in krypton with U = 8 kv and C = 4 μf at different pressures: 1 and 4: 6 atmos, 2 and 5: 4 atmos. 3 and 6: 2 atmos. Curves 1-3 - brightness; 4-6 - diameter.

At a certain discharge voltage the peak instantaneous brightness reaches a limiting, maximum value; any further increase in the voltage does not increase the initial peak brightness but results only in a rise of the succeeding brightness peaks (Fig. 2) produced by the oscillatory discharge. This brightness saturation was observed for all the investigated gases. At a pressure of 2 atmospheres and with the circuit employed the limiting value of the peak brightness is attained at 5 kv in xenon, at 6.5 kv in krypton and only at 10 kv in argon. The absolute values of the saturation peak brightness are the same for all three gases.

Since, as may be seen from Fig. 1, the discharge diameter is greater in argon than in krypton and xenon, one might expect the peak instantaneous luminous flux from the argon discharge to be greatest. This was confirmed by experiment. On the other hand the summary luminous flux - flux integrated over the discharge time - is greatest from a xenon tube[2], even though the peak instantaneous luminous flux from xenon is the lowest. This is explained by the character of the variation of brightness with time curves (Fig. 1) which show that the emission falls off most rapidly in argon.

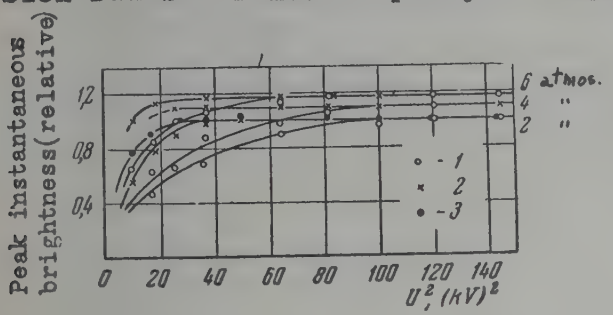

Fig. 4. Variation of the maximum instantaneous brightness of pulse discharges in argon (1), krypton (2) and xenon (3) with the square on the voltage of the discharge capacitor (C = 4 μf) at different gas pressures.

Curves showing the variation in brightness with time in krypton at different gas pressures are reproduced in Fig. 3. It will be seen that the time to peak brightness depends on the pressure, the peak value being reached earlier at higher pressures. A similar effect is observed in all three of the investigated gases. The voltage dependence of the peak brightness in all three gases at different pressures is shown in Fig. 4. It will be seen that the limiting brightness at a given pressure does not depend on the kind of gas. The peak brightness attains the saturation value at somewhat lower voltages as the pressure is increased. The limiting value of the instantaneous brightness in the investigated region of the spectrum increases only very slightly with increasing pressure.

The above facts would appear to indicate that the temperature and energy density in a pulse discharge also have limiting, saturation values. If we assume further that the release of energy in the discharge channel is independent of the type of gas, this would explain the diverse experimental results cited above (the different intervals to peak instantaneous brightness, the attainment of the limiting brightness in xenon at a lower voltage than in the other two gases and so on). As the supply of energy is increased, a saturation state is reached where further increase in energy released does not enhance the brightness but leads only to widening of the discharge channel.

The question of whether the temperature is uniform over the discharge cross section or is higher at the center than near the edges still remains open.

All-Union Scientific Research Institute
of Light Technology

1. K.S.Vul'fson & I.Sh.Libin, Zhur. eksp. i teor.fiz., 21, 570 (1951).
2. K.S.Vul'fson, Elektrichestvo, 11 (1946).

INFLUENCE OF THE CHEMICAL COMPOSITION OF THE ELECTRODES AND THE DISCHARGE CONDITIONS ON THE RELATIVE RATE OF VOLATILIZATION

- G. E. Zolotukhin

The present report gives the results of comparative studies of the variation of the relative concentration of particles, ΔN, in an AC arc with the thermal effects accompanying the process of vaporization. We used electrodes of platinum and platinum-silver (50% Ag) alloys and of copper and copper-gold (50% Au) alloys. Admixtures of elements differing from platinum as regards melting and boiling points were introduced into the platinum and its alloys in amounts of up to 0.1%: in one experiment, Pd or Au, in the other Rh or Ru. In the case of the copper alloys we made an attempt to establish the influence of an increase in the Au content on the relative rate of vaporization of Pt, Pd, Rh, Ir, Ru and Cu as a function of the power of the discharge. The value of ΔN was determined by measuring the intensity of the appropriate spectrum lines and the temperature in the electrode gap.

The thermal effects were investigated by means of a procedure which will be described in a future article. The temperature near the heated surface of the electrodes was calculated by means of the following equation for stable thermal equilibrium:

$$\varkappa \cdot F \frac{\partial T}{\partial x} = C \cdot \rho \cdot F \int \frac{\partial T}{\partial t} dl + q, \qquad (1)$$

where $\varkappa$ is the thermal conductivity of the substance, F is the cross section area of the electrode, $\frac{\partial T}{\partial x}$ is the temperature gradient, q is the heat carried off by the cooling liquid and $C \cdot \rho \cdot F \int \frac{\partial T}{\partial t} dl = \Sigma$ is a quantity characterizing the variation in heat content with time.

Equation (1) can be used to find $\partial T/\partial x$ at different distances x from the "white spot" on the electrode; $\varkappa$, C, ρ, q and Σ are assumed to be constant quantities, while F is variable.

The relative values of the logarithm of the ratio of the concentration of the admixtures (Pd, Au, Rh and Ru) to the concentration of platinum found for different electrode gaps h and different electrode polarities are listed in Table 1. The value of $\log \Delta N_{h=4}$ is arbitrarily set equal to zero. It will be seen from the table that the concentration of Pd and Au particles increases as the gap length is decreased, while the concentration of Rh and Ru particle decreases relative to the Pt concentration as the gap is narrowed.

The results of analogous observations made using Pt-Ag (50%) electrodes and AC arcs only are summarized in Table 2. The experiments with the platinum-silver electrodes showed that the value of $\partial T/\partial x$ is virtually independent of h.

We also conducted similar tests with Cu-Au alloy electrodes. As a result of these we established that the presence of gold noticeably reduces the effect of oxide films on the vaporization of the electrodes.

Changes in the strength of the discharge were accompanied by changes in the temperature gradient between the heated and cooled surfaces of the electrodes. The dependence of log T on R for platinum electrodes is shown in Table 3 and in the figure below. In Table 3 we give the values of log T for spheres of different radii R inside the electrode with their centers at the center of the "white spot."

Table 1

Concentration of Pd, Rh, Ru and Au relative to the Pt concentration in arcs formed between electrodes of platinum containing admixtures of the element, at different gap lengths and electrode polarities.

h, мм	Pt-Pd			Pt-Rh			Pt-Ru			Pt-Au		
	Anod.	Cath.	AC	Anod.	Cath.	AC	Anod.	Cath.	AC	Anod.	Cath	AC
1	+0,10	+0,21	+0,09	—0,02	—0,10	—0,08	—0,17	—0,16	—0,28	+0,27	—	+0,38
2	+0,05	+0,14	+0,00	—0,03	—0,03	—0,02	—0,14	—0,10	—0,28	+0,09	—	+0,07
4	0	0	0	0	0	0	0	0	0	0		0

Table 2

Concentrations of Pd, Rh, Ru and Au relative to Pt-Ag alloy present in AC arcs between platinum-silver alloy electrodes at different gap lengths.

h, мм	Pt-Ag-Pd		Pt-Ag-Rh		Pt-Ag-Ru		Pt-Ag-Au	
	lg ΔI	lg ΔN	lg ΔI	lg ΔN	lg ΔI	lg ΔN	lg ΔI	lg ΔN
1	+0,02	0,00	—0,21	—0,09	—0,16	—0,04	+0,10	+0,06
2	+0,02	0,00	—0,13	—0,05	—0,07	—0,01	+0,02	0,00
4	0	0	0	0	0	0	0	0

Table 3

Temperature (log T) distribution inside platinum electrode under different discharge conditions

h, мм \ R, см	0,006	0,012	0,025	0,050	0,075	0,100	0,150	0,200	0,300
4	3,38	3,14	2,95	2,81	2,74	2,70	2,68	2,66	2,62
2	3,19	3,01	2,85	2,72	2,67	2,64	2,62	2,60	2,57
1	3,07	2,81	2,77	2,65	2,60	2,56	2,54	2,52	2,50

As may be seen from Table 3 and the figure the temperature distribution is dependent on h. It is interesting to note that the dependence on h is weaker in the case of Pt-Ag alloy electrodes (see figure).

We calculated the minimum radius R of the sphere for which equation (1) remains valid. To this end we computed the rate of change of T and the temperature variation ΔT during the interruption in the discharge (between-cycle pause, taken equal to $4 \cdot 10^{-3}$ sec) for different values of R with the center of the "white spot" as origin. We used the following equation

$$\frac{dT}{dt} = \frac{\varkappa \frac{\partial T}{\partial x}}{C \cdot \rho}. \qquad (2)$$

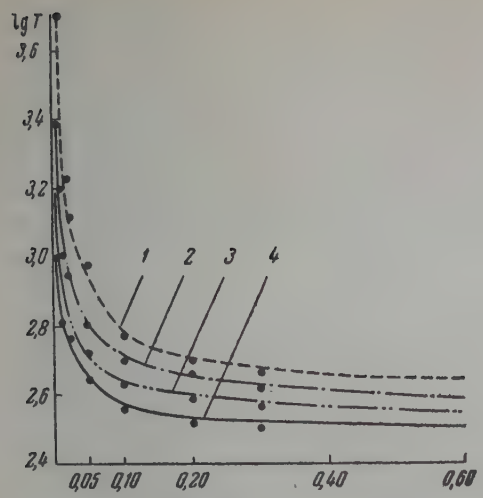

Distance from heated surface, R, cm

Variation of log T with R in Pt and Pt-Ag alloy electrodes at different inter-electrode distance h. 1) Pt-Ag alloy, h = 2 and 4 mm; 2) Pt, h = 4 mm; 3) Pt, h = 2 mm; 4) Pt, h = 1 mm.

The computed values of dT/dt and ΔT (for an interval $t = 4 \cdot 10^{-3}$ sec) are listed in Table 4. Thus an AC arc may be considered to be a continuous source of heat when R > 0.06 cm. In the case of electrode spheres of smaller radius there will be evident a relatively rapid temperature fluctuation during the "pauses" in the discharge.

In the light of our experimental results and calculations one can estimate what portion of the heat released at the surface of an electrode in an arc discharge is expended on vaporization of the electrode material. Let us designate this quantity through α. At a given frequency of the AC current the dependence of α on the physical properties of the electrode and the electrode cooling conditions is characterized by

$$\alpha = \frac{\Sigma m\lambda}{F\frac{\partial T}{\partial x}\cdot x + C} = \frac{\Sigma m\lambda}{a\cdot x + C},$$

where m is the mass of the volatilized material, λ is the heat of vaporization, ax is the quantity of heat transported in consequence of the thermal conductivity of the electrode and C is a small correction for thermal losses not otherwise accounted for.

Table 4

Electrode	R, см.	0,370	[?]	0,060	0,030	0,015
Platinum	$\frac{dT}{dt}$, sec^{-1} . . .	44	131	580	3100	11 800
	ΔT, deg. . . .	0,17	0,53	2,3	12,4	47
Pt-Ag Alloy	$\frac{dT}{dt}$, sec^{-1} . . .	50	129	815	3100	12 000
	ΔT, deg. . . .	0,2	0,51	3,2	12,4	48

The calculated values of α for Pt and Pt-Ag electrodes at different values of h are given in Table 5.

Table 5

Electrode	h, мм	m, mg/sec	$m\lambda$	ax	$\alpha \cdot 10^2$
Platinum	4	$1{,}5 \cdot 10^{-2}$	$0{,}91 \cdot 10^{-2}$	15,9	0,57
	2	$1{,}0 \cdot 10^{-2}$	$0{,}61 \cdot 10^{-2}$	13,0	0,47
	1	$0{,}67 \cdot 10^{-2}$	$0{,}40 \cdot 10^{-2}$	10,9	0,36
Pt-Ag Alloy	4	$6{,}4 \cdot 10^{-2}$	$4{,}1 \cdot 10^{-2}$	13,2	3,10
	1	$2{,}5 \cdot 10^{-2}$	$1{,}6 \cdot 10^{-2}$	11,3	2,21

Calculations of the rate of vaporization, made using the equation of Langmuir et al[1], showed that the part played by fractional vaporization in an AC arc between cooled electrodes is normally small and can be further reduced by using electrodes of alloys having a low value of $\varkappa$ and a relatively high value of α, instead of pure metal electrodes. In this case the volatilization or, more accurately speaking, the transport of the particles into the arc is explosive in character and the inter-electrode space becomes filled with particles having the same ratio of components as the solid phase (i.e., as the electrode material).

Reference

1. H. A. Jones, J. Langmuir & G. Macney, Phys. Rev., 30, 201 (1927).

* * * * * *

ON THE KINETICS OF VAPORIZATION IN AN ELECTRIC ARC

- Ia. D. Raikhbaum

In connection with the development of photoelectric methods of spectrum analysis of ores we undertook an investigation of the kinetics of vaporization of material in the crater of an arc electrode. One of the methods used was based on measuring the duration of emission of intense spectrum lines of the vaporized material; this was assumed to be equal to the time of vaporization of the sample. The use of a DG-1 arc generator assured good reproducibility of the vaporization conditions. Measurements made with different metals and metal compounds showed that vaporization time is related to the weight of the sample by the expression

$$t = a \cdot m^k \qquad (1)$$

The values of the parameter a — the vaporization time for a 1 mg sample — were found to be consistent with the thermal constants of the material. Experiments showed that this parameter serves as a reliable index in making quantitative comparisons of the volatility of different substances in an arc discharge.

The measured values of k for the investigated materials varied between 0.3 and 1. Analysis of the relationship (1) indicates that the magnitude of k characterizes the type of vapor formation. Thus, for metals with a high vapor pressure (Pb, Sn, Sb, Zn and Cd) and many of their compounds k fell between 0.6 and 0.75. Such values of k denote superficial vaporization in which diffusion and heat transfer in the vapor layers adjoining the sample play a dominant role. In the case of a small, spherical sample, the kinetics of the process are characterized by Sreznevski's law:

$$\frac{dS}{dt} = c,$$

where S is the surface area of the body (sample); k in this case equals 2/3.

In an arc in an atmosphere of hydrogen we noted an appreciable increase in the magnitude of the parameters a and k for zinc, cadmium and mercury; this is presumably connected with an increase in the diffusion and thermal conductivity coefficients and the absence of an oxide film.

Measurements made with mercury and cadmium at high electrode temperatures yielded values of k in the vicinity of 1/3, indicating a transition to pellicular boiling or a spheroid state.

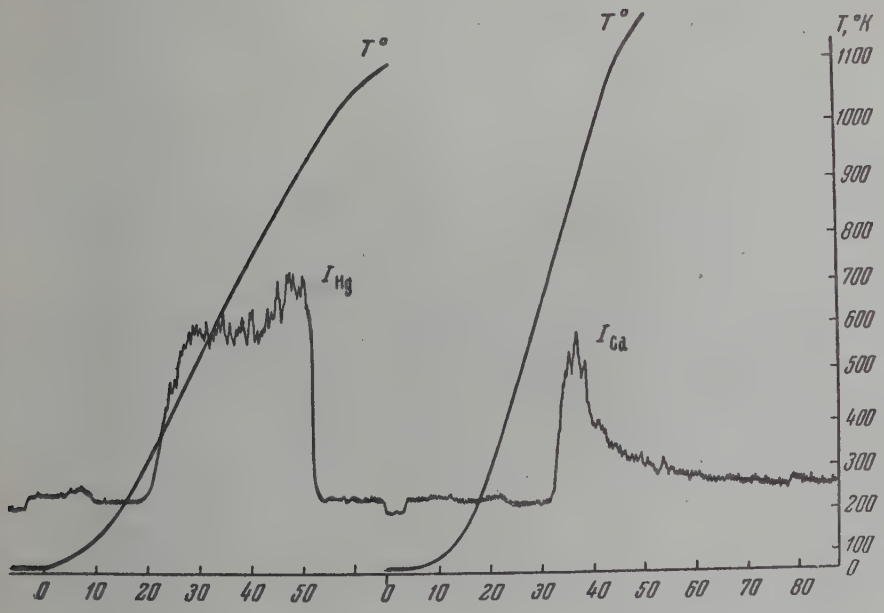

Photogram of the vaporization of Hg and Cd from a deep (18 mm) crater with increasing temperature of the electrode due to heating. The vaporization rates were evaluated from the intensity of the Hg 4358.35 A and Cd 5085.82 A lines.

In our experiments the volatilization of metals with a low vapor pressure (Fe, Cu and Ag) proceeded at a uniform rate and k equalled unity. Presumably this may be attributed to localization of a discharge of constant power on the surface of the sample.

Our deductions were verified by direct observation and measurement of samples in the electrode crater. The measurements were made by means of a microscope sighted through an opening in the upper electrode. On the basis of these measurements we were able to establish the rate of change of the diameter of the sample for different values of k.

We studied the kinetics of vaporization with the aid of an electrode equipped with a special, separate heater. The vapor from the crater of the controlled temperature electrode was drawn into the gap of a low-power spark; the intensities of the characteristic spectrum lines in the vapor were measured by means of a spectrograph with a FEU-17 photomultiplier. The photocurrent and the current from thermocouples inserted into the electrode were recorded on the same photogram; hence the complete record showed the variation of the line intensity with time and the temperature in the electrode crater. Measurements of the photogram record verified the validity of (1) and showed that the changes in the rate of vaporization (as indicated by the intensity of the spectrum lines) were in accord with the values of k.

In the case of a number of metals (Zn, Cd) and compounds the intensity of the characteristic line rose sharply when the temperature in the crater of the heated electrode reached the boiling point of the sample (see figure); in this way the boiling point of various substances could be determined with an accuracy of within 10-20°.

The described methods of investigating the kinetics of vaporization are applicable to substances of complex chemical composition and should prove useful in connection with various methodological studies.

* * * * *

THE USE OF PULSE DISCHARGES FOR SPECTRUM ANALYSIS OF GAS MIXTURES

- O. P. Bochkova and E. Ia. Shreider

Ordinarily when two components are present in the mixture of gases in a discharge tube only the emission of the component having the lower ionization potential is discernable in the positive column. Special conditions must be provided to achieve excitation of the other component. Suitable sources for this purpose are hollow-cathode tubes and quartz glow discharge tubes with a capillary section, supplied from a suitable high-frequency generator. With such tubes it has proved feasible to detect a few tenths of a percent of a hard-to-excite component in gas mixtures[1].

We investigated the possibility of using a pulse source[2] with a view to enhancing the sensitivity of analysis and simplifying the analytic procedure. A capacitor assembly (C = 2 to 70 μf) was charged through a high resistance from a high-voltage rectifier (1.5-3 kv) and then discharged through the glow discharge tube with cylindrical nickel electrodes. The enlarged portions, containing the electrodes, were connected by a constricted section some 10-15 mm in diameter. The shape of the tube and the gas pressure maintained prevented breakdown prior to ignition which was effected by means of a Tesla coil.

In pulse discharges, the electrodes in the tube neither absorb nor liberate gas to any appreciable extent (i.e., do not affect the composition of the mixture), due to the extremely short duration of the flash. If the capacitance of the discharge circuit is properly selected, the spectrum of a mixture of two gases with highly different ionization potentials will comprise the arc lines of the higher ionization potential component and the spark lines of the low ionization potential component.

We worked with the following mixtures: argon with helium, nitrogen with helium and air with neon. We plotted the calibration curve for the nitrogen-helium mixtures using the intensity ratio of the He 5876 and N II 5767 A lines (see accompanying figure) for a range of helium concentrations from 0.04 to 3.5%. The discharge conditions employed were C = 12 μf, V = 3 kv and P = 8 mm Hg col. The reproducibility was evaluated by checking individual values against the average for 60 determinations. The probable error for an individual determination was found to be about 5%.

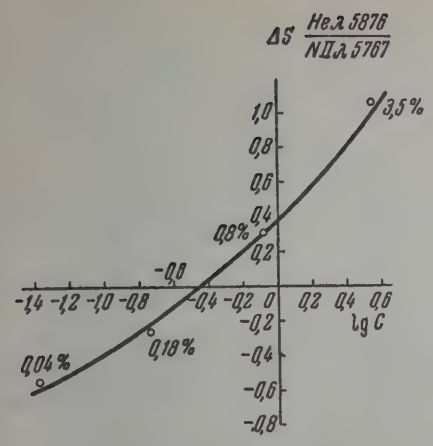

Calibration curve for determining small concentrations of He in N.

Analogous curves were plotted for the argon-helium and air-neon mixtures. In order to raise the sensitivity of the determination of helium in argon to the requisite level it was found necessary to increase the power of the discharge by increasing the capacitor voltage. Premature breakdown was prevented by connecting an auxiliary spark gap in series with the tube.

In the case of the air-neon mixtures the sensitivity where the determination of neon (according to the 6402 A line) is concerned could not be increased above 0.2% regardless of the gas pressure and circuit capacitance tried. However, the sensitivity of determination can be increased about ten-fold by photographing the glow inside the hollow electrode during the pulse discharge.

Rapid-sequence photographic studies of pulse discharges[3] show that the peak emissions of the arc and spark lines do not coincide in time. Hence, the sensitivity of the analysis can be enhanced by photographing the pulse discharge at different stages of its development to record the respective peaks.

Better reproducibility can doubtless be achieved by using a thyratron instead of the auxiliary spark gap.

Physical Institute of
Leningrad State University

References

1. S.E.Frish & E.Ia.Shreider, Izv. AN SSSR, Ser.fiz., 13, 465 (1949); S.E.Frish, Vestnik LGU (Review, Leningrad State University), 6, 26 (1950).
2. M.Laporte & Mlle Pierrejean, Journ. de Phys.et Rad.,7,6,248 (1931).
3. K.S.Vul'fson, Izv. AN SSSR, Ser. fiz., 9, 3, 239 (1945).

* * * * *

NEW METHODS OF USING MULTIPLEX ETALONS IN HIGH RESOLUTION SPECTROSCOPY

- F. A. Korolev

The intensity distribution in compound etalons - now commonly termed multiplex etalons and used for high-resolution spectroscopy- when the assembly is properly adjusted, is characterized by

$$I = \frac{\pi p^2 B \vartheta^2 \vartheta'^2}{\left\{(1-R)^2 + 4R\sin^2\frac{\Phi}{2}\right\}\left\{(1-R')^2 + 4R'\sin^2\frac{\Phi'}{2}\right\}}, \qquad (1)$$

where p is the radius of the multiplex etalon aperture, B is the brightness of the source, taking into account all losses in the optical system except the losses in the mirrors and the separating layers in the etalon, R and R' are the reflection coefficients of the first and second etalon component mirrors, respectively, ϑ and ϑ' are the transmission coefficients of the respective mirrors and Φ and Φ' are the phase differences of two consecutive beams for the first and second components of the etalon. In this case

$$\Phi = \frac{4\pi h}{\lambda}\cos\psi + \delta_1 + \delta_2 \quad \text{and} \quad \Phi' = \frac{4\pi h'}{\lambda}\cos\psi + \delta_1' + \delta_2',$$

where h and h' are the thicknesses of the first and second etalon components, $\delta_1 \neq \delta_2$ and $\delta_1' \neq \delta_2'$ are the phase "jumps" at the first and second component mirrors, λ is the wavelength and ψ is the observation angle.

The intensity at the maximum is given by

$$I_m = \frac{\pi p^2 B \vartheta^2 \vartheta'^2}{(1-R)^2(1-R')^2}. \qquad (2)$$

The angular dispersion of a multiplex etalon is the same as that of a conventional etalon. The limit of resolution in the case of etalons with components of markedly different thickness is practically equal to the limit of the thicker component while the region of dispersion is equivalent to that for the thinner component.

In the case of multiplex etalons with components of equal thickness, the limit of resolution of the multiplex etalon equals 0.64 of the limiting value for one of the etalon components, while the contrast factor

$$C = \left(\frac{1+R}{1-R}\right)^4. \qquad (3)$$

By virtue of this a multiplex etalon with equal-thickness components is advantageous for use in resolving lines of unequal intensity.

For many applications multiplex etalons with components of almost equal thickness will be found preferable. Where there is a small difference Δh between the thicknesses of the two components, the dispersion region is increased by a factor $m = h/\Delta h$ (where h is the thickness of one component) over the dispersion region with exactly equal thickness components. At the same time the limit of resolution is decreased (while the resolving power is increased) by a factor of 0.64 compared with the value for the individual components. Hence, almost-equal-thickness multiplex etalons may be said to reunite the advantages of multiplex etalons with components of different thickness with the positive features of equal-thickness etalons.

As we showed in an earlier contribution[2] a satisfactory multiplex etalon can be realized even with components whose thicknesses are not simple multiples of each other; this, of course, greatly simplifies construction of the etalon. In view of what has been stated above and bearing in mind the possibility of utilizing dielectric mirrors we can safely say that it should be possible to make use of compound etalons in a wide range of line intensity ratios and to attain limits of resolution equal to or even less than the natural breadth of the spectrum lines while retaining a sufficiently wide region of dispersion.

Department of Physics of
Moscow State University

References

1. F. A. Korolev, Spektroskopiia vysokoi razreshaiushchei sily (High Resolution Spectroscopy). M.-L. 1953.
2. F. A. Korolev, Vestnik MGU (Moscow State University Review), 3, 105 (1953).

* * * * *

EXCITATION OF SPECTRA BY ELECTRIC DISCHARGES IN A LIQUID MEDIUM*

- N. S. Sventitski and K. I. Taganov

Electric discharges in a liquid medium, in addition to their familiar use as a continuum source, can serve as a source for emission spectrum analysis. This method of excitation can be advantageously applied in a number of cases, such as 1) for observing the spectrum of a flowing liquid without taking samples, 2) analyzing parts of underwater structures, 3) when it is essential to isolate the discharge cloud from the surrounding medium, 4) when it is desired to localize the influence of the discharge or restrict it to a small section of the electrodes, and 5) in studying spark-hardening of metals and similar processes in a liquid.

Observations of the emission of discharges in liquids have shown that changing the parameters of the discharge circuit has a very appreciable effect on the emitted spectrum. Specifically, in the case of a low-voltage pulse discharge one can effectively suppress the continuous spectrum and obtain conditions favorable to observing line spectra and effecting emission analyses.

In the analysis of brass for zinc content the initial portions of the line intensities curves (corresponding to the burning in period of the electrodes) differ for discharges in air and in CCl_4 due to differences in the character of the oxidation process. The influence of "third" components is also markedly reduced in the case of discharges in a liquid medium. For example, tests on two samples of brass, both containing 15% zinc, but one with 5% lead, the other with 5% silicon, showed the following differences as regards the logarithm of the relative intensities of the Zn I 4680 and Cu I 4651 A lines: 0.56 in air, 0.14 in hexane and 0.10 in carbon tetrachloride (in all cases the Zn line was more intense in the spectrum of the sample containing 5% silicon). Thus it will be seen that the influence of silicon on the Zn line intensity is very strong in discharges in air and that it diminishes appreciably in discharges in a liquid.

The relative intensity of the Cu II 4556 A and Cu I 4587 A lines is increased by a factor of 4.4 in discharges in CCl_4 as compared with discharges in air, which indicates that the excitation temperature in CCl_4 is considerably higher.

When the spectrum is excited in carbon tetrachloride or hexane one can detect the presence of gases, such as hydrogen and nitrogen, in the electrode material.

---

* M. G. Mal'tsev and V. N. Filimonov took part in the experimental work.

The pronounced inhomogeneities of the temperature and vapor density distributions in discharges under a layer of liquid result in conditions favorable to self-reversal of spectrum lines. Thus excitation in a liquid medium provides a ready means of demonstrating the effect and may well serve as a convenient experimental procedure in determining the characteristics of individual lines. Thus, for example, in the visible region of the spectrum of a pulse discharge between iron electrodes in water one can observe over 60 fully reversed iron lines, associated with the lower energy levels.

* * * * *

DIELECTRIC MIRRORS AND THEIR USE IN FABRY-PEROT ETALONS

- F. A. Korolev and V. V. Sukhanovski

The recent development of dielectric mirrors, having virtually negligible absorption over a considerable portion of the spectrum, has made it possible to effect a substantial improvement in the optical characteristics of Fabry-Perot etalons.

A theoretical analysis of the reflection of a plane wave front from multiple-layer, two-component dielectric coatings consisting of 2m + 1 transparent and isotropic films and a careful review of Frau's investigation of this problem[1] have enabled us to develop a theory which avoids certain errors present in Frau's work and is free of his restrictions on the order in which the dielectric layers are applied and on the magnitude of the indices of refraction of the dielectric materials forming the coatings (n_1 and n_2, the support (n) and the surrounding medium (n_0). The results of our theory are in satisfactory agreement with experiment.

According to our theory the transmission T of a dielectric coating consisting of 2m + 1 layers of equal optical thickness ($n_1d_1 = n_2d_2 = a$) is given by

$$T = \frac{n_0}{n} \cdot \frac{1}{C^2[(a_2^2 - a_1^2)\sin^2\delta + a_1^2] + S^2 g_1 + CS g_2},$$

where

$$g_1 = \frac{1}{b_1^2 \operatorname{tg}^2\delta - 1}\left[(a_2^2 - a_1^2) b_2^2 \cos^2\delta + \frac{a_3^2 b_1^2}{\cos^2\delta} + 2a_2a_3b_1b_2 + a_1^2b_2^2\right],$$

$$g_2 = \frac{1}{\sqrt{b_1^2 \operatorname{tg}^2\delta - 1}}\left[(a_2^2 - a_1^2) b_2 |\sin 2\delta| + 2a_2a_3b_1b_2 |\operatorname{tg}\delta|\right],$$

$$a_1 = \frac{n + n_0}{2n}, \quad a_2 = \frac{nn_0 + n_1^2}{2nn_1}, \quad a_3 = \frac{nn_0 - n_1^2}{2nn_1},$$

$$b_1 = \frac{n_1 - n_2}{2\sqrt{n_1n_2}}, \quad b_2 = \frac{n_1 + n_2}{2\sqrt{n_1n_2}}, \quad \delta = \frac{2\pi}{\lambda} a,$$

and

$$\left.\begin{aligned} C &= (-1)^m \cos m\varphi \\ S &= (-1)^{m+1} i \sin m\varphi \\ \varphi &= \operatorname{arc\,tg} \frac{\sqrt{1 - z_{11}^2}}{-z_{11}} \end{aligned}\right\} \text{ when } |z_{11}| < 1$$

or

$$\left.\begin{aligned} C &= (-1)^m \operatorname{ch} m\Phi \\ S &= (-1)^{m+1} \operatorname{sh} m\Phi \\ \Phi &= \operatorname{arg\,th} \frac{\sqrt{z_{11}^2 - 1}}{-z_{11}} \end{aligned}\right\} \text{when} |z_{11}| > 1,$$

while

$$z_{11} = 1 - \frac{(n_1 + n_2)^2}{2n_1 n_2} \sin^2 \delta.$$

A theoretical analysis of the optical characteristics of different two-component multiple-layer dielectric coatings showed that quarter-wave ($a = \lambda/4$) multiple-layer coatings would be most suitable for Fabry-Perot interferometer mirror.

We produced such reflecting surfaces with 3, 5, 7, 9 and 11 layers for different regions of the spectrum by vaporizing zinc sulfide ($n_1 = 2.3$) and cryolite ($AlF_3 \cdot 3NaF$ — $n_2 = 1.35$) under vacuum on to a glass support. Seven-layer dielectric mirrors having an optical thickness of each layer a = 1450 A and a reflection coefficient R = 0.94 and a transmission coefficient T = 0.06 at λ = 5461 A were used in making a Fabry-Perot etalon which was then employed to observe the hyperfine structure of the 5461 A green mercury line. The sample etalon was compared with an analogous interferometer having conventional silvered reflecting surfaces (R = 0.92 and T = 0.04 at λ = 5461 A). The comparison showed that the use of dielectric mirrors increases the transmission by a factor of 4 and the contrast by almost 2 and effects an improvement of about 35% as regards resolving power. The superiorities of the dielectric mirror etalon stand out clearly in the comparison microphotograms: there is appreciably greater blackening with half the exposure time in the strip obtained with the dielectric mirror etalon; furthermore, at least seven lines are resolved in the dielectric mirror etalon photogram strip as against the six separated by the conventional silvered surfaces etalon.

It will be seen, therefore, that etalons with quarter-wave, multiple layer dielectric mirrors are superior to those with silvered mirrors as regards all the principal characteristics: transmission, contrast and resolution. Hence, such etalons provide an effective means for extending the experimental scope of high-resolution spectroscopy.

Department of Physics of
Moscow State University

Reference

1. K. Frau, Revue d'Optique, 31, 4, 161 (1952).

A TWO-PRISM DISPERSING SYSTEM WITH AN INTERMEDIATE MIRROR

- B. A. Shapochnik

It is known that turning individual prisms of a dispersing system away from the minimum deviation angle position results in an appreciable increase in the angular and, consequently, in the linear dispersion[1]. This makes it possible 1) to obtain a higher true resolving power in spectrographs, 2) to attain an increase in resolution with wide slits in spectroscopes and to obtain a brighter spectrum with an increase in linear dispersion than is obtained by increasing the focal length of the camera or the power of the eyepiece[2] and 3) to utilize more fully the dispersing properties of the prism at the limiting angles of the incident and emerging beams in a wide spectral range.

The factors restricting the deflection of prisms from the minimum deviation position in practice are worsening of the quality of the spectrum due to increased influence of inhomogeneity of the material and aberrational errors, increased light loss due to reflection and increased curvature of the spectrum lines.

In individual prism system designs where deflection from the minimum position is used[3,4] the turned prism is usually fixed in the deflected position. The realization of a dispersing system in which the angular positions of the prisms can be varied to obtain a variable dispersion (without changing the angle of deflection of the spectrum) would make possible a more universal and flexible spectroscopic instrument.

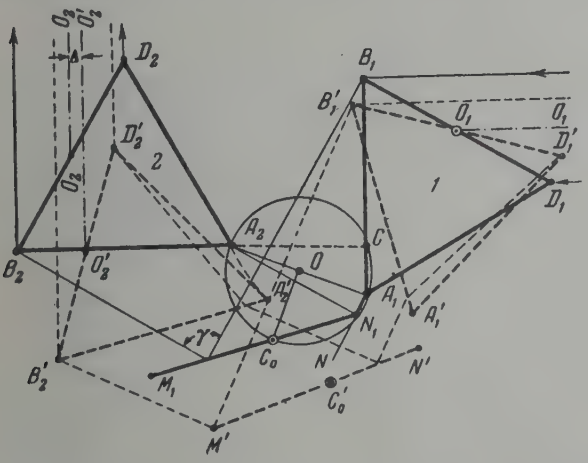

Two-prism dispersing system with intermediate mirror: 1 & 2 prisms, M_1N_1 intermediate mirror, C_0 axis of rotation of mirror for shifting wavelengths, O_1 axis of rotation of entire system from the minimum deviation position. Solid lines indicate initial position of the optical elements; dash lines show position after rotation about O_1.

A possible variable dispersion system is one consisting of two identical prisms 1 and 2 and an intermediate mirror M_1N_1 arranged as shown in the accompanying diagram[5]. To go from one region of the spectrum to another, one need only rotate the mirror M_1N_1 about an axis through point C_0, leaving the prisms undisturbed. Point C_0 is located so that it bisects the arc $A_1N_1A_2$ of the circle passing through A_1, A_2 and C (point C is the intersection of the extension of the face B_2A_2 of prism 2 and the face B_1A_1 of prism 1.

The deviation of the collimated beam by the system as a whole depends on the angle γ at the mirror and is the same for different wavelengths inasmuch as the deviations introduced by the two prisms are equal and compensate each other. The angle γ

depends only on the relative orientation of the prisms and equals the angle between two corresponding faces of the prisms.

The prisms can be swung away from the minimum deviation position (without altering their relative orientation) in a number of ways. Two possible procedures, for example, are 1) rotating the prisms through equal angles about their corresponding edges A_1 and A_2 and 2) turning the entire system about a common axis (for instance, about O_1; the resultant positions of the elements in the latter case are indicated by dash lines in the figure). It must be borne in mind that such rotation away from the minimum deviation position will shift the spectrum to some extent, necessitating a compensatory shift of the camera or eyepiece. The described system can also be made to work as a constant minimum deviation system; to this end the angular displacements or rates of rotation of the prisms and the mirror must be in the ratio of 1:2.

It is also possible to design a four-prism dispersing system patterned on the described two-prism arrangement. Such a system would have a more convenient (as regards both construction and operation of the instrument) total deviation angle in the vicinity of 180°. It should be possible to minimize vignetting (fading) of the side beams in the dispersing system by proper positioning of the prisms relative to each other.

Our experiments with one version of two-prism system with an intermediate mirror carried out in conjunction with an UM-3 monochromator showed that such systems are practicable and worthy of further development.

"Bauman" Moscow Higher Technical School

References

1. V.I.Malyshev, Izv. AN SSSR, Ser. fiz., 14, 746 (1950).
2. A.Shuster, Vvedenie v teoreticheskuiu optiku (Introduction to Theoretical Optics), p. 159, M.-L. 1935.
3. V.M.Chulanovski, Vvedenie v molekularnyi spektral'nyi analiz (Introduction to Molecular Spectrum Analysis), p. 300, M.-L. 1950.
4. F.S.Baryshanskaia, Izv. AN SSSR, Ser. fiz., 9, 657 (1945).
5. S.Makishma & others, Journ. Opt. Soc. Am., 41, 4, 249 (1951).

* * * *

INVESTIGATION OF HIGH-CURRENT PULSED ARCS

- M. E. Britske

In recent years pulsed spectroscopic light sources have come into widespread use, yet their physical properties have not been fully investigated.

In our report to the Eighth Conference on Spectroscopy we pointed out that a heavy-current pulsed arc has a higher arc-flame temperature and an enhanced overall brightness.

Subsequent studies have shown that the density of the arc current mounts to a peak value at the initial instant of burning and then

falls off with time, asymptotically approaching the value characteristic of a stationary discharge. As the strength of the current is increased, there is an appreciable increase in the current density. The maximum attainable current densities are of the order of 10^5 amp/cm^2.

In our investigation we determined the diameter of the arc channel by two methods: from photographs obtained with the aid of a stroboscope synchronized with the ignition of the arc and by measuring the trace of the anode and cathode spots on the electrodes. An oscilloscope was used to measure the strength of the current.

Our experimental results are in good agreement with the published data of other investigators on the current density in pulsed discharges of different durations.

Study of the spatial distribution of the emission of a pulsed high-current arc showed that the absolute and relative intensities of atomic and ionic lines remain virtually constant over the entire length of the inter-electrode gap (Fig. A, p. 75). The intensification of lines due to ions in the vicinity of the electrodes, common to the spectra of low-current arcs, was not observed in our spectra of high-current pulsed arcs. (See Fig. B, p. 75.)

The relative intensities of the lines due to atoms and ions in the central part of the cloud of a high-current pulsed arc proved to be nearly the same as their relative intensities in the vicinity of the electrodes in weak-current arcs. This indicates that the enhancement of the relative intensities of the ionic lines in a high-current pulsed arc is due to an increase in their absolute intensities in the central region of the discharge.

The relative intensity of pairs of atomic lines, having different upper-level energies, which serves to characterize the atom temperature T_a of the arc flame, remains constant over the length of the gap in both pulsed and low-current arcs. Hence, the entire region of the arc flame can be characterized by a single value of T_a. T_a rises as the strength of the current is increased. The value of T_a measured by Ornstein's method on the basis of the relative intensity of the 5105 and 5153 A lines of Cu proved to be 8500°K with a current strength on the order of 200 amperes at the pulse peak, as compared with 5100°K for a constant arc with a current of 5 amperes.

We also found that the relative intensity of ionic lines with different upper-level energies, which may be said to characterize the ion temperature T_i, remains constant over the length of the gap in a pulsed arc; i.e., the ion temperature in the entire volume of the arc cloud can be characterized by a single value of T_i. In contrast, in steady low-current arcs T_i is much lower in the central zone than near the electrodes.

The distinctive features of the spatial luminescence distribution in high-current arcs can be explained if we assume that the electrode material is carried or blown into the arc flame by a jet mechanism.

The fact that vapor jets - the luminescence of which persists for some time outside the electric field - are formed in such discharges was proved experimentally: vapor jets were obtained both by artificially directing the vapor stream and under natural conditions. The jet spectrum proved to be identical with that of the inter-electrode region of a pulsed arc.

State Scientific Research Institute
for Non-Ferrous Metals

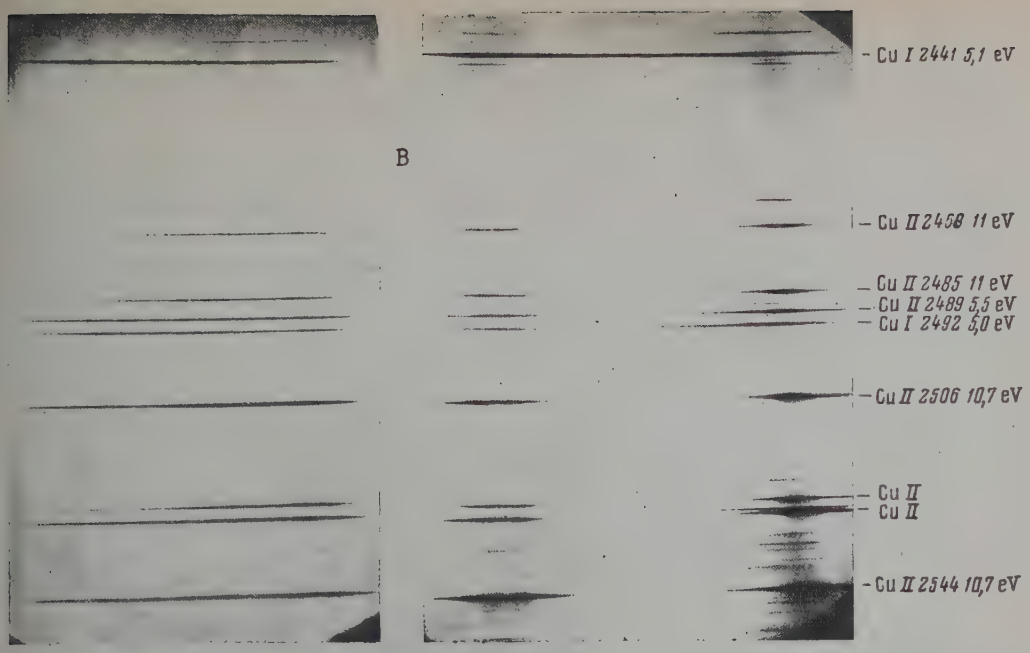

See page 73.

Spatial distribution of intensities in arc spectra:
A - spectrum of high-current pulsed arc (I = 100 a); B - low-current arc (I = 5 a).

See page 76.

Spectra of sparks between iron electrodes obtained with a metal spark-hardening unit at different spark temperatures produced by varying the capacitance of the unit.

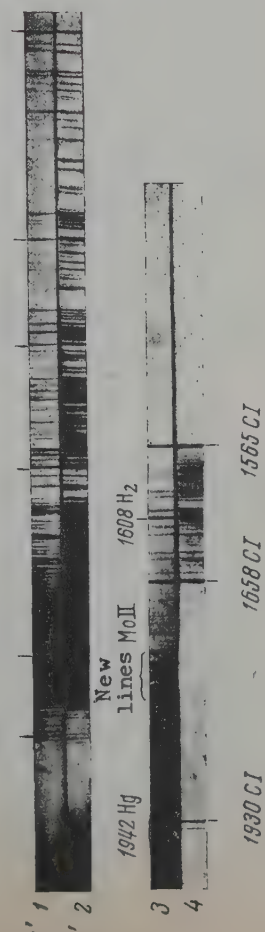

Spectrograms obtained on the vacuum fluorite spectrograph: 1 - high-voltage discharge in hydrogen, photographed on panchromatic film; 2 - same, but on emulsion developed by the authors; 3 - discharge in hollow cathode of Mo in an atmosphere of Ar with H; 4 - same as 3 but in an atmosphere of He with an admixture of H. See page 77.

INVESTIGATION OF THE TEMPERATURE OF THE SPARK PRODUCED BY A METAL-HARDENING SPARK GENERATOR

- A. N. Liulichev and L. S. Palatnik

The present investigation is a continuation of our study of electric-spark working of metals using the techniques of spectrum analysis[1] and was devoted to measuring the temperature of the vapor phase of the spark discharge formed in the process of electric-spark surface-working of metals. The spectra of sparks produced by a spark hardening unit[2] were photographed with the aid of a ISP-22 spectrograph.

The spark temperatures were determined by Ornstein's method and by the "comparison method" proposed by the present authors (see below). For the determinations by Ornstein's method we selected 10 lines of Fe II in the 2562-2756 A interval; the data on the transition probabilities and the upper level energy values for these lines were taken from Sobolev[3]. In our investigation we assumed that the spectral sensitivity and the gamma of the photographic plates used remain constant in the wavelength range in question[4,5].

The temperature determinations by our "comparison method" are based on the relative intensities of spark and arc lines of iron. We made use of four pairs of Fe I - Fe II lines in the 2560-2750 A region. Our procedure for approximate evaluation of the temperature involves visual comparison of arc and spark spectrograms. In the 6000-9000°K interval temperatures can be determined by the "comparison method" to within ±3%.

The spark temperature remained constant within the limits of the measurement error when the supply voltage was varied from 70 to 220 v and the short-circuit current increased from 1 to 3 amperes. Temperature measurements showed, however, that as the capacitance of the condenser assembly is reduced from 280 μf to 0.25 μf the spark temperature falls from 10,200 to 7200°K. This is evinced in the spectra photographs (see p. 75) by the increase in the relative intensity of the arc lines (the 2594, 2733 and 2735 A lines, for example). The observed variation is satisfactorily described by the following empirical equation (within the investigated ranges):

$$T = 720 + 450\sqrt[3]{C}.$$

Reduction of the electrode diameter leads to an increase in the spark temperature. Thus, for sparks with a capacitance of 10 and 20 μf in the discharge circuit, a decrease of the diameter of the electrodes from 4 to 1 mm brings the spark temperature up about 1500°.

We measured the temperature of sparks between the following electrode pairs: Fe-Fe, Fe-W, Fe-Cu, Fe-Al and FeC at spark circuit capacitances of 280, 140, 80, 40, 20, 10 and 3 μf. For most pairs the observed temperatures for like capacitances were the same within the limits of the measurement error. In the case of the Fe-C pair, however, we obtained temperature values running 600-1000° below the corresponding temperatures for the Fe-Fe pair.

The "comparison method" of measuring spark temperatures can be used to advantage in checking or setting the operating regime of the generator unit in spark metal-working equipment.

"A. M. Gor'ki" Kharkov State University

References

1. A.N.Liulichev & L.S.Palatnik, Izv. (Bulletin) AN SSSR, Ser.fiz., 18, 259 (1954). [Translation available from C.T.T.]
2. B.R. & N.I.Lazarenko, Elektricheskaia erosia metallov (Electric erosion of metals), M. 1946.
3. N.N.Sobolev, Zhur. eksp. i teor. fiz., 13, 131, 137 (1943).
4. I.I.Breido, Zhur. tekh. fiz., 14, 199 (1944).
5. V.K.Prokof'ev, Fotograficheskie metody kolichestvennogo spektral'nogo analiza metallov i splavov (Photographic methods of quantitative spectrum analysis of metals and alloys), M.-L. 1951.

* * * * * *

THE VACUUM FLUORITE SPECTROGRAPH, PHOTOGRAPHIC EMULSIONS FOR IT AND SOME EXPERIMENTAL RESULTS OBTAINED WITH THE INSTRUMENT

- A. V. Iakovleva, I. I. Gromova and I. R. Protas

The optical system of the new vacuum spectrograph [see p. 331 and Fig. 2, p. 332, Trans. No. 6, Vol. 18 of the Bulletin] consists of a 60° fluorite prism, 20 mm high, and two simple fluorite lenses 17 and 22 mm in diameter. In order to enhance the resolving power one surface of each of the lenses is ground parabolic, which effectively reduces spherical aberration. The speed of the instrument for λ = 1600 A is 1:10. The instrument has provision for moving the diaphragm relative to the slit, adjusting the cassette and varying the slit width between 0.01 and 0.36 mm without disturbing the vacuum. The spectrograph is supplied with two cassettes: a flat and a concave one. The entire spectral range of the instrument - 1300 to 2100 A - can be clearly focused only on the concave cassette. Four spectrograms obtained with the instrument are reproduced on p. 75 ; these represent: 1) a high-voltage discharge in hydrogen photographed on panchromatic film, 2) an identical discharge photographed on an emulsion developed by the authors (see below), 3) a discharge in a hollow-cathode of molybdenum in an atmosphere of argon with an admixture of hydrogen, and 4) a similar discharge in an atmosphere of helium with an admixture of hydrogen.

We used hollow cathodes of Mo, Ni, Fe, Zn, Cu and C as sources of vacuum ultraviolet radiation. Fewer metal lines are observed in discharges in helium due to the fact that there is least evaporation from the cathode in helium and, hence, fewer metal atoms in the discharge. On the other hand, many metal lines are present in discharges in argon. In the spectrum of the discharge with a molybdenum cathode in argon we detected a group of relatively intense lines in the vicinity of 1750 A, which are not mentioned in published lists of Mo lines (see Table 2).

Although our experimental data is inadequate for positive identification of these lines, we believe they should be attributed to Mo II. The lines appear in spectrogram 4.

To obtain the spectra of the various metals a small sample of the investigated metal was placed in the cathode made of a more refractory metal (molybdenum, for example).

It was established that the intensity distribution in the molecular spectrum of hydrogen differs, depending on the material of the

Table 1

Molybdenum lines detected by the authors in the spectrum of a discharge in argon with a molybdenum hollow cathode

№ n/n	λ, Å	I	λ, Å according to Kayser	№ n/n	λ, Å	I	λ, Å according to Kayser
1	1769,60	1		12	1733,00	15	
2	1767,61	1		13	1732,20	25	
3	1754,40	10	1754,4	14	1731,11	35	1731,9
4	1749,85	10		15	1722,40	10	
5	1747,88	5		16	1721,24	1	
6	1746,95	7	1746,7	17	1719,89	10	
7	1745,66	20		18	1718,08	1	
8	1742,77	25	1742,2	19	1704,72	5	
9	1741,18	25		20	1702,90	5	
10	1737,49	50	1737,3	21	1701,63	1	
11	1735,10	10		22	1699,00	1	

cathode and the nature of the other gas present in the discharge tube. This is due apparently to collisions of the second order between hydrogen molecules and atoms of the metal in some cases and atoms of the extraneous gas in other cases.

The spectra were photographed on ordinary panchromatic film and on positive film. Transformer oil was used for sensitizing the emulsions. We determined the fluorescence region (3100-4300 A) and the absorption characteristics of the oil. In addition a number of photographs were made on film coated with special emulsion we developed for this purpose (see spectrogram 2).

In developing this new emulsion we carried out an investigation of the various factors affecting the sensitivity of emulsions in the vacuum ultraviolet region. We discovered that the speed of emulsions in the vacuum ultraviolet can be increased by means of the chemical sensitization procedures employed for sensitization of emulsions to the visible range of the spectrum. As a result of our studies we developed an emulsion which, like Schumann's[1] plates, contains a high proportion of silver halide and a very small amount of gelatin. The emulsion is applied in layers not exceeding 2-3 microns in thickness.

Table 2 shows the relative values of the speed and gamma at λ = 1402 A determined for our film, for an emulsion prepared according to Schumann's formula and for "Type II, Spectral" plates sensitized with oil. In addition the values of the resolving power R for λ = 4360 A and the fog density D_o are compared in the table.

Table 2

Comparison of photographic characteristics of three emulsions

Photographic material	$S_{rel} = \left(\frac{1}{min}\right)_{D_o+0.2}$	γ	D_o	R, mm^{-1}
Spectral plates, Type II sensitized with trans. oil	0.9	1.05	0.02	180
Schumann emulsion	1.5	0.60	0.02	--
Emulsion developed by the authors	7.0	1.10	0.02	300

The data in Table 2 and spectrogram 2 (p.75) show that in the vacuum ultraviolet our new emulsion is far more sensitive than the materials used hitherto and, in addition, is superior as regards resolving power.

The described spectrograph was designed by G. I. Zavodchikov, V. I. Aleksandrov and N. I. Kulikovskaia. V. L. Abritalin, G. A. Karkeshkina and E. D. Pazumova, graduate students at LIKI, participated in the experimental work involved in the development of the new emulsion.

Reference

1. V. Schumann, Ann. de Phys., 349 (1901).

* * * * * * *

A VACUUM FLUORITE MONOCHROMATOR

- S. A. Kulikov and A. V. Iakovleva

We constructed a vacuum fluorite monochromator with a photoelectric radiation receiver. By adding a special attachment it can be converted to a double monochromator. Both the basic monochromator and the attachment employ a Wadsworth mounting, consisting of a 60° prism and an aluminized mirror. The lenses are planoconvex fluorite lenses 15 mm in diameter; they are moved simultaneously with rotation of the prism by the same handwheel. For covering the 2500 to 1300 A range the prism is turned 10°30', the corresponding travel of the lenses being 71 mm. The average speed of the instrument is 1:12. The width of the slits can be adjusted from 0 to 1 mm without disturbing the vacuum. The instrument has appropriate flanges for airtight connection to the light source and the receiver. The vacuum line coupling and valve are located in the base of the monochromator.

In converting to the double monochromator, the attachment, which has a mating flange, is mounted behind the exit slit of the basic instrument. A condensing lens is mounted at the intermediate slit to insure better filling of the second monochromator lens with radiation. The wavelength controls for the two monochromators are separate and each is adjusted individually. The wavelength drum of the basic monochromator was graduated photographically according to the spectrum of a spark between aluminum and zinc electrodes and the line spectrum of hydrogen; the wavelength drum of the attachment was graduated by means of the photoelectric radiation receiver. The working range of the single monochromator extends from 2500 to 1350 A; that of the double, from 2500 to 1400 A. Below the indicated limits the intensity drops off sharply due to radiation losses in the instrument. From comparative measurements of the intensity at the exit slits of the single and double instruments the loss in the attachment was estimated to be 50% at 2500 A and 85% at 1500 A. It may be assumed that the losses in the basic monochromator are of the same order.

Two different types of photoelectric receivers were used with the monochromator: a FEU-19 (photomultiplier) with a sodium salicylate screen and photon [Geiger] counters with fluorite windows. In working with the photomultiplier, the exit slit of the monochromator

was hermetically covered with a fluorescent screen and the end of the photomultiplier tube was set flush against this screen. The photocurrent was measured by means of a "Multiplex" galvanometer after amplification by a DC bridge amplifier designed about a 6Zh1Zh tube.

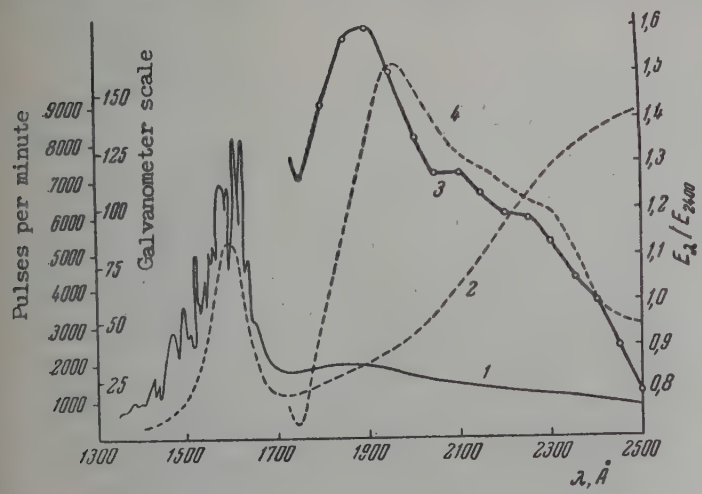

Spectra of a hydrogen discharge tube obtained by means of the single (basic) monochromator 1) with a photon counter and 2) with the photomultiplier. The intensity distribution in the emission of the tube as measured by the photomultiplier is given by curve 3; the distribution found by the photographic method, by curve 4.

The photon counters were built by us in the laboratory. The anodes were made of 0.1 mm diameter tungsten filament, the cathodes were cylinders 11 mm in diameter and 50 mm in height of oxidized copper or iron covered with molybdenum oxide. An opening 5 x 8 mm was cut in the cylinders and the fluorite window was cemented to the envelope opposite this opening. The counter tubes were filled with hydrogen at 100 mm Hg col; the photoelectric threshold of the counters was located at about 2600-2700 A. The counter plateau was about 250 v wide with a slope of 0.2% per 1 v.

The figure shows the curves of the variation in the number of photon counter pulses and in the FEU photomultiplier current with the wavelength obtained for a GOI hydrogen discharge tube (Curves 1 and 2). The intensity distribution in the emission of this tube in the 1700 to 2500 A interval as determined on the monochromator by means of a photomultiplier with a fluorescent screen is represented by Curve 3. Curve 4 is the distribution determined photographically on a ISP-18 spectrograph[1]. It will be seen that down to about 2000 A the two distribution curves nearly coincide; the divergence at shorter wavelengths is explained by the fact that with the photographic procedure it was impossible to take account of the light loss in the instrument.

Reference

1. M.K. Ivanov and Iakovleva, Izv.(Bulletin)AN SSSR,Ser.fiz.,14,561 (1950).

A NEW HIGH RADIANCE HYDROGEN DISCHARGE TUBE

- I. I. Kondilenko and M. P. Lisitsa

We developed a new design for a hydrogen tube of high effective brightness. A sectional view of the tube is shown in the accompanying figure.

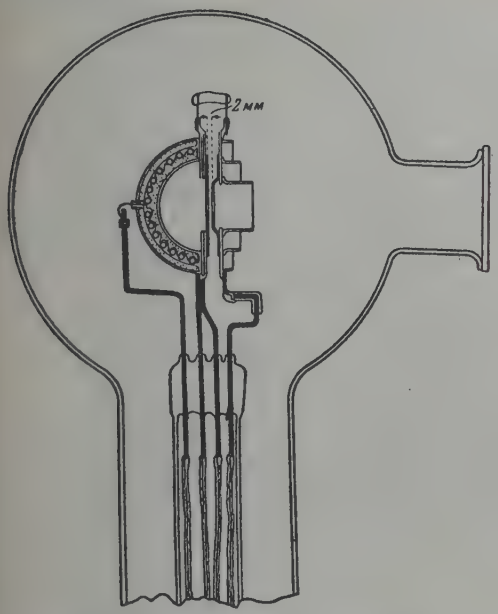

Sectional view of the new high-brightness hydrogen discharge tube.

The present version differs from the earlier types of this type in the design of the cathode, which in this tube is a metallic hemisphere with an oxide coating on the inside surface. This shape insures a high emission and makes it possible to use heavy discharge currents: with water cooling current densities well in excess of 200 amp/cm^2 should be attainable.

The cathode is heated by means of a special heater consisting of two insulating cups and a molybdenum or tungsten wire spiral fitted into a helical recess between the cups. The preheating current does not exceed 2-3 amperes; once the tube is in operation the heater current is cut off.

Tests showed that the operation of the tube is stable in the 2 to 17 ampere discharge current range (due to the fact that the prototype tube had no water cooling, heavier currents were not used). Under our test conditions the maximum current density attained was 240 amp/cm^2.

The useful life of the tube has not been ascertained but it can safely be asserted that it is not less than 100 hours. During the tests, the tube was operated continuously for three days and nights at a 7 ampere discharge current.

An investigation of the variation of discharge current with the hydrogen pressure in the tube showed that the range of most favorable pressures lies between 1.6 and 4.2 mm Hg col. That is, the radiation yield is highest in this interval. A study of the pressure dependence of the intensity of emission at different wavelengths showed that the intensity reaches a peak at pressures in the vicinity of 2 mm Hg col. In view of the inevitable aging effects it is best to fill the tube initially to a pressure a few millimeters above the optimum.

Further, tests showed that the energy distribution over the spectrum is virtually independent of the strength of the discharge current, while the intensity of emission is proportional to the current.

The described tube differs from other hydrogen tubes not only as regards design details but also in having high spectral qualities. Due to the greater spectral density of the tube's emission it should prove particularly advantageous for use in recording spectroscopic instruments for all regions of the ultraviolet, including the vacuum region.

Department of Experimental Physics and Optics
"T. G. Shavchenko" Kiev State University

AN ELECTRONICALLY CONTROLLED LOW-VOLTAGE ARC AND SPARK GENERATOR

- M.I.Demidov, N.N.Ogurtsova & I.V.Podmoshenski

The purpose of the present project was to develop and test a low-voltage arc and spark generator with electronic control. The developed generator is capable of producing 1) an AC arc or 2) a low-voltage spark. The inductance of the discharge circuit can be varied between 10 and 50 microhenries; the capacitance between 10 and 40 microfarads.

The discharge can be initiated each 2nd, 4th, 8th, 16th, 64th or 128th half-cycle. For arc operation the circuit is supplied directly from the 220 volt AC line. For spark operation an autotransformer is coupled into the charging circuit in order to control the potential on the capacitor. The discharge is regulated through control of the firing pulse.

A schematic of the generator circuit is shown in the accompanying figure. This circuit design insures positive functioning under all operating regimes with discharge gaps up to 3 mm.

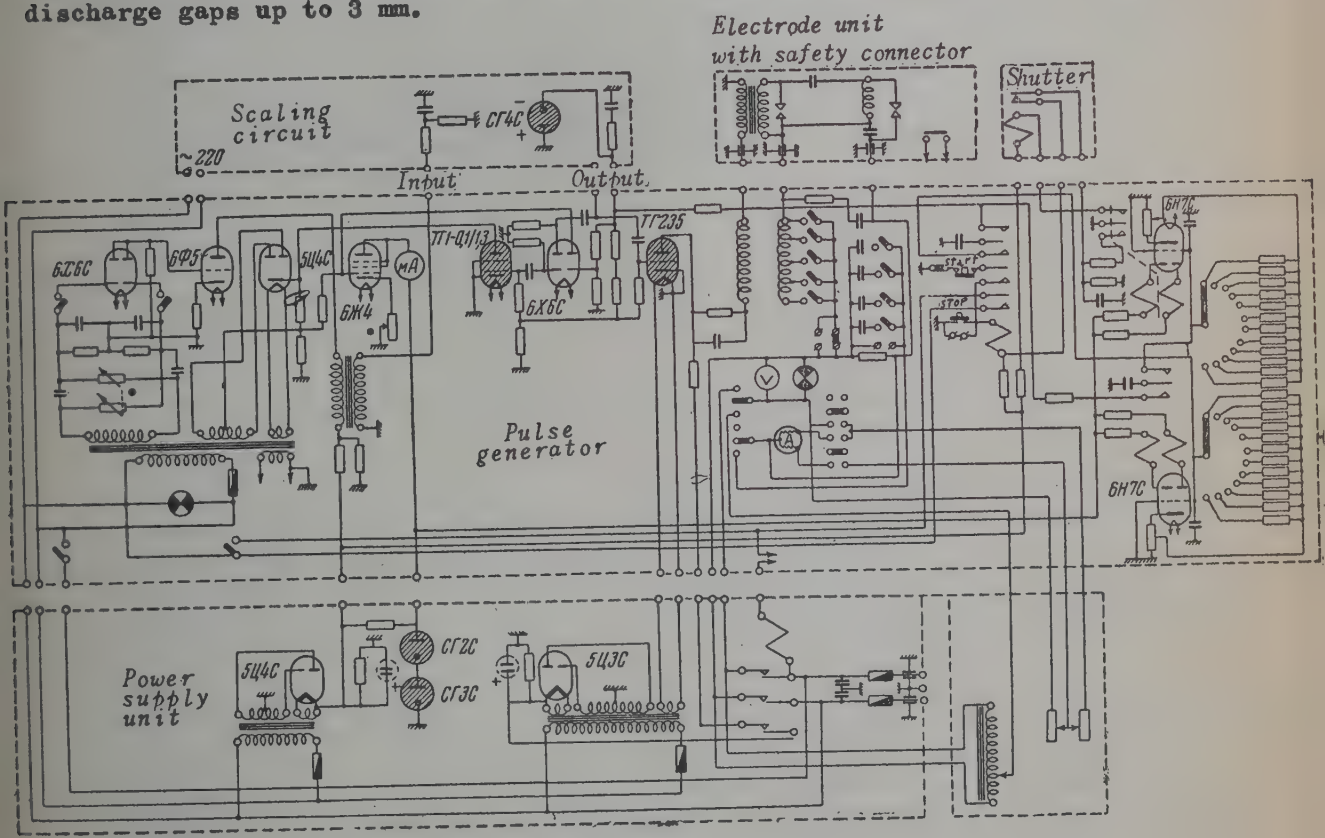

Schematic diagram of the low-voltage arc and spark generator with electronic control

The phase of the discharge (relative to the phase of the supply voltage) can be varied smoothly over the entire range from 10 to 170°. A special circuit was developed for measuring and indicating the phase. The phase is set according to a magneto-electric indicator with an accuracy to within 2°.

The generator incorporates an electronic relay linked to a mechanical shutter mounted in front of the spectrograph slit; this permits automatic actuation of the source for a preset firing and exposure time. The following discharge and exposure times can be set: 1, 2, 5, 7, 10, 15, 20, 30, 45, 60, 90, 120, 180 or 240 seconds.

The error in setting the exposure does not exceed 2%.

The generator is assembled in a single cabinet: all controls are brought out to the front panel.

A special mount for the high-voltage part of the firing circuit was designed be S.P.Rozov. The entire high-voltage assembly is enclosed in a silicon-aluminum alloy housing. The cable leading to the generator is shielded. This design greatly reduced external interference from the generator. The housing also protects the operator against ultraviolet radiation, deadens the noise and makes exhaust ventilation of the region of the discharge feasible. A safety switch interlocked with the cover safeguards personnel against accidental contact with the electrodes or other high-voltage units.

Comparison of the spark discharges of this generator with those of the IG-2 high-voltage spark generator showed that the "hardness" of the excited spectra as determined on the basis of the relative intensities of lines of Cu I, Cu II and Cu III is virtually the same. The relative level of the background is somewhat lower with the electronically controlled generator, while the overall intensity of the spectrum is about twice as high. Moreover, the generator with electronic control permits of gradual variation of the "hardness", from "hard" spark to arc.

Extensive electrical and spectral tests have shown that the generator with electronic control assures better reproducibility of analyses than the DG-1 (arc) and IG-1 (spark) generators.

* * * * * * *

INVESTIGATION OF THE SPARK REGIMES OF THE DG-1 GENERATOR

- G.A.Soboleva

The present paper deals with an investigation of the character of the excitation produced by the DG-1 generator in spark operation and determinations of the energy liberated in the discharge gap and at the electrodes.

1. By varying the parameters of the discharge circuit (L from 5 to 180 microhenries and C from 15 to 130 microfarads) one can either obtain intense arc lines or achieve the excitation of spark lines associated with different degrees of ionization of the atoms.

The appearance in the spectrum of lines characteristic of Cu III, Cd III, Al III, Fe III, O II, N II and C III (2296.89 A and others) proves that conditions permitting observation of spectrum lines associated with transitions from 45-50 ev levels are realized in the discharge gap with the "hardest" spark regimes.

2. The operating regimes of the generator were characterized by the relative intensities of lines having different excitation potentials (to $\Delta E \simeq 30$ ev).

The corresponding durations, current amplitudes and current densities of the discharges were measured by means of an oscillograph.

We also determined the "excitation temperature" by the optical method, according to the intensities of Fe II lines having known transition probabilities[1].

Characteristics of some generator regimes

a) An appreciable change in the relative intensity of the spectrum lines is observed as the inductance of the discharge circuit is increased from 5 to 180 microhenries. The intensity of lines associated with high excitation potentials decreases, which corresponds to a drop in the density of the discharge current.

For example, with C = 51 μf, the current density falls off from $80 \cdot 10^4$ amp/cm^2 at L = 5 microhenries to $7 \cdot 10^4$ amp/cm^2 at L = 51 microhenries; at the same time the "excitation temperature" decreases by about 1200° K.

Further, with C = 51 μf, the amplitude of the discharge current decreases from I_o = 660 amp at L = 5 microhenries (duration of discharge $\tau = 0.6 \cdot 10^4$ sec) to about 100 amp at L = 180 microhenries ($\tau = 3 \cdot 10^{-4}$ sec).

b) On the other hand, with L = 50 microhenries, increasing C from 15 to 100 μf results in a decrease in the current density from $30 \cdot 10^4$ amp/cm^2 to $4 \cdot 10^4$ amp/cm^2; concurrently the "excitation temperature" goes down from 7800 to 6800°K. The discharge interval increases in proportion to $\sqrt{C}$ from about $1 \cdot 10^{-4}$ to $3 \cdot 10^{-4}$ sec.

c) With L = 5 microhenries, increasing C from 15 to 100 μf is accompanied by a decrease of the "excitation temperature" from 9000 to 7800°K; the duration of the discharge again increases in proportion to $\sqrt{C}$ from $2.5 \cdot 10^{-5}$ sec with C = 15 μf to $8 \cdot 10^{-5}$ sec with C = 100 μf. At C = 60 μf, $I_{o\ max}$ = 670 amp.

3. To determine the variation of the energy released in the spark gap and at the electrodes with the mode of operation, the energy values were measured by the calorimetric method. In addition, the energy liberated in the discharge gap was calculated from oscillograms of the discharge current and the electrode voltage.

At a constant value of the inductance, the quantity of energy liberated in the gap per discharge increases with increasing capacitance.

Influence of the capacitance of the discharge capacitor on the energy distribution

$C_{\mu f}$	Q_g/Q_c, %	Q_e/Q_g, %
15	28	55
43	35	60
59	40	62
99	45	78
129	68	88

The accompanying table lists values of the ratios Q_g/Q_c and Q_e/Q_g in percent of the values for the arc between copper electrodes with L = 50 microhenries; here Q_g is the energy released in the gap per discharge, Q_c is the energy stored in the capacitor and Q_e is the energy expended on heating both electrodes per discharge. When L is increased from 50 to 180 microhenries (with C = 50 μf) Q_g remains virtually constant at 0.57-0.60 J, which amounts to about 38% of the energy stored in the capacitor Q_c; Q_e/Q_g increases from 58 to 84% due to increase in the discharge time.

The same ratios were also measured with the DG-1 operated as an arc generator.

With a spark gap of 0.5 mm in the high-frequency circuit, Q_g increases from 0.74 to 3.6 J as the strength of the current is increased from 2 to 8 amperes; the value of Q_e/Q_p remains constant at about 75% of the copper electrode value.

4. Measurements of the energy consumed on heating the electrodes were made for electrodes made of Cu, Zn, Cd, Al, Fe, Ti, Ni, and C with L = 57 microhenries and C = 30 μf.

The energy expended on heating the electrodes depends on the energy of the discharge and on the duration of the current pulse. The energy of the discharge differs somewhat for metals with different physical-chemical properties and is determined primarily by the potential necessary to maintain the mechanism of the discharge with the given current strength. The influence of the physical-chemical properties is manifested through their effect on the burning voltage of the discharge. As regards the burning voltage the various metals may be arranged in the following ascending series: Cd, Zn, Cu, Fe, Ni, W, Ti and Al.

The thermal conductivity of the electrode material has a direct bearing on the discharge characteristics, inasmuch as metals with a lower conductivity heat up more in the vicinity of the discharge. As a result, all the surface processes proceed more intensely. Thus, for example, slag formation is more intensive on

iron as compared with copper electrodes.

In conclusion the writer wishes to thank V.K.Prokof'ev for his guidance.

Leningrad Institute of
Precision Mechanics and Optics

References

1. N.N.Sobolev, Zhur. eksp. i teor. fiz., 13, 131 (1943).

* * * * * * *

THE ISP-67 HIGH-DISPERSION AND HIGH-RESOLUTION SPECTROGRAPH

- A.I.Ryskin

The ISP-67 three prism, glass spectrograph is a universal type instrument (see Fig. 10, p. 335, preceding issue of the Bulletin). The spectrograph comes with four interchangeable cameras with focal lengths of f_1 = 180 mm, f_2 = 500 mm (both used with an f' = 400 mm collimator), f_3 = 1500 mm (used with an f" = 1000 mm collimator) and f_4 = 3000 mm (autocollimation setting). The two longer focus cameras are intended for spectroscopic investigation of the fine structure of lines, while the short focus, large aperture cameras can be used for studying luminescence, photochemical effects, Raman spectra, etc.

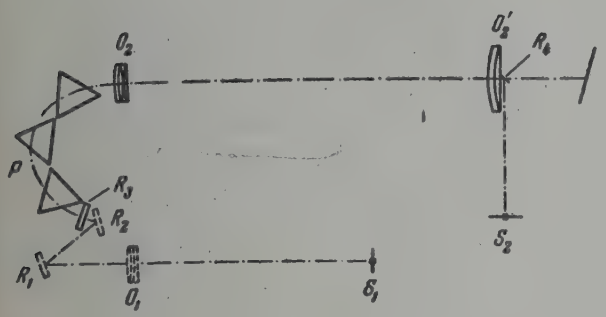

Fig. 1. Diagram of the ISP-67 3-prism glass spectrograph. S_1 and S_2 - slits; O_1, O_2 and O_2'-lenses; R_1, R_2, R_3, and R_4 - mirrors; P - dispersing system.

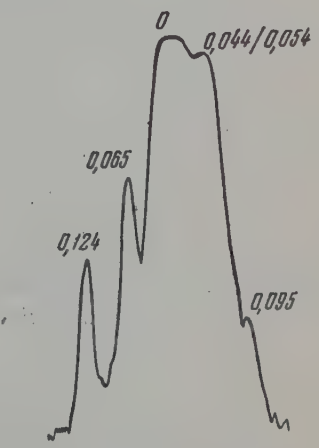

Fig. 2. Trace of 4046 A mercury line made on an MF-4 microphotometer from photograph made with a IPS-67 spectrograph. The hyperfine structure is clearly resolved. Figures indicate displacement of auxiliary peaks relative to the principal peak (0) in Angstroms.

The optical system of the ISP-67 is pictured in Fig. 1. The components O_1, R_1 and R_2, indicated by dotted lines, are used only in the direct setting. In the autocollimation setting, the light from the slit S_2 is reflected from the rotatable mirror R_4, goes through the lenses O_2' and O_2 to the dispersing system P consisting

of three prisms (base of individual prism 150 mm, height 95 mm, refracting angle 63°) and is finally thrown on the autocollimation mirror R_3.

The desired section of the spectrum is brought to the center of the photographic plate by rotating the prism assembly together with mirror R_3. In shifting from the autocollimation to the direct setting the mirror R_3 is swung out of the way of the beam.

The long-focus autocollimation camera has an aperature ratio of 30. The theoretical resolving power with this camera is 280,000 at λ = 4046 A; the dispersion 0.88 A/mm. The resolving power of the spectrograph with the autocollimation camera is much higher than that of all other domestic (Soviet) instruments. It is great enough to resolve the hyperfine structure of mercury lines. By way of illustration the record of the 4046 A mercury line made with a MF-4 microphotometer from a photograph obtained with the ISP-67 spectrograph is reproduced in Fig. 2. It will be seen that the structure of this line is fully resolved despite the great difference in the relative intensities of the individual components.

The mechanism of the autocollimation camera is fully automatic, i.e., in shifting from one section of the spectrum to another the prisms are rotated, the plate holder shifted to the appropriate position and the lens refocused on the plane of the plate by one unified control. The use of an achromatic main lens O_2 in conjunction with the field lens O_2' near the focal plane makes it possible to obtain a virtually flat spectrum on a plate 18 cm long.

The main lens throws two pencil beams, one of which is focused on the plane of the photographic plate and extinguished by means of a special diaphragm while the other falls on a pin-point diaphragm mounted in the tube joining the plate-holder section with the prism section of the instrument. To make full use of the great resolving power of the spectrograph with the autocollimation camera the instrument should be located in a room with thermostatic temperature control.

The 1500 mm focal length camera has an aperature ratio of 15. The theoretical resolving power with this camera is 140,000 at 4046 A; the dispersion, 3.5 A/mm. As regards speed and resolving power this camera is superior to the 1300 mm focal length camera used with the ISP-51 spectrograph; its dispersion, however, is somewhat lower. In view of the low dispersion of the spectrum lines, fine-grain emulsions should be used in working with this camera.

The 500 mm focal length camera has a relative aperture of 5 and a dispersion of 28 A/mm at 4861 A; the respective values for the 180 mm camera are 2 and 70 A/mm. As regards speed, dispersion and resolving power, these cameras are superior, respectively, to the f = 270 and 120 mm cameras of the ISP-51 spectrograph.

* * * * * * *

[Start of proceedings of Section III of the Conference]

SPECTROSCOPIC ANALYSIS OF SLAGS
Survey and Evaluation of Analytic Procedures

- N.V.Buianov

At present a number of different methods and procedures are used in spectrochemical analysis of metallurgical slags. We feel the time has come to make a critical appraisal of these analytic methods with a view to selecting the best among them.

1. Survey of Spectroscopic Methods of Slag Analysis

Sift-through method. This method was originated and first used by Nedler[1] in 1938. The material is first ground to 80-100 mesh powder, thoroughly mixed to in-

sure uniformity and then a sample is weighed out. By means of a special device this sample is allowed to trickle through a condensed spark or arc discharge at a set rate, the sift-through time being made equal to the exposure time.

The sift-through method was utilized by Veselovskaia in developing an analytic procedure for open-hearth slags. This procedure was introduced at the Magnitogorsk Metallurgical Combine (MMK)[2,3] and at the Stalingrad "Krasnyi Oktiabr'" Plant. At the Magnitogorsk Combine the procedure was subsequently modified somewhat and in this form used through 1943-1945. However, the accuracy of analysis was found to be low and the Magnitogorsk laboratories changed to the briquetting method.

The "Krasnyi Oktiabr'" Plant still uses the sift-through method for the analysis of open-hearth slags for calcium and silicon oxides. The accuracy is relatively low (about 5-10%).

Although a number of investigators[4,5] have improved and refined the sift-through technique, the method suffers from a number of inherent shortcomings: the unavoidable influence of the mineralogical structure of the slag, the impossibility of accurate control of the time the powder particles remain in the discharge proper, etc.

Spectral energy method. The spectral energy [total-energy] method was proposed by Slavin[6] in 1938. Later Rusanov[5] conclusively proved that Slavin's method is in principle unsuitable for quantitative spectrum analysis of ores of different composition.[7]

At present the spectral energy method is used with the following modifications: 1) a quantity of a comparison element is introduced into the powder sample, 2) the sample is diluted with a "spectroscopic buffer" to stabilize the flame temperature and 3) special procedures are employed to prevent the powder from being thrown out of the electrode cup during the discharge.

Korzh utilized the spectral energy method in developing a procedure for analyzing for all components in open-hearth slags[9]; however, this procedure has so far not been applied in practice. Matveev and Mikhailov[10] used the method for determining cobalt in converter slags; according to these authors the accuracy of analysis varies between 3 and 10%.

Although the spectral energy method has been used from time to time by other investigators for analysis of slags[11-13], it is not regularly employed in any Soviet ferrous-metallurgy plant.

Moving lower electrode method. This traverse method was first applied to the analysis of slags by Buianov[14] in 1946. The basic procedure is the following: a quantity of the slag is ground to 200 mesh and thoroughly mixed; a sample of 0.2 to 0.5 grams is spread in a uniform layer on a flat stage, serving as the lower electrode. With the arc turned on, the stage is moved at a uniform rate under the stationary upper electrode during the exposure period. The stage is usually made of pure nickel or copper. In some cases when the liquified slag tends to stick to the upper electrode, it is expedient to make the upper electrode of pure carbon and to increase the arc gap.

The method is extensively used in two plants: the Cheliabinsk Ferrous Alloy Plant and the Chusovsk Metallurgical Plant.

In the former the method has been used since 1948 for analysis of:

a) chrome slag obtained in the production of carbide-free ferrochromium for all components (silicon, aluminum, calcium, iron, chromium and magnesium oxides),

b) 75% ferrosilicon for aluminum, chromium and manganese oxides,

c) ferrotitanium for aluminum, copper, titanium and silicon.

At the Chusovsk plant the method has been used since 1950 for analysis[15] of:

a) blast-furnace slags of cast iron (for steel manufacture) for the oxides of calcium, iron, silicon, aluminum, magnesium and manganese,

b) blast-furnace slags of vanadium cast irons for the oxides of silicon, aluminum, iron, manganese, calcium, magnesium, titanium and vanadium,

c) sinter cake for chromium and vanadium oxides.

The accuracy of the spectroscopic analyses is reported to be equal to that attainable by chemical methods[14,16,17].

Molten slag method. In 1951 Noskov, Skorniakov and Chukina proposed a new method of analysis for slags[18]. The slag sample is first fused with borax in the ratio of 1:3; the product has a relatively low melting temperature and in the molten state is sufficiently conducting to maintain a stable arc. The fused sample is kept molten by means of a gasoline blow torch. This method has not been used much in industry, hence it is difficult to evaluate its worth.

Briquetting method. This is one of the more commonly employed methods of spectrum analysis of powdered substances in general and slags in particular[2,19-29].

The method is based on compressing a weighed sample of the powder, pure metal or metal shavings to form a hard, stable briquet. In the case of powders, a suitable binding and conducting agent is added before compressing. In addition, a quantity of an appropriate element to serve as an internal standard is introduced at the same time. The further analytic procedure with such briquetted electrodes is the same as with metallic electrodes in a condensed spark.

The first descriptions of the application of the briquetting method to spectroscopic analysis of slags appeared in 1941[20,21]. The second reference (Deitert) is concerned with the analysis of cobalt slag; briquettes, compressed of a mixture of 0.25 grams slag and 0.75 grams iron powder, were used for both electrodes.

In the Soviet Union the briquetting method was first applied by Veselovskaia[2]. Subsequently Sychev's[23] work contributed much to the development of this method. Sychev showed that the electric conductivity of the briquet increases in direct proportion to the briquetting pressure employed. He asserts that the optimum pressure for compressing the electrodes is 9000-10,000 atmospheres.

At present the briquetting technique is employed at a number of plants and mills (the Magnitogorsk and Beloretsk Metallurgical Combines, the "Serp i molot", "Azovstal'", Cheliabinsk Metallurgical, Novo-Tulsk, Kazakh Metallurgical and other plants) for analysis of blast-furnace and open-hearth slags.

Tube electrode method. This method was proposed by Zimina[30] in 1952 and has been adopted in the Verkh-Iset and Serov Metallurgical plants.

The procedure is the following: the slag sample is thoroughly pulverized and 0.25 grams of the powder are placed in a tube of electrolytic copper. The dimensions of the tube, which is open at one end, are: length 55 mm, diameter 8-9 mm, thickness of side walls and bottom 1.0-1.5 mm. The electrode-tube is mounted horizontally; before being clamped the tube is rotated slowly so that a thin layer of powdered slag comes to the mouth of the tube. A brass rod 8-9 mm in diameter serves as the other electrode.

The tubes are re-usable; after analysis the tubes are cleaned in a 1:1 solution of HCL and then washed in water.

Solution method. The greatest success in this line has been achieved by the group of spectroscopists headed by Granovski at the "Stalin" (Donbas) Plant[19]. They have developed procedures by which a number of slags can be completely dissolved in a matter of 2-3 minutes. The resultant solution is placed in a special fulgurator and then an AC arc is ignited between it and the upper electrode. Potassium bichromate is introduced into the solution to serve as an internal standard. Procedures have been developed for determining silicon, manganese, calcium, iron, magnesium and aluminum oxides. The plant laboratory has been making determinations of the first four oxides by this method for about two years.

2. Recommended Methods of Spectrum Analysis of Slags

Of the spectroscopic methods examined above, the sift-through and the spectral energy methods cannot be recommended for analysis of fused slags.

The last method, i.e., the method based on bringing the slag into solution, has undoubted potentialities but still requires further development and improvement.

Accuracy and reproducibility of the recommended methods

Briquetting method. The comparative results of analyses by the spectroscopic-briquetting and chemical methods reported by a number of plant laboratories are listed in Table 1.

Table 1

Difference between the results of spectroscopic analysis by the briquetting method and determinations by chemical analysis reported by different plants.

Plant Laboratory	SiO_2	CaO	FeO_{all}	MnO	Basicity
Beloretsk Metallurgical	3.4	2.9	-	-	-
Cheliabinsk Metallurgical	-	2.9	-	-	-
Novo-Tulsk Metallurgical	2.4	4.0	2.4	3.1	-
"Azovstal' "	6.6	3.4	-	-	-
Kazakh Metallurgical	-	5.2	8.0	-	4.8
Same Plant*	3.3	4.9	6.4	5.1	-

*Data for analysis with spectrograph; other data are for analyses using steelometers.

We checked the reproducibility of the briquetting method by photographing the spectrum of the same chrome ore sample 24 times. The briquettes were all compressed on a Brinell press at a pressure of 3000 kg/cm^2. The following deviations ($\delta \Delta S$) from the mean value were noted for individual determinations of the difference in blackening of analytic line pairs (densities relative to the standard): for Cr $\pm$0.015; Mg $\pm$0.012; Al $\pm$0.026; Fe $\pm$0.016; Si $\pm$0.018. The reproducibility deteriorates (variation increases 2 to 3-fold) if the briquetting pressure is reduced to 200-250 kg/cm^2. It will be noted that the reproducibility with an adequately high briquetting pressure is not appreciably inferior to that common to industrial analyses of steels and alloys.

It will be seen from Table 1 that the accuracy of analysis as reported by different laboratories varies considerably; in this connection we note an unjustifiable lack of standardization of the procedure followed in preparing the briquets. For example, in the "Azovstal' " laboratory the powdered slag sample is mixed with graphite in the proportion of 1:5; this use of graphite instead of the copper powder employed at the other plants does not appear to be justified by any increase in accuracy.

In the interests of greater accuracy and standardization it is suggested that:

1) the representative sample be pulverized to 150-200 mesh;

2) the filler should be copper powder in the proportion of 2.5-3 parts to 1 part slag by weight. (In some cases it may be expedient to add zinc oxide to the mixture; where this is done the oxide should be added in an amount of not less than 0.1 gram per gram of copper-slag powder mixture in order to insure uniform distribution of the zinc oxide throughout the briquet.)

3) in forming the briquets the pressure should not be less than 1500-2000 kg/cm^2 and should be applied at a uniform rate;

4) massive briquet-electrode holders and minimal values of the current and discharge circuit inductance should be employed to minimize heating of the briquets;

5) where possible the internal standard used should be an element already present in the slag.

Tube electrode method. Comparison of the data obtained by this spectroscopic method with the results of chemical analyses (Verkh-Iset Plant laboratory) shows that the relative error in determinations of silicon dioxide is 3.6%; of calcium oxide it is 4%.

We suggested the following modifications in the procedure: a) mounting the tube vertically rather than horizontally in the electrode holder, b) using a tube 20 mm long and 7 mm in diameter, instead of 50 and 8-9 mm, (the wall and bottom thickness remaining 1-1.5 mm), c) using a counter electrode 7 mm, rather than 9-10 mm, in diameter, d) charging the tube with a mixture of powdered slag with copper powder in the ratio of 1:3, instead of the slag alone, and using a standard charge of 0.5 grams. Employing the outlined procedure, we checked the reproducibility on a sample of open-hearth slag by photographing the spectrum of the same sample thirty times. The deviations of individual determinations of the relative blackening of analytic line pairs were: Ca ±0.014; Si ±0.015; Fe ±0.017; Mg ±0.013; Mn ±0.017. A similar reproducibility was obtained in a series of analyses of slag formed in the production of chrome-silicon alloy.

It will be seen that as regards accuracy and reproducibility the tube electrode method stands up well in comparison with the briquetting method.

Moving lower electrode method. The reproducibility of this traverse method may be evaluated from the figures in Table 2 (deviations from arithmetic mean).

Table 2

Reproducibility of moving lower electrode method

Type of slag	Oxides of V	Cr	Si	Al	Ca	Mg	Fe	Mn
Vanadium	5.0	—	3.9	5.4	5.5	4.7	2.5	—
Chrome from flux process	—	4.4	2.8	4.0	1.7	3.3	4.5	—
Chrome from fluxless process	—	2.7	3.1	5.5	6.0	3.0	5.5	—
Open hearth	—	4.6	2.6	4.3	1.6	4.5	4.5	3.5

It must be noted that the recommended methods are not universal, i.e., are not applicable to the analysis of all types of slags.

Central Scientific Research Institute
for Ferrous Metals

References

1. V.V.Nedler, Zavod.labor., 12, 1469 (1936).
2. I.M.Veselovskaia, Kartoteka TEKhSO (Technical Advice Card Index) Description of efficiency increasing suggestions awarded prizes in the first People's Commissariat of Ferrous Metallurgy contest. 1944.
3. M.N.Shtutman, Izv. (Bulletin) AN SSSR, Ser.fiz., 12, 444 (1948).
4. S.I.Safonov, Zavod.labor., 2, 187 (1940).
5. A.K.Rusanov, Spektral'nyi analiz rud i mineralov (Spectrum analysis of ores and minerals), Chapt. III. M. 1948.
6. M.Slavin, Ind. Eng.Chem., Anal. Ed., 10, 407 (1938).
7. Ia.D.Raikhbaum, Zhur. tekh. fiz., 15, 485 (1945).
8. Ia.D.Raikhbaum, Zavod.labor., 6, 601 (1939).
9. P.D.Korzh, Izv.(Bulletin) AN SSSR, Ser.fiz., 9, 665 (1945).
10. N.I.Matveev & P.M.Mikhailov, Zavod.labor., 9, 1090 (1951).
11. J.T.Kozsa, Metal Progress, 4, 593 (1947).
12. K.G.Carlson, Journ of Iron & Steel Inst., 4, 273 (1950).
13. T.Gillis, Spectrochemica Acta, 4 (1951).
14. N.V.Buianov, Spektral'nyi analiz shlakov (Spectrum analysis of slags) TsNIIChM Otchety (Reports) 1946; Zavod.labor.,5, 565 (1948); Trudy (proceedings) TsNIIChM, Issue 1, 85 (1948).
15. Z.N.Kuznetsova, Biulleten' (Bulletin) Chusov branch of the NITOM and the Technical Soviet of the Plant, January 1951.
16. N.V.Buianov, Popova,Babaev & Nazarenko, Zavod.labor., 3,299 (1952).

17. N.V.Buianov, Izv.(Bulletin) AN SSSR, Ser.fiz., 12, 439 (1948).
18. M.M.Noskov, Skorniakov & Chukina, Zavod.labor., 4, 429 (1951).
19. N.V.Buianov, Zavod.labor., 5, 554 (1953).
20. Concrete, 55, 4, 14 (1941).
21. H.W.Dietert, JOSA, 31, 693 (1941).
22. E.J.Fitz & W.W.Murray, Ind.Eng.Chem., Anal.Ed., 17, 145 (1945).
23. V.P.Sychev, Zhur.tekh.fiz., 16, 10, 1181 (1946).
24. I.M.Veselovskaia, Zavod.labor., 2, 219 (1947).
25. K.A.Shisterman & Z.A.Ustalova, Zavod.labor., 4, 500 (1948).
26. M.M.Kler & M.I.Rezvova, Izv.(Bulletin) AN SSSR,Ser.fiz.,12,481 (1948).
27. V.V.Nalimov & K.I.Ionova, Zavod. labor., 3, 301 (1952).
28. V.V.Nalimov & K.I.Ionova, Zavod. labor., 3, 305 (1952).
29. V.V.Nalimov, Kombulatov & Ionova, Zavod. labor., 11, 1354 (1954).
30. A.A.Zimina, Zavod. labor., 1, 39 (1953).

Zavod.labor. = The Plant Laboratory

* * * *

METHODS OF SPECTROCHEMICAL ANALYSIS OF OPEN-HEARTH SLAGS FOR ALL BASIC COMPONENTS

- O. I. Nikitina

The purpose of the present project was to develop methods of analysis obviating the influence of third elements and of the mineralogical composition.

1. Method of spectrographic analysis of slag in the solid state (briquets)*

In order to select the best source we investigated the analytic conditions in an activated AC arc a) with the method of complete vaporization of the sample and b) with the method of partial vaporization from a moving flat electrode-stage and in a high-voltage condensed spark with vaporization of the sample from briquets compressed with a graphite filler.

It was established that for determinations of calcium in slags of varying basicity systematic errors are absent with all the enumerated sources. Deviations from the mean value (random experimental errors) are minimal with condensed spark excitation. We also investigated the influence of the degree of dilution of the slag and of grain size of the slag powder on the accuracy of determination of the elements present in the slag.

On the basis of the results obtained, the following standard electrical conditions were established for determination of the principal elements in slags from one photograph of the spectrum: excitation by means of an IG-2 spark generator, complex circuit setting, 220 v and 0.8-1.0 amp in primary, C = 0.006 μf, L = 0.55 mH, gap = 2.0 mm, pre-exposure sparking - 2.0 min; upper electrode - graphite rod, 5.5-6.0 mm main diameter, tapered to a cone truncated to form a 1.5-2.0 mm diameter flat; lower electrode - 0.1 gm slag, 0.3 gm titanium dioxide (or 0.1 gm chromium trioxide); internal standard - 2.0 gm spectrally pure graphite; briquetting pressure - 3000 kg/cm^2; diameter of briquet - 12 mm; degree of pulverization - 200 mesh.

The analytic line pairs and the limits of the range of determinable concentrations are listed in Table 1. As noted above, titanium or chromium (introduced in the form of oxides) served as the internal standard.

It was established that the results of analysis do not depend on the physical state of the slag; however, in view of the fact that alterations in the chemical

---

* M. S. Tovstenko, I. V. Zhigalovski, E. I. Malitskaia and O. M. Sheichenko participated in this part of the program.

composition of the slag may occur in the process of crystallization, it is essential that the sample be taken in the form of a small cake not over 5 mm thick and cooled rapidly.

Table 1

Range of determinable concentrations and line pairs used in analysis of slags formed into briquets

Range of concentrations, %	Analytic line of element, A	Ti line, A	Cr line, A
CaO 17÷58	Ca II 3158,87	II 3194,76	II 3147,23
SiO_2 6÷25	Si I 2881,6	I 2956,13	—
	Si I 2516,12	—	I 2571,74
MnO 2÷25	Mn II 2939,31	II 2938,7	II 2935,14
FeO 6÷30	Fe II 2755,74	II 2764,8	II 2756,30
Al_2O_3 2÷13	Al I 3092,71	I 3101,52	I 3034,19
	Mg I 2852,12	I 2948,26	—
MgO 2÷12	Mg II 2798,02	II 2810,30	—
	Mg II 2790,78	—	II 2789,30

The influence of third elements - introduced in our tests in the form of Fe_2O_3, MgO, Al_2O_3 and CaO, as mechanical admixtures into the sample and in the molten state - is negligible. The accuracy of the briquetting method as described is characterized in Table 2.

Table 2

Accuracy of briquetting method of slag analysis

Basis of evaluation	No. of determ.	Error, rel. arithmetic mean, %					
		CaO	SiO_2	FeO_{tot}	MnO	MgO	Al_2O_3
Reproducibility (individual determ.)	27	4.9	2.4	5.1	3.7	4.7	5.2
Comp. with chem. anal. (average for three)	8	4.3	8.0	7.7	3.7	8.2	--

2. Method of spectrographic analysis of open-hearth slag in solution*

In analysis by this method 0.25 gm of slag are mixed with 1.25 gm of flux consisting of 2 parts Na_2CO_3 and 3 parts $Na_2B_2O_7$ and sintered in a muffle furnace at 900-1000° C for 2 minutes; the product is dissolved in 75 cc hydrochloric acid (1:3) with the application of heat. Finally distilled water is added to make 250 cc. In the process all elements of the slag go into solution. Chromium or vanadium is added to serve as the internal standard.

The discharge conditions described above are used to excite the spectrum. The lower electrode used in this case is a porous graphite rod (heated to 900-950° C for 3 minutes beforehand). The electrode is immersed to the level of its flat tip in the cup containing the slag solution.

The analytic lines are listed in Table 3.

Third elements added to the slag in the form of oxides prior to fusing with the flux do not affect the analytic results. The accuracy of the method may be evaluated

Table 3

Elements determined and analytic line pairs in analysis of slags in solution

Element	Analytic line, A	Cr line A	V line A
Ca	II 3158,87	I 3147,23	II 3136,52
Si	I 2881,6	—	I 2990,94
	I 2516,12	I 2571,74	I 2870
Fe all	II 2755,74	II 2756,30	II 2777,73
Mn	II 2939,31	II 2935,14	II 2938,25
Mg	II 2790,78	II 2789,30	II 2781,45
Al	I 3092,71	II 3034,19	I 3073,82

* M. S. Tovstenko participated in this part of the program.

from Table 4.

The concentrations of the slags analyzed by the solution method extended over the same range as those of the slags analyzed by the briquetting method.

Table 4

Accuracy of analysis in solution

Basis of evaluation	No. of determ.	Error, rel. arithmetic mean, %					
		CaO	SiO_2	MnO	FeO_{tot}	Al_2O_3	MgO
Reproducibility (individual determ.)	20	3.2	4.1	4.2	4.2	5.8	3.4
Comp. with chem. anal. (average for three)	8	2.2	6.7	5.7	2.2	6.5	3.7

* * * * * * *

SPECTROSCOPIC ANALYSIS OF NICKEL SLAGS IN A WIDE RANGE OF COMPONENT CONCENTRATIONS

- D. M. Shvarts and I. S. Nilova

1. Analysis of Briquetted Samples

The analytic procedure we used is the following: The slag sample is powdered and mixed with copper oxide powder in the ratio of 1:100 by weight. Briquets weighing one gram are compressed of the mixture.

A briquet is placed on a copper stand which forms the cathode of a DC arc (supply voltage 400 v)[1]. A copper rod terminating in a truncated cone is used as the counter electrode. The pre-exposure burn-in time is 1.5 min; the arc current - 5.5 amp; the exposure - 20 sec. Instrument data: ISP-22 spectrograph, 0.01 mm slit, three-lens condenser with an intermediate diaphragm having a 1.2 mm cutout. Photographic plates: Spectral, Type I, Speed 6° H&D. The plates are processed in the conventional manner.

The analytic lines are listed in the table below.

Analytic line pairs used in spectrum analyses of slags

Briquettes	Solutions
Ni I 3050,82 — Cu I 3156,63	Ni I 3414,76 — Mo 3195,96
Co I 3502,28 — Cu I 3156,63	Co I 3405,12 — Mo 3195,96
Fe I 3047,61 — Cu I 3156,63	Fe I 2599,57 — Mo 2775,40
Ca II 3179,33 — Cu I 3088,13	Ca II 3179,33 — Mo 3195,96
Si I 2503,90 / Si I 2516,12 — Cu I 3088,13	Si I 2881,58 — Mo II 2871,51
Al I 3082,16 — Cu I 3156,63	Al I 3092,71 — Mo 3195,96
Mg 2779,83 / Mg II 2795,53 — Cu I 3088,13	Mg II 2802,70 / Mg II 2795,53 — Mo II 2816,15
	Cu I 3247,54 — Mo 3195,96

The described procedure allows of plotting a single calibration curve for samples of different composition over the entire requisite range of concentrations: Ni ~ 0.2--10%, Co ~ 0.2-10%, FeO 2-60%, SiO_2 ~ 5-40%, CaO ~ 1-25%, MgO ~ 1-20% and Al_2O_3 ~ 1-15%. The procedure can also be used for analyzing certain other substances (ores and refractories) with a mean square error for individual determinations between 7 and 14%.

2. Analysis in solutions

The sample is fused in a platinum crucible with an excess of borax (1 part slag to 10 parts borax); the product is dissolved in a buffer solution consisting of 50 cc 40% citric acid and 20 cc 20% sodium citrate solution (for an 0.3 gm sample of slag).

Molybdenum is used as the internal standard; this is introduced in the form of ammonium molybdate (2 cc of 5% molybdate solution per 70 cc of the analytic solution).

Three drops of the solution are placed on the flat ends of both carbon electrodes. The spark spectrum is excited by means of an IG-2 spark generator. Circuit parameters: C = 0.005 μf, L = 0.55 mH, I = 1.8-2.0 amp, auxiliary gap - 3 mm, main spark gap - 2.5 mm. Spectrograph data: ISP-22, three lens condenser illuminating 0.015 mm width slit. No pre-sparking; exposure - 3 min. Plates: Spectral, Type I, speed - 6° H&D.

The analytic line pairs are listed in the table.

The outlined procedure permits carrying out all quantitative determinations over the range of concentrations encountered in nickel-production slags with reference to a single calibration curve. The mean square error for individual analyses does not exceed 5%.

Institute of the Nickel-Cobalt Industry
"Gipronikel' "

Reference

1. L.N.Filimonov, Zavod. labor (The Plant Laboratory) 10, 1200 (1950).

* * * * * * *

SPECTROSCOPIC ANALYSIS OF SLAGS USING FUSING AGENTS

- E.N.Lesnikova

The purpose of the present investigation was to eliminate the influence of "third" components in the analysis of slags. The work was carried out on open-hearth slags specially prepared for the purpose. Only standard spectroscopic equipment was used; the spectra were excited in an AC arc.

Our studies showed that the effect of "third" components may be due to a number of factors:

1) The burning of the sample in the arc is often accompanied by a fractional or selective distillation effect which leads to a change in the temperature of the source and, consequently, to a change in the intensity of the spectrum lines.

2) Where an element with a low ionization potential is present, it acts to lower the temperature of the arc flame, the depressing effect increasing with the concentration of the element; thus, for example, increasing the concentration of calcium in the sample from 0.5 to 50% reduces the temperature by some 1000-1500°. Of the elements commonly encountered in slags Ca and Al have the lowest ionization potentials (6.113 ev and 5.985 ev, resp.). In the case of the artificial slag samples prepared for our tests, we noted an appreciable decrease in the intensity of the Mg 2781.4 A line (ionization potential of Mg = 7.17 ev) with increasing calcium concentration. Hence, the intensity of spectrum lines associated with high excitation potentials decreases with increased calcium concentration (i.e., with increased alkalinity of the slag).

3) Often slags differ as regards mineralogical composition: the same element may be present in the form of different compounds in different slags. The lines of elements present in the form of readily volatilized compounds are intensified, while the lines of elements present in the form of less volatile compounds are weakened.

In order to obviate the influence of these "third" component factors we used the fusing method first proposed by the author in 1952. Anhydrous borax was selected as the flux. It may safely be assumed that when the slag sample is fused with borax all elements and their compounds in the slag, except silicon, go over into borates; the silicon is converted to sodium silicate. Under the influence of the high temperature of the arc these compounds decompose into the oxides, the behavior and characteristics of which then determine the rate at which the various elements enter the arc. Thus the elements are vaporized at a more uniform rate than when present in different compounds. The effect of fractional distillation is further reduced through stabilization of the arc temperature by the continuous entry of sodium from the dissociating excess borax.

In the light of the above we developed a new procedure for spectroscopic determination of Ca, Al, Mn, Mg, Si and Fe in slags. The essential steps are the following. The slag sample is mixed with anhydrous borax in the proportion of 1:4. The mixture is placed on a copper ring plate and fused for 4 minutes in a muffle furnace at 800-850°C. The copper ring carrying the fused sample serves as one electrode; during the exposure it is continuously moved by means of a small electric motor. The stationary electrode is made of carbon, with a hemispherical point. The analysis is effected by the method of three standards, the comparison lines are lines of copper, while the analytic lines are the characteristic lines of the elements usually utilized in the analysis of slags.

Our investigations showed that instead of the copper comparison lines one can use the background, due to the flux, in the same region for all the elements.

The developed procedure was checked by analysis of standard slag samples Nos. 79 and 80 put out by the Ural Institute of Ferrous Metals. These samples can also be utilized as spectroscopic standards. The average relative errors in the determinations of the various elements were: Si ~ 5.2%, Ca ~ 5.6%, Al ~ 6.7%, Mg ~ 6.2%, Mn ~ 4% and Fe~4%.

The applicability of the procedure was also verified on industrial samples; with minor modifications it can be employed for the analysis of various powdered substances.

"A.M.Gor'ki" Ural State University

* * * * * * *

QUANTITATIVE SPECTRUM ANALYSIS OF THE RAW MATERIAL AND CLINKER USED IN THE PRODUCTION OF CEMENT

- T. K. Massil'on

The substances subject to analysis in the cement industry are commonly received by the laboratory in the form of fine powders. In our laboratory we use the moving lower electrode method to bring such samples into the source. A certain weight of the sample is moistened with ethyl alcohol and then coated in a thin layer on the copper plate which serves as the stage electrode. The stage is moved at a uniform rate during the exposure by means of an electric motor. The upper electrode is a copper rod, 10 mm in diameter, with a truncated cone point (diameter of flat ~ 2-3 mm).

The concentrations of the different elements are determined by the method of three standards: three samples of the substance in question, having a sufficiently wide range of concentrations, are selected; the concentration of the various components is determined by two-fold chemical analysis and the samples are then used as the standards for plotting the calibration curve.

Comparison of the results of spectroscopic determinations of CaO in six cement slag mixtures with the results of chemical analysis

Sample 22			Sample № 30			Sample № 21			Sample № 3			Sample № 7			Sample № 6		
Result, chem. anal. 43.4%			Result, chem. anal. 42.9%			Result, chem. anal. 42.4%			Result, chem. anal. 42.6%			Result, chem. anal. 42.7%			Result, chem. anal. 43.2%		
Result, spec. anal.	Error, %		Result, spec. anal.	Error, %		Result, spec. anal.	Error, %		Result, spec. anal.	Error, %		Result, spec. anal.	Error, %		Result, spec. anal.	Error, %	
	abs.	rel.		abs.	rel.		abs.	rel.		abs.	rel.		abs.	rel.		abs.	rel.
41,7	—1,4	3,3	42,4	—0,3	0,7	43,4	+1,1	2,5	42,2	—0,4	0,9	43,6	+0,7	1,6	42,1	—0,8	1,9
43,5	+0,4	0,9	42,3	—0,4	0,9	41,1	—1,2	2,9	42,0	—0,6	1,4	42,5	—0,4	0,9	43,6	+0,7	1,6
44,5	+1,4	3,1	42,8	+0,1	0,2	42,1	—0,2	0,4	42,8	+0,2	0,5	42,5	—0,4	0,9	42,6	—0,3	0,7
43,1	0,0	0	43,6	+0,9	2,1	42,2	—0,1	0,2	42,9	+0,3	0,7	42,9	0,0	0	42,9	0	0
42,	—1,0	2,3	42,9	+0,2	0,5	43,0	+0,7	1,6	43,5	+0,9	2,1	43,7	+0,8	1,8	43,2	+0,3	0,7
42,9	—0,2	0,4	42,6	—0,1	0,2	42,1	—0,2	0,4	42,3	—0,3	0,7	42,3	—0,6	1,4	43,0	+0,1	0,2
42,5	—0,6	1,4	—	—	—	—	—	—	—	—	—	—	—	—	—	—	—
43,7	+0,6	1,3	—	—	—	—	—	—	—	—	—	—	—	—	—	—	—
43,3	+0,2	0,4	—	—	—	—	—	—	—	—	—	—	—	—	—	—	—
43,8	+0,7	1,5	—	—	—	—	—	—	—	—	—	—	—	—	—	—	—
AVERAGES																	
43,1	±0,7	±1,5	42,7	±0,3	±0,7	42,3	±0,6	±1,3	42,6	±0,4	±1,0	42,9	±0,5	±1,0	42,9	±0,4	±0,8

Analysis is complicated by the fact that each different type of material requires a different set of standards. However, we have successfully used the described procedure for determining Al_2O_3, Fe_2O_3, MgO and TiO_2 in cements with an ISP-22 spectrograph, using the moving electrode method with a 6.5 ampere AC arc.*

Later we used a KS-55 spectrograph in conjunction with an AC arc (I = 5 amp) to determine CaO and SiO_2 in raw material mixtures according to the relative intensities of the Ca 3179.3 & Cu 3194.1 A and the Si 2881.6 & Cu 2882.9 A lines.

The results of determinations of CaO in six mixtures with slag are listed in Table 1. The mean absolute deviation from the average for all the spectroscopic analyses is 0.5%.

In the production of cement from aluminum-production waste (nepheline sludge) it is necessary to make rapid checks on the alkali metal content, running up to 3%. Since the ratio of Na to K in nepheline sludge is fairly constant and Na is the predominant element of the pair, one can readily ascertain the total alkali content by photometry of a single Na line.

The determinations are made on an ISP-22 spectrograph using the moving electrode technique; a spark is used

*The analyses were carried out by T.K. Aidarov.

for the raw sludge, an arc for clinker, inasmuch as it is impossible to obtain adequate blackening of the Na line with a spark in the case of clinker. The divergence between successive determinations for the same sample does not exceed 0.2% (absolute value). The results obtained in spectroscopic determinations of alkali metals in nepheline sludge samples by different technicians are listed in Table 2.

Table 2

Alkali metal concentrations in nepheline sludge found by different laboratory technicians by the method of photometric interpolation

Lab. tech.	Sample No.					
	517	520	524	209	210	211
1	2,2	2,5	2,2	2,0	3,1	1,4
2	2,3	2,5	2,4	2,0	3,15	1,4
3	2,25	2,4	2,25	2,0	3,15	1,4
4	2,15	2,5	2,4	2,0	3,2	1,5
5	2,15	2,4	2,1	2,1	3,0	—
6	2,3	2,5	2,3	1,9	3,2	—
Averages	2,2	2,5	2,3	2,0	3,15	1,4

"Giprotsement" Institute

* * * * * * *

QUANTITATIVE SPECTROGRAPHIC ANALYSIS OF CEMENTS AND RAW MATERIALS

- Z. A. Kel'tseva

The procedure we employ for analyzing clinker differs in principle from the techniques proposed by Buianov[1] and Nikitina[2] for slag analysis. We use an ISP-22 spectrograph, an AC arc and make our determinations by the method of three standards. The arc current used is 7 amp, the gap 2 mm, the exposure time 1.5 min. The standards are suitable production samples, analyzed for us in two different chemical laboratories. We use copper electrodes; the time required for a complete analysis is 1 hour 20 minutes.

The analytic line pairs we use are listed in the table below.

Analytic lines, A		Comparison line, A		Range of concentrations, %	Accuracy, %
Ca	3158,90	Cu	3142,44	CaO 58,0 ÷ 66,0	± 1,1
Si	2881,58	Cu	2882,93	SiO_2 18,0 ÷ 23,0	± 3,4
Al	3082,15	Cu	3073,80	Al_2O_3 4,0 ÷ 7,5	± 7,2
Fe	3075,78	Cu	3073,80	Fe_2O_3 2,0 ÷ 7,0	± 6,0
Fe	2382,03	Cu	2400,11	Fe_2O_3 in white cement 0,2 ÷ 1,0	± 5,5
Mg	2779,80	Cu	2768,87	MgO to 4,5	± 4,5
Mg	2779,80	Cu	2768,87	MgO to 10,0 in magnesia Portland cement	± 5,0
Mg	2802,69	Ca	3158,90		± 5,5
Mn	2801,06	Cu	2882,93	MnO to 0,5	±12,0
Na	3302,60	Cu	3142,44	Na_2O to 0,3	

General calibration curves plotted for the products and raw materials of all cement plants cannot be used, since the use of such general curves introduces systematic errors. In fact there is some displacement of the calibration curves for different types of materials used in one and the same plant. For example, in developing a procedure for determining MgO in magnesia Portland cement sludge containing over five different constituents (limestone, chalk, dolomite, clay, pyrite cinders, etc.) it proved impossible, in an arc, to obtain a straight line calibration curve. At the same time synthetic samples containing only two calcareous components (from two different uniform benches of the quarry) show a linear variation of log C with ΔS.

In view of this we developed a special procedure for determining Mg, using a condensed spark (IG-2 spark generator). Both carbon and copper electrodes were used; with the former the Mg 2802.39 A line was compared to the C 3158.90 A line; with the latter the Mg 2779.80 and Cu 2768.87 line pair was compared. The spectrographic conditions were: L = 0.05 mH, C = 0.01 μf, I = 1.6-1.8 amp, auxiliary gap - 3 mm, electrode gap - 2 mm, exposure - 30 sec, photographic plates - Spectral, Type I, speed 0.1 units GOST; photo-processing - standard procedure. The sample material was moistened with glycerin or an alcohol solution of "kleol" [= "cementall"] and applied to the electrodes in this form. The accuracy of determination of Mg is $\pm 5\%$ (referred to the results of chemical analysis).

During an investigation of possible procedures for determining coloring oxides (Fe_2O_3 and MnO) in white cement it was established that among other factors the results of analysis are greatly dependent on the type of limestone used in making the clinker, the calibration curves for clinkers based on different types of limestone being parallel but displaced relative to one another. Using the appropriate curves (selected by means of control standards) and a copper electrode arc for exciting the spectrum we attained an accuracy of within 5.5% for a range of Fe_2O_3 concentrations between 0.2 and 1% and MnO concentrations to 0.04%.

NIITsement
(Cement Scientific Research Institute)

References

1. N.V.Buianov, Zavod. labor. (The Plant Laboratory) 14, 565 (1948).
2. O.I.Nikitina, Izv. (Bulletin) AN SSSR, Ser. fiz., 18, 285 (1954).

* * * * * * *

QUANTITATIVE SPECTRUM ANALYSIS OF MAGNESITE AND MAGNESITE REFRACTORY MATERIALS*

- G. A. Pedan

We developed a spectrographic procedure for determining the SiO_2, Al_2O_3, CaO and Fe_2O_3 content in magnesite and refractory materials derived from it.

The spectra were photographed on an ISP-22 spectrograph. The slit width was 0.04 mm; the height of the cutout in the intermediate diaphragm of the three-lens condenser was 0.5 mm. A natural size image of the arc was obtained in the plane of the intermediate diaphragm. Photographic plates: Spectral, Type I, speed rating 0.5 units GOST. The samples and standards were pulverized to pass through a 10,000 mesh per cm^2 sieve. The raw magnesite powder was calcined in a muffle furnace at 1000°C for one hour. The standards were selected samples of magnesite and refractory materials derived therefrom, whose composition had been determined by careful

* N.P.Krilovskaia participated in the development work.

chemical analysis.

The samples were vaporized and the spectra excited in an AC arc. The powdered material was spread in an even layer (0.13 mm thick) on a copper plate which served as the lower electrode and was moved at a uniform rate during the exposure. The upper electrode was of carbon. Exposure - 90 sec; current - 14 amp, arc gap - 1.5 mm; rate of displacement of stage electrode - 3 cm/min; activator spark gap - 0.3 mm. The analytic line pairs employed are listed in the accompanying table.

Analytic line pairs

Analytic lines, A	Comparison line, A	Range of concent. (%)
Fe 2973,13/23	Mg 2938,54	0,1 ÷ 5,0
Fe 2501,127	Cu 2492,15	0,1 ÷ 5,0
Si 2881,58	Mg 2938,54	0,1 ÷ 5,0
Si 2514,33	Cu 2492,15	0,1 ÷ 2,5
Si 2435.159	Cu 2441,64	2,0 ÷ 5,0
Ca 3158.87	Cu 3142,44	1,5 ÷ 5,0
Ca 3158,87	Cu 3146,82	0,1 ÷ 2,5
Ca 3179,38*	Background	0,1 ÷ 1,5
Al 3961,53	Cu 4022,7	0,1 ÷ 2,0

*The Ca 3179.3 A line can be used when the Fe_2O_3 content does not exceed 0.5%.

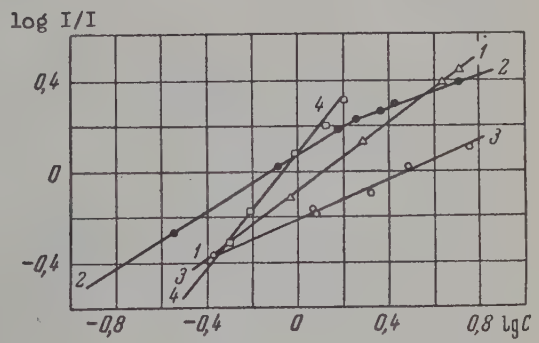

Calibration curves for determining admixtures in magnesite: 1) SiO_2 according to the Si 2881.58 - Mg 2938.54 A pair; 2) Fe_2O_3 from the Fe 2973.13/23 - Mg 2938.54 A pair; 3) CaO from the Ca 3158.8 - Cu 3146.82 A pair; Al_2O_3 from the Al 3961.53 - Cu 4022.7 A pair.

To weaken the Al 3961.53, Cu 4022.7, Si 28881.58, Mg 2938.54 and Fe 2973.13/23 A lines a diaphragm with half its cutout covered with a smoked glass plate 0.16 mm thick (passing an appreciable proportion of the ultraviolet radiation) was mounted in front of the spectrograph slit.

The mean relative errors (deviations) as determined on the basis of 10 analyses were 3.64% for SiO_2 (absolute content 2.20%), 4.5% for Fe_2O_3 (1.58%), 5.5% for CaO (1.15%) and 4.4% for Al_2O_3 (0.54%). The calibration curves used for the determinations are shown in the figure.

The divergences between the results of spectrographic and chemical analyses do not exceed the maximum divergences between the findings of two chemical laboratories allowed by State Standards (GOST).

In conclusion I wish to thank R.I.Garber for his interest and many helpful suggestions.

* * * * * * *

SPECTRUM ANALYSIS OF ALUMINA*

- L.V.Drutskaia

We developed the following procedure for spectroscopic analysis of alumina. Two sources are used: a controlled spark and an AC arc.

Controlled spark data. IG-2 spark generator, Model 1, circuit capacitance -

*E. A. Drutman participated in the development of the analytic procedure.

0.01 μf, inductance - 0.15 mH; auxiliary gap - 2.8 mm; electrodes - carbon, set for 2.5 mm gap; current - 2.5 amp. Lower electrode - hollow, with well for sample; upper electrode - flat face. The pre-exposure procedure consists of switching on the spark a number of times for 2-3 sec and adding more material in between the pre-sparkings until the well in the lower electrode is adequately filled with the sample (usually 4-5 filling-sparking cycles are sufficient). The exposure is effected by turning on the generator 5 to 10 times for a period of 5 seconds, again introducing additional amounts of the sample material into the lower electrode between sparkings; the total exposure time (i.e., the number of cycles) depends on the speed of the photographic plates used.

AC arc data. PS-39 arc generator; current - 5 amp; analytic gap - 2 mm. Lower electrode - as above; upper electrode - truncated cone point. The exposure is comprised of several arcings of 3-4 sec each, with additions of sample material between arcings.

The use of two different sources was found necessary due to the influence of the type of the compounds present in alumina on the analytic results.

The accompanying figure shows the distribution of the experimental points, using in plotting the calibration curves, for artifical samples of alumina with controlled admixtures of quartz, clay, sand and clay, chamotte (fire clay), white slime and sodium silicate.

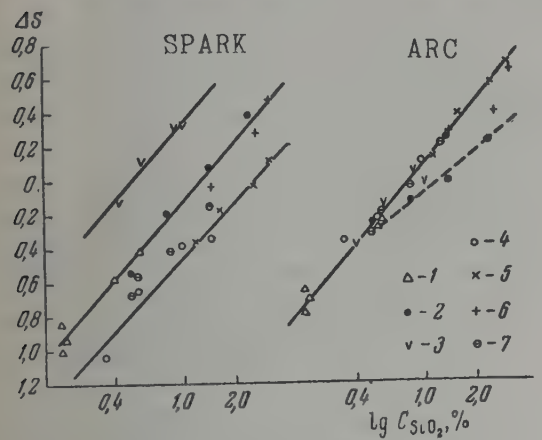

Calibration curves for determining SiO_2 in alumina and alumina with admixtures from the relative density of the Al 2652.5 and Si 2435.2 A lines in arc and spark spectra: 1) Al_2O_3; 2) Al_2O_3 + slime, 3) Al_2O_3 + clay, 4) Al_2O_3 + quartz, 5) Al_2O_3 + chamotte, 6) Al_2O_3 + sodium silicate, 7) Al_2O_3 + sand & clay mixture.

Obviously, correct results with the spark will be obtained only when the sample contains only white slime or sodium silicate; the determinations of all other admixtures will comprise a large error.

On the other hand, in the arc all experimental points fall on one common curve, with the exception of those for samples containing white slime (sludge). This series requires additional verification.

In order to evaluate the influence of the mineralogical composition and structure of alumina on the analytic results we prepared special mixtures of alumina with the hydrate. The test results showed that changes in the composition of the sample had little effect on the determination of iron and silicon in the spark. In the arc we noted a minor apparent increase in the determined silicon content in going from the hydrate to anhydrous Al_2O_3; however, the increase lies within the limits of the analytic error. On the other hand, the apparent sodium oxide concentration is dependent on the composition of the sample; the influence is particularly pronounced in the case of arc spectra, for which the calibration curve is less steep. In order to find the reason for the increase in the relative intensity of the Na line in going from the hydrate to alumina, we made an additional series of tests. The hydrate was heated at different temperatures to determine the effect of gradual elimination of the water of crystallization on the analytic results. In addition, a sample of the same hydrate was heated to temperatures at which the structure of alumina changes (the γ-form is transformed into the α-modification).

The variation of the apparent sodium concentration with the heating temperature corresponds to the transition from the hydrate to anhydrous aluminum oxide.

Consequently in the analysis of mixtures it is essential to reduce the crystallization water in the sample to a minimum.

In a spark, the results of determination of sodium oxide do not vary to the point of complete dehydration (about 900°); at this point there is a small apparent increase and then no further change with temperature. In an arc, on the other hand, the apparent sodium oxide content increases monotonously up to the same temperature and then remains constant despite the fact that as the temperature is increased further the structure of alumina changes, from the γ - to the α-modification.

The present investigation made it possible to adopt an analytic procedure based on the use of a single standard, taking advantage of the fact that the difference between the apparent concentrations of sodium oxide according to the alumina and hydrate calibrations curves for the spark remains constant.

Since the predominant admixture in alumina is chamotte, all samples are photographed in the arc as well as in the spark in order to avoid under-estimating the silicon dioxide content.

* * * * * * *

SPECTRUM ANALYSIS OF MAGNESITE AND OPEN HEARTH-BOTTOM MATERIAL

- A.E.Noshchenko

Basic data. In our procedure a weighed sample is brought into solution. Chromium, introduced in the form of potassium chromate, serves as the internal standard. We use an ISP-22 spectrograph and an IG-2 spark generator. The relative line intensities are determined by the method of photometric interpolation.

Dissolving the sample. The test material is first ground to a fine powder in an agate mortar; a 0.2 gm sample is then dropped into a 250 ml flask containing 2-3 ml cold distilled water, while shaking the flask. Next 25 ml hot distilled water and then 10 ml 1.19 sp. gr. hydrochloric acid are added and the contents are heated gently until the sample is fully dissolved. The solution is allowed to cool to room temperature and is then transferred to a 100 ml graduate cylinder. To this 5 ml of a 0.08 gm per 1 ml solution of potassium chromate (pure, analytic grade) and distilled water to bring the contents to the 100 ml mark are added. The contents are thoroughly stirred.

Fulgurator. The fulgurator pictured on the next page is used for exciting the spectrum. In it the spark discharge is formed between the flat face of the upper carbon electrode and the lower electrode with a 1 mm central capillary (both electrodes are 6 mm in outside diameter). The lower electrode fits tightly into a rubber bushing in one end of the U-tube (7 mm dia). The prepared solution is introduced into the U-tube by means of a 5 ml pipette, the height of the meniscus being adjusted so that the liquid level in the capillary will be just at the edge of the upper opening. This is accomplished with the aid of a templet and marks on the glass tube. Usually the solution level in the tube is some 12 mm below that in the capillary. The fulgurator is mounted on a suitable stand; its arms have positioning stops.

Excitation conditions. The IG-2 generator is used in the complex circuit setting; C = 0.01 μf; L = 0.15 mH; I = 2.0 amp; V = 220 v; control electrode gap - 3.5 mm, main electrode gap - 2.5 mm. The sample is pre-sparked for about 2 min; approximately 0.2 ml of solution are evaporated during this time. At the end of the pre-sparking interval, the generator is switched off and the 1-2 drops of

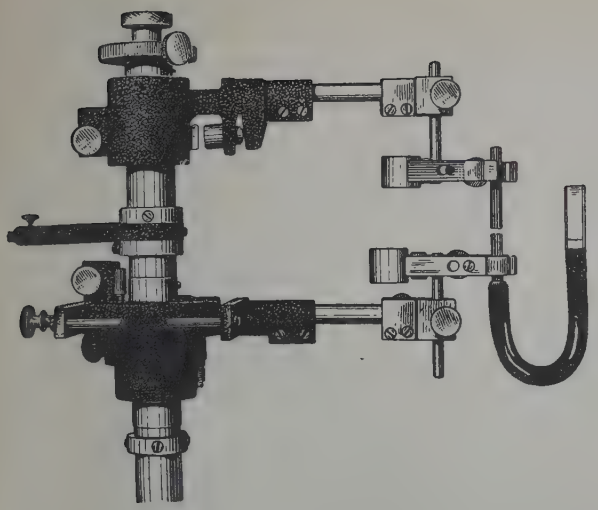

solution necessary to bring it back to the initial level are added. The 2 minute exposure is then made. The slit width used is 0.15 mm, the electrode to slit distance is 200 mm. The spectrum of each sample is photographed three times, using Spectral, Type I plates (speed - 0.5 units GOST). The plates are developed in the conventional manner in metol-hydroquinone developer.

Standards. The calibration curve is plotted with reference to standard solutions of magnesium oxide, made up of the analytic grade reagent, heated to 1000°C before making up the solutions. The standard solutions, having magnesium oxide concentrations of 55, 60, 70, 80 and 100%, were prepared under the same conditions as the analytic samples. The lines compared are Mg 2776.7 and Cr 2785.7 A.

The MgO content in the samples analyzed varied between 55 and 95%. Data characterizing the reproducibility are given in the table. The deviation from the mean value amounted to $\pm 1.0\%_{abs}$.

Reproducibility of analysis for MgO (%)

Material	Results of spectrum analyses						Mean	Chem. Anal.
Magnesite brick, S.O. No 82	93.3	91.4	96.3	91.4	91.8	92.1	92.7	93.1
Hearth bottom, Fe 4.3%	78.5	78.5	75.2	77.2	77.2	76.5	76.9	76.7
Hearth bottom, Fe 22.2%	57.6	57.9	56.8	57.6	57.8	56.4	57.6	57.0

The presence of iron in concentrations within the range from 5 to 25% does not affect the relative intensity of the analytic line pair.

The described procedure makes it feasible to make MgO determinations in the course of fettling a furnace (the analysis requires only 35-40 minutes) and is sufficiently accurate for this purpose.

"S.M.Karpov" Metallurgical Plant

* * * * * * *

VARIATION OF THERMAL EXCITATION CONDITIONS IN ARC SPECTRUM ANALYSIS OF ORES AND MINERALS

- A. K. Rusanov

The principal difficulties encountered in spectrum analysis of ores, minerals, slags and other powdered substances of varying composition stem from the fact that the intensity of the analytic lines depends not only on the concentration of the element in the sample but also on the chemical composition of the material.[1] That

is, any change in the composition of the sample alters the conditions of vaporization of the elements and compounds with a consequent change in the concentration of the atoms in the vapor cloud and in the conditions of emission (flame temperature, reabsorption, etc.).

The source commonly used in the analysis of powder samples is the carbon arc; the basic regularities governing the order of vaporization of the elements in carbon arcs are known (exemplified by volatility series)[2] as is the general variation of the arc temperature as a function of the ionization potentials of the elements and the concentration of atoms in the arc cloud[3].

In the case of vaporization of ores, minerals and similar substances of complex composition from the core of a carbon electrode, fractional vaporization with preferential entry of the different elements into the arc cloud is the rule; hence there is always a gradual change in the concentration of the various elements in the arc and a variation of the arc temperature. This leads to a continuous alteration in the intensity of the spectrum lines and, in many cases, to the appearance or disappearance of individual lines with time[1,4].

It must be admitted that our knowledge and understanding of the various factors - including the temperature - determining the conditions of emission in an arc cloud are far from what they ought to be in view of the present widespread and general use of arc spectra for the analysis of ores, minerals, slags, etc.

The paucity of information available on thermal excitation conditions in carbon arcs is to a considerable extent due to the complexity of the processes involved in fractional vaporization. As we know the temperature is usually determined from the relative intensities of lines for which the excitation potentials and transition probabilities are known[5]. Usually these "thermal indicator" lines are the characteristic lines of elements introduced into the electrode or added to the sample specifically for this purpose. Hence their appearance in the arc spectrum is limited to the interval of the preferential vaporization of the given elements, which means that their relative intensity cannot be used to find the temperature at different times during the entire arcing period. Furthermore, the reliability of determinations of the relative intensity of the "indicator" lines is seriously impaired by the variation of their absolute intensity, due to the fractional nature of the vaporization process.

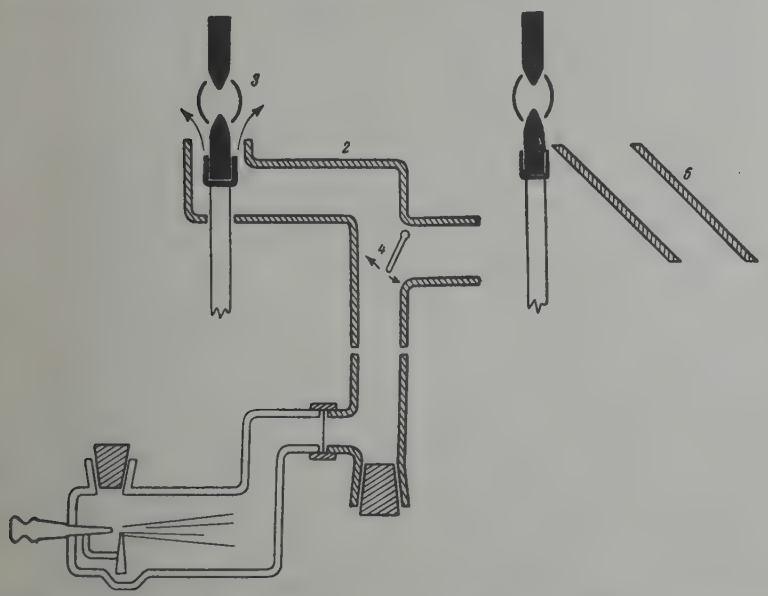

Fig. 1. Atomizer for introducing solutions of salts into the arc: 1) glass atomizer, 2) brass tube,3)arc, 4) flap valve regulating flow of mist to the arc, 5) alternate arrangement: inclined tube feeding the atomized solution into the arc at an angle.

These shortcomings of the conventional method of determining arc temperatures are largely obviated by introducing the "indicator" elements into the arc flame over a period of time, in small amounts by means of a solution atomizer. In addition this method of introducing the elements allows of a wider choice of "indicator" substances

and permits of closer control of the concentration of the desired atoms in the arc.

We used the vaporizer pictured in Fig. 1. The solution reduced to a fine mist by the glass atomizer 1 is carried through the brass tube 2 into the arc 3. Satisfactory results were also obtained with an inclined feed tube as shown at 5. The flow of atomized solution into the arc is regulated either by varying the air pressure to the atomizer or by turning the flap valve 4 in the brass tube.

The suspended solution droplets evaporate in approaching the arc and salt enters the arc in the form of minute particles, which assures complete and virtually instantaneous vaporization. With our atomizer operating normally at a pressure of 0.5 atmospheres about 0.001 mg of the dissolved salts together with 1 mg water vapor enter the arc per second.

Measurements of the relative intensity of the arc lines during the operation of the atomizer and after the atomizer is shut off indicate that over 98% of the material fed into the arc is vaporized in the arc flame.

Evaluations of the relative intensities of the Bi I 2938.32 and Bi I 2989.0 A [6] and the V I 3185.4 and V II 3110.7 A [7] lines, carried out by V. M. Alekseeva, showed that the introduction of the solution does not result in any appreciable decrease in the arc temperature, even when the solution contains elements with low ionization potentials.

We photographed the spectrum of the central portion of the arc flame with a medium dispersion quartz spectrograph (ISP-22) and also with a Hilger autocollimating quartz spectrograph. The line intensities were determined from the degree of blackening on the basis of the characteristic curves of the plates used, taking into account the background density. The effect of self-absorption could be discounted in view of the small amounts of the elements introduced.

There is a marked divergence between the values for the temperature in carbon arcs reported by different investigators. For example, for the case of vaporization of NaCl from the anode in a carbon arc under similar conditions we find the following range of values in the literature: 3900° (Ref. 3), 4527° (Ref. 8), 5200° (Ref. 6), 4600° (Ref. 5) and 4700°K (Ref. 7). As may be seen from the curves of Fig. 2 these differences may be explained by the rapid vaporization of NaCl from the electrode and the corresponding rapid rise in the temperature of the arc. Further examples of the rapid rise in arc temperature in case of relatively volatile substances are furnished by KCl and PbS; the curves for these salts in Fig. 2 show to what extent the results of temperature determinations depend on the time of observation. The fourth curve - for SiO_2 - is characteristic of substances having a medium volatility.

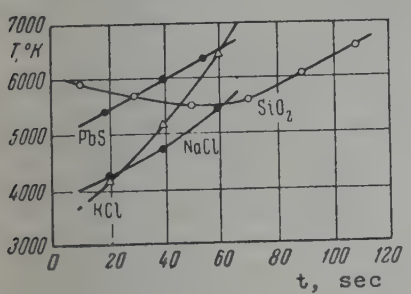

Fig. 2. Variation of the temperature in a carbon arc during vaporization of KCl, NaCl, PbS and SiO_2 from the core of the anode.

An idea of the variation in thermal excitation conditions in a carbon arc with changes in the composition of the vaporized sample may be gained from the curves of Fig. 3. These curves pertain to the vaporization from the anode of samples of different chemical composition but all containing 0.3% vanadium (in the form of the pentoxide) and encompass the full effective burning time of the arc for vanadium (the effective burning time[1] is here understood to be the time during which the lines of the element -- vanadium in this case -- are present in the spectrum of the arc flame). The character of the curves shows that the thermal excitation conditions in a carbon arc change in a complex manner during the vaporization of the sample and that the temperature may vary by as much as 1000-2000°. Since this has a direct effect on the emission conditions, measuring the mean temperature over the effective burning time does not, in general, enable us to determine the true relationship between the temperature and the intensity of the spectrum lines.

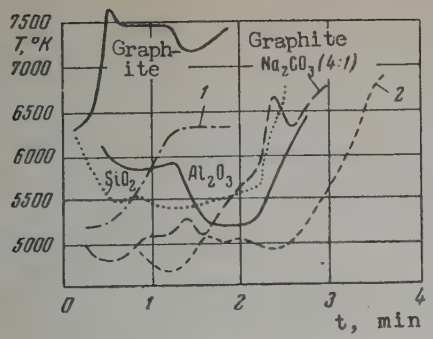

Fig. 3. Variation of the carbon arc temperature incident to vaporization of samples of different composition from the anode core: 1) 18% MgO & 18% Fe_2O_3 & 18% Al_2O_3 & 36% SiO_2 & 10% CaO; 2) same mixture but diluted 4 to 1 with $NaCO_3$.

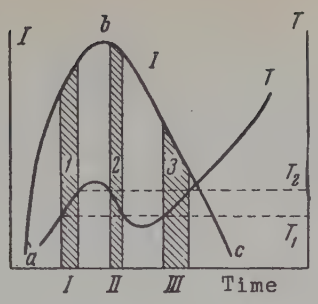

Fig. 4. Variation of the carbon arc temperature and of the line intensities during vaporization of the sample. T_1-T_2 is the temperature interval in which the emission of the line occurred; I, II and III are the time intervals in which the emission took place.

We can get a better idea of the influence of the temperature on the line intensity by juxtaposing the temperature vs time curve with the corresponding line intensity curve and determining in what temperature interval most of the emission at the given line frequency occurred. It will be seen from Fig. 4, where temperature and intensity curves are plotted to the same time scale, that in the given case emission occurred three times — during the time intervals I, II and III — in the temperature range between T_1 and T_2. By finding the total energy of the emission Σ_A (the area under the curve abc) and the energy of the emission Σ_a during the intervals I, II and III (sum of areas 1, 2 and 3) we can readily compute the relative energy of the emission $100\ \Sigma_A/\Sigma_a$ for the temperature interval T_2-T_1.

Analogous calculations made by T. I. Tarasova for the V I 3185.4 A line on the basis of the temperature curves shown in Fig. 3 confirmed that the temperatures at which the most intense emission of the lines occurs may differ appreciably from the mean temperature.

Table 1 gives the distribution of relative emission energy values over successive temperature intervals, the effective burning times for vanadium, the temperature variation range and the mean temperature as determined for samples of different composition.

The distribution of the elements in the Mendeleev periodic table as regards volatility in a carbon arc and ionization potentials is shown in Fig. 5. The elements having the highest volatility and lowest ionization potentials and, hence, reducing the arc temperature to the greatest degree are indicated by the darkest hatching. From a comparison of the upper and lower parts of the figure it will be evident that the most appreciable but short term decrease in the arc temperature will occur in the presence of the alkali elements as well as of such rare elements as thallium, indium and gallium.

It should be noted, however, that the last three elements, like the other rare members of the table (Hf, Re, Ge, Sc, Se, Te, etc.) are seldom encountered in practice and are, therefore, not likely to affect the arc temperature in ordinary ore and mineral analyses. One can also exclude from the class of temperature depressing elements those grouped at the right end of the table, since although highly volatile they are all characterized by high ionization potentials.

In Fig. 6 the elements present in common types of ores and minerals are arranged in descending volatility series. The relative ionization potentials of the elements in each series is indicated by the hatching; the darkest hatching indicates

TEMPERATURE DISTRIBUTION OF RELATIVE EMISSION ENERGY IN VAPORIZATION OF SAMPLES OF DIFFERENT COMPOSITION

Composition of material vaporized in the arc	Effective burning time for V, sec.	Mean arc temp, °K	Range of arc temp. variation °K	Distribution of relative emission energy over temperature intervals, %				Σ_a/Σ_A
Graphite $_{MK}$ + Na_2CO_3 (4:1)	170	7100	6300 ÷ 7600	—	—	—	—	—
SiO_2	210	5600	4800 ÷ 6700	—	—	—	—	—
	230	5700	5350 ÷ 6300	—	5350 } 85%	5600 } 10%	5800 } 5%	
					5600	5800	6300	
Al_2O_3	230	5650	5200 ÷ 6500	5200 } 59%	5400 } 21%	5650 } 10%	5800 } 10%	
				5400	5650	5800	6500	
Oxide mixture*	170	5900	5200 ÷ 6300	5200 } 45%	5450 } 20%	5700 } 16%	5950 } 19%	
				5450	5700	5950	6300	
Oxide mixture* + Na_2CO_3 (4:1)	280	5250	4750 ÷ 6800	4750 } 50%	4950 } 30%	5200 } 9%	5500 } 11%	
				4950	5200	5500	6800	

* Oxide mixture: 18% Al_2O_3 + 18% Fe_2O_3 + 18% MgO + 10% CaO + 36% SiO_2.

the lowest ionization potentials. The latter are the elements most likely (depending on their position in the series) to cause an appreciable reduction of the arc temperature. The elements most commonly encountered in the ores and minerals of the given type are enclosed in heavy-line squares: □

Observations of the variation in arc temperature in the process of vaporization of the listed minerals and compounds in a DC arc (220 v, 10 amp) were made under the conditions usually prevailing in conventional quantitative analysis of ores (powdered sample mixed 1-to-1 with graphite, packed into the 2 mm diameter, 5 mm deep core opening in a 3.5 mm diameter carbon anode.) The temperature measurements were made primarily for the easily volatilized elements and for elements with low ionization potentials. The results obtained, taken in conjunction with appropriate data in the literature on carbon arc temperatures, may be taken as a guide to the probable changes in the arc temperature during the vaporization in it of the common groups of ores and minerals listed in Figs. 6 and 7. The temperature variation data are presented graphically in Fig. 7, where the most commonly

Fig.5. Distribution of elements in the periodic system according to ionization potential and according to volatility (rate of entry into arc from the core of a carbon electrode during analysis of ores and minerals).

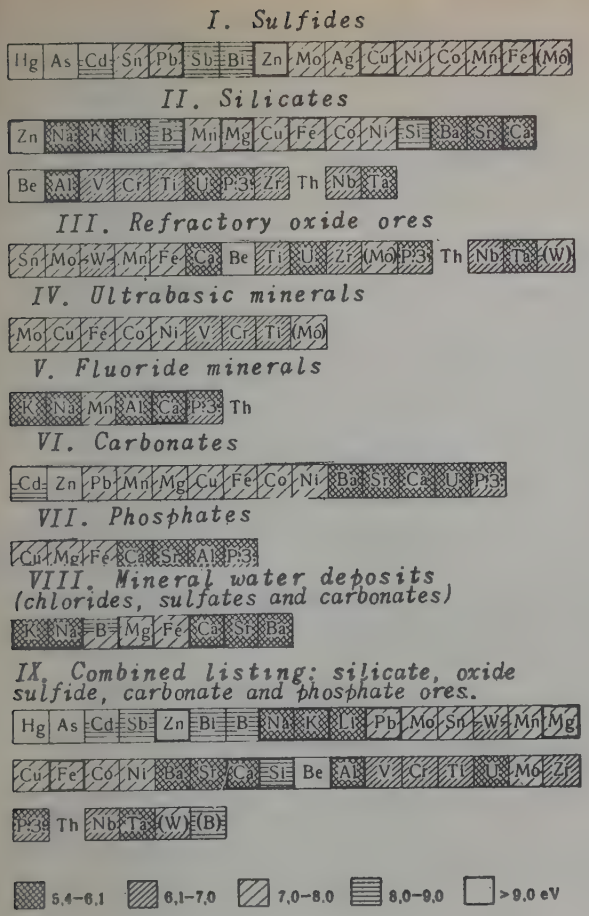

Fig. 6. Volatility series: sequence in which the various elements enter the arc from the core of a carbon electrode in the analysis of the more common types of ores and minerals. Ionization potentials indicated by hatching.

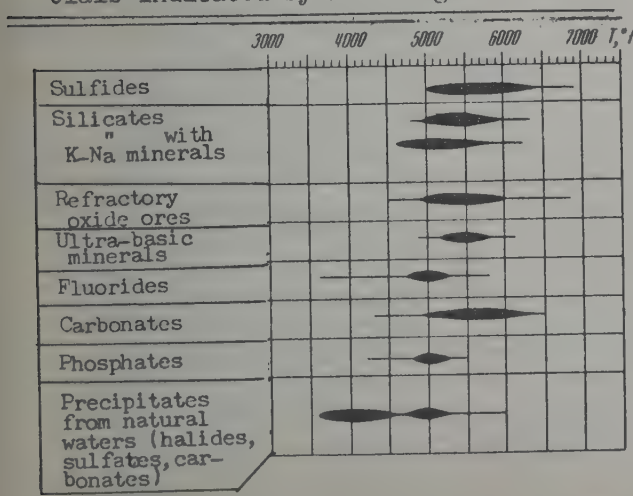

Fig. 7. Range of observed temperature variations during the vaporization of ores and minerals from the core of a carbon electrode.

observed temperature range is indicated by a thickened line. It should be borne in mind that the last stage of vaporization is characterized by a rise in temperature, which may reach a peak value of 7100–7400°K immediately subsequent to complete vaporization of the substance. This temperature rise during the ultimate instants was not taken into account in plotting the diagram of Fig. 7.

An examination of the diagram will show that in the analysis of ores and minerals one generally has to deal with a temperature variation in a fairly wide interval (from 4700 to 5800–6500°K). In the analysis of mineral waters containing a high concentration of alkali group elements the arc temperature during the initial stages of vaporization is frequently below 3700°K.

We have already noted that the addition of compounds of elements with low ionization potentials to the sample does not always assure a constant arc temperature because of fractional or preferential vaporization of the elements[1]. In practice it is common to compare lines which are far from being true homologous line pairs; hence it must be admitted that the variation in the temperature of the carbon arc is, together with the variation in the concentration of atoms in the arc flame, one of the principle causes of error in the analysis of substances of varying composition[9].

Until reliable means for stabilizing the carbon arc temperature and minimizing the effects of preferential vaporization are discovered one must always bear in mind the possibility of systematic errors in analyses of such substances. Among the more dependable methods of eliminating or reducing such errors are altering the chemical composition of the sample in the requisite direction prior to spectrum analysis[1] and the method of additions described by Prokof'ev[10].

The immediate and urgent problems facing spectroscopists working with ores and minerals are development of a constant temperature excitation source and of methods of minimizing the effect of selective vaporization

(for example, by the introduction of the sample material in small, quickly and fully vaporized portions). No less important is the development of rapid spectrochemical methods of preparing samples for spectrographic analysis.

All-Union Institute of Mineral Resources

References

1. A.K.Rusanov, Spektral'nyi analiz rud i mineralov (Spectrum analysis of ores and minerals) pp. 42, 105, Gosgeologizdat, M. 1948.
2. A.K.Rusanov, Izv. AN SSSR, Ser. fiz., 9, 6, 707 (1945).
3. O.P.Semenova, Izv. AN SSSR, Ser. fiz., 9.6.715 (1945).
4. A.K.Rusanov & V.M.Alekseeva, Zavod. Labor. (The Plant Lab), 1, 51 (1941).
5. L.Ornstein, H.Brinkman & Hengstum, Physica, 5, 145 (1938).
6. N.N.Sobolev, Zhur. eksp. i teor. fiz., 13, 130 (1943).
7. S.A.Shipitsyn, Izv. AN SSSR, Ser. fiz., 14, 677 (1950).
8. V.S.Mel'chenko, Trudy Sib. fiz, tekh. in-ta. (Proceedings of the Siberian Physics & Technology Institute) 2, 195 (1950).
9. N.A.Prilezhaeva, Ibid., 32, 15 (1953).
10. V.K.Prokof'ev, Fotograficheskie metody kolichestvennogo spektral'nogo analiza (Photographic methods of quantitative spectrum analysis) M.-L. 1951.

* * * * * * *

INFLUENCE OF COMPOSITION ON THE ACCURACY OF SPECTRUM ANALYSIS OF ORES

- V. V. Nedler

The widely employed method of complete vaporization of the sample from a well in one of the arc electrodes does not insure the accuracy often required in the analysis of ores. This is due primarily to the variation from sample to sample of the chemical and physical composition of the ore material and the consequent poor reproducibility of the vaporization conditions for both the analyzed components and the comparison elements.

In view of this we undertook a series of experiments aimed at evaluating the possible quantitative effect of these factors in the determination of Pb, W, Cu, Sn and Bi in ores. Samples containing the mentioned elements in the form of their oxides were divided into two parts: one part remained in its natural state, while 20% NaCl by weight was added to the other part. The densities of the characteristic lines of the enumerated elements were evaluated in the spectrograms obtained, Sn being provisionally taken as the comparison element. The results of measurement are summarized in the table.

We detected an appreciable shift in the relative intensities of the analytic lines. In order to take account of the part of the shift due to temperature changes and the degree of ionization in the electrode gap we measured the temperature on the basis of the relative intensities of three pairs of lines and then computed the change in relative intensities of the analytic pairs corresponding to the determined temperature difference. Even after the introduction of these corrections, there still remained a residual shift in the relative intensities, which was different for different elements.

Photographic scanning experiments (photographing the spectrum of the sample in process of vaporization on a moving plate) showed that the addition of NaCl to the samples produces an appreciable change in the rate of volatilization of the

Composition of sample	Concent. of both elements	No. of tests	Logarithm of intensity ratio of compared lines			
			Pb 2833 – Sn 2863	W 2897 – Sn 2863	Bi 2898 – Sn 2863	Cu 2824 – Sn 2863
$SiO_2 + C$	0,39	15	$-0,35 \pm 0,03$	—	—	$-0,21 \pm 0,02$
$SiO_2 + C + NaCl$ . .	0,39	15	$-0,08 \pm 0,04$	—	—	$-0,26 \pm 0,02$
$SiO_2 + C$	0,78	15	$-0,35 \pm 0,01$	$-0,47 \pm 0,04$	$-0,29 \pm 0,02$	$-0,23 \pm 0,04$
$SiO_2 + C + NaCl$ . .	0,78	15	$-0,10 \pm 0,04$	$-0,26 \pm 0,03$	$-0,45 \pm 0,02$	$-0,33 \pm 0,03$
$SiO_2 + C$	1,17	15	$-0,33 \pm 0,02$	$-0,45 \pm 0,05$	$-0,33 \pm 0,03$	$-0,25 \pm 0,01$
$SiO_2 + C + NaCl$ . .	1,17	15	$-0,13 \pm 0,02$	$-0,12 \pm 0,03$	$-0,53 \pm 0,02$	$-0,32 \pm 0,02$
$SiO_2 + C$	1,17	15	$-0,37 \pm 0,04$	$-0,42 \pm 0,03$	$-0,23 \pm 0,02$	$-0,15 \pm 0,02$
$SiO_2 + C + NaCl$ . .	1,17	15	$-0,10 \pm 0,03$	$-0,19 \pm 0,04$	$-0,55 \pm 0,04$	$-0,33 \pm 0,03$

different elements. The greater this change in vaporization rate, the larger the alteration in the intensity of the lines of the element in question relative to the intensity of the lines of the other elements.

The processes of solid-to-vapor phase transformation and spectrum excitation in an arc differ markedly from these processes in a spark and spark-like discharges between metal electrodes. Whereas in spark type discharges the vapor is expelled from the surface of the electrode at a temperature on the order of 10,000° and cools down as it moves further from the electrode, in arcs the vapor rises from the surface of the molten phase at a temperature not exceeding 2000-3000°K. Obviously, under these conditions only a part of the vapor released enters the region of the luminous arc channel. Depending on the rate of evaporation at any instant, a greater or lesser proportion of the released vapor passes through the luminous region and the total energy of the emission of the various analytic components varies accordingly. The above mentioned photographic scanning experiments confirm this.

It is evident that changes in the rate of vaporization may occur not only due to the presence of admixtures capable of affecting the vaporization regime, but also as the result of wandering of the arc discharge, local hot spots in the sample, inhomogeneities and similar factors. All such changes lead to changes in the relative intensities of the compared lines and, consequently, to analytic errors. In view of the fact that most of the factors causing variation in the rate of vaporization cannot be controlled in the conventional electrode-well method, it is clear that to eliminate such analytic errors it is essential to develop new methods of introducing samples into the arc, methods free of the shortcomings inherent in the conventional procedure.

* * * * * * *

ON THE ABSOLUTE SENSITIVITY IN DETERMINING RARE-EARTH METALS

– T.N.Zhigalovskaia

Emission spectrum analysis, particularly with medium dispersion instruments, is seldom used in practice for determining the rare-earth elements, partly because of the numerous lines present in the spectra of these metals and partly because of the low absolute sensitivity of this method. In view of this we undertook a series

of experiments designed to determine the threshold of sensitivity for the rare earths and to compare it with the sensitivity threshold for certain other elements having filled s- and d-shells. The experiments were made with an AC carbon arc, in a circuit developed by N.S.Sventitski, in conjunction with an ISP-22 spectrograph. The metal oxides were applied in a thin layer to the surface of the carbon electrodes. The following elements were investigated: with filled s-levels - Mg, Ca, Sr and Ba; with "filling" d-levels - Cr, Nb and W; Mn, Mo, Re, Y and La; and with "filling" f-levels - Ce, Pr, Nd, Sm and Yb.

The following conclusions may be drawn from the experimental results.

1. The threshold of the absolute sensitivity depends on the position of the element in the Mendeleev table. For a given value of the quantum number l, the sensitivity rises with increasing quantum number n. At a given value of n and l, the sensitivity rises with the difference between number of electrons actually in the outer shell and the number required for the outer shell to be completely filled or half filled. For the rare-earth metals investigated the threshold of sensitivity is lower, the lower the quantum number l for the ground term.

2. The threshold of sensitivity in determining the rare-earth elements by emission analysis also depends to a considerable extent on the presence in the sample of other elements. Thus the presence of an appreciable concentration of NaCl or KCl (5 mg in the samples used) may reduce the sensitivity by a factor of 100 or more. On the other hand the presence of AgCl increases the sensitivity with the thin-layer procedure used by a factor of 2.

A very appreciable increase in sensitivity (about 100-fold) was observed as the result of adding NH_4NO_3 in the amount of 50% by weight and AgCl in the amount of up to 5% by weight to the sample. With these additions the threshold of sensitivity for Ce, Pr and Nd proved to be on the order of 10^{-3}%.

Geological Institute of the
Tadzhik SSR Academy of Sciences

* * * * * * *

A SEMI-QUANTITATIVE SPECTROSCOPIC PROCEDURE FOR DETERMINING 40-50 ELEMENTS IN ROCKS AND MINERALS

- V.V.Khokhlov, V.N.Protopopov, L.I.Denisenko, E.Ia.Smirnova & Z.G.Timonina

The line-weakening spectro-analytical procedure developed by M.M.Kler*, by virtue of its simplicity and the fact that it is readily learned by semi-qualified personnel, is now widely used by various geological enterprises, expeditions, prospecting parties, etc.

However, the accuracy of the line-weakening method is inadequate for the solution of certain petrographic, geological and chemical problems. In view of this

---

*See Izv. (Bulletin) AN SSSR, 18, #2, 291 (1954).

Trans. Editor's Note: As described by Kler the procedure consists of photographing the spectrum through a logarithmic step-sector or rotating disk. The elements are determined on the basis of a single line by reference to a chart or calibration curves showing how many steps of the line characteristic of the given element appear at different concentrations. The relative accuracy is claimed to be ±13-25% for samples of the same type of mineral, but the error may be much greater "in unfavorable cases" (cases of great variation in the nature and composition of the samples).

Also see the next article in the present issue. Ed.

the spectroscopic staff of the Geological Institute laboratory conducted a series of investigations aimed at enhancing the accuracy of the procedure.

Experimental data, based on a large number of determinations made by the laboratory staff, indicate that the influence of the host or parent material is not great enough to cause a radical change in the evaluated content of the important elements. This is confirmed by the results of determinations of Bi, Sn, Y, Pb and Mo in granite, pegmatite, Rapakivi granite, dolomite, calcite, diabase, nepheline syenite, skarn, peridotite and diopside, all according to a single calibration curve for each element. On the average, the probable (relative) analytic error amounted to ±43.1% (for concentrations ranging between 0.001 and 0.1%).

On the basis of a large number of determinations (several hundred) we evaluated the accuracy of the improved procedure as compared with the results of chemical analyses for a wide range of concentrations (the possible errors in chemical analysis were not taken into account in making the evaluation). The mean arithmetic error of determination was found to be 60%, which betokens a higher accuracy as compared with the original procedure in which the analytic results were obtained only in terms of concentration intervals (i.e., between 0.001 and 0.01, 0.01 and 0.1%, etc.).

The conditions to be observed in order to attain the indicated degree of accuracy do not complicate the basic procedure and may be summarized as follows:

1. The standards used in plotting the calibration curves should be prepared on the basis of natural compounds found in the minerals to be analyzed, according to groups of genetically related elements.

2. When working in a wide range of concentrations one should use a series of calibration curves for different more and less sensitive lines.

3. The content of the elements should always be determined directly from the appropriate calibration curve, using only the straight line section thereof (i.e., never by interpolation and similar approximate procedures).

To facilitate the introduction and application of this improved analytic procedure in geological institutions and agencies we offer an instruction manual covering approximate spectroscopic analysis of minerals for 40-50 elements. The manual comprises a set of spectrum line charts for which the lines were photographed on an ISP-22 spectrograph.

All-Union Scientific Research
Geological Institute

* * * * * * *

APPROXIMATE QUANTITATIVE SPECTRUM ANALYSIS OF MINERALS

- M.M.Kler

In analyzing natural minerals and metal oxides for admixtures we use an AC arc with a current of up to 20 amperes. In our procedure a 20 mg sample is completely vaporized from the core of a carbon electrode. The relative error as computed on the basis of the reproducibility of determinations of Sn, Y and other elements in granites amounted to ±13%, with visual evaluation of the line intensities to the nearest 0.1 step.

The accuracy may deteriorate sharply in analyzing samples of different types of minerals using the same calibration curve, since element-concentration curves for different mineral formations are shifted relative to one another. We investigated the question of the position of the analytic curves, their slope and relative

shift in the case of analysis of metal oxides for admixtures. We worked with 16 different elements in 5 different host materials (SiO_2, CaO, Al_2O_3, ZnO and coal powder). The average angle of slope of the calibration curves for the analytic lines used in all five host materials was 34.3°. The deviation from this mean value for a given line in different host materials is small (1.6° on the average). In studying the positions of the calibration curves we did note some parallel displacement of the curves. In his monograph on the subject, Harvey (1950) recommends two constant slopes for the calibration curves: 33.7° for resonance lines and 45° for non-resonance lines (lines associated with high-lying lower level). It will be seen that the former value is very close to the value obtained in our investigation (34.3°). We find nothing in our data to indicate use of a 45° slope calibration curve; nor does our experimental data support Harvey's hypothesis regarding the dependence of the slope of the calibration curve on the type of line (energy of the lower level). We have verified this by careful measurement of 140 analytic curves for the determination of 27 different elements in zinc oxide. We found the average slope angle of the curves for resonance lines and lines with a lower level energy of up to 1 ev (112 lines in all) to be 32.8°, while the value for 29 lines with a high-lying lower level averages 32.0°.

We are currently compiling tables to be used in making corrections for the lateral shift of the calibration curves; this is, however, a very laborious project and the tables are applicable only to the analysis of certain typical samples (i.e., certain specific types of minerals allied to the mineral for which the basic calibration curve is plotted).

In order to obtain universal calibration curves for each element suitable for approximate quantitative analysis regardless of the host material we applied the method of introducing a new host material (diluting the sample) and the method of stabilizing the arc temperature by the introduction of sodium. As a result we succeeded in obtaining general curves for the determination of Bi, Cd, Mo, As, Sn, Sb, Pb, Ag and P in different host materials (oxides).

On the basis of the accumulated experimental data we have also compiled tables of the suitable analytic lines and giving the difference in wavelengths between these and the nearest lines of interfering elements.

Department of Chemistry of
Leningrad State University

* * * * * * *

QUANTITATIVE SPECTRUM ANALYSIS FOR GEOLOGICAL WORK

- Iu. A. Sherstkov

In the analysis of ores the physical and chemical properties of the sample have a pronounced effect on the appearance of the spectrum. We had to deal with this effect in developing a procedure for quantitative analysis of limestones for Si, Al and Fe. We used the briquetting with graphite method and spark excitation. In the course of the work we noted that the introduction of third components into the sample changed the results of analysis, the extent of the change depending on the mineral composition of the additive.

Thus our observations again confirmed that one of the principal difficulties in quantitative spectrum analysis of ores and minerals stems from the variation

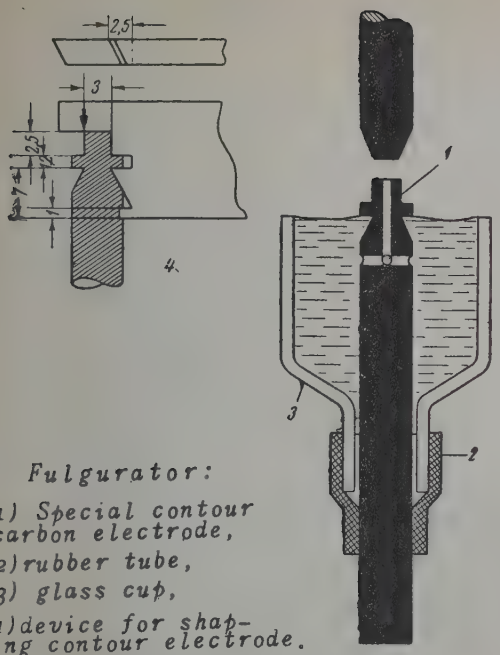

Fulgurator:

1) Special contour carbon electrode,
2) rubber tube,
3) glass cup,
4) device for shaping contour electrode.

of the appearance of the spectrum with the mineralogical composition of the samples. The difficulty can be obviated by bringing the samples into solution.

Hence the theoretical aspects of the problem, developed by V.V.Nalimov and K.I. Ionova, are of great practical interest. One of the possible procedures which would permit use of quantitative spectrum analysis in geological work consists of using aliquot parts of the solution after determining the silica content chemically.

We bore this in mind in developing a method of analysis of fire clays (chamotte) for the Fe, Ti, Ca and Mg content. We used a special fulgurator (see accompanying figure). The spectra were photographed on an ISP-22 spectrograph with a 0.03 mm wide slit, illuminated by means of the standard three-lens condenser. Source data: IG-2 spark generator; C = 0.01 μf, L = 0.01 H; analytic gap - 2.5 mm, auxiliary gap - 3 mm. Plates: positive, speed - 0.7 units GOST. Pre-exposure sparking - 30 sec; exposure - 1 min.

The analytic line pairs used are listed in Table 1. Cobalt was used as the comparison element, 5 ml of 7% solution of $CoCl_2$ being added to 20 ml of sample solution.

The calibration curves were plotted by the method of three standards, using synthetic standard solutions. The spectra of each solution were photographed two times using the same special profile electrode. The solution and upper electrode were changed between photographs. With the method of excitation used, the variation of ΔS for all the analytic line pairs averaged ±0.01-0.02.

The reproducibility was checked by repeated analysis of Standard Sample No.55. The results are listed in Table 2.

Comparison of our analytic results with those of chemical analysis of Standard Sample No. 55 shows that where determination of calcium and magnesium is concerned the accuracy of our spectrographic method is appreciably higher.

Table 1

Concentration ranges determined and analytic line pairs used

Elements	Wavelength, A		Range of concentrations, %
	Cobalt		
Fe II	2599,39	I, II 2648,63	1 ÷ 10
Ti II	3349,04	I 3354,38	0,6 ÷ 2,5
Ca II	3968,47	I 3894,08	0,05 ÷ 1,5
Mg II	2802,7	II 2663,68	0,05 ÷ 1,2

Table 2

Reproducibility of spectrum analysis (Repeated analyses of Standard Sample No. 55)

Test No.	Content, %			
	TiO_2	Fe_2O_3	MgO	CaO
As per certificate				
	1,33	1,56	0,84	0,47
Found by spectroscopic analysis				
1	1,33	1,53	0,85	0,41
2	1,33	1,62	0,81	0,54
3	1,38	1,64	0,87	0,49
4	1,19	1,52	0,80	0,47
5	1,25	1,60	0,84	0,45
6	1,26	1,67	0,93	0,47
7	1,26	1,55	0,84	0,43

* * * * * * *

THE EFFECT OF GRAPHITE IN SPECTROSCOPIC ANALYSIS OF ALLOYS

- A.V.Kozlova & P.D.Korzh

The influence of third elements, frequently observed in spectrum analysis of alloys, is due to the modifications they produce in the processes occurring on the surface of metallic electrodes and in the excitation conditions in the discharge. The effects connected with surface processes can be minimized to a certain extent by providing conditions assuring simultaneous entry of all the elements of the sample into the discharge. Such conditions can be realized by diluting the sample with graphite powder and then vaporizing the mixture from the core of a carbon electrode in an AC arc.

The action of the graphite powder may be explained as follows. In the absence of graphite, the sample material is fused and forms a globule. The temperature of the globule depends not on the strength of the discharge current but mainly on the composition of the sample and generally remains much lower than the temperature of the plasma. Hence we have fractional vaporization of the sample components, with the result that the concentrations of the elements in the discharge differ from their concentrations in the sample.

On the other hand, in the presence of graphite powder the sample material vaporizes without first forming a drop or globule, the temperature of the electrode rises and more favorable conditions for the simultaneous sublimation of more and less volatile components are created. Thus the influence of the gross composition of the sample is weakened.

Range of concentrations of some elements in the analyzed alloys:-

Alloy	Concentration,%		
	Cr	Ni	Mn
Stainless steel	17-25	8-20	0.8-1.6
Chrome-aluminum	12-25	0.2-0.4	0.5-1.6
Ni-Cr-Fe alloy	15-22	60-80	0.4-1.2

We utilized this method of introducing alloy samples into an AC arc in analyzing different grades of stainless steels, chrome-aluminum and nickel-chromium-iron (nichrome) alloys. The range of concentrations of Cr, Ni and Mn in these alloys is given in the accompanying table.

The procedure used was the following: the powdered sample, NH_4VO_3 (the vanadium served as the internal standard) and graphite powder, sifted through a 200 mesh screen, were mixed in the proportions of 1:1:2. The thoroughly stirred mixture was packed into the core of the lower electrode (core well: 1.5 mm deep, 1.5 mm in diameter, 0.2-0.3 thick walls); the upper electrode was a spectrally pure carbon rod. The spectra were photographed on positive plates using an arc current of 7 amperes. The exposure, which was determined by the time required for complete burning of the sample, equalled 1.5-2.0 min.

The calibration curve for Cr, showing the distribution of the experimental points for the different alloys, is reproduced in the accompanying figure. A similar pattern was obtained for Mn. It will be seen that all the points fall in one straight line, whereas with the conventional vaporization procedure (without graphite) it is necessary to plot separate calibration curves for each type of alloy.

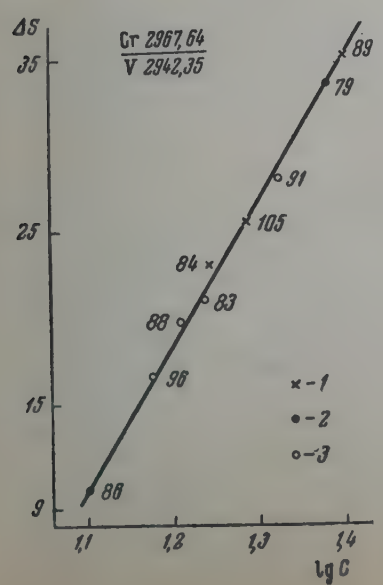

Figure: Calibration curve for determination of Cr in 1) Stainless steels, 2) Cr-Al alloys, 3) Ni-Cr-Fe alloys.

Magnitogorsk Metallurgical Institute

THE EFFECT OF GRAPHITE POWDER IN SPECTRUM ANALYSIS OF ORES

- K.Z.Finkin

In spectroscopic analysis of ores, aside from errors due to non-uniform distribution of the elements through the material of the sample, we also have the possibility of errors due to the influence of the molecular composition of the predominant component. This is at least one of the factors making it difficult, and in some cases impossible, to analyze ores of different origins by the same spectrographic procedure.

Studies of the vaporization from core electrodes have shown that the sample fuses into a molten globule from the surface of which the different elements are selectively vaporized. Under such conditions the influence of the molecular composition of the principal ore component and other factors aggravating the analytic error becomes particularly strong. The effect of these factors can be largely eliminated by vaporizing the ore in the form of a mixture with graphite powder. The graphite separates the ore particles and prevents the micro-droplets from coalescing into a macro-globule. At the same time the rate of vaporization of the ore is increased due to the fact that the total surface area of the micro-droplets is much greater than the surface area of the equivalent globule and the fact that the vapor tension over the minute droplets is higher than over the large globule.

Also, in the absence of graphite, oxides may form in the molten globule, whereas when graphite is present the droplets are composed almost entirely of free elements.

A proportion of one part graphite to one part ore is already sufficient to insure uniform vaporization of the entire mixture. Under these conditions each element enters the arc at approximately the same rate, regardless of the initial chemical and molecular composition of the sample.

We investigated the influence of graphite powder in determining Mn (20.5 to 52% content) and Si (6.3 to 41% SiO_2) in manganese ores of three different origins and in determining Fe, Si and Al in iron ores from the Ural, Kerch, Krivorog and other regions. The source was a Sventinski activated arc; the current 6.5–7.0 amperes. The electrodes were spectrally pure graphite rods. The calibration curves were plotted in ΔS *vs* log C coordinates by the method of three standards. Ni, introduced in the form of $NiCO_3$, served as the internal standard. A representative sample of ore was pulverized to 200 mesh and the $NiCO_3$, powdered to the same degree of fineness, was added in the ratio of 1:1; then the graphite powder was added to the mixture, again in the ratio of one part graphite to one part mixture.

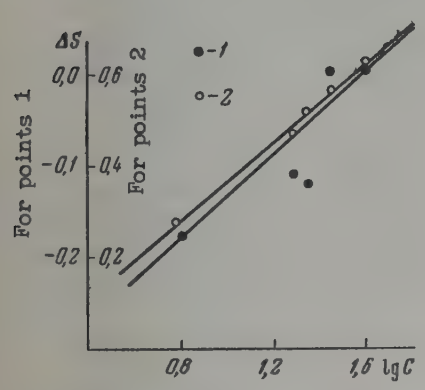

Calibration curves for determining Si in manganese ore: 1) without graphite, 2) with graphite powder added in the proportion of 1 to 1.

The analyzed ores differed greatly from each other as regards mineralogical composition and physical and chemical properties.

By way of illustration, the calibration curves for the Si content in manganese ores for vaporization with and without graphite powder are reproduced in the accompanying figure. It will be seen that without graphite the points are scattered, with graphite all the points fall on a straight-line calibration curve.

In conclusion it might be noted that the results of our investigation may prove useful in the development of new universal methods of spectrum analysis of ores.

Magnitogorsk Metallurgical Institute

SPECTRUM ANALYSIS OF POWDERS WITH REFERENCE TO A SINGLE STANDARD

- A. M. Shavrin

In earlier reports* we showed that, using the dilution method, one can make determinations of vanadium in ores by means of a single calibration curve, regardless of the composition of the analyzed samples. This curve can be plotted (straight line with a 45° slope) on the basis of a single standard, provided the vanadium concentrations are relatively low (self-absorption of the vanadium lines is absent), if the density of the continuous background is taken into account.

The feasibility of plotting calibration curves on the basis of a single standard was verified experimentally on four standard samples (differing only as regards vanadium content) having the following compositions: 1) $SiO_2.aq$ + 0.025% V + 0.5% Mo, 2) $SiO_2.aq$ + 0.05%V + 0.5% Mo, 3) $SiO_2.aq$ + 0.1% V + 0.5% Mo and 4) SiO_2aq + 0.2% V + 0.5% Mo. The exposure conditions were chosen so that the spectrogram would have a sufficiently blackened background to permit determining its density according to the same characteristic curve as that used for evaluating the line intensities. Positive plates having a GOST speed rating of 3 units were used. The standard samples were vaporized in an AC arc, using a current of 5 ± 0.5 amp. The samples were packed into a cup in the lower copper electrode. Spectrograph slit width - 0.03 mm; exposure - 30 sec. The relative intensities of the V 3110.71 and Mo 3112.12 A line pair were measured.

The resultant curve, plotted in log $I_V/\log I_{Mo}$ *vs* log C coordinates, taking into account the background and the gamma of the plates, was a straight line with a slope of 45°.

Thus the experiments proved the absence of self-absorption of the V 3110.71 A line in the range of concentrations from 0.025 to 0.20% and showed that it is possible to plot a calibration curve on the basis of one point (one standard), by drawing a 45° straight line through this point. The described procedure was further verified by determinations of vanadium in copper-bearing sandstones. The accuracy of determination was within ± 10%.

"A.M.Gor'ki" Molotov State University

* * * * * * *

THE INFLUENCE OF CERTAIN SUBSTANCES ON THE INTENSITY OF THE SPECTRUM LINES OF MOLYBDENUM, INDIUM AND THALLIUM

- L.A.Spektorov, I.K.Klavdienko & A.I.Poguliaeva

We investigated the effect of additions of compounds of K, Na, Li, Ba, Sr, Al, Zn, Cd, Hg, Cu and Fe on the intensity of a number of lines of Mo, In and Tl in the spectra of MoS_2, $InCl_3$ and Tl_2SO_4. To this end mixtures of these compounds with carbon powder with and without the various additives were packed into the core of carbon electrodes.

In the case of MoS_2 a 20 mg sample was used and the depth of packing (cup in electrode) was 8mm; for $InCl_3$ and Tl_2SO_4 the sample weight was 30 mg and the depth 12 mm. The spectra were excited by means of a DG-1 arc generator with a current of 5 amperes and photographed on an ISP-22 spectrograph. The exposures, equal to

---

*A.M.Shavrin, Zavod. labor. (The Plant Laboratory), 1, 66 (1949); Izv. (Bulletin) AN SSSR, Ser. fiz., 15, 673 (1950).

the full vaporization time, were 6 min for MoS_2 and 3.5 min for $InCl_3$ and Tl_2SO_4. The spectrograms were compared on an MF-2 microphotometer.

The results of the investigation showed that:

1) the addition of readily ionized substances (K, Na and Li) causes a relative intensification of the Mo 3902, 3194, 3170, 3158 and 3132 A lines, which is apparently connected with a certain weakening of the continuous background and of the CN bands in the region of 3000 A and above;

2) the addition of Sr, Li and Ba produces a less appreciable increase in the intensity of the Mo lines; addition of the other elements listed results in some weakening of the Mo lines;

3) the greatest increase in the intensity of the In and Tl lines is also caused by the addition of K, Na and Li; additions of Fe and Cu produce no appreciable change in the intensity of the In and Tl lines.

It should be noted that self-absorption plays an important part in the change in intensity of the Mo, In and Tl lines; consequently, the extent of the change produced by the same addition varies for different lines of each element.

It should be possible to take advantage of the increase in the intensity of Mo, In and Tl lines produced by the addition of alkali metals for purposes of analysis.

Kirgiz State University

* * * * * * *

VARIATION OF THE INTENSITY OF COPPER AND NICKEL LINES WITH THE CONCENTRATION OF THESE METALS IN Cu-Ni ALLOYS

- N.K.Rudnevski & G.I.Golitsyn

We investigated copper-nickel alloys containing from 1 to 79% Ni, 0.2% Mn and 0.15 to 0.40% Fe. To insure homogeneity of structure all the alloys were heated at 700°C for 4 hours.[1] Both the upper and lower electrodes were made of the same alloy, in the form of rods 8 mm in diameter and 12 cm in length. Both electrode tips were shaped, according to the same templet, to a blunt-end cone. The source used was an AC arc; 5 amp; 2 mm gap. The spectra were photographed on an ISP-22 spectrograph , with a 20 second exposure without pre-arcing. The spectrograms were processed on an MF-2 microphotometer. The experimental results are shown in the form of curves: Fig. 1 for copper and Fig. 2 for nickel. It will be seen that the intensities of the copper arc lines (Curves 2, 3 & 4) pass through a maximum at a Cu content of 80-85%, whereas the intensity of the spark lines (Curve 1) increases continuously over the entire investigated range of concentrations. The rise in the spark line intensities is particularly rapid in the range of high copper concentrations (80 to 100% Cu content). The relative intensity of the Cu I 3093.99 and Cu I 2492.15 A lines (Curve 5) also exhibits considerable variation, passing through a peak at a Cu concentration of 80-85%.

The variation of the intensity of the arc and spark lines of nickel with the concentration of this metal in the alloy has a number of distinctive features. For example, the slope (tangent) of the initial straight-line portion of the Ni I 3080.76 A arc line curve (Curve 1 in Fig. 2) in the 1 to 8% Ni concentration interval is greater than unity and steeper than the slope of the Ni II 2416.16 A spark line (Curve 2). The increase in "concentrational sensitivity" of the arc and spark nickel lines in the 30 to 80% interval of Ni concentrations is rather interesting. The greatest "concentrational sensitivity" is betrayed by the line

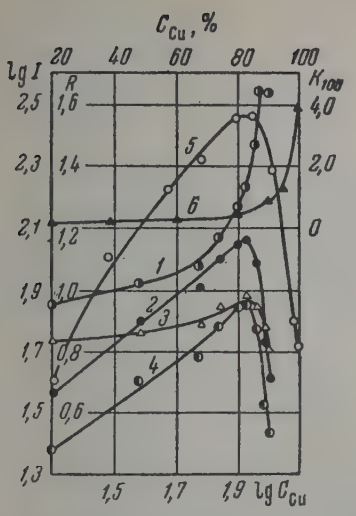

Fig. 1. Variation of the line intensity with the Cu content in alloy: 1) Cu II 2369.89, 2) Cu I 3093.99, 3) Cu I 2492.15, 4) Cu I 3073.8; 5) variation of relative intensity (R) of Cu I 3093.99 & Cu I 2492.15 A lines with the Cu concentration in the alloy; 6) variation of the thermal conductivity coef. K at 100° with the Cu concentration.

pairs in which the comparison line is a spark line of copper.

The observed variation of the relative intensity of the Cu I 3093.99 and Cu I 2492.15 A lines cannot be attributed solely to alterations of the arc temperature. Thus, if we assume the temperature of the copper arc to be 6000°K, the theoretical change in temperature for the 80 to 100% Cu concentration interval computed on the basis of the observed change in the relative intensity of the lines amounts to $\Delta T \approx 6600°$, which is obviously an impossibly high value. It can be shown that the relative intensity R of two homologous arc or spark lines of the same element, having different values of the coefficient b characterizing the self-absorption of the line, will depend on the number N of atoms of the element in the source cloud:

$$R = A \cdot N^{(b_1 - b_2)}.$$

The Cu I 3093.99 and Cu I 2492.15 A conform fairly well with this relationship. Hence Curve 5 of Fig. 1 reflects with reasonable accuracy the variation in the number of copper atoms entering the arc cloud at different concentrations of copper in the alloy. Thus the variation in the intensity of the copper lines in the arc follows the variation in the amount of copper being carried into the arc. It will be noted that for the Cu I 2492.15 A line (Curve 3) the variation is less pronounced than for the Cu I 3093.99 and Cu I 3073.8 A lines (Curves 2 and 4). This is explained by the fact that the 2492.15 A line, ending at the ground level, is more subject to self-absorption. The sharp increase in the intensity of the copper spark lines as the copper concentration is increased from 80 to 100% is apparently connected with an appreciable rise of the discharge temperature in this concentration interval.

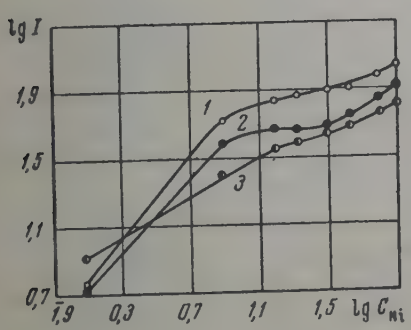

Fig. 2. Variation of intensity of Ni lines with Ni content in the alloy: 1) Ni I 3080.76; 2) Ni II 2416.14; 3) Ni I 3050.82 A.

As in the case of Al-Si alloys[2], the intensity of the Cu and Ni lines is determined to an appreciable extent by the characteristics peculiar to the process of vaporization of the alloy. The characteristics of the vaporization process (i.e., the rate of entry of the Cu-Ni alloy material into the arc) are apparently connected with variations in thermal conductivity of the alloy (see following article). The variation of the thermal conductivity coefficient K at 100°C (taken from Ref. 3) with the copper content of the alloy is shown by Curve 6 (Fig. 1). It will be seen that the thermal conductivity falls off sharply as the Cu content is reduced from 100 to 85%; this leads to more intense heating and, obviously, more rapid vaporization of the alloy in the areas where the arc is concentrated.

In conclusion, we wish to thank V.K.Prokof'ev and S.E.Frish for their interest in the project and valuable advice.

Scientific Research Institute for Chemistry
at Gor'ki State University

References

1. N.S.Kurnakov, Sobranie izbrannykh rabot (Selected Papers), M. 1938.
2. N.K.Rudnevski & G.A.Mukhin, Iav. (Bulletin) AN SSSR, Ser.fiz.,18, 258 (1954).
3. Tekhnicheskaia entsiklopediia, Spravochnik, etc. (Technical encyclopedia, Handbook of physical, chemical and technological data) Pub. "Sovietskaia entsiklopediia", Moscow 1931.

*** *** *** *** *** *** ***

INVESTIGATION OF THE RATE OF ENTRY OF COPPER-NICKEL ALLOYS INTO THE CLOUD OF AN ELECTRIC ARC

- N.K.Rudnevski, A.I.Matiunin & E.S.Obukhova

The amounts of the Cu-Ni alloy and of its constituent elements entering the arc cloud were determined in the following manner. The alloy electrodes, formed with truncated cone tips, were mounted horizontally in a glass vessel. The design of the vessel assured free access of air to the arc and complete collection of the electrode material. The burning of the arc proceeded under conditions analogous to those obtaining in the investigation of the Cu and Ni line intensities (see preceding article). Thanks to convection and diffusion, the electrode material entering the arc was deposited in the form of oxides on the inside walls of the enclosing vessel. To permit averaging results and accumulate a sufficient amount of oxides for purposes of analysis each pair of electrodes was arced a number of times; prior to each burning period the electrodes were re-machined to the initial shape. The deposited oxides were collected and analyzed for copper and nickel content. The copper was determined by the iodometric method, while the nickel was determined by the gravimetric method, based on precipitation of the element by dimethyl glyoxime.

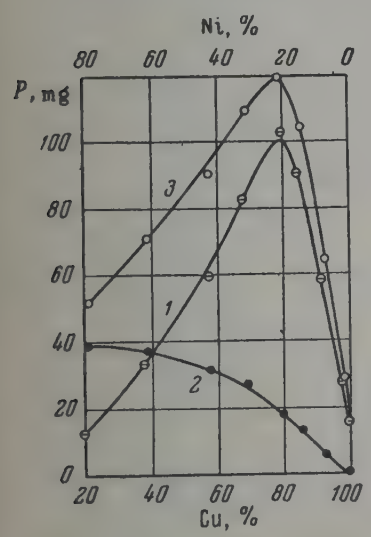

Variation of the amount of alloy and of copper and nickel entering the arc cloud with the composition of the alloy: 1) Cu, 2) Ni, 3) both.

In the accompanying figure curves 1 and 2 characterize the variation of the amounts of Cu and Ni entering the arc cloud with the composition of the alloy. Curve 3 shows the variation of the total amount of material (Cu + Ni). All data are averaged values for 30 arcings. As may be seen from curve 1, the amount of copper entering the arc passes through a maximum at about 80% copper content in the alloy. Then from 80 to 100% copper concentration the amount of copper entering the arc falls off by a factor of about 6.5. The amount of nickel entering the arc, also, is not a linear function of the nickel concentration in the alloy. The curve for the total amount of material brought into the

arc (nickel + copper) exhibits a peak in the vicinity of 20% nickel content. It will be seen that over most of the investigated range the concentration of nickel in the arc cloud does not vary linearly with the nickel concentration in the alloy; only between 1 and 15% nickel does the concentration of nickel in the arc vapor coincide with the nickel concentration in the alloy. In the 15 to 80% range of nickel concentrations in the alloy, the nickel concentration in the arc cloud remains some 5–8% lower than in the alloy. The increased rate of entry of the alloy material (Cu + Ni) when the copper content of the alloy is between 80 and 100% is due to the reduced thermal conductivity of the alloy in this concentration range.

In conclusion, we wish to thank V.K.Prokof'ev for his interest and advice in connection with the investigation.

Scientific Research Institute for Chemistry
at Gor'ki State University

* * * * * * *

THE INFLUENCE OF HEAT TREATMENT ON THE ENTRY OF ALUMINUM-SILICON ALLOYS INTO AN ELECTRIC ARC

– G.A.Mukhin & N.K.Rudnevski

In an earlier report[1] it was shown that the heat treatment (hardening or annealing) to which a binary Al-Si alloy is subjected affects the absolute and relative intensities of the aluminum and silicon lines in an AC arc.

In the present investigation we determined the amount and composition of the alloy material entering the arc after different heat treatments of the alloys. The alloys studied contained 4 to 14% silicon. The heat treatments consisted of a) hardening by heating at 560°C followed by rapid cooling and b) annealing at 340°C for 4 hours followed by slow cooling. To collect the material entering the arc we used the method of electric transfer of the material to carbon counter electrodes with hemispherical tips. Each individual transfer period was 40 sec with a current strength of 5 amperes and an electrode gap of 2.5 mm. To insure averaged values and to obtain sufficient quantities of the deposited oxides for purposes of analysis the process was repeated 30 times, using a new carbon electrode for each run. The oxides were carefully scraped into a porcelain dish and then heated at 1100°C for a sufficient time to burn out the carbon. The residual oxides were weighed and then brought into solution, the SiO_2 content of which was then determined by the photocalorimetric method. Obviously, knowing the combined weight of the oxides and the SiO_2 content, we could readily find the amount of aluminum oxide by subtraction.

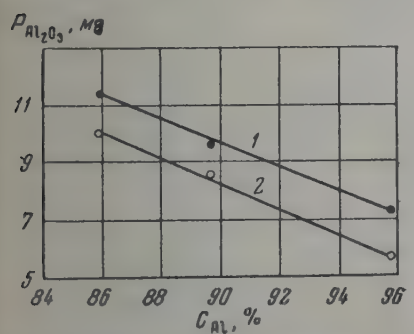

Variation of the amount of Al_2O_3 carried over to the carbon electrode with the aluminum concentration in the alloy: 1) for hardened alloys; 2) for annealed alloys.

The analytic results showed that the total amount of oxides carried to the carbon electrode is greater in the case of hardened alloys; the amount of aluminum oxide transferred to the carbon electrode is also greater in the case of hardened alloys (see figure). It was also established that the concentra-

tion of silicon in the oxides is higher in the case of annealed alloys.

Inasmuch as the oxides are deposited on the carbon electrodes from the arc vapor cloud, it may safely be assumed that composition of the deposits is representative of the composition of the cloud vapor. It may, therefore, be concluded that the amount of aluminum entering the arc cloud is greater for hardened alloys than for annealed Al-Si alloys. The concentration of silicon in the arc cloud, although lower in the case of annealed than in that of hardened alloys, in every case exceeds the Si concentration in the alloy composing the electrode.

The above results help explain the variations in the spectrum of aluminum-silicon alloys observed previously.

"M.I.Kalinin" Plant
and the
Scientific Research Institute for Chemistry
at Gor'ki State University

Reference

1. N.K.Rudnevski & A.K.Zueva, Izv. AN SSSR, Ser.fiz., 12, 4, 416 (1948).

* * * * * * *

APPLICATION OF NOMOGRAPHIC METHODS OF COMPUTATION TO SPECTRUM ANALYSIS

- R.N.Rubenshtein & N.G.Karpel'

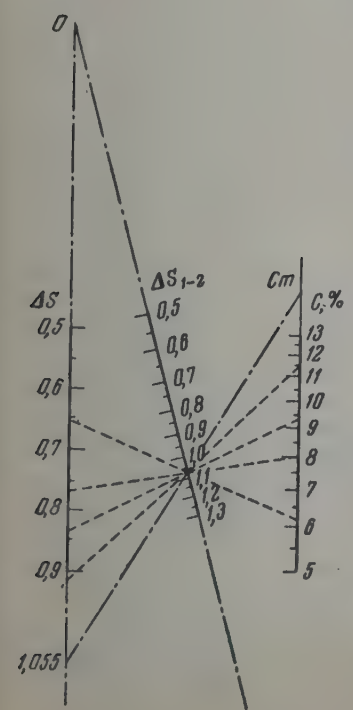

Fig. 1. Calibration curve nomogram

In the region of normal exposures the variation in the difference in blackening S of the compared lines with the concentration C of the analyzed-for element is given by

$$\Delta S = A \log C + B \qquad (1)$$

where A and B are constants.

The nomogram based on this expression, giving the relationship between ΔS and log C, is reproduced in Fig. 1*.

A nomogram of this type can be used for computation when employing the method of three standards, the method of a single standard, the method of two spectrum lines, the method of a constant calibration curve with a varying conversion factor or the method of a control standard.

To allow calculations in the region of under-exposures we have constructed the universal nomogram of Fig. 2, based on the equation for the full characteristic curve of photographic emulsions:

$$\log I = \frac{S}{\gamma} - q \cdot \varphi (S), \qquad (2)$$

where γ and q are parameters characterizing the photographic emulsion in the given spectral region and $\varphi(S)$ is a universal blackening function.

---

* The nomogram is based on data taken from V.K.Prokof'ev, "Fotograficheskie metody kolichestvennogo spektral'nogo analiza metallov i splavov" (Photographic methods of quantitative analysis of metals and alloys). Vol.II, p.155. M.-L.1953.

This nomogram makes it possible to determine the following without the need for plotting the characteristic curve of the plates in the region of under-exposures:

a) the logarithm of the intensity of the sought analytic line from the degree of blackening of three lines (S_1, S_2 and S_3) or from the blackenings corresponding to three steps of a step-weakener, having a known ratio of transmission coefficients;

b) the logarithm of the concentration of the analyzed-for substance on the basis of three standards having known concentrations directly (without intermediate determination of the respective intensities);

c) the absolute values of the intensity of the background or of superposed lines.

A simple computation chart-board can readily be constructed on the basis of the nomogram of Fig. 2; a logarithmic slide rule built into the chart-board would permit of taking account of the background or superposed lines without recourse to special tables.

Similar nomographic procedures can also be applied to determining the wavelength of an analytic line both in the case of narrow wavelength ranges in which linear interpolation is allowable and in the case of a wide interval, where the dispersion curve must be regarded as parabolic.

Calculations with the aid of the described nomograms have shown that the use of nomographic methods is practical, simple and efficient. It is particularly worthwhile in plant laboratories performing a large number of routine analyses.

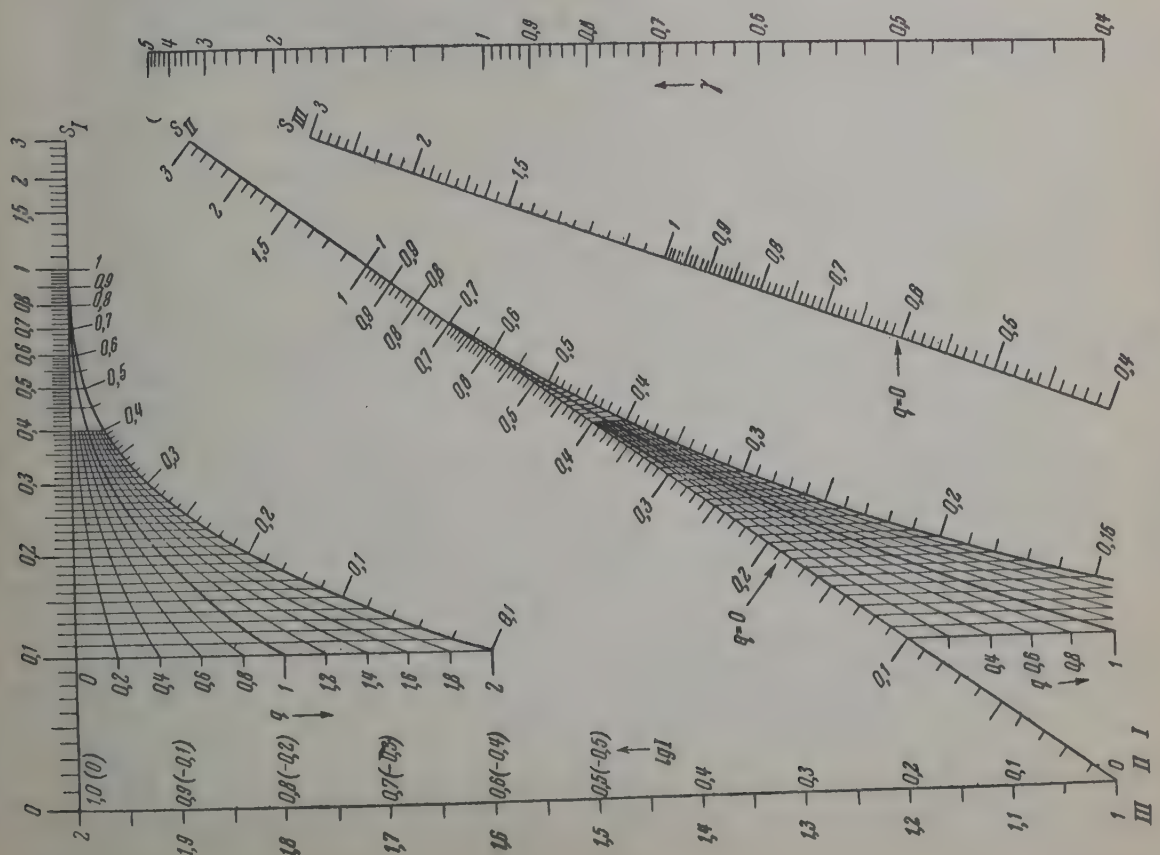

Fig. 2. Nomogram for calculations in the region of underexposures.

* * * * * * *

STATISTICAL INVESTIGATION OF THE ACCURACY OF SPECTROGRAPHIC ANALYSIS OF CARBON STEELS

- K.I.Ionova & V.V.Nalimov

Applying statistical methods to the results of spectrographic analyses of twenty grading-type 2 kg samples of carbon steel we investigated the following errors: e_{pho} - the photometry error, e_{pl} - the plate error, $e_{s\&i}$ - the error due to the source and inhomogeneity of the sample, e_{cc} - the error connected with plotting and using the calibration curves, e_{ps} - the error due to the physical state peculiar to the sample and e_{tot} - the total or overall error, equal to

$$e_{tot} = \sqrt{\frac{e_{pho}^2}{n} + \frac{e_{pl}^2}{n} + \frac{e_{s\&i}^2}{n} + e_{cc}^2 + e_{ps}^2}$$

where n is the number of spectrograms on which the analytic results are based.

The spectrographic analysis was effected in a spark discharge (IG-2 generator employing a Raiski circuit) for Si, Mn and Cu and in an arc (DG-1 and Tekhsnab AN SSSR generators) for Si, Mn, Cr and Ni. The analytic line pairs recommended in the literature were employed.

The results showed that e_{pho} = 1.6% and e_{pl} = 1.13-1.55% for a line separation of 0.20 mm and that e_{pl} = 3.09-2.62% for lines 2.8 to 1.4 mm apart. (Plates - Spectral, Types I and II).

The magnitude of $e_{s\&i}$ was determined for different pre-arcing (pre-sparking) and exposure times with a view to selecting the optimum conditions. To indicate the dependence of $e_{s\&i}$ on t_{pre} and t_{ex} we can cite the following data: 1) in the arc, with t_{pre} = 0 and t_{ex} = 7 sec, $e_{s\&i}$ = 5-9%, while with t_{pre} = 0 and t_{ex} = = 20 sec, $e_{s\&i}$ = 3.6-6.0%; in the spark, with t_{pre} = 20 and t_{ex} = 10 sec, $e_{s\&i}$ = = 4.0-4.8%, while with t_{pre} = 60 and t_{ex} = 60 sec, $e_{s\&i}$ = 2.5-4.4%. Analysis of the deviations (reproducibility) shows that even under the most favorable conditions 50-70% of the total error is due to $e_{s\&i}$.

The magnitude of e_{ps} fluctuates between 1.7 and 5% for different elements and line pairs. We also found that there is some liquation on the surface of the cast samples; this separation and segregation of the elements results in a difference between the superficial and interior regions of the sample which leads to an error on the order of 5-8%.

Under favorable conditions when using the control standard method one can obtain the following minimal values for e_{cc}: in the arc (DG-1 generator) 1.5% for Mn and 5% for Si; in the spark 5.5% for Si, 4.3% for Mn and 6.1% for Cu. The three-standards method, when $\log C_1 - \log C_2 = 0.7-1.0$ for the two end standards, yields more accurate results; however, this method is too slow and cumbersome for general plant laboratory practice.

If the control standard method is employed and the analytic result is taken as the average of four spectrograms, the overall error, e_{tot}, varies between 4.0 and 7.0%, with 50 to 70% of this being attributable to e_{cc} and e_{ps}. With the three-standards method, e_{tot} = 4.5-4.7%, again with 50-70% of the total error being due to e_{cc} and e_{ps}.

On the basis of the results of our analysis we submit that spectroscopic analysis can be used for determining the Mn, Si, Cr, Ni and Cu content of carbon (non-alloy) steels for grading purposes. Given proper selection of the exposure and discharge conditions, the accuracy of the spectrographic analysis is not inferior to that of routine chemical grading analysis. Nevertheless, it must be noted that if the permissible error specified in GOST All-Union State Standard

2331-41 is interpreted as being equal to 3 e where e is our e_{tot}, spectrographic analysis cannot meet the GOST requirements. However, if the allowable error specified in the Standard is assumed to be equal to 3 e, routine grading chemical analysis also fails to meet the GOST requirements; in fact, where the accuracy in determining Si is concerned, under this interpretation even the high-accuracy analysis used in preparing standard samples does not satisfy the GOST requirements.

Kazakh Metallurgical Institute

* * * * * * *

INVESTIGATION OF THE PHOTOMETRIC PROPERTIES OF "SPECTRAL" PHOTOGRAPHIC PLATES TYPES I, II AND III PRODUCED BY PLANT No. 2

- A.A.Frishberg

In the present study we investigated the dependence of gamma on the wavelength of the incident light, determined the point of the beginning of the region of normal blackening (i.e., the beginning of the straight-line portion of the characteristic curve) and the micro- and macro-inhomogeneity of the emulsion of "Spectral" Type I, II and III plates.

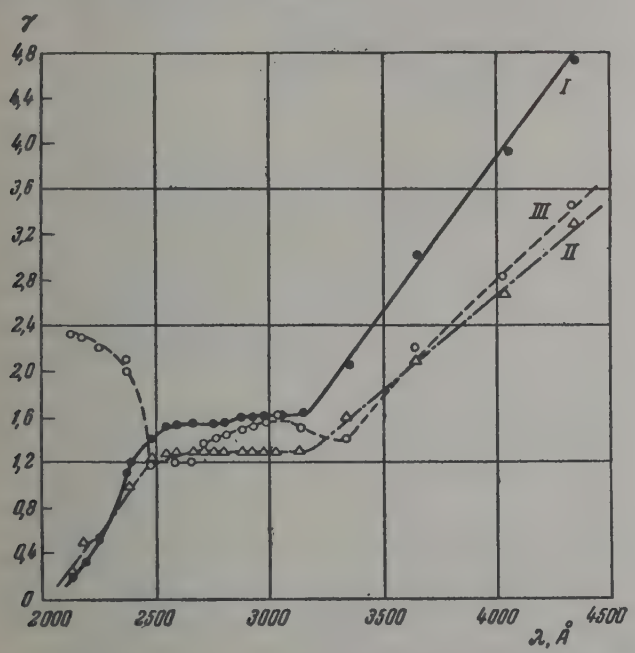

Variation of gamma (γ) with the wavelength of "Spectral" Type I, II and III plates.

The gamma was determined from the slope of the straight-line portion of the characteristic curve, plotted for equal times of exposure. The calibration marks were imposed by means of standard wire-gauze screens and a platinum step weakener. The light sources were a PRK-5 mercury tube and a condensed spark, operated in a stabilized circuit. The light discriminator was an ISP-22 spectrograph.

The plates were developed in standard No. 1 developer with continuous agitation. The developing time was 4 minutes, insuring gamma values close to the maximum. In all we obtained 520 characteristic curves for 21 different wavelengths in the range from 2100 to 4400 A. The diagram showing the variation of gamma with the wavelength for the three types of plates is reproduced in the figure. It will be seen that the curves for Type I and Type II plates have a horizontal section in the 2500 to 3100 A interval.

Examination of the characteristic curves obtained shows that in the 2500 to 3300 A region the normal blackening section begins at S = 0.4-0.5 for plates of Types I and II and at S = 0.7-0.8 for plates of Type III. The region of "over-exposure" for the Spectral plates put out by Plant No. 2 begins at blackenings exceeding S = 3.

For investigating the macro-inhomogeneity, the plates were uniformly exposed to visible light in one series of tests and to ultraviolet (2536 A) in another series. The blackening was approximately the same over the entire exposed surface and lay within the region of normal blackening at all points. The densities of individual areas were measured with a recording microphotometer. The resultant photograms showed that the macro-inhomogeneity is independent of the wavelength but differs for plates of the different types. The macro-inhomogeneity is most pronounced in the case of Type I plates, attaining an average deviation of 0.05 relative to the mean. All the plates are acceptable for spectrographic use only over the area 1 cm in from the edges.

The micro-inhomogeneity of Type I plates is such as to introduce an error of up to 0.8-1.0% in the spectrographically determined value of the concentration; the micro-inhomogeneity of Type II plates may introduce an error of 1.5-2.0%; that of Type III plates, an error of 2.0-2.5%.

In conclusion I want to thank S.L.Mandel'stam and S.M.Raiski for their advice and aid in the investigation.

Commission on Spectroscopy at the
OFMN of the USSR Academy of Sciences

* * * * * * *

EVALUATION OF THE ERRORS ARISING IN DIFFERENT PARTS OF THE SPECTRO-ANALYTIC PROCESS

- E.L.Grinzaid

The dispersion of the results of spectrographic analysis generally conforms to the normal distribution law. However, we know of only a few investigations[1,2] in which the relative importance of the various sources of error has been determined experimentally. Moreover, the methods of dividing or classifying the deviations used in these investigations are unduly complicated, while the results arrived at are somewhat contradictory and cannot be applied directly under our usual analytic conditions.

In the present investigation we shall limit ourselves to dividing the entire spectro-analytic process into two parts or "links": 1) the emission of the source and 2) reception of the radiation emitted, which we will hereinafter term the "photolink". The photolink will be understood to comprise both the photography and the photometry.

The dispersion of the analytic results due solely to the instability of the emission can be characterized by the root mean square deviation σ_e — the emission error. Analogously, the dispersion of results originating in the photolink can be characterized by σ_p - the photo error.

The emission error may be said to reflect the joint influence of inhomogeneity of the sample, non-uniformity of vaporization and variation in the excitation conditions. The photo error comprises errors due to inhomogeneity of the emulsion, non-uniformity of development and errors in photometry.

The total or overall error σ_t of analysis, in this case, equals

$$\sigma_t = \sqrt{\sigma_e^2 - \sigma_p^2}.$$

To determine the proportions of the total error attributable to the emission

error and to the photo error we employed the method of double photometry[3] in height in conjunction with a simplified statistical processing procedure (control of the range of variation). This method of dividing the total error into its two components (σ_e and σ_p) was applied to spectroscopic analyses of tool steel and primary aluminum (see table). (The analytic procedures employed differed little from those recommended by the agencies preparing steel and aluminum standard samples: LSO -- Laboratory of Standard Samples and VAMI -- All-Union Aluminum-Magnesium Institute.)

Mean root square errors (% rel) in analyses of aluminum and steel

Aluminum						Steel					
Si 2516 / Al 2669			Fe 2598 / Al 2669			V 3063 / Fe 3062			Cr 2792 / Fe 2794		
σ_t	σ_e	σ_p	σ_t	σ_e	σ_p	σ_t	σ_e	σ_p	σ_t	σ_e	σ_p
5.5	3.1	4.7	3.3	2.0	2.7	3.3	3.0	1.5	2.0	1.4	1.4

The table shows that it is feasible to identify the weak "link" where reproducibility of the spectrographic analysis is concerned. Thus it can be seen that in determining vanadium in steel the reproducibility can be enhanced only by improving the stability of the source. In analyses for silicon in aluminum, on the other hand, it is necessary to give priority to reducing the photo error.

In practice there are cases when the disparity between the two error components is even greater than in the cases characterized in the table. When the ratio of their magnitudes exceeds 2, the smaller of the components can be safely neglected.

In a large number of measurements made by the writer, σ_p never fell below 1.5-2.0%; not over 1% of this can be attributed to errors in photometry. Hence when the total error in spectrographic determinations approaches 1.5-2.0%, further improvement of the reproducibility can be attained only through reducing the error in the photolink.

Department of Analytic Chemistry of
"M.I.Kalinin" Leningrad Polytechnical Institute

References

1. R.A.Sawyer, Eksperimental'naia spektroskopiia M. 1953 (Experimental Spectroscopy - N.Y. 1944.

2. H.Shirley, E.Elliott & J.Meeds, J. Iron & Steel Inst., 157, 391 (1947).

3. E.L.Grinzaid, Rol' fotograficheskogo zvena v rasseianii rezultatov spektral'nogo analiza (The role of the photographic link in the dispersion of the results of spectrum analysis). LDNTP Information pamphlet No. 59, June 1954.

* * * * * * *

REPRODUCIBILITY OF SPECTRUM LINE INTENSITIES IN ACTIVATED AC ARCS

- V.P.Borzov & N.S.Sventitski

The reproducibility of the emitted line intensities is one of the important characteristics of radiation sources for spectrum analysis. The reproducibility should be evaluated by repeated measurement of the spectrum of the same substance. In order not to complicate the evaluation by having to take into account the influence of the composition of the electrodes and differences in the superficial processes on them, it is preferable to use copper electrodes in all cases. As a criterion of the stability of the excitation conditions one may take the resultant error in a nominal analysis effected according to the intensities of lines characteristic of different excitations, for example, Cu I 2492.15 and Cu II 2489.65 A.

Experience shows that the error in determining an admixture element in actual spectrum analyses is often nearly equal to the error in such a nominal analysis and that when a change in the excitation conditions produces an appreciable increase or decrease in the nominal analysis error, the error in the actual determination changes accordingly. This is illustrated by the results of analyses of samples of AL-2 aluminum alloy. Thus, in the case when the probable deviation of the nominal analysis equalled ±1.8%, the probable errors in determining the admixtures in the AL-2 alloy were ±1.7% for Si and 2.5% for Fe. When the excitation conditions were modified for the worse to bring the probable error of the nominal analysis up to ±9.7%, the probable deviations for Si and Fe increased to ±8.4 and ±9.2% respectively.

We investigated the reproducibility characteristics of several types of AC arc generators: standard model PS-39 generators, a DG-1, a new PS-39 model generator with an improved discharger and a generator prototype with electronic firing (developed by I.V.Podmoshenski). The old series (1947-1948) PS-39 generators had a poor reproducibility (deviations up to 12%). However, certain modifications, designed to stabilize the process of spark-formation in the discharger, reduced the nominal analysis error appreciably.* The results of the reproducibility evaluation tests are summarized in the accompanying table.

Generator type	Operating characteristics	Probable error of nominal analysis, %
PS-39 original	5 amp current	7.9
PS-39 modified*	same	3.0
PS-39 improved (new prototype)	5 amp current	1.4
	2 amp current	1.4
	5 amp, interrupted arc	2.3
New generator with electronic firing device	5 amp, long flashes	1.6
	5 amp, short flashes	1.5
	2 amp	1.6
	5 amp, interrupted arc	2.0
DG-1 generator	5 amp current	2.7
	2 amp current	1.6

These results show that an AC arc does assure the requisite reproducibility of line intensities and hence can safely be used as a source in quantitative spectrum analysis.

*See "Nekotorye priemy regulirovki i kontrolia raboty generatorov aktivizirovannoi dugi peremennogo toka dlia spektral'nogo analiza" (Certain techniques for regulating and controlling the operation of activated AC arc generators for spectrum analysis). LDNTP Information pamphlet No. 98 (243) Leningrad 1950.

* * * * * * *

ON THE ACTUAL VALUE OF THE REABSORPTION COEFFICIENT b IN CONDENSED SPARK SPECTRA

- I.S.Fishman

The reabsorption coefficient b can, in principle, be determined experimentally from the slope of the calibration curves plotted in terms of ΔS *vs* log C. In order to obtain the true value of the coefficient, however, it is necessary to eliminate the influence on the slope of the curve of the following factors: the vaporization, the spectrum background, the gamma of the photographic plate and the dilution of the host material of the sample. The effect of the last three can be allowed for by using appropriate, experimentally determined correction factors. The influence of the vaporization factor can be minimized by satisfying certain conditions where excitation of the spectra is concerned, namely,

a) limiting the concentrations to a range in which the physical properties of the alloy (sample) remain unaltered;

b) selecting a set of standards having uniform properties and similar "overlapping" characteristics of their spectra;

c) photographing the spectrum in the stable region of the "sparking curve" (i.e. after "sparking-off").

The reabsorption coefficient may be characterized by the expression

$$b = \frac{\tan \alpha_b}{\gamma k \beta},$$

where $\tan \alpha_b$ is the angular coefficient of the characteristic curve; γ is the contrast (gamma) of the photographic plate (we determined the gamma from the spectrum photographed with a nine-step weakener, after introducing certain necessary corrections for non-uniformity of illumination of the spectrograph slit), β is a factor taking into account the dilution of the host material (it is given by $\beta = 1 + (C/C_{host})$, where C is the concentration of the determined element and C_{host} is the concentration of the principal element in the alloy); and k is a factor taking into account the spectrum background, which can be computed by means of the following equation[1]:

$$k = \frac{I_\ell}{I_\ell + I_b} = 1 - 10^{-\Delta S^*/\gamma},$$

here $\Delta S^* = S^*_{\ell+b} - S^*_b$, where $S^*_{\ell+b}$ and S^*_b are so-called converted blackening values[2] of the line plus background and of the background, found from the amount of blackening determined in the conventional manner.

For the purpose of determining the value of b experimentally, we# photographed the spectra of the standards a number of times on the same plate together with the additional spectra, required for determining the values of k and γ.

The results obtained for 13 analytic lines of different elements in two alloys (low-alloy steel and duraluminum) are summarized in the table. Each value represents the average of 2-4 independent determinations. The reproducibility of the analytic results is ± 0.02. In the last column we list the excitation potentials of the lower level associated with the given line. It may be tentatively concluded from the table that with the conventional method of exciting the spectrum by a condensed spark in air the reabsorption coefficient for lines ending at an excited or metastable level is close to unity, while for lines associated with transitions to the ground level the coefficient is less than unity.

The above results were utilized for further development of our idea of using standard calibration curves for spectroscopic analysis. Thus, assuming that

---

V.M.Zimin participated in the experimental work.

Values of the reabsorption coefficient b

Alloy	Analytic line	Reabsorp. coef. b	Excitation potential of lower level
Steel	Cr 2677,1	0,96	Not determined
	Ni I 3101,55/87	0,99	0,12/0,43
	Ni I 3414,76	0,59	0
	Si I 2516,1	0,90	0
	Mn 2939,3	1,02	Not determined
Dural	Cu II 2369,89	1,03	0,52
	Mg I 2852,1	0,69	0
	Mg 2779,83	1,0	Not determined
	Fe II 2599,39	0,97	0
	Fe II 2749,3	0,92	1,08
	Si I 2516,1	0,75	0
	Mn 2939,3	0,94	Not determined
	Mn II 2593,7	0,81	0

b = 1 for lines with excited or metastable lower levels and having determined the values of k and γ from photographs of spectra on a test plate, one can calculate the angular coefficient of the calibration curve in the conventional ΔS *vs* log C coordinates by means of the equation

$$\tan \alpha_b' = k'\gamma'\varrho' b.$$

The procedure for plotting the calibration curve on the basis of the determined angular coefficient and its subsequent use for analysis follow from the general operating technique when using the control standard method[3]; the value of $\Delta S_{1,2}$, needed to take into account the specific characteristics of the photographic plates employed, can readily be found by photometry of appropriate line pairs in the spectra of the sample or the control standard, photographed on the same plate.

The earlier described procedure for plotting and using standard calibration curves[4] remains valid for lines associated with transitions to the ground level; in this connection it is still essential to take into account the absolute intensity of the analytic lines, which we accomplished by means of the so-called "standard arc" [an AC arc between Cu electrodes of specified dimensions].

References

1. V.M.Zimin & I.S.Fishman, Uchenye zapiski KGU (Scientific Records of Kiev State University), 113. 9, 155 (1953).
2. I.S.Fishman, Ibid, p. 137.
3. I.S.Fishman, Zavod. labor. (The Plant Laboratory) 9, 1106 (1951).
4. I.S.Fishman, Izv. (Bulletin) AN SSSR, Ser. fiz., 18, 269 (1954).

* * * * * * *

ON THE NATURE OF THE SPARKING-OFF EFFECT IN SPECTRUM ANALYSIS OF METAL ALLOYS

- E.S.Kudelia

The entry of the component materials of the sample into the luminous cloud of a spark discharge is an extremely complex physical-chemical process. A number of different effects are closely associated with this process; these include the sparking-off effect, the influence of structure and the effect of third components.

There are many, diverse opinions regarding the nature and relative importance of these effects. Currently many investigators have favored Filimonov's theory, according to which the predominant role in all phenomena associated with sparking-off is played by oxidation-reduction reactions proceeding in the surface layer of the sample and at the metal-luminous cloud boundary. However, this theory fails to explain many well-known facts such as the absence of sparking-off effect and of the influence of structure when the sample is preheated to 1000-1100°C, the ap-

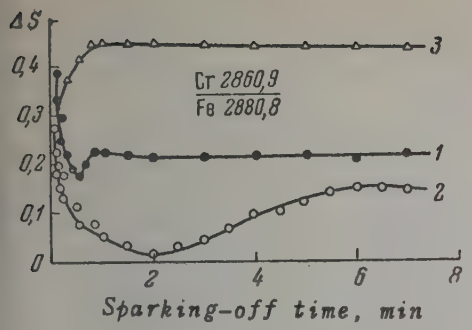

Sparking-off curves, obtained 1) under ordinary conditions, 2) after cooling the sample (the sparking-off is extended in time), 3) after heating the sample (the initial portion of the curve is characterized by an increase in relative intensity, due to weakening of the comparison line). To prevent overlap the curves are shifted along the S axis.

preciable weakening of the effect of third components in the case of such preheating, effect of the mass of the sample on the intensity of the spectrum lines, the presence of maxima and minima in the sparking-off (line intensity *vs* time) curves, etc.

Yet all the effects accompanying the play of the spark over the electrodes during the unstable sparking interval (i.e., the phenomena referred to collectively as the sparking-off effect) can readily be explained if we regard them as deriving from two processes: 1) selective oxidation of the elements in the thin surface layer and 2) diffusion of the elements from the interior to the surface of the sample (specifically, the rates of diffusion of the various components). From this point of view the sparking-off effect can be explained by the difference between the rate of "consumption" of the element as a result of oxidation in the surface layer and the rate of its diffusion to the surface from the depths of the sample. The influence of structure is explained by predominance of diffusion along the boundaries over volumetric diffusion and the effect of third components, by their influence on the rate of diffusion of the determined element and their general diluent action.

Confirmation of the diffusional nature of the phenomena accompanying sparking-off is furnished by the results of experiments in which the rate of diffusion was slowed and speeded up by altering the temperature (cooling the sample in liquid oxygen in one case and preheating to 1200° C in the other). The curves for chromium in steel obtained under these different conditions are shown in the accompanying figure.

The writer recommends the following measures for minimizing the sparking-off effect: 1) the use of high-frequency sources combining a relatively low consumption of the electrode material with rapid heating of the surface layers (the rapid heating accelerates the diffusion in the surface layer with the result that equilibrium between the consumption and the rate of "supply" of the analytic elements in the superficial reaction zone is established more quickly); 2) the use of powerful pulsed sources with localization of the discharge by means of insulating bushings and similar devices ; 3) heating the samples to just below the melting point (by induction heating, for example) which has the effect of greatly increasing the rate of diffusion of the components.

The application of the recommended measures in conjunction with the procedure for taking account of diluent action of third components developed by Sorokina[1] should make it possible to reduce the number of spectroscopic standards well below the total now prepared and stocked.

"E.O.Paton" Electric Welding Institute
of the Academy of Sciences of the Ukranian SSR

Reference

1. N.N.Sorokina, Izv. (Bulletin) AN SSSR, Ser. fiz., 18, 277 (1954).

* * * * * * *

ON TAKING INTO ACCOUNT THE BACKGROUND IN MEASURING THE INTENSITY OF SPECTRUM LINES BY THE PHOTOGRAPHIC METHOD

- S.A.Shipitsyn

In spectroscopic practice it is customary to take into account the properties of the photographic plates by imposing blackening marks and plotting a characteristic curve converting densities into intensity values. It is open to question whether this procedure wholly eliminates the influence of the photographic process in cases when the background densities of the spectrogram and of the blackening calibration marks are different. This is no reason to assume that allowing for the background on the basis of $I_{l+b} = I_l + I_b$ (where I_l = the intensity of the line and I_b that of the background) as determined by photometry will necessarily yield the true value of I_l, since the separate effects of light of intensities I_l and I_b need not be exactly equivalent to the effect of light of intensity I_{l+b}.

We checked this experimentally. We designed a special set-up for illuminating the slit by two sources so as to obtain simultaneously on one spectrogram blackenings S_{l+b}, S_l and S_b. The line spectrum source used was an arc, mounted in line with the optical axis of the Hilger Model E-492 large spectrograph. The light of the arc was thrown by a condenser on an intermediate diaphragm which had two horizontal slits, each 7 mm long and 1 mm wide, located 4 mm one above the other. The lower slit was unobstructed, while the upper was blocked by a mirror, set at 45° to the plane of the diaphragm. This mirror received light from an incandescent bulb and reflected it through the upper slit to the entry slit of the spectrograph (see figure).

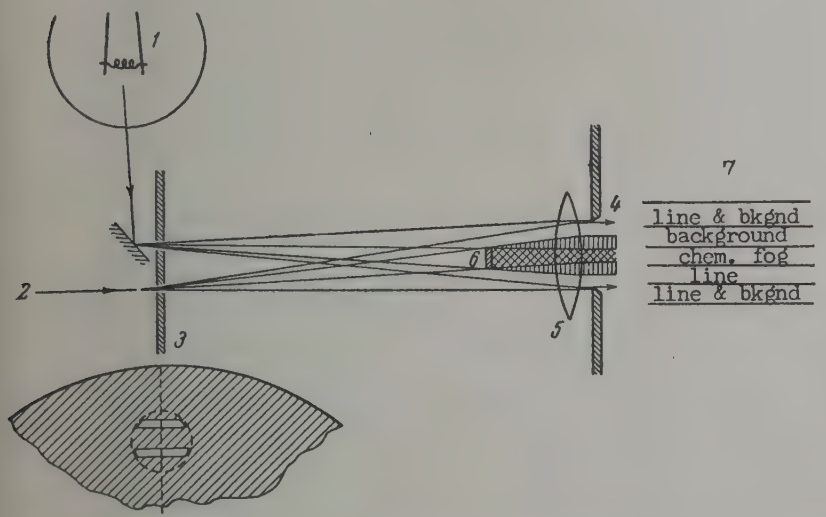

Illumination of the slit by two sources: 1) continuum source, 2) light from arc, 3) slit diaphragm, 4) entry slit of spectrograph, 5) lens forming image of diaphragm 3 in the plane of the collimator slit, 6) wedge-shaped shield, 7) pattern of spectrum strips obtained.

A special wedge-shaped shield mounted in front of the slit blocked out part of the beams making it possible to photograph separately the background (i.e., the continuum emitted by the incandescent bulb), the background + the lines and the line spectrum; in addition a strip of the plate remained unexposed.

The intensities of the background areas and lines were measured by means of a photometer with reference to characteristic curves plotted on the basis of a line spectrum photographed through a step weakener disk.

All characteristic curves were adjusted to bring the inertia point over $\log I = 1$. This procedure made it possible to make direct comparison between intensity measurements obtained from different plates and facilitated development of a graphic method for taking the background into account.

It was found that when the background is strong and the line intensities are moderately high, photometric measurements give $I_{l+b} < I_l + I_b$. The difference in some cases amounts to as much as 35–40%. It is possible that the density of the l+b area is reduced as a result of increased bromine concentration in the region of intensive development (the Eberhard effect).

On the other hand, in the case of a low density background and weak lines, we have $I_{l+b} > I_l + I_b$. Among other possible explanations, it has been suggested that the difference in this case may be connected with the role of sublatent-image centers forming in the emulsion.

From calibration curves plotted for the Cu 5105.54 A line it was established that the slope of the curve is less steep in the case of a heavier background (the background, in this case, was determined as $I_b = I_{l+b} - I_l$).

To facilitate correction for the background we plotted curves, based on the experimental data, in log I_l vs log I_{l+b} coordinates for different background levels. Such curves – "iso-backgrounds" – permit graphic conversion directly from log I_{l+b} to I_l once the background density is determined. The investigations were carried out in the visible region of the spectrum, using iso-ortho plates.

"A. A. Zhdanov" Irkutsk State University

* * * * * * *

As mentioned in the prefatory note in the preceding issue (No. 6, Vol. 18), the reports on emission analysis, presented at Section III of the Ninth All-Union Conference on Spectroscopy, will be continued in the next issue of the Bulletin (No. 2, Vol. 19). Translation Editor.

COLUMBIA TECHNICAL TRANSLATIONS
5 VERMONT AVENUE
WHITE PLAINS, N. Y.

BULLETIN of the Academy of Sciences of the USSR - Physical Series

Vol. 19, No. 1, 1955 - Conference on Spectroscopy (Tartu, 1954)

(Continued from Vol. 18, No. 6)

TABLE OF CONTENTS

	Page Orig.	Trans.
The role of cascade transitions in the excitation of spectral lines - S.E.Frish & I.P.Zapesochnyi	5	1
Ratio of line intensities in the visible triplet of mercury - V.V.Lebedeva & V.A.Fabrikant	7	2
Determining the oscillator strengths (f-numbers) in the spectra of iron and nickel - G.F.Parchevski & N.P.Penkin	8	4
Diagram of periodic system of atomic ionization potentials - A.A.Dibrova	10	6
On conditions under which Kirchhoff's law is applicable to the radiation of the plasma of a gas discharge - S.L.Mandel'shtam & N.K.Sukhodrev	11	7
Optical determination of changes in the density and composition of vapor mixtures in a discharge gap - A.M.Shukhtin	15	10
On determining the concentration of excited mercury atoms in discharges in a mixture of mercury vapor with inert gases - N.P.Penkin & M.N. Palladin	16	12
Spectroscopic investigation of high-frequency discharges in gases and in a flame at atmospheric pressure - V.S.Rossikhin & I.L.Tsikora	18	14
Investigation of the distribution of molecules over the vibrational states in a glow discharge - T.N.Popova & N.A.Prilezhaeva	20	15
Determining the dissociation energy of SrO, CaO and MgO from the intensity of the resonance lines of the metal atoms in flame spectra - I.V.Veits, L.V.Gurvich & V.V.Korobov	21	16
Spectrometry of some early-stage stars - M.V.Dolidze	23	18
On the applicability of statistical theory to pressure and Doppler broadening of spectrum lines - I.I.Sobel'man	24	19
Calibration curves and the breadth of spectrum lines in an AC arc discharge - I.M.Nagibina	25	20
Investigation of the shape and breadth of spectrum lines in DC arcs - V.F.Kitaeva	27	22
The effect of self-absorption on the intensity of spectrum lines in a DC arc - V.S.Mel'chenko	30	24
Hyperfine structure of the spectrum lines and the nuclear spins of U^{233} and Pu^{239} - L.A.Korostyleva, A.R.Striganov & N.M.Iashin	31	26
Isotope shift in the spectrum of plutonium - A.R.Striganov, L.A.Korostyleva & Iu.P.Dontsov	34	28
The effect of light from a mercury arc on the emission of a flame - S.M.Kishko & V.S.Miliianchuk	19	29
Diffraction grating replicas - A.A.Nizhin & F.Z.Pedos	35	32
Atlas of spectrum lines for glass prism spectrographs - S.K.Kalinin	42	33
Some characteristics of low-voltage pulse discharges - D.B.Gurevich, R.A.Esin & V.K.Prokof'ev	64	34
The DFS-2 and DFS-3 diffraction grating spectrographs - R.I.Tveriankina	28	36
A photoelectric spectrograph for quantitative spectrum analysis - I.V.Podmoshenski & L.D.Kondrasheva	36	37
Use of an electrometer with a dynamic capacitor for recording spectra - L.P.Maliavkin & I.S.Abramson	40	38
The use of a high flux monochromator in conjunction with photoelectric recording in Raman spectroscopy - Ia.S.Bobovich & D.B.Gurevich	48	41

	Page Orig.	Trans.
The ST-7 Steelometer - E.L.Berman	38	42
Atlas of arc and spark spectra of the elements (2100-6600 A) - A.K.Rusanov, E.V.Gusiatskaia & N.V.Il'iasova	44	45
Photoelectric recording instruments - T.K.Fal'k	45	46
The IKS-11 and IKS-6 infrared spectrometers - L.V.Smirnova	52	48
Certain operating characteristics of photoelectric spectrum scanning equipment - I.S.Abramson & A.N.Mogilevski	49	48
A method of recording rapidly varying processes by means of inertia receivers - A.M.Bonch-Bruevich & Ia.I.Imas	54	52
The SF-2m recording spectrophotometer - V.N.Osipova	55	53
The MF-4 recording microphotometer - G.Ia.Kossov	56	54
Vaporization of metal electrodes in a DC arc - G.P.Skorniakov	57	55
Further results of photoelectric investigation of spark spectra - S.L.Mandel'shtam & I.P.Tindo	60	57
Investigation of the instantaneous brightness of pulse discharge in inert gases - K.S.Vul'fson, I.Sh.Libin & F.A.Charnaia	61	58
Influence of the chemical composition of the electrodes and the discharge conditions on the relative rate of volatilization - G.E.Zolotukhin	67	61
On the kinetics of vaporization in an electric arc - Ia.D.Raikhbaum	70	64
The use of pulse discharges for spectrum analysis of gas mixtures - O.P.Bochkova & E.Ia.Shreider	75	66
New methods of using multiplex etalons in high resolution spectroscopy - F.A.Korolev	78	67
Excitation of spectra by electric discharges in a liquid medium - N.S.Sventitski & K.I.Taganov	77	69
Dielectric mirrors and their use in Fabry-Perot etalons - F.A.Korolev & V.V.Sukhanovski	79	70
A two-prism dispersing system with an intermediate mirror - B.A.Shapochnik	82	72
Investigation of high-current pulsed arcs - M.E.Britske	58	73
Investigation of the temperature of the spark produced by a metal-hardening spark generator - A.N.Liulichev & L.S.Palatnik	66	76
The vacuum fluorite spectrograph, photographic emulsions for it and some experimental results obtained with the instrument - A.V.Iakovleva, I.I.Gromova & I.R.Protas	84	77
A vacuum fluorite monochromator - S.A.Kulikov & A.V.Iakovleva	86	79
A new high radiance hydrogen discharge tube - I.I.Kondilenko & M.P.Lisitsa	87	81
An electronically controlled low-voltage arc and spark generator - M.I.Demidov, N.N.Ogurtsova & I.V.Podmoshenski	72	82
Investigation of the spark regimes of the DG-1 generator - G.A.Soboleva	74	83
The ISP-67 high-dispersion and high-resolution spectrograph - A.I.Ryskin	81	85
Spectroscopic analysis of slags (survey) - N.V.Buianov	89	86
Methods of spectrochemical analysis of open-hearth slags for all basic components - O.I.Nikitina	94	91
Spectroscopic analysis of slags using fusing agents - E.N.Lesnikova	97	94
Quantitative spectrum analysis of the raw material and clinker used in the production of cement - T.K.Massil'on	98	95
Quantitative spectrographic analysis of cements and raw materials - Z.A.Kel'tseva	100	97
Quantitative spectrum analysis of magnesite and magnesite refractory materials - G.A.Pedan	102	98
Spectrum analysis of alumina - L.V.Drutskaia	103	99
Spectrum analysis of magnesite and open hearth-bottom material - A.E.Noshchenko	104	101

	Page Orig.	Trans.
Variation of thermal excitation conditions in arc spectrum analysis of ores and minerals - A.K.Rusanov	106	102
Influence of composition on the accuracy of spectrum analysis of ores - V.V.Nedler	113	108
On the absolute sensitivity in determining rare-earth metals - T.N.Zhigalovskaia	115	109
A semi-quantitative spectroscopic procedure for determining 40-50 elements in rocks and minerals - V.V.Khokhlov, V.N.Protopopov, L.I.Denisenko, E.Ia.Smirnova & Z.G.Timonina	115	110
Approximate quantitative spectrum analysis of minerals - M.M.Kler	116	111
Quantitative spectrum analysis for geological work - Iu.A.Sherstkov	117	112
The effect of graphite in spectroscopic analysis of alloys - A.V. Kozlova & P.D.Korzh	119	114
The effect of graphite powder in spectrum analysis of ores - K.Z.Finkin	120	115
Spectrum analysis of powders with reference to a single standard - A.M.Shavrin	122	116
The influence of certain substances on the intensity of the spectrum lines of molybdenum, indium and thallium - L.A.Spektorov, I.K.Klavdienko & A.I.Poguliaeva	122	116
Variation of the intensity of copper and nickel lines with the concentration of these metals in Cu-Ni alloys - N.K.Rudnevski & G.I.Golitsyn	123	117
Investigation of the rate of entry of copper-nickel alloys into the cloud of an electric arc - N.K.Rudnevski, A.I.Matiunin & E.S.Obukhova	125	119
The influence of heat treatment on the entry of aluminum-silicon alloys into an electric arc - G.A.Mukhin & N.K.Rudnevski	126	120
Application of nomographic methods of computation to spectrum analysis - R.N.Rubinshtein & N.G.Karpel'	128	121
Statistical investigation of the accuracy of spectrographic analysis of carbon steels - K.I.Ionova & V.V.Nalimov	129	123
Investigation of the photometric properties of "spectral" photographic plates types I, II and III produced by plant No. 2 - A.A.Frishberg	131	124
Evaluation of the errors arising in different parts of the spectro-analytic process - E.L.Grinzaid	132	125
Reproducibility of spectrum line intensities in activated AC arcs - V.P.Borzov & N.S.Sventitski	133	127
On the actual value of the reabsorption coefficient b in condensed spark spectra - I.S.Fishman	135	128
On the nature of the sparking-off effect in spectrum analysis of metal alloys - E.S.Kudelia	136	129
On taking into account the background in measuring the intensity of spectrum lines by the photographic method - S.A.Shipitsyn	138	131

Translated in 1956 by
Columbia Technical Translations
5 Vermont Ave., White Plains, N.Y.

SPECTROSCOPIC DETERMINATION OF HYDROGEN IN METALS

- N.G.Gerasimova, T.F.Ivanova, N.S.Sventitskii, G.P. Startsev, K.I.Taganov, M.E.Trantovius *

The spectra were excited by high- and low-voltage single pulse discharges. Discharges of short duration were chosen in order to minimize the time of contact of the luminous cloud with the surrounding medium in view of the fact that it is not always feasible to have the latter entirely free of traces of hydrogen.

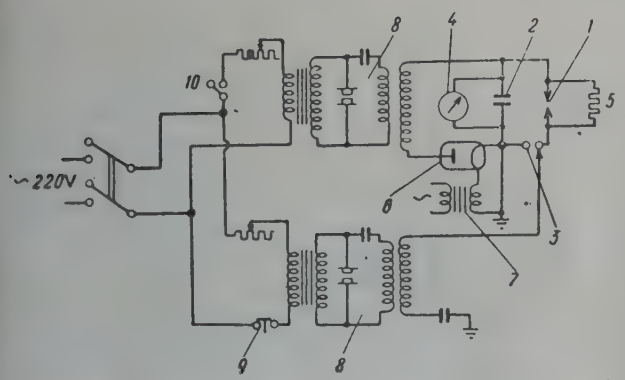

Fig. 1 High-voltage pulse generator: 1) analytic discharge gap, 2) capacitor assembly - 6 μf, 6 kv, 3) auxiliary spark gap - 1.5 mm, 4) kilovoltmeter, 5) 400 ohm resistance, 6) kenotron, 7) kenotron heater supply transformer, 8) PS-39 generator, 9) push button setting off spark across gap 3, triggering main discharge across gap 1, 10) switch.

In the high-voltage discharge circuit (Fig. 1) a 6 μf capacitor assembly was charged to 6 kv. The spectrum of the high-voltage flash produced by the discharge at ordinary pressures is characterized by a strong background; however, reducing the pressure to 100 mm Hg weakens the background appreciably so that the 6562 A hydrogen line selected for analysis stands out clearly. With the high current density obtaining, this line was considerably broadened; near it one could distinguish the 6578.03 and 6582.85 A diffuse lines of carbon. We employed the background intensity in the 6500 A region as the internal standard. The spectra were photographed with an UF-85 camera on an ISP-55 spectrograph. The investigated samples were pieces of metal of any shape with a clean flat formed in the area of the discharge. The counter electrodes were pointed tungsten or copper rods. The inter-electrode gap was adjusted to 0.3 mm. One flash (pulse) sufficed to obtain a record of the spectrum on "Panchrom-10" type film.

Under these conditions the working curve was rather flat (slope about 0.15-0.20). The use of other media (such as carbon dioxide, argon, chlorine, carbon tetrachloride vapor and silicon tetrachloride vapor), although it allows of simultaneous determination of oxygen and nitrogen in the metal, gives no increase in the sensitivity of analysis as regards detection of hydrogen.

Excitation of the spectrum by means of a low-voltage discharge (see Fig. 2) in air at atmospheric pressure proved to be a simpler and equally effective procedure. Experiments with other media showed no significant improvement in sensitivity.

Contamination of the surface of the electrode and sample with organic substances leads to a great increase in the intensity of the hydrogen line, and, consequently, to highly misleading analytic results. Hence the sample surfaces must be cleaned off with a grease-free cutting tool or file and protected against dirt, oil, etc.

The preparation of suitable standards is a particularly difficult matter. Ordinary steels gradually lose hydrogen and are, therefore, unsuitable. KhN-60 [ХН-80] alloys liberate hydrogen more slowly, while KhN-80 [ХН-80] alloys retain

---

*Graduate students I.V.Dvornikova, B.V.Zakharchenia and A.A.Petrov participated in the experiments.

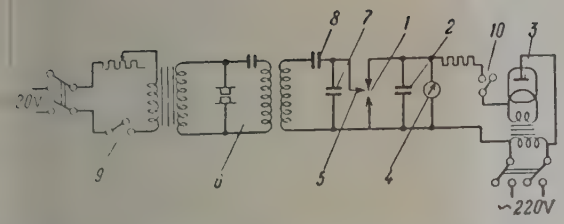

g. 2. Low-voltage pulse generator:
analytic gap, 2) electrolytic capacitor
sembly, having a total capacitance of
00 μf, charged to 250-280 v, 3) kenotron
r charging capacitors, 4) voltmeter,
auxiliary electrode for triggering
scharge from PS-39 generator (6),
100 μf capacitor, rated for potentials
er 10 kv, 8) separating capacitor, 0.01-
1 μf, 300 v, 9) pushbutton, depressing
ich initiates the discharge across gap 1
ien switch 10 is closed.

it satisfactorily and can be used for the preparation of standards[1]. Undoubtedly metals forming stable hydrides could also serve for the preparation of standards.

Most of our experiments were carried out with KhN-80 alloys. By heating pieces to different temperatures and for different times we obtained samples with different amounts of hydrogen. The hydrogen content in the prepared samples was determined by the method of melting under vacuum. Exhaustive experiments with samples and standards of KhN-80 alloy showed that with excitation of the spectrum by a low-voltage pulse discharge one can obtain a dependable calibration curve with a slope of about 0.3. The probable deviation in making determinations by the method of three standards in the 0.2 to 1.5 ml/kg range of concentrations is about 20%.

We wish to thank Iu. A. Kliachko, A.G.Atlasov, E.M.Chistiakova, S.M.Ianovski
id S.Ia.Reznikova for their assistance in selecting and analyzing the samples and
andards.

Reference

1. Iu. A. Kliachko, A.G.Atlasov & M.M.Shapiro, Analiz gazov i vkluchenii v
tali (Analysis of gases and inclusions in steel), M. 1950.

* * * * * * *

SPECTROSCOPIC DETERMINATION OF OXYGEN IN STEEL

- O.B.Fal'kova

In developing a spectroscopic method of determining oxygen in steels a number f difficulties had to be overcome. The principal ones were:

a) the difficulty of exciting the spectrum lines of oxygen (to obviate this e had to develop a special source) and

b) difficulties connected with the physical and chemical properties peculiar o oxygen in steel (as is known, oxygen is present in steel primarily in the form f different oxides, characterized by a high degree of chemical stability and dif- erent dissociation temperatures).

In the analytic procedure developed by the writer the sample is utilized as ne of the electrodes of a powerful low-voltage discharge, produced in an atmos- here of hydrogen at pressure of 270 mm Hg. The permanent electrode (a carbon rod) nd the sample are mounted inside a special discharge chamber which is evacuated o a pressure of 10^{-2} mm Hg before being filled with hydrogen. Apparently the ydrogen, introduced in this manner, reduces the various oxides present in the etal, thereby insuring a normal concentrational sensitivity.

The spectrum is photographed on an ISP-51 spectrograph. The oxygen concentration is determined according to the logarithm of the ratio of the intensity of the 4641.8 A oxygen line to the background intensity by means of a suitable calibration curve. The standards used for plotting the curve were samples analyzed by the melting under vacuum method.

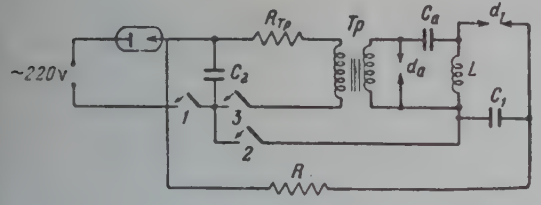

Low-voltage pulsed spark circuit

The source can be either a high-voltage or a low-voltage pulsed spark. For the former one can employ a conventional Raiski circuit two sparkgap circuit with a resistance and a kenotron for controlling the pulse frequency connected into the circuit of the transformer secondary winding.

The low-voltage pulsed spark circuit is shown in the accompanying figure. When knife switches 1 and 2 are closed and switch 3 is open the capacitors C_1 (700 μf) and C_2 (40 μf) are charged through the thyratron (TG-162). Switches 1 and 2 are then opened, disconnecting the capacitors C_1 and C_2 from the charging circuit. Finally closing switch 3 causes C_2 to discharge through the primary winding of the transformer Tp thereby giving rise to a pulse across the gap d_1 which triggers the discharge of capacitor C_1 across this gap.

Both circuits (high- and low-voltage) provide for satisfactory determination of oxygen in a range of concentrations from 0.005 to 0.2% with a deviation (reproducibility) of about 25%.

The productive capacity of the described set-up allows of making three-fold analyses of 5-6 samples per working shift. The developed procedure is now being used in the "Stalin" Metallurgical Plant in the city of Stalino.

"I.V.Stalin" Moscow Steel Institute

Reference

1. S.L.Mandel'shtam & O.B.Fal'kova, Zvod. labor. (The Plant Lab), 4, 430 (1950).

* * * * * * *

QUANTITATIVE DETERMINATION OF CERTAIN DIFFICULT-TO-EXCITE ELEMENTS BY MEANS OF A SQUARE-PULSE GENERATOR

- A.N.Vorsin

It is known that the square waveform of pulses is the most favorable for the excitation of spectra of many hard-to-excite elements.

We designed a pulse generator employing an artificial-line type circuit which produces nearly square pulses having virtually constant parameters. The charging potential is about 12 kv. The line consists of four cells, having a capacitance of 0.1 μf each. The generator is readily tuned by varying the discharge resistance with the operation being monitored by an oscillograph.

The substance being analyzed (solution or salt) is spread over a copper disk 30 mm in diameter, which serves as the lower electrode. The upper electrode is a copper rod 4 mm in diameter. A simple electromagnetic device rotates the disk through a predetermined angle after each charging of the line. The device also serves as a pulse counter.

We developed a procedure based on the use of the designed generator for quantitative determinations of Br, I and S in the range of concentrations from 0.1 to 1.0% with the accuracy common to spectroscopic analysis.

West Siberian Branch of the
Academy of Sciences of the USSR

* * * * * * *

SPECTRO-CHEMICAL DETERMINATION OF CARBON IN IRON ALLOYS

- E.S.Kudelia & A.S.Dem'ianchuk

We established through a series of investigations that the principal causes hindering spectro-chemical determinations of carbon in iron alloys are 1) intensive oxidation of the carbon as a result of exchange reactions with the components of the oxide film forming on the surface of the sample in the area subjected to the spark, 2) direct oxidation of the carbon by atmospheric oxygen, 3) diffusion of the gaseous carbon oxides through the air surrounding the discharge and 4) reduction of the concentrational sensitivity of the C III 2296.8 A line under the influence of carbon in the atmosphere during prolonged exposures.

The use of a magnesium counter electrode reduced the effect of these causes to an appreciable extent. Magnesium, having a strong affinity for oxygen, prevents the formation of thick oxide films, lowers the rate of oxidation of the carbon and thereby reduces the rate of diffusion of carbon oxides into the surrounding gaseous medium. As a result, the proportion of carbon entering the discharge proper increases and the intensity of its analytic line is enhanced accordingly. This makes it possible to use exposures on the order of 20-30 sec which are short enough to make the influence of atmospheric carbon on the concentrational sensitivity of the C III 2296.8 A line virtually negligible. In addition, the use of a magnesium counter electrode appreciably reduced the intensity of the interfering nickel lines.

We recommend the use of the following iron lines for comparison: the 2304.7 A line for low-alloy steels, the 2279.9 A line for alloy steels and the 2327.4 A line for cast irons. Our investigation established that use of the absolute intensity of the C III 2296.8 A line makes it feasible to determine carbon in all types of steel and cast iron by means of one and the same, common calibration curve.

By way of excitation source we recommend a high-frequency discharge such as that obtained with a DG-1 generator. The minimal determinable concentration of carbon in this case is 0.01-0.02%. When a condensed spark is employed the minimal concentration for reasonably accurate determinations of carbon is about 0.03-0.04%.

"E.A.Paton" Electric Welding Institute
of the Ukranian Academy of Sciences

* * * * * * *

LOCAL SPECTRUM ANALYSIS

- N.G.Isaev

In 1950 we described a new principle of qualitative and quantitative local spectrum analysis[1]. An instrument designed on the basis of this principle was successfully used to solve a number of practical problems involving spectrum analyses with a localization of approximately 0.2 mm. The work done showed that it is feasible to apply the same principle to qualitative analysis with a localization of about 20 μ.

Observation of the localized spark (in our case, dispersed linearly) under a microscope shows that it should be possible to duplicate the method of conventional qualitative analysis while retaining a high degree of localization ($\sim$ 20 μ). Thus, under the microscope all the minute jets, produced on the surface of the sample by the action of the spark, appear as bright flashes localized within circles not exceeding 20 μ in diameter. Hence analysis could be effected by projecting an image of the sparked sample surface, magnified 20–25 times, on the spectrograph slit. In this case surface areas 20 μ across would correspond to spectrum line segments some 0.4–0.5 mm in length, which could readily be recorded and measured. Where analytic conditions permit, the spectrograph slit could be widened appreciably.

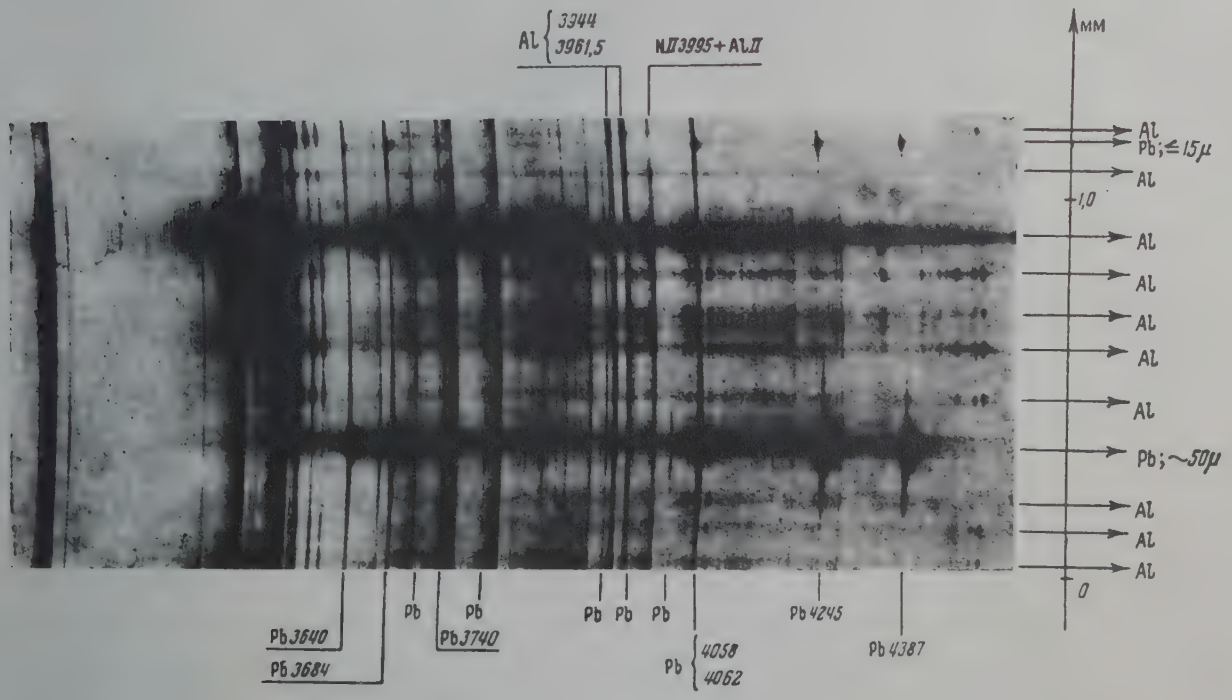

Spectrogram of artifical sample consisting of a stack of aluminum and lead foil acted upon by a dispersed spark. Photographic data: counter electrode - aluminum foil; plates - non-sensitized, 600° H&D, exposure - 15 min; development - 3 min. Overall enlargement - 56 X (magnification on slit - 15 X, magnification in spectrograph - 1.24 X, enlargement in printing - 3 X.

The results of an experiment along these lines using an artifical sample consisting of a stack of copper, aluminum and lead foil are shown in the accompanying photograph. The spectrogram shows that layers of aluminum and lead foil 10–20 μ

nick are faithfully recorded. In this experiment we used the wavelengths to nich the silver bromide emulsion is most sensitive and a wide slit (70-80 μ) order to bring the exposure time to an acceptable interval (15-20 min). For e camera lens we used a 10 X 0.30 achromatic glass micro-objective. (In case photography in the ultraviolet region below 3600 A we recommend that an OK-10 ns be used.) The magnification on the spectrograph slit was approximately 15 X.

On the basis of our experiments it may be asserted that the described method local spectrum analysis using a linearly dispersed low-power spark discharge practical, simple and merits general application.

Reference

1. N.G.Isaev, Izv. AN SSSR, Ser. fiz., 14, 689 (1950).

* * * * * * *

LOCAL ANALYSIS OF WELDS OF HIGH-ALLOY STEELS AND HEAT-STABLE ALLOYS

- A.G.Komarovski

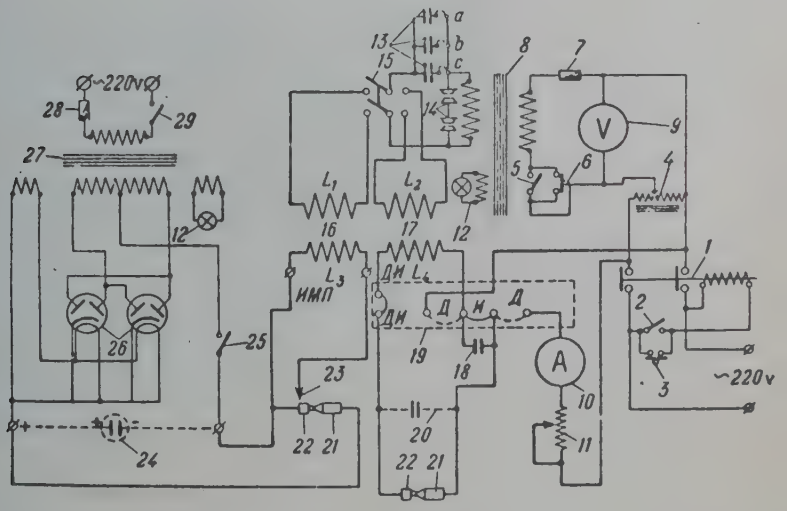

cuit diagram of source generator: 1) magnetic starter, 5 amp, 220 v, 2) rter switch on generator control panel, 3) remote control starter button, 2 amp autotransformer, 5) high-voltage transformer switch, 6) remote pulse trol button, 7) 2 amp fuse, 8) 220/5000 v, 0.2 kva transformer, 9) 250 v tmeter, 10) 10 amp ammeter, 11) 40 ohm, 10 amp rheostat, 12) indicator lamp, capacitor assembly (one 0.0023 μf and two 0.01 μf, all rated 10 kv), 14) twin charge gap unit, 15) high frequency transformer selector switch, 16) h-f trans- mer in pulsed spark circuit, 17) h-f transformer in arc and spark discharge cuit, 18) 0.025 μf, 500 v blocking capacitor, 19) generator operation selection trol panel, 20) 100 μf shunting capacitor, 21) permanent electrode, 22) sample, pulse-exciting (triggering) spark, 24) set of electrolytic capacitors having otal capacitance of 4000 μf, 450 v, 25) switch in rectifier plate circuit, kenotrons (5Ts4S - 5Ц4С), 27) rectifier transformer, 28) 1 amp fuse, 29) tch in line to rectifier transformer.

We developed and built a special generator for carrying out local analyses of welds. This generator permits of obtaining different types of discharge (high-frequency spark, a low-voltage, high-current pulse spark discharge, a pulsed AC arc as well as conventional arc and spark discharges) by simple switching without modifying the basic circuit of the unit. The circuit of the developed generator is pictured in the preceding diagram.

A high-frequency discharge permits effecting local analyses of the surface layers of heat cracks developing in welds of high-alloy steels and heat-stable alloys.

Table

Sample No.	Elements	Concentration, % in surface layer of heat cracks	Concentration, % in the weld metal
1	Silicon	6.30	2.24
	Manganese	1.81	1.50
	Molybdenum	5.50	4.65
2	Silicon	2.09	0.80
	Manganese	1.24	1.23
	Molybdenum	5.30	5.10
3	Niobium	1.59	0.85

By way of illustration the determined concentrations of the alloying elements, Nb, Mo, Si and Mn, in the surface layer of the thermal cracks and in the weld proper are listed in the table.

The spectra obtained with the high-frequency spark are distinguished by sharp lines and a virtual absence of the background characteristic of the spectra obtained by means of all the other sources.

On the other hand, the low-voltage, powerful pulse spark-discharge used in conjunction with an insulating bushing to limit the area affected by the discharge makes it possible to obtain a spectrogram with a single flash. With this type of discharge a large amount of energy is released within a brief interval with the result that an appreciable quantity of metal is ejected from the sample in the form of an explosive jet. This method of exciting the spectrum makes it possible 1) to determine the composition of small areas on the surface of the weld or the investigated metal and 2) to dispense with preliminary treatment of the electrode (heating, pre-arcing, etc.) since in this case the role of oxidizing processes is negligible. Pulse discharge spectra differ markedly as regards their nature and appearance from ordinary spectra; they comprise new lines which are not excited in conventional spectrographic sources.

* * * * * * *

USE OF EMISSION SPECTRUM ANALYSIS IN BIOLOGY AND MEDICINE*

- A.O.Voinar

Despite the fact that the so-called micro-elements are present in extremely minute quantities in living organisms (10^{-3}–10^{-12}%), these mineral components play an important part in various biological processes, such as growth, reproduction, tissue metabolism, replacement of blood, ossification and so on, since they are intimately connected with a number of organic compounds - vitamins, hormones,

---

* Based on investigations by Iu.G.Antonov, G.A.Babenko, G.A.Belykh, A.O.Voinar, V.N.Garlakhova, V.A.Del'va, L.S.Dinevich, M.M.Kovalev and N.B.Nasel'ski.

enzymes and the like - either entering into the composition of these substances or exerting a certain influence on their activity.

Determination of the content of these micro-elements in the fluids and tissues of the body requires special measures for enriching the analyzed ash of other samples and enhancement of the sensitivity of the spectroscopic method employed. In our work enrichment of the ash samples was effected primarily by the method of precipitation with various reagents.

It has been established that the content of micro-elements in different organs varies, depending on the age of the organism, the state of the nervous system and many other factors. For example, the introduction of a physiological concentration of copper into chicken eggs in the process of incubation significantly accelerates the growth rate of the chicks, whereas the introduction of lithium salts inhibits their development. Under the influence of narcotics, the content of Ti, Cu and Ag in the nuclei of nerve cells decreases, while the content of Mn, Pb, Al, Ni, Cr and other elements rises.

These few examples will suffice to indicate the great importance of accumulating data on micro-elements in living organisms. The use of spectrum analysis has already helped solve a number of problems concerning the distribution and the biological role of some micro-elements in the bodies of men and animals, both in a state of normal health and when suffering from certain diseases.

"A.M.Gor'ki" Stalinsk State Medical Institute

* * * * * * * .

THE OXYHEMOMETER - A PHOTOELECTRIC INSTRUMENT FOR BLOODLESS AND CONTINUOUS DETERMINATION OF THE OXYGEN CONTENT OF BLOOD*

- M.S.Shipalov

Until recently the only extant methods of determining the degree of oxygen saturation in arterial blood were based on taking blood samples with subsequent chemical (gasometric) analysis. Obviously any method involving the taking of samples by means of a needle, whether from arteries, veins or capillaries, suffers from serious disadvantages.

Yet an examination of the spectral characteristics of (deoxidized) hemoglobin and oxyhemoglobin shows that in the red region of the spectrum (640-650 mμ) the difference between absorption of light by hemoglobin and oxyhemoglobin is very appreciable, attaining about 70% relative to the total transmission of the oxyhemoglobin. At 800 mμ the transmission curves for the two forms of hemoglobin intersect, which makes it feasible to evaluate the total amount of hemoglobin in the blood by measurements in this region of the spectrum.

Taking advantage of these spectral properties of hemoglobin and oxyhemoglobin a number of investigators have used photoelectric methods for determining the degree of saturation of hemoglobin with oxygen in solutions of hemoglobin or hemolyzed blood. However, these methods, too, are based on taking blood samples from the living organism. Obviously it was necessary to seek another way of studying the oxygen saturation of blood, a way of measuring it in vivo continuously and without the necessity of puncturing the body to take samples. A solution was found in the method of oxyhemometry based on continuous observation of the spectral characteristics of hemoglobin in human tissue.

---

* The design of the instrument was developed by E.M.Kreps, M.S.Shipalov and E.A.Bolotinski.

To this end a data-transmitter is attached to the fossa of the subject's ear (see illustration). The unit consists of a small incandescent lamp housed in a special case and two photoelectric cells, each with a light filter covering the light-sensitive surface. The data-transmitter is clipped over the helix so that the lamp is on one side and the case containing the light filters and photocells is on the other side of the ear. The filters separate out the requisite more or less monochromatic portions of the spectrum 1) in the region where the spectral characteristics of the hemoglobin are determined by the oxygen saturation (red filter) and in the region where the absorption of hemoglobin and oxyhemoglobin is the same (green - infrared filter). The data-transmitter is connected by means of a flexible multiple-conductor cable with the receiver-measuring unit of the instrument. When the instrument is turned on, the transmitter unit lamp goes on. The light beam passes through the ear tissue and filters, being partially absorbed and scattered in the process, and falls on the photocells. The photocurrent generated by the photocells is measured by a galvanometer in the receiver unit. The arrangement of the measuring circuit is such that, provided the ratio of the two photocurrents remains within certain limits, the indication of the galvanometer depends only on the degree of oxygen saturation of the blood, regardless of the amount of blood present in the ear tissue of the subject.

Photoelectric data-transmitter [sensing element] for continuous measurement of the degree of oxygen saturation of the blood.

Thus after suitable adjustment the instrument gives a continuous record of the oxygen concentration in the blood of the subject without sampling. The scale of the instrument is graduated directly in percent saturation of the blood with oxygen.

In view of the fact that we are here dealing with live tissue, it is essential to bear in mind that live tissue normally contains arterial, capillary and venous blood. Hence to determine the oxygen saturation of arterial blood one should contrive to transform the blood in the examined tissue to as nearly arterial as feasible. This is accomplished by expanding the capillaries by the application of heat in order to accelerate the flow of blood. The heat source is actually the same incandescent lamp serving as the light source.

Our Soviet industry is now producing two instruments for oxyhemometric studies: the cathode 0-26 oxyhemometer and the 0-38 oxyhemograph. They consist of a data-transmitter and a receiving-recording and power supply unit. The power supply unit is plugged into the regular AC line. There are also special models for use under field or other non-laboratory conditions (in ships, aircraft, etc.) with power supply units designed for other electric sources (storage batteries or other). The oxyhemometers are now extensively used in physiological and medical institutes.

"A.N.Bakh" Institute of Biochemistry of the Academy of Sciences of the USSR

* * * * *

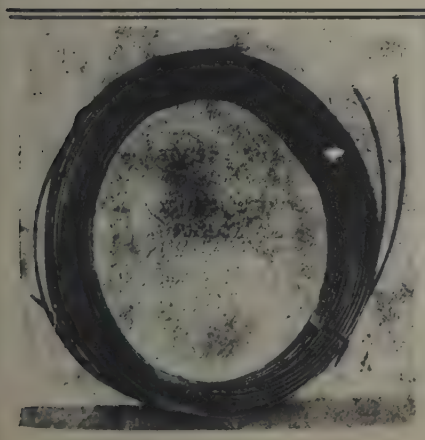

← Fig. 1. Coil of aluminum wire produced by continuous casting for the preparation of spectroscopic standards.

[See article starting on page 145.]

PREPARATION AND INVESTIGATION OF SPECTROSCOPIC STANDARDS OF DIFFERENT ALLOYS

- K.A.Sukhenko, I.O.Mladentseva, N.P.Gorozhankina, Z.S.Platonova, A.V.Aksenova & S.M.Il'ina

The use and application of spectroscopic analysis in industry have increased tremendously in recent years. The growth in the number and activities of spectroscopic laboratories has been accompanied by a corresponding rise in the demand for standard samples of different alloys.

At present spectroscopic standards are being made by the Standard Samples Laboratory at the Ural Institute of Metals, the MAP Institute (p/ia 126), the Ministry of the Ship Building Industry and a number of agencies under the Ministry of Non-Ferrous Metallurgy (the State Institute for Processing of Non-Ferrous Metals, the All-Union Aluminum-Magnesium Institute, the Gintsvetmet [State Institute of Non-Ferrous Metals], the Institute of the "Gipronikel'" [State Institute for the Planning of Nickel Plants], and others).

The Standard Samples Laboratory at the U.I.M. has on hand or in preparation for issue in 1954-55 the following standards; 11 sets of steel standards, 2 sets of ferrous alloy standards, standards for steeloscopic analysis, and a set of standard counter electrodes; these are all of high quality and available to all industrial and scientific laboratories. The laboratories of the Ministry of Non-Ferrous Metallurgy produce only a limited number of standards, intended primarily for the use of agencies and establishments under the Ministry. The Ministry laboratories and agencies produce and use primary aluminum and magnesium standards, standards of aluminum alloys (secondary silumin), a set of standards for testing various grades of nickel, lead, zinc, and copper for purity and conformity to grade, and brass standards. These standards are of high quality but they are not generally available to industry.

We feel that it is important for all organizations preparing standards to increase their production in order to satisfy the growing demands not only of allied and supplier-plants but of other consumers as well. The standard Samples Laboratory at the U.I.M. must increase the scope of its standards work and expand its production plan to include the preparation of standards of different grades and types of bronze and other alloys.

Since 1942 the MAP Institute has put out over 30 sets of different standards for use in analysis for cobalt, nickel, aluminum, magnesium, iron and copper.

In producing standards one of the more difficult problems is the casting of a large number of chemically uniform standard samples (400 or more rods 7 to 16 mm in diameter) from a single melt or batch. Also in fabricating standards one must make sure that the chemical composition of the standard rods does not differ from that of the ingot from which a shaving is taken for chemical analysis; furthermore, it is desirable that the casting conditions be as similar as possible to the conditions under which the samples are cast in the plants using the standards for analysis. If the casting conditions differ appreciably, special tests should be run to make sure that the differences will not affect the results.

The last point may be illustrated by the example of the duraluminum and nickel alloy standards prepared some time ago by our laboratory in the form of cast rods (6-7 mm in dia. in the case of duraluminum and 8 and 16 mm in the case of nickel and cobalt alloys). The plant laboratories, on the other hand, receive not only castings but also pieces which have undergone different types of heat treatment (sheets, wire, blades and so on). On the basis of investigations by M.S.Alpatov, I.A.Grikit and others we established the feasibility of analyzing heat treated samples and pieces of AL4 and AL5 duraluminum and of nickel alloys with reference to cast standards.

In preparing the standards we used different methods of casting and processing. Al, Mg, Ni, Co and Cu alloys as well as steels and cast irons were cast

directly into chill molds of different shapes. In addition, duraluminum and silicon-aluminum alloy standards were successfully formed by the method of continuous casting in the form of a drawn wire and also (in the case of MA8 alloy) by the method of stamping and rolling cast ingots.

The continuous casting method makes it possible to produce a large number of uniform standards of metal entirely free of pores, blow holes, blisters, etc. A coil of standard wire produced by continuous casting is shown in Fig. 1 (p. 144). The main shortcoming of this method is the possibility of some change in the chemical composition of the wire in the course of prolonged drawing. Nevertheless, provided certain casting conditions are observed, the standards obtained by this method are fully homogeneous. To check the uniformity about 100 samples were taken from different sections of each coil of standard wire. The results of tests on these samples were compared with the results of 50 repeated analyses of a single sample.

The results of an investigation of the uniformity of Standard No. 19 of AL9 alloy produced by the method of continuous casting are shown in Table 1 in the form of mean arithmetic deviations. The calibration curves based on the standards of this alloy are reproduced in Fig. 2. These standards are now widely used by industrial laboratories.

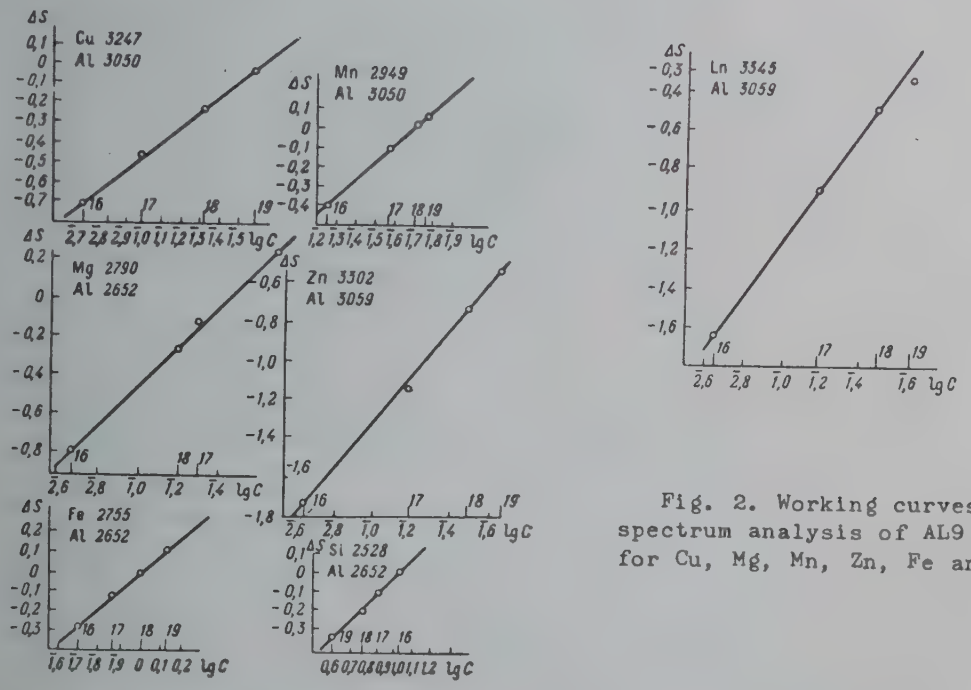

Fig. 2. Working curves for spectrum analysis of AL9 alloy for Cu, Mg, Mn, Zn, Fe and Si.

We produced standard samples of nickel alloys with various concentrations of tin, lead, antimony, arsenic and bismuth in cooperation with the "Electrostal'" Plant; these standards were produced in the form of plates (sheet billets). In view of the brittleness of these alloys, this method of casting was the only one by means of which it was possible to obtain uniform standards free of porosity, cavities and similar defects.

A difficulty in investigating these standards lies in establishing the exact chemical content of the admixture elements which are present in concentrations ranging from 0.0005 to 0.01%. Ten different agencies participated in the preparatory work; extensive use was made both of spectroscopic methods of analysis using solutions and powders and of chemical and physico-chemical analytic procedures.

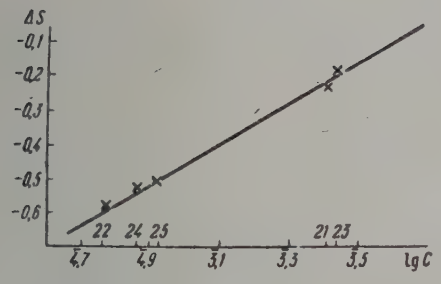

Fig. 3. Working curve for analysis of nickel alloy for lead with reference to the Pb 2833 - Cr 2840 line pair.

By way of illustration the final calibration curve for determining the lead content in the solid standards is shown in Fig. 3; the chemical composition of the standard samples was established on the basis of numerous spectroscopic and chemical analyses made by the laboratories of the different agencies participating in the development work.

Table 1 below shows the results of an investigation of the uniformity of Standard No. 19 of AL9 as mentioned previously. The results of uniformity tests on the nickel alloy standards containing admixtures of Cr, Al, Ti, Fe and Mn are shown in Table 2.

Table 1

Results of uniformity test on Standard No. 19 of AL9 alloy: averages for 100 different samples compared with averages for 50 analyses of one sample.

	Analytic elements and line pairs					
	Cu 3247— Al 3050	Mn 2949— Al 3050	Si 2528— Al 2652	Mg 2790— Al 2652	Fe 2755— Al 2652	Zn 3345— Al 3050
Lot	3,65	6,7	3,2	1,8	6,65	5,0
One sample	2,90	3,6	3,3	2,7	4,8	6,1
Difference	0,75	3,1	0,1	—0,9	1,85	—1,1
Permissible error	0,90	1,2	1,1	0,9	1,65	2,03

Table 2

Results of uniformity test on Standard No. 21 of nickel alloy: averages for 100 different samples from one batch compared with averages for 50 analyses of one sample.

	Analytic elements and line pairs					
	Cr 3147— Ni 3080	Al 3082— Ni 3080	Ti 3073— Ni 3080	Cr 2853— Ni 2863	Fe 2598— Ni 2584	Mn 2594— Ni 2584
Lot	4,0	9,9	11,3	3,2	3,6	6,6
One sample	3,6	6,6	9,2	2,4	3,1	4,0
Difference	0,4	3,3	2,1	0,8	0,5	2,6
Permissible error	1,2	2,2	3,07	0,8	1,03	1,33

* * * * * * *

METHODS OF SPECTRUM ANALYSIS EMPLOYED AT THE "SEVERONIKEL' " COMBINE

- O.Ch.Velichko

This report is devoted to a description of the rapid control methods for intermediate products by means of steeloscopes and steelometers and of the more accurate quality control methods employing a KS-55 spectrograph developed at our plants.

Steeloscope Analyses

Determination of Fe in the 1-5% range in bessemerized copper-nickel sulfide. The sample is taken from the converter with a ladle, cooled with water and broken into several pieces, one of which is then taken for analysis. The source is a 5 amp AC arc; the counter electrode is a 10 mm diameter, 150 mm long nickel rod, having an ion content under 0.002-0.003 %. The entire process including sampling takes 5-6 minutes. The analytic lines and concentration values are listed in Table 1. Fig. 1 shows a diagram of the spectrum region in question.

Table 1

Analytic lines and concentration values

Sample	Element	λ, Å	Fe content %	Evaluation
1	Fe	4383,5	0,5	1≤4
				2<4
2	Fe	4404,7	1,0	1≥4
				2≤4
3	Fe	4375,9	1,5	1=5
				2=4
4	Ni	4384,5	2,2	1≥5
				2=5
5	Ni	4359,5	5,0	1=6
				2≤6
6	Ni	4401,5		3=4

Determination of Co in the 1-10% range in cobalt alloys. The sample is taken through the mouth of the converter by means of a sampling bar, cooled with water and broken off the bar. A 20 by 20 mm flat is then cleaned off on a slag-free piece by means of an emery wheel.

A 220 v, 5 amp DC arc is used as the source. The sample serves as the cathode, while the permanent anode is an iron rod 6 mm in diameter and 150 mm long. The entire procedure including sampling requires 4-5 minutes. A diagram of the spectrum region used is shown in Fig. 2; the analytic lines and concentration indications are listed in Table 2. (see next page)

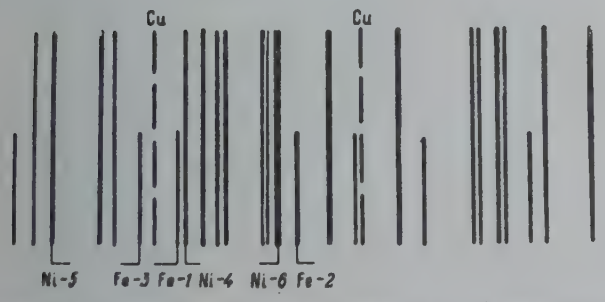

Fig. 1. Spectrum region used in determining Fe in copper-nickel sulfide product.

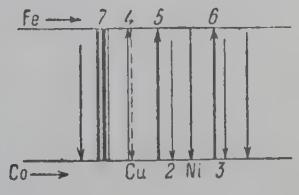

Fig. 2. Spectrum region used in determining Co in cobalt alloys.

Steelometer Analyses

Determination of Ni in the 0.4-3.0% range in the initial flotation product. Here the source used is a DC arc with a 6 amp current. The powdered sample is mixed with iron oxide powder in the ratio of 1:1 and the mixture is briquetted. The resultant briquet (7 mm in diameter & 4 mm high) is placed on a carbon support which is connected as the cathode; a 6 mm diameter, 150 mm long iron rod serves as the anode.

Table 2

Analytic lines and concentration values

Sample	Element	λ, A	Co content, %	Evaluation
1	Co	4663,4	1,0	1—None
2	Co	4683,4	2,0	1=7
3	Co	4693,2	3,0	1<4
4	Fe	4673,2	4,0	1=4
				2=7
5	Fe	4678,8	5,3	1≥4
				2=4
6	Fe	4691,4	6,0	1=6
				2≥4
7	Fe	4669,2	7,0	1≤5
				1≥6
				3=4
			8,0	1=5
				2=6
			9—10,0	1>5

The analytic line pair used is Ni 5115 & Fe 5090. The relative deviation (error) is 5-10%. The analysis time = 15 min.

Determination of S in the 0.4-13.0 % range in nickelous oxide. The nickelous oxide powder is mixed with powdered metallic copper 1 to 1 and the mixture is formed into cylindrical briquets (5 mm diameter, 7-8 mm high). A briquet is used as one electrode; the counter electrode is a carbon rod 6 mm in diameter, 40-45 mm long with a truncated cone point (end area = 3 mm^2). The spectrum is excited by means of an IG-2 spark generator employing the complex circuit hook-up; the circuit parameters are: L = 0, C = 0.005 μf, auxiliary gap = 3 mm, analytic gap = 3 mm, current in transformer primary = 3 amp, voltage = 220 v. Sparking off time = 2 min.

The analytic line pair used is S 5606.13 & Ni 5535.39 A.

When the sulfur content is over 4%, the sample is diluted 1:2 with copper powder.

Analyses on the KS-55 Spectrograph

Determination of Cr content in the 0.0005 to 0.2% range in nickel carbonate. The sample, prepared in the form of 0.2 gram briquet compressed of a 1 to 1 mixture of the carbonate and copper powder, is placed on a carbon support and serves as the lower electrode; the upper electrode is a carbon rod. The DC arc is operated with a current of 4-5.5 amp. As a first step the sample is connected as the anode and the arc is operated until the briquet fuses and any sodium present is burned out. Then the polarity is reversed and the 25 sec exposure made. The analytic line pair used is Cr 3578.7 & Ni 3561.75 A.

Determination of small amounts (0.9-0.2 mg/liter) of Zn in nickel catholyte. The nickel-production catholyte in question is a nickel sulfate solution containing free sulfuric acid, sodium sulfate, boric acid and a small admixture of organic substances. Direct spectroscopic analysis of such solutions is very difficult. Hence we evolved a procedure based on preliminary extraction of the zinc by a chemical method. The extraction is accomplished by means of isoamyl alcohol in the form of a thiocyanate complex; only 15 minutes time are required for the extraction of two samples. A measured quantity of the solution containing the extracted zinc is added to a definite amount of a nitric acid solution of high-purity nickel. The resultant solution is evaporated to dryness and the residue is roasted to the formation of nickelic oxide. Finally the zinc content of the oxide is determined in accordance with GOST (State All-Union Standard) 6012-51. The comparison standards used are samples of cathode nickel, repeatedly analyzed for zinc both according to GOST 6012-51 and chemically.

We feel that the present GOST 6012-51 should be modified to indicate that determinations can be made on a KS-55 spectrograph and extended to include cobalt so that the full list of elements for which cathode nickel is analyzed will be comprised in the spectroscopic procedure.

* * * * * * *

METHODS OF SPECTROSCOPIC ANALYSIS USED AT THE MOSCOW SECONDARY-ALUMINUM PLANT IN 1952-1954

- N.P.Rubina

Quality control in production

The spectroscopic laboratory of the plant performs analyses of aluminum and copper-base alloys. The control stages are a) raw materials, b) molten lots in production (rapid analysis of melt samples) and c) finished products. The equipment comprises an ISP-22 spectrograph , an IG-2 spark generator, a Feissner generator (modified to produce a simple spark) and a PS-39 AC arc source.

The elements being determined and the corresponding concentration ranges are a) in the aluminum alloys: Fe - 0.4-2.5%, Zn - 0.2-7.0%, Si - 0.4-8.0%, Mg - 0.1-1.5%, Mn - 0.1-1.5%, Ni - 0.04-0.50%; b) in the copper-base alloys (tin bronzes): Fe - to 0.5%, Sb - to 0.6%, Si - to 0.05%, Ni - 0.5-1.5%, Al - to 0.05% and Zn - 2-10%. All determinations are made according to standardized calibration curves.

The time required for the rapid analysis of an aluminum alloy sample (determining 6 elements, using two sparking regimes) is 25 minutes; the time for bronze samples (7 elements, two sparking regimes) is 22-25 minutes.

Development of new procedures

Recently we developed a new rapid-analysis procedure for determining the Sn content (in the 2-7% range) in OTsS bronzes. The spectra are photographed on the ISP-22 spectrograph. The source is an IG-2 generator connected in a Raiski circuit; L = 0.05 mH, C = 0.02 μf, current - 3-3.5 amp, permanent electrode - carbon rod with truncated cone point (2 mm diameter flat), sample - 70 x 20 x 20 mm ingot; analytic gap - 2 mm, auxiliary gap - 3 mm. Analytic line pair: Cu 2824 & Sn 2839 A. The accuracy of determination when the tin content is between 2 and 6 % and composition of the sample is uniform (as regards Sn) is within ±0.2% (absolute value).

* * * * * * *

ENHANCING THE SENSITIVITY OF SPECTRUM ANALYSIS OF POWDERS

-A.N.Bronshtein

It is known that, other conditions being equal, the minimum detectable concentration of an element depends to a great extent on the composition of the base or host material of the sample. We attempted to utilize this fact by artificially altering the composition of the sample. We discovered that the introduction of a number of substances, despite the fact that it reduces the relative concentration of the admixture element being determined (by dilution) actually results in an increase in sensitivity by one or two orders of magnitude. The maximum sensitivity is attained at a certain degree of dilution (sometimes as great as 4-5-fold).

Using zinc sulfide as the diluent in the analysis of certain ore samples we noted an appreciable increase in the sensitivity in determining Ga, In, Ge, Fe, Co and Mn in the ores.

For example, we utilized the described dilution method in developing a procedure for the analysis of powdered samples for gallium. The procedure makes it possible to determine concentrations of gallium down to 0.001% whereas by conventional methods it is impossible to detect concentrations of 0.01% (see figure on next page).

The peak sensitivity is reached when the samples are diluted with zinc sulfide

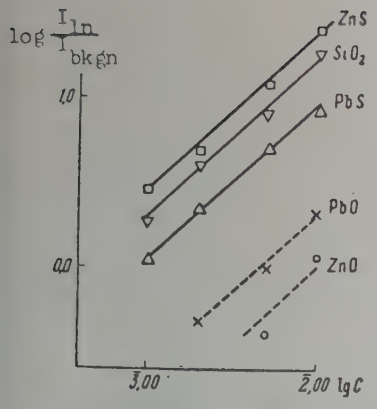

Influence of the composition of the base of the sample on the sensitivity of analysis for gallium

in the ratio of 1:2. However, in this case the calibration curves for samples of different original composition are displaced relative to each other. When the dilution is increased to 1:5, the calibration curves for different samples coincide.

The samples were spread on a brass stage electrode which moved at the rate of 5 cm/min. The source was an AC arc with a current of 5 amp. The spectra were photographed on a KS-55 spectrograph. Analysis was carried out by the method of three standards [straight-line calibration curve plotted on the basis of three standards], the measured line being the Ga 4172.06 A line. Potassium was introduced as the internal standard; at the same time it served to stabilize the arc flame temperature. The comparison line was the K 4044.14 A line.

* * * * * * *.

USE OF SPECTROSCOPIC METHODS OF ANALYSIS AT THE KUZNETSK METALLURGICAL COMBINE

- L.P. Andreeva

The development and introduction of spectroscopic analysis at the Kuznetsk Metallurgical Combine has proceeded along the lines of replacing the more laborious or less dependable chemical procedures.

Analysis for aluminum

Grading analysis for aluminum in 38KhMIuA [38XMIOA], catalytic and silicon-aluminum steels (Al content 0.4 to 2.0%) and determination of residual aluminum in all steels (a few hundredths or thousandths of a percent) are carried out on an ISP-22 spectrograph with an AC arc source, employing the method of three standards. For the higher range of concentrations (0.4-2.0%) we use the Al 3082.16 - Fe 3087.74 A line pair, the absolute error in this case being within ±0.02%; for residual aluminum the line pair is Al 3082.2 - Fe 3080.0 A and the absolute error is ±0.002-0.003%.

In the residual aluminum analyses the current strength is 8 amp. A very important factor in the analysis is proper cleaning of the sample; failure to clean the sample thoroughly leads to an appreciable increase in the error.

The introduction of spectrographic to replace chemical analysis has greatly simplified the procedure, reduced the time required from several days to 1-2 hours and increased the accuracy of the results.

Analysis for zirconium, titanium and magnesium

Determinations of zirconium in steel (0.1-0.6% concentrations) and magnesium in cast iron (some hundredths of a percent) are made by the method of three standards on an ISP-22 spectrograph with an AC arc source. The analytic pair for Zr is Zr 2571.4 - Fe 2572.0 A; the absolute error, ±0.03%.

The Mg 2802.7 - Fe 2804.5 A line pair is used for determining the small amounts

of Mg in cast iron.

For standards employed in the above-mentioned analyses - except for magnesium - we used selected samples carefully analyzed chemically in the main control laboratory of the Combine. The magnesium standards were prepared by a combination of spectroscopic and chemical methods: preliminary standards, analyzed spectroscopically, were prepared by adding known quantities of a titrated magnesium solution into artificial standard solutions of magnesium-free cast iron; subsequently solid samples, analyzed both chemically and spectroscopically, with reference to the preliminary standards, were selected for use as standards in the routine analyses.

The accuracy of spectroscopic analysis for magnesium is no lower than that of chemical methods.

Analysis of electrolytes for zinc

The spectroscopic laboratory was faced with the task of developing a procedure for determining zinc in electrolytes. The electrolyte in question, used in nickel plating, consisted of a 30% solution of nickel sulfate. The presence of zinc in concentrations of 0.01-0.02 gm/liter has a negative effect on the plating process. Chemical analysis is lengthy, complicated and not accurate enough. Direct spectrum analysis of solution samples was impossible, since with the given concentrations the zinc lines did not appear in the spectrum. Consequently it was necessary to evaporate samples to dryness and then burn the residue in the crater of a carbon electrode.

Zinc determinations are carried out by the method of three standards, using an AC arc. The standard samples are prepared by adding appropriate quantities of titrated zinc solution to fresh batches of 30% nickel sulfate solution.

The analytic line is Zn 3345.02 A; the background on the short-wave side of the line is used as the internal standard. The accuracy is within 0.004 gm/liter.

Analysis of steel during smelting

At present work is being carried out at the Kuznetsk Metallurgical Combine to develop and introduce rapid spectrum analysis of steels in production. Rapid procedures for determination of chromium and molybdenum in open-hearth steel were put into effect in 1945. Determinations of chromium in concentrations to 0.25% are being made with a steeloscope, according to a procedure developed by Smirnov, to within 0.02-0.03% absolute. Chromium concentrations in the 0.25-0.85% range in steel are determined spectrographically by the method of photometric interpolation on an ISP-22 spectrograph used in conjunction with an IG-2 spark generator (complex circuit setting). Here the analytic line pair is Cr 2677.15 & Fe 2689.212 A; the time required - 12-15 minutes; the accuracy - ±4-6% relative.

In analyzing for molybdenum (in the 0.01 to 0.35% range) in open-hearth steels the laboratory uses a PS-39 generator. Analytic line pair - Mo 3170.34 & Fe 3175.443 A; time required - 10-12 min; accuracy - ±5-7%.

The substitution of rapid spectroscopic methods for chemical procedures always reduced the time required without sacrifice in accuracy; in some cases, in fact the accuracy was enhanced.

However, to make even more effective use of spectroscopic methods in the rapid-analysis laboratory there is still need for the development of unified procedures providing for the simultaneous determination of several components.

* * * * * * *

INVESTIGATION OF THE SPECTRAL CHARACTERISTICS OF SPECTROSCOPIC STANDARDS PREPARED BY COMPRESSING METAL POWDERS

- V.V.Poliakova

The purpose of the present research project was to study the distinctive characteristics of the spectra of standards prepared by briquetting powders of technical grade copper, nickel, lead, tin, bismuth, zinc, cadmium and aluminum containing some hundredths or thousandths of a percent of admixtures and to determine the principal causes of such characteristics.

We recorded and compared the spectra of cast and briquetted (at a pressure on the order of 10 tons/cm^2) electrodes, 10 mm in diameter and 20–30 mm in length, of all the enumerated metals.

The logarithms of the relative intensities of the lines of various admixture elements in the spectra of cast and briquetted samples of the different metals listed are juxtaposed in the accompanying table.

The spectra were excited in an AC arc with a current strength of 7 amperes, with a flash period of 0.004 sec and a stabilized ignition phase. The interval between flashes was varied between 0.004 and 0.6 sec for the different metals. The figures in the table show an appreciable modification of the relative intensity of the admixture lines in briquets as compared to cast samples for most metals. Only in the case of lead and tin are the spectra of cast and briquetted electrodes virtually identical. Through further experiments we established that in going from cast to briquetted samples there is a change in the intensity of the characteristic lines of the admixture elements and in the intensity of the spectrum background. Furthermore, the experiments showed that spectra of the basic metal of cast and briquetted electrodes may differ considerably as regards absolute intensity. Finally, in the spectra of copper and nickel electrodes we observed some change in the relative intensity of the reference-pair components in going from one type of electrodes to the other.

Calibration curves plotted for briquetted and cast samples have the same slope but in a number of cases are shifted laterally an appreciable distance. The briquetted samples retain their peculiar spectral characteristics even when the material is formed into small (one gram) briquets and burned in the core of a carbon electrode in an AC arc.

Comparison of the relative intensities of impurity element lines in the spectra of cast and briquetted samples

Base metal of sample	Logarithms of the relative line intensities																									
	As		Cd		Zn		Bi		Sb		Pb		Mn		Ag		Sn		Cu		Ni	
	C	B	C	B	C	B	C	B	C	B	C	B	C	B	C	B	C	B	C	B	C	B	C	B	C	B
Cadmium	—	—	—	—	−0.78	−0.50	−0.90	−0.91	−1.45	−1.52	−0.80	−0.80	—	—	−0.34	−0.42	−0.39	−0.33	−0.60	−0.66	−1.15	−1.28
Zinc	−0.95	−1.18	+0.02	+0.05	—	—	—	—	−1.23	−1.01	−0.82	−0.90	—	—	−1.55	−1.52	−0.56	−0.73	+0.20	0	—	—
Bismuth	—	—	−0.43	−0.63	−0.09	+0.11	—	—	−0.88	−0.91	−0.10	−0.12	—	—	−0.12	−0.25	—	—	−0.72	−0.72	−0.70	−0.76
Lead	−0.52	−0.53	−0.37	−0.34	−0.82	−0.80	+0.60	+0.63	−0.17	−0.17	—	—	—	—	+0.55	+0.54	−0.42	−0.39	−0.67	−0.65	—	—
Aluminum	—	—	—	—	−0.46	−0.37	—	—	—	—	—	—	+0.32	+0.37	—	—	—	—	+0.25	+0.14	−0.14	−0.90
Tin	—	—	−0.16	−0.16	−1.76	−1.73	−0.43	−0.38	−0.48	−0.45	−0.33	−0.37	—	—	−0.93	−0.93	—	—	−0.48	−0.49	−0.96	−1.01
Copper	−1.20	−0.81	—	—	—	—	−0.70	−0.63	+0.11	−0.50	−0.65	−0.17	+0.11	+0.17	−0.23	−0.14	0	+0.13	—	—	−0.35	−0.38
Nickel	—	—	−0.89	−0.62	—	—	—	—	—	—	−0.52	−0.45	+0.03	+0.30	—	—	—	—	+0.34	+0.88	—	—

C = cast. B = briquetted.

In order to evaluate the influence of oxidation on the spectral characteristics of both types of electrodes, the oxygen content in the air surrounding the arc was varied between 0.5 and 25%. Variation of the oxidation conditions had little effect on the spectra of either type and the characteristics peculiar to briquet spectra persisted throughout the entire range.

We also established that the spectra of briquets approach closer to those of cast electrodes as the briquetting pressure is increased. By combining pressing with simultaneous heating of the metal to about 800°C we succeeded in obtaining copper briquets with a spectrum undistinguishable from that of cast copper electrodes.

Our experiments showed that single discharge pulses have a stronger destructive effect on the surface of briquetted electrodes due to their lower thermal conductivity and tend to fuse out more metal from the surface than do like pulses on the surface of cast electrodes. This naturally results in different vaporization conditions and leads to a change in the composition of the vapor mixture in the arc. The spectra of single pulse discharges between briquetted electrodes exhibit the same distinctive characteristics as the spectra of more or less prolonged arcs between such electrodes.

Thus the features peculiar to the spectra of briquets become manifest from the first instant of ignition of the arc, inasmuch as the energy of the initial discharge is localized in a relatively smaller area on the end face of the briquets with a consequent modification of the conditions of vaporization.

* * * * * * *

ON THE USE OF THE METHOD OF PARALLEL WORKING CURVES IN SPECTRUM ANALYSIS OF STEELS

- Iu. M. Buravlev

We investigated the parallelism of the working curves plotted for analysis of high-alloy type Kh12M, 15Kh5MA, N5A, R9, R18, 38KhMIuA and IalT [Х12М, 15Х5МА, Н5А, Р9, Р18, 38ХМЮА + Я1Т] steels, using arc or spark sources with a view to evaluating the feasibility of issuing "control" standards for use in spectroscopic analysis of these steels.

We found that the slope of the working curves for determining most elements in these steels is not invariable. In fact, the slope of the curves depends to an appreciable extent on the composition of the alloy, its structure, the preexposure arcing or sparking time and a number of other factors. Our results show that the assertion of certain investigators (I.S.Fishman, K.A.Sukhenko and others) that the working curves for the same extraneous element in different base alloys are parallel is not borne out in many cases. The originators of the "control" standard method which is based on the assumption that the working curves are parallel claim far more general occurrence of parallelism than is justified in practice. We feel that it is essential to take into account the actual conditions of analysis in each particular case and the differences in the course of the physical-chemical processes on the surfaces of electrodes of different alloys.

The results of analyses of standard samples of steels 38KhMIuA, R9 and R18 carried out on the basis of the absolute blackening show that the blackening of the lines characteristic of the principal components of the alloy differ for different standards, depending on the content of the alloying elements (with virtually the same iron content), and moreover depend greatly on the physical structure of the sample.

In our opinion the equation for the working curve at any instant t in the parking (or arcing) process for a narrow interval of admixture element concentrations in alloys with a similar structure can be written in the form

$$\Delta S_t = \gamma b \beta_t \log C + a_1$$

here β_t is a coefficient characterizing the ratio between the concentration of he element in the initial sample (i.e. before sparking) and the concentration of he element in the luminous cloud.

aboratory of Standard Samples at the
Ural Institute of Metals.

* * * * * * *

RAPID METHOD OF QUANTITATIVE SPECTRUM ANALYSIS OF HIGH-ALLOY STEELS AND ALLOYS

- A.G.Komarovski

We developed a rapid procedure of quantitative analysis of high-alloy steels and heat-resistant alloys for Si, Mn, Cr, Ni, Mo, Ti, W, V, Co, Al B and Nb. The procedure can be used with either a spark or an arc source.

The working curves were plotted by the method of photometric interpolation. With this method, as in the case of photographic photometry[1], we noted a definite regularity in the lateral (parallel) shift of the working curves for any given set of different grades or types of steels and alloys relative to the working curves for binary systems.

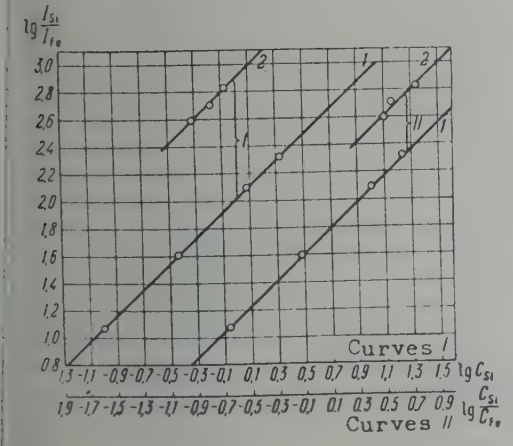

Working curves for determining Si in ordinary steels (1) and high-alloy steels (2) plotted in log I_{Si}/I_{Fe} *vs* log C (I) and log I_{Si}/I_{Fe} *vs* log C_{Si}/C_{Fe} (II) coordinates. Line pair: Si2506.9 & Fe2498.9A

The curves were plotted both in terms of $\log \frac{I_{det}}{I_{comp}}$ *vs* C and in $\log \frac{I_{det}}{I_{comp}}$ *vs* $\log \frac{C_{det}}{C_{comp}}$ coordinates; in the former case the concentration C was expressed in %weight, in the latter in %atomic. By way of illustration the working curves for determining silicon in ordinary and high-alloy steels in both systems of coordinates are shown in the accompanying figure. In both systems in going from ordinary steels (Curve 1) to steels of complex composition (Curve 2) there is a definite parallel displacement of the curve; the shift is somewhat smaller in log I_{Si}/I_{Fe} *vs* log C_{Si}/C_{Fe} coordinates.

We made a very thorough study of the effect of third elements on the analytic results which, as we know, is one of the major factors hindering wider acceptance of spectroscopic methods.

We have proposed a method of taking quantitative account of this effect and suggested an appropriate classification of steels and alloys (see table).

The fact that there is a predictable regularity in the parallel displacement of the working curves and the suggested distribution

of steels and alloys into "working curve" classes should be of practical and theoretical value since it would permit solving the problem of providing spectroscopic standards of steels and alloys in a simpler and more efficient manner.

Distribution of steels and alloys into classes as regards working curves

Determined element	Class No.	Concentration (%) ranges of alloying elements entering into the composition of the alloy of the given class.
Silicon . . .	1	Si 0,3÷1,0; Cr 15,0÷22,0; Ni 7,0÷24,0; Mo 1,5÷4,0; W 0,8÷4,0; Ti 0,2÷1,0; V 0,4÷1,5; Co 9,0÷21,0; Nb 1,0÷3,0
	2	Si 0,2÷1,56+ i.a.o.e.
Manganese . .	1	Mn 0,2÷2,1; Cr 2,0÷7,0; W 4,0÷21,0; Mo 0,2÷1,5
	2	Mn 0,3÷8,6; Cr 0,5÷7,0; Ni 6,0÷25,0; Mo 0,2÷1,0; W 0,9÷7,0; V 0,2÷1,6; Si 0,6÷1,5; Co 0,4÷2,25
	3	Mn 0,3÷28,0+ i.a.o.e.
Chromium . .	1	Cr 4,4÷25,0; Mn 0,4÷7,0; Si 0,2÷1,5; Ni 6,0÷22,0; Mo 2,0÷7,0; W 0,2÷6,0; V 0,2÷2,0
	2	Cr 1,6÷8,0; Mo 0,2÷1,3; W 1,0÷23,0; V 0,4÷1,5
	3	Cr 0,3÷30,0+ i.a.o.e.
Nickel . . .	1	Ni 10,0÷30,0; Cr 12,0÷20,0; Mo 1,2÷3,5; W 0,7÷3,5; Ti 0,25÷1,0; V 0,2÷1,3; Co 3,0÷21,0; Nb 1,0÷3,0
	2	Ni 10÷34,0+ i.a.o.e.
Molybdenum .	1	Mo 0,4÷3,0; Cr 15,0÷19,0; Ni 45,0÷70,0; W 1,0÷3,0; Ti 1,0÷2,0; Co 3,0÷10,0; Nb 1,0÷2,0
	2	Mo 0,5÷6,5; Cr 7,0÷18,0; Ni 7,0÷24,0; W 1,0÷3,0
	3	Mo 0,3÷5,0+ i.a.o.e.
Tungsten . .	1	W 1,5÷17,0; Cr 15,0÷20,0; Ni 15,0÷20,0; Mo 1,0÷3,0; Co 10,0÷19,0
	2	W 1,5÷20,0+ i.a.o.e.
Titanium . .	1	Ti 0,1÷3,5; Cr 9,0÷16,0; Ni 8,0÷24,0; Mo 0,3÷2,6; W 0,3÷1,5; Al 0,1÷2,5; Co 0,5÷3,0
	2	Ti 0,15÷6,75+ i.a.o.e.
Vanadium . .	1	V 0,18÷2,5; Cr 14,0÷22,0; Ni 15,0÷24,0; Mo 1,0÷3,0; Co 10,0÷20,0; Nb 0,6÷3,0
	2	V 0,18÷3,0; Cr 3,0÷9,0
	3	V 0,18÷3,5+ i.a.o.e.
Cobalt . . .	2	Co 4,0÷40,0; Cr 14,0÷20,0; Ni 15,0÷20,0; Mo 2,0÷3,5; W 1,0÷4,0; V 1,2÷2,5; Nb 1,0÷2,5
	1	Co 5,0÷48,0+ i.a.o.e.
Aluminum . .	1	Al 0,01÷1,53; Cr 14,0÷19,0; Ni 15,0÷25,0; W 1,0÷4,3; Ti 0,12÷3,0; Nb 0,6÷2,6
	2	Al 0,01÷2,5+ i.a.o.e.
Boron . . .	1	B 0,001÷0,15; Cr 12,0÷18,0; Ni 45,0÷75,0; Mo 1,5÷4,0; W 3,0÷6,0; Ti 1,5÷2,5; Al 1,0÷2,0; Co 3,0÷10,0
	2	B 0,001÷0,15; Cr 12,0÷18,0; Ni 15,0÷25,0
	3	B 0,001÷0,25+ i.a.o.e.
Niobium . . .	1	Nb 0,1÷3,16; Cr 8,0÷20,0; Ni 9,0÷20,0; Mo 1,0÷4,5; W 0,8÷4,0; Co 10,0÷20,0
	2	Nb 0,1÷3,5; Cr 8,0÷15,0; Ni 9,0÷16,0
	3	Nb 0,1÷4,6+ i.a.o.e.

i.a.o.e. = insignificant amounts of other elements

According to the developed procedure the determination of one element in a sample requires 9 minutes when using an arc and 10 minutes in a spark; the determination of each additional element in the same sample requires one more minute in an arc and one and a half minutes in a spark.

Central Scientific Research Institute
for Technology and Machine Building

Reference

1. A.G.Komarovski, Nauchno-tekhnicheskaia informatsiia (Scientific-Technical Information) No. 13, Mashingiz 1952; Inform.-tekhnicheski listok, LNDTP (Technical Information Pamphlet, Leningrad House of Scientific & Technical Propoganda) No. 71 (1952).

ON THE INTERSECTION OF THE WORKING CURVES OF DIFFERENT SETS OF ALUMINUM-BASE ALLOY STANDARDS

- A.M.Borbat & N.G.Liakhovich

The method of three standards, now widely used in spectroscopic practice, has a number of shortcomings. Consequently a number of investigators have studied the possibility of going over to methods dispensing with the use of standards. Back in 1941 Prokof'ev showed that in the basic analytic expression $\log I_1/I_2 = b \log C + \log a$, the value of b determining the slope of the working curve does not depend on the base material of the alloy[1]. Prokof'ev suggested the idea of carrying out analyses according to a "control" sample, using available standards of alloys with another base. Subsequently Komarovski[2] and Sorokina[3] showed that the magnitude of b is also independent of the physical state of the sample, i.e., that the working curves for solid standards and for standards brought into a liquid state or composed of solutions of the appropriate salts all have the same slope. Hence it may be assumed that the working curves for determining the same element plotted for different sets of standards of alloys of the same base-metal should coincide or at any rate be parallel.

To check this assumption we compared and analyzed the working curves of nine sets of different aluminum-base alloy standards: AL4, AL5, an automobile engine piston alloy, zinc silumin, silumin silicon-aluminum alloy , primary aluminum (two sets of different origin), duraluminum and motorcycle piston alloy. We found that the working curves for determining all elements in the two different sets of primary aluminum standards coincide fully. As for the other alloys, the curves for determining iron, manganese and magnesium all coincide closely; on the other hand the curves for determining silicon and copper in the different alloys intersect at angles ranging from 5 through 20° (see figure).

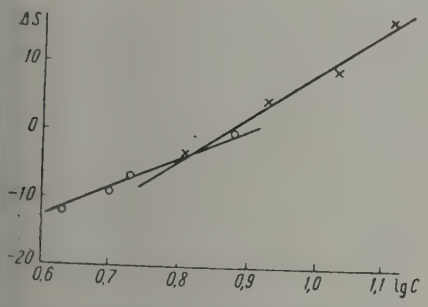

Intersection of working curves for determining Si in silumin and in piston alloy. Source: ordinary spark.

The fact that the working curves intersect (i.e., are not parallel or superposed) cannot be explained as being due to the influence of third elements inasmuch as the same elements are present in most cases. Moreover in the few cases where elements not common to all alloys are present (zinc silumin and silumin) the character of the intersection is the same. Nor can the intersection of the curves be attributed to the diluent action of the third elements since it occurs when these are present in the alloys whose curves intersect in approximately the same total amounts. Further, it cannot be explained by the effect of background or the peculiarities of the analytic line pairs, for it also occurs when the limiting concentrations of the determined element in both sets of standards are about equal. Finally, the intersection cannot be blamed on differences of heat treatment or physical structure of the standards. Our tests showed that preliminary heat treatment has no effect on the results of analyses of AL4 and AL5 alloy samples. The annealing curves for these two alloys also coincide.

In view of the above we made the tentative assumption that the presence of intersection, i.e., the deviation from the regularity discovered by Prokof'ev, is due to systematic errors in chemical analysis. Check analyses of the composition of the set of motorcycle piston alloy standards made at two different chemical laboratories (at the Kiev and the Irbitsk Motorcycle Plants) showed deviations in the chemical composition only as regards silicon and copper. In other words the working curves plotted according to the data of each of the laboratories coincided

for Mg, Mn and Fe, while the Si and Cu curves intersected. This tends to confirm our assumption regarding the presence of systematic errors in the results of chemical analyses for Si and Cu.

Kiev Motorcycle Plant

References

1. V.K.Prokof'ev, Izv. AN SSSR, Ser. fiz., 5, 366 (1941).
2. A.G.Komarovski, Inform.-tekhnicheski listok, LDNTP (Technical Information Pamphlet, Leningrad House of Scientific & Technical Propaganda) No. 70 (1952).
3. N.N.Sorokina, Izv., AN SSSR, Ser. fiz., 14, 567 (1950).

* * * * * * *

INVESTIGATION OF THE INFLUENCE OF STRUCTURE ON THE RESULTS OF SPECTRUM ANALYSIS OF R9, R18 and 38KhMIuA STEELS

- Iu.M.Buravlev

The conclusions arrived at by different authors of reports devoted to investigations of the influence of structure on the results of spectrum analysis of medium- and high-alloy steels are often contradictory and incomplete.

The present investigation was initiated in connection with the work of the Laboratory of Standard Samples preparatory to issuing spectroscopic standards of multiple-component alloy steels. The purpose of the investigation was to determine the influence of structure resulting from different heat treatments (quenching and annealing) on the results of spectrum analysis of R9, R18 and 38KhMIuA [P9, P18 & 38XMIOA] type steels, using domestic equipment (ISP spectrograph, IG-2 spark generator and MF microphotometer).

We found that the effect of structure can lead, in individual cases, to systematic deviations of up to 15-20% (relative). Structure affects the degree of blackening (relative and absolute) of the spectrum lines of both the alloying elements and the basic material which results in a change in the angle of the working curves and a shift in the position of the curves for hardened samples relative to the curves for soft ones.

The magnitude of the effect of structure on the results of analysis depends to some extent on the conditions of analysis: the pre-sparking time, the material of the counter electrode, the composition of the alloy, etc.

We also established that changes in structure due to cold working of Type IalT [1I1T] stainless steels affect the results of spectrum analysis of such steels (the resultant change for some elements may be as great as 10-15% relative).

Laboratory of Standard Samples
at the Ural Institute of Metals

* * * * * * *

THE INFLUENCE OF HEAT TREATMENT AND DEFORMATION ON THE RESULTS OF SPECTRUM ANALYSIS OF R18 HIGH-SPEED TOOL STEEL

- I.A.Grikit

Deformation (forging, rolling) and heat treatment of R18 [P18] steel - commonly used to improve its cutting characteristics - have an appreciable effect on the results of spectrum analysis of this steel for W, V and Cr (using Laboratory of Standard Samples Standards Nos. 60, 61, 64 & 68): in the case of cast samples the results of spectrum analysis are appreciably higher than the values determined by chemical analysis.

To investigate the reasons for the observed difference we had cylindrical bars (20 mm in diameter) cast from two production lots of the R18 steel. The bars were cut in half: one half was left in its initial state; the other was subjected to deformation by forging. Three samples were then prepared of each piece: one pair of samples (one cast, one forged) was hardened; a second pair was annealed (in each case the heat treatment procedure was analogous to that employed in production) while the third pair was left without heat treatment.

The spectra were photographed on the same plate 20 times each on an ISP-22 spectrograph. The source was an IG-2 spark generator connected in a Raiski circuit.

Analysis of the experimental data (see table) brings out the influence of change in structure produced by deformation on the results of spectrum analysis. The determined values of tungsten and vanadium are higher for the cast as compared with the forged samples. On the other hand, heat treatment has no noticeable effect on the results in either the cast or the forged state.

Results of analysis of cast and forged samples of R18 steel for W, V and Cr (arithmetic mean for 20 measurements - %)

Determined element	Melt No.	In cast state			In forged state		
		no heat treatment Sample #3	annealed Sample #4	hardened &tmpred Sample #5	no heat treatment Sample #6	annealed Sample #7	hardened & tempered Sample #8
W	1	17,52	17,60	17,64	16,65	16,68	16,59
	2	15,63	16,28	16,42	15,35	15,38	15,31
Cr	1	4,35	4,40	4,42	4,35	4,23	4,30
	2	4,66	4,50	4,57	4,33	4,25	4,42
V	1	2,11	2,17	2,22	2,03	1,93	1,99
	2	2,17	2,15	2,19	1,92	1,82	1,99

The deviation of the results for samples in the cast state (C_1) from the results for samples in the forged state (C_2) cannot be explained as being due to accidental experimental errors since the difference $C_1 - C_2$ for W and V exceeds the maximum possible error $3m_K$. The root mean square error m_K based on 20 determinations amounts to 0.12% for W, 0.02% for V and 0.04% for Cr. Hence the deviation between cast and forged samples as regards the determined W and V content must be attributed to differences in structure.

In analyzing the same samples in an arc (PS-39 generator source) we failed to detect any noticeable influence of changes in structure due to deformation and heat treatment on the analytic results.

We also obtained sparking-off curves for some of the samples, maintaining a continuous spark and moving the plate holder at the end of every three minutes (the exposure time). Thus the preceding total exposure time equalled the pre-sparking time for each successive photograph.

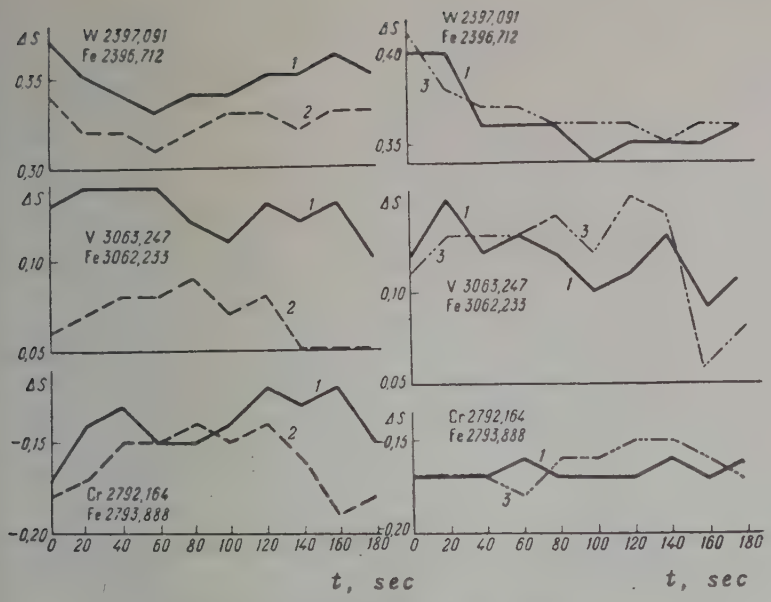

Sparking curves (ΔS vs time) for samples of R18 steel with different structure (resulting from mechanical and heat treatment) obtained in determining W, V and Cr: 1) Sample No. 4 (cast & annealed); 2) No. 7 (forged & annealed); 3) No. 5 (cast and hardened).

The resultant curves (see figure) show that the relative intensities of the W and V lines in the cast samples are appreciably greater than in the forged samples and that this difference persists even after prolonged sparking. On the other hand the relative intensities of the Cr lines differ little in cast and forged samples.

The relative intensity of the analytic line pairs used is affected little if at all by heat treatment in the case of either forged or cast samples.

Metallographic studies have established that the cast and forged samples differ in structure. The cast samples have free carbides in the form of an eutectic material, surrounding the grains and constituting large inclusions of typical "skeletal" form; high-alloy austenite with a thin carbide network fills the interdendritic spaces. The forged samples, in contrast, have a structure characterized by a uniform distribution of fine carbide particles with a broken down cementite-austenite eutectic network; the Laboratory of Standard Samples standards also have this type of structure.

* * * * * * *

ON THE WORK OF A STEEL WIRE PLANT SPECTROSCOPIC LABORATORY

- A.V.Sokolova

Most present-day spectroscopic procedures for steels have been developed for analyzing samples over 10 mm in diameter. In our laboratory - since our plant produces steel wire - we have to deal with samples well under 10 mm in diameter.

With the aid of the Physics Department of the Magnitogorsk Mining-Metallurgical Institute[1] and by virtue of studies carried out in the laboratory since 1948 we have developed a method of sorting (grading) analysis for chromium by means of a steeloscope. This method is now used for inspection of steel wire down to 0.01 mm in diameter made of the following types of steel: Kh20N80, Kh20N80T, Kh20N80TZ, Kh15N60, Kh25N20, Kh25N15, 1Kh18N9T, 0Kh18N9, Kh20N10T6, EI464, Kh25Iu5, Kh17Iu5, Kh13Iu4, EZh1, R18, 50KhFA, 20KhMA, ShKh6ShKh10* and carbon steel. Wires 0.01 to

* = X20H80, X20H80T, X20H80T3, X15H60, X25H20, X25H15, 1X18H9T, 0X18H9, X20H10T6, ЭИ464, X25I05, X17I05, X13I04, ЭЖ1, Р18, 50ХФА, 20ХМА, ШХ6ШХ10

1.5 mm in diameter are twisted into a bundle of several lengths; 1.6 to 3.0 mm wires require no special preparation while samples of wire over 3.0 mm are sharpened to a point. The spark is ignited between the end of the sample and a copper disk electrode. The analytic indications do not vary with the wire diameter.

Utilizing the experience gained in sorting analysis, the laboratory has recently developed a method for determining manganese in the 0.9 to 1.2% range in 35G steel wire 1.0-3.0 mm in diameter. The source is a Raiski circuit spark generator supplying a 2.0 mm spark gap.

We use the method of photometric interpolation; analyses are made on an ISP-22 spectrograph with a 0.02 mm slit setting. The slit is illuminated by a single lens condenser in the standard setting. The Mn 2939.3 and Fe 2936.58 A lines serve as the analytic pair. Photographic plates: positive, speed - 0.25 GOST. Exposure - 10 sec. Standards: selected production samples.

For 1.6 to 3.0 mm diameter samples the upper (counter) electrode is an 8-9 mm diameter copper rod tapered at the point to a 1 mm diameter flat; the standards are 2.0 mm diameter samples. Pre-sparking has no effect on the relative intensity of the selected line pair. Samples 1.0 to 1.5 mm in diameter are twisted into bundles consisting of 3 to 6 pieces of wire and the spark end of the bundle is sanded flat. Here the wire bundle is the upper electrode, while the permanent, lower electrode is a spectroscopic carbon rod tapered to a 1.0 mm flat at the tip. Standards are 1.0-1.2 mm samples. The sample is pre-sparked 60 seconds. The working curves for both types of samples are shown in the figure. There is good agreement between the results of spectroscopic determinations and those of chemical analysis. The mean relative error amounts to ±1.7%.

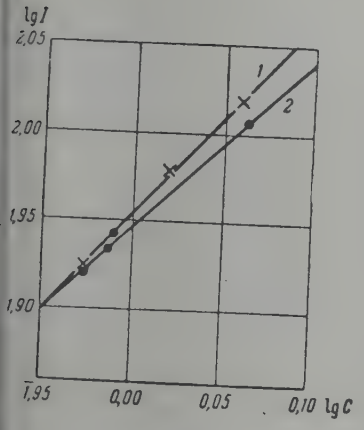

orking curves for determining Mn (0.9-1.2%) n steel wire: 1) in 1 o 1.5 mm wire; 2) in .6 to 8.0 mm samples.

We also developed a method (using the same excitation and illumination conditions) for determining copper (0.10 to 0.25% range) in carbon steels in the form of rolled wire 6-8 mm in diameter. The analytic pair used for copper is Cu 3273.96 & Fe 3286.76 A. The premanent electrode is a carbon rod tapered to a 1 mm flat at the tip. Both the main and auxiliary gap equal 2.5 mm. Preliminary sparking has no appreciable effect on the relative intensity of the selected analytic pair. The sparked area is a circle 3.0-3.5 mm in diameter. Plates: Spectral, Type I. Exposure: 25 sec. The intensity easurements are made by the method of photometric interpolation. The mean relaive error is 2.8%.

Reference

1. V.V.Borovkov & P.D.Korzh, Zavod. labor (The Plant Laboratory) 6, 744 (1949).

* * * * *

SPECTROGRAPHIC ANALYSIS OF CARBON AND LOW-ALLOY STEELS AND PIG IRON

- N.V.Buianov

Analysis of low-alloy and carbon steels

The present instructions apply to the determination of Mn, Si, Cr, Ni, Al, Mo and Ti. The analytic line pairs and corresponding concentration intervals are listed in the table. These instructions are also applicable to medium-alloy steels, provided the amount of admixtures and alloying elements does not exceed 5-6%.

Analytic line pairs and concentrations

λ, Å		Range of concentrations, %
Determined element	Comparison element	
Mn 2933,06	Fe 2920,69	0,20 ÷ 1,20
Si 2528,52	Fe 2530,69	0,03 ÷ 0,50
Si 2881,58	Fe 2869,31	0,01 ÷ 0,50
Cr 2677,15	Fe 2684,76	0,02 ÷ 1,20
Ni 3050,82	Fe 3055,26	0,05 ÷ 1,20
Al 3092,71	Fe 3055,26	0,01 ÷ 0,30
Mo 3170,35	Fe 3178,02	0,01 ÷ 0,30
Ti 3088,02	Fe 3055,26	0,02 ÷ 0,30

Sampling and preparation of sample. Sampling is accomplished by casting into a cast iron chill mold in the shape of a truncated pyramid: bases - 50 and 80 mm squares, height - 120 mm. The sample is deoxidized with aluminum and forged into a square in the longitudinal sense. The forged sample should be 35 x 35 mm square and 250 mm long. The weight of the sample should not be less than 100 grams.

A layer some 2-3 mm thick is ground off an area 30 x 30 mm on the surface of the sample with an abrasive wheel; the area is then cleaned with a smooth-out file to remove all defects and leave a smooth and even surface*.

Counter electrode. A rod of electrolytic copper is used as the permanent electrode; the rod is 8 mm in diameter and is tapered to a diameter of 1.5-2.0 mm at the tip.

Where copper electrodes are not available spectroscopic carbons 6 mm in diameter may be used; these are pointed by means of a special sharpener (like a pencil sharpener) to a 45° cone. The tip of the cone is then blunted with a file to obtain a 2.0-2.5 diameter flat. However, it should be borne in mind that when a carbon counter electrode is used the reproducibility deteriorates by $0.005-0.008 \cdot \Delta S$.

Photography. The spectra are photographed on an ISP-22 spectrograph with a slit width of 0.015 mm. The source and the elements of the illuminating system must be located at the standard distances from the slit specified in the ISP-22 instruction manual. Or a single f = 214 mm condenser lens may be used for illuminating the slit; in this case the slit to source distance is determined experimentally (200 to 400 mm), to suit the speed of the photographic plates employed.

The DG-1 arc generator, operated at 5 amp and 220 v should be used for the source (if this is not available a PS-39 source unit may be used). The current in the primary of the transformer should be 0.2 amp; the discharger gap 0.6-0.8 mm (the selected setting should be rigorously maintained). The sample to counter electrode distance should be 1.5 mm; the pre-arcing time - 10 sec; exposure - 40-60 sec, depending on the speed of the plates.

The spectra are photographed on Spectral Type I plates, with a speed rating of 0.5 or 1.0 GOST. The plates are developed in metol-hydroquinone developer for

---

* a) In preparation for determining titanium it is not permissible to use an abrasive wheel containing this element. b) The emery wheel and file must be kept scrupulously clean and should not be used for any other purposes. c) Where defects cannot be removed by grinding and filing, the sample should be discarded.

13 minutes at 19-21°; after being washed in pure running water the plates are fixed in acid hypo.

In the case of rapid analysis each sample is photographed at least two times; in grading analysis - at least three times. If the results of photometry of the analytic lines in the several spectrograms differ by more than 0.05, the photography (analysis) is repeated.

Photometry. Photometry is effected by interpolation by means of a nine-step spectrum weakener. Usually the interpolation is accomplished on a PS-18 spectrum projector; however, in some cases (for example, in cases of samples on the border line between grades or when the analytic lines compared differ as regards contour) it is more convenient to use a microphotometer.

In carrying out grading analyses the plate should be dried for 1.5-2 min in a vacuum drier or for 4-6 min in a stream of warm air obtained by means of a fan blowing over an electric hot-plate.

Plotting the working curves. The working curves are constant curves, i.e., are independent of the gamma of the photographic plate. The curves are plotted in a logarithmic scale in terms of log I_x/I_{Fe} *vs* log C. Each of the standards or control samples used for plotting the working curves must be photographed 15-18 times on 5-6 different plates. The average value of log I_x/I_{Fe} (from the 15-18 spectrograms) is used in plotting.

As a rule working curves to be used for grading analysis should be based on standard samples. For rapid, in-production analysis (and if necessary in some cases for grading analysis) the working curves may be plotted on the basis of analyzed samples. "Analyzed samples" are here understood to mean samples taken from the production of the given plant and repeatedly and carefully analyzed by different chemical methods. These samples should also be checked for homogeneity.

In order to verify the validity of the curves (i.e., the stability of the analytic process) 1-2 standards should be photographed at least once each working shift.

Speed and accuracy of analysis. The normal time for rapid analysis of a sample for 2-3 elements is 14-17 minutes; the time for a like grading analysis is 17-19 minutes. In case the concentration of an element is just on the border line between grades, the photography should be repeated and, in this case, the time for analysis increases accordingly.

The accuracy of analysis meets the GOST (All-Union State Standards) requirements for rapid and grading analyses. The required accuracy as regards determination of aluminum in concentrations from 0.01 to 0.3% is not specified in the GOST; however, the determination of this element is guaranteed to the same degree of accuracy as that of molybdenum.

Spectrographic analysis of pig iron

The present instructions apply to the determination of manganese and silicon in pig iron in the 0.80-4.40% range for Mn and 0.20-1.50% for Si. The analytic line pairs are Mn 2889.58 - Fe 2883.7 A and Si 2516.12 - Fe 2518.10 A.

Sampling and preparation. The sample is cast in a special chill mold, producing a small ingot with 4-6 fingers, 6 mm in diameter. The fingers are broken off for spectrum analysis, while the main part of the ingot remains for a check chemical analysis where necessary. The base end of the broken off finger is ground on an abrasive wheel to remove all defects and obtain a smooth even surface.

Counter electrode. The permanent electrode is a 6-8 mm diameter rod of electrolytic copper with a truncated cone tip (1 mm diameter flat).

Equipment, photography, photometry and working curves. The equipment and procedure as regards photography, preparation of the working curves and photometry remain the same as described above for steels, except as follows:

The source employed is an IG-2 spark generator operated at 1.5 amp and 220 volts (set for one discharge train per half-cycle). C = 0.01 μf; L = 0.01 μH; discharger (auxiliary) gap = 3 mm; gap between electrodes = 2 mm; pre-sparking -

45 sec; exposure - 45-60 sec.

Photographic plates - Spectral Type I, speed 0.5-1.0 GOST. Development and fixing as above.

Speed and accuracy. The normal time for rapid analysis of one sample is 15-16 min; the time for grading analysis is 17-18 min. When the sample turns out to be on the border line between neighboring grades it is rephotographed and the time required increases accordingly.

The accuracy meets the GOST specifications for the corresponding types of analyses.

Spectrographic determination of copper in carbon and low-alloy steels

Copper is determined in the 0.04 to 0.40% range of concentrations according to the Cu 3273.96 - Fe 3286.76 A line pair. The method of taking and preparing the sample, the spectroscopic equipment, photography, photometry and curve plotting procedure remain the same as in analyzing the steels for Mn, Si, Cr, etc.

Counter electrode. A spectroscopic carbon rod 6 mm in diameter is used as the permanent electrode. The electrodes are shaped by means of a special sharpener (similar to a pencil sharpener) to a 45° cone point. The tip is filed to a 1.5-2.0mm diameter flat.

Photographing conditions. Source: IG-2 spark generator; current and voltage - 1.7 amp, 220 v; C = 0.01 μf; L = 0.01 μH (one discharge train per half-cycle); discharger (auxiliary) gap - 3 mm; main gap - 2 mm; pre-sparking time 30 sec; exposure - 60 sec. The photographic plates and processing remain the same as above.

Speed and accuracy. The normal time for rapid analysis of one sample is 11-13 min; the time for grading analysis is 14-15 min. In border line cases the photography is repeated and the time required increases accordingly. The accuracy of analysis for concentrations to 0.1% is guaranteed to within 0.01%; for concentrations between 0.1 and 0.4%, to within 0.02%.

Central Scientific Research Institute
of Ferrous Metals

* * * * * * *

OPERATIONS OF THE LABORATORY OF STANDARD SAMPLES CONCERNED WITH THE PREPARATION OF STANDARDS FOR SPECTRUM ANALYSIS

- V.V.Stepin

At present the Laboratory is producing the following spectroscopic standards:

a) Set V - low and medium-alloy steels having the following concentrations of alloying elements: Mn - 0.25-1.95, Si - 0.11-2.09, Cu - 0.24-0.49, Cr - 0.23-4.25, Ni - 0.19-4.80, W - 0.71-2.91, Mo - 0.23-0.71, Ti - 0.027-0.31%.

b) Set VI - type R9, R18, EI262 & EI347 steels [Р9, Р18, ЭИ262, ЭИ347].

c) Set VII - Bessemer pig irons, having 0.43-1.98 Mn and 0.69-2.23% Si.

d) Set IX - EIalP steels [ЭЯ1П].

e) Set X - 38KhIuA steels [38ХМЮА].

f) Set XI - ferrochrome.

Before the end of 1954 the Laboratory will issue two more sets: XII - carbon steels and XIII - ferromanganese.

In addition the Laboratory has available for steeloscopic analysis standard samples of the following grades of steel: 5KhVG, 18KhVA, 5KhVGS, KhV5, R18,

45KhIMFA, 3AKhGSA, Kh18N123G, Kh10S2M, 4Kh14, N14VGM [5XBГ, 18XBA, 5XBГC, XB5, P18, 45XHMФA, 3AXГCA, X18H12M3Г, X10C2M, 4X14, H14BГM] and steel with niobium.

Investigations at the Laboratory have established that spectroscopic analyses of samples of EIa1P [ЭИ1П] steel in its ordinary state (after hot deformation) and after cold working (cold plastic deformation) yield divergent results.

Studies of the standards comprised in Set X have shown that changes in structure produced by different heat treatments (hardening, annealing, etc.) have an appreciable effect on the results of spectrum analysis of these steels. In view of this the Laboratory has started issuing the standards of Set X in three states: after rolling without further heat treatment, after hardening and after annealing (according to the GOST procedure). In order to minimize the influence of structure the Laboratory recommends the use of spark excitation with a continuous flow of oxygen through the gap (supplied through a special auxiliary electrode) in analyzing samples with an unknown thermal history.

The Laboratory has developed a procedure for investigating the homogeneity of standards, based on taking account of metrological requirements and metallurgical regularities involved in the formation of defects and inhomogeneities in the metal. The Laboratory is also conducting research aimed at developing more efficient methods of preparing and analyzing spectroscopic standards, particularly as regards spectroscopic methods for determining the chemical composition of standard samples with reference to synthetic solutions.

In 1955 the Laboratory plans to add the following to its list of available standards: a) Set XIV - high chrome steels, b) Set XVII - nickel steels, c) Set XVIII - pig irons for the production of steel, d) Set XIX - cast irons, e) Set XX - silicon steels and f) Set XXI - chrome-silicon steels.

Laboratory of Standard Samples
at the Ural Institute of Metals

* * * * * * *

SPECTRUM ANALYSIS OF TITANIUM FOR IMPURITIES

- Sh.G.Melamed, M.A.Notkina & S.M.Solodovnik

The metallic titanium is transformed into the dioxide by heating in air in a muffle furnace at 1000°C (the actual temperature in the reaction zone is appreciably higher and depends on the particle size of the metal powder). Control experiments showed that there is no loss of the admixture elements incident to the burning process. When the sample is in the form of titanium tetrachloride it is converted to the dioxide by hydrolysis. The advantage of converting to the dioxide is that this makes it possible to prepare standards synthetically. We prepared all the necessary standards (except for P) by adding oxides of the appropriate elements to pure dioxide of titanium. In the case of phosphorus, the standards were prepared by adding magnesium pyrophosphate to the pure dioxide. The titanium dioxide, free of magnesium and calcium, was prepared by hydrolisis of the tetrachloride; the dioxide free of silicon was made by partial distillation of the tetrachloride and hydrolysis of the less volatile fraction (the boiling point of $SiCl_4$ is 57° whereas that of $TiCl_4$ is 137°, hence the former distills over first).

We recommend three different methods of exciting the spectrum, the choice depending on the volatility of the determined elements and the analytic sensitivity required.

The first method is intended for determining phosphorus and consists of vaporizing the phosphorus from a deep cup (6 mm deep, 2 mm diameter) in a carbon electrode in a DC arc. We photographed the spectrum on an ISP-22 spectrograph equipped with a three-lens condenser. Very little titanium enters the flame of the arc and only a few titanium lines appear in the spectrum obtained. The determination is based on the absolute blackening of the P I 2553.28 A line. Under our conditions the more intense P I 2535.65 A line could not be used since with the dispersion of the ISP-22 spectrograph it is overlapped by the very sensitive Ti II 2535.87 A line.

We found that the formation of TiC in the electrode core does not further the supression of the titanium spectrum.

The sensitivity of phosphorus determination is 0.01%. The relative error is ±8%. In the KS-55 spectrograph the P I 2535.65 and Ti II 2535.87 A lines are resolved so that phosphorus concentrations down to 0.005% can be detected with the aid of this instrument.

The second method is intended for determining silicon and magnesium and consists of simultaneous vaporization of the admixtures and the titanium dioxide from the core of a carbon electrode, connected as the anode in a DC arc. A mixture consisting of 15 mg of the TiO_2 sample, 7.5 mg of carbon powder and 7.5 nickel oxide was packed into the electrode cup. The spectra were photographed on an ISP-22 spectrograph with a three-lens condenser. The Si content was determined on the basis of the relative blackening of the Si I 2516.12 and Ni 2540.02 A lines. The sensitivity for Si is 0.01%. Mg was determined from the relative blackening of the Mg II 2795.83 and Ti II 2784.64 A lines in the 0.001 to 0.03% range and from the relative blackening of the Mg 2779.83 and Ti II 2784.64 A lines in the 0.03% up range. The relative deviations of single determinations were computed to be ±8% for Si and ±9% for Mg.

The third method is intended for determining Si, Mg and Ca and is based on the use of a spark source. A mixture consisting of 100 mg of the TiO_2 sample and 800 mg of powdered copper was compressed in a split mold at a pressure of 6000 kg/cm^2. The resultant 9 mm diameter briquet was then mounted on a copper stage electrode. The upper electrode was a carbon rod. The spark spectrum was photographed on an ISP-22 spectrograph. The spark was supplied by means of an IG-2 generator, connected in a complex (Raiski) circuit and adjusted for the maximum inductance (0.55 mH) and minimal capacitance (0.005 μf). The current in the transformer primary was 0.5 amp.

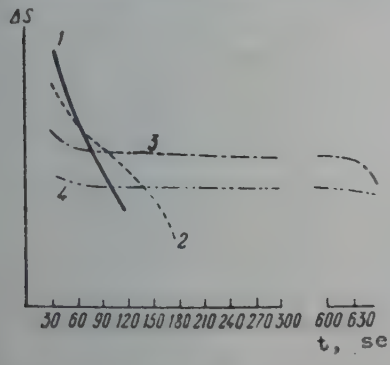

Influence of the relative Cu content on the blackening of the Mg line. Ratios of TiO_2 to Cu: 1) 1:1, 2) 1:2, 3) 1:3, 4) 1:16.

The ratio of the amount of copper to the amount of titanium in the briquet has an appreciable effect on the relative intensity of the lines of the determined elements and on the stability of the relative and absolute blackening (see figure). As may be seen from the curves the optimum TiO_2 to Cu ratio is about 1:8. With this ratio the relative blackening of the Mg line remains constant over a period of 10 minutes. A like effect obtains for Si and Ca. The determinations were made on the basis of the relative degrees of blackening of the following line pairs: Mg II 2795.53 - Ti II 2805.01 A and Ca II 3968.47 - Ti 3958.21 A.

The sensitivity as regards Si is 0.1%; Mg 0.003% and Ca 0.01%. The relative deviation of an individual analysis is ±5%.

The three described methods can be extended to analyses for other impurities. The relative sensitivity of each will vary, depending on the determined elements. With three alternatives to choose among, the most suitable may be selected for each particular case.

* * * * *

SPECTROSCOPIC DETERMINATION OF IMPURITIES IN VANADIUM PENTOXIDE

- P.M.Polikov & A.K.Rusanov

The purpose of the present project was the development of methods of quantitative spectroscopic determination of the extraneous elements most commonly encountered in vanadium compounds. Given appropriate spectrum excitation and sample vaporization conditions the impurities common to vanadium compounds can be determined by means of a medium dispersion quartz spectrograph (the ISP-22) and a glass spectrograph (the ISP-51). The most satisfactory results were obtained in analyzing the spectra of vanadium pentoxide, into which metallic vanadium and most vanadium compounds can be easily converted.

Use of the pentoxide eliminates the difficulties that may otherwise be encountered in connection with non-uniform distribution of the impurities through the sample; also use of the pentoxide simplifies the preparation of standards, since they can be easily made by adding appropriate quantities of compounds of the determined elements to pure vanadium pentoxide.

We found the best universal source to be a carbon arc (AC or DC). Vaporization of 20 mg of the pentoxide from the core of the anode in a carbon arc (220 v, 10 amp) permits of detecting a considerable number of impurity elements with the following sensitivities: Be, Cd, Mg, Mn, Cu and Sn to 0.001%, Al, As, and Sb to 0.003%, Ba, Bi, Ge, Fe, Co, Si, Ni, Pb, Cr and Zn to 0.01%, W, Mo, Nb, Ta and Zr to 0.003%.

Quantitative procedures were developed for determining the following: Al, Bi, Fe, Co, Ca, Si, Mn, Mg, Cu, As, Pb, Sb and P.

Analytic pairs, concentration ranges and probable deviations

Determined element & analytic line pair (λ, A)	Internal standard & percent introduced into the pentoxide	Range of determined concentrations, (%)	Type arc	Probable deviation, (%)
AlI 3961,53—VII 3951,97	—	0,001÷0,1	DC	±12
BiI 2897,98—SnI 2594,42	SnO_2—0,5	0,01 ÷0,3	DC	±11
FeI 2599,70—NiII 2437,89	NiO—4	0,01 ÷0,3	AC	±12
SiI 2519,2 —NiI 2540,02	NiO—4	0,01 ÷0,3	AC	± 9
CdI 2288,02—SnI 2286,68	SnO_2—0,5	0,001÷0,04	DC	±11
MnII 2593,73—NiII 2437,89	NiO—4	0,002÷0,3	AC	±10
MgII 2795,53—NiI 2821,29	NiO—4	0,001÷0,1	AC	±10
CuI 3247,54—NiI 2821,29	NiO—4	0,001÷0,1	AC	±11
AsI 2349,84—SnI 2354,85	SnO_2—0,5	0,004÷1,0	DC	±12
SbI 2598,06—SnI 2594,42	SnO_2—0,5	0,001÷0,3	DC	±12
PbI 2833,07—SnI 2594,42	SnO_2—0,5	0,004÷1,0	DC	±12
PI 2535,65— backgnd	—	0,02 ÷1,0	DC	±11
ZnI 3302,59— backgnd	—	0,01 ÷1,0	DC	±11

Instruments: Aluminum - ISP-51 glass spectrograph; all others - ISP-22 quartz spectrograph.

The procedure for the determination of aluminum is based on complete vaporization of the sample of vanadium pentoxide mixed with carbon powder from the anode (well 2 mm in dia., 5 mm deep; tip of electrode tapered to 3.5 mm); the determination is made on the basis of the difference in blackening of selected Al and V lines. The procedure for Fe, Mn, Mg, Si and Cu consists of vaporizing a 70 mg sample mixed with carbon powder from the cores of two vertical carbon electrodes in an AC arc (wells 3 mm in dia., 5 mm deep; tip tapered to 4 mm). The determinations are based on the difference in blackening between selected lines of these elements and appropriate nickel lines. The procedure for the more volatile elements (Sn, Bi, As, Ca, Pb and Zn) calls for complete vaporization of a 40 mg sample from the core of the anode (well 4 mm in dia., 6 mm deep; outside diameter of electrode 6 mm). The determination is based on comparison of the blackening of the element lines with that of near lines of tin. For determining phosphorus use is made of selective vaporization of the element from a sample packed into a deep well in the anode (well 2 mm in dia., 7 mm deep). The determination is based on measurement of the absolute blackening of the analytic P line. It was established that when iron is present in concentrations above 0.03% it vaporizes simultaneously with the phosphorus and interferes with the determination due to superposition of the Fe I 2535 A line on the analytic P I 2535.65 line. The analytic pairs for the determined elements, the ranges of determined concentrations and the probable deviations are listed in the accompanying table.

* * * * * * *

DETERMINATION OF ANTIMONY IN ITS ORES AND OF IMPURITIES IN ANTIMONY TRIOXIDE AND METALLIC ANTIMONY

- S.M.Solodovnik

The present report is concerned with various analytic procedures developed to facilitate production control of antimony, ranging from spectrum analysis of antimony ores through analysis of the finished product - metallic antimony. All the analytic work was done on an ISP-22 spectrograph.

Determination of antimony in ores

The composition of antimony ores is fairly uniform: the principal component of most antimony minerals is silica, the content of which varies between 50 and 80%.

The spectrum source was a DC carbon arc (8 amp, 180 v), the sample being vaporized from the core of the cathode (2 mm in dia., 5 mm deep). The determinations were based on the variation of the relative blackening of the Sb 2877.91 and the internal standard, Cd 2868.2 A, lines. The standards were either chemically analyzed ore samples or synthetic samples prepared with a base similar in composition to that of the analyzed samples.

Determinations were made in a range of concentrations from 0.03 to 2% with a probable deviation of 9-11% for individual analyses. It was established that the presence of barite and fluorite does not affect the analytic results. The presence of a large proportion of feldspar (over 20%) results in an under-evaluation of the Sb content, presumably due to reduction of the arc temperature by the potassium and sodium common in feldspars.

Determination of impurities in antimony trioxide

Our Soviet industry produces optical and phosphor grades of antimony oxide. The latter must meet particularly exacting requirements: according to the provisional technical specifications the maximum allowable amounts of impurities are lead - 0.01%, copper - 0.001%, iron - 0.002% and nickel - 0.001%.

The procedure developed meets these requirements as regards sensitivity. For analysis the oxide powder is vaporized from the core (2.5 mm dia., 5 mm deep) of a carbon electrode (4 mm outside diameter). The analytic line pairs, concentration ranges and relative deviations are listed in Table 1. The spectroscopic values show satisfactory agreement with the results of chemical analyses.

Table 1

Analytic line pairs, concentration ranges and accuracy of determining impurities in antimony trioxide

Impurity	Analytic lines (A): Impurity	Analytic lines (A): Antimony	Range of concentrat.%	Accuracy of method
PbI . . .	2833,07	2858,04	0,003 ÷ 1,0	± 9,0
FeI . . .	3020,64	2858,04	0,001 ÷ 1,0	±12,0
NiI . . .	3050,82	2858,04	0,001 ÷ 1,0	±12,0
Cu I . . .	3247,55	2858,04	0,001 ÷ 0,1	± 7,0

Determination of impurities in metallic antimony

Some time ago we developed a procedure for determining Pb, As, Bi, Sn, Cu, Ag, Zn, Co, Mn, Ni and Fe in metallic antimony using a spark source[1]. The sensitivity of detection corresponds to the technical specifications for Grade SuO [CyO = Antimony, Optical] antimony.

In view of the need for determining even lower concentrations we developed a more sensitive procedure based on the use of an interrupted AC arc.

With both procedures the standards are prepared in the following manner: the main standard is prepared by melting antimony with an appropriate quantity of the impurity elements in a stream of hydrogen; the other standards are then prepared by grinding each preceding standard with an additional quantity of pure antimony. The successively diluted mixtures are formed into cylindrical electrodes (6-8 mm in dia.) by compression at 6000-7000 kg/cm^2 in a suitable mold by means of a manual hydraulic press.

The quantitative determinations are based on the relative blackening of the impurity lines as compared with an appropriate Sb line. The analytic line pairs, concentration ranges and deviations are listed in Table 2.

Table 2

Same as Table 1 but for analysis of metallic antimony

Impurity	Analytic lines (A): Impurity	Analytic lines (A): Antimony	Range of concentrations %	Accuracy of method, %
Pb . . .	2833,07	2851,10	0,001 ÷ 0,3	±3,8
Bi . . .	3067,72	3232,52	0,0004 ÷ 0,3	±3,8
Cu . . .	3247,55	3232,52	0,001 ÷ 0,3	±5,1
Ag . . .	3280,67	3232,52	0,0004 ÷ 0,1	±4,3
As . . .	2780,20	2851,1	0,003 ÷ 0,3	±3,9
Zn . . .	3345,0	3232,52	0,001 ÷ 0,3	±3,8
Co . . .	3405,12	3383,15	0,002 ÷ 0,5	±3,3
Ni . . .	3619,39	3637,83	0,002 ÷ 0,5	±3,9
Mn . . .	2794,82	2769,94	0,002 ÷ 0,5	±5,0
Sn . . .	3175,02	3232,52	0,0004 ÷ 0,3	±3,9

We also developed a quantitative spectroscopic method for determining a few thousandths of one percent of sodium in antimony after converting the latter into the oxide by dissolving it in nitric acid and then heating the precipitate. The Na concentration is determined in the arc spectrum obtained in vaporizing the oxide sample from the core (4 mm dia; 8 mm deep) of a carbon electrode (anode) into the flame of a DC arc.

The determination is based on measuring the difference in blackening of the sodium doublet, Na I 5889.95 and Na I 5895.92 A, and the background in the vicinity of these lines. By this procedure Na can be determined in concentrations ranging from 0.005 to 1% with a relative error of 10-12%.

Reference

1. S.M.Solodovnik & A.M.Rusanov, Izv. AN SSSR, Ser.Fiz., 9, 635 (1945).

* * * * * * *

SPECTROSCOPIC DETERMINATION OF Cd, Pb, Cu & Fe in GRADE Ts-V, Ts-0 AND Ts-1 ZINCS BY THE METHOD OF PHOTOMETRIC INTERPOLATION WITH SHIFTED SPECTRA

- B.P.Pashevkin

In view of the limited number of Cd, Pb, Cu and Fe lines appearing in the spectra of zinc of Grades Ts-V, Ts-0 and Ts-1 [Ц-В, Ц-О, Ц-1 – ц is the initial letter of zinc in Russian] it is necessary to use the analytic lines Fe 3581.2 - Cd 2288.02 A, whose wavelengths lie in regions characterized by different values of the gamma and spectral response of photographic plates. This makes it difficult to apply methods based on the use of a permanent working curve and makes it necessary to have recourse to the method of three standards which, where analysis of individual samples is involved, cannot be termed a rapid-analysis method. The fact that the spectrum of zinc has relatively few lines and the absence in the spectra of the above mentioned grades of zinc of all cadmium lines except the Cd 2288.02 A line restricts the choice of comparison lines to the self-reversing Zn 2138.56 A line (in which case measurements are made at one side of its contour[1]) or the Zn 2712.5 and Zn 2670.53 A lines which lie in regions characterized by a different gamma of the plate[2]. For our analyses we used the method of shifted spectra[3] in which conventional photometry on a microphotometer is replaced by visual photometric interpolation.

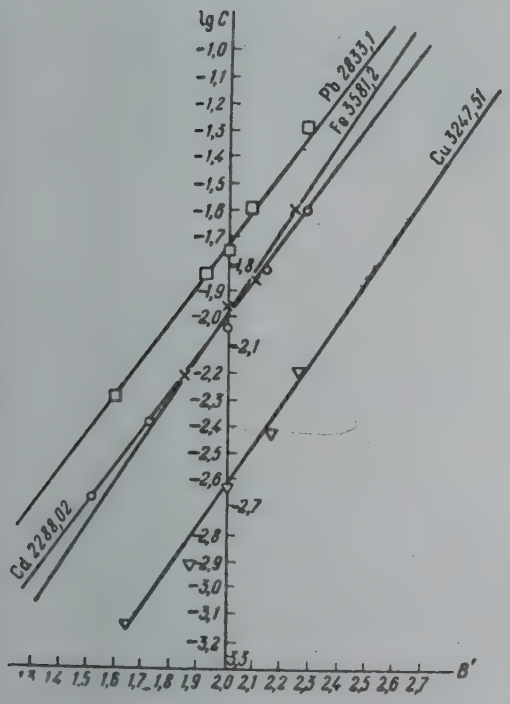

Working curves for determining Ca, Pb, Cu and Fe in zinc by the method of shifted spectra. Comparison line is Zn 2670,53 A.

The working curves, plotted in terms of B' vs log C are shown in the accompanying figure. Here

$$B' = B + (2.00 - A) = B - A + 2.00$$

where $B = I_{sam}/I_{sta}$ and $A = I'_{sam}/I'_{sta}$; I_{sam} and I_{sta} are intensities of the analytic line in the spectrum of the sample and of the control standard respectively and I'_{sam} and I'_{sta} are the intensities of the internal standard (Zn) line in the sample and control standard spectra.

The spectra of the sample and of the control standard photographed through a nine-step weakener, are located side by side on the same plate which facilitates visual evaluation of A and B. Use of a microphotometer does not lead to any appreciable increase in accuracy. The method described is applicable to blackenings in the region of under-exposure. The procedure, however, does require careful calibration of the weakener for different wavelengths.

Table

Melt No.	Fe, %		Cu, %		Pb, %		Cd, %	
	Determination		Determination		Determination		Determination	
	I	II	I	II	I	II	I	II
1	0,007	0,006	0,001	0,001	0,015	0,015	0,006	0,007
2	0,003	0,003	0,005	0,006	0,049	0,046	0,003	0,003
3	0,017	0,015	0,005	0,004	0,005	0,004	0,002	0,002
4	0,006	0,006	0,004	0,004	0,023	0,023	0,015	0,018
5	0,009	0,009	0,004	0,003	0,005	0,006	0,003	0,003
6	0,004	0,003	0,002	0,002	0,005	0,005	0,002	0,003
7	0,003	0,004	0,003	0,002	0,003	0,004	0,005	0,005
8	0,003	0,004	0,002	0,002	0,005	0,006	0,005	0,004
9	0,005	0,004	0,003	0,002	0,004	0,004	0,006	0,006
10	0,004	0,005	0,001	0,002	0,005	0,005	0,007	0,008
11	0,005	0,005	0,002	0,002	0,004	0,004	0,005	0,005
12	0,005	0,005	0,002	0,002	0,005	0,005	0,005	0,006

The spectra were excited by means of a PS-39 AC arc generator incorporating an additional 12 μf blocking capacitor. Excitation conditions were analogous to those employed by the authors of Refs. 1 and 2.

The analytic lines used for determining the magnitude of B were Fe 3581.2, Cu 3247.51, Pb 2833.1 and Cd 2288.02 A. The comparison line for evaluating A in analyzing the samples for all four impurity elements was the Zn 2670.53 A line.

The accuracy of the method may be judged from the accompanying table where the results (each value is the average for two spectrograms) of two separate determinations on a number of different samples are juxtaposed.

References

1. L.E.Neimark & Alekseeva, Zavod.labor (The Plant Laboratory), 16, 1511 (1950).
2. M.E.Britske, L.I.Varshavskaia & L.M.Ivantsov, Ibid., 16, 1207 (1950).
3. V.K.Prokof'ev, Fotograficheskie metody kolichestvennogo analiza metallov i splavov (Photographic methods of quantitative analysis of metals and alloys) p. 166, Part II, Moscow-Leningrad 1951.

* * * * * * *

USE OF SPECTROSCOPIC TECHNIQUES FOR DETERMINING THE CHARACTER OF ARSENIC DISTRIBUTION IN STEEL

- O.I.Nikitina*

Where ores containing arsenic are used for the production of steel it becomes important to know both the concentration and distribution of this impurity in the final product. The spectroscopic procedure for determining As in steel which we developed some time ago[1] and which is currently being used for this purpose in a metallurgical plant is not suitable for investigating the distribution of As in small volumes. Below we describe a method developed to study the As distribution in cast and hot-worked steels. We tested two variants of the procedure for determining arsenic with minimal destruction of the analyzed surface.

In the first variant the source was an AC arc (PS-39 generator with attachment; 1 amp current). The analytic lines were the As I 2288.12 A and Fe 2289.03 A pair. The counter electrode was of copper. The instrument was an ISP-22 spectro-

* M.G.Skliar and L.V.Al'tman participated in the investigation.

graph with the slit illuminated by means of a spherical-cylindrical lens. The working curve is shown in Fig. 1.

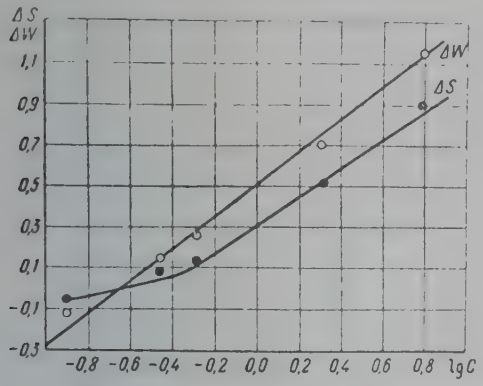

Fig. 1. Working curves for the determination of As in steel in an AC arc (PS-39 arc source with attachment) according to the As I 2288.12 - Fe 2289.03 A line pair

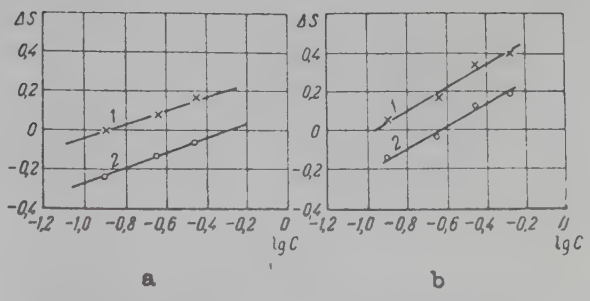

Fig. 1. Working curves for determining As in steel in a spark (IG-2 generator) according to the AsI 2288.12 - Fe 2287.63 A (Curves 1) and the AsI 2288.12-Fe 2287.24 A (Curves 2) line pairs. a) sparked surface not limited; b) sparked area limited by means of a mica overlay.

In the second variant the source was a spark supplied by an IG-22 generator (C = 0.005 μf, L = 0.55 mH; current in transformer primary: 0.8-1.0 amp). Counter electrode: copper. In one series of tests the sparked area was limited by means of a mica overlay. The analytic line pair was As I 2288.12 - Fe 2287.63 A (& Fe 2287.24 A - see Fig. 2). The working curves are shown in Fig. 2.

The first object studied was a longitudinal section through an ingot of No. 3 rimming steel. Quantitative analyses for arsenic were made at different levels through the ingot. The analyses showed the following:

1) The arsenic in rimming steel is distributed non-uniformly. At the lower levels (near the bottom surface) the As concentration is below the average; at the upper levels the As concentration in going from the ingot edges to the central zone increases two-fold and at some points three-fold.

2) The region of above-average concentration of arsenic coincides with that of the liquation of sulfur (as determined from a sulfur print), which indicates that the arsenic tends to concentrate in the common impurities liquation zone.

The subjects of further studies were cross sections of rolled shapes of rimming and killed No. 3 steels. The analytic results showed that the As distribution in rolled plates of killed steel is virtually uniform whereas in rolled rimming steel plates the arsenic content in the liquation zone is twice that elsewhere in the section.

We also investigated the influence of an increased (as compared with No. 3 steel) carbon content on the arsenic distribution. The studies were made on sections through rolled rails. The results indicated a fairly uniform As distribution. Somewhat above average (about 1½ times) concentrations were found only in the intermediate region of the rail head and in the center of the web and base. In the absence of a clear-cut liquation zone (judging from the sulfur print) for the other impurity elements there is no such sharp variation in the As content over the cross section of a rolled rail as was observed in the case of soft rimming steel.

The experimental results described above demonstrate that spectrographic analysis provides a simple and convenient method for investigating macroliquation in alloys.

In the second part of the investigation we applied the spectrographic procedure to determining arsenic in thin metallic layers. It was known from the data of

chemical and spectroscopic analyses that there is generally an above-average arsenic content at the surface of specimens subjected to heat treatment. In view of this we investigated a series of samples of No. 3 and rail steel in the initial state and after prolonged annealing in vacuum and in air (for the same length of time).

Traces of arsenic were detected in the loose scale of both the soft and rail steel samples. In the metal proper the highest concentration was found at a depth of 20-25 microns below the surface; the concentration fell off to the average value at a depth of 50-70 microns.

An increase in the carbon content to 0.7% in the steel (rail steel) does not alter the character of the arsenic distribution in the superficial layers of the metal; however, it does retard oxidation and in this way operates against concentration of arsenic at the surface. The increased arsenic concentration in the surface layer of the pure metal depends solely on the depth of the oxide layer and is independent of both the type of steel and the final As concentration in it. The appreciable increase (to 5-10 times the average value) in the arsenic concentration in the superficial layers may be the cause of the surface defects peculiar to arseniferous steels.

Further we studied the joint effect of carbon and arsenic on the diffusion of these elements in iron; the investigation was carried out on samples of double refined (pure industrial) iron free of As and containing various concentrations of As (0.5 to 2.6%) as well as samples of low-carbon and medium-carbon steels. It was established that increasing the As content reduces the rate of diffusion of carbon in steel; increasing the carbon content lowers the rate of diffusion of arsenic. These results are consistent with the data regarding the distribution of arsenic in the superficial layer when the sample is subject to oxidation (annealing in air).

Ural Scientific Research Institute of Metals

Reference

1. O.I.Nikitina, Zavod.labor.(The Plant Laboratory) 13, 885 (1947).

* * * * * * *

A SPECTROGRAPHIC PROCEDURE FOR THE DETERMINATION OF ARSENIC IN STEEL AND ITS APPLICATIONS

- E.F.Nikiforova

We found only one report in literature on spectroscopic analysis of arseniferous steel[1] and this describes a procedure based on visual photometric interpolation. In the present article we describe a technique based on objective photometry.

The standards used were selected samples of arseniferous steel carefully analyzed by chemical methods as well as spectroscopically by means of synthetic solutions prepared by adding measured quantities of a solution of an arsenic salt to arsenic-free steel.

The line pair used was As 2349.84 and Fe 2350.39 A. The spectrum was excited by means of PS-39 AC arc generator (arc current - 9 amp). The spectra were photographed on an ISP-22 spectrograph, using a source to slit distance of 17 cm and an exposure of 20 sec without pre-arcing. The arc gap was 2 mm; the counter electrode was a spectroscopic carbon rod with the point tapered to a 2 mm diameter flat. The positive plates (speed: 0.5 GOST) were processed in the conventional manner.

The density measurements were made on a MF-2 microphotometer. The working curves were plotted according to the method of three standards.

The spectra of the standards were photographed three times; those of the

Bauman sulfur print of cross section thru part of sheet of rimming steel.

Point No.	As, %
1	0,171
2	0,181
3	0,254
4	0,292
5	0,197
6	0,246
7	0,240
8	0,184
9	0,191
10	0,191

samples, at least four times in the case of small samples and more than four times in the case of large samples. In every case different portions of the sample were arced for successive exposures in order to minimize the effect of liquation. The analytic results were based on the average for each series of measurements. The accuracy was evaluated by checking against the results of chemical analysis. In the 0.10 to 0.30% range of As concentrations the average absolute error was computed to be 0.005%.

The developed spectrographic method was used to study the distribution of arsenic in arseniferous steel: it was found that the distribution is not homogeneous. The liquation of arsenic, characterized in terms of a variation coefficient V ($V = -(\sigma/x)\ 100$, where σ is the root mean square deviation and x is the arithmetic mean value of the As content in the sample as a whole) had an average value of 10.9% in cross sections of steel sheets and 9.5% in steel rails and forged specimens.

We established that there is a correlation between the distribution of arsenic and of sulfur by juxtaposing the results of our zonal analyses with Baumann sulfur prints. The As distribution parallels that of S and, like sulfur, arsenic tends to accumulate at the boundaries of the liquation zones. By way of illustration a Baumann print of part of a cross section of a rimming steel sheet with indications of the arsenic content at different points is reproduced in the accompanying figure.

All-Union Scientific Research Institute of Railroad Transport

Reference

1. O.I.Nikitina, Zavod.labor. (The Plant Laboratory) 13, 885 (1947).

* * * * * * *

MORE REGARDING BESSEMER FLAME SPECTRA

- K.S.Garger, V.D.Ummov & G.D.Krivulia

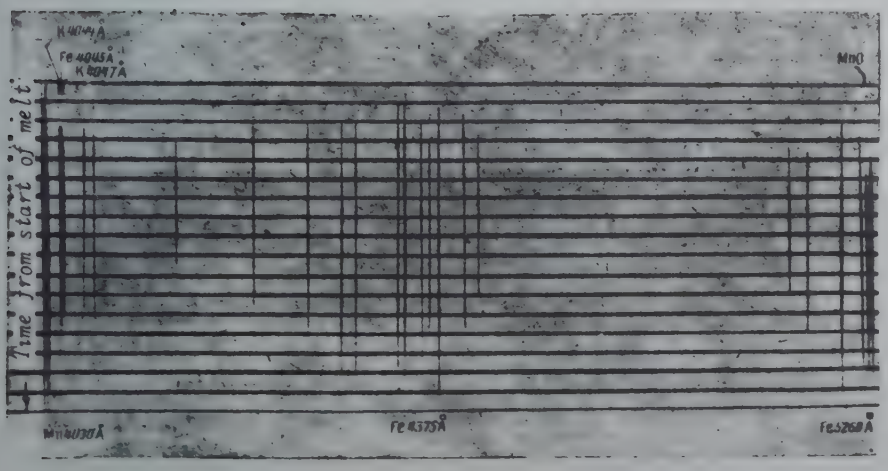

Changes in a Bessemer flame spectrum with time. Photographing rate : two exposures per minute. Photodrawing from isoortho plates.

Earlier one of the present authors investigated the 5000-6750 A interval of the spectrum of a Bessemer flame[1]. It was shown that during the latter half of the blow-through period Fe O bands and Fe I lines predominate in the spectrum. These observations serve to explain the results obtained by Chernov[2] and Glazer[3].

Below we give the results of an investigation of the short-wave portion of the visible region of the Bessemer flame spectrum. For recording the spectrograms we employed an SL-3 Steeloscope, equipped with a Hartmann diaphragm and a new, improved photo-attachment which is installed in place of the eyepiece housing of the Steeloscope and permits step-by-step photography of the spectrograms during the Bessemer process. The vertical feed has a ball-type detent. The comparison spectrum was obtained by means of a Cu - Fe electrode arc.

We detected and definitely identified 38 Fe I lines with excitation potentials of 2.4 to 4.65 ev as well as Mn and K lines in the 3960 to 5500 A interval (see figure on preceding page). Lines of other elements, recorded for the Thomas (basic Bessemer) process[4], were not observed.

We established experimentally that it is feasible to utilize certain violet lines of iron to fix the time for stopping the Bessemer process at a high carbon content, which is in accord with the indications given by Grum-Grzhimailo[5]; for example, the 4482, 4143 and 4063 A lines disappear when the carbon content reaches 0.5-0.7% while the 4375 A line fades out when the carbon content of the batch equals 0.3%.

The observed sequence in which the lines of the different elements appear as the process develops and the temperature rises is Na, Mn, Fe, K, Li instead of K, Na, Li, Mn, Fe as might have been expected. This as well as the great intensity of the Fe I lines and Fe O bands is evidence of the important part played by chemiluminescence in the emission of the flame.

We have come to the conclusion that the iron in a converter goes through a process of fractional distillation with the formation of intermediate carbonyl compounds. It proved possible to elucidate some of the steps in their formation in the light of Kholmayer's study[6]. When taking gas samples we found brown flakes, containing iron oxides and reminiscent of the iron carbonyl described by Mittasch[7], in the sampler tube. Analogous results are reported by Andreev[8] who remarks on the presence of deposits containing ferric oxide in the sampling tube.

Simultaneously with photographing the spectra we recorded the total emission in different spectral intervals. We found that the intensity curves for the near infrared (0.8 - 3.0 μ) differ from the curves for blue-green radiation (0.4 - 0.6 μ) as regards slope (rate of increase in intensity). In view of this we assumed that the difference between the photocurrent of a selenium and of a silver sulfate cell should vary in a consistent manner with the progress of the conversion process, since the former (selenium photocell with a green filter) responds primarily to the visible radiation of the flame while the latter (Model FESS with an ebonite filter) is sensitive mainly to the thermal. Experiments confirmed this assumption.

We also showed that this differential method can be used for checking on and controlling the Bessemer process and has certain advantages over the photoelectric methods now sometimes employed.

In conclusion we wish to express our thanks to G.L.Landsberg and S.L.Mandel'shtam for their interest in the work and their valuable advice.

"Arsenichev" Dneprodzerzhinsk
Metallurgical Evening-Study Institute

References

1. K.S.Gurger, Zhur. tekh. fiz., 22, 606 (1952).
2. "D.K.Chernov i nauka o metallakh" (D.K.Chernov and the science of metals). Symposium, 1950.
3. L.Glazer, Stahl und Eisen, 1920.

4. B.Breckpot et al in symposium "Problemy sovremennoi metallurgii" (Problems of modern metallurgy), Moscow 1953.
5. V.E.Grum-Grzhimailo, Proizvodstvo stali (Steel production), M.-L. 1931.
6. E.Kholmayer, Geisserei, 38, 4, 73 (1951).
7. A.Mittasch, ZS. f. angew. Chem., 41, 30, 827 (1928).
8. B.Andreev, Stal' (Steel) 13, 2, 129 (1953).

* * * * * * *

SPECTROGRAPHIC DETERMINATION OF ARSENIC IN ORDINARY CARBON STEELS

- V.V.Sukhovalova

A spectroscopic procedure for analyzing open hearth steels for the arsenic content in the 0.04 to 0.18% range of concentrations has been developed in the laboratory of the "Azovstal'" Metallurgical Plant.

The samples for analysis were taken in accordance with GOST State Standard 380-50 and worked by forging in all cases. The final weight of the forged pieces was 700-800 grams. In obtaining the preliminary experimental data for comparing the results of chemical and spectrographic analyses the spectrum analysis was carried out on the section of the sample from which the shaving for chemical analysis was cut.

The spectra were excited by means of a PS-39 AC arc generator. The counter electrode was a copper rod 8 mm in diameter, tapered at the tip to a 1-1.5 mm flat. The electrode gap was 2.5 mm; the arc current - 6 amp.

The spectra were photographed on an ISP-22 spectrograph equipped with a single lens condenser. The source to condenser lens distance was 165 mm; the source to spectrograph distance - 860 mm.

The arsenic determinations were made both according to the method of three standards and by the method of photometric interpolation. For the latter the slit was illuminated through a nine-step weakener.

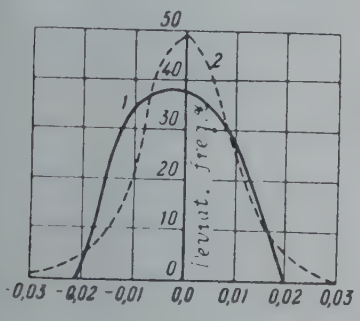

Distribution of deviations of the results of spectrum analysis from those of chemical analysis: 1) by the three standards method (230 determinations) 2) by the method of photometric interpolation (965 determinations).

The As I 2288.12 and Fe I 2291.6 A lines were selected as the analytic pair. This As line has the requisite absolute intensity and good concentration sensitivity. In the spectra of the plant samples with the discharge parameters employed the line is free of overlapping. The spectra were photographed on Spectral Type I plates.

Exhaustive tests of the developed procedure showed that it has a definite advantage over chemical analysis as regards speed. In fact with the interpolation method the determination is five to seven times faster than through chemical analysis. As regards accuracy the developed spectrographic procedure meets the requirements of GOST 2604-44-1950. The mean relative error computed on the basis of 60 independent determinations equals 9.1%.

The error distribution curves characterizing the deviation between the results of individual spectrum analyses and the content determined by chemical analysis (assumed to be the true value) for a number of samples are shown in the accompanying figure.

The proposed procedure is also suitable for the

determination of arsenic in low-alloy steels containing up to 1% chromium, nickel and copper.

"Azovstal'" Plant

* * * * * * *

DETERMINING NICKEL, VANADIUM, CHROMIUM AND COPPER IN CLAYS BY SPECTRUM ANALYSIS
- N.V.Astaf'ev, R.S.Rubinovich & S.A.Iakovleva

In connection with studies of sedimentary formations it became necessary to obtain quantitative data on the content of nickel, vanadium, chromium and copper in specimens collected in the field. Below we describe a procedure which assured rapid and sufficiently accurate determination of these elements in clays, in concentrations ranging from 0.002 to 0.050%.

The source employed was a DC carbon arc powered from a VAR-24 [BAP-24] rectifier (operating voltage - 180 v; current - 6.5 amp).

The sample was packed into a cup (3 mm in diameter; 2 mm deep) in the lower electrode (4.2 mm in diameter) which was connected as the cathode. The interelectrode gap was kept constant at 2.5 mm throughout the exposure; the gap length was monitored and adjusted according to the image of the incandescent electrode tips thrown on a screen by means of a lens.

The spectra were photographed by means of an ISP-22 spectrograph on positive plates, having a speed rating of 0.25 GOST. Up to 54 spectra were recorded on one plate. The width of the spectrograph slit was 0.01 mm. It was illuminated by a single lens condenser. In order to reduce the background the emission from the incandescent electrode tips was cut off by means of a suitable diaphragm. The line densities were measured on a microphotometer. The analyses were carried out by the method of three standards with both the samples and standards being burned completely (exposure time - 3 min 15 sec).

The base for the standards was prepared by mixing chemically pure reagents in proportions duplicating the average composition of the clay samples. The analytic elements were introduced into the base material in the form of their oxides: Ni_2O_3, V_2O_5, Cr_2O_3 and CuO.

The working curves were plotted on the basis of standards containing the following concentrations of the analytic elements: 0.0025, 0.0050, 0.010, 0.020 and 0.050%.

Cobalt was utilized as the comparison element. It was introduced into the samples and standards in the form of a solution of cobalt acetate in proper amounts to obtain a concentration of 0.06% cobalt by weight. The working curves were plotted in the usual ΔS *vs* log C coordinates. The following line pairs were used: V 3183.98 - Co 3044.01, Ni 3414.77 - Co 3409.18, Ni 3050.82 - Co 3044.01, Cr 4254.35 - Co 3409.18, and Cu 3273.96 - Co 3409.18 A.

The natural cobalt content of the analyzed samples generally did not exceed 0.006%. At such concentrations the Co lines used for comparison do not appear in the spectrum. There was no danger of superposition of the Co 3414.74 line on the analytic Ni 3414.77 line since, as we established by tests, this line is not manifest in the spectrum at cobalt concentrations of 0.06-0.08%. The working curves are shown in the accompanying figure.

The mean deviation for individual determinations as computed on the basis of the results of 50 analyses is 8% for Ni, 9% for V, 10% for Cr and 11% for Cu.

To verify the feasibility of effecting analyses of natural clays with reference

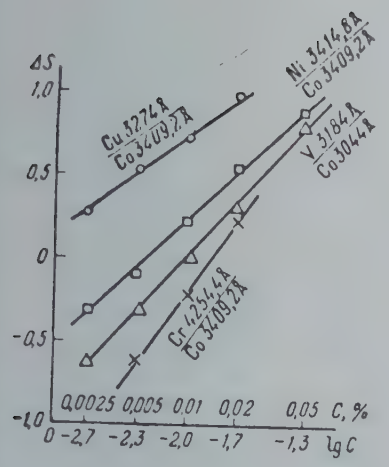

Working curves for determining V, Ni, Cr & Cu in clays by the method of three standards.

to artificial standards we carried out analyses of typical samples of clay for Ni and V by the method of additions. The results of these were in agreement, within the experimental error, with the results of analyses with reference to the artificial standards.

Experiments set up to evaluate the possible influence of iron, sodium and calcium on the intensity of the analytic lines of V, Ni, Cr, Cu and Co showed that the absolute and relative densities of the lines remain constant when the Fe content of the base is varied between 2 and 7%, the Na content between 2 and 6% and the Ca content between 2 and 7%. When the Ca content is increased above 10% there is a noticeable increase in the intensity of the background and a weakening of the analytic lines of V, Ni, Cu and Co. Working curves plotted according to standards with a high calcium content had a very flat slope. In view of this we did not analyze samples with an elevated calcium content. Such samples can readily be recognized both from the general appearance of their spectrum and from the way in which the material burns in the arc.

The described procedure has been successfully used in our laboratory for the analysis of numerous clay samples for over a year. The results have proved valuable for geological mapping and similar work.

Scientific Research Institute for
Geology of the Arctic

* * * * * * *

SPECTRUM ANALYSIS OF CLAYS FOR PRINCIPAL COMPONENTS

- E.E.Vainshtein, T.F.Borovik-Romanova & V.V.Korolev

The purpose of this report is to describe a spectroscopic procedure for the determination of Si, Al, Ca, Fe and Mg oxides in clays of different geologic origins. The ranges of the determinable contents are SiO_2 30-75%, Al_2O_3 6-35%, MgO 1-15%, Fe_2O_3 1-20% and CaO 0.5-30%. In developing the procedure we used the method of dilution in order to minimize the effect of third components. Cupric oxide and carbon powder were used as the diluting and stabilizing agents. The optimum proportions of the components of the analytic mixture were determined experimentally. The proportions of sample to CuO to carbon powder finally selected for the mixture were 1:39:80. Before mixing, the samples were dried at 105-110°C to drive off any water present.

The mixture made up in the above proportions was then thoroughly ground in an agate mortar and a 30 mg portion was packed into the core (3.5 mm dia, 4 mm deep) of the lower electrode which was connected as the anode. To minimize sputtering the sample was covered with a thin layer of carbon powder. The upper electrode of the DC arc (10 amp, 250 v) was a carbon rod tapered to a point. The exposure time was 60 sec. During this interval the elements enter the arc at a uniform rate.

The analytic lines were Si 2514.3, Al 3082.2, Ca 4226.7 and Ca 3179.3, Mg 2779.8 and Mg 2802.7, and Fe 2599.6 A. The comparison lines were the three copper lines: 4275.1, 3073.8 and 2441.6 A. The central portion of the arc (limited by a suitable diaphragm) was projected on the slit of a Q-24 spectrograph by means of a three-lens condenser. Plates: positive, speed 0.5 GOST. Developer: D-19. The standards employed for plotting the working curves were selected samples of clay whose composition had been determined by accurate chemical analysis. The curves were plotted in the conventional ΔS *vs* log C coordinates. The arithmetic mean error of determination did not exceed 6% (1.4% for Al_2O_3, 2.5% for Fe oxides, 4.3% for CaO, 4.5% for SiO_2 and 5.8% for MgO). Tests showed that the influence of varying amounts of the analytic elements on the determination of the others was negligible. To test the reliability of the procedure we analyzed 35 samples of clays whose composition was also determined chemically. The spectrographic and chemical results agreed within 4-6%.

At present work is in progress to extend the analytic procedure to include other elements present in clays, particularly potassium and sodium.

"V.I.Vernadski" Institute of Geochemistry
and Analytic Chemistry at the Academy of
Sciences of the USSR

* * * * * * *

SPECTROSCOPIC DETERMINATION OF LEAD AND OTHER ELEMENTS IN NATURAL WATERS

- E.B.Gusiatskaia & L.G.Loginova

Analysis of natural waters for their content of microelements, the concentrations of which frequently do not exceed 10^{-5}-10^{-7}%, can generally be effected by spectrum analysis of their dry residues acidified with H_2SO_4. After treatment with sulfuric acid the remaining product consists primarily of the sulfates of calcium, magnesium, the alkali metals and, in some cases, iron. Vaporization of a mixture of these salts from the core of a carbon electrode is characterized by preferential entry of the various microelements into the flame of the arc in accordance with the following volatility series Cd, Zn, Sb, Pb, Bi, Mo, Na, Sn, W, Mn, Fe, Co, Ni, Cr, Ti, Zr, Mo, W.

By vaporizing 10-20 mg of the dry residue from the anode of a carbon arc and taking advantage of the fractional nature of the vaporization process it is feasible to attain the following high sensitivities in detecting the various elements: Fe - $1\cdot10^{-3}$, Mn - $3\cdot10^{-4}$, Cr - $3\cdot10^{-3}$, Cu - $1\cdot10^{-4}$, Ni - $1\cdot10^{-3}$, Ti - $1\cdot10^{-3}$, Mo - $3\cdot10^{-4}$, Pb - $1\cdot10^{-3}$, Co - $3\cdot10^{-3}$, V - $1\cdot10^{-3}$, W - $3\cdot10^{-3}$, Ag - $3\cdot10^{-4}$, Sb - $3\cdot10^{-3}$, Zn - $5\cdot10^{-2}$, Ge - $1\cdot10^{-3}$, Mg - $1\cdot10^{-3}$, Bi - $1\cdot10^{-3}$, Cd - $3\cdot10^{-3}$, Ga - $1\cdot10^{-3}$, Ca - $5\cdot10^{-2}$, As - $1\cdot10^{-1}$, Sn - $1\cdot10^{-3}$, Be - $3\cdot10^{-3}$, Ba - $3\cdot10^{-4}$%.

By photographing the spectrum of the sample on the same plate with the spectra of standard-powder mixtures of Ca, Mg, Na, k and Fe sulfates it is possible to make approximate determinations of the concentrations of these elements in the dry residues in the concentration ranges from 0.001 to 0.003% and from 0.01 to 0.03% by visual comparison of the line densities.

Measurements of the absolute and relative intensities of the analytic lines by means of a microphotometer showed that the principal obstacle to more accurate determination of the microelements is the influence of "third elements" - calcium, magnesium and particularly sodium - the concentrations of which in the dry residues vary to an appreciable extent. Changes in the quantity of these elements in the

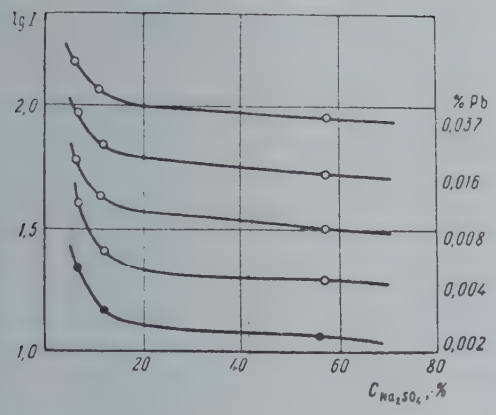

Variation of the intensity of the Pb 2833.1 A line for different Pb concentrations with the Na_2SO_4 content of the sample.

sample lead, as a rule, to alterations not only of the absolute but also in the relative intensities of the analytic lines with a resultant shift of the working curves and, consequently, introduction of systematic errors.

The influence of the sulfates of alkali metals is particularly pronounced at relatively low concentrations of these salts in the sample (under 10-15%).

As may be seen from the curves reproduced in the accompanying figure, further increases in the Na_2SO_4 concentration above 30% have relatively little effect on the intensity of the Pb I 2833.1 A line. This suggests a means of obviating the effect of possible variations in the sodium content of the samples: dilution of the sample material 1:1 with sodium sulfate. When this is done the working curves for dry residues having different initial Na concentrations virtually coincide, provided the iron content of such residues does not exceed 5%, which is usually the case with residues of natural waters.

In our tests the best analytic results were obtained in vaporizing 25 mg samples from the well (3 mm dia; 4 mm deep) of a carbon electrode in an AC arc (8 amp, 220 v). The photography was effected during the first 20 seconds after ignition of the arc. If standard spectrum-excitation conditions are rigorously maintained it is feasible to determine the lead content on the basis of the absolute intensity of the Pb I 2833.1 A line. The probable relative error in determining Pb in the 0.001 to 0.04% range of concentrations is ±12%.

All-Union Scientific Research Institute
of Hydrogeology and Engineering Geology
"Vsegingeo"

* * * * * * *

ON THE USE OF AN ACTIVATED AC ARC FOR SPECTROSCOPIC DETERMINATIONS OF ALKALI AND ALKALI EARTH ELEMENTS IN NATURAL WATERS

- T.F.Borovik-Romanova, V.V.Korolev, Iu.I.Kutsenko and M.M.Farafonov

The present report is devoted to a description of a spectrographic procedure for the analysis of natural waters. The microelements contained in the waters of seas, rivers, lakes and springs have been the objects of numerous investigations. The results of such investigations have facilitated the solution of many geochemical problems, such as problems connected with determining the source of water courses, the migration or interchange of elements in solution, etc.[1,2]

Our immediate project called for developing a procedure for determining strontium and lithium in certain natural waters. The Sr contents of the waters in question varies between $1 \cdot 10^{-5}$ and $1 \cdot 10^{-2}$%, while the range of variation in

the Li content is $1 \cdot 10^{-7}$ to $1 \cdot 10^{-4}$%. The analytic procedure evolved is actually a further development of the spectrographic method proposed earlier by S.A.Borovik and one of the present authors.[3]

The source employed was an activated AC arc (PS-39 generator, operated at 120 v and about 2 amp). The solutions were brought into the arc flame by means of the fulgurator described in Ref. 3. The design of the fulgurator electrode was modified to the extent of making the electrode somewhat longer (4 mm) and having it protrude through the bottom of the vessel containing the solution so that the electrode proper could be clamped in the electrode holder. The upper electrode was a carbon rod, 6 mm in diameter, with a plain wedge-shaped tip. The spectrograms were taken on an ISP-51 three-prism glass spectrograph equipped with a 270 mm focal length camera. The slit width was 0.02 mm. A two-step weakener attenuating the spectrum intensity by a factor of three was mounted in front of the slit. The electrode gap was 4 mm. The exposure time was 2 min. The arc was burned for one minute (with the slit covered) prior to making the exposure, to allow the fulgurator to reach a steady state of operation (i.e. to insure a steady rate of entry of the solution into the arc during the exposure).

The investigated waters were for the most part similar as regards the qualitative composition of their mineral content, but differed as regards its concentration. By appropriate dilution and evaporation the investigated samples were brought to the same total concentration of the dissolved salts: 0.015 gm/cm^3. The composition and concentrations of the standard solutions were close to those of the samples; the analytic elements were introduced in the form of $SrCl_2$ and LiCl (the Sr content in the standards varied between $7.1 \cdot 10^{-5}$ and $6.3 \cdot 10^{-3}$%; the corresponding range for lithium was $4.9 \cdot 10^{-4}$ to $6 \cdot 10^{-6}$%.

The analytic lines were Sr 4607.331 and Li 6707.844 A. The caesium was used as the internal standard; 1½% solution of caesium nitrate was added to both the samples and the standards in the proportion of 2:1. The comparison lines were Cs 4593.177 and Cs 6723.279 A.

The plate holder was loaded simultaneously with a panchromatic plate having a speed of 1200 H&D (for determination of lithium) and an isoortho-line plate having a speed of 2 GOST (for determination of strontium). The calibration curves were plotted in the conventional ΔS *vs* log C coordinates. The range of the determined concentrations of lithium was $2 \cdot 10^{-5}$ to $5 \cdot 10^{-4}$%; that of strontium was $2.3 \cdot 10^{-4}$ to $6 \cdot 10^{-3}$%. The sensitivity of the procedure for Sr was $1 \cdot 10^{-5}$%; for the detection of lithium, $3 \cdot 10^{-6}$% using 1200 H&D panchromatic plates or $9 \cdot 10^{-7}$% when panchromatic plates having a speed rating of 1900 H&D were used. The relative error was evaluated as 6-8%.

"V.I.Vernadski" Institute of Geochemistry
and Analytic Chemistry at the Academy of
Sciences of the USSR

References

1. A.P.Vinogradov, Usp. khim., 13, 3 (1944).

2. A.P.Vinogradov, Trudy Biogeokhimicheskoi laboratorii (Transactions of the Bio-geo-chemical Laboratory) Vol. 9, AN SSSR, M.-L. 1949.

3. S.A.Borovik & T.F.Borovik-Romanova, Doklady AN SSSR, 73, 683 (1950); Izv. AN SSSR, Ser. fiz., 14, 665 (1950).

* * * * * * *

FACTORS AFFECTING LINE INTENSITIES IN SPECTRUM ANALYSIS OF SOLUTIONS

- Kh. I. Zil'bershtein

We investigated the dependence of the spectrum line intensities of six elements (Zn, Be, Si, Bi, Mn and La), differing as regards ionization potential and volatility, on the location of the dry residue of the analyzed solution in the carbon electrodes of an AC arc. Three variants of affixing the sample to the electrode where employed: the dry residue was located 1) in a thick layer of unprotected carbon, 2) on the end face of the carbon electrode, previously treated with polystyrene, and 3) in the thin end-face layer of the carbon electrode[1]. The location of the sample in the electrode was verified in each case by X-ray examination. In the case of very dilute solutions the intensity of the analytic lines is increased by a factor ranging from 2 to 9 in going from the first to the second variant; the greatest gain is observed for spark lines and arc lines ending at a high energy level. In the case of a concentrated solution containing a large quantity of aluminum in addition to the above-listed elements there remains, after evaporation of the solvent, an appreciable amount of dry residue and, in this case, in going from the first variant of fixing the sample to the second, the intensity of the analytic lines of Zn, Si, Bi, Mn and La increases only slightly while the intensity of the Be and Al lines diminishes. The method of fixing the dry residue in the thin end-face layer of the electrode developed by the writer[1] assures a two to six-fold increase in the intensity of all the analytic lines as compared with the intensity obtained with the first variant in the case of both dilute and concentrated solutions. Further enhancement of the line intensities can be attained by reducing the arc temperature through the introduction of Na into the discharge (0.3 mg placed on both electrodes). The overall increases in line intensity achieved by introducing Na and by replacing the first with the

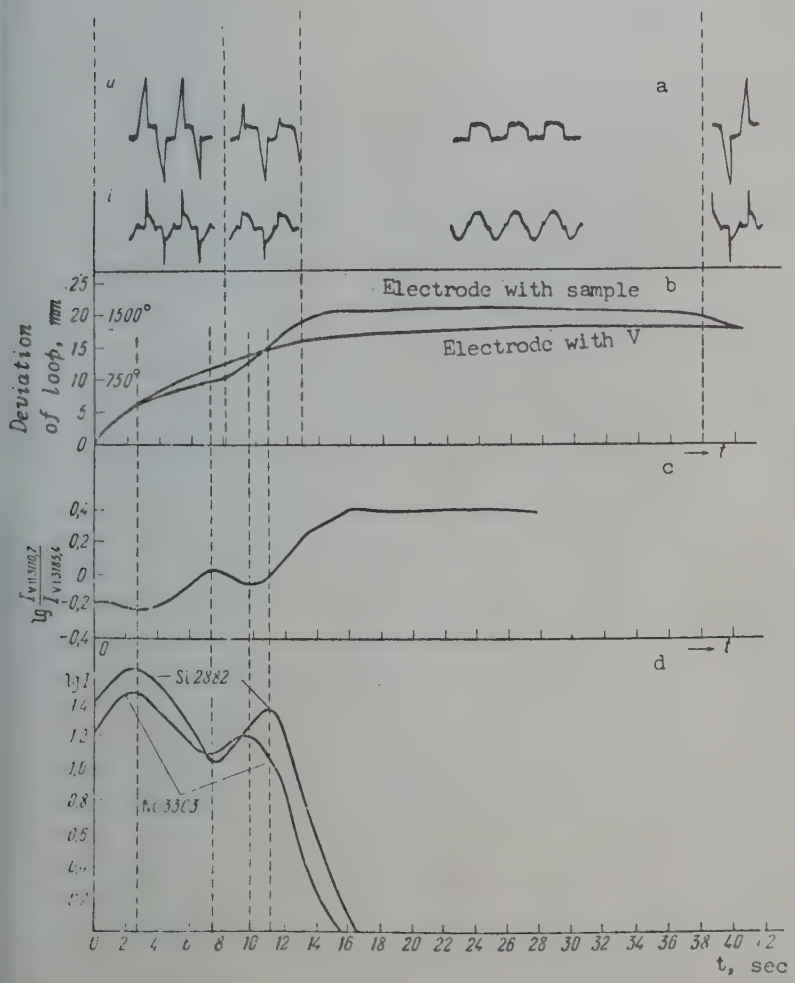

Time scan of the process of burning (complete vaporization) of Si and Na fixed in a thin layer in the end-face of a carbon electrode in an AC arc: a) electric characteristics of the arc (v and i), b) electrode temperature (1 mm 75°), c) qualitative characteristic of discharge temperature variation, d) variation of intensity of Si and Na lines.

third variant of affixing the sample are indicated by the following figures: In I 3345 - 15 X, Be I 2345.7 - 5 X, Si I 2881.6 - 8 X, Bi I 3067.7 - 12 X, Mn 2801.1 - 23 X, and La II 3337.5 A - 35 X. As a result, the errors in quantitative determinations are reduced by 50-60%. According to our data, based on determinations of 26 different elements, the described procedure is characterized by a sensitivity, as regards both detection and determination, equal or, in some cases, superior to that of all other methods. For example, the sensitivity threshold as regards detection of elements in the sample mounted in the electrode is $8 \cdot 10^{-11}$ gm for Be, $4 \cdot 10^{-8}$ gm for Zn, $5 \cdot 10^{-8}$ gm for Sb, $5 \cdot 10^{-9}$ gm for Cr, La and Co, $4 \cdot 10^{-10}$ gm for Ag, and $1 \cdot 10^{-8}$ gm for Zr and Pd. Tests showed that the presence of large amounts of aluminum (from 20 to 10,000 times the quantity of the determined elements) in most cases does not affect the results of quantitative determinations of low concentrations of Zn, Be, Si, Bi, Mn and La. Nor was any effect due to anions observed.

We also studied the process of burning (complete volatilization) of the dry residues of sodium silicate and certain other solutions in an AC arc with the different variant ways of affixing the sample. To this end we obtained a time-scan record of the spectrum of the sample and of the spectrum of vanadium, a small amount of which was introduced into the second electrode (not containing the sample). We used the V I 3185.4 and V II 3110.7 A lines to evaluate the discharge temperature. At the same time we made an oscillograph record of the temperature of the sample-bearing electrode by means of a Pt/PtRh thermocouple mounted 2 mm from the end of the electrode and of voltage-current characteristics of the arc. The synchronized records show little evidence of preferential vaporization, particularly in the case of the third variant of holding the dry residue (see figure). This, together with the high temperature of the end-face layer of the electrode and the stability of the arc temperature due to the introduction of sodium, explains the great sensitivity of our analytic method and the absence of the influence of other elements present on the results. The differences in the variation of the Si and Na line intensities during the arcing when different variants of fixing the dry residue in the electrode are employed are connected with thermal effects obtaining on the electrode surfaces, the depth to which the sample material is imbedded in the electrode and changes in the electric regime of the arc. Electric transfer of the material of the sample (i.e., the fact that a greater or lesser amount of material is carried to the counter electrode) may also be a contributing factor.

Institute of the Chemistry of Silicates
at the Academy of Sciences of the USSR

References

1. Kh.I.Zil'bershtein, Zavod. labor. (The Plant Laboratory) 19, 443 (1953); Kh.I.Zil'bershtein & O.N.Nikitina, Izv. AN SSSR, Ser. fiz., 18, 295 (1954).

* * * * * * *

SPECTROSCOPIC DETERMINATION OF CERTAIN METALLIC ELEMENTS IN QUARTZ AND OTHER SILICEOUS SUBSTANCES

- O.N.Nikitina

We developed a sensitive spectrographic method for determining Fe, Co, Mn, Ni, Ti and Cr in sand, quartz and other forms of silica. The work was effected on an ISP-22 quartz spectrograph with a three-lens condenser; the slit width was 0.01 mm. The spectra were photographed on positive plates, having a speed rating of 3° H&D. The samples were packed into the core of the carbon electrode serving as the anode in a DC arc (10 amp current, 2 mm gap). To drive off superficial impurities the electrodes were pre-heated for 5-10 seconds in a 25-27 amp arc prior to packing the sample.

Scan photography of the sample spectra on a moving plate showed that the impurities and the base material of the sample are volatilized at about the same rate and that both are entirely consumed at the end of about the same interval. Hence we used the method of complete burning of the sample with the main element - silicon - being utilized as the internal standard.

The standards were prepared by moistening "pure" silica with solutions of salts of the determined elements followed by heating the moistened powder at 1100°C. So-called "chemically pure" silicic acid, rock crystal or quartz could not serve as the base since these natural materials contain too high a percentage of impurities. Pure silicon dioxide free of all impurities (except traces of titanium) was prepared by hydrolysis of distilled silicon tetrachloride.

Two variant procedures were evolved:

1) With the first, in order to attain a high sensitivity (detection of concentrations to 0.0001%) approximately 100 mg of the sample are burned in the arc. In this case a fairly intense line-band spectrum characteristic of SiO and CN molecules is superposed on the analytic lines of the determined elements. Quantitative determinations were made taking account of the intensity of the background in the following manner. First, photometric measurements were made of the background intensity at the point where analytic lines appear; then a nearby section of background having the same intensity was located. Finally, in photometry of the spectra of the samples, the heightened intensity in the region of the analytic lines was compared with the intensity of the area of the "equal-intensity" background. The absolute sensitivity of the procedure is such as to permit detection of 10^{-7} grams of the impurity in a 100 mg sample. The working curves were plotted in terms of log $(I_{line+backgrd} - I_{backgrnd})/I_{Si}$ *vs* log C. The working curves proved to be straight lines in a rather wide range of concentrations (0.0003-0.1%).

b) In the second procedure, intended for determining impurity concentrations exceeding 0.001%, smaller samples (20 mg) were used; in this case the SiO bands did not obtrude in the spectrum. The optimum dimensions of the carbon electrode core proved to be 2.5 mm dia, 3 mm deep, 0.3 mm wall thickness. The electrodes were prepared with the aid of a special device designed for this purpose. These dimensions assured effective weakening of the CN bands and simultaneous complete burning of the sample and of the electrode-core walls.

In this case the working curves were plotted in the conventional coordinates of relative intensities of the analytic lines *vs* concentration, without taking the background into account.

The reliability of the procedure was checked by comparing the spectrographic results with the results of colorimetric analyses for iron. The agreement was satisfactory.

Institute of the Chemistry of Silicates
at the Academy of Sciences of the USSR

* * * * * * *

APPLICATIONS OF SPECTRUM ANALYSIS IN PETROLEUM GEOLOGY

- A. A. Geiro

In exploring an oil-bearing region for commercial accumulations of petroleum and natural gas, the prospecting geologist must be able to compare samples of petroleum and bitumen encountered in different strata. Spectrum analysis provides a solution to this problem in that it permits determining the content of metal-porphyrins and other natural dyes, as well as of ash elements, for purposes of comparison.

We investigated 53 samples of petroleum and 40 samples of bituminous minerals from one oil region. All the petroleum samples of Devonian origin were found to contain 2 to 100 μgm of vanadium porphyrin per gram of petroleum. In petroleum from a sandy stratum of the Lower Carboniferous Period, in addition to a high vanadium porphyrin content, we also detected traces of nickel porphyrin. The vanadium porphyrin was determined in alcohol extracts according to the 572 mμ absorption band; nickel porphyrin was detected on the basis of the 550 mμ band. The other bands characteristic of these compounds were eclipsed by the absorption of other colored substances extracted from the petroleum together with the porphyrins. In addition to the 572 mμ band, we observed a strong absorption band with a peak at 630 mμ. The nature of the dyes responsible for this band has not yet been elucidated.

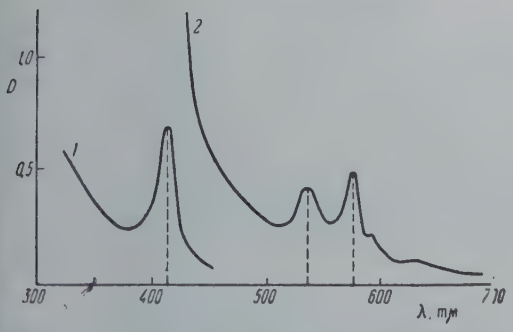

Fig. 1. Absorption spectrum of vanadium porphyrin observed in chloroform extracts from bituminous minerals.

In order to make quantitative determinations of the metal porphyrins it is necessary to separate their absorption from the absorption of the other coloring substances. It has been established that the optical density of metal porphyrins, as measured according to the height of their band peaks above the absorption curve for the attenuating components, is linearly dependent on their concentration; hence determinations can be based on Beer's Law.

Extensive tests have shown that within the limits of the same geological region the concentration of metal porphyrins and particularly the ratio between the concentration of metal porphyrins and the dyes having the absorption band at 630 mμ are constant, identifying characteristics of petroleums from a given stratum.

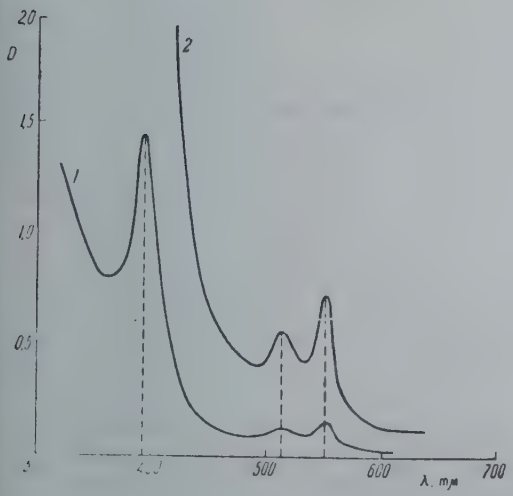

Fig. 2. Same as Fig. 1 but of nickel porphyrin.

We investigated the distribution of metal porphyrins in Devonian bitumens over the profiles of three bore holes and detected the presence of the following in chloroform extracts from the bituminous samples: vanadium porphyrin with absorption bands at 410, 534 and 575 mμ (see Fig. 1) and nickel porphyrin with absorption bands at 394-395, 508-516 and 552 mμ (see Fig. 2). We measured the ratio of the optical densities of the characteristic bands and obtained the following values: for vanadium porphyrin - D_{410}/D_{575} = = 16; for nickel porphyrin - D_{395}/D_{552} = 9.

All studies were made on an SF-4 spectrophotometer.

Analysis of the porphyrin distributions in the bituminous formations shows that nickel porphyrin predominates in Domanik layer bitumens while vanadium porphyrin predominates in Mendym and Sargaev strata. There is a reversal in the relative contents of nickel and vanadium porphyrin at the boundary between the Domanik and Mendym and between the Domanik and Sargaev strata. The noted difference between the metal porphyrins in the petroleums of the productive Devonian strata and in the bitumens of the Domanik formation (predominance of vanadium porphyrin in the petroleums and of nickel porphyrin in the bitumens) confirms the views of Ukhta geologists regarding the independent evolution of the bitumen-bearing Domanik deposits.

Thus our "porphyrin coring", the first investigation of the quantitative distribution of metal porphyrins along the profiles of three test holes, has demonstrated the potentialities of this spectroscopic method for comparing the petroleums and bitumens encountered in exploring sedimentary strata.

Central Scientific Research Laboratory at the
Ukhta Combine of the Komi A.S.S.R.

* * * * * * *

EMISSION SPECTRUM ANALYSIS OVER A PROFILE OF THE DEVONIAN AND CARBONIFEROUS SEDIMENTARY STRATA IN THE TROITSK-PECHORSK REGION OF THE KOMI A.S.S.R.

- S.S.Geiro

In prospecting for useful minerals associated with sedimentary strata it is important to know the paleo-geographic conditions obtaining at the time and place of their formation and subsequent geo-chemical history of the deposits. To investigate these the geologist has at his disposal samples of minerals formed during certain geological periods, collected at different levels in bore holes or from eroded or otherwise exposed surfaces. Carrying out such profile-sampling study by spectroscopic means involves making numerous simultaneous quantitative determinations of a considerable number of different elements in samples of varying composition.

The subjects of our investigation were the profiles of two exploratory bore holes - Zelenetz No. 1 and Nizhniaia Omara No. 1 - penetrating sedimentary strata of the Devonian and Carboniferous Periods some 2000 meters thick. The spectra were photographed on an ISP-22 spectrograph equipped with a three-lens condenser. The samples were burned in the cores of carbon electrodes in an activated AC arc operated with a current of 30 amps and giving an exposure time of 50 sec.

The following elements were detected in the investigated samples: Fe, Ca, Mg, Si, Al, B, Na, Mn, Ba, Sr, Ti, Cr, V, Ni, K, Cu, Be, Zr, Pb, Sn, Mo, Co, Cd, and Zn. The distribution and association of a number of individual elements were studied. The most common of the micro-elements are Mn and Sr, next in frequency of occurence are Na, Ba, Ti and Cu. A further increase in the number of elements present in a sample is usually due to K, V, Cr and Ni; the last three always occur together and as a rule only in samples also containing K. Be was detected only in the Stalinogorsk horizon represented by sandy-clay deposits with streaks of carbonized organic matter.

The number of micro-elements present varies not only with the age of the strata but also with their mineralogical composition: the micro-complex increases with increasing argillaceousness of the samples. Generally the samples with the

greatest number of different micro-elements also bear the heaviest concentrations of such elements and, conversely, those with the fewest elements exhibit the lowest micro-element concentrations.

The variation of the micro-element complex over the profile is not chaotic. By plotting the results of analyses in a stratographic column one can readily distinguish zones characterized by different qualitative and quantitative contents of micro-components. These zones correspond to geological ages of different duration; often their boundaries coincide with the recognized stratographic ones.

Comparison of the results obtained for the two bore holes, which are located about 50 kilometers apart, shows 1) that the basic micro-element complex is the same for both holes, 2) that the various distinctive zones in the two profiles are similar as regards composition of the corresponding zones and their vertical sequence and 3) horizons bearing the same geological designation are comprised in zones of the same type.

Thus it will be seen that study of the distribution of micro-elements over geological profiles by means of spectrum analysis facilitates more detailed investigation of different formations; the presence or absence of various micro-elements and their varying concentrations can be utilized in correlating different strata. In our case the variation of the micro-component complex over the investigated profile as a whole indicates that the geochemical conditions over the period of accumulation of the sedimentary strata did not remain static; in fact there is a distinctly cyclic character in the nature of the variation of the micro-element complex.

Ukhta Combine of the Komi A.S.S.R.

* * * * * * *

SPECTRUM ANALYSIS OF THE ELECTROLYTE IN ZINC AND NICKEL PLATING BATHS

- M.P.Grishchenko & A.B.Shaevich

The application of protective coatings by plating with zinc or nickel is extensively practiced in the machine tool and consumer goods industries.

Rapid and dependable control of the composition of the plating baths is essential for efficient production. Chemical methods of analysis are neither fast nor dependable enough. On the other hand, spectrum analysis of the electrolytes used in zinc and nickel plating is rendered somewhat difficult by the high concentrations of the salts and in the case of zinc plating baths by the presence of

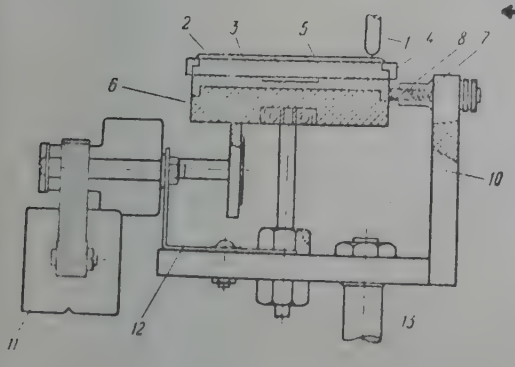

← Set-up for spectrum analysis of solutions: 1) counter electrode, 2) ashless filter paper impregnated with the analytic solution, 3) disk (lower electrode), 4) ring serving to retain filter paper on disk 3, 5) contact plate carrying current to disk, 6) insulating disk with bearing, 7) nest for electric brush with wire terminal, 8) brush, 10) stand, mounting brush assembly, 11) SD-2 motor with rubber-rim drive wheel, 12) slide for positioning motor, 13) supporting rod for mounting entire assembly on the optical bench.

dextrin; consequently conventional spectroscopic methods have failed to yield satisfactory results.

We developed a procedure in which the solution is brought into the discharge from a sheet of ashless filter paper, impregnated with the solution and mounted on a rotating disk electrode (see figure). This procedure insures a constant rate of entry of the sample into the discharge zone, enhances the sensitivity and reproducibility of the determinations, simplifies and accelerates the analytic procedure and eliminates the spraying and spattering that commonly occur when an ordinary fulgurator is used.

The developed procedure is applicable to the determination of Zn and Al in the acid electrolyte of zinc plating baths and of Ni, Mg and B in nickel plating solutions.

We used synthetic standards. The source was a PS-39 generator set for spark operation (the inductance in the arc circuit was not cut out). The analytic line pairs used were Zn 2800.9 - Fe 2787.9, Al 3082.1 - Fe 3047.6, Ni 2394.5 - Fe 2395.6, Mg 2790.8 - Fe 2783.7 and B 2496.7 - Fe 2493.3 A.

The mean deviations (%, relative) were 1.9 for Zn, 6.7 for Al, 2.1 for Ni, 2.8 for Mg and 3.2 for B. The accuracy is superior to that attained by chemical methods. The time required for a complete spectrum analysis is only 2-3 hours, as compared with the 15-18 hours needed for chemical analysis.

* * * * * * *

SPECTRUM ANALYSIS OF ELECTROLYTIC BATHS

- V.P.Golovchenko

There is relatively little in spectroscopic literature on analysis of electrolytic baths[1,2]. We developed procedures for the analysis of the following electrolytes: acid zinc plating, nickel plating*, chrome plating and copper stripping.

The analyzed solution is either introduced into a channel drilled in the carbon electrode by means of a tube from a communicating vessel or applied to the surface of a carbon or metal electrode. To assure good reproducibility in analysis for metals the solution must be applied to permeate a relatively thin surface layer of the electrode, but no salt deposits should remain on the electrode surface. To this end it is preferable to apply the solution to predampened electrodes. The spectra of sulfur and chlorine were excited by means of a carefully adjusted autotransformer-circuit AC arc generator with a stabilized ignition circuit (high-frequency spark excitation is also feasible). It was established that intensity of the spectra of chlorine, bromine and, particularly, sulfur and iodine can be appreciably enhanced by taking advantage of their high volatility to induce preferential entry of these elements into the plasma of the discharge. This desirable effect is achieved by the selected method of introducing the electrolyte into the gap. The spectra of the other elements were excited by a conventional low-current (2-3 amp) AC arc.

In all cases an internal standard was introduced into the analytic solution (although in some cases the background can be used for comparison). Tests showed that the reproducibility depends not only on the excitation conditions and the homology of the analytic lines but also to a considerable extent on the comparison element used and the method of bringing the electrolyte into the gap.

---

* I.B.Blankman, graduate student of Kiev State University, participated in analyses of this bath.

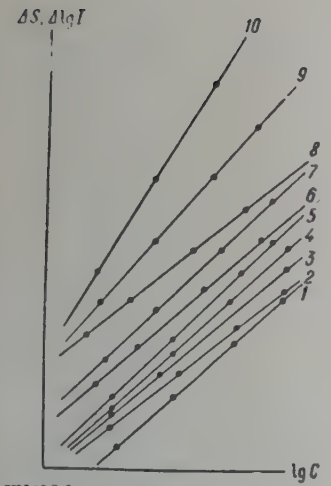

Figure:

Typical working curves: 1) S 5453.9 - I 5464.6 A, 2) Ni 3054.3 - Mn 2801 A, 3) Mg 2802.7 - Mn 2801 A, 4)Cl 4794.5 - Br 4785.5 A, 5) [?] 2496.7 - Mo 2775.4 A, 6) Al 3082.4 - Mg 3096.9 A, 7) Zn 3284.3 - Cd 3261 A, 8) Cr 2677.1 - Mn 2605 A, 9) Na 5688.2 - Cu 5782.1 A, 10) Na 6154.2 - background.

Tests also showed that the influence of third elements is manifested by a lateral shift of the working curves; this influence, however, can be minimized or obviated by proper selection of the comparison element, the pre-arcing time and the method of introducing the solution into the discharge.

The accompanying figure shows typical working curves. The probable deviation varies, depending on the determined element, between 2.5 and 5%.

For the determination of many plating bath components it is feasible to use a Steeloscope, utilizing the method of homologous pairs. In burning precipitates one can obviously make a rough evaluation of the concentration of elements in them on the basis of the time required for complete consumption (duration of their line spectra in the arc).

"T.G.Shevchenko" Kiev State University

References

1. Informatsionno-tekhnicheskii listok (Technical Information Pamphlet) No. 41, (499). Leningrad.
2. V.K.Prokof'ev, Izv. AN SSSR, Ser. fiz., 9, 691 (1945).

* * * * * * *

SPECTRUM ANALYSIS OF METALS AND ALLOYS UTILIZING SPARK-CONTACT SAMPLING

- M.G.Mal'tsev & K.I.Taganov

The spark-contact material transfer procedure developed by one of the present authors[1] has extended the possibilities of analyzing objects located outside the laboratory.

We developed a procedure based on electric spark transfer of material for analysis of low-alloy, complex and high-speed steels, grey cast iron and certain non-ferrous metals. The analysis is effected with the aid of a special portable spark unit having the following parameters: C of capacitor in the discharge circuit - 60 μf; voltage of rectified current - 200 v, short-circuit current - 0.25 amp. The vibrator is powered from the regular 50 cycle AC line.

The sample is collected on to cylindrical copper electrodes, 6 mm in diameter, having hemispherical tips. About one minute is required to coat the spherical tip with the sample material.

The transferred material is then burned for analysis in an AC arc (5.5 amp). The spectra were photographed on positive plates in an ISP-22 spectrograph with a slit width of 0.03 mm. The electrode gap was 2.5 mm. The exposure was 40 sec.

The spark-contact method of taking the sample is applicable to a wide range of concentrations: from 0.1% (Si in duraluminum) to 20% (Cr in EIaIT [illegible] steel).

The developed procedure was also adapted to determining the thickness of

cadmium (9 to 16 μ) and copper (5 to 35 μ) coatings on steel. In this case the sample is sparked on to a copper electrode for 10 sec. The spectra were photographed as described above.

The increased superficial concentration of sample material obtained with spark sampling enhances the sensitivity of analysis, hence when fast plates are used (for example, Spectral, Type II) the conventional spectroanalytic procedure can be followed with only minor modifications.

Tests have shown that the error with spark-contact sampling virtually does not exceed that common to conventional analytic methods. On the contrary, in a number of cases the slope of the working curves is increased (for example, in determining W in high-speed steels the steepness of the working curve is more than doubled).

We also discovered that in some cases the spark-contact method of sampling reduces the influence of the structure and overall composition of the alloy. Furthermore, the fact that the amount of sample material transferred on to the electrodes can be varied and controlled makes it possible to increase or decrease the relative intensity of the various analytic lines, corresponding to different concentration ranges in the sample, i.e., provides a means of preparing artificial standards. This would indicate that the spark-contact procedure has diverse potentialities in spectrum analysis.

Reference

1. K.I.Taganov, Izv. (Bulletin) AN SSSR, Ser. fiz., 18, 299 (1954).

* + * + *

DETERMINATION OF TIN IN COMPLEX ELECTROPLATED COATINGS ON RADIATOR TUBES

- L.S.Evlashin

Proper technological control of the process of tinning radiator tubes requires rapid analyses of the electroplated coating. According to the pertinent technical specifications, the cathode deposit should contain 15-25% tin and 85-75% lead.

Chemical analysis prior to starting operation was unsatisfactory, for it held up production since such analysis for tin requires 3-4 hours. The spectroscopic methods described in the literature and in particular the procedure developed by Kogan[1] could not meet the requirements imposed in our case. Attempts to determine the tin concentration in a coating 15-20 μ thick directly on the plated tube failed to yield acceptable results since the spark quickly burned through the coating to the base. Reducing the current and varying the parameters of the spark generator to eliminate burn-through led to poor stability of the discharge and spectrum. Hence we were forced to resort to analysis of removed coatings.

Two special plates of stainless steel were immersed in the plating bath and received the coating. The deposited film is easily stripped from such plates. The high tin content of the film (10-30%) reduces the concentration sensitivity of the analytic lines. Hence to increase the accuracy of analysis we reduce the tin concentration to about one-third by fusing the stripped-off film with a weighed amount of pure granular lead.

The standards were prepared in the laboratory; they were made up to obtain tin concentrations of approximately 2, 4, 6, 8 and 10%. The actual tin content of each standard was determined by chemical analysis. The standards were checked for homogeneity.

The tin determinations were made on a Zeiss spectrograph. The slit width was 0.06 mm; the condenser to source distance was 100 mm. The spectra were excited by

a simple condensed spark generator; voltage - 6 kv, current in transformer primary - 0.4 amp, inductance - 6.9 turns, capacitance - 0.002 μf. A spectroscopic carbon rod of 5.5 mm in diameter served as the permanent electrode. The gap was 2 mm. Pre-sparking time - 15 sec; exposure - 30 sec; plates - positive. The analytic line pair was Sn 2421.69 - Pb 2401.96 A.

The line densities were measured on a microphotometer built in the laboratory. The determinations were effected by the method of three standards.

The results were multiplied by three (in view of the initial dilution of sample with lead). Comparison of the results with those of chemical analysis showed that the accuracy of the spectrographic analysis was within ±1%. The time required for a spectrographic analysis is one hour.

The speed and accuracy of the spectroscopic procedure meet the industrial requirements.

Kirov Plant

Reference

1. A.I.Kogan, Zavod. labor. (The Plant Laboratory), 17, 1100 (1951).

* * * * * * *

DETERMINATION OF THE THICKNESS OF OXIDE COATINGS ON ALUMINUM ALLOYS

- V.P.Borzov & E.V.Il'ina

The determinations of the thickness of oxide films on aluminum alloys were carried out according to the relative intensity of the line pair: filler - base; to this end potassium bichromate was introduced into the pores of the coating to serve as the filler. For purposes of the determination we assumed that the pores are all equal in depth and completely filled by the bichromate and that the porosity of the coatings is fairly uniform. The investigation was carried out on AL8 aluminum alloy and duraluminum. The thickness of the coating on the standards was determined in two ways: by weighing and metallographically.

Straightforward weighing could not be utilized inasmuch as the percent porosity was unknown. The introduction of the filler made it possible to find the thickness by solving a system of equations. The sequence of operations in preparing the standards was the following: 1) oxidation, drying in an exsiccator, weighing (p_1); 2) introduction of the filler, drying, weighing (p_2); 3) removal of the coating from part of the standard, drying, weighing (p_3); 4) measurement of the total surface and of the area from which the coating was stripped. The thickness was then computed according to the equation:

$$h = \frac{(p_1 - p_2)d_f + k(p_2 - p_1)d_f + (1 - k)(p_2 - p_1)d_c}{(1 - k)d_c \cdot d_f \cdot s}$$

where k is the ratio of the area of the remaining coating to the total area of the standard, d_f and d_c are the specific weights of the filler and coating, respectively, s is the total surface area of the standard and h is the sought thickness.

The validity of the weighing method is confirmed by the good agreement of the results obtained by it with the results of metallographic determinations.

The spectra were excited in an AC arc (1.3 amp). The upper electrode was of copper. The spectra were photographed on an ISP-22 spectrograph; slit setting - 0.2 mm; exposure - 90 sec. Analytical pair Cr II 2835.6 - Al II 2816.2 A.

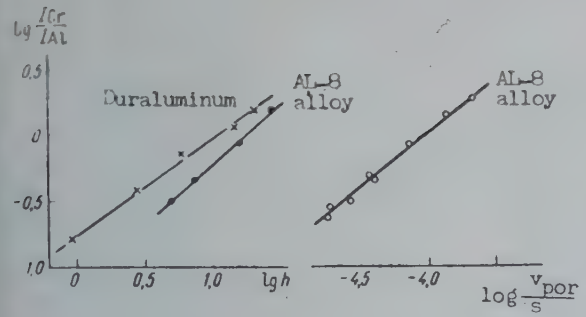

Working curves for determining the thickness and porosity of oxide coatings. Analytic pair: Cr II 2835.6 - Al II 2816.2 A.

The permanent curves for both alloys are shown in the accompanying figure. The probable error of an individual determination is ±3.0%. This indicates that our initial assumptions are justified.

Since the porosity of the coatings may vary we felt it important to determine the range of allowable porosities within which the above curves are applicable. To this end we prepared samples with coatings having different porosities. The points for all these did not fall on a common curve. Calculations of the degree of porosity by means of the equation:

$$v_{por}/v = (p_2 - p_1)/d_f s \cdot h$$

showed that only the points for samples having a coating porosity within ±20% of the average value fall on the working curve. Hence a necessary requirement is that the porosity of the standards must not differ by more than 20% from that of the samples analyzed.

The variation of the intensity of the filler spectrum with the volume of the pores in the coating can be utilized for determining the percent porosity if the thickness of the coating is known or determined beforehand by some other method.

The curve showing the variations of log (I_{Cr}/I_{Al}) with log v_{por}/s) is given at the right in the figure. Having determined v_{por}/s from the curve and knowing the thickness of the coating we can readily compute the porosity by simple division. The possibility of determining the porosity of oxide coatings may be of as much interest to industry as measurement of coating thicknesses.

* * * * * * *

QUANTITATIVE SPECTRUM ANALYSIS FOR METALLIC IMPURITIES IN LUBRICATING OILS

- V.P.Borzov & E.V.Il'ina

It is often necessary to analyze samples of new oil when additives containing metals are employed. In many cases analysis of used oil may also be of considerable interest. In determining the metal concentration in oil by spectroscopic methods one can either introduce the oil directly into the discharge or analyze the dry residue. In the first case analysis is rendered difficult by the presence of a strong background and the necessity of continuously agitating the oil sample[1-3]. These difficulties are obviated when the analysis is effected by the dry residue; however, great care must be taken to avoid the loss of metal in preparing the residue[4,5].

We were specifically interested in determining the elements entering into the composition of copper alloys present in vaseline oil. The procedure was based on burning the dry residue in a carbon arc. In preparing the standards the requisite admixtures were introduced in the form of CuO, ZnO, PbO, SiO_2, Al_2O_3, $SnCl_2$, $FeSO_4$ and $MnSO_4$. Appropriate amounts of these compounds were thoroughly mixed with a carefully weighed portion of graphite powder. The mixture was placed into porcelain crucibles and equal quantities of the vaseline oil thinned with gasoline were

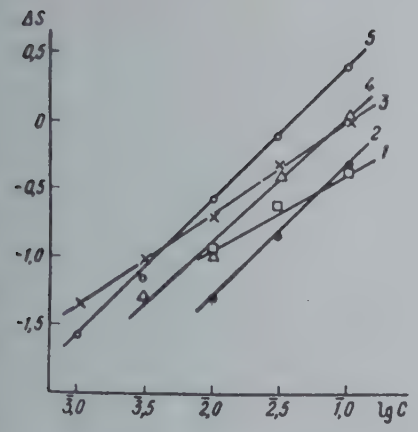

Curves for determining Pb, Zn, Al, Sn, Mn in lubricating oils according to the lines: 1) Pb 2833.1, 2) Zn 3345.3, 3) Al 3082.2, 4) Sn 3262.3, 5) Mn 2949.2 A. The comparison line in all cases was Ni 3080.8 A.

added to each lot. A quantity of organic salts of Ni (the comparison element) and Ba (for stabilizing the discharge) were dissolved in the gasoline beforehand. The final mixture was evaporated to dryness in a furnace at 800°C. Lastly, powdered graphite was added to the residue in suitable amounts to obtain the following concentrations of the analytic elements: 0.001, 0.003, 0.01, 0.03 and 0.1%. The investigated oil samples were processed in the same manner with appropriate additions of graphite and gasoline.

The work was carried out on an ISP-22 spectrograph. The spectra were excited in an AC arc by means of a DG-1 generator. The samples were packed into the core of the lower carbon electrode. Photographic conditions: slit - 0.02 mm, current - 2.5 amp, plates - positive, exposure - 80 sec, gap - 1.5 mm. The working curves for a number of elements are shown in the accompanying figure. The probable deviation of individual determinations is ±12%.

References

1. Gambrill, Anal. Chem., 23, 1365 (1951).
2. Pagliasotti & Porsch, Anal.Chem.,23,198(1951).
3. Clark, Anal. Chem., 23, 1349 (1951).
4. Hansen, Anal. Chem, 23, 1360 (1951).
5. Mecker & Pomatti, Anal. Chem, 25, 154 (1953).

* * * * * * *

SPECTRUM ANALYSIS OF BLACK TIN

- V.D.Pisarev, A.V.Kornilov & Z.P.Kostrova

We employed spectrum analysis to determine Pb, Cu, Sb, Fe and As. In preparing samples for analysis we made use of the property of tin of going over, at 161°C, into the rhombic (γ) modification characterized by great brittleness.

The tin shavings taken as the sample were heated to 180-200°C and then crumbled by hand while wearing canvas gloves. The tin powder was thoroughly mixed and then briquetted at a pressure of 3000-5000 kg/cm^2 into small cylinders which served as the electrodes.

Table 1

Element	Analytic line pairs λ, Å	Range of concentrations, %
Lead	Pb 2833,0 — Sn 2785,0	0,05 ÷ 2,0
Copper	Cu 3273,9 — Sn 3223,5	0,05 ÷ 0,4
"	Cu 2369,8 — Sn 2368,2	0,4 ÷ 2,0
Antimony	Sb 2528,5 — Sn 2368,2	0,01 ÷ 0,2
Iron	Fe 2746,9 — Sn 2785,0	0,1 ÷ 0,8
"	Fe 2719,0 — Sn 2785,0	0,8 ÷ 2,0
Arsenic	As 2349,8 — Sn 2368,2	0,1 ÷ 1,0

The spectra were photographed on an ISP-22 spectrograph. The excitation source was an IG-2 generator, connected for complex circuit operation: C = 0.02 μf; L = 0.01 μH; current - 3 amp; analytic gap - 2 mm; auxiliary gap 2.5 mm. The spectra were photographed on plates having a speed rating of 11 units GOST; exposure - 1 minute (2 mm diameter aperature in the intermediate diaphragm); development - 2 minutes at 18°C. The analysis was effected by

Table 2

Sample No.	Results of chemical analysis,%					Results of spectrum analysis (average of 10 determ.),%				
	Pb	Cu	Sb	Fe	As	Pb	Cu	Sb	Fe	As
1	0,90	1,17	0,14	0,023	0,21	0,89	1,05	0,13	0,025	0,22
2	0,75	1,08	0,16	0,035	0,17	0,68	1,03	0,13	0,036	0,19
3	0,21	0,21	0,053	1,69	0,14	0,18	0,18	0,056	1,68	0,15
4	0,61	0,69	0,08	0,94	0,25	0,61	0,75	0,093	0,85	0,25
5	0,80	0,95	0,096	0,24	0,31	0,78	0,91	0,10	0,23	0,30
Mean error	—	—	—	—	—	±5,4	±8,4	±10,8	±5,9	±6,4

the method of three standards. The line densities were measured on an MF-2 microphotometer. The standards were selected samples subjected to repeated chemical analysis. The analytic line pairs used and the concentration ranges of the determined elements are listed in Table 1.

The results of chemical spectrum analysis are juxtaposed in Table 2, where we also list the arithmetic mean errors as computed on the basis of ten repeat analyses of all samples. The developed procedure satisfies the requirements of the industry and is now being employed in some plant laboratories.

Novosibirsk Institute of
Railroad Transport Engineers

* * * * * * *

SPECTROGRAPHIC DETERMINATION OF MINOR IMPURITIES IN CERTAIN RAW MATERIALS, INTERMEDIATE PRODUCTS AND PURE METALS ENCOUNTERED IN COPPER-NICKEL PRODUCTION

- V.L.Ginzburg, I.N.Gramenitski, S.E.Kashlinskaia & D.M.Livshits

Analysis of copper ores, slags, etc., for gold, platinum and palladium

In the copper refining industry materials containing as little as 1-2 grams per ton of platinum, palladium and gold may be of industrial value. Direct spectroscopic determination of such minute quantities of these metals is impossible: samples must be enriched 30-50 times.

To this end a 5-10 gram portion of the finely broken-up gross sample is heated and then decomposed in aqua regia. Next sulfuric acid is added and the solution is twice heated to the point of evolution of sulfuric acid fumes. The solution is cooled and 15-20 ml hydrochloric acid and 0.3 gm potassium chlorate are added to it. The solution is heated to drive off most of the chlorine, diluted with hot water and filtered. A solution of copper sulphate is added to the filtrate in an amount to bring the copper content in the solution to 0.1-0.2 gm. The resultant solution is heated to the boiling point and then the copper together with gold, platinum and palladium are precipitated by the addition of a 40% solution of sodium thiosulfate.

The precipitate is filtered out and heated in a muffle furnace; the oxides obtained are reduced in a stream of hydrogen in a tubular furnace at 300-400°C. The resultant "sponge" is transferred to a graphite crucible and fused in another furnace into an assay button, which is then subjected to spectrum analysis.

We introduced the assay button into an AC arc between spectroscopic carbon electrodes. The electrode gap measured 2-2.5 mm; the current was 4 amp; the voltage - 220 v. The spectra were photographed on an ISP-22 spectrograph using a slit

width of 0.01 mm. The slit was illuminated by means of a single lens condenser, having a focal length of 75 mm. The condenser to slit distance was 315 mm; the arc to condenser distance was 100 mm. Analysis was effected by the method of three standards. The spectra were photographed on Spectral Type II plates, using an exposure of 30-60 sec, after 30 sec pre-arcing.

We utilized the following lines: Au 2675.95, Pt 2659.45, Pd 2447.91; internal standard - Cu 2630.00 or Cu 2627.30 A.

From the results of the analysis of the button one can readily compute the content of platinum, palladium and gold in the gross sample.

Under the described conditions the determination threshold for gold was 0.003%, for platinum 0.001% and for palladium 0.003%. The average relative error was 8% for gold, 6% for platinum and 11% for palladium. In view of the losses incident to chemical decomposition and processing, the overall analytical error is estimated to be within±20%.

The standards were prepared by fusing appropriate amounts of Au, Pd and Pt with pure copper; the poorer standards were made by successive dilution of rich standards with spectrally pure copper.

We carried out a series of tests to verify the efficacy of the described procedure of extracting the noble metals; the results were satisfactory. Another series of tests showed that variation of the weight of the assay buttons between 0.1 and 0.2 gm does not affect the analytical results.

We also investigated the possibility of using similar small (5-10 gm) samples for the determination of noble metals diffused in sulfide ores. Among several thousand parallel spectrographic and conventional chemical analyses (the latter using assay samples of 100-200 gm) less than 2% yielded results diverging by more than the allowable value.

Determination of small amounts of silver in copper-nickel matte

Copper-nickel matte (Feinstein) is an alloy of copper and nickel sulfides, containing 2-3 percent iron sulfide and some hundredths or thousandths of one percent of other admixtures. The content of copper, like that of nickel, varies in different mattes from 7 to 70%, but the content of both together always adds up to about 77%.

In our analyses of mattes for silver, either copper or nickel served as the internal standard. We determined the so-called reduced silver concentrations (i.e., the Ag concentrations referred to the Cu or the Ni content).

We prepared several series of samples of nickel and copper sulfide alloys with different proportions of these two components but with the same Ag content relative to the copper or the nickel. These alloys were subjected to spectrum analysis in an activated AC arc. The samples, in the form of 0.1-0.2 gm buttons, were introduced into the gap between two spectroscopic carbon electrodes. The spectra were photographed on Spectral, Type II plates, using an exposure of 10-20 sec, without preliminary arcing. Other spectrographic conditions were the same as outlined above.

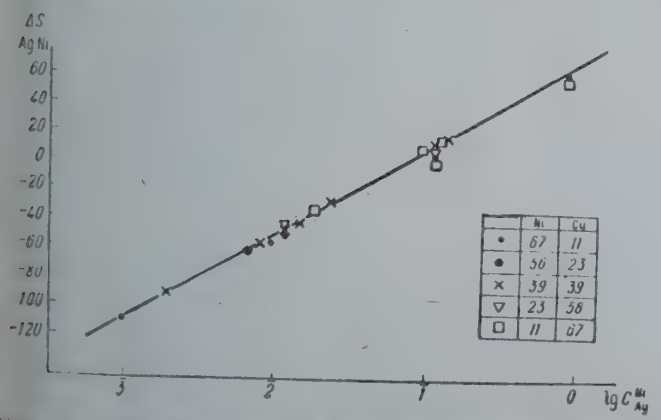

Fig. 1. Working curve for analysis of Cu-Ni matte with different proportions of Ni and Cu for small amounts of silver according to the Ag 3383 - Ni 3371 A line pair.

The Ag 3382.89 - Ni 3371.99 A line pair was used in determining the Ag concentration referred to nickel and the Ag 3280.68 -

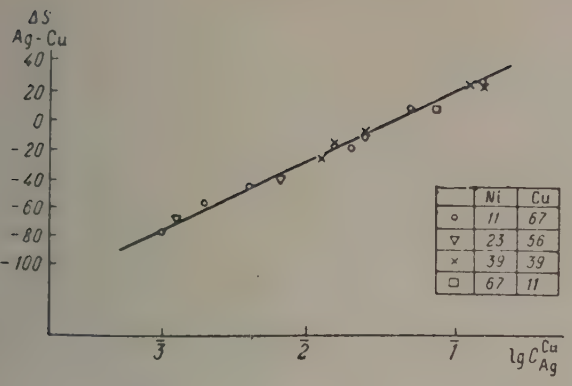

Fig. 2. Same as Fig. 1, but for analysis on the basis of the Ag 3280 - Cu 3279 A line pair.

Cu 3279.82 A pair was employed for determining the concentration referred to nickel. The working curves, plotted in ΔS *vs* log C_{Ag}^{Cu} and ΔS *vs* log C_{Ag}^{Ni} coordinates (here C_{Ag}^{Cu} and C_{Ag}^{Ni} are the silver concentrations referred to the copper and nickel contents, respectively) are shown in Figs. 1 and 2. It will be noted that all the points fall on the same straight line, regardless of the proportions of nickel to copper, which shows that variation of the Ni-Cu ratio does not affect the determination of the reduced silver concentration.

Knowing C_{Ag}^{Cu} or C_{Ag}^{Ni}, we can readily find C_{Ag}, the silver content in the sample from:

$$C_{Ag} = \frac{C_{Ag}^{Ni} \cdot C_{Ni}}{100} \quad \text{or} \quad C_{Ag} = \frac{C_{Ag}^{Cu} \cdot C_{Cu}}{100}.$$

Assuming the total copper plus nickel content of the samples to be constant:

$$C_{Ni} + C_{Cu} \approx 77,$$

we obtain as the solution of the above three equations:

$$C_{Ag} = \frac{C_{Ag}^{Ni} \cdot C_{Ag}^{Cu}}{C_{Ag}^{Ni} + C_{Ag}^{Cu}} \cdot 0.77.$$

This procedure does not require preliminary determination of Ni and Cu in the matte and presumably can be used for determining any other minor impurities in complex sulfide alloys.

Analysis of metallic copper and cobalt for minor metals

In developing the procedure we strove a) to provide for the determination of all metallic impurities as required by the pertinent State Standard (or the applicable technical specifications), b) to obtain an accuracy and sensitivity not inferior to those of current chemical methods and c) to arrive at a simple procedure suitable for use in any industrial laboratory.

Both the samples and standards were in the form of metallic electrodes 6-7 mm in diameter and 25-30 mm in length.

The standards for the determinations of Ni, Fe, Mn and Si in cobalt were prepared by fusing appropriate quantities of these metals with pure cobalt; the poorer standards were obtained by adding pure cobalt to the richer alloys. The alloys were fused in graphite crucibles in a resistance furnace (carburization of the cobalt does not have a deleterious effect).

The standards for determination of Pb, Sb, As and Al were prepared by fusing these metals with pure cobalt with subsequent chemical analysis. The concentration of Ni, Fe, Mn and Si in cast

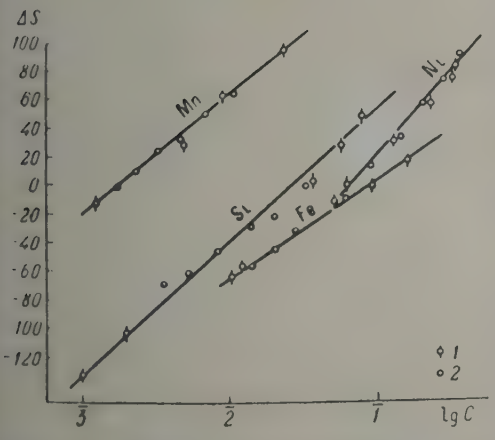

Fig. 3. Working curves for the determination of Ni, Fe, Mn, and Si in 1) cast cobalt electrodes, 2) powdered oxide standards.

cobalt electrodes can be checked (without converting the metals to their oxides) spectrographically with reference to powdered oxide standards. Fig. 3 shows the working curves for the determination of these elements, plotted on the basis of cast cobalt and powdered oxide standards. (The oxide standards were prepared by Gipronikel.) As may be seen, the points for both types of standards fall on the same straight-line curves.

When the metal is produced in the form of cast ingots the samples are taken at the time of casting, an appropriate amount of the molten metal being poured into sectional steel molds. Samples of cathode copper are taken in the form of shavings in accordance with the specified procedure for such sampling; then the shavings are melted to form an electrode of the requisite size in a graphite crucible in an arc or resistance furnace. Tests showed that this fusing does not produce any noticeable changes in the composition of samples of high purity grades of copper, for which this sampling procedure is commonly employed.

In analyzing copper we use Spectral Type II plates; in analyzing cobalt, Spectral Type I plates. Copper samples were pre-arced 2 min; cobalt samples - 30 sec. In the analysis of cobalt, the upper electrode was a spectroscopic carbon rod. The other conditions remained as described above. The analysis was effected by the method of three standards. The analytic line pairs employed are listed in Tables 1 & 2.

Table 1

Analytic line pairs for analysis of copper

Determined element	Wavelengths, Å		Range of concentrations %
	Analytic line	Comparison line (Cu)	
Nickel	3054,32	3022,61	0,01 ÷ 0,2
	3050,8	3022,61	0,005 ÷ 0,02
	3050,8	3050,3	0,001 ÷ 0,006
Iron	3020,64	3022,61	0,005 ÷ 0,05
	2599,40 57	2627,36	0,001 ÷ 0,01
Antimony	2598,06	2627,36	0,001 ÷ 0,02
Bismuth	3067,72	3022,61	0,001 ÷ 0,01
Lead	2833,07	2858,73	0,001 ÷ 0,02
Zinc	3345,02	3329,64	0,001 ÷ 0,05
Tin	2839,99	2858,73	0,001 ÷ 0,05
Arsenic	2860,45	2858,73	0,001 ÷ 0,02
	2780,19	2782,60	0,005 ÷ 0,05

Table 2

Analytic line pairs for analysis of cobalt

Determined element	Wavelengths, Å		Range of concentrations %
	Analytic line	Comparison line (Co)	
Nickel	3003,62	2975,46	0,03 ÷ 0,4
	3012,00	3013,59	0,03 ÷ 0,4
Iron	2719,03	2719,58	0,002 ÷ 0,25
	2966,90	2975,46	0,002 ÷ 0,25
Silicon	2516,12	2512,31	0,001 ÷ 0,1
	2514,12	2512,31	0,01 ÷ 0,3
Manganese	2794,82	2787,02	0,0005 : 0,03
	2576,10	2578,93	0,005 ÷ 0,2
Lead	2833,07	2833,93	0,001 ÷ 0,02
Antimony	2598,06	2578,93	0,001 ÷ 0,02
Arsenic	2349,84	2345,50	0,002 : 0,02
Aluminum	3092,71	2975,46	0,005 ÷ 0,1

In developing the analytical procedure for cobalt we made a detailed study of its spectrum. In the 2345 - 3600 A interval we observed over 130 lines which are certainly associated with cobalt but which are not listed in published wavelength tables. Furthermore, we discovered that a number of lines commonly ascribed to cobalt do not appear in the spectrum of the pure metal and consequently must be due to impurities; these are the following:

Lines ascribed to Co	Pertain to	Corrected value	Lines ascribed to Co	Pertain to	Corrected value
2576.10	Mn	-	2802.71	Mg	2802.70
2750.14	Fe	-	2881.58	Si	-
2794.82	Mn	-	2966.90	Fe	-
2798.65	Ni or Mn	2798.27			

We use some of these Mn and Fe lines as analytic lines in our procedure inasmuch as they are free of overlapping.

The mean error in the analysis of copper is ±12%. The mean error in the analysis of cobalt varies from ±3 to ±8% for the different minor elements.

References

1. A.N.Zeidel', V.K.Prokof'ev & S.N.Raiski, Tablitsy spektral'nikh linii (Tables of spectrum lines), Gostekhizdat, L. -M. 1952.

2. S.L.Mandel'shtam, Vvedenie v spektral'nyi analiz (Introduction to spectrum analysis) M. -L. 1946.

3. V.K.Prokofev', Fotograficheskie metody kolichestvennogo spektral'nogo analiza metallov i splavov (Photographic methods of spectrum analysis of metals and alloys). M. -L. 1951.

4. D.M.Shvarts & I.S.Nilova, Izv. AN SSSR, 18, 280 (1954).

5. L.N.Filimonov, Zavod. labor. (The Plant Laboratory), 16, 1200 (1950).

* * * * * * *

SPECTROGRAPHIC DETERMINATION OF TIN IN NATURAL MINERALS

- M.L.Shilling

According to our procedure for the determination of Sn in natural minerals, the powdered sample is mixed with an equal amount of antimonyl potassium tartarate (tartar emetic). The mixture is packed into a well (2-2.5 mm dia., 3 mm deep) in a 5-6 mm diameter carbon electrode, tapered to a thin lip at the well edge. It is preferable to use an ordinary (unrefined) carbon rod for the upper electrode, for the low thermal conductivity of unrefined carbon and the impurities in it assure more stable burning of the arc.

The presence of potassium in the sample in the amount of 5.5% (in the mixture with tartar emetic) stabilizes the arc temperature. Analysis was effected on an ISP-22 spectrograph by the method of three standards. The slit width was 0.017 mm. We used an AC arc (220 v, 12 amp). The spectra were photographed on positive or line-reproduction plates processed in the conventional manner. Antimony served as a comparison element, the analytic pair being Sn 2429.5 and Sb 2426.4 A. Each sample was photographed three times. The tin content was determined from a working curve plotted in terms of ΔS *vs* log C.

Since tin is commonly encountered in nature in the form of cassiterite (SnO_2), it appeared logical to prepare standards by the introduction of measured quantities of SnO_2 into minerals similar to the samples as regards gross composition, but free of tin. However, in trying various other tin compounds we found that equally satisfactory results are obtained by the introduction of $SnCl_2 \cdot 2H_2O$ in the form of an alcohol solution. The use of this compound also insures more stable standards.

In order to determine the possible influence of the principal components of tin ores and minerals on the analytical results we also prepared standards with silicate, silicate-iron and sulfide bases. Tin is rarely found in any other types of minerals. The curves obtained virtually coincided, which simplified the analytical procedure.

Concentrations ranging from 0.01 to 2.0% can be determined according to the Sn 2429.5 A line employed.

In order to evaluate the errors we carried out forty analyses on each of the three samples. The average tin concentrations were 0.27, 1.04 and 4.25%. The mean probable deviations were calculated to be±9.4, 6.0, and 11.8%.

* * * * * * *

RAPID SPECTRUM ANALYSIS FOR FLUORINE

- I.I.Smoliak

The spectrum of fluorine is not excited in a carbon arc, which renders determination of fluorine on the basis of its atomic spectrum difficult in conventional spectrographic analysis. However, fluorine can be determined indirectly on the basis of the molecular spectrum of the CaF^- radical. This spectrum appears under favorable excitation conditions when the analytic sample contains compounds of both calcium and fluorine or when other conditions favorable to the formation of the radical in the arc flame obtain. The equilibrium point of the CaF^- formation reaction and, consequently, the intensity of the spectrum depend on the amount of calcium entering the arc and on the arc temperature.

In our procedure the spectrum was excited in an AC arc (220 v, 16 amp). The sample was packed into the core (4 mm diameter, 4 mm deep) of the lower carbon electrode. The calcium was introduced from the upper electrode in the form of calcite. To this end a longitudinal slot 4.5 mm deep was hacksawed in the upper electrode (6 mm diameter, 15 cm long); lateral grooves were scratched in the bottom and sides of the slot to insure retention of the calcite. The slot was filled with calcite, moistened with water and dried. The upper electrode with the calcite inlay was mounted in the holder at an angle of 15° to the horizontal with the slot uppermost.

We employed the most intense characteristic bands of the molecular spectrum of the radical for determining fluorine: 5291 A (10), 5830 A (5), 6064.4 A (10) and 6256.6 A (4); these are located in the visible range of the spectrum and hence are convenient for observation. The determinations were effected visually on an ISP-22 spectrograph, using a slit width of 0.01 cm (eyepiece magnification - 10 X).

The rate of entry of the calcium into the arc was monitored visually according to the intensity of the green CaO 5473 A line group. In addition, a supplementary check on the arc regime was furnished by the intensity of the spectrum of a special control standard burned simultaneously with the samples. To provide a basis of comparison for quantitative determination of fluorine we burned standard powders

having concentrations of fluorine (in the form of fluorite) of 0.001, 0.003, 0.01 and so on up to 30%.

Fluorine was detected first in the samples according to the most sensitive 5291 A line, which is virtually free of surposition.

The analysis of a large number of samples showed that drift material over ore bodies commonly contains 1% or more of fluorine.

The expedient of introducing the calcium into the upper carbon electrode eliminates the onerous and time consuming operation of mixing each individual sample with calcium.

Although the outlined procedure suffers from the shortcoming that the entry of calcium into the arc is somewhat irregular, which gives rise to certain errors, the results are accurate enough for many practical purposes.

* * * * * * *

CALCULATION AND INTERPRETATION OF THE VIBRATIONAL SPECTRA OF CERTAIN MONOALKYLBENZENES AND POLYMETHYLBENZENES

- M.A.Kovner

The development of molecular spectrum analysis of petroleums, petroleum products and engine fuels has brought the need for theoretical calculation and systematization of the vibrational spectra of alkylbenzenes.

In our previous investigations we determined the entire system of bond force constants characterizing the benzene ring. We utilized this system in the present investigation to compute the vibrational frequencies of alkylbenzenes. Solution of the corresponding secular equations for toluene and ethylbenzene has made it possible to give an almost complete interpretation of the vibrational spectra of these substances, to identify and supply a theoretical basis for the characteristic and noncharacteristic ring frequencies. We computed the values of the noncharacteristic frequency coefficients derived by Maiants; the computed values are in agreement with the experimental data on the frequency variation in the series of normal monoalkylbenzenes. We also showed that the lowest frequencies have the greatest variability; these are the frequencies of the deformation vibrations of the angles marked in the accompanying figure and of the angles characterizing the departure of the C—R bond from the plane of the ring. These low frequencies can be utilized as an analytic indication to distinguish between different radicals. However, to justify such use theoretically it is essential to evaluate the force constants of the interaction of the alkyl group with the ring. Apparently this can be done only on the basis of the spectrum of $C_6D_5CD_3$. We computed the vibrational frequencies and fully interpreted the vibrational spectra of paraxylene, mesitylene and durene, including a classification of the overtones and component frequencies. In connection with this we utilized all the data we could find in the literature on the Raman and infrared spectra of these compounds. With the exception of the values for some of the low frequencies of the type mentioned above the agreement of the calculated with observed frequency values is satisfactory.

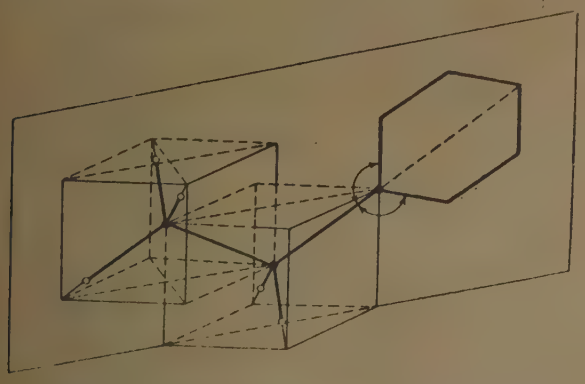

Model of ethylbenzene molecule

Thus, we investigated the spectra of representative mono-, di-, tri- and tetra-substituted alkylbenzenes. It is to be hoped, therefore, that our interpretation of their spectra can be utilized in the future to determine the general regularities and characteristic frequencies in the spectra of polyalkylbenzenes.

A preliminary examination of the spectra of diphenyl shows that they comprise many of the frequencies of benzene. This led us to attempt to compute the vibrational frequencies of diphenyl on the basis of the system of force constants of benzene. While our results must still be regarded as tentative, they would indicate that the force constant of the C—C bond has a somewhat lower value than those associated with the other bonds. This may be attributed to the influence of the π-electrons of the two linked rings, which acts to weaken the intraring π-bonds. The force constant of the interring bond equals 7.02, which indicates that this is a single bond. The angles adjacent to this bond differ from tetrahedral angles and from the C—CH angles in benzene, and should be characterized by different force constants, the values of which can be determined only on the basis of the spectra of deuterodiphenyls.

In conclusion the writer feels duty bound to thank G.S.Landsberg for his interest in the investigation and his very valuable advice.

"N.G.Chernyshevski" Saratov State University

* * * * * * *

TEMPERATURE DEPENDENCE OF THE INTENSITY OF FIRST ORDER STOKES LINES

- Ia.S.Bobovich

Despite the fact that the effect is contrary to the predictions of currently accepted theory, we know that the intensity of the Stokes lines in Raman spectra of the first order decreases with increasing temperature of the scattering substance. In view of this we undertook a systematic investigation aimed at accumulating experimental data for the purpose of eventual revision of the pertinent theory.

The change in intensity over the relatively narrow temperature range readily attainable in the laboratory is small; hence, its investigation necessitates the use of precision methods. In our investigation we used a special sensitive photoelectric set-up.

We investigated the spectra of eighteen different compounds, including four in the solid state. The measurements were made at +14° and +55°C.

The results may be summarized as follows:

1) The intensity anomaly really exists; it cannot be explained away by Lorentz broadening or by reduction in the number of scattering centers due to thermal expansion of the liquid.

2) The anomalous intensity change does not parallel the frequency shift associated with molecular interaction.

3) There is no apparent correlation between the line frequency and the magnitude of the observed anomaly.

4) The anomaly is apparently not connected with the molecule having a dipole moment, for it is also observed in the case of symmetrical molecules (although to a lesser degree).

5) Lines associated with deformation vibrations undergo a particularly great change in intensity.

6) Lines associated with valence vibrations are less affected by temperature

variation than those connected with the deformation vibrations of the same atoms.

7) Multiple bonds are also less subject to the influence of temperature than are single bonds; in the particular case when the molecule contains large atoms blocking the multiple bond, the anomaly is virtually unnoticeable.

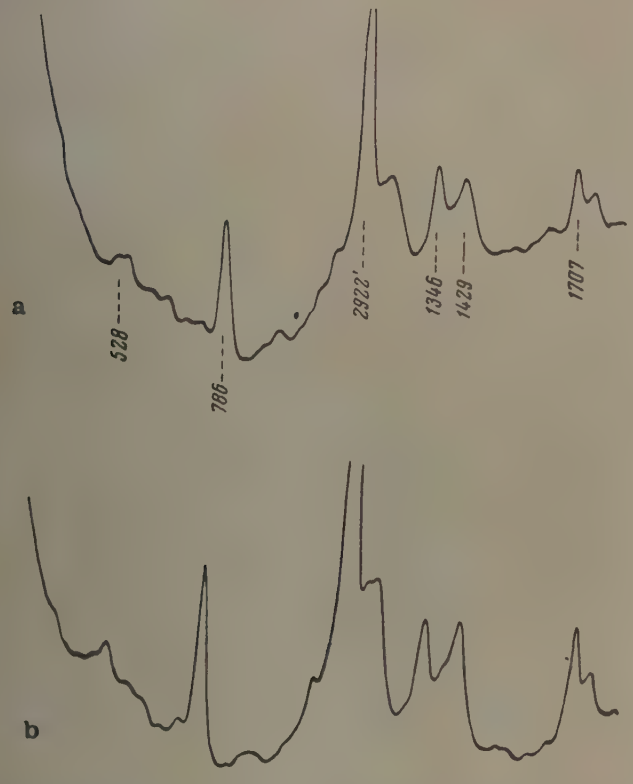

Photoelectric record of the spectrum of acetone: a) at 55°; b) at 14°C.

Analysis of the experimental data indicates that the temperature dependence anomaly is a composite effect due to intermolecular interaction as well as to the attributes of the chemical bonds and purely steric conditions.

The observed effects can be explained with the aid of the concept of the mutual deformation of the potential curves for the excited electronic levels. Frank and Aiken have successfully employed a similar approach to explain, at least qualitatively, observed differences in the effectiveness of particle collisions as regards exchange of translational and vibrational energies. The existence of a strong temperature dependence of these quantities for ground energy states has been established experimentally and theoretically by Henry, Richards and Reade, by Huntington and by Aiken and his collaborators. In the expression for the derivative of the polarization, characterizing the influence of the parameters of the potential curve for the excited state, we consider the determining factor to be $\left(\frac{\partial \nu_e}{\partial q}\right)_0$, where ν_e is the virtual transition frequency and q is the normal coordinate.

The above deductions are supported by the records of infrared spectra made at different temperatures and by the measured line intensities in the Raman spectra of twenty pure liquids and different mixtures at room temperature.

The photoelectric records of the spectrum of acetone obtained at 14 and 55°C are reproduced in the accompanying figure.

* * * * * * *

EFFECT OF CARBURIZATION AND NITRIDATION ON THE RESULTS OF SPECTRUM ANALYSIS*

- I. A. Grikit

A metallurgical plant laboratory may receive for spectrum analysis iron and steel products not only in the ordinary untreated state but also pieces subjected to carburizing and nitriding. It is, therefore, essential to know to what extent carburization or nitridation may distort the results of analyses effected under conditions selected for samples and standards that have not undergone thermo-chemical treatment.

As far as we know this question has been studied only by Filimonov[1,2] who gives only a qualitative picture of the effects of such treatment and discusses the general nature of these effects. Filimonov's reports do not contain any specific quantitative data on the magnitude of the distortion introduced into the analytic results by nitridation and carburization.

We therefore deemed it desirable to investigate the matter in more detail. The investigation was carried out on an ISP-22 spectrograph, using a condensed spark as the source (power = 0.5 kw, voltage-8 kv, C = 0.02 μf, L = 0.025 mH).

In the first part of the investigation we determined the magnitude and sign of the errors introduced by carburization and nitridation into the results of spectrum analysis carried out with reference to standards prepared by the Ural Institute of Metals and under the conditions specified for untreated samples. We worked with samples of Grade 12Kh2N4A, 12KhN3A, 13N2A, 18KhNVA and 13N5A [12X2H4A, 12XH3A, 13H2A, 18XHBA and 13H5A] steels for carburizing and Grade 40KhNMA and 38KhMIuA [40XHMA and 38XMIOA] steels for nitriding. Two sample plates of identical size were taken from each melt: the first remained as is, while the second was subjected to the appropriate thermo-chemical treatment in accordance with the regular production procedure. Specifically, the treatment for the five samples of the first group of steels was gas carburizing with pyrobenzol, with the pyrobenzol being supplied at the rate of 140-200 drops per minute during carburization and the sample held at 920°C for 5-6 hours. As a result of the treatment there was obtained a hypereutectoid carbon concentration of up to 1% with a case of 0.8-1.1 mm. Inasmuch as some grades of steel have a tendency to self-hardening when cooled in air after treatment, all the samples were annealed for 2 hours at 650° after carburization. The 40KhNMA and 38KhMIuA steel samples were nitrided in ammonia gas at 525° (25 hours; degree of dissociation of ammonia - 25-35%) or at 540° (30-35 hours; degree of dissociation - 40-50%). The nitrogen saturation of the nitrided surface attained 0.8%; the depth of case was 0.4-0.7 mm).

Each pair of samples (treated and untreated) was photographed on the same plate with the appropriate Ural Institute of Metals standards. Eighteen spectrograms were recorded for each of the investigated specimens. Then the mean (arithmetic) values of the concentrations of the impurity elements were determined from working curves plotted on the basis of standard samples. In order to allow for the possible influence of the counter electrode material measurements were made using carbon, copper and iron counter electrodes. With carbon counter electrodes the pre-sparking time was 10 sec; the exposure 60 sec; with copper - pre-sparking 40 sec, exposure 60 sec; with iron - pre-sparking

---

* Report presented at the Eighth All-Union Conference on Spectroscopy.

50 sec, exposure 60 sec.

The results show a persistent but varying deviation of the data for carburized and nitrided samples as compared to samples in the initial state. Referred to the respective concentrations in the untreated samples, the Ni and Mn contents of carburized samples were 2-10% lower; the Cr content in 12Kh2N4A steel was 5-10% higher, while in 12KhN3A the apparent Cr content was 2-3% lower with all three counter electrode materials. In the nitrided samples (compared with the corresponding untreated samples) the apparent Al, Mn and Cr contents were 5-20% lower, while the Ni content was somewhat higher when the analyses were made with a carbon counter electrode. In the case of analyses with a copper electrode the Al and Mn concentrations were as much as 9% lower while the Cr and Ni concentrations were 3 to 30% higher. With iron counter electrodes, higher values were obtained for the concentrations of all the impurity elements. In all cases the intensity of the spectrum of the nitrided samples was 1.5-2 times greater than that of the untreated samples.

Thus it will be seen that carburization and nitridation do have an appreciable influence on the results of spectrographic determinations of impurities, throwing the results off by over 10% in many cases. The material of the counter electrode has considerable bearing on the magnitude and direction of the deviations in analyzing nitrided samples and only a negligible effect in analyzing carburized samples.

The obtained data on the influence of carburization (specifically, an excessively high Cr and erroneously low Ni concentration in 12Kh2N4A and 18KhVA steels) are in conformity with Filimonov's deductions regarding the influence of a deoxidizing agent (carbon). On the other hand the below-actual values for Cr in 12KhN3A steel and Mn in all the steels are in conflict with Filimonov's data.

The second part of our investigation was concerned with the influence of hardening with subsequent tempering of nitrided and carburized samples (the prescribed industrial procedure was followed in treating the different grades of steel). This part of the investigation was undertaken in view of the contradictory data in literature on the actual effect of structure on analytic results.

In this part of the investigation, the spectra of samples from the same melt in three different states - 1) carburized, 2) carburized and annealed for 2 hours at 650° and 3) carburized, hardened and tempered - were photographed on the same plate together with the spectrum of the appropriate Ural Institute of Metals standards. Eight to eleven spectrograms for each sample were recorded; two series of measurements were made, one with carbon, the other with copper counter electrodes.

A similar procedure was followed in studying the effect of hardening with subsequent tempering on nitrided specimens, except that in this case the three samples were 1) untreated, 2) nitrided, and 3) nitrided, hardened and tempered. The spectra of this group were recorded only with carbon counter electrodes.

The results showed that the hardening-tempering treatment after carburization does have an appreciable effect on the nickel determination; thus while for carburized and annealed samplesthe apparent nickel concentration was low, that for carburized, hardened and tempered samples was high. The deviations were more pronounced in the case of analyses with carbon electrodes, in which the pre-sparking period was shortest. As regards the other impurity elements the deviations of the results of analyses of carburized, hardened and tempered samples (from the true values) are approximately equal to the deviations of the analytic results for samples subjected to carburization and annealing.

Hardening with subsequent tempering of nitrided samples leads to approximately the same deviations from the true values as does nitriding without subsequent heat treatment.

We also studied the sparking-off effect and determined the pre-sparking time at which the influence of carburization, nitridation and hardening-tempering after case-hardening disappears.

We found that where the determination of Cr, Mn and Si is concerned the effect of carburization with annealing and carburization with hardening and tempering diminishes rapidly with sparking time and becomes virtually negligible after 3-4 minutes of sparking. On the other hand where the Ni concentration in carburized and annealed samples is concerned the effect persists even after 10 minutes pre-sparking while the effect of carburization, hardening and tempering diminishes with sparking time. The sparking-off curve for carburized, hardened and tempered samples lies between the variation of apparent Ni concentration with sparking time curves for carburized only and carburized and annealed samples. The position and shape of the sparking-off curves for carburized samples are not affected by changing the material of the counter electrode.

The effect of nitridation and nitridation with subsequent hardening and tempering on the determined content of all the investigated elements diminishes with increasing sparking time and becomes virtually negligible after 3-4 minutes. The position of the initial part (0 to 3-4 min.) of the sparking-off curves is noticeably affected by the counter electrode material. Thus the apparent Al, Mn, Cr and Si concentration curves for nitrided samples lie below and the Ni concentration curve lies above the corresponding curves for non-nitrided specimens when a carbon counter electrode is used. With a copper counter electrode the Al and Mn concentration curves for nitrided samples are situated below and the Cr and Si curves above the corresponding curves for samples in the non-nitrided state. Lastly, with iron electrodes the curves for all the determined elements lie higher in the case of nitrided samples.

The writer wishes to express his profound gratitude to K. A. Sukhenko for his guidance and advice in connection with the investigation.

References

1. L.N.Filimonov, Izv. AN SSSR, Ser. fiz., 12, 402 (1948).
2. L.N.Filimonov, Zavod. labor. (The Plant Laboratory) 15, 1178 (1949).

* * * * *

SPECTROSCOPIC DETERMINATION OF SILICON AND LEAD IN POWDER USED FOR THE PRODUCTION OF SYNTHETIC CORUNDUM*

- O. P. Malkova and N. K. Rudnevski

We developed a procedure for analyzing the powder used for the production of corundum for its lead and silicon content by the method of three standards. The powder is brought into the AC arc by means of a stage electrode traversed at a uniform rate. The stage was made of spectroscopic grade carbon electrode material. The upper electrode was a carbon rod 5 cm in length.

* Condensation of report presented at the Eighth All-Union Conference on Spectroscopy (1952).

The arc current was 6 amp; the electrode gap - 2.5 mm; the exposure time - 40 sec. The probable deviation in determining Si according to the Si 2516.12 - Al 2652.49 A line pair was ±11%; the line pair used for lead was Pb 2614.17 - Al 2652.49 and the probable error ±12%.

Scientific Research Institute for Chemistry
at Gor'ki State University.

* * * * * *

REPORT NO. 8. RAMAN SPECTRA OF CERTAIN AROMATIC HYDROCARBONS*

- V. T. Aleksanian, Kh. E. Stepin, A. L. Liberman, E. A. Mikhailova, M. A. Prianishnikova and B. A. Kazanski

It is known that there are lines in the Raman spectra of mono-, di- and tri-alkyl substituted benzene whose lines are characteristic of the type of replacement in the benzene ring.[1,2] Recently in comparing published data on the spectra of aromatic compounds, we noted that the intensity of lines associated with a given type of replacement does not vary much for different substituents.[3] Translator's Note: Ref. 3 is translated in No. 6, Vol. 18 of the Bulletin. We concluded, therefore, that the intensity of such lines, averaged for different compounds, may be regarded as a characteristic of the type of substitution for a certain boiling point interval. In the same contribution[3] we described an attempt to utilize these characteristic lines for purposes of narrow-group analysis of the aromatic components of ligroin. However, for some types of substitutions the number of spectra available in literature was inadequate for establishing the corresponding characteristic lines. In addition some of the data in literature appeared to be somewhat doubtful. In view of this we undertook the project of obtaining and investigating the spectra of 13 aromatic hydrocarbons; 6 of these have not been studied hitherto.

The Raman spectra were recorded by means of an ISP-22 quartz spectrograph with the 270 mm focal length camera and were excited by the blue mercury line (4358A). We shifted the middle of the spectrum from the minimum deviation position bringing the reciprocal dispersion at 4500 A to 100 cm^{-1} per mm. That is, the dispersion was increased by a factor of one and a half compared to that at the minimum deviation setting which resulted in somewhat better resolution of close lines on the photographic plate.[4] Special tests showed that with the dispersion increased in this manner and the slit width kept constant the ratios of the line intensities in the spectrum of cyclohexane remains unaltered within the limits of the experimental error.

The frequencies of the Raman spectrum lines were determined by linear interpolation with reference to the iron spectrum; the distance between neighboring reference marks in no case exceeded 150 cm^{-1}. The spectra, photographed with a slit width of 0.025-0.035 mm, were measured on an IZA-2 comparator (reading to 0.001 mm) at least five times each. The mean deviation in determining frequencies did not exceed ±1 cm^{-1} for bright lines and ±3 cm^{-1} for weak and diffuse lines.

---

* The preceding report was published in Izv. AN SSSR, Otd. khim. nauk, No. 4, 709 (1954).

t_{boil} = 152.4-152.6 (760 mm); n_D^{20} = 1.4912; d_4^{20} = 0.8619; according to Rossini et al[5]: t_{boil} = 152.39; n_D^{20} = 1.49145; d_4^{20} = 0.86179.

$\Delta\nu$ (cm^{-1}): 144 (50), 311 (20,w), 359 (4), 405 (3,w), 461 (22,p), 564 (15), 591 (2), 622 (39,r), 662 (2), 742 (96,p) 761 (12), 789 (2). 817 (2), 840 (10), 868 (1), 892 (15), 956 (8), 989 (8), 1002 (410,p), 1029 (87,p), 1083 (13), 1106 (14), 1143 (1), 1156 (31), 1183 (35), 1212 (57,p), 1281 (5), 1306 (15), 1326 (2), 1346 (2), 1383 (4), 1406 (2), 1445 (20,w), 1464 (18,w), 1527 (2), 1583 (22), 1606 (70), 2870 (60), 2888 (40,bkgd), 2906 (60,bkgd), 2936 (60,bkgd), 2966 (100), 2980 (10), 3002 (30), 3038 (30,w), 3054 (140), 3064 (120).

n-BUTYLBENZENE. Separated in the same manner as the isopropylbenzene except that final distillation was under vacuum.

t_{boil} = 76.6° (20 mm); n_D^{20} =1.4897; d_4^{20} = 0.8603; according to Rossini et al[5] t_{boil} = 183.270° (760 mm); n_D^{20} = 1.48979; d_4^{20} = 0.86013.

$\Delta\nu$ (cm^{-1}): 172 (10,w), 226 (15,w), 287 (20,w), 335 (0), 402 (0), 443 (3), 499 (10,w), 512 (0), 588 (4), 606 (0), 624 (47), 747 (22,d,w), 783 (23,p), 809 (15), 821 (32), 843 (9), 877 (15), 894 (15), 911 (12,w), 991 (5,bkgd), 1003 (265,p), 1033 (73,p), 1052 (25,w), 1106 (33,w), 1148 (0), 1157 (29), 1181 (23), 1203 (65,w,p), 1255 (2), 1283 (0), 1302 (20,w), 1336 (10,w), 1441 (42,w), 1456 (35,w), 1466 (5,w,bkgd), 1585 (29), 1606 (80), 2859 (80,w), 2877 (90,w,bkgd), 2904 (90,w,bkgd), 2917 (90,w,bkgd), 2936 (90,w,bkgd), 2964 (30), 3002 (20), 3033 (50), 3045 (120,w), 3065 (90,w).

SECONDARY BUTYLBENZENE. Obtained by alkylation of benzene with butyl in the presence of sulfuric acid and separated by chromatographic absorption in a large amount of silica gel. In view of the small quantity of this hydrocarbon available it was not distilled.

n_D^{20} = 1.4902; d_4^{20} = 0.8624; according to Rossini et al[5]; t_{boil} = 173.305° (760 mm); n_D^{20} = 1.49020; d_4^{20} = 0.86207.

$\Delta\nu$ (cm^{-1}): 148 (40,w), 203 (3,d), 232 (20,d), 259 (3), 272 (3), 312 (6), 330 (8), 362 (0), 385 (0), 407 (2,w), 435 (0), 465 (14), 478 (1), 488 (0), 505 (2), 543 (2), 580 (0), 595 (2), 608 (0), 623 (37,p), 643 (1), 706 (3), 732 (40,p), 749 (13), 764 (8), 791 (5), 809 (11), 841 (8), 856 (14), 959 (8), 991 (2,bkgd), 1002 (230), 1019 (3,bkgd), 1031 (77,p), 1057 (4), 1084 (8), 1097 (12), 1121 (4), 1157 (25,p), 1182 (22,p), 1207 (54,p), 1244 (4), 1259 (2), 1284 (4), 1295 (4,bkgd), 1307 (3,bkgd), 1327 (4), 1338 (4), 1358 (6), 1377 (4), 1442 (10), 1455 (39), 1483 (0,bkgd), 1583 (21), 1606 (69), 2829 (10), 2864 (50), 2877 (80), 2908 (60,w,bkgd), 2934 (100,w), 2965 (80), 2974 (70), 3003 (60), 3035 (70), 3055 (130,w), 3065 (130,w).

1-METHYL-2-ETHYLBENZENE. Obtained from o-acetotoluide carefully separated from its isomers[6], converted to o-bromotoluene according to Sandmeyer's reaction, then to 1-methyl-2-ethylbenzene by the Wurtz-Fittig reaction; final purification by distillation in a column rated at about 80 theoretical plates.

t_{boil} = 165.5° (760 mm); n_D^{20} = 1.5045; d_4^{20} = 0.8804; according to Rossini et al[5]; t_{boil} = 165.153° (760 mm); n_D^{20} = 1.50456; d_4^{20} = 0.88069.

$\Delta\nu$ (cm^{-1}): 144 (150,w), 221 (30,w), 240 (10), 324 (15,w), 342 (7), 394 (2), 409 (0), 451 (8), 462 (8), 497 (29), 514 (1), 551 (28), 587 (68), 602 (1), 698 (0), 718 (115), 731 (115), 756 (8), 780 (0),

822 (13), 863 (7), 935 (5), 963 (24), 990 (20), 1001 (8), 1033 (58), 1040 (10), 1060 (98), 1124 (2), 1159 (43), 1181 (1), 1217 (145), 1245 (4), 1271 (3), 1287 (4), 1306 (2), 1326 (15), 1380 (35), 1400 (0), 1452 (39,w,d), 1492 (3), 1579 (35), 1606 (100), 2734 (5), 2873 (90), 2894 (20), 2912 (100), 2932 (140), 2970 (90), 2994 (20), 3025 (50), 3047 (50), 3075 (40).

1,2-DIISOPROPYLBENZENE. Prepared from technical grade diisopropylbenzene by distillation under vacuum in a column having a rating of 25 theoretical plates, followed by sulfonation with subsequent hydrolysis of the sulfo acids under conditions under which the sulfonic acids of 1,3- and 1,4-diisopropylbenzene underwent hydrolysis first and that of 1,2-diisopropylbenzene hydrolyzed later at a higher temperature. The 1,2-isomer concentrate was then distilled under vacuum in a column having a rating of 100 theoretical plates. The final fraction contained 95.4% of the 1,2-isomer.

t_{boil} = 92.0° (18 mm); t_{freeze} = -58.7°; n_D^{20} 1.4964; d_4^{20} = 0.8711; according to Melpolder et al[7]: t_{boil} = 203.75°(760 mm); t_{melt} = -56.68°, n_D^{20} = 1.49603; d_4^{20} = 0.87007.

As noted above the following optical data are to be regarded as tentative.

$\Delta\nu$ (cm^{-1}): 155 (120,w), 186 (15,w), 262 (3), 290 (3), 315 (30,p), 339 (5), 369 (2), 395 (2), 422 (2), 449 (24), 475 (13), 522 (3), 554 (4), 564 (3),592 (26), 622 (1), 707 (125,p), 757 (15), 798 (1), 865 (5), 885 (36,p), 895 (18), 957 (15), 1001 (7)*, 1030 (205,p), 1048 (3), 1082 (3), 1108 (36,p), 1140 (3), 1164 (40,p), 1185 (3), 1201 (1), 1226 (73,p), 1263 (1), 1280 (1), 1305 (18,w), 1331 (1), 1363 (10), 1384 (6), 1445 (37,p), 1464 (39,p), 1488 (1), 1578 (21), 1603 (67,p), 2868 (80,p), 2887 (30), 2908 (100,w,p), 2934 (100,w,bkgd,p), 2965 (150,w,p), 2995 (10), 3029 (20), 3055 (90,w), 3068 (30).

1,3-DIISOPROPYLBENZENE. Separated with the preceding; the 1,3-isomer concentrate obtained in the hydrolysis of the sulfonic acids was again subjected to sulfonation and hydrolysis and then purified by distillation in a column having a rating of 100 theoreticalplates.

t_{boil} = 133.7° (100 mm); n_D^{20} = 1.4893; d_4^{20} = 0.8562; according to Melpolder et al[7]: t_{boil} = 133.4 (100 mm); n_D^{20} = 1.48883; d_4^{20} = 0.85593.

$\Delta\nu$ (cm^{-1}): 152 (100,w,bkgd), 271 (10,w), 317 (8,w), 354 (1), 437 (4), 463 (3), 472 (14), 517 (2), 545 (7), 575 (10), 601 (3), 638 (12), 670 (0), 696 (12), 703 (52), 734 (0), 759 (0), 795 (5), 810 (2), 855 (0), 885 (27), 921 (6), 957 (14), 973 (1), 989 (3), 1002 (235), 1028 (1), 1051 (13), 1070 (4), 1087 (9), 1107 (19,d), 1133 (2), 1149 (2), 1173 (15), 1187 (3), 1229 (23), 1242 (17), 1284 (8), 1308 (20,w), 1328 (1), 1347 (2), 1362 (3), 1383 (8), 1444 (23), 1463 (30,w), 1487 (1), 1587 (17), 1607 (36), 2713 (10), 2756 (5),2868 (100), 2886 (50,bkgd), 2904 (100,w,bkgd), 2935 (70,bkgd), 2963 (160,w,bkgd,d), 3001 (10), 3041 (40,w), 3059 (50,w).

1,4-DIISOPROPYLBENZENE. Separated with the preceding products; the 1,4-isomer concentrate was subjected to repeated crystallization from ether at a low temperature and then distilled in a column rated at 100 theoretical plates. The final product was 99.8% pure (on the basis of the cooling curve).

t_{boil} = 96.5° (18 mm); t_{freeze} = -17.1°; n_D^{20} = 1.4900; d_4^{20} = 0.8568;

---

* This line is presumably associated with the 1,3-isomer.

according to Melpolder et al[7]: t_{boil} = 210.37° (760 mm); t_{freeze} = -17.07°; n_D^{20} = 1.48983; d_4^{20} = 0.85676.

$\Delta\nu$ (cm^{-1}): 163 (80,w), 170 (50,w), 264 (25,w), 282 (3), 313 (4, w),348 (2), 403 (2,w), 433 (27), 443 (27), 470 (1), 485 (1), 500 (2), 514 (1), 607 (1), 623 (1), 642 (48,p), 660 (1), 706 (3), 745 (8), 763 (0), 780 (210), 792 (3), 812 (8,w), 832 (8,w), 855 (0), 872 (0), 892 (26), 922 (5), 953 (17), 1019 (2), 1045 (33), 1058 (52), 1072 (1), 1094 (8), 1104 (26,w), 1120 (5), 1138 (8,w), 1190 (37), 1213 (72,p), 1255 (4), 1278 (7), 1296 (16), 1308 (23), 1326 (2), 1347 (6), 1354 (4), 1384 (10), 1401 (6), 1422 (6), 1444 (28,w), 1463 (40,w), 1485 (2), 1535 (2), 1576 (5), 1584 (3), 1616 (125), 1636 (2), 1661 (3,w), 2869 (120,w), 2890 (70,w,bkgd), 2905 (100,w,bkgd), 2933 (100,w,bkgd), 2963 (180,w), 3009 (50), 3033 (30), 3056 (70).

1,2,4-TRIMETHYLBENZENE (Pseudocumene). Prepared from 2,4-dimethyl-1-formylcyclohexane-3 through hydrazone by decomposition of which according to Kijner we obtained 1,3,4-trimethylcyclohexene-1. The pseudocumene obtained by dehydrogenation of the latter over platinized carbon was purified by chromatographic absorption with silica gel and vacuum distillation in a column rated at 40 theoretical plates.

t_{boil} = 79.8-79.9° (38.5 mm); n_D^{20} = 1.5050; d_4^{20} = 0.8757; according to Rossini et al[5]: t_{boil} = 169.351° (760 mm); n_D^{20} = 1.50484; d_4^{20} = 0.87582.

$\Delta\nu$ (cm^{-1}): 210 (30,w,p), 235 (0), 285 (12), 320 (70,w), 349 (0,w), 387 (1,w), 438 (21), 478 (97,p,p), 519 (0), 540 (6), 555 (150,p,p), 586 (1), 705 (5), 718 (67,p,p), 746 (205,p,p), 806 (12,w), 833 (1), 908 (5), 925 (51,p,p), 957 (1,w), 982 (3,w), 1023 (5,w), 1044 (2,w), 1103 (3), 1125 (16,p), 1155 (12), 1212 (10), 1246 (135,p,p), 1271 (3), 1289 (9), 1348 (1), 1374 (25,), 1383 (82,p,), 1406 (5,w), 1438 (15,w,bkgd), 1451 (20,w,bkgd), 1507 (3,w), 1581 (18,w), 1620 (79), 2859 (70), 2885 (25,w,bkgd), 2920 (190, w,bkgd,p), 2972 (25,bkgd), 3000 (25,bkgd) 3042 (80),

1,2,3,5-TETRAMETHYLBENZENE (Durene). (Note: The spectra were obtained at 93°C.) Prepared from commercial grade durene by repeated recrystallization first from alcohol and then from ether. Purity of final product - 99.8% (based on cooling curve).

t_{freeze} = 79.1; according to Rossini et al[5]: t_{melt} = 79.24°.

$\Delta\nu$ (cm^{-1}): 262 (69,w), 315 (3), 333 (3), 349 (61), 372 (4), 431 1 (30), 465 (4), 508 (175), 518 (40,bkgd), 556 (2), 583 (3), 624 (5), 660 (5), 703 (12), 738 (385,p), 1020 (5,w), 1042 (5,w), 1107 (4,w), 1148 (2), 1157 (4), 1246 (2), 1267 (140), 1306 (3), 1347 (3), 1371 (43), 1385 (110,p), 1402 (5), 1446 (39,w), 1471 (7), 1501 (3), 1516 (4), 1567 (33,w), 1622 (75), 2725 (25), 2757 (10), 2824 (10), 2861 (100), 2886 (50), 2920 (230), 2938 (100), 2968 (80), 2990 (60), 3031 (40).

1,3,5-TRIMETHYL-2-ETHYLBENZENE (Ethylmesitylene). Prepared from thoroughly purified mesitylene through 2-bromomesitylene; the ethylmesitylene was obtained from the latter with diethylsulfate by the Grignard reaction. The product was purified by chromatographic absorption with silica gel, distillation in a column rated at about 50 theoretical plates and finally by crystallization from ether at low temperature. The degree of purity was 99.7% (according to the cooling curve).

t_{boil} = 99.3° (20 mm); t_{freeze} = -12.1°; n_D^{20} = 1.5103; d_4^{20} = 0.8859; according to Bruck et al[8]: t_{boil} = 88.5° (11.8); t_{freeze} = -12.2°;

n_D^{20} = 1.5101; d_4^{18} = 0.888.

$\Delta\nu$ (cm^{-1}): 173 (15,w), 231 (80,w), 260 (2), 278 (15), 320 (5,w), 394 (59), 416 (3), 444 (3), 473 (34), 496 (5,w), 516 (30), 546 (58,p), 575 (250), 684 (0,w), 710 (52,p), 728 (1), 746 (5), 767 (3), 816 (3), 850 (2), 881 (2), 950 (30), 970 (44), 1026 (4,w), 1062 (54), 1095 (3, w), 1106 (3), 1142 (15), 1152 (15), 1179 (1), 1209 (22,p), 1239 (10), 1256 (3), 1295 (110), 1320 (32), 1379 (99,w), 1411 (5,w), 1443 (7,w, bkgd), 1453 (44,w,bkgd), 1483 (10,w), 1581 (22,w), 1615 (78), 2857 (70), 2871 (100,w,bkgd,p), 2902 (70,w,bkgd), 2921 (250,w,bkgd,p), 2945 (50, bkgd), 2967 (125,w,bkgd), 3011 (70,w).

1,3,5-TRIMETHYL-2-PROPYLBENZENE (Propylmesitylene). Obtained like the preceding product, except that as the second component in the Grignard reaction we used propyl n-toluenesulfonate. The hydrocarbon was purified by chromatographic absorption in silica gel and vacuum distillation in a column rated at 50 theoretical plates. Purity of final product - 99.7% (based on cooling curve).

t_{boil} = 99.6° (11.5 mm); t_{freeze} = -20.5°; n_D^{20} = 1.5052; d_4^{20} = 0.8782. The data on this hydrocarbon given by Töhl[9] (t_{boil} = 220-221°; d_4^{20} = 0.8773) are for a less pure product with a freezing point below -20°.

$\Delta\nu$ (cm^{-1}): 170 (10,w), 204 (15,w), 233 (64,w), 280 (29), 314 (10), 340 (14), 385 (45), 423 (0), 479 (3), 504 (18), 516 (19), 527 (0), 547 (49), 570 (145), 578 (145), 675 (0), 702 (7), 721 (16), 740 (0), 762(0), 784 (10), 808 (2), 856 (12), 878 (5), 892 (28), 932 (3), 961 (33), 1008 (0), 1034 (24), 1071 (0), 1092 (31), 1120 (1), 1142 (24), 1179 (2), 1206 (15), 1262 (3), 1280 (27), 1296 (68), 1331 (5), 1346 (16), 1379 (98), 1408 (8), 1445 (35), 1454 (35), 1471 (5), 1486 (15), 1534 (3), 1581 (15), 1615 (70), 2731 (20), 2867 (100), 2918 (220), 2948 (80), 2962 (110), 3012 (70), 3037 (20),

1,3,5-TRIMETHYL-2-ALLYLBENZENE (Allylmesitylene). Prepared like the foregoing by the Grignard reaction using allyl chloride as the second component. Purified by vacuum distillation in a column rated at about 50 theoretical plates and then recrystallization from ether at low temperature. Purity - 98.9% (based on the cooling curve). This is the first time this hydrocarbon has been synthetized.

t_{boil} = 105.5° (16 mm); t_{freeze} = 2.1°; n_D^{20} = 1.5194; d_4^{20} = 0.8989.

$\Delta\nu$ (cm^{-1}): 176 (10), 205 (10), 234 (70), 279 (20), 304 (3), 328 (3), 360 (28), 383 (30), 405 (5), 420 (29), 451 (3), 492 (5), 516 (25), 541 (42), 575 (240), 620 (5), 653 (2), 716 (19), 792 (18,d), 853 (1), 881 (3,w), 909 (14), 922 (11), 940 (0), 961 (40), 995 (5), 1034 (2), 1062 (3), 1108 (2), 1143 (34), 1165 (0), 1188 (2), 1204 (19), 1238 (16), 1296 (160), 1321 (32), 1379 (105), 1406 (26), 1447 (30,w), 1456 (30,w), 1483 (10), 1580 (26), 1614 (77,p), 1638 (70), 2864 (60,w), 2896 (10, bkgd), 2918 (180,w,bkgd), 2948 (110,bkgd), 2976 (70,bkgd), 3003 (120, w,bkgd), 3015 (10), 3081 (20).

β-METHYLNAPHTHALENE. Separated from the commercial product by repeated treatment with concentrated sulfuric acid in benzene solution, distillation and crystallization from ethyl alcohol. Note: The spectra were recorded at 75° since at lower temperatures the liquid appears cloudy, presumably due to the poor solubility of residual traces of ethyl alcohol.

t_{melt} = 34.5°; according to Olivier & Wit[10]: t_{melt} = 34.5°.

$\Delta\nu$ (cm^{-1}): 190 (20), 210 (20), 233 (15), 246 (15), 266 (20), 285 (25), 406 (49), 451 (260), 476 (10), 485 (20), 520 (320), 546 (10), 565 (10), 590 (10), 621 (15), 648 (15), 705 (45), 743 (25), 771 (650), 791 (30), 813 (15), 850 (10), 886 (20,w), 918 (10), 927 (10), 952 (35, w), 1023 (180), 1043 (10), 1085 (50), 1110 (5), 1126 (25), 1143 (15), 1157 (15), 1174 (66), 1199 (5), 1219 (10), 1236 (5), 1255 (20), 1380 (1750), 1432 (69), 1466 (185,p), 1478 (78,w), 1506 (10), 1534 (15), 1578 (190), 1603 (10), 1634 (25,w), 2864 (20), 2919 (90), 3017 (70), 3050 (190), 3057 (190).

Discussion of Results

Of the thirteen hydrocarbons listed the spectra of three diisopropylbenzenes and three alkyl- and alkenylmesitylenes were studied for the first time. The spectra of the others have been investigated previously[2,11-18]. However, the spectra recorded by us are more complete; in view of the high degree of purity of the compounds used we feel safe in assuming that the newly discovered lines are not due to impurities. Judging by descriptions of the procedure given by earlier investigators the most reliable values are probably those given in Ref. 17. The data of Fenske et al[2] & [18] were obtained by photoelectric recording and in view of this, despite certain merits, have a number of shortcomings. Among these is deviation of the frequency values (by 5-8 and in some cases by as much as 10-12 cm^{-1}) from the commonly accepted values, obtained by photographic methods (for example, for benzene and toluene). Furthermore, the photoelectric photometer employed could not record the weakest lines or resolve lines differing by less than 10-15 cm^{-1}. A considerable number of aromatic hydrocarbon spectra has been investigated by Fromhertz et al[13] by the method of photographic recording, with the intensity being evaluated visually in a 15 point scale. For purposes of comparison the frequencies and intensities of the lines of isopropylbenzene given in Ref. 17 are listed next to our values in Table 1.

Diisopropylbenzenes. In our preceding investigation[3] we noted the following characteristic lines in the spectra of dialkylbenzenes (figures in parentheses are intensity values referred to cyclohexane):

1,2-dialkylbenzenes: 586 (35), 714 (130), 1039 (200), 1220 (150);
1,3-dialkylbenzenes: 525 (80), 716 (140), 1002 (400), 1247 (65);
1,4-dialkylbenzenes: 642 (50), 780-810 (250), 1204 (100).

Of these the following characteristic lines were also found in the spectra of diisopropylbenzenes:

1,2-diisopropylbenzene: 592 (125), 707 (125), 1030 (205), 1226 (73);
1,3-diisopropylbenzene: - - 703 (52), 1002 (235), 1242 (17);
1,4-diisopropylbenzene: 642 (48), 780 (210), 1190 (37), 1213 (72)

Thus the spectra of ortho- and para-diisopropylbenzenes confirm our findings regarding lines characteristic of substitutions. The meta-isomer is an exception: it lacks the line in the vicinity of 520-530 cm^{-1} which we took to be characteristic for 1,3-dialkyl- homologues of benzene. In addition the line intensities of the meta-isomer are appreciably lower than those of the other hydrocarbons of this type. In view of this, further investigation of the characteristic substitution-indications of the 1,3-dialkyl-homologues of benzene, using new samples, is indicated.

Ethyl-, propyl and allylmesitylenes. A number of lines having stable frequency and intensity values were observed in the spectra of these compounds as well as that of isodurene (see Table 2). An excep-

Table 1

Raman spectra of isopropylbenzene (cumene)

Catalog Ref. 17		Our data		Catalog Ref. 17		Our data	
Δν, cm⁻¹	Inten.*	Δν, cm⁻¹	Inten.	Δν, cm⁻¹	Inten.*	Δν, cm⁻¹	Inten.
140	160	144	50	1156	31	1156	31
290	weak	—	—	1182	27	1183	25
310	24	311	20, w	1213	79	1212	57, p
—	—	359	4	—	—	—	—
437	weak	405	3, w	1287	27	1281	5
460	20	461	22, p	—	—	1306	15
564	12	564	15	—	—	1326	2
—	—	591	2	—	—	1346	2
621	47	622	39, r	1355	weak	—	—
—	—	662	2	—	—	1383	4
741	110	742	96, p	—	—	1406	2
760	8	761	12	1445	31	1445	20, w
791	4	789	2	1466	39	1464	18, w
—	—	817	2	—	—	1527	2
839	12	840	10	1583	35	1583	22
—	—	868	1	1606	130	1606	70
891	20	892	15	2870	138	2870	60
902**	20	—	—	2892	weak	2888	40, bkgd
923	weak	—	—	2906	106	2906	60, bkgd
942**	16	—	—	2935	8	2936	60, bkgd
955	12	956	8	2962	weak	—	—
989	weak	989	8	2969	197	2966	100
—	—	—	—	—	—	2980	40
1002	394	1002	410, p	3002	weak	3002	30
1029	110	1029	87, p	3038	weak	3038	30, w
1082	12	1083	13	3055	95	3054	140
1113	20	1106	14	3064	130	3064	120
—	—	1143	1	3162***	27	—	—
—	—	—	—	3212***	—	—	—

*In the intensity scale employed in the Catalog of Ref. 17 for cumene the intensity of the 459 cm⁻¹ line of CCl_4 is assigned a value of 94. The values listed in the table are converted to our cyclohexane scale. According to our measurements the intensity of the above CCl_4 line equals 400 in our scale.

** Repetition of the 1002 cm⁻¹ lines due to the second and third components of the mercury triplet.

*** Mercury lines erroneously ascribed to cumene.

tion here is the 1296 cm^{-1} line in the spectrum of allylmesitylene which has twice the intensity of the same characteristic lines in the spectra of ethyl- and propylmesitylene. Nevertheless these lines can safely be assumed to be characteristic of this type of substitution, particularly since they are also present in the spectrum of isodurene[12]. It is interesting to note that most of the brightest lines of the alkylmesitylenes and of mesitylene proper coincide (Table 2), although the intense 999 cm^{-1} line observed in the spectra of 1,3,5-substituted compounds does not appear in the spectra of isodurene and its homologues.

Table 2

Characteristic lines of isodurene and its homologues

Compound	Δν, cm⁻¹	I	Δν, cm⁻¹	I	Δν, cm⁻¹	I	Δν, cm⁻¹	I	Δν, cm⁻¹	I
Mesitylene (Ref. 19)	231	245	276	62	517	191	—	—	578	360
Isodurene (Ref. 14)*	232	7	275	3	512	3	546	4	573	12
Ethylmesitylene	231	80	278	15	516	30	546	58	575	250
Allylmesitylene	234	70	279	20	516	25	541	42	575	230
Propylmesitylene	233	64	280	29	516	19	547	49	578	145
Mesitylene** (Ref. 19)	—	—	—	—	1301	96	1379	85	1607	61
Isodurene (Ref. 14)*	959	9	1212	3	1293	8	1380	9	1614	7
Ethylmesitylene	970	44	1209	22	1295	110	1379	99	1615	78
Allylmesitylene	961	40	1204	19	1296	160	1379	105	1614	77
Propylmesitylene	961	33	1206	15	1296	68	1379	98	1615	70

* The intensities are given in the visual scale.

** Mesitylene also has an intense (336) line at 999 cm^{-1}, which is not exhibited by the other homologues of isodurene.

We also observed a line at 1638 cm^{-1} having an intensity of 70 in the spectrum of allylmesitylene. This line is due to a double bond in the side chain. Its frequency and intensity are consonant with the position (at the end of the side chain) ascribed to the double bond by Goubeau indicating that the structure suggested by Goubeau is the correct one.

The spectrum of β-methylnaphthalene includes a very intense line at 1380 cm^{-1} which is characteristic of naphthalene and its derivatives[14,21].

A noteworthy feature of the investigated spectra is that in the 2700-3100 cm^{-1} frequency range an increase in the number of substituents is accompanied by weakening of the lines in the 3045-3065 cm^{-1} interval (the frequencies ascribed to the valence vibration of the C_{arom}-H group) and a simultaneous increase in the intensity of other lines, particularly the 2920 cm^{-1} line (in the spectra of tri- and tetraalkyl-homologues of benzene). The 3035 cm^{-1} line observed in the spectra of all monoalkyl-homologues of benzene is weakened or vanishes entirely as the number of substituent groups increases. In addition, in the spectrum of allylmesitylene we observed a 3081 cm^{-1} line which like the 1638 cm^{-1} line, characteristic of the valence vibration of the C═C group, is connected with the presence of a double bond at the end of the side chain[20].

In concluding we wish to thank G. S. Landsberg and S. A. Ukholin for their help in the present investigation and valuable discussion of the results.

Commission on Spectroscopy and
The "N. D. Zelinski" Institute of Organic Chemistry
at the Academy of Sciences of the USSR.

References

1. M.M.Sushchinski, Izv. AN SSSR, Ser. fiz., 17, 608 (1953).
2. M.R.Fenske et al , Anal. Chem., 19, 700 (1947).
3. B.A.Kazanski, Liberman, Landsberg, Aleksanian, Bulanova, Mikhailova, Plate, Sterin & Ukholin, Izv. AN SSSR, Ser. fiz., 18, 704 (1954). Translation in BULLETIN, 18, # 6, 386. CTT.
4. V.I.Mylishev, Izv. AN SSSR, Ser. fiz., 14 746 (1950).
5. D.F.Rossini & others, Selected values of physical and thermodynamic properties of hydrocarbons and related compounds. Pittsburgh 1953.
6. A.L.Liberman, Sterligov, Lapshina & Kazanski, Doklady AN, 91, 845 (1953).
7. F.Melpolder, J.Woodbrige & C.Headington, J.Am.Chem.Soc., 70, 935 (1948).
8. F.Bruck, K.Coles, G.Kennedey & F.Morton, J.Am.Chem.Soc., 71, 2377 (1949).
9. A.Töhl, Ber., 28, 2459 (1895).
10. S.Olivier & J.Wit, Rec. Trav. Chem., 57, 90 (1938).
11. G.Dupont & R.Dulou, Bull.Soc. chim.France, 3, 1639 (1936).
12. K.Kohlrausch & A.Pongratz, Mh.Chem., 64, 361, 374 (1934).
13. H.Fromherz, H.Bueren & L.Thaler, Angew.Chem., A59, 142 (1947).
14. H.Luther & C.Reichei, ZS phys. Chem., 195, 103 (1950).
15. J.Goubeau, Ber. deutsch. Chem.Ges., 75, 65 (1942).
16. E.Pendl & G.Radinger, Mh. Chem., 72, 382 (1939).
17. Catalog of Selected Raman Spectral Data, Amer.Petr.Inst.Research Project No.44, National Bureau of Standards, Washington 1948.
18. W.Braun, D.Spooner & M.Fenske, Anal.Chem., 22, 1074 (1950).
19. P.A.Bazhulin, Ukholin, Liberman, Novikov & Kazanski, Izv. AN SSSR, Otd. khim. nauk, 5, 501 (1950).
20. J.Goubeau, Die Ramanspektren von Olefinen, Beihilfe zu der "ZS Angew. Chem.", No. 56 (1948).
21. K.Kohlrausch, Spektry kombinatsionnogo rasseianiia (Raman spectra),M.-L.1952.

Transactions of the Division of Physical-Mathematical Sciences of the USSR Academy of Sciences
Paper presented at the meeting of 14 April 1954.

CAUSALITY CONDITIONS IN QUANTUM FIELD THEORY

- N. N. Bogoliubov

We know that grave difficulties are encountered in attempts to extend the quantum theory of fields in its present-day localized form, particularly where treatment of problems of meson-nucleon interaction is concerned.

This situation has led many investigators to seek solutions outside the framework of the theory, for example, in the direction of dispensing with strict localization or with rigorous conformity to the law of causality, etc.

It would be desirable, therefore, to evolve a formulation of the quatum theory of fields that would put into clear evidence the basic physical concepts upon which the present-day theory is actually founded so as to make manifest in just what directions it is permissible to generalize them.

In the usual representation of the theory, based on the Hamiltonian formalism, these basic concepts are not given full and due consideration.

In our opinion it is most advantageous to proceed from the scheme proposed by Stueckelberg[1,2,3], in which a generalized S-matrix is introduced without resorting to the Hamiltonian formalism. Its role in the derivation of a concrete form of S-matrix is taken by clearly defined physical conditions, among which the condition of causality is fundamental.

However, Stueckelberg failed to arrive at a sufficiently clear and general formulation of this condition; in view of this his ideas have not received wide recognition.

With a view to developing these ideas further, we shall attempt, in the present article, to work out a new formulation of causaltiy conditions and a method of elaborating the quantum field theory on the basis of this formulation.

We must note that in our formulation of the quantum field theory, as in all its other formulations, it is necessary to introduce fictitious, non-interacting particles and to treat interaction as a sort of supplementary factor which alters the properties of the dynamic system, a factor which can be "engaged" or "disengaged" ["einschalten" and "ausschalten"]. Obviously, from the physical point of view, this treatment of interaction between fields is highly unsatisfactory; hence, we feel it necessary to emphasize the important role that this treatment is nevertheless called upon to play in modern field theory.

To describe mathematically the "interaction engaging operation," let us, following Stueckelberg, introduce a function $g(x)$ with values from 0 to 1, characterizing the degree of "engagement" of the interaction. Then in space-time regions where $g(x) = 0$, interaction is entirely absent; in regions where $g(x) = 1$, the interaction is fully "engaged," while where $0 < g(x) < 1$ the interaction is only partially "engaged."

Now let $g(x)$ differ from zero only in some finite space-time region. In this case, at a sufficiently remote past or future time the fields will be free and, hence, in operating with the interaction concept we can characterize the initial and final states of our dynamic system by constant state amplitudes: $\Phi(-\infty)$ and $\Phi(+\infty)$.

These amplitudes must evidently be related by some operator $S(g)$, capable of transforming $\Phi(-\infty)$ into $\Phi(+\infty)$ and dependent on the behavior of the function $g(x)$. Setting the initial state amplitude

we can consider the final state amplitude to be a functional of g:

$$\Phi(g) = S(g)\Phi. \qquad (1)$$

In view of the above definition, S(g) may be interpreted as the scattering operator for the case when the interaction is engaged with an intensity g(x).

The "real" case where interaction is fully engaged over all space-time, must be treated in this scheme by letting the region where g(x) = 1 expand without restriction and encompass all space-time at the limit. If there are limiting, finite values for even a few of the matrix elements of the operator S(g), they must, in this case, be regarded as the corresponding elements of the conventional scattering matrix S.

We must emphasize that the generalized S-operator S(g) gives more detailed information concerning the behavior of the dynamic system than does the usual S-operator, for S(g) comprises the function g(x) which makes it possible to separate out individual space-time regions. In connection with this, it can be shown that the "Hamiltonian of the system" can also be expressed directly through S(g).

Let us now formulate the basic physical conditions which the operator S(g) must satisfy. Thus, to assure covariance we must specify that the operator must transform like a scalar, i.e., that

$$S(Lg) = U_L S(g) U_L^*, \qquad (2)$$

where $Lg = g(Lx)$ and U_L is the unitary operator by means of which the quantum wave functions of free fields are transformed in L transformations from Lorentz groups and translations.

Further, to maintain the norm of the state amplitude in the transition (1) from the initial to the final state, we must specify that the operator S(g) be unitary:

$$S(g)S^*(g) = 1. \qquad (3)$$

Let us now take into account the causality condition in accordance with which a given event in the system can influence the evolution of the system only in the future and cannot affect the behavior of the system in the past, i.e., at any instants of time preceding the given event. We must postulate, therefore, that any change in the interaction law in any space-time region can affect motion only at subsequent instants of time.

To formulate this condition mathematically, let us imagine that in an infinitely small region in the vicinity of space-time point y the function g receives an infinitesimal increment δg.

Then the limit state amplitude $\Phi(g)$ will experience an increment

$$\delta\Phi(g) = \delta S(g)\cdot\Phi = [\delta S(g)\cdot S^*(g)]\,\Phi(g).$$

In accordance with the principle of causality, a change in g in the infinitesimal region near point y can affect the motion only for $x^0 > y^0$ and therefore the operator.

$$1 + \delta S(g)\cdot S^*(g),$$

transforming $\Phi(g)$ into $\Phi(g + \delta g)$ must not depend on the behavior of the function g(x) when $x^0 < y^0$.

Consequently, from covariance considerations, it follows that this operator must also be independent of the behavior of the function g(x) where $x \sim y$ ($\sim$ denotes spatial similarity).

Thus, the causality condition is formulated by the equality:

$$\frac{\delta}{\delta g_x}\left(\frac{\delta S(g)}{\delta g_y} S^*(g)\right) = 0, \qquad \text{with } y \gtrless x. \tag{4}$$

To arrive at the actual form of this operator, satisfying all the above requirements, let us make use of the formal functional expansion in powers (degrees) of g:

$$S(g) = 1 + \sum_{(n \geqslant 1)} \frac{1}{n!} \int S_n(x_1, \ldots, x_n)\, g(x_1) \cdots g(x_n) dx_1 \cdots dx_n, \tag{5}$$

in which $S_n(x_1, \ldots, x_n)$ are poli-local operators, i.e., operator expressions of the form

$$S_n(x_1, \ldots, x_n) = \sum K_{\alpha_1, \ldots, \alpha_n}(x_1, \ldots, x_n)\, \Psi_{\alpha_1}(x_1) \cdots \Psi_{\alpha_s}(x_s), \tag{6}$$

dependent on the total field functions and on their partial derivatives $\psi_\alpha(x)$ at points (x). To maintain the scalar character of S_n, only the even combinations of the Fermi-operators should enter into these expressions. The K's are non-quantized c-functions, which we shall hereinafter term coefficient functions.

It must be emphasized that the requirement that S_n depend on the field functions as a whole, rather than on their separate positive and negative frequency portions, is a physical condition. When it is satisfied the following relationship holds:

$$[S_n(x_1, \ldots, x_n);\ S_m(y_1, \ldots, y_m)] = 0,$$

when all the x_i's are spatially similar to any y_j.

Hence, if two functions $g_1(x)$ and $g_2(x)$ are localized in two space-time regions such that any point in one region is spatially similar to all points of the other region, $S(g_1)$ will commute with $S(g_2)$. In essence this is an expression of the fact that a signal cannot be propagated with a speed exceeding that of light and that the interaction-engagement processes in mutually spatially-similar regions do not interfere with each other.

We note that in general the coefficient functions K are always singular.

Consequently, to insure convergence of the individual terms of the expansion (5) in the class of g(x) functions sufficiently smooth and diminishing at a sufficiently fast rate at infinity, we must require that the K's be defined as integrable, singular functions, i.e., that rules be given for integrating them with functions that are sufficiently smooth and vanish at infinity at a sufficiently fast rate.

A convenient means for such determination of the coefficient functions is improper transition to the limit and juxtaposition with them of linear functionals, prescribed in a corresponding linear space of sufficiently regular functions.

We have just mentioned the need for insuring convergence of the individual terms of expansion (5). Obviously, convergence of the individual terms has nothing to do with convergence of the series as a whole. In fact, in the light of a number of recently published investigations, there are good reasons to expect expansion (5) to be divergent.

At best, if the interaction is weak we can hope that a few terms of the expansion will yield an approximation, whose accuracy will be the greater, the weaker the interaction. In other words, in certain cases series (5) can be regarded as a source of asymptotic approximations.

One such case, important from the practical standpoint, is that of electrodynamics.

However, even when the interaction is known not to be weak (for example, in the case of meson-nucleon interaction) a study of the above formal expansion may be of interest, since it offers a means of determining a number of qualitative, as well as quantitative, properties of the operator S(g), so that we can then attempt to establish these properties on a more rigorous basis. Furthermore, this expansion is most appropriate to the present-day state of the theory of fields, wherein it is still impossible to dispense with various formal expansions in terms of the extent of interaction (powers of g) and wherein all the basic results obtained so far have been with the aid of such expansions.

Before proceeding to the successive determination of the polilocal operators S_n, let us relate the first term, S_1, with the Lagrangian interaction in accordance with the correspondence principle. Let the interaction be engaged with only an infinitesimal intensity. We can then write

$$S(g) = 1 + \int S_1(x)\, g(x)\, dx. \tag{7}$$

Let us now examine the analogous situation in classical theory. Let us introduce an action A into the classical system in the case when the interaction is engaged with infinitely small intensity g(x). We have

$$A = \int \{\mathcal{L}_0(x) + g(x)\, \mathcal{L}_1(x)\}\, dx, \tag{8}$$

where $\mathcal{L}_0(x)$ is the Lagrangian of the free field and $\mathcal{L}_1(x)$ is the Lagrangian of the interaction.

Here we substituted field functions satisfying the pertinent equations of motion.

In particular, if we regard g(x) as a first-order infinitesimal, our field functions will differ from free field functions also by infinitesimals of the first order. On the other hand, in view of the fact that the free field equations are derived from the variational principle

$$\delta \int \mathcal{L}_0(x)\, dx = 0,$$

it follows that if the field functions are taken in the integral

$$\int \mathcal{L}_0(x)\, dx$$

with an error of first-order smallness, the integral itself will differ from its true value by a second-order small quantity. Further, the second term in (8) will have a first-order accuracy and changes in the field functions comprised in it by a first-order quantity will result in an error of the second-order of smallness. Therefore, to an accuracy to within a second-order magnitude we can substitute free field wave functions in the classical action equation (8).

Thus when the interaction is engaged with an infinitely small intensity g(x), the action A will be augmented by an increment

$$\delta A = \int g(x)\, \mathcal{L}_1(x)\, dx,$$

in which the field functions introduced into the interaction Lagrangian $\mathcal{L}_1(x)$ are free field functions.

We must now note that in going over from classical to quantum theory, the expression e^{iA} must be replaced by a quantum-mechanical wave function or, in field theory terminology, by the state amplitude. In accordance with this correspondence principle, we see that, when the interaction is engaged with an infinitesimal intensity, the state amplitude experiences an increment

$$(e^{i\delta A} - 1)\Phi = i\delta A\Phi = i\int g(x)\,\mathscr{L}_1(x)\,dx\,\Phi.$$

On the other hand, from (7) the increment in the examined case will be

$$\int S_1(x)\,g(x)\,dx\,\Phi.$$

Whence, we have

$$S_1(x) = i\mathscr{L}_1(x).$$

Thus, the first term of the expansion (5) is defined by the interaction Lagrangian $\mathscr{L}_1(x)$.

We can now proceed to the successive determination of the poli-local operators $S_n(x_1, \ldots, x_n)$ for $n > 1$.

We note, first, that in view of the symmetry of the weighting factors $g(x_1)\ldots g(x_n)$ comprised in the terms of the expansion (5), we can assume, without sacrifice in generality, that these operator functions are symmetrical with respect to the arguments $x_1, \ldots, x_n$.

Let us insert expansion (5) in equations (2)-(4), defining the conditions of covariance, unitarity and causality.

In this way we obtain the following system of conditions for determining the poli-local operators:

$$S_n(Lx_1, \ldots, Lx_n) = U_L^* S_n(x_1, \ldots, x_n) U_L, \tag{9}$$

$$S_n(x_1, \ldots, x_n) + S_n^*(x_1, \ldots, x_n) +$$

$$+ \sum_{(1 \leqslant k \leqslant n-1)} P\left(\frac{x_1, \ldots, x_k}{x_{k+1}, \ldots, x_n}\right) S_k(x_1, \ldots, x_k)\, S_{n-k}^*(x_{k+1}, \ldots, x_n) = 0, \tag{10}$$

$$S_{n+1}(x, x_1, \ldots, x_n) +$$

$$+ \sum_{(1 \leqslant k \leqslant n-1)} P\left(\frac{x_1, \ldots, x_k}{x_{k+1}, \ldots, x_n}\right) S_{k+1}(x, x_1, \ldots, x_k)\, S_{n-k}^*(x_{k+1}, \ldots, x_n) = 0, \tag{11}$$

provided that $x \succ x_j$ for at least one of the values of $j = 1, \ldots, n$.

Here

$$P\left(\frac{x_1, \ldots, x_k}{x_{k+1}, \ldots, x_n}\right)$$

denotes the symmetrization of the full set of n points into two subsets of k and $n-k$ points over all the possible $\frac{n!}{k!\,(n-k)!}$ subdivisions.

Let us now evaluate the degree of arbitrariness with which these conditions permit determining S_{n+1} starting with the already determined expressions for $S_1, \ldots S_n$.

We note that in view of condition (11) the difference

$$\Delta S_{n+1}(x_1, x_2, \ldots, x_{n+1}) \tag{12}$$

between two possible values of S_{n+1} with the identical given values for $S_1, \ldots, S_n$ has the property

$$\Delta S_{n+1}(x_1, x_2, \ldots, x_{n+1}) = 0,$$

provided $x_1 \succ x_j$ for at least one of the values of $j = 2, \ldots, n+1$.

Since, furthermore, the difference (12) must be a symmetrical function of all the arguments $x_1, \ldots, x_{n+1}$, we see that

$$\Delta S_{n+1}(x_1, x_2, \ldots, x_{n+1}) = 0, \tag{13}$$

if there exists at least one pair of unequal arguments: $x_a \neq x_b$.

Let us agree to designate as "quasi-local" those poli-local operators which possess this property of vanishing everywhere except in the infinitesimal region about the point where all the arguments fully coincide.

In the light of this definition, a characteristic feature of quasi-local operators is the fact that their coefficient functions $K(x_1,\ldots,x_{n+1})$ are expressions of the type

$$Z\left(\cdots\frac{\partial}{\partial x}\cdots\right)\delta(x_1-x_2)\cdots\delta(x_1-x_{n+1}),$$

where $Z\left(\cdots\frac{\partial}{\partial x}\cdots\right)$ are polynomials, where the differentiation operations are concerned.

It is precisely because of this property that the quasi-local operators, like the local ones, depend on the behavior of the field functions only in the infinitesimal region in the vicinity of a single point.

As we just established in (13), the expression S_{n+1} is determined by the causality conditions (11) in accordance with the given values for the preceding expressions for $S_1,\ldots,S_n$ with an accuracy to within an arbitrary quasi-local operator.

By virtue of the symmetry and covariance conditions, this quasi-local operator must be symmetrical and transform as a scaler.

We now turn to the unitarity conditions (10), from which it follows that the sum $S_{n+1} + S^*_{n+1}$ is completely defined by the preceding expressions for $S_1,\ldots,S_n$. Whence it follows that the above-mentioned quasi-local operator must be anti-Hermetian.

Thus, by means of our conditions, S_{n+1} is determined from the expressions for $S_1,\ldots,S_n$ with an accuracy to within the additive term

$$iA_{n+1}(x_1,\ldots,x_{n+1}), \tag{14}$$

in which A_n is a scalar quasi-local operator with symmetrical and Hermetian properties.

If, in addition to the above, S_n were required to satisfy other, supplementary conditions (for example, gradient invariance), corresponding further restrictions would be imposed on the choice of

Taking some scalar, Hermetian, local operator, we note that expressions

$$S_n(x_1,\ldots,x_n) = i^n T\{L(x_1),\ldots,L(x_n)\}$$

with a chronologically ordered T-product formally satisfy all our conditions.

An expression corresponding to this formulation of S_n is

$$S(g) = T\left\{e^{i\int\mathscr{L}(x)\,g(x)\,dx}\right\}.$$

Let us now examine a somewhat more general form

$$S(g) = T\left\{e^{i\int\mathscr{L}(x;\,g)\,g(x)\,dx}\right\}, \tag{15}$$

in which

$$\mathscr{L}(x;g) = \mathscr{L}(x) + \sum_{(n\geqslant 1)}\frac{1}{(n+1)!}\int A_{n+1}(x,x_1,\ldots,x_n)\,g(x_1)\cdots g(x_n)\,dx_1\cdots dx_n \tag{16}$$

and A_n are scalar quasi-local operators with symmetrical and Hermetian properties.

Leaving aside, as we do throughout this article, the question of convergence of expansions in powers of g (assuming, for example, that

the sum (16) consists of a finite number of terms), we note that $\mathcal{Z}(x;g)$ will be a local operator like $\mathcal{Z}(x)$, but also dependent on the "classical field" g(x). In view of this, expression (15), or, more precisely speaking, its coefficients in the expansion in powers of g, also satisfies the conditions (9)-(11).

Carrying out an expansion in powers of g on the basis of (15) and (16), we obtain

$$S_n(x_1, \ldots, x_n) = i^n T(\mathcal{Z}(x_1) \cdot \ldots \cdot \mathcal{Z}(x_n)) + \sum_{\substack{2 \leqslant m \leqslant n-1 \\ (\sum \nu_j = n,\ \nu \geqslant 1)}} \frac{i^m}{m!} P(x_1, \ldots, x_{\nu_1} | \ldots | \ldots x_n)\, T\{\Lambda_{\nu_1}(x_1, \ldots, x_{\nu_1}) \ldots \Lambda_{\nu_m}(\ldots, x_n)\} + i\Lambda_n(x_1, \ldots, x_n); \quad \Lambda_1(x) = \mathcal{Z}(x), \tag{17}$$

where

$$P(x_1, \ldots, x_{\nu_1} | \ldots \ldots, x_n)$$

denotes a symmetrization operation over all $\frac{n!}{\nu_1! \ldots \nu_m!}$ subdivisions of the set of n points $x_1, \ldots, x_n$ into m systems of $\nu_1, \ldots, \nu_m$ points.

We note, incidentally, that it is possible to verify whether (17) satisfies the conditions imposed by (9)-(11) directly, without recourse to the "creation functional" S(g) (15).

It can readily be seen, moreover, that equation (17) yields the most general expression for S_n consistent with the imposed requirements, inasmuch as in addition to the $\Lambda_1, \ldots, \Lambda_{n-1}$ terms, comprised in $S_1, \ldots, S_{n-1}$ as well, S_n contains additive terms of the type defined by (14); and we have already established above that S_n is determined through $S_1, \ldots, S_{n-1}$ with an accuracy to within such an additive term.

It appears that the examined dynamic system is characterized not simply by a single Lagrangian but by a string of Lagrangians:

$$\Lambda_1(x), \ldots, \Lambda_n(x_1, \ldots, x_n), \ldots$$

In this connection it must be noted, however, that in general the only physically meaningful state is the one in which the interaction is fully engaged, i.e., where g = 1. In this case, as may be seen from (15)

$$S = T\left\{e^{i\int L_e(x)\,dx}\right\}, \tag{18}$$

where

$$L_e(x) = \mathcal{Z}(x) + \sum_{(\nu \geqslant 2)} \frac{1}{\nu!} \int \Lambda_\nu(x, x_1, \ldots, x_{\nu-1})\, dx_1 \ldots dx_{\nu-1}. \tag{19}$$

Thus the "real" scattering operator S is actually determined by a single Lagrangian $L_e(x)$. We can arbitrarily assign different parts of this effective Lagrangian to terms of different orders in the sum (19), altering thereby only the mathematical operation of "engaging and disengaging the interaction;" this should not influence the physical quantities characterizing the dynamic system, insofar as they pertain to the actual state of "fully engaged" interaction.

We now turn to the question of the integrability of the derived poli-local operators $S_n(x_1, \ldots, x_n)$.

It must be noted, as Stuckelberg points out, that the usual determination of the S-product by introducing a chronological order in the succession of the operators is valid only when there is no coincidence of the arguments $x_1, \ldots, x_n$, while in view of the singularity of the corresponding coefficient functions, these are not "predetermined" in the regions where the arguments coincide. Such "predetermination" presents an entirely different, separate problem.

We note further, that, strictly speaking, the problem here is not one of determining the coefficient functions of the operators $S_n(x_1,\ldots,x_n)$ in regions where $x_r = x_s$, but rather one of establishing integration rules for them in the infinitesimal vicinities of such regions, inasmuch as we must determine the coefficient functions S_n not as ordinary functions but as integrable singular functions, the "nuclei" of the corresponding functional.[4]

If we disregard this difficulty and formally invoke Wick's theorem, we arrive at expressions of the following form:

$$\prod_{a<b} D^c(x_a - x_b), \tag{20}$$

consisting of the products of causal D^c-functions.

Changing to a Fourier representation, we obtain integrals with the familiar "ultraviolet" divergences. This is a consequence and manifestation of the fact that the product of the singular causal functions (20) has not been effectively defined as an integrable singular function.

It is interesting to note that this difficulty does not arise in the case when we are dealing with an ordinary operator product.

Thus, for example, the coefficient functions of the ordinary product of local operators

$$\mathcal{L}(x_1)\cdots\mathcal{L}(x_n)$$

are represented by products

$$\prod_{a<b} D^{(-)}(x_a - x_b) \tag{21}$$

of the negative-frequency parts of the D-functions and are directly determinable as integrable singular functions.

The significant point here is the fact that in changing over to the Fourier representation the resultant integrals for the Fourier transform of (21) are actually taken over a finite momentum region and, therefore, prove to be convergent.

In view of this we can establish a more general theorem to the effect that if the poli-local operators

$$A(x_1,\ldots,x_r),\quad B(x_{r+1},\ldots,x_n)$$

with independent arguments are integrable, the poli-local operators representing their usual product

$$A(x_1,\ldots,x_r)\,B(x_{r+1},\ldots,x_n), \tag{22}$$

will also be integrable. Moreover, it is permissible to carry out an improper transition to the limit in expressions of type (22).

Thus, the problem of "predetermination" does not arise for the ordinary operator products; the fact that it comes up here is due to chronological ordering operation. It can be solved for the case of T-products in the following manner.

Let us regularize the D-functions, for example, by introducing additional masses M, after Pauli and Villars. By doing this we make the coefficient functions in the expression

$$S_n^M(x_1,\ldots,x_n)\,T^{\mathrm{reg}_M}(L(x_1)\cdots L(x_n)) \tag{23}$$

continuous. In this case, given finite, fixed values of M, the problem of predetermination of the T-products does not arise and consequently the poli-local operators of (23) satisfy all our conditions.

Difficulties appear when we proceed to remove the regularization, when the additional fictional masses tend to infinity. It turns out then that the coefficient functions of operators (22) do not approach a limit, even in the improper sense, and, hence, we cannot determine S_n as

$$\lim_{M\to\infty} S_n^M(x_1, \ldots, x_n).$$

It can, however, be shown that for a given Lagrangian L(x) it is feasible to construct a string of quasi-local operators

$$\Lambda_2^M(x_1, x_2), \ldots, \Lambda_n^M(x_1, \ldots, x_n),$$

with coefficients dependent upon the M's in such a manner that expressions of the type (17):

$$S_n^M(x_1, \ldots, x_n) = i^n \operatorname{reg}_M T(L(x_1)\cdots L(x_n)) + \cdots + \sum_{\substack{2\le m\le n-1 \\ (\sum \nu_j = n,\ \nu\ge 1)}} \frac{i^m}{m!} P(x_1, \ldots, x_{\nu_1}|\ldots|\ldots, x_n) \operatorname{reg}_M \times T\{\Lambda_{\nu_1}^M(x_1, \ldots, x_{\nu_1})\cdots\Lambda_{\nu_m}^M(\ldots, x_n)\} + i\Lambda_n^M(x_1, \ldots, x_n) \qquad (24)$$

become convergent in the improper sense.

In view of this we can agree to define $S_n(x_1, \ldots, x_n)$ as the improper limit of the expression (24) as $M \to \infty$.

The poli-local operators obtained in this manner are integrable by definition. Moreover, they satisfy all the conditions of (9)-(11).

Actually expressions (24) satisfy these conditions for finite values of M; the possibility of transition to the limit in (9) is trivial; in the case of expressions (10) and (11) the possibility is assured by the theorem on the properties of the ordinary product of two poli-local operators with independent arguments.

This general definition of integrable poli-local operators S_n is reflected in practice in the case of Feyman diagrams in the form of an application of a special subtraction procedure[5], analogous to the Dyson-Salam procedure.

We must note that two different (but actually equivalent) points of view are possible here. Thus, it may be held that proceeding in the above manner we effect "predetermination" of the T-product in the sense of Stueckelberg and thereby obtain a new T'-product leading automatically to integrable poli-local operators:

$$S_n = i^n T'(L(x_1)\cdots L(x_n)).$$

From this point of view, we have symbolically

$$S = T'(e^{i\int L(x)dx}).$$

We would be equally justified, however, in holding to the usual definition of T-products, which is fully meaningful in operating with regularized causal functions before passing to the limit. In this case, symbolically

$$S = \lim_{M\to\infty} \operatorname{reg}_M T(e^{i\int (L(x) + L_c(x))\,dx}),$$

where

$$L_c(x) = \sum_{(\nu\ge 2)} \frac{1}{\nu!} \int \Lambda_\nu^M(x, x_1, \ldots, x_{\nu-1})\,dx_1\cdots dx_{\nu-1}. \qquad (25)$$

From this latter point of view, the given "priming" Lagrangian $L(x)$ must be supplemented by "counter-terms" $L_c(x)$. Their coefficients in expansion (25) are finite for fixed values of M, but in general tend to infinity as $M \to \infty$.

These divergences in $L_c(x)$ thus serve to compensate the divergences produced by $L(x)$ in the scattering operator.

References

1. E.C.G.Stueckelberg & D.Rivier, Helv. Phys. Acta, 23, Suppl.3,236 (1950).
2. E.C.G.Stueckelberg & T.A.Green, Helv. Phys. Acta, 24, 153 (1951).
3. E.C.G.Stueckelberg & A.Peterman, Helv. Phys. Acta, 26, 499 (1953).
4. N.N.Bogoliubov & O.S.Parasiuk, Doklady AN SSSR, 1 (1954).
5. N.N.Bogoliubov & O.S.Parasiuk, Doklady AN SSSR, 2 (1954).

Note from C.T.T.-

This issue completes our first year of translation of the BULLETIN.

We would like to take this occasion to thank all the friends, acquaintances and strangers who have helped, aided and abetted the undertaking. Space does not allow of listing all the names, for neither least nor last on such a list would be every single one of our subscribers.

However, special thanks are due to Mrs. J. Norris and Mrs. O. Davidson without whose painstaking and careful typing these pages would carry a great many more errors and your editor's head would bear many more grey hairs.

Eugene J. Rosen

BULLETIN of the Academy of Sciences of the USSR - Physical Series

Vol. 19, No. 2, 1955 - Conference on Spectroscopy (Tartu, 1954)

(Continued from Vol. 18, No. 6 and Vol. 19, No. 1)

TABLE OF CONTENTS

	Page Orig.	Trans.
Spectroscopic determination of hydrogen in metals - N.G.Gerasimova, T.F.Ivanova, N.S.Sventitskii, G.P.Startsev, K.I.Taganov & M.E.Trantovius	147	136
Spectroscopic determination of oxygen in steel - O.B.Fal'kova	149	137
Quantitative determination of certain difficult-to-excite elements by means of a square-pulse generator - A.N.Vorsin	150	138
Spectro-chemical determination of carbon in iron alloys - E.S.Kudelia & A.S.Demianchuk	150	139
Local spectrum analysis - N.G.Isaev	151	140
Local analysis of welds of high-alloy steels and heat-stable alloys - A.G.Komarovski	152	141
Use of emission spectrum analysis in biology and medicine - A.O.Voinar	153	142
The oxyhemometer - a photoelectric instrument for bloodless and continuous determination of the oxygen content of blood - M.S.Shipalov	154	143
Preparation and investigation of spectroscopic standards of different alloys - K.A.Sukhenko, I.O.Mladentseva, N.P.Gorozhankina, Z.S.Platonova, A.V.Aksenova & S.M.Il'ina	161	145
Methods of spectrum analysis employed at the "Severonikel" Combine - O.Ch.Velichko	156	148
Methods of spectroscopic analysis used at the Moscow Secondary-Aluminum Plant in 1952-1954 - N.P.Rubina	158	150
Enhancing the sensitivity of spectrum analysis of powders - A.N.Bronshtein	159	150
Use of spectroscopic methods of analysis at the Kuznetsk Metallurgical Combine - L.P.Andreeva	160	151
Investigation of the spectral characteristics of spectroscopic standards prepared by compressing metal powders - V.V.Poliakova	165	153
On the use of the method of parallel working curves in spectrum analysis of steels - Iu.M.Buravlev	166	154
A rapid method of quantitative spectrum analysis of high-alloy steels and alloys - A.G.Komarovski	167	155
On the intersection of the working curves of different sets of aluminum-base alloy standards - A.M.Borbat & N.G.Liakhovich	169	157
Investigation of the influence of structure on the results of spectrum analysis of R9, R18 and 38KhMIuA steels - Iu.M.Buravlev	170	158
The influence of heat treatment and deformation of the results of spectrum analysis of R18 high-speed tool steel - I.A.Grikit	171	159
On the work of a steel wire plant spectroscopic laboratory - A.V.Sokolova	173	160
Spectrographic analysis of carbon and low-alloy steels and pig iron - N.V.Buianov	174	162
Operations of the Laboratory of Standard Samples concerned with the preparation of standards for spectrum analysis - V.V.Stepin	178	164
Spectrum analysis of titanium for impurities - Sh.G.Melamed, M.A.Notkina & S.M.Solovodnik	179	165
Spectroscopic determination of impurities in vanadium pentoxide - P.M.Poliakov & A.K.Rusanov	180	167

	Page Orig.	Trans.
Determination of antimony in its ores and of impurities in antimony trioxide and metallic antimony - S.M.Solodovnik	182	168
Spectroscopic determination of Dc, Pb, Cu and Fe grade Ts-V, Ts-O and Ts-1 zincs by the method of photometric interpolation with shifted spectra - B.P.Pashevkin	185	170
Use of spectroscopic techniques for determining the character of arsenic distribution in steel - O.I.Nikitina	188	171
A spectrographic procedure for the determination of arsenic in steel and its applications - E.F.Nikiforova	190	173
More regarding Bessemer flame spectra - K.S.Garger, V.D.Umnov & G.D.Krivulia	186	174
Spectrographic determination of arsenic in ordinary carbon steels - V.V.Sukhovalova	191	176
Determining nickel, vanadium, chromium and copper in clays by spectrum analysis - N.V.Astaf'ev, R.S.Rubinovich & S.A.Iakovleva	192	177
Spectrum analysis of clays for principal components - E.E.Vainshtein, T.F.Borovik-Romanova & V.V.Korolev	194	178
Spectroscopic determination of lead and other elements in natural waters - E.B.Gusiatskaia & L.G.Loginova	194	179
On the use of an activated AC arc for spectroscopic determinations of alkali and alkali earth elements in natural waters - T.F.Borovik-Romanova, V.V.Korolev, Iu.I.Kutsenko & M.M.Farafonov	196	180
Factors affecting line intensities in spectrum analysis of solutions - Kh.I.Zil'bershtein	197	182
Spectroscopic determination of certain metallic elements in quartz and other siliceous substances - O.M.Nikitina	199	184
Applications of spectrum analysis in petroleum geology - A.A.Geiro	201	185
Emission spectrum analysis over a profile of the Devonian and Carboniferous sedimentary strata in the Troitsk-Pechorsk Region of the Komi A.S.S.R. - S.S.Geiro	200	186
Spectrum analysis of the electrolyte in zinc and nickel plating baths - M.P.Grishchenko & A.B.Shaevich	203	187
Spectrum analysis of electrolytic baths - V.P.Golovchenko	204	188
Spectrum analysis of metals and alloys utilizing spark-contact sampling - M.G.Mal'tsev & K.I.Taganov	205	189
Determination of tin in complex electroplated coatings on radiator tubes - L.S.Evlashin	206	190
Determination of the thickness of oxide coatings on aluminum alloys - V.P.Borzov & E.V.Il'ina	207	191
Quantitative spectrum analysis for metallic impurities in lubricating oils - V.P.Borzov & E.V.Il'ina	209	192
Spectrum analysis of black tin - V.D.Pisarev, A.V.Kornilov & Z.P.Kostrova	210	193
Spectrographic determination of minor impurities in certain raw materials, intermediate products and pure metals encountered in copper-nickel production - V.L.Ginzburg, I.N.Gramenitski, S.E.Kashlinskaia & D.M.Livshits	211	194
Spectrographic determination of tin in natural minerals-M.L.Shilling	216	198
Rapid spectrum analysis for fluorine - I.I.Smoliak	217	199
Calculation and interpretation of the vibrational spectra of certain monoalkylbenzenes and polymethylbenzenes - M.A.Kovner	218	200
Temperature dependence of the intensity of first order Stokes lines - Ia.S.Bobovich	219	201

	Page Orig.	Trans.
Effect of carburization and nitridation on the results of spectrum analysis - I.A.Grikit	221	203
Spectroscopic determination of silicon and lead in powder used for the production of synthetic corundum - O.P.Malkova & N.K.Rudnevski	224	205
Report No. 8. Raman spectra of certain aromatic hydrocarbons - V.T.Aleksanian, Kh.E.Stepin, A.L.Liberman, E.A.Mikhailova, M.A.Prianishnikova & B.A.Kazanski	225	206

Transactions of the Division of Physical-Mathematical Sciences of the USSR Academy of Sciences

Causality conditions in quantum field theory - N.N.Bogoliubov	237	215

Translated in 1956 by
Columbia Technical Translations
5 Vermont Ave., White Plains, N.Y.

GAMMA-EMISSION AND DECAY OF LANTHANUM^{140}

- L. V. Arkhangel'ski, B. C. Dzhelepov, N. N. Zhukovski, V. P. Prikhodtseva & Iu. V. Khol'nov

1. Introduction

The decay of La^{140} has been the subject of many investigations;[1-26,40] The results of these investigations may be summarized as follows:

1. Half-life. The half-life of La^{140} has been measured by 13 workers.[1-13] The most accurate measurements were apparently those made by Maurer:[13] T = 40.22 ± 0.02 hours.

Lanthanum samples commonly encountered in laboratories contain impurities - rare earth elements - which are difficult to separate out. Hence La^{140} obtained by means of the (n,γ) reaction is usually contaminated with other radioactive substances. Separation of the La after bombardment is extremely difficult, which presumably explains the errors in the determination of the half-life. However, relatively pure lanthanum after bombardment with neutrons exhibits an activity that falls off according to the exponential law over a period of 320 hours.[8]

The decay of La^{140} obtained by deuteron bombardment has been followed over 11 periods[13] and has proved to be simple.

La^{140} can be separated out from solutions containing Ba^{140}, produced by the fission of heavy elements. The decay of La^{140} obtained in this manner has been followed for 574 hours[13] and also proved to be simple.

Formation of La^{140} has also been observed in bombardment of Ba^{138} by thermal neutrons; successive capture of two neutrons leads to Ba^{140} which breaks down to La^{140}.

2. Continuous β-spectrum of La^{140}. The continuous β-spectrum has been studied by means of magnetic spectrometers in four investigations.[9,14-16] The conclusions on which all investigators agree are the following:

a) The end-point energy of the hardest β-ray lies between 2.12 and 2.26 Mev (according to Ref. 9, E_{ep} = 2.20 ± 0.02 Mev).

b) The relative intensity of this component is 7-10% (according to Ref. 9: 8 ± 1%).

c) The Fermi plot for La^{140} is curvilinear over almost its entire length.

The positions and relative intensities of the soft β-spectrum components reported in the above-mentioned investigations differ. It can, however, be safely asserted that there are components with an energy of 1.6-1.7 Mev and 1.3-1.4 Mev. The following components are listed in Refs. 9 and 16 (end-point energies):

Bashilov et al[9]		Peacock et al[16]	
E_{ep} = 2.20 ± 0.02 Mev	(8 ± 1%)	E_{ep} = 2.15 Mev	(7%)
= 1.62 ± 0.02 "	(14 ± 1%)	= 1.67 "	(10%)
= 1.36 ± 0.02 "	(30 ± 2%)	= 1.34 "	(45%)
= 1.15 ± 0.03 "	(20 ± 1%)	= 1.10 "	(26%)
= 0.86 ± 0.03 "	(12 ± 2%)	= 0.83 "	(12%)
= 0.42 ± 0.04 "	(16 ± 2%)		

The original report was presented at the Beta- and Gamma-Spectroscopy Conference on 20 February 1954. However, in the written article we take into account the results of investigations published subsequent to this date.

The energy values and relative intensities of the components of so complex a β-spectrum cannot be determined accurately directly from the shape of the spectrum since the true shape of the hard components (which must be separated out) is not known. In this case only experimental separation of partial β-spectra by means of β-γ coincidences can yield sufficiently accurate information.

For the hardest component of the La^{140} β-spectrum $fT \approx 10^9$; this value indicates that the associated transition is highly forbidden. For the softer components fT is smaller but still exceeds $2 \cdot 10^7$; consequently, the corresponding transitions are also forbidden.

3. Conversion electrons. The γ-radiation from La^{140} is complex; Cork et al[17] observed conversion lines corresponding to 15 γ-rays. However, all the conversion lines of La^{140} have a low intensity. Comparison of the β-particle counts for pure Ba^{140} and for Ba^{140} in equilibrium with La^{140} yields a value of about 6% of the number of disintegrations for the total number of La^{140} conversion electrons.[10] A more accurate value can be deduced from the conversion electron spectrum. According to Bashilov et al[9], the total of all conversion electrons in the 200 to 2000 kev range comes to 1.9% of the number of β-particles; the corresponding percentage for the energy range under 200 kev, according to Ref. 17 is about 1%. Thus conversion electrons appear in less than 3% of the disintegrations. The data on the energy and relative intensity of the conversion electron lines are listed in Table 4.

4. γ-emission. The relative intensity of the γ-lines has until now been determined only by observation of photoelectrons[14,15,18,19,21-24] The results are listed in Table 1; as may be seen, they are conflicting.

Table 1

Relative intensity of γ-rays from La^{140}, as reported by different investigators on the basis of photoelectron and photoneutron observations.

γ-ray energy, Kev	Ref. 14	Ref. 18	Ref. 19	Refs. 20 & 40	Ref. 16
328,6	0,20	0,01	0,03	0,05	0,10
486,4	0,20	0,10	0,07	0,39	0,10
815,6	0,20	0,20	0,13	0,20	0,10
1597	1,00	1,00	1,00	1,00	1,00
2520	0,20	0,05	0,08	0,05	—

5. β-γ coincidences. These were studied in 5 investigations[14,20,21,25,26] From the results of the investigations carried out by means of counters not differentiating the β- and γ-rays according to energies,[14,21,25] one can conclude only that the "integral" β-γ coincidences depend little on the filtration of β-particles. Robinson and Madansky,[26] who used two crystal counters, discriminated between γ-ray energies. They arrived at the very important conclusion that "the 1.60 Mev γ-ray is in coincidence with the most energetic β-particles."

6. γ-γ coincidences. These were measured in the investigations of Refs. 14, 21, 25 but were studied with separation by energies only in the investigations of Refs. 20, and 26. It was found that the γ-lines of energies 816 and 1597 kev yield γ-γ coincidences, while their angular correlation agrees with that theoretically computed for transitions between levels with consecutive spins of 4 - 2 - 0. According to Rall and Wilkinson,[20] 1597 kev γ-quanta also give coincidences with 328 and 486 kev γ-quanta, but do not yield coincidences with any γ-rays having energies above 816 kev. We question this statement, since according to our scheme the 1597 kev γ-line should give coincidences with the weak 926 kev γ-ray.

7. Decay schemes of La^{140}. Three different decay schemes have been proposed.[15-17]. The schemes suggested by Beach et al[15] and by Cork et al[17] are invalidated by the latest data. The scheme given by Peacock et al[16] is in the main in agreement with the diagram based on the present investigation, which will be discussed in more detail in Section 4 below.

2. Investigation of the γ-Spectrum of La^{140}

We investigated the γ-ray spectrum of La^{140} by means of the Ritron, a spectrometer utilizing recoil electrons.[27,28] The principal measurements (two series) were carried out under conditions similar to those obtaining in the investigations of the γ-spectra of Fe^{59}, Co^{60}, Cu^{64}, Br^{82}, Cs^{134}, Sb^{124}, Ag^{110} and Ir^{192} (Refs. 29 through 35a).

A cellophane film 50 μ thick (6.15 mg/cm^2) served as the target; both slits of the spectrometer were 2 mm wide. In the first series of experiments the instrument was filled with pure helium at a pressure of 32 cm Hg; the windows of the first counter were covered with a cellophane film 17 μ thick (i.e., the same conditions as obtained in the investigations of Refs. 29-35a). For the second series of measurements the instrument was filled with a mixture of 96% He and 4% CH_4 (total pressure - 32 cm Hg); to minimize scattering the counter windows were covered with thinner (1-2 μ) cellophane film. These modified conditions led to more stable operation of the counters while the half-width of the γ-lines changed only slightly: at 815.6 kev it became equal to 10.5% instead of 13%. This made it possible to extend the measurements down to 250 kev, whereas previously the threshold was at about 400 kev.

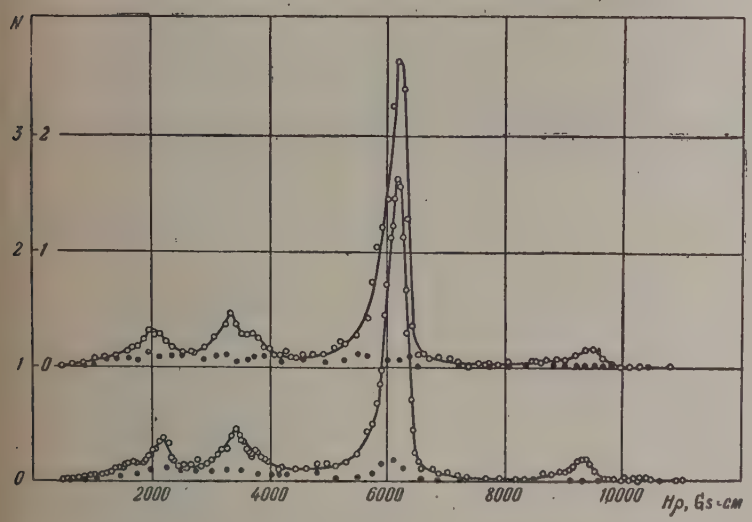

Fig. 1. γ-spectrum of La^{140}. Experimental curves: upper - first series of measurements; lower - second series.

The radiation source was a sample of La_2O_3, bombarded with neutrons. The weight of the sample in the first series was 1.9 g; in the second series - 2.5 g. The source was a disc 14 mm in diameter. The experimental curves for both series are reproduced in Fig. 1, where the horizontal axis is scaled in Hρ values and the vertical axis in coincidences per unit time. The circles are the number of coincidences with the target in place; the black dots are the background, i.e., the number of coincidences with the target lowered out of the beam.

The same spectra but in processed form are shown in Fig. 2, i.e. after taking into account the background, correcting for differences in counter efficiency, conversion to equal energy intervals and, finally, resolution of the separate lines. The resolution was effected taking into account the dependence of the line shape on the energy, for which purpose single lines of Au^{198}, Zn^{65} and Cu^{64} were utilized as references. After separation we determined the intensity of each component and introduced appropriate corrections for attenuation of

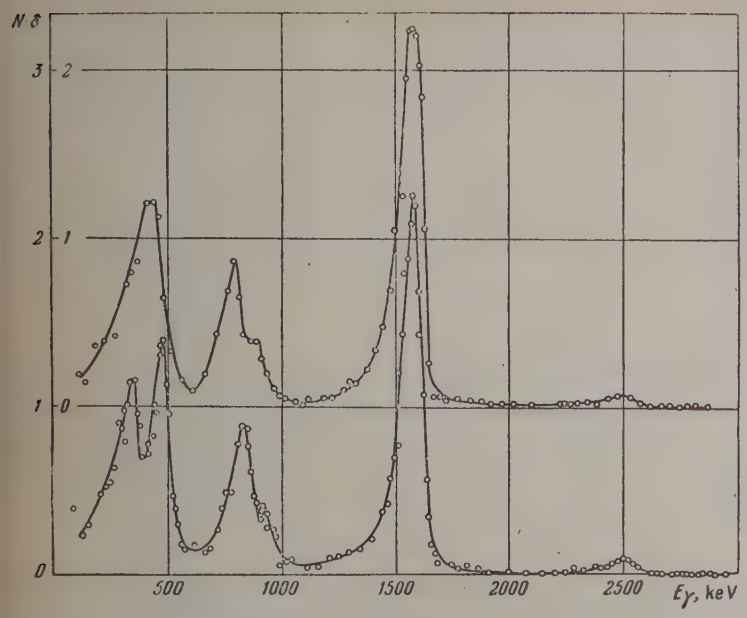

Fig. 2. Same as Fig. 1 but in processed form.

the γ-rays in the source, the tube containing the sample and the entry window of the instrument (up to 14% for hν = 335 kev) as well as corrections for the spectral response of the instrument (according to the curve given in Ref. 28). Finally all the corrected components were recombined.

The γ-ray energies were determined by the position of the peaks (intersection of the tangents to the sides of the line contours) with reference to the calibration curve reproduced in Ref. 28. [See trans. Bulletin No. 5, Vol. 18, p. 285.]

The relative γ-line intensities are listed in Table 2.

Table 2

Results of energy and intensity measurements of γ-rays from La^{140} made on the Ritron

γ-ray energy, Kev *	Relative intensities of γ-lines				Number of photons per 100 disintegrations (see page 236)
	Series I	Series II	Series III**	Best value	
335 (328,6)	0,49	0,19	—	0,19	18
482 (486,4)		0,41	—	0,41	39
822 (815,6)	0,26	0,37	—	0,37	35***
918 (926)	0,17	0,12	—	0,12	11
1597 (1597)	1,00	1,00	1,00	1,00	94
2535 ± 30	0,043	0,062	0,050	0,058	5,5
> 2700 (2900 [24])	—	—	<0,002	<0,002	<0,2

* Mean values for all our measurements; the figures in parentheses are the values given by Cork et al.[17]

** Supplementary series of measurements (see below).

*** Possibly 3-5% of the disintegrations should be attributed to the 751.8 Kev line detected by Cork et al by observing conversion electrons.

The variation of the relative half-widths of the lines with γ-ray energy under the conditions of the first and second series of experiments is shown in Fig. 3. The curves are taken from Ref. 28; the points correspond with the observed La^{140} lines. It will be seen that the points fall above the corresponding curves; this is apparently

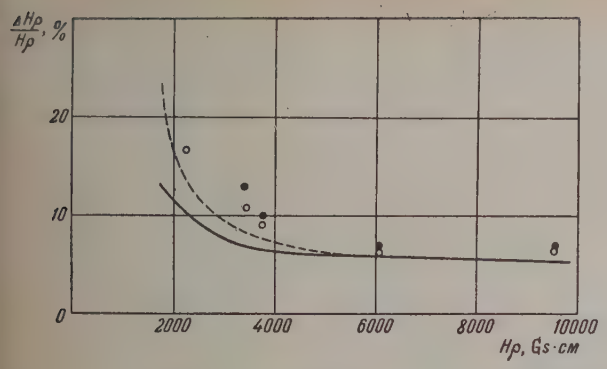

Fig. 3. Relative half-width of La^{140} lines. Dots and dash-line pertain to the measurement of Series I; the circles and solid line, Series II. The curves are taken from Ref. 28.

connected with the greater diameter of the γ-ray source. In order to make sure that none of the investigated lines are due to impurities their intensities were measured repeatedly over a period of about 80 hours. This enabled us to determine the half-life period for each line. The results are given in Fig. 4; the solid straight line corresponds to a half-life of 40 hours while the points pertain to the different γ-lines.

Supplementary series of measurements with a thick target

In the curves of Figs. 1 and 2 there is no indication of the existence of the faint 2.9 Mev γ-line detected in earlier experiments with photoprotons.[23] We attempted to verify the existence of this line and to this end carried out a supplementary series of observations under the following modified conditions: the cellophane target was replaced by a beryllium target about 400 μ thick and the two slits were widened to 7 mm. Under these conditions while the line width is increased to some extent (by a factor of about two for the 1597 kev line) the transmission of the instrument is greatly enhanced: the counting rate at the peak of the 1597 kev line goes up 22 times and the area under the contour is increased 47 times.

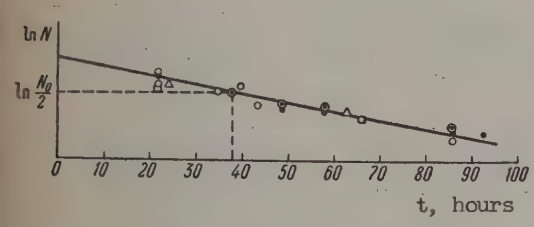

Fig. 4. La^{140} activity curve. The points pertain to the different observed γ-lines.

The experimental results are shown in Fig. 5. It will be noted that there is still no sign of the 2.9 Mev line; it is possible, however, that it is very weak and is masked in the trailing edge of the 2535 kev line. To clarify this it was necessary to investigate the falling off of the 2535 kev line quantitavely. To this end we recorded the well-known 2514 kev line of ThC" under the same conditions. It may be assumed that the shape of this line is similar to that of the 2535 kev La^{140} line. On the basis of this assumption one can "inscribe" the ThC" line into the experimental plot of the 2535 kev La^{140} line as shown (black dots) in Fig. 5. The two curves diverge in the $H\rho >$ 10,300 Gs·cm region. This region is shown to an enlarged scale in the insert of Fig. 5. The difference between the curves exceeds the limits of the statistical fluctuations. However, the ambiguity connected with the subtraction of plotted lines does not permit reasonably accurate evaluation of the energy and relative intensity of the weak hard line. It may safely be said, however, that the energy of the quanta exceeds 2700 kev and the intensity of the line is less than 1/30th the intensity of the 2535 kev La^{140} line and accordingly under 0.2% of intensity of the 1597 kev La^{140} line.

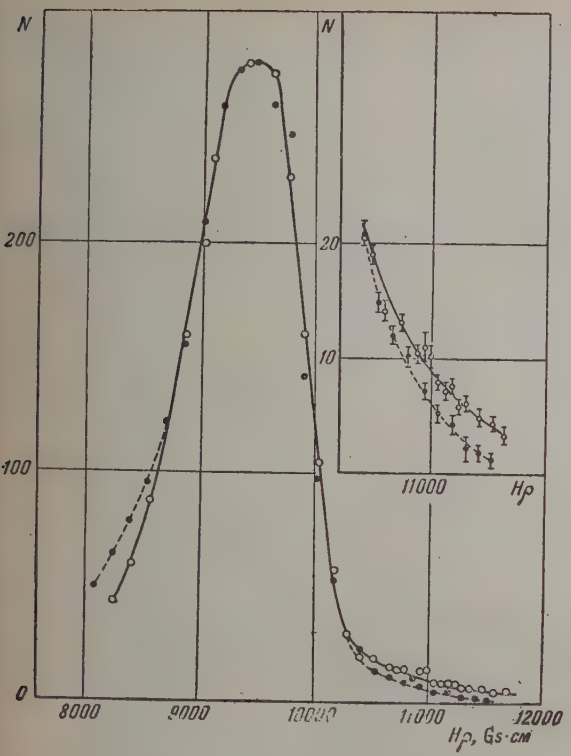

Fig. 5. Circles and solid curve: hard part of La^{140} spectrum as recorded under high-transmission conditions (Be target and wide slits). Black dots and dash-line: 2614 kev ThC" γ-line recorded under the same conditions.

3. Discussion of Experimental Results

1. All the investigated γ-lines have been discovered earlier by observation of conversion electrons or photoneutrons.

2. The intensity of the investigated γ-lines falls off with a period of approximately 40 hours; it may be therefore assumed that all these lines belong to La^{140}.

3. The γ-ray energies are measured most accurately by observation of conversion electrons: conversion lines are usually narrower than photoelectron and recoil electron lines. Hence, in what follows we will assume that the energy values reported in the latest publication of Cork et al[17] are the most reliable ones (see Table 4 below). The scales of Cork's magnetic spectrometer[36] and of DuMond's curved crystal spectrometer[37] coincide with an accuracy of within ±0.2%. Hedgran and Lind[38] measured photoelectron energies by means of a double focusing β-spectrometer and obtained values agreeing with Cork's data to within 0.06%. It may be assumed therefore that the energies of the lines measured by Cork are known accurately to within 0.1%.

Data obtained by Vashilov et al[9] agree with Cork's data to within 1%. Our data obtained on the Ritron do not diverge from Cork's values by more than 2.2%.

4. Our values for the relative intensities of the γ-lines are probably closer to the true values than those obtained observing photoelectrons[14-16,18,19] inasmuch as the lines are better resolved on the Ritron and the spectral response of the instrument can be determined more accurately.

4. The Decay Scheme of La^{140}

1. Building the decay scheme of La^{140} presents certain difficulties inasmuch as the β-spectrum of La^{140} is complex and has not been satisfactorily resolved into components, the γ-spectrum has not yet been studied over the full necessary energy range and the conversion spectrum is very complicated; moreover many of the conversion lines have been observed only photographically to date. It is expedient in such cases to first sketch in the framework of the decay scheme on the basis of the observed predominant disintegrations and then supplement and fill in this framework by indicating the transitions characterized by lower probabilities.

2. In the spectrum of La^{140} there are apparently 5 γ-lines that appear in more than 10% of the disintegrations. These are the lines of energies 328.6, 486.4, 815.6, 926 and 1597 kev. All the other lines have a lower intensity; as regards the soft lines this will be shown below (Para. 18 & Table 4); where the hard lines (>300 kev) are concerned this is evinced by analysis the γ-spectra.

The γ— line of energy 1597 kev is undoubtedly the most intense. In attempting to connect the data relative to this line with β-decay data we can safely make use of the assertion of Robinson and Madansky[26], who studied β-γ coincidences, to the effect that "this experiment indicated that the 1.60 Mev γ-ray is in coincidence with the most energetic β-rays." Robinson and Madansky were aware of the fact that the hardest component of the β-spectrum (~ 2.2 Mev) has an intensity of only 8%, nevertheless in their report they assert that the 1597 kev γ-transition follows this hard β-emission.

In view of the fact that many of the deduction of the present investigation are based on this observation by Robinson and Madansky it would be desirable to verify it.

3. No other single γ-transition can follow the γ-transition with $h\nu = 1597$ kev since all the known γ-lines have considerably lower intensities (see Tables 1 & 2).

4. Among the more intense γ-lines listed in Tables 1 and 2, we note one case where the sum of the energies of two lines is almost exactly equal to the energy of a third line:

$$328.6 + 486.4 = 815.0 \sim 815.6 \text{ kev}.$$

Apparently we have here a case of competition between a direct and cascade transition (Fig. 6). Let us see in what sequence the 328.6 and 486.4 kev quanta are emitted. Let us compare available data on the intensity of these lines.

While there is appreciable scattering of values where photoeffect data are concerned (Table 1), the average ratio of their intensities is calculated to be 1:2.2, which coincides with our experimental value (Table 2). Thus there can be no doubt that the γ-line of energy 486.4 kev is much more intense than the 328.6 kev line.

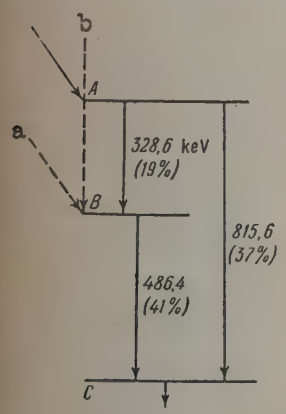

Fig. 6. Part of La^{140} decay scheme.

In view of this intensity ratio we must conclude that the transition with 486.4 kev energy occurs between the levels B and C (Fig. 6), i.e. is the second in cascade. If it were the first the γ-spectrum of La^{140} should include another γ-line associated with a transition from the B level; this line should begin at the B level and have an intensity approximately equal to that of the 486.4 kev line. This "missing" line cannot be the 1597 kev γ-line since these γ-quanta show a coincidence with the quanta of energy 815.6 kev; there are no other sufficiently intense lines in the γ-spectrum of La^{140}.

Having accepted the fact that the 486.4 kev transition is second in cascade we must conclude that the intermediate B state is produced not only as the result of a γ-transition from level A, but also as a consequence of either a β-decay directly to this level (dash-line a in Fig. 6) or a γ-transition from some higher level (dash-line b in Fig. 6). We shall examine this question further in Para. 7 below.

5. The γ-lines of energies 1597 and 815.6 kev give γ-γ coincidences; consequently these transitions do not occur in parallel and the entire group of lines shown in Fig. 6 either follows the 1597 kev

line or precedes it. We note that according to Table 2 the sum of the intensities of the 815.6 and 486.4 kev γ-lines equals 0.78 the intensity of the γ-line of energy 1597 kev.

If we should place this group of lines below the 1597 kev line we would be faced with the problem of how the states associated with the soft components of the β-spectrum pass to the ground level. All the other γ-lines, except those of energies 329, 486, 816 and 1597 kev, taken together have an intensity not exceeding 0.57 that of the 1597 kev line, i.e. appear as the result not more than 54% of disintegrations, while the β-spectrum components softer than the components ending at the 1597 kev level occur in 90-92% of the disintegrations. It follows that we must locate the line group of Fig. 6 above the 1597 kev γ-line in our scheme.

Inasmuch as there are no other γ-lines with measurable intensities we can logically locate this group immediately above the 1597 kev γ-line. In this respect we depart from the scheme of Beach et al.[15]

6. Having accepted the reasoning of Paragraphs 3 and 5 above we must assume that the γ-line of energy 1597 kev extends directly to the ground level of Ce^{140}: there are no single or group transitions following this line. We have thus arrived at the skeletal scheme pictured in Fig. 7.

In accordance with this scheme the mass difference between the ground states of La^{140} and Ce^{140} corresponds to an energy emission of 2200 + 1597 ≃ 3800 kev.

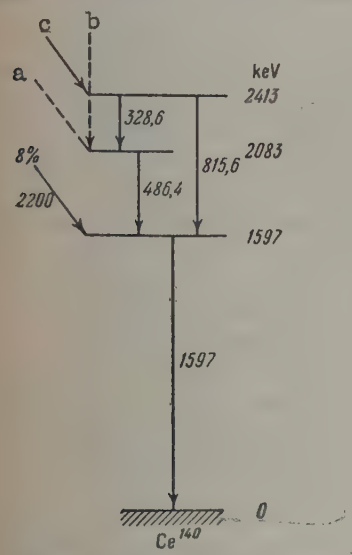

Fig. 7. Skeletal decay scheme for La^{140}.

7. Let us now attempt to determine the number of quanta per disintegration associated with each of the lines in Fig. 7.

The 1597 kev γ-line, according to Robinson and Madansky[26] gives coincidences with the fastest β-particles. But does it yield coincidences with all the other β-emissions? The experiments do not answer this question. Yet coincidences with not all β-particles could occur in three cases:

A) If aside from the 1597 kev γ-transition the 1597 kev level of Ce^{140} decays through a cascade emission of 2 or 3 quanta (Case A, Fig. 8).

B) If some excited state of Ce^{140} decays by a direct transition to the ground level of Ce^{140} (Case B).

C) If some excited state of Ce^{140} decays by a cascade transition not comprising the 1597 kev γ-line (Case C). Let us examine these cases in turn.

Case A. In this case the γ-spectrum should comprise 2 or 3 lines with energies adding up to 1597 kev. Examination of the most complete list of known γ-lines (Table 4) shows that no pair of $h\nu$ values add up to 1597 kev (within 2 kev). However we do find a triplet totaling close to the sought value: 241.4 + 431.3 + 926 = 1598.7 kev.

This may be a fortuitous coincidence: this possibility should not be discounted in view of the large number of different combinations involved. However, with the present state of our knowledge, we cannot exclude the possibility of this cascade. The 241.4 kev line has a low intensity; it appears as a result of less than 2.6% of the disintegrations (see Table 4); hence the cascade cannot occur in more than 2.6% of the disintegrations. In any case, we can provisionally disregard it.

Case B. In this case there should be observed γ-lines of higher energies than 1597 kev. Such lines are present in the γ-spectrum: $h\nu$ = 2535 kev (0.058 the intensity of the 1597 kev line) and, possibly, $h\nu$ = 2900 kev (< 0.002 the intensity the 1597 kev line). It can safely be said, however, that the associated transitions occur in parallel rather than in sequence with the 1597 kev transition; the 1597 kev γ-ray does not give γ-γ coincidences with any harder γ-rays.[20]

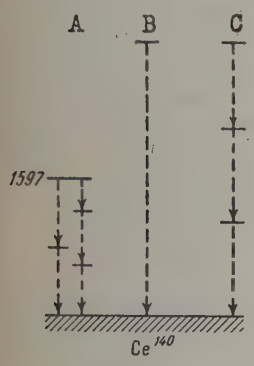

Fig. 8. Decay cases (see text).

Case C. This case is more ambiguous than the preceding two inasmuch as γ-lines of different energies may be involved. However, after assigning locations to the γ-lines with energies 328.6, 486.4, 815.6, 1597, 2535 and 2900 kev in the decay scheme, we have left only one intense γ-line, that with an energy of 918 (926) kev and having an intensity of 0.12 relative to the 1597 kev line. There are no other lines with the intensity above 6% with which we can combine this line into a cascade (if we assume that the above listed lines are all single). This in itself indicates that not more than 6% of the disintegrations can lead to cascades of this type. As for the "left over" 926 kev line we can find a place for it in another part of the decay scheme (see Para. 8).

Summing up, we can state that the existence of type A and C cascades is not proved, although they are possible and that the number of disintegrations leading to these branches amounts to no more than 10% of the number of disintegrations following the main branch (see Fig. 7). Direct transitions of type B exist and their intensity amounts to 0.058 of the intensity of the 1597 kev transition. Inasmuch as the sum of all the transmissions to the ground level of Ce^{140} must equal 100% we arrive at the following distribution:

the 1597 kev line appears in 94 ± 9% of the disintegrations;
the 2535 kev line appears in 5.5 ± 0.8% of the disintegrations;
the 2900 kev line appears in < 0.2% of the disintegrations.

The above margin of error for the intensity of the 1597 kev line is based on the possibility of the existence of as yet unknown cascade transitions; the margin for the 2535 kev line is based on the measured intensities and the error for the 1597 kev line. The number of quanta per disintegration associated with the other γ-lines can be evaluated from the relative intensities of the γ-lines listed in Table 2 and the number of quanta per disintegration associated with the 1597 kev line. The computed values are listed in the last column of Table 2.

8. The 2535 ± 30 kev line, undoubtedly, and the 2900 kev line, possibly, appear in direct transitions from excited levels to the ground level of Ce^{140}. The photon energies give a direct indication of the excitation energies.

Let us examine the 2535 kev state of Ce^{140}. In the conversion and γ-ray spectra we observe lines which may correspond to transitions from this level of Ce^{140} to excited levels of energies 2413, 2083 and 1597 kev (see Fig. 7). Transitions from the 2535 ± 30 kev level to these levels should give rise to γ-lines having energies 122 ± 30, 452 ± 30 and 939 ± 30 kev; and actually from observations of conversion lines we know of transitions with energies equal to these values within the limits to the experimental error: $h\nu$ = 109.2, 110.4, 130.7, 431.3, 486.4 and 926 kev.

In order to obtain the best agreement with the observed lines one must assume that the actual excitation energy of the level in question is 2535 kev; in this case the 109-110 and 926 kev lines fit well into our decay scheme.

The indefiniteness of the experimental data where the energy of the hardest γ-rays of La^{140} (2900 kev) is concerned does not permit locating the corresponding level with adequate accuracy. It is interesting to note, however, that if the actual excitation energy of this level proved to be 3009 kev the transitions to the 2535 and 2083 kev levels would have energies of 486 and 926 kev, respectively, i.e. would coincide as regards energy with transitions actually observed in the γ-spectrum but now assigned other locations in the decay scheme. However, this coincidence - if it exists - may be entirely fortuitous.

9. As a result of the amplifications introduced in the preceding paragraphs our decay scheme acquires the appearance shown in Fig. 9. At this point one may ask whether the additional lines observed in the conversion electron spectrum are not associated with transitions between some of the levels pictured in Fig. 9. Re-examining all the possible transitions between the indicated levels, we do not find a single one which would agree even within 5 kev with the remaining lines listed by Cork et al[17]: 68.7, 109.2, 130.7, 173.0, 241.4, 265.4, 431.3, 751.8 and 1904 kev.

In order to fit these γ-lines into the scheme we must introduce additional levels; in some cases we can locate them in the scheme with the aid of the following equalities, indicating cascade transitions:

$$\left.\begin{aligned} 68.7 + 173.0 &= 241.7) \\ 110.4 + 130.7 &= 241.1) \end{aligned}\right\}$$ a 241.4 kev line is listed;

$$265.4 + 486.4 = 751.8$$ - a 751.8 kev line is listed.

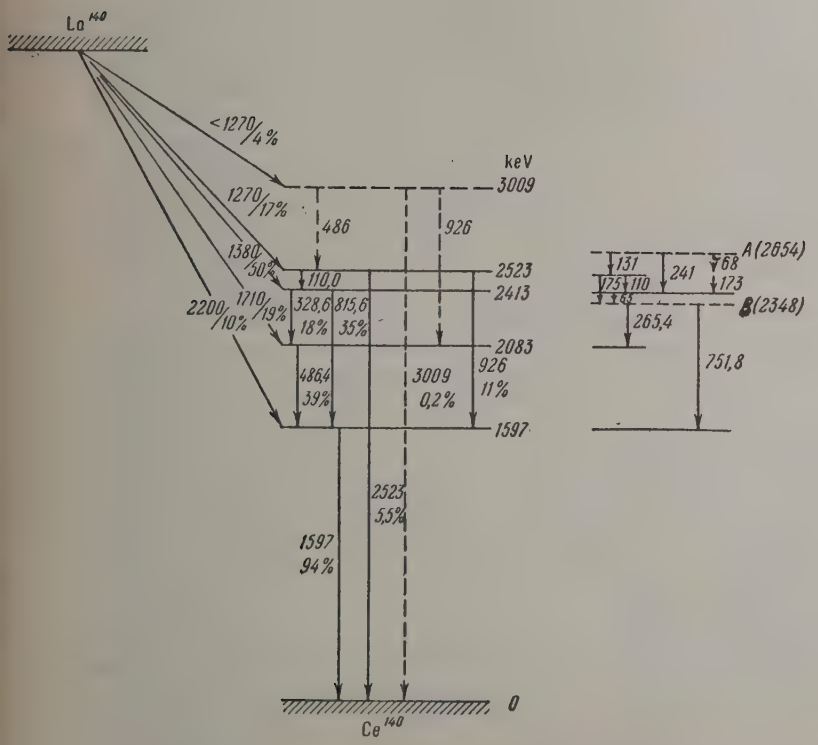

Fig. 9. Decay scheme of La^{140}.

Two such additional levels, designated by A and B in Fig. 9, can account for six of Cork's lines. the location of the still remaining 109.2, 431.3 and 1904 kev lines still remains unclear.

10. Let us now evaluate the intensity balance for the different levels of Ce^{140}. Since we have already established in Para. 7 above that the 1597 kev γ-line appears in 94% of the disintegrations, the intensities of all the other γ-lines can also be expressed directly in percent disintegration. The results of our calculations listed in the last column of Table 2.

11. As noted, 94 ± 9% of the disintegrations must lead to the 5197 kev level of Ce^{140}. Of these, 8 ± 1% must be attributed to the hardest component of the β-spectrum; the remaining 86% must be associated with γ-lines having energies of 486.4 (39%), 815.6 (35%) and 926 kev (11%).

The sum of the intensities of these lines is 85% which is in good agreement with the expected value.

12. Next we turn to the 2083 kev level. Thirty nine percent of the disintegrations start from this level. To balance these we have the following ending at this level: a) the second component of the β-spectrum present in 14% of the disintegrations, b) the γ-line of energy 328.6 kev appearing in 18% of the disintegrations, and c) possibly the weak 265.4 kev γ-line departing from level B (Fig. 9), present in not more than 4.2% of the disintegrations (see Table 4). These total 32-36%, giving a reasonably good balance.

13. Next the 2413 kev level. Departing from it we have the 328.6 and 815.6 kev lines, appearing in 53% of the disintegrations and possibly a weak 65 kev line. Ending at this level, we have a) the third β-spectrum component with E_{ep} = 1360, present in 30 ± 2% of the disintegrations and b) the weak γ-rays of energies 241 and 173 kev, the total intensity of which according to Cork et al[17] and the data of Table 4 does not exceed 3.5%.

Thus, we have a considerable deficit to account for: in order to maintain equilibrium we would have to increase the intensity of the β-decays to about 50%.

14. Starting from the 2535 kev level we have three γ-lines (110, 926 and 2535 kev) occurring all together in about 17% of the disintegrations. We do not know whether any γ-lines end at this level (possibly the 131 kev line from level A of Fig. 9 or the 486 kev line from a hypothetical 3009 kev level), but if they do, they are extremely weak. We must assume, therefore, that the energy balance is maintained primarily by β-decays to this level.

15. According to Bashilov et al[9], 48% of the β-disintegrations of La^{140} lead to Ce^{140} in an excited state with an energy above 2523 kev. Yet all the known γ-lines with relative intensities over 5% have already been fitted into scheme of transitions between lower levels; "undetected" γ-lines can appear (see Table 4) as a result of not over 25% of the disintegrations. Thus it is hard to see how the transitions from the high levels are accomplished; in view of this the provisional resolution of the β-spectrum into Fermi components, given in Ref. 9, becomes questionable.

16. The data on the energy and intensity of the β-components deduced from the location of the energy levels and the balance of intensities are summarized in Table 3. The values in columns 1 and 2 and 3 and 4 were arrived at by two independent methods, neither of which, incidentally, can be regarded aa highly accurate. Nevertheless, it will be seen that there is satisfactory agreement where the hard components are concerned. The errors inherent in both methods mount rapidly as we go into the softer components.

17. Let us determine the multipole order of the 1597 kev transition. According to the empirical rule given by Goldhaber and Sunyar,[39] the first excited state of Ce^{140}, which has N and Z even, must be 2+. If this is the case, the 1597 kev transition must be an electric quadrupole (E2). The results of the experiments of Bishop and Jorba[40], who studied the angular correlation between the 815.6 and 1597 kev and the 486.4 and 1597 kev γ-rays and the polarizational correlation between the (328.6 + 486.4 + 815.6) and the 1597 kev γ-rays, favor an assignment of 2+ and 4+ for the first two states of Ce^{140}. The

Table 3

Energy and intensity of the components of the β-spectrum of La^{140} (approximate data).

From separation of the β-spectrum into Fermi components[19]		From intensity balance in the decay scheme		
Energy, kev	%	Energy, kev	%	fT
1	2	3	4	5
2200 ± 20	8	E_{ep} = 2200	~10	$1{,}1 \cdot 10^9$
1620 ± 20	14	= 1710	~19	$2{,}2 \cdot 10^8$
1360 ± 20	30	= 1380	~50	$3{,}6 \cdot 10^7$
1150 ± 30	20	= 1270	17	$7{,}9 \cdot 10^7$
860 ± 30	12	< 1270	4	—
420 ± 40	16			

relative number of conversion electrons for the 1597 kev transition measured by Bashilov et al[9] in 1951 indicated a greater conversion coefficient than is associated with E2 transitions; however later control experiments show that their original value was overestimated.

Summing up, we feel that the available data justifies a spin and parity assignment of 2+ to the 1597 kev state of Ce^{140}. The data on the intensity of the γ-rays from Pr^{140} support this assignment (see Section 7 below).

The question of the multipole order of the other transitions and of the spin and parity of the second and higher excited states of Ce^{140} and the ground state of La^{140} remains open.

18. Let us now turn to the question of the intensity of transitions detected by conversion electrons but not evinced by γ-rays.

Cork et al[17] list the relative intensities of the conversion lines. Although these values must be regarded as only approximate we shall use these for evaluating the maximum possible intensity of these lines.

The experimental data relative to conversion at the K-shell are listed in column 2 of Table 4.

Let us denote the γ-line intensities, expressed in the number of quanta per disintegration, through p_i; the conversion coefficients at the K-shell, through α_i; and the intensity of the conversion electrons (the number of electrons per disintegration) through n_i. Then

$$n_i = p_i \alpha_i .$$

If we know the multipole order and the number of quanta per disintegration for any one of the γ-lines, we can compute the value of p_i for the other lines, assuming an appropriate multipole order, according to the equation

$$p_i = p_o \frac{n_i}{n_o} \frac{\alpha_o}{\alpha_i} .$$

If we then assume a multipole order for the transition, yielding a minimal value of α_i (i.e. assume an electric dipole transition), we will obtain the maximum value of p_i.

In carrying out our calculations we used the following:

a) values of α_i, obtained by interpolation of Rose's tables and listed in columns 3 through 10 of Table 4;

b) a value of $\alpha = 6.9 \cdot 10^{-4}$ for $h\nu$ = 1597 kev, obtained for an E3 transition in the same manner;

c) the experimental values of n_i/n_o given by Cork et al[17];

d) a value of p_o = 94% for the 1597 kev line.

If we assume that the 1597 kev transition is an electric quadrupole one (E2) we obtain the values for p_i listed in columns 11-15 of Table 4.

Examining Table 4, we note the following:

1) For the α-lines of energies 109.2, 110.4, 130.7, 173.0, 241.4 and 265.4 kev, all p_i's are under 4.2%; consequently every one of these γ- lines appears in less than 4.2% of the disintegrations (as we assumed above).

TABLE 4

Maximum possible intensities of γ-lines not actually observed in the spectrum of La^{140} but assumed to exist on the basis of the conversion spectrum recorded by Cork et al

hν, keV	Relative intensity K - line acc. Cork	Theoretical K conversion coefficients (x 100) for different multipole orders								Intensity of γ-transitions of the indicated types in terms of % disintegrations, assuming the 1597 kev transition is E2					Maximum possible intensity of the γ-line, %
		E1	E2	E3	E4	M1	M2	M3	M4	E1	E2	E3	M1	M2	
1	2	3	4	5	6	7	8	9	10	11	12	13	14	15	16
109,2	40	21	105	—	—	78	—	—	—	0,4	0,09	—	0,11	—	0,4
110,4	10	21	105	—	—	78	—	—	—	0,1	0,02	—	0,03	—	0,1
130,7	70	8,7	52	—	—	39	—	—	—	1,8	0,3	—	0,1	—	1,8
173,0	20	4,9	24	81	350	23	91	570	3160	0,9	0,2	0,05	0,2	0,05	0,9
241,4	30	2,5	8,6	28	97	8,9	43	138	680	2,6	0,8	0,2	0,7	0,2	2,6
265,4	30	1,55	6,4	21	65	6,8	34	93	450	4,2	1,0	0,3	10	0,2	4,2
431,3	20	0,44	1,38	3,9	10,3	1,55	7,1	16,4	54	10	3,2	1,1	2,8	0,6	6*
751,8	10	0,138	0,35	0,76	1,56	0,48	1,47	3,4	7,1	16	6,3	2,9	4,6	1,5	<5**
1904	10	0,024	0,046	0,090	0,14	0,056	0,121	0,19	0,23	92	48	25	40	18	<4**
1597	30	0,033	0,069	0,129	0,22	0,092	0,19	0,35	—	—	—	—	—	—	—

* Value based on observation of photoelectrons.

** Value based on the experimental curve of Fig. 2.

2) For the 431.3 kev line, p(E1) = 10%; this means that if this were an E1 transition, the observed manner of conversion electrons could appear only in connection with a γ-transition occurring in 10% of the disintegrations. A γ-line of such intensity would undoubtedly be observed in photoelectron spectra, since it would have an intensity almost equal to that of the 328.6 kev line and would be well separated from the other lines; it would also have been noted in observations with the Ritron. Since this line has not been detected, it must be assumed that this transition is of a higher multipole order and that, consequently, the intensity of the associated γ-rays is less than 3.2%.

3) The 751.8 and 1904 kev lines in the case of an E1 transition would have a sufficiently great intensity to be readily detected in observations with the Ritron; hence, if such transitions do exist they are either characterized by a higher multipole order (than E1) or have an appreciably smaller number of conversion electrons per disintegration.

5. $La^{140} \rightarrow Ce^{140}$ Decay and Shell Theory

The very high excitation energy of the first level of Ce^{140} may appear surprising: as a rule the first excited state of nuclei with $Z > 50$ has an energy under 500 kev. The exceptional case of Ce^{140} is explained by the fact that this nucleus with 82 neutrons has a closed neutron shell. The first excited level is always anomalously high in nuclei with closed shells. This is clearly evidence in Fig. 10, taken from Goldhaber[41] It will be seen that Ce^{140} is located at the very top of one of the peaks. Ford[42] explains the character of the curve in Fig. 10 by the fact that nuclei with closed shells are exceptionally symmetrical and that it is particularly difficult to disturb this symmetry.

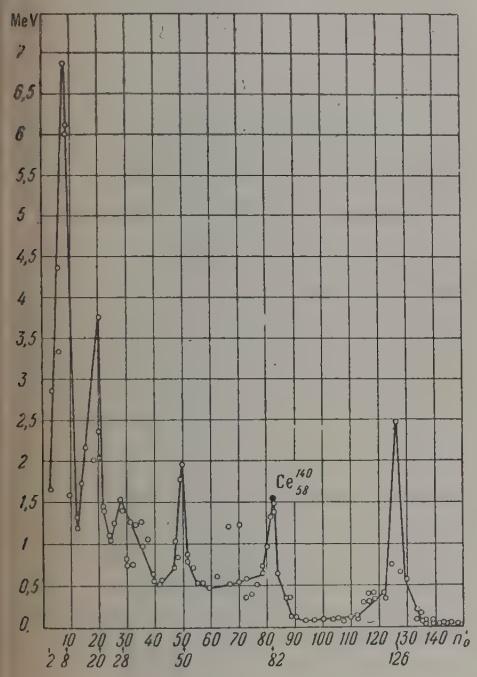

Fig. 10. Energies of first excited state of even-even nuclei according to Goldhaber.[41]

Some investigators are of the opinion that the first excited states of even-even nuclei are 2+ and are the first collective motions levels. However, in the case of two other nuclei with closed shells - $_8O^{16}$ and ThC($_{82}Pb^{208}$) - the first level also turns out not to be 2+: in the case of O^{16} of the first state is 0+ while the second is 3- (Ajzenberg et al[43]); in the case of Pb^{208}, the first level is of type 3- and the next are 5- and 4-. A different situation obtains in the case of Ce^{140}. If the 1597 kev level is actually a rotational level, the next collective level should lie very high - above 5 Mev - and consequently all the other observed levels should be excited as a result of superposition of individual-particle motions on collective motions.

6. Comments on Earlier Investigations

It must be noted that many of the investigations of radioactivity from La^{140} contain serious errors. Some of these are worth mentioning to show the need for great care in drawing conclusions from experimental data:

1) One of the earliest errors is that of Fermi et al[45] who, in writing of lanthanum in the classical work on neutron activation, state that "After intense bombardment under water no sign of activity was detected." Yet we now know that the activation cross section of La^{140} in the slow neutron region is appreciable: 8.4 ± 1.7 barns.[46,47]

2) Even after the publication of reports on numerous investigations of the radiation from La^{140} clearly establishing the fact that its β- and γ-spectra are complex, Cork et al[48] wrote in 1948 that after prolonged bombardment in a pile La did not exhibit conversion lines. Yet three years later the same investigators reported[17] that using the same procedure they detected 24 conversion lines.

3) Weimer, Pool and Kurbatov[6] found that the absorbtion of γ-rays from La^{140} in lead is exponential; whence they concluded that the γ-radiation from the La^{140} is monoenergetic.

4) Mandeville[49] studied the γ-spectrum of La^{140} by observing Compton electrons ejected from a thick target and "confirmed" the conclusion of earlier investigators regarding the monoenergetic nature of the γ-radiation from La^{140}; "The γ-rays appear to be monochromatic, and their energy computed from the end-point of the momentum distribution is 2.04 ± 0.04 Mev. . ."

5) In 1948 Mandeville and Scherb[25] reported that a line of energy 2.3 Mev follows each β-particle. Yet we now know it follows only about 5.5% of the disintegrations.

6) A number of authors asserted, on the basis of β-γ coincidence studies, that the β-spectrum of La^{140} is simple[21] and that the number of β-γ coincidences per recorded β-particle is independent of the β-ray energy.[25] We know that the β-spectrum actually comprises more than three components.

7) Cork et al[17] in their 1951 report give a La^{140} decay scheme from which it follows that the total intensity of the 265.4 + 751.8 kev γ-lines as well as of the 241.4 + 173.0 + 110.4 kev lines equals 100% of the disintegrations yet in the same article they list the relative intensities of the conversion lines associated with these γ-lines from an analysis of which one can readily see that the total intensity of the 265.4 + 751.8 kev γ-lines cannot exceed 13% while that of the latter group of three lines is inferior to 7%.

8) The authors of Ref. 9 are also guilty of errors: as noted above they reported excessively high values for the intensity of the 238.6 and 1597 kev conversion lines.

9) In analyzing results of their correlation experiments Bishop and Jorba[40] failed to take into account the rather intense γ-lines of energy 926 kev.

7. Other Isobars with Mass Number 140

In addition to La^{140} five other radioactive isotopes having a mass number of 140 are known: Xe^{140}, Cs^{140}, Ba^{140}, Pr^{140} and Nd^{140}.

The established decay scheme for La^{140} permits drawing a number of deductions regarding the properties of these isotopes and elucidating certain details concerning the shape of the energy surface in the A = 140 region.

Ba^{140} (β^-, T = 12.8 days)

This isotope of Ba has been extensively studied since it is easily obtained (good yield in the fission of heavy elements) and has a rather long half-life. The latest decay scheme is shown in Fig. 11 (Hollander et al[50]).

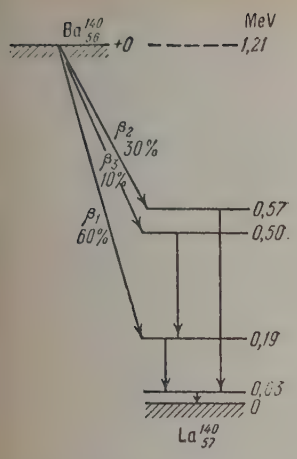

Fig. 11. Decay scheme for Ba^{140}.

The absence of a direct transition between the ground levels of Ba^{140} and La^{140} is to be expected inasmuch as this must be a highly forbidden transition. Regardless of the spin and parity of the ground state of La^{140} there is reason to assume that the β-transitions from Ba^{140} 0+ to the ground state of La^{140} and from this state to Ce^{140} 0+ must have approximately equal fT values. If the transition to the ground level in the β-spectrum of La^{140} has an intensity $< 1\%$ (and otherwise it would have been detected), the fT value for it should be greater than $1.3 \cdot 10^{11}$. Assuming the decay scheme of Fig. 11 to be correct, we may conclude that the hardest component in the β-spectrum of Ba^{140} must have an energy of 1.21 Mev; then with $fT > 1.3 \cdot 10^{11}$, it should have $T_{part} > 1.6 \cdot 10^9$ sec, i.e. a relative intensity $< 0.071\%$. Of course, in practice it would be virtually impossible to detect so weak a component against the background of the harder spectrum of the daughter nuclide, La^{140}.

Ba^{140} is an even-even nucleus: according to the empirical rule of Goldhaber and Sunyar[39], its first excited state should be 2+ and, according to Fig. 10, it should lie at a level of about 1300 kev; it is possible that this is the first collective level of the Ba^{140} nucleus.

Cs^{140} (β^-, T = 9.5 min); Xe^{140} (β^-, T = 10-16 sec)

We have no data on radiation from these isotopes. From the energy diagram of Fig. 12 the γ-spectrum of Cs^{140} may be expected to have a γ-line with an energy of about 1300 kev.

Pr^{140} (β^+, K, T = 3.4 min)

We know the following regarding radiation from Pr^{140}:

1) Pr^{140} emits positrons, the end-point energy of the spectrum being 2.23 ± 0.02 Mev[51] (according to earlier data 2.40 ± 0.15 Mev[51,52]).

2) Pr^{140} captures atomic electrons. According to Browne et al[51], Pr^{140} decays 37% by K-capture, 5% by L-capture and 58% by positron emission. According to Wilkinson et al[53] K-capture accounts for 66% of the decay.

3) Aside from annhilation radiation the above investigators observed only low intensity γ-rays of energy 1-1.2 Mev,[51,53] appearing in approximately 2% of the disintegrations.[53]

4) A search for conversion lines by means of a double focusing magnetic spectrometer failed to yield positive results.[51]

In light of the above data we can draw certain conclusions regarding the type of the principal transition involved in the decay of Pr^{140}.

Inasmuch as no nuclear γ-quanta in amounts commensurate with the total number of disintegrations are observed it must be assumed that most of the transformations occur between the ground states of Pr^{140} and Ce^{140}.

For $E_{ep} = 2.23 \pm 0.02$ Mev, $\beta^+ = 58\%$ and $T = 3.4 \pm 0.1$ min, we obtain $fT = 1.4 \cdot 10^4$, which identifies the transition as an allowed one. The Fermi plot of the β^+-spectrum given by Browne[51] confirms this deduction. A further confirmation is furnished by the magnitude of the ratio β^+/K for this transition. According to theory, for $Z = 58$ and $W_o = 5.37\ m_o c^2$ the ratio should equal unity; in practice, according to Browne

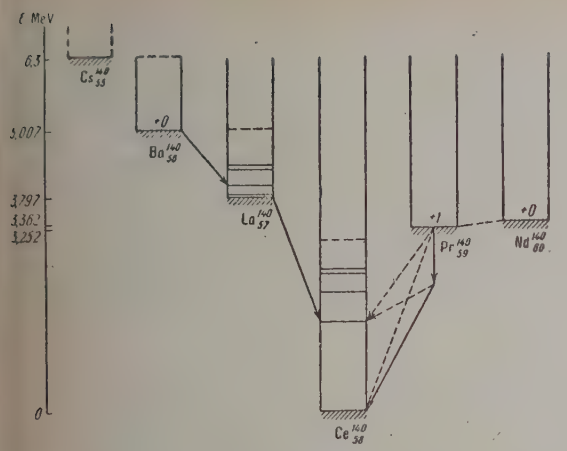

Fig. 12. Energy diagram of ground and excited states of isobars and a mass number of 140.

et al[51], $\beta^+/K = 58/37 = 1.6$; according to Wilkinson and Hicks[53], $\beta^+/K = 34/66 = 0.52$. In all probability, neither value is accurate, nevertheless both differ markedly from the theoretical.

Inasmuch as the ground state of Ce^{140} (even-even nucleus) is probably 0+, the ground state of Pr^{140} must be 1+ if Teller's selection rule applies or 0+ if Fermi's rule is applicable. Shell theory does not afford a unique prediction of the state of nuclei with two odd particles. Although Pr^{140} belongs in this category, we can nevertheless make certain deductions. The spin of Pr^{141}, which is determined by the behaviour of the 59th proton, equals 5/2; shell theory indicates type $j_{5/2}$. The spin of Ba^{137}, which is determined by the behaviour of the 81st neutron, equals 3/2; hence shell theory indicates type $d_{3/2}$. Pr^{140} has 59 protons and 81 neutrons; hence it is natural to attempt combining these types. According to Nordheim's empirical rule the addition of $j_1 = l_1 + 1/2$ and $j_2 = l_2 - 1/2$ leads to a state with a total momentum $(j_1 - j_2)$. In this case the state is 1+, in accordance with the data on β-decay (see below). If this conclusion is correct the transformation of Pr^{140} is produced by tensor or axial-vector forces in the presence of which transitions of the 1+ ⟶ 0+ type are allowed.

In addition to the transition to the ground state of Ce^{140}, Pr^{140} must also undergo transitions to the first excited level of Ce^{140}, having an excitation energy of 1597 kev, spin 2 and even parity. It may be noted that the 1+→2+ type β-transition is allowed according to Teller's selection rule. Determination of the fT value of this transition may prove decisive for making the spin and parity assignment for this state.

According to Wilkinson and Hicks[53] hard γ-rays appear in about 2% of the disintegrations of Pr^{140}. Consequently for the positron transition to the 1597 kev level of Ce^{140}:

$$T(\beta_2) = 50\, T_{exp}\left(1 + \frac{\lambda_{K_2}}{\lambda_{\beta_2}}\right)$$

and

$$E(\beta_2) = 2.23 - 1.597 = 0.63 \text{ Mev}.$$

Assuming $\frac{\lambda_{K_2}}{\lambda_{\beta_2}} = 71$ and $f(\beta_2) = 0.16$ (according to the curve in Ref. 54), we obtain $fT(\beta_2) = 50 \cdot 204 \cdot 72 \cdot 0.16 = 1.2 \cdot 10^5$, i.e. a value typical for allowed β-disintegrations. Thus the presence of hard γ-quanta as a result of 2% of the disintegrations of Pr^{140} is evidence in favor of a 2+ assignment for the 159 kev state of Ce^{140}. Unfortunately the data on these γ-rays is only approximate.

It must be noted that if the ground state of Pr^{140} were of type 0+, the 0+ ⟶ 2+ transition would be twice forbidden and in this case γ-rays would be virtually absent.

Nd^{140} (electron capture, T = 3.3 ± 0.1 days)

Nd^{140} has been produced twice[51,53], in both cases by the Pr^{141} (d, 3n) reaction. Apparently the product does not emit any particles or γ-rays but only captures atomic electrons (according to Browne et al[51]: 74% K-capture and 26% L-capture). Since Nd^{140} has even numbers of protons and neutrons, its ground state should be 0+. Hence, transitions to the ground state of Pr^{140} (1+) should be allowed.

Assuming that the fT value for this transition (0+ → 1+) is equal to that for the $Pr^{140} \rightarrow Ce^{140}$ transition (1+ → 0+), we can find the disintegration energy and the mass difference between the Nd^{140} and Pr^{140}:

$$f_K T = 1.4 \cdot 10^4, \quad T = 2.85 \cdot 10^5 \text{ sec and } f_K = 0.049.$$

By extrapolation of the curves for $f_K = f(\Delta E)$, given by Landolt-Bornstein,[55] we obtain

$$Nd^{140} - Pr^{140} \lesssim 110 \text{ kev}.$$

The relative positions of the masses of Ba^{140}, La^{140}, Ce^{140}, Pr^{140} and Nd^{140} in a unified energy scale can be seen from the data of Fig. 12. The anomalously tight packing of Ce^{140} is probably connected with the fact that this nucleus has a closed shell of 82 neutrons.

"V. G. Khlopin" Radium Institute of
the Academy of Sciences of the USSR

References

1. I. Marsh & S. Sugden, Nature, 136, 102 (1935).
2. M. Pool & L. Quill, Phys. Rev., 53, 437 (1938).
3. O. Hahn & F. Strassman, Naturwiss., 27, 529 (1939); 28, 61 (1940).
4. O. Hahn & F. Strassman, Naturwiss., 28, 543 (1940).
5. K. Mounce, M. Pool & J. Kurbatov, Phys. Rev., 61, 389 (1942).
6. K. Weimer, M. Pool & J. Kurbatov, Phys. Rev., 63, 67 (1943).
7. C. Mandeville, Phys. Rev., 64, 147 (1943).
8. J. Cork, H. Keller, W. Rutledge & A. Studdard, Phys. Rev., 76, 1886 (1949).
9. A. Bashilov, B. Dzhelepov & L. Chervinskaia, Izv. AN SSSR, Ser. fiz., 18, 88 (1951).
10. G. Reed & A. Turkevich, Phys. Rev., 92, 1473 (1953).
11. K. Philipp & J. Riedhammer, ZS.f. Naturforsch., 1, 372 (1946).
12. H. Kirby & M. Salutsky, Phys. Rev., 93, 1051 (1954).
13. W. Maurer, ZS. f. Naturforsch., 2a, 586 (1947).
14. R. Osborne & W. Peacock, Phys. Rev., 69, 679 (1946).
15. L. Beach, L. Peacock & R. Wilkinson, Phys. Rev., 76, 1624 (1949).
16. C. Peacock, J. Quinn & A. Oser, Phys. Rev., 94, 372 (1954).
17. J. Cork, J. Le Blanc, A. Stoddard, D. Martin, C. Branyan & W. Childs, Phys. Rev., 83, 856 (1951).
18. L. Miller & L. Curtiss, Phys. Rev., 70, 983 (1946).
19. W. Rall & R. Wilkinson, Phys. Rev., 71, 321 (1947).
20. R. Bannerman, G. Lewis & S. Curran, Phil. Mag., 42, 1097 (1951).
21. A. Mitchell, L. Langer & L. Brown, Phys. Rev., 71, 140 (1947).
22. A. Hanson, Phys. Rev., 75, 1794 (1949).
23. C. Bishop, R. Wilson & H. Halban, Phys. Rev., 77, 416 (1949).
24. A. Wattenberg, Phys. Rev., 74, 497 (1947).
25. C. Mandeville & M. Scherb, Phys. Rev., 73, 1434 (1948).

26. B. Robinson & L. Madansky, Phys. Rev., 84, 1067 (1951).
27. B. Dzhelepov & M. Orbeli, Doklady AN SSSR, 62, 615 (1948).
28. B. Dzhelepov, N. Zhukovski & Iu. Khol'nov, Izv. AN SSSR, Ser. fiz., 18, 599 (1954).
29. B. Dzhelepov, N. Zhukovski & Iu. Khol'nov, Doklady AN SSSR, 86, 497 (1952).
30. B. Dzhelepov, N. Zhukovski & Iu. Khol'nov, Doklady AN SSSR, 77, 233 (1951).
31. B. Dzhelepov, N. Zhukovski, V. Prikhodtseva & Iu. Khol'nov, Izv. AN SSSR, Ser. fiz., 17, 4, 511 (1953).
32. B. Dzhelepov & A. Silant'ev, Doklady AN SSSR, 85, 533 (1952).
33. K. Gromov & B. Dzhelepov, Doklady AN SSSR, 85, 299 (1952).
34. K. Gromov, B. Dzhelepov, N. Zhukovski, A. Silant'ev & Iu. Khol'nov, Doklady AN SSSR, 86, 255 (1952).
35. B. Dzhelepov, N. Zhukovski & Iu. Khol'nov, Doklady AN SSSR, 77, 597 (1951).
35a. N. Glazûnov, B. Dzhelepov & Iu. Khol'nov, Izv. AN SSSR, Ser. fiz., 19, 3, 294 (1955).
36. J. Cork, M. Brice, W. Nester, J. Le Blanc & D. Martin, Phys. Rev., 89, 1291 (1953).
37. D. Muller, H. Hoyt, D. Klein & J. DuMond, Phys. Rev., 88, 775 (1952).
38. A. Hedgran & D. Lind, Arkiv för Fysik, 5, 177 (1952).
39. M. Goldhaber & A. Sunyar, Phys. Rev., 83, 906 (1951).
40. G. Bishop & J. Jorba, Phys. Rev., 98, 89 (1955).
41. G. Goldhaber, Phys. Rev., 90, 587 (1953).
42. K. Ford, Phys. Rev., 90, 29 (1953).
43. F. Aizenberg & T. Lauritzen, Rev. Mod. Phys., 24, 321 (1952).
44. L. Elliott, R. Graham, J. Walker & J. Wolfson, Phys. Rev., 93, 356 (1954).
45. E. Amaldi, O. d'Agostino, E. Fermi, B. Pontecorvo, R. Rasetti & E. Segre, Proc. Roy. Soc., A149, 522 (1935).
46. K. Sinma & F, Yamasaki, Phys. Rev., 59, 402 (1941).
47. L. Seren, H. Friedlander & S. Turkel, Phys. Rev., 72, 888 (1947).
48. J. Cork, R. Shreffler & C. Fowler, Phys. Rev., 74, 240 (1948).
49. C. Mandeville, Phys. Rev., 63, 387 (1943).
50. J. Hollander, I. Perlman & G. Seaborg, Rev. Mod. Phys., 25, 556 (1953).
51. C. Brown, J. Rosmussen, J. Surls & D. Martin, Phys. Rev., 85, 146 (1952).
52. J. De Wire, M. Pool & J. Kurbatov, Phys. Rev., 61, 544, 564 (1942).
53. G. Wilkinson & H. Hicks, Phys. Rev., 75, 1687 (1949).
54. G. Glasoe & J. Steigman, Phys. Rev., 58, 1 (1940).
55. Landolt-Börnstein, 6 Aufl., Bd. 1/5.

GAMMA-RADIATION FROM Au^{198}

- B. S. Dzhelepov, N. N. Zhukovski, V. P. Prikhodtseva and Iu. V. Khol'nov

1. Introduction

By 1950 the decay scheme of Au^{198} appeared to be definitively established: it was generally accepted that the β—spectrum of Au^{198} is simple, has a linear Fermi plot and leads to the 411 kev level of Hg^{198}, which in turn passes to the ground state by an electric quadrupole transition. The experimental bases for this scheme were set forth in detail by Anton'eva, Bashilov, Dzhelepov and Zolotavin.[1]

In recent years, however, many new investigations devoted to the activity of Au^{198} have appeared in scientific literature. The most important results of these are detection of two new γ-lines having energies of 676 and 1089 kev, determination of their characteristics and recording of the β-γ and γ-γ coincidences associated with them. In view of these results and the renewed interest in the decay scheme for Au^{198}, we undertook a study of the γ-spectrum of Au^{198} by means of the Ritron.

2. Investigation of the γ-spectrum of Au^{198}

The purpose of our experiments was a more accurate determination of the relative intensities of the γ-lines of Au^{198} than had been attained by preceding investigators. The measurements were made on the Ritron.[2] The source was a gold cylinder 3 mm in diameter and 6 mm long, bombarded with neutrons and having an activity of about 2 curies.

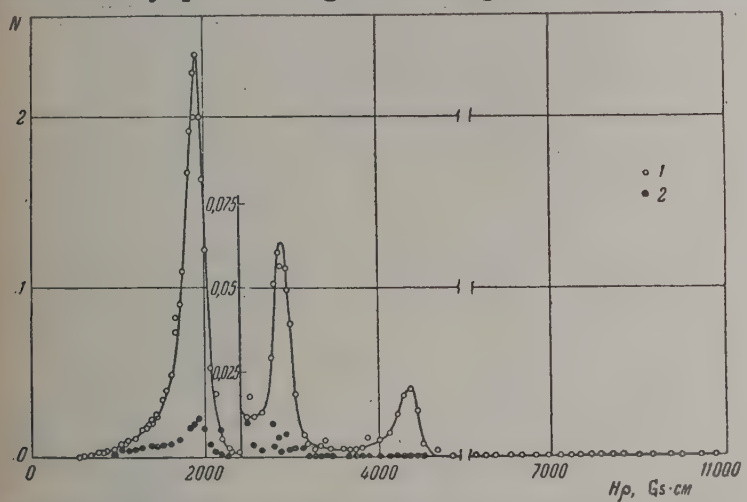

Fig. 1. γ-Spectrum of Au^{198}, experimental curves: 1) points obtained with target in beam; 2) points with target out of beam (background).

Fig. 1 shows the experimental curve. The two hard -lines are plotted to an enlarged scale (20 X).

Fig. 2 shows the resultant spectrum after processing: subtraction of background, reduction to equal energy intervals, introduction of appropriate corrections for the absorption of γ-rays in the source and walls of the instrument, and taking into account the spectral sensitivity of the instrument and the variation of counter efficiency with electron energy.[2]

In order to eliminate the possible influence of the gas filling the instrument on the height of the observed peaks, we carried out three series of measurements at different pressures of the 96% helium + 4% methane mixture: 32, 16 and 7 mm Hg. The results of all three series agree within 6%. The average values of the energies and

intensities obtained in the three series are listed in the table below.

To make sure that the gold sample does not emit even harder γ-rays we extended the main series to 3000 kev; no additional γ-rays were detected. We also carried out a supplementary series of measurements under conditions of enhanced transmission (increased 25-fold, using a 0.4 mm beryllium target and opening the slits to 7 mm - see Ref. 2).

The tests showed that the intensity of γ-rays having energies in the 1100 to 3000 kev range does not exceed $1.5 \cdot 10^{-3}$ quanta per disintegration.

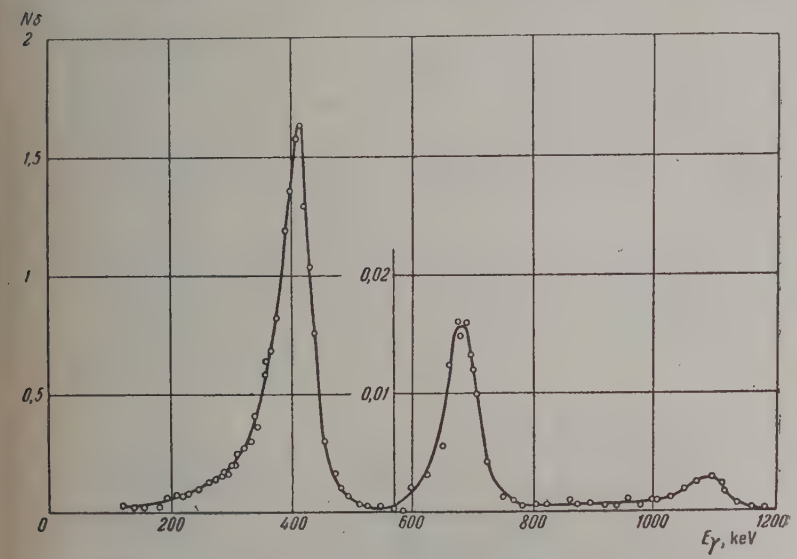

Fig. 2. Same as Fig. 1 but after processing.

3. Discussion

The hard lines in the γ-spectrum of Au^{198} were discovered in 1951 by Cavanagh, Turner, Booker and Dunster.[6] Since then the relative intensity of the γ-lines has been measured in six investigations, the results of which are summarized in the table below.

ENERGIES AND RELATIVE INTENSITIES OF THE GAMMA-LINES OF Au^{198} ACCORDING TO THE DATA OF DIFFERENT INVESTIGATORS

E_γ, keV	Relative intensity	E_γ, keV	Relative intensity	E_γ, keV	Relative intensity
Elliot et al[3] - 1951		Brosi et al[4] - 1951		Elliot et al[7] - 1954	
411,77	100	411	100	411,77	100
675,7 ± 1,5	0,48 ± 0,1	680	1	676,5 ± 0,8	0,842 ± 0,056
1087 ± 2	0,13 ± 0,2	1090	0,2	1088,9 ± 0,9	0,17 ± 0,012
Hubert[5] - 1951		Cavanagh et al[6] - 1951		Maeder et al[8] - 1954	
411	100	410 ± 6	100	410 ± 2	100
673 ± 3	1,4 ± 0,1	671 ± 9	1,5	680	1,3
1075 ± 7	0,25 ± 0,05	1092 ± 13	0,4	1090	0,25

Our data

E_γ, keV	Relative intensity Series I (32 cm Hg)	Relative intensity Series II (16 cm Hg)	Relative intensity Series III (7 cm Hg)	Accepted best rel. intensity value
412 ± 4	100	100	100	100
680 ± 7	1,14	1,07	1,10	1,11 ± 0,05
1088 ± 10	0,26	—	—	0,26 ± 0,02

In the investigations of Refs. 4 and 6 the γ-spectrum was studied by means of a scintillation spectrometer; the accuracy of such measurements is relatively low.

Hence, the comparable data are primarily those of Elliot et al[7] and our own. The values differ far more than is consistent with the limits of experimental error indicated by the respective authors.

The energy of the strongest γ-line of Au^{198} was measured most accurately by Muller, DuMond et al[9], who report a value of 411.77 ± 0.036 kev. The most accurate measurements of the hard lines are those of Elliot, Preston and Wolfson:[7] 676.5 ± 0.8 and 1088.9 ± 0.9 kev. Gamma-rays with energies of 411.1 and 675 kev have also been observed in conjunction with K-capture in Tl^{198} (Ref. 10). This proves that the transitions occur in Hg^{198}. This is further confirmed by the fact that the difference between the energies of the conversion electrons ejected from the K and L shells equals 68.5 kev for $h\nu$ = 411 kev,[1] 67.9 ± 0.6 kev for $h\nu$ = 676 kev and 68.0 ± 0.5 kev for $h\nu$ = 1089 kev.[10] while the difference K - L should be 64.2 for Pt, 66.1 kev for Au and 68.1 kev for Hg.

4. Decay Scheme of Au^{198}

Below we shall systematize the data on the decay of Au^{198} accumulated to date (1 October 1954).

1. The principal component of the β-spectrum has an end-point energy 958.8 ± 1.6 kev (weighted average based on the results of Refs. 1, 3, 7, 11-15). The Fermi plot is linear.[1,7] The soft (E = 290 kev) and hard (E = 1371 kev) components of the β-spectrum are of such low intensity that they cannot produce any noticeable deviations from linearity of the Kurie plot.

2. The soft component of the β-spectrum was discovered by Cavanagh[16] in studying β-γ coincidences for Au^{198}. In this investigation a scintillation spectrometer was adjusted to the hard γ-line (1086 kev) while the β-particles were recorded by a G-M counter. Cavanagh investigated the variation of the number of coincidences with the thickness of an absorber (Al) mounted in front of the β-counter. The coincidences disappear at an absorber thickness corresponding to an end-point energy of 295 kev. This soft β-component leads to the second excited level of Hg^{198}. A maximum energy value of 290 ± 15 kev was obtained by Brosi et al[4] who studied coincidences between γ-quanta of energy 680 kev (detected by a scintillation spectrometer) and β-particles, discriminated by means of a lens spectrometer.

3. The hard component of the β-spectrum was discovered by Elliot et al.[7] It has an end-point energy of 1371 ± 4 kev and a relative intensity of $(2.5 \pm 0.5)\cdot 10^{-4}$ β-particles per disintegration. Since this energy value agrees almost exactly with the sum of the energies of the principal β-component and γ-line (1370.5 ± 1.7 kev), it is natural to assume that this hard component is produced in the transition of Au^{198} to the ground level of Hg^{198}. The shape of this weak β-component was investigated by Elliot et al;[7] its Fermi plot was found to be non-linear.

4. The β- and γ-spectrum data listed above formed the basis of the decay scheme pictured in Fig. 3.[7] The results of β-γ coincidence[4,16] and γ-γ coincidence measurements tend to support this scheme.

5. The ground state of Hg^{198} - an even-even nucleus - is probably 0+.

6. The quantum characteristics of the first excited state of Hg^{198} follow from a) the absolute magnitude of the K conversion coefficient of the 411 kev γ-ray, b) the value of the ratio K/L and

c) the value of L_{II}/L_{III} for the same line. The magnitude of α_K was determined in the investigations of Refs. 1, 3, 5, 15, 17 and 18). The most accurate determination (within 1%) is that by Simons:[18] $\alpha_K = 0.0307 \pm 0.0003$. This value is in excellent agreement with the theoretical value of 0.031 for an electric quadrupole transition (interpolated value based on relativistic calculations for a pure Coulomb field[19]) ($\alpha_K = 0.012$ for E1, $\alpha_K = 0.16$ for M1, $\alpha_K = 0.082$ for E3, E4, ..., α_K 0.43 for M2, M3, ...).

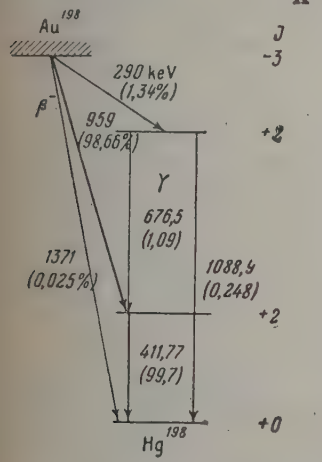

Fig. 3. Decay scheme for Au^{198}.

According to Simons' data K/L = 0.0307/0.0103 ≈ 3.0; the value for this ratio taken from the curve of Goldhaber and Sunyar[20] for an E2 transition is 2.7.

Swan and Hill[21] determined the ratio of the probabilities of conversion of the 411 kev γ-rays at the L_{II} and L_{III} sublevels; according to their data, $L_{II}/L_{III} = 2.53$, which is in agreement with the theoretical value of 2.73 for E2 radiation.[22]

Hence, it must be assumed that the ground state of Hg^{198} is 2+.

7. The 2+ assignment for the 411 kev state of Hg^{198} does not conflict with the lifetime of the state as measured by Graham and Bell[23] and Malmfors[24] (according to the latter, $\tau = 1.6 \cdot 10^{-11}$ sec.

8. The spin and parity of the 1089 kev state of Hg^{198} may be deduced from 1) measurements of α_K and 2) measurements of K/L for the direct transition to the ground state of Hg^{198}.

According to Elliot et al,[7] $\alpha_K = 0.00450 \pm 0.00034$, which is in excellent agreement with the theoretical value (Rose et al[25]) for an E2 transition: 0.00453 (for E1, $\alpha_K = 0.00173$; for E3, 0.0097; for M1, 0.0184; for M2, 0.030).

Elliot et al[7] also give an experimental value for the ratio K/L of 6.3 ± 0.5, which is in excellent agreement with value 6.8 obtained by extrapolation of the curve given by Goldhaber and Sunyar[20] for E2 radiation. Thus the second excited level of Hg^{198}, like the first, has spin 2 and even parity.

9. These identifications of the first and second levels are confirmed by comparison of the 676 kev γ-ray conversion coefficient determined experimentally by Elliot et al[7] with the theoretical value. The experimental value is $\alpha_K = 0.0224 \pm 0.0019$ which agrees with the theoretical value[25] for a mixture of (32 ± 6)% M1 and (68 ± 6)% E2 radiation (for M1, $\alpha_K = 0.047$, while for E2, $\alpha_K = 0.0111$).

10. The above identification of the states of Au^{198} is in good agreement with the results of measurements of angular γ-γ correlation of the 411 and 676 kev γ-rays.[26-28] The assignments for the 411 and 1089 kev states of Hg^{198} are also supported by the nearness of the fT values for the transitions of Au^{198} to these two levels (see below).

11. Direct measurements of the spin of Au^{198} made by Reynolds et al[29] resulted in a value of 2. Thus the β-transition of Au^{198} to the ground state of Hg^{198} is of the $2 \rightarrow 0+$ type. For this transition the end-point energy E = 1371 kev and $\beta^+ = 0.025\%$ and, consequently, $\log fT = 11.7$. So high an fT value indicates that this must be at least a second forbidden transition. If Au^{198} were 2-, the transition would be a first forbidden one, hence it must be assumed that the ground state of Au^{198} is presumably 2+. Both the β-transitions

to the excited states of Hg^{198} are of the $2+ \rightarrow 2+$ type, i.e. must be allowed. The values of log fT for these transitions (7.4 and 7.6) are in poor agreement with this deduction. However, there are now known to be other cases where allowed transitions have an anomalously high fT value, presumably due to differences in the structure of the initial and final nuclei.

12. The following data are available regarding the transformation $Au^{198} \rightarrow Pt^{198}$:

Mims and Halban[30] determined the upper limit for the ratio $\beta^+/\beta^-: < 3 \cdot 10^{-5}$.

Cavanagh et al,[6] using a lens spectrometer to observe photoelectrons, detected two soft γ-lines having energies of 66.5 ± 1 and 78.0 ± 1 kev. They failed to detect the corresponding conversion lines and came to the conclusion that these are X-rays. These are produced 1) as a result of the ejection of conversion electrons in the decay of Au^{198} and 2) due to ionization of the atoms of the source by β-particles. These investigators give a value of 6% for the upper limit of the intensity of the K-capture branch.

The investigators of Ref. 31 evaluated the intensity of the K-branch by the method of selective absorption of the X-rays produced in the K-capture. They established that if K-capture does occur in Au^{198}, its probability is less than 0.4% of the probability of β-disintegration.

"V. G. Khlopin" Radium Institute of
the Academy of Sciences of the USSR

References

1. N.Anton'eva, A.Bashilov, B.Dzhelepov & A.Zolotavin, Izv. AN SSSR, Ser. fiz., 14, 299 (1950).
2. B.Dzhelepov, N.Zhukovski & Iu.Khol'nov, Izv. AN SSSR, Ser. fiz., 18, 5, 599 (1954). Trans. BULLETIN, Vol. 18, No. 5, p. 285.
3. L. Elliot & J.Wolfson, Phys. Rev., 82, 333 (1951).
4. A.Brosi, B.Ketelle, H.Zeldes & E.Fairstein, Phys. Rev., 84, 586 (1951).
5. M.Hubert, C. R., 232, 2201 (1951).
6. P.Cavanagh, J.Turner, D.Booker & H.Dunster, Proc. Phys. Soc., 64A, 13 (1951).
7. L.Elliot, M.Preston & J.Wolfson, Canad. J. Phys., 32, 153 (1954).
8. D.Maeder, R.Mueller & V.Wintersteiger, Helv. Phys. Acta, 27, 3 (1954).
9. D.Mueller, H.Hoyt, D.Klein & J.Du Mond, Phys. Rev., 88, 775 (1952).
10. I.Bergström, R.Hill & G.Pasquali, Phys. Rev., 92, 918 (1953).
11. P.Levy & E.Greuling, Phys. Rev., 73, 83 (1948); 75, 819 (1949).
12. D.Saxon, Phys. Rev., 73, 811 (1948).
13. R.Steffen, O.Huber & F.Humbel, Helv. Phys. Acta, 22, 167 (1949).
14. L.Langer & H.Price, Phys. Rev., 76, 641 (1949).
15. C.Fan, Phys. Rev., 87, 252 (1952).
16. P.Cavanagh, Phys. Rev., 82, 791 (1951).
17. C.Fan, Phys. Rev., 81, 300 (1951).
18. L.Simons, Phys. Rev., 86, 570 (1952).
19. M.Rose, G.Goertzel & B.Spinrad, Phys. Rev., 83, 79 (1951).
20. M.Goldhaber & A.Sunyar, Phys. Rev., 83, 906 (1951).
21. J.Swan & R.Hill, Phys. Rev., 91, 424 (1953).
22. H.Gellman, B.Griffith & J.Stanley, Phys. Rev., 85, 944 (1952).
23. R.Graham & R.Bell, Phys. Rev., 84, 380 (1951).
24. K.Malmfors, Ark. f. Fys., 6, 49 (1952).
25. M.Rose, G.Goertzel & C.Perry, ORNL Report, 1023 (1951).
26. C.Schrader, E.Nelson & J.Jacobs, Phys. Rev., 90, 159 (1953).

27. D.Schiff & F.Metzger, Phys. Rev., 90, 849 (1953).
28. C.Schrader, Phys. Rev., 92, 928 (1953).
29. J.Reynolds, R.Christensen, D.Hamilton, A.Lemonick, F.Pipkin & H.Stroke, Bull. Am. Phys. Soc., 30, 13 (1955).
30. W.Mims & H.Halban, Proc. Phys. Soc., 64A, 311 (1951).
31. Gerard-Andre Renard, C. R., 228, 387 (1949).

* * * *

INVESTIGATION OF THE ENERGY LEVELS OF LIGHT NUCLEI BY THE METHOD OF MAGNETIC ANALYSIS

- L. M. Khromchenko

Investigation of the spectra of the products of nuclear reactions is one of the most effective methods of nuclear spectroscopy. Determination of the energies of charged particles formed in nuclear reactions by means of magnetic analysis has made it possible to increase the resolution of spectroscopic instruments and enhance the accuracy of the experimental results in studying nuclear energy levels.

However, in a number of cases such investigations were effected in only a narrow range of excitation energies. Thus, for example, Buechner et al[1] used deuterons with an energy of only 2 Mev for bombarding the targets in their experiments. Hence, although the experimental accuracy was relatively high, the experiments yielded information only on the lower lying excited levels of the investigated nuclei. One must also note the extreme laboriousness of the method of recording the charged particles employed by these investigators: counting and measuring the length of tracks on photographic plates; the intensities of the investigated particle groups were evaluated from the number of tracks, while the track lengths indicated the nature of the particles.

In the present report we shall summarize the results of a series of experiments.[2-5] The purpose of these experiments was investigation of the levels of some light nuclei in the region of higher excitation energies than had hitherto been studied.

Experimental Procedure

In our experiments the energy of the products of nuclear reaction was also determined by means of magnetic analysis. The experimental set-up, however, differed from that of Buechner et al. In our apparatus the beam of monoenergetic deuterons with an energy of up to 4.7 Mev fell on the target A (Fig. 1). The charged particles, produced in the target by the deuteron reactions and ejected therefrom, described circular trajectories in the strong and homogeneous magnetic field (perpendicular to the plane of the drawing) and passing through the narrow slit B fell on the detector. The last was a thin-emulsion photographic plate, located on the bottom of the instrument. The radius of curvature of particle paths obviously varied with their momentum so that particles having different momenta fell on the plate at different points: C_1, C_2, C_3, etc., the distance from the target increasing with momentum. The conditions of the experiment were such that we obtained on the plate at the sites of localization of discrete groups of particles distinct lines discernible with the naked eye, rather than single tracks.

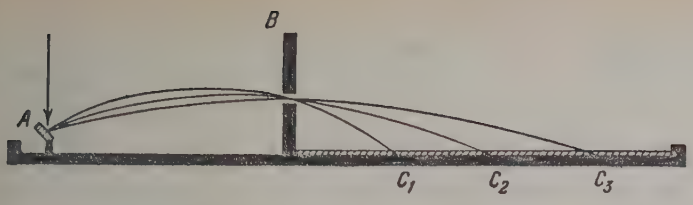

Fig. 1. Diagram of spectrograph: A) target, B) slit, C_1-C_3) points at which particles fall on plate.

Knowing the geometry of the instrument and the intensity of the magnetic field, the energy of the particles making up any given group could be determined by the position of the corresponding line on the plate, provided the nature of the particles, i.e., the e/m ratio, was known.

At the suggestion of Nemilov, to insure rapid and unequivocal identification of the particles we employed a differentiating filter (absorber), representing a modification of the selective wedge developed by him.[6] The filter was placed over the plate so that it covered its entire length and half its width. The filter was prepared of layers of aluminum foil, its thickness being increased in steps in such a manner as to completely stop all deuterons and similar particles at every point along the plate but pass protons. Thus one-half the plate (without the filter) recorded all the charged particles emitted by the target in a narrow range of scattering angles, while the other part (protected by the filter) recorded only the spectrum of the protons produced by the (d, p) reaction in the investigated target. The dependability of this method of identification was checked in yet another manner: the energy spectrum of each nucleus was investigated at a number of different energies of the bombarding deuterons.

The greatest advantage of our method is the high statistical reliability of the observed particle groups: going over from counting individual tracks to lines, observable visually, necessitated increasing the concentration of the tracks by at least three orders of magnitude.

Another advantage of the described experimental set-up is that both spectra in a rather wide range of excitation energy values are obtained simultaneously and on the same photographic plate. This did away with the troublesome operation, forced upon Buechner at al, of "assembling" the overall curve from many individual plates (in some cases up to 20), each of which encompassed only a small portion of the investigated energy region. In view of this, any instability of the deuteron beam in our experiments was less critical inasmuch as it simultaneously affected all the particle groups in the spectrum.

The form of the energy spectrograms obtained made it possible to accelerate greatly the processing of the plates: instead of counting individual tracks we could measure the relative intensities of the groups by means of a microphotometer. The enhanced rapidity of processing, in turn, made it possible to investigate a whole series of spectrograms for each of the studied elements. Also thanks to repeated checking of the reproducibility of the results it was feasible to eliminate most of the accidental factors from the final data.

The focussing and dispersion in our spectrograph were not optimal, inasmuch as the analyzed particles were deflected far less than 180^0. Because of this and the fact that we used thicker targets, the resolving power of the instrument and the accuracy of our results were lower than obtained in the experiments of Buechner et al. The energy of most of the levels was determined with an accuracy of within approximately 20-30 kev. In the cases when thicker targets were used (for example in investigating magnesium and silicon) the probable error increased to 40-50 kev, while when thinner targets were employed (carbon and oxygen) it was reduced to 10-15 kev.

One shortcoming of our procedure is that only the relative intensities of the different particle groups can be evaluated from microspectrograms, whereas counting tracks makes it possible to determine the absolute intensities. On the other hand it must be noted that in the experiments of Buechner et al the reliability of this determination was reduced somewhat due to the fact that individual portions of the spectrum were photographed successively so that any variation in the intensity of the deuteron beam from exposure to exposure distorted the true intensity values.

The energy of the deuterons bombarding the target in our experiments was determined from energy measurements of the recoil deuterons elastically scattered from the nuclei of the target. In the case of targets of complex composition, i.e., in the presence of several groups of elastically scattered deuterons, we took the mean value of the individual measurements for each plate.

In the tables below, summarizing the energy-level data for the investigated nuclei, we list mean values averaged over a series of plates; the statistical weight of the individual measurements was taken into account in computing the mean values. The relative weight was evaluated on the basis of the intensity of the corresponding peaks in the microphotograms. Energy values which we consider to be less reliable than the other data, in view of poorer reproducibility of the spectrum lines, are enclosed in parentheses ( ) in the tables.

The Systems of Excited Levels of some Light Nuclei

Of the investigated light nuclei two - carbon and oxygen - were studied both for the purpose of calibrating and testing the instrument and because they were present in the form of impurities in almost all the other target materials. The energy spectra of the other nuclei were, obviously, studied for their intrinsic interest.

Typical plates showing the energy spectra of the investigated nuclei are reproduced in Fig. 2. As may be noted from a comparison of the photographs the spectra of carbon and oxygen are the simplest of the entire series.

Carbon

In the experiments with carbon, the target was a layer of soot, coated on a copper foil support 0.5 μ thick. A bright line due to the deuterons elastically scattered from the copper can be clearly seen in the spectrum photograph (Fig. 2a). It appears in the upper half of the plate, exposed without the absorber, and is absent in the lower half which was covered by the aluminum foil filter-absorber. Microphotograms of both halves of this plate are shown in Fig. 3. It will be seen that the investigated energy interval comprises four groups of protons from the $C^{12}(d,p)C^{13}$ reaction. One of these groups, identified as $C^{13}(0)$, is associated with the transition of the C^{13} nucleus to the ground state; the remaining three characterize excited states of this nucleus. At a bombarding deuteron energy of 4.4 Mev this $C^{13}(0)$ group of protons coincided as regards position with the group of deuterons elastically scattered from the C^{12} nucleus. Hence in Curve I (representing the spectrum of the unprotected part of the photographic plate) this peak carries both identifications.

Both the mass of the C^{12} nucleus and the Q-value of the $C^{12}(d,p)C^{13}$ reaction are known with good accuracy, having been determined by two independent methods: from magnetic analysis of the products of the

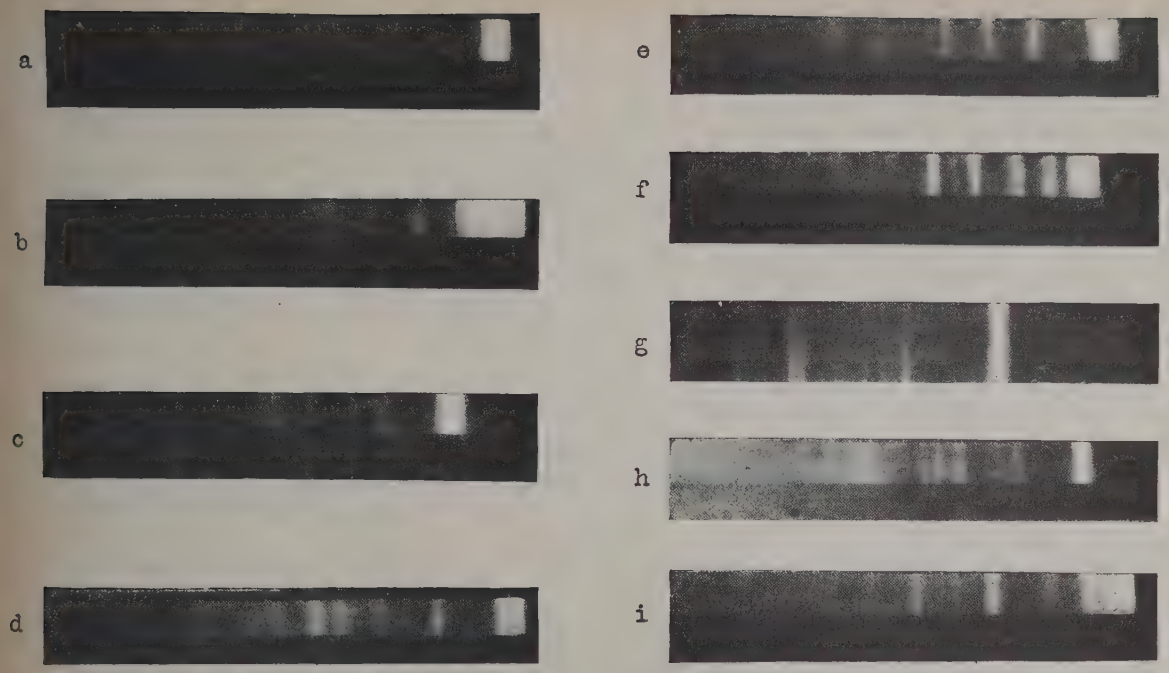

Fig. 2. Energy spectra: a) carbon, b) oxygen, c) lithium - E_d = 3.76 Mev, d) lithium - E_d = 4.69 Mev, e) boron, f) magnesium, g) aluminum - E_d = 3.048 Mev, h) aluminum - E_d = 4.308 Mev, i) silicon.

reaction[7] and by mass-spectrometric measurements.[8] At the suggestion of Lukirski, we used the Q-value for this reaction as the reference in calibrating our spectrograph.

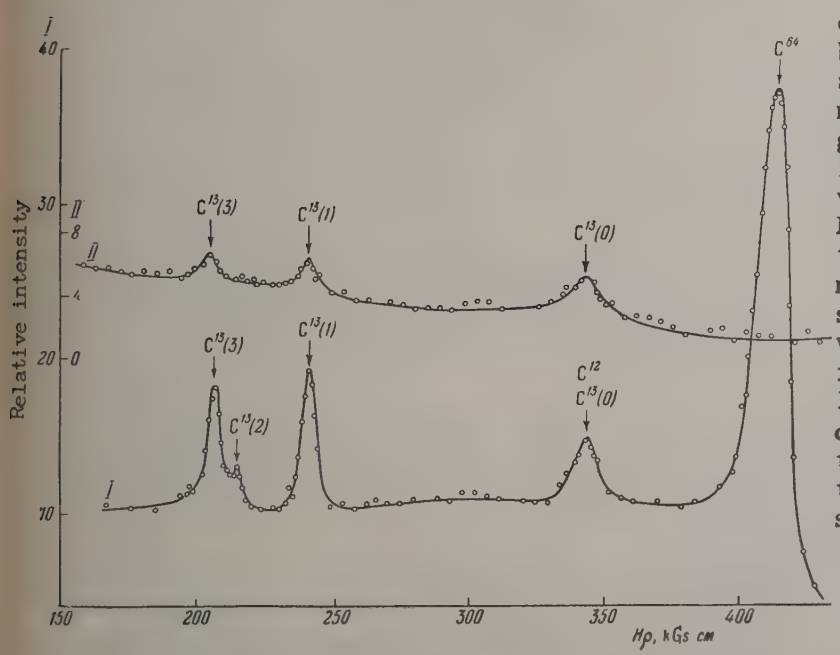

Fig. 3. Microphotogram of carbon spectrum (E_d = 4.40 Mev): I - spectrum on part of plate without absorber, II - spectrum on covered portion of plate.

The data on the energy levels of C^{13} based on our results as well as the measurements of other investigators are summarized in Table 1. In the investigation of Van Patter the energy of the levels was determined by magnetic analysis; in the other investigations, by measuring the proton tracks. In view of the simplicity of the carbon spectrum we analyzed only three plates with this spectrum.

Oxygen

For studying the spectrum for oxygen we used targets of tungsten oxide deposited on a copper foil support. In addition we made use

Table 1

Excitation levels of C^{13} (in Mev)

Group No.	Present Invest	Ref. 9	Ref.10	Ref.11
1	$3,10_7$	3,086	3,11	3,14
2	$3,69_9$	3,686	3,683	—
3	$3,86_9$	—	3,884	4,13

of the data obtained in deuteron bombardment of metallic magnesium. The magnesium samples were appreciably oxidized, hence the spectrum of oxygen appears fairly clearly in the magnesium spectrograms.

One of the photographs of the oxygen spectrum obtained with the tungsten oxide target is shown in Fig. 2b. The microphotograms of this plate are reproduced in Fig. 4. The most intense peaks at the right in Curve I are due to deuterons elastically scattered from the tungsten and copper. The third less intense group of peaks is due to deuterons elastically scattered by the oxygen.

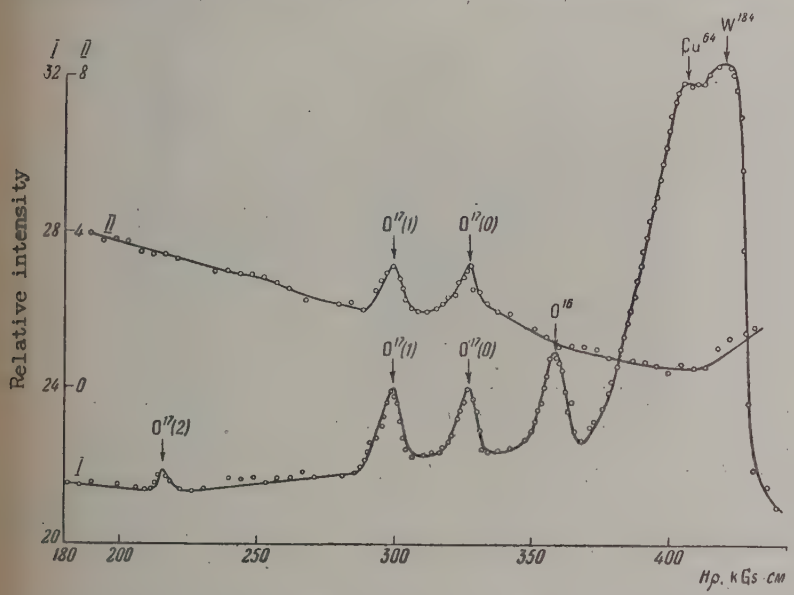

Fig. 4. Microphotogram of oxygen spectrum (E_d = 4.32 Mev: I - spectrum on portion of plate without absorber, II - spectrum on covered portion of plate.

The proton spectrum of oxygen consists of two intense groups - $O^{17}(0)$ and $O^{17}(1)$ - which are comparable in intensity with the $O^{16}(d,d)O^{16}$ group, and two weaker groups. The last of these, $O^{17}(3)$, did not come out on the microphotogram although it was observed visually and its position could readily be established.

The excitation energies of the levels of O^{17} obtained in our investigation are listed in Table 2. They are based on measurements on three plates with the spectrum of oxygen from tungsten oxide and four plates obtained with oxidized magnesium. The values reported by other investigators are shown in the Table for purposes of comparison. The latter values were obtained as a result of studies of the $O^{16}(d,p)O^{17}$ reaction as well as of the $F^{19}(d,\alpha)O^{17}$ reaction yielding the same final nucleus. For the group of protons corresponding to the transition of the O^{17} nucleus to the ground state we obtained an energy balance of the $O^{16}(d,p)O^{17}$ reaction equal to 1.88_5 Mev. The most reliable values in the literature are Q_0 = 1.93 Mev (Burrows and Powell[12]) and 1.918 Mev (Klema and Phillips[14]). The last was obtained by the method of magnetic analysis and

Table 2

Excitation levels of O^{17} (in Mev)

Group No.	Present invest.	Ref. 12	Ref.13
1	$0,89_3$	0,87	0,883
2	$3,00_5$	3,07	3,069
3	$3,85_3$	3,87	3,856

is given with greater accuracy than the former.

Lithium*

The targets for these investigations were prepared by depositing a layer of lithium oxide, obtained by burning metallic lithium in the air, on a copper support. These targets were bombarded by deuterons with $E_d \approx 3.7$-4.7 Mev. Two photographs of the lithium spectrum obtained with different deuteron energies are shown in Fig. 2 c and d. The corresponding microphotograms appear in Figs. 5 and 6.

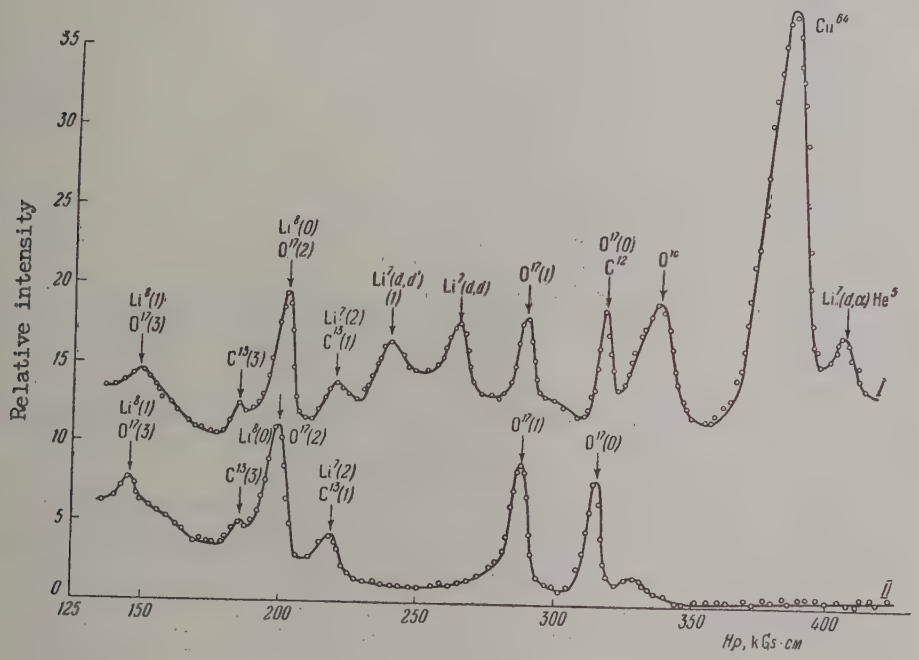

Fig. 5. Same as Fig. 4 but for lithium (E_d = 3.76 Mev).

It will be seen that these spectra exhibit appreciable differences as regards composition: in addition to deuterons elastically scattered from the copper, oxygen and lithium we have registered a number of groups of protons from the (d,p) reaction on Li^6, Li^7, O^{16} and C^{12}, a group of deuterons inelastically scattered from Li^7 and a group of α-particles.

In view of the fact that lithium occurs in the form of two isotopes, - Li^7 with an abundance of 92.48% and Li^6 having an abundance of 7.52% - we could identify the levels only through comparison with the more reliable data in the literature.

The energy level data for Li^7 derived by us from analysis of six photographic plates with lithium spectra are listed in Table 3. These data are juxtaposed with the results of other investigators who determined the energies of these levels in investigating the (d,p) as well as other nuclear reactions. The proton groups associated with the transitions of Li^{7*} to the ground and the first excited state of this nucleus are not discernible in our spectrograms. This is probably due to the relatively low abundance of the Li^6 isotope and

---

* V. A. Blinov, a student of Leningrad Polytechnical Institute, participated in the investigation of lithium.

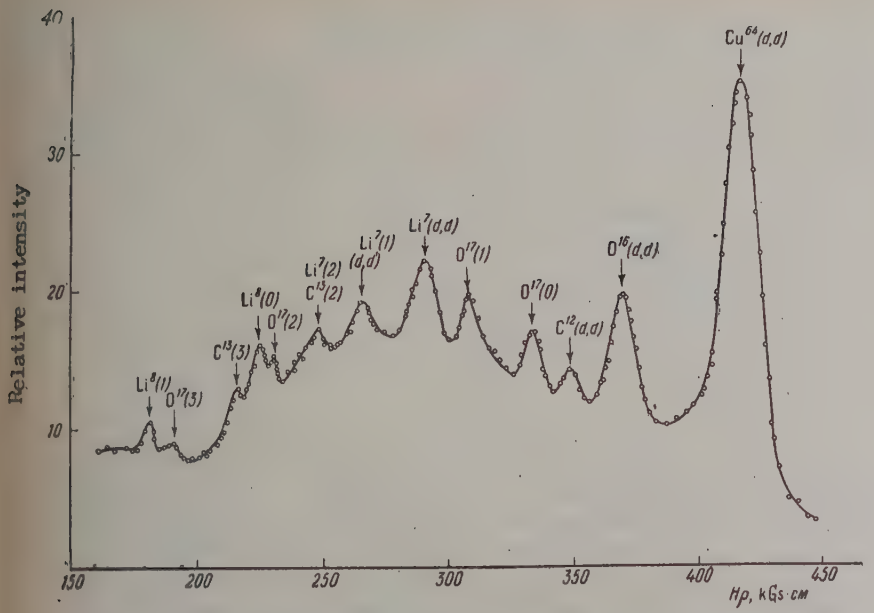

Fig. 6. Microphotogram of the lithium spectrum (E_d = 4.69 Mev) on uncovered portion of plate.

microphotograms and proved to be rather intense.

Table 3

Excitation levels of Li^7 (in Mev)

Group No.	Our results		Data of other investigators		
	Q	E*	E*	Reaction	
1	$-0,47_0$	$0,47_0$ from(d, d')	0,483 0,477 0,478	(d, p) γ-rays (p, p') & (d, d')	Ref. 1 Ref. 15 Ref. 16
2	$(0,58_0)$	$(4,45_4)$ from(d, p)	4,56 4,61	(p, p') (d, p)	Ref. 17 Ref. 18
3	$-4,51_0$	$6,53_0$ from(d, p)	6,56	(p, p')	Ref. 17

the small cross section of the $Li^6(d,p)Li^7$ reaction for these transitions. Hence for computing the levels of Li^7 we assumed the Q-value to be 5.020 Mev, as reported by Strait et al.[7] However, we determined the energy of the first excited level of Li^7 from a different type of reaction: inelastic scattering of deuterons from Li^7 nuclei in the ground state. The group of deuterons associated with the $Li^7(d,d')Li^{7*}$ reaction was clearly visible in all the

The Li^{7*} level at 6.53 Mev had previously been observed only in connection with the inelastic scattering of protons.[17] It was recorded from the $Li^6(d,p)Li^{7*}$ reaction for the first time in our experiments.[3]

The data on the levels of Li^8 obtained as a result of the $Li^7(d,p)Li^8$ reaction are summarized in Table 4. The proton group characterizing the transition of the Li^8 nucleus to the ground state was very intense. The Q-value for this reaction measured in our investigation is in good agreement with the data of a number of other investigators, using diverse experimental procedures. Our results definitely prove the existence of an excited level with $E^* = 1.0 \pm 0.2$ Mev in Li^8, hitherto regarded as somewhat doubtful.

At an energy of the bombarding deuterons of about 3.7 Mev, a group of particles effectively blocked by the foil appears in the lithium spectrum on the uncovered plate (at right in Fig. 5). Special control experiments using thick-emulsion photographic plates showed that this group consists of α-particles from the $Li^7(d,\alpha)He^5$ reaction. The energy of this reaction, as determined from analysis of five plates,

Table 4

Excitation levels of Li^8 (in Mev)

Group No.	Our invest.		Data of other investigators			
	Q	E*	Q	E*	Method	Investigators
0	$-0,18_3$	0	$-0,187$	0	Angular thresh.	Paul[19]
			$-0,188$	0	Magnetic spectrograph	Strait et al[7]
			$-0,192$	0	Electrostatic analyzer	Williamson et al[16]
1	$-1,16_0$	$0,97_7$	—	(1,0)	—	Gove & Harvey[20]

proved to be Q = 13.71_9Mev. The Q-values reported by earlier investigators vary between 13.43 and 14.3 Mev; these were determined by less accurate methods; consequently our value can be used for a more accurate evaluation of the mass of the He^5 nucleus. Assuming the values for the masses of the reacting nuclei given by Dzhelepov and Zyrianova[24] in their survey article, we obtain

$$M_{He^5} = 5.014353 \text{ amu.}$$

Boron

For the experiments with boron, the targets were prepared of finely powdered boron having a natural isotope composition (B^{10} - 18.45% and B^{11} - 81.55%) coated on copper foil. One of the photographs of the boron spectrum is shown in Fig. 2e. The corresponding microphotogram appears in Fig. 7. In it, curve I (section of plate not covered by aluminum foil) comprises three peaks due to deuterons elastically scattered from the copper and the contaminants, magnesium and oxygen. At this energy (4.153 Mev) of the bombarding deuterons, the group of deuterons elastically scattered from the boron proper coincided with the O^{17} (1) group. For determining the levels of boron we analyzed

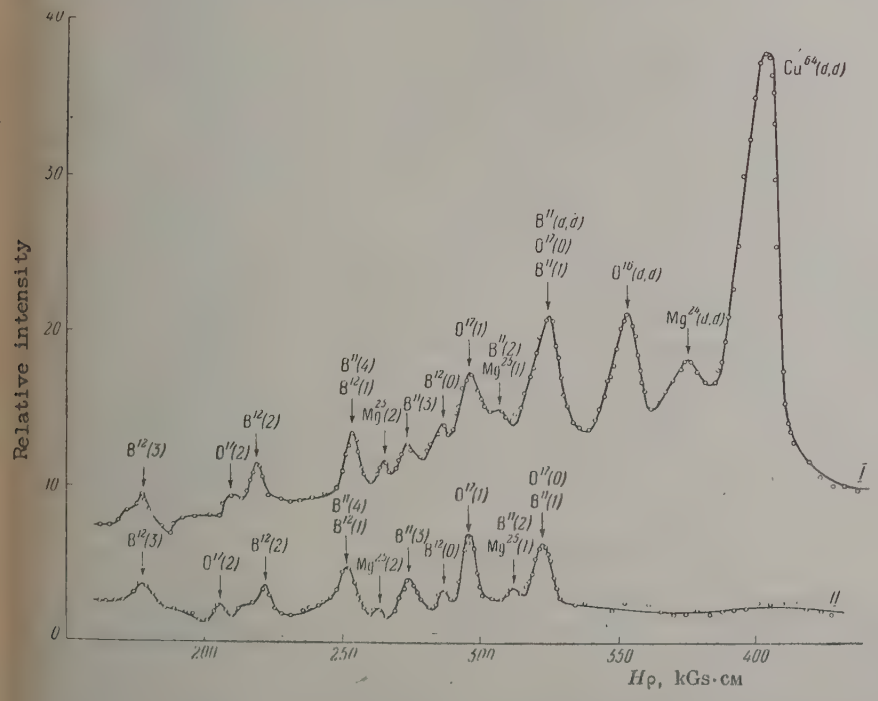

Fig. 7. Same as Fig. 4 but for boron (E_d = 4.153 Mev).

three plates with the spectrum of this element. In identifying the observed levels as belonging to B^{11} or B^{12} we also drew on the data of other investigators, based on experiments with enriched isotopes.

Table 5

Excitation levels of B^{11} (Q in Mev)

Group No.	Our data	Ref.25	Ref. 9
1	$2,44_5$	—	2,447
—	—	—	2,427
—	—	1,36	—
2	$(1,98_5)$	—	1,937
3	$0,84_5$	0,70	0,667
4	$0,27_8$	0,320	0,309

Table 6

Excitation levels of B^{12} (in Mev)

Group No.	Our data	Ref. 15	Ref. 28
1	$0,94_0$	0,950	0,951
2	$1,66_4$	1,65	1,674
—	—	1,82	—
3	$2,56_2$	—	2,618

The Q-values obtained by us for the $B^{10}(d,p)B^{11}$ reaction are listed in Table 5 together with the corresponding values reported by Bateson[25] and by Van Patter et al.[5] Our investigation comprised only the range of energies corresponding to the higher levels of B^{11}, hence Q-values and levels near the ground state do not appear in our spectrograms.

In Table 6 we list the levels of B^{12} resulting from the (d,p) reaction with the main boron isotope. Our data are juxtaposed with those of other authors, as collated by Ajzenberg and Lauritsen.[15]

The value of Q_0 for the $B^{11}(d,p)B^{12}$ reaction reported by Buechner et al[26] is $Q_0 = 1.136$ Mev. In our experiments we obtained a value of 1.10 Mev for the same reaction. Buechner et al also recorded a proton group corresponding to the first excited state of B^{12} ($E^* = 0.947$ Mev).

Our experiments confirmed the existence of two previously reported levels in B^{12}: $E^* = 0.94_0$ and 1.66_4 Mev. We did not observe the 1.82 Mev level in the (d,p) reaction. In addition to the above levels we also recorded a proton group characterizing a new level in boron. If this group is interpreted as a result of the (d,p) reaction on the main isotope, the energy of the corresponding product level of B^{12} comes out to be $E^* = 2.56_2$ Mev.

Elkind, in an article[28] devoted to an investigation of the levels of aluminum and boron and published after the present report was first submitted to the editors, reports recording the levels of B^{12} detected in our experiments and, in addition, two new higher-energy excited levels (in Elkind's experiments $E_d = 8.5$ Mev). As in our case, in Elkind's investigation no level with $E^* = 1.82$ in B^{12} was observed from the (d,p) reaction. Hence either the very existence of this level must be regarded as open to question or it must be assumed that the transition to this state in the (d,p) reaction is highly forbidden.

Magnesium

We prepared the magnesium targets by evaporation of natural magnesium onto copper foil supports. These targets were appreciably thicker than those for the above-listed elements and were noticeably oxidized. One of the spectrum photographs is reproduced in Fig. 2f. A section of the microphotogram from this plate is shown in Fig. 8.

It will be seen that the spectrum of magnesium is considerably more complex than the spectra of the preceding elements. It is

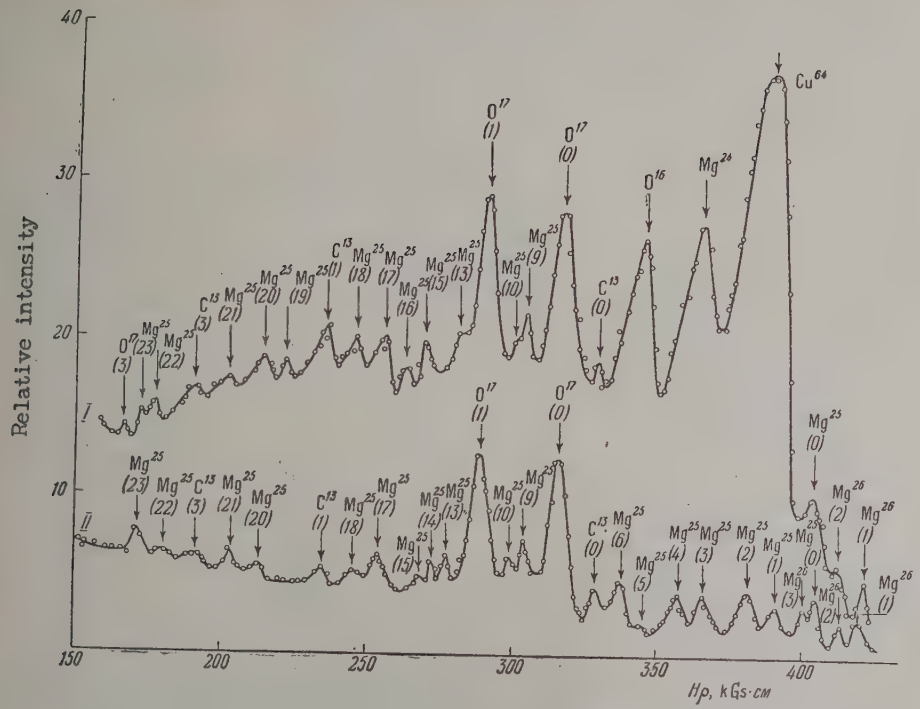

Fig. 8. Same as Fig. 4 but for magnesium (E_d = 4.04 Mev).

interesting to contrast the right-hand parts of the two curves: Curve II (proton spectrum of magnesium) contains a whole series of low but clearly resolved proton peaks in the region dominated in Curve I (spectrum of all the charged particles) by intense peaks of deuterons elastically scattered from the copper, magnesium and oxygen. Thus it is evident that our aluminum foil filter made it possible not only to discriminate between different types of particles but also to discern the weak proton group structure otherwise masked by the strong deuteron background.

Identification of the levels in the case of magnesium was also complicated by the presence of three isotopes in the natural product (relative abundances: Mg^{24} - 78.60%, Mg^{25} - 10.11% and Mg^{26} - 11.29%). Inasmuch as normally the cross section of the (d,p) reaction does not exhibit any pronounced anomalies in going from one isotope to the next, it would be logical to ascribe the observed levels to the reaction involving the main isotope: $Mg^{24}(d,p)Mg^{25}$. However, the relative intensities of the different groups can vary markedly with changes in the bombarding deuteron energy, hence this criterion is not always valid.

A pertinent example is furnished by the observed groups of protons that are faster than the protons associated with the transition of Mg^{25} to the ground state. These fast proton groups are characteristic of the levels of Mg^{26}, in which the transition to the ground state is accompanied by a greater liberation of energy than in the case of Mg^{25}: Q_0 = 8.88 Mev.[29]

In Table 7 we list the levels of Mg^{25} determined from analysis of six plates with magnesium spectra together with the data of Endt et al,[30] who studied the products of the (d,p) reaction with separate magnesium isotopes by means of a magnetic spectrograph. Comparison

of the data (within the interval of excitation energies where such comparison is possible) shows that all the levels observed by us are results of the reaction on the main isotope with the exception of the three above-mentioned levels of Mg^{26}).

Table 7

Excitation levels of Mg^{25} (in Mev)

Group No.	Our data	Endt et al Ref.30	Group No.	Our data
1	$0,50_3$	0,582	13	$4,62_2$
2	$0,99_8$	0,976	14	$4,85_7$
3	$(1,58_1)$	1,612	15	$4,96_0$
4	$2,02_2$	1,957	16	$5,14_7$
5	$(2,47_1)$	2,565	17	$5,34_1$
6	$2,69_5$	2,742	18	$5,53_6$
7	$(2,87_1)$	2,806	19	$6,08_7$
8	—	3,405	20	$6,24_9$
9	$3,92_4$	3,899	21	$6,54_2$
10	$4,03_0$	3,972	22	$6,94_8$
11	—	(4,265)	23	$7,07_4$
12	—	(4,421)		

In addition to the levels of Mg^{25} observed by Endt et al[30] from the (d,p) reaction we recorded a number of new, higher levels (Groups 13-23). By analogy with the preceding, lower groups, these new groups may be identified as resulting from the (d,p) reaction with the main isotope of magnesium.

Some of these levels ($E^* = 4.857$, 5.536 and 6.948 Mev) have been detected in investigating a different type of reaction - $Al^{27}(d,\alpha)Mg^{25}$ - by Schelberg et al[40] and Toops et al.[41] Holt and Marsham[42] (report published after the appearance of our preliminary article[2]) also investigated the products of the $Mg^{24}(d,p)Mg^{25}$ reaction. They determined the proton energies by the method of absorbing filters. The range of excitation energies used by Holt and Marsham was greater than in our experiments ($E_d = 8$ Mev). In the region of groups 13-23 (Table 7) they recorded four levels of Mg^{25}. One of these, the level at 4.62 Mev, coincides with the level of our group 13.

For the transition of the Mg^{25} nucleus to the ground state we derived a value of $Q_o = 5.022$ Mev. The previously published values are 5.097 (Van Patter et al[31]) and 5.03 (Allan and Wilkinson[32]).

Aluminum

The target in our investigations of the $Al^{27}(d,p)Al^{28}$ reaction was aluminum foil having a superficial density of up to 0.46 mg/cm^2. The spectra of Al^{28} were studied at two energies of the bombarding deuterons - about 3 and 4 Mev. Two of the photographs are reproduced in Fig. 2g and h: the corresponding microphotograms are shown in Fig. 9. We see that Al^{28} has a very dense system of levels. The highest peak (Al^{27}) is due to elastic scattering of neutrons from aluminum nuclei. The other peaks (identified by Al^{28}) are due to protons from the $Al^{27}(d,p)Al^{28}$ reaction, with the sole exception of the peak in Curve II marked Mg^{28}. This group should be attributed to the first excited level of Mg^{25} ($E^* = 0.5$ Mev), formed as a result of the $Al^{27}(d,\alpha)Mg^{25}$ reaction. This group is observed at $E_d \simeq 4$ Mev, but disappears when the deuteron energy is reduced to 3 Mev.

The mean values of the energy of the excited levels of Al^{28}, obtained through analysis of nine photographs of aluminum spectra, are listed in Table 8. Our results are compared in the table with those of Keller[33] who investigated the same reaction in a somewhat wider range of bombardment energies but with appreciably lower accuracy and resolving power of the instrument. Hence Keller recorded 14 proton groups, while we were able to detect 28 groups in the narrower energy interval. [Table 8 - on page 264]

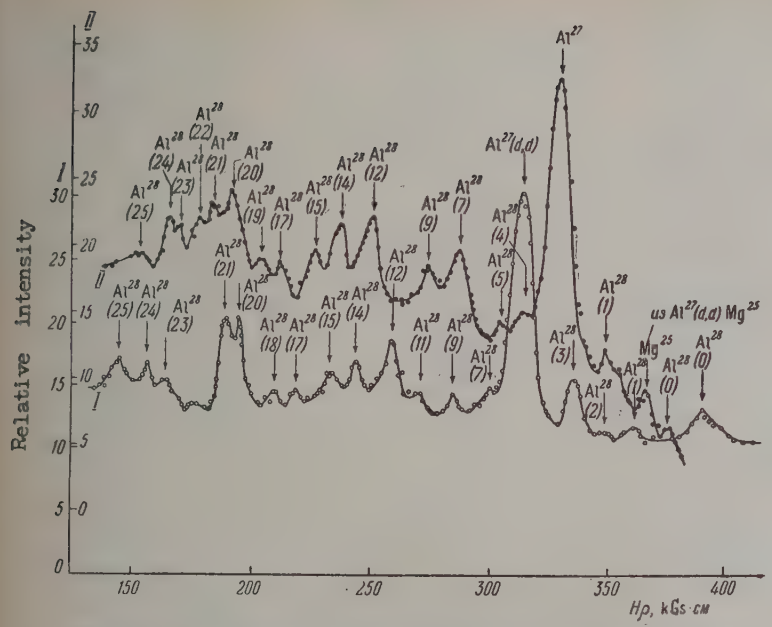

Fig. 9. Microphotograms of aluminum spectra at different deuteron energies: I - E_d = 3.048 Mev, II - E_d = 4.308 Mev.

In the fourth column of the table we list, for purposes of comparison, the data reported by Enge, Buechner and Sperduto.[34] Their report, which was published while we were working on aluminum, gives an even more detailed picture of the levels of Al^{28} and lists 50 levels of the nucleus (only part of them are given in Table 8). We feel, however, that some of these are doubtful, being based on very weakly evinced peaks. The level scheme of Enge et al breaks off at a lower excitation energy than Keller's and ours.

We found an energy value of $Q_o = 5.47_5$ Mev for the $Al^{27}(d,p)Al^{28}$ reaction. Keller reports $Q_o = 5.53$ Mev; Enge et al, $Q_o = 5.494$ Mev.

Comparison of the data in Table 8 shows that in addition to the levels detected earlier by other investigators we observed four new levels in Al^{28} (proton groups 22, 24, 25 and 27). There is some uncertainty as regards identification of the last level. The low intensity of the group makes it impossible to wholly exclude the possibility of its belonging to Al^{27}.

The 7.59_9 Mev level was also observed for the first time from the (d,p) reaction in our experiments. A near-lying level of Al^{28} was known previously from the (Al^{27} + n) reaction.[35]

Silicon

The targets were prepared of natural silicon (Si^{28} - 92.27%, Si^{29} - 4.68% and Si^{30} - 3.05%). The silicon was finely ground in a mortar and a suspension of the lightest particles in alcohol was coated on a copper foil support. The targets were bombarded with deuterons of energies up to 4.4 Mev. One of the photographs of the silicon spectrum is reproduced in Fig. 2i; the corresponding microphotogram is shown in Fig. 10. The three deuteron groups (d,d) are due to deuterons elastically scattered from the copper, silicon and oxygen. The complex nature of the proton spectrum is evinced by Curve II. Six photographic plates were analyzed in determining the levels of silicon. The analytic results are listed and compared with the data of Van Patter and Buechner[36] in Table 9. The investigation of Van Patter and Buechner is the latest and most accurate of a series of studies devoted to the levels of silicon. The (d,p) reaction was studied using enriched silicon isotopes by the method of magnetic analysis. The energy levels of Si^{29}, Si^{30} and Si^{31} were determined

Table 8

Excitation levels of Al^{28} (in Mev)

Group No.	Our data	Ref. 33	Ref. 34
1	$0,98_0$	1,04	0,974 1,015
2	$1,59_7$	1,58	1,625
3	$2,15_2$	2,17	2,137
4	$2,57_4$	2,52	2,578
5	$2,92_9$	—	2,980
6	$3,33_4$	—	3,342
7	$3,52_0$	3,47	3,532
8	$(3,74_7)$	—	3,695
9	$3,93_4$	3,98	3,932
10	$4,27_7$	—	4,307
11	$4,46_9$	—	4,457
12	$4,72_0$	—	4,759
13	$(4,88_3)$	4,83	4,898
14	$5,17_0$	5,16	5,169
15	$5,39_6$	—	5,372
16	$5,64_3$	—	5,735
17	$5,78_4$	5,80	5,792
18	$5,96_8$	—	6,011
19	$6,14_8$	6,10	6,190
20	$6,29_8$	—	6,307
21	$6,43_8$	6,40	—
22	$6,64_1$	—	—
23	$6,85_5$	6,90	—
24	$7,01_3$	—	—
25	$7,19_7$	—	—
—	—	7,40	—
26	$(7,59_9)$	—	—
27	$7,89_6$	—	—
—	—	8,50	—

with high accuracy but in a comparatively narrow range of excitation energies. In the interval where comparable data are available all the levels observed by us proved to be due to the deuteron reaction on the main isotope: $Si^{28}(d,p)Si^{29}$. Hence we attributed the groups 11-17, observed for the first time in our experiments, to the same reaction. Level 15 was detected for the first time from the (d,p) reaction by us. This level may, however, be identical with the Si^{29} level of approximately equal energy previously observed by Freier et al[37] in studying the (Si^{28} + n) reaction.

In the investigation of silicon we used relatively thick targets, which resulted in somewhat greater experimental errors than in the other cases: the deviations of the individual values from the mean attained 40-50 kev.

We found an energy value for the investigated reaction of $Q_0 = 6.22_9$ Mev; Van Patter and Buechner give $Q_0 = 6.246$ Mev.

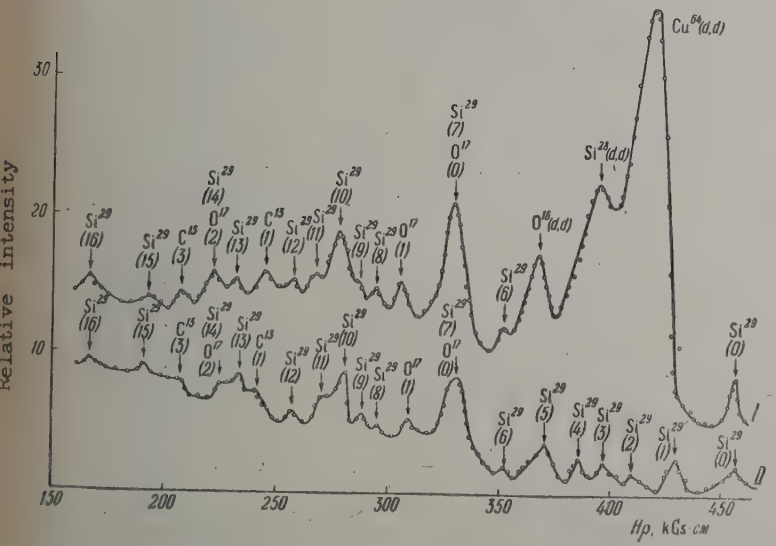

Fig. 10. Microphotogram of silicon spectrum (E_d = 4.44 Mev): I - spectrum on uncovered part of plate; II - spectrum on covered part.

Table 9

Excitation levels of Si^{29} (in Mev)

Group No.	Our data	Ref. 36
1	$1,23_7$	1,278
2	$2,03_8$	2,027
3	$2,41_6$	2,426
4	$3,08_3$	3,070
5	$3,66_2$	3,623
6	$4,22_3$	4,078
7	$4,93_1$	4,840 4,897 4,934
8	$5,94_4$	5,946
9	$6,13_8$	6,105
10	$6,45_3$	6,380
11	$6,72_8$	
12	$7,00_0$	
13	$7,57_7$	—
14	$7,82_0$	
15	$8,35_4$	—
16	$8,83_2$	
17	$(9,11_2)$	

Discussion of Results

Analysis of the systems of levels of light nuclei shows that of the diverse reactions which may occur in the bombardment of these nuclei by deuterons of medium energies the most likely is the (d,p) reaction. In the entire series of experiments we recorded over 100 levels in the different nuclei studied. Only in one case did we observe the reaction of inelastic scattering of deuterons (in the lithium spectrum) and in two cases, the (d,α) reaction (in lithium and aluminum). In all the other cases the observed levels were obtained as a result of the (d,p) reaction.

In the bombardment of nuclei by deuterons, seven different types of reactions could occur: (d,n), (d,pn), (d,p), (d,d'), (d,α), (d,He^3) and (d,H^3). The first two were virtually not recorded in our experiments. The (d,α) reaction is limited to a greater extent than the others by the height of the barrier for the emitted particles. This circumstance reduces the number of possible states of the final nucleus, i.e., lowers the probability of this type of reaction.

The last two reactions and the (d,d') reaction, if we assume it to pass through an intermediate, compound nucleus stage, are unlikely from energy considerations. The investigation of the angular distribution of deuterons inelastically scattered from magnesium, carried out by Mullin and Guth,[38] showed that inelastic scattering of deuterons probably involves a different process (rather than the formation of a compound nucleus): better agreement with experiment is obtained if the scattering is regarded as a process of electromagnetic excitation of the nucleus by the field of the charged particle. The low frequency of the (d,d') reaction observed in our experiments may be due to the disadvantageous observation angle (about 110°) and the relatively low energy of the bombarding deuterons. It must be noted that the investigations in which large inelastic deuteron scattering cross sections were noted were all carried out at high deuteron energies - 7.5 to 14 Mev.

It will readily be seen that of the investigated nine nuclei - Li^7, Li^8, B^{11}, B^{12}, C^{13}, O^{17}, Mg^{25}, Al^{28} and Si^{29} - the last three have a relatively complex energy spectrum, while the others exhibit a much simpler one. In connection with this it may be noted that in the first six nuclei the second neutron shell (N = 8) is being filled, while in the last three, the third shell begins to fill. Analysis of the positions of the first excited levels of light nuclei in the investigated N interval shows that the beginning of filling of the second neutron shell is characterized by an excitation energy of the first level on the order of 0.5-2.5 Mev. As the second shell becomes filled (i.e. as $N \rightarrow 8$), the first level excitation energy of a number of nuclei (for example, C^{13} and O^{15}) increases. The filled shell condition is characterized by an exceptionally high energy of the first excited level: thus, C^{14}, N^{15} and O^{16} have their first excited level at 5-6 Mev. At the point where the third neutron shell begins to fill we find a sharp drop in the excitation energy of the first level of most nuclei in this N range.

Thus the regularities noted in the range of heavier nuclei[39] are also apparent in the examined N range. The above may help explain the complexity of the spectra of the Mg^{25}, Al^{28} and Si^{29} nuclei, in which the third neutron shell is beginning to fill and which are, therefore, characterized by easier deformability and readier excitation.

The present investigation owes its inception to the initiative of the late P. I. Lukirski. Lukirski's interest in the work and many valuable suggestions have been of inestimable aid to the writer. The writer is also obligated to Iu. A. Nemilov for his advice and support in connection with the investigation.

"V. G. Khlopin" Radium Institute of the
Academy of Sciences of the USSR

References

1. W.Büchner, E.Strait et al., Phys. Rev., 74, 1569 (1948).
2. L.Khromchenko, Doklady AN SSSR, 93, 451 (1953).
3. L.Khromchenko, Doklady AN SSSR, 94, 1037 (1954).
4. L.Khromchenko, Doklady AN SSSR, 98, 761 (1954).
5. L.Khromchenko & V.Blinof, Zhur. eksp. i teor. fiz.,28, 741 (1955).
6. Iu.Nemilov, Izv. AN SSSR, Ser. fiz., 14, 319 (1950).
7. E.Strait, D.Van Patter et al., Phys. Rev., 81, 747 (1951).
8. K.Ogata & H.Matsuda, Phys. Rev., 89, 27 (1953).
9. D.Van Patter, A.Sperduto & W.Büchner, Phys. Rev., 82, 248 (1951).
10. T.Rotblatt, Nature, 167, 1027 (1951).
11. D.Cowie, N. Heydenburg & G.Phillips, Phys. Rev., 87, 304 (1952).
12. H.Burrows & C.Powell, Proc. Roy. Soc., 209, 479 (1951).
13. H.Watson & W.Büchner, Phys. Rev., 88, 1324 (1952).
14. E.Klema & G.Phillips, Phys. Rev., 86, 951 (1952).
15. F.Ajzenberg & T.Lauritsen, Rev. Mod. Phys., 24, 321 (1952).
16. R.Williamson, C.Browne et al., Phys. Rev., 84, 731 (1951).
17. W.Frenzen & J.Likely, Phys. Rev., 87, 667 (1952).
18. R.Gelinas & S.Hanna, Phys. Rev., 86, 253 (1952).
19. E.Paul, Phil. Mag., 41, 942 (1950).
20. H.Gove & J.Harvey, Phys. Rev., 82, 658 (1951).
21. J.Williams, W.Shepherd & R.Haxby, Phys. Rev., 52, 390 (1937).
22. G.Lattes, P.Fowler & P.Cüer, Proc. Roy. Soc., 59A, 883 (1947).
23. A.French & P.Treacy, Proc. Roy. Soc., 64A, 452 (1951).
24. B.Dzhelepov & L.Zyrianova, Usp. fiz. nauk, 47, 512 (1952).
25. W. Bateson, Phys. Rev., 80. 982 (1950).
26. W.Büchner, D.Van Patter et al., Phys. Rev., 79, 262 (1950).
27. W.MacMinn, M.Sampson & V.Rasmussen, Phys. Rev., 84, 963 (1951).
28. M.Elkind, Phys. Rev., 92, 127 (1953).
29. P.Endt, T.Haffner & D.Van Patter, Phys. Rev., 86, 518 (1952).
30. P.Endt, H.Enge et al, Phys. Rev., 87, 27 (1952).
31. D.Van Patter, Sperduto et al., Phys. Rev., 85, 142 (1952).
32. H.Allan & C.Wilkinson, Proc. Roy. Soc., A194, 131 (1948).
33. K.Keller, Phys. Rev., 84, 884 (1951).
34. H.Enge, W.Büchner & A.Sperduto, Phys. Rev., 88, 963 (1953).
35. D.Alburger & E.Haffner, Rev. Mod. Phys., 22, 373 (1950).
36. D.Van Patter & W.Büchner, Phys. Rev., 87, 51 (1952).
37. G.Freier, M.Fulk et al., Phys. Rev., 78, 508 (1950).
38. C.Mullin & E.Guth, Phys. Rev., 82, 141 (1951).
39. L.Sliv & L.Peker, Doklady AN SSSR, 94, 849 (1954).
40. A.Schelberg, M.Sampson & R.Cochran, Phys. Rev., 80, 574 (1950).
41. E.Toops, M.Sampson & F.Steigert, Phys. Rev., 85, 280 (1952).
42. J.Holt & T.Marsham, Proc. Phys. Soc., A66, 258 (1953).

* * * *

THE GAMMA-SPECTRUM OF Ir^{192}

- M. P. Glazunov, B. S. Dzhelepov, and Iu. V. Khol'nov

The γ-radiation from Ir^{192} is characterized by a highly complex spectrum. It has been established that Ir^{192} emits γ-quanta of no less than fourteen different energies in the 100 to 1000 kev interval.

A survey of the experimental data on the emission from Ir^{192} is comprised in an article by Bashilov, Anton'eva and Dzhelepov,[1] who also give a tentative decay scheme and a full bibliography of contributions published prior to 1952. Since that date three more investigations devoted to the radiation from this radioactive isotope have appeared in scientific literature.[2,3,4] These results, however, have not necessitated any major modification of the proposed decay scheme.

Muller et al[3] give the results of new precision measurements of the energies of eleven γ-rays from Ir^{192} (to 612.87 kev). In the investigation of Pringle and associates[2,4] the γ-spectrum of Ir^{192} was studied by means of a scintillation spectrometer; the investigators determined the relative intensities of the hardest γ-lines: 605, 788, 883, 1080 and 1210 kev.

The energies and relative intensities of the γ-lines investigated by Bashilov et al[1] and Pringle et al[4] are listed in the accompanying table.

ENERGIES AND RELATIVE INTENSITIES OF THE GAMMA-LINES OF Ir^{192}

Ref. 1		Ref. 4		Our measurements				
					Intensities			
Energy γ-line, kev	Relative Intensity	Energy γ-line, kev	Relative Intensity	Energy γ-line, kev	Series I 32 cm Hg	Series II 17 cm Hg	Series III 8 cm Hg	Assumed best value
206±1	0,27							
280±3	—							
296±1	3,0	311	—	(314)	7,56	9,17	8,97	9,09
308±2	3,1							
316±1	7,7							
417±2	—	—	—	—	—	—	—	—
468±1	4,1	471	—	466	4,62	4,79	4,23	4,58
486±4	—	—	—	—	—	—	—	—
589±2	0,33							
605±1	1,0	605	1,74	(612)	1,74	1,74	1,74	1,74
613±2	0,41							
—	—	788	3,3	788?	<0,002	—	—	<0,002
880±4	—	883	1,6	898	0,037	0,037	—	0,037
—	—	1080	0,6	1053	0,0085	0,0122	—	0,0098
—	—	1210	0,1	—	—	—	—	—

The purpose of the present investigation was to determine the relative intensities of the hard γ-lines and a group of soft γ-lines by means of the Ritron.[5] An Ir^{192} source of approximately 0.1 gm in the form of a disk 1 cm in diameter was used in the experiments.

Original report presented in February 1954 at the Conference on Beta- and Gamma- Spectroscopy; the present article has been amplified by references to the investigations of Refs. 4 & 5 published subsequent to that date.

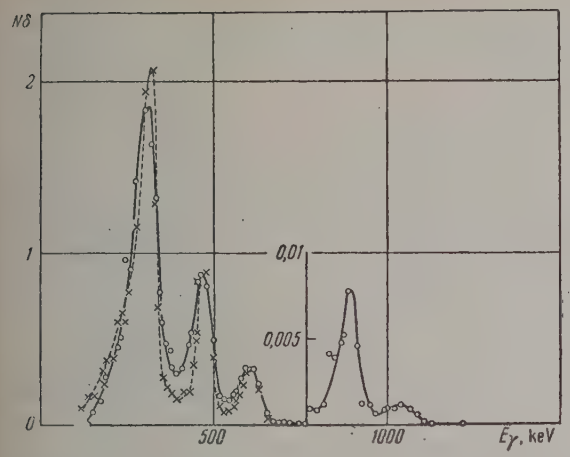

Gamma-spectrum of Ir^{192}: o - results of 1st series of measurements; x - results of 3rd series of measurements.

In order to allow for the influence of the scattering of recoil electrons in the gas filling the instrument we carried out three series of experiments at different pressures of the helium + methane mixture used (32, 17 and 8 cm Hg).

The results of the first and third series of measurements are shown in the accompanying figure. The spectrum is shown in processed form: the experimental curves reduced to equal energy intervals and appropriate corrections made for variation of the spectral sensitivity of the Ritron, absorption in the source and the energy dependence of the counter efficiency. The curves were adjusted to coincide in height at E = 605 kev. It will be noted that the hard 898 and 1053 kev lines are clearly resolved.

The 206, 280, 296, 308 and 316 kev and the 589, 605 and 613 kev lines were not separated but appear as two composite groups with effective energies of 314 and 612 kev, respectively.

Our experimental results are summarized in the right-hand side of the table.

To facilitate comparison with the data of Ref. 1, the total intensity of the group of lines of energies 589, 605 and 613 has been taken equal to 1.74. The total intensity of the group of softer lines was determined from the results of the second and third series of measurements in which the influence of the gas filling the instrument was weaker. The intensities of the remaining γ-lines were arrived at by averaging the results of the first and second series of measurements.

The intensity of the 880 kev line, detected for the first time in the investigation of Ref. 1, proved to be appreciably greater than indicated in the decay scheme proposed in Ref. 1. The 1210 kev line, detected by Pringle et al,[4] can readily be fitted into that decay scheme, but the 1053 kev line discovered by us and confirmed by Pringle et al[4] necessitates the introduction of an additional level. In a series of check experiments using higher transmission conditions we did not detect any γ-lines with an intensity above $2 \cdot 10^{-4}$ quanta per disintegration (our detection threshold) in the 1600 to 2500 kev region.

Radium Institute of the
Academy of Sciences of the USSR

References

1. A.Bashilov, N. Anton'eva & B.Dzhelepov, Izv. AN SSSR,Ser.fiz., 16,264 (1952).
2. K.Roulston & R.Pringle, Phys. Rev., 87, 930 (1952).
3. D.Müller, H.Hoyt & J.DuMond, Phys. Rev., 88, 775 (1954).
4. R.Pringle, W.Turchinetz & H.Taylor, Phys. Rev., 95, 115 (1954).
5. B.Dzhelepov, N.Zhukovski & Iu.Khol'nov, Izv. AN SSSR, Ser. fiz., 18, 599 (1954). Trans. Bulletin, Vol. 18, No. 5, p. 285.

GAMMA-RADIATION FROM Eu^{152} AND Eu^{154}

- B. S. Dzhelepov, N. N. Zhukovski and V. G. Nedovesov

When europium is irradiated with thermal neutrons there are obtained two long-period isotopes[1-3] of mass numbers 152 and 154, having roughly equal periods (13 and 16 years, respectively);[4] the decay of both isotopes is accompanied by γ-radiation.

We investigated this radiation by means of the Elotron,[5] a γ-spectrometer with improved focusing, utilizing recoil electrons.

The experimental curve obtained with a cellophane target 17 μ thick (superficial density - 1.88 mg/cm^2) is reproduced in Fig. 1. The vertical scale is laid off in coincidences per unit time (N/min). Nine lines stand out clearly in the record; in addition there is a distinct rise above the background in the region of $H\rho$ = 2200-2900 Gs·cm. An investigation of this spectrum interval using a 50 μ thick target confirmed the presence of one or more γ-lines in this interval (points 3 in figure).

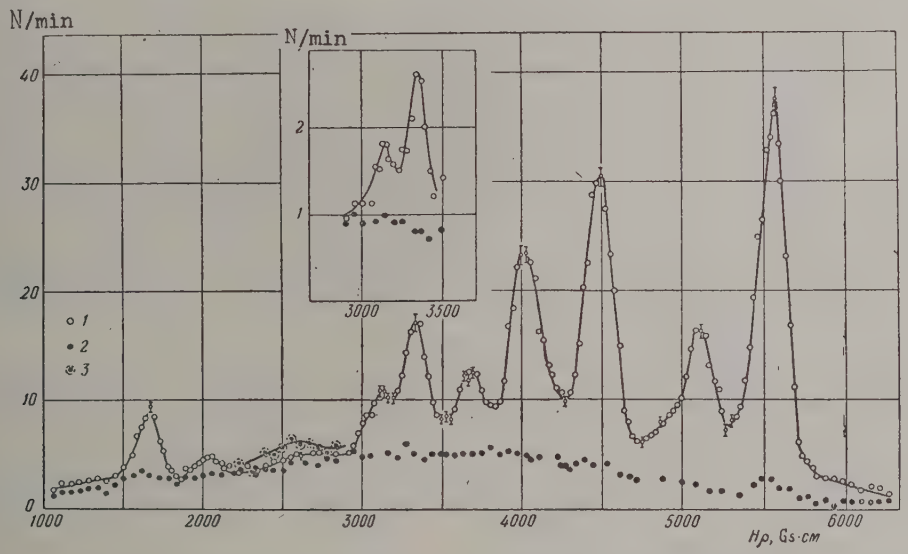

Fig. 1. Gamma-spectrum of Eu^{152} and Eu^{154} obtained on the Elotron with 17 μ thick cellophane target: 1 - coincidences with target in beam; 2 - with target out of beam (background); 3 - with 50 μ target in beam.

A special series of measurements was made in the 2900 to 3500 Gs·cm region under conditions of enhanced resolution of the instrument in order to secure better separation of the two lines in this region. The results are shown in the insert.

To facilitate determining the relative intensities of the γ-lines the $Eu^{152,154}$ spectrum was also investigated on the Ritron[6] whose spectral sensitivity is known.

The curves of Fig. 2 show the spectra of Eu^{152} and Eu^{154} in processed form, i.e., after allowing for the background, converting to equal energy intervals, and introducing the appropriate corrections for absorption in the window of the instrument (2 mm brass) (it was

not necessary to correct for absorption in the source inasmuch as attenuation of the beam in the source and source container is negligibly small - about 0.5%); corrections for variation in counter efficiency were made in determining the relative intensities of the γ-lines.

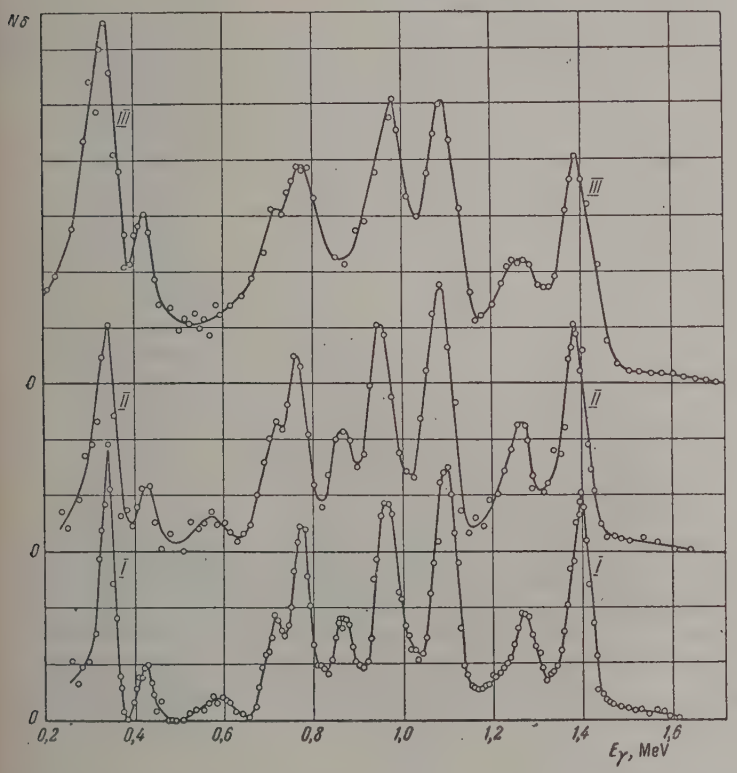

Fig. 2. Gamma-spectrum of Eu^{152} & Eu^{154} in processed form: I - recorded on the Elotron with 17 μ cellophane target; II - same but with 50 μ thick target; III - recorded on the Ritron with 50 μ thick target. Ordinates are numbers of -quanta reduced to equal energy intervals.

Curves I and II were obtained with the Elotron using 17 and 50 μ thick cellophane targets, respectively; curve III was obtained on the Ritron under the usual conditions employed with this instrument.

It will be seen from the figure that the Elotron has a higher resolution as compared with the Ritron; the transmission of the instruments is of the same order.

The curves I and II were resolved into individual lines with the aid of calibration γ-lines from Co^{60}, Zn^{65} and ThC" recorded specifically for this purpose on the Elotron under the same conditions as the europium spectra. Curve III was separated into its components by means of the calibration lines given in Ref. 6.

The ratios of the areas under the individual peaks in the spectra obtained on the Elotron and the Ritron are equal within the limits of the experimental error (i.e., to within 5-6%); hence the spectral sensitivity values calculated for the Ritron can be used for the Elotron as well.[6]

The values of the energy and relative intensities of the γ-lines of Eu^{152} and Eu^{154} are listed in the accompanying table. We believe the relative intensities have been measured for the first time in the present investigation.

The most reliable relative intensity values are those obtained with the 17 μ thick target.

All the observed γ-lines in the spectrum of Eu^{152} and Eu^{154} have been reported previously. Our energy values for the γ-rays are in good agreement with the results of a number of investigators;[7-11] the 1086 and 1116 kev lines, observed by Cork et al[8] and Katz and Lee[12], were not resolved by us in view of the inadequate resolution of our instrument.

Relative intensities of the gamma-lines of Eu^{152} & 154

E_γ from our measurements, kev	Elotron				Ritron		Values of E_γ determined by observation of conversion electrons	
	17 μ target		50 μ target		50μ target			
	area under contour	relat. intens.	area under contour	relat. intens.	area under contour	relat. intens.	Shull [7]	Cork et al [8]
341	47	0,86	48	0,87	53	0;86	342	337; 344
427	8	0,14	12	0,20	18	0,31	416; 442	408; 412; 448
593	7	0,10	9	0,15				584; 587; 608; 612; 720,4
717	14	0,21	62	0,89	—	—	772; 774	778
779	43	0,60						
871	25	0,34	24	0,33				868; 871
958	73	0,93	72	0,92	75	0,93	959	963; 964
1106	101	1,19	104	1,22	106	1,21	1082	1086; 1116
1281	41	0,43	43	0,46	39	0,41	—	—
1409	100	1,00	100	1,00	100	1,00	1402	—

According to Cork et al,[8] there are four weak lines in the 550-650 kev interval (see table). In this region we obtained a rise in the curve above the level of the background, indicating that these lines exist; their total intensity is listed in the table opposite provisionally assumed value of $h\nu = 593$ kev.

In view of the fact that the activity periods of the two isotopes of europium are nearly equal it is impossible to identify the γ-rays as belonging to one or the other isotope by decay measurements. In order to determine which γ-rays accompany the disintegration of each of the isotopes it would be necessary to investigate sources consisting entirely of the separate isotopes or at least greatly enriched with one of them. There are, however, indications[12] that the 344 kev line is associated with the decay of Eu^{152} and that the 1116 kev line accompanies the disintegration of Eu^{154}.

"V. G. Khlopin" Radium Institute of
the Academy of Sciences of the USSR

References

1. K.Fajans & D.Steward, Phys. Rev., 56, 625 (1939).
2. R.Hayden, J.Reynolds & M.Inghram, Phys. Rev., 75, 1500 (1949).
3. M.Inghram & R.Hayden, Phys. Rev., 71, 130 (1947).
4. D.Karraker, R.Hayden & M.Inghram, Phys.Rev., 87, 901 (1952).
5. B.Dzhelepov, N.Zhukovski, A.Karamian & S.Shestopalova, Izv. AN SSSR, Ser. fiz., 17, 518 (1953)
6. B.Dzhelepov, N.Zhukovski & Iu.Khol'nov, Izv. AN SSSR, Ser.fiz., 18, 599 (1954) Trans. BULLETIN, Vol. 18, No. 5, p. 285.
7. F.Shull, Phys. Rev., 74, 917 (1948).
8. J.Cork, H.Keller, W.Rutledge & A.Stoddard, Phys.Rev., 77, 848 (1950).
9. R.Hill & L.Shepard, Proc. Phys. Soc., 63A, 126 (1950).
10. L.Shavtalov, Zhur. eksp. i teor. fiz., 23, 611 (1952).
11. B.Kettel, ORNL - 607, 50 (1950).
12. R.Katz & M.Lee, Phys. Rev., 85, 1038 (1952).
13. H.Keller & J.Cork, Phys. Rev., 84, 1079 (1951).

INVESTIGATION OF CERTAIN CASES OF ANGULAR CORRELATION

- A. P. Grinberg and I. Kh. Lemberg

β-γ Angular Correlation in the $Sb^{124} \rightarrow Te^{124}$ Transition

1. Introduction

In many cases of β-decay the ejection of the β-particle from the nucleus is accompanied by the emission of γ-quanta. Investigation of the variation of the number of β-γ coincidences with the angle θ between the directions of emission of the β-particles and γ-quanta at different β-particle energies (i.e., experimental determination of the β-γ correlation function)can yield certain information regarding the quantum characteristics (spins and parities) of the nuclear levels involved, the degree of forbiddenness of the β-transition and the type of interaction between nucleons and light particles in β-decay.[1] An experiment in which the energy of the β-particles entering the counter is limited to a narrow interval (E_1 to $E_1 - \Delta E$) gives the so-called differential β-γ correlation function. If in a given case the β-γ coincidence distribution is anisotropic, the highest degree of anisotropy will be observed at $E_1 \approx E_{ep}$ (E_{ep} is the end-point energy of the β-spectrum).

Depending on the experimental conditions the differential β-γ correlation function will be obtained either in the form $W(\theta)$ with $E_1 = \text{const}$, or in the form $W(\theta) = f(E_1)$ with $\theta = \text{const}$. In order to enhance the experimental accuracy it is expedient to select $E_1 \approx E_{ep}$ in the first case and $\theta = 180^\circ$ in the second.

The number of cases in which anisotropy in the distribution of β-γ coincidences has been observed in correlation measurements is still very small. However, pronounced anisotropy is known to obtain in the case of the β-transition of Sb^{124} (60 day) to Te^{124}.

Beta-gamma correlation for Sb^{124} has been studied by a number of investigators. The integral β-γ correlation function has been determined in the investigations of Refs. 2-5. The results of these investigations are generally in good agreement. The most detailed (at 10° intervals) curve for $W(\theta)$ was recorded by Darby.[4] He found that in recording β-particles with $E > 0.9$ Mev, $W(\theta) = 1 - 0.23 \cos^2 \theta$

The differential β-γ correlation function for Sb^{124} was studied by Stevenson and Deutsch[1] and Darby.[4] The former determined $W(180^\circ) = f(E_1)$ in the region $E_1 \approx 1$-2 Mev by means of a thin-lens magnetic spectrometer: at $E_1 \approx 2$ Mev, $W(180^\circ) = 0.58 \pm 0.07$. Darby selected the energy interval of the β-particles by means of a scintillation spectrometer and a 12-channel pulse-height analyzer. In this investigation, too, $W(180^\circ)$ was determined as a function of the energy in the $E_1 \approx 1$-2.17 Mev region: with $E_1 \approx 2.17$ Mev, $W(180^\circ) = 0.56 \pm 0.06$.

In the particular case of the $Sb^{124} \rightarrow Te^{124}$ transition there is little to be gained from determining the β-γ correlation function in the $W(180^\circ) = f(E_1)$ form, since the β-spectrum associated with this transition comprises at least five components; the end-point energy of the hardest of these is about 2.3 Mev, while that of the next hardest equals about 1.6 Mev. In determining the β-γ correlation function one should arrange to record the γ-ray coincidences with only the β-particles of one component, for otherwise the experimental results will represent a mixture of correlation functions.

Consequently, in the case of Sb^{124} there is only a very narrow interval of β-energy values ($1.6 < E_1 < 2.3$ Mev) for which one can

determine the relationship $W(180^{o}) = f(E_1)$ experimentally. Hence, we considered it more expedient to add to the extant correlation data by determining the β-γ correlation function for Sb^{124} in the form $W = W(\theta)$ with $E_1 \lesssim E_{ep} \lesssim 2.3$ Mev.

2. Apparatus

A block diagram of the experimental set-up used in determining the differential β-γ correlation function is shown in Fig. 1. For selecting the β-particles we used a thin lens magnetic β-spectrometer. Its principle parameters are: distance from source to detector L = 1.04 meters; inside diameter of tube = 200 mm, maximum relative solid angle of acceptance $\omega = 0.88\%$. The β-particles are detected by a stilbene crystal in the shape of a disk 8 mm in diameter and about 2 mm thick. The scintillations in the crystal are conducted to the photomultiplier (FEU), located outside the vacuum chamber, by a plastic rod 30 mm in diameter and 100 mm long. To forestall evaporation of the silbene the crystal is capped by a glass cover having a window $\sim$10 μ thick.

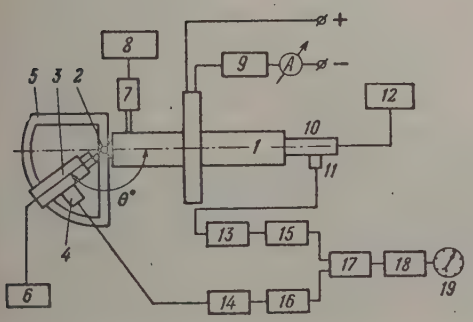

Fig. 1. Block diagram of apparatus: 1) magnetic spectrometer; 2) source chamber; 3) γ-counter; 4 & 11) preamplifiers; 5) graduated aluminum sector; 6 & 12) dry cells (1.4 v); 8) vacuum gage; 9) rheostat; 10) β-counter; 13 & 14) linear amplifiers with negative feedback (K = 100); 15 & 16) discriminators; 17) coincidence circuit; 18) scaling circuit with scaling factor up to 8192; 19) electromagnetic register.

In the γ-counter we used a stilbene crystal in the form of a cylinder some 30 mm in length. In view of the fact that the dimensions of the FEU photomultiplier tube precluded mounting it against the crystal at 90° to the axis of the spectrometer, we used a plastic light-conductor 30 mm in diameter and 85 mm long to attain the requisite orientation of the photomultiplier. The solid angle at which the γ-counter is viewed from the source (acceptance angle) is $\omega = 1/135 = 0.74\%$ of 4π.

The photomultipliers of the β- and γ-counters are enclosed in housings, each consisting of three concentric soft iron cylinders, to shield them from the magnetic field of the spectrometer.

The brass cylindrical container housing the source has a 12 mm high slit covered with brass foil 100 μ thick (γ-ray window). The protruding part of the housing enclosing the γ-counter scintillator is shielded with a lead cap (4 mm side walls, 2 mm front wall).

3. Experimental procedure

The Sb^{124} source was prepared by depositing a layer of Sb_2S_3, 5 mm in diameter and 1.8 mg/cm^2 thick, from an alcohol suspension on an aluminum foil strip having a superficial density of 3 mg/cm^2. The activity of the source was 62 μcurie. The resolving time of the coincidence circuit was $(1.6\text{-}1.7)\cdot 10^{-7}$ sec.

We investigated the angular correlation between the β-particles of the hardest component of the Sb^{124} spectrum and the 0.6 Mev γ-

quanta following these. The magnetic spectrometer was adjusted so that the 1.78 Mev β-particles would be focused on the center of the β-counter. In view of the known abberation of the instrument it may be assumed that β-particles of energy $E_\beta = 1.78 \pm 0.22$ Mev entered the counter. The β-γ coincidence rate was measured at four values of θ: 90, 120, 150 and 180°. The purpose of each measurement was to determine the angular correlation coefficient

$$A(\theta) = \frac{W(\theta)}{W(90^\circ)} = \frac{N(\theta)}{N(90^\circ)} \qquad (1)$$

where N is the rate of the β-γ coincidences at the given values of θ.

The coincidences were recorded alternately for each angle and 90°; in each measurement 100 coincidences (true and chance) were recorded for each θ and for 90°, i.e. counting was continued to $N_{t+c} = 100$. Before and after each measurement of the number of coincidences we recorded the counting rate of the β- and γ-counters. In the subsequent calculations we used the arithmetic average of each pair of rates (N_β and N_γ). In all we made 16 measurements at $\theta = 180^\circ$, 14 at $\theta = 150^\circ$ and 13 at $\theta = 120^\circ$. Prior to each series of measurement we determined the resolving time τ of the coincidence circuit; the determined value was used in computing the number of chance coincidences (N_c) in the measurements of the given series. For the value of N(θ) in equation (1) we used the converted coincidence count rate, i.e. the counting rate for true coincidences, referred to the product $N_\beta \cdot N_\gamma$. Since $N_c = 2N_\beta \cdot N_\gamma \tau$,

$$N(\theta) = \frac{N_t}{N_\beta \cdot N_\gamma} = \frac{N_{t+c}}{N_\beta \cdot N_\gamma} - 2$$

The value of A(θ) was determined according to equation (1) for each measurement. The final value of A(θ) was found as the arithmetic mean of the series of computed values for the given angle θ.

4. Results of measurement

The following results were obtained: $A(120^\circ) = 0.912 \pm 0.029$; $A(150^\circ) = 0.658 \pm 0.026$; $A(180^\circ) = 0.553 \pm 0.034$ (the indicated deviations are mean square errors). These values are plotted in Fig. 2.

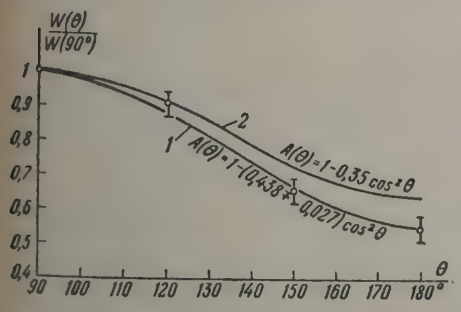

Fig.2. Differential β-γ correlation functions for Sb^{124}: 1) experimental curve; 2) theoretical curve corrected for the angular resolution of the apparatus.

The hardest component of the β-spectrum of Sb^{124} is commonly attributed to a first forbidden transition. In this case the β-γ correlation function should have the form

$$W(\theta) = 1 + a \cos^2 \theta \qquad (2)$$

Consequently the experimental points should fit a curve described by $A(\theta) = 1 + a \cos^2 \theta$. Proceeding from this and using the method of least squares we found that for our experimental points $a = -0.438 \pm 0.027$.

In comparing the theoretical curves for W(θ) with the experimental one, each theoretical curve must first be corrected for the angular resolution of the experimental set-up. We computed the corrections

according to the equations of Alkhazov et al.[6] The correction factors are

$$\alpha_2^{(\gamma)} = 0.98 \quad \text{and} \quad \alpha_2^{(\beta)} = 0.976.$$

5. Discussion of results

a) The system of levels and transitions involved in the $Sb^{124} \rightarrow Te^{124}$ process is exceptionally complex so that despite the large number of investigations devoted to its elucidation only its general outlines are known so far. Many of the data in the literature are conflicting.[7-14] The scheme proposed in one of the more recent investigations[7] devoted to the radiation from Sb^{124} is shown in Fig. 3 (also see Ref. 15 in which the proposed scheme is amplified in the light of data reported by Gromov et al.[8]) However, the existence of the $B_5 \rightarrow \gamma_1$ cascade has been definitely established so that the uncertainties of the scheme as a whole have no bearing on our measurements.

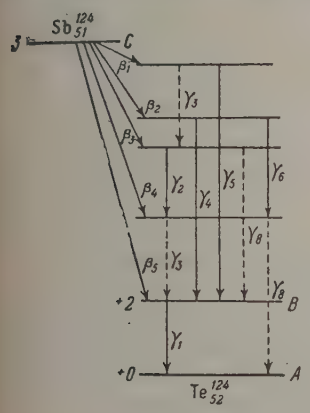

Fig. 3. Scheme of levels and transitions for the Sb124 → Te124 process. End-point energies: $\beta_1 = 0.24$, $\beta_2 = 0.610$, $\beta_3 = 0.966$, $\beta_4 = 1.602$, $\beta_5 = 2.317$ Mev. γ-ray energies: $\gamma_1 = 0.603$, $\gamma_2 = 0.641$, $\gamma_3 = 0.716$, $\gamma_4 = 1.68$, $\gamma_5 = 2.09$, $\gamma_6 = 0.958$, $\gamma_7 = 1.052$ (there is no place for this transition[8] in the scheme), $\gamma_8 = 1.347$ Mev. Dash lines indicate alternate positions.

b) It was suggested in 1951, on the basis of an investigation of the shape of the β_5-spectrum,[16] that this component is associated with a once forbidden transition and is a spectrum of the α-type and that the sequence of transitions in the β_5-γ_1 cascade is characterized by the formula $3(I) \rightarrow 1(1)0$ (here I denotes the first degree of forbiddenness). In transitions of the α-type the β-interaction is described by the B_{ij} matrix element alone.

The results of several β-γ correlation studies showed, however, that the $3(I) \rightarrow 1(1)0$ transition hypothesis is unacceptable.[3,4,1] Subsequently a number of investigators established conclusively that the γ_1-transition is of the E2 type. Since it may be taken for granted that for the ground state of the even-even Te^{124} nucleus $J^*_A = 0+$, it must be assumed that $J^*_B = 2+$ (see Fig. 3). Hence the formula for the β-γ cascade we are dealing with should be of the form $X \rightarrow 2(2)0$; the results of the β-γ correlation measurements should be analyzed in the light of this deduction.

If one persists in the hypothesis that the β_5-spectrum is of the α-type and associated with a first forbidden transition, ΔJ in the transition should be 2, i.e., J_C should equal 0 or 4.

Using the equations of Dolginov[19] and data from various other theoretical studies,[20-22] we computed the angular correlation function for the variants $0(I)2(2)0$ and $4(I)2(2)0$ with tensor interaction and a B_{ij} matrix element, assuming $E_\beta = 1.78$ Mev. After introduction of the appropriate corrections for the angular resolution of the apparatus we obtained the following results: for the first variant $A(\theta) = 1 + 0.9 \cos^2 \theta$ and for the second variant $A(\theta) = 1 + 0.35 \cos^2 \theta$. Thus in the case of both variants the function $A(\theta)$ differs appreciably from the one determined experimentally. Consequently the idea that the β_5 component is of the α-type and pertains to a

first forbidden transition must be rejected. Furthermore, there are certain considerations which make $J_C = 0$ or 4 appear doubtful; in fact there are good reasons to assume that $J_C = 3$. If one persists in regarding the transition associated with β_5 as a first forbidden one (although there is no very convincing evidence in favor of this), then according to the Gamow-Teller selection rules this should be a "yes" transition; hence, since $J^*_B = 2+$, presumably, J^*_C should equal 3-.

Making use of the same theoretical equations we computed the β-correlation function for the variant 3(I)2(2)O assuming tensor interaction, a B_{ij} matrix element and $E_\beta = 1.78$ Mev. The result, after appropriate correction for the angular resolution of the apparatus, was $A(\theta) = 1 - 0.35 \cos^2 \theta$ (see Fig. 2).

It will be seen that the theoretical coefficient a_{theo} in front of $\cos^2 \theta$ differs somewhat from the experimental value $a_{exp} = -0.439 \pm 0.027$, i.e., $0.411 \leqslant |a_{exp}| \leqslant 0.465$. In view of the fact that $|a_{exp}| > |a_{theo}|$, the divergence can hardly be blamed on distortion of the $A(\theta)$ curve by some experimental factor (for example, scattering of the β-particles).

In other investigations of β-γ correlation for Sb^{124}, the investigators compared the experimental curve for $W(180^o) = f(E_1)$ with the results of theoretical calculations also carried out for the variant 3(I)2(2)o and only a B_{ij} matrix element.[1,4] As in our case, the theoretical curve was close to the experimental one but did not fully coincide with it.

Apparently these divergences are not connected with any experimental shortcomings; hence it may be asserted that the β_5 transition in Sb^{124} cannot be described by a single B_{ij} matrix element with tensor type interaction. One could attempt to obtain closer agreement of theory with experiment by using, in the calculations, a mixture of matrix elements with either some one form of interaction (tensor, axial vector, etc.) or a combination of several forms; moreover the calculations should be carried out not only for the first degree of forbiddenness of the β_5 transition but also assuming that this transition is twice forbidden. However, such calculations comprise many arbitrary or uncertainly known parameters (for example, ratios of the amplitudes and phases of the different matrix elements) so that it is often possible to make different variants fit the experimental curves through appropriate selection of the parameter values.

This clearly evinced in the investigations of Morita and Yamada. In one contribution[23] these investigators showed that one can theoretically explain both the shape of the β_5 spectrum and the experimental data on β-γ correlation in the $\beta_5 \rightarrow \gamma_1$ cascade if one assumes a linear combination of matrix elements $\int \beta\alpha$, $\int \vec{\beta} \cdot \vec{r}$ and B_{ij} with tensor interaction and a first degree of forbiddenness. In a later article[24] the same authors showed that equally satisfactory agreement is obtained on the assumption (proposed by Langer et al[7]) of a combination of S + T + P interactions with $\Delta J = 1$. In both cases the β-γ cascade is characterized by the formula 3-(I)2+(2)O+.

Thus it can only be stated that the experimentally determined differential β-γ correlation function for Sb^{124} with $E_\beta = 1.78$ Mev definitely invalidates the assumption that the transition associated with the β_5 component is a first forbidden, α-type transition.

In order to obtain more precise and detailed data on the character of the β_5 transition (i.e., to determine the degree of forbiddenness, the form of the matrix elements characterizing the transition, etc.) one must greatly enhance the experimental accuracy in determining the shape of the β_5-spectrum and the form of the β-γ correlation

function. In particular, reliable confirmation of the absence of a $\cos^4\theta$ term in the expression for $W(\theta)$ would serve to prove that the β_5 transition is actually a first forbidden one.

Angular Correlation of Gamma-Rays from ThD

The scheme for the ThC"$(Tl^{208}) \rightarrow$ ThD(Pb^{208}) process has not yet been definitively established. The data given in Refs. 25-28 diverge to considerable extent; however, all these investigations confirm the finding that the γ_1- (0.58 Mev) and γ_2-rays (2.62 Mev) are emitted in cascade. According to Ref. 26 this two-step transition occurs in about 70% of the disintegrations. The decay scheme based on the data of Refs. 27 and 28 is shown in Fig. 4.

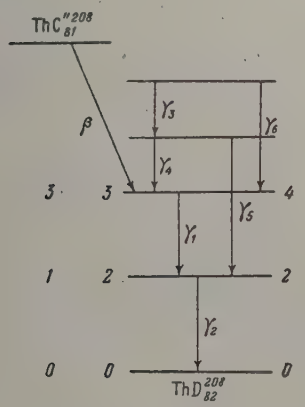

Fig. 4. Partial diagram of the system of levels and transitions for ThC" → ThD. γ-ray energies: γ_1 - 0.58, γ_2 - 2.62, γ_3 - 0.233. γ_4 - 0.277, γ_5 - 0.859, γ_6 - 0.51 Mev. Figures at left are spins according to Ref. 28 (1st column) and Ref. 29 (2nd column). Figures at right are the probable spins deduced from our data.

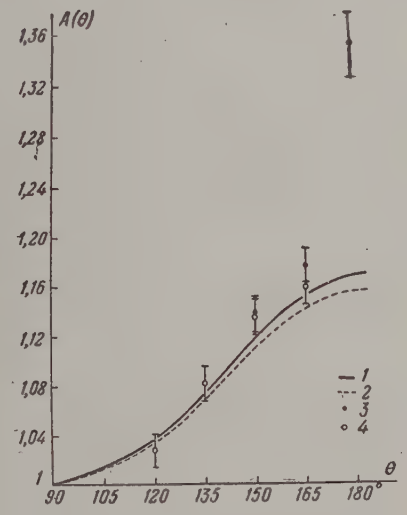

Fig. 5. Correlation between γ-quanta from ThD: 1) theoretical curve for the transition sequence variant 4(2)2(2)0; 2) theoretical curve corrected for angular resolution; 3) uncorrected experimental data; 4) values 3 corrected for the influence of annihilation radiation.

Analysis of the results of the above-mentioned investigations indicates that the intensity of the γ_3- (0.233 Mev), γ_4- (0.277 Mev) and γ_5- (0.859 Mev) rays is low compared to that of the γ_1- and γ_2-rays (in addition lead caps with 2 mm thick walls used in the spectrometer reduce the relative efficiency of recording the γ_3- and $_4$-quanta) while the intensity of the γ_6-(0.51 Mev) ray is about 1/3 that of γ_1. The spins of the ground and two excited states of ThD according to the data of Refs. 28 and 29 are also shown in Fig. 4.

In our investigation we measured the magnitude of the angular correlation coefficient $A(\theta) = W(\theta)/W(90^\circ)$ for θ = 120, 135, 150, 165 and 180°. The following modifications were made in the set-up for measuring γ-γ angular correlation described in Ref. 6: 1) the stilbene scintillator crystals were replaced by NaI·Tl crystals (enclosed in a sealed plastic container with a glass window); 2) the photomultiplier output pulses instead of being applied directly to the coincidence circuit were first amplified by means of an amplifier having a factor of 100 and a frequency response extending to 2

megacycles. In connection with these modifications, in studying the angular correlation of γ-quanta from ThD we utilized a Rossi coincidence circuit with appropriate preliminary shaping of the pulses. The resolving time τ of the coincidence circuit was $1.8 \cdot 10^{-7}$ sec. In view of the rapid decay of the source (T = 10.2 hours) each measurement was effected within a 10 minute period; the measurements were made alternately for the given angle between the counter axes and for 90°. Not less than 10,000 true coincidences were registered for each angle.

The source consisted of a deposit of active thorium on an aluminum support. The intensity of the source was selected so that the ratio of chance to true coincidences would be 1/4 to 1/5 at the beginning of the day and about 1/10 at the end of the day's work. The experimental results were corrected to allow for chance coincidences and annihilation radiation. The effect of the annihilation quanta was taken into account by means of an experimentally determined curve for the variation of the counting rate for annihilation quanta from Cu^{64} with the angle θ between the counter axes.

This same curve was also utilized in introducing the corrections for the angular resolution of the apparatus into the theoretical angular correlation function. The results of our determinations of A are shown in Fig. 5. They confirm the results of Petch and Johns.[30] One may assume the transition sequence variant 4(2)2(2)0 for ThD, i.e., that the spins of the successive levels are 4, 2 and 0 and that the transitions between them are quadrupole ones. The variants 3(2)2(1)0, 3(2)2(2)0 and 3(1)2(2)0, suggested by Oppenheimer[25] and Arnoult,[29] would lead to values of A less than unity (see Fig. 2 in Ref. 6) and must, therefore, be rejected. The circumstance that the presence of γ_6 does not noticeably affect the shape of the observed function may be explained by assuming that the spin of the upper level (decaying with the emission of the γ_6-ray) is 6 and that the transition is quadrupole. In this case the resulting function coincides with the angular correlation function for the 4(2)2(2)0 variant.

It must be noted, however, that the above assignment of the spins for the first excited levels of ThD and multipole orders for the transitions between them must not be regarded as definitive.

According to the data of Latyshev[31] the emission of γ-quanta in cascade is possible in the radioactive decay of ThC to ThC'. The existence of such a cascade and of a three-step cascade $(\gamma_6 - \gamma_1 - \gamma_2)$ in the decay of ThC" may make it necessary to modify our interpretation of the experimentally determined angular correlation function.

Cascade Transition in Nb^{95}

Shpinel'[32] gives a decay scheme for $Zr^{95} \rightarrow Nb^{95}$ which indicates that the 365 kev β-transition having a relative intensity of 95% goes to an excited level of Nb^{95} and that the following transition to the ground state of Nb^{95} occurs either in the form of a cascade with the emission of two γ-rays of energies 230 and 730 kev or directly, the relative intensity of the direct transition being only 7%.

On the other hand, in the schemes for the $Zr^{95} \rightarrow Nb^{95}$ transformation given by Slätis and Zappa[33] and Mandeville et al[34] the cascade transition from the excited to the ground state of Nb^{95} is missing. Hence we deemed it necessary before investigating the γ-γ angular correlation for Zr^{95} to determine whether this two-step transition actually occurs.

In order to increase the efficiency of detection of 230 kev γ-rays we replaced the lead caps covering the projecting part of the

photomultiplier housings in our apparatus for measuring angular correlation by aluminum caps with 3 mm thick front walls. This, we subsequently discovered, was a mistake since it resulted in a great increase in coincidences due to scattering of the γ-quanta in the counters, so that quanta scattered in one counter were registered in the other. We, therefore, arrived at misleading conclusions regarding the number of true γ-γ coincidences in the decay of Zr^{95} and the anisotropy in the distribution of these coincidences. The error came to light in the course of control experiments with samples (Co^{60} and Sb^{124}) for which the angular correlation function is known.

We then ran a new series of measurements after replacing the aluminum caps by conical lead ones. The installation of the new caps sharply reduced the count of γ-quanta scattered from one counter to the other with $\theta = 180^{\circ}$ and virtually eliminated this effect for $\theta < 165^{\circ}$. An aluminum plate 1.5 mm thick was mounted in front of each scintillator; this thickness is sufficient for the absorption of all β-rays from Zr^{95} and Nb^{95}. The resolving time of the coincidence circuit in the experiments with Zr^{95} was 10^{-7} sec. The results of our measurements showed that the relative intensity of this cascade branch (if it does exist) does not exceed 1% of the intensity of the direct γ-transitions to the ground state.

We desire to thank D. G. Alkhazonov and A. Z. Dolginov for discussion of the results and S. G. Tsepakin, G. I. Mishin, Iu. A. Shalashov and K. I. Erokhina for their help in carrying out the measurements.

Leningrad Physico-Technical Institute of
the Academy of Sciences of the USSR

References

1. D.Stevenson & M.Deutsch, Phys. Rev., 83, 1202 (1951).
2. S.Ridgway, Phys. Rev., 78, 821 (1950).
3. J.Beyster & M.Wiedenbeck, Phys. Rev., 79, 169 (L), 728 (L) (1950).
4. E.Darby, Canad. J. Phys., 29, 569 (1951).
5. R.Kloepper, E.Lennox & M.Wiedenbeck, Phys. Rev., 88, 695 (1952).
6. D.Alkhazov, I.Lemberg & A.Grinberg, Izv. AN SSSR, Ser. fiz., 17, 487 (1953).
7. L.Langer, N.Lazar & R.Moffat, Phys. Rev., 91, 338 (1953).
8. K.Gromov, B.Dzhelepov, N.Zhukovski, A.Silant'ev & Iu.Khol'nov, Doklady AN SSSR, 86, 255 (1952).
9. F.Metzger, Phys. Rev., 90, 328 (L) (1953).
10. R.Maerker & R.Birkhoff, Phys. Rev., 89, 1159 (L) (1953).
11. D.Hutchinson & M.Wiedenbeck, Phys. Rev., 88, 699 (1952).
12. E.Tomlinson, S.Ridgway & Gopalakrishnan, Phys. Rev., 91, 484 (1953).
13. J.Kraushaar & M.Goldhaber, Phys. Rev., 89, 1081 (1953).
14. A.Zolotavin, Izv. AN SSSR, Ser. fiz., 18, 127 (1954).
15. L.Langer & J.Starner, Phys. Rev., 93, 253 (L) (1954).
16. L.Langer, Phys. Rev., 84, 1059 (L) (1951).
17. R.Stump, Phys. Rev., 86, 249 (L) (1952).
18. F.Metzger, Phys. Rev., 86, 435 (L) (1952).
19. A.Dolginov, Zhur. eksp. i teor. fiz., 22, 668 (1952).
20. K.Alder, Helv. Phys. Acta, 25, 235 (1952).
21. Condon & Shortley, Theory of Atomic Spectra (Russ. trans.), M. 1949.
22. H.Jahn, Proc. Roy. Soc., 205A, 192 (1951).
23. M.Morita & M.Yamada, Progr. Theor. Phys., 8, 449 (1952).
24. M.Morita & M.Yamada, Progr. Theor. Phys., 10, 111 (1953).
25. F.Oppenheimer, Proc. Cambr. Phil. Soc., 32, 328 (1936).

26. J.Surugue, Ann. de Phys., 8, 484 (1937).
27. H.Richardson, Nature, 161, 516 (1948).
28. G.Martin & H.Richardson, Proc. Phys. Soc., 63A, 223 (1950).
29. R.Arnoult, Ann. de Phys., 12, 241 (1939).
30. H.Petch & M.Johns, Phys. Rev., 80, 478 (1950).
31. G.Latyshev & L.Kul'chitski, Zhur. eksp. i teor. fiz., 11, 200 (1941).
32. V.Shpinel', Zhur. eksp. i teor. fiz., 21, 1370 (1951).
33. H.Slätis & L.Zappa, Ark. Fys., 6, 81 (1953).
34. C.Mandeville, E.Shapiro, R.Mendenhall, E.Zucker & G.Conklin, Phys. Rev., 89, 559 (1953).

* * * *

ANGULAR CORRELATION BETWEEN INTERNAL CONVERSION ELECTRONS FROM Ba^{80*}

- B. A. Shakhbazian and
L. I. Rusinov

Investigation of the angular correlation between conversion electrons emitted incident to cascade transitions make it feasible to determine from the results of the same experiment both the nuclear spin of the excited states and the parity of these states. Thus in the conversion electron angular correlation function

$$W(\theta) = 1 + \sum_{k=0}^{k_{max}} A_k b_k^{(1)} b_k^{(2)} P_k(\cos\theta) \qquad (1)$$

the factors $b_k^{(1)}$ and $b_k^{(2)}$ depend both on the multipolarity of the successive transitions and on the type of the transitions, i.e., on the spin and parity of the excited states involved. A_k depends only on the mulitpole orders of the transitions and is the coefficient of the γ-γ angular correlation for the given nucleus. The summation limit k_{max} is determined from the condition

$$k_{max} \leqslant 2l_1,\ 2l_2,\ 2J_2,$$

where l_1 and l_2 are the multipole orders of the successive transitions and J_2 is the spin of the nucleus in the intermediate state.

When $J_2 = 0$ or $\pm 1/2$, the angular correlation effect is absent. The investigations of Refs. 2 and 3 are devoted to a study of the conversion electron angular correlation in Ta^{181} and Hg^{197*}. The existence of angular correlation is established in these investigations, but the authors do not attempt to make any spin and parity assignments. The fact that angular correlation between internal conversion electrons is observed in the case of Br^{80*} was established by Rusinov and Chuikina.[4]

In the present investigation we have determined the angular correlation function of the K and L conversion electrons from Br^{80*} and have drawn certain deductions regarding the spins and parities of the excited states of the nucleus therefrom. The decay scheme for Br^{80*} is shown in Fig. 1.

The internal conversion coefficient of the $Br^{80*} \rightarrow Br^{80'}$ transition is very large while that of the $Br^{80'} \rightarrow Br^{80}$ transition is somewhat greater than unity (according to our results - 1.44 ± 0.23). The energies of the K and L electrons of the former transition are 35.5 and 47.5, respectively, while for the latter transition the respective energy values are 23.5 and 33.5.

Investigation of angular correlation consists of determining the variation in the number of coincidences between internal conversion electrons emitted in successive transitions with the angle between the directions in which the electrons are ejected.

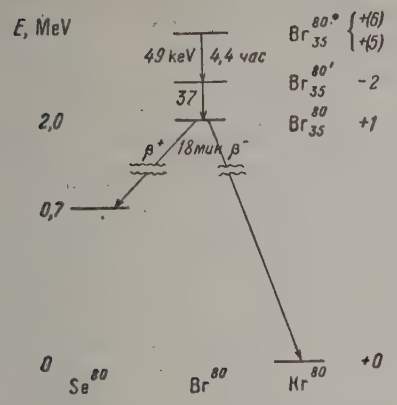

Fig. 1. Decay scheme for Br^{80*}.

Apparatus

Chamber with counters and source. A diagram of the apparatus used for the conversion electron angular correlation measurements is shown in Fig. 2. The main chamber 1 is formed by a spherical glass vessel 200 mm in diameter. One of the end-window electron counters 2 was fixed as regards position while the other counter 3 was mounted so that it could be rotated about the source 4 as the center. The source and the absorber 5 were set on separate adjustable supports.

In all measurements the source was positioned so that the angle between the normal to its surface and the axis of the stationary counter would be 45°. The source-to-counter window distance was 50 mm; the diameter of the counter window - 10 mm. Measurements were made at angles of 90, 75, 60, 45 and 30°. The chamber and counters were filled with a mixture of 90% helium and 10% ethyl alcohol vapor at a total pressure of about 50 mm Hg in which scattering of the conversion electrons from bromine is minimal. Under these conditions, according to the Williams-Bethe[5] multiple scattering theory, the square root of the root mean square deviation of 23.5 kev electrons passing through a 50 mm thick layer of the gaseous mixture equals about 2.7 mm. Hence the correction for the coefficient A_2 in the conversion electron angular correlation function of the form $1 + A_2 \cos^2 \theta$ when $A_2 \leq 0.5$ equalled about 3.5%.

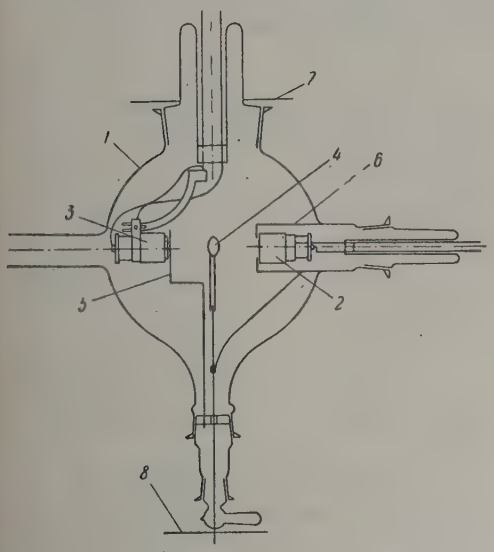

Fig. 2. Diagram of apparatus used for studying angular correlation between conversion electrons from boron: 1) chamber, 2) stationary counter, 3) movable counter, 4) source, 5) absorber (superficial density 4.2 mg/cm²), 6) electrostatic shield, 7) scale for setting angle, 8) scale.

In order to eliminate background coincidences between internal conversion and Auger electrons from Br^{80*}, the windows of the counters were covered with an organic film having a superficial density of 0.25 mg/cm². The superficial density of the gas filling the instrument was 0.14 mg/cm². This thickness is somewhat greater than the path length of the fastest Auger electrons of bromine whose maximum energy does not exceed 13.5 kev.

The slope of the counter plateaus was 1.25% per 100 v. The efficiency of the counters equalled 80% of the efficiency of the same counters when filled with a mixture of 90% argon and 10% ethyl alcohol vapor at 100 mm Hg pressure. A shield 4.2 mg/cm^2 in thickness, absorbing all conversion electrons from the radioactive bromine, was used in determining the coincidence background due to all other radiation from the decay of Br^{80*}.

The pulses from the electron counters were applied to a two-channel amplifier, shaped in appropriate trigger circuits and after differentiation applied to the coincidence circuit. Simultaneously with the number of coincidences we also recorded the number of pulses from the individual counters, for which purpose the pulses from the first trigger tubes were applied, through cathode followers, to separate scaling circuits. The resolving time of the coincidence circuit was $3.5 \cdot 10^{-7}$ sec.

Radioactive source. The source was prepared in the form of a spot of AgBr with a superficial density of under 0.06 mg/cm^2 on a cellophane film having a density under 0.04 mg/cm^2.

Control tests showed that the total superficial density of the active layer plus the support was less than 0.1 mg/cm^2 and that the angular distribution of the electron emission is isotropic (Fig. 3). This is evidence that the absorption and scattering of the electrons in the active layer are minimal and that there is little reflective scattering of the electrons from the support.

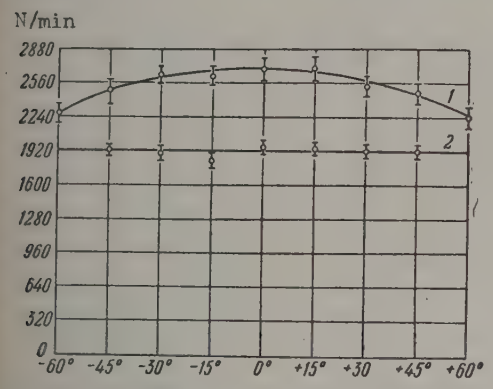

Fig. 3. Angular distribution of electron emission from the radioactive bromine source at different total thicknesses of the source plus the cellophane support: 1) 105 mg/cm^2; 2) 0.1 mg/cm^2.

Hence, in view of the selected dimensions of the source and geometry of the experiment it was assumed that the number of pulses in the movable counter was independent of the angle between the counter axes.

Given the 10 mm diameter of the counter window and the 50 mm source-to-counter distance, the solid angle of acceptance (angle of the counter window viewed from the source) was 0.00248 of the 4π solid angle and varied less than 0.01% incident to variation of the angle between the counter axes.

Experimental Results

In order to obtain the conversion electron angular correlation function from the recorded data it was necessary to determine the background due to chance coincidences and coincidences from other types of radiation. The experimental procedure was the following. At each value of the angle θ_i between counter axes, the number of coincidences and loads on each counter was recorded for a period of 10 minutes. Then the window of the movable counter was covered with the 4.2 mg/cm^2 thick absorber-shield and the coincidences and individual counter pulses were again recorded for 10 minutes. This double series of measurements was repeated three times for each angle setting.

The total number N of coincidences recorded without the absorber in front of the counter is comprised of the number of coincidences

between conversion electrons — $N(e^- - e^-)$, the number of coincidences between internal conversion electrons and Roentgen and γ-quanta from the Br^{80*} — $N(e^- - R,\gamma)$, the number of coincidences of all the Roentgen quanta with each other and with the γ-quanta from the Br^{80*} — $N(R - R,\gamma)$, the number of chance coincidences — $N_{c.c.}$ and the number of γ-γ and β-γ coincidences from the disintegration of $Br^{82} \rightarrow N_{82}$.

$$N = N(e^- - e^-) + N(e^- - R,\gamma) + N(R - R,\gamma) + N_{c.c} + N_{82}. \qquad (2)$$

The thickness of the absorber-shield used in the experiments was great enough to stop all conversion electrons from the source, hence in the measurements with the absorber-shield in front of the counter the first term in the above expression vanishes while the second is halved because the probability of recording an $(e^- - R,\gamma)$ coincidence is reduced by a factor of 2 when one counter is shielded.

Measurements showed that under our experimental conditions the background from Br^{80*} amounts to 14.9% of the total count, with the $(e^- - R,\gamma)$ coincidences making up about 94% of this percentage. The number of $(R - R,\gamma)$ coincidences comes to less than 1.5% of the total number of coincidences at $\theta = 90^o$. The number of coincidences with the absorber in front of the counter is characterized by

$$N' = \frac{1}{2} N(e^- - R,\gamma) + N(R - R,\gamma) N'_{c.c} + N'_{82}. \qquad (3)$$

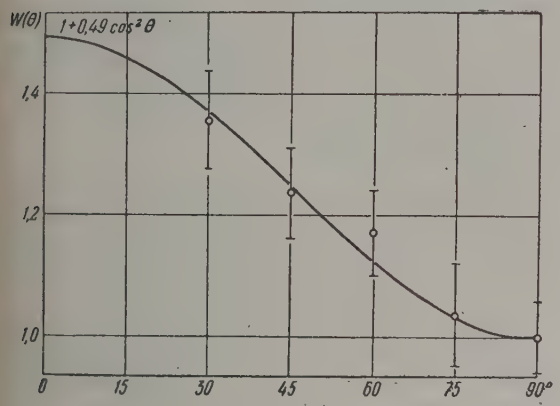

Fig. 4. K- and L-conversion electron angular correlation function for Br^{80*}

The numbers N_{82} and N'_{82} were measured 48 hours after the beginning of the experiment in accordance with the known 36 hour half-life of Br^{82}. The absorption of the X- and γ-rays in the absorber is practically negligible.

The number of coincidences per unit time between conversion electrons from Br^{80*} is given by the following expression

$$n(0) = \frac{1}{T} \sum \{(N - N_{c.c.} - N_{82}) - 2(N' - N'_{c.c} - N'_{82})\}, \qquad (4)$$

where T is the measurement time at the given angle θ_i. In our experiments T = 30 min. The number $N(R - R,\gamma)$ introduced in multiplying the second parenthesis by two is negligibly small. Thus equation (4) shows that under the given experimental conditions one can readily separate the number of true coincidences between conversion electrons from the background of chance coincidences and coincidences due to other forms of radiation. To determine the most probable value of $n(\theta_i)$ from each series of measurements of varying accuracy we computed the weighted averages of the results obtained for each angle, the individual values of $n(\theta_i)$ being reduced to the time of initiation of the experiment. The values of the angular correlation function were then determined as the ratio

$$W(\theta_i) = \frac{n_{av}(\theta_i)}{n_{av}(90^o)}$$

In a number of cases we introduced corrections for off-center location of the source (determined experimentally). Finally we

computed the weighted averages of the series of values of the angular correlation function obtained in all the experiments.

The final results of four separate series of experiments are listed in the accompanying table. The relative error (deviation) in the listed values of the angular correlation function is 6%.

Values of the conversion electron angular correlation function $W(\theta_i)$ for Br^{80*} obtained as the result of four series of experiments

θ_i	Measurement series				Weighted average of the results of all 4 series
	№ 1	№ 2	№ 3	№ 4	
90°	1±0,23	1±0,11	1±0,1	1±0,14	1±0,06
75°	0,99±0,25	1,07±0,11	1,08±0,11	1,01±0,13	1,04±0,06
60°	1,06±0,25	1,25±0,13	1,17±0,11	1,12±0,15	1,17±0,07
45°	1,28±0,28	1,27±0,13	1,18±0,12	1,28±0,16	1,24±0,07
30°	1,37±0,28	1,36±0,14	1,36±0,13	1,32±0,17	1,35±0,08
$W(\theta)$	$1+0{,}49\cos^2\theta$	$1+0{,}54\cos^2\theta$	$1+0{,}47\cos^2\theta$	$1+0{,}47\cos^2\theta$	$1+0{,}49\cos^2\theta$

Lastly, we determined the functions $1 + A\cos^2\theta$ for each series of experiments by the method of least squares. The resultant curve is shown in Fig. 4.

Comparison of Experimental Results with Theoretical Calculations and Conclusions

The angular correlation functions obtained as the result of our experiments were compared with the possible theoretical values of the conversion electron angular correlation function for bromine computed for cascade transitions of different types and multipole orders.

The calculations were made according to the equations derived by Ter-Martirosian (see Appendix) by summation of the general expression of Berestetski[6] for the internal conversion angular correlation function over the magnetic quantum numbers and reduction of the general expression to the form of equation (1).

The various equations for the angular correlation and internal conversion coefficients derived by Ter-Martirosian in the non-relativistic approximation are listed, with his kind permission, in the Appendix to the present article.

Some of the calculated values of the function for Br^{80*} are shown in Fig. 5 together with the experimentally determined values of the internal conversion angular correlation function. We introduced appropriate corrections into the calculated theoretical values of the internal conversion angular correlation function to allow for the finite solid angle subtended by the electron counter windows, for electron absorption in the windows and the gas filling the instrument and for multiple scattering of the electrons in the gas.

The following conclusions may be drawn from a comparison of the experimental results with the calculated angular correlation functions for different variants of the $Br^{80*} \rightarrow Br^{80'} \rightarrow Br^{80}$ cascade:

1. The $Br^{80'} \rightarrow Br^{80}$ transition is El, Electric, since for all magnetic multipoles the theoretical angular correlation function decreases as the angle is decreased from 90° to 0°, i.e., the sign of

A_2 is negative, which conflicts with the experimental data. The possibility of the $Br^{80'} \rightarrow Br^{80}$ transition being of a higher order (magnetic or electric) is excluded by the magnitude of the total conversion coefficient. The experimental value of the total conversion coefficient N_e/N_γ for the transition is 1.44 ± 0.23. The computed values (non-relativistic approximation) of N_e/N_γ for E1 and M1 transitions are 1.54 and 1.23, respectively. The probable error in calculating the conversion coefficient for a transition energy of 37 kev does not exceed 20%. At the same time the values of the conversion coefficient assuming the $Br^{80'} \rightarrow Br^{80}$ to be quadropole as against dipole differ by a factor of over 20. Hence, there can be no doubt that this must be a dipole transition.

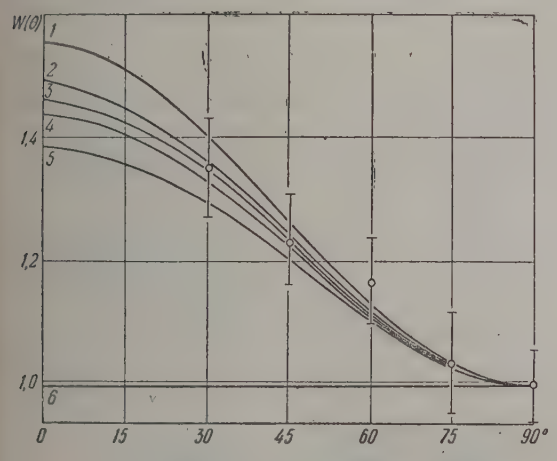

Fig. 5. Comparison of experimental (points) and theoretical (curves) data on angular correlation between K- and L-electrons from Br^{80*}. The theoretical curves were computed for different types of correlating transitions: 1) E1 - E2, $W(\theta) = 1 + 0490 \cos^2\theta + 0.0585 \cos^4\theta$; 2) E4 - E1, $W(\theta) = 1 + 0.487 \cos^2\theta$; 3) M4 - E1, $W(\theta) = 1 + 0.460 \cos^2\theta$; 4) E3 - E1, $W(\theta) = 1 + 0.438 \cos^2\theta$; 5) M3 - E1, $W(\theta) = 1 + 0.382 \cos^2\theta$; 6) M3 - M1, $W(\theta) = 1 - 0.0073 \cos^2\theta$.

Thus the character of the increase of the internal conversion angular correlation function for Br^{80*} indicates that $Br^{80'} \rightarrow Br^{80}$ is an electric dipole transition. This is in contradiction to Berthelot's[7] indication that this transition is of the magnetic dipole type.

2. According the Fig. 5 the order of the $Br^{80*} \rightarrow Br^{80'}$ transition should not be below the octupole. An assignment of E4, M4, E3 or M3 is possible within the limits of the experimental error where the values of the angular correlation function are concerned. However, according to the data of Rusinov and Iusefovich[8] the value of the relative internal conversion coefficient (K/L ratio) for this transition is 2.2 ± 0.2, while according to our non-relativistic calculations the theoretical values are 0.7 for E4, 2.15 for M4, 1.8 for E3 and 4.29 for M3. We conclude therefrom that the M4 assignment is the most probable for this transition. However, in view of the errors inherent in the calculations the possibility of its being E3 is not entirely precluded.

According to the selection rules for β-decay the state of the Br^{80} nucleus is 1+. Consequently the changes in spin and parity in the $Br^{80*} \rightarrow Br^{80'} \rightarrow Br^{80}$ decay process must be described by one of the following schemes:

$$6+ \xrightarrow{M4} 2- \xrightarrow{E1} 1+ \qquad \text{or} \qquad 5+ \xrightarrow{E3} 2- \xrightarrow{E1} 1+.$$

3. The presence of coincidences produced by internal conversion electrons omitted in the $Br^{80*} \rightarrow Br^{80'} \rightarrow Br^{80}$ transitions indicates that the mean lifetime of the $Br^{80'}$ nucleus is shorter than the resolving time of the coincidence circuit:

$$\tau_{Br_{35}^{80'}} < 3{,}5 \cdot 10^{-7} \text{ sec.}$$

4. The minimal lifetime τ_H of the $Br^{80'}$ nucleus calculated from optical data on the hyperfine splitting of the bromine spectrum lines is[9]

$$\tau_H \approx 10^{-10} \text{ sec.}$$

It is known[10] that for the distortion of the angular correlation to be negligibly small the condition

$$\tau_H > 10^{-11} \text{ sec.}$$

must be satisfied. This condition is fulfilled for bromine.

On the other hand the existence of angular correlation between internal conversion electrons from Br^{80*} indicates that the lifetime of bromine in the $Br^{80'}$ state is less than 10^{-10} sec.

It should be noted that investigation of the radiation angular correlation in certain cases can yield information on the upper limit of the lifetime of compound nuclei.

The authors wish to thank K. A. Ter-Martirosian for his great help on questions of theory.

References

1. M.Rose, L.Briedenharn & G.Arfken, Phys. Rev., 85, 5 (1952).
2. A.Ward & D.Walker, Nature, 163, 168 (1949).
3. O.Huber, M.Walter & W.Zuentli, Helv. Phys. Acta, 23, 855 (1950).
4. L.Rusinov & E.Chuikin, Doklady AN SSSR, 68, 1029 (1949).
5. H.Bethe, Phys. Rev., 70, 821 (1946).
6. V.Berestetski, Zhur. eksp. i teor. fiz., 18, 1070 (1948).
7. A.Berthelot, Ann. de Phys., 19, 219 (1944).
8. L.Rusinov & A.Iuzefovich, Journ. Phys. USSR, 3, 281 (1940).
9. S.Tolansky & S.Trivedi, Proc. Roy. Soc., 175, 366 (1940).
10. D.Hamilton, Phys. Rev., 58, 122 (1940).

Appendix

NON-RELATIVISTIC EQUATION FOR COMPUTING COEFFICIENTS OF ANGULAR CORRELATION BETWEEN INTERNAL CONVERSION ELECTRONS AND INTERNAL CONVERSION COEFFICIENTS

(derived by K. A. Ter-Martirosian)

Electric 2^l-pole transition

Internal conversion coefficients

$$\gamma_K^{2l+2}\alpha_K^{(l)} = \frac{l}{l+1} q(l, n_K),$$

$$\gamma_L^{2l+2}\alpha_{L_I}^{(l)} = \frac{l}{l+1} q_0(l, n_L),$$

$$\gamma_L^{2l+2}\alpha_{L_{II,III}}^{(l)} = \frac{l}{l+1}\left[\frac{l}{2l+1} q_{-1}(l, n_L) + \frac{l+1}{2l+1} q_1(l, n_L)\right].$$

Conversion electron angular correlation coefficients

$$b_k(K) = 1 + \frac{k(k+1)}{2l(l+1) - k(k+1)},$$

$$b_k(L_I) = b_k(K),$$

$$b_k(L_{II,III}) = 1 + \frac{k(k+1)}{2l(l+1) - k(k+1)} \cdot \frac{l(l+1)}{2l+1} \cdot \frac{1 - 2T_l \cos(\eta_{l+1} - \eta_l) + T_l^2}{l+1+lT_l^2}.$$

Magnetic 2^l-pole transition

Internal conversion coefficients

$$\gamma_K^{2l}\beta_K^{(l)} = \lambda + \mu_1,$$

$$\gamma_L^{2l}\beta_{L\,\mathrm{I}}^{(l)} = \frac{\left(1+\frac{n_L^2}{4}\right)^2}{16n_L^4}\left[\frac{l+1}{2l+1}\Lambda_0 + \frac{l}{2l+1}q_0(l+1, n_L)\right],$$

$$\gamma_L^{2l}\beta_{L\,\mathrm{II,\,III}}^{(l)} = \frac{\left(1+\frac{n_L^2}{4}\right)^2}{16n_L^4}\left\{\frac{l^2-1}{4l^2-1}\Lambda_1 + \frac{l(l+2)}{(2l+1)(2l+3)}q_1(l+1, n_L) + \right.$$

$$\left. + \left[\frac{l(l+1)}{(2l+1)(2l+3)} + \frac{4}{(2l+1)^2}\right]q_{-1}(l+1, n_L)\right\}.$$

Conversion electron angular correlation coefficients

$$b_k(K) = 1 + \frac{k(k+1)}{2l(l+1)-k(k+1)} \cdot \frac{l(l+1)}{2l+1} \cdot \frac{1-2\tau_m\cos(\eta_{l+1}-\eta_l)+\tau_m^2}{l+1+l\tau_m^2},$$

$$b_k(L_{\mathrm{I}}) = 1 + \frac{k(k+1)}{2l(l+1)-k(k+1)} \cdot \frac{l(l+1)}{2l+1} \cdot \frac{1-2T_m\cos(\eta_{l+1}-\eta_{l-1})+T_m^2}{l+1+lT_m^2},$$

$$b_k(L_{\mathrm{II,\,III}}) = 1 +$$

$$+ \frac{k(k+1)\left\{\left[\frac{l(l+1)}{3(2l+1)} + \frac{l^2+8}{2(2l+1)}\right]\gamma_1(kll1,\ ll) + \frac{l^2(2l-1)}{6(2l+1)(2l+3)}\gamma_1(kll2,\ ll)\right]q_{-1}(l+1, n_L)}{[2l(l+1)-k(k+1)]\left[\left(\frac{(l+1)l}{2l+3}+\frac{4}{2l+1}\right)q_{-1}(l+1, n_L) + \frac{l^2-1}{2l-1}\Lambda_1 + \frac{l(l+2)}{2l+3}q_1(l+1,\ n_L)\right]} +$$

$$+ \frac{\frac{l^2-1}{2l-1}\gamma_1(kll-2k,\ ll-2)\Lambda_1 + \frac{l(l+2)}{2l+3}\gamma_1(kll+22,\ ll+2)q_1(l+1, n_L)\Big\}}{[2l(l+1)-k(k+1)]\left[\left(\frac{(l+1)l}{2l+3}+\frac{4}{2l+1}\right)q_{-1}(l+1, n_L) + \frac{l^2-1}{2l-1}\Lambda_1 + \frac{l(l+2)}{2l+3}q_1(l+1, n_L)\right]} +$$

$$+ \frac{2\sqrt{\frac{l^2(l^2-1)}{6(2l+1)(2l+3)}}\sqrt{\Lambda_1 q_{-1}}\cos(\eta_l-\eta_{l-2})\,\gamma(kll2,\ ll-2) +}{[2l(l+1)-k(k+1)]\left[\left(\frac{(l+1)l}{2l+3}+\frac{4}{2l+1}\right)q_{-1}(l+1, n_L) + \frac{l^2-1}{2l-1}\Lambda_1 + \frac{l(l+2)}{2l+3}q_1(l+1,\ n_L)\right]} +$$

$$+ \frac{+2\sqrt{\frac{l^3(l+2)(2l-1)}{6(2l+1)(2l+3)^2}}\sqrt{q_1 q_{-1}}\cos(\eta_{l+2}-\eta_l)\,\gamma(kll2,\ ll+2)}{[2l(l+1)-k(k+1)]\left[\left(\frac{(l+1)l}{2l+3}+\frac{4}{2l+1}\right)q_{-1}(l+1, n_L) + \frac{l^2-1}{2l-1}\Lambda_1 + \frac{l(l+2)}{2l+3}q_1(l+1,\ n_L)\right]} +$$

$$+ \frac{2\sqrt{\frac{(l^2-1)(l+2)l}{(2l-1)(2l+3)}}\sqrt{q_1\Lambda_1}\cos(\eta_{l+2}-\eta_{l-2})\,\gamma(kll+22,\ ll-2)}{[2l(l+1)-k(k+1)]\left[\left(\frac{(l+1)l}{2l+3}+\frac{4}{2l+1}\right)q_{-1}(l+1, n_L) + \frac{l^2-1}{2l-1}\Lambda_1 + \frac{l(l+2)}{2l+3}q_1(l+1,\ n_L)\right]}.$$

Note: $q(l, n_K)$, $q_0(l, n_L)$, $q_1(l, n_L)$, $q_{-1}(l, n_L)$, V_l, B_l^+, B_l^-, B_l, T_l, T_m, τ_m, Λ_0, Λ_1, λ, μ_1, γ_K, γ_L, n_K, n_L, $\cos(\eta_{l+1}-\eta_{l-1})$, $\cos(\eta_l-\eta_{l-2})$, $\cos(\eta_{l+2}-\eta_l)$, $\cos(\eta_{l+2}-\eta_{l-2})$, γ, γ_1 *in the above equations denote:*

$$q(l, n_K) = \frac{64\pi}{137}\cdot\frac{[(2l-1)!!]^2 n_K^{2l+6}}{(1+n_K^2)^{2l-1}}\cdot\frac{\left[(l+1)(1+n_K^2)^{l-2}e^{-2n_K\,\mathrm{arcctg}\frac{n_K}{2}} - V_l\right]^2}{(1-e^{-2\pi n_K})\prod_{j=1}^{l}(j^2+n_K^2)},$$

$$q_0(l, n_L) = \frac{2\pi}{137}\cdot\frac{[(2l-1)!!]^2 n_L^{2L+6}}{\left(1+\frac{n_L}{4}\right)^3}\cdot\frac{\left[2(l+1)\dfrac{1+\frac{l+3}{4}n_L^2}{1+\frac{n_L^2}{4}}e^{-2n_L\mathrm{arcctg}\frac{n_L}{2}} - B_l\right]^2}{(1-e^{-2\pi n_L})\prod_{j=1}^{l}(j^2+n_L^2)},$$

$$q_1(l, n_L) = \frac{9\pi}{2\cdot 137}\cdot\frac{[(2l-1)!!]^2 n_L^{2l+3}}{\left(1+\frac{n_L^2}{4}\right)^3}\times\frac{\left\{\frac{3l^2+9l+4+\frac{n_L^2}{4}(2l^3+15l^2+31l+16)}{3\left(1+\frac{n_L^2}{4}\right)}e^{-2n_L\operatorname{arcctg}\frac{n_L}{2}}-B_l^+\right\}^2}{(1-e^{-2\pi n_L})\prod\limits_{j=1}^{l+1}(j^2+n_L^2)},$$

$$q_{-1}(l, n_L) = \frac{2\pi}{137}\cdot\frac{[(2l-1)!!]^2 n_L^{2l+3}}{\left(1+\frac{n_L^2}{4}\right)^5}\cdot\frac{\left[(l+1)e^{-2n_L\operatorname{arcctg}\frac{n_L}{2}}+B_l^-\right]^2}{(1-e^{-2\pi n_L})\prod\limits_{j=1}^{l-1}(j^2+n_L^2)};$$

$$V_{l+1} = \frac{l+2}{l+1}(1+n_h^2)V_l + \frac{\prod\limits_{j=1}^{l}(j^2+n_K^2)}{1+n_K^2}\cdot\frac{l\cdot 2^{2l+1}}{(2l+2)!};$$

$$B_1 = 0,\quad B_2 = \frac{2}{3},\quad B_3 = \frac{4}{15}\cdot\frac{6+n_L^2}{1+\frac{n_L^2}{4}},\ldots;$$

$$B_1^+ = 0,\ B_2^+ = \frac{2}{3},\ B_3^+ = \frac{1}{30}\cdot\frac{68+13n_L^2}{1+\frac{n_L^2}{4}},\ldots;$$

$$B_1^- = 0,\ B_2^- = 1,\ B_3^- = \frac{4}{3},\ldots;$$

$$T_l = \frac{l+1}{l}\sqrt{\frac{q_1(l, n_L)}{q_{-1}(l, n_L)}},\quad T_m = \sqrt{\frac{q_0(l+1, n_L)}{\Lambda_0}},\quad \tau_m = \sqrt{\frac{l+1}{l}\cdot\frac{\mu_1}{\lambda}};$$

$$\mu_1 = \frac{l}{2l+1}\cdot\frac{(1+n_K^2)^2}{16n_K^4}q(l+1, n_K);$$

$$\lambda = \frac{l+1}{2l+1}\cdot\frac{\pi}{137}\left[\frac{(2l-1)!!}{(2l-1)!}\right]^2\frac{\prod\limits_{j=1}^{l-1}(j^2+n_K^2)}{1-e^{-2\pi n_K}}\cdot\frac{n_K^{2l+4}2^{4l+2}}{(1+n_K^2)^{2l+1}};$$

$$\frac{\left(1+\frac{n_L^2}{4}\right)^2}{16n_L^4}\Lambda_0 = \frac{\pi}{137}\left[\frac{(2l-1)!!}{(2l-1)!}\right]^2\frac{\prod\limits_{j=1}^{l-1}(j^2+n_L^2)}{1-e^{-2\pi n_L}}\cdot\frac{2^{4l-1}n_L^{2l+4}}{\left(1+\frac{n_L^2}{4}\right)^{2l+1}},$$

$$\frac{\left(1+\frac{n_L^2}{4}\right)^2}{16n_L^4}\Lambda_1 = \frac{\pi}{137}\left[\frac{(2l-1)!!}{(2l-3)!}\right]^2\frac{\prod\limits_{j=1}^{l-2}(j^2+n_L^2)}{1-e^{-2\pi n_L}}\cdot\frac{2^{4l-5}n_L^{2l+6}}{\left(1+\frac{n_L^2}{4}\right)^{2l+1}};$$

$$\cos(\eta_{l+1}-\eta_{l-1}) = \frac{l(l+1)-n_L^2}{\sqrt{[(l+1)^2+n_L^2](l^2+n_L^2)}},$$

$$\cos(\eta_{l+2}-\eta_l) = \frac{(l+1)(l+2)-n_L^2}{\sqrt{[(l+1)^2+n_L^2][(l+2)^2+n_L^2]}},$$

$$\cos(\eta_{l+2}-\eta_{l-2}) = \frac{[(l+1)(l+2)-n_L^2][l(l-1)-n_L^2]-(2l-1)(2l+3)n_L^2}{\{[(l+2)^2+n_L^2][(l+1)^2+n_L^2](l^2+n_L^2)[(l-1)^2+n_L^2]\}^{1/8}},$$

$$\cos(\eta_l-\eta_{l-2}) = \frac{(l-1)l-n_L^2}{(l^2+n_L^2)^{\frac{1}{2}}[(l-1)^2+n_L^2]^{\frac{1}{2}}};$$

$$n_K = \frac{Z_{ef}^{(K)}}{137\frac{v}{c}},\quad n_L = \frac{Z_{ef}^{(L)}}{137\frac{v}{c}};\quad \gamma_K = \frac{Z_{ef}^{(K)}}{137},\quad \gamma_L = \frac{Z_{ef}^{(L)}}{137},$$

$$Z_{ef}^{(K)} = Z-\sigma^{(K)},\ Z_{ef}^{(L)} = Z-\sigma^{(L)};\ \sigma^{(K)} = 0{,}3;\ \sigma^{(L)} = 4{,}15;$$

$$\gamma(klj_1^2,\ lj_2) = \sqrt{(2j_1+1)(2j_2+1)}\,W(klj_{11}^2, lj_2)\frac{C_{j_10j_20}^{k0}}{C_{l0l0}^{k0}};\quad \gamma_1 = \gamma-1.$$

INVESTIGATION OF THE RADIATION FROM Tb^{160} BY THE METHOD OF COINCIDENCES

– I. P. Stepanenko & L. Ia. Shavtvalov

The radiation from terbium 160 has been studied by a number of investigators both by absorption methods and with the aid of magnetic spectrometers. The γ-ray spectrum has been recorded, the end-point energies of the β-spectrum components have been determined and two decay schemes have been proposed.[1,2] In addition Shatalov[3] made coincidence measurements by means of a twin β-spectrometer.

In view of the fact the conversion coefficients for the γ-rays from Tb^{160}, having energies over 85 kev, are relatively small Shatalov was unable to record coincidences between these harder γ-rays and the particles of the continuous β-spectrum. In such cases it is preferable to record the γ-rays by observing photoelectrons rather than by detecting the conversion electrons.[4,5]

In order to study β-γ and γ-γ coincidences in cases when the internal conversion coefficient is small we designed and constructed a scintillation γ-spectrometer employing an NaI.Tl crystal.

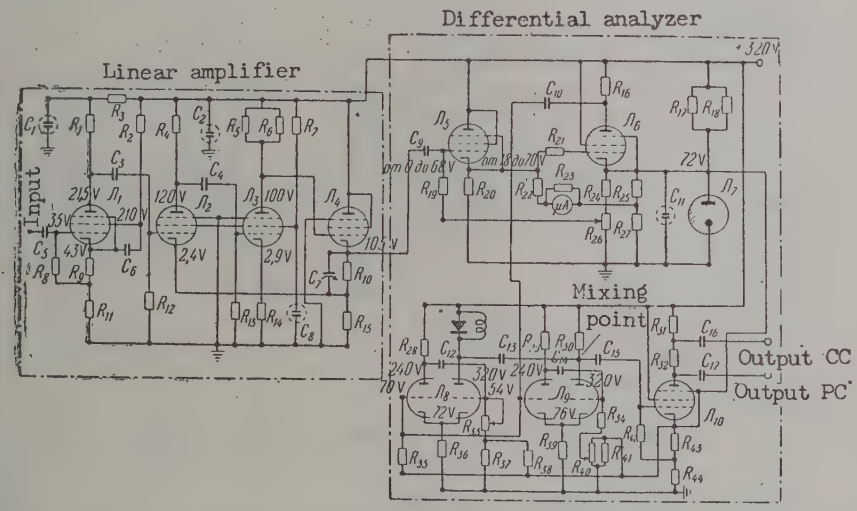

Fig. 1. Schematic of linear amplifier and differential analyzer used in the scintillation gamma-spectrometer

Resistors: R_1, R_{11} – 4 kΩ, R_3 – 4,7 kΩ, R_2 – 32 kΩ, R_4 – R_7, R_{17}, R_{18}, R_{44} – 22 kΩ, R_8, R_{13}, R_{19} – 300 kΩ, R_9 – 220 Ω, R_{10}, R_{28}, R_{29}, R_{36}, R_{39} – 12 kΩ, R_{12} – 270 kΩ, R_{14}, R_{15} – 120 Ω, R_{16} – 200 Ω, R_{20} – 3 kΩ, R_{21} – 2kΩ, R_{22} – 50 kΩ, R_{24} – 2,5 kΩ R_{25}, R_{31} – 500 Ω, R_{26} – 25 kΩ, R_{27} – 20 kΩ, R_{30} – 5,1 kΩ, R_{32} – 1,5 kΩ, R_{33} – 68 kΩ, R_{34} – 220 kΩ, R_{35} – 470 kΩ, R_{37} – 24 kΩ, R_{38} – 8,2 kΩ, R_{40}, R_{41} – 100 kΩ, R_{42} – 200 kΩ, R_{43} – 39 kΩ; Capacitors: C_1, C_2, C_8, C_{11} – 10 μF, C_3 – C_6, C_{10}, C_{15}, C_{17} – 0,01 μF, C_7 – 10 pF, C_9 – 400 pF, C_{12} – C_{14} – 50 pF, C_{13} – 300 pF; Tubes Л-1, Л-2, Л-4, Л-6, Л-10 – 6Ж4, Л-3, Л-5 – 6П9, Л-7 – СГ2С, Л-8, Л-9 – 6Н15П

The potentialities of this method are severely limited by the relatively poor resolution of scintillation spectrometers.[6,7,8] Measurements are feasible only when the γ-lines are far apart as regards energy.

The linear amplifier and single channel differential analyzer used in our investigation are shown schematically in Fig. 1. The two-stage amplifier with negative feedback has a response band of 1 mc and an amplification factor of 100. The differential analyzer consisted of

two pulse-height discriminators, incorporating the Л-8 and Л-9 tubes, connected to operate as monovibrators with a fixed operating level, and an amplifying-limiting stage, using a normally non-conducting Л-6 tube, performing the functions of an integral analyzer with a variable limiting level monitored by a microammeter. This design, as can be shown, makes the analyzer channel width more stable, i.e. minimizes the effects of drift of the characteristics of the Л-8 and Л-9 tubes. Our circuit has no anticoincidence stage (common to most analyzers); its functions are taken over by the branch circuit C_{13} - R_{30}.

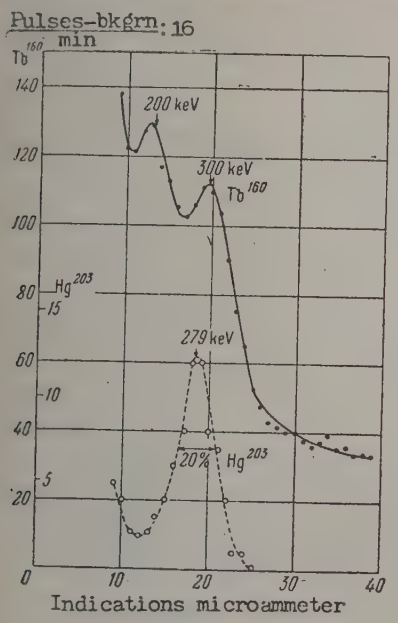

Fig. 2. Gamma-spectra of Tb^{160} and Hg^{203} recorded by means of the scintillation spectrometer.

The calibration measurements were effected using a sample of Hg^{203}. As a result of the measurements, adjustments and matching of the photomultipliers we were able to obtain a resolution equal to 20% at a γ-ray energy of 280 kev. In Fig. 2 the solid line represents the recorded spectrum of Tb^{180}. the dash line, the γ-spectrum of Hg^{203}. The experimental arrangement is shown schematically in Fig. 3. Under these conditions, however, the efficiency of the original scintillation spectrometer was not high enough to permit studying β-γ coincidences. By substituting a thicker crystal (18 x 22 x 22 mm) and reducing the collimation we were able to increase the luminous efficiency of the instrument sufficiently to permit of such observations. Naturally the resolution was impaired: the half-width of the line of the 280 kev γ-rays went down from 20% to 30%. The two photoelectron peaks due to the 200 and 300 kev γ-rays merged into one. However, by making use of the γ-spectrum of Hg^{203} obtained under the same conditions one can select the operating point (level) so that only the 300 kev but virtually none of the 200 kev γ-rays are recorded. Unfortunately in this case, because of the diffuse character (energy spread) of the Compton electron spectrum about

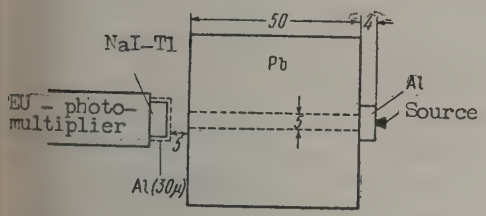

Fig. 3. Diagram of the scintillation -spectrometer. Dimensions in mm.

half the recorded intensity will be due to the hard γ-rays (870 and 960 kev). We arrived at this evaluation on the basis of supplementary measurements of the γ-spectra of Zn^{65}, Tb^{160} and Hg^{203} (Fig. 4). As may readily be deduced from the curves of Fig. 4, at a microammeter indication corresponding to 300 kev energy the ratio of the number of pulses due to the γ-rays from Tb^{160} to the number of pulses due to the γ-rays from Zn^{65} equals about 1.6 (the spectra of Zn^{65} and Tb^{160} have been plotted to coincide in the high-energy region). Inasmuch as the energy of the γ-rays from Zn^{65} (1,118 kev) is close to the energy of the hard γ-rays from Tb^{160} (960 and 870 kev) the shape of the Compton

electron spectrum associated with the γ-rays from Zn^{65} must be nearly identical with that obtained for the hard γ-rays from Tb^{160}. It is not difficult to select the operating point of the spectrometer so that only the hard γ-rays will be recorded.

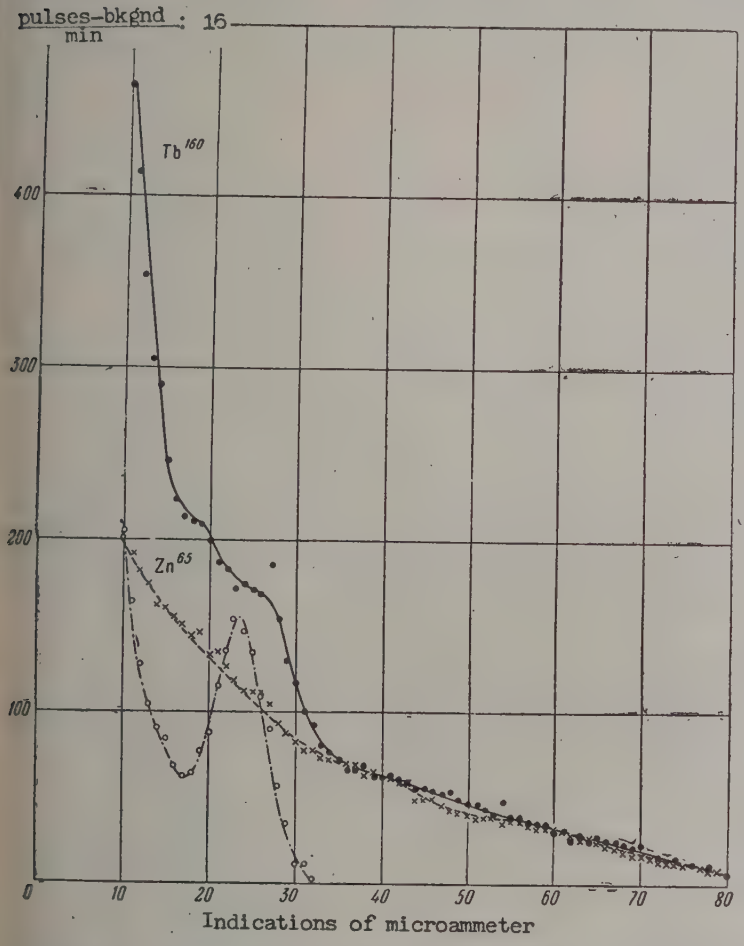

Fig. 4. Gamma-spectra of Tb^{160}, Hg^{203} and Zn^{65} recorded by means of the γ-spectrometer under high-luminosity conditions.

Our procedure in measuring the coincidences between the electrons of the continuous β-spectrum of Tb^{160} and the hard γ-rays (870 and 960 kev) was the following. The electrons of the primary spectrum were detected by means of a Geiger-Müller counter in a magnetic β-spectrometer, while the γ-rays were recorded by means of the described γ-spectrometer by detecting the Compton recoil electrons of 500 kev energy. In order to obviate the influence of the magnetic field, produced by the β-spectrometer lens, on the photomultiplier, this field was neutralized in the region of the photomultiplier by means of a second magnetic lens, the direction of the current in the winding of the latter being opposite to that in the spectrometer coil. The general arrangement of the vacuum chamber, magnetic lenses and photomultiplier is illustrated in Fig. 5. The pulses from the G-M counter and from the photomultiplier were applied to a coincidence circuit with a resolving time of about 0.4 microsec.

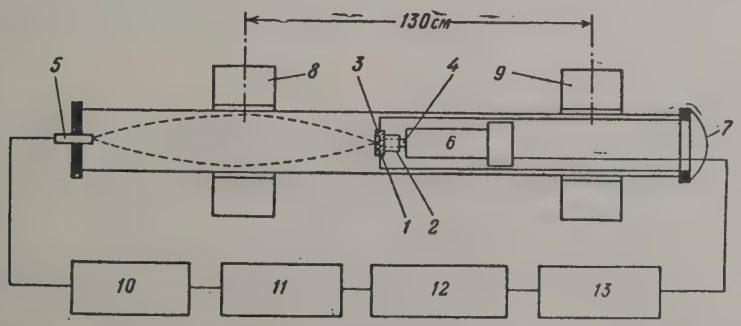

Fig. 5. Diagram of set-up used in measuring β-γ and γ-γ coincidences for Tb^{160}: 1) source, 2) lead shield, 3) aluminum, 4) NaI.Tl crystal, 5) counter, 6) photomultiplier, 7) opaque cap, 8) magnetic lens No. 1, 9) magnetic lens No. 2 - compensating lens, 10) preamplifier, 11) intermediate stage, 12) coincidence circuit, 13) linear amplifier & differential analyzer.

In Fig. 6 the solid line represents the primary β-spectrum correlating with the hard γ-rays. The Fermi plot of this spectrum is shown by the solid lines in Fig. 7. It will be seen that the β-spectrum is complex and consists of two components of approximately equal intensity with end-point energies of 550 and 880 kev.

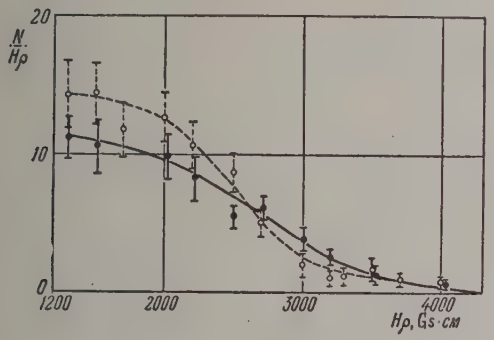

Fig. 6. β-spectrum of Tb^{160}. Solid line - spectrum correlating with the hard 870 & 960 kev γ-rays; dash line - spectrum correlating with the 300 kev and the 870 & 960 kev γ-rays.

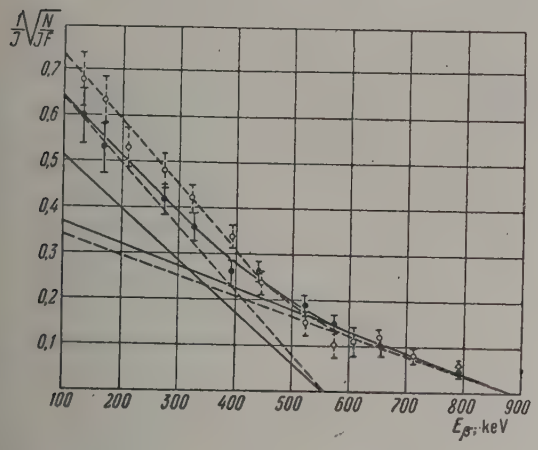

Fig. 7. Fermi plots and separation into components of the β-spectra of Fig. 6.

Thus it follows from our experimental results that the hard γ-rays from Tb^{160} correlate about equally with both components of the β-spectrum. This deduction is in conflict with both published decay schemes.[1,2]

Then, using the analyzer of the scintillation γ-spectrometer as an integral analyzer (cutting out the discriminator),[9] we counted the coincidences between the hard γ-rays and the β-particles. The observed β-spectrum was the same as in working with the differential analyzer. However, the number of true and chance coincidences increased about 4 times.

In studying the coincidences between the 300 kev γ-rays from Tb^{160} and the electrons from β-decay the scintillation spectrometer was adjusted to a γ-ray energy of about 300 kev. The spectrum of the β-particles correlating with the 300 kev as well as with the harder (870 and 960 kev) γ-rays is shown by the dash-line curve in Fig. 6. In these experiments the number of genuine coincidences for electrons with $H\rho$ = 2000 Gs·cm equalled 25.5 pulses/hour while the number of chance coincidences was 33.5 pulses/hour. The Fermi plot of the spectrum represented by the dash line in Fig. 6 is shown by dash lines in Fig. 7. It will be seen that the β-spectrum is complex and consists of two components with end-point energies of 550 and 880 kev. From a comparison of the dash and solid line curves in Fig. 6 it may be concluded that the 300 kev γ-rays correlate to a somewhat greater extent with the softer (550 kev) component of the β-spectrum. A prerequisite for obtaining more dependable and decisive results would be a substantial improvement in the resolving power of the scintillation γ-spectrometer. We note that the indication that there may be correlation between the 300 kev γ-rays and the softer (550 kev end-point energy) β-spectrum component is also in conflict with both the published decay schemes.

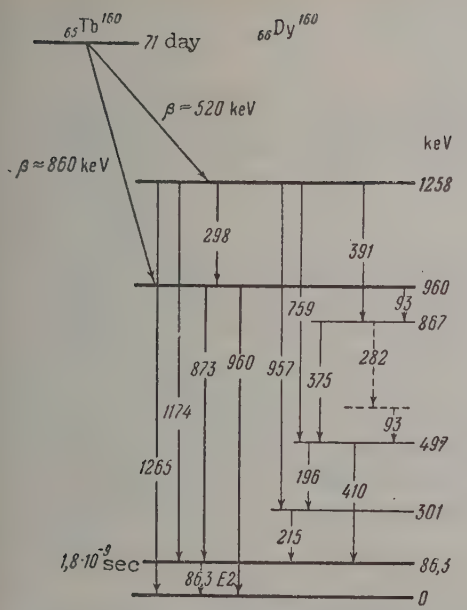

Fig. 8. Decay scheme for Tb^{160} proposed by Burson et al[10] in 1954.

In the decay scheme given by Cork et al[2] there are listed γ-rays of energies close to 400 kev. However, the investigators give no data on their intensity. As may be seen from the γ-spectra recorded by us (Figs. 2 and 4), these γ-rays, if they exist at all, are rather weak. Hence they cannot have any appreciable effect on our results.

Finally we investigated the coincidences between the 85 kev and the hard (870 and 960 kev) γ-rays. In these measurements the 85 kev γ-rays were recorded by observing conversion electrons with the magnetic β-spectrometer while the hard γ-rays were recorded by the scintillation spectrometer. These measurements were alternated with control experiments in which the current in the β-spectrometer magnet was adjusted so that the instrument would detect electrons of the continuous β-spectrum with energies ($H\rho$ = 1000 Gs·cm) somewhat greater than the energy of the conversion electrons.

Thus if there were no correlation between the 85 kev and the hard γ-rays the number of true coincidences in the control measurements should have been approximately the same as when the β-spectrometer was detecting conversion electrons due to the 85 kev γ-quanta. Actually the number of coincidences registered in the latter case was 5-6 times greater than in the control measurements.

Consequently there is undoubted correlation between the 85 kev and the hard (870 and 960 kev) γ-rays.

To be able to establish the decay scheme for Tb^{160} fully and reliably it would be necessary to measure the relative intensities of the observed γ-rays and their internal conversion coefficients as well as to investigate the angular correlation. In addition it would be desirable to investigate some of the other types of β-γ and γ-γ coincidences, which we were unable to do in the present study in view of the inadequate resolving power of the scintillation γ-spectrometer.

Some time after completion of the present investigation, Burston, Jordan and LeBlanc[10] published the results of their investigation in which the emission from Tb^{160} was studied by means of two scintillation spectrometers, connected to a coincidence circuit, as well as a magnetic β-spectrometer. On the basis of their coincidence measurements the investigators propose the new decay scheme shown in Fig. 8. It may be noted that our results are in agreement with this new scheme.

References

1. S.Burson, K.Blair & D.Saxon, Phys. Rev., 77, 403 (1950).
2. J.Cork, Branyan, Rutledge et al., Phys. Rev., 78, 304 (1950).
3. L.Shavtalov, Izv. AN SSSR, Ser. fiz., 17, 503 (1953).
4. A.Brosi, Ketelle, Zeldes & Fairstein, Phys. Rev., 84, 586 (1951).
5. B.Ketelle, A.Brosi & F.Porter, Phys. Rev., 90, 567 (1953).
6. R.Pringle, H.Taylor & K.Roulston, Phys. Rev., 87, 1016 (1952).
7. T.Strickler & W.Wadey, Rev. Scient. Instr., 24, 13 (1953).
8. I.McIntyre & R.Hofstadter, Phys. Rev., 78, 617 (1950).
9. R.Hofstadter & I.McIntyre, Nucleonics, 7, 32 (1950).
10. S.Burson, W.Jordan & J.Le Blanc, Phys. Rev., 94, 103 (1954).

INVESTIGATION OF THE NUCLEAR ISOMERISM OF Zn^{69*}, Se^{79*}, Se^{81*}, Rh^{103*} & Ba^{137*}

- G.M.Drabkin, V.I.Orlov & L.I.Rusinov

The regularities of the distribution of nuclear isomers among the isotopes of the periodic system are connected with the system of energy levels ensuing from the structure of nuclear shells. This system of levels is applicable to the ground states of the nuclei as well as to the metastable states having a relatively low excitation energy.

In connection with this, it is of interest to investigate the multipole order of γ-radiation from isomeric nuclei and to compare the spins and parities of the isomeric states with those of the system of levels, deduced from the nuclear shell model. Further, we can advantageously compare the experimental lifetimes of isomeric nuclei with the theoretical values computed on the basis of different assumptions regarding nuclear structure.

In the present study we investigated the isomeric nuclei Zn^{69*}, Se^{79*}, Se^{81*}, Nb^{95*}, Rh^{103*} and Ba^{137*}. The multipole orders of the γ-radiation from these isomers were determined by investigating the internal conversion coefficients and K/L ratios. The radioactive decay schemes for a number of the isomers were verified and refined.

Zn^{69*}

In the decay scheme suggested by Livingood and Seaborg[1] the metastable Zn^{69*} nuclei pass to the ground state of Zn^{69} (T = 13.8 hours), which then decays by β-transition to the ground state of Ga^{69} (T = 57 min).

In the present investigation we carried out a series of measurements by means of a β-spectrometer having a homogeneous magnetic field, aimed at verifying this decay scheme. To this end we checked the persistence in time of the shape of the β-spectrum. The shape of the β-spectrum of Zn^{69} did not change, within the limits of the experimental error, over a period of 50 hours. Our observations confirm the existence of two half-life periods: 57 min and 13.8 hours.

The experimental data also confirm the fact that the β-decay of Zn^{69} with T = 57 min corresponds to the transition from the ground state of Zn^{69} to that of Ga^{69}, while the β-decay with the 13.8 hour period occurs as a result of attainment of radioactive equilibrium between the metastable Zn^{69*} nuclei (13.8 hours) and the Zn^{69} nuclei in the ground state (57 min).

The transition of the metastable Zn^{69*} nuclei to the ground state is accompanied by an intense emission of γ-rays as well as conversion electrons. Absorption experiments, using absorbers of different thickness, showed that the energy of these γ-rays equals 430±20 kev.

The β-spectrum and the conversion electron spectrum of Zn^{69} were studied by means of a magnetic β-spectrometer with a transverse field. The superficial density of the source was about 0.6 mg/cm^2. The electrons were recorded by means of a shielded counter with an end window of an 0.1 μ thick organic film.

The results of the β-spectrum measurements are shown in Fig. 1. The end-point energy as determined from the Kurie plot is 920±20 kev. The conversion electron energies equal 429±3 and 437±3 kev, which corresponds with a transition of energy 439±3 kev at the K- and L-shells of the zinc atom. The energy value obtained is in agreement with the value determined by γ-radiation absorption studies.

When Zn^{69*} and Zn^{69} are in radioactive equilibrium, the number of β-particles emitted per unit time equals the number of isomeric transitions. The value of the K-conversion coefficient, α_K, was determined from the ratio of the number of K-conversion electrons to the total number of electrons making up the β-spectrum. In the low energy region the shape of the β-spectrum was determined from the Kurie plot. We obtained the following values: $\alpha_K = 0.04 \pm 0.005$ and K/L = 7.5±1.

According to the theoretical calculations of Rose et al[2] the values of α_K for Z = 30 and E_γ = 439 kev are ∽0.027 for E4, ∽0.074 for E5, ∽0.018 for M3, ∽0.052 for M4 and ∽0.164 for M5.

Comparison of experimental and theoretical data on the conversion coefficients shows that the best agreement is obtained in the case when it is assumed that the Zn^{69*} decay is an M4 transition. This deduction is supported by comparison of the 7.5±1 value for K/L found in the present investigation with curve given by Goldhaber and Sunyar[3] according to which K/L = = 8 for Z = 30 and E_γ = 439 kev in the case of M4 transitions.

The nuclei of stable Ga^{69} are in the $p_{3/2}$ state. The Fermi plot of the β-spectrum of Zn^{69} is linear, consequently the nuclei of Zn^{69} may be assigned state $p_{1/2}$. In accordance with the multipole order of the radiation from Zn^{69} indicated above, the metastable nuclei of the isotope should be assigned state $g_{9/2}$.

The decay scheme for Zn^{69*} is pictured in Fig. 1.

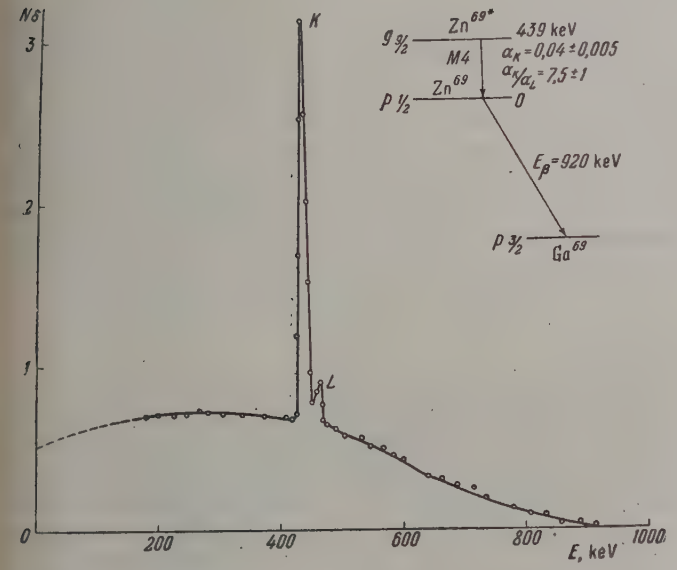

Fig. 1. β-spectrum and decay scheme of Zn^{69*}

Se^{79*}

Investigation of the isomeric transitions of Se^{79*} and Se^{81*} is of particular interest in view of the fact that interpretation of the energy levels of these isomers may have a direct bearing on the further development of the nuclear shell model.

The metastable Se^{79*} nucleus transforms with a half-life of about 3.9 min, to Se^{79}, which decays by -emission (T = 6.5·10⁴ years) to stable Br^{79} (Ref. 4).

In our experiments we used a source having a superficial density of 0.3 mg/cm². In view of the short life of Se^{79*} the sample was intro-

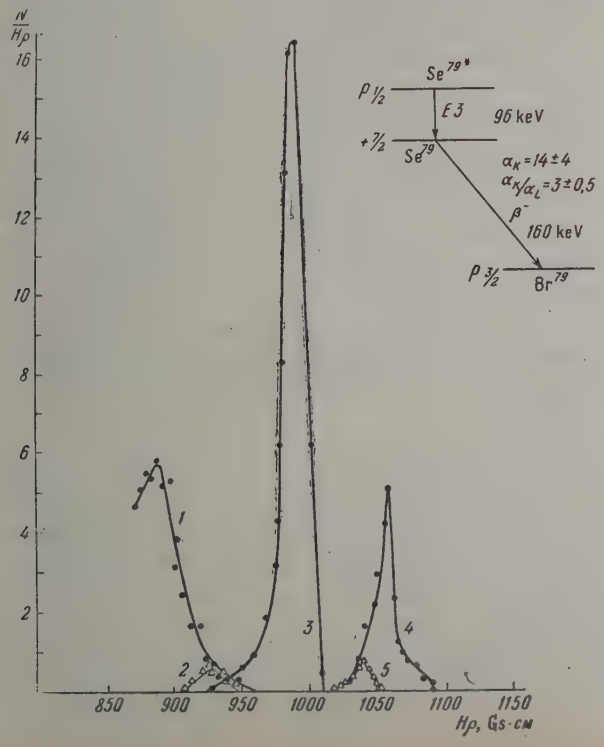

Fig. 2. Conversion and photoelectron lines of Se^{79*} and Se^{81*}: 1) line of photoeffect at the K-shell of tin due to the 96 kev γ-ray emitted in the isomeric transition of Se^{79*}; 2) photoeffect line (K-shell of tin) due to the 103 kev γ-ray emitted in the isomeric transition of Se^{81*}; 3 & 4) K- and L-conversion lines of the isomeric transition of Se^{81*}. Upper right of figure: Decay scheme of Se^{79*}.

duced into the β-spectrometer chamber through a vacuum gate. We developed a special electronic power circuit for the electric magnet designed to permit rapid changes of the magnetic field.

The results of the conversion line measurements are shown in Fig. 2. The peaks 3 & 4 correspond with the energy of the K- and L-conversion lines of the isomeric transition of Se^{79*}; the energies of these conversion electrons are 84 ± 1 and 94 ± 1 kev, respectively. The excitation energy of the metastable state of the isomer, according to our data, is 96 ± 1 kev; the K/L ratio equals 3 ± 0.5.

We used the method of conversion described by Drabkin & Rusinov[5] for determining α_K. To this end we determine the ratio of the intensities of the K-electrons emitted by radioactive samples of Se^{79*} and Se^{81*} under identical conditions by means of a β-spectrometer. In our determination we utilized the difference in the half-life periods of these isomers (T for Se^{81*} = 56 min). The value of α_K for Se^{81*} has been determined earlier by comparison[5] with the isomer Ag^{109*} in radioactive equilibrium with long-lived Cd^{109*}. The ratio of the intensities of the γ-radiation in the isomeric transitions of Se^{79*} and Se^{81*} was determined with the aid of a magnetic spectrometer by observing the photoelectrons ejected from a tin radiator. The results are shown in Fig. 2.

The internal conversion coefficient of Se^{79*} was determined from the expression

$$\alpha_{K_{Se^{79*}}} = \alpha_{K_{Se^{81*}}} \frac{K_e}{K_\gamma},$$

where K_e is the ratio of the number of K-electrons of Se^{79*} and Se^{81*} and K_γ is the ratio of intensities of the γ-lines as determined by observation of the photoelectric lines of these two isomers. According to Drabkin & Rusinov[5], α_K for Se^{81*} equals 7.1 ± 1.5. We carried out several series of measurements, from which we computed a mean value of 10 ± 4 for the K-coefficient of Se^{79*}.

The values of the coefficient for Se^{79} computed by extrapolation of the data of Rose et al[2] are ~ 0.5 for E2 and M2 transitions, ~ 7 for E3, ~ 5 for M3 and ~ 30 for M4.

Comparison of these values with the experimental one shows that the closest agreement is obtained in the case when the isomeric transition of Se^{79*} is assumed to be E3. The residual divergence may be due to inaccuracy in extrapolating in the ~ 100 kev energy region. We also made use of the data of Goldhaber & Sunyar[3] on K/L ratios for determining the multipole order of the transition. For Z = 34 and E_γ = 96, Goldhaber & Sunyar give the following values: ~ 9 for M2, ~ 6 for M3, ~ 4 for E2, ~ 3 for E3 and ~ 1 for E4. Here again the best agreement of our experimental value with the theoretical one is obtained if we assume that the isomeric transition is accompanied by E3 radiation.

The ground state of Br^{79} may be identified as a $p_{3/2}$ level.[6] According to the β-decay data, the ground state of Se^{79} should be assigned a spin and parity of $7/2+$. Hence, in accordance with the deduced data on the multipole order of the γ-radiation, the metastable Se^{79*} nucleus can be attributed a $p_{1/2}$ configuration.

The decay scheme of Se^{79*} is pictured in Fig. 2.

Se^{81*}

The half-life of the metastable Se^{79*} nuclei is 56 min. The excitation energy is 103 kev.[7] Our experiments showed that the shape of the β-spectrum associated with the radioactivity of Se^{81} (T = 16 min) and Se^{81*} (T = 56 min) does not change over a period of several hours (within the limits of the experimental error). This indicates that the β-emission with T = 56 min is due to the decay of Se^{81} nuclei to the ground state. The isomeric Se^{81*} nuclei decay with T = 56 first to the ground state of Se^{81} ($Se^{81*} \rightarrow Se^{81} \rightarrow Br$).

In studying Se^{81*} we detected γ-radiation of energy 100 kev (T=56 min) emitted during the isomeric transition.

The conversion coefficient $_K$ was determined by the comparison method,[5] the comparison element selected being Ag^{109*} in radioactive equilibrium with Cd^{109} (T = 470 days).

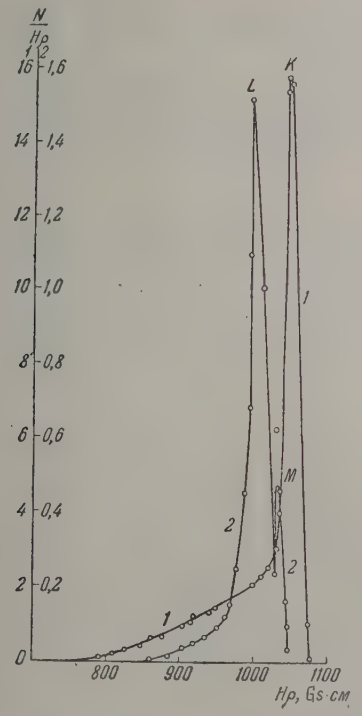

Fig. 3. K-electron lines of Se^{81*} (Curve 1) and L + M-electron spectrum of Ag^{109*} (Curve 2).

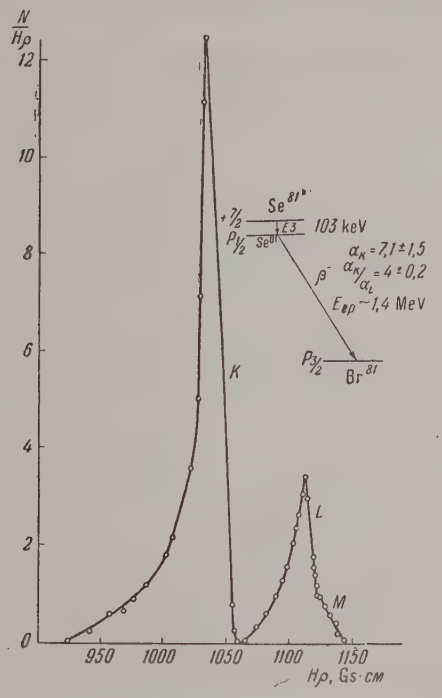

Fig. 4. Internal conversion spectrum and decay scheme of Se^{81*}.

We determined the ratio of the number of K-electrons emitted by the Se^{81*} sample to the number of L + M-electrons emitted by Ag^{109*} under identical experimental conditions by means of a magnetic β-spectrometer. The results of the internal conversion line measurements are shown in Fig. 3. The value of the conversion coefficient was determined from the equation

$$\alpha_{K_{Se^{81*}}} = \alpha_{(L+M)_{Ag^{109*}}} \frac{K_e}{K_\gamma},$$

where K_e is the ratio defined in the preceding paragraph and K_γ is the ratio of the intensities of the γ-rays of the isomeric transitions Se^{81*} to Se^{81} and Ag^{109*} to Ag^{109}. We assumed a value of 12±0.5 as given by Brunner and Huber,[8] for α_{L+M} for Ag^{109*}.

As a result of the measurements and computation we obtained a value of $\alpha_K = 8.6 \pm 2.4$.

In studying the conversion electron lines of Se^{81*} we used a selenium source having a superficial density of about 0.15 mg/cm^2. The results are shown in Fig. 4. We obtained a value of 4.0±0.2 for K/L. The values of α_K for Se^{81*} computed according to Rose et al[2] for different multipole orders are ~0.5 for E2 and M2, ~6 for E3, ~4 for M3, ~50 for E4 and ~30 for M4.

In view of the fact that there are no theoretical calculations of the value of K/L based on relativistic equations, we used the curves for this ratio given by Goldhaber & Sunyar.[3] According to these curves, for Z = 34 and E_γ = 103 kev, the values of K/L for the different multipole orders are ~8 for M2, ~6 for M3, ~3 for M4, ~4 for E2, ~3 for E3 and ~1 for E4.

The value of α_K obtained in the present investigation was averaged with the values found by Drabkin & Rusinov:[5] the resultant mean value of α_K for Se^{81*} was 7.1±1.5.

The experimental values for α_K and K/L as defined above are both found to be in closest agreement with the theoretical values if the isomeric transition is assumed to be E3.

The ground state of Se^{81} is $p_{1/2}$. Accepting the above identification of the isomeric transition (E3), the metastable Se^{81*} nuclei should be ascribed state 7/2+.

The decay scheme for Se^{81*} is given in Fig. 4.

Nb^{95*}

The isomer Nb^{95*} was obtained as a result of β-decay of Zr^{95}(T = 65 days). The half-life of this isomer is about 90 hours; Nb^{95} is transformed into Mo^{95} by β^--decay (T = 35 days). The decay series $Zr^{95} \rightarrow Nb^{95} \rightarrow Mo^{95}$ gives rise to several groups of γ-rays and a complex β-spectrum.[9-12]

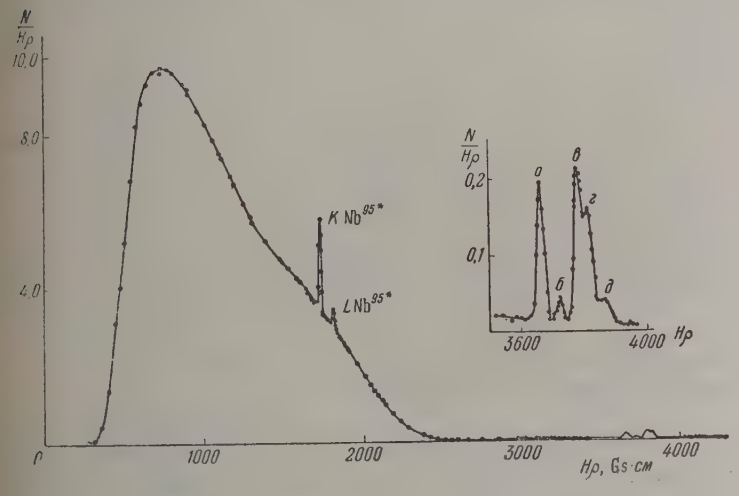

Fig. 5. β-Spectrum of Zr^{95*}

In order to elucidate the characteristics of the isomeric transition of Nb^{95*} it was essential to make a detailed study of the decay series $Zr^{95} \rightarrow Nb^{95*} \rightarrow Nb^{95} \rightarrow Mo^{95}$.

To this end we recorded the β-spectrum of Zr^{95} by means of a β-spectrometer, using a radioactive product consisting of Zr^{95} + Nb^{95}. The measurements were initiated after the two components had reached radioactive equilibrium ($T_{\frac{1}{2}}$ = 90 hours). The electrons were recorded by means of two counters connected in a coincidence circuit. In investigating the β-spectra and conversion lines in the low-energy region, the electrons were recorded by a single counter with a window having a superficial density of about 0.01 mg/cm^2. The superficial density of the source containing the Zr^{95} was under 0.1 mg/cm^2.

The results of measurement are shown in Fig. 5. The K- and L-lines associated with the isomeric transition of Nb^{95*} of energy 237 kev stand out clearly. In addition the β-spectrum has a number of distinct peaks (a, b, c, d and e in enlarged-scale insert).

These conversion maxima may be identified as follows: a and b) K- and L-conversion lines of Zr^{95} with E = 726±2 kev; c) K-line of Zr^{95} with E = 760±3 kev; d) K-line of Nb^{95} with E = 770±3 kev; e) unresolved group of L-conversion lines associated with γ-rays from Nb^{95} of energy 770 kev and from Zr^{95} of energy 760 kev. The identification of these conversion lines was accomplished by running a series of control measurements using sources with different proportions of Zr^{95} and Nb^{95}.

Analysis of the Kurie plot of the observed β-spectrum (Fig. 6) discloses the presence of three components due to Zr^{95}, having end-point energies of 885±10, 396±5 and 360±5 kev and relative intensities of 2±0.5, 55±5 and 43±5%, respectively, and of a soft component associated with Nb^{95}.

The data relative to the β-spectrum of Zr^{95} and the γ-line energies can be used to construct the decay scheme of the nuclide shown in Fig. 6. From the ratios of the number of conversion electrons to the number of electrons in the correspond-

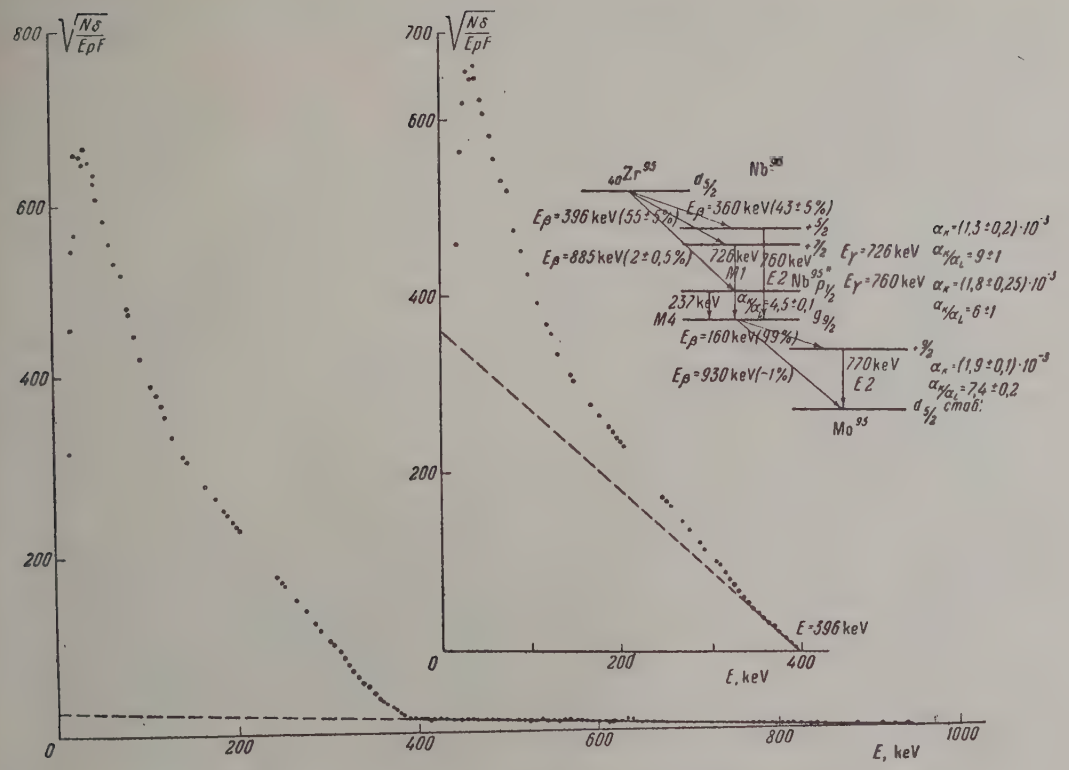

Fig. 6. Kurie plot of the β-spectrum of Zr^{95} and the decay scheme of this nuclide

ing components of the β-spectrum of Zr^{95} we calculated the following values for the K-conversion coefficients and the K/L ratios:

E_γ = 726±3 kev, $\alpha_K = (1.3\pm0.2)\cdot10^{-3}$, K/L = 9±1;
E_γ = 760±3 kev, $\alpha_K = (1.8\pm0.25)\cdot10^{-3}$, K/L = 6±1.

It should be noted that because of the closeness in the spectrum of the L-lines of the 760 kev γ-rays from Zr^{95} and of the 770 kev γ-rays from Nb^{95}, the value of the ratio K/L for the 760 kev γ-line of Zr^{95} was calculated on the basis of the experimentally determined value of this ratio for the 770 kev γ-line of Nb^{95}. Using the experimental data on the K- and L-conversion lines of Nb^{95} that appear in the tail-end of the β-spectrum of Zr^{95}, we calculated the value of K/L for the isomeric transition of Nb^{95*}; it proved to be 4.5±0.5,

For the purpose of recording the β-spectrum of Nb^{95} (T = 35 days) we had prepared a radioactive Nb^{95} sample free of Zr^{95}. The experimental results are shown in Fig. 7.

The K- and L-lines associated with the γ-rays of energy 237 kev pertain to the isomeric transition of Nb^{95*}. The intensity of these lines fell off with a period of 90±2 hours. The K/L ratio for this transition was found to be 4.5±0.1 (this value agrees with the results obtained earlier, but is more accurate).

The K- and L-conversion peaks associated with the γ-rays of energy 770±2 kev may be seen in Fig. 7. The intensity of these lines fell off with a period of about 35 days, corresponding to the decay of Nb^{95}.

Fig. 7 also shows the Kurie plot; analysis of the plot indicates the presence

of two components in the β-spectrum of Nb^{95}:

E_γ = 160±3 kev (99±0.5%) and E_γ = 930±20 kev (1±0.5%).

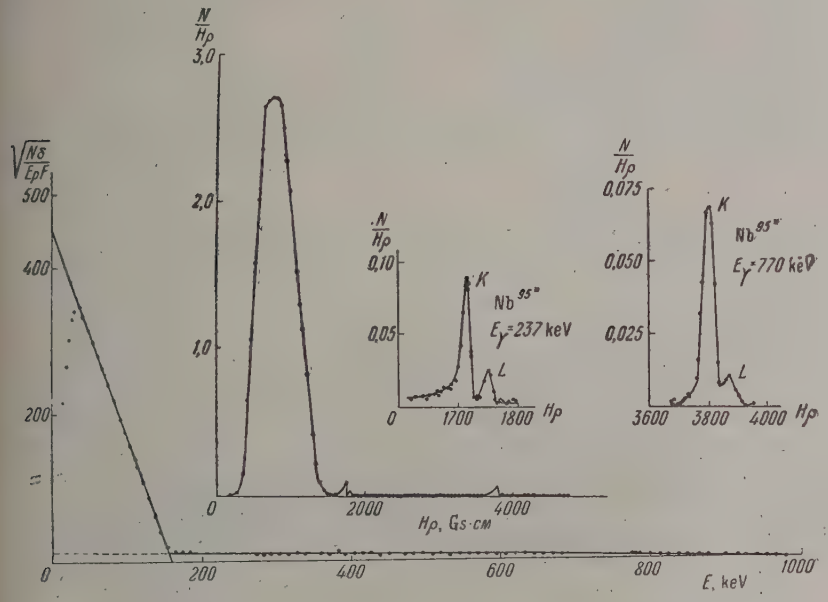

Fig. 7. β-spectrum of Nb^{95} and the Kurie plot.

The presence of the hard component was confirmed by a supplementary series of measurements using a stronger Nb^{95} source (but one with a greater superficial density). In these measurements the intensity of the hard component was enhanced. On the basis of the data obtained we propose the decay scheme for $Nb^{95} \rightarrow Mo^{95}$ pictured in Fig. 6. The following values of α_K and K/L were found for the γ-rays from Nb^{95}: $\alpha_K = (1.9\pm0.1)\cdot10^{-3}$ and K/L = 7.4±0.2.

Thus as a result of the investigation we suggest an overall scheme for the decay series $Zr^{95} \rightarrow Nb^{95} \rightarrow Mo^{95}$ in which the metastable Nb^{95*} nuclei decay by γ-transition to the ground state of Nb^{95}.

According to the curves of Goldhaber & Sunyar,[3] we find the following values of the ratio K/L for the isomeric transition of Nb^{95*} (Z = 41 and E_γ = 237 kev) corresponding to different multipole orders of the γ-radiation: ~ 4.15 for E3, ~ 2.2 for E4, ~ 7.3 for M3 and ~ 4.7 for M4.

Juxtaposing these values with our experimental data for this transition, we are justified in identifying it as type M4, although the possibility of its being E3 is not entirely excluded. To check this identification by means of Weisskopf's equations,[13] we calculated the lifetimes of the metastable state of Nb^{95*} (E_γ = = 237 kev) assuming γ-radiation of different multipole orders. The computed values were compared with the experimental lifetimes, determined taking internal conversion into account.

The internal conversion coefficients for Nb^{95*} used for determining the mean lifetime of the metastable nucleus τ_{exp} were computed according to the table given by Rose et al.[2]

The results of our calculations are presented in Table 1.

Table 1

Type transition	E3	E4	E5	M3	M4
τ_γ theo *sec*	$2\cdot10^{-4}$	$3{,}6\cdot10^{-4}$	$8{,}7\cdot10^{10}$	2,2	$3{,}9\cdot10^{5}$
τ_γ exp *sec*	$5{,}8\cdot10^{5}$	$1\cdot10^{6}$	$3{,}5\cdot10^{6}$	$5\cdot10^{5}$	$17\cdot10^{5}$

In the light of our experimental value for K/L and the data of Table 1, the isomeric transition of Nb^{95*} should be of type M4.

Comparing the experimentally determined values of the internal conversion coefficients for the other γ-transitions of Nb^{95} and Zr^{95} with the theoretical ones, computed as described above, we arrived at the following multipole orders:

E = 726 kev γ-line of Zr^{95} — M1 transition;
E = 760 kev γ-line of Zr^{95} — E2 transition;
E = 770 kev γ-line of Nb^{95} — E2 transition.

The multipole orders are indicated accordingly in the decay scheme for Zr^{95} and Nb^{95} diagrammed in Fig. 6.

Rh^{103*}

The isomeric Rh^{103*} nuclei were obtained as a result of β-decay of Ru^{103} with a half-life period of 40 days. The metastable Rh^{103*} nuclei pass to Rh^{103} with T = 57 min.

The $Ru^{103} \rightarrow Rh^{103}$ decay series has a complex β-spectrum and, in all probability, emits several groups of γ-rays. The data in the literature regarding the decay scheme of Ru^{103} is somewhat conflicting.[14, 15]

In the present investigation we carried out a detailed study of the decay of Ru^{103} in connection with the investigation of the isomeric transition of Rh^{103*}. The β-spectrum of Ru^{103} was observed by means of a magnetic β-spectrometer. The superficial density of the source was about 0.1 mg/cm^2. The electrons were recorded by counter with a window covered by a film having a superficial density under 0.1 mg/cm^2.

The experimental results are shown in Fig. 8.

Three peaks stand out in the β-spectrum; these are the K-, L- and M-lines associated with the isomeric transition of Rh^{103*} (40 kev); the conversion ratios are K/L = 0.18±0.03 and L/M = 7±1.

In addition to these conversion peaks we detected K- and L-lines corresponding to γ-rays from Ru^{103}, having an energy of 498 kev. In the series of measurements with a thicker source we also observed a conversion line corresponding to E_γ = 610 kev (see Fig. 8).

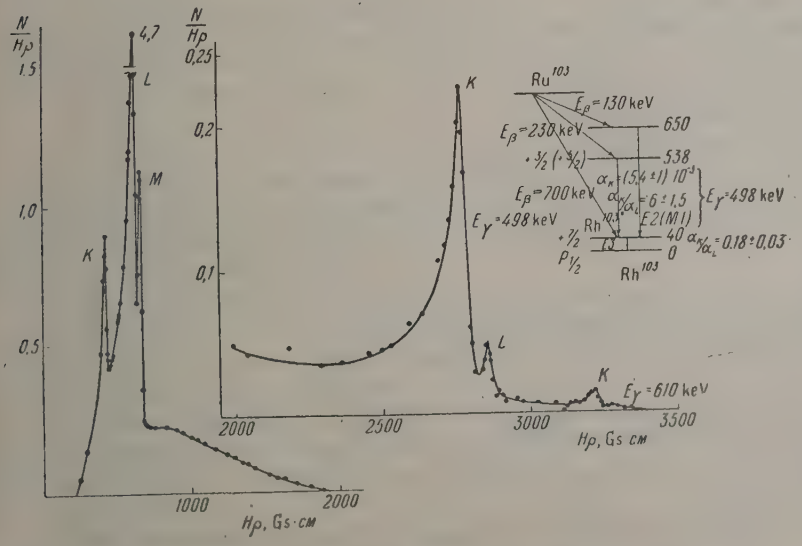

Fig. 8. β-spectrum and decay scheme of Ru^{103}.

From an analysis of the Kurie plot it follows that the β-spectrum of Ru^{103} is complex and apparently comprises three components having end-point energies:

E = 700 kev (5±1 %)
E = 230 kev } (95 %).
E = 120 kev }

Since in the present investigation we used relatively thick sources, the existence of the soft component having an end-point energy of ~120 kev cannot be considered as definitely proved.

On the basis of the data obtained we propose the decay scheme presented

in Fig. 8. We evaluated the relative intensity of the 230 kev end-point energy component as 75±20%. On the basis of the decay scheme shown in Fig. 8 the computed values of α_K and K/L for the 498 kev γ-rays from Ru^{103} are $\alpha_K = (5.4\pm1)\cdot10^{-3}$ and K/L = 6±1.5.

From a comparison of these data with the results of theoretical calculations it follows that the 498 kev γ-transition is either an electric quadrupole or a magnetic dipole one.

From the fact that the ratio of the number of conversion electrons corresponding to the isomeric transition of Rh^{103*} to the number of β-particles in the spectrum of Ru^{103} is nearly equal to unity it follows that the decay of all the excited levels of Rh^{103} leads to the formation of metastable Rh^{103*} nuclei which then transform to the stable Rh^{103} nuclei with a period of 57 min and a transition energy of 40 kev.

The theoretical values of K/L arrived at by the nonrelativistic method of calculation described by Hebb & Nelson[16] are listed in Table 2.

Table 2

Type transition	*E*	*E3*	*E4*	*E5*	*M4*	*M3*	*M2*
α_K/α_L	1,8	0,18	0,038	0,0074	0,21	0,85	3,5

From these data it may be concluded that the isomeric transition of Rh^{103*} is probably E3, although the possibility of its being M4 is not excluded. To clarify this point we compare the experimental mean lifetime τ_γ of the metastable state of Rh^{103} referred to γ-emission with the values computed by means of Weisskopf's equations.[13] The values of the internal conversion coefficients used in determining τ_{exp} were calculated according to the data of Lowen & Tralli.[17] The results are summarized in Table 3.

Table 3

Type transition	*E3*	*E4*	*M4*
$\tau_{\gamma\ exp}$ *sec*	$4\cdot10^6$	$1{,}4\cdot10^8$	$4\cdot10^8$
$\tau_{\gamma\ theor}$ *sec*	$4{,}4\cdot10^3$	$2{,}5\cdot10^{11}$	$3\cdot10^{12}$

From Table 3 and the conversion data it follows that the isomeric transition must be of type E3, since τ_{exp} can only be greater than τ_{theo} [13] (precluding E2 transitions).

Ba^{137*}

The radioactive isotope Cs^{137} decays by β-emission to Ba^{137} (T = 33 years). In 98% of a total number of disintegrations the β-decay of Cs^{137} leads to the formation of the metastable Ba^{137*} nuclei which have a half-life of 2.6 min.

The electron spectrum of Cs^{137} and Ba^{137*} obtained by us is shown in Fig. 9.* The continuous β-spectrum with end-point energy of 540±10 kev belongs to Cs^{137}. The K-, L- and M-lines are associated with the isomeric transitions of Ba^{137*} of energy 661±2 kev.

From the ratio of the number of electrons to the number of the β-particles in the spectrum of Cs^{137} we determined the internal conversion coefficient for the isomeric transition of Ba^{137} and the ratios K/L and L/M: $\alpha_K = 0.11\pm0.01$; K/L = = 6.0±0.1 and L/M = 4.1±0.4.

According to Rose et al[2] the values of α_K for Z = 56 and E_γ = 661 kev for different multipole orders are ~0.0095 for E3, ~0.025 for E4, ~0.045 for M3, ~0.1 for M4 and ~0.25 for M5. It follows that the isomeric transition of Ba^{137*}

---

* B.M.Dolishniuk participated in the investigation of Ba^{137}.

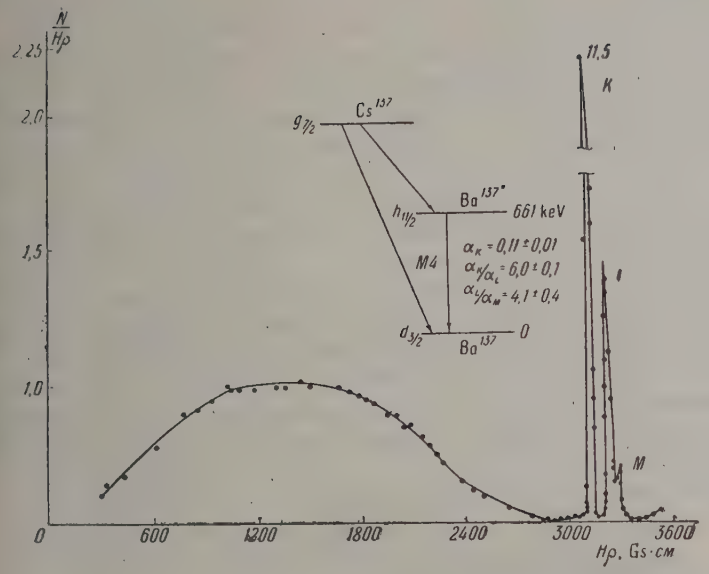

Fig. 9. β-spectrum and decay scheme of Cs^{137}.

is of type M4. The experimental value of K/L = 6.0±0.1 is in agreement with the value of 6 for M4 transitions from the curves of Goldhaber and Sunyar.[3] The decay scheme for Cs^{137} is pictured in Fig. 9. The state of the stable Ba^{137} nucleus is $d_{3/2}$; the metastable state of Ba^{137*} is $h_{11/2}$.

Conclusions

As a result of our investigation of the isomers Zn^{69*}, Se^{79*}, Se^{81*}, Nb^{95*}, Rh^{103*} and Ba^{137*}, having an odd number of protons or neutrons, we determined the multipole order of the radiation of these isomers. The principle characteristics of the isomeric transitions and the data on the levels corresponding to the ground and metastable states of the nuclei are summarized in Table 4. The transitions of Zn^{69*}, Nb^{95*} and Nb^{137*} to the ground state are accompanied by M4 radiation which is in agreement with the system of levels ensuing from the nuclear shell model.

Table 4

Principal characteristics of the isomeric transitions and levels of the metastable nuclei Zn^{69*}, Se^{79*}, Se^{81*}, Nb^{95*}, Rh^{103*} and Ba^{137*}

Nuclide	Half-life	E_γ, keV	α_K exp.	α_K theo.	α_K/α_L exp.	α_K/α_L comp	Type transition	Ground state	Metastable state	$\frac{\tau_\gamma \text{ exp.}}{\tau_\gamma \text{ theo.}}$
Zn^{69*}	13,8 hr	439	0,04±0,005	0,05	7,5±1,5	8	M4	$p_{1/2}$	$g_{9/2}$	~1
Se^{79*}	4 min	96	10	7	3±0,5	3	E3	$+^7/_2$	$p_{1/2}$	$\sim 10^3$
Se^{81*}	56 min	103	7,1±1,5	6	4±0,1	3	E3	$p_{1/2}$	$+^7/_2$	$\sim 10^3$
Nb^{95*}	90 hr	237	—	—	4,5±0,1	4,7	M4	$g_{9/2}$	$p_{1/2}$	~1
Rh^{103*}	57 min	40	—	—	0,18±0,03	0,18	E3	$p_{1/2}$	$+^7/_2$	$\sim 10^3$
Ba^{137*}	2,6 min	661	0,11±0,01	0,1	6±0,1	6,0	M4	$d_{3/2}$	$h_{11/2}$	~1

In the case of Se^{79*}, Se^{81*} and Rh^{103*}, the isomeric transition is accompanied by E3 radiation. To account for the transition being of type E3 in the case of these isomers one must assume the formation of a 7/2+ level in the third nuclear shell. It may be assumed that this level is formed as a result of the interaction of several odd nucleons located at the g-level of this nuclear shell.

It should be noted that for Se^{79*} the ground level is 7/2+, while the metastable state is $p_{1/2}$; for Se^{81*} the ground level is $p_{1/2}$ while the metastable one is 7/2+. The ground state of Zn^{69} may be designated as a $p_{1/2}$ level and the metastable state as $g_{9/2}$. The ground state of Nb^{95} must be assigned a $g_{9/2}$ con-

figuration; the metastable state, a $p_{1/2}$. These data are connected with the character of the filling of the levels in accordance with the nuclear shell model.

The last column of the table lists the ratios of the experimental lifetimes referred to the γ-radiation (taking conversion into account) to the lifetimes computed on the basis of the one-particle model of Weisskopf.[13] It will be seen that there is satisfactory agreement (i.e., a ratio close to unity) in the case of M4 transitions; this agreement is in accord with the one-particle model of radiation transitions in nuclei.

On the other hand in the case of E3 transitions (Se^{79*}, Se^{81*} and Rh^{103*}) the experimental lifetime values are some two-three orders of magnitude greater than the theoretical values. It might be assumed that in these nuclei the radiation occurs in accordance with the independent particle model, if we bear in mind the assumptions made in deriving the equations used in computing the lifetimes.

The greater than predicted by theory lifetimes may be due to deformations of the nucleus tending to prolong the life of excited nuclear states. Further accumulation of experimental data on the transformations of isomeric nuclei should help clarify some of the peculiarities and characteristics of the structure of nuclear shells.

In conclusion the authors desire to thank P.A.Zabelin and V.I.Sharalapov for their help in the investigation.

References

1. I.Livingood & C.Seaborg, Phys. Rev., 55, 457 (1939).
2. M.Rose, G.Goertzel, B.Spinrad, J.Harr, P.Strong, Phys. Rev., 83, 79 (1951).
3. M.Goldhaber, A.Sunyar, Phys. Rev., 83, 906 (1951).
4. W.Rutledge, J.Cork, S.Burson, Phys. Rev., 86, 775 (1952).
5. G.Dravkin & L.Rusinov, Doklady AN SSSR, 97, 417 (1954).
6. M.Goldhaber, R.Hill, Rev. Mod. Phys., 24, 179 (1952).
7. I.Bergstrom, S.Thulin, Phys. Rev., 76, 1718 (1949).
8. I.Brunner, O.Huber, Helv. Phys. Acta, 26, 588 (1953).
9. B.Dolishniuk, G.Drabkin, V.Orlov & L.Rusinov, Doklady AN SSSR, 92,1141(1953).
10. V.Shpinel', Zhur. eksp. i teor. fiz., 21, 1370 (1951).
11. H.Slatis, L.Zappa, Ark. Fys., 5, 26 (1952).
12. J.Cork, J.LeBlanc, R.Stump, W.Nester, Phys. Rev., 86, 575 (1952).
13. V.Weisskopf, Phys. Rev., 83, 1073 (1951).
14. E.Kondaiah, Phys. Rev., 79, 891 (1950).
15. J.Cork, J.LeBlanc, D.Martin, W.Nester, M.Brice, Phys. Rev., 90, 579 (1953).
16. M.Hebb, E.Nelson, Phys. Rev., 58, 486 (1940).
17. I.Lowen, N.Tralli, Phys. Rev., 75, 529 (1949); Phys. Rev., 76, 1541 (1949).

* * * * * * *

LIFETIMES OF THE EXCITED STATES OF CERTAIN NUCLEI

- E.E.Berlovich

Introduction

The range of lifetimes of excited nuclear states is very wide, extending from intervals on the order of 10^{-18}–10^{-17} sec (for example, levels formed in radiative neutron capture) to several years. The long period states are commonly called metastable, the criterion being that the lifetime is susceptible of measurement. Actually, however, the lower limit of measurement is gradually being reduced, so that there can be no distinction in principle between ordinary nuclear states and metastable (or isomeric) ones.

At present it is possible to measure lifetimes of the order of 10^{-9}–10^{-10} sec with fair accuracy and to evaluate even shorter ones. Such brief lifetimes are measured by means of coincidence circuits with a small resolving time, having provision for introducing a variable delay into either counter circuit.[1-7]

Below we describe a coincidence circuit, not unlike that used by Bell, Graham and Petch,[6] constructed in our laboratory and give some results of measurements of the periods of excited states of nuclei in the 10^{-10} to 10^{-8} sec range.

Description of the Equipment

A block diagram of the experimental set-up showing the more important units is reproduced in Fig. 1. Negative pulses from the plates of the two photomultiplier tubes (F1 and F2) are applied through suitable capacitors to the grids of

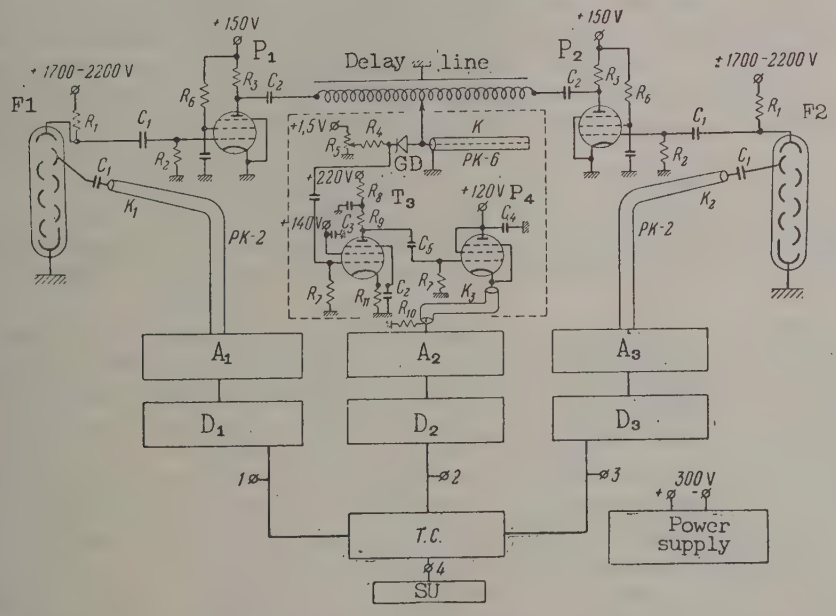

Fig. 1. Block diagram of the experimental set-up (the part of the circuit enclosed by the dash line is mounted on the delay-line carriage); F1 and F2) photomultipliers, P_1 & P_2) 6Zh1P pentodes, K) short-circuited shaping cable, K_1, K_2 & K_3) coupling cables, GD) germanium diode, D_1, D_2 & D_3) discriminators, A_1 & A_3) amplifiers (μ_A= 4000; band ~ 3.5 mc, A_2) amplifier (μ_A= 6000; band ~ 3.5 mc), T.C.) triple coincidence circuit (τ = 0.3 sec), SU) scaling unit, R_1 - 8.2 kΩ, R_2 - 200 kΩ, R_3 - 100Ω, R_4 - 3 kΩ, R_5 - R_6 - 33 kΩ, R_7 - 1 MΩ, R_8 - 5 KΩ, R_9 - 10 KΩ, R_{10} - 100Ω, R_{11} - 500Ω, C_1 - C_2 - 0.01 μf, C_3 - 1 μf, C_4 - 2 μf, C_5 - 2.5 μf.

the pentodes P_1 and P_2 (Tube type: 6Zh1P), cutting them off and thus giving rise to positive pulses of standard amplitude in the pentode plate circuits. These pulses are applied to the opposite ends of the variable delay line: a rheochord, i.e., a copper conductor wound over a helical groove in a brass cylinder. The conductor is laid on polystyrene blocks mounted along the groove at regular intervals. The entire rheochord cylinder can be rotated by means of a hand wheel driving a worm pair, thus displacing the delay-line carriage which engages in the helical groove on the cylinder. All the circuit components enclosed by the dash line in Fig. 1 are mounted on the carriage and travel with it. The rheochord slider, making contact with the central conductor, is connected to the short-circuited shaping cable K, whose effective length (twice the actual) determines the resolving time of the coincidence circuit. The shaped pulses of 2t' sec (t' is the transmission time of the pulse in one direction in the cable) duration go through the germanium diode GD to the amplifier tube T_3 and the cathode follower P_4. By virtue of the non-linearity of the diode characteristic, its cut-off potential can be adjusted by means of potentiometer R_5 so that after the diode the individual pulses from each of the photomultipliers will be small compared with two pulses in coincidence from both photomultipliers. In this manner one can obtain a selection factor for double coincidences equal to 4-5.

In operation the rheochord slider is displaced by means of the hand wheel to find the position where the pulses from the two photomultipliers coincide. Thus if the pulses in both photomultipliers originate simultaneously, coincidences will be recorded with the slider near the middle of the central conductor. If the pulses are separated by some time interval, the natural delay of the second pulse must be compensated for by introducing an equal delay in the path of the pulse from the first photomultiplier, i.e., by moving the slider an appropriate distance in the appropriate direction, for coincidence to be obtained.

From the output of tube P_4 the pulses go to the amplifier A_2 and the discriminator D_2, which serves to limit individual pulses passing through the capacitance of the diode GD.

At the same time the signals from the final emitters of the photomultiplier tubes are carried through cables K_1 and K_2 to the amplifiers A_1 and A_3 and thence to the discriminators D_1 and D_3. Finally all three pulses are applied to the triple coincidence circuit T.C., which in turn is coupled to the scaling unit SU, connected to the mechanical counter.

The use of the triple coincidence circuit enhances the reliability of the system and increases the coincidence counting efficiency. For maximum coincidence counting efficiency the discrimination of the diode should be minimal. This is necessary in order to obtain coincidences from weak pulses which might not fully cut off P_1 (or P_2). On the other hand, with a minimal discrimination adjustment, a single strong pulse might be recorded as a double one (i.e, a coincidence). This possibility is obviated by the triple coincidence circuit. Furthermore, the discriminators D_1 and D_3 permit cutting off a considerable proportion of the noise pulses from the photomultipliers, which might otherwise give accidental coincidences. This is particularly important in the case of the described circuit for it operates with a rather high voltage (1700-2200 v) on the photomultiplier tubes. The use of the high voltage is dictated 1) by the necessity of insuring a sufficiently high pulse amplitude (several volts) to cut off the limiting pentodes and 2) the need for reducing the fluctuations of the pulse front in the photomultiplier in order to minimize the resolving time of the double coincidence circuit.

A distinctive feature of the described coincidence system is that it operates on the narrow initial portion of the pulse fronts. The entire pulse due to the flash of light in the phosphor viewed by the photocathode of the multiplier has a duration equal to the luminescence time of the phosphor and the resultant ejection of electrons from the photocathode. However, with a high amplification of the multiplier the blocking pentode P_1 (or P_2) will cut off at the initial stage of the development of the flash in the phosphor, so that the rest of the pulse will not be

"sensed" by the tube (the tube operates - cuts in - with a time constant on the order of 10^{-7} sec). In principle with high photomultiplier amplification the pentode may be cut off by the first electron ejected from the photocathode. Naturally even in this case the shorter the luminescence period of the phosphor, the briefer will be the attainable resolving time of the coincidence circuit, since with the shorter luminescence time the "first" electron will be ejected earlier. The effect of these factors on the resolving time is examined in detail by Post & Schiff.[8]

Tuning and adjustment of the system involves careful selection and matching of the photomultiplier tubes (we used Type FEU-19), the voltage divider in the multiplier supply line and the diode and blocking pentodes. The values and parameters of the circuit components, including the amplifiers, are indicated in Fig. 1.

The voltage divider supplying the photomultipliers is characterized by the following data (the resistors are numbered beginning with the one nearest the photocathode):

$$\frac{r_1}{r_{3-11}} = 3{,}5; \quad \frac{r_2}{r_{4-11}} = 3{,}2; \quad \frac{r_3}{r_{4-11}} = 0{,}2; \quad \frac{r_{12-14}}{r_{4-11}} = 2; \quad \frac{r_{15}}{r_{4-11}} = 2{,}5.$$

The low value of the third resistance is dictated by the design characteristics of the photomultiplier tube.

It will be noted that the described circuit does not necessitate the use of wide-band amplifiers, common to circuits with a small resolving time.

Measurement of the Lifetimes of Excited States of Nuclei

In cases when the excited state of the nucleus is produced as a result of α- or β-decay, or after a preceding radiative transition to the given level, or by a transfer of energy to an atomic electron (internal conversion), the lifetime of the investigated level can be determined by measuring the number of α-γ, β-γ γ-γ or e^--γ coincidences (as the case may be) as a function of the delay time introduced into one of the branches of the coincidence circuit. If the excited state decays by the ejection of a conversion electron, the coincidences of the α, β, γ or e-rays with these electrons are determined.

Suppose, for example, that the nuclei of the source U, a substance with an atomic number Z, are transformed by β^--decay to nuclei with atomic number Z + 1 (or Z - 1 in the case of β^+-decay) in an excited state, which then decays to a lower or the ground state by the emission of one or more γ-quanta (see Fig. 2).

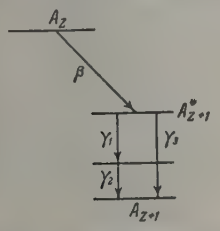

Fig. 2. Diagram illustrating equation (1).

In our set-up (Fig. 3), the source is placed between the two photomultipliers (FI and FII), with plates cut from a single crystal of stilbene cemented to their photocathodes. An aluminum foil absorbing all electrons is mounted between the source U and the photomultiplier FI. Thus the FI multiplier receives only light flashes induced in the phosphor by photons, while the other, FII, receives light pulses due both to β-particles and the γ-rays.

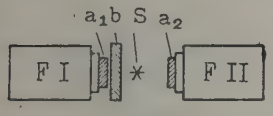

Fig. 3. Arrangement of source and detectors: FI and FII) photomultipliers; a) phosphors, b) absorber, S) source.

Let the solid angles (with apexes at the source) subtended by the phosphors a_1 and a_2 be ω_1 and ω_2; the number of quanta γ_1, γ_2, .., γ_n per decay be p_1, p_2, .., p_n, respectively, and the respective efficiencies in recording these be ε_1, ε_2, .., ε_n. The emission of photons beginning with the instant of formation of the excited state must proceed according to the exponential law. If the disintegration constant is λ, the resolving time of the coincidence circuit is 2τ, the number of decay events in the source per unit time is N_0 and the delay time introduced into the branch recording β-particles

is t, then, provided $\tau \ll 1/\lambda$, the number of coincidences per unit time will be

$$C = 2\tau N_0 \omega_1 \omega_2 (p_1\varepsilon_1 + p_2\varepsilon_2 + \ldots + p_n\varepsilon_n)\lambda e^{-\lambda t}. \qquad (1)$$

The above equation is based on the obvious assumption that the number of disintegrating (by γ-emission) atoms is proportional to the number of atoms of the given type present. The number of atoms capable of emitting γ-quanta present is determined by the number of β-decays per unit time, since the "γ-active" atoms are formed by the β-decay process. It is also assumed that only the higher initial state is metastable, while the lower excited levels have appreciably shorter lifetimes.

In cases when the condition $\tau \ll 1/\lambda$ is not fulfilled the number of coincidences recorded per unit time will depend on the shape of the pulses. The influence of different pulse forms (triangular and gaussian) is analyzed in Refs. 9, 10 & 11 and it is shown that in this case, with t greater than τ, the coincidence count rate also falls off exponentially as a function of the delay time.

It follows from the above that to determine the lifetime of an excited state one must investigate the variation of the number of coincidences with the delay time. Then, having plotted the curve for this variation in semilogarithmic coordinates, one can readily find the disintegration constant λ from the slope of the straight line so obtained.

If the lifetime of the investigated state is short compared to the resolving time of the coincidence circuit, one cannot obtain the exponential curve. In this case the sought lifetime can be evaluated from the shift of the coincidence curve relative to the center of gravity of a fast coincidence curve obtained for a cascade transition, passing through an intermediate state known to have a very brief lifetime. In order to enhance the sensitivity of this procedure it is advantageous to effect the measurements with the β-particle absorber in two positions: first in front of one photomultiplier and then in front of the other. Through this expedient the magnitude of the shift is doubled.

Isomeric State of Ta^{181}

Fig. 4 shows the $Hf^{181} \rightarrow Ta^{181}$ decay scheme deduced from investigations of the radiation from Hf^{181}. 12&13 It will be seen that the β-decay of Hf^{181} leads to a metastable state of Ta^{181} with a half-life of $2.2 \cdot 10^{-5}$ sec and an excitation energy of 611 kev. Aside from a low-intensity γ-transition directly to the ground level, there is an intense transition passing through the intermediate 481 kev level, which, according to Barber,[14] has a period of $1.08 \cdot 10^{-8}$ sec. According to Jensen[13] the 133 kev transition between the two metastable levels is strongly converted: the internal conversion coefficient is computed to be about 11. Hence it is feasible to observe the coincidence of the 64 and 122 kev electrons associated with this transition with the 481, 344 and 136 kev γ-rays. In order to reduce the number of fast γ-γ coincidences due to the 344 and 136 kev cascade quanta, we installed a lead absorber 3 mm thick between the source and the first photomultiplier; this absorber greatly attenuated the 136 kev rays, partially absorbed the 344 kev radiation and only slightly weakened the emission of the main branch (70%), having an energy of 481 kev.

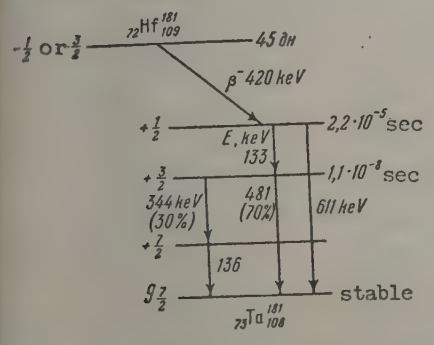

Fig. 4. $Hf^{181} \rightarrow Ta^{181}$ scheme.

In this experiment a thick stilbene crystal (h = 25 mm; dia. = 33 mm) was cemented over the FI photomultiplier, recording the γ-rays (Fig. 3). The source was prepared by coating the bottom of a

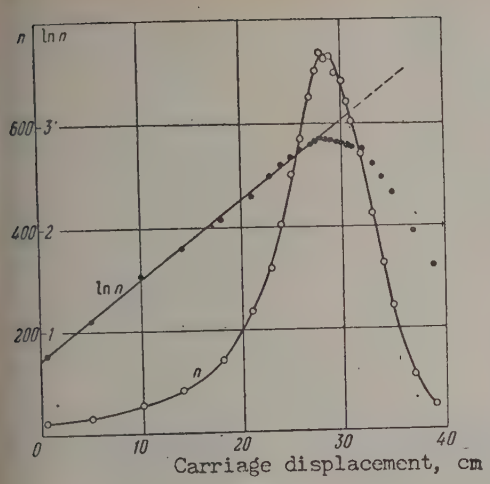

Fig. 5. Variation of the number of coincidences for the 481 kev level of Ta^{181} with delay time.

shallow, flat plexiglass dish (3 mm thick) with a layer of hafnium oxide.

The variation of the number of coincidences with the delay time introduced into the circuit branch recording conversion electrons is shown, plotted in conventional and logarithmic coordinates, in Fig. 5. The time was gaged from the displacement of an indicator, mounted on the delay-line carriage, relative to a stationary scale. Since the rate of propogation of a pulse in the delay line is equal to the speed of light, knowing the displacement of the contact slider corresponding to one division of the indicator scale one can calibrate the scale accordingly. However, in practice it is more convenient to introduce an additional section of cable into one of the channels and observe the resultant shift of the coincidence curve. The delay time is found from the wave impedance (ρ) and the capacitance (C) of the cable by means of the equation

$$t = \rho C. \qquad (2)$$

In this calibration procedure pulses from the same photomultiplier were fed into both channels of the coincidence circuit and the coincidence curves made of minimal width. The accuracy of the calibration is determined by the accuracy with which the values of ρ and C are known; in our case it is calculated to be within 3%.

The half-life of the investigated level of Ta^{181} as determined from the slope of the logarithmic curve is $(0.86 \pm 0.10) \cdot 10^{-8}$. This result is in agreement with the values obtained by Barber.[14]

Excited State of Sr^{86}

The scheme for $Rb^{86} \rightarrow Sr^{86}$ as established by a number of investigators[15-17] is shown in Fig. 6. The ground state of the even-even Sr^{86} nucleus may be assumed to have spin 0 and even parity.

It follows from the unique shape of the hard β-spectrum, corresponding to the transition to the ground level of Sr^{86}, that the ground state of the Rb^{86} must be assigned spin 2 and odd parity. This spin value has also been obtained experimentally.[18] From analysis of the β-γ angular correlation data in the literature and of the results of measurement of the soft β-spectrum associated with the transition ending at the excited level of Sr^{86} Muether & Ridgeway[16] conclude that the possible spin assignments for these levels are 1, 2 or 3.

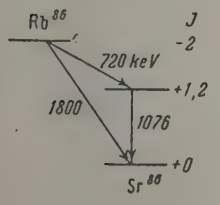

Fig. 6. $Rb^{86} \rightarrow Sr^{86}$ scheme.

The results of our measurements of the variation in the number of β-γ coincidences with the delay time are shown in Fig. 7. In one case (solid dots) the β-ray absorber was located to the left of the source; in the other case (circles), to the right (Fig. 3). As may be seen both curves (normalized to the same height) are fully symmetrical relative to the midpoint of the rheochord and exhibit no lateral shift relative to each other. Each one millimeter division on the scale of our instrument has a value of $2.2 \cdot 10^{-10}$ sec. If the lifetime of the investigated level of Sr^{86} were equal to this interval, the relative shift of the curves would be equivalent to $4.4 \cdot 10^{-10}$ sec which would be readily noticeable with the

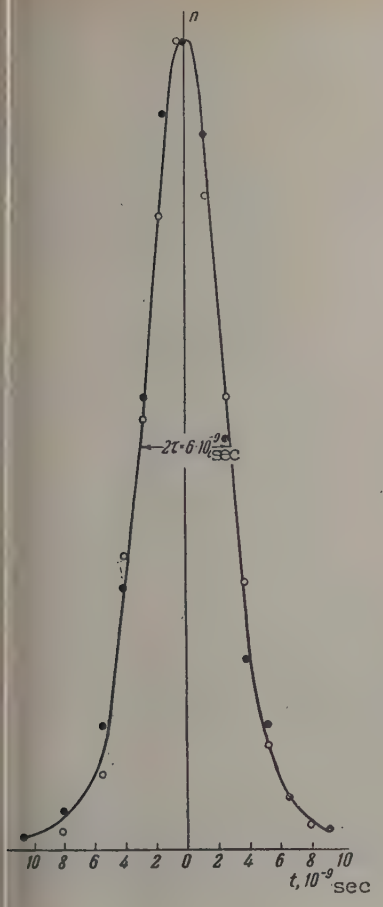

Fig. 7. Variation in number of coincidences for the excited level of Sr^{86} with delay time.

widths of the resolving curves employed. It may be concluded, therefore, that the lifetime of the excited Sr^{86} level is under 10^{-10} sec.

The results of our determination of τ_γ from the curves given by Moszkowski[19] lead to the following values for the possible spins and parities of the excited state of Sr^{86}:

Spin and parity	Type transition	τ_γ, sec
1+	M1	$5\cdot10^{-13}$
2+	E2	$6\cdot10^{-12}$
3+	E3	$6\cdot10^{-4}$

It follows from these data that the value of 3 for the spin must be rejected, since it is entirely inconsistent with our evaluation of the upper limit of the lifetime of this state.

Excited State of Tl^{203}

Radioactive Hg^{203} has a simple β-spectrum, characterizing the transition to the sole excited level of the Tl^{203} nucleus (Fig. 8). We carried out $\beta-\gamma$ coincidence measurements using the same procedure as described above (β-ray absorber first on one side and then on the other of the source). The results are shown in Fig. 9. It will be seen that the two curves are shifted relative to each other; the distance between the cg's of the two curves is about $1.2\cdot10^{-9}$ sec. Consequently, the mean lifetime of the excited state of the Tl^{203} nucleus is about 6.10^{-10} sec, and the half-life, $T_{\frac{1}{2}} = 4.1\cdot10^{-10}$ sec. In view of the smallness of this value it should probably be regarded as the upper limit of the period of the investigated state. Our value is in agreement with the upper limit for the lifetime of this state set by McGowan.[20]

From the curves of Mozskowski[19] for radiation of different types and multipole orders we find the following values for the mean lifetime, assuming the energy of the transition to be 280 kev:

Type transition	τ_γ, sec
E1	$6\cdot10^{-16}$
M1	$1\cdot10^{-11}$
E2	$4\cdot10^{-10}$

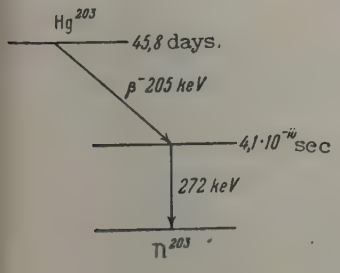

Fig. 8. $Hg^{203} \rightarrow Tl^{203}$ scheme.

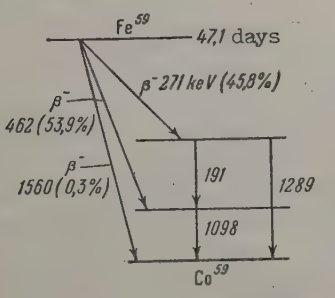

Fig. 10. $Fe^{59} \rightarrow Co^{59}$ scheme.

Hence the electric quadrupole assignment is in best agreement with our value for the upper limit of the lifetime of the excited state of Tl^{203}. However, our value does not preclude the possibility of its being either M1 or a mixed M1 + E2 transition.

The data in the literature on the interval conversion coefficient (0.19 in Ref. 21 and 0.23 in Ref. 22) and on the ratio of the K and L coefficients

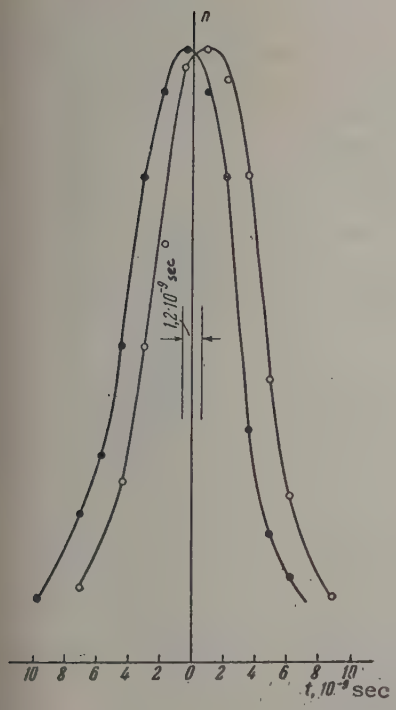

Fig. 9. Variation in the number of coincidences for Tl^{203} with the delay time.

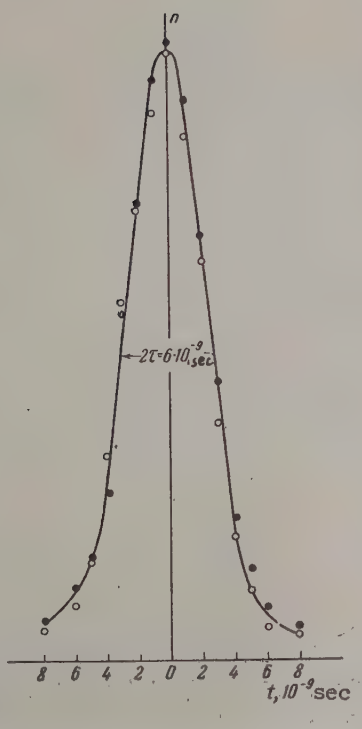

Fig. 11. Variation in number of coincidences for the levels of Co^{59} with the delay time.

(K/L = 3, according to Ref. 23) also does not permit of making an unequivocal selection between E2 and M1. Thus, according to the theoretical analysis of Rose et al[24] α_K for Tl^{203} in the case of E2 radiation should have a value somewhat under 0.1, while for M1 the approximate value is 0.65. This would appear to favor identification of this transition as a mixed M1 + E2 transition.

$Fe^{59} \rightarrow Co^{59}$

The scheme of this transition is pictured in Fig. 10.[25] In this case we investigated both $\gamma-\gamma$ coincidences and $\beta-\gamma$ coincidences; in some of the latter measurement we filtered out the soft (271 kev) β-component and thus investigated the $\beta-\gamma$ coincidences corresponding to the lower excited state. The described measurement procedure with the absorber to the right and left of the source did not, however, result in any noticeable relative displacement of the experimental curves. The dots and circles in Fig. 11 identify the results of the two series of measurements of $\beta-\gamma$ coincidences for the hard portion of the β-spectrum. Apparently the lifetime of the level is appreciably under 10^{-10} sec.

We wish to express our gratitude to V. Filimonov, graduate student of LPI (Leningrad Polytechnical Institute), for his help in making the measurements, K. Shilkov, student of LPI, for assistance in assembly of the apparatus, and A. Savateev, student of LPI, and D.M.Khai, member of the Leningrad Physico-Technical Institute, for aid in selecting and matching the voltage divider for the photomultipliers.

Leningrad Physico-Technical Institute
of the USSR Academy of Sciences

References

1. S.DeBenedetti & F.McGowan, Phys. Rev., 74, 728 (1948).
2. J.Bowe, M.Goldhaber et al, Phys. Rev. 73, 1219 (1948).
3. P.Bittencourt & M.Goldhaber, Phys. Rev. , 70, 780 (1946).
4. F.McGowan, Phys. Rev., 77, 138 (1950).
5. M.Deutsch & W.Wright, Phys. Rev., 77, 139 (1950).
6. R.Bell, R.Graham, H.Petch, Canad. Journ, Phys., 30, No. 1, 35 (1952).
7. S.DeBenedetti & H.Richings, Rev. Sci, Instr., 23, No. 1, 37 (1952).
8. R.Post & L.Schiff, Phys. Rev., 80, 1113 (1950).
9. F.Van Name, Phys. Rev., 75, 100 (1949).
10. D.Binder, Phys. Rev., 76, 856 (1946).

11. T. Newton, Phys. Rev., 78, 490 (1950).
12. K.Chu & M.Wiedenbeck, Phys. Rev., 75, 226 (1949).
13. E.Jensen, Phys. Rev., 76, 958 (1949).
14. W.Barber, Phys. Rev., 80, 332 (1950).
15. D.Zaffarano, B.Kern & A.Mitchell, Phys. Rev., 74, 682 (1948).
16. H.Muether, & S.Ridgeway, Phys. Rev., 80, 750 (1950).
17. A.Dmitriev & P.Zarubin, Izv. AN SSSR, Ser. Fiz. 18, 580 (1950). Trans. Bulletin, Vol. 18, No. 5, p.264.
18. E.Bellamy & K.Smith, Phil. Mag., 7 (44), 33 (1955).
19. S.Moszkowski, Phys. Rev., 83, 1071 (1951).
20. F.McGowan, Phys. Rev., 85, 142 (1952).
21. H.Wilson & S.Curran, Phil. Mag., 42, 768 (1951).
22. R.Heath & P.Bell., Phys. Rev., 87A, 176 (1952).
23. D.Saxon, Phys. Rev., 74, 849 (1948).
24. M.Rose, G.Goertzel et al, Phys. Rev., 88, 79 (1951).
25. A.Nesmeianov, A.Lapitski & N.Rudenko, Poluchenie radioaktivnykh izotopov (Preparation of radioactive isotopes), p. 151, M. 1954.

* * * * * * *

DETECTION OF SHORT PERIOD ISOMERS

- P.A.Iampol'ski, O.I.Leipunski, M.Ia.Gen & A.M.Tikhomirov

Detection of short period activities, ranging from a few microseconds to a fraction of a second, is hampered by a number of difficulties. The detection of activities of even shorter periods is now a familiar experimental procedure by virtue of the development of delayed coincidence techniques. These techniques, however, are no longer applicable in the case of activities with a period of an appreciable fraction of a millisecond or greater, since in this case it is necessary to have a recording instrument with low resolution which leads to the presence of a strong accidental-coincidence background. Increasing the activity of the sample does not solve the problem since the background intensity is increased in proportion.

In view of the experimental difficulties there are relatively few investigations devoted to activities in this time interval. Yet there can be no doubt that searches in this region might bring out a considerable number of hitherto unknown activities. Thus, for example, we know that the isotopes of light nuclei with N = = (Z - 1) are unstable and that their period drops off rapidly with increasing atomic number. The last of the known members of this series, Ti^{43}, has a half-life of 0.58 sec.[1] Undoubtedly if appropriate recording procedures were available we could detect the next, shorter-period members of the series. Martin & Brackon[2] investigated the isotopes of certain nuclei with equal numbers of protons and neutrons, produced by the (p,n) reaction. They discovered new short-lived isotopes having half-lives of a few tenths of a second. The equipment used by these investigators was not suitable for the measurement of shorter periods.

Up to the present, there has not been detected a single isomer with a half-life in the interval between 0.40 sec (Ta^{182*}) and $2 \cdot 10^{-5}$ sec (Ta^{181*}). This fact has been remarked on by a number of authors. Goldhaber & Sunyar[3] computed the energy regions where millisecond activities may be expected. For a multipole order of 3, the energy should be about 800 kev, i.e., such isomers should be relatively easy to detect. The absence of such isomers cannot be satisfactorily explained by present day theory.

In the opinion of O.I.Leipunski the dearth of information on the existence of short period (0.1 - 0.0001 sec) isomers was probably connected with methodological difficulties, specifically with the necessity of using powerful pulse sources for exciting the nuclei. Such sources had not hitherto been used for this purpose; hence, Leipunski suggested that work on the application of neutron, proton and γ-ray pulse sources might advantageously be initiated with a search for short period isomers.

The present report deals with the preliminary results of an investigation of short period activities resulting from bombardment of suitable targets with neutron bursts.

For the purpose of this investigation we developed a pulse source of neutrons having an energy of 14 Mev. The source is an ion tube with a potential of 150 kev. By virtue of the use of a pulsed ion source we obtained deuteron pulses of 1.3 millisec duration. The pulse form was square; the current I = 10 ma. The deuteron beam was used to bombard a zirconium target saturated with tritium;~14 Mev neutrons were formed as result of this bombardment.

The substances investigated for the presence of short period activities induced by fast neutrons were mounted immediately under the target. The γ-radiation produced by neutron bombardment of the investigated substance was recorded by means of a scintillation counter; the signals from the counter after appropriate amplification were applied to a cathode-ray oscillograph with a held-back sweep. The sweep was triggered by a special unit, the start of the sweep being exactly synchronized with the final instant of the deuteron pulse.

To permit verifying the absence of X-ray afterglow, the tube had provision for introducing a brass shield into the deuteron beam in front of the zirconium target. The verification was effected by means of a dual beam oscillograph: one beam recorded the deuteron beam; the other, the signal from the scintillation counter. The tests showed that the radiation ceased immediately upon interruption of the deuteron beam.

Furthermore the measurements showed that the efficiency of the scintillation counter + coupled amplifier as regards response to γ-radiation did not change upon termination of the neutron pulse.

Thus the set-up recorded only γ-rays emitted after bombardment of the sample with neutrons and was not affected by the X-rays connected with the operation of the tube or the instantaneous γ-radiation originating incident to the interaction of neutrons with the material of the sample. The available range of sweep times of the cathode-ray oscillograph permitted detecting activities with periods in the 10^{-4} to 10^{-1} sec interval. A loop oscillograph was used for recording and measuring longer half-lives.

When the deuteron beam was incident on the target the scintillation counter indicated a very intense afterglow even in the absence of a sample between the target and the scintillation counter. Judging by the magnitude of the pulses the afterglow consisted of γ-rays rather than X-rays. The afterglow intensity varied markedly with changes in the distance between the target and counter (possibly, inversely as the square of the distance). Whence it follows that the source of the γ-radiation was located in the immediate proximity of the target or crystal. Thus the tests show that the detected γ-radiation could not be a result of capture of neutrons slowed down in the shielding.

In the absence of a neutron-bombarded target we detected γ-rays emitted with the following periods: 1) 0.45-1.5 millisec, 2) 5.5 millisec, 3) 27-30 millisec and 4) 3-4 sec.

All measurements were made using organic crystals on the scintillation counter. When an NaI.Tl crystal was installed on the counter, in addition to the above listed periods we observed γ-rays whose intensity dropped off with a period of 12 sec; this activity was a result of the $Na(n,\alpha)F$ reaction with the sodium of the crystal.

None of the elements entering into the composition of the ion tube and photomultiplier is known to form isotopes having such decay periods as a result of neutron reactions.

The activity with the 27 millisec period could be due to the presence of B^{12} (T = 27 millisec, E_β = 13.43 Mev); B^{12} could conceivably form as a result of the $N^{15}(n,\alpha)$ or $C^{12}(n,p)$ reactions. However, no noticeable increase of intensity of this radiation followed the introduction of specimens containing nitrogen and carbon between the target and counter.

We placed samples containing Fe, Cu, Al, N, H, Zr and W between the target and the crystal of the photomultiplier; none of these substances produced any appreciable difference in the character of the afterglow. So far we have not been able to establish what elements are responsible for this radiation.

The energy of the radiation was roughly evaluated by varying the discrimination of the pulses reaching the trigger.

Of the detected activities with periods T = 27, 5.5 and 0.45-1.5 millisec, the shortest period activity was characterized by the hardest radiation; the longest period activity, by the softest.

From the displacement of the discriminator, which was calibrated by means of γ-radiation from Au^{198}, Co^{60} and Na^{24} it may be assumed that the energy of the shortest activity γ-rays was about 2.5 Mev. We believe the detected γ-radiation cannot be attributed to any known radioactive isotope but is rather the emission of some new, as yet unknown isomers produced in the inelastic scattering of 14 Mev neutrons by some element.

Possibly the short period γ-radiation observed by a number of investigators and as yet unexplained may be due to such formation of isomers. Thus Brolley et al,[4] searching for short period activities while using a pulsed neutron source (Be + d; E_d = 11 Mev), observed a short period background with a half-life of some tenths of a millisec. In another investigation,[5] effected with neutrons from the (Li + d) reaction (E_d = 0.9 Mev; $E_n \simeq$ 14 Mev), the investigators detected γ-radiation with a period of 25-30 millisec. It is interesting to note that when in the last investigation the lithium target was replaced by one of boron (i.e., when the neutron energy was reduced), the short period background disappeared.

Studies aimed at elucidating the nature of the formed isomers and the character of the nuclear reactions resulting in their formation are now under way.

In addition to the elements listed above we also investigated lead and bismuth. Campbell & Goodrich[6] detected a short period isomer of lead, Pb^{207*}, with a 0.9 sec activity. This isomer was obtained by bombardment of lead with slow neutrons in a reactor: $Pb^{208}(n,\gamma)Pb^{207*}$. In a later investigation[7] it was shown that the period of Pb^{207*} was actually 0.82 sec. We discovered a short period activity from lead bombarded with 14 Mev neutrons, having a period of 0.83 sec.

Our set-up was repeatedly calibrated with reference to the known energies of the emission from Pb^{207*} (1.07 and 0.56 Mev) for the purpose of determining the energy of the short period γ-radiation. To this end we measured the number of pulses on the screen of the oscillograph in the absence of an absorber and with aluminum absorbers of different thickness. By way of monitor we used an ionization chamber arranged to measure the current produced by the α-particles from the tritium target.

We also discovered that when a bismuth sample is placed between the target and the photomultiplier there is obtained a γ-ray activity with a period of 2.3-2.4 millisec. The energy of this γ-radiation as determined from the absorption by aluminum is about 2.5 Mev.

We must now ask to what isotope of bismuth should this radiation be ascribed?

Bismuth has one stable isotope - Bi^{209}. At present all the isotopes of bismuth from Bi^{197} to Bi^{214} with the one exception of Bi^{208} have been isolated or observed. In Seaborg's[8] tables there is mention that, according to a private communication from Neuman and Perlmann, this isotope has a short period. However,

these authors later withdrew this statement. Moreover there is reason to assume that Bi^{208} must have a long period,[9] since the spin of Bi^{208} is 5 while the spin of Pb^{208} is 0. In considering the interaction of 14 Mev neutrons with the Bi or Pb nucleus we can confine our examination to the (n,2n) and (n,n') reactions.

According to statistical nuclear theory[10]

$$\sigma_{n,2n} = \sigma_i [1 - (1 + \Delta E / T) e^{-\Delta E / T}],$$

where σ_i is the inelastic scattering cross section, ΔE is the difference between the neutron energy and the binding energy and T is the "temperature" of the nucleus.

According to the data of Graves & Rosen,[11] the "temperature" of the Bi nucleus in interaction with 14 Mev neutrons is about 0.95 Mev. Assuming ΔE = 7.5 Mev,[12] we find that for Bi $\sigma_{n,2n} \approx \sigma_i \approx \pi R^2$.

This is in agreement with the results of Clarke[13] who compared the experimental values of $\sigma_{n,2n}$ with the values computed from statistical theory for a number of elements. Thus it must be assumed that under bombardment by fast neutrons, Bi with mass number 208 does form. The radiation in question, however, cannot be ascribed to the β-decay of Bi^{208}, since this is a highly forbidden transition (J = 5) and with so high a disintegration constant the disintegration energy must be very great. We believe, rather, that the detected γ-radiation is associated with the isomeric transition of Bi^{208*}, formed in the excited state. This is all the more credible in view of the fact that the number of neutrons in Bi^{208} (125) is one less than the magic number (126), just as in Pb^{207}.

Vendries[7] in his investigation obtained the isomer Pb^{207} from the (n,n') reaction with neutrons from a Be + d source (E_d = 0.9 Mev). He found that the Pb^{207*} formation cross section equals $1.5 \cdot 10^{-26} cm^2$. If we accept that the inelastic scattering cross section is $2.7 \cdot 10^{-24} cm^2$, we see that only 5% of the nuclei participating in the reaction end in the isomeric state.

We made an attempt to evaluate the Pb^{207*} and Bi^{208*} formation cross sections in the (n,2n) reaction with 14 Mev neutrons. Our evaluation was necessarily rough since a number of factors (the absolute efficiency of recording, measurement energy, etc.) were not accurately known. It appears, however, that the yield of the isomeric state is near to unity, i.e., every or nearly every Pb^{207} or Bi^{208} nucleus formed as a result of the (n,2n) reaction is in the isomeric state. In the case of the (n,n') reaction with slower neutrons the probability of formation of isomeric nuclei is considerably lower.

In the interaction with fast neutrons, a nucleus may acquire an additional orbital momentum, proportional to $l \leq R/\lambda$, where R is the radius of the nucleus and λ is the wavelength of the neutron. For Bi and Pb and neutrons of 14 Mev energy, $R/\lambda > 7$. If the (n,2n) reaction occurs, 7-8 Mev of the energy brought by the neutron is expended on ejecting the second neutron from the nucleus.

The energy distribution of the neutrons emitted from Pb or Bi is Maxwellian with a maximum of about 1.5-2.0 Mev.[11,14] Thus, in the (n,2n) reaction the orbital momentum which can be removed from the nucleus by the two comparatively slow neutrons is, as a rule, lower than the momentum brought into the nucleus by the incident fast neutron. Hence there is a high probability that the residual nucleus will be left in a state with a higher (excess) orbital momentum as compared with the initial state; i.e., the probability of formation of the isomeric state as a result of the (n,2n) reaction is high.

The above reasoning may serve to explain the different activities observed from molybdenum. Mo^{91} obtained from the $Mo^{92}(\gamma,n)$ reaction decays with two periods: 16 min (E_β = 3.3 Mev) and 75 sec (E_β = 3.0 Mev).[15] According to the decay scheme given by the investigators the 16 min activity is due to the decay of the isomer Mo^{91*}. On the other hand an investigation of the $Mo^{92}(n,2n)Mo^{91}$ reaction with bombarding neutron energies up to 18 Mev showed that at these energies the short period activity is absent;[16] i.e., in the case of the (n,2n) reaction the molybdenum nuclei are formed predominantly in the isomeric state. We note that in

Mo^{91}, too, the number of neutrons is one less than a magic number.

References

1. A.Schalberg et al, Rev. Sci. Inst., 19, 459 (1948).
2. W.Martin & S.Brackon, Canad. J. Phys., 30, 643 (1952).
3. M.Goldhaber & A.Sunyar, Phys. Rev., 83, 906 (1951).
4. J.E.Brolley et al, Phys. Rev., 83, 990 (1951).
5. I.Jelly & E.Paul, Proc.Cambr. Phil. Soc., 44, 133 (1948).
6. C.Campbell & M.Goodrich, Phys. Rev., 78, 640 (1950).
7. G.Vendries, Ann. de Phys., 7, 656 (1952).
8. G.Seaborg, Rev. Mod. Phys., 20, 85 (1948).
9. M.Pryse, Proc. Phys. Soc., A65, 773 (1952).
10. V.Weisskopf, Statisticheskaia teoria iadrenykh reaktsii (Statistical Theory of Nuclear Reactions) M. 1952.
11. E.Graves & L.Rosen, Phys. Rev., 89, 343 (1953).
12. B.Kansey, G.Bartholomew & W.Walker, Phys. Rev., 82, 380 (1951).
13. P.Clarke, Canad. J. Phys., 31, 267 (1953).
14. B.Whitmore & G.Dennis, Phys. Rev., 84, 296 (1951).
15. R.Katz, a. oth., Canad. J. Phys., 31, 2, 250 (1953).
16. J.Brolley, Phys. Rev., 89, 876 (1953).

* * * * * * *

ON THE RESOLVING POWER OF A SCINTILLATION SPECTROMETER

- I.F.Barchuk, E.M.Galkin, M.V.Pasechnik & N.N.Pucherov

In recent years there have been great advances in the development of magnetic spectrometers having high resolution[1] and scintillation spectrometers having high transmission, advances which have made it possible to expand the scope of investigations of the energy spectra of atomic nuclei.

One obstacle in the way of wider application of single crystal scintillation spectrometers has been their low resolving power. The half-width of the spectral line in the best of the instruments described in the literature[2,3] is only 5-10% (for the γ-rays from Co^{60}). Our measurements showed that a single crystal scintillation spectrometer employing a Type FEU-19* photomultiplier tube has an even lower resolution. Attempts to increase the resolution by selection and matching of crystals and FEU tubes were not particularly successful.

We undertook two series of experiments for the purpose of bringing out the reasons for the inferior resolving power. In one of the series the scintillation spectrometer served as the "counter" of a magnetic spectrometer which was employed as an electron monochromator. In these measurements we evaluated the degree of monochromatization of the electron beam, which was determined by the resolving power of the magnetic spectrometer. In the second series of tests we recorded the spectral composition of the electron beam by means of the scintillation spectrometer.

It turned out that when the spread of the electron energies is 1%, the spread of the pulse heights at the FEU-19 photomultiplier output varies between 10 and 30%, depending on the energy of the electrons and the operating regime of the photomultiplier.

---

*FEU (ФЭУ) = Foto Electronnyi Umnozhitel - photo electronic multiplier. Trans.Ed.

We constructed a special set-up for testing FEU multiplier tubes, i.e., for determining their response to light pulses incident on the photocathode. A Kerr cell, which may be regarded as an essentially inertialess shutter, was employed to modulate the light.

The principal components of the set-up for determining the spread (scatter) of the pulses in height comprised a light source, the Kerr cell, the FEU-19 photomultiplier, an amplifier and a 50 channel analyzer. Each component was carefully checked beforehand; the stability and linearity of the amplifier section were systematically tested and verified. We also checked the stability of the generator; to this end the Kerr cell and FEU were cut out of the circuit and the pulses from the generator, appropriately reduced by means of a voltage divider, were applied to the amplifier and analyzer. Since in this case the pulses remained over a prolonged period of operation in one and the same channel of the analyzer it was assumed that the generator could be depended upon to produce pulses of constant amplitude (less than 2% spread in height).

The amplitudes of the light pulses used in the tests were determined upon in the following manner. A thallium-activated sodium iodide crystal with the usual reflector was mounted on the FEU-19 photocathode and the maximum pulse obtained with irradiation of the crystal with γ-rays from Co^{60} was measured. Next the crystal was removed and 750 volt pulses of the same shape and duration as those initially obtained from the photomultiplier were applied to the Kerr cell by means of the generator. The filament voltage of the light source lamp was regulated so that the height of the pulses at the output of the amplifier due to the light pulses from the Kerr cell would be equal to or differ by a known factor from the pulses produced by the scintillation of the NaI·Tl crystal under the influence of the γ-rays from Co^{60}.

Thus for each set filament voltage (brightness) we studied the spectrum of the electric pulses at the photomultiplier output with the photocathode illuminated by a modulated wide beam of light. It must be noted that if a narrow beam were used the results might be affected by inhomogeneities of the photocathode; in general these probably contribute to the scatter of pulse heights.

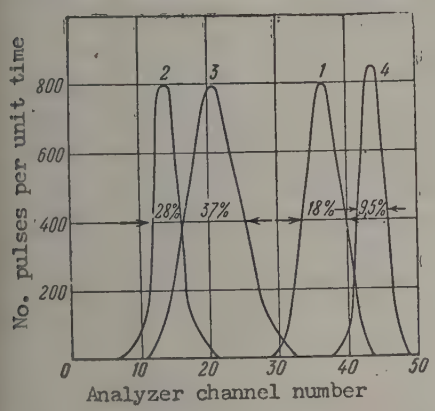

Fig. 1. Distribution of output pulses from the FEU-19 photomultiplier with light pulses of different intensity applied to the photocathode: 1) pulses equal to the maximum scintillation in the NaI·Tl crystal due to γ-rays from Co^{60}, 2) light 2.5 times weaker, 3) light 5 times weaker, 4) light 2.5 times stronger than for Curve 1.

The curves of Fig. 1 show the observed distribution of output pulse heights with input light pulses corresponding in intensity to the maximum scintillations in the NaI·Tl crystal produced by γ-rays from Co^{60} (Curve 1), with "light 2.5 times weaker" (Curve 2), "5 times weaker" (Curve 3) and "2.5 times stronger" (Curve 4), referred to the intensity for Curve 1. In view of the fact that with weak light intensities the counts came primarily in the first (side) channels of the analyzer, which situation could result in errors in determining the actual pulse-height spread, we increased the amplification and recorded the weaker input intensity curves at amplifications which brought the major part of the pulses into the higher-number (middle) channels of the analyzer. In the figures we give only the ratio of the half-widths to the height (in %). The particular curves shown in the figure were obtained for one of the tested FEU-19 tubes with a uniform distribution of potentials on the photocathode and emitters.

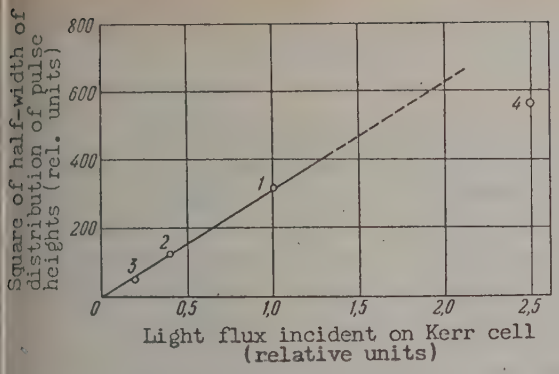

Fig. 2. Variation of the square of the half-width of the pulse spread curve with the height of the pulses. The figures correspond to the numbers of the curves in Fig. 1.

Fig. 2 shows the variation of the half-width of the peaks squared with the value of the light flux incident on the Kerr cell (position of maximum on the amplitude scale) for the four curves of Fig. 1 normalized to the same amplification factor. The point (4) at 2.5 on the light flux scale falls below the common straight line because of nonlinear distortion of the FEU due to space charges between the last emitters with a heavy current in the last stages.

It may be concluded from the cited data that the spread of pulse heights at the output of a scintillation spectrometer is due to statistical fluctuations in the number of electrons striking the first emitter as well as to fluctuation in the magnitude of the secondary emission coefficient. Consequently in order to increase the resolution of our scintillation spectrometers it would be necessary to have phosphors with a higher light yield and photocathodes with a higher quantum yield than are now available. Also further improvement of the electron optics of the first dynodes is indicated. As for the photomultiplier as a whole, it would appear that by proper selection of the potentials of the cathode-diaphragm-dynode system the parameters of the multiplier can be enhanced to some extent. In the case of some individual photomultiplier tubes we were able to reduce the spread by 20-50% through such selection and matching of the applied voltages.

We tested several dozen FEU-19 tubes both of the old and new design. It developed that the spread of pulse heights of different individual tubes varies appreciably: between 15 and 35% for light input pulses corresponding to the maximum scintillation of the NaI·Tl crystal irradiated by the γ-rays from Co^{60}.

For a few individual tubes we tried various adjustments of the voltages on the emitters, photocathode, focusing diaphragm and anode and in some cases succeeded in bringing down the pulse height spread to 6-10%. The optimum distribution of potentials proved to be different for different individual photomultipliers. For example, for one particular FEU-19 tube the optimum voltage proved to be 1080 v, distributed among the emitters by means of a dividing potentiometer with the following parameters: R_1 = 90 k , R_2 = 200 kΩ, R_3 = 19.5 kΩ, $R_4 \rightarrow R_{14}$ = 120 kΩ, R_{15} = 300 kΩ and R_{p1} = 75 kΩ. The pulse height spread did not alter appreciably when the characterized voltage divider was replaced by another having different absolute values but the same relative values of the resistors.

Physics Institute of the
Academy of Sciences of the USSR

References

1. A.Bashilov, B.Dzhelepov & L.Chervinskaia, Izv. AN SSSR, Ser. fiz., 17, 428 (1953); N.Anton'eva, A.Bashilov, B.Dzhelepov & V.Orlov, Izv. AN SSSR, Ser. fiz., 18, 93 (1954).
2. C.Borkowsky & R.Clark, Rev. Sci. Inst., 24, 1046 (1953).
3. R.Kiehn & C.Goodman, Phys. Rev., 95, 989 (1954).

ON DETERMINING THE DEFORMATION OF THE NUCLEAR SURFACE

- L.A.Sliv & L.K.Peker

As we know the nuclear shell model has been useful in explaining many features of nuclear structure and nuclear levels on the basis of the independence of individual nucleons. However the difficulties encountered in accounting for the large quadrupole moments and certain properties of the levels of even-even nuclei stimulated the development of a more general model - the collective model - capable of obviating these difficulties. The collective model allows not only for the independent motion of individual nucleons in a certain average, effective field but also for distortion of the nuclear surface and the rise of collective rotational and vibrational motions. This model yields a consistent explanation of both small and large quadrupole moments as well as of various deviations in the magnetic moments and, in addition, points to the existence of nuclear levels of a special type: the so-called rotational levels.[1] Analysis of earlier data and the results of certain specific experiments led to the discovery of a system of levels in the rare earth and heavier radioactive elements, the energy of which in even-even nuclei is characterized by the simple formula:

$$E = \frac{\hbar^2}{2J} I(I+1), \tag{1}$$

where J is the moment of inertia of the rotating part of the nucleus and I is the spin or angular momentum of the rotation.

The measured lifetimes of such levels proved to be shorter than the lifetimes of other, single particle levels, which is also indicative of the exceptional nature of these levels. The moment of inertia J, according to the theory,[1,2] is

$$J = 3\beta^2 B, \tag{2}$$

where

$$B = \frac{3}{8\pi} MAR_0^2; \tag{2'}$$

here M is the nucleon mass, A is the atomic weight, R_0 is the radius of the equivalent sphere and β is a deformation parameter, determined in the case of the simplest assumption that the nucleus is a spheroid from

$$R = R_0 [1 + \beta Y_{2,0}(\theta)], \tag{3}$$

where $Y_{2,0}(\theta)$ is the normalized spherical function.

The internal quadrupole moment of such a nucleus also depends on β and equals

$$Q_0 = \frac{3}{\sqrt{5\pi}} ZR_0^2\beta. \tag{4}$$

The spectroscopic value of the quadrupole moment

$$Q_s = PQ_0,$$

where

$$P = \frac{I(2I-1)}{(I+1)(2I+3)} \tag{4'}$$

Thus a relation between the energy of the rotational level and the quadrupole moment is established. However, if we determine β first from the experimental values of Q_s and then from the energy E_1 of the first rotational level, we obtain results diverging by a factor of 2-3 (See Table 1 in Ref. 3). Moreover, from E_1, using equation (1), we arrive at values of β for strongly deformed nuclei close to

Table 1

Values of the deformation parameter derived from the energy of the first levels of even-even nuclei(β_E), from the lifetimes of these levels (β_T) and from the quadrupole moments (β_Q)

Nucleus	β_E	β_T	β_Q
Dy^{160}	0,77	0,41	—
Er^{166}	0,76	0,30	—
Yb^{170}	0,74	0,31	0,46 (Yb^{173})
Hf^{176}	0,69	0,23	0,59 (Lu^{175})
Os^{186}	0,52	0,21	0,30 (Re^{185})
Os^{188}	0,49	0,13	0,36 (Os^{189})
Hg^{198}	0,30	0,11	0,07 (Hg^{201})
Po^{214}	0,22	0,062	—
Pu^{242}	0,82	—	—

unity. If this is true, the entire theory developed by Bohr[1] on the assumption that β is very small is invalidated.

It should be noted that equation (1) is deduced from theory as a first approximation for the case of strong coupling between the nuclear surface and the nucleons outside the closed shells (individual nucleons). When account is taken of the non-diagonal terms in the Hamiltonian and of the admixture of states with K = 1 or 2 (K is the projection of I on the nuclear axis of symmetry Z) the value of β is reduced to some extent; however, the decrease removes only a small part of the divergence and disturbs the proportionality $E \backsim I(I+1)$.

Let us determine β in yet a third way: from the lifetime of the rotational levels. Making use of equation (VII.17) from Ref. 2, we obtain the values (β_T) listed in the third column of Table 1. It will be seen that the values of the parameter found in this manner are smaller than those in the other two ways.

What method of determining β yields the correct value? Before attempting to answer this question let us turn to another phenomenon which at first glance bears no relation to the problem under discussion. Let us examine the β-transitions with equal degrees of forbiddenness to the ground and first excited levels of even nuclei with a large quadrupole moment. From the condition of the applicability of (1) it follows that there is no change in the deformation parameter β, or in the state of the individual nucleons, incident to a transition from the ground level. This greatly simplifies computation of the matrix elements for the β-transitions, inasmuch as the nucleonic wave functions are identical in both cases.

The wave function of the deformed nucleus is written as the product of the functions

$$\Psi = \sqrt{\frac{2I+1}{8\pi^2}}\,\varphi(\beta)\,D^I_{MK}(\theta_i)\cdot\sum_p \chi_p, \qquad (5)$$

where χ_p is the wave function of the individual nucleons, $\varphi(\beta)$ describes the oscillations of the surface relative to the equilibrium position and D^I_{MK} is the eigenfunction of a symmetrical top.[2] The normalization of the function is such that D gives a unitary transformation from the fixed coordinate system to the nuclear. Assuming that for the initial state the spin $I_i = 1$ and $K_i = 1$, for the ground state of the even nucleus $I_f = 0$ and $K_f = 0$ and for the excited state $I_f = 2$ and $K_f = 0$, we obtain, after integration, for the ratio of the squares of the matrix elements

$$\rho = \frac{|M(1\to 2)|^2}{|M(1\to 0)|^2} = \frac{1}{2} \qquad (6)$$

The initial state may contain an admixture of the state with $I_i = 1$ and $K_i = 0$ (or consist entirely of the latter). In this case $\rho = 2$. Thus, on condition that β = const. we find that $\rho \geqslant \frac{1}{2}$. Data on the ft-values for the transitions of interest to us here are assembled in Table 2. The experimental values of ρ are listed in the last column of the table. As may be seen from the table, $\rho < \frac{1}{2}$ and

Table 2

Data on -transitions to levels of even-even nuclei

Nucleus & emission	Type of transition	lg(ft)	ρ_{exp}
	Allowed transitions		
Rh^{104}; β^-	+1→+0	4,7	0,39
	+1→+2	5,11	
Ag^{106}; β^+, k	+1→+0	4,9	0,50
	+1→+2	5,2	
Ag^{108}; β^+, k	+1→+0	4,8	0,06
	+1→+2	6,0	
Ag^{108}; β^-	+1→+0	4,6	0,04
	+1→+2	6,0	
In^{114}; β^+, k	+1→+0	5,0	<0,5
	+1→+2	>5,3	
J^{128}; β^-	+1→+0	5,9	0,20
	+1→+2	6,6	
	Forbidden transitions		
Pr^{144}; β^-	−1→+0	6,5	0,03
	−1→+2	8,1	
Tu^{170}; β^-	−1→+0	8,9	0,16
	−1→+2	9,7	
Re^{186}; β^-	−1→+0	7,7	0,22
	−1→+2	8,35	

on the average equals 0.1.* This means that the integral over the nucleonic wave functions is not the same for the two β-transitions mentioned above. The difference in the values of the integral could result only because there is interaction between the rotation and the motion of individual nucleons, i.e. the motion of the nucleons follows the rotation non-adiabatically.

In the transition from the ground to the excited state of the even nucleus there is a small increment $(\Delta\beta)$ in the deformation of the nucleus. The small change in the surface leads to small changes in the states of the individual nucleons; although the changes are minor, the integral over the coordinates of many particles may be reduced several-fold.

The increased distortion incident to the transition to the excited state leads to another effect which has a direct bearing on the problem under discussion. The binding energy of the nucleons increases with the deformation of the nucleus and can, at some point, become greater than the increment of surface energy. As a result, in distortion there is liberated an energy

$$E_d = \sum_p \Delta E_p - \Delta V \cdot (surface) \qquad (7)$$

Hence the experimentally observed energy E of the level is the rotational energy E_{rot} less the released energy E_d:

$$E = E_{rot} - E_d. \qquad (8)$$

Consequently the rotational energy will always be greater than the actual energy of the level and hence the values of β obtained from the energy of the first levels were over-estimated. The true values of β should be calculated from the spectroscopic quadrupole moments, the probability of α-decay[4] and other experimental data.

It now remains to be seen why the energy of the levels of even nuclei in the region where the strong coupling approximation is applicable actually does conform

---

*Analysis of β-transitions of a different type, for example, $2- \rightarrow \begin{cases} 2+ \\ 0+ \end{cases}$, also leads to the conclusion that $|M(2\rightarrow 2)|^2$ is on the average an order of magnitude smaller for such transitions than for analogous transitions but proceeding to a one-particle level. The value of $|M(2\rightarrow 0)|^2$ has a normal order of magnitude.

with equation (1), i.e., an equation for purely rotational levels. In the transition from the ground to an excited state of an even nucleus the increment in the deformation parameter may be caused by centrifugal forces; hence it is reasonable to propose the following relationship for $\Delta\beta$:

$$\Delta\beta = \eta \frac{k}{C} I(I+1), \qquad (9)$$

where η is a proportionality factor, k is the nucleon-surface coupling constant and C is a surface coefficient characterized by

$$C = 4R_0^2 s - \frac{3}{10\pi} \cdot \frac{Ze^2}{R_0},$$

where s is the surface tension coefficient.

Then from equation (II.21) of Ref. 2 we obtain the following expression for E_d:

$$E_d = \left[\sqrt{\frac{5}{4\pi}} k \sum_p \left| \frac{3\Omega_p^2 - j_p(j_p+1)}{4j_p(j_p+1)} \right| - C_\beta \right] \eta \frac{k}{C} I(I+1), \qquad (10)$$

where Ω_p is the projection of the angular momentum of the nucleons on the symmetry axis of the nucleus and j_p is the angular momentum of a single particle. It will be seen from (10) that E_d, too, is proportional to $I(I+1)$. This explains why the energy of the levels is correctly given by equation (1). Only now J should be the effective moment of inertia.*

The hypothesis of increased deformation of the nucleus incident to rotation is supported by the data on the lifetimes of rotational levels τ_γ relative to E2 transitions. In this case τ_γ is inversely proportional to the square of the quadrupole moment Q_0 (equation (VII.17) in Ref. 2). If one takes into account incomplete superposition of the wave functions of the initial and final states the probability of the transition is greatly decreased relative to that obtained on the basis of the referred to equation. Experimental data on the Coulomb excitation of nuclei also support this deduction.

Thus, the divergences between the values of β determined in different ways have been obviated. If the computed values of β obtained do not exceed 0.5 (i.e., if $\Delta R \leqslant 0.3$), the assumption that the nuclear deformation is small will be validated.

It would be most desirable to have more accurate spectroscopic data on the quadrupole moments of nuclei in the region of the rare earths and heavy elements as well as more precise information on the deformation of nuclei from the point of view of the theory of α-decay.

Leningrad Physico-Technical Institute
of the USSR Academy of Sciences

References

1. A.Bohr, Dan. Mat. Fys. Medd., 26, 14 (1952).
2. A.Bohr & B.R.Mottelson, Dan. Mat. Fys. Medd., 27, 16 (1953).
3. K.Ford, Phys. Rev., 90, 1250 (1953).
4. R.King & D.Peaslee, Phys. Rev., 94, 1284 (1954).

*In odd nuclei interaction of the rotation with the motion of the odd nucleon may result in so-called Λ-doubling of the rotational levels.

STRUCTURE OF THE SECOND EXCITED LEVEL OF He^5 AND Li^5

- A.I.Baz'

It has recently become increasingly clear that the states of the nucleons in the case of the lightest nuclei, such as H^3, He^3, He^4, He^5 and Li^5, can be characterized by the values of their total and orbital angular momenta (shell model). This means that each low-energy state of the nucleus can be assigned a definite configuration. Thus the configuration of ground states of H^3 and He^3 is $(1s)^3$; that of the ground state of He^4 is $(1s)^4$; of the first excited state of He^4 - $(1s)^3 1p_{3/2}$. As for Li^5 and He^5, we know that their ground states (3/2 -) have the configuration $(1s)^4 1p_{3/2}$, while the first excited states ($\frac{1}{2}$ -) are assigned the configuration $(1s)^4 1p_{1/2}$. This identification of the first excited states of Li^5 and He^5 (below we shall speak only of Li^5, bearing in mind that Li^5 and He^5 are mirror nuclei with similar systems of levels) is in full agreement with most experimental data pertaining to heavier nuclei.

Let us see how one should identify, from this point of view, the excited level of Li^5, having an energy of 16.7 Mev.

This level is formed in two reactions:

1) $He^3 + d \rightarrow He^4 + p$. [1] The reaction cross section vs energy curve shows a resonance at E_d = 420 kev. The width of the resonance curve turns out to be unexpectedly small for so high an excitation energy and so light a nucleus: only about 400 kev. Moreover the greater part of this width (about 300 kev) is connected with the Coulomb repulsion of the protons in Li^5. This is apparent from the fact that the widths of the corresponding level in He^5, which has only two protons, is less than ~100 kev (it may be recalled that width of the ground and first excited levels of He^5 and Li^5 is of the order of 1 Mev.). The spin (3/2) and parity (even) of the excited Li^5 level formed in this reaction have been established from the angular distribution of the reaction products, from the magnitude of the absolute cross section and from the fact that only deuterons with $l = 0$ participate in the reaction (deuterons with $l > 1$ cannot take part in the reaction at the energies obtaining in this case because of the high centrifugal barrier).

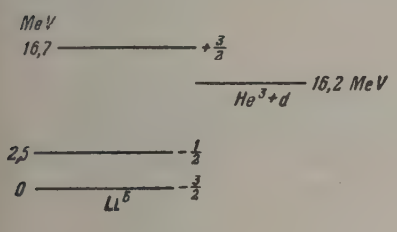

2) $He^3 + d \rightarrow Li^5 + \gamma$. Hintz, Briar & Van Peter[2] found that when He^3 is bombarded with deuterons hard γ-quanta are emitted and that the photon yield curve has a maximum at E_d = 0.46 Mev. The end-point of the γ-ray spectrum at this bombarding energy is 16.6 ± 0.2 Mev.

On the basis of these data the hard γ-quanta must be attributed to the $He^3 + d \rightarrow Li^5 + \gamma$ reaction in which the excited state of Li^5 with energy 16.7 Mev decays to the ground state with the emission of a γ-quantum.

The above data, taken in conjunction, permit determining the structure of the 16.7 Mev state of Li^5. That this state decays to the ground state by the emission of a γ-ray indicates that the configurations of the two states differ only by the transition of one nucleon to a different state. This follows from the fact that the electromagnetic transition operator has the form $F = \sum_i f_i$, where f_i is an operator acting only on the coordinates of the i^{th} nucleon and the summation is carried out over all the nucleons of the nucleus. It can readily be shown that the matrix elements of such an operator do not equal zero only for transitions in which the state of not more than one nucleon changes. Whence it follows that inasmuch as the configuration of the ground state is $(1s)^4 1p_{3/2}$, the configuration of the second excited state can only be either $(1s)^4 nl_j$, which corresponds to a transition of the outside nucleon from the state $1p_{3/2}$ to some higher state nl_j, or $(1s)^3 1p_{2/3} nl_j$, which corresponds to the transition of the outside nucleon from the 1s state to a higher state. The first alternative can be immediately eliminated since in this

case it is impossible to explain the comparatively small width of this level relative to the disintegration into He^4 + p in the He^3 + d $\rightarrow$ He^4 + p reaction. Hence there remains only the second possibility, i.e., the configuration $(1s)^3 p_{3/2} nl_j$. The most logical assumption is that a 1s shell nucleon is excited to the $1p_{3/2}$ state since the other possible states have a higher energy. Consequently the 16.7 Mev level must be assigned the configuration $(1s)^3(1p_{3/2})^2$, which serves to explain the spin and parity as well as the small width of this level.

It is interesting to note that the 16.7 Mev (second excited) level of Li^5 has certain traits in common with the first excited level of He^4, the configuration of which is $(1s)^3 1p_{3/2}$. Both these states are formed as a result of the transition of one nucleon from the closed $(1s)^4$ shell to the $1p_{3/2}$ state and consequently we can evaluate the excitation energy of the closed $(1S)^4$ shell in two independent ways: from the data on the first excited level of He^4 (Ref. 3) and from the data on the excited state of Li^5. Calculated on the basis of the energy of the first excited level of He^4, the excitation energy of the $(1s)^4$ shell proves to be about 22 Mev.

An analogous value is obtained from the data on the state of Li^5 with E = 16.7 Mev. Thus, in the first approximation, the energy difference between the ground and the 16.7 Mev excited states of Li^5 equals the difference between the energies of the $(1s)^4$ and $(1s)^3 1p_{3/2}$ configurations minus the binding energy of two nucleons in the $1p_{3/2}$ state (we neglect the interaction between the nucleons in the 1p state and the nucleons in the 1S state inasmuch as this interaction is comparatively weak; this is evidenced by the fact that the difference in energy between (He^4 + n) and He^5, as well as between He^{4*} and (He^3 + n) does not exceed 1-2 Mev). The binding energy of two nucleons in the $1p_{3/2}$ state can be taken equal to about 4.7 Mev from the difference in the masses of (He^5 + p) and Li^6. Whence we find that the excitation energy of the closed $(1s)^4$ shell equals approximately (16.7 + 4.7) = 21.4 Mev.

This close agreement (21.4 and 22 Mev) further confirms the validity of our deductions regarding the structure of the excited state of Li^5 with E = 16.7 Mev.

I consider it my duty to thank Ia. A. Smorodinski for his interest in the investigation and his valuable advice and N. A. Vlasov for a number of important comments.

References

1. J.Yarnell, R.Lowberg & W.Stratton, Phys. Rev., 90, 292 (1953).
2. N.Hintz, J.Briar & D.Van Peter, Phys. Rev., 93, 924 (1954).
3. A.Baz' & Ia.Smorodinski, Zhur. eksp. i teor. fiz., 27, 382 (1954).

* * * * * * *

THE SHELL MODEL WITH INTERMEDIATE COUPLING AND BETA-DECAY OF He^6

- A.I.Baz'

In the region of light nuclei the shell model with intermediate coupling gives the best agreement with experiment. According to this model the nucleons are in states with a definite orbital momentum, while the character of the coupling of the momenta of the individual nucleons into the total momentum of the nucleus is intermediate between the two extreme cases of LS-coupling and jj-coupling. This model has proved useful for explaining such properties of light nuclei as the ordering of the excited levels, the energy differences between the levels, the values of the magnetic moments and so on. In the present investigation the shell model with intermediate coupling is applied to calculating the nuclear matrix elements for the β-decay, $He^8 \longrightarrow Li^6$. It must be noted that the increased accuracy of β-spectroscopy determinations calls for a more precise evaluation of the nuclear matrix elements than has hitherto been made. This more precise evaluation is needed both for a more accurate determination of the constants in the theory of β-decay and for the purpose of checking the present-day concepts regarding the structure of light nuclei. In our calculations we shall not take into account the exchange character of nuclear forces. It can be shown that taking account of exchange forces would not alter the qualitative deductions and would lead only to an insignificant modification of the numerical results.

The spins of the ground states of Li^6 and He^6 are, respectively, 1 and 0. Inasmuch as both states have even parity and ΔJ for the transition equals 1, the transition is an allowed one; the matrix element $\int 1$ is identically equal to zero, hence it is necessary to compute only the matrix element $\int \vec{\sigma}$. For this computation we must know the wave functions of the ground states of He^6 and Li^6; we shall use the ordinary methods of atomic spectroscopy to construct these wave functions.

According to the shell model with intermediate coupling the configuration of the ground states of He^6 and Li^6 is $(1s)^4(1p)^2$ and the wave functions are a superposition of wave functions with different orbital momenta and spins:

$$\left.\begin{array}{ll} \text{of } He^6 & \psi_{He} = \alpha\psi(^1S_0) + \beta\psi(^3P_0), \\ \text{of } Li^6 & \psi_{Li} = a\psi(^3S_1) + b\psi(^1P_1) + c\psi(^3D_1). \end{array}\right\} \qquad (1)$$

Here $\psi(^3S_1)$, for example, is the wave function of the $^3S_1$ state. The coefficients a, b, c and α and β were found from a solution of the corresponding secular equations. The values of these coefficients depend on the parameter y, which characterizes the type of coupling (y = 0 for LS-coupling, $y = \infty$ for jj-coupling and has intermediate values for intermediate coupling) and is determined as $y = \xi/F_2$, where ξ is the spin-orbital interaction constant and $F_2 = \int R^2(r_1) V_1 R^2(r_2) r_1^2 r_2^2 dr_1 dr_2$; here R is the radial wave function of a nucleon on the p-shell and V_1 is the coefficient of P_1 in the expansion of the nucleon interaction potential in Legendre polynomials:

$$V(\mathbf{r}_1 - \mathbf{r}_2) = \sum_{k=0}^{\infty} P_k(\cos\omega) V_k$$

(ω is the angle between the radii vectors $\mathbf{r}_1$ and $\mathbf{r}_2$ of the first and second nucleons) On the basis of the invariance of charge hypothesis the value of y should be identical for both He^6 and Li^6. It can be evaluated from a comparison of the experimental value of the magnetic moment, $M_{exp} = 0.82$ with its theoretical value which is a function of y and equals

$$M_{theo} = 0{,}88a^2 + 0{,}50b^2 + 0{,}31c^2.$$

Computing M_{theo} for different values of y, we find that $M_{theo} = M_{exp}$ for y = 1.5. That is, the data on the magnetic moment of Li^6 lead to a value of y = 1.5.

Now making use of (1) we can readily evaluate the matrix element $\int\vec{\sigma}$. We obtain the following expression for the square of the modulus of the matrix element:

$$|\int\sigma|^2=\Sigma|\int\psi^*_{\mathrm{Li}}(\sigma_1+\sigma_2)\psi_{\mathrm{He}}|^2=6\left(a\alpha-\frac{b\beta}{\sqrt{3}}\right)^2$$

In the case of pure LS-coupling ($y=0$), $a=\alpha=1$ and $b=\beta=0$ and the numerical value of the expression is 6. In the case of pure jj-coupling ($y=\infty$), $a=0.611$, $b=0.745$, $\alpha=\sqrt{2/3}$ and $\beta=\sqrt{1/3}$ and for $|\int\vec{\sigma}|^2$ we get 3.34. For the value of $y=1.5$, obtained above from the data on the magnetic moment of Li^6, we find $|\int\vec{\sigma}|^2=5.25$. This value is in agreement with the latest data on the ft-values for the β-decay of H^3 and O^{12} (Refs. 1 & 2). It is precisely from the now known value of $ft=815\pm70$ for He^3 (Ref. 3) that we are now able to assert that $|\int\vec{\sigma}|^2$ cannot be greater than 5.5.

We note that this limitation on $|\int\vec{\sigma}|^2$ decisively refutes the formerly suggested $(1S)^4(2S)^2$ configuration for Li^6 since in this case we would have $|\int\vec{\sigma}|^2=6$.

We also calculated the electric quadrupole moment of Li^6, for which we obtained the following expression

$$Q=-e\overline{r^2}\{0{,}35\,c^2-0{,}50\,b^2+0{,}90\,ac\}\cdot\frac{4}{15},$$

where $\overline{r^2}$ is the mean square of the radius of the orbit of a proton in the p-state and e is the charge of the proton. For $y=1.5$, we obtain $Q=0.040\,\overline{r^2}\cdot e$ cm^2, which does not conflict with the experimental evaluation $|Q|<0{,}0009\cdot e\cdot10^{-24}$ cm^2.

Our deductions may be summarized as follows: the data on the β-decay of He^6 and on the magnetic and quadrupole moments of Li^6 can be interpreted in the framework of the shell model with intermediate coupling. The close agreement of the calculated value of $y=1.5$ with the value of 1.3 obtained from data on the energy difference between the lower levels of Li^6, reported by Juglis,[4] also speaks in favor of this model.

In conclusion I wish to thank Ia.A.Smorodinski, who suggested the subject of this study, for many valuable comments.

References

1. L.Langer & R.Moffat, Phys. Rev., 88, 689 (1952).
2. J.Gerhart, Phys. Rev., 95, 288 (1954).
3. C.Wu, B.Rustad, V.Perez-Mendez & L.Lidovsky, Phys. Rev., 87, 1140 (1952).
4. R.Juglis, Rev. Mod. Phys., 25, 390 (1953).

* * * * * * *

ON THE THEORY OF DOUBLE BETA-DECAY

- L.A.Maksimov & Ia.A.Smorodinski

1. Introduction

Investigation of double β-decay may throw light on whether the neutrino and anti-neutrino are identical. Recently double β-decay was detected in Ca^{48} by McCarthy.[1] The results of experimental studies of double β-disintegration in different nuclei were analyzed and compared with theory by Zel'dovich, Luk'ianov & Smorodinski.[2] These authors note that the double decay of Ca^{48} is of particular interest since among all the known isotopes of the periodic system for which double β-decay is energetically possible Ca^{48} has the highest disintegration energy (4.3

Mev).* On the other hand Ca^{48} and its decay product Ti^{48} are characterized by an identical nuclear structure: both nuclei have eight nucleons in the $f_{7/2}$ state above the closed Ca^{40} shell. Hence the nuclear matrix element for the decay of Ca^{48} must be large compared with those for the decay of heavier elements. For this particular case one can compute the matrix element for the transition of the two nucleons from shell theory. This is the purpose of the present article. The effect of interaction with the other nucleons (the core) can be taken into account by the introduction of a correction factor, as will be shown below in Section 7.

The probability of a neutrinoless double β-decay is strongly dependent on the energy of the transition; in view of this only ground state to ground state transitions are of practical interest. Hence in the present investigation we shall confine our analysis to such transitions.

Thus our problem is to compute, on the basis of the independent particle model, the nuclear matrix elements for scalar interaction:

$$\int 1 \int 1 \equiv \langle F | \sum_{i \neq k} \tau_i^+ \tau_k^+ | I \rangle \qquad (1)$$

and for tensor interaction:

$$\int \sigma \int \sigma \equiv \langle F | \sum_{i \neq k} \tau_i^+ \tau_k^+ (\vec{\sigma}_i \vec{\sigma}_k) | I \rangle \qquad (2)$$

Here τ_i^+ is the operator of the transition of the i^{th} neutron to a proton, $\vec{\sigma}_i$ is the spin operator of the i^{th} nucleon and I and F are the initial (Ca^{48}) and final (Ti^{48}) states of the nucleus. Both states have an identical inner kernel - Ca^{40} - which does not participate in the process and hence can be disregarded in the present analysis. Thus the initial state I is a state comprising eight neutrons with individual momenta $j = 7/2$, i.e., a $f_{7/2}^8$ shell closed with regard to neutrons. The isotopic spin of this state is $T = 4$ with an isotopic projection $T_\zeta = 4$. The total momentum of the initial nucleus is, of course, $J = 0$. Inasmuch as Ti^{48} is an even-even nucleus, the total angular momentum of the final ground state F is also zero. The incompletely filled $f_{7/2}$ shell of Ti^{48} is populated by two protons and six neutrons, i.e., the isotopic projection of this state is $T_\zeta = 2$.

Flowers[3] worked out the general classification of the states of n equivalent nucleons with $j = 7/2$. For $T_\zeta = 2$ there are only four states with $J = 0$:

I.	$J = 0$	$T = 4$	$s = 0$	III.	$J = 0$	$T = 2$	$s = 4$	(3)
II.	$J = 0$	$T = 2$	$s = 0$	IV.	$J = 0$	$T = 2$	$s = 4$**	

Here s is a supplementary quantum number - the "seniority".

We are safe in assuming that the ground state of Ti^{48} is the state II(3) which satisfies the requirement that the ground state have a minimal isotopic spin.

In the present investigation we shall compute the matrix elements (1) and (2) for transitions to the states I and II (3) and indirectly evaluate the half-sum of the matrix elements of the transitions to the two states with $s = 4$.

2. Construction of the wave functions

In the shell theory it is feasible to introduce the individual states of the

---

* N.Kolesnikov[7] has also remarked on the importance of studying Ca^{48}.

** The absence of a state with $T = 3$ has a general meaning and can be proved in general form. Briefly, this is connected with the impossibility of constructing a scalar function symmetrical relative to an odd number of particle pairs.

nucleons. We shall describe the state of the ith nucleon with a total momentum j = 7/2 and a projection of the momentum m by the normalized wave function-spinor of rank 7 $\varphi_m(i)$ and the isotopic wave function $\chi_1(i)$ if the nucleon is in the charge-state of a neutron or $\chi_{-1}(i)$ if the nucleon is a proton. In constructing the end states we shall use functions of the form

$$\chi(12) \equiv \chi_{-1}(1)\chi_{-1}(2)\chi_1(3)\cdots\chi_1(8). \tag{4}$$

χ (12) corresponds to the state in which the first and second nucleons are protons.

The total wave function is constructed from the individual wave functions in the conventional manner. Thus we can immediately write the initial wave function, characterizing the $f_{7/2}$ shell of eight neutrons:

$$\Psi_I(J=0,\ T=4,\ T_\zeta=4) = \Phi_0 \cdot \chi_1(1)\chi_1(2)\cdots\chi_1(8), \tag{5}$$

where

$$\Phi_0 = \frac{1}{\sqrt{8!}}\Sigma \pm \varphi_{7/2}(1)\,\varphi_{5/2}(2)\cdots\varphi_{-7/2}(8) \tag{6}$$

is a fully antisymmetric function and

$$\chi_1(1)\chi_1(2)\cdots\chi_1(8)$$

is the isotopic function of the state with T = 4 and T_ζ = 4.

We can as readily construct the wave function of the state with two protons and six neutrons, corresponding to T = 4 and T_ζ = 2. The isotopic function of this state is fully symmetric:

$$\frac{1}{\sqrt{28}}\sum_{i<k}\chi(ik), \tag{7}$$

while the spatial-spin function coincides with the initial Φ_0. Hence

$$\Psi_F(J=0,\ T=4,\ T_\zeta=4) = \Phi_0 \cdot \frac{1}{\sqrt{28}}\sum_{i<k}\chi(ik). \tag{8}$$

As may readily be seen Young's scheme a (see figure) corresponds to this function. The scheme b must correspond to the wave function of the state with T = 2 and T_ζ = 2.

The function Φ_F (12), corresponding to Young's scheme c, can be constructed from some arbitrary function Φ by symmetrization of the latter with respect to the nucleons (13) and (24) with subsequent antisymmetrization over the groups (12) and (345678). In the general case the function Φ can be set up by the method indicated by Mizushima & Umezawa.[4] Inasmuch as we are interested in the state with T = 0, we can select for Φ any scalar function that does not vanish upon symmetrization with reference to Young's scheme. This is where the multiplicity of the states with the given values of J and T becomes evident. For further classification of the states one must introduce the quantum number s. It is convenient to regard s as the number indicating how many nucleons do not enter into the wave function of the state of n equivalent nucleons

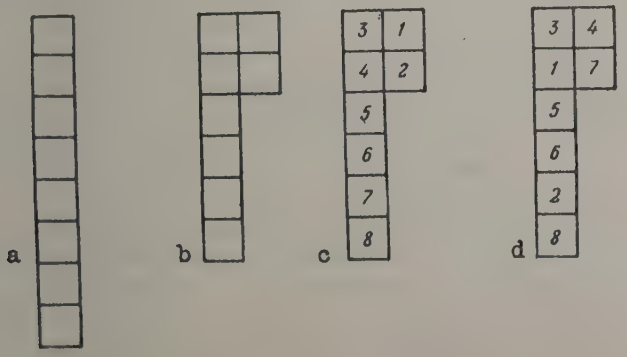

Young's scheme

in the scalar combination

$$\begin{bmatrix} i \\ k \end{bmatrix} \equiv \Sigma (-1)^{m+\frac{1}{2}} \varphi_m(i)\, \varphi_{-m}(k). \tag{9}$$

Clearly, if $s < n$, the wave function of the n nucleons is reduced (from the point of view of spatial symmetry) to a function of s nucleons.

The construction of the generating function Φ is simplest in the case where $s = 0$. It then has the form

$$\Phi = \begin{bmatrix} 1 \\ 2 \end{bmatrix} \cdot \begin{bmatrix} 3 \\ 4 \end{bmatrix} \cdot \begin{bmatrix} 5 \\ 6 \end{bmatrix} \cdot \begin{bmatrix} 7 \\ 8 \end{bmatrix}, \tag{10}$$

where the brackets denote scalar products of (9).

As noted above, we use this function to construct Φ_F (12). To facilitate further calculations it is convenient to write our function in the form

$$\Phi_F(12) = N_6 \hat{A}_6 \left(2 \begin{bmatrix} 1 \\ 2 \end{bmatrix} \begin{bmatrix} 3 \\ 4 \end{bmatrix} + \begin{bmatrix} 1 \\ 3 \end{bmatrix} \begin{bmatrix} 2 \\ 4 \end{bmatrix} - \begin{bmatrix} 1 \\ 4 \end{bmatrix} \begin{bmatrix} 2 \\ 3 \end{bmatrix}\right)\left(\begin{bmatrix} 5 \\ 6 \end{bmatrix} \begin{bmatrix} 7 \\ 8 \end{bmatrix} - \begin{bmatrix} 5 \\ 7 \end{bmatrix} \begin{bmatrix} 6 \\ 8 \end{bmatrix} + \begin{bmatrix} 5 \\ 8 \end{bmatrix} \begin{bmatrix} 6 \\ 7 \end{bmatrix}\right). \tag{11}$$

Here we have effected explicit antisymmetrization with respect to the groups (12), (34) and (5678); $\hat{A}_6$ is the antisymmetrization with respect to (345678); it reduces to $6!/(2!4!) = 15$ terms; N_6 is the normalization. It is worth noting that the functions in the brackets are functions of four nucleons, corresponding to isotopic spins $T = 0$ and $T = 2$:

$$\varphi_{T=0}(12|34) \equiv 2 \begin{bmatrix} 1 \\ 2 \end{bmatrix} \begin{bmatrix} 3 \\ 4 \end{bmatrix} + \begin{bmatrix} 1 \\ 3 \end{bmatrix} \begin{bmatrix} 2 \\ 4 \end{bmatrix} - \begin{bmatrix} 1 \\ 4 \end{bmatrix} \begin{bmatrix} 2 \\ 3 \end{bmatrix} \tag{12}$$

(the vertical bar in $\varphi_{T=0}(12|34)$ separates the groups inside which $\varphi_{T=0}$ is antisymmetric) and

$$\varphi_{T=2}(5678) \equiv \begin{bmatrix} 5 \\ 6 \end{bmatrix} \begin{bmatrix} 7 \\ 8 \end{bmatrix} - \begin{bmatrix} 5 \\ 7 \end{bmatrix} \begin{bmatrix} 6 \\ 8 \end{bmatrix} + \begin{bmatrix} 5 \\ 8 \end{bmatrix} \begin{bmatrix} 6 \\ 7 \end{bmatrix}. \tag{13}$$

The fully antisymmetric total function of the state with $J = 0$, $T = 2$, $T_\zeta = 2$ and $s = 0$ can easily be constructed from functions of the form of $\Phi(12)$ and $\chi(12)$ (see (4)):

$$\Psi_F(J = 0,\ T = 2,\ T_\zeta = 2,\ s = 0) = \frac{1}{\sqrt{28}} \sum_{i<k} \pm \chi(ik)\, \Phi_F(ik) =$$

$$= \frac{1}{\sqrt{28}} \{\chi(12)\, \Phi_F(12) - \chi(13)\, \Phi_F(13) - \ldots + \chi(34)\, \Phi_F(34) + \ldots\}, \tag{14}$$

where $\Phi_F(ik)$ is obtained from $\Phi_F(12)$ by a simple change in numeration. Thus, for example, the function $\Phi_F(47)$ is represented by Young's scheme d in the figure.

Only two states from (3) - I and II - correspond to the set of quantum numbers $J = 0$, $T_\zeta = 2$ and $s = 0$. The first state is described by function (8). The function (14) is orthogonal to (8), which can be proved by computing the scalar product of the functions, although it should be obvious from the fact that these functions pertain to different Young's schemes. Consequently, the function (14) actually describes the $T = 2$ state.

The two functions corresponding to $T = 2$ and $s = 4$ have the form of (14) but with a more complex $\Phi_F(ik)$. The problem of constructing these functions can be reduced to the problem of four particles, representing the new $\Phi_F(ik)$ functions in the form of (11), but now the functions in the first bracket will not have the simple meaning $[\,][\,] = [\,] \times [\,]$, that obtained in the case when $s = 0$. We shall not attempt to construct the functions for $s = 4$ here, but will only note that by constructing the four particle functions by the method of Mizushima & Umezawa[4] one can show convincingly that the functions (3) do exhaust the possible sets of functions with $T_\zeta = 2$.

3. Normalization

In order to make use of function (14) one must also compute the normalization factor N_6. This calculation is not trivial since, in view of $\hat{A}_6$ some terms in $\Phi_F(12)$, for example,

$$\varphi_{1/2}(1)\,\varphi_{-1/2}(2)\,\varphi_{1/2}(3)\,\varphi_{-1/2}(4)\,\varphi_{1/2}(5)\,\varphi_{-1/2}(6)\,\varphi_{1/2}(7)\,\varphi_{-1/2}(8),$$

appear three times, while others cancel each other out.

Let us carry out an explicit antisymmetrization of $\hat{A}_6$ with respect to (345678). For this it is convenient to write (11) as

$$\Phi_F(12) = N_6 \hat{A}_6 \varphi_{T=0}(12\,|\,34)\,\varphi_{T=2}(5678). \tag{15}$$

The vertical bars here separate groups inside which explicit antisymmetrization has already been effected.

We obtain (form A):

$$\begin{aligned}
\Phi_F(12) = N_6 \{ & \varphi_{T=0}(12\,|\,34)\,\varphi_{T=2}(5678) \quad \text{1 term} \\
& - \varphi_{T=0}(12\,|\,\underline{35})\,\varphi_{T=2}(\underline{46}78) \\
& - \varphi_{T=0}(12\,|\,\underline{36})\,\varphi_{T=2}(\underline{54}78) \quad \text{4 terms} \\
& - \quad \ldots\ldots\ldots \\
& - \varphi_{T=0}(12\,|\,\underline{54})\,\varphi_{T=2}(\underline{36}78) \\
& - \varphi_{T=0}(12\,|\,\underline{56})\,\varphi_{T=2}(\underline{34}78) \quad \text{4 terms} \\
& - \quad \ldots\ldots\ldots \\
& + \varphi_{T=0}(12\,|\,\underline{56})\,\varphi_{T=2}(\underline{34}78) \\
& + \varphi_{T=0}(12\,|\,\underline{57})\,\varphi_{T=2}(\underline{36}48) \quad \text{6 terms} \\
& + \quad \ldots\ldots\ldots\ldots \}
\end{aligned} \tag{16a}$$

(we have underlined the numbers with respect to which the transposition is effected) or (form B):

$$\begin{aligned}
\Phi_F(12) = - N_6 \{ & \varphi_{T=0}(12\,|\,35)\,\varphi_{T=2}(46\,78) \\
& - \varphi_{T=0}(12\,|\,\underline{34})\,\varphi_{T=2}(\underline{56}78) \\
& - \varphi_{T=0}(12\,|\,\underline{36})\,\varphi_{T=2}(\underline{45}78) \\
& \mp \quad \ldots\ldots\ldots\ldots \}
\end{aligned} \tag{16b}$$

We obtain the following equalities

$$\begin{aligned}
(\Phi_F(12),\ \Phi(12)) &= N_6 (\varphi_{T=0}(12\,|\,34)\,\varphi_{T=2}(5678),\ \Phi_F(12,\ \text{form } A)) - \\
&- N_6 (\varphi_{T=0}(12\,|\,35)\,\varphi_{T=2}(4678),\ \Phi_F(12,\ \text{form } B)) \mp \ldots = \\
&= 15 N_6 (\varphi_{T=0}(12\,|\,34)\,\varphi_{T=2}(5678),\ \Phi_F(12,\ \text{form } A)).
\end{aligned} \tag{17}$$

Here, as usual, (Φ_1, Φ_2) denotes a scalar product.

Let us introduce the notation

$$\begin{aligned}
\varphi^2_{T=0} &= (\varphi^1_{T=0}(12\,|\,34),\ \varphi_{T=0}(12\,|\,34)) \\
\varphi^2_{T=2} &= (\varphi_{T=2}(5678),\ \varphi_{T=2}(5678)) \\
p &= (\varphi_{T=0}(12\,|\,\underline{34})\,\varphi_{T=2}(\underline{56}78),\ \varphi_{T=0}(12\,|\,\underline{35})\,\varphi_{T=2}(\underline{46}78)) \\
q &= (\varphi_{T=0}(12\,|\,\underline{34})\,\varphi_{T=2}(\underline{56}78),\ \varphi_{T=0}(12\,|\,\underline{56})\,\varphi_{T=2}(\underline{34}78)).
\end{aligned} \tag{18}$$

Then, in view of the fact that

$$(\varphi_{T=0}(12|34)\varphi_{T=2}(5678),\quad \varphi_{T=0}(12|36)\varphi_{T=2}(5478)) = (-1)^2 p \tag{19}$$

and so on, we obtain

$$(\Phi_F(12), \Phi_F(12)) = 15N_6^2(\varphi_{T=0}^2 \cdot \varphi_{T=2}^2 - 8p + 6q). \tag{20}$$

The calculation of $\varphi_{T=0}^2$, $\varphi_{T=2}^2$, p and q is greatly facilitated by the fact that in $\varphi_{T=0}(12|34)\varphi_{T=2}(5678)$ only the terms not comprising equal projections of the individual momenta inside each group of nucleons need be taken into account.

Hereinafter we shall use the equations

$$\left(\underbrace{\left[\ \right]\cdots\left[\begin{smallmatrix} i \\ k \end{smallmatrix}\right]}_{n},\ \underbrace{\left[\ \right]\cdots\left[\begin{smallmatrix} i \\ k \end{smallmatrix}\right]}_{n}\right) = 8\left(\underbrace{\left[\ \right]\cdots}_{n-1}\ \underbrace{\left[\ \right]\cdots}_{n-1}\right) \tag{21}$$

if there is an identical pair and

$$\left(\underbrace{\left[\ \right]\cdots\left[\ \right]}_{n},\ \underbrace{\left[\ \right]\cdots\left[\ \right]}_{n}\right) = \pm 8, \tag{22}$$

when there are no identical pairs. The sign $(\pm)$ is determined by whether the sum $n + \Sigma m + \Sigma m'$ is odd or even, as will become clear in actual computations (n is the number of scalar pairs).

Let us prove (22) for the particular case of $n = 2$. We find the scalar product for the functions

$$\left[\begin{smallmatrix} 1 \\ 2 \end{smallmatrix}\right]\left[\begin{smallmatrix} 3 \\ 4 \end{smallmatrix}\right] = \sum (-1)^{m_1+m_2+1} \varphi_{m_1}(1)\varphi_{-m_1}(2)\varphi_{m_2}(3)\varphi_{-m_2}(4)$$

and

$$\left[\begin{smallmatrix} 1 \\ 4 \end{smallmatrix}\right]\left[\begin{smallmatrix} 2 \\ 3 \end{smallmatrix}\right] = \sum (-1)^{m_1'+m_2'+1} \varphi_{m_1'}(1)\varphi_{m_2'}(2)\varphi_{-m_2'}(3)\varphi_{-m_1'}(4).$$

Bearing in mind that

$$(\varphi_m(i),\ \varphi_{m'}(k)) = \delta_{ik}\delta_{mm'}, \tag{23}$$

we obtain

$$\left(\left[\begin{smallmatrix} 1 \\ 2 \end{smallmatrix}\right]\left[\begin{smallmatrix} 3 \\ 4 \end{smallmatrix}\right],\ \left[\begin{smallmatrix} 1 \\ 4 \end{smallmatrix}\right]\left[\begin{smallmatrix} 2 \\ 3 \end{smallmatrix}\right]\right) = \sum_{m_1=m_1'=-m_2'=m_2} (-1)^{m_1+m_2+m_1'+m_2'+2} = \sum (-1)^{2m+2} = -8. \tag{24}$$

Below we shall abbreviate the above as

$$^{2+}\left(\left[\begin{smallmatrix} m \\ 1 \\ 2 \end{smallmatrix}\right]\left[\begin{smallmatrix} m \\ 3 \\ 4 \end{smallmatrix}\right],\ \left[\begin{smallmatrix} m \\ 1 \\ 4 \end{smallmatrix}\right]\left[\begin{smallmatrix} -m \\ 2 \\ 3 \end{smallmatrix}\right]\right) = -8 \qquad (2m+2 \text{ is odd.})$$

Over the scalar product we have inscribed the sum $(n + \sum m + \sum m')$ taking (23) into account.

$$\varphi_{T=0}^2 = 2^4 \cdot 3^3 \quad \text{and} \quad \varphi_{T=2}^2 = 2^4 \cdot 3^2$$

are easy to compute. The calculation of p is somewhat more complicated. Let us write it out in full

$$p = \left(\left\{2\left[\begin{smallmatrix} 1 \\ 2 \end{smallmatrix}\right]\left[\begin{smallmatrix} 3 \\ 4 \end{smallmatrix}\right] + \left[\begin{smallmatrix} 1 \\ 3 \end{smallmatrix}\right]\left[\begin{smallmatrix} 2 \\ 4 \end{smallmatrix}\right] - \left[\begin{smallmatrix} 1 \\ 4 \end{smallmatrix}\right]\left[\begin{smallmatrix} 2 \\ 3 \end{smallmatrix}\right]\right\}\left\{\left[\begin{smallmatrix} 5 \\ 6 \end{smallmatrix}\right]\left[\begin{smallmatrix} 7 \\ 8 \end{smallmatrix}\right] - \left[\begin{smallmatrix} 5 \\ 7 \end{smallmatrix}\right]\left[\begin{smallmatrix} 6 \\ 8 \end{smallmatrix}\right] + \left[\begin{smallmatrix} 5 \\ 8 \end{smallmatrix}\right]\left[\begin{smallmatrix} 6 \\ 7 \end{smallmatrix}\right]\right\},$$
$$\left\{2\left[\begin{smallmatrix} 1 \\ 2 \end{smallmatrix}\right]\left[\begin{smallmatrix} 3 \\ 5 \end{smallmatrix}\right] + \left[\begin{smallmatrix} 1 \\ 3 \end{smallmatrix}\right]\left[\begin{smallmatrix} 2 \\ 5 \end{smallmatrix}\right] - \left[\begin{smallmatrix} 1 \\ 5 \end{smallmatrix}\right]\left[\begin{smallmatrix} 2 \\ 3 \end{smallmatrix}\right]\right\}\left\{\left[\begin{smallmatrix} 4 \\ 6 \end{smallmatrix}\right]\left[\begin{smallmatrix} 7 \\ 8 \end{smallmatrix}\right] - \left[\begin{smallmatrix} 4 \\ 7 \end{smallmatrix}\right]\left[\begin{smallmatrix} 6 \\ 8 \end{smallmatrix}\right] + \left[\begin{smallmatrix} 4 \\ 8 \end{smallmatrix}\right]\left[\begin{smallmatrix} 6 \\ 7 \end{smallmatrix}\right]\right\}\right)$$

The scalar products which do not cancel out are

$$^{2+}\left(\begin{bmatrix}1\\2\end{bmatrix}\begin{bmatrix}3\\4\end{bmatrix}^{m}\begin{bmatrix}5\\6\end{bmatrix}^{-m}\begin{bmatrix}7\\8\end{bmatrix},\ \begin{bmatrix}1\\2\end{bmatrix}\begin{bmatrix}3\\5\end{bmatrix}^{m}\begin{bmatrix}4\\6\end{bmatrix}^{-m}\begin{bmatrix}7\\8\end{bmatrix}\right)=+8\cdot 8^2 \qquad (2=\text{even})$$

$$^{3+}\left(\begin{bmatrix}1\\2\end{bmatrix}^{m}\begin{bmatrix}3\\4\end{bmatrix}^{-m}\begin{bmatrix}5\\6\end{bmatrix}^{m}\begin{bmatrix}7\\8\end{bmatrix},\ \begin{bmatrix}1\\3\end{bmatrix}^{m}\begin{bmatrix}2\\5\end{bmatrix}^{-m}\begin{bmatrix}4\\6\end{bmatrix}^{m}\begin{bmatrix}7\\8\end{bmatrix}\right)=+8\cdot 8 \quad (3+2m=\text{even})$$

$$^{3+}\left(\begin{bmatrix}1\\2\end{bmatrix}^{m}\begin{bmatrix}3\\4\end{bmatrix}^{m}\begin{bmatrix}5\\6\end{bmatrix}^{-m}\begin{bmatrix}7\\8\end{bmatrix},\ \begin{bmatrix}1\\5\end{bmatrix}^{m}\begin{bmatrix}2\\3\end{bmatrix}^{-m}\begin{bmatrix}4\\6\end{bmatrix}^{-m}\begin{bmatrix}7\\8\end{bmatrix}\right)=-8\cdot 8 \quad (3=\text{odd})$$

Here all the computations are similar to those of (24).

Again taking advantage of the fact that a scalar product is not changed as a result of a change in designations, we obtain the quantity

$$p=2(2\cdot 8^3+8^2+8^2)\cdot 3+(2\cdot 8^2+8^3)\cdot 3+(2\cdot 8^2+8^3)\cdot 3=3\cdot 7\cdot 2^9.$$

The three added terms correspond to the summands of the function $\varphi_{T=0}(12|34)$. The factor 3 is due to functions of the type $\varphi_{T=2}$: the only important terms here are the ones containing identical pairs $\begin{bmatrix}7\\8\end{bmatrix}, \begin{bmatrix}6\\8\end{bmatrix}$ and $\begin{bmatrix}6\\7\end{bmatrix}$, for example, $\left(\dots\begin{bmatrix}7\\8\end{bmatrix},\dots\begin{bmatrix}7\\8\end{bmatrix}\right)$.

Now let us evaluate q:

$$\begin{aligned}q=&\left(\left\{2\begin{bmatrix}1\\2\end{bmatrix}\begin{bmatrix}3\\4\end{bmatrix}+\begin{bmatrix}1\\3\end{bmatrix}\begin{bmatrix}2\\4\end{bmatrix}-\begin{bmatrix}1\\4\end{bmatrix}\begin{bmatrix}2\\3\end{bmatrix}\right\}\left\{\begin{bmatrix}5\\6\end{bmatrix}\begin{bmatrix}7\\8\end{bmatrix}-\begin{bmatrix}5\\7\end{bmatrix}\begin{bmatrix}6\\8\end{bmatrix}+\begin{bmatrix}5\\8\end{bmatrix}\begin{bmatrix}6\\7\end{bmatrix}\right\},\right.\\&\left.\left\{2\begin{bmatrix}1\\2\end{bmatrix}\begin{bmatrix}5\\6\end{bmatrix}+\begin{bmatrix}1\\5\end{bmatrix}\begin{bmatrix}2\\6\end{bmatrix}-\begin{bmatrix}1\\6\end{bmatrix}\begin{bmatrix}2\\5\end{bmatrix}\right\}\left\{\begin{bmatrix}3\\4\end{bmatrix}\begin{bmatrix}7\\8\end{bmatrix}-\begin{bmatrix}3\\7\end{bmatrix}\begin{bmatrix}4\\8\end{bmatrix}+\begin{bmatrix}3\\8\end{bmatrix}\begin{bmatrix}4\\7\end{bmatrix}\right\}\right)=\\=&\left(\left\{2\begin{bmatrix}1\\2\end{bmatrix}\begin{bmatrix}3\\4\end{bmatrix}+\begin{bmatrix}1\\3\end{bmatrix}\begin{bmatrix}2\\4\end{bmatrix}-\begin{bmatrix}1\\4\end{bmatrix}\begin{bmatrix}2\\3\end{bmatrix}\right\}\begin{bmatrix}5\\6\end{bmatrix}\begin{bmatrix}7\\8\end{bmatrix},\right.\\&\left.\left\{2\begin{bmatrix}1\\2\end{bmatrix}\begin{bmatrix}5\\6\end{bmatrix}+\begin{bmatrix}1\\5\end{bmatrix}\begin{bmatrix}2\\6\end{bmatrix}-\begin{bmatrix}1\\6\end{bmatrix}\begin{bmatrix}2\\5\end{bmatrix}\right\}\begin{bmatrix}3\\4\end{bmatrix}\begin{bmatrix}7\\8\end{bmatrix}\right).\end{aligned}$$

The other terms cancel out inasmuch as they contain equal projections in the nucleon group (5678). The significant terms are

$$\left(\begin{bmatrix}1\\2\end{bmatrix}\begin{bmatrix}3\\4\end{bmatrix}\begin{bmatrix}5\\6\end{bmatrix}\begin{bmatrix}7\\8\end{bmatrix},\ \begin{bmatrix}1\\2\end{bmatrix}\begin{bmatrix}5\\6\end{bmatrix}\begin{bmatrix}3\\4\end{bmatrix}\begin{bmatrix}7\\8\end{bmatrix}\right)=8^4;\quad \left(\begin{bmatrix}1\\2\end{bmatrix}\begin{bmatrix}3\\4\end{bmatrix}\begin{bmatrix}5\\6\end{bmatrix}\begin{bmatrix}7\\8\end{bmatrix},\ \begin{bmatrix}1\\5\end{bmatrix}\begin{bmatrix}2\\6\end{bmatrix}\begin{bmatrix}3\\4\end{bmatrix}\begin{bmatrix}7\\8\end{bmatrix}\right)=+8^3;$$

$$\left(\begin{bmatrix}1\\2\end{bmatrix}\begin{bmatrix}3\\4\end{bmatrix}\begin{bmatrix}5\\6\end{bmatrix}\begin{bmatrix}7\\8\end{bmatrix},\ \begin{bmatrix}1\\6\end{bmatrix}\begin{bmatrix}2\\5\end{bmatrix}\begin{bmatrix}3\\4\end{bmatrix}\begin{bmatrix}7\\8\end{bmatrix}\right)=-8^3;$$

$$\left(\begin{bmatrix}1\\3\end{bmatrix}\begin{bmatrix}2\\4\end{bmatrix}\begin{bmatrix}5\\6\end{bmatrix}\begin{bmatrix}7\\8\end{bmatrix},\ \begin{bmatrix}1\\5\end{bmatrix}\begin{bmatrix}2\\6\end{bmatrix}\begin{bmatrix}3\\4\end{bmatrix}\begin{bmatrix}7\\8\end{bmatrix}\right)=+8^2;$$

$$\left(\begin{bmatrix}1\\3\end{bmatrix}\begin{bmatrix}2\\4\end{bmatrix}\begin{bmatrix}5\\6\end{bmatrix}\begin{bmatrix}7\\8\end{bmatrix},\ \begin{bmatrix}1\\6\end{bmatrix}\begin{bmatrix}2\\5\end{bmatrix}\begin{bmatrix}3\\4\end{bmatrix}\begin{bmatrix}7\\8\end{bmatrix}\right)=-8^2.$$

Whence we obtain

$$q=2(2\cdot 8^4+8^3+8^3)+(2\cdot 8^3+8^2+8^2)+(2\cdot 8^3+8^2+8^2)=2^8\cdot 3^4.$$

Substituting the computed values in (20), we find the normalization factor for the function $\Phi_F(12)$:

$$N_6^2=\frac{1}{81}\cdot\frac{7}{2\cdot 131}. \qquad (25)$$

4. Computation of the matrix element $\int 1 \int 1$

The matrix element $\int 1 \int 1$ is easy to compute. Clearly the operator $\sum_{i\neq k}\tau_i^+\tau_k^+$

does not act on the spatial-spin function, hence only the T = 4 → T = 4 transition differs from zero. Substituting the appropriate functions (5) and (8) in (1) we get

$$\int 1 \int 1 \equiv \langle F | \sum_{i<k} \tau_i^+ \tau_k^+ | I \rangle = \langle J=0,\ T=4,\ T_\zeta = 2 \left| \sum_{i<k} \tau_i^+ \tau_k^+ \right| J=0,\ T=4,\ T_\zeta = 4 \rangle =$$

$$= \frac{56}{\sqrt{28}} (\Phi_0, \Phi_0) = 2\sqrt{28}. \qquad (26)$$

5. Computation of the matrix elements $\int \sigma \int \sigma_-$

Operator $\hat{L} = \sum_{i<k} \tau_i^+ \tau_k^+ (\vec{\sigma}_i \vec{\sigma}_k)$ comprises the one-particle spin operators $\vec{\sigma}_i$:

$$(\vec{\sigma}_i \vec{\sigma}_k) = \sigma_z(i)\,\sigma_z(k) + \frac{1}{2}\sigma_+(i)\,\sigma_-(k) + \frac{1}{2}\sigma_-(i)\,\sigma_+(k), \qquad (27)$$

where

$$\sigma_+ \equiv \sigma_x + i\sigma_y;\quad \sigma_- \equiv \sigma_x - i\sigma_y.$$

We are concerned with transitions in the $f_{7/2}$ shell, hence in our case the total orbital momenta of each nucleon prior to and after the transition are j = 7/2 and l = 3, respectively. Hence[5]

$$\left.\begin{aligned} \sigma_z \varphi_m &= \frac{1}{7} m \varphi_m, \\ \sigma_+ \varphi_m &= \frac{1}{7} f(m+1)\,\varphi_{m+1}, \\ \sigma_- \varphi_m &= \frac{1}{7} f(m)\,\varphi_{m-1}, \end{aligned}\right\} \qquad (28)$$

where

$$f(m) \equiv \sqrt{(j-m+1)(j+m)} = \sqrt{(^9/_2 - m)(^7/_2 + m)}. \qquad (29)$$

Below we shall make use of the equalities

$$\left.\begin{aligned} &\sum m^2 = 42;\ \sum m^4 = {}^1/_2\,777; \\ &\sum_{m_1+m_2} m_1 m_2 = -42;\ \sum_{|m_1|+|m_2|} m_1 m_2 = 0;\ \sum_{m_1+m_2} m_1^2 m_2^2 = {}^1/_2\,2751; \\ &f(-m) = f(m+1);\ \sum f^2(m) = 84; \\ &\sum f^2(m+1) f^2(m) = 1008;\ \sum m(m-1) f^2(m) = 231. \end{aligned}\right\} \qquad (30)$$

It is convenient to write the matrix elements from the operator $\hat{L}$ as a scalar product:

$$\int \sigma \int \sigma \equiv \langle F | \hat{L} | I \rangle = (\Psi_F, \hat{L}\Psi_I). \qquad (31)$$

Let us compute this matrix element for the transition

$$J=0,\ T=4,\ T_\zeta = 4 \to J=0,\ T=2,\ T_\zeta = 2,\ s=0.$$

The result of the action of the operators $\tau_i^+ \tau_k^+$ is obviously

$$(\Psi_F (T=2,\ s=0),\ \hat{L}\Psi_I) = \frac{56}{\sqrt{28}} (\Phi_F(12),\ \vec{\sigma}_1 \vec{\sigma}_2 \Phi_0). \qquad (32)$$

The operator $\vec{\sigma}_1 \vec{\sigma}_2$ acts on the individual functions of the first and second nucleons. Hence in computing the matrix elements, we shall explicity write out only that part of functions Φ_0 and Φ_F (12) which contains the first and second nucleons. In doing so it must be borne in mind that Φ_0 is fully antisymmetric

and does not contain terms with equal projections of the momenta in the two nucleons. Obviously, in this abbreviated notation the equalities must be understood symbolically. Let us once more write out the function

$$\Phi_F(12) = N_6 \hat{A}_6 \left\{2\begin{bmatrix}1\\2\end{bmatrix}\begin{bmatrix}3\\4\end{bmatrix} + \begin{bmatrix}1\\3\end{bmatrix}\begin{bmatrix}2\\4\end{bmatrix} - \begin{bmatrix}1\\4\end{bmatrix}\begin{bmatrix}2\\3\end{bmatrix}\right\}\left\{\begin{bmatrix}5\\6\end{bmatrix}\begin{bmatrix}7\\8\end{bmatrix} - \begin{bmatrix}5\\7\end{bmatrix}\begin{bmatrix}6\\8\end{bmatrix} + \begin{bmatrix}5\\8\end{bmatrix}\begin{bmatrix}6\\7\end{bmatrix}\right\}.$$

It is convenient to represent the initial function in the form

$$\Phi_0 = \frac{1}{\sqrt{8!}} \Sigma \pm \begin{bmatrix}1\\2\end{bmatrix}\begin{bmatrix}3\\4\end{bmatrix}\begin{bmatrix}5\\6\end{bmatrix}\begin{bmatrix}7\\8\end{bmatrix}, \tag{33}$$

where the summation is carried out over essentially different functions, not equivalent to each other to within the sign. Thus the computation of the matrix element from $\sigma_z\sigma_z$ comes down to finding the following elements

$$\left(\begin{bmatrix}1\\2\end{bmatrix},\ \sigma_z(1)\,\sigma_z(2)\begin{bmatrix}1\\2\end{bmatrix}\right) = \left(\frac{1}{7}\right)^2 \sum_{m_1 \neq m_2} m_1 m_2 = -\frac{42}{49},$$

$$\left(\begin{bmatrix}1\\3\end{bmatrix}\begin{bmatrix}2\\4\end{bmatrix},\ \sigma_z(1)\,\sigma_z(2)\begin{bmatrix}1\\3\end{bmatrix}\begin{bmatrix}2\\4\end{bmatrix}\right) = \sum_{|m_1| \neq |m_2|} m_1 m_2 = 0.$$

Whence

$$(\Phi_F(12),\ \sigma_z(1)\,\sigma_z(2)\,\Phi_0) = \frac{N_6}{\sqrt{8!}}\, 2\left(-\frac{42}{49}\right)\cdot 6\cdot 4!\cdot 15; \tag{34}$$

here N_6 and $\frac{1}{\sqrt{8!}}$ are normalizations, 2 is the factor at $\begin{bmatrix}1\\2\end{bmatrix}\begin{bmatrix}3\\4\end{bmatrix}$, 6 is the number of terms from $\begin{bmatrix}3\\4\end{bmatrix}$ with the given $\varphi_m(1)\varphi_{-m}(2)$ from $\begin{bmatrix}1\\2\end{bmatrix}$, 4! is the number of terms from the antisymmetric function from (5678) and 15 is the factor due to $\hat{A}_6$.

We shall compute the matrix element from $\sigma_+\sigma_-$ in a somewhat more detailed manner:

$$\left(\begin{bmatrix}1\\2\end{bmatrix},\ \sigma_+(1)\,\sigma_-(2)\begin{bmatrix}1\\2\end{bmatrix}\right) = \Big(\Sigma(-1)^{m+\frac{1}{2}}\varphi_m(1)\,\varphi_{-m}(2),$$

$$\left(\frac{1}{7}\right)^2 \sum (-1)^{m'+\frac{1}{2}} f(m'+1) f(-m')\,\varphi_{m'+1}(1)\,\varphi_{-m'-1}(2)\Big) =$$

$$= \left(\frac{1}{7}\right)^2 \sum_{m=m'+1} (-1)^{m+m'+1} f(m'+1) f(-m') = -\left(\frac{1}{7}\right)^2 \sum f^2(m) = -\frac{84}{49}, \tag{35}$$

$$\sigma_+\sigma_-\begin{bmatrix}1\\3\end{bmatrix}\begin{bmatrix}2\\4\end{bmatrix} = \left(\frac{1}{7}\right)^2 \sum_{|m_1| \neq |m_2|} (-1)^{m_1+m_1+1} f(m_1+1) f(m_2)\,\varphi_{m_1+1}(1)\varphi_{m_2-1}(2)\,\varphi_{-m_1}(3)\varphi_{-m_2}(4). \tag{36}$$

Again the equality is written taking into account that actually in $\begin{bmatrix}1\\3\end{bmatrix}\begin{bmatrix}2\\4\end{bmatrix}$, regarded as a part of Φ_0, there are present only terms which did not vanish in antisymmetrization with respect to (1234).

Obviously

$$\left(\begin{bmatrix}1\\3\end{bmatrix}\begin{bmatrix}2\\4\end{bmatrix},\ \sigma_+\sigma_-\begin{bmatrix}1\\3\end{bmatrix}\begin{bmatrix}2\\4\end{bmatrix}\right) = 0, \tag{37}$$

while the term differing from zero is

$$\left(\begin{bmatrix}1\\4\end{bmatrix}\begin{bmatrix}2\\3\end{bmatrix},\ \sigma_+\sigma_-\begin{bmatrix}1\\3\end{bmatrix}\begin{bmatrix}2\\4\end{bmatrix}\right) = \left(\frac{1}{7}\right)^2 \sum_{m_1+1=m_2} (-1)^{m_1+m_2+1+(m_1+1)+(m_2-1)+1} f(m_1+1) f(m_2) = +\frac{84}{49}. \tag{38}$$

Collecting the similar terms, we obtain

$$(\Phi_F(12),\ \sigma_+(1)\,\sigma_-(2)\,\Phi_0) = \frac{N_6}{\sqrt{8!}}\left\{2\left(-\frac{84}{49}\right)6+\left(\frac{84}{49}\right)+\left(\frac{84}{49}\right)\right\}\cdot 4!\cdot 15. \qquad (39)$$

It must be borne in mind that the sign of the $\begin{bmatrix}1\\i\end{bmatrix}\begin{bmatrix}2\\k\end{bmatrix}$ terms in $\Phi_F(12)$ is opposite to the "parity" of the transposition. Finally we get

$$(\Phi_F(12),\ \sigma_+(1)\,\sigma_-(2)\,\Phi_0) = -\frac{N_6}{\sqrt{8!}}\cdot\frac{84}{49}\cdot 10\cdot 4!\cdot 15. \qquad (40)$$

It will readily be seen that

$$(\Phi_F(12),\ \sigma_+(1)\,\sigma_-(2)\,\Phi_0) = (\Phi_F(12),\ \sigma_-(1)\,\sigma_+(2)\,\Phi_0). \qquad (41)$$

The ratio of the matrix elements (34) and (40) equals

$$\frac{(\Phi_F(12),\ \sigma_z\sigma_z\Phi_0)}{(\Phi_F(12),\ \sigma_+\sigma_-\Phi_0)} = \frac{3}{5}. \qquad (42)$$

Now we can write the total matrix element:

$$M_2 \equiv (\Psi_F(T=2,\ s=0),\ \sum_{i\neq k}\tau_i^+\tau_k^+\,(\vec{\sigma}_i\vec{\sigma}_k)\,\Psi_I) = -\frac{N_6\sqrt{8!}\cdot 48}{7\sqrt{7}}, \qquad (43)$$

$$M_2^2 = \frac{36\cdot 32}{49\cdot 131} = 0{,}18. \qquad (44)$$

In a like manner for the transition in $\Psi_F(T=4)$ we find

$$(\Phi_0,\ \sigma_z\sigma_z\Phi_0) = \left(\frac{1}{7}\right)^2\frac{1}{8!}\sum_{m_1\neq m_2} m_1m_2\cdot 6! = -\frac{1}{56}\cdot\frac{42}{49} \qquad (45)$$

and

$$(\Phi_0,\ \sigma_+\sigma_-\Phi_0) = -\left(\frac{1}{7}\right)^2\frac{1}{56}\sum_m f^2(m) = -\frac{1}{56}\cdot\frac{84}{49}. \qquad (46)$$

The minus sign in (46) is obtained in view of the fact that the result, not vanishing because of the antisymmetry of Φ_0 differs from zero only for $m\leftrightarrow m-1$ transitions, which change the "parity" of the transposition. Finally, from (45) and (46) we find

$$M_1 \equiv (\Psi_F(T=4),\ \sum_{i\neq k}\tau_i^+\tau_k^+\,(\vec{\sigma}_i\vec{\sigma}_k)\,\Phi_I) = -\frac{9}{7\sqrt{7}}, \qquad (47)$$

$$M_1^2 = 0{,}24. \qquad (48)$$

6. Transitions to states with s = 4

As can readily be shown the operator $\hat{L} = \Sigma\tau_i^+\tau_k^+\,(\vec{\sigma}_i\vec{\sigma}_k)$ commutes with the total momentum operator $\vec{J} = \Sigma(\vec{l}_i + \vec{\sigma}_i)$, where $\vec{l}_i$ and $\vec{\sigma}_i$ are the operators of the orbital and spin momenta of the i^{th} nucleon. This circumstance makes it possible to deduce indirectly certain information on the transitions to the two states with s = 4, namely, to evaluate the half-sum of the squares of the matrix elements in these states.

Thus from the fact that the total momentum is conserved we can write the following expansion

$$\hat{L}\Psi_I\ (J=0,\ T=4,\ T_\zeta=4) = M_1\Psi_F(J=0,\ T=4,\ T_\zeta=4) + \\ + M_2\Psi_F(J=0,\ T=2,\ T_\zeta=2,\ s=0) + \\ + M_3\Psi_F^{(1)}(J=0,\ T=2,\ T_\zeta=2,\ s=4) + \\ + M_4'\Psi_F^{(2)}(J=0,\ T=2,\ T_\zeta=2,\ s=4). \qquad (49)$$

This expansion is complete, since, as has already been noted, there are no other states with J = 0 and T_ζ = 2. If the functions Ψ_F are normalized to 1, clearly M_1, M_2, M_3 and M_4 will be the matrix elements of the transitions to the corresponding states.

Let us find the scalar product of (49) multiplied by itself:

$$(\hat{L}\Psi_I\ ,\ \hat{L}\Psi_I) = M_1^2 + M_2^2 + M_3^2 + M_4^2 \qquad (50)$$

or.

$$M_3^2 + M_4^2 = (\hat{L}\Psi_I',\ \hat{L}\Psi_I) - M_1^2 - M_2^2. \qquad (51)$$

Equation (51) permits finding the half-sum $^1/_2(M_3^2 + M_4^2)$ without using complicated functions with s = 4.

The computation of $(\hat{L}\Psi_I\ ,\ \hat{L}\Psi_I\ )$ is fully analogous to that carried out in Section 5 above and yields

$$(\hat{L}\Psi_I,\ \hat{L}\Psi_I) = 1{,}43. \qquad (52)$$

Whence

$$^1/_2(M_3^2 + M_4^2) \approx 0{,}5. \qquad (53)$$

7. Results

Computed values of the squares of the matrix elements

Matrix element	Initial state	Final state	Sq. of matrix element
$\int 1 \int 1$	$J=0,\ T=4,\ T_\zeta=4$	$J=0,\ T=4,\ T_\zeta=2$	112
$\int\sigma\int\sigma$	$J=0,\ T=4,\ T_\zeta=4$	$J=0,\ T=4,\ T_\zeta=2,\ s=0$	0,24
		$J=0,\ T=2,\ T_\zeta=2,\ s=0$	0,18
		$J=0,\ T=2,\ T_\zeta=2,\ s=4$	0,5
		$J=0,\ T=2,\ T_\zeta=2,\ s=4$	0,5

The computed values of the squares of the matrix elements are listed in the accompanying table. The figures for the last two transitions are the half-sums.

It will be seen that the most probable value of the square of the nuclear matrix element is 0.2.

It must be emphasized, however, that this is not the true value of the matrix element. As is known, calculations on the basis of the independent particle model lead to a correct value of the matrix element only in the case of the lightest nuclei. The divergence in other cases is due, presumably, to deformation of the nucleus in the process of β-decay. An analysis carried out by Bohr & Mottelson[6] shows that in the region of the $f_{7/2}$ shell the experimental lifetime exceeds the theoretical by a factor of about 100 (100 in the case of Ca^{48}; 80 in the case of Sc^{49}). This factor must, apparently, be introduced into the matrix element of double β-decay as well. One might think that in the case of double β-decay this deformation factor should be squared. This,

however, is not so. The transition to the intermediate state (after emission of one neutron) must proceed without deformation of the nucleus (for reasons analogous to the Condon-Shortley principle) and deformation can take place only in the final state of the nucleus, since the transition must occur between the given ground states of the nuclei.*

In view of the above considerations we can at best expect the theoretical equation to give only an approximate evaluation of the lifetime. The theoretical value should, however, be indicative of the lower limit of the lifetime inasmuch as all deviations from the independent particle model should only prolong the lifetime. On the other hand, it is improbable that the factor can be appreciably under 100. Comparison of experimental results with the theoretical value will permit evaluating this deformation factor and hence should be of particular interest.

The equation for calculating the half-life is given in Ref. 2; it is

$$T_{1/2} \approx 7 \cdot 10^{19} Z^{-4/3} (1 - e^{-Z/22})^2 \frac{1}{|M|^2 f(x)} \text{ years;}$$

$f(x)$ for an energy of 4.3 Mev equals $7 \cdot 10^4$.

Substituting the numerical values for the other quantities in the above equation we obtain

$$T_{\frac{1}{2}} = 0.5 \cdot 10^{16} \text{ years (for 4.3 Mev energy).}$$

In view of the possible computation errors the actual period may be one order of magnitude greater.

In conclusion we wish to thank Ia.Zel'dovich and A.Baz' for helpful discussions of the work.

Note added in proof. McCarthy[1] in 1955 published a new value for the period: $T_{\frac{1}{2}} = \overline{(1.6 \pm 0.7) \cdot 10^{17} \cdot \ln 2} = (1 \pm 0.5) \cdot 10^{17}$ years; this gives a value of 500-1000 for the deformation factor.

References

1. J.McCarthy, Phys. Rev., 97, 1234 (1955).
2. Ia.Zel'dovich, S.Luk'ianov & Ia.Smorodinski, Usp. fiz. nauk, 54, 361 (1954)
3. B.Flowers, Proc. Royal Soc., A212, 248 (1952).
4. M.Mizushima & M.Umezawa, Phys. Rev., 85, 37 (1952).
5. L.Landau & E.Lifshits, Kvantovaia mekhanika (Quantum mechanics) M.-L. 1948.
6. A.Bohn & B.Mottelson, Dan. Mat. Fys. Medd., 27, No. 16 (1953).
7. D.Ivanenko & N.Kolesnikov, Doklady AN SSSR, 81, 5, 771 (1951).

*The argument here is admittedly rough and intended only to indicate that the multiplication factor in double decay must be less than the square of the factor in ordinary decay. The fact that two even-even nuclei differ less as regards shape than an even-even and an even-odd nucleus also speaks in favor of our contention.

* * * * * * *

NEW DATA ON THE BINDING ENERGIES OF INTERMEDIATE NUCLEI

- V.A.Kravtsov

The great amount of experimental data on the mass of doublets, the energy of nuclear reactions and the energy of the products of radioactive disintegration allows of thorough cross checking in calculating the atomic masses and the binding energies of nuclei. In the region of nuclei of intermediate mass ($20 \leqslant Z \leqslant 78$) one can check the experimental data by comparing binding energy differences. In a number of cases comparison of the differences in binding energy computed from the results of two different experimental measurements makes both the measured values appear doubtful, so that it is impossible to establish the true value of the energy difference.

In Ref. 1 we showed that study of energy surface sections may be useful in establishing the reliability of experimental data. This method has made it possible to resolve certain doubtful cases and select the more reliable experimental data from among divergent reported values.[1,2] As is known the dependence of the nuclear binding energy E on the atomic number Z and the mass number A can be represented in the form of four energy surfaces in (E, Z, A) space: surfaces for even-even, even-odd, odd-even and odd-odd nuclei. For convenience in plotting it is advantageous to operate with energy surfaces with a reduced slope; for example, in the case of light and intermediate nuclei, surfaces described by the equation

$$9A - E(Z, A) \text{ Mev} = \text{const.}$$

It is generally convenient to examine the sections of these surfaces cut by the planes Z = const. (isotopic sections), N = A - Z = const. (isoneutron sections) and T = A - 2Z = const. (sections through nuclei with equal neutron excesses). As we showed in our earlier article,[1] the energy surface sections possess a number of properties which can be used to good advantage in checking doubtful binding energies by comparing them with other binding energies. These useful properties are the following:

1) The surfaces for even-even and odd-odd nuclei do not intersect with each other or with either of the two other surfaces.

2) Surfaces of different parity (i.e., odd vs even numbers of N, Z, etc.) largely follow the same topography, i.e., exhibit similar curves.

3) Sections of the same parity for neighboring values of Z, N or T (i.e., in going from Z to Z±2, N to N±2 and T to T±2) retain a certain similarity as regards the shape and relative position of the curves.

4) The curves of the isotopic (Z = const.) and isoneutron (N = const.) sections are convex only towards the A or Z axis.

As a result of analysis and critical comparison of available experimental data we compiled tables of the atomic masses and total binding energies of the intermediate nuclides.[1] The publication of new, more accurate mass-spectroscopy measurements[3] and other data[4-9] makes it possible to refine and revise the earlier values for nuclides with mass numbers in the 68-104 range. Hence the purpose of the present article is a revision of the results arrived at in the investigation of Ref. 1 in the light of this new, more accurate data (see table in Appendix).

Our checking showed that the binding energy values for Sc^{48}, V^{48}, Ni^{57} and Ge^{69} published in Ref. 1 remain unchanged. On the other hand, in the light of the data reported by Collins et al[3] the original deductions concerning the binding energies of nuclei with A = 85 proved to be in need of considerable modification.

Let us examine the inconsistencies disclosed in calculations of the binding energies of nuclei with A = 85. The binding energy of the "last" neutron in the Kr^{85} nucleus is $e_n = 5.95 \pm 0.08$ Mev if computed from the energy of the $Kr^{84}(d,p)Kr^{85}$

reaction as reported by Wheeler et al[10]; on the other hand, $e_n = 6.90 \pm 0.09$ Mev when computed from the mass-spectroscopy data for Kr^{84} and Rb^{85} of Collins et al[3] and from the energy of the β-decay of Kr^{85} (T = 9.4 years) found by a number of investigators.[11-13] The divergence of 0.95 ± 0.12 Mev exceeds the experimental error by a factor of 8.

The binding energy of the "last" neutron in the Sr^{86} nucleus equals 9.5 ± 0.2 Mev if we assume it to be equal to the threshold energy of the $Sr^{86}(\gamma,n)Sr^{85}$ reaction as measured by Sher et al.[14] The upper limit of the binding energy of the Sr^{85} nucleus can be evaluated from the total binding energy of Rb^{85}, computed from mass spectroscopy data,[3] making use of the decay scheme for Sr^{85} (T = 65 days) published in Refs. 11, 15 and 16. The binding energy of the stable Sr^{86} nucleus is known from mass-spectroscopy data;[3] subtracting the upper limit of the binding energy of Sr^{85} from this value we find that the binding energy of the "last" neutron in Sr^{86} is not less than 11.0 ± 0.1 Mev. Thus we find that the lower limit of the "last" neutron in Sr^{86} derived from mass-spectroscopy measurements is 1.5 ± 0.3 Mev greater than the value calculated from the (γ,n) reaction.

Among the various values used in our calculations the most dependable are the energy of the β^--decay of Kr^{85} measured independently by three groups of investigators[11-13] and the lower limit of the energy of electron capture in Sr^{85} also determined in three investigations.[11,15,16] Our value for the mass of the stable Sr^{86} nucleus is fully consistent with the mass-spectroscopy values for the masses of Kr^{86}, Rb^{87}, Sr^{87}, Sr^{88}, Y^{89}, Zr^{90} and Nb^{93} reported by Collins et al[3] and the available data on reaction and disintegration energies. The value of the mass of Sr^{86} was deduced by the method of least squares from these masses and reaction energies and, hence, is presumably virtually free of systematic errors. Our value of the binding energy of Kr^{84} falls on the various curves, described below; in view of this it may safely be assumed that the systematic error in its determination is less than 0.3 Mev. Now, the source of the divergence between the values of the binding energy of the "last" neutrons can be 1) the energy of the $Kr^{84}(d,p)Kr^{85}$ reaction from Ref. 10, 2) the mass of Rb^{85} from Ref. 3 or 3) the threshold energy of the $Sr^{86}(\gamma,n)Sr^{85}$ reaction from Ref. 14.

Let us turn to Fig. 1, representing the isotopic section at Z = 36, comprising the binding energies of the isotopes of krypton. Curve 2 is for even-odd nuclei. The solid-line branch of the curve is drawn through the point corresponding to the value of the binding energy of Kr^{85} as computed from the mass of Rb^{85} reported by Collins et al,[3] while the dash-line portion is plotted to pass through point 3, corresponding to the value of the binding energy of Kr^{85} computed from the energy of the $Kr^{84}(d,p)$ reaction and the mass of Kr^{84}. It will be seen that the dash-line branch has an inflection with an upward convexity, something which has not hitherto been observed in any isotopic section. On the other hand, the solid line curve shows no such abnormal inflection. This would indicate that an error has crept into the measurement of the (d,p) reaction energy in the investigation of Ref. 10. This is also evinced in Fig. 2, showing the isoneutron section (N = 49), comprising the binding energy of Kr^{85}. Here again the dash-line drawn through point 3, representing the binding energy value computed from the reported energy of the (d,p) reaction, exhibits an abnormal inflection and an upward bulge.

To check the binding energy of Rb^{85} we turn to Fig. 3 showing the isoneutron section for N = 48. The dash-line part of curve 2 and point 3 in the figure are plotted for the value of the binding energy of Rb^{85} computed from the energy of the (d,p) reaction. The solid-line part of curve 2 and the points on it pertain to odd-even nuclei and the binding energy of Rb^{85} calculated on the basis of mass-spectroscopy data. Again, the curves indicate that the binding energy value from the (d,p) reaction is erroneous and that the value of the mass of Rb^{85} measured by Collins et al[3] is correct.

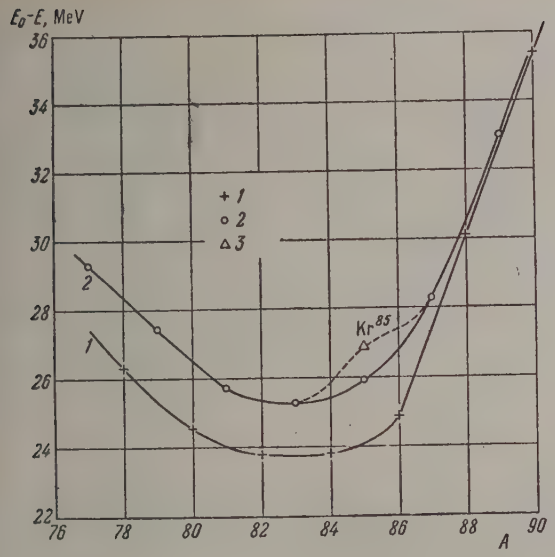

Fig. 1. Isotopic section through energy surfaces with reduced slope for krypton isotopes (Z = 36): 1) points representing binding energy values of even-even nuclei; 2) points representing binding energy values of even-odd nuclei and values for krypton computed from the mass of Rb^{85}; 3) point for Kr^{85} binding energy computed from the energy of the (d,p) reaction.

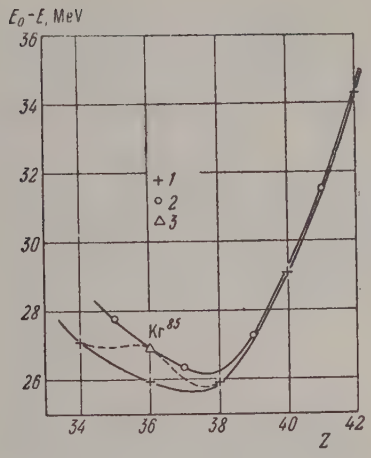

Fig. 2. Isoneutron section through energy surfaces with reduced slope for nuclei with N = 49: 1) points plotted for even-odd nuclei and for Kr^{85} on the basis of the mass of Rb^{85}; 2) points for odd-odd nuclei; 3) point representing the binding energy of Kr^{85} computed from the reported energy of the (d,p) reaction.

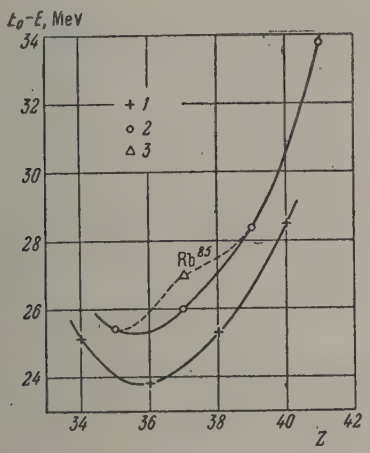

Fig. 3. Isoneutron section through energy surfaces with reduced slope for nuclei with N = 48: 1) points for even-even nuclei; 2) points for odd-even nuclei and from Rb^{85} from mass-spectroscopy data; 3) point representing binding energy of Rb^{85} calculated from the mass of Kr^{84} and the energy of the (d,p) reaction.

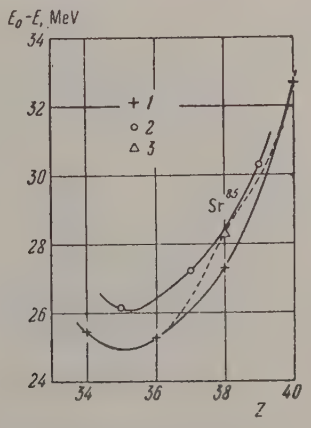

Fig. 4. Isoneutron section through energy surfaces with reduced slope for N = 47: 1) points for even-odd nuclei and Sr^{85} computed from the mass of Rb^{85}; 2) points for odd-odd nuclei; 3) point for the binding energy of Sr^{85} based on the mass of Sr^{86} and the energy of the (γ,n) reaction.

In like manner the isoneutron section for N = 47 reproduced in Fig. 4 can be used as a check on the value of the energy of the $Sr^{86}(\gamma,n)Sr^{85}$ reaction. Here the dash-line branch of curve 1 is plotted to pass through point 3, representing the binding energy value derived from the reported energy of the (γ,n) reaction, while the solid-line branch of curve 1 and the points on it pertain to even-odd nuclei and the binding energy of Sr^{85} computed from the mass of Rb^{85}. The upward convexity of the dash-line indicates that the reported experimental value for the energy of the $Sr^{86}(\gamma,n)Sr^{85}$ reaction is erroneous.

Thus all the energy-surface sections reproduced in the accompanying figures, as well as all the other pertinent sections (not shown), establish the presence of errors in the measurements of the energy of the $Kr^{84}(d,p)Kr^{86}$ and $Sr^{86}(\gamma,n)Sr^{85}$ reactions and confirm the value for the mass of Rb^{85} as measured by Collins et al.[3] Thus, it may be safely assumed that the binding energy values for the last neutrons are

$$e_n(Kr^{85}) = 6.90 \pm 0.09 \text{ Mev}$$

$$e_n(Sr^{86}) = 11.0 \pm 0.3 \text{ Mev}$$

It will be noted that these values are at variance with the deductions regarding the neutron binding energies in Kr^{85} and Sr^{86} arrived at in Ref. 1. This difference is due to the new mass measurements by Collins et al.[3] and, specifically, the revised value for the mass of Kr^{83}, superseding the earlier value published by Collins.[17] Our new deductions are in good agreement with other new experimental data: for example, the energy of the β^--decay of Br^{82} reported by Lu et al.[9] The new, revised binding energy values listed in the table below yield smoother curves for all three energy surface sections. It may be asserted, therefore, that these new mass and binding energy values for nuclei in the interval $68 \leqslant A \leqslant 104$ are more accurate than those published earlier in Ref. 1.

"M.I.Kalinin" Leningrad Polytechnical Institute

References

1. V.Kravtsov, Zhur. eksp. i teor. fiz., 25, 630 (1953).
2. V.Kravtsov, Usp. fiz. nauk, 54, 3 (1954).
3. T.Collins, W.Johnson & A.Nier, Phys. Rev., 94, 398 (1954).
4. L.Rietjens, H.Van den Bold & P.Endt, Physica, 20, 107 (1954).
5. B.Haldar & E.Wiig, Phys. Rev., 94, 1713 (1954).
6. L.Marquez, Phys. Rev., 95, 67 (1954).
7. D.Kochendorfer & D.Farmer, Bull. Am. Phys. Soc., 29, No. 6, 20 (1954).
8. R.Diamond, Phys. Rev., 95, 410 (1954).
9. D.Lu, W.Kelley & M.Wiedenbeck, Phys. Rev., 95, 1533 (1954).
10. G.Wheeler, R.Schwartz & W.Watson, Phys. Rev., 92, 121 (1953).
11. A.Sunyar, J.Mihelich, G.Scharff-Goldhaber, M.Goldhaber, N.Wall & M.Deutsch, Phys. Rev., 86, 1023 (1952).
12. H.Zeldes, B.Ketelle & A.Brosi, Phys. Rev., 79, 901 (1950).
13. I.Bergstrom, Ark. Fys., 5, 191 (1952).
14. R.Sher, J.Halpern & A.Mann, Phys. Rev., 84, 387 (1951).
15. M.Ter-Pogossian & F.Porter, Phys. Rev., 81, 1057 (1951).
16. W.Emmerich & J.Kurbatov, Phys. Rev., 85, 149 (1952).
17. T.Collins, Mass-spectroscopy in Physics Research, Nat. Bur. Stand. USA. Circular, 522, 67 (1953).
18. C.Levi & L.Papineau, C.R., 1038, 1407 (1954).

APPENDIX

ATOMIC MASSES AND TOTAL NUCLEAR BINDING ENERGIES OF THE NUCLEI FROM Zn TO Cd as revised in the light of the mass-spectroscopy data of Refs. 3-8 & 18

Atomic number Z and element	Mass number A	Neutron number N	Form of activity	Atomic mass, amu	Total nuclear binding energy, Mev
1	2	3	4	5	6
30 — Zn	68	38	stable	67,946 71±11	595,10±0,10 нк
	69	39	β^-	68,948 68±6	601,61±0,06 нк
	70	40	stable	69,947 59±8	611,01±0,08 нк
	71	41	β^-	70,949 7 ± 3	617,4 ± 0,3
	72	42	β^-	71,950 5 ± 3	625,0 ± 0,3
31 — Ga	68	37	β^+	67,949 83±11	591,42±0,19 нк
	69	38	stable	68,947 72±6	601,73±0,06 нк
	70	39	β^-, э.з.	69,948 27±8	609,59±0,08 нк
	71	40	stable	70,947 42±15	618,75±0,14 пк
	72	41	β^-	71,948 79±7	625,85±0,07
	73	42	β^-	72,948 1 ± 2	634,8 ± 0,2
32 — Ge	69	37	β^+	68,950 12±7	598,71±0,07 нк
	70	38	stable	69,946 40±10	610,55±0,09 нк
	71	39	э.з.	70,947 74±16	617,67±0,15
	72	40	stable	71,944 49±6	629,07±0,05
	73	41	stable	72,946 54±4	635,52±0,04
	74	42	stable	73,944 62±9	645,68±0,09
	75	43	β^-	74,946 76±5	652,04±0,05
	76	44	stable	75,945 44±5	661,65±0,05
	77	45	β^-	76,947 86±5	667,76±0,05
	78	46	β^-	77,947 6 ± 3	676,4 ± 0,3
33 — As	71	38	β^+	70,949 90±16	614,88±0,15
	72	39	β^+	71,949 17±6	623,93±0,05
	73	40	β^+	72,946 8 ± 2	634,5 ±0,2 и
	74	41	β^+, β^-	73,947 38±9	642,33±0,09
	75	42	stable	74,945 54±5	652,40±0,05
	76	43	β^-	75,946 68±7	659,71±0,07
	77	44	β^-	76,947 86±5	669,44±0,05
	78	45	β^-	77,946 6 ± 2	676,5 ± 0,2
	79	46	β^-	78,946 0 ± 3	685,5 ± 0,2
34 — Se	73	39	β^+	72,949 7 ± 2	631,0 ± 0,2 и
	74	40	stable	73,945 99±8	642,84±0,08
	75	41	э.з.	74,946 48±8	650,75±0,05
	76	42	stable	75,943 45±5	661,94±0,05
	77	43	stable	76,944 47±5	669,36±0,05
	78	44	stable	77,942 20±5	679,84±0,05
	79	45	β^-	78,943 67±6	686,84±0,06
	80	46	stable	79,941 92±5	696,83±0,05
	81	47	β^-	80,943 68±8	703,57±0,08
	82	48	stable	81,942 68±5	712,85±0,05
	83	49	β^-	82,944 1 ± 2	719,9 ± 0,2
35 — Br	75	40	β^+	74,949 40±5	647,25±0,05
	76	41	β^+	75,948 38±9	656,57±0,08
	77	42	β^+	76,945 93±5	667,22±0,05
	78	43	β^+	77,945 88±10	675,63±0,09
	79	44	stable	78,943 50±6	686,21±0,06
	80	45	β^+, β^-	79,943 95±5	694,16±0,05
	81	46	stable	80,942 17±6	704,18±0,06

Key: э.з. - electron capture; и - binding energy and atomic mass values obtained by interpolation from curves; нк - values deduced from experimental data by the method of least squares.

Atomic number Z and element	Mass number A	Neutron number N	Form of activity	Atomic mass, amu	Total nuclear binding energy, Mev
1	2	3	4	5	6
	82	47	β^-	81,942 90±8	711,86±0,08
	83	48	β^-	82,941 49±6	721,44±0,06
	84	49	β^-	83,943 24±6	728,28±0,06
	85	50	β^-	84,942 5 ± 2	737,4 ± 0,2
	87	52	β^-	86,949 6 ± 5	747,5 ± 0,5
36 — Kr	77	41	β^+	76,949 8 ± 2	663,7 ± 0,2
	78	42	stable	77,944 98±5	675,78±0,05
	79	43	β^+	78,945 52±6	683,55±0,06
	80	44	stable	79,941 74±7	695,44±0,06
	81	45	э.з.	80,942 3 ± 2	703,3 ± 0,2 и
	82	46	stable	81,939 52±7	714,23±0,06
	83	47	stable	82,940 44±6	721,75±0,06
	84	48	stable	83,938 21±6	732,18±0,06
	85	49	β^-	84,939 80±7	739,08±0,07
	86	50	stable	85,937 99±13	749,12±0,12 нк
	87	51	β^-	86,940 98±14	754,70±0,13 нк
	88	52	β^-	87,942 34±17	761,82±0,17
	89	53	β^-	88,944 7 ± 4	768,0 ± 0,4
	90	54	β^-	89,946 6 ± 6	774,6 ± 0,3 и
37 — Rb	81	44	β^+	80,944 4 ± 3	700,5 ± 0,3 и
	82	45	β^+	81,943 9 ± 3	709,4 ± 0,3 и
	83	46	э.з.	82,941 5 ± 2	720,0 ± 0,2 и
	84	47	$+\beta$	83,941 06±6	728,75±0,06
	85	48	stable	84,939 05±7	738,99±0,07
	86	49	β^-	85,938 70±11	747,67±0,10
	87	50	nat.β^-	86,937 00±11	757,63±0,10 нк
	88	51	β^-	87,939 31±17	763,86±0,15
	89	52	β^-	88,940 5 ± 4	771,1 ± 0,4
	90	53	β^-	89,942 0 ± 5	777,6 ± 0,4
	82	44	β^+	81,948 3 ± 4	704,5 ± 0,4 и
	83	45	β^+	82,943 9 ± 4	717,0 ± 0,4 и
	84	46	stable	83,939 95±16	729,00±0,16
	85	47	э.з.	84,939 6 ± 3	737,7 ± 0,3
38 — Sr	86	48	stable	85,936 78±11	748,69±0,10 нк
	87	49	stable	86,936 71±11	757,12±0,10 нк
	88	50	stable	87,933 75±14	768,23±0,14 нк
	89	51	β^-	88,935 67±16	774,81±0,16 нк
	90	52	β^-	89,935 91±24	782,95±0,24
	91	53	β^-	90,938 63±25	788,79±0,23
	86	47	β^+	85,941 3 ± 4	743,7 ± 0,4 и
	87	48	β^+	86,938 6 ± 3	754,6 ± 0,3 и
	88	49	β^+	87,936 67±16	764,75±0,16
39 — Y	89	50	stable	88,934 09±17	775,50±0,16 нк
	90	51	β^-	89,935 27±24	782,77±0,23
	91	52	β^-	90,935 77±25	790,67±0,23
	92	53	β^-	91,938 7 ± 4	796,2 ± 0,4
	93	54	β^-	92,938 8 ± 5	804,6 ± 0,5
	94	55	β^-	93,943 0 ± 6	809,0 ± 0,6 и
	87	47	β^+	86,942 4 ± 3	750,3 ± 0,3 и
	88	48	э. з.	87,937 2 ± 3	763,5 ± 0,3
	89	49	β^+	88,937 10±18	771,92±0,17 нк
	90	50	stable	89,932 88±24	784,22±0,22 нк
40 — Zr	91	51	stable	90,934 11±25	791,44±0,23 нк
	92	52	stable	91,933 74±26	800,15±0,24 нк
	93	53	β^-	92,935 46±20	806,92±0,20 нк
	94	54	stable	93,935 87±28	814,90±0,26 и
	95	55	β^-	94,938 3 ± 4	821,0 ± 0,4 и
	96	56	stable	95,938 9 ± 5	828,8 ± 0,5 и
	97	57	β^-	96,941 7 ± 5	834,6 ± 0,5 и

Key: э.з. - electron capture; и - binding energy and atomic mass values obtained by interpolation from curves; нк - values deduced from experimental data by the method of least squares.

Atomic number Z and element	Mass number A	Neutron number N	Form of activity	Atomic mass, amu	Total nuclear binding energy, Mev
1	2	3	4	5	6
	89	48	β^+	88,941 3 ± 5	767,2 ± 0,5
	90	49	β^+	89,938 2 ± 5	778,5 ± 0,5
	91	50	э. з.	90,935 0 ± 3	789,8 ± 0,3
	92	51	э. з.	91,935 85±28	797,40±0,28 нк
41 — Nb	93	52	stable	92,935 39±20	806,20±0,20 нк
	94	53	β^-	93,936 63±20	813,41±0,20 нк
	95	54	β^-	94,936 9 ± 4	821,5 ± 0,4 и
	96	55	β^-	95,938 5 ± 4	828,4 ± 0,4 и
	97	56	β^-	96,938 8 ± 5	836,4 ± 0,5 и
	99	58	β^-	98,942 0 ± 5	850,2 ± 0,5 и
	91	49	β^+	90,939 66±29	784,71±0,27
	92	50	stable	91,934 51±27	797,87±0,25
	93	51	э. з.	92,935 3 ± 5	805,5 ± 0,5 и
	94	52	stable	93,934 37±20	814,74±0,18
	95	53	stable	94,936 0 ± 4	821,6 ± 0,4 и
	96	54	stable	95,935 2 ± 4	830,75±0,40 и
	97	55	stable	96,936 8 ± 5	837,6 ± 0,5 и
	98	56	stable	97,936 0 ± 4	846,7 ± 0,4 и
	99	57	β^-	98,938 6 ± 5	852,6 ± 0,5 и
	100	58	stable	99,938 4 ± 3	861,2 ± 0,3
	101	59	β^-	100,941 2 ± 5	866,9 ± 0,5 и
	93	50	β^+	92,938 6 ± 5	801,6 ± 0,5 и
	94	51	β^+	93,938 98±22	809,66±0,21
	95	52	э. з.	94,937 5 ± 4	819,4 ± 0,4 и
	96	53	э. з.	95,938 1 ± 5	827,2 ± 0,5 и
	97	54	э. з.	96,936 9 ± 5	836,7 ± 0,5 и
	(98)	55	(э. з.)	97,937 7 ± 6	844,3 ± 0,6 и
	99	56	β^-	98,937 2 ± 5	853,2 ± 0,5 и
	100	57	β^-	99,938 6 ± 6	860,2 ± 0,6 и
	101	58	β^-	100,938 8 ± 6	868,4 ± 0,6 и
44 — Ru	95	51	β^+	94,940 3 ± 6	816,0 ± 0,6 и
	96	52	stable	95,938 1 ± 5	826,4 ± 0,5 и
	97	53	э. з.	96,937 8 ± 6	835,1 ± 0,6 и
	98	54	stable	97,936 2 ± 7	844,9 ± 0,7 и
	99	55	stable	98,936 8 ± 7	852,7 ± 0,7 и
	100	56	stable	99,935 6 ± 8	862,2 ± 0,8 и
	101	57	stable	100,937 1 ± 6	869,2 ± 0,6 и
	102	58	stable	101,936 10±9	878,50±0,09
	103	59	β^-	102,938 3 ± 2	884,8 ± 0,2
	104	60	stable	103,937 6 ± 3	893,8 ± 0,3 и
45 — Rh	98	53	β^+	97,941 6 ± 8	839,1 ± 0,8 и
	99	54	β^+	98,938 7 ± 7	850,2 ± 0,7 и
	100	55	β^+	99,939 5 ± 8	857,8 ± 0,8 и
	101	56	э. з.	100,937 4 ± 6	868,1 ± 0,6 и
	102	57	β^+, β^-	101,938 55±9	875,44±0,09
	103	58	stable	102,937 42±12	884,85±0,12
	104	59	β^-	103,939 11±12	891,64±0,12
46 — Pd	100	54	э. з.	99,941 5 ± 8	855,2 ± 0,8 и
	101	55	β^+	100,941 0 ± 8	864,0 ± 0,8 и
	102	56	stable	101,937 34±9	875,78±0,09
	103	57	э. з.	102,938 02±12	883,51±0,12
	104	58	stable	103,936 34±10	893,44±0,10
47 — Ag	103	56	β^+	102,941 2 ± 3	879,8 ± 0,3
	104	57	β^+	103,940 94±12	888,38±0,12
48 — Cd	104	65	β^+	103,942 98 ±14	885,75±0,14

Key: э.з. - electron capture; и - binding energy and atomic mass values obtained by interpolation from curves; нк - values deduced from experimental data by the method of least squares.

BULLETIN of the Academy of Sciences of the USSR - Physical Series
Vol. 19, No. 3, 1955 - Conference on Beta- and Gamma-Spectroscopy (1954)
(Continued from Vol. 18, No. 5)

TABLE OF CONTENTS

	Page Orig.	Trans.
Gamma-emission and decay of lanthanum^{140} - L.V.Arkhangel'ski, B.C.Dzhelepov, N.N.Zhukovski, V.P.Prikhodtseva & Iu.V.Khol'nov	251	228
Gamma-radiation from Au^{198} - B.S.Dzhelepov, N.N.Zhukovski, V.P.Prikhodtseva & Iu.V.Khol'nov	271	247
Investigation of the energy levels of light nuclei by the method of magnetic analysis - L.M.Khromchenko	277	252
The gamma-spectrum of Ir^{192} - M.P.Glazunov, B.S.Dzhelepov & Iu.V.Khol'nov	294	267
Gamma-radiation from Eu^{152} and Eu^{154} - B.S.Dzhelepov, N.N. Zhukovski & V.G.Nedovesov	296	269
Investigation of certain cases of angular correlation - A.P.Grinberg & I.Kh.Lemberg	300	272
Angular correlation between internal conversion electrons from Ba^{80} - B.A.Shakhbazian & L.I.Rusinov	308	280
Investigation of the radiation from Tb^{160} by the method of coincidences - I.P.Stepanenko & L.Ia.Shavtvalov	318	289
Investigation of the nuclear isomerism of Zn^{69}, Se^{79}, Se^{81}, Rh^{103} and Ba^{137} - G.M.Drabkin, V.I.Orlov & L.I.Rusinov	324	294
Lifetimes of the excited states of certain nuclei - E.E.Berlovich	343	305
Detection of short period isomers - P.A.Iampol'ski, O.I.Leipunski, M.Ia.Gen & A.M.Tikhomirov	338	312
On the resolving power of a scintillation spectrometer - I.F.Barchuk, E.M.Galkin, M.V.Pasechnik & N.N.Pucherov	352	316
On determining the deformation of the nuclear surface - L.A.Sliv & L.K.Peker	355	319
Structure of the second excited level of He^5 & Li^5 - A.I.Baz'	360	323
The shell model with intermediate coupling and beta-decay of He^6 - A.I.Baz'	363	325
On the theory of double beta-decay-L.A.Maksimov & Ia.A.Smorodinski	365	326
New data on the binding energies of intermediate nuclei - V.A.Kravtsov	377	338

Translated in 1956 by
Columbia Technical Translations,
5 Vermont Ave., White Plains, N.Y.

CONFERENCE ON MAGNETISM AT LOW TEMPERATURES

- S.V.Vonsovski

A conference on the problems of low-temperature magnetism was held July 1-3, 1954 in Kharkov under the joint auspices of the Commission on Magnetism of the Ural Branch of the USSR Academy of Sciences, the Physico-Technical Institute of the Ukranian SSR and the Imeni "S.I.Vavilov" Institute for Physical Problems of the USSR Academy.

This Conference, the second conference in the history of Soviet physics devoted to the problems of cryogenic physics, reunited both specialists in the field of low-temperature physics and experts in the physics of magnetic phenomena. This Conference, too, was the first conference on magnetism at which primary attention was given to ferromagnetics and other magnetic materials. The Conference heard and discussed reports on experimental and theoretical investigations of the magnetic and galvanomagnetic properties of diverse substances at low temperatures, carried out over the past 5-6 years. The great number of conferees present (over 150 physicists from Kharkov, Moscow, Sverdlovsk, Leningrad, Kiev and other cities of the Soviet Union) and the enthusiastic and active discussion of the reports presented are evidence of the advances achieved by Soviet physics in the field of cryogenic magnetism. In all, twenty reports were heard at the five plenary sessions of the Conference.

The experimental reports were devoted to the results of investigations of the magnetic, galvanomagnetic, photomagnetic and thermal characteristics of different weakly magnetic substances at low temperatures.

In his report, Magnetic Properties of Metals at Low Temperatures, B.I.Verkin summarized and analyzed the results of numerous researches of the Kharkov group of physicists on this subject. These included the investigations of B.I.Verkin, B.G. Lazarev and N.S.Rudenko (1950) in the course of which these investigators discovered the effect of the periodic field dependence of the parallel, perpendicular and differential ($\Delta\chi = \chi_{\parallel} - \chi_{\perp}$) magnetic susceptibilities of single crystals of zinc, cadmium, beryllium, magnesium, indium, tin, antimony and mercury and, also, brought to light anisotropy of the magnetic properties of bismuth, zinc, beryllium and antimony single crystals in the basal plane. B.I.Verkin and I.F.Mikhailov (1953) developed a superior compensation method for measuring $\Delta\chi$ and detected and made a detailed study of the dependence of this parameter in a zinc single crystal on the intensity of the magnetic field and the temperature in a range extending from room temperatures down to cryogenic ones. In addition, these investigators discovered the "hyperfine structure" of the dependence of $\Delta\chi$ on the field in beryllium single crystals (for fields ranging from 1500 to 20,000 oersteds at $T \lesssim 2^{\circ}K$). Comparison of the experimental "hyperfine structure" data with the theory of Landau yields a value of $3.5 \cdot 10^{-2}$ for the number of electrons [responsible for the effect] per atom (calculations taking into account the experimental data of E.S.Borovik on the magnitude of galvanomagnetic effects give a value $4 \cdot 10^{-2}$ electrons per atom). Verkin and Mikhailov made an exhaustive study of a magnesium single crystal. Analysis of the oscillation curves in fields of up to 20,000 oersted at $T = 4.2^{\circ}K$ indicated the existence of two close oscillation frequencies. The investigators noted the great difficulties encountered in attempting to carry out a harmonic analysis of the experimental oscillation curves for $\Delta\chi(H)$. In an investigation by B.I. Verkin and I.M.Dmitremko* a detailed study was made of a zinc single crystal: The field dependence of $\Delta\chi$ in the crystal was studied for sixteen different relative directions of the field in the range from 1500 to 20,000 oersteds and at temperatures from 1.5 to 4.2°K. The investigators detected fine structure of the dependence of $\Delta\chi$ on H and noted the presence of two widely separated frequencies.

---

*See below in the present issue of the Bulletin.

The investigators determined the dependence of the period of each component on the orientation of the field relative to the principal crystal axis or, in other words, the dependence of the maximum Fermi energy surface sections, for two groups of electrons, perpendicular to the field vector, on the angle between the vector and the principal axis of the crystal. It was shown that for the fundamental (low) frequency the relationship of the effective masses is characterized by $m_3 \gg m_1$, while for the high frequency of the "fine" structure, $m_3 \ll m_1$. This deduction, in the opinion of Verkin, is evidence in favor of the existence of different "groups" of electrons responsible for the complex periodicity of the field dependence of the permeability.

Verkin's report called forth a lively discussion particularly as regards questions of theoretical interpretation of the observed "fine and hyperfine structure" of the oscillation of the magnetic permeability.

Great interest was aroused at the conference by the report of E.S.Borovik on Galvanomagnetic Effects and the Properties of Conduction Electrons in Metals (see below). It has been known since the time of the basic work of P.L.Kapitsa (1929) on the increase of resistance of metals in magnetic fields up to $3 \cdot 10^5$ oersteds that the effect becomes stronger with decreasing temperature. For example, in a later investigation of bismuth it was found that at 2-4°K and fields on the order of $3 \cdot 10^4$ oersteds the specific resistance arrises by a factor of 10^6. This increase is due primarily to the fact that the free path time of conduction electrons increases with decreasing temperature (which is equivalent to an increase in the perturbing effect of the external magnetic field, i.e., an increase in the effective intensity of the field). It appears that the investigated metals can be divided into two classes: 1) metals characterized by an unlimited increase of the resistance in the magnetic field (cadmium, gallium, bismuth, tungsten, etc.) and 2) metals in which the effect exhibits saturation (aluminum, indium, sodium, etc.). Attempts were made to explain these phenomena by recourse to the concept of mixed conductivity (electron and hole) and the influence of the Hall effect. However, investigations of the Hall effect and of the variation of the electric resistance in a magnetic field were, as a rule, carried out separately so that the interdependence of these effects was not elucidated. Borovik investigated these phenomena jointly and analyzed their interdependence at low temperatures in pure metals. The effects were studied in copper, beryllium, magnesium, zinc, aluminum, indium, tin and lead. The investigator emphasizes that in the case of metals with a sharply rising resistance in magnetic fields the Hall constant is no longer fixed, but varies in a complex manner with the intensity of the field and other parameters; hence in such cases it is more expedient to characterize the Hall effect by the ratio of the Hall field (potential) E_y to the intensity of the electric field in the direction of the current E_x, i.e., by E_y/E_x. In such materials as beryllium, magnesium, zinc, cadmium, lead, tin, graphite and bismuth E_y/E_x passes through a maximum at a certain field strength and then falls off as the field is further increased. In aluminum, indium, copper and sodium E_y/E_x increases without limit with increasing field intensity. At the same time in the metals of the first group the relative change in electric resistance $\Delta\rho/\rho$ increases with field intensity without limit whereas in the second group $\Delta\rho/\rho$ tends to a definite limit with increasing field strength. Furthermore, Borovik detected finer traits in both effects (anisotropy, quantum oscillations, etc.) and established certain regularities in the relationships between them.

In the second part of his report, Borovik compared the experimental results with the quantum theory of metals. In the main, the theoretical interpretation is based on the work of D.I.Blokhintsev and L.Nordheim (1933) and its subsequent development. There is satisfactory qualitative agreement between the deductions of theory and the experimental results. However, a number of difficulties are encountered in effecting the comparison. In order to overcome these, the author proposes to complicate the theoretical metal model by the introduction of the hypothesis of the existence of several (two) types or groups of holes in some metals.

This hypothesis is not in conflict with the current concepts of one-electron zonal theory on the structure of energy bands and state zones, for example, in metals with hexagonal symmetry. In the conclusion of his report, Borovik compares his experimental results with the results of experimental studies of other properties of conduction electrons (determinations of the free path length, measurements of the electronic specific heat and deviations from Ohm's law).

Borovik's report called forth a lively exchange of views. The speakers called particular attention to the need for further development of the quantum theory of metals and overcoming the limitations of the one-electron model through extension of multiple electron theory based on the method of elementary excitations. Other speakers stressed the importance of complex investigations of metals, i.e., of studying their physical properties jointly and in relation to each other.

In their report N.E.Alekseevski and N.B.Brandt, The Influence of Volumetric Compression on Galvanomagnetic Effects in Bismuth and its Alloys, noted that the results of their investigation of the displacement of the critical temperature T_c in a number of superconducting alloys composed of non-superconducting components under the influence of compression have made it possible to establish the existence of two signs for the variation of T_c with the pressure p. For example, in alloys poor in bismuth $\partial T_c/\partial p < 0$, while in the case of high bismuth content alloys $\partial T_c/\partial p > 0$. The existence of two signs ($\pm$) for $\partial T_c/\partial p$ in superconductors is to be explained, in the opinion of the investigators, by the influence of the conduction-electron density on the character of the shift of T_c. From the work of Borovik (preceding report) it follows that study of galvanomagnetic effects in pure metals should make it possible to deduce certain information on the parameters characterizing conduction electrons in metals. Hence Alekseevski and Brandt felt it would be of interest to investigate the influence of volumetric compression on galvanomagnetic effects in superconducting alloys and their components. The measurements were made on single crystal specimens in the form of spheres and on polycrystalline plates. The specimens were subjected to compression in a constant-volume bomb by freezing water in accordance with the procedure developed by B.G.Lazarev and his co-workers. It was discovered that volumetric compression exerts a strong reversible influence on galvanomagnetic effects and on the temperature dependence of the electrical resistance of bismuth. The pronounced influence of volumetric compression on galvanomagnetic effects was also observed in a number of superconducting intermetallic compounds of bismuth.

In the discussion following the report the most animated exchange of views occurred in connection with the theoretical interpretation of the experimental results obtained by Alekseevsk and Brandt. Again many speakers emphasized the great importance of further development of the multiple electron theory of metals.

The report, Photomagnetic Effect in Cuprous Oxide Crystals at Low Temperatures (see below), by A.P.Komar, N.M.Reinov and S.S.Shalyt was devoted to an exposition of the results of further experimental investigation of the Kinoin-Noskov effect. The earlier works of I.K.Kinoin and his colleagues showed that the photomagnetic emf increases linearly with the magnetic field intensity H at T = 77°K, up through fields on the order of $4 \cdot 10^3$ oersteds. Theory predicts, however, that this linear dependence should obtain only on condition that $(\mu H/c)^2 \ll 1$ (where μ is the mobility of the current carriers and c is the speed of light); hence it was of interest to investigate the effect for the case when $(\mu H/c)^2 \sim 1$. The experiments were made at T = 77° and 4.2°K in fields of up to about $25 \cdot 10^3$ oersteds. The results showed that the photomagnetic emf vs field intensity curve at T = 77°K departs from a straight line when the field strength reaches about 10^4 oersteds, and at 4.2°K at about $4 \cdot 10^3$ oersteds. The mobility of the current carriers can be evaluated from the observed variation of the photomagnetic emf with the field intensity.

In the course of the ensuing discussion a number of speakers stressed the desirability of extending the investigation to diverse semiconductors and other materials.

In their report entitled, Magnetic and Thermal Properties of Condensed Oxygen, A.S.Borovik-Romanov, M.P.Orlova and P.G.Strelkov gave the results of measurements of the magnetic susceptibility of solid oxygen in the 14 to 18°K interval. The results showed that the properties of the γ-modification of solid oxygen are similar to those of liquid oxygen. The susceptibility of the β-modification of the solid decreases with decreasing temperature. This together with appreciable absolute magnitude of the (negative) Curie constant observed for oxygen at higher temperatures favors the hypothesis that the two low-temperature modifications of solid oxygen are antiferromagnetic. In addition the investigators also made a calorimetric study of the character of the phase transformations. The results of these studies and the shape of the specific heat curve indicate that the transformation from the α- to the β-modification is a transition of the second type. Antiferromagnetism in solid oxygen becomes manifest in the transition from the γ- to the β-modification this transition is of the first type, involving a considerable rearrangement of the crystal lattice.

The desirability of further investigations of the magnetic properties of the different forms of solid oxygen with a view to a more detailed determination of the antiferromagnetic properties of the element was noted in the ensuing discussion.

In Magnetic Properties of Trivalent Europium and Samarium by A.C.Borovik-Romanov and N.M.Kreines the speaker reported on the results of their investigation of the temperature dependence of the magnetic susceptibility of Eu_2O_3 and Sm_2O_3 in the 11 to 300°K temperature range and fields ranging to $6 \cdot 10^3$ oersteds by means of a highly sensitive magnetic balance developed expressly for this purpose. The susceptibility values were measured at intervals of only 5-10° which made it possible to bring out the shape of the temperature dependence curve with fair precision. The data for Eu_2O_3 are in fair agreement with the theory of Van Vleck and allow of determining the multiplet splitting for the Eu^{+++} ions. In the case of Sm_2O_3 the agreement at higher temperatures was more qualitative in character, while at the lowest temperatures the divergence between theory and experiment was very great. This divergence may be due to the influence of impurities and crystal electric fields on the magnetic properties of the samarium ions.

The report of M.O.Kostriukov, Investigation of the Specific Heat and the Temperature Dependence of the Magnetic Susceptibility of Anhydrous Manganese Chloride Below 4.2°K, was devoted to the results of the author's work, in the course of which he found that manganese chloride exhibits antiferromagnetism in the 4.2-1.4°K interval. The specific heat vs temperature curve disclosed an anomaly, with the specific heat passing through a maximum at 1.96°K. This anomaly is associated, according to the author, with transition of the compound from a paramagnetic to an antiferromagnetic state. This view is supported by the variation of the temperature dependence of the susceptibility in the same temperature region: the specific heat exhibits a maximum at the 1.6-1.95°K interval. On the basis of his experimental data the author evaluated the specific entropy of the transition from the fully ordered antiferromagnetic state to the fully disordered paramagnetic state; the resultant value was 13.1 ± 1.1 J mol^{-1} $degree^{-1}$ (the theoretical value is 14.86 J mol^{-1} $degree^{-1}$).

In the animated discussion following the last three reports, a number of speakers (I.M.Lifshits and others) dwelt on the question of the character of the anomalies of the different physical parameters, evinced in phase transformations of the second type. It was noted that the deductions from the statistical-thermodynamic theory of L.D.Landau (on the assumption that the dependence of the thermodynamic potential on the thermodynamic variables in the vicinity of a phase transition point is analytic in character) regarding the finite nature of the "jumps" is in need of critical re-examination in the light of the latest findings of Onsager et al. It was also noted in the discussion that as the accuracy of measurement of the quantities undergoing "jumps" incident to phase transitions has increased the height of the maximum of the observed anomalies has risen; this may be taken as an

indirect confirmation of the "infinitely large" value of the "jumps", which has been predicted by theory for the particular case of a linear chain and plane lattice.

The reports on theoretical problems connected with cryogenic magnetism were concerned with general quantum-mechanical theory of condensed systems (method of quasi-particles), quantum theory of the oscillation of the magnetic susceptibility in weakly magnetic metals, the theory of magnetic susceptibility in thin metallic lamina at low temperatures, the theory of the anamolous skin effect in magnetic fields for weakly magnetic materials, and the theory of this effect in ferromagnetics; a series of reports was devoted to consideration of the theory electronic relaxation effects at low temperatures in ferromagnetic dielectrics and ferromagnetic metals, the theory of magnetic cooling, the kinetics of the magnetization of solutions of He^3 in He^4, the theory of the temperature dependence of the spontaneous magnetization of metals and alloys at cryogenic temperatures, theoretical problems having to do with the magnetic attributes of antiferromagnetic substances, the scattering of neutrons in ferromagnetics and theory of the thermal properties of ferromagnetic bodies.

The report, Certain Problems of the Quantum-Mechanical Theory of Crystals at Low Temperatures (see below) by S.V.Vonsovski comprised an exposition of the general principles of the method of quasi-particles and gave illustrations of the application this method to specific problems of multiple electron theory of crystals (ferromagnetism of transition metals, semi-conductors, etc.).

Numerous questions were asked in connection with this report and a lively discussion ensued. I.M.Lifshits drew attention to the difficulties arising in dealing with systems of interacting micro-particles, particularly in connection with the problem of the diagonalization of the energy operator of a multiple electron system, in the course of which there is a danger of obtaining divergent results, rendering the entire calculation worthless. At the same time it was emphasized in the discussion that the method of quasi-particles offers a promising approach to the investigation of systems of interacting micro-particles. There was also an extensive exchange of views regarding the statistics of elementary excitations, the difference between the statistics of the initial particles of a system and quasi-particles, the nature of the kinetic processes involving quasi-particles and similar problems.

In the report, A Contribution to the Theory of the Magnetic Susceptibility of Metals with an Arbitrary Dispersion Law, by I.M.Lifshits, A.V.Pogorelov and A.M. Kosevich it was pointed out that the conduction electrons of metals interacting with each other and with the ionic lattice may, at low temperatures, be regarded from the thermodynamic point of view, as equivalent to an ideal gas of Fermi quasi-particles obeying a complex dispersion law, relating their energies (frequencies) with the quasi-momentum (wave vector). Consequently, to investigate the electronic diamagnetism of metals at low temperatures one should construct the thermodynamic potentials and find the magnetic momentum of the gas in the external magnetic field. The investigators determined the quasi-classical energy levels of quasi-particles with an arbitrary dispersion law in the magnetic field, computed the thermodynamic potentials and determined the magnetic susceptibility of the Fermi gas taking spin paramagnetism into account. They determined the amplitudes and periods of the oscillation of the susceptibility, which are expressed through the characteristics of the Fermi energy surface for the quasi-particles. Further, they analyzed the roles played by the different groups of electrons in the oscillation effect and examined the limiting cases for the derived equations. In addition the investigators made an attempt to determine the shape of the Fermi surfaces and the velocities of the electrons in the metal from the variation of the period and amplitude of the oscillation of the magnetic moment on the orientation of the magnetic field. They succeeded in deriving certain simple equations describing the Fermi surface in terms of the oscillation period and showed that determination of the temperature dependence of the amplitude of oscillation makes it possible to evaluate the electron velocity.

In the ensuing discussion particular attention was drawn to the advantages of the method of quasi-particles in the theoretical treatment of the electric and magnetic properties of metals.

In his report, Analysis of Oscillation Effects in Magnetic Fields on the Assumption of a Quadratic Dispersion Law [see Oscillation Effects in Magnetic Fields] below , G.E.Zil'berman presented the results of a series of theoretical investigations. The author emphasized the fact that the quadratic law approximation is not limited to the free electron model but can legitimately be utilized in the framework of the one-electron zonal scheme as well as in certain multiple electron problems. In the latter case the quadratic dispersion law applies to the quasi-particles of the system of electrons. The theory based on the assumption of the quadratic dispersion law yields qualitative agreement with experiment in certain temperature and field intensity ranges. However, from the quantitative standpoint there are encountered certain difficulties stemming from the anomalously small values of the Fermi brim energy and the effective mass of the quasi-particles. These difficulties must be obviated in further development of the theory.

The report called forth a considerable number of questions; many speakers remarked on the desirability of extending and developing these investigations in view of their importance in the cryogenic physics of metals.

The report by I.M.Lifshits and A.M.Kosevich, On the Magnetic Susceptibility of Thin Metal Lamina at Low Temperatures, was devoted to an exposition of the results of an investigation into the influence of the shape and size of the specimen on the oscillation of the magnetic susceptibility of the metal. The effect becomes appreciable when the thickness of the layer is commensurate with the radius of the Larmor electron orbit and is manifested through the dependence of the period and amplitude of the susceptibility oscillations on the dimensions (i.e. thickness) of the metal lamina. The investigators derived expressions for the magnetic moment of such a metallic lamina both for the case of a quadratic and any arbitrary dispersion law.

In their report, Contribution to the Theory of the Anomalous Skin Effect in Magnetic Fields, M.Ia.Azbel' and M.I.Kaganov gave the results of their investigation of the influence of the magnetic field on the magnitude of the surface impedance of metals. They showed that in the region of the anomalous skin effect the impedance is independent of the magnetic field. In the case of resonance the reflected wave is elliptically polarized and the metal can be characterized by two reflection coefficients, one corresponding to the normal, the other to the anomalous skin effect.

A.V.Sokolov and R.Zigenlaub in their report entitled, On the Distinctive Features of the Anomalous Skin Effect in Ferromagnetic Metals, drew attention to the specific influence of the ferromagnetic state on the characteristics of the skin effect. Taking into account elastic collisions between conduction electrons and ferromagnons the authors derived an expression for the surface impedance of ferromagnetic metals. They also derived expressions for the optical parameters (index of refraction, absorption coefficient, etc.) of ferromagnetic metals in the near infrared and red region of the spectrum.

The last three reports evoked numerous questions and an animated discussion. Part of the report by Sokolov and Zigenlaub was severely criticized by M.I.Kaganov who pointed out an inadmissible inconsistency in computing the part of the impedance due to the collisions of electrons with ferromagnons. The discussion brought out the importance of developing a rigorous quantitative theory for computing the impedance of metals at low temperatures.

In an extensive report A.I.Akhiezer summarized the results of three studies relating to relaxation effects in the condensed phase at low temperatures: 1) Relaxation Effects in Ferromagnetic Dielectrics at Low Temperatures (A.I.Akhiezer), 2) Establishment of Equilibrium between the Spins and the Lattice in Magnetic Cooling (A.I.Akhiezer & I.Ia.Pomeranchuk), 3) Kinetics of Magnetization of Solutions of He^3 in He^4 (A.I.Akhiezer & V.F.Aleksin). The first of these studies was con-

cerned with relaxation effects in ferromagnetic dielectrics, due to collisions of ferromagnons with each other and with the phonons of the lattice. The relaxation times were determined as functions of the temperature and a number of characteristic "constants" (the Debye temperature & Curie point). In the second study the time to attainment of equilibrium between the spins of the electrons of the system and the lattice in magnetic cooling was determined as a function of the temperature and other parameters. It was shown that this time is rather short. The investigators also evaluated the relaxation time in utilizing nuclear magnetism for obtaining cryogenic temperatures. Finally, in the third study, the variation of the magnetization time of weak solutions He^3 in He^4 with the temperature and the concentration of He^3 was determined.

In his report, Relaxation Effects in Ferromagnetic Metals at Low Temperatures (see below), E.A.Turov stated that analysis of the results of experimental investigations of relaxation effects in ferromagnetic metals indicates the necessity of taking into account spin-electron relaxation due to collisions between ferromagnons and conduction electrons. On the basis of the exchange model of interacting outer and inner electrons in ferromagnetic transition metals, the author computed the relaxation times for different types of collisions between conduction electrons and ferromagnons, an important part in which is played by the collision processes due to spin-orbital interaction between the inner and outer electrons of the ferromagnetic materials. Investigation of the process of attainment of equilibrium in a ferromagnon-conduction electron system leads to the conclusion that the spin-electron relaxation may be an important factor in determining the breadth of ferromagnetic resonance absorption lines. The method of calculation used by the author also makes it possible to compute the temperature dependence of the additional resistance of ferromagnetic metals due to collisions of the conduction electrons with the ferromagnons; this resistance proves to be directly proportional to the temperature and, consequently, at sufficiently low temperatures may become greater than the electrical resistance due to collisions between conduction electrons and phonons.

Numerous questions were asked in connection with the last two reports and an animated discussion ensued, in the course of which a number of speakers remarked on the importance of further development of the theory of relaxation processes particularly in ferromagnetic and antiferromagnetic materials.

In their report, On the Theory of the Temperature Dependence of the Spontaneous Magnetization of Metals and Alloys at Cryogenic Temperatures, E.I.Kondorski and A.S.Pakhomov gave the results of their investigation in which they extended the theory of ferromagnetism to the case of metals each atom in which has several electrons with uncompensated magnetic moments, rather than only one such electron in the unfilled electron shell. The authors derived an equation for the temperature dependence of the spontaneous magnetization at low temperatures in a ferromagnetic material of the indicated type in the case of two electrons with uncompensated magnetic moments per atom. The authors also indicated a method for solving the general problem (more than two electrons in the shell) and analyzed the probable character of the temperature dependence of the spontaneous magnetization in the general case. They derived equations for this dependence for ordered binary ferromagnetic alloys with equal or different numbers of electrons having uncompensated spin magnetic moments in the atoms of each of the component metals.

In the ensuing discussion particular attention was given to the problem of evaluating the different variables in the equations and the possibility of determining experimentally the additional terms in the expression for the spontaneous magnetization, derived by the investigators.

K.B.Vlasov presented a report entitled Anisotropy of the Susceptibility and the Magnetocaloric Effect in Antiferromagnetic Materials (see below). The author, using the method of the energy centers of gravity and taking into account magnetic dipole-dipole interaction, computed the free energy of a magneto-uniaxial antiferromagnetic single crystal. From this it was possible to determine the aniso-

tropy of the magnetic susceptibility as well as its dependence on the temperature and field in a wide range of field intensities and for temperatures extending to the antiferromagnetic Curie point. The derived regularities in turn permitted determining the temperature dependence of the critical field (intensity above which the anisotropy of the susceptibility begins to decrease) as well as giving a theoretical explanation for the anisotropy of the antiferromagnetic Curie point and computing the magnitude of the magnetocaloric effect in antiferromagnetics.

Many questions were asked in connection with this report and the subsequent discussion showed the urgent necessity of more extensive and intensive theoretical and experimental investigations of antiferromagnetic phenomena.

In his report, Thermal Properties of Ferromagnetic Dielectrics, L.M.Shishkin described the results of his determinations of the specific heat and thermal conductivity of ferromagnetic dielectrics as a function of the temperature.

The report, Neutron Scattering in Ferromagnetics, by S.B.Maleev was devoted to the problem of determining the neutron scattering cross section in ferromagnetic crystals with emission and absorption of ferromagnons.

In the ensuing discussion a number of speakers asked questions and commented on various points in connection with these reports.

* * * * * * *

ON THE OSCILLATIONS OF THE THERMODYNAMIC PARAMETERS OF A DEGENERATE FERMI GAS AT LOW TEMPERATURES

- I.M.Lifshits & A.M.Kosevich

As we know, quantization of the electron energy levels in a magnetic field leads to oscillation of the thermodynamic parameters of a degenerate Fermi gas and, specifically, is the cause of the periodic field dependence of the magnetic susceptibility of an electron gas (the de Haas-van Alphen effect).[1] It is evident that the thermodynamic parameters of a degenerate Fermi gas consisting of particles with quantized energy levels will always exhibit an oscillatory dependence on the quantities that determine the energy levels, whenever factors producing quantization of the levels are present (for example, limited volume, external field with an increasing potential, etc.).

Below we shall compute the oscillating terms of the thermodynamic potential that are responsible for the entire effect, basing our calculations on quite general assumptions regarding the energy spectrum of the particles (or quasiparticles) forming an ideal degenerate Fermi gas.

1. Calculation of the Oscillating Component of the Thermodynamic Potential

Let us assume that the "classical" problem of the energy displacement of a particle is solved. Then the energy $\mathcal{E}$ of this particle can be expressed in terms of the action variables I_i:

$$\mathcal{E} = \mathcal{E}(I_1, I_2, I_3). \tag{1}$$

Inasmuch as at low temperatures the oscillations of the thermodynamic parameters are determined by the energy spectrum near the Fermi brim, we are interested only in the higher energy levels and can, therefore, use the quasi-classical approximation for quantizing the motion of the particles. The quasi-classical quantization of a system with several degrees of freedom and comprising finite motions is given by the following condition:[2]

$$I_i=(n_i+\gamma_i)h, \qquad 0<\gamma_i<1, \tag{2}$$

and the quantized levels of energy E are obtained from (1) by substituting $(n_i+\gamma_i)h$ for I_i:

$$E(\mathrm{n})=\mathcal{E}[(n_1+\gamma_1)h,\ (n_2+\gamma_2)h,\ (n_3+\gamma_3)h],$$

(here we use n to denote a vector with integer components n_1, n_2, and n_3).

The thermodynamic potential Ω which it is convenient to use in calculating the thermodynamic parameters is given by

$$\Omega=-\theta\sum_{\mathrm{n}}\ln\{1+e^{[\zeta-E(\mathrm{n})]/\theta}\},$$

where $\theta=kT$, ζ is the chemical potential and the summation is carried out over all possible values of n.

To separate out the oscillating part of Ω we invoke a three-dimensional analogue of Poisson's equation replacing the summation over n by integration

$$\Omega=\int f[\zeta-E(\mathrm{n})]\,d\mathrm{n}+2\,\mathrm{Re}\sum_{\mathrm{k}}\mathscr{L}_{\mathrm{k}}=\frac{1}{h^3}\int f[\zeta-\mathcal{E}(I_1,I_2,I_3,)]\,dI_1\,dI_2\,dI_3+2\,\mathrm{Re}\sum_{\mathrm{k}}\mathscr{L}_{\mathrm{k}}, \tag{3}$$

where

$$f(x)=-\theta\ln(1+e^{x/\theta}).$$

The vector k is understood to mean the aggregate of three integer indices: k_1, k_2, k_3; the summation over k is carried out over all non-negative values of k_1, k_2 and k_3, with the exception of $\mathrm{k}=0$. The symbol $\mathscr{L}_{\mathrm{k}}$ denotes the integral:

$$\mathscr{L}_{\mathrm{k}}=\int f[\zeta-E(\mathrm{n})]\,e^{2\pi i\mathrm{kn}}\,d\mathrm{n}.$$

The oscillating part of Ω is comprised in the second term of (3).

Before proceeding to evaluate the integrals $\mathscr{L}_{\mathrm{k}}$ contained in (3), we must note that the integration with respect to n is carried out only in the first octant (from $n_i=0$ to $n_i=\infty$). By virtue of this, owing to the discontinuity in the integrand at the boundary of the region of integration, the result will contain two- and one-dimensional integrals along with the three-dimensional integrals $\mathscr{L}_{\mathrm{k}}$. Hence the equation evaluating the oscillating component of Ω will have the following form:

$$\Omega_{\mathrm{osc}}=2\,\mathrm{Re}\sum_{\mathrm{k}}{}'\mathscr{L}_{\mathrm{k}}+\mathrm{Re}\left\{\sum_{k_1k_2}{}'P_{k_1k_2}+\sum_{k_1k_3}{}'P_{k_1k_3}+\sum_{k_2k_3}{}'P_{k_2k_3}\right\}+\frac{1}{2}\,\mathrm{Re}\left\{\sum_{k_1}{}'Q_{k_1}+\sum_{k_2}{}'Q_{k_2}+\sum_{k_3}{}'Q_{k_3}\right\}, \tag{4}$$

where the two-dimensional integral $P_{k_1k_2}$ is defined as follows:

$$P_{k_1k_2}=\iint f[\zeta-E(n_1,n_2,0)]\,e^{2\pi i(k_1n_1+k_2n_2)}\,dn_1dn_2,$$

$P_{k_1k_3}$ and $P_{k_2k_3}$ are similarly defined, while the one-dimensional integrals Q_{k_1}, Q_{k_2} and Q_{k_3} are given by expressions of the following type:

$$Q_{k_1}=\int f[\zeta-E(n_1,0,0)]\,e^{2\pi ik_1n_1}\,dn_1.$$

The primed summation sign (Σ') in (4) signifies that the terms with $\mathrm{k}=0$ ($k_1=k_2=k_3=0$) are excluded from the summation over all the indicated indices from 0 to ∞.

The integral $\mathscr{L}_k$, can evidently be transformed to:

$$\mathscr{L}_k = \int f(\zeta - E) \left\{ \int\limits_{\substack{E(n)=E \\ n_i \geqslant 0}} \frac{e^{2\pi i k n} d\Omega_n}{|\nabla E(n)|} \right\} dE,$$

where $d\Omega_n$ denotes an element of the constant-energy surface

$$E(n) = E, \tag{5}$$

having the same orientation as n. The surface integral in the braces is evaluated over the portion of the constant-energy surface (5) located in the first octant.

Invoking the initial assumption that the quantum numbers are large $(kn \gg 1)$, we can obtain an asymptotic value for the integral:[3]

$$\mathscr{L}_k \approx \int dE f(\zeta - E) \sum_\nu \frac{\exp\{2\pi k n i_\nu \pm i\pi/4 \pm i\pi/4\}}{|k|\,|\nabla E(n_\nu)|\sqrt{|K_\nu(E)|}};$$

here $n_\nu = n_\nu(k, E)$ denotes the radius vectors in n space of all the points on the surface (5), at which the normal to the surface is parallel to k; $K_\nu(E)$ is the Gaussian curvature of the surface at these points and the summation is carried out over all such points in the first octant. The phases $i\pi/4$ entering into the exponent all have the same sign if the point n_ν is elliptic; the sign is minus if the surface at the given point is convex toward k and plus if convexity is in the opposite direction. In the case of a hyperbolic point, the phases $i\pi/4$ in the exponent have different signs.

Assuming $\partial n_\nu/\partial E \neq 0$ and the obvious condition that $\theta \ll \zeta$, the principal contribution to the oscillating portion of $\mathscr{L}_k$ results from integration over the region where the Fermi distribution function df/dE is sharply non-stationary, i.e., over the boundary of $E = \zeta$. Taking this into account, let us expand $n_\nu(k, E)$ in the exponent in powers of $E - \zeta$ and carry out the integration:

$$(\mathscr{L}_k)_{osc} \approx \frac{1}{(2\pi)^2\sqrt{k_1^2 + k_2^2 + k_3^2}} \sum_\nu \frac{\Psi(\lambda_k)\exp\{2\pi i k n_\nu(k,\zeta) \pm i\pi/4 \pm i\pi/4\}}{(k, \partial n_\nu/\partial\zeta)^2\,|\nabla E(n_\nu)|\sqrt{|K_\nu(\zeta)|}},$$

$$\Psi(\lambda) = \lambda/\mathrm{sh}\lambda; \quad \lambda_k = 2\pi^2 (k, \partial n_\nu/\partial\zeta)\,\theta.$$

The two- and one-dimensional integrals are evaluated in an analogous manner. We give the final equations for these integrals below:

$$(P_{k_1k_2})_{osc} \approx \frac{1}{(2\pi)^2 (k_1^2 + k_2^2)^{1/2}} \times \sum_\mu \frac{\Psi(\lambda_{k_1k_2})\exp\{2\pi i (k_1 n_{\mu 1} + k_2 n_{\mu 2}) \pm i\pi/4\}}{\left(k_1\frac{\partial n_{\mu 1}}{\partial\zeta} + k_2\frac{\partial n_{\mu 2}}{\partial\zeta}\right)^2 \left[\left(\frac{\partial E}{\partial n_1}\right)^2 + \left(\frac{\partial E}{\partial n_2}\right)^2\right]^{1/2} \sqrt{|K_{12\mu}(\zeta)|}};$$

$$\lambda_{k_1k_2} = 2\pi^2\theta\left(k_1\frac{\partial n_{\mu 1}}{\partial\zeta} + k_2\frac{\partial n_{\mu 2}}{\partial\zeta}\right).$$

Here $n_{\mu 1}(\zeta) = n_{\mu 1}(k_1, k_2, \zeta)$ denote the coordinates of those points on the plane curve

$$E(n_1, n_2, 0) = \zeta, \tag{6}$$

at which the normal to the curve is parallel to the two dimensional vector (k_1, k_2); $K_{12\mu}(\zeta)$ is the curvature of curve (6) at these points; the summation is carried out over all such points in the first quadrant. The phase $i\pi/4$ in the exponent has a minus sign if the curve (6) is convex toward (k_1, k_2) at the point $(n_{\mu 1}, n_{\mu 2})$ and a plus sign if the convexity is in the opposite direction.

The one-dimensional integral is

$$(Q_{k_1})_{osc} \approx \frac{\Psi(\lambda_{k_1})}{(2\pi k)^2\,\partial n_1/\partial\zeta} e^{2\pi i k_1 n_1(\zeta)};$$

$$\lambda_{k_1} = 2\pi^2\theta\,(k_1\,\partial n_1/\partial\zeta);$$

here $n_1(\zeta)$ denotes that value of n_1 for which $E(n_1, 0, 0) = \zeta$.

The equations for $P_{k_1k_3}$, $P_{k_2k_3}$, Q_{k_2}, and Q_{k_3} are similar in form.

Substituting the asymptotic expressions obtained for $\mathscr{L}_k$, P, and Q into (4) we obtain the oscillating component of Ω. It turns out that Ω_{osc} contains several terms, each having its own period of oscillation. Each of these periods can be determined from the dependence of the arguments of the corresponding exponents on the parameters that determine the locations of the energy levels. It should be noted that since the ratios between the periods of the various terms may, in general, have any arbitrary value, the form of the oscillations becomes quite complicated if (4) comprises several terms of the same order of magnitude.

The "classical" problem of obtaining the energy of a particle in the form of (1) is virtually intractable in the general case and can be readily solved only when the variables are separable.

We shall cite several simple examples in which the oscillating part of the thermodynamic potentials can be calculated completely and the periods of the corresponding oscillations obtained.

2. Electron Gas in Three-Dimensional Potential Box

Let us consider an electron gas with an arbitrary dispersion law

$$\mathscr{E} = \mathscr{E}(p_1, p_2, p_3) \tag{7}$$

in an infinitely high potential box having the dimensions L_1, L_2 and L_3 along the axes. In this case conditions (2) reduce to

$$2p_i L_i = n_i h,$$

and, therefore, the quantization of the energy level has the following form:

$$E(\mathrm{n}) = \mathscr{E}\left(\frac{n_1 h}{2L_1}, \frac{n_2 h}{2L_2}, \frac{n_3 h}{2L_3}\right). \tag{8}$$

Using (8) and carrying out the calculations by means of the equations of Section 1, we can readily find all the terms of the oscillating part of the thermodynamic potential Ω (the right half of the expression for Ω must be multiplied by 2 to take into account the two possible orientations of the electron spin). It turns out here that if the anomalously high anisotropy of the boundary surface $\mathscr{E}(\mathrm{p}) = \zeta$ is excluded, the following expression holds when L_1, L_2 and L_3 are all of the same order of magnitude and equal, say L:

$$\frac{\mathscr{L}_k}{P} \approx \frac{P}{Q} \approx L^{1/2} \Big/ \left(\frac{h\,\partial^2\mathscr{E}/\partial p^2}{\partial\mathscr{E}/\partial p}\right)^{1/2},$$

where the $\frac{h\,\partial^2\mathscr{E}/\partial p^2}{\partial\mathscr{E}/\partial p}$ equals the de Broglie electron wavelength λ_B. Assuming $L \gg \lambda_B$ we need leave in expression (4) for Ω_{osc} only the terms containing $\mathscr{L}_k$. Then

$$\Omega_{osc} = \Omega_1 + \Omega_2 + \Omega_3. \tag{9}$$

Here

$$\Omega_1 = L_1 L_2 L_3 \frac{1}{\pi^2}\left\{\sum_{\nu}\sum_{k_1=1}^{\infty} \beta^2(\mathrm{k}) \frac{\Psi(\lambda_k)\cos(2\pi k_1 n_{\nu 1} \pm \pi/4 \pm \pi/4)}{V\,|D(k_1, 0, 0)|} + \sum\sum \ldots + \sum\sum \ldots\right\}.$$

The dots under the summation sign stand for expressions analogous to the preceding terms in the braces; $\mathrm{n}_\nu(k_1)$ is the radius vector of the point on the boundary surface $E(\mathrm{n}) = \zeta$ at which the normal to the surface is parallel to the vector characterized by the components $(k_1, 0, 0)$. $\mathrm{n}_{\nu'}(k_2)$ and $\mathrm{n}_{\nu''}(k_3)$ are similarly determined.

$$\Omega_2 = L_1 L_2 L_3 \frac{1}{(2\pi)^2}\left\{\sum_{\mu}\sum_{k_1 k_2=1}^{\infty}\beta^2(\mathbf{k})\frac{\Psi(2\lambda_{\mathbf{k}})\cos[2\pi(k_1 n_{\mu 1}+k_2 n_{\mu 2})\pm\pi/4\pm\pi/4]}{\sqrt{|D(k_1,k_2,0)|}}+\sum_{\mu'}\sum_{k_1 k_3=1}^{\infty}\cdots+\sum_{\mu''}\sum_{k_2 k_3=1}^{\infty}\cdots\right\},$$

where $\mathbf{n}_\mu(k_1, k_2)$ is the radius vector of the point at which the normal to the boundary surface $E(\mathbf{n})=\zeta$ is parallel to the vector $(k_1, k_2, 0)$. $\mathbf{n}_{\mu'}(k_1, k_3)$ and $\mathbf{n}_{\mu''}(k_2, k_3)$ are determined similarly.

$$\Omega_3 = L_1 L_2 L_3 \frac{1}{(3\pi)^2}\sum_{\rho}\sum_{k_1,k_2,k_3=1}^{\infty}\beta^2(\mathbf{k})\frac{\Psi(3\lambda_{\mathbf{k}})\cos(2\pi k n_\rho \pm\pi/4\pm\pi/4)}{\sqrt{|D(k_1,k_2,k_3)|}},$$

where $\mathbf{n}_\rho(k_1, k_2, k_3)$ is the radius vector of the point at which the normal to the boundary surface is parallel to the vector $\mathbf{k}$:

$$\lambda_{\mathbf{k}} = (2\pi)^2\theta/h\beta(\mathbf{k});$$

$$D(k_1,k_2,k_3)=\begin{vmatrix}\partial^2\mathcal{E}/\partial p_1^2 & \partial^2\mathcal{E}/\partial p_1\partial p_2 & \partial^2\mathcal{E}/\partial p_1\partial p_3 & K_1L_1\\ \partial^2\mathcal{E}/\partial p_1\partial p_2 & \partial^2\mathcal{E}/\partial p_2^2 & \partial^2\mathcal{E}/\partial p_2\partial p_3 & k_2L_2\\ \partial^2\mathcal{E}/\partial p_1\partial p_3 & \partial^2\mathcal{E}/\partial p_2\partial p_3 & \partial^2\mathcal{E}/\partial p_3^2 & k_3L_3\\ k_1L_1 & k_2L_2 & k_3L_3 & 0\end{vmatrix}.$$

The values of $\lambda_{\mathbf{k}}$ and $D(k_1, k_2, k_3)$ are taken at the corresponding points on the boundary surface.

Here we used $\beta(\mathbf{k})$ to denote the ratios

$$\frac{\partial\mathcal{E}/\partial p_1}{k_1L_1}=\frac{\partial\mathcal{E}/\partial p_2}{k_2L_2}=\frac{\partial\mathcal{E}/\partial p_3}{k_3L_3} \qquad (10)$$

taken at the same points.

If we assume $L_3 \gg L_1 \approx L_2$, the expression (9) for Ω_{osc} is simplified. If L_3 is infinitely large, it follows from (10) that $k_3 = 0$, and, therefore, Ω_3 in (9) vanishes so that only the terms with summations over k_1 and k_2 remain in the equations for Ω_1 and Ω_2.

Lastly, if we assume $L_2 \approx L_3 \gg L_1$, i.e., in the case of an electron gas confined between two infinitely high walls, we have:

$$\Omega_{\text{osc}} = \Omega_1 = \frac{L_2L_3}{L_1^2}\cdot\frac{1}{\pi^2}\sum_{\nu}\sum_{k=1}^{\infty}\frac{(\partial\mathcal{E}/\partial p_1)^2\Psi\left(\frac{4\pi^2kL_1\theta}{h\partial\mathcal{E}/\partial p_1}\right)}{k^3\left|\frac{\partial^2\mathcal{E}}{\partial p_2^2}\cdot\frac{\partial^2\mathcal{E}}{\partial p_3^2}-\left(\frac{\partial^2\mathcal{E}}{\partial p_2\partial p_3}\right)^2\right|^{1/2}}\cos\left(2\pi k n_{\nu_1}\pm\frac{\pi}{4}\pm\frac{\pi}{4}\right). \qquad (11)$$

The equations given above for the oscillating part of Ω assume the simplest form in the case of an electron gas with a quadratic law dispersion:

$$\mathcal{E}=\frac{p^2}{2m}\equiv\frac{p_x^2+p_y^2+p_z^2}{2m},$$

in a cubic potential box

$$(L_1 = L_2 = L_3 = L).$$

In this case the terms in (9) assume the following form:

$$\Omega_1 = \frac{6\zeta}{\pi^2}\sum_{k=1}^{\infty}\frac{1}{k^3}\Psi\left(2\sqrt{2}\,\pi^2k\frac{\sqrt{m}\,\theta L}{h\sqrt{\zeta}}\right)\sin\left(4\pi kL\frac{\sqrt{2m\zeta}}{h}\right);$$

$$\Omega_2 = \frac{6\zeta}{(2\pi)^2}\sum_{k_1,k_2=1}^{\infty}\frac{1}{(k_1^2+k_2^2)^{3/2}}\Psi\left(4\sqrt{2}\,\pi^2\sqrt{k_1^2+k_2^2}\frac{\sqrt{m}\,\theta L}{h\sqrt{\zeta}}\right)\times\sin\left(4\pi\sqrt{k_1^2+k_2^2}L\frac{\sqrt{2m\zeta}}{h}\right);$$

$$\Omega_3 = \frac{2\zeta}{(3\pi)^2}\sum_{k_1,k_2,k_3=1}\frac{1}{|\mathbf{k}|^3}\Psi\left(6\sqrt{2}\,\pi^2|\mathbf{k}|\frac{\sqrt{m}\,\theta L}{h\sqrt{\zeta}}\right)\times\sin\left(4\pi|\mathbf{k}|L\frac{\sqrt{2m\zeta}}{h}\right).$$

If the gas temperature is very low or the potential box very small, so that $\lambda_k \equiv 2\sqrt{2}\,\pi^2 \frac{\sqrt{m}\,\theta L}{h\sqrt{\zeta}} \ll 1$, the function $\Psi(\lambda_k)$ can be replaced by unity. On the other hand, if the potential box is large and $\lambda_k \gg 1$, we have $\Psi(\lambda_k) \approx 2\lambda_k e^{-\lambda_k}$ and we need retain only the first term in the sum for Ω_1 in (9):

$$\Omega_{osc} \approx 24\,\theta L \frac{\sqrt{2m\zeta}}{h} \exp\left\{-2\sqrt{2}\,\pi^2 \frac{\sqrt{m}\,\theta L}{h\sqrt{\zeta}}\right\} \sin\left(4\pi L \frac{\sqrt{2m\zeta}}{h}\right).$$

It is evident from the last expression that with alterations of the linear dimensions of the potential box, the thermodynamic potential Ω will oscillate with a period

$$\Delta L = \frac{h}{2\sqrt{2m\zeta}},$$

which is independent of the magnitude of L. We note that this period is equivalent to half the de Broglie wavelength for an electron at the Fermi surface. Since the number $h/2\sqrt{2m\zeta}$ of the de Broglie half waves contained between the potential walls determines the number of the limiting stationary states, each "oscillation" of Ω is associated with a change of 1 in the number of states below the "limiting" Fermi energy level.

3. Electron Gas in a Potential Box in Magnetic Field.

We now turn to an electron gas, characterized by an arbitrary dispersion law (7), enclosed in a potential box as described above in Section 2, but placed in a homogeneous magnetic field H directed along the x_3 axis. If the vector potential is chosen to be $A_1 = -Hx_2$ and $A_2 = A_3 = 0$, two of the conditions of (2) reduce to the obvious relationships:

$$2p_1 L_1 = n_1 h \quad \text{and} \quad 2p_3 L_3 = n_3 h.$$

The third condition can be written as[4]

$$S\left(E, \frac{n_1 h}{2L_1}, \frac{n_3 h}{2L_3}; H\right) = (n_2 + \gamma)\frac{ehH}{c}, \qquad (12)$$

where $S(E, p_x, p_z; H)$ is the area of the cross section of the constant-energy surface

$$\mathcal{E}(P_1, P_2, P_3) = E, \quad p_x - \frac{|e|H}{c}\cdot\frac{L_2}{2} < P_1 < p_x + \frac{|e|H}{c}\cdot\frac{L_2}{2}$$

cut by the plane $P_3 = p_z = \text{const}$.

The levels of energy E are given by the expression, derivable from (12):

$$E = E(n_1, n_2, n_3; H).$$

Taking the dimension L_2 to be small, we can assume that the mean diameter of the classical orbit of an electron in the magnetic field is greater than L_2. In that case E is determined from various analytic expressions, depending on the ratio of the diameter of the curve $\mathcal{E}(P_1, P_2, p_z) = E$, (where $p_z = \frac{n_3 h}{2L_3} = \text{const}$) to the quantity $\left|\frac{n_1 h}{L_1} \pm \frac{eH}{c} L_2\right|$.

Using (12) and the equations deduced in Section 1 (taking the electron spin into account) we can find all the terms of the oscillating part of the thermodynamic potential Ω. Comparison of the terms containing $\mathcal{L}_k$, P and Q shows that, if $L_1 \approx L_3 = L$, their ratios are of the following order of magnitude:

$$\frac{\mathcal{L}_k}{P} \approx \frac{P}{Q} \approx \frac{L}{(ch/eH)^{1/2}},$$

where the quantity $(ch/eH)^{1/2}$ has a simple physical meaning: it is equivalent to the radius of the classical orbit of an electron in a magnetic field, $r_0(H)$, corresponding to the lowest energy level ($n_2 = 0$). In fact, since the expansion of (7) need not be carried out beyond the square term for small values of p, the lowest levels of the energy of motion of an electron in a magnetic field have the following form $E_{n_2} = \left(n_2 + \frac{1}{2}\right)\frac{ehH}{m^* c}$, where m^* is the effective mass; therefore

$$r_0(H) = \frac{c\sqrt{2m^* E_0}}{eH} = \left(\frac{ch}{eH}\right)^{1/2}.$$

Assuming that $L \gg r_0(H)$, we can leave, as in Section 2, only the terms containing $\mathscr{L}_k$ in the expression for Ω_{osc}:

$$\Omega_{osc} = \Omega^{(1)} + \Omega^{(2)} + \Omega^{(3)};$$

here

$$\Omega^{(1)} = L_1 L_3 \left(\frac{eH}{c}\right)^2 \frac{4}{\pi^2} \sum_m \sum_{k_2=1}^{\infty} \frac{\Psi(\lambda_{k_2}) \cos\left[\frac{2\pi k_2 c S_m(H)}{ehH} \pm \frac{\pi}{4} \pm \frac{\pi}{4} - 2\pi k_2 \gamma\right]}{k_2^3 \Phi(\zeta, n_m)},$$

$n_m(H)$ is the radius vector of the point at which $S(\zeta, p_x, p_z; H)$ has the extremal value $S_m(H)$ with ζ constant; $\partial S/\partial p_x|_m = \partial S/\partial p_z|_m = 0$; the normal to the surface

$$E(n_1, n_2, n_3; H) = \zeta \qquad (13)$$

is parallel at this point to the n_2 axis;

$$\Omega^{(2)} = L_1 L_3 \left(\frac{eH}{c}\right)^2 \frac{1}{\pi^2} \left\{ \sum_{\mu} \sum_{k_2=1}^{\infty} \frac{1}{k_2^3} \sum_{k_1=1}^{\infty} \frac{\Psi(2\lambda_{k_2}) \cos\left[2\pi(k_1 n_{\mu 1} + k_2 n_{\mu 2}) \pm \frac{\pi}{4} \pm \frac{\pi}{4}\right]}{\Phi[\zeta, n_\mu(k_1, k_2)]} + \right.$$

$$\left. + \sum_{\mu'} \sum_{k_2=1}^{\infty} \frac{1}{k_2^3} \sum_{k_3=1}^{\infty} \frac{\Psi(2\lambda_{k_2}) \cos\left[2\pi(k_3 n_{\mu' 3} + k_2 n_{\mu' 2} \pm \frac{\pi}{4} \pm \frac{\pi}{4}\right]}{\Phi[\zeta, n_{\mu'}(k_3, k_2)]} \right\};$$

$n_\rho(k_1, k_2; H)$ is the radius vector of the point at which the normal to the surface (13) is parallel to the vector $(k_1, k_2, 0)$; $n_{\mu'}(k_3, k_2; H)$ is similarly defined;

$$\Omega^{(3)} = L_1 L_3 \left(\frac{eH}{c}\right)^2 \left(\frac{2}{3\pi}\right)^2 \sum_{\rho} \sum_{k_2=1}^{\infty} \frac{1}{k_2^3} \sum_{k_1, k_3=1}^{\infty} \frac{\Psi(3\lambda_{k_2}) \cos\left[2\pi \mathbf{k} n_\rho(\mathbf{k}) \pm \frac{\pi}{4} \pm \frac{\pi}{4}\right]}{\Phi[\zeta, n_\rho(\mathbf{k})]};$$

$n_\rho(\mathbf{k}, H)$ is the radius vector of the point at which the normal to the surface (13) is parallel to the vector $\mathbf{k}$;

$$\lambda_{k_2} = 2\pi^2 k_2 \frac{c\theta}{ehH}\left(\frac{\partial S}{\partial \zeta}\right), \quad \Phi(\zeta, \mathbf{n}) = \left|\frac{\partial S}{\partial \zeta}\right| \left|\frac{\partial^2 S}{\partial p_x^2} \cdot \frac{\partial^2 S}{\partial p_z^2} - \left(\frac{\partial^2 S}{\partial p_x \partial p_z}\right)^2\right|^{1/2}.$$

The values of λ_{k_2} and $\Phi(\zeta, \mathbf{n})$ are taken at the corresponding points.

We must add, that if any of the above points lies in a coordinate plane of the n space, the corresponding term is multiplied by 1/2; if, however, this point lies on one of the coordinate axes, it is necessary to multiply the corresponding term by 1/4.

The equation for Ω_{osc} simplifies in two limiting cases: if $\lambda_{k_2} \ll 1$, the function $\Psi(\lambda_{k_2})$ can be replaced by unity; if $\lambda_{k_2} \gg 1$, $\Psi(\lambda_{k_2}) \approx 2\lambda_{k_2} e^{-\lambda_{k_2}}$, and therefore only the first terms should be left in the summations over k. The latter case corresponds to strengthening of the inequality

$$\frac{c\theta}{ehH}\left(\frac{\partial S}{\partial \zeta}\right) \gg 1, \qquad (14)$$

which inequality can be given a simple physical meaning. It follows from (12) that the mean spacing between neighboring energy levels with quantum numbers n_2 and $n_2 + 1$ near the Fermi level becomes

$$\Delta E_{n_2} = \frac{ehH}{c} \Big/ (\partial S / \partial \zeta),$$

and therefore inequality (14) corresponds to

$$\zeta \gg \theta \gg \Delta E_{n_2}.$$

If this inequality is satisfied, Ω_{osc} is comprised of terms of the form:

$$\Omega_{osc} \sim B(L_1, L_2, L_3; H, \zeta) \cos[2\pi n(L_1, L_2, L_3; H, \zeta) \pm \pi/4 \pm \pi/4].$$

The amplitude B and phase $2\pi n$ of the oscillations have the following form for $\Omega^{(j)}$ (j = 1, 2, 3):

$$B(L_1, L_2, L_3; H, \zeta) = L_1 L_2 \frac{16}{j} \cdot \frac{eH\theta}{ch} \left(\frac{\partial S}{\partial \zeta}\right) \frac{\exp\left(-j\, 2\pi^2 \frac{c\theta}{ehH} \cdot \frac{\partial S}{\partial \zeta}\right)}{\Phi(\zeta, n)} \quad (j = 1, 2, 3),$$

$$n = \frac{cS_m(H)}{ehH} - 2\pi\gamma \qquad \text{with } j = 1,$$

$$n = n_{\mu 1}(L_1, L_2, L_3; H, \zeta) + n_{\mu 2}(L_1, L_2, L_3; H, \zeta) \qquad \text{with } j = 2,$$

$$n = n_{\rho 1}(L_1, L_2, L_3; H, \zeta) + n_{\rho 2}(L_1, L_2, L_3; H, \zeta) + n_{\rho 3}(L_1, L_2, L_3; H, \zeta), \qquad \text{with } j = 3.$$

The dependence of the phase $2\pi n$ on the magnetic field intensity H and on the dimensions L_1, L_2, L_3 of the potential box determines the variation of the periods of oscillation with these parameters.

It is readily seen that the variation of the oscillation periods of the terms in Ω_{osc} with H are given by the following expressions:

1) for $\Omega^{(1)}$

$$\Delta\left(\frac{1}{H}\right) = \frac{eh/c}{|S_m(H) - H\,\partial S_m/\partial H|},$$

2) for $\Omega^{(2)}$

$$\Delta\left(\frac{1}{H}\right) = \frac{eh/c}{2|S(n_\mu, H) - H\,\partial S_\mu/\partial H|},$$

3) for $\Omega^{(3)}$

$$\Delta\left(\frac{1}{H}\right) = \frac{eh/c}{3|S(n_\rho, H) - H\partial S_\rho/\partial H|}.$$

The variation of the oscillation periods with L_1, L_2 and L_3 can be obtained in a similar manner.

If we take $L_3 \gg L_1$, we must assume $k_3 = 0$, and the following expression holds for Ω_{osc}:

$$\Omega_{osc} = \Omega_1 + L_1 L_3 \left(\frac{eH}{c}\right)^2 \frac{1}{\pi^2} \sum_\mu \sum_{k_2=1}^{\infty} \frac{1}{k_2^3} \sum_{k_1=1}^{\infty} \Psi(2\lambda_{k_2}) \times \frac{\cos[2\pi(k_1 n_{\mu 1} + k_2 n_{\mu 2}) \pm \pi/4 \pm \pi/4]}{\Phi[\zeta, n_\mu(k_2, k_2)]}.$$

Lastly, if we assume $L_1 \gg L_2$ and $L_3 \gg L_2$, only the first term (Ω_1) remains in the expression for Ω_{osc}:

$$\Omega_{osc} = \Omega_1 = L_1 L_3 \left(\frac{eH}{c}\right)^2 \frac{4}{\pi^2} \times \sum_m \sum_{k_2=1}^{\infty} \frac{\Psi(\lambda_{k_2}) \cos\left[\frac{2\pi k_2 cS_m(H)}{ehH} \pm \frac{\pi}{4} \pm \frac{\pi}{4} - 2\pi k_2 \gamma\right]}{k_2^3 \Phi(\zeta, n_m)}, \qquad (15)$$

and this agrees with the expression obtained by the authors[4] for a one-dimensional infinitely-deep potential well, using a somewhat different method*.

*In Ref. 4 we obtained an expression for the oscillating component M_{osc} of the magnetic moment of an electron gas directly. Using $M = -\partial\Omega/\partial H$ and noting that in (15) the factor in front of the cosine need not be differentiated, it is easy to verify that the two equations are equivalent.

It can readily be shown in the limiting case where $H \longrightarrow 0$ equation (15) transforms into (11).

Physico-Technical Institute of the
Ukranian SSR Academy of Sciences &
Chernovtsi State University

References

1. R. Peierls, Zs.f. Phys., 81, 186 (1933); L.Landau, Communication concerning article by D.Schoenberg, Proc. Roy. Soc. A 170, 341 (1939); A.Akhiezer, Doklady AN SSSR, 23, 872, (1939); I.Lifshits & A.Kosevich, Doklady AN SSSR, 96, 963 (1954).
2. L.Landau & E.Lifshits, Kvantovaia mekhanika (Quantum Mechanics), M. 1948.
3. I.Lifshits, Zhur. eksp. i teor. fiz., 18, 293 (1948).
4. A.Kosevich, Zhur. eksp. i teor. fiz., 29, 12 (1955).

* * * * * * *

OSCILLATION EFFECTS IN MAGNETIC FIELDS

- G.E.Zil'berman

1. Introduction

If an electron gas* is in a potential well of sufficiently small dimensions or under conditions equivalent to such a well, in the sense of formation of discreet energy levels, the number of states per energy interval will prove to be a quantity that oscillates when any of the parameters characterizing the well is changed.

The reason for this is that any change in the external parameters results in a displacement of the energy levels and a change in the degree of degeneracy of each level. When one of the levels intersects the Fermi energy level E_0 the number of states having an energy from 0 to E_0 changes abruptly ("jumps"). When the external parameters are altered such changes will occur periodically, hence the number of states will oscillate. This oscillation of the number of states will lead, in turn, to oscillation of all the physical quantities dependent upon the distribution of electrons among the quantized energy levels.

The connection between the periodicity of the changes of these quantities and the spacing of the energy levels offers a means for direct experimental investigation of the energy spectrum of the electrons in a crystal. If, as is sometimes the case, the oscillating quantity can be represented in the form of the sum of oscillating quantities with different frequencies this may be taken as evidence of the complex structure of the energy spectrum of the electrons in the crystal; in the mathematical treatment this is commonly spoken of as the existence of "electron groups" in different regions of K-space.

Thus investigation of oscillation effects is one of the most powerful and refined means of studying the energy spectra of electrons.

The most important of these oscillation effects are those which are manifested when a crystal is placed in a magnetic field. As is known[1], the energy of

*The term "electron gas" should be understood to mean a Fermi gas of quasi-particles in an electronic fluid.

a free electron in a magnetic field may be described by

$$E_{nk_3} = \mu H\left(n + \frac{1}{2}\right) + \frac{\hbar^2 k_3^2}{2m}, \qquad (1)$$

where

$$\mu = \frac{e\hbar}{mc}.$$

The spacing between levels equals μH. This, therefore, is the quantity determining the period of oscillation.

The different oscillating parameters which have been investigated theoretically include the magnetic susceptibility of metals at low[2-5] and medium[6] temperatures, the specific heat of metals in a magnetic field, the electric resistance[3,8,9], the Hall field[9], and the thermal emf[9].

Oscillation of the magnetic susceptibility, discovered by de Haas & van Alpen[10], has been investigated in greatest detail by Verkin, Lazarev & Rudenko[11]. Oscillation of the resistance has been observed by Schubnikov & de Haas[12] and Lazarev, Nakhimovich & Parfenova[13]. Oscillation of the Hall field has been detected by Borokik[14], while oscillation of the thermal emf has been observed by Steel & Babiskin[15].

2. Different approximations of the law characterizing the dispersion of electrons in the magnetic field

The number of energy states is determined by the dispersion law. Hence investigation of the law characterizing the dispersion of the electrons in the magnetic field is one of the most important aspects of any theoretical consideration of the oscillation effects. As of the present, the following approximations have been investigated:

a) Entirely free electrons[1] - see equation (1).

b) Electrons in a weak periodic electric and a homogeneous magnetic field[16]. The magnetic field operator is included in the principal Hamiltonian, while the periodic field of the crystal is regarded as a perturbation. The energy of such a weakly coupled electron in the lower levels of the zone is characterized by

$$E_{k_1 nk_3} = \mu^* H\left(n + \frac{1}{2}\right) + \frac{\hbar^2 k_3^2}{2m_3^*} + \sum_{l=1}^{\infty} A \cos\left(4\pi l \frac{\alpha_0^2}{a} k_1\right), \qquad (2)$$

where $\mu^* = \frac{e\hbar}{m^* c}$, m^* and m_3^* are the effective masses and $\alpha_0 = \sqrt{\frac{\hbar c}{eH}}$.

If we neglect the small last term, equation (2) shows that in this case use of the method of effective masses is admissable. The last term, containing the wave vector k_1, leads to broadening of each of the n energy levels into a narrow zone. The possible influence of this broadening has not yet been investigated.

c) Strongly coupled electrons in a magnetic field[17, 9]. In this case the applicable approximation is fully analogous to the usual approximation of Bloch for strongly coupled electrons. If one takes into account only the exchange interaction of electrons in nearest neighbor atoms, the energy of motion of an electron in the plane perpendicular to the direction of the magnetic field is determined as the eigenvalue of the differential equation

$$(\lambda - 2\cos\varepsilon x)\,\varphi(x) = \varphi(x + \varepsilon) + \varphi(x - \varepsilon), \qquad (3)$$

where $\varepsilon = \frac{a}{\alpha_0}$, a being the lattice constant.

For the lower levels of the energy zone this equation again has a solution in the form of (1) with the effective masses expressed through the appropriate exchange integrals. For levels near the middle of the energy zone, we again have

broadening of the levels into narrow bands similar to that obtaining for weakly coupled electrons.

d) Polar model of a metal in a magnetic field[19]. In this model, as is known, the electrons do not have their proper wave functions and we consider the wave functions of the entire crystal as a whole. In this case the dispersion law for the quasi-particles is again determined by equation (3).

e) Weakly interacting electrons[21]. If we subtract from the energy of the Coulomb interaction of the electrons the energy of their interaction with the electric charge, distributed with average density throughout the crystal, we can construct an interaction operator which under certain conditions can be regarded as a perturbation. The criterion of smallness for the latter is the inequality:

$$\frac{m^* e^2}{\pi^2 \hbar^2}\left(\frac{\pi}{3n}\right)^{1/3} \ll 1, \qquad (4)$$

where n is the electron concentration and m^* is the effective mass. Perturbation theory then permits of finding the dispersion law for quasi-particles in the absence of and in a magnetic field:

$$E_{nk_3} = \mu^* H\left(n+\frac{1}{2}\right) + \frac{\hbar^2 k_3^2}{2m^*} - \frac{4}{5}\sqrt{\left[\mu^* H\left(n+\frac{1}{2}\right) + \frac{\hbar^2 k_3^2}{2m^*}\right]\frac{m^* e^4}{2\pi^2\hbar^2}}. \qquad (5)$$

f) Recently Lifshits and his colleagues have succeeded in developing a theory in the quasi-classical approximation in which the dispersion law for electrons in a magnetic field is determined from the dispersion in the absence of the field; the dispersion in the absence of a field can be arbitrary[4, 20].

3. Oscillation of the magnetic susceptibility and the specific heat in a magnetic field

Oscillations of the susceptibility were first investigated in the theoretical studies of Landau[2] and Akhiezer[3] on the assumption that the electron dispersion law is quadratic. The same assumption was utilized by the present author in the investigation of Ref. 5, the equations of which reduce to the equations of Refs. 2 and 3 in the corresponding limiting cases. In the developed theory, in addition to diamagnetism - expressed by equation (1) - spin paramagnetism is also taken into account. The theory is qualitatively and in a number of cases quantitatively in agreement with experiment if it is assumed that the experimentally observed effect of the oscillation of susceptibility is due to electrons with very small effective masses and a low Fermi energy E_0. The principal comparable quantities are the dependence of the period of oscillation on the intensity of the field and its orientation with respect to the crystal axes and the dependence of the amplitude of oscillation on these variables. Some experimental results, for example, the field dependence of the amplitude in strong magnetic fields, cannot, apparently, be wholly explained on the assumption of a quadratic dispersion law, but will require more general assumptions[4]. Through a detailed comparison of theory with experiment it should be possible, as Lifshits and Pogorelov[20] have shown, to reproduce the Fermi surface for electrons and elucidate the dispersion law in the vicinity of this surface.

The "fine structure" of the oscillation, observed in many metals, particularly in the strong fields, can, as has been noted, be regarded as due to the presence of several electron groups. Separation of the "fine structure" part from the fundamental frequency, where this is feasible, permits determining the parameters characterizing such groups.

At present theory is not yet in full conformity with experiment and obviously stands in need of further development. It must also be noted that quantitative comparison of theory with experiment is often extremely difficult in view of the great complexity of the theoretical and experimental data.

The oscillation effects gradually vanish as the temperature is increased. Verkin and Mikhailov[22] showed that (for zinc) the magnetic susceptibility is field dependent up to room temperatures. The theory for the variation of the susceptibility with the field intensity in a wide range of temperatures developed in Ref. 6 on the assumption of a quadratic dispersion law gives satisfactory qualitative agreement with experiment.

The electron specific heat in a magnetic field also oscillates when the field intensity is changed. Theoretical calculations for this oscillation have been carried out in Ref. 4 (in the framework of the quasi-classical approximation) both for the assumption of a quadratic dispersion law and for the case of any arbitrary dispersion law. This effect has not yet been observed. Experimental measurements are extremely difficult inasmuch as the oscillating part of the specific heat amounts to only a few percent of the total electron specific heat.

4. Oscillations of the resistance, Hall field and thermal emf

The great variation of the resistance of metals in a magnetic field can, as is known[7, 8, 18], be explained with the aid of the so-called two-zone metal model, in which it is assumed that the electrons of two overlapping zones - a thinly populated one and an almost filled one - participate in the kinetic effects. On the other hand, in view of the fact that the oscillations are observed only in sufficiently strong fields satisfying the inequality,

$$\omega\tau \gg 1, \tag{6}$$

where $\omega = \frac{eH}{mc}$ and τ is the free path time, the calculations cannot be based on the kinetic equation which, rigorously speaking, is valid only in the case when $\omega\tau \ll 1$. In the investigation of Ref. 9 the kinetic effects in the magnetic field have been computed on the basis of the two-zone model and on the assumption that inequality (6) holds. Explicit expressions for the resistance, the Hall field and the thermal emf in a magnetic field were derived. All these proved to be oscillating quantities in strong magnetic fields. The resistance is given by

$$\rho_H = \frac{CH^2(f_1+f_2)}{ec^2H^2(N_1-N_2)^2 + eC^2(f_1+f_2)^2}, \tag{7}$$

where

$$f_1 = \frac{8}{3}E_0^2 m_1^4\left[1 + a\mu_1 H - \frac{5\pi^2\sqrt{2}}{\sqrt{\mu_1 H E_0}}\exp\left(-\frac{2\pi^2 kT}{\mu_1 H}\right)\cos\left(\frac{2\pi E_0}{\mu_1 H} - \frac{\pi}{4}\right) + \ldots\right]; \tag{8}$$

the expression for f_2 is obtained from (8) by substituting m_2 for m_1 and $A - E_0$ for E_0 (E_0 is the Fermi brim energy and A is the overlap of the zones), N_1 and N_2 are, respectively, the concentrations of the electrons in the upper zone and of the holes in the part of the lower zone overlapping it, and C and a are constants.

As may be seen from (7) the oscillations of the resistance are superposed on its increase in the magnetic field.

The oscillations of the Hall field are similar to those of the resistance but differ from the former in phase by π; this has been experimentally confirmed by Borovik[14]. Soon after submission of Ref. 9 to the editors, Steel and Babiskin[15] reported detecting oscillations of the thermal emf experimentally.

Thus all the oscillation effects mentioned in this report have already been observed experimentally. However, it must be noted that whereas oscillation of the magnetic susceptibility has been investigated in great detail, experimental investigation of the oscillations of the other physical quantities is at present only in the initial stages and there has been virtually no effective comparison of theory with experiment. At the same time such investigation is essential for a detailed study of the energy spectrum of electrons in crystals.

References

1. L.D.Landau, ZS. f. Phys., 64, 629 (1930).
2. L.D.Landau, Communication concerning D.Shoenberg's article, Proc. Roy. Soc., A170, 341 (1939).
3. A.I.Akhiezer, Doklady AN SSSR, 23, 872 (1939).
4. I.M.Lifshits & A.M.Kosevich, Doklady AN SSSR, 96, 963 (1954).
5. G.E.Zil'berman, Zhur. eksp. i teor. fiz., 21, 1209 (1951).
6. G.E.Zil'berman, Zhur. eksp. i teor. fiz., 25, 713 (1953).
7. D.Blokhintsev & L.Nordheim, ZS. f. Phys., 84, 168 (1933).
8. B.I.Davydov & I.Ia.Pomeranchuk, Zhur. eksp. i teor. fiz., 9,1295 (1939).
9. G.E.Zil'berman, Zhur. eksp. i teor. fiz. (forthcoming issue).
10. W.I. de Haas & P.M. van Alphen, Leid. Comm., No.212a (1930;No.220d (1932).
11. B.I.Verkin, Lazarev & Rudenko, Zhur. eksp. i teor. fiz., 20, 93, 995 (1950) & 25, 471 (1953); Doklady AN SSSR, 69, 773 (1949), 73, 59 (1950), 81, 529 (1951); in Sbornik (Symposium) "In Memorium of S.I.Vavilov,p.344,M.L. 1952.
12. L.W.Shubnikow & W.I. de Haas, Leid.Comm., No.207a,d & No.210a (1930).
13. B.G.Lazarev, N.M.Nakhimovich & E.A.Parfenova, Zhur.eksp. i teor. fiz., 9, 1169 (1939).
14. E.S.Borovik, Thesis, Kharkov State University, 1954.
15. M.C.Steel & I.Babiskin, Phys. Rev., 94, 1394 (1954).
16. G.E.Zil'berman, Zhur. eksp. i teor. fiz., 23, 49 (1952).
17. R.Peirls, ZS. f. Phys. 80, 763 (1933).
18. M.Kohler, Ann. d. Phys. 6, 18 (1949).
19. G.E.Zil'berman, Zhur. eksp. i teor. fiz., 25, 313 (1953).
20. I.M.Lifshits & A.V.Pogorelov, Doklady AN SSSR, 96, 1143 (1954).
21. G.E.Zil'berman, Zhur. eksp. i teor.fiz., 25, 549 (1954).
22. B.I.Verkin & I.F.Mikhailov, Zhur.eksp. i teor.fiz., 24, 342 (1953).

* * * * * * *

ANISOTROPY OF THE MAGNETIC PROPERTIES OF ZINC SINGLE CRYSTALS AT LOW TEMPERATURES

- B.I.Verkin & I.M.Dmitrenko

1. Introduction

Prior to 1930 it was generally assumed, on the basis of the available experimental data and in accord with the accepted theory of the metallic state, that the magnetic susceptibility of all diamagnetic and most paramagnetic metals is independent of the magnetic field in a wide range of temperatures.

In 1930 the Leiden Laboratory group discovered that at low temperatures ($T \leq 20.4^{\circ}K$) the resistivity of highly pure bismuth single crystals changes in a complex steplike manner with the external magnetic field[1] and that the susceptibility of such crystals varies with the intensity of the external field in a complicated periodic fashion[2].

A quantitative theory for the complex periodic field dependence of the magnetic susceptibility at low temperatures (the so-called de Haas-van Alphen effect) was proposed first by Landau[3] on the basis of the free electron model, i.e., for the case of an almost non-interacting electron gas with a quadratic dispersion law. The interaction of the electrons and the periodic field of the lattice were taken into account only through a self-consistent field by the introduction of "effective masses." Later Akhiezer[4] gave a generalization of this theory taking account of spin paramagnetism and Zil'berman[5] deduced the basic theoretical equations in a form

applicable to the anisotropic case and more convenient for comparison with experiment. As a result of such comparison one can deduce the values of the parameters of theory: the three principal values of the effective mass tensor, the Fermi energy E_0 and the number of electrons per metal atom, participating in the effect. Comparison of the experimental data obtained in investigations of the de Haas-van Alphen effect in bismuth (a metal with an abnormally small number of conduction electrons) with theory[6] showed that with values of the parameters in satisfactory agreement with the results of other investigations (for example, investigations of the galvanomagnetic properties of bismuth[7, 8]) the theory correctly reflects the main quantitative regularities of the periodic field dependence of the susceptibility at low temperatures.

A series of experimental studies carried out over the past eight years has shown that in addition to bismuth there are at least fourteen other metals -- single crystals of zinc[9], tin, cadmium, beryllium, indium, magnesium, antimony, mercury[10], gallium, thallium, aluminum, lead, graphite[11, 12] and arsenic[13] — in which the difference between the principal susceptibilities depends in a complex periodic manner on the external field intensity at low temperatures. The location of these metals in the Mendeleev periodic table will be clear from an examination of Fig. 1. Thus it has been found that the effect in question is generally common to the nontransition metals of Groups 2, 3, 4 and 5. This attribute, which is a consequence of the diamagnetism of the electrons in the metal, is manifest at low temperatures and, probably depends on the particular characteristics of the electronic structure of each individual metal. It is important to note that not one of the univalent metals of Group 1, which have been investigated down to very low temperatures ($<1^\circ$K) and in very strong fields ($\leq 9 \cdot 10^4$ oersteds) exhibits periodicity of the susceptibility under these experimental conditions. Analysis of the physical properties of the metals exhibiting the de Haas-van Alphen effect shows that the effect is observed in diamagnets (Zn, Bi, Be, etc.) and in paramagnets (Sn and Mg), in superconductors (Sn, In, Zn, etc.) and in non-superconductors (Sb, As, graphite, etc.), in metals with an unlimited increase in electric resistance in magnetic fields (Bi, Sn, Zn, etc.) and in metals exhibiting saturation of the resistance in increasing fields (In). Important for understanding the role of the interaction of the electrons with the lattice is the fact that in metals crystallizing into like lattices (Zn and Cd) the de Haas-van Alphen effect becomes manifest at a temperature proportional to the Debye characteristic temperature of the metal, i.e., the lower the Debye temperature, the lower the temperature at which the effect becomes apparent[10].

Numerous comparisons of the experimental data relating to the various metals listed above with theory based on the free electron model[5, 11] all lead to small values of the effective mass, the Fermi energy E_0 and the number of the electrons participating in the effect. The number of electrons participating in the effect is some 5-6 orders of magnitude inferior to the number of electrons responsible for the magnitude of the electronic specific heat of the metal and the values of the principal parameters characterizing observed galvanomagnetic effects. Another difficulty is the fact that if we select our parameters by two independent methods, comparing theory with two basically different experiments (for example, investigations of the dependence of the magnetic susceptibility on the intensity of the field, on the one hand, and on its direction on the other) we end up with divergent results.

Further experimental studies of the anisotropy of Be and Zn crystals[14] led to the discovery of "fine" and "hyperfine" structure of the complex periodic field dependence of the magnetic susceptibility (the experimental curve for $\Delta\chi(1/H)$ appears to be the result of the superposition of several curves of the form $A_k(T, \theta) H^{-3/2} e^{-B_k(T, \theta) \cdot 1/H} \sin\left[\omega_k(\theta) \frac{1}{H} - \delta_k\right]$ with markedly different values of ω_k which are

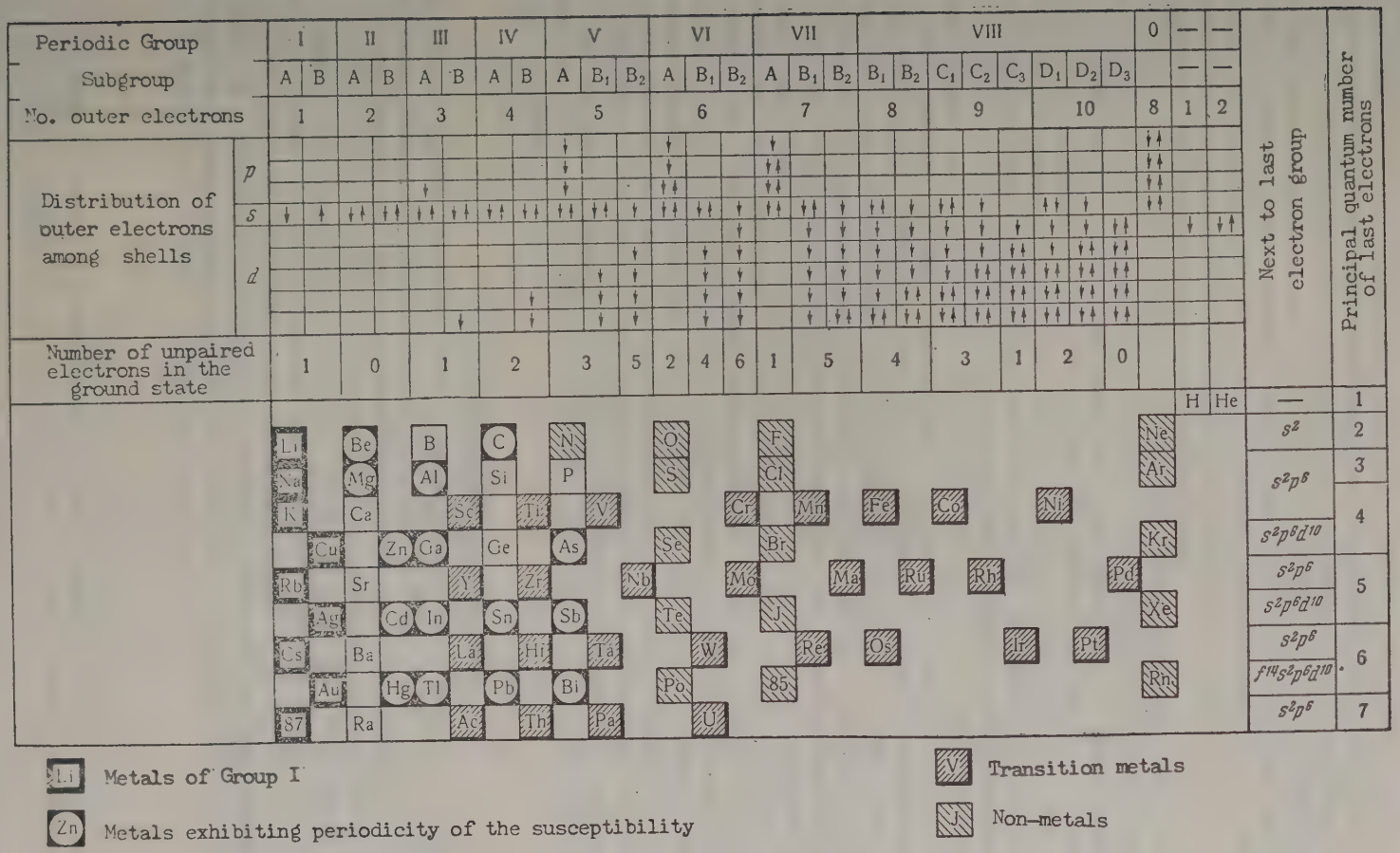

Fig. 1. Position in the periodic table of metals exhibiting "periodic" field dependence of the magnetic susceptibility.

not whole multiples of each other*). The discovery of fine and superfine structure together with the results of comparisons of theory with the experimental data for the curves with minimal values of ω_k (bearing witness to the smallness of the number of electrons responsible for the effect described by the said curve) confirmed the earlier suggested hypothesis of the existence in the metal of several groups of elcctrons that successively, as the field intensity is increased, further the development of the periodic field dependence of the susceptibility, observed at low temperatures. It should be noted that the previously known complex structure of the $\Delta\chi(1/H)$ curves for Al and Pb[11,12](as well as for Mg[14]) can, without special investigation of highly anisotropic crystals, be explained within the framework of the aforementioned theory by the complexity of the structure of the energy surface of a single group of electrons.

The theory of the de Haas-van Alphen effect has been further developed in the publications of Lifshits, Kosevich and Pogorelov who connected the problem of the effect in metals with the problem of the electron energy spectrum in metals, one of the pivotal problems in modern physical theory of metals. Proceeding from the fact that at low temperatures the metal electrons, interacting with each other and with the lattice can be regarded and treated as an ideal Fermi gas of charged quasi-particles with some (unknown) dispersion law, Lifshits and Kosevich deduced an expression for the energy levels of such a particle in a magnetic field and computed the magnetic moment of this quasi-particle gas[15]. The results of these investigations theoretically indicate the way in which it should be feasible to elucidate the principal characteristics of the energy spectrum of the quasi-particles (the form of the Fermi surface and the electron velocities in the vicinity of this surface) from the results of experimental studies of the angular dependence of the period and amplitude of the oscillation of the magnetic susceptibility on the orientation of the magnetic field vector relative to the crystal axes.[16]

Since there was not enough experimental data available to decide whether it was possible to solve the problem of determining the Fermi surface, we undertook the present investigation for the purpose of making a thorough study of the angular dependence of the periods and amplitudes of the oscillation of the susceptibility on the orientation of the field, comparing the experimental results with the character of the angular dependence predicted by theory based on the free electron model and, finally, clarifying the possibility of utilizing these data for reproducing the Fermi surface.

2. Experimental conditions

We investigated the magnetic properties of zinc single crystals in fields ranging from 1500 to 20,000 oersteds at $T \leqslant 4.2^{\circ}K$.

The procedure, as in our preceding studies, consisted in measuring the turning couple acting on the crystal suspended, in a homogeneous magnetic field, from a thin, elastic galvanometer filament. Depending on the magnitude of the turning couple, its value could be determined either from the angle of twist or from the voltage drop V_N over a known resistance R_N after compensation of the deflection of the system by sending the requisite current through the galvanometer.[17] According to which method was employed, the differential susceptibility was computed by means of one or the other of the following equations:

$$\Delta\chi = \frac{2K}{m \sin 2\theta} \cdot \frac{\Delta\alpha}{H^2}, \qquad (1)$$

where K is the elasticity constant of the filament, $\Delta\alpha$ is the angle of rotation of the suspended system due to the action of the field H, oriented at an angle θ

*Here and below θ is the angle between the field vector and the principal axis of the crystal Z.

to the principal axis of the crystal, on the crystal of mass m; or

$$\Delta\chi = \frac{2K}{mGR_N \sin 2\theta} \cdot \frac{V_N}{H^2}, \qquad (2)$$

where, in addition, G is the dynamic constant of the galvanometer.

The spherical zinc single crystals were grown by the method of Obreimov-Shubnikov from Hilger Spectroscopic metal. The quality of the crystals was checked by X-ray analysis. The orientation of the crystals was determined and their placement when attached to the suspension was checked with the aid of a Chapski goniometer especially modified for this purpose (see Ref. 18). The appropriately etched crystals were fixed in the crystal holder so that the reflecting facet ("signal"), normal to the principal axis, would also be normal to the axis of the screw raising and lowering the stand. After careful centering (to insure complete immobility of the "signal" when the stand was rotated), measurement of the angles between the normals to the reflecting planes parallel to the vertical graduated circle and setting one of the binary axes of the crystal along the axis of the vertical circle, a thin quartz rod was oriented parallel to the axis of the graduated circle and affixed to the crystal at the point of exit of a binary axis by means of a drop of Zapon cement. With the above procedure the error in the orientation of the axes of the crystal relative to the axis of the suspension does not exceed ±30'.

We used two methods in orienting the crystal relative to the suspension axis:

1) The binary axis Y passing through the centers of the side faces of the crystal was set parallel to the suspension axis; this was the first orientation (see Fig. 2 a). In this case the field vector, the principal axis Z and the binary axis X of the crystal were all in the horizontal plane and the quantity measured was $\Delta\chi = \chi_3 - \chi_1$.

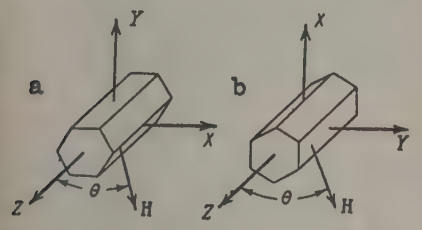

Fig.2.Orientation of crystal: Z - sixth order axis; X & Y - binary axes; a) first orientation, b) second orientation.

2) The binary axis X passing through the center points of the edges of the hexahedron was set parallel to the axis of the suspension; this was the second orientation (see Fig. 2 b). In this case the field vector, the principal axis Z and the binary axis Y were in the horizontal plane and the measured differential susceptibility was $\Delta\chi = \chi_3 - \chi_2$.

It may be mentioned that we investigated yet a third orientation of the crystal in which the principal axis Z is set parallel to the suspension axis and the field vector is in the basal plane. However, in view of the great difficulties in processing and, consequently, in interpreting the results of this series of measurements, we shall not discuss them in this report.

The magnetic field was produced by a large Weiss electromagnet which could be rotated by means of a motor about the cryogenic part of the apparatus, mounted on a stationary stand independent of the magnet. The fine orientation of the Z axis relative to the graduated circle of the magnet was determined from the variation of the turning couple C at room temperature. The error in the magnitude of the angle between the field vector and the principal axis of the crystal did not exceed ±30'.

3. Angular dependence of the couple acting on the crystal at a constant magnetic field intensity

Most of the investigators of the periodic field dependence of the susceptibility have confined themselves to a determination of only a few curves for $\Delta\chi(1/H)$, corresponding to a few values of θ, without bothering to study the angular dependence of the couple acting on the crystal with H = const.

We know from trustworthy experimental data[6] that an error in the orientation of the crystal leads to distortion of the $\Delta\chi(1/H)$ curves, distortion differing in character for different values of θ. In such cases, the investigator is compelled to disregard such "distorted" curves, which means that a considerable portion of his work loses value. Furthermore, we must bear in mind that even a weak mosaic structure of the crystal may result in "distortion" (diffusion or masking) of oscillations with a short period and small amplitude.[15]

All these "distortions" will necessarily be manifest in the curve of the angular dependence of the turning moment acting on the crystal in a constant field. Moreover, examination of such a curve allows of detecting the presence of ferromagnetic or strongly paramagnetic impurities often anisotropically distributed through the crystal. The above indicates the desirability of a preliminary investigation of the curve for $C(\theta)$ or $\Delta\chi(\theta)$ with H = const. for the purpose of preselecting the best specimens for the subsequent investigations; of course, in a number of cases the data so obtained may prove useful for the theoretical interpretation.[5, 19]

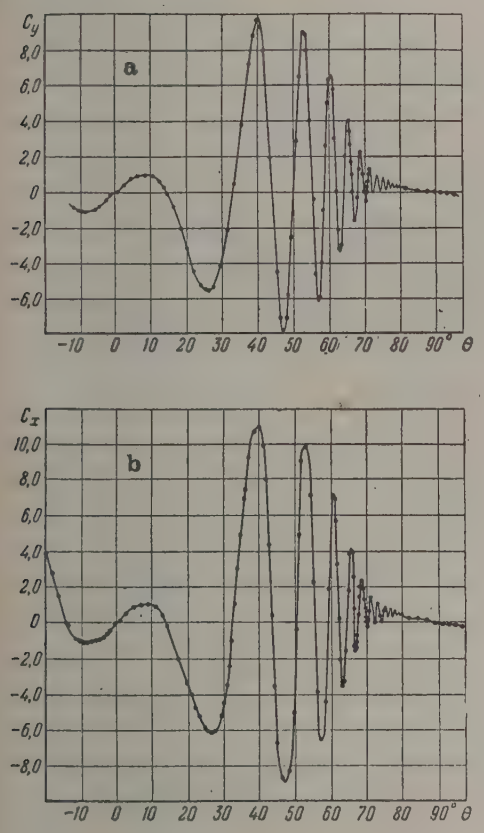

Fig.3. Variation of the couple acting on the zinc crystal with the angle θ between the field vector and the principal crystal axis: a) first orientation, b) second orientation of crystal.

The curve for $C_y(\theta)$ for one of the Zn crystals we studied, obtained in a constant field of 5600 oersteds, is shown in Fig. 3 a; the $C_x(\theta)$ curve for the same crystal in the same field is shown in Fig. 3 b.

The smooth character of the median line and the envelopes of the curves and the absence of any obvious "distortions" even at the minimal values of the period show that the mosaicity of the given crystal is negligibly small, that the error in orienting it was minimal and that it contains virtually no anisotropically distributed impurities. All the experimental data discussed below were obtained as a result of further investigations of this particular zinc single crystal.

The two curves are generally similar: at small angles, the period and amplitude of the angular oscillation are comparatively great and fall off rapidly as θ approaches 90°. The curves are distinguished only by a small difference in the magnitude of the periods and amplitudes at corresponding angles.

The character of the curves for $C(\theta)$ is evidence that in this case the Fermi surface is elongated along the principal Z axis of the crystal, while in the direction of X and Y axes its dimensions are considerably smaller and almost if not entirely equal. With reference to the theory based on the free electron gas model this means[5] that $m_3 \gg m_1$, $m_3 \gg m_2$ and $m_1 \neq m_2$ (m_1, m_2 and m_3 are the principal values of the effective mass tensor). The fact that $m_1 \neq m_2$ is even more convincingly confirmed by the presence of a noticeable magnetic anisotropy in the basal plane of the crystal at liquid helium temperature. The $C_z(\varphi)$ curve for this case, which we recorded, has the same character as the corresponding curve for zinc reproduced in our earlier report[20] (φ is the angle between the field vector, located on the basal plane, and one of the binary axes of the crystal).

4. Field dependence of the principal differential susceptibilities

First orientation of crystal (Fig. 2 a). We determined the variation of $\Delta\chi$ with $1/H$ with the crystal in the first orientation and T = 4.2°K for nineteen different values of θ. The resultant experimental data are presented graphically in Figs. 4 and 5.*

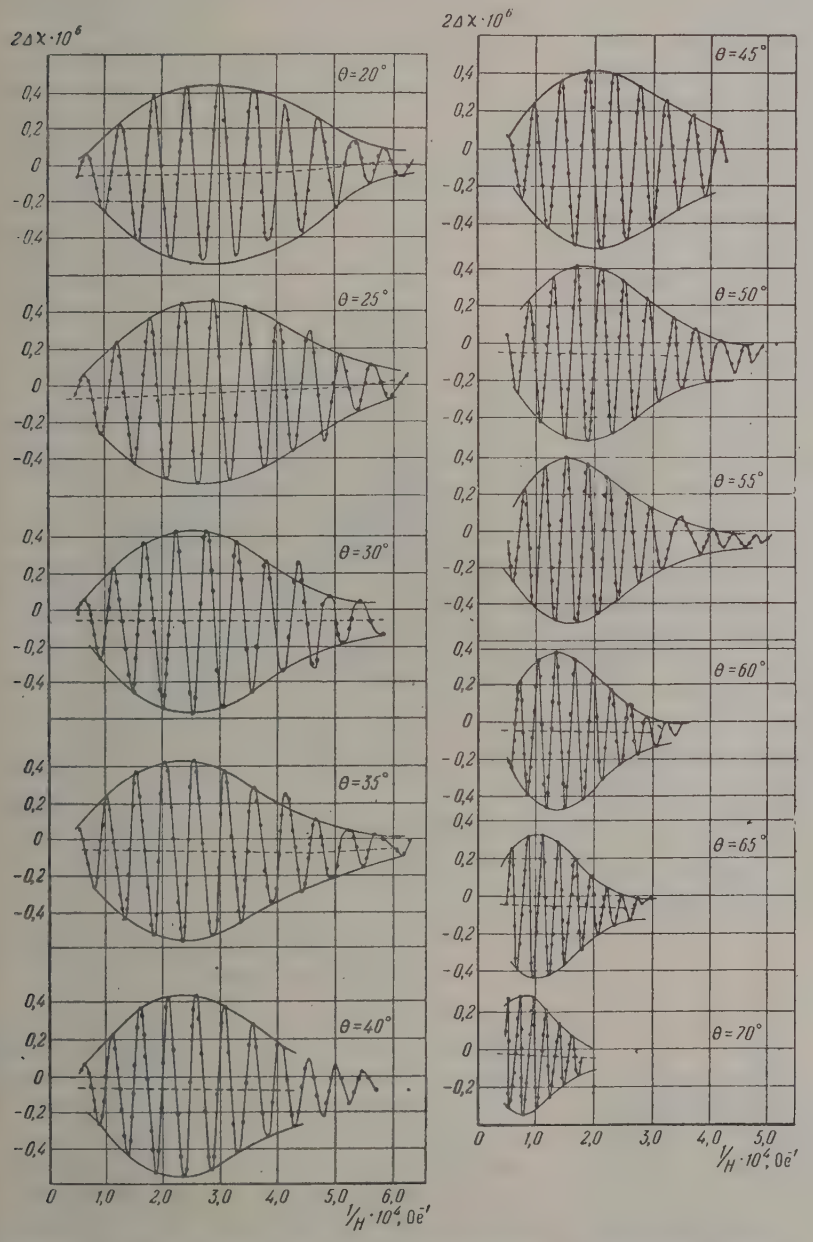

Fig.4. Variation of the differential magnetic susceptibility $(\chi_3-\chi_1)$ of the zinc crystal in the first orientation and with T = 4.2°K with the external field for θ = 20 to 70°.

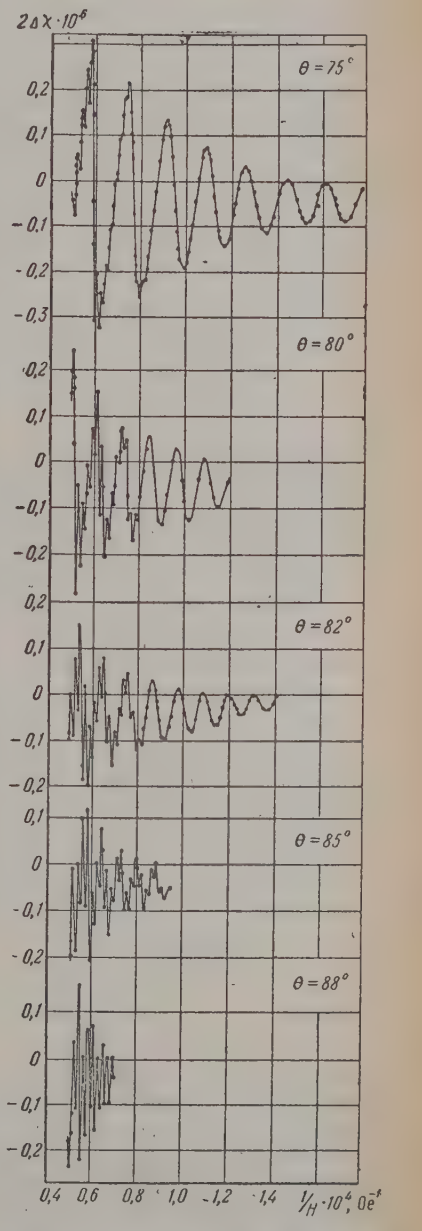

Fig. 5. Same as Fig. 4 but for θ = 75–88°.

*In addition to the angles shown in Figs. 4 and 5, measurements were also carried out at θ = 5, 10 and 15°.

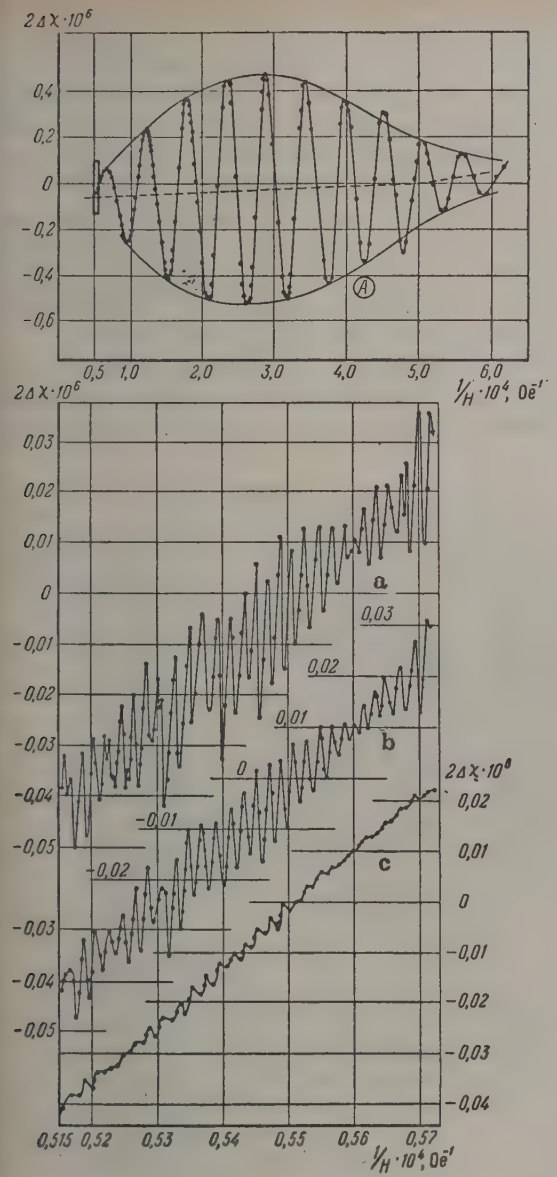

Fig.6 Variation of the differential susceptibility $(\chi_3 - \chi_1)$ **of the zinc crystal in the first orientation and** $\theta = 25^\circ$ **with the external field at different temperatures: A) 4.2°K; a) 1.45°K, b) 2.0°K, c) 4.2°K. Curve c represents an enlarged (both coordinates) plot of the section of A enclosed in the rectangle; curves a and b are for the same 1/H interval as c but lower temperatures.**

As will be shown below, for a number of reasons it is impossible to make a reasonably full comparison of the experimental data with theory at present and, hence, in this report we give all our reliable experimental data in full, so that when certain difficulties (which will also be indicated below) are obviated these data will be readily available for comparison with the theoretical formulae.

All the differential susceptibility curves are curves varying periodically about a more or less constant median value of $\Delta\chi$ that represents the difference $\chi_3 - \chi_1$ at small values of the field. The slight variation of the median line in weak fields is attributable to errors in measurement of the field intensity and the magnitude of the turning couple, errors which are proportionately greater in weak fields.

In the range of small angles ($\theta \leqslant 70^\circ$) the envelopes of all the $\Delta\chi$ vs 1/H curves have a maximum; the field H_{max} corresponding to the maximum of the envelope depends on the angle: as θ increases the maximum of the envelope is shifted to the side of stronger fields. From the shape and characteristics of the differential susceptibility curves (i.e., the fact that the envelopes have a maximum, that the period of oscillation is fairly constant, that the peaks and dips of the $\Delta\chi$ curves are smooth and occur at equal field value intervals) it follows that with $\theta \leqslant 70^\circ$ each curve in a wide range of fields can be described by an equation of the form

$$\Delta\chi = -A + B_1^1(T, \theta) H^{-3/2} e^{-B_2^1(T,\theta)\frac{1}{H}} \times \sin\left[\omega^1(\theta)\frac{1}{H} - \delta^1\right]. \qquad (3)$$

At angles over 70°, at first in strong fields and then, as θ increases in fields of lesser intensity, the so-called "fine structure" of the effect begins to come through: a higher frequency component begins to appear against the background of the fundamental frequency of the oscillation of $\Delta\chi$ (1/H). Whereas the "period" of the fundamental component noticeably falls off with increasing θ. The periods of the two high-frequency components are close at small angles (to θ = 30-35°) and markedly different when $\theta \to 90^\circ$.

The curves of Fig. 6 illustrated the complexity of the "fine structure" of the effect in Zn crystals. The small section at the beginning of curve A (recorded

for θ = 25°), identified by the rectangle, is shown to a greatly enlarged scale below at c. Examination of the curve c shows the presence of high-frequency components at low angles as well: two components in this case, for the pattern of beats is clearly apparent. Lowering the temperature (curves a and b in Fig. 6) leads to the appearance of an even greater number of high-frequency components, which, of course, tends to complicate analysis of the experimental curves.

The fine structure of the effect was investigated in detail at all the aforementioned values of θ and T = 4.2°K. Taking advantage of the fact that only two high-frequency components are present, the clearness of the beat pattern at small angles and the relatively short periods and low amplitudes of the high-frequency components, it proved possible to separate the three components.

It may be mentioned that the dependability and reproducibility of the results is assured by results of measurements on two other zinc single crystals, equally pure and free of "distortion" and repeat measurements on the same crystal after remounting it in the suspension according to the above described procedure.

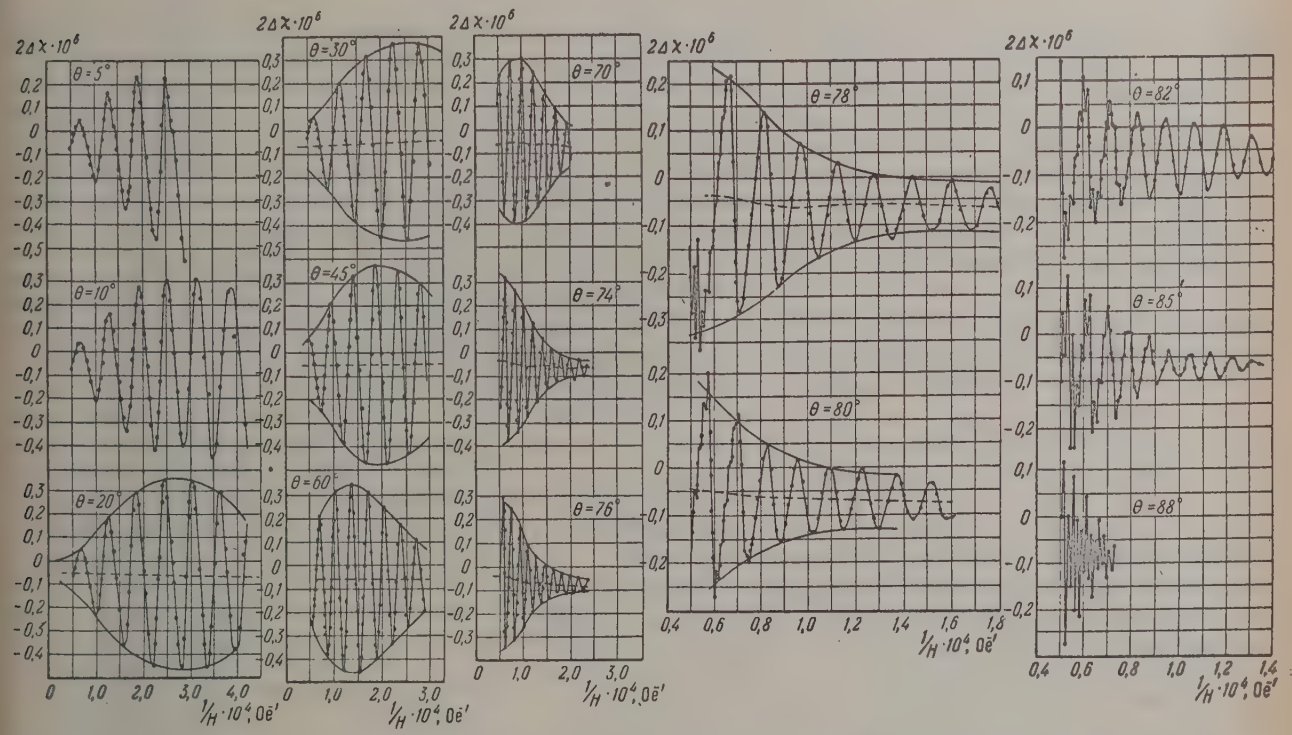

Fig. 7. Variation of differential susceptibility $(\chi_3 - \chi_2)$ of the zinc single crystal in the second orientation and with T = 4.2°K with the intensity of the external field for angles θ from 5 to 88°.

Second orientation of the crystal (Fig. 2 b). With the crystal in the second orientation we measured the variation of $\Delta\chi = \chi_3 - \chi_2$ with 1/H at 4.2°K for fourteen different values of the angle θ. The resultant experimental curves are shown in Fig. 7. The region of large angles was investigated in particular detail with the crystal in the second orientation.

The principal characteristics of the second orientation curves are similar to those of the first orientation curves, as described above. Moreover, the values of the parameters characterizing each pair of curves recorded for the same θ but different orientations are very close.

5. Angular dependence of the "period" of oscillation.

First orientation of the crystal. As we mentioned above, by virtue of the presence of only two high-frequency components and the fact that their periods and amplitudes are small compared with those of the fundamental component it is feasible to separate the three components and analyze the experimental curve as the sum of three curves:

$$\Delta\chi_{exp} = \Delta\chi^0 + \Delta\chi^{I} + \Delta\chi^{II}, \tag{4}$$

the first of which is described by equation (3) while the other two are characterized only by the periodic term in (3), with different values and possibly with a different angular dependence of the quantities B_1^0, B_1^I, B_1^{II}, B_2^0, B_2^I, B_2^{II} and ω^0, ω^I, ω^{II}.

Each of the components vanishes on condition that

$$\omega^i(\theta)\frac{1}{H} - \delta^i = n^i\pi, \tag{5}$$

where $n = 0, 1, 2, \ldots$, and $i = 0, I, II$.

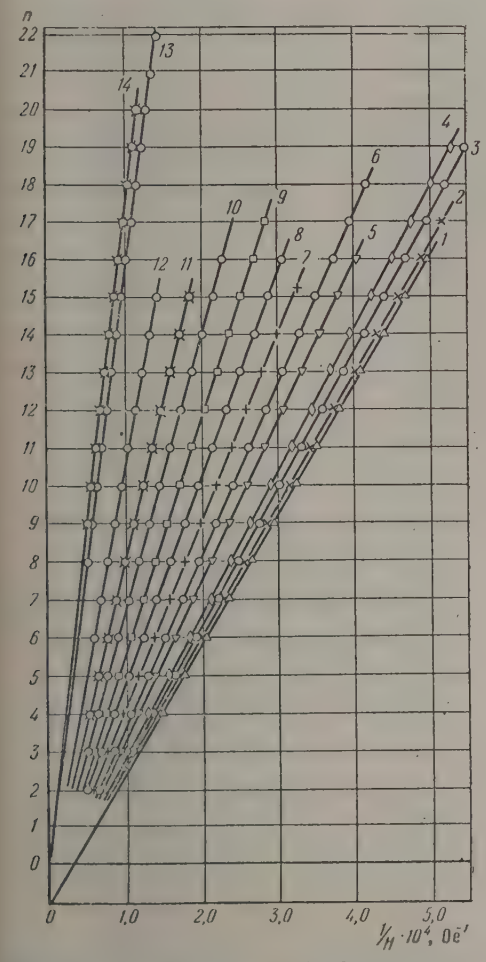

Fig. 8. Curves of $n(1/H)$ for the first orientation and different angles θ: 1) 15°, 2) 20°, 3) 25°, 4) 30°, 5) 40°, 6) 45°, 7) 50° 8) 55°, 9) 60°, 10) 65°, 11) 70°, 12) 75°, 13) 80°, 14) 82°.

If we plot a curve of $n = n(1/H)$ for θ = const, we should obtain a straight line whose angular coefficient will equal $\frac{\omega^i(\theta)}{\pi} = \frac{2}{\Delta(1/H)}$ (here $\Delta(1/H$ is the period of oscillation of the differential susceptibility at the selected θ) while the free term will equal δ^i/π.. In plotting the $n(1/H)$ curve it is essential to be guided by the following:

a) There must exist a region of super-strong fields within which $\Delta\chi$ no longer varies periodically with the field intensity[24], i.e. $n = 0$ when $1/H > 0$.

b) With $\delta > \pi$ one must take into account the change in the sign of $\sin\left[\omega^i(\theta)\frac{1}{H} - \delta^i\right]$ in equation (3).

The curves of $n(1/H)$ for the fundamental component of $\Delta\chi_{exp}(1/H)$ with the crystal in the first orientation and different values of θ are shown in Fig. 8. As may be seen the points actually do fall on straight lines. At small angles (lines 1-4), the experimental points in weak fields lie on the appropriate straight lines, while in strong fields they fall above the extension of the line, i.e., the period increases. On the other hand, at angles close to π/2 (lines 13 & 14), in strong fields the experimental points fall below the extension of the lines, i.e., the period of oscillation is reduced. These deviations in the dependence of n on 1/H from linearity, which are connected with the weak dependence of ω on H in strong fields, are more clearly evinced in Fig. 9, in which the pertinent portions of Fig. 8 are drawn to a larger scale.

In the first approximations (neglecting these deviations for the moment) we can safely draw a straight line through most of the experi-

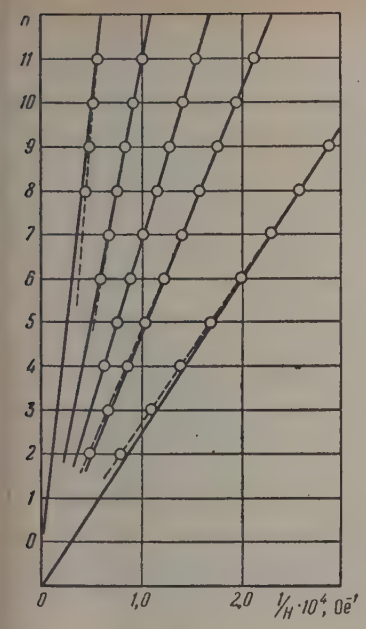

Fig. 9. Deviation of the curves for $n(1/H)$ from linearity in strong magnetic fields.

mental points corresponding to weak through moderate fields, i.e., not too small values of n. The angular coefficient of each such straight line will give the period of oscillation of $\Delta\chi$ at the given angle θ.

It should be noted that the initial phase of δ^i, determinable by extrapolation of the straight lines into the region of infinitely strong fields ($1/H \to 0$), depends on θ and in the interval $0 < \theta < \pi/2$ varies within the limits $0 \leqslant |\delta| \leqslant \pi$.

The curves of Fig. 10 show the angular dependence of the periods of the three components of $\Delta\chi_{exp}$ for the first orientation of the zinc crystal. Curve 1 characterizes the angular dependence of the fundamental component period, Curves 2 & 3, the angular dependence of the periods of the high-frequency components, comprising the "fine structure" of the effect. Even a casual glance shows the markedly different character of the angular dependences of the periods of the three components, particularly of the fundamental component as compared with that of the high-frequency one represented by Curve 2. In addition, we note the presence of a small but clearly pronounced periodicity in the variation of $\Delta\chi(1/H)$ with θ in the angular interval approaching $\pi/2$* (actually starting from $\theta \simeq 60°$).

Second orientation of the crystal. All the experimental curves for the variation of $\Delta\chi_{exp}$ with $(1/H)$ plotted as a result of investigations of the second orientation of the crystal at T = 4.2°K can also be viewed as comprised of the sum of three curves - see equation (4). Proceeding as before, i.e., separating the individual components and plotting curves of n^i vs 1/H for different values of θ, we can readily determine the period of oscillation of the differential susceptibility $\Delta\chi^i$ at the various given angles.

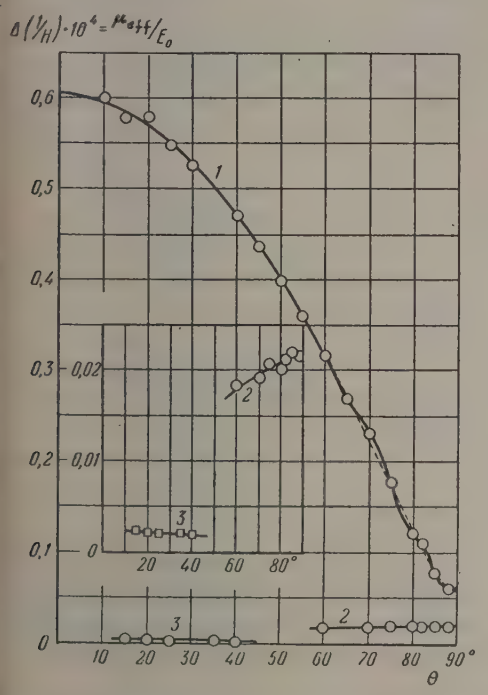

Fig. 10. Variation of the period of oscillation of the differential susceptibility ($\chi_3 - \chi_1$) of the zinc crystal in the first orientation and with T = 2.4°K with θ: 1) fundamental (low-frequency) component, 2 & 3) high-frequency components.

The curves of Fig. 11 show the angular dependence of the periods of the three components of $\Delta\chi_{exp}(1/H)$ with the crystal in the second orientation. Curve 1 characterizes the dependence of the period of the fundamental component; Curves 2 & 3, the angular dependence of the periods of the components comprising the fine structure of the effect. As in the case of the first orientation, the angular dependences of the three components differ markedly, the difference between those characterized by Curves 1 and 2 being the most pronounced. A weak periodicity of the angular dependence of the period is apparent in the region of large angles ($60° \to 90°$).

In general the curves of Figs. 10 & 11 are largely similar; the differences between the corresponding curves are mainly quantitative.

*At small angles, where $\theta \to 0$, the absolute error in determining the period becomes large due to the smallness of the couple acting on the crystal.

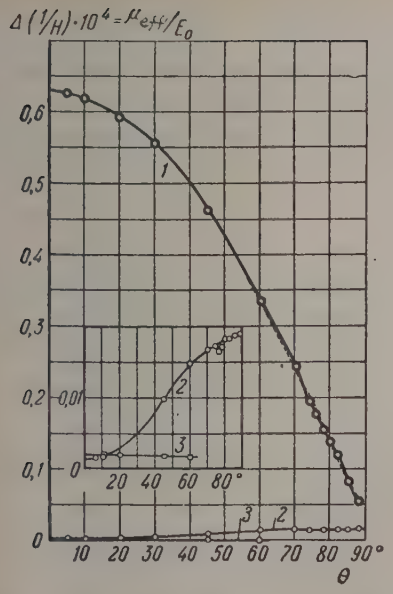

Fig. 11. Same as Fig.10 but for the second orientation of the crystal.

Thus, the period of the fundamental component with $0 \rightarrow 0^\circ$ is greater for the second orientation than for the first, while with $\theta \rightarrow 90^\circ$, on the contrary, the period for the first orientation is greater.

6. Angular dependence of the amplitude of the differential susceptibility curves in a constant field

The theory of the effect, based on the free electron model, predicts a definite angular dependence not only of the period but also of the amplitude of the $\Delta\chi(1/H)$ curves.

First orientation. The curves of Fig. 12 show the angular dependence of the amplitude of oscillation of the fundamental component in four different constant fields. In the weakest field (Curve 1) the amplitude changes little with the angle in the range from 0 to 30° and then falls off rapidly as θ is further increased. In stronger fields the character of the angular dependence becomes more complicated; maxima and minima appear in the curves. The location of the maximum is field dependent: as the field increases the maximum is reduced in height and shifted to the side of larger angles.

Second orientation. The angular dependence of the amplitude of oscillation of the fundamental component with the crystal in the second orientation is shown for the same four values of the external field in Fig. 13. In this case even the curve for the weakest investigated field exhibits a maximum; as in the former case the maxima are displaced in the direction of larger angles with increasing field intensity. In contrast to the first orientation curves, those for the second orientation do not have minima.

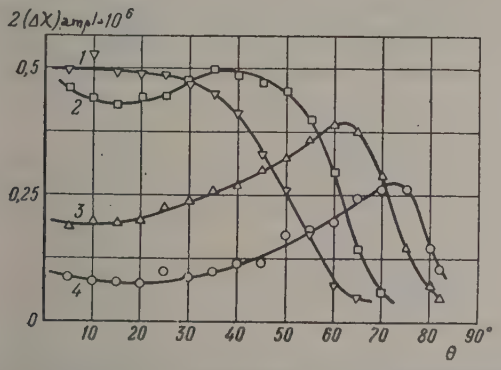

Fig. 12. Angular dependence of the differential susceptibility of the crystal in first orientation (T = 4.2°).

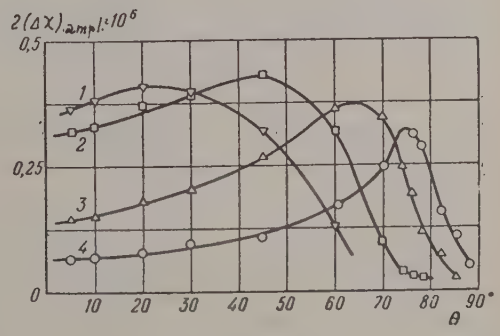

Fig. 13. Same as Fig. 12 but for the crystal in the second orientation.

Fields (both figures): 1) 3300, 2) 5000, 3) 10,000 and 4) 20,000 oersteds.

Analogous curves for the high-frequency components do not have maxima or minima: thus the amplitude of the component whose period is represented by Curves 2 in Figs. 10 and 11, increases smoothly with the angle in constant fields.

7. Discussion of results

Investigation of the magnetic properties of Zn single crystals in the basal

plane shows that the couple $C_z(\varphi)$ has a period equal to $\pi/3$.[20] It is customary to explain this experimental fact by assuming that the constant energy surface consists not of one but of three triaxial ellipsoids which fully coincide with each other when rotated through $2\pi/3$ in the basal plane.[5] On this assumption the theory of the effect based on the free electron model and suitably modified for the anisotropic case correctly describes the symmetry of C_z relative to the binary axes and, provided that

$$\frac{kT}{E_0} \ll 1, \quad \frac{\mu_{\text{eff}} H}{E_0} \ll 1, \quad \frac{2\pi^2 kT}{\mu_{\text{eff}} H} \gg 1 \tag{6}$$

leads to the following basic relationships for the two orientations of the crystal investigated in the present experimental study:
for $\varphi = 0$ (first orientation):

$$C_y = (\chi_3 - \chi_1) H^2 \sin\theta\cos\theta = \gamma H^2 \sin\theta\cos\theta \left\{(m_3 - m_1)\,\psi\,[\alpha H \beta(\theta, 0)] + \frac{4m_3 - m_1 - 3m_2}{2}\,\psi\left[\alpha H \beta\left(0, \frac{\pi}{3}\right)\right]\right\} \tag{7}$$

and for $\varphi = \pi/2$ (second orientation):

$$C_x = -(\chi_3 - \chi_2) H^2 \sin\theta\cos\theta = -\gamma H^2 \sin\theta\cos\theta \left\{(m_3 - m_2)\psi\left[\alpha H \beta\left(\theta, \frac{\pi}{2}\right)\right] + \frac{4m_3 - 3m_1 - m_2}{2}\,\psi\left[\alpha H \beta\left(0, \frac{\pi}{6}\right)\right]\right\}. \tag{8}$$

Here

$$\psi[\alpha, H, \beta] = \beta^{-3/2} \exp\left\{-\frac{2\pi^2 kT}{\mu H}\right\} \frac{4\pi kT}{E_0 (\alpha H)^{3/2}} \sin\left(\frac{2\pi E_0}{\mu H} - \frac{\pi}{4}\right) \cos\left(\frac{\pi \sqrt{m_1 m_2 m_3}}{m_0 \beta}\right), \tag{9}$$

$$\alpha = \frac{e\hbar}{cE_0\sqrt{m_1 m_2 m_3}}, \quad \gamma = \frac{e^2}{2\pi^2 \hbar c^2} \sqrt{\frac{E_0}{m_1 m_2 m_3}}, \quad \mu = E_0 \alpha\beta; \tag{10}$$

$$\beta(\theta, \varphi) = \sqrt{m_1 \sin^2\theta\cos^2\varphi + m_2 \sin^2\theta\sin^2\varphi + m_3 \cos^2\theta}. \tag{11}$$

It must be noted that in most comparisons of theory with experiment[6, 11] only one term, assumed to be a function of the largest β is left in the expression of C_x or C_y. This is somewhat arbitrary and, for the general case, wrong since for strongly anisotropic masses, when $m_3 \gg m_1$, $m_3 \gg m_2$ and $m_2 \neq m_1$ (Zn),

$$\frac{\beta(\theta, 0)}{\beta\left(\theta, \frac{\pi}{2}\right)} = \frac{\sqrt{m_1 \sin^2\theta + m_3 \cos^2\theta}}{\sqrt{(1/4 m_1 + 3/4 m_2)\sin^2\theta + m_3 \cos^2\theta}}$$

and

$$\frac{\beta\left(\theta, \frac{\pi}{2}\right)}{\beta\left(\theta, \frac{\pi}{6}\right)} = \frac{\sqrt{m_2 \sin^2\theta + m_3 \cos^2\theta}}{\sqrt{(1/4 m_2 + 3/4 m_1)\sin^2\theta + m_3 \cos^2\theta}}$$

are of the order of unity, at least at small values of θ; in the same region of small angles, when the periods are close, the amplitudes of the two additive terms in the expressions of C_x and C_y differ by a factor of about 2. The situation is further complicated by the fact that ratios of the periods and amplitudes of the two terms when $\theta \to \pi/2$ are not known, which, of course, hampers comparison of the experimental data with theory.

The ratios of the periods and amplitudes of the two terms in (7) and (8) when $\theta \to \pi/2$ are determined by the ratio of the effective masses m_1 and m_2 and extent to which $\frac{2\pi^2 kT}{\mu_{\text{eff}} H} > 1$. If $\frac{2\pi^2 kT}{\mu_{\text{eff}} H} \gg 1$, then the character of the angular dependence of each of the terms is determined by the exponential factor: the amplitude decreases monotonously with increasing θ (if $m_3 \gg m_1$ and $m_3 \gg m_2$).

When $m_2 \gg m_1$, the amplitude of the second term in the expression for C_y for

the first orientation of the crystal remains larger than that of the first term for all values of θ (to $\pi/2$); the first term will be the smaller, the larger m_2 compared to m_1, and, for a given ratio m_2/m_1, the greater $\frac{2\pi^2 kT}{\mu_{eff} H}$ is compared with unity. At the same time (i.e., when $m_2 \geqslant m_1$) the amplitudes of both terms in the expression for C_x for the second orientation of the crystal become equal at some value of θ, while at values of $\theta \to \pi/2$ the amplitude of the first term becomes greater than that of the second, the difference being greater, the greater m_2/m_1 and $\frac{2\pi^2 kT}{\mu_{eff} H}$.

If $m_2 \leqslant m_1$, then, on the contrary, for the second orientation of the crystal the amplitude of the second term in the expression for C_x remains larger than that of the first term for all values of θ (to $\pi/2$), while the amplitudes of the two terms in the expression for C_y for the first orientation of the crystal are equalized at some value of θ and when $\theta \to \pi/2$ the amplitude of the first term becomes greater than that of the second.

If $m_2/m_1 \neq 1$, but differs little from 1 (slightly larger or slightly smaller), the second terms in the expressions for C_x and C_y become the dominant ones at all values of θ for both orientations of the crystal. The range of values of $m_2/m_1 \neq 1$ satisfying this condition will be the greater, the smaller the inequality $\frac{2\pi^2 kT}{\mu H} > 1$.

Hence knowing that each component of the experimental curve of $\Delta\chi(1/H)$ (including the fundamental one) is the result of the addition of two components of type (7) or (8) with close periods but different amplitudes, we can assume that the total curve has the same apparent frequency as the component having the greater amplitude at the given value of θ. Then making use of the data of Figs. 10 and 11 for values of $\theta \to 0$ and $\theta \to \pi/2$ and assuming that $\frac{2\pi^2 kT}{\mu H} > 1$ at all values of the angle θ, we can say that the following equalities obtain for the fundamental component of $\Delta\chi(1/H)$:

$$\frac{\Delta(1/H)_{\theta\to 0}}{\Delta(1/H)_{\theta\to \pi/2}} = 9{,}8 = \begin{cases} 2\sqrt{\frac{m_3}{m_1}} \cdot \frac{1}{\sqrt{1+3\frac{m_2}{m_1}}}, & \text{when } m_2 \geqslant m_1 \\ \sqrt{\frac{m_3}{m_1}}, & \text{when } m_2 \leqslant m_1 \end{cases} \quad \text{first orientation of the crystal}$$

$$\frac{\Delta(1/H)_{\theta\to 0}}{\Delta(1/H)_{\theta\to \pi/2}} = 11{,}8 = \begin{cases} \sqrt{\frac{m_3}{m_2}}, & \text{when } m_2 \geqslant m_1 \\ 2\sqrt{\frac{m_3}{m_2}} \cdot \frac{1}{\sqrt{1+3\frac{m_1}{m_2}}}, & \text{when } m_2 \leqslant m_1 \end{cases} \quad \text{second orientation of the crystal}$$

$$\frac{\Delta(1/H)^{I}_{\theta\to \pi/2}}{\Delta(1/H)^{II}_{\theta\to \pi/2}} = 1{,}1 = \frac{\sqrt{m_1+3m_2}}{\sqrt{m_2+3m_1}}, \quad \text{when } \frac{m_2}{m_1} \neq 1, \text{ (small inequality)}$$

Assuming one or the other of the alternative relationships between m_1 and m_2, we can readily compute the ratio of the masses by means of the first two equations. However, such calculations lead either to a result contrary to the initial assumption regarding the ratio of the masses or to a negative value for one of the ratios. The last of the three equations leads to $m_2/m_1 \approx 1{,}4$.

It must be concluded from the above that although each of the Curves 1 of Figs. 10 and 11 considered separately can be satisfactorily described by a function of the form

$$\mu/E_0 = \frac{e\hbar\sqrt{M\sin^2\theta + m_3\cos^2\theta}}{c\sqrt{m_1 m_2 m_3 E_0}}$$

(where M equals m_1 or $^1/_4 m_1 + {}^3/_4 m_2$ for the first orientation or m_2 or $^1/_4 m_2 + {}^3/_4 m_1$ for the second orientation) in a wide range of values of θ (up to 45–50°), the

curves considered in conjunction can be described by equations (7) and (8) only in the region of large angles ($\theta \to \pi/2$).

This deduction is even more convincingly confirmed by the character of the angular dependence of the amplitude of oscillation (Figs. 12 & 13). The function $\psi[\alpha, H, \beta]$ depends on θ, attaining a maximum at a value of θ satisfying the following condition

$$\frac{2\pi^2 kT}{\mu H} = \frac{3}{2}.$$

When $m_3 \gg m_1$ and $m_3 \gg m_2$ (which is the case for Zn single crystals), the derivative of the curve of the angular dependence of the amplitude of each term in the expressions for C_x and C_y is negative when $\frac{2\pi^2 kT}{\mu H} > 1$ The positions of the maxima in the curves of Figs. 12 and 13 determine the limit of the applicability of equations (7) and (8) to the cited experimental data. Inasmuch as $m_2/m_1 \neq 1$, but differs little from unity, we can assume that the portions of these curves corresponding to large values of θ (i.e., to the right of the maxima, where the derivative is negative) are also determined to some extent by the second terms in the expressions for C_x and C_y.

A usual step in the comparison of the experimental curves for $\Delta\chi(1/H)$ with θ = const. is comparison of the shape of their envelopes with the shape predicted by theory. According to theory, if $\Delta\chi(1/H)$ is described by one of the terms of (7) or (8),

$$\ln(\Delta\chi)_{ampl} + \frac{3}{2}\ln H = \text{const} - \frac{2\pi^2 kT}{\mu}\cdot\frac{1}{H}. \qquad (12)$$

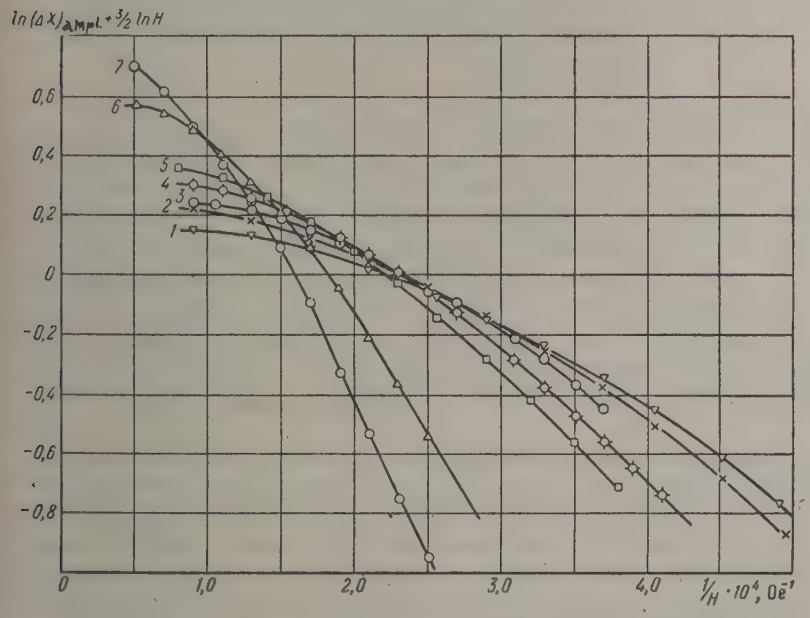

Fig. 14. Variation of $\ln(\Delta\chi)_{ampl} + \frac{3}{2}\ln H$ on 1/H with the first orientation of the crystal and T = 4.2°K for the following values of θ: 1) 15°, 2) 25°, 3) 30°, 4) 40°, 5) 45°, 6) 60° and 7) 65°.

The curves of Fig. 14 show the dependence of the experimental values of $\ln(\Delta\chi)_{ampl} + \frac{3}{2}\ln H$ on 1/H for a number of angles; 1-3 have no straight-line portions; in the case of large angles the curves deviate from linearity in the region of strong fields. It is important to note that this deviation from linearity indicates the presence of a maximum and sections of the angular dependence of the amplitude curves with a positive derivative, where $\frac{2\pi^2 kT}{\mu H} < 1$.

We note that the curves of Fig. 14 can be satisfactorily described by an equation of the type shown below

$$\ln(\Delta\chi)_{ampl} + \frac{3}{2}\ln H = \text{const} - a\frac{1}{H} - bH + cH^2. \qquad (13)$$

Thus the presence of maxima in the curves for the angular dependence of the amplitudes, which are similar in character for the first and second orientations of the crystal, the non-linearity of the variation of $\ln(\Delta\chi)_{ампл} + \frac{3}{2}\ln H$ with 1/H

at small angles θ and the closeness of the values of m_1 and m_2, deduced directly from the experimental data and confirmed by analysis of the curves of the angular dependence of the period of oscillation of the fundamental period of the magnetic susceptibility, taken all together permit us to assert that in the region of large angles ($0 \to \pi/2$) the experimental results are described by equations (7) and (8) in which the principal dominant factor (factor with the larger amplitude) is the second term. In the region of small angles ($\theta \to 0$), the inequality $\frac{2\pi^2 kT}{\mu H} > 1$ does not hold and instead of (7) and (8) it is, apparently, necessary to use the general equation for the magnetic moment of a unit volume:

$$M = \frac{\mu}{2\pi^2}\left(\frac{\sqrt{mE_0}}{\hbar}\right)^3 \left\{ \frac{\sqrt{2}}{6}\left[-1 + 3\left(\frac{m}{m_0}\right)^2\right]\frac{\mu H}{E_0} - \frac{2\pi^2 kT}{\sqrt{\mu H E_0}} \sum_{p=}^{\infty} (-1)^p \frac{\sin\left(\frac{2\pi pE_0}{\mu H} - \frac{\pi}{4}\right)\cos\left(p\pi\frac{m}{m_0}\right)}{\sqrt{p}\,\mathrm{sh}\left(\frac{2\pi^2 pkT}{\mu H}\right)} \right\}, \qquad (14)$$

Nothing can be said at present regarding the form of this equation for the anisotropic case and the feasibility of comparing it with experimental data.

Where planning further experimental studies is concerned, the above conclusions indicate 1) the necessity of detailed investigation of each component of the experimental dependence of $\Delta\chi$ on $1/H$ in appropriate weak fields so that $\frac{2\pi^2 kT}{\mu H}$ would be greater than unity for all orientations of the crystal and the experimental data can be compared with the simplest theoretical expressions of the type of (7) and (8) and 2) the need for attempting to find such theoretical parameters as would permit of describing the angular dependence of the periods and amplitudes at all possible values of θ and φ.

In the theory based on the assumption of an arbitrary dispersion law for the quasi-particles that are responsible for the de Haas-van Alphen effect:[15]

$$\Delta\left(\frac{1}{H}\right) = \frac{eh}{c}\cdot\frac{1}{S_m(\xi)}, \qquad (15)$$

where $S_m(\xi)$ is the maximum area of the Fermi energy surface in a plane normal to the field vector. Thus, the curves of Figs. 10 and 11 represent the angular dependence of this maximal cross section for the two orientations of the crystal. The different nature of the angular dependences characterized by the respective curves of the two figures may be taken as evidence in favor of the hypothesis that the different components of the $\Delta\chi(1/H)$ curves for zinc correspond to different electron groups, or, more accurately speaking, to different unfilled energy zones in the metal, in each of which the motion of the electrons is independent of their motions in the other zones. Each such group of electrons is characterized by its own value of $S_m(\xi)$, the angular dependence of which is determined by the curves of Figs. 10 and 11.

To solve the problem of reproducing the shape of the Fermi surface on the basis of the experimental data obtained in the present investigation one must first resolve the question of the structure of this surface for each of the electron groups. In other words, we must first ascertain whether we can speak of a single Fermi surface of complicated shape, capable of assuring the observed periodicity of $C_z(\varphi)$ or must hold to the concept of the presence, for each electron group, of three Fermi surfaces, coinciding when rotated through $\pi/3$ in the basal plane. In the latter case the theoretical equations are inconvenient for comparison with experiment even when

$$\lambda = \frac{\pi c\, kT}{|e|\hbar H}\left(\frac{\partial S_m}{\partial E}\right)_\zeta \gg 1. \qquad (16)$$

Among the difficulties in the way of solving the problem of the reproducibility of the Fermi surface are the lack of a suitable procedure for separating the indivi-

dual "fine structure" components in a wide range of fields*, the difficulty of comparing the experimental data for each component with theory when $\lambda \gg 1$ but the orientation of the crystal is arbitrary, so that the number of terms in the expressions for the magnetic moment is greater than two (as a result of the complexity of the structure of the surface; actually, too, there are probably three surfaces rather than one), the impossibility of utilizing the experimental data corresponding to strong fields (small quantum numbers) for each component, when $\lambda \backsim 1$ and, possibly, $\zeta/\mu H \sim 1$ as well.

The fact that it is feasible to describe the observed results for the zinc crystal in two orientations for large values of θ (where $\lambda \gg 1$) by means of the equation derived from the theory based on the free electron model gives reason to assume that the Fermi surface is nearly ellipsoidal, although the dispersion law may differ somewhat from the quadratic.

Lastly, we must mention that to determine the theoretical (free electron model) parameters we made use of the experimental results obtained at large values of θ. The following values were obtained:

a) for the fundamental component of the effect (group with the fewest of electrons) —

$$m_1 \approx 0{,}016\, m_0, \quad m_2 \approx 0{,}023\, m_0, \quad m_3 \approx 2{,}5\, m_0, \quad E_0 \approx 0{,}01\ \text{eV}, \quad n \approx 6 \cdot 10^{-6};$$

b) for one of the components of the fine structure of the effect — curves 2 in Figs. 10 & 11 $\left(\frac{2\pi^2 kT}{\mu H} > 1 \text{ at all values of } \theta\right)$ —

$$m_1 \approx 1{,}7\, m_0, \quad m_2 \approx 0{,}42\, m_0, \quad m_3 \approx 0{,}011\, m_0, \quad E_0 \approx 0{,}045\ \text{eV}, \quad n \approx 2 \cdot 10^{-4}.$$

As G.E.Zil'berman pointed out the periodicity of the curves of $\Delta\left(\frac{1}{H}\right) = \frac{\mu}{E_0}(\theta)$ in the region of large values of θ can be explained by taking into account the dependence of E_0 on H.[22] Then

$$\frac{\mu}{E_0} = \frac{\mu}{E_{00}}\left[1 - \sqrt{2\pi^3}\frac{kT}{\sqrt{E_{00}\mu H}} \exp\left\{-\frac{2\pi^2 kT}{\mu H}\right\} \cos\left(\frac{2\pi E_{00}}{\mu H} - \frac{\pi}{4}\right)\right], \qquad (17)$$

so that the amplitude of the periodic term when $\frac{E_{00}}{\mu H} \sim 3 \div 4$ and $\frac{kT}{\mu H} \sim \frac{1}{\pi^2}$, for example, amounts to several percent of the magnitude of the first term.

8. Conclusions

Investigating the field dependence of the differential magnetic susceptibility of zinc single crystals for two orientations of the crystal in the field, we observed the presence of "fine" and "hyperfine" structure of the effect and obtained curves of the angular dependence of the periods and amplitudes of three components of the effect. The different character of the angular dependence of the periods $\left(\frac{\mu}{E_0} \text{ or } \frac{eh}{c}\cdot\frac{1}{S_{m(\xi)}}\right)$ of the three components is essentially the first experimental evidence in favor of the existence of different groups of electrons, each of which is partially responsible for the de Haas-van Alphen effect. We ascertained that in the region of large angles between the field vector and the principal axis of the crystal the value of $\frac{\mu}{E_0}\left(\text{or } \frac{eh}{c}\cdot\frac{1}{S_{m(\xi)}}\right)$ varies periodically with the angle and detected the presence of peaks in the curves for the variation of the amplitudes with θ with H = const, peaks which are shifted to the side of larger angles as the field intensity is increased. These maxima in the angular dependence of the amplitudes correspond to the deviation from linearity of the variation of $\ln(\Delta\chi)_{ampl} + \frac{3}{2}\ln H$ with 1/H.

We also observed a deviation from linearity of $n(1/H)$ in the region of small

*The need for such a procedure is particularly great in analyzing and interpreting the results of experimental studies of weakly anisotropic metals.

values of n (strong fields).

We compared our results with the theory of the effect based on the free electron model; they are in satisfactory agreement in the region of large angles (for the fundamental component, i.e., for the electron group with the smallest number of electrons).

The experimental results can be utilized for the problem of reproducing the shape of the Fermi limiting-energy surface after a number of difficulties (enumerated in the report) have been overcome.

In further experimental studies and to permit dependable comparison of the resultant experimental data with theory it is essential to investigate the angular dependence of the periods and amplitudes of each component in appropriately weak fields.

In conclusion we wish to express our gratitude to B.G.Lazarev for his interest in the investigation, I.M.Lifshits and G.E.Zil'berman for valuable discussions and E.K.Pogrebniak for his help in processing the experimental data.

Physico-Technical Institute of the
Academy of Sciences of the USSR

References

1. L.Schubnikov & W. de Haas, Leid. Comm., No.207 d & No.210 a (1930).
2. W. de Haas & P. van Alphen, Leid. Comm., No.212 a & No. 220 d (1932).
3. L.Landau, ZS. f. Phys., 64, 629 (1930); communication concerning D.Shoenberg's article, Proc. Roy. Soc.,A170, 341 (1939).
4. A.Akhiezer, Doklady AN SSSR, 23, 872 (1930).
5. G.Zil'berman, Zhur. eksp. i teor. fiz., 21, 1209 (1951).
6. D.Shoenberg, Zhur. eksp. i teor. fiz., 8, 1271 (1938).
7. B.Davydov & I.Pomeranchuk, Zhur. eksp. i teor. fiz., 9, 1294 (1939).
8. E.Borovik, Zhur. eksp. i teor. fiz., 23, 91 (1952).
9. J.Marcus, Phys. Rev., 71, 559 (1947).
10. B.Verkin, Lazarev & Rudenko, Zhur.eksp. i teor. fiz., 20, 995 (1950); 21, 658 (1951); Doklady AN SSSR, 80, 45 (1951).
11. D.Shoenberg, Phil. Trans. of the Roy. Soc., A245, 1 (1952).
12. D.Shoenberg, Physica, 19, 791 (1953).
13. T.Berlincourt, Phys. Rev., 92, 1068 (1953).
14. B.Verkin, Dmitrenko & Mikhailov, Doklady AN SSSR, 101, 34 (1955).
15. I.Lifshits & A.Kosevich, Doklady AN SSSR, 96, 963 (1954).
16. I.Lifshits & A.Pogorelov, Doklady AN SSSR, 96, 1143 (1954).
17. B.Verkin & I.Mikhailov, Zhur. eksp. i teor. fiz., 25, 471 (1953).
18. E.E.Flint, Geometric crystallography handbook ("Prakticheskoe rukovodstvo po geometricheskoi kristallografii"), M. 1948.
19. S.Sidoriak & D.Robinson, Phys. Rev., 75, 118 (1949).
20. B.Verkin, B.Lazarev & N.Rudenko, Doklady AN SSSR, 73, 59 (1950).
21. Iu.Rumer, Zhur. eksp. i teor. fiz., 18, 1081 (1948).
22. G.Zil'berman, Zhur. eksp. i teor.fiz., 25, 713 (1953).

GALVANOMAGNETIC EFFECTS AND THE PROPERTIES OF CONDUCTION ELECTRONS IN METALS

- E.S.Borovik

Introduction

Subsequent to the original work of P.L.Kapitsa,[1] who investigated the change of the resistance of most metals in fields to $3 \cdot 10^5$ oersteds at temperatures down to the boiling point of liquid nitrogen, it was discovered that the effect is greatly intensified with further reduction of temperature provided sufficiently pure metals are used.[2-4] At temperatures of 2-4°K and fields of about 10^4 oersteds the resistance of many pure metals increases hundreds and thousands of times, while for bismuth the factor is in the millions. The great increase is explained by a 10^3-10^4-fold increase in the length of the free path of the electrons in pure metals at these temperatures. Inasmuch as the influence of the magnetic field is determined by the magnitude of the perturbation in the motion of the electrons produced by it, the increase in the length of the free path may be regarded as equivalent to a corresponding increase in the effective strength of the magnetic field. This point of view is supported by the curve obtained if, as suggested by Kohler,[5] we plot the relative increase in resistance against the product of the magnetic field intensity by the conductivity (rather than simply the field intensity); in these coordinates experimental data obtained at different temperatures all nearly fit a common single curve.

Thus investigations of galvanomagnetic effects at low temperatures should be regarded primarily as measurements in large effective fields and the specific influence of low temperatures recognized and analyzed as a secondary factor. This specific influence of low temperatures is manifested, for example, in the superposition of a certain periodic field dependence of the resistance on the principal smooth curve characterizing the increase in resistance with field intensity. This particular periodic effect was discovered in bismuth by Schubnikov and de Haas,[2] and subsequently observed by Lazarev, Nakhimovich and Parfenova in zinc[3] and the author in tin.[6]

The available extensive experimental data on the resistance behavior of metals at low temperatures permitted Justi[4,7] to divide metals into two classes: metals in which there is an unlimited increase of the resistance in magnetic fields (Bi, Cd, Ga, W, etc.) and metals in which saturation is observed, i.e., in which the resistance approaches a certain limiting value (Al, In and Na). The difficulties in the way of a theoretical explanation of the large increase in resistance in magnetic fields have been resolved by the introduction of a concept that conduction in metals is due to two kinds of quasi-particles with opposite charges,[8,9] whose existence is predicated on the assumption that the Brillouin zones overlap. The unlimited increase in resistance occurs in the metals in which the mobile charges of both signs are present in equal numbers. However, experimental data confirming the hypothesis that the limited growth of the resistance is connected with the influence of the unlimited increase in the intensity of the Hall field are virtually lacking inasmuch as since the investigations of Kamerlingh Onnes and Hof[10] back in 1914 there have appeared only individual studies of the Hall effect in bismuth,[11] sodium,[12] and graphite[13] satisfying the condition of obtaining large effective fields, i.e., investigations of sufficiently pure metals at low temperatures.

Moreover, investigations of the Hall effect and of the variation of the resistance in magnetic fields have as a rule been made separately, i.e., the connection between the two effects was not studied. In view of the strong influence of impurities on the conductivity of metals at low temperatures accurate information on the relationship between the galvanomagnetic effects can be obtained only through concurrent investigation of them in the same specimen.

1. Experimental Data

The present investigation is devoted to an experimental study of galvanomagnetic effects at low temperatures and determination of the properties of conduction electrons in metals on the basis of the results obtained.

We carried out joint investigations of the Hall effect and the variation of the resistance in a magnetic field in eight metals, comprising one metal in the first group of the periodic table (Cu), three in the second group (Be, Mg and Zn), two in the third group (Al and In) and two in the fourth group (Sn and Pb).[14-16] The use of pure metals and a sufficiently low temperature insured attaining the region of large effective fields in which the period of the Larmor precession is shorter than the average time between collisions of the electrons with the lattice.

Commonly, in both experimental and theoretical investigations the Hall effect is characterized by the Hall constant R. The general result of experimental investigations where the Hall constant is concerned may be summarized as follows: R is independent of the magnetic field only in metals in which the increase in resistance in magnetic fields is insignificant.[14,15] In the presence of an appreciable increase in the resistance, the magnitude of the Hall constant depends upon the field intensity. The alkali metals are a possible exception to this rule.

The field dependence of the Hall constant is generally rather complex and differs in detail for different metals.[14,15] It is difficult to formulate any general regularity common to individual groups of metals. This is a natural consequence of the fact that in strong fields R is simultaneously a function of both the Hall effect and the variation in resistance.[14]

An appreciably clearer pattern emerges if we characterize the Hall effect in the region of strong fields by a dimensionless parameter: the ratio of the Hall field (E_y) to the electric field in the direction of the current (E_x), i.e., by E_y/E_x. We measured E_y/E_x directly in our investigation. The value of this parameter can also be deduced from the data in the literature on the Hall effect for Bi[11], C (graphite)[13], Cd[10] and Na[12] in conjunction with the results of measurements of the resistance. However, the values obtained in this manner are not particularly accurate since the results of the respective separate investigations are for different specimens.

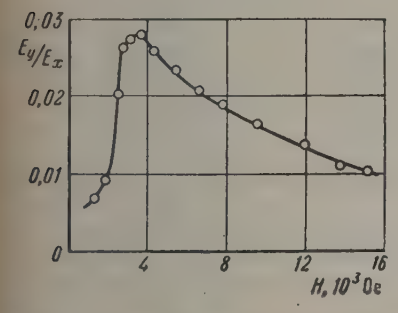

Fig. 1. Hall effect in zinc sample Zn-2 at 4.22°K.

The investigated metals can be divided into two classes, according to the nature of the field dependence of the ratio E_y/E_x: in the metals of the first class, which includes Be, Mg, Zn, Cd, Sn, Pb, C (graphite) and Bi, the absolute value of E_y/E_x increases to a maximum and then falls off as the field is increased (Fig. 1); in those of the second class, which comprises Al, In, Cu and Na, the absolute value of E_y/E_x increases without limit with the field intensity (Fig. 2, Curve 1). Furthermore, whereas in the metals of the first class the magnitude of E_y/E_x seldom exceeds some tenths or hudredths of unity, in those of the second class the value of the Hall field may be greater than the value of the electric field; for example, $E_y/E_x > 2$ for Al in the strongest fields used. It is also interesting to note that in In, Al, Mg and, for certain orientations of the crystal, in some Zn single crystals[18] the Hall effect changes sign as the temperature is reduced and at the very lowest temperatures as the field intensity is increased.

As a result of concurrent investigations of the Hall effect and the field dependence of the resistance, we are able to establish a definite connection between the form of the field dependence of E_y/E_x and the character of the field dependence of the resistance: in metals in which the Hall effect is observed to fall off in

strong fields (Fig. 1), the resistance increases without limit (Fig. 3, Curve II); in metals in which the Hall field increases without limit (Fig. 2, Curve 1), the resistance in magnetic fields tends to approach a limiting value (Fig. 2, Curve 3).

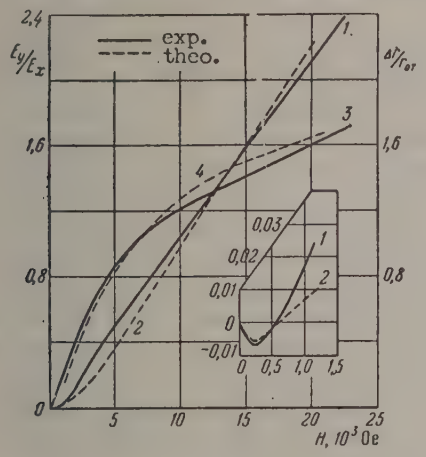

Fig. 2. Comparison of the experimental and calculated values of the Hall field and the change in resistance in magnetic fields for aluminum. Sample Al-4; T = 4.22°K. Curves 1 & 2 - E_y/E_x; curves 3 & 4- r/r_{0T}.

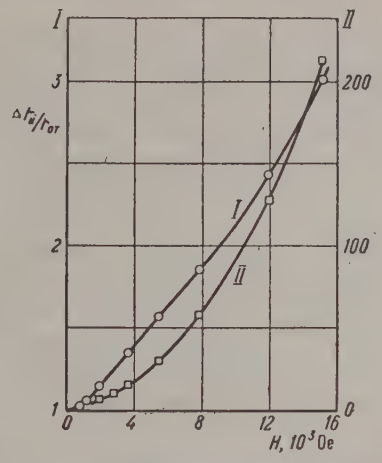

Fig. 3. Field dependence of the change in resistance of sample Zn-2: I - at 20.4°K, II - at 4.22°K (H normal to the plane of the plate).

If, following Justi, we classify the metals according to the character of their change in resistance in strong fields, at present we should include the following in the list of metals exhibiting an unlimited growth in resistance: Bi, Sb, As, Ga, W, Cd, Be, Zn, Pb, Sn, C and Mg(Refs. 1 & 2. 1, 1, 19, 20, 21, 22, 3, 23, 6, 15 & 15, resp.). Presumably Mo and Ba also belong in this class, although in the fields used in the investigations of these metals,[24 & 25] the increase in resistance amounted to only a few units. The metals are listed above in the chronological order of the discovery of the large(10^2-10^3-fold) increase in their resistance in strong fields. It has been established experimentally that the resistance of Al, In and Na (Refs. 4, 12 and 15) increases slowly with increasing field intensity and apparently tends to a limiting value.

As a result of comparison of our data and those in literature it may be stated that for metals, which have been investigated in strong fields, the curve characterizing the change in resistance $\Delta r/r_{0T}$ in magnetic fields has the following form:* at values of $\Delta r/r_{0T} < 10^{-2}$ the increase in $\Delta r/r_{0T}$ is approximately quadratic; then in the interval $10^{-2} < \Delta r/r_{0T} < 10$ the rate of increase falls off and in the case of a number of metals becomes linear (the linear field dependence was first observed by Kapitsa[1]). This linear portion is clearly discernable in Fig. 3 (Curve I) for Zn at T = 20.4°K.

For metals of the class comprising aluminum, indium and so on, at $\Delta r/r_{0T} \sim 1$ the increase in resistance is slowed down to an even greater extent and the resistance becomes almost independent of the field.

In the case of Sn, Zn and other metals, after the practically linear section of the curve, at still higher fields the dependence again becomes quadratic. This "second" quadratic dependence persists in the entire range of investigated strong fields.[15] The coefficient in this "second" quadratic variation region is appreciably smaller than the coefficient associated with the "first" quadratic variation in weaker fields with $\Delta r/r_{0T} < 10^{-2}$. As will be shown below this feature of the resistance-increase curves enables us to make certain important deductions when we come to compare experiment with theory.

* Δr is the increment in resistance in the magnetic field; r_{0T} is the resistance at H = 0 and the temperature of the experiment.

All the aforesaid applies to the average effect (increase in resistance) in a transverse magnetic field. Experiments on single crystals show that, while the general regularities noted above hold, the ratio of the coefficients in the quadratic-dependence regions in strong and weak fields differs for different orientations of the single crystal.

Thus investigation of the change in resistance of a tin single crystal rotated about its longitudinal axis - oriented parallel to the direction of the current in the crystal and perpendicular to the magnetic field - showed that the anisotropy of the resistance in a magnetic field is very pronounced;[6] presumably this holds for all crystals of this type in which the fourth order symmetry axis is perpendicular to the principal axis. At 4.2°K and in a field of $2 \cdot 10^4$ oersteds the resistance of the crystal varies by a factor of about 20 as the crystal is rotated; the minimum resistance is observed when the fourth order axis of symmetry is aligned with the magnetic field. The anisotropy increases with increasing field strength. Such anomalously low resistance minima have been observed previously at certain orientations of Ga, Zn, Ca (Refs. 19, 3 and 3 & 26) and possibly Au (Ref. 17) crystals. The appearance of such deep minima is rather unexpected, since it is known that the anisotropy of the conductivity of tin in the absence of a magnetic field amounts to only about 40% and is even smaller in other metals.

In the orientations of the crystal in which such anomalous minima are manifest, not only is the resistance lowered but there is also usually an alteration in the form of the field dependence of the resistance. In such cases the resistance increases more slowly with the field than for other orientations. It has been shown that this slower growth of the resistance with the field intensity is due to the influence of the strong Hall field obtaining in such cases. In this connection it may be assumed that the low value of the resistance in a magnetic field and the change in the character of its field dependence at certain orientations of metal crystals are also due to the influence of the Hall field.

In view of this we undertook an investigation of the anisotropy of the Hall effect in tin and zinc and, for purposes of comparison, in indium, in which the anisotropy of the resistance in magnetic fields is small. The anisotropy of the Hall effect at liquid helium temperatures had not been studied hitherto.

In indium the anisotropy of the Hall effect, like that of its resistance in magnetic fields, proved to be small.[16] The rotation diagrams (Hall effect and change in resistance *vs* angle of the crystal) for Sn and Zn are shown in Figs. 4 and 5. The anisotropy of the Hall effect is at least as great and possibly greater than the anisotropy of the resistance. In absolute magnitude the maximum values of the Hall field exceed the minimum values tens of times. The component E_z of the Hall field parallel to the magnetic field differs from zero, hence the resultant Hall field is not perpendicular to the magnetic field. The Hall field becomes perpendicular to the magnetic field only when the latter is in line with one of the principal axes of the crystal. It will be noted that the resistance minima correspond to the maxima in the absolute value of the Hall field; the magnitude of E_y/E_x corresponding to the orientations at which the anomalously deep resistance minima observed may even exceed unity.

In view of the complex character of the anisotropy of the Hall field in a strong magnetic field, investigation of the effect cannot be restricted to the principal orientations; it is essential to record a complete rotation diagram.

In the case of zinc, when the hexagonal axis is parallel to the magnetic field, the E_y/E_x curve becomes irregular, i.e., oscillations are superposed on the smooth basic curve (see Fig. 6). The location of these oscillations is analogous to that observed earlier in the curve for the variation of resistance;[3] however, in this case the oscillations are appreciably more pronounced. Comparisons of Curves 1 & 2 with Curves 5 & 6 shows that the period of oscillation of E_y/E_x is of the same order of magnitude as the period of oscillation of the susceptibility.[27, 28] Although we cannot conclude that the oscillation of the Hall effect is directly

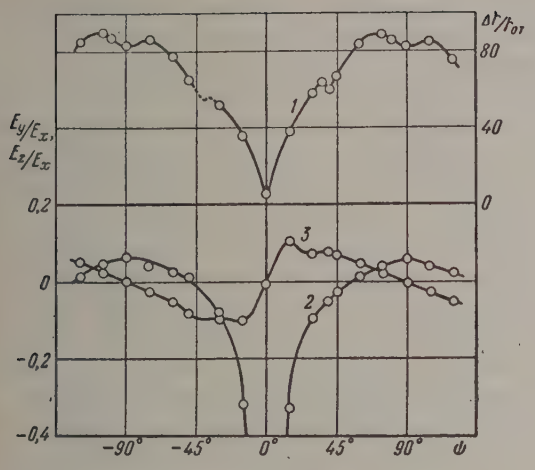

Fig. 4. Hall effect and change in resistance in tin. Sample Sn-6; T = 4.22°K; H = 14,880 oersteds. Curve 1 - r/r_{0T}; 2 - E_y/E_x; 3 - E_z/E_x; ψ - angle between fourth order symmetry axis and magnetic field. (At ψ = 0°, E_y/E_x = -2.46.)

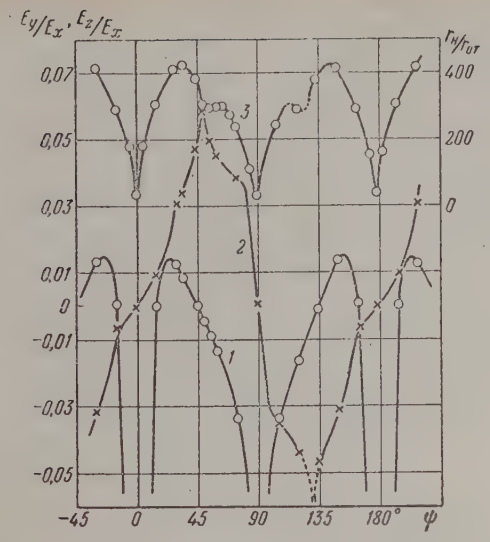

Fig.5. Same as Fig. 4 but for zinc. Sample Zn-10, T = 4.22°K, H = 22,200 oersteds. Curve 1 - E_y/E_x; 2 - E_z/E_x; 3 - r_H/r_{0T}; ψ -angle between sixth order symmetry axis and field. (At ψ = 0°, E_y/E_x = -0.69; at ψ = 90°, E_y/E_x = -0.47.)

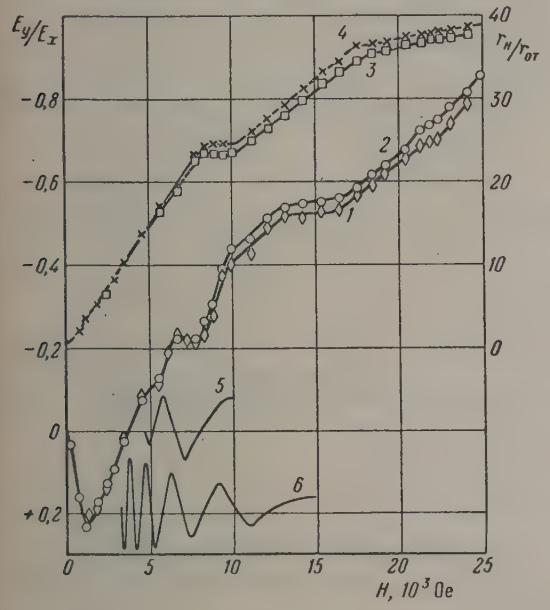

Fig. 6. Field dependence of the Hall field and change in resistance for sample Zn-10 at = 0. Curves 1 & 3 recorded at 1.81°K; Curves 2 & 4 at 4.22°K. Curves 1 & 2 - E_y/E_x, 3 & 4 - r/r_{0T}; 5 - magnetic susceptibility χ (ψ = 0°, T = 14°K - Ref. 27; 6 - difference of principal susceptibilities $\Delta\chi$ (4.22°K; Ref. 28).

connected with the oscillation of the susceptibility, we are fairly safe in assuming that the two stem from the same cause, witness the presence of an oscillating term in the expression for the thermodynamic potential of an electron gas in a magnetic field, as derived from the theory of Landau. We shall not here further discuss the question of quantum oscillations inasmuch as this lies beyond the proper scope of this investigation.

2. Comparison of Experimental Data with Theory

Let us see how the results of experiment compare with the deductions of modern theory. Until recently there were difficulties in explaining the unlimited increase in resistance in a magnetic field, observed in most metals. Theory yielded a curve with saturation. The main difficulty stemmed from the fact that theoretical calculations indicated an unlimited linear increase in the value of the Hall field with increasing magnetic field intensity. This difficulty can be obviated only by recourse to the two-zone model with

an equal number of holes and electrons. It should be noted that an equal number of holes and electrons is naturally obtained for the metals of the even numbered groups of the periodic system, having the simplest lattice, and for a number of metals of the odd numbered groups, having a more complex lattice. The two-zone model was first proposed by Blokhintsev and Nordheim[8] and subsequently used by a number of other investigators;[29-32] however, it has become clear as a result of the latest investigations[9,33] that the requisite result is obtained from this model regardless of the assumptions made concerning the anisotropy of the metal and the method of taking a number of other, secondary factors into account. The theory[9] is formulated for an isotropic metal on the assumption of a quadratic relationship between the quasi-momentum and the energy of the electrons, so that formally the departure from free electron theory amounts essentially to introduction of the effective mass concept and assumption of the existence of particles with both negative and positive charges. The theory has been developed for a fully degenerate electron gas. The theoretical results as regard the Hall effect are given by Sondheimer[34] in the form of an expression for the Hall constant. However, a simple expression for E_y/E_x can readily be deduced from Sondheimer's theoretical results.

Let the conduction electrons in the isotropic metal be distributed between two Brillouin zones so that the number of vacancies per unit volume in the lower, almost filled zone equals n_1, while in the upper, almost empty zone there are n_2 electrons per unit volume. The behavior of the electrons in the lower zone may be considered as equivalent to the behavior of n_1 particles with a charge $+e$ and a certain effective mass m_1. We denote the mean time between the collisions of these particles with the lattice through τ_1. We denote the corresponding quantities for the n_2 electrons with a charge $-e$ through m_2 and τ_2, respectively.

Taking into account both groups of mobile charges, the electric conductivity in the absence of a magnetic field is

$$\sigma_{0T} = n_1 \frac{e^2\tau_1}{m_1} + n_2 \frac{e^2\tau_2}{m_2} = \sigma_{01} + \sigma_{02}, \tag{1}$$

and the conductivity in a magnetic field is

$$\sigma_H = \left(\frac{\sigma_{01}}{1+\varphi_1^2} + \frac{\sigma_{02}}{1+\varphi_2^2}\right)\left[1 + \left(\frac{E_y}{E_x}\right)^2\right], \tag{2}$$

where $\varphi_1 = \frac{eH\tau_1}{m_1 c}$ and $\varphi_2 = \frac{eH\tau_2}{m_2 c}$. For the Hall field we have

$$\frac{E_y}{E_x} = \frac{\dfrac{n_1\varphi_1^2}{1+\varphi_1^2} - \dfrac{n_2\varphi_2^2}{1+\varphi_2^2}}{\dfrac{n_1\varphi_1}{1+\varphi_1^2} + \dfrac{n_2\varphi_2}{1+\varphi_2^2}} \tag{3}$$

or in a less symmetrical but more convenient for computation form

$$\frac{E_y}{E_x} = \frac{\left(\frac{n_1}{n_2} - 1\right)\varphi_1^2\varphi_2^2 + \left(\frac{n_1}{n_2}\varphi_1^2 - \varphi_2^2\right)}{\left(\frac{n_1}{n_2}\varphi_1 + \varphi_2\right) + \left(\frac{n_1}{n_2}\varphi_2 + \varphi_1\right)\varphi_1\varphi_2}. \tag{4}$$

If the number of holes equals the number of electrons, i.e., when $n_1 = n_2 = \frac{n}{2}$, equation (4) reduces to

$$\frac{E_y}{E_x} = \frac{\varphi_1 - \varphi_2}{1 + \varphi_1\varphi_2}. \tag{5}$$

After substitution from (5) in (2) and certain transformations we get

$$\frac{\Delta r}{r_{0T}} = \frac{\sigma_{0T}}{\sigma_H} - 1 = \varphi_1\varphi_2. \tag{6}$$

It will be seen from the above equations that E_y/E_x and σ_H/σ_{0T} are functions of the dimensionless parameters φ_1 and φ_2. These parameters can serve as a measure

of the effective magnetic field. The quantity φ for the free electrons is a simple physical meaning: it represents the angle of deflection of the electron's path during the interval τ.

In weak fields $\varphi_1, \varphi_2 \ll 1$ there is little difference between the behavior of metals with $n_1 \neq n_2$ and $n_1 = n_2$ In both cases the Hall field increases directly and the resistance as the square of the magnetic field.

In strong fields $\varphi_1, \varphi_2 \gg 1$ for metals with $n_1 = n_2$ we have $E_y/E_x \sim 1/H$ and $\Delta r/r_{0T} \sim H^2$; for metals with $n_1 \neq n_2$, $E_y/E_x \sim H$. In consequence of the linear increase of the Hall field, in these metals, σ_H/σ_{0T} does not fall off without limit as in the preceding case but tends to approach a limit:

$$\left(\frac{\sigma_H}{\sigma_{0T}}\right)_{\varphi \gg 1} \approx \frac{(n_1 - n_2)^2}{n_1^2 + n_2^2 + n_1 n_2 (\varphi_1/\varphi_2 + \varphi_2/\varphi_1)} . \qquad (7)$$

Thus it will be seen that qualitatively the properties of the two models with an equal and an unequal number of holes and electrons correspond to the behavior of the aforementioned two groups of metals.

Metals in which the number of holes equals the number of electrons are characterized by a Hall field falling off an intensity in strong magnetic fields and a resistance increasing without limit (Zn, Be, etc.). Metals in which the number of holes is not equal to the number of electrons are characterized by a Hall field increasing without limit and a resistance exhibiting saturation in strong magnetic fields (In & Al).

Despite the fact that the described theory is only approximate, a detailed qualitative comparison with the results of experiment and is worthwhile. Juxtaposing the experimental data for E_y/E_x and $\Delta r/r_{0T}$ with equations (1)-(6) we can compute the parameters φ_1 and φ_2 and, consequently, evaluate the mobility of the holes and electrons. Then comparing the resultant mobility data and the experimental values of the electric conductivity in the absence of a magnetic field we can, by means of equation (1), compute the concentrations of the mobile particles.

Aluminum and indium are among the metals with $n_1 \neq n_2$. In this case theory can be compared with experiment over the entire range of the investigated fields. The calculations are facilitated by the fact that for both metals measurements have been extended into fields where the growth of E_y/E_x becomes linear and the resistance approaches its saturation value. For copper the picture is not as clear[15], however, the observed large value of the Hall effect and the attenuated increase in the resistance in magnetic fields give reason to assume that copper also belongs in the group of metals in which $n_1 \neq n_2$. This is in accord with the position of Cu in the periodic table. In making the calculations the different parameters in (2), (3) and (4) are selected so that the theoretical curves will fit the experimental ones as well as possible. The calculated and experimental curves for aluminum, indium and copper are reproduced in Figs. 2, 7 and 8. It will be seen that the agreement is generally satisfactory although there is a certain divergence between the curves in the region of medium fields. The incomplete agreement indicates that, while the theory is qualitatively correct, it cannot in its present stage accurately describe all the features of the experimental curves.

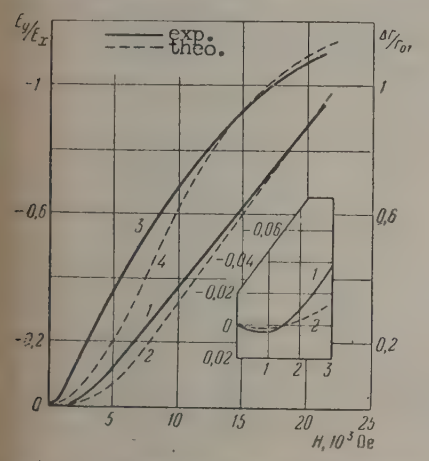

Fig. 7. Comparison of experimental and calculated values of the Hall field and change in resistance in a magnetic field for sample In-4 at T = 4.22°K. 1 & 2 - E_y/E_x; 3 & 4 - $\Delta r/r_{0T}$.

In making a quantitative comparison with theory for metals with an equal number of holes and electrons it should be borne in mind that equations (5)

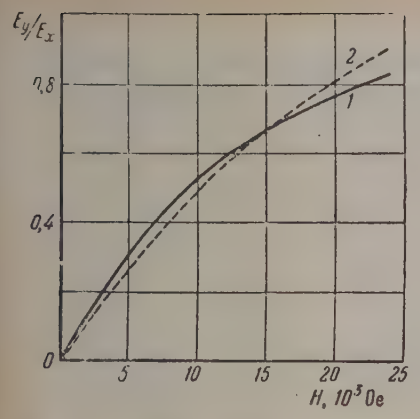

Fig. 8. Comparison of experimental (1) and theoretical (2) values of the Hall field for sample Cu-14 at 4.22°K.

and (6) do not allow for the experimentally observed retardation in the rate of increase of the resistance in medium fields or the field dependence of the Hall constant. The theory characterizes the experimental data more accurately in the region of strong fields. Hence, in making comparisons with theory for metals with $n_1 = n_2$ one should take the values for E_y/E_x and $\Delta r/r_{0T}$ in the strongest fields investigated.

The values of the mobility and concentration of the mobile charges computed on the basis of the experimental data for E_y/E_x, $\Delta r/r_{0T}$ and σ_{0T} by means of equations (1)-(4) for Cu, Al, and In and equations (1), (5) and (6) for Be, Zn, Sn, Pb and Bi are listed in Table 1. The data for Be, Zn, Sn, and Bi pertain to single crystals. The orientations of the single crystals were selected so that the magnitude of the observed effects would not differ greatly from the average values. The other data are for polycrystals.

For metals with an unlimited increase of the resistance in a magnetic field — in which according to theory $n_1 = n_2$ — one can obtain certain information regarding the mobility and concentration of the mobile charges even when only the variation in resistance with the field has been investigated. From the change in resistance one can compute the geometric mean of the mobilities of the holes and the electrons — $\sqrt{(\tau_1/m_1)(\tau_2/m_2)}$ — according to equation (6) and then, substituting this value in (1) instead of the arithmetic mean, obtain the approximate concentration of the mobile particles. Comparison of the values obtained in this way with the data of Table 1 shows that the error involved is not great. Computations should be carried out for the strongest magnetic fields, in the region of the "second" quadratic dependence. The results of such calculations are shown in Table 2. The listed data are for polycrystals and averaged values for single crystals.

Table 1

Values of the mobility and concentration of the mobile particles computed on the basis of the experimental data for E_y/E_x

Sample	T, °K	$\frac{r_{0T}}{r_{00}}$*	$\frac{\tau_1}{m_1} \cdot 10^{-16}$	$\frac{\tau_2}{m_2} \cdot 10^{-16}$	$\frac{n_2}{n_1}$	$\frac{n_1}{n_A}$	$\frac{n_2}{n_A}$
Cu-14	4,22	$6,4 \cdot 10^{-3}$	0,25	0,47	2,5	0,32	0,81
In-4	4,22	$1,7 \cdot 10^{-3}$	0,94	0,44	4,8	0,23	1,1
Al-4	4,22	$1,6 \cdot 10^{-3}$	1,1	2,1	0,23	1,1	0,26
Be-1	20,4	$1,1 \cdot 10^{-2}$	1,9	0,8	1	0,028	0,028
Zn-2	4,22	$4,7 \cdot 10^{-4}$	6,5	5,6	1	0,16	0,16
Pb-1	1,86	$1,7 \cdot 10^{-5}$	6,2	6,8	1	0,5	0,5
Sn-6	4,22	$4,3 \cdot 10^{-4}$	5,0	2,7	1	0,35	0,35
Bi VII **	64	0,312	5,2	5,1	1	$0,42 \cdot 10^{-4}$	$0,42 \cdot 10^{-4}$

* $\frac{r_{0T}}{r_{00}}$ is the ratio of the resistance of the sample at the temperature of the experiment to its resistance at 0°C; $\frac{n_2}{n_1}$ is the ratio of the concentrations of the electrons and holes; $\frac{n_1}{n_A}$ is the number of holes per atom and $\frac{n_2}{n_A}$ is the number of electrons per atom.

** According to the data of Refs. 11 and 2.

Table 2

Values of the mobility and concentration of the mobile particles computed according to equation (1) on the basis of data in the literature

Metal	T, °K	$\frac{r_{0T}}{r_{00}}$	$\sqrt{\frac{\tau_1}{m_1}\cdot\frac{\tau_2}{m_2}}\cdot 10^{-16}$	n/n_A	Ref. No.
Sb	80	0,33	0,134	$7\cdot10^{-3}$	[1]
Cd	4,22	$2{,}9\cdot10^{-4}$	9,8	0,38	[15]
Ba	4,22	$7{,}87\cdot10^{-3}$	0,32	0,16	[25]
Ga	4,22	$1\cdot10^{-3}$	3,3	0,04	[19]
Mo	14	$7{,}68\cdot10^{-3}$	0,36	0,42	[24]
W	4,22	$3{,}47\cdot10^{-4}$	9,4	0,38	[20]

For most of the metals listed in Tables 1 and 2, calculations of the number of mobile charges per atom yield values between 0.1 and 1, i.e., values that may reasonably be expected assuming an appreciable overlapping of the zones.

Substantially lower concentration values are obtained for Bi, Be, Ga and Sb; however, these may also be regarded as realistic in view of the strong influence of impurities on the conductivity of these metals. The average values of the mobility, if they are compared at temperatures equal to the Debye temperature, prove equal for metals with equal concentrations of mobile particles. The mobility increases with decreasing concentration approximately as $n^{-1/3}$.

In general it can be said that the theory fits the experimental data fairly well. It must be recalled, however, that for metals with an equal concentration of holes and electrons close agreement obtains only in the regions of strong fields and the theory is incapable of correctly describing the entire change in resistance *vs* magnetic field curve, while where the Hall effect is concerned the agreement is only qualitative.

Let us examine these difficulties and shortcomings of theory.

The form of the E_y/E_x and $\Delta r/r_{0T}$ curves for magnesium[15] in the strongest fields used in the investigation shows that magnesium belongs to the group of metals with an equal number of holes and electrons. This is in accord with the position of Mg in the periodic table. However, the character of the curves in medium fields is not in conformity with the properties ensuing from the above described simple model with two groups of mobile charges. Thus according to equation (5), at the given temperature E_y/E_x should not change sign as the field is increased. Actually the sign of E_y/E_x does change in magnesium (see Fig. 9). The linear section of the curve of $\Delta r/r_{0T}$ as a function of the field for magnesium extends to $\Delta r/r_{0T} \simeq 20$ (Fig. 10). As noted previously, this feature of the variation in resistance is not constant with the given model, which predicts a quadratic increase in resistance in all magnetic fields.

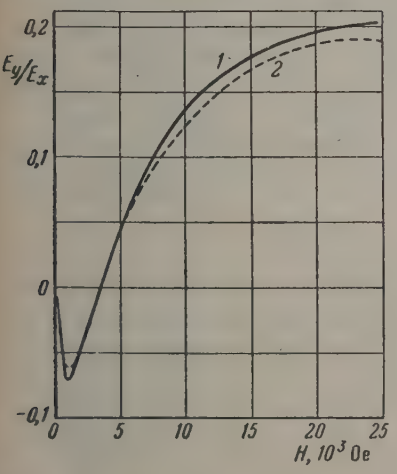

Fig. 9. Comparison of experimental (1) and theoretical (2) values of the Hall field for sample Mg-6 at 4.22°K.

The difficulty can be obviated by recourse to a somewhat more complicated model. Let us assume that instead of one group of holes and one group of electrons the isotropic metal has two groups of holes having concentrations n_1 and

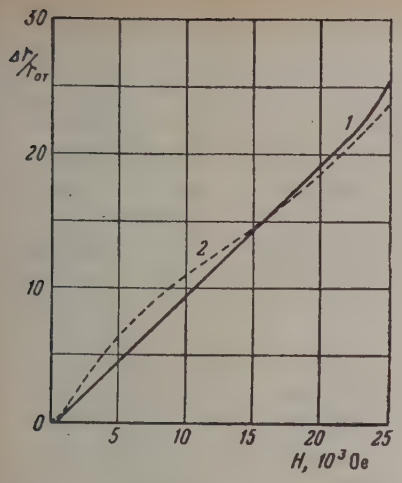

Fig. 10. Comparison of experimental (1) and calculated (2) values of the change in resistance in magnetic fields for sample Mg-6 at 4.22°K.

n_3, effective masses m_1 and m_3, and with mean times between collisions τ_1 and τ_3, and two groups of electrons similarly characterized by n_2 and n_4, m_2 and m_4, and τ_2 and τ_4. Let us examine the case of a metal in which the concentrations of group pairs are equal, i.e., $n_1 = n_2$ and $n_3 = n_4$. For this model equations (1)-(7) are modified accordingly and it becomes possible to fit the theoretical values to the experimental curves in the entire investigated range of fields and to obtain the experimentally observed change in sign of the Hall effect and the section with the slowed-down growth of resistance.

The equations for the conductivity and Hall field for this paired-group model have the following form:

$$\sigma_{0T} = \sum_{i=1}^{i=4} \frac{n_i e^2 \tau_i}{m_i} = \sum_{i=1}^{i=4} \sigma_{0i}, \tag{8}$$

$$\sigma_H = \left[1 + \left(\frac{E_y}{E_x}\right)^2\right] \sum_{i=1}^{4} \frac{\sigma_{0i}}{1+\varphi_i^2}, \tag{9}$$

$$\frac{E_y}{E_x} = \frac{\frac{n_1}{n_3}(\varphi_1^2 - \varphi_2^2)(1+\varphi_3^2)(1+\varphi_4^2) + (\varphi_3^2 - \varphi_4^2)(1+\varphi_1^2)(1+\varphi_2^2)}{\frac{n_1}{n_3}(\varphi_1+\varphi_2)(1+\varphi_1\varphi_2)(1+\varphi_3^2)(1+\varphi_4^2) + (\varphi_3+\varphi_4)(1+\varphi_3\varphi_4)(1+\varphi_1^2)(1+\varphi_2^2)}, \tag{10}$$

where

$$\varphi_1 = \frac{eH\tau_1}{m_1 c}, \quad \varphi_2 = \frac{eH\tau_2}{m_2 c}, \quad \varphi_3 = \frac{eH\tau_3}{m_3 c}, \quad \varphi_4 = \frac{eH\tau_4}{m_4 c}.$$

From the data for magnesium sample Mg-6 at 4.22°K[15] and equations (8)-(10) we arrive at the values of the mobility and concentrations of the mobile charges listed in Table 3.

At T = 4.22°K, $r_{00}/r_{0T} = 2.24 \cdot 10^{-3}$.

Thus for magnesium we get two groups of holes and electrons — 1,2 and 3,4 — differing markedly as regards mobility but having almost the same mobility of the holes and electrons in each pair of groups. Taken in conjunction, the properties of these groups of charges satisfactorily account for both the shape of the resistance curve for magnesium in a magnetic field and the observed variation of E_y/E_x. The curves for the variation of the resistance and the Hall field, computed on the basis of these parameters, are juxtaposed with the experimental curves for the magnesium sample in Figs. 9 and 10. It will be seen that the fit, in general, is satisfactory.

Table 3

Mobilities and concentrations of the mobile particles for magnesium sample Mg-6 at 4.22°

No. of group of charges	τ_i/m_i	n_i/n_A
1	$4{,}4 \cdot 10^{16}$	0,09
2	$5{,}2 \cdot 10^{16}$	0,09
3	$2{,}5 \cdot 10^{15}$	0,15
4	$2{,}3 \cdot 10^{15}$	0,15

It should be noted that if in the framework of this model we relax the requirement that $n_1 = n_2$ and $n_3 = n_4$ and retain only the condition of the total number of holes equal the total number of electrons, i.e., that $n_1 + n_3 = n_2 + n_4$, we obtain an additional "free" parameter, through selection of which it is possible to secure an even closer agreement of the theoretical results with the experimental data. However, even without recourse to this added complication fairly good agreement is obtained. The properties of the described

model, on the whole, satisfactorily reflect the features and characteristics peculiar to the group of metals with an unlimited increase in resistance in a magnetic field. From an analysis of equations (9) and (10) it will be seen that in weak fields there is obtained 1) a quadratic variation of the resistance with the field, characterized by a coefficient determined by the group with the maximum mobility, 2) a linear field dependence of the Hall effect and 3) an unvarying Hall constant. In strong fields, when the parameter $\varphi_i > 1$ even for the group of charges with the minimal mobility, the field dependence of the resistance is also quadratic but characterized by a coefficient determined roughly by the geometric mean of all the mobilities. The Hall effect in large fields decreases in proportion to $1/H^2$, while the Hall constant remains virtually constant. In medium fields there is a slow increase in resistance and a strong dependence of the Hall constant on the field; in particular, the constant can change sign. Thus the described properties of this model correspond to the observed attributes of metals with an unlimited growth of the resistance in magnetic fields.

The hypothesis of the existence of two groups of electrons and holes with distinctly different mobilities is not in conflict with current concepts regarding the structure of the energy zones of metals with hexagonal symmetry. The mobilities of the electrons in the second zone, near the base and the lateral sides of the polyhedron of the first zone, as well as the mobilities of the holes near the edges of the base and of the sides of the first zone polyhedron, can differ substantially.

The results obtained for magnesium, presumably, have a general significance. Two groups of electrons and holes, but with a smaller difference between mobilities than in magnesium, apparently, also exist in zinc and in cadmium; the smaller difference accounts for the less clearly pronounced linear section in the resistance vs field curves for these metals. Furthermore, even for cubic crystals, where all six electron groups in the second zone have identical properties, we can obtain different mobilities for the different groups if we allow for anisotropy of the effective masses and differences in the orientation of the effective mass tensor relative to the field for electron groups near different planes at the boundary with the first zone.

In comparing theory with the results of investigations of the anisotropy of the Hall effect and the variation in resistance in tin and zinc it turns out that here, too, the model with two groups of mobile particles — holes and electrons — characterized by anisotropy of the effective masses, is inadequate for interpretation of the experimental data. For tin one can obtain curves for the variation in resistance and the Hall effect for the two principal orientations that are in fair agreement with the experimental curves, on the basis of the model with four groups of mobile particles: two groups of electrons and two groups of holes with anisotropic effective masses.[18] Thus this model can help explain the appearance of a very large anisotropy of the resistance in a magnetic field in certain cases as well as the usual observed anisotropy, manifested in a simple rotation diagram with the usual maxima and minima for the principal crystallographic orientations. However, this model is incapable of explaining the additional minima which appear in the resistance rotation diagram recorded in very strong fields. The experimental data show that these additional minima appear at the orientations of the crystal in which one of the crystal surfaces with the highest density of atoms is turned perpendicularly to the field. In another publication[18] we show that this effect can be qualitatively explained in the framework of the zone theory.

3. Comparison of Experimental Data with the Results of other Methods of Investigating the Properties of Conduction Electrons

a) Comparison with free path length determinations. At present three methods are used for determining the length of the free path of the mobile charges: In chronological order of application these are 1) the method based on determining the influence of the dimensions of the sample on the conductivity,[35] 2) the method

of the anomalous skin effect[36] and 3) the method based on the effect of the shape and dimensions of the sample on its resistance in a magnetic field. This method was developed by the writer in collaboration with B.G.Lazarev.[37]

Assuming a quadratic relationship between the quasi-momentum and the energy of the mobile particles, we can, on the basis of the mobility data obtained from measurements of the galvanomagnetic effects, also compute the free path length for the particles of each of the aforementioned groups and then, having averaged the results, compare the resultant mean value with values obtained by other methods. Comparison of the data derived in this way with those arrived at by the different methods mentioned above shows good agreement. For example, the values of the free path length at 0°C determined on the basis of the anomalous skin effect are $\lambda_0 = 4.2 \cdot 10^{-6}$ cm in copper, $1.95 \cdot 10^{-6}$ cm in aluminum and $0.55 \cdot 10^{-6}$ cm in lead; the corresponding values computed on the basis of data for galvanomagnetic effects are $3.3 \cdot 10^{-6}$ cm for Cu, $2.4 \cdot 10^{-6}$ cm for Al and $0.48 \cdot 10^{-6}$ cm for Pb. For cadmium the value obtained by the method based on determining the effect of the dimensions of the sample on the conductivity is $2.9 \cdot 10^{-6}$ cm, that derived from the anomalous skin effect $2.25 \cdot 10^{-6}$ cm, while the value arrived at on the basis of the galvanomagnetic effects is $2.4 \cdot 10^{-6}$ cm.[15]

b) Comparison with experimental data on the electronic specific heat. Experimental data on the electronic specific heat have hitherto been compared only with free electron theory. The electron concentration was usually computed from the valence of the metal and the atomic volume. The effective mass was determined by comparing the calculated and experimental data. Obviously, this method of comparing theory with experiment is not satisfactory, but until recently it was the only feasible one. Our data on the concentration of the mobile charges permit of making a more satisfactory, if still rather rough, comparison of the theoretical data with the results of specific heat measurements.

If the electronic specific heat per gram-atom is characterized by

$$C_{V_e} = \alpha RT, \tag{11}$$

then, according to free electron theory the value of α is given by the expression

$$\alpha = \frac{n}{n_A} \cdot \frac{\pi^2}{2} \cdot \frac{k}{\varepsilon_0^1} = \frac{n}{n_A} \cdot \frac{\pi^2}{2} \cdot \frac{8km_0}{h^2 \left(\frac{3n}{\pi}\right)^{2/3}}, \tag{12}$$

where n is the number of electrons and n_A is the number of atoms per unit volume. If we are dealing with several groups of mobile charges, the electronic specific heat will, obviously, be the sum of the specific heats of the individual groups:

$$C_{V_e} = \alpha RT = RT\Sigma\alpha_i.$$

We computed the values of α_i both for the holes and the electrons by means of equation (12), using the concentration data listed in Tables 1, 2 and 3.

Table 4

Metal	n_1/n_A	n_2/n_A	$\alpha\ (=\Sigma\alpha_i) \cdot 10^4$	$\alpha_{exp} \cdot 10^4$	m^*/m_0	Ref. No.
Cu	0,32	0,81	0,97	0,90	0,93	[38]
Be	0,028	0,0028	0,38	0,27	0,71	[39]
Mg	0,09	0,15	1,16	1,64	1,41	[38]
Zn	0,17	0,17	0,78	$0,68_5$	0,88	[40]
Cd	0,18	0,18	1,05	0,85	0,81	[41]
Al	0,85	0,28	1,21	1,30	1,08	[40]
In	0,25	1,1	1,72	1,76	1,02	[42]
Sn	0,34	0,34	1,47	2,0	1,36	[43]
Pb	0,50	0,50	1,78	3,77	2,1	[44]
Bi	$4,2 \cdot 10^{-6}$	$4,2 \cdot 10^{-5}$	0,178	0,094	0,53	[45]

Then we deduced the value of m^*/m_0 (the ratio of the effective mass of the charge to the mass of a free electron) by comparing the calculated with the experimental data for α. Obviously the resulting values of m^*/m_0 are only mean values that give no clue to the actual differences between the effective masses of the particles comprising the different individual groups. The results of our calculations are summarized in Table 4.

In the table n_1/n_A are the relative concentrations of the holes and n_2/n_A, the relative concentrations of the electrons (for Mg read $\frac{n_1}{n_A}$ and $\frac{n_3}{n_A}$ — see Table 3); the values of $\alpha = \Sigma\alpha_i$ are computed according to equation (12) and the concentration data; the experimental values of α_{exp} are taken from the references listed in brackets in the last column. The values of $\frac{m^*}{m_0} = \frac{\alpha_{exp}}{\alpha}$.

With few exceptions the values of m^*/m_0 are very close to unity. Although these are only average values we can safely conclude that there are no effective masses greatly (by as much as an order of magnitude) exceeding unity and that in at least one of the groups of mobile particles the value of the effective mass must be close to unity (the reference unit mass is that of a free electron).

The above deductions also apply to beryllium in which the electron concentration, according to our data, amounts to approximately 10^{-2} per atom. For bismuth the mean value of the effective mass is about 0.5; this is not in conflict with the assumption regarding the smallness of the effective masses of the electrons[33] provided the effective mass of the holes is close to unity.

Conclusions

We have shown that combined investigations of the diverse galvanomagnetic effects in sufficiently pure metals at low temperatures yield detailed information on the properties of conduction electrons in metals. The investigated metals may be divided into two classes according to the character of the observed galvanomagnetic effects. The first class comprises metals in which the value of the Hall field (E_y/E_x) in strong fields decreases with increasing field intensity while the resistance increases without limit. The second class comprises metals in which the Hall field increases without limit in the magnetic field while the resistance tends to approach a finite saturation value. In order to explain the experimental results obtained it is necessary to assume that there is overlapping of the Brillouin zones in all the investigated metals (except the alkali metals) and that the conductivity is due to quasi-particles with opposite signs: holes and electrons. In metals belonging in the first class the number of holes equals the number of electrons, while in metals of the second class the numbers are not equal. For a more detailed interpretation of the experimental data it is necessary to postulate a model with several distinct groups of holes and electrons.

Further refinement of the theory of the metallic state is essential for complete utilization of the experimental data obtained. However, even with the present state of the theory, the results of investigations of the galvanometric effects can be used to evaluate the order of magnitude of the mobilities and concentrations of the mobile particles (charges) in metals.

References

1. P.L.Kapitsa, Proc. Roy. Soc., A123, 292 (1929).
2. W. de Haas & L.Schubnikov, Leid. Comm. No. 207 & No. 210 (1930).
3. B.G.Lazarev, Nakhimovich & Parfenova, Zhur. eksp. i teor, fiz. 9, 1169 (1939).
4. E.Justi, Phys. ZS., 41, 563 (1940).
5. M.Kohler, Ann d. Phys., 32, 211 (1938).
6. E.S.Borovik, Doklady AN SSSR, 69, 767 (1949).
7. E.Justi, Leitfähigkeit & Leitungsmechanismus festerStoffe, Gött. 1948.

8. D.Blokhintsev & L.Nordheim, Zs. f. Phys., 84, 168 (1933).
9. E.Sondheimer & A.Wilson, Proc. Roy. Soc., 190, 435 (1947).
10. Onnes H.Kamerlingh, H of K. Leid. Comm., No. 1426 (1914).
11. A.N.Geritzen & W.I.Haas, Physica, 7, 802 (1940).
12. E.Justi, Ann. d. Phys., 3, 183 (1948).
13. G.H.Kinchin, Proc. Roy. Soc., A217, 9 (1953).
14. E.S.Borovik, Doklady AN SSSR, 70, 601 (1950); 75, 639 (1950).
15. E.S.Borovik, Zhur. eksp. i teor. fiz. 23,83 (1953); 27, 355 (1954).
16. E.S.Borovik, Doklady AN SSSR, 96, 485 (1954).
17. E.Justi & H.Scheffers, Phys. ZS., 37, 475 (1936).
18. E.S.Borovik, Zhur. eksp. i teor. fiz. (forthcoming issue).
19. W. de Haas & J.Blom, Physica, 1, 134 (1934).
20. E.Justi & H.Scheffers, Phys. ZS., 37, 700 (1936); 38, 981 (1937).
21. C.Milner, Proc. Roy. Soc., 160, 207 (1937).
22. E.Grüneisen & H.Adenstat, Ann. d. Phys., 32, 211 (1938).
23. E.Justi, Ann. d. Phys., 41, 486 (1940).
24. A.Forroud & E.Justi, Phys., Zs, 41, 113 (1940).
25. A.Forroud & E.Justi & J.Kramer, Phys. ZS., 41, 308 (1940).
26. E.Justi, J.Kramer & R.Schulze, Phys. ZS., 41, 308 (1940).
27. J.A.Marcus, Phys. Rev., 76, 412 (1949).
28. B.I.Verkin, Doklady AN SSSR, 81, 529 (1951).
29. T.A.Kontorova & Ia.I.Frenkel', Zhur. eksp. o teor. fiz., 5, 405 (1935).
30. H.Jones, Proc. Roy. Soc., A155, 653 (1936).
31. M.Köhler, Ann. d. Phys., 22, 129 (1938).
32. B.I.Davydov & A.Ia.Pomeranchuk, Zhur. eksp. i teor. fiz., 9, 1295 (1939).
33. M.Köhler, Ann. d. Phys., 6, 186 (1949).
34. E.Sondheimer, Proc. Roy. Soc., A193, 484 (1948).
35. A.Eucken & F.Forster, Nachr. Ges. d. Wiss. Göttingen, 1, 43 (1934).
36. A.B.Pipard, Proc. Roy. Soc., A 191, 385 (1947).
37. E.S.Borovik & B.G.Lazarev, Doklady AN SSSR, 62, 611 (1948).
38. J.Esterman, S.A.Fridberg & J.E.Goldman, Phys. Rev., 87, 582 (1952).
39. R.W.Hill & P.L.Smith, Phil. Mag., 44, 636 (1953).
40. J.G.Danut & C.V.Neer, Phys. Rev., 76, 1113 (1949).
41. B.N.Samoilov, Doklady AN SSSR., 86, 281 (1952).
42. A.D.Misener & H.H.Wills, Proc. Roy. Soc., A 174, 262 (1940).
43. W.H.Keesom & P.H.VanLaer, Physica, 5, 193 (1938).
44. M.Horovitz & A.A.Silvidi, Phys. Rev., 88, 1182 (1952).
45. W.H.Keesom & N.Realman, Phys. Rev., 96, 897 (1954).

* * * * * * *

INVESTIGATION OF THE PHOTO-MAGNETOELECTRIC EFFECT IN CUPROUS OXIDE AT LOW TEMPERATURES

- A.P.Komar, N.M.Reinov & S.S.Shalyt

The present work is a continuation of the investigation of the photo-magnetoelectric effect in cuprous oxide, but at lower temperatures and in stronger fields than were employed in the original investigation by the discoverers of the effect.[1]

The Kikoin-Noskov photo-magnetoelectric effect consists of the following: if a plate of a semiconducting material, illuminated by light incident normal to its surface, is placed in a magnetic field there develops a potential difference, due to the internal photoeffect in a direction perpendicular to the magnetic field. Kinkoin and Noskov illuminated samples of Cu_2O with white light at 77° K and in individual cases obtained voltage differences of up to 20 v with an electric field gradient on the order of 5 v/cm. It was established that the photo-magnetoelectric difference of potential falls off rapidly with increasing temperature and at room temperatures is reduced to the sensitivity threshold of available measuring instruments.

Subsequent investigations by Kinkoin and others[2] showed that the field dependence of the photo-magnetoelectric difference of potential at the temperature of liquid nitrogen is linear up to fields of about $4 \cdot 10^3$ oersteds. A theoretical explanation of the effect was proposed by Frenkel'.[3] Briefly, the effect is interpreted as follows: the light incident on the specimen frees an electron-hole pair in the layer at the surface; the electron and hole start to diffuse into the material. The applied magnetic field changes the direction of their motion, thus giving rise to the photo-magnetoelectric effect.

Theory predicts that the field dependence of the effect should be linear when $(\mu H/c) \ll 1$, where μ is the mobility of the current carrier, H is the field and c is the speed of light.

It follows from theory that with an accuracy to within the first non-linear term of the expansion the above dependence of the photo-magnetoelectric emf on the magnetic field has the form

$$V = \frac{aH}{1 + (\mu H/c)^2}.$$

No investigations of cuprous oxide under conditions when the parameter $\mu H/c$ is commensurate with unity have been until now. The mobility of the current carriers under these conditions can be evaluated from the dependence of the photo-magnetoelectric emf on the intensity of the magnetic field.

According to the data of Engelhard[4] the values of μ in Cu_2O, computed from the conductivity and the Hall effect, are $\mu = 4 \cdot 10^4$ cgs at 200° K and $\mu = 4 \cdot 10^5$ at 80° K.

From the cited data we may conclude that the non-linear dependence of the emf at the temperature of liquid nitrogen should become manifest in fields of about 10^5 oersteds. Taking into account the fact that the mobility increases with decreasing temperature one may expect that at liquid helium temperatures the deviation from linearity will become apparent even at the field intensities used in the investigation of Kinkoin and Noskov.[1]

Thus the curves of the field dependence of the photo-magnetoelectric effects in fields to $H \geqslant c/\mu$ recorded at different temperatures can serve for experimental evaluation of the temperature dependence of the mobility of current carriers.

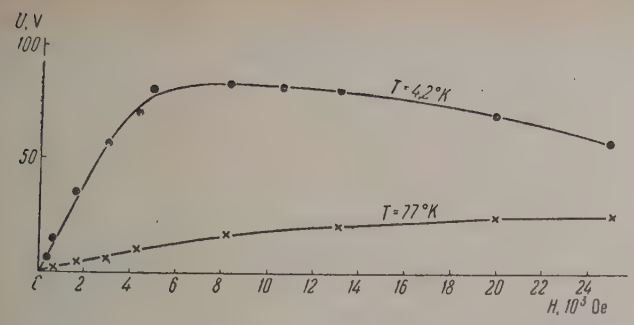

Variation of the photo-magnetoelectric effect in a sample of cuprous oxide with the magnetic field at 77° K and 4.2° K.

The cuprous oxide specimens we investigated were in the form of parallelepipeds measuring 0.4 x 10 x 40 mm. The specimens were illuminated by a conventional 500 watt incandescent bulb, directly or through a blue filter. Illumination with blue light enhanced the effect almost two-fold.

The specimens were investigated at two temperatures — 77° K and 4.2° K — and in fields of up to $2.5 \cdot 10^4$ oersteds. The results are shown in the accompanying figure. It will be seen that the deviation from linearity at 77° K starts in fields on the order of $6 \cdot 10^3$ oersteds and at 4.2° K in fields on the order of $3 \cdot 10^3$ oersteds.[5]

These data permitted evaluating the magnitude of the mobility of current carriers at the two indicated temperatures —

$$\mu_{77^\circ K} \approx 1.2 \cdot 10^6 \text{ cgs and } \mu_{4.2^\circ K} \approx 3.6 \cdot 10^6 \text{ cgs}$$

— and comparing the results with those of Engelhard.[4]

Bearing in mind the difficulty of obtaining samples of cuprous oxide with reasonably equal values of the mobility (usually the mobilities for different specimens of Cu_2O differ by an appreciable factor), the agreement between the values obtained by our method and that of Engelhard for the temperature of liquid nitrogen may be considered satisfactory.

It is interesting to note that the photo-magnetoelectric effect in our specimens attained 90 volts. The experimental results have been theoretically interpreted by A. I. Ansel'm.

Physico-Technical Institute of
the Academy of Sciences of the USSR

References

1. I.K.Kikoin & M.M.Noskov, Sow. Phys., 5, 586 (1934).
2. E.Lifshits, Sow. Phys., 9, 641 (1936); V.E.Lashkarev, Zhur. eksp. i teor. fiz., 18, 917,(1948); 18, 953 (1948); K.B.Tolpygo, Trudy Instituta fiziki AN USSR (Proceedings of the Physics Institute of the Ukrainian SSR Academy of Sciences), 3, 52 (1952); P.Agrain & H.Bulliard, C.R., 236, 6, 595 (1953); T.S.Moss, L.Pincherle & A.M.Woodward, Proc. Phys. Soc., B66, 743 (1953); H.Bulliard, Ann. de phys., 9, 52 (1954).
3. Ia.I.Frenkel', Sow. Phys., 5, 597 (1934).
4. E.Engelhard, Ann. de phys., 17, 501 (1933).
5. A.P.Komar, N.M.Reinov & S.S.Shalyt, Doklady AN SSSR, 96, 1, 47 (1954).
6. A.I.Ansel'm, Zhur. tekh. fiz., 24, 2064 (1954).

CERTAIN PROBLEMS RELATING TO THE QUANTUM-MECHANICAL THEORY OF CRYSTALS AT LOW TEMPERATURES

- S. V. Vonsovski

1

At low temperatures, when kT, the mean thermal energy per atom, becomes small compared with the energy of interaction between the atomic particles in a body, the body assumes a condensed state, either liquid (amorphous) or solid (crystalline). The dominant role, in this case, is played by the electric interaction between the atomic nuclei and the electrons. The weak magnetic interaction can, in the majority of cases, be considered as a small perturbation. From the mathematical viewpoint, the problem reduces to solution of the wave equation, which has the following form in the coordinate representation:

$$i\hbar \frac{\partial \Psi(\mathbf{r}_1, \ldots, \mathbf{r}_n; \mathbf{R}_1, \ldots, \mathbf{R}_N)}{\partial t} = \hat{H} \cdot \Psi(\mathbf{r}_1, \ldots, \mathbf{r}_n; \mathbf{R}_1, \ldots, \mathbf{R}_N), \quad (1.1) \qquad (1.1)$$

where Ψ is the wave function of the coordinates $\mathbf{r}_j$ of n electrons and the coordinates $\mathbf{R}_i$, of N nuclei; $h = 2\pi\hbar$ is a quantum of action and $\hat{H}$ is the Hamiltonian operator of the system, defined by

$$\hat{H} = -\frac{\hbar^2}{2M} \sum_{i=1}^{N} \Delta_{\mathbf{R}_i} - \frac{\hbar^2}{2m} \sum_{j=1}^{n} \Delta_{\mathbf{r}_j} + \hat{V}(\mathbf{r}_1, \ldots, \mathbf{r}_n; \mathbf{R}_1, \ldots, \mathbf{R}_N). \qquad (1.2)$$

Here M and m are, respectively, the nucleus and electron masses, $\Delta_{\mathbf{R}_i}$ and $\Delta_{\mathbf{r}_j}$ are Laplacian operators, and $\hat{V}$ the potential-energy operator of the electric interaction between particles. In the case of stationary states, (1.1) assumes the simpler form:

$$H \cdot \Psi = E\Psi, \qquad (1.3)$$

where E is the energy of the entire system. In view of understandable mathematical difficulties, it is impossible to solve (1.3) exactly or even approximately for the general case. The main cause of the mathematical difficulties is the "entanglement" of the coordinates of the micro-particles in the potential $\hat{V}$. Physically, this difficulty is due to the complexity of the couplings between the particles in the system. Unless simplifying assumptions are made concerning the form of the function $\hat{V}$, it is impossible to obtain any information on the general properties of solutions of (1.3) and (1.1). It is, therefore, necessary to resort to different approximate computation methods. Thus, for example, the fact that condensed systems have a discrete x-ray spectrum in the range of frequencies corresponding to electron transitions between the lowest levels of the atoms is frequently the basis of an approximation by which the condensed phase is considered to consist of two "autonomous" subsytems, namely, an aggregate of charged ions and collectivized electrons (former valence electrons of the gas atoms). The principal difference between the two subsystems is the difference between the masses of the ions and electrons. Using the ratio of the electron mass to that of an ion as a small dimsionless parameter, it is possible to effect in (1.3) an expansion in powers of this parameter and to develop an approximate theory, which is called the adiabatic approximation. It is assumed, in this treatment, that at any given instant the moving

electron system is described by a wave function that corresponds to an "immutable" distribution of the high-inertia ions. The adiabatic approximation can be applied only to condensed-body phenomena, in which the ion system does not play an active, "dynamic" part. That is, the ions are considered to be either perfectly stationary or, at most, undergoing small oscillations about "fixed" equilibrium positions. These oscillations are commonly regarded as a small perturbation, capable of causing only quantum transitions of the electron system between its stationary states, corresponding to an immutable configuration of the ion system. The adiabatic approximation precludes a consistent quantum-mechanical treatment of such effects as diffusion and plastic deformation, effects which in turn characterize the nature of structural phase transformations in condensed bodies. The active role of ionic motion must be taken into account even in the analysis of purely electronic effects. An illustrative example is furnished by the isotopic effect in superconductors.

Leaving open, for the time being, the question of overcoming the difficulties inherent in the adiabatic approximation, let us explore the theoretical possibilities of this approximation. To this end, in lieu of (1.3), we must attempt to solve the simpler equation

$$\hat{H}_{el}\Psi_{el} = E_{el}(\mathbf{R}_1, \ldots, \mathbf{R}_N)\,\Psi_{el}, \tag{1.4}$$

in which the wave function depends only on the electron coordinates, while the ion coordinates enter as parameters both in the wave function and in the energy of the electron system. The energy operator (1.4) does not contain operators associated with the kinetic energy of the ions or the potential energy of interaction between the ions. Solution of (1.4) in the usual coordinate representation comes up against serious mathematical difficulties.* Hence, a solution of (1.4) is usually sought in other representations. As was already mentioned, the main difficulty in solving (1.4) stems from the "entanglement" of the electron coordinates. If we disregard the interaction energy, the variables in (1.4) become separable, and the problem reduces to the solution of monotypic one-electron equations. The energy of the system is then the arithmetic sum of the energies of the individual electrons, and the wave function assumes the form of an antisymmmetrized sum of products of the single-electron functions. This one-electron approximation deprives us of the possibility of subsequently taking into account the properties of the system that stem from the existence of electron interaction.

The inherent limitations of the one-electron (zonal) approximation indicate the great need for development of a multi-electron theory of solid bodies. In the multi-electron treatment, the system wave function is usually sought in the form of a series of antisymmetrized products of one-electron functions:

$$\Psi_{el}(\mathbf{r}_1, \ldots, \mathbf{r}_n) = \sum_{\alpha_1, \ldots, \alpha_n} a(\alpha_1, \ldots, \alpha_n)\,\psi_{\alpha_1, \ldots, \alpha_n}(\mathbf{r}_1, \ldots, \mathbf{r}_n), \tag{1.5}$$

---

* The sole exceptions are the so-called one-dimensional problems (linear atomic chains) which in themselves are of little physical interest, and sometimes lead to erroneous results if attempts are made to generalize the resultant solutions to actual three-dimensional systems.

where $\alpha_1, \alpha_2, \ldots, \alpha_n$ are quantum numbers, defining the one-electron states, which are chosen as generalized coordinates of the system under investigation. If the orthonormalized functions $\psi_{\alpha_1, \ldots, \alpha_n}(r_1, \ldots, r_n)$ form a complete set, expansion (1.5) is exact and the coefficients $a(\alpha_1, \ldots, \alpha_n)$ are the exact wave function of the system in the new representation. Using the standard methods of the theory of unitary transformations, we can rewrite (1.4) in terms of the new representation. The energy operator in the usual representation has the form:

$$\hat{H}_{el} = -\frac{\hbar^2}{2m}\sum_{j=1}^{n}\Delta_{r_j} + \sum_{i,j} G(|r_j - R_i|) + \frac{1}{2}\sum_{j \neq j'} V(|r_j - r_{j'}|), \qquad (1.6)$$

i.e., it consists of an additive part (the kinetic energy and potential energy of electrons r_j in the ion field R_i, i.e. $G(|r_j - R_i|)$) and a binary part (energy of interactions between electrons, $V(|r_j - r_{j'}|)$). If the coordinates chosen for the new representations are the occupation numbers n_α of the single-electron states, operator (1.6) assumes the following form:

$$\hat{H}_{el}^{(\alpha)} = \sum_{\alpha, \alpha'} L(\alpha, \alpha')\hat{a}_\alpha + \hat{a}_{\alpha'} + \sum_{\alpha_1\alpha_2;\ \alpha_1'\alpha_2'} F(\alpha_1\alpha_2;\ \alpha_1'\alpha_2')\hat{a}_{\alpha_1}^{+}\hat{a}_{\alpha_2}^{+}\hat{a}_{\alpha_1'}\hat{a}_{\alpha_2'}, \qquad (1.7)$$

where L and F are the matrix elements of the individual components of the additive and binary parts of (1.6), respectively, calculated by means of the one-electron functions, and $\hat{a}_\alpha^{+}$ and $\hat{a}_\alpha$ are the operator second-quantization Fermi-amplitudes, acting on the wave functions from the occupation numbers. The product of these operators yields the state occupation number operator $\hat{n}_\alpha$, which in the given representation is diagonal:

$$\hat{a}_\alpha^{+}\hat{a}_\alpha = \hat{n}_\alpha; \qquad (1.8)$$

its eigenvalues are 0, 1, 2, 3, . . . The Fermi operators obey the anti-commutation rules:

$$\hat{a}_\alpha^{+}\hat{a}_{\alpha'} + a_{\alpha'}\hat{a}_\alpha^{+} = \delta_{\alpha\alpha'}. \qquad (1.9)$$

The principal theoretical problem lies in finding the eigenvalues of the energy operator (1.7). To solve such a problem is in general also virtually impossible, even in the second-quantization representation. It is more expedient to seek approximate solutions. It is possible to determine directly the eigenvalues of the operator (1.7) for the case when the operator has the form of the additive sum of the occupation-number operators. The energy of the system then becomes the sum of the energies of the effective "field" oscillators. representing the initial system of interacting particles. In solid-state theory, such a solution was first obtained in an investigation of the thermal motion of crystals, which can be treated as a gas comprised of elementary excitations: i.e., phonons. This method was employed even earlier in electromagnetic field theory, in which photons were assumed to be quantum oscillators of this type. In connection with these results, it must be borne in mind that even though the energy of the initial micro-particle system is characterized by the sum of the energies of the individual elementary oscillators, one should not identify the individual operators with the motions of individual initial particles, for such an oscillator represents the collective motion of the entire system as a whole.

Even if we discard the terms in (1.7) describing the interaction between the electrons, we still will be dealing, after diagonalization, not with the motion of the "free" particles of the initial system, but rather with the motion of a system consisting of the particle + the external field. For example, the energy of an electron in a crystal lattice is not simply the energy of a single electron, but of the electron and the lattice (only in case of vanishingly weak interaction between the electron and lattice can this energy be considered identical with that of a truly "free" electron).

It is evident, from the cited examples, that in studying the motion of a complicated system of interacting micro-particles we have to do with collective degrees of freedom, in which the motion of the system as a whole is dominant, while the individual attributes of the initial particles are secondary. As a consequence of the interaction between the particles of the initial system, there is established a definite correlation in the motion of the particles throughout the system, i.e., ordered oscillations of the density of the particles (or their charge, their spins, etc.). These collective degrees of freedom do not exhaust all the possible types of motions of a system of interacting particles. Other degrees of freedom, reminiscent in character of the individual motions of the initial system particles, also exist. Here, the correlation through the system does not come to the forefront, and we have to do with an analogue of the random thermal motions of molecules in a gas. In fact, we deal, in this case, with the motion of a single interacting collective of initial particles, and the abovementioned subdivision of the degrees of freedom of the system into collective and individual degrees of freedom is only approximate.

This raises an important question: in what cases and how is it permissible to effect such classifications of the "overtones" of the complex motion of a micro-system? Experience with theoretical calculations shows that this can be done when the system oscillates about some ground or normal state of equilibrium for the given type of oscillations. This condition is satisfied, for example, in the case of the thermal motion of a crystal lattice at low temperatures. In the case of ferromagnets it is feasible, we know, to consider small deviations from a ground state having spin saturation. In this case the elementary excitations of the electron system have the character of spin waves or ferromagnons. In semiconductors deviation from the normal state of the system on the part of the outer electrons is in the nature of elementary excitations, namely, different types of excitons (conducting or non-conducting), etc.

Thus, in the treatment of atomic systems comprised of many interacting particles it is possible to separate out collective degrees of freedom, which, provided the system is weakly excited in the vicinity of appropriate "homogeneous" ground states, can be represented in the form of "ideal" gases composed of quasi-particles.

By separating out in the Hamiltonian (1.7) of the system the terms of the second power relative to the second-quantization operators, we cannot completely eliminate the higher-order terms of these operators (cubic, fourth-power, etc.). We can merely say that if the system is weakly excited (relative to the homogeneous ground state) these higher-order terms are small. In the first approximation, they characterize the collision processes between quasi-particles, i.e., quantum transitions in the system between its stationary weakly-excited states. This gives us the possibility not only of determining the energy spectrum of the system (i.e., the dispersion

relationship between the energy — or frequency — and the quasi-momentum — or wave number — of the quasi-particles) and of computing the equilibrium values of the thermodynamic variables of the system, but also of successively solving a great number of kinetic problems for condensed phases in a state near the ground state, i.e., the region of cryogenic temperatures.

2

Use of the quasi-particle method, particularly where kinetic problems are concerned, naturally involves question of the type of statistics applicable to the quasi-particles. Without resolving this question it is impossible to write correctly the kinetic equation for any given problem. The choice is between Fermi or Bose statistics. In view of tne great diversity of the collective and individual degrees of freedom of complex systems of interacting electrons and ions, one can expect the motion of these systems to be represented by a combination of Bose and Fermi elementary-excitation gases.

Simplified or "graphic" methods are sometimes employed to determine the type of statistics. For example, it is known that in the case of a phonon gas any number of phonons (having the same value of quasi-momentum) can be excited simultaneously in a lattice; whence it follow that the phonons obey Bose statistics. Moreover, for particles obeying these statistics (bosons) the projection of the spin moment must be integral. In the case of phonons it equals zero, while for ferromagnons the projection equals unity, for every time a ferromagnon is created one electron with opposite spin appears in the system, and consequently the projection of the system spin changes by unity. In like manner it can be shown that in semiconductors, as a rule, excitons of different types form a boson gas.

The problem of the appearance of excitations obeying Fermi statistics (ferions) is more complicated. The distinctive features of these excitations are the half-integral value of the spin projections, their paired creation and annihilation, and the existence of a certain "boundary value" of the quasi-momentum. In the case of an ideal gas of non-interacting electrons the bound of the quasi-momentum is uniquely determined by the density of the gas; such uniqueness may not obtain for quasi-particles.

The type of statistics of the quasi-particles can be determined rigorously and uniquely by considering the commutation or anti-commutation relations of the second-quantization operators, corresponding to the given type of quasi-particles. If the relationship is of the type of (1.9), the quasi-particles are fermions; if it has the form

$$\hat{b}_f^{\dagger}\hat{b}_{f'} - \hat{b}_{f'}\hat{b}_f^{\dagger} = \delta_{ff'}, \qquad (2.1)$$

we are dealing with a boson gas.

The problem under consideration automatically brings up another problem, that of the connection between the statistics obeyed by the particles of the initial microsystem and the statistics of the elementary excitations. Thus, for example, the elementary excitation in liquid He^4 and He^3 have the forms of bosons and fermions, respectively.[1] But in the general case the initial system of Fermi particles can apparently have excitations of both types, while a system of Bose particles can comprise only Bose excitations. It must be noted that this problem is not yet definitively solved.[1]

Recently D. N. Zubarev[2] proposed a general method for separating the two branches of the elementary-excitation spectrum in systems of interacting electrons on the basis of a new method of transforming the initial Hamiltonian of the system (method of extra variables). Prior to this investigation it was assumed that the collective degrees of freedom in the initial fermion system are always of the boson type[3]. Zubarov was able to show, however, that this is not necessarily so and that the two different excitation branches (Fermi and Bose) can exist simultaneously.

Mention must also be made of another approach in the development in the theory, involving the application of methods developed in the theory of charged plasma[4,5] to the "collective" description of systems of interacting electrons and ions. This approach is of great promise where the quantum theory of condensed systems is concerned.

3

Inasmuch as this Conference is concerned with magnetism, we shall illustrate the method described by a treatment of ferromagnetic and antiferromagnetic transition metals. The characteristic feature of these metals is that their physical and chemical properties are affected not only by the former valence electrons, but also by the electrons of the internal unfilled layers of the electron shells of isolated atoms. Even through elementary analysis[6] it can be shown that the electrostatic exchange interaction between the outer (4s) and inner (3d) electrons in a ferromagnetic transition metal leads to a change in the s-electron energy, which becomes dependent on the direction of the spin projection relative to the magnetization of the inner d-electrons. This leads to dependence of the effective mass of the conduction electrons on the magnetization of the ferromagnetic. This magnetization, in turn, determines all the so-called "anomalies" of ferromagnets in the vicinity of the Curie point.[6,7] The s-d exchange interaction is also an important factor where the properties peculiar to ferromagnets at low temperatures in general are concerned.

Recently, it has proved feasible to generalize the theory of s-d exchange interaction by use of the method of second quantization,[9] as well as by taking magnetic interaction into account.[10-12] When the latter is taken into account the potential energy operator in (1.6), relating to the interaction of two electrons, proves to be dependent not only on the relative separation of the electrons but also on the vector operators of the momenta $\hat{\mathbf{p}}_j$ and $\hat{\mathbf{p}}_{j'}$ and the spin vector operators $\hat{\mathbf{s}}_j$ and $\hat{\mathbf{s}}_{j'}$:

$$\hat{\Phi}(j, j') \equiv V(|\mathbf{r}_j - \mathbf{r}_{j'}|;\ \hat{\mathbf{p}}_j,\ \hat{\mathbf{p}}_{j'};\ \hat{\mathbf{s}}_j,\ \hat{\mathbf{s}}_{j'}). \tag{3.1}$$

At sufficiently low temperatures (magnetic quasi-saturation) the total Hamiltonian of the system of the interacting outer and inner electrons can be represented as the sum of three terms:

$$\hat{H} = \hat{H}_0 + \hat{H}_{dd} + \hat{H}_{sd}. \tag{3.2}$$

When the first term, which is the principal part of operator (3.2) is diagonalized, it represents, to the first approximation, the energy spectrum of the system in the form of the sum of energies of two types of quasi-particles — ferromagnons (Bose branch) and conduction electrons (Fermi branch):

$$\hat{H}_0 = \sum_g \varepsilon_g \hat{n}_g + \sum_{k\sigma} E_{k\sigma} \hat{n}_{k\sigma} + U_0, \tag{3.3}$$

where U_0 is a constant independent of the state,

$$\varepsilon_g = \sqrt{A_g^2 + |B_g|^2} \tag{3.4}$$

is the energy of a ferromagnon with quasi-momentum g,

$$E_{k\sigma} = E_k^0 + \frac{1}{2}[D(k^+, k^+) + D(k^-, k^-)] + \sigma \sqrt{[D(k^+, k^+) - D(k^-, k^-)]^2 - 4|D(k^+, k^-)|^2} \tag{3.5}$$

is the energy of the conduction electron, dependent not only on its quasi-momentum k, but also on the spin projection σ (which can equal $\pm 1/2$), and E_k^0 is the energy of the conduction electron disregarding s-d interaction.

The second term of (3.2) describes the processes of creation and annihilation of ferromagnons due to their mutual collisions:

$$\hat{H}_{dd} = \sum_{g, g'} C_g \hat{b}_{g'}^+ \hat{b}_{g'+g} \hat{b}_g^+ + C_g^+ \hat{b}_{g'+g}^+ \hat{b}_{g'} \hat{b}_g, \tag{3.6}$$

where $\hat{b}_g^+$ and $\hat{b}_g$ are the Bose annihilation and creation operators, which conform to the commutation relationship (2.1); in addition, they are related to the ferromagnon number operator $\hat{n}_g$ by the equation: $\hat{b}_g^+ \hat{b}_g = \hat{n}_g$.

The last term of (3.2) pertains to the collision processes between the ferromagnons and the conduction electrons:

$$\begin{aligned}
\hat{H}_{sd} = &\sum_{(k, g)} C_+^{(0)}(k, g) \hat{b}_g^+ \hat{a}_{k-g}^+ (-1/2) \hat{a}_k (1/2) + \\
&+ \sum_{(k, g)} C_+^{(0)}(k, g) \hat{b}_g \hat{a}_{k+g}^+ (1/2) \hat{a}_k (-1/2) + \\
&+ \sum_{(k\sigma, g)} C_+^{(1)}(k\sigma, g) \hat{b}_g^+ \hat{a}_{k-g}^+ (\sigma) \hat{a}_k (\sigma) + \sum_{(k\sigma, g)} C_+^{(1)}(k\sigma, g) \hat{b}_g \hat{a}_{k+g}^+ (\sigma) \hat{a}_k (\sigma) + \\
&+ \sum_{(k, g)} C_+^{(2)}(k, g) \hat{b}_g^+ \hat{a}_{k-g}^+ (1/2) \hat{a}_k (-1/2) + \sum_{(k, g)} C_+^{(2)}(k, g) \hat{b}_g \hat{a}_{k+g}^+ (-1/2) \hat{a}_k (1/2).
\end{aligned} \tag{3.7}$$

The terms in (3.7) define the absorption and emission of ferromagnons by conduction electrons. It is easy to see that the first, second, and third lines of (3.7) describe processes characterized by

$$\Delta m = 0, \quad \Delta m = \pm 1 \text{ and } \Delta m = \pm 2,$$

respectively, where Δm is the change in the total magnetic quantum number of the system.

Higher-order terms, comprising the products of four or more $\hat{a}$ and $\hat{b}$ operators, are not included in operators (3.6) and (3.7); they correspond to more complex and hence less probable (assuming weak excitation) "collision" processes.

The actual forms of the coefficients A_g, B_g and $D(k\sigma, k\sigma')$, entering into (3.4) and (3.5), as well as the forms of the collision probability amplitudes C_g, $C_+^{(0)}(k, g)$, etc., in (3.6) and (3.7), are determined by the form of the interaction operator (3.1).

Let us examine the case when in addition to the electric interaction between electrons their magnetic spin-spin interaction is taken into account, i.e., when (3.1) has the form

$$\hat{\Phi}(jj') = V(r_{jj'}) + 4\mathfrak{M}^2 [r_{jj'}^2 (\hat{S}_j \hat{S}_{j'}) - 3(r_{jj'} \hat{S}_j)(r_{jj'} \hat{S}_{j'})] r_{jj'}^{-5}; \tag{3.8}$$

here $\hat{S}$ is the vector spin operator (in $\hbar$ units), $r_{jj'} = |\mathbf{r}_j - \mathbf{r}_{j'}|$ and $\mathfrak{M} = e\hbar/2mc$ is the Bohr magneton.

In this case the coefficients entering into (3.3), (3.4) and (3.5) are determined as follows:

$$A_g = I_n(1 - e^{igr_n}) + 3\sum_n (J_n - E_n) - \sum_n (J_n - E_n)(1 - e^{-igr_n}) + 2\mathfrak{M}H, \tag{3.9}$$

where

$$I_n = \int \varphi^*(\mathbf{r}_1)\varphi^*(\mathbf{r}_2 - \mathbf{n})\,V(r_{12})\,\varphi(\mathbf{r}_2)\,\varphi(\mathbf{r}_1 - \mathbf{n})\,d\mathbf{r}_1\,d\mathbf{r}_2, \tag{3.10}$$

$$E_n = \mathfrak{M}^2 \int |\varphi(\mathbf{r}_1)|^2 r_{12}^{-3}\left(1 - 3\frac{z_{12}^2}{r_{12}^2}\right)|\varphi(\mathbf{r}_2 - \mathbf{n})|^2\,d\mathbf{r}_1\,d\mathbf{r}_2, \tag{3.11}$$

$$J_n = \mathfrak{M}^2 \int \varphi^*(\mathbf{r}_1)\varphi^*(\mathbf{r}_2 - \mathbf{n})\,r_{12}^{-3}\left(1 - 3\frac{z_{12}^2}{r_{12}^2}\right)\varphi(\mathbf{r}_2)\,\varphi(\mathbf{r}_1 - \mathbf{n})\,d\mathbf{r}_1\,d\mathbf{r}_2, \tag{3.12}$$

H is the external magnetic field, and $\varphi(\mathbf{r})$ is the atomic wave function of the d-electron;

$$B_g = \sum_n e^{igr_n}\left[(J_n^{xx} - E_n^{xx}) - (J_n^{yy} - E_n^{yy}) - 2i(J_n^{xy} - E_n^{xy})\right], \tag{3.13}$$

where E_n^{jl} and J_n^{jl} $(j, l \equiv x, y, z)$ are obtained from (3.11) and (3.12) respectively by replacing $r_{12}^{-3}\left(1 - 3\frac{z_{12}^2}{r_{12}^2}\right)$ with $3r_{12}^{-5}(\mathbf{r}_{12})_j(\mathbf{r}_{12})_l$;

$$D(\mathbf{k}\sigma; \mathbf{k}\sigma) = C(\mathbf{k}) - \frac{1}{2}I(\mathbf{k}, \mathbf{k}) + \sigma\{I(\mathbf{k}, \mathbf{k}) - 2[K(\mathbf{k}, \mathbf{k}) - R(\mathbf{k}, \mathbf{k})]\}, \tag{3.14}$$

$$D(\mathbf{k}^+, \mathbf{k}^-) = D^*(\mathbf{k}^-, \mathbf{k}^+) = [(R^{xz}(\mathbf{k}, \mathbf{k}) - K^{xz}(\mathbf{k}, \mathbf{k})) - i(R^{yz}(\mathbf{k}, \mathbf{k}) - K^{yz}(\mathbf{k}, \mathbf{k}))], \tag{3.15}$$

where

$$C(\mathbf{k}) = N\int |\varphi(\mathbf{r}_1)|^2 V(r_{12})\,|\psi_k(\mathbf{r}_2)|^2\,d\mathbf{r}_1\,d\mathbf{r}_2, \tag{3.16}$$

$$I(\mathbf{k}_1, \mathbf{k}_2) = N\int \varphi^*(\mathbf{r}_1)\,\psi_{\mathbf{k}_1}^*(\mathbf{r}_2)\,V(r_{12})\,\varphi(\mathbf{r}_2)\,\psi_{\mathbf{k}_2}(\mathbf{r}_1)\,d\mathbf{r}_1\,d\mathbf{r}_2, \tag{3.17}$$

$$K(\mathbf{k}_1, \mathbf{k}_2) = N\mathfrak{M}^2\int |\varphi(\mathbf{r}_1)|^2\,r_{12}^{-3}\left(1 - 3\frac{z_{12}^2}{r_{12}^2}\right)\psi_{\mathbf{k}_1}^*(\mathbf{r}_2)\,\psi_{\mathbf{k}_2}(\mathbf{r}_2)\,d\mathbf{r}_1\,d\mathbf{r}_2, \tag{3.18}$$

$$R(\mathbf{k}_1, \mathbf{k}_2) = N\mathfrak{M}^2\int \varphi^*(\mathbf{r}_1)\,\psi_{\mathbf{k}_1}^*(\mathbf{r}_2)\,r_{12}^{-3}\left(1 - 3\frac{z_{12}^2}{r_{12}^2}\right)\varphi(\mathbf{r}_2)\,\psi_{\mathbf{k}_2}(\mathbf{r}_1)\,d\mathbf{r}_1\,d\mathbf{r}_2, \tag{3.19}$$

($\psi_k(\mathbf{r})$ is the non-localized wave function of the s-electron in the lattice), and $K^{jl}(\mathbf{k}_1, \mathbf{k}_2)$ and $R^{jl}(\mathbf{k}_1, \mathbf{k}_2)$ are obtained respectively from $K(\mathbf{k}_1, \mathbf{k}_2)$ and $R(\mathbf{k}_1, \mathbf{k}_2)$ by replacing $r_{12}^{-3}\left(1 - 3\frac{z_{12}^2}{r_{12}^2}\right)$ with $3r_{12}^{-5}(\mathbf{r}_{12})_j(\mathbf{r}_{12})_l$; ; lastly, we have in (3.6) and (3.7)

$$C_g = \frac{2}{V\overline{N}}\sum_n e^{igr_n}\left[(J_n^{xz} - E_n^{xz}) + i(J_n^{yz} - E_n^{yz})\right], \tag{3.20}$$

$$C_{\mp}^{(0)}(\mathbf{k}, \mathbf{g}) = -\frac{1}{V\overline{N}}[I(\mathbf{k}, \mathbf{k} \mp \mathbf{g}) + K(\mathbf{k}, \mathbf{k} \mp \mathbf{g}) - R(\mathbf{k}, \mathbf{k} \mp \mathbf{g})], \tag{3.21}$$

$$\begin{aligned} C_-^{(1)}(\mathbf{k}^+, \mathbf{g}) = C_+^{(1)*}(\mathbf{k}^+, -\mathbf{g}) = -C_-^{(1)}(\mathbf{k}^-, \mathbf{g}) = -C_+^{(1)*}(\mathbf{k}^-, -\mathbf{g}) = \\ = \frac{1}{V\overline{N}}\{[R^{xz}(\mathbf{k} - \mathbf{g}, \mathbf{k}) - iR^{yz}(\mathbf{k} - \mathbf{g}, \mathbf{k})] - \\ - [K^{xz}(\mathbf{k} - \mathbf{g}, \mathbf{k}) - iK^{yz}(\mathbf{k} - \mathbf{g}, \mathbf{k})]\}, \end{aligned} \tag{3.22}$$

$$C_{-}^{(2)}(\mathbf{k}, \mathbf{g}) = C_{+}^{(2)*}(\mathbf{k}, -\mathbf{g}) = \frac{1}{\sqrt{N}} \{[R^{xx}(\mathbf{k}-\mathbf{g}, \mathbf{k}) - R^{yy}(\mathbf{k}-\mathbf{g}, \mathbf{k}) + 2iR^{xy}(\mathbf{k}-\mathbf{g}, \mathbf{k})] - [K^{xx}(\mathbf{k}-\mathbf{g}, \mathbf{k}) - K^{yy}(\mathbf{k}-\mathbf{g}, \mathbf{k}) + 2iK^{xy}(\mathbf{k}-\mathbf{g}, \mathbf{k})]\}. \quad (3.23)$$

Using equations (3.10) to (3.19) we can deduce specific expressions for the ferromagnon energy (3.4) and the energy of a conduction electron (3.5).

We note that the coefficients (3.9) and (3.13) are expressed in terms of two types of integrals: quasi-classical (E_n and E_n^{jl}) and exchange (I_n, J_n and J_n^{jl}). If we assume, as is usually done,[13] that the magnetic moments of the d-electrons are "bound" to the corresponding lattice sites (which is formally equivalent to replacing the square of the modulus of the atomic function $\varphi(r)$ by a delta function: $|\varphi(r)|^2 = \delta(r)$), then discarding the terms with the magnetic exchange integrals J_n and J_n^{jl} makes the coefficients A_g and B_g exactly equal to the corresponding values obtained in Ref. 13. The advantage of the calculation method employed here is that it permits of taking into account simultaneously and automatically both the quasi-classic and the anisotropic (magnetic) exchange interaction.

The integrals E_n and E_n^{jl} diminish relatively slowly with the distance (n) between the lattice sites and the nearest-neighbor approximation cannot be employed for their sums in (3.9) and (3.13). In Ref. 13 the summation was replaced in this case by integration over the entire volume of the crystal. The exchange-type integrals I_n, J_n and J_n^{jl}, on the contrary, decrease rapidly with the distance between sites and consequently the nearest-neighbor approximation can be used to calculate the portions of coefficients A_g and B_g corresponding to these integrals (in other words, when g is small, the exponents in (3.9) and (3.13) can be expanded into a series in powers of (gn)). Thus, for example, for a cubic lattice, assuming weak excitation ($ag \ll 1$), we obtain*

$$A_g = [I - J(1 - 3\cos^2\theta_g)](ag)^2 + 4\pi \mathfrak{M} M_0 \sin^2\theta_g + 2\mathfrak{M} H, \quad (3.24)$$

$$B_g = [4\pi \mathfrak{M} M_0 - \sqrt{(J^2 + J'^2)}(ag)^2] \sin^2\theta_g e^{2i\varphi_g}, \quad (3.25)$$

where θ_g and φ_g are the polar and azimuthal angles of the vector g, respectively, a is the lattice constant, $M_0 = \mathfrak{M} a^{-3}$ is the magnetic moment per unit volume at T = 0°K, $I = \frac{1}{2}\sum n^{(x)s} I_n$ is a quantity of the order of magnitude of the integral relating to the electrostatic exchange interaction between the nearest neighbors, and

$$J = \frac{1}{2}\sum_n (n^{(x)s} - n^{(y)s}) J_n^{xx} \quad \text{and} \quad J' = \sum_n n^{(x)} n^{(y)} J_n^{xy}$$

are quantities characterizing the magnetic exchange interaction.

If we restrict the examination to the temperature region in which $\overline{J(ag)^2} \sim xT \gg \frac{\mathfrak{M}^2}{a^3}$, i.e., T $\gg 0.1$°K (on the other hand, of course, T $\ll T_C$, where T_C is the Curie point), we have $A_g \gg |B_g|$ and, conse-

---

* In this case the components of the vector n are $n^{(x)}a$, $n^{(y)}a$, $n^{(z)}a$.

quently, according to (3.4), $\varepsilon_g \approx A_g$. Furthermore, if we are not interested in magnetic anisotropy effects, the last expression can be simplified even more by neglecting the angular dependence contained therein, (by replacing $\cos^2\theta_g$ and $\sin^2\theta_g$ in (3.24) by their values averaged over the entire quasi-momentum space, i.e., by 1/3 and 2/3, respectively). In this approximation we get

$$\varepsilon_g = I(ag)^2 + 2\mathfrak{M}H', \tag{3.26}$$

where

$$H' = H + \frac{4\pi}{3}M_0.$$

The magnetic interaction between the electrons is thus considered as merely the cause of a certain average (Lorentz) internal field $(4\pi/3)M_0$, superposed on the external field.

In calculating the conduction-electron energy from equation (3.5) we must take into account the fact that the electrostatic exchange integral $I(\mathbf{k}, \mathbf{k})$ is considerably greater than the magnetic exchange integrals $K^{jl}(\mathbf{k}, \mathbf{k})$ and $R^{jl}(\mathbf{k}, \mathbf{k})$ and, consequently,

$$D(\mathbf{k}^+, \mathbf{k}^+) - D(\mathbf{k}^-, \mathbf{k}^-) \gg |D(\mathbf{k}^+, \mathbf{k}^-)|.$$

We can, therefore, assume approximately that

$$E_{\mathbf{k}\sigma} = E^0_{\mathbf{k}} + \frac{1}{2}(1+2\sigma)D(\mathbf{k}^+, \mathbf{k}^+) + \frac{1}{2}(1-2\sigma)D(\mathbf{k}^-, \mathbf{k}^-). \tag{3.27}$$

Let us now represent the electron wave function $\psi_{\mathbf{k}}(\mathbf{r})$ in (3.16) to (3.19) in form of a series in terms of the "atomic" functions of the s-state:

$$\psi_{\mathbf{k}}(\mathbf{r}) = N^{-1/2}\sum_{\mathbf{n}} e^{i\mathbf{k}\mathbf{n}}\chi(\mathbf{r}-\mathbf{n}). \tag{3.28}$$

Integrals in (3.16) to (3.19) will then appear in the form of double summations over the lattice sites. Here we can restrict ourselves to the nearest-neighbor approximation for exchange-type integrals $I(\mathbf{k}_1, \mathbf{k}_2)$, $R(\mathbf{k}_1, \mathbf{k}_2)$, and $R^{jl}(\mathbf{k}_1, \mathbf{k}_2)$ in both summations. In the integrals of the quasi-classical type $E(\mathbf{k})$, $K(\mathbf{k}_1, \mathbf{k}_2)$, $C(\mathbf{k})$, and $K^{jl}(\mathbf{k}_1, \mathbf{k}_2)$ this approximation can be used in only one of the summations, while the second summation must be carried out over the entire volume of the crystal. In the case of the integrals $K(\mathbf{k}_1, \mathbf{k}_2)$ and $K^{jl}(\mathbf{k}_1, \mathbf{k}_2)$ the last summation can be replaced by integration. Let us also invoke the effective-mass approximation, i.e., in those cases where the nearest-neighbor approximation can be used, let us expand $e^{i\mathbf{k}\mathbf{n}}$ in powers of $\mathbf{k}\mathbf{n}$ and neglect terms of order higher than the second. In this case, we obtain for (3.27):[12]

$$E_{\mathbf{k}\sigma} = 2\sigma(\alpha' + \mathfrak{M}H') + \frac{\hbar^2(k_x^2+k_y^2)}{2m^\sigma_\perp} + \frac{\hbar^2 k_z^2}{2m^\sigma_\parallel}, \tag{3.29}$$

where

$$m^\sigma_\perp = \frac{\hbar^2}{2a^2[\beta - 2\sigma(\beta' + R)]} \tag{3.30}$$

is the "transverse" effective mass, and

$$m^\sigma_\parallel = \frac{\hbar^2}{2a^2[\beta - 2\sigma(\beta' - 2R)]} \tag{3.31}$$

is the "longitudinal" effective mass of the conduction electrons. Thus the effective mass of conduction electrons in a ferromagnetic transition metal proves to be an anisotropic quantity while the effective-mass tensor has axial symmetry (in a cubic crystal!). A

similar expression for the effective mass can also apparently be used for an isotropic polycrystalline specimen, magnetized to saturation along the z-axis. This result may help to explain the difference between the values of the longitudinal and transverse resistivity of a ferromagnetic metal, magnetized to saturation[14*].

If we neglect the added anisotropic terms, (3.29) takes the following form:

$$E_{k\sigma} = 2\sigma(\alpha' + \mathfrak{M}H') + (\beta - 2\beta')(ak)^2. \tag{3.32}$$

For H' = 0, this expression agrees with the corresponding expression given in Ref. 9.

Lastly, let us write the expressions for the amplitudes of the transition probabilities (3.20)-(3.23), computed on the basis of the same assumptions as made above. Here, for one of the polar angles for $C_{\pm}^{(1)}(k, g)$ and $C_{\pm}^{(2)}(k, g)$ we choose the angle between vectors k and g. We obtain, with an accuracy to within the first non-vanishing terms of the expansion in powers of g and to within terms of an order not higher than the second in the expansion in powers of k:

a) For collisions between ferromagnons:

$$C_g = -\frac{1}{V\overline{N}}[4\pi W_0 + J'(ag)^2]\sin 2\theta_g e^{-i\varphi_g}, \tag{3.33}$$

where $W_0 = \mathfrak{M}^2 a^{-3}$. This expression differs from the corresponding expression given by A. I. Akhiezer[15] in that it contains within the brackets a second term that appears due to the fact that here magnetic exchange interaction is taken into account. Since the average value of $(ag)^2$ equals $\varkappa T/I \sim T/T_C$, the effect of the anisotropic exchange on the collision probability diminishes with decreasing temperatures and becomes negligibly small compared with the effect of the quasi-classical magnetic interaction at $T \ll (W_0/J')T_C$. Assuming that the magnetic exchange integral J' has the same order of magnitude as W_0, this will hold for the entire temperature range $T \ll T_C$ under consideration. On the other hand, if we assume that J' is one order of magnitude (or even two) greater than W_0, as is sometimes done in explanations of the magnetic anisotropy, the effect of the anisotropic exchange will be appreciable over a rather wide range of low temperatures.

b) For collisions between ferromagnons and conduction electrons: with $\Delta m = 0$:

$$C_{\pm}^{0}(k, g) = -\frac{1}{V\overline{N}}\{2\alpha' - \beta' a^2[k^2 - (k \pm g)^2]\}; \tag{3.34}$$

terms due to magnetic interaction are omitted here, since they exhibit the same dependences on k and g as the terms in (3.34) but are much smaller in magnitude;
with $\Delta m = \pm 1$:

$$C_{\pm}^{(1)}(k, g) = -\frac{R}{V\overline{N}}(ak)^2 \sin\theta_{kg}\left(\cos\theta_{kg} \pm \frac{g}{2k}\right)e^{-i\varphi_k}, \tag{3.35}$$

---

* A similar analysis of the conduction-electron energy could be carried out for temperatures near the Curie point, by employing the energy centroid approximation for the d-electrons.[11] In this case σ in (3.29) must be replaced by $\sigma\mu$, where μ is the magnetization (in Bohr magnetons) per site.

with $\Delta m = \pm 2$:

$$C_{\pm}^{(2)}(\mathbf{k}, \mathbf{g}) = -\frac{1}{\sqrt{N}}(ak)^2 \sin^2 \theta_{kg}(R\cos 2\varphi_k - iR'\sin 2\varphi_k). \tag{3.36}$$

Another type of magnetic interaction that can be treated in the framework of the model employed here is the interaction of the magnetic spin moments of d-electrons with the magnetic fields associated with the movement of the conduction electrons (this interaction might be termed "spin-orbital" interaction). The operator (3.1), corresponding to this interaction, assumes the form

$$\hat{\Phi}_{s\text{-}o}(jj') = -i4\mathfrak{M}^2 r_{jj'}^{-3}[\mathbf{r}_{jj'} \cdot \nabla_{j'}]\hat{\mathbf{S}}_j, \tag{3.37}$$

where the index j pertains to the d-electron and j' pertains to the s-electron. Under the approximations employed, this interaction has no effect on value of the ferromagnon energy or the conduction electron energy, for the non-vanishing matrix elements of operator (3.37) enter only into the expressions for the probability amplitudes of collisions between the ferromagnons and the conduction electrons, and do not appear in (3.26) or (3.29). Such an interaction between the d- and s-electrons can lead only to collision processes of the $\Delta m = \pm 1$ type (this is due to the linearity of the operator (3.37) relative to $\hat{S}_j$. Approximate calculations give the following expression for the collision probability (in the first approximation):

$$C_{\pm}^{(1)}(\mathbf{k}, \mathbf{g}) = \pm\frac{8\pi W_0 Lk}{\sqrt{N}g}\sin\theta_{kg}e^{i\varphi_k}, \tag{3.38}$$

where

$$L = a\sum_{\mathbf{n}} n^{(x)}\int \chi(\mathbf{r})\frac{\partial}{\partial x}\chi(\mathbf{r}-\mathbf{n})\,d\mathbf{r}.$$

If, instead of (3.28) we take the ordinary wave functions of a free electron (plane waves) for the wave functions of the s-electrons, L in expression (3.38) becomes equal to unity.

The above results of our calculations of the energy spectrum of the system of outer and inner electrons of a ferromagnetic transition metal, and of the probability of quantum transitions in this system, permit of developing a theory of relaxation processes and a theory of electric conductivity of ferromagnetics at low temperatures. These topics are covered in two papers by E. A. Turov.[16]

The entire scheme given above can be generalized to include the anti-ferromagnetic transition metals.[17] In these metals the zero state is a single state with an antiparallel ordered distribution of the spins over the lattice sites. We have as yet no proof that such a state is really the lowest energy state. However, neutron diffraction experiments[18] favor the hypothesis of ordered magnetic sublattices. In the case of antiferromagnetic materials small deviations from full magnetic ordering in the region of low temperatures also have the nature of spin waves, or antiferromagnons. However, the dispersion law for these excitations differs from that for ferromagnets. Specifically, we have in lieu of (3.26) a "linear" law:

$$\varepsilon_g \approx \alpha g. \tag{3.39}$$

The temperature dependence of the resistance of antiferromagnetic metals of the transition group differs from that of ferromagnetic metals. This difference stems from the difference in that part of the resistance which is due to collisions of conduction

electrons with antiferromagnons in antiferromagnets and with ferromagnons in ferromagnets. Specifically, in antiferromagnets

$$\rho_{\text{antifm}} = a_1 T^2 + a_2 T^4 \tag{3.40}$$

while in ferromagnets the "ferromagnon" part of the resistance is given by

$$\rho_{\text{fm}} = b_1 T + b_2 T^2 \tag{3.41}$$

It was assumed in the foregoing discussion that terms relating to interaction between conduction electrons are absent from the operator (3.2). Actually such terms do exist and are characterized by

$$\hat{H}_{ss} = \sum_{k_1, k_2, k_1', k_2', \sigma_1, \sigma_2} F(k_1, k_2; k_1', k_2') \hat{a}^+_{k_1\sigma_1} \hat{a}^+_{k_2\sigma_2} \hat{a}_{k_2'\sigma_2} \hat{a}_{k_1'\sigma_1}. \tag{3.42}$$

If (3.42) can be regarded as a perturbation, this term in the Hamiltonian can be considered as the cause of collisions between conduction electrons. These collisions also affect the resistance of the metal. The temperature dependence of this part of the resistance is described by[19]:

$$\rho_{ss} = \alpha T^2 + \beta T^3 \tag{3.43}$$

This problem was treated by L. D. Landau and I. Ia. Pomeranchuk in the framework of the one-electron theory of metals.

Since the resulting expressions for the temperature dependence of resistance of transition metals are of complicated "polynomial" form, very careful experimental verification of these theoretical expressions is indicated. It would be desirable to devise an experimental arrangement which would permit "turning on" or "off" the mechanisms responsible for the different terms in the expression for the resistance. Presumably the realization of such experiments would lean rather heavily on the methods of magnetic radio spectroscopy and ferromagnetic resonance.

4

Hitherto it has generally been assumed that the quasi-particles — current carriers — in metals are free (conduction) electrons subject to Fermi statistics. A strong argument in favor of this assumption was the apparently universal character of the temperature dependence of the resistance of metals at low temperatures (the familiar "T^5 law"). However, a more careful examination of the experimental data indicates that the "T^5 law" is not quite so universal as has been assumed. One of the reasons for departures from the law in normal (not transition group) metals may be that the current carriers are not fermions but bosons. In connection with this we must dwell briefly on the so-called polar model of metals (see Ref. 21), semiconductors and semimetals. It is known that semiconductors differ from metals in that in the ground state of the former the electron charge distribution is uniform throughout the crystal, and is not altered by the imposition of an external field (provided the field is not strong enough to cause ionization).

However, deviations from this uniform distribution are possible. These deviations may vary in character: there may be fluctuations in charge density, in the distribution of single-electron states over

the sites, in the spins, etc. An example of the first type of fluctuation is furnished by the elementary excitations that result from ionization of the individual lattice sites. Each such ionization leads to the appearance of two quasi-particles in the crystal — "doublets" and "holes" — which by virtue of translational symmetry will propagate freely through the lattice and carry an electric charge. Since there is no limiting momentum in this case and no restriction whatever on the number of such particles with any given quasi-momentum, these particles obviously obey Bose statistics. We can distinguish two subgroups among these quasi-particles: excitations of the "adhering" double and hole type (analogue of elliptic orbits in atoms), which carry no current, and excitations of the "free" hole and doublet type, capable of carrying current (hyperbolic orbits!). In addition to such "non-excited" doublets (where both electrons are in the same orbital state but have opposite spin projections), one can conceive of a disturbance in the homogeneity of the electron charge distribution in the crystal produced by excitation waves or "excitons." In this case there is excitation of the electrons near the lattice sites. Here either only an excitation wave carrying no charge (Frenkel currentless excitons) may be propagated through the lattice or an electron in an excited state may travel from site to site, regardless of the presence of another valence electron at the sites (current-carrying excitons). In the latter case, the hole left by the excited electron also migrates through the crystal by virtue of "relay-race" transitions of electrons from neighboring sites.

All these considerations can be extended to the case of metals and semimetals. In semiconductors excitons of all types are absent at absolute zero. In metals, on the other hand, a finite current is possible even at 0°K. This means that there is no energy gate between the excited and ground state and the current states adjoin the lowest level. We may expect spontaneous polarization to obtain in the electron system and, therefore, even the lowest energy state will be characterized by a finite number of doublets, holes or current-carrying excitons. It is difficult to explain the spontaneous polarization in the light of classical theory. Quantum mechanics, however, predicts the possibility of spontaneous polarization in the case when the lowest energy band, corresponding to the polarized states, lies below the deepest level of the uniform charge distribution band, even though according to classical theory the centroids of these energy bands should always lie higher for polarized states.

We can distinguish between two cases: that of a weakly polarized metal (small number of doublets and holes) and that of a strongly polarized metal (number of holes and doublets approaching the maximum possible). In either case one can postulate quasi-particles, characterizing deviations from the homogeneous electron charge distribution. These quasi-particles will obey Bose statistics.

Analyses show that in both a weakly[22] and strongly[23] polarized metal with a Bose electron energy spectrum the temperature dependence of the resistance differs markedly from the "T^5 law", namely,

$$\begin{aligned} \rho &= aT \quad \text{with} \quad T < \theta_1 \\ \rho &= bT^2 \quad \text{with} \quad \theta_1 < T < \theta \end{aligned} \tag{4.1}$$

where $\theta_1 \sim$ 1-10°K and θ is the Debye temperature. This temperature dependence obtains for "poor" metals: hafnium, graphite, zirconium, caesium, tungsten, potassium, arsenic, etc.

We have examined a number of properties of semiconductors in the light of the polar-exciton model. Our analysis indicates that in the case of ferromagnetic semiconductors, in which spontaneous magnetization is determined by the excited states, the spontaneous magnetization should disappear not only at the Curie point but also at 0°K.[24] This dependence will not obtain if the dominant role in the magnetization is played by the normal states (homogeneous as regards the excited states but not with respect to spins) of the electron system in the crystal. It also proved possible to evaluate, in the framework of this model, the temperature dependence of the conductivity of atomic semiconductors free of impurities.[25]

This model helps explain the existence of so-called semimetals, i.e., substances in which the temperature dependence is that of a metal or that of a semiconductor, depending on the temperature. Spontaneous polarization at low temperatures results in a metallic type resistance variation; as the temperature increases, excitation effects, due to new groups of conduction electrons, assume the dominant role, leading to a temperature dependence of the resistance characteristic of semiconductors. Examples of such substances are the selenides of lead, chromium, sulfur, etc.

The quasi-particle method has also proved applicable to the investigation of the electric and magnetic properties of crystal systems, more complicated than those of pure metals and semiconductors. Thus, it was possible to show, for example, that in the case of ferromagnetic ferrites the spontaneous magnetization in the low temperature region varies not as $T^{3/2}$ but as T^2, which is substantiated by Pauthenet's[27] experimental studies of iron, nickel and cobalt ferrites.

5

The quasi-particle method, as applied in quantum theory treatment of the condensed phase, is admittedly an approximate method. However, in the region of low temperatures it yields satisfactorily accurate predictions regarding the general properties and the character of the regularities in the behavior of solids. A thorough check on the deductions from theory and its further refinement are necessary; this calls for careful and systematic experimental investigations of the physical properties of crystals at low and ultra-low temperatures. One can safely predict that the results of extensive experimental studies of solids at cryogenic temperatures will largely determine the future development of our theoretical concepts concerning the attributes of condensed systems.

Institute of the Physics of Metals
of the Ural Branch of the USSR
Academy of Sciences

References

1. L.D.Landau & E.M.Lifshits, Statisticheskaia fizika (Statistical Physics), M-L. 1951.
2. D.N.Zubarev, Zhur. eksp. i teor. fiz., 25, 548 (1953).
3. S. Tomonaga, Progr. Theor. Phys., 5, 544 (1950).
4. D.Bohm & D.Pines, Phys. Rev., 82, 625 (1951);85, 338 (1952); 92, 609 (1952).
5. P.S.Zyrianov, Zhur. eksp. i teor. fiz., 25, 411 (1953).
6. S.V.Vonsovski, Zhur. eksp. i teor. fiz., 16, 981 (1946).
7. S.V.Vonsovski, Sovremennoe uchenie o magnetizme (Modern Magnetism), Sec. 17, M.-L. 1953.

8. S.V.Vonsovski, Zhur. eksp. i teor. fiz., 18, 145 (1948).
9. S.V.Vonsovski, & E.A.Turov, Zhur. eksp. i teor. fiz., 24, 419 (1953).
10. E.A.Turov, Doklady AN SSSR, 98, 945 (1954).
11. S.V.Vonsovski, K.B.Vlasov & E.A.Turov, Zhur. eksp. i teor. fiz., 29, 37 (1955).
12. E.A.Turov, Thesis, Sverdlovsk, 1955.
13. T.Holstein & H.Primakoff, Phys. Rev., 58, 1098 (1940).
14. S.V.Vonsovski & K.P.Rodionov, Doklady AN SSSR, 75, 643 (1950).
15. A.I.Akhiezer, Journ. of Phys., 10, 217 (1946).
16. E.A.Turov, present issue of the Bulletin (the two following articles).
17. A.A.Berdyshev & S.V.Vonsovski, Izv. AN SSSR, Ser. fiz., 18, 328 (1954) - Trans. Bulletin Vol. 18, No. 3, p. 23.
18. C.G.Schull & I.S.Smart, Phys. Rev., 76, 1256 (1949).
19. S.V.Vonsovski & A.A.Berdyshev, Zhur. eksp. i teor. fiz., 25, 723 (1953).
20. L.D.Landau & I.Ia.Pomeranchuk, Zhur. eksp. i teor. fiz., 7, 379 (1937).
21. S.P.Shubin & S.V.Vonsovski, Sow.Phys., 7, 292 (1935).
22. S.V.Vonsovski, K.B.Vlasov & A.V.Sokolov, Zhur. eksp. i teor. fiz., 21, 1185 (1951).
23. S.V.Vonsovski & B.V.Paduchev, Zhur. eksp. i teor. fiz., 25, 571 (1953).
24. S.V.Vonsovski & V.S.Galishev, Zhur. eksp. i teor. fiz., 25, 584 (1953).
25. S.V.Vonsovski & E.N.Agafonova, Symposium in honor of the 70th birthday of Academician A.F.Ioffe, USSR Acad. Sci., M.-L. 1950.
26. S.V.Vonsovski & Iu.M.Seidov, Izv. AN SSSR, Ser. fiz., 18, 319 (1954) - Trans. Bulletin Vol. 18, No. 3, p. 14.
27. R.Pauthenet, Ann. de phys., 7, 710 (1952).

* * * * *

RELAXATION PROCESSES IN FERROMAGNETIC METALS AT LOW TEMPERATURES

- E. A. Turov

1. It is the purpose of this investigation to generalize the theory of relaxation processes in ferromagnetics, developed for ferro-dielectrics by A. I. Akhiezer[1] to include ferromagnetic metals. The generalization consists, essentially, of taking into account the active role of conduction electrons in these processes.

The simplest model of a ferromagnetic, suitable for the solution of the above problem, is the s-d-exchange model of transition metals.[2] In treating relaxation processes in the framework of this model, one must take into account, in addition to the electrostatic interaction of the ferromagnetic electrons with each other and with conductivity electrons, the magnetic (anisotropic) interaction between them. The question of systematically taking account of the magnetic interaction within the framework of this model is discussed in two articles, one by S. V. Vonsovski[3] and the other by the author.[4]*

---

* Before Ref. 4 can be used, the following misprints and errors must be corrected: 1) replace $\hat{a}_{n\sigma'_1}$ in the last term of eq. (3) by $\hat{a}_{n\sigma'_1}$; 2) correct $\hat{b}^{+}_{g}$ in the last term of eq. (10) to read $\hat{b}^{+}_{g_1}$; 3) change the + sign to a - sign in the expression for $A_{\underline{g}}$ on p. 947 (sixth line from the top), in front of the term $F(0^+, n^-; n^+, 0^-)$ and close the square bracket after this term; 4) the square bracket in the following line should be opened not ahead of the exponential term $e^{i\underline{g}\underline{n}}$, but following it; 5) insert a - sign in the first of eq. (11")

(footnote continued on p. 414)

Hereinafter we shall have occasion to refer to the equations of the article by S. V. Vonsovski;[3] these references will be identified by a Roman numeral I preceding the appropriate equation number of Ref. 3.

2. At low temperatures, an ideal ferromagnetic metal can be regarded as an aggregate of three subsystems of quasi-particles; ferromagnons (or spin waves), phonons (or lattice vibrations) and conduction electrons. Relaxation phenomena in such a mixture of quasi-particles are determined by the collision processes between these particles.

Let a system of ferromagnons be brought out of its equilibrium state in some manner (for example, by a rapid change of the external magnetizing field or by "heating" the spin system incident to resonant absorption of energy from a microwave magnetic field). The collisions between the ferromagnons themselves and between the ferromagnons and phonons and the conduction electrons will restore the system to its equilibrium state after a certain time interval, which we shall term the "total relaxation time τ of the ferromagnetic system." If the initial departure from equilibrium is small, τ will be approximately equal to the mean lifetime of each of the excess ferromagnons (for the sake of clarity in the present discussion we are assuming that the spin system is "heated"). This lifetime, in turn, is the reciprocal of the average probability of the splitting of the ferromagnon per second (naturally, taking into account the creation process). We shall call this probability the average relaxation frequency $\bar{w}$.

The expression for the total relaxation frequency may be comprised of several terms, each corresponding to one of the possible collision mechanisms. In general, therefore, the relaxation time can be defined with the aid of the following equation:

$$\frac{1}{\tau} = \sum_i \bar{w}^{(i)}, \qquad (1)$$

where $\bar{w}^{(i)}$ is the mean relaxation frequency corresponding to the i'th collision mechanism.

The relaxation frequencies $\bar{w}_{c\text{-}c}$ and $\bar{w}_{c\text{-}p}$ for collisions of ferromagnons with other ferromagnons and with lattice vibrations, respectively, (spin-spin and spin-lattice relaxations) were computed by Akhiezer.[1] It turned out there that at sufficiently low temperatures (according to Akhiezer at $T < 10^{\circ}K$) the equilibrium between the ferromagnons themselves is established much more quickly than equilibrium between ferromagnons and phonons, *i.e.* $\bar{w}_{c\text{-}c} \gg \bar{w}_{c\text{-}p}$. Consequently, the $\bar{w}_{c\text{-}p}$ in (1) may be considered negligible as compared with $\bar{w}_{c\text{-}c}$.

The outstanding characteristic of metal ferromagnetics, as compared with ferrodielectrics, is the appearance in (1) of terms due to collisions between ferromagnons and conduction electrons.

The main purposes of this investigation are to compute the average relaxation frequencies $\bar{w}^{(i)}_{c\text{-}e}$ (spin-electron relaxation) that correspond to the various ferromagnon-conduction electron collision mechanisms, to compare these frequencies in order to determine the principal collision mechanism, and to evaluate the role of conduction electrons in ferromagnetic relaxation.

(footnote continued from p. 413) ahead of the (1/2) inside the bracket, and reverse the sign of the power of the exponential in the second eq. (11"); 6) add the conditions $l_+ > 0$, $l_- < 0$ to eq. (11'); 7) replace eq. (14) by

$$E_{k\sigma} = E_k + \frac{1}{2}[D(k^+, k^+) + D(k^-, k^-)] + \sigma\sqrt{[D(k^+, k^+) - D(k^-, k^-)]^2 + 4|D(k^+, k^-)|^2}.$$

2. Mean Frequency $\overline{w}_{c\text{-}э}^{(i)}$ of the Spin-Electron Relaxation

1. The collision processes between ferromagnons and conduction electrons, which for brevity we shall call spin-electron collisions, are characterized by an operator given in Ref. 4 (equation 10); the first two terms therein are due to "absorption" and "emission" of ferromagnons by the conduction electrons (inelastic collisions) and the last term is associated with mutual scattering of ferromagnons and conduction electrons without an ensuing change in the number of quasi-particles (elastic collisions). Here we shall consider only inelastic collisions, i.e., only collisions incident to which the number of ferromagnons in the system may be altered.

The portion of the energy operator corresponding to these collisions is represented in a more expanded form by expression (I, 3.7); in this expression the first three lines describe, respectively, processes of the following type: 1) $\Delta m = 0$, 2) $\Delta m = \pm 1$, and 3) $\Delta m = \pm 2$, i.e., processes in which the quantum number m of the entire system is 1) unchanged, 2) changed by one unit, or 3) changed by two.

The average frequency of the spin-electron relaxation will be determined for collision processes of the i'th type (i = 0, 1, 2) from relationships of the form:

$$\overline{w}_{c\text{-}э}^{(i)} = \left(\sum_g \overline{N}_g\right)^{-1} \sum_g w_g^{(i)} \overline{N}_g, \tag{2}$$

$$w_g^{(i)} = -(\Delta N_g)^{-1} \frac{d}{dt} \Delta N_g, \tag{3}$$

where ΔN_g is the deviation of the number of ferromagnons in state g from the equilibrium value

$$\overline{N}_g = (e^{\varepsilon_g/\varkappa T} - 1)^{-1}. \tag{4}$$

Equations (3) are obtained by linearizing the right half of the corresponding kinetic equations (with respect to ΔN_g):

$$\frac{d}{dt} \Delta N_g = b_i - a_i,$$

that describe the changes produced by collision processes of a given type in the number of ferromagnons (b_i and a_i are, respectively, the number of ferromagnons with quasi-momentum g emitted and absorbed by the conduction electrons per second).

For actual calculations of the spin-electron relaxation frequencies, one must know 1) the dispersion law for the energies of the quasi-particles and 2) the amplitudes of the probabilities of the corresponding quantum transitions. Both obviously depend on the actual form of the electron interaction energy operator $\hat{\Phi}(j, j')$ (see I, 3.7).

We shall consider the following types of interaction between electrons: 1) electrostatic interaction of d-electrons with each other and with conduction electrons, 2) magnetic spin-spin interaction of d-electrons with each other and with conduction electrons, and 3) interactions of the magnetic spin moments of the d-electrons with the magnetic field, associated with the motion of the conduction electrons (spin-orbital interaction).

Approximate expressions for the energy of the ferromagnons (ε_g) the energy of the conduction electrons ($E_{k\sigma}$), and the probability amplitudes of the collisions between ferromagnons and conduction electrons, taking the above interactions into account, are given in Ref. 3: (I, 3.26), (I, 3.32), and (I, 3.34) to (I, 3.38). These

---

Key to subscripts: c - spin; p - lattice; э - electron.

expressions are valid for the temperature range defined by the inequality $2\mathfrak{M}H' \ll \varkappa T \ll \varkappa T_k$. All the following calculations will, therefore, be valid only for this temperature interval.

2. According to the first line of (I, 3.37), the kinetic equation for the variation of ΔN_g with time due to collisions of the $\Delta m = 0$ type has the following form:

$$\frac{d}{dt}\Delta N_g = \frac{2\pi}{\hbar}\sum_k |C_-^{(0)}(k,g)|^2 [(N_g+1)(1-N_{k-g}^-)N_k^+ - N_g(1-N_k^+)N_{k-g}^-]\,\delta(E_k^+ - E_{k-g}^- - \varepsilon_g), \quad (5)$$

where $C^{(0)}(k,g)$ is given by (I, 3.34) and the following notation is used:

$$N_k^+ = N_k\left(\tfrac{1}{2}\right),\quad N_k^- = N_k\left(-\tfrac{1}{2}\right),\quad E_k^+ = E_k\left(\tfrac{1}{2}\right),\quad E_k^- = E_k\left(-\tfrac{1}{2}\right)$$

In this case it is possible to neglect $\mathfrak{M}H'$ compared with α' in the expression (I, 3.32) for the energy $E_{k\sigma}$.

Putting in the right half of (5) $N_g = \bar{N}_g + \Delta N_g$ and $\bar{N}_{k\sigma} = (e^{(Ek\sigma-\varepsilon_0)/\varkappa T}+1)^{-1}$ for $N_{k\sigma}$, we obtain, according to (3), the value of $w_g^{(0)}$ as the coefficient of ΔN_g:

$$w_g^{(0)} = \frac{2\pi}{N\hbar}\sum_k \{2\alpha' - \beta'[(ak)^2 + (ak-ag)^2]\}^2 \times (N_{k-g}^- - N_k^+)\,\delta(E_k^+ - E_{k-g}^- - \varepsilon_g). \quad (6)$$

We next carry out the following calculations:

1) average $w_g^{(0)}$ over all states g in accordance with (2);

2) replace the summation with respect to k and g by integration in the quasi-momentum space (with the direction of vector g serving as a polar axis for the vector k);

3) carry out the integration with respect to the angles, using the delta function to remove the integration with respect to θ_{kg}, and bearing in mind that

$$\delta(E_k^+ - E_{k-g}^- - \varepsilon_g) = [2(\beta+\beta')akag]^{-1} \times \delta\left[\cos\theta_{kg} + \frac{2\alpha' - 2\beta'(ak)^2 - (\beta+\beta'+J)(ag)^2}{2(\beta+\beta')akag}\right]$$

(we note that the condition $|\cos\theta| \leqslant 1$ restricts the integration region to the planes (ak, ag), thereby greatly complicating all the computations);

4) replace in the resulting equation the remaining integration variables ak and ag with

$$x = \frac{(\beta-\beta')(ak)^2 - \bar{\varepsilon}}{\varkappa T} \quad \text{and} \quad y = \frac{J(ag)^2}{\varkappa T},$$

where, according to reference 2,*

$$\bar{\varepsilon} = \varepsilon_0 - \alpha' = \lambda(\beta-\beta')(1-d)^{2/3},\quad d = \frac{3(\alpha'-\lambda\beta')}{2\lambda\beta} \ll 1 \quad \text{and} \quad \lambda = (3\pi^2)^{2/3}; \quad (7)$$

5) integrate with respect to y; here it is possible to substitute infinity for the upper integration limit.

As a final result we obtain:

$$\bar{w}_{c-g}^{(0)} = D\int_{-\bar{\varepsilon}/\varkappa T}^{\infty} \frac{\left[2\alpha'\beta - \frac{2\beta\beta'}{\beta-\beta'}(\bar{\varepsilon}+\varkappa Tx)\right]^2 \ln(e^{x-y_1(\bar{\varepsilon}+\varkappa Tx)}+1)}{e^x+1}\,dx,$$

where

$$D = \frac{(J\varkappa T)^{3/2}}{10{,}4\pi^{3/2}\hbar(\beta+\beta')^3(\beta-\beta')},$$

$$y_1(\bar{\varepsilon}+\varkappa Tx) = \frac{J}{\varkappa T}\left[\frac{(\beta+\beta')\sqrt{\frac{\bar{\varepsilon}+\varkappa Tx}{\beta-\beta'}} - \sqrt{\frac{\delta(\bar{\varepsilon}+\varkappa Tx)}{\beta-\beta'} + 2\alpha'(\beta+\beta'+J)}}{\beta+\beta'+J}\right]^2$$

---

* We assume that there is, on the average, one conduction electron for each lattice site.

(here $\delta = \beta^2 - \beta'^2 - 2\beta' J$).

The last integral is of a standard form $\int_{-\bar{\varepsilon}/\varkappa T}^{\infty} \frac{f(x)\,dx}{e^x+1}$ employed in statistical physics (where $f(x)$ is a slowly varying function of x) and is given by a series in powers of T (Ref. 5).

Considering that $\varkappa T \ll J$ and $\beta, \alpha' \ll \bar{\varepsilon}$, $\beta' < \beta$, , we obtain by straightforward though onerous computations:

$$\bar{w}^{(0)}_{c\text{-}e} = \frac{J(\alpha' - \lambda\beta')^2}{2{,}6\pi^{3/2}\hbar(\beta - \beta'^2)}\left(\frac{T}{T_K}\right)^{3/2}[B_1(T) + B_2(T)],$$

where $T_K = \frac{J}{\varkappa}$ is a temperature on the order of the Curie point. Here we used the approximate relationship

$$2\beta\left(\alpha' - \frac{\beta'\bar{\varepsilon}}{\beta - \beta'}\right) \approx 2(\beta + \beta')(\alpha' - \lambda\beta'),$$

obtained with the aid of (7), and introduced the following notation

$$B_1(T) = \sum_{n=1}^{\infty} \frac{(-1)^{n+1}}{n^2} e^{-nT_0/T} \quad \text{and} \quad B_2(T) = \frac{\pi^2 e^{-T_0/T}}{6(1 + e^{-T_0/T})},$$

where

$$T_0 = T y_1(\bar{\varepsilon}) \approx \lambda\left(\frac{\alpha'}{\bar{\varepsilon}}\right)^2 T_K. \tag{8}$$

Let us examine the two limiting cases: $T \gg T_0$ and $T \ll T_0$. In the former case $B_1(T) \approx B_2(T) \approx \frac{\pi^2}{12}$, and in the latter case

$$B_1(T) \approx e^{-T_0/T}, \quad B_2(T) \approx \frac{\pi^2}{6} e^{-T_0/T}.$$

We finally obtain the following expressions for the average spin-electron relaxation frequency due to processes of the $\Delta m = 0$ type:

$$\bar{w}^{(0)}_{c\text{-}e} \approx \frac{\sqrt{\pi} J(\alpha' - \lambda\beta')^2}{15{,}6\hbar(\beta^2 - \beta'^2)}\left(\frac{T}{T_K}\right)^{3/2} \quad \text{with } T \gg T_0, \tag{9}$$

$$\bar{w}^{(0)}_{c\text{-}e} \approx \frac{J(\alpha' - \lambda\beta')^2}{\pi^{3/2}\hbar(\beta^2 - \beta'^2)}\left(\frac{T}{T_K}\right)^{3/2} e^{-T_0/T} \quad \text{with } T \ll T_0. \tag{9'}$$

According to (8) the critical temperature T_0, below which the value of $\bar{w}^{(0)}_{c\text{-}e}$ diminishes very rapidly, depends to a large extent on the value of the s-d-exchange integral α'. Yet the exact order of magnitude of α' remains unknown.

If we assume, following Bloembergen,[6] that $\alpha' \sim 10^{-14}$ erg, and furthermore that $J \sim \beta \sim 10^{-12}$ erg and $\bar{\varepsilon} \sim 10^{-12}$ erg, we get $T_0 \sim 1^{\circ}K$, and, consequently, for $T \gg 1^{\circ}K$, we have

$$\bar{w}^{(0)}_{c\text{-}e} \sim 4 \cdot 10^9 \sqrt{T} \ \text{sec}^{-1} \tag{10}$$

At $10^{\circ}K$, for example, $\bar{w}^{(0)}_{c\text{-}e} \sim 10^{10}$ sec^{-1}.

An entirely different result is obtained if we assume that α' is of another possible order of magnitude — namely, $\alpha' \sim J \sim 10^{-13}$ erg.[7] In this case $T_0 \sim 100^{\circ}K$, and, consequently, for $T \ll 100^{\circ}K$, we have

$$\bar{w}^{(0)}_{c\text{-}e} \sim 6 \cdot 10^{11} \sqrt{T} \cdot e^{-100^{\circ}/T} \ \text{sec}^{-1} \tag{10'}$$

At $10^{\circ}K$, for example, $\bar{w}^{(0)}_{c\text{-}e} \sim 10^8$ sec^{-1}.

There are several considerations in favor of the first estimate for the exchange integral α'.[8]

Key to subscripts: c - spin; p - lattice; e - electron.

3. According to line 2 of (I, 3.7), the kinetic equation for processes of the $\Delta m = \pm 1$ type is of the form:

$$\frac{d}{dt}\Delta N_g = \frac{2\pi}{\hbar}\sum_{k\sigma}|C_-^{(1)}(k, g)|^2[(N_g+1)(1-N_{k-g,\sigma})N_{k\sigma} - N_g(1-N_{k\sigma})N_{k-g,\sigma}]\delta(E_{k\sigma}-E_{k-g,\sigma}-\varepsilon_g), \quad (11)$$

where $C_-^{(1)}(k, g)$ is given by either (I, 3.35) or (I, 3.38), depending on whether we are dealing with spin-spin or spin-orbital magnetic interaction. The average relaxation frequency for processes of this type is therefore

$$\bar{w}_{c-s}^{(1)} = \frac{2\pi}{\hbar}\left(\sum_g \bar{N}_g\right)^{-1}\sum_{k\sigma}|C_-^{(1)}(k, g)|^2(\bar{N}_{k-g,\sigma}-\bar{N}_{k\sigma})\delta(E_{k\sigma}-E_{k-g,\sigma}-\varepsilon_g).$$

Consider first the spin-orbital interaction. Applying transformations analogous to those carried out in the preceding subsection and introducing the following integration variables

$$x = \frac{(\beta - 2\sigma\beta')(ak)^2}{\varkappa T} \quad \text{and} \quad y = \frac{J(ag)^2}{\varkappa T} \quad (12)$$

we obtain:

$$\bar{w}_{c-s}^{(1)} = \sum_\sigma B_\sigma \int \frac{x - p_\sigma(y)}{y(e^{y+u}-1)}\left(\frac{1}{e^{x-y-u-v_\sigma}+1} - \frac{1}{e^{x-v_\sigma}+1}\right)dx\,dy, \quad (13)$$

where

$$B_\sigma = \frac{6{,}15\sqrt{\pi}(LW_0)^2J^2}{\hbar(\beta-2\sigma\beta')^3}\left(\frac{T}{T_K}\right)^{1/2};$$

$$v_\sigma = \frac{\varepsilon_0 - 2\sigma(\alpha' + \mathfrak{M}H')}{\varkappa T} = \frac{\varepsilon_\sigma}{\varkappa T};$$

$$u = \frac{2\mathfrak{M}H'}{\varkappa T};$$

$$p_\sigma(y) = \frac{1}{A_\sigma}\left(\frac{1+A_\sigma}{2}\right)^2 y + \frac{(1+A_\sigma)u}{2} + \frac{A_\sigma u^2}{4y}, \quad \text{here } \left(A_\sigma = \frac{J}{\beta - 2\sigma\beta'}\right).$$

The range of integration in (13) is defined by the inequality $x \geqslant p_\sigma(y)$, i.e., is the portion of the (x, y) plane bounded by the parabola $x = p_\sigma(y)$. It appears that this parabola can be replaced without much loss in accuracy by the two intersecting straight lines

$$y = \frac{A_\sigma u^2}{4v_\sigma} = l \quad \text{and} \quad x = \frac{1}{A_\sigma}\left(\frac{1+A_\sigma}{2}\right)^2 y + \frac{(1+A_\sigma)u}{2} = by + h.$$

In this approximation we have

$$\bar{w}_{c-s}^{(1)} \sum_\sigma B_\sigma \int_l^\infty \frac{dy}{y(e^{y+u}-1)} \int_{by+h}^\infty (x - by - h)\left(\frac{1}{e^{x-y-u-v_\sigma}+1} - \frac{1}{e^{x-v_\sigma}+1}\right)dx. \quad (14)$$

The integrals with respect to x can be converted to integrals of the form:

$$i(\eta) = \int_0^\infty \frac{z\,dz}{e^{z-\eta}+1}.$$

If $\eta \gg 1$, which condition obtains, in our case, the value of the last integral is approximately $\eta^2/2$. This yields in lieu of (14):

$$\bar{w}_{c-s}^{(1)} = \sum_\sigma B_\sigma v_\sigma \int_l^\infty \frac{(y+u)\,dy}{y(e^{y+u}-1)}.$$

If again we restrict ourselves to the case when $2\mathfrak{M}H' \ll \varkappa T$ (i.e., $l \ll u \ll 1$), we finally obtain, upon approximate evaluation of this integral:

$$\bar{w}^{(1)}_{c\text{-}e} \approx \sum_{\sigma} \frac{6{,}15\sqrt{\pi}(LW_0)^2\varepsilon_\sigma \varkappa T_K}{\hbar(\beta - 2\sigma\beta')^3}\left(\frac{T_K}{T}\right)^{1/2} \ln\frac{\varepsilon_\sigma \varkappa T}{A_\sigma(\mathfrak{M}H')^2}. \qquad (15)$$

For example, if again we put $J \sim 10^{-13}$ erg, $(\beta - 2\sigma\beta') \sim 10^{-13}$ erg, and $\varepsilon_\sigma \sim 10^{-12}$ erg, we obtain for T = 100K and $H' \sim 10^3$ oersteds:

$$\bar{w}^{(1)}_{c\text{-}e} \sim 4 \cdot 10^{10} \quad \text{sec}^{-1}.$$

It is worth noting that $\bar{w}^{(1)}_{c\text{-}e}$, unlike $\bar{w}^{(0)}_{c\text{-}e}$, does not increase with the temperature, but, on the contrary, falls off rather slowly.

The value of $\bar{w}^{(1)}_{c\text{-}e}$ for the case of spin-spin interaction between s- and d-electrons is obtained in a fully analogous manner and equals:

$$\bar{w}^{(1)}_{c\text{-}e} \approx \sum_{\sigma} \frac{0{,}7 \cdot R'^2 (J\varkappa T)^{3/2}\varepsilon_\sigma}{\pi^{3/2}\hbar(\beta - 2\sigma\beta')^5}. \qquad (16)$$

Equation (16) yields a very low value of the spin-electron relaxation frequency as compared with (15), even if the most favorable value of the parameter R' is chosen. Thus, for example, assuming $R' \sim 10^{-16}$ erg, we obtain

$$\bar{w}^{(1)}_{c\text{-}e} \sim 10^3 T^{9/2} \quad \text{sec}^{-1}$$

This result shows that collision processes of the $\Delta m = \pm 1$ type are due primarily to spin-orbital interaction, at least in the temperature range where our calculation is valid.

4. Lastly, let us consider the collision processes of the $\Delta m = \pm 2$ type. According to line 3 of (I, 3.7), the corresponding kinetic equation is:

$$\frac{d}{dt}\Delta N_g = \frac{2\pi}{\hbar}\sum_k |C^{(2)}(k,g)|^2 [(N_g + 1)(1 - N^+_{k-g})N^-_k - N_g(1 - N^-_k)N^+_{k-g}]\,\delta(E^-_k - E^+_{k-g} - \varepsilon_g), \qquad (17)$$

where, according to (I, 3.36),

$$|C^{(2)}_-(k,g)|^2 = \frac{1}{N}(ak)^4 \sin^4\theta_{kg}(R^2\cos^2 2\varphi_k + R'^2\sin^2 2\varphi_k).$$

From (17) we again obtain the average relaxation frequency:

$$\bar{w}^{(2)}_{c\text{-}e} = \left(\sum_g \bar{N}_g\right)^{-1}\frac{2\pi}{\hbar}\sum_{k,g}|C^{(2)}_-(k,g)|^2\bar{N}_g(\bar{N}^+_{k-g} - N^-_k)\,\delta(E^+_{k-g} - E^-_k + \varepsilon_g). \qquad (18)$$

A rigorous continuation of the calculations of $\bar{w}^{(2)}_{c\text{-}e}$ involves no particular difficulty: they differ little from the analogous calculations of Section 2 above. To avoid cumbersome computations, which in the final analysis are superfluous, we shall restrict ourselves to proving that even the excessively high value of $\bar{w}^{(2)}_{c\text{-}e}$ obtained in this case is still negligibly small compared with the value of $\bar{w}^{(0)}_{c\text{-}e}$, deriving from electric exchange interaction. To prove this, we replace the factor $\sin^4\theta_{kg}$ in (18) by its maximum value — unity — and will neglect in the changeover from summation to integration the restriction imposed by the laws of conservation of energy and quasi-momentum on the range of integration ($|\cos\theta_{kg}| \leqslant 1$). Since the integrand is positive for all values of k and g between zero and infinity, this can result only in a larger value for the integral.

Introducing the following variables of integration

$$x = \frac{\beta + \beta'(ak)^2 - \bar{\varepsilon}}{\varkappa T} \quad \text{and} \quad y = \frac{\varepsilon_g}{\varkappa T}$$

and integration with respect to y, taking the above into account, we obtain (neglecting terms of the order of $\frac{2\mathfrak{M}H'}{\varkappa T}$):

Key to subscripts: c - spin; p - lattice; e - electron.

$$\bar{w}^{(2)}_{c\text{-}э} < \frac{(R^2+R'^2)J}{20{,}8\pi^{3/2}\hbar(\beta^2-\beta'^2)(\beta+\beta')^2}\left(\frac{T}{T_K}\right)^{1/2}\int\limits_{-\bar{\varepsilon}/\varkappa T}^{\infty}\frac{(\bar{\varepsilon}+\varkappa T x)^2\ln(e^x+1)}{e^x+1}\,dx.$$

The approximate value of this integral is $\frac{\pi^2}{4}\bar{\varepsilon}^2$. We finally obtain

$$\bar{w}^{(2)}_{c\text{-}э} < \frac{\sqrt{\pi}(R^2+R'^2)J\bar{\varepsilon}^2}{83{,}2(\beta^2-\beta'^2)(\beta+\beta')^2\hbar}\left(\frac{T}{T_K}\right)^{1/2}. \qquad (19)$$

As in the case of $\bar{w}^{(0)}_{c\text{-}э}$, if the restrictions on the integration range are taken into account, the right half of (19) will contain a factor e^{-T/T_0} for temperatures $T \ll T_0$.

It follows from measurements of the resistance anisotropy in ferromagnets that a reasonable order of magnitude for $R^2 + R'^2$ would be 10^{-32} erg^2. Assuming for the remaining quantities in (19) the same values as indicated in subsections 2 and 3, we obtain:

$$\bar{w}^{(2)}_{c\text{-}э} < 10^6\sqrt{T}\ \ \text{sec}^{-1}. \qquad (20)$$

Thus comparison of (20) and (10) indicates that $\bar{w}^{(2)}_{c\text{-}э}$ is indeed much smaller than $\bar{w}^{(0)}_{c\text{-}э}$.

3. Spin-Electron Relaxation Time

1. It is evident from the above calculations and evaluations that in the temperature range in question, the spin-electron relaxation frequency is affected primarily by processes of the $\Delta m = 0$ type, which are due principally to electric exchange interaction, and processes of the $\Delta m = \pm 1$ type, due principally to magnetic spin-orbital interaction. The total spin-electron relaxation frequency can be written as the sum of expressions (9) and (15), i.e.,

$$\bar{w}_{c\text{-}э} = \bar{w}^{(0)}_{c\text{-}э} + \bar{w}^{(1)}_{c\text{-}э}. \qquad (21)$$

What is remarkable is that as the temperature decreases the first term in this sum diminishes slowly (approximately as $\sqrt{T}$) while the second increases slowly (approximately as $1/\sqrt{T}$), and that both terms are of the same order of magnitude. Consequently, over a wide temperature range, $\bar{w}_{c\text{-}э}$ may retain a nearly constant value which should be not less than 10^9 sec^{-1}.

We note, for purposes of comparison, that the value computed by Akhiezer for the spin-spin relaxation frequency $\bar{w}_{c\text{-}c}$ is approximately 10^7 sec^{-1} at T = 10°K and increases with temperature as $(T/T_K)^{1/2}\left(\ln\frac{\varkappa T_c}{2\mathfrak{M}H'}\right)^2$.

One could apparently conclude that $\bar{w}_{c\text{-}э} \gg \bar{w}_{c\text{-}c}$ and that in contrast to the case in ferrodielectrics, equilibrium in the ferromagnetic spin systems of ferromagnetic metals is attained not through collisions between ferromagnons, but primarily through collisions of ferromagnons with conduction electrons. In this case the relaxation time of the ferromagnetic system would be described by

$$\frac{1}{\tau} = \bar{w}_{c\text{-}э}. \qquad (22)$$

The conclusion, however, would be premature, since in the computation of $\bar{w}_{c\text{-}c}$ we took into account only the dipole-dipole spin-spin interaction, and did not allow for the interactions associated with orbital motion of the d-electrons (spin-orbital, orbital-orbital, and

Key to subscripts: c – spin; p – lattice; э – electron.

other interactions). There is no basis for assuming that these types of magnetic interaction yield the same value of spin-relaxation frequency as the dipole-dipole interaction. It is known, for example, that in ferromagnetic anisotropy the dominant role is played not by the spin-spin interaction between the ferromagnetic electrons, but by the spin-orbital interaction between them. Apparently this interaction also plays a decisive role in collision processes between ferromagnons. It is conceivable that it leads to a spin-spin relaxation frequency not only comparable with the spin-electron relaxation frequency, but possibly greater than the latter.

2. To allow to some extent for this possibility, let us examine the case when $\bar{w}_{c\text{-}c} \gg \bar{w}_{c\text{-}э}$. In this case $1/\tau \approx \bar{w}_{c\text{-}c}$, and since equilibrium is restored within the ferromagnon subsystem itself much more quickly than the equilibrium between the subsystem and the conduction electrons, it becomes logical to introduce the concept of a ferromagnon-gas temperature $T_ф$, differing from the electron-conduction temperature T.

To describe the process of attainment of thermal equilibrium between these two subsystems we can now introduce still another characteristic time, i.e., the spin-electron relaxation time $\tau_{c\text{-}э}$, defined by analogy with the spin-lattice relaxation time[1] by the relationship

$$\frac{d(T_ф - T)}{dt} = -\frac{T_ф - T}{\tau_{c\text{-}э}}. \tag{23}$$

Denoting the specific heat of the ferromagnon and conduction-electron subsystems by $C_ф$ and $C_э$, respectively, we obtain, in accord with the equations

$$-dQ = C_ф dT_ф \quad \text{and} \quad dQ = C_э dT, \tag{23'}$$

the following expression for the quantity of heat transferred from the ferromagnons to the electrons:

$$\frac{dQ}{dt} = \frac{\bar{C}}{\tau_{c\text{-}э}} \Delta T, \tag{24}$$

where

$$\Delta T = T_ф - T, \quad \frac{1}{\bar{C}} = \frac{1}{C_ф} + \frac{1}{C_э}.$$

To determine $\tau_{c\text{-}э}$ it is therefore necessary to find the value of dQ/dt, which in the first approximation (for small values of ΔT) is evidently proportional to ΔT, i.e.,

$$\frac{dQ}{dt} = D\Delta T, \tag{25}$$

where the proportionality coefficient D can be called the "coefficient of heat transfer" between the ferromagnon and electron systems. If D is known, we have from (24) and (25)

$$\tau_{c\text{-}э} = \frac{C}{D}. \tag{26}$$

3. The energy exchange between the ferromagnetic spin system and the electron system occurs through the "absorption" and "emission of ferromagnons by the conduction electrons. The energy transferred from the spin system to the electron system per unit time is

$$\frac{dQ}{dt} = \sum_g \varepsilon_g \frac{dN_g}{dt}. \tag{27}$$

Key to subscripts: c - spin; p - lattice; э - electron; ф - ferromagnon.

Since the most probable processes of absorption and emission of ferromagnons by the conduction electrons at low temperatures are the processes of the $\Delta m = \pm 1$ type, due primarily to spin-orbital interactions, the value of dN_g/dt must be determined from equation (11), in which $C_{-}^{(1)}(k, g)$ should be assigned the value given in (I, 3.36). As a result after replacing the summation by integration, we obtain instead of (27)

$$\frac{dQ}{dt} = \frac{16N(LW_0)^2}{\pi\hbar} \sum_{\sigma} \int \varepsilon_g \sin^3\theta_{kg} \left[(N_g + 1) N_{k\sigma}(1 - N_{k-g,\sigma}) - \right.$$
$$\left. - N_g N_{k-g,\sigma}(1 - N_{k\sigma})\right] (ak)^4 \delta(E_{k\sigma} - E_{k-g,\sigma} - \varepsilon_g)\, d(ak)\, d(ag)\, d\theta_{kg}.$$

According to the assumptions that $(\overline{w}_{c\text{-}c} \gg \overline{w}_{c\text{-}э})$, the values of $N_{k\sigma}$ and N_g used in this equation must be the equilibrium values $\overline{N}_{k\sigma}$ and $\overline{N}_g$, referred to the temperatures T and T + ΔT, respectively, it being assumed that the spin system is "heated" ΔT degrees above the electron system.

Taking this into account, we expand $\overline{N}_g$ in powers of ΔT, cutting off the expansion at the linear term. Comparison of the resultant expression with (26) gives us the "coefficient of heat transfer:"

$$D = \frac{16N(LW_0)^2}{\pi\hbar\varkappa T^2} \sum_{\sigma} \int \frac{\varepsilon_g^2\, e^{\varepsilon_g/\varkappa T} (\overline{N}_{k-g,\sigma} - \overline{N}_{k\sigma}) \sin^3\theta_{kg}}{(e^{\varepsilon_g/\varkappa T} - 1)^2} \times$$
$$\times (ak)^4 \delta(E_{k\delta} - E_{k-g,\sigma} - \varepsilon_g)\, d(ak)\, d(ag)\, d\theta_{kg}. \qquad (28)$$

It is possible to put H' = 0 in the expressions employed here for the ferromagnon energy ε_g (I, 3.26) and the conduction electron energy $E_{k\sigma}$ (I, 3.32), inasmuch as where the condition $2\mathfrak{M}H' \ll \varkappa T$ holds, taking account of the external magnetic field H (or H') introduces only a negligibly small correction.

The integration with respect to θ_{kg} can be removed from (28) by using the delta function. If this is followed by the change of variables (12), the remaining integrals also become quite simple.

We finally obtain for the "heat-transfer coefficient:"

$$D = \sum_{\sigma} \frac{N(LW_0)^2 \varepsilon_\sigma \varkappa^2 T}{3\hbar(\beta - 2\sigma\beta')^3}. \qquad (29)$$

Using the same evaluations as in Section 2, we obtain

$$D \approx 10^{-12} NT \quad \text{erg/degree/sec.} \qquad (30)$$

4. To determine the spin-electron relaxation time $\tau_{c\text{-}э}$ according to (26), one must know the specific heats of the ferromagnon and electron subsystems. The specific heat of the ferromagnons, as is known,[1] equals

$$C_\Phi = \frac{15\sqrt{\pi}}{8(2\pi)^2} \varkappa N \left(\frac{T}{T_K}\right)^{3/2} \approx 10^{-21} NT^{3/2} \quad \text{erg/degree,} \qquad (31)$$

while for the electron specific heat let us take the experimental values obtained for nickel by Keith and Clark:[9]

$$C_э = 8{,}72 \cdot 10^{-4} N\varkappa T \approx 10^{-19} NT \quad \text{erg/degree.} \qquad (31')$$

Thus $C_э \gg C_\Phi$ in the temperature range under consideration, and, therefore, the conduction-electron temperature T can be assumed constant and equal to the lattice temperature. Hence, we can write $C = C_\Phi$.

Consequently, equations (26), (30), and (31) yield for the spin-electron relaxation time:

Key to subscripts: c - spin; p - lattice; э - electron; Φ - ferromagnon.

$$\tau_{c\text{-}e} \approx 10^{-9}\sqrt{T} \quad \text{sec.} \tag{32}$$

Let us note that $\tau_{c\text{-}e}$ is several orders of magnitude smaller than the spin-lattice relaxation time $\tau_{c\text{-}p}$, computed by Akhiezer.[1] Furthermore, $\tau_{c\text{-}e}$ falls off with decreasing temperature, while $\tau_{c\text{-}p}$ grows very rapidly: $\left(\tau_{c\text{-}p} \sim \frac{1}{T} e^{\text{const}/T}\right)$.

Consequently, one can expect the ferromagnetic metals and non-metals (such as ferrites) to exhibit a different behavior with regard to effects involving spin-lattice relaxation.

4. Line Breadth of Ferromagnetic Resonance Absorption

1. The above spin-electron relaxation mechanism may serve as one of the causes of the broadening of the ferromagnetic resonance absorption lines in metals.[10] Since there is still no satisfactory theory of line broadening, it may be of interest to evaluate the effect that one spin-electron relaxation could exert on the line breadth, neglecting other attenuation mechanisms.

The theory should explain the following basic experimental facts: 1) great breadth of the line $\Delta\omega \sim 10^9$-10^{10} sec^{-1}, and 2) its independence of the temperature, at least as regards order of magnitude, at room temperatures and below.

If we identify $\Delta\omega$ with the total mean spin-electron relaxation frequency $\overline{w}_{c\text{-}e} = \overline{w}^{(0)}_{c\text{-}e} + \overline{w}^{(1)}_{c\text{-}e}$, these facts and the theoretical deductions are in general agreement both as regards the order of magnitude and the weak temperature dependence.

There is little point in attempting a more detailed comparison with experiment, inasmuch as, rigorously speaking, our calculations are valid only for temperatures considerably below the Curie point, while the available experimental data[11] are limited primarily to room temperatures and above.

Although our evaluation of the spin-electron relaxation can fully account for the line breadth observed in metals, we do not have the temerity to assert that this relaxation mechanism is the determining cause of the broadening, for this would make it difficult to explain the cause of similar broadening in non-metallic ferromagnets.

Furthermore, our method of computing the relaxation frequency (by averaging over all ferromagnon states) is subject to the critical observation by Polder[12] that the true relaxation frequency for the spin waves that are active in resonance absorption is considerably lower than the usually computed "average" frequency.

Nevertheless, there is apparently no reason for doubting that spin-electron relaxation can have a substantial effect on the line breadth, and this effect must be allowed for in investigation of those line-breadth regularities that distinguish metallic from non-metallic ferromagnetic materials.

At present there is still no convincing experimental evidence of any substantial difference in the line breadth for metallic and non-metallic ferromagnets. However, it follows from data of Ref. 11 that above room temperature ferrites behave differently from ferromagnetic metals as regards the temperature dependence of the line breadth. With rising temperature the line breadth remains constant for ferrites, but rises for supermalloy and nickel, first slowly, and then faster as the Curie point is approached. This fact does not contradict our results, for it is in agreement with the corres-

ponding increase in the spin-electron relaxation frequency for processes of the $\Delta m = 0$ type, particularly if the next-order terms in T/T_K are taken into account in calculating $\overline{w}^{(0)}_{c\text{-}s}$.

2. To resolve conclusively the problem of the mechanism of line broadening in ferromagnetic resonance absorption it would be essential to carry out systematic measurements of the line breadth of both metallic and non-metallic ferromagnetics over a wide range of low temperatures. On the theoretical end it is necessary to extend the calculations of the spin-spin relaxation frequency to comprise successive evaluation of all the interactions associated with the orbital motions of ferromagnetic electrons.

Conclusions

1. We used the s-d-exchange model of ferromagnetic metals to compute the average probabilities (relaxation frequencies) corresponding to various types of collision processes between ferromagnons and conduction electrons. It emerged that the spin-electron relaxation frequency is most strongly affected by two types of processes: 1) absorption and emission of ferromagnons by conduction electrons in which the total magnetic quantum number is unchanged and those in which the total magnetic quantum number changes by unity. The former processes are due primarily to electric exchange interaction; the latter by magnetic spin-orbital interactions. The relaxation frequencies corresponding to the former and latter are, respectively, directly and inversely proportional to $\sqrt{T}$; both frequencies are of approximately the same order of magnitude, namely, 10^9-10^{10} sec^{-1}.

2. Assuming that equilibrium is established much more quickly within the ferromagnon subsystem than between this subsystem and the conduction-electron subsystem, we computed the time required to attain thermal equilibrium between the two subsystems. This time is of the order of magnitude of $10^{-9}\sqrt{T}$ sec.

3. We utilized the computed average spin-electron relaxation frequency in examining the question of the role played by collisions between ferromagnons and conduction electrons in the broadening of ferromagnetic resonance-absorption lines. The line breadth obtained on the basis of this relaxation mechanism agrees satisfactorily with the principal experimental data both as regards the order of magnitude and the weak temperature dependence. One can safely conclude that spin-electron relaxation is one of the dominant factors affecting the line breadth observed in ferromagnetic materials.

In conclusion I wish to express my deep gratitude to S. V. Vonsovski for suggesting the topic of this investigation and continuous guidance in carrying it out.

References

1. A.I.Akhiezer, Sow. Phys., 10, 217 (1946).
2. S.V.Vonsovski & E.A.Turov, Zhur. eksp. i teor. fiz., 24, 419 (1953).
3. S.V.Vonsovski, this issue of the Bulletin, p. 399 (of trans.).
4. E.A.Turov, Doklady AN SSSR, 98, 945 (1954).
5. L.D.Landau & E.M.Lifshits, Statisticheskaia fizika (Statistical Physics), M.-L. 1951.
6. N.Bloembergen, Phys. Rev., 78, 572 (1950).
7. K.Zener, in Problemy sovremennoi fiziki (Problems of Modern Physics), V - Ferromagnetism, p. 33, M. 1952.
8. E.A.Turov, Zhur. eksp. i teor. fiz., 25, 352 (1953).
9. F.Seitz, The Modern Theory of Solids (Russian trans. M.-L. 1949).
10. E.A.Turov & S.V.Vonsovski, Zhur. eksp. i teor. fiz., 24, 501 (1953).
11. N.Bloembergen & S.Wang, Phys. Rev., 93, 72 (1954).
12. D.Polder, Phil. Mag., 40, 99 (1949).

ELECTRIC CONDUCTIVITY OF FERROMAGNETIC METALS AT LOW TEMPERATURES

- E. A. Turov

1. It is commonly assumed that in ordinary (non-ferromagnetic) metals electric resistance is due to collisions of conduction electrons with lattice vibrations (phonons). As a result of the competition of two effects - acceleration by the external electric field and slowing-down due to collisions with phonons - the system of electrons arrives at a stationary (stable-current) state. The electron-phonon collision processes determine the temperature dependence of the resistance at low temperatures; this dependence characterized by the "T^5 law" (i.e. the resistivity ρ is proportional to T^5).

The existence of a ferromagnon branch of the energy spectrum in ferromagnets creates a supplementary "reservoir" in which the energy of the conduction electrons accelerated by the electric field can accumulate. Inasmuch as the laws of dispersion of the energy of ferromagnons and of the probability of collisions with ferromagnons differ from those for phonons, generally speaking, one may expect spin-electron relaxation to result in an additional resistance of ferromagnets, so that the temperature dependence of their resistance will differ from the "T^5 law." In fact, it is entirely possible that in some temperature interval the "ferromagnon" part of the resistance may even predominate over the "phonon" part.

These considerations regarding the additional resistance of ferromagnetic metals at low temperatures were first advanced by Vonsovski in 1948.[1] On the basis of certain assumptions regarding the collision mechanism he deduced a T^3 law for the electric resistance specific for ferromagnets.

The second attempt at calculating the additional resistance in ferromagnetic metals was made by Samoilovich and Iakovlev[2] who computed the "free path time" for collisions of conduction electrons with ferromagnons, due to s- and d-electron spin-orbital interaction (see Refs. 3 and 4). However, the uncritical use of the "free path time" concept, which at low temperatures does not have an unambiguous meaning, led these investigators to an erroneous result (the nature of the error will be clarified below). Moreover, in their investigation Samoilovich and Iakovlev make use of a very doubtful method of cutting off the lower limit of integration over the quasi-momentum of the ferromagnons, as a result of which their "free path time" proved to be strongly dependent upon the size of the crystal. Samoilovich and Iakovlev found that the additional resistance is proportional to T^2.

At present, thanks to the development of the mathematical apparatus of the s-d-exchange model of a ferromagnetic metal (see Refs. 5, 6 and 3), it is possible to investigate more rigorously and in greater detail the electric resistance due to collisions of conduction electrons with ferromagnons. This is the aim of the present investigation.

2. We shall concern ourselves with such collision processes between conduction electrons and ferromagnons as are accompanied by a change in the number of ferromagnons in the system ("emission" and "absorption"of ferromagnons by conduction electrons).

As we showed in an earlier report,[4] among such processes the most probable are processes of the $\Delta m = 0$ and the $\Delta m = \pm 1$ types (Δm is the change in the magnetic quantum number of the system incident to an individual collision between quasi-particles). Processes of the first type are due primarily to exchange electrostatic interaction, those of the second type, to magnetic spin-orbital interaction between

the outer and inner electrons of the ferromagnet. The corresponding amplitudes of the transition probabilities are calculated in Ref. 3.*

As in Ref. 1, we shall confine our examination to the region of low temperatures in which $T \ll T_к$ ($T_к$ is the Curie point) and, on the other hand, $T \gg \frac{\overline{W}_0}{\varkappa}$, where $\overline{W}_0 \approx \frac{\mathfrak{M}^2}{a^3}$ is a quantity of the order of the energy of the magnetic dipolar interaction between the magnetic spins of neighboring atoms in the crystal lattice. In this temperature region the energy of a ferromagnon with a quasi-momentum g can be represented, according to equation (I, 3.26), in the form

$$\varepsilon_g = J(ag)^2 + W_0, \qquad (1)$$

where J is the d-d exchange integral and is the lattice constant.

Invoking equation (I, 3.7) for the part of the energy operator characterizing conduction electron-ferromagnon collision processes, and equations (I, 3.34), (I, 3.38), (I, 3.32) and (1), we can write and solve the kinetic equation determining the change in the quasi-momentum distribution function of the conduction electrons under the influence of the electric field and collisions of any given type. Knowing this function we can calculate the electric resistances associated with the collision processes of each type.

3. The qualitative variation of the resistance with the temperature due to any specific electron-ferromagnon collision mechanism can be deduced from general physical considerations without solving the kinetic equation. Effecting some generalization of the common assumptions made for the qualitative derivation of the "T^5 law" for the resistance at low temperatures,[7] this can be accomplished in the following manner.

If a conduction electron gave up in every collision with a ferromagnon (or phonon) the entire momentum acquired under the influence of the electric field, the resistance would be directly proportional to the number of collisions, i.e., to the integral

$$\int \overline{N}_g w(g)\, \delta(E_{k\sigma} - E_{k-g,\,\sigma'} - \varepsilon_g)\, dg, \qquad (2)$$

where $\overline{N}_g$ is the average number of ferromagnons (phonons) having momentum g (Bose distribution function), $w(g)\,\delta(E_{k\sigma} - E_{k-g,\,\sigma'} - \varepsilon_g)$ is the probability of an elementary collision event in which the electron loses an energy $E_{k\sigma} - E_{k-g,\,\sigma'} = \varepsilon_g$ and momentum g; here the first factor - $w(g)$ - in the product is the square of the matrix element modulus, corresponding to the given quantum transition and the second factor - the δ-function - provides for the conservation of energy and momentum. However, at low temperatures the transfer-of-momentum process is a "slow process" (diffusion in momentum space); in each collision, the component of the momentum in the direction of the field changes by an amount directly proportional to g^2.[8] Consequently, the expression under the integral in (2) must also be divided by the number of collisions in the course of which a conduction electron loses its entire momentum in the direction of the field. This number will, obviously, be inversely proportional to g^2.

---

* Hereinafter we shall have occasion to refer to the equations in this reference (Ref. 3); to denote these we will use the original equation number preceded by the Roman numeral I.

In other words, the resistance must be directly proportional to the number indicating how many times per second the entire momentum of the electron directed along the field can be reduced to zero as the result of collisions, i.e.,

$$\rho = \int \overline{N}_g^{\mathbf{k}} w(g)\, \delta(E_{\mathbf{k}\sigma} - E_{\mathbf{k}-g,\,\sigma'} - \varepsilon_g)\, g^2\, dg, \tag{3}$$

where integration is carried out over the entire g momentum space.

If we neglect the difference between the energies of conduction electrons in states with opposite spins, i.e., assume that $E_{\mathbf{k}\sigma} \approx E_{\mathbf{k}\sigma'} = E_{\mathbf{k}}$ and also assume that $E_{\mathbf{k}}$ depends only on $|\mathbf{k}| \equiv k$, we can write the following approximate equality:

$$E_{\mathbf{k}} - E_{\mathbf{k}-g} \approx \frac{dE_{\mathbf{k}}}{dk}\, g\left(\cos\theta_{\mathbf{k}g} - \frac{g}{2k}\right), \tag{4}$$

where $\theta_{\mathbf{k}g}$ is the polar angle of the vector g, measured from the direction of vector k.

After transformation to spherical coordinates and integration - taking (4) into account - equation (3) assumes the form

$$\rho = C \int \overline{N}_g\, w(g)\, (ag)^3\, d(ag) = C \int \frac{w(g)\,(ag)^3\, d(ag)}{\exp(\varepsilon_g / \varkappa T) - 1}, \tag{5}$$

here C is a constant independent of the temperature and the following substitution in the function under the integral is indicated

$$\cos\theta_{\mathbf{k}g} = \frac{g}{2k} + \frac{\varepsilon_g}{g\,(dE_{\mathbf{k}}/dk)}. \tag{6}$$

(In general, the condition $|\cos\theta_{\mathbf{k}g}| \leqslant 1$ must limit the region of integration over g).

By means of equation (5), bearing in mind the substitution (6), we can determine the form of the temperature dependence of the resistance of a metal for any given specific mechanism of the collision of conduction electrons with Bose quasi-particles (phonons or ferromagnons). It also proves feasible to evaluate the possible contribution of each of the different mechanisms.

4. First, let us derive from (5) the "T^5 law" for the resistance ρ_{lat} of the lattice due to the collision of conduction electrons with phonons. In this case

$$\varepsilon_g = \varkappa T_D \frac{g}{g_0}, \tag{7}$$

and

$$w(g) = \frac{2\overline{\mathcal{E}}^2 \hbar^2 g_0 g}{9M\varkappa T_D}, \tag{8}$$

where T_D is the Debye temperature; $g_0 = \sqrt[3]{6\pi^2}/a$ for a cubic lattice having a lattice constant a; $\overline{\mathcal{E}}$ is the mean kinetic energy of a conduction electron (this is of the same order of magnitude as the Fermi energy), and M is the mass of a metal atom.

Hence,

$$\rho_{lat} = \frac{2C\overline{\mathcal{E}}^2 \hbar^2 g_0}{9M\varkappa T_D a} \int_0^\infty \frac{(ag)^4\, d(ag)}{\exp(\varepsilon_g/\varkappa T) - 1}.$$

The last equation, after replacement of the integration variable

$$\varepsilon_g / \varkappa T = y \tag{9}$$

and taking tabular integral, assumes the form

$$\rho_{lat} \approx C \frac{10^2 \pi^4 \overline{\mathcal{E}}^2 \hbar^2}{Ma^2 \varkappa T_D} \left(\frac{T}{T_D}\right)^5. \tag{10}$$

5. Now let us consider the collisions of conduction electrons with ferromagnons.

For processes of the $\Delta m = 0$ type, due to electrostatic exchange interaction, according to (I, 3.34),

$$w(g) \approx |2(\alpha' - \lambda\beta')|^2, \quad *$$

and, consequently,

$$\rho_0 = 2C(\alpha' - \lambda\beta')^2 \int \frac{(ag)^2 d(ag)^2}{\exp(\varepsilon_g/\varkappa T) - 1}.$$

Here the constant term W_0 in the expression (1) for the energy ε_g introduces only an insignificant correction on the order of $(W_0/\varkappa T) \ll 1$ into ρ_0 ; hence, in the first approximation we can set $W_0 = 0$ and, after substitution according to (9), integrate between the limits of 0 and ∞. As the result we get

$$\rho_0 \approx C\frac{\pi^2}{3}(\alpha' - \lambda\beta')^2\left(\frac{T}{T_K}\right)^2. \qquad (11)$$

We note that in this case one should, as a general rule, take into account the dependence of the conduction electron energy on the orientation of the spin σ (see (I, 3.32)). This would lead to the appearance in (11) of a factor of the form $\exp\left(-\frac{T_0}{T}\right)$, where $T_0 \approx \left(\frac{\alpha'}{\varepsilon}\right)^2 \lambda T_K$. However, on condition of weak polarization of the conduction electrons $(\alpha'/\varepsilon \ll 1)$ in the temperature region in question, $T \gg T_0$ and, consequently, the said factor is close to unity.

6. For collision processes of the $\Delta m = \pm 1$ type, due to magnetic spin-orbital interaction between the s- and d-electrons, according to (I, 3.38),

$$w(g) = \frac{(8\pi L W_0 k \sin\theta_{kg})^2}{Ng^2}. \qquad (12)$$

As simple calculations show, the principal contribution to the magnitude of the electric resistance due to collisions of this type is made by the expression derived from (5), taking (1) and (12) into account, if we assume that $\cos\theta_{kg} \sim 0$ (i.e., set $\sin^2\theta_{kg}$ equal to unity). This, according to (6), obtains in the temperature interval $W_0/\varkappa \ll T \ll T_K$. In this approximation, after the substitution of the integration variable (9), we obtain**

$$\rho_1 \approx C\frac{(8\pi L W_0)^2 \lambda T}{2NT_K}\int_{W_0/\varkappa T}^{\infty}\frac{dy}{e^y - 1} \approx C\frac{\lambda(8\pi L W_0)^2 T}{2NT_K}\ln\frac{\varkappa T}{W_0}. \qquad (13)$$

---

* Here we take all the functions of the conduction electron quasi-momentum for their value at the Fermi brim.

** The aforementioned error in Ref. 2 amounts, essentially, to the following: the authors took into account the factor g^2, distinguishing the expressions under the integral in (2) and (3), only after computing the integral of (2), setting $g^2 \sim T$. In consequence, instead of the integral in (13), they obtained an integral of the form

$$\int_{\text{const}/T}\frac{dy}{y(e^y - 1)} \sim T,$$

which led to the T^2 law for ρ_1.

Thus in the case of magnetic dipolar interaction, collision processes of the $\Delta m = \pm 1$ type yield an additional resistance directly proportional to T^3. Hence, the original calculations of Vonsovski[1] pertain to this particular case.

7. More rigorous calculations of the electric resistance of ferromagnetic metals based on solving the kinetic equations corresponding to each of the collision mechanisms give results fully analogous to those cited above.* It turns out, however, that the "constant" coefficients C differ for the different type processes; namely, the different coefficients bear the same relationship as the exponents of the temperature in the expressions for the temperature dependence of the resistance. Thus, for example, for ρ_{lat} ($\sim T^5$) the constant C is five times greater than for ρ_1 ($\sim T$); for ρ_0 ($\sim T^2$) C is two times greater than for ρ_1, etc. Hence, in using equation (5) for evaluating the relative contributions to the resistance of the different collision mechanisms one must introduce an appropriate factor p, equal to the exponent temperature in the temperature dependence law operating in the given case.

(Mathematically, this follows from the fact that the above-described approximate method of evaluating the temperature dependence of the resistance involves replacement of integrals of the $I_p = \int_0^\infty \frac{x^p dx}{(e^x-1)(1-e^{-x})}$ type by integrals of the form $I_1 = \int_0^\infty \frac{x^{p-1}dx}{e^x-1}$, which, as may readily be seen, are linked by the relation $I_p = pI_1$ - exactly for $p \geq 2$ and approximately for $p = 1$, taking into account the limitation in the integration interval imposed by the inequality $|\cos\theta_{kg}| \leqslant 1$ and provided $\varkappa T \gg W_0$.)

8. From the form of the temperature dependence of the resistance of ferromagnetic metals due to collisions of conduction electrons with ferromagnons - equations (11) and (13) - it follows that at sufficiently low temperatures this part of the resistance will predominate over the ordinary "phonon" resistance characterized by the "T^5 law." We still have to determine, however, whether the critical temperature at which the "ferromagnon" part of the resistance becomes noticeable is high enough for this attribute of ferromagnetic metals to be of practical experimental interest.

To this end let us attempt at least a rough quantitative comparison of the "ferromagnon" and "phonon" portions of the resistance and, at the same time, try to evaluate the relative contributions to the resistance due to $\Delta m = 0$ and $\Delta m = \pm 1$ collision processes.

Invoking equations (10), (11) and (13) and taking into account the remarks regarding the factor p under Section 7 above, we find

$$\frac{\rho_0}{\rho_{lat}} = \frac{(\alpha' - \lambda\beta')^2 Ma^2 \varkappa T_D^6}{750\pi^2 \bar{\mathcal{E}}^2 \hbar^2 T_K^2 T^3}, \qquad (14)$$

$$\frac{\rho_1}{\rho_{lat}} = \frac{8\lambda (LW_0)^2 Ma^2 \varkappa T_D^6}{125\pi^2 \bar{\mathcal{E}}^2 \hbar^2 T_K T^4} \ln \frac{\varkappa T}{W_0}, \qquad (15)$$

$$\frac{\rho_1}{\rho_0} = \frac{48\lambda (LW_0)^2 T_K}{(\alpha' - \lambda\beta')^2 T} \ln \frac{\varkappa T}{W_0}. \qquad (16)$$

Assuming, for example, that $M \sim 10^{-22}$ gm, $T_D \sim 500^\circ$K (iron), $T_K \sim 1000^\circ$K, $a^2 \sim 10^{-15}$ cm^2, $\bar{\mathcal{E}} \sim 10^{-12}$ ergs, $(\alpha' - \lambda\beta') \sim 10^{-14}$ ergs,

---

* The kinetic equation for type $\Delta m = 0$ processes was solved by A. A. Berdichev.[9]

and $LW_0 \sim 10^{-17}$ ergs, we obtain for (14), (15) and (16), respectively

$$\rho_0/\rho_{lat} \sim \frac{10^3}{T^3}, \quad \rho_1/\rho_{lat} \sim \frac{10^3}{T^4}\ln(10T), \quad \text{and} \quad \rho_1/\rho_0 \sim \frac{\ln(10T)}{T}.$$

These results indicate that at temperatures of a few degrees Kelvin the electric resistance peculiar to ferromagnetic metals not only becomes commensurate with the ordinary "phonon" resistance but may appreciably exceed it.

The above evaluations, in view of their highly approximate character, cannot, of course, be taken as definitive proof that the additional "ferromagnon" resistance effect will always be manifest at the low temperatures readily available in cryogenic laboratories (for example, at liquid helium temperatures). However, they do give reason to hope that the effect can be observed experimentally at least in some ferromagnetic metals.

We feel that a series of systematic measurements of the electric resistance of both ferromagnetic and non-ferromagnetic metals in the region of cryogenic temperatures, with a view to proving or disproving the above deductions regarding the distinctive features of the temperature dependence of the resistance of ferromagnetic metals, would be highly desirable and of great theoretical interest.

9. The only experimental study we know of from which one can gain some useful information regarding the peculiarities of the temperature dependence of the resistance of ferromagnets (specifically, iron) in the region of liquid helium temperatures is the investigation of Maissner and Voight.[10] The accompanying figure shows the variation of the resistance of one of the iron specimens* in the temperature interval from 1.29 to 4.21°K, converted to the case of a pure metal (i.e., residual resistance subtracted). As may be seen from the figure, in the given temperature interval, the experimental results are in good agreement with theoretical temperature dependence of the part of the resistance of a ferromagnet that is due to $\Delta m = \pm 1$ type processes (spin-orbital interaction; equation (13)).

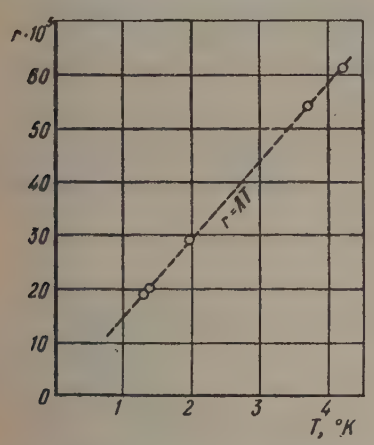

Variation of the resistance of iron (Sample 10) with the temperature at liquid He temperatures, after Maissner and Voight, recalculated for the pure metal. Points from experimental data. $r = R/R_0$; R_0 = resistance at 0°C.

Although the above evidence, which is illustrative of the value and interest presented by experimental investigations in this field, is favorable, it is not in itself sufficient to prove the validity of our theoretical predictions regarding the additional resistance peculiar to ferromagnetic metals.

10. It may be of interest to note that the ferromagnetic spin-system can be excited ("heated") independently of the lattice by magnetic rather than thermal methods, for example, in ferromagnetic resonance.

---

* We chose Maissner and Voight's data for specimen No. 10 for our illustrative example since the results for it are more accurate than for the other specimens studied.

In sufficiently strong microwave resonance fields, an effect termed saturation of ferromagnetic resonance absorption is observed; in particular, this effect is evinced experimentally by a falling off of the longitudinal component of the magnetization with increasing intensity of the microwave magnetic field.[11] The increase in the number of ferromagnons over the "equilibrium" number corresponding to the given temperature should, presumably, lead to an increase in the "ferromagnon" part of the resistance of specimen under the influence of the microwave resonance field. It is possible that this effect can be utilized to study and evaluate the resistance of ferromagnetic metals, due to the collisions of conduction electrons with ferromagnons.

Conclusions

1. Ferromagnetic metals, in view of their having a ferromagnon spectrum branch, must have an additional resistance, peculiar to ferromagnets and due to collisions of conduction electrons with ferromagnons.

2. This additional resistance, which is characterized by a temperature dependence of the form $\rho \sim C_1T + C_2T^2$, may at sufficiently low temperatures (possibly, at liquid helium temperatures) exceed the ordinary "lattice" ("phonon") resistance, which is proportional to T^5.

It may be feasible to separate the "ferromagnon" part of the resistance by non-thermal excitation of the ferromagnetic spin-system.

In conclusion the writer wishes to thank S. V. Vonsovski for his interest and aid in the investigation.

Institute of the Physics of Metals
at the Ural Branch of the
Academy of Sciences of the U.S.S.R.

References

1. S.V.Vonsovski, Zhur. eksp. i teor. fiz., 18, 219 (1948).
2. A.G.Samoilovich & V.A.Iakovlev, Zhur. eksp. i teor. fiz., 22, 350 (1952).
3. S.V.Vonsovski, present issue of the Bulletin.
4. E.A.Turov, present issue of the Bulletin.
5. S.V.Vonsovski & E.A.Turov, Zhur. eksp. i teor. fiz., 24, 419 (1953).
6. E.A.Turov, Doklady AN SSSR, 98, 6, 945 (1954).
7. H.Bethe & A.Sommerfeld, Electron Theory of Metals (in Russian trans.), M.-L. 1938.
8. L.E.Gurevich, Osnovy fizicheskoi kinetiki (Fundamentals of physical kinetics), M.-L. 1940.
9. A.A.Berdyshev, thesis, Sverdlovsk, Ural State University, 1954.
10. W.Maissner & B.Voigt, Ann. de phys., (5), 7, 892 (1930).
11. N.Bloembergen & S.Wang, Phys. Rev., 93, 72 (1954).

ANISOTROPY OF THE SUSCEPTIBILITY AND THE MAGNETOCALORIC EFFECT IN ANTIFERROMAGNETIC MATERIALS

- K. B. Vlasov

The stable macroscopic magnetic state of an antiferromagnet is determined by the minimum level of its thermodynamic potential (for example, the free energy). In computing the part of the free energy associated with the magnetic state of an antiferromagnet, one must take into account the energy of the antiferromagnet in the external magnetic field, the magnetic interaction energy of the elementary magnetic moments and the energy of the electrostatic exchange interaction (see Ref. 1). The familiar antiparallel orientation of the elementary magnetic moments - spins - is due to the exchange interaction.

Hereinafter we shall consider the behavior of antiferromagnetic materials in the range of field intensities in which the energy in the external field is much smaller than the exchange energy but can exceed the magnetic interaction energy of the elementary magnetic moments. In this case we can assume that the spins and, accordingly, the vectors of the spontaneous magnetization of the sublattices* remain antiparallel to each other in the entire field-intensity interval. We shall designate the directions of these vectors through the unit vectors $\mathbf{p}_1(\alpha_1, \alpha_2, \alpha_3)$ and $\mathbf{p}_2(\mathbf{p}_2 \approx -\mathbf{p}_1)$ and the direction of the external field by the unit vector $\mathbf{h}(\beta_1, \beta_2, \beta_3)$.

1. Let us start by establishing the relationships which can be deduced from general thermodynamic considerations.

We resolve the field intensity vector into two components: one parallel, the other perpendicular to the orientation of the magnetic moments. These components will give rise to parallel and perpendicular components of the magnetization (paraprocess):

$$I_{\parallel} = \chi_{\parallel} H \cos\psi$$

and

$$I_{\perp} = \chi_{\perp} H \sin\psi,$$

where $\chi_{\parallel}$ and $\chi_{\perp}$ are, respectively, the parallel and perpendicular susceptibility (in the field intensity interval in question, they may be regarded as independent of the field intensity), ψ is the acute angle between the direction of the field and of the magnetic moments:

$$\cos\psi = (\mathbf{h}, \mathbf{p}) = \cos\alpha_1 \cos\beta_1 + \cos\alpha_2 \cos\beta_2 + \cos\alpha_3 \cos\beta_3.$$

The resultant magnetization, here, in the direction of the field equals

$$I = H(\chi_{\parallel} \cos^2\psi + \chi_{\perp} \sin^2\psi), \qquad (1)$$

the susceptibility equals

$$\chi = \frac{I}{H} = \chi_{\parallel} \cos^2\psi + \chi_{\perp} \sin^2\psi \qquad (2)$$

and the free energy in the external magnetic field is

---

* As in Ref. 1, we shall assume here that the lattice of an antiferromagnet can be regarded, from the magnetic point of view, as divided into two sublattices, both having spontaneous magnetization.

$$F_M = -(\mathrm{I}\,\mathrm{H}) = -(\chi_\parallel \cos^2\psi + \chi_\perp \sin^2\psi) H^2 = H^2(\chi_\perp - \chi_\parallel)\cos^2\psi - \chi_\perp H^2. \quad (3)$$

In view of the magnetic interaction between the elementary magnetic moments, the free energy of the antiferromagnet is dependent on the orientation of the magnetic moments relative to the crystal axes. From considerations of symmetry the part of the free energy termed the free energy of the crystallographic magnetic anisotropy, for single crystals of the rhombic, tetragonal, trigonal and hexagonal systems, can be written in the first approximation as

$$F_K = -(K_x \cos^2\alpha_1 + K_y \cos^2\alpha_2 + K_z \cos^2\alpha_3),$$

where K_x, K_y and K_z are crystallographic magnetic anisotropy constants. In single crystals belonging to the tetragonal, trigonal and hexagonal systems $K_y = K_z$.

We find the equilibrium values of the angles α_1, α_2 and α_3 and, consequently, of ψ from the conditions for the lowest total free energy $F = F_M + F_K$, which, taking account of the additional condition $\cos^2\alpha_1 + \cos^2\alpha_2 + \cos^2\alpha_3 = 1$, are given by

$$\left.\begin{aligned}
(\cos^2\alpha_1 - 1)\frac{\partial F}{\partial \cos\alpha_1} + \cos\alpha_1\cos\alpha_2\frac{\partial F}{\partial \cos\alpha_2} + \cos\alpha_1\cos\alpha_3\frac{\partial F}{\partial \cos\alpha_3} = 0,\\
\cos\alpha_2\cos\alpha_1\frac{\partial F}{\partial \cos\alpha_1} + (\cos^2\alpha_2 - 1)\frac{\partial F}{\partial \cos\alpha_2} + \cos\alpha_2\cos\alpha_3\frac{\partial F}{\partial \cos\alpha_3} = 0,\\
\cos\alpha_3\cos\alpha_1\frac{\partial F}{\partial \cos\alpha_1} + \cos\alpha_3\cos\alpha_2\frac{\partial F}{\partial \cos\alpha_2} + (\cos^2\alpha_3 - 1)\frac{\partial F}{\partial \cos\alpha_3} = 0.
\end{aligned}\right\} \quad (5)$$

Substituting from (3) and (4) in (5) and selecting the orientation of the coordinate axes so that the condition $K_x > K_y > K_z$ is fulfilled, we obtain

$$\left.\begin{aligned}
H^2_{0XY}\cos\alpha_1\cos\alpha_2 + H^2\cos\psi(\cos\alpha_1\cos\beta_2 - \cos\alpha_2\cos\beta_1) = 0,\\
H^2_{0XZ}\cos\alpha_1\cos\alpha_3 + H^2\cos\psi(\cos\alpha_1\cos\beta_3 - \cos\alpha_3\cos\beta_1) = 0,\\
H^2_{0YZ}\cos\alpha_2\cos\alpha_3 + H^2\cos\psi(\cos\alpha_2\cos\beta_3 - \cos\alpha_3\cos\beta_2) = 0,
\end{aligned}\right\} \quad (6)$$

where H_{0XY}, H_{0XZ} and H_{0YZ} are the critical fields characterized by

$$H^2_{0XY} = \frac{K_X - K_Y}{\chi_\perp - \chi_\parallel} = \frac{K_1}{\chi_\perp - \chi_\parallel};\quad H^2_{0XZ} = \frac{K_X - K_Z}{\chi_\perp - \chi_\parallel} = \frac{K_2}{\chi_\perp - \chi_\parallel};\quad H^2_{0YZ} = \frac{K_Y - K_Z}{\chi_\perp - \chi_\parallel} = \frac{K_3}{\chi_\perp - \chi_\parallel}, \quad (7)$$

and

$$H^2_{0XZ} = H^2_{0YZ} + H^2_{0XY}.$$

The solutions of (6) have been analyzed by Gorter and Haatjes (Ref. 2).* In the field intensity interval in question one solution - designated as Type A by Gorter and Haatjes - satisfies the minimal free energy condition. This solution corresponds to the case of opposite orientations of the vectors P and $-$P, characterizing the direction of the vectors of the spontaneous magnetization of the sublattices. At zero field the magnetic moments are directed along the X axis. As the field intensity is increased the magnetic moments tend to orient themselves perpendicularly to the direction of the field (rotation process).

---

* Gorter and Haatjes carried out the calculations for a temperature equal to absolute zero, utilizing the molecular field method. This restriction is not imposed in the present investigation.

When the field vector lies in the XZ plane, the solution of (6) has certain distinctive features, namely, when the values of the magnetic field intensity satisfy the equation of a hyperbola

$$\frac{H_X^2}{H_{0_{XY}}^2} - \frac{H_Z^2}{H_{0_{YZ}}^2} = 1, \qquad (8)$$

the magnetic moments suddenly change direction and orient themselves along the Y axis. If the field vector lies in the XY plane, the solution of equation (6) has the form

$$\operatorname{tg} 2\psi = \frac{\sin 2\beta}{\cos 2\beta - \frac{H^2}{H_{0_{XY}}^2}}, \qquad (9)$$

where β is the acute angle between the field vector and the X axis. When the field vector lies in the XZ plane, ψ is determined by equation (9), in which $H_{0_{XZ}}^2$ should be substituted for $H_{0_{XY}}^2$. However, in this case (9) is applicable only up to values of the field intensity satisfying the equation of the hyperbola (8), when $\left|\frac{H_Z}{H_X}\right| < \frac{H_{0_{YZ}}}{H_{0_{XY}}}$.

When the field vector lies in the YZ plane the magnetic moments remain oriented along the X axis.

For crystals having tetragonal, trigonal and hexagonal symmetry solution (9) is valid for any crystallographic orientation.

Equations (2) and (6) or, in the particular case when the field vector lies in the XY plane, equation (9) wholly determine the anisotropy and the field dependence of the susceptibility in antiferromagnetic single crystals. An analysis of these dependences for the particular case when $K_Y - K_Z = 0$ is given in Ref. 1.

Let us now compute, on the basis of the above relationships, the temperature change which should occur incident to adiabatic-isochoric magnetization of an antiferromagnet (magnetocaloric effect).

It follows from thermodynamic considerations[3] that

$$\delta T = -\frac{T\left(\frac{\partial I}{\partial T}\right)_{H,V}}{C_{H,V}} dH = f(H, T)\, dH. \qquad (10)$$

Going over to finite temperature changes incident to an increase of the magnetic field intensity from 0 to H, we obtain

$$T = T_0 + \int_0^H f(H, T)\, dH. \qquad (11)$$

Inasmuch as we cannot, in the general case, determine the explicit form of the temperature dependence of the parameters $\chi_\parallel$, $\chi_\perp$ and K in terms of which the derivative $\left(\frac{\partial I}{\partial T}\right)_{H,V}$ and the specific heat C_H are expressed from thermodynamic considerations alone, we cannot solve (11) for the general case. We can, however, obtain an approximate solution of (11) by the method of successive approximations for the case when $\Delta T = T - T_0 \ll T_0$; this, as will be seen below, is the case which virtually always obtains in the field intensity interval in question and at temperatures not in the immediate proximity of absolute zero. Let us examine the case when the magnetization is described by equations (1) and (9). For the zero approximation we select the solution $T = T_0$. Substituting from (1) and (9) in (11),

assuming that in the first approximation the specific heat C_H is independent of the field intensity and going over from integration over H from 0 to H to integration over ψ from β to ψ, we obtain the following expression for ΔT in the first approximation:

$$\Delta T = -\frac{1}{2}\cdot\frac{T_0}{C_H}\left[\frac{\partial\chi_\parallel}{\partial T}H_{0XY}^2\cos\beta\frac{\sin(\psi-\beta)}{\sin\psi}+\frac{\partial\chi_\perp}{\partial T}H_{0XY}^2\sin\beta\frac{\sin(\psi-\beta)}{\cos\psi}+\right.$$

$$\left.+H_{0XY}^4(\chi_\perp-\chi_\parallel)\frac{\partial\left(1/H_{0XY}^2\right)}{\partial T}\sin^2(\psi-\beta)\right], \qquad (12)$$

where C_H, $\frac{\partial\chi_\parallel}{\partial T}$, H_0, $\frac{\partial\chi_\perp}{\partial T}$, $(\chi_\perp-\chi_\parallel)$ and $\frac{\partial\left(1/H_{0XY}^2\right)}{\partial T}$ taken for $T = T_0$.

In view of (7) we can go over from the derivative $\frac{\partial\left(1/H_{0XY}^2\right)}{\partial T}$ to the derivative of the magnetic crystallographic anisotropy constant with respect to the temperature. Then instead of (12) we obtain

$$\Delta T = -\frac{1}{2}\frac{T}{C_H}[A(T)f_1(H)+B(T)f_2(H)+D(T)f_3(H)], \qquad (13)$$

where

$$A(T)=\frac{\partial\chi_\parallel}{\partial T}H_0^2,\quad B(T)=\frac{\partial\chi_\perp}{\partial T}H_0^2,\quad D(T)=-\frac{\partial K_1}{\partial T}; \qquad (14)$$

$$\left.\begin{aligned} f_1(H)&=\left[\cos\beta\frac{\sin(\psi-\beta)}{\sin\psi}-\sin^2(\psi-\beta)\right],\\ f_2(H)&=\left[\sin\beta\frac{\sin(\psi-\beta)}{\cos\psi}+\sin^2(\psi-\beta)\right],\\ f_3(H)&=\sin^2(\psi-\beta). \end{aligned}\right\} \qquad (15)$$

These equations describe the dependence of the change in temperature, incident to adiabatic magnetization of an antiferromagnet, on the magnetic field intensity (when the values of A(T), B(T) and D(T) are known from other magnetic measurements) and on the crystallographic direction in which the field is applied (anisotropy of the magnetocaloric effect).

Let us analyze the field dependence of the factors $f_1(H)$, $f_2(H)$ $f_3(H)$ on the field intensity.

Let us assume that the field is applied in the natural direction of magnetization of the sublattices* ($\beta = 0$). In this case these factors vary in the following manner: when $H < H_0$, the factor $f_1(H) = H^2/H_0^2$; when $H = H_0$, $f_1(H)$ drops from unity to zero and when $H > H_0$, $f_1(H) = 0$ (solid curve in accompanying figure a). When $H < H_0$, $f_2(H) = 0$; when $H = H_0$, $f_2(H)$ jumps up from zero to unity and when $H > H_0$, $f_2(H) = H^2/H_0^2$ (solid curve in figure b). When $H < H_0$, $f_3(H) = 0$; when $H = H_0$, $f_3(H)$ jumps from zero to unity and when $H > H_0$, $f_3(H) = 1$ (solid curve in figure c).

Let the field be applied perpendicularly to the natural direction of magnetization of the sublattices ($\beta = 90^\circ$). In this case in the entire field interval in question: $f_1(H) = 0$; $f_2(H) = H^2/H_0^2$ and $f_3(H) = 0$ (dotted line curve in figure b; in figures a and c this

---

* Here the natural direction of magnetization of the sublattice is understood to mean the crystallographic direction in which the magnetic moments (magnetizations) are oriented in the absence of an external magnetic field. In Ref. 1 - and certain other investigations - this direction is termed the direction of preferred magnetization.

for the temperature dependence of $\chi_\parallel$, $\chi_\perp$ and K_1:

$$\chi_\parallel = \frac{N\mu_0^2(1-y^2)}{kT_K\left[\tau + \frac{0}{T_K}(1-y^2)\right]}, \tag{16}$$

$$\chi_\perp = \frac{N\mu_0^2}{k(T_K+\theta)}, \tag{17}$$

$$K_1 = K_1(0)\,y^2, \tag{18}$$

where $\tau = T/T_K$ and y is the magnetization of the sublattices in relative units, with

$$y = \text{th}\frac{y}{\tau}. \tag{19}$$

T_K is the antiferromagnetic Curie point above which antiferromagnetism vanishes and θ is the paramagnetic Curie point;

$$T_K = \frac{1}{k}[(P-Q)+(P'-Q')\cos^2(\psi-\beta)], \tag{20}$$

$$\theta = -\frac{1}{k}[(P+Q)+(P'+Q')\cos^2(\psi-\beta)], \tag{21}$$

Where P and Q are the sums of the integrals, characterizing the magnitude of the electrostatic, quasi-classical exchange interaction and the magnetic exchange interaction and P' and Q' are the sums of the integrals characterizing the quasi-classical and magnetic exchange interaction between electrons of one sublattice and both sublattices, respectively.

It follows from (20) that the temperature of the antiferromagnetic Curie point is dependent on the orientation of the elementary magnetic moments relative to the crystal axes (anisotropy of the Curie point). The maximum spread of the Curie points, resulting from differences in orientation can readily be related[1] to the value of the critical field at absolute zero (i.e., $H_0(0)$) and the perpendicular susceptibility:

$$\Delta T_{K\,max} = \frac{\chi_\perp H_0^2(0)}{R}, \tag{22}$$

where R is the gas constant.

In evaluating the magnitude of the magnetocaloric effect, one must bear in mind that in experimental studies of the field dependence of the magnetic susceptibility and of the change in temperature incident to adiabatic magnetization it is necessary to employ antiferromagnetic materials with a low Curie point (i.e., to make the measurements at low temperatures). This, as follows from (7) and (17) is due to the fact that the critical value of the field, in the vicinity of which the most interesting effects should be observed, is proportional to the Curie temperature. It is not impossible, of course, that there may exist or can be prepared antiferromagnetic materials having low values of the anisotropy constants. Such antiferromagnets could, according to (7), be characterized by a relatively low value of the critical field even if they should have comparatively high Curie points.

The most complete experimental data are available at present for a $CuCl_2 \cdot 2H_2O$ single crystal ($T_K = 4.3^\circ K$ and $H_0(0) \approx 6500$ oersted).[4] Our further calculations will pertain specifically to this material. In antiferromagnetic substances with so low a Curie point, as follows from theory and is confirmed by experiment,[4] the specific heat is

curve obviously coincides with the horizontal axis.

The curves in the accompanying figures also show the field dependences of these factors in the cases when $\beta = 6^\circ$ and $\beta = 45^\circ$.

Thus analysis of the change in temperature, incident to adiabatic magnetization with the field intensity makes it possible to determine the magnitudes and, consequently, if measurements are made at different temperatures, also the temperature dependences of the parameters H_0, $\frac{\partial \chi_\parallel}{\partial T}$, $\frac{\partial \chi_\perp}{\partial T}$ and K_1. To do this one must, of course, first determine the temperature dependence of the specific heat C_H. Thus, if we plot the dependence of the change in temperature due to the magnetocaloric effect on the square of the relative magnetic field intensity H^2/H_0^2, the slope of the $\Delta T = T(H^2/H_0^2)$ line constructed for $\beta = 0^\circ$ in the field intensity interval $0 < H < H_0$ will give us the value of $\frac{1}{2} \cdot \frac{T}{C_H} H_0 \frac{\partial \chi_\parallel}{\partial T}$. In the $H > H_0$ field interval, the slope of the line will give us $\frac{1}{2} \cdot \frac{T}{C_H} H_0 \frac{\partial \chi_\perp}{\partial T}$, while extrapolation of this line to the point where $H = 0$ will give the value of $\frac{1}{2} \cdot \frac{T}{C_H} \cdot \frac{\partial K_1}{\partial T}$. The slope of the ΔT line recorded for $\beta = 90^\circ$ will give the value of $\frac{1}{2} \cdot \frac{T}{C_H} H_0 \frac{\partial \chi_\perp}{\partial T}$.

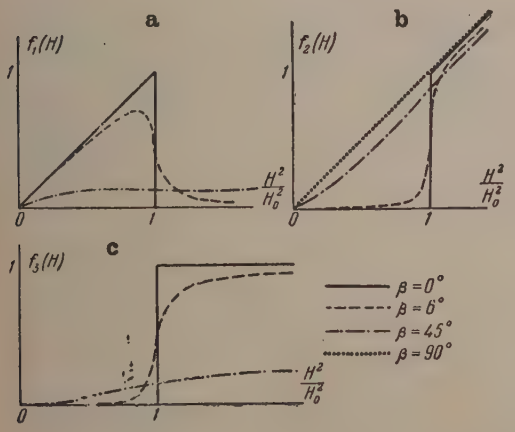

Dependence of the factors $f_1(H)$, $f_2(H)$ and $f_3(H)$, determining the magnitude of the magnetocaloric effect on the relative value of the square of the field intensity for different orientations of the field vector relative to the natural direction of magnetization of the sublattices. H_0 - critical field; β - angle between field vector and natural direction of sublattice magnetization.

2. In order to establish the temperature dependence of the change in temperature that must occur incident to adiabatic magnetization and evaluate its magnitude theoretically we must know the explicit form of the temperature dependence of H_0, $\chi_\parallel$, $\chi_\perp$ and K_1. This requires microscopic analysis. Such an analysis was carried out in Ref. 1, for example, in which the following model was employed. The lattice of the antiferromagnet was divided into two sublattices, magnetized in opposite directions at temperatures below the antiferromagnetic Curie point. In the calculations we used the method of energy centers of gravity, which, rigorously speaking, is valid only for temperatures near and above the Curie point, and took into account dipole-dipole magnetic interaction. We obtained an expression for the part of the free energy of an antiferromagnet, dependent upon the magnetic state of the system, from the minimum conditions which can be defined by the relationships (2), (4), (7) and (9)*, as well as expressions

---

* These relationships were deduced for the particular case when $K_y = K_z$. However, as may readily be seen, if in the calculations it is assumed that the lattice is characterized by rhombic, rather than tetragonal or hexagonal symmetry expressions of the type of (4) and (7) will be obtained.

determined primarily by the presence of antiferromagnetic ordering of the magnetic moments. Knowing the form of the dependence of the free energy on the magnetic state of the antiferromagnet,[1] we can deduce an expression for the specific heat:

$$C_H = -\frac{R}{2} \cdot \frac{\partial y^2}{\partial \tau}. \qquad (23)$$

Substituting from (23), (14) and (18) in (13), taking (7) and (22) into account and recalling that, according to (17), the perpendicular susceptibility is temperature independent, we arrive at the following expression for the temperature change which should occur incident to adiabatic magnetization:

$$\Delta T = -\left[\tau \frac{A(T)}{D(T)} f_1(H) + \tau f_3(H)\right] \Delta T_{C_{max}}. \qquad (24)$$

All the quantities entering into (24) can be evaluated by means of (14), (7), (16), (18) and (19). Calculations show that as the temperature goes down below the Curie point the factor $\tau \frac{A(T)}{D(T)}$ should increase (from unity at the Curie point to 1.15, for example, at $\tau = 0.8$ and 1.45 at $\tau = 0.5$). Hence, if the specific heat of an antiferromagnetic material is determined primarily by its magnetic state, the change in temperature produced by the paraprocess (first term in (24)) must increase with decreasing temperature, while the change due to the process of rotation (second term in (24)) must decrease. When the field is increased from zero to H, the change in temperature from some initial value T should vary in the following manner in the case when the direction of the field coincides with the natural direction of magnetization of the sublattices ($\beta = 0$): At field intensities $H < H_0$, the absolute magnitude of the temperature change will be proportional to H^2, at $H = H_0$ the change will attain the value $\tau \frac{A(T)}{D(T)} \Delta T_{\kappa_{max}}$, then precipitatedly drop to $\tau \Delta T_{\kappa_{max}}$ and remain equal to this last value in fields $H > H_0$. For other orientations of the external field relative to the natural direction of magnetization, the absolute value of the temperature change will be smaller and its dependence on the field intensity will be more complicated (specifically, the peak in the temperature-change curve should be less pronounced).

It must be borne in mind, however, that calculations based on the method of energy centers of gravity can be expected to give results agreeing with experiment only in the vicinity of the Curie point; in contrast our computations of the field dependence of the magnetocaloric effect (see (13)) are valid in a wider temperature range (except, of course, for the region in the immediate proximity of absolute zero). Thus, for instance, comparison of the temperature dependence of the specific heat characterized by (23) with the experimental dependence found by Gorter[4] shows that the specific heat falls off more rapidly with decreasing temperature than the equation predicts. Moreover, it is possible that the crystallographic magnetic anisotropy constant varies with the temperature in a more complex manner than is indicated by (18) (as is the case, for instance, in ferromagnets), inasmuch as in deriving (18) only magnetic dipole-dipole interaction was taken into account. We can conclude with certainty that in antiferromagnets, in contrast to the case in para-

magnetic materials, one can expect to observe cooling incident to adiabatic magnetization below the Curie point. The decrease in temperature which should occur incident to such magnetization 1) will depend on the initial temperature of the material, and 2) should depend in a complex manner on both the strength of the magnetic field and its orientation relative to the crystal axes. We can judge of the magnitude of the temperature change which one might expect to observe in the antiferromagnetic temperature region on the basis of the data on the maximum variation of the Curie point as a function of the orientation of the field relative to the crystal axes in $CuC_2 \cdot 2H_2O$ which Poulis and Hardeman[5] report equal to 0.04°K.

In conclusion I desire to thank S. V. Vonsovski for valuable discussion of the work.

References

1. K.B.Vlasov, Izv. AN SSSR, Ser. fiz., 18, 339 (1954). (Trans. in BULLETIN Vol. 18, No. 3, p. 35.)
2. C.J.Gorter & J.Haatjes, Physica, 18, 285 (1952).
3. S.V.Vonsovski & Ia.S.Shur, Ferromagnetizm (Ferromagnetism), M.-L. 1948.
4. C.J.Gorter, Rev. Mod. Phys., 25, 332 (1953).
5. N.J.Poulis & G.E.G.Hardeman, Physica, 18, 429 (1952).

BULLETIN of the Academy of Sciences of the USSR - Physical Series
Vol. 19, No. 4, 1955 - Conference on Cryogenic Magnetism (1-3 July 1954)

TABLE OF CONTENTS

	Page Orig.	Trans.
Conference on magnetism at low temperatures (introduction and summary of conference papers) - S.V.Vonsovski	387	346
On the oscillations of the thermodynamic parameters of a degenerate Fermi gas at low temperatures - I.M.Lifshits & A.M.Kosevich	395	353
Oscillation effects in magnetic fields - G.E.Zil'berman	404	361
Anisotropy of the magnetic properties of zinc single crystals at low temperatures - B.I.Verkin & I.M.Dmitrenko	409	365
Galvanometric effects and the properties of conduction electrons in metals - E.S.Borovik	429	383
Investigation of the photo-magnetoelectric effect in cuprous oxide at low temperatures - A.P.Komar, N.M.Reinov & S.S.Shalyt	444	397
Certain problems relating to the quantum-mechanical theory of crystals at low temperatures - S.V.Vonsovski	447	399
Relaxation processes in ferromagnetic metals at low temperatures - E.A.Turov	462	414
Electric conductivity of ferromagnetic metals at low temperatures - E.A.Turov	474	426
Anisotropy of the susceptibility and the magnetocaloric effect in antiferromagnetic materials - K.B.Vlasov	481	433

Translated in 1956 by
Columbia Technical Translations
5 Vermont Ave., White Plains, N. Y.

TRANSACTIONS OF THE THIRD ALL-UNION CONFERENCE ON THE PHYSICS OF COSMIC RAYS

The Third All-Union Conference on the Physics of Cosmic Rays was held December 15-23, 1954, in Moscow. The program of the Conference comprised reports in the following categories:

1) Interaction of cosmic ray particles having energies of the order of 10^{10} ev with atomic nuclei.

2) Interaction of nucleons and photons of energies under 10^{9} ev with nucleons and atomic nuclei.

3) Theory of high-energy processes.

4) Interaction of particles at ultra-high energies.

5) New particles.

6) Variations and origin of cosmic rays.

The transactions of the Conference in the form of reports, revised and corrected by their authors, will be published in the BULLETIN (Izvestiia) of the USSR Academy of Sciences - Physical Series - Vol. 19, No. 5 - i.e., the present issue (Categories 1 and 2), and No. 6 (Categories 3-5) and Vol. 20, No. 1 (Category 6). In cases when the full report is not made available the material will appear in the form of an abstract. The published transactions will not include the lecture "On the Multiple Formation of Particles" by L. D. Landau or the survey on "New Particles" by A. O. Vaisenberg.

The following participated in editing and preparing the transactions for publication: M. A. Adamovich (interaction of photons from a synchrotron with matter), N. P. Bogachev (interaction of particles accelerated by a synchrocyclotron with matter), M. I. Daion (new particles, studies conducted by means of magnetic mass-spectrometers and methodological investigations), L. I. Dorman (variations in the intensity of cosmic rays), I. P. Ivanenko (theoretical investigations), V. S. Mursin (investigations carried out in the stratosphere), L. I. Sarycheva (interactions at ultra-high energies), M. I. Fradkin (origin of cosmic rays).

S. N. Vernov

Chairman of the Organizing Committee of the Third All-Union Conference on the Physics of Cosmic Rays, Associate Member of the Academy of Sciences.

OPENING ADDRESS

- S.N.Vernov

The Third All-Union Conference on the Physics of Cosmic Rays is declared open.

We all know what important discoveries have been made thanks to investigations of cosmic rays. Aside from positrons and μ-mesons, whose discovery dates back to the nineteen thirties, most of the new elementary particles detected in recent years have been discovered as a result of cosmic ray studies.

Scientists working in the field of cosmic radiation have established the basic nature of the elementary event of genesis of new particles and have thrown light on the characteristics of electronic-nuclear showers. The presence in cosmic rays of particles with extremely high energies makes it feasible to investigate any nuclear processes, no matter how high their energetic threshold. In view of the extreme shortness of the wavelengths corresponding to cosmic radiation particles we can now hope to "penetrate" into the nuclei of elementary particles. We may, perhaps, succeed in elucidating the structure of elementary particles, in determining the nature of the fundamental "building blocks" forming the elementary particles - or, let us say rather, of the particles which at the present stage of development of physics we call elementary. It can well be that in the near future entirely new physical laws will be discovered, that the next step -- comparable in importance to the development of quantum mechanics and the theory of relativity -- will be taken. I believe that cosmic rays will play a very important part in deciphering the mysteries of matter.

For the first time at this Third Conference, in addition to reports on investigations of cosmic rays, we shall hear and discuss the great achievements of our physicists working with particle accelerators. The Conference will learn of the results obtained by the group of physicists headed by M.G.Meshcheriakov and the studies carried out under the leadership of V.I.Veksler. Thus we shall discuss here the properties of nucleons, mesons and photons obtained in accelerators and having energies close to those of cosmic ray particles. The consideration of such data at a conference on cosmic rays is important, for experiments with accelerators alone or with cosmic rays alone will not suffice for the successful development of the physics of high-energy particles. Only through the proper conjunction of the results of investigations of cosmic rays and of artificial beams of high-energy particles will efficient progress be achieved.

The investigation of cosmic ray particles permits studying the interactions of particles of energies to 10^{17} ev with atomic nuclei and nucleons. It is obvious that such studies can yield very valuable results. But in order to understand such processes and clarify the nature of the elementary interaction events at these elevated energies we must know the attributes and characteristics of elementary particles in the region of lower energies. In this respect experiments with accelerators can greatly aid in investigations at ultra-high energies as well.

At the same time, in studying cosmic rays one can come upon new, as yet unknown effects and hence suggest new approaches to scientists working with particle accelerators. There is good reason to hope that at the present Conference physicists working in the field of cosmic rays and physicists operating with accelerators will acquaint us with new phenomena that will be of great significance for Physics as a whole.

I should like to express my hope that this Conference will hear truly creative discussions, that the conferees will boldly put forth new ideas and hypotheses. It matters little if some of the hypotheses advanced should later prove wrong. It is important only that in such cases their authors should not persist in their errors, but should abandon their erroneous assumptions in time.

As you know from the distributed program (abstracts) we shall first discuss the results of investigations of 10^{10}-10^{12} ev energy particles with atomic nuclei. Next we shall hear reports on phenomena in the energy range below 10^9 ev, according to data obtained on accelerators. Following this, we shall discuss theoretical investigations. Then we shall return to experiment and learn of investigations of the complex but highly important processes occurring at ultra-high energies. Next we shall consider data on new elementary particles. Finally the Conference will hear of new hypotheses regarding the origin of cosmic rays and of the first, but highly successful attempts to utilize the results of continuous recording of the intensity of cosmic rays for the investigation of the processes in which cosmic rays are involved on their path to the Earth.

L.D.Landau's lecture "On the Multiple Formation of Particles" will be read at the Conference. This lecture will serve to acquaint the conferees with Landau's theory and introduce them to many of the theoretical problems with which the Conference will be concerned.

One and a half years have elapsed since our previous Conference on Cosmic Rays. During this interval our physicists working on cosmic rays have accomplished much. They have carried out many new investigations and deepened and extended their theoretical analyses of the effects produced in matter by cosmic radiation. It is a pleasure to report that in the interim the scientific collectives working in other cities of our land, including those of the different Soviet Republics, have been materially strengthened. It must be noted, however, that both the scope and conditions of scientific work outside Moscow are still far from being fully adequate. I sincerely hope that the present Conference and a number of organizational measures now being undertaken will help remedy the situation.

* * * * * * *

than the ionization produced by a relativistic particle, traversing the diameter of the chamber, it was possible to establish reliably the number of relativistic particles at high altitudes and thus substantiate the afore-described method of determining the number of electrons.

Fig. 2 shows a diagram of the equipment used by Rapoport[9] for measuring the air-lead transition effect and one of the transition curves obtained at 10 km.

The results of measurements of the electronic-photonic energy flux at 51 and 31° N together with the difference between the resultant curves are shown in Fig. 3. As may be seen from the figure, at 31° the energy flux of the electronic-photonic component slowly falls off as the depth of the atmosphere penetrated by the radiation increases (Curve 2). On the other hand the differential curve (3) falls off more rapidly with increasing depth. The difference between curves 2 and 3 is due to the fact that at high energy of the primary particles (at latitude 31° N, the mean energy of the primary protons equals 20 Bev) an appreciable part of the energy, after collision with a nucleus, is retained by the nucleon and thus is carried further into the depth of the atmosphere, where π^0 mesons are produced.

Knowing the electron-photon energy flux and the number of electrons, we can easily compute $E_{ep}(p)$ by means of equation (1). Fig. 4 shows the altitude dependence of the ratio $E_{ep}(p)/\Delta N_0(p)$, where $\Delta N_0(p)$ is the number of primary particles which have interacted in the thickness of the atmosphere above the pressure altitude p. Curve 1 pertains to measurements made at 31°N; curve 2 represents the difference between the values for 51 and 31° N. The rise of the curves indicates that neutral pi mesons are effectively produced not only by primary but also by secondary particles. If only primaries created π^0 mesons the curves of Fig. 4 would be parallel to the p-axis. The threefold increase observed at 31° N indicates that the energy transferred to mesons in each nuclear collision event does not exceed 1/3 the energy of the incident nucleon.

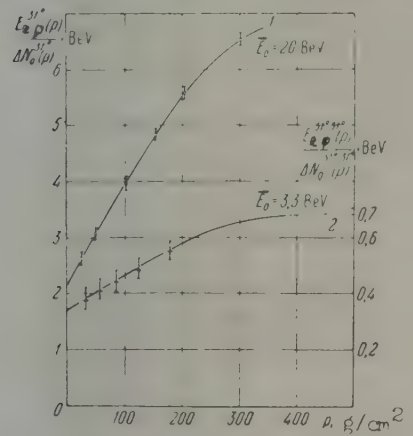

Fig. 4. Variation of the ratio $E_{ep}(p)/N_0(p)$ with depth in the atmosphere (p) 1) results of measurements at 31° N; 2) difference between results at 51 & 31°.

The data for the highest altitudes permit us to evaluate the fraction of the proton energy transferred to π^0 mesons in the first collision of the primary proton with an atomic nucleus. From Fig. 4 we deduce that at latitude 31° the electronic-photonic component receives about 2.2 Bev energy, which amounts to 11% of the mean energy of the primaries. Assuming that twice as much energy is transferred to the $\pi^{\pm}$ mesons as to the π^0 mesons and taking into account the formation of the electronic-photonic component from the disintegration of the mu mesons, we obtain

$$\varkappa_\pi = \frac{E_{\pi^0} + E_{\pi^\pm}}{E_0} = \begin{cases} (21 \pm 5)\,\% & \text{for } E_0 = 3 \text{ BeV}, \\ (28 \pm 3)\,\% & \text{for } E_0 = 20 \text{ BeV}. \end{cases}$$

where $\varkappa_\pi$ is the average fraction of the energy of the primary particle transferred to the pi mesons in a collision with a light nucleus. At 31° N approximately 75% of the total primaries energy is contributed by particles of energies exceeding 14 Bev; hence for particles with energies over 14 Bev (E_0 = 40 Bev) we should also obtain $\varkappa_\pi \gtrsim 30\%$.

In determining the energy transferred to the π^0 mesons a correction (on the order of 20%) was introduced to take account of the energy of the mu-meson

INVESTIGATION OF THE INTERACTION OF NUCLEONS WITH LIGHT NUCLEI AT ENERGIES OF 10^9-10^{12} EV

- S.N.Vernov, N.L.Grigorov, G.T.Zatsepin & A.E.Chudakov

Investigation of the different components of cosmic rays, carried out in the stratosphere at different latitudes, can help elucidate the general characteristics of the interaction of nucleons, having diverse energies, with light atomic nuclei. From these characteristics in turn we can deduce the nature and features of the effects occuring in the collision of high-energy particles with each other.

Reports on studies of the different components of cosmic radiation in the stratosphere at geomagnetic latitudes of 51, 31 and 2° N were presented at the preceding Conference on Cosmic Rays. The components investigated included

1) high-energy ($\gtrsim$ 3 Bev) protons;[2]
2) electrons and photons;[3]
3) mu mesons;[1]
4) components producing nuclear disintegration.[1,4]

By virtue of the fact that the investigations were made at different latitudes one can determine the character of the production of the different components listed by primary particles, having energies between certain bounds, by subtracting the values obtained at lower latitudes from those for higher latitudes.

Pi mesons are created in the collision of a proton with an atomic nucleus. Neutral pi mesons give rise to the electronic-photonic component.[5] Thus measurement of this component at great altitudes permits investigating the generation of π^0 mesons incident to collisions of nucleons with light nuclei. Analogous measurements of mu mesons, produced in almost all cases of pi-meson decay, yield information on the generation of π^+ mesons incident to the encounter of nucleons with light nuclei. It follows from an analysis of the experimental data that after collision most of the energy of the primary particle is carried off by one of the nucleons; in view of this the absorption of high-energy nucleons is a multiple rather than a single-event process. Finally in collisions of the nucleon with nuclei some of the energy is expended on nuclear splitting. Investigations in the stratosphere of pulses in an ionization chamber and the ionization produced by non-relativistic particles have made it possible to evaluate the values of the energy transferred by primary particles of different energies to the disintegration products of light nuclei.

The present report is devoted to a summary of the experimental data and their analysis. In computations the interaction free path for nucleons in the atmosphere is assumed to be equal to 60-70 g/cm^2, in accordance with a number of experimental studies.[6] We shall consider the various components in turn.

1. High-energy protons. The arrangement of counters used and the results obtained by Charakhch'ian[2] are shown in Fig. 1. The apparatus consisted of a telescope and 17 hodoscopic counters. A 10 cm lead absorber, consisting of two plates, was located between the counters. The interaction of a proton having an energy over 3 Bev with a lead nucleus results in an electronic-nuclear shower that is recorded by coincidences in the discharges of the telescope and hodographic counters. The number of δ-showers produced by penetrating particles was subtracted from the total number of showers recorded. At high altitudes this correction is small.[2] Curve 1 pertains to measurements at the equator. Curve 2 gives the difference between the variations in the number of E > 3 Bev protons with altitude, observed at 51 and 31° latitude. The marked difference between the curves indicates that primary protons with an average energy of 40 Bev lose their entire energy in a single event. Calculations show that to explain these data it must be assumed that in the encounter of the primary proton with a nitrogen nucleus 70% of the energy is retained by one nucleon.[7]

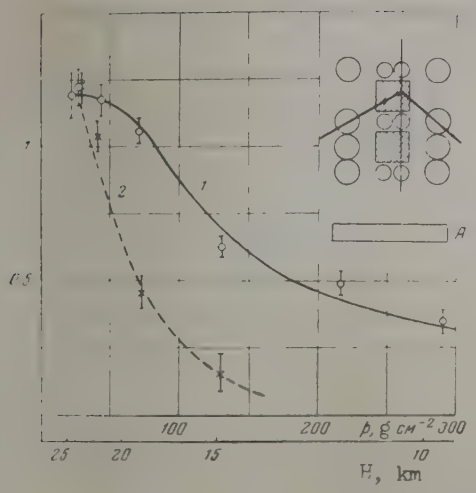

Fig. 1. Absorption of protons of over 3 Bev energy in the atmosphere: 1) variation of the number of protons with altitude near the equator ($E_0 = 40 \cdot 10^9$ ev); 2) difference between the altitude dependence curves at 51° and 31° N ($E_0 = 4 \cdot 10^9$ ev). Upper right: diagram of apparatus; row A consisted of 9 hodoscopic counters whose axes are parallel to the plane of the drawing.

2. Electronic-photonic component. The portion of the energy transferred in the collision of a nucleon with a light nucleus to π^0 mesons is determined by measuring the number of electrons and the energy flux of the electronic-photonic component at different latitudes and altitudes:

$$E_{ep}(p) = \left(\frac{dE}{dp}\right)_{ion} \int_0^p N_e(p)\,dp + S^{hor}(p), \qquad (1)$$

where $E_{ep}(p)$ is the energy transferred to the electronic-photonic component at altitudes above the pressure altitude p; $N_e(p)$ is the number of electrons at the pressure altitude p; $S^{hor}(p)$ is the electron-photon energy flux through a 1 cm^2 horizontal area.

Measurements[3] of the air-lead transition effect permit finding the energy flux of the electronic-photonic component passing through a 1 cm^2 cross section sphere ($S^{glob}(p)$) from the height of the peak or the area under the transition curve.

As has been shown by Grigorov,[8] the following equation can be used:

$$S^{hor}(p) = S^{glob}(p) - \int_0^{\pi/2} S^{glob}(p/\cos\theta)\cos\theta\sin\theta\,d\theta, \qquad (2)$$

where θ is the angle with the vertical.

$N_e(p)$ was determined by measuring the number of soft component particles at different altitudes and latitudes.

Rapoport[9] used a pulse ionization chamber to determine the ionization produced by an individual particle in the stratosphere. Inasmuch as the minimal ionization Rapoport's apparatus was capable of recording was appreciably less

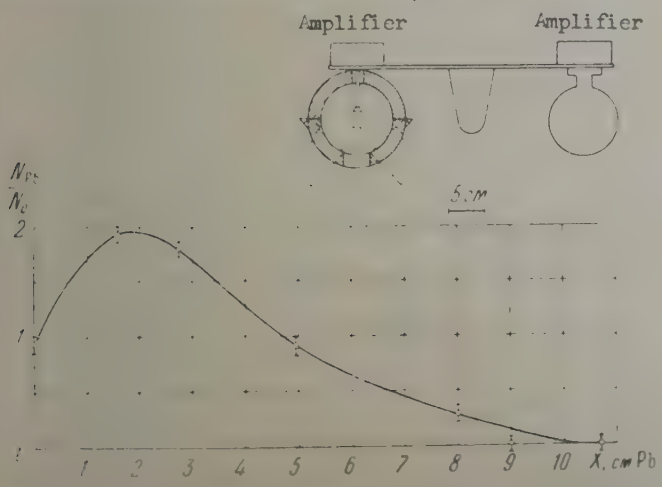

Fig. 2. Air-lead transition curve obtained for the soft component of cosmic radiation at 10 km by means of a counter. Above: diagram of the apparatus.

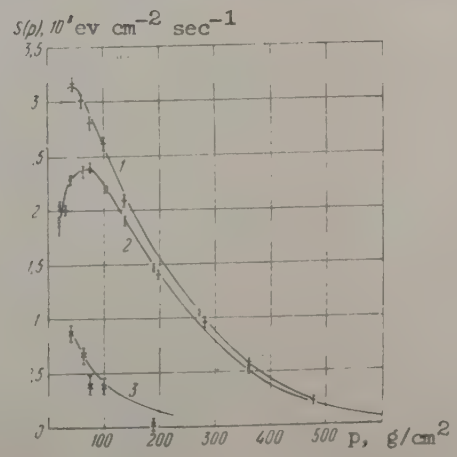

Fig. 3. Variation of electronic-photonic component energy flux with atmospheric depth: 1) 51°N, 2) 31° N, 3) difference between curves 1 and 2.

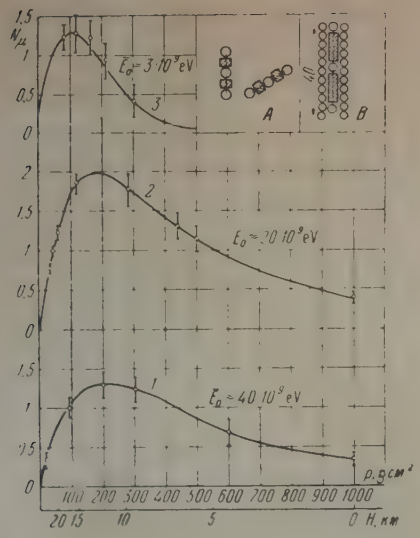

Fig. 5. Altitude dependence of mu-meson intensity: 1 & 2) results of measurements at latitudes 2° and 31°; 3) difference between results at 51 and 31° N. A & B: diagrams of apparatus used for measuring mu-meson intensity (see text).

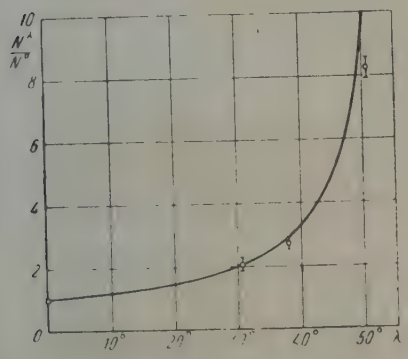

Fig. 6. Variation of number of pulses in ionization chamber at 40 g/cm² pressure altitude with latitude.

decay electrons. The number of mesons at different altitudes was measured by Charakh-ch'ian.[10] Mu mesons were separated from the general cosmic radiation by measuring the number of penetrating particles passing in the vertical direction and at 60° to the vertical (see Fig. 5, A; in this case mu-meson decay was utilized) and by counting the number of particles passing through 32 cm of lead without generating showers (see Fig. 5, B; here advantage was taken of the fact that mu-mesons virtually do not interact with atomic nuclei). As the result of these measurements and analysis of the composition of cosmic radiation at different latitudes the data on mu mesons shown in Fig. 5 were obtained. Knowing the number of mu mesons at different altitudes and latitudes, the investigators could determine the energy of the electrons produced in the decay of mu mesons; this is the energy that must be subtracted from the total electronic-photonic component energy in order to obtain the energy transferred to mesons. The results of mu-meson intensity measurements are in accord with the above-mentioned assumption that twice as much energy is transferred to $\pi^{\pm}$ mesons as to π^{0} mesons. Studies of high-energy protons and the electronic-photonic component thus lead us to conclude that only a small portion (30%) of the energy of the primary particle is transmitted to pi mesons in each collision.

In addition to the energy going into the formation of pi mesons in the collision of a high-energy nucleon with an atomic nucleus, some portion of the nucleon's energy is expended on nuclear disintegration. Appropriate pulse ionization chamber measurements were carried out by Grigorov and Murzin at latitudes 51, 31 and 2° in order to study this nuclear splitting (the results are presented in Fig. 7 of their report - see Ref. 1).

Fig. 6 shows the latitude dependence of the number of pulses at an altitude corresponding to a pressure of 40 g/cm². The points in Fig. 6 are the experimentally measured number of pulses; the solid line curve indicates the number of primary particles. It will be seen that the number of pulses is proportional to the number of primary particles. Yet, as measurements made by Murzin by means of a pulse ionization chamber surrounded by hodoscopic counters have shown, at an altitude corresponding to 40 g/cm² pressure most of the pulses are due to nuclear disintegrations produced in the chamber walls by neutrons of relatively low energy.

The proportionality of the number of pulses to the number of primaries at the different latitudes indicates that the collisions of the primary particles of different energies with nitrogen nuclei result in the formation of approximately the same number of neutrons having an energy of the order of 10^8 ev.

This alone shows that the primary particles of mean energies ranging between 3 and 40 Bev produce roughly identical nuclear effects. A study of these disintegrations has made it possible to evaluate the average energy expended on splitting of a light nucleus.[8] It appears that this energy is about 400 Mev and is independent of the energy of the incident particle. It follows that in a collision of a high-energy nucleon with a light nucleus the part of the initial primary particle energy not expended on the formation of mesons (about 70%) is, as a rule, carried off by one nucleon; it has been estimated that the probability of a transfer of 1-2 Bev energy to a recoil nucleon is not greater than 1/4. As a result it can be deduced that the cross section for nucleon-nucleon collisions involving transfer of a high energy to the recoil nucleon is not larger than 0.1 of the geometric cross section πr_0^2 (here $r_0 = \hbar/\mu c$; where μ is the meson rest mass).

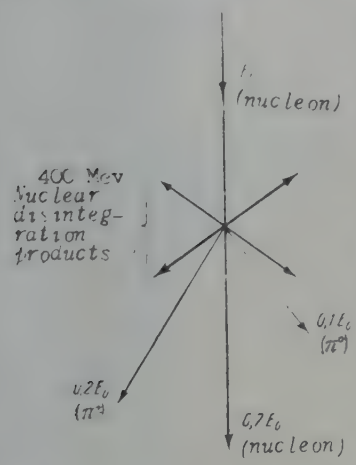

Fig. 7. Distribution of the energy of the incident nucleon among the particles formed as the result of a collision of a high-energy nucleon with a light nucleus.

Thus the general pattern of the interaction of primary particles with light nuclei appears to be as diagrammed in Fig. 7. About 400 Mev are expended on splitting the struck nucleus; this, given the high energies obtaining, amounts to only a small fraction of the primary particle energy.

The fact that the energy expended on nuclear disintegration is apparently independent of the energy of the primary particle can be interpreted as follows. If it be assumed that the splitting of the nucleus occurs at the expense of the energy the recoil nucleon received from the incident particle, then the experimental results can be taken to mean that the recoil nucleons receive the same energy regardless of the energy of the primary particle (at least in the range of average energies from 3 to 40 Bev). This leads to the conclusion that the angular distribution, in the center of mass system, of the nucleons shooting out after the collision will be highly anisotropic. On the basis of the experimental data then available, we predicted back in 1953 the anisotropy of scattering, starting with incident particle energies of about 3 Bev. Data recently obtained on the cosmotron confirm that at an incident particle energy of $2 \cdot 10^9$ ev and with inelastic nucleon-nucleon collisions there is pronounced anisotropy of the scattered particles in the center of mass system (in this case we can even speak of quantitative agreement of experiment with the mean scattering angle of about 30° in the center of mass system, predicted by us).

M.G.Meshcheriakov and his colleagues[11] showed, even before the results of the cosmotron experiments appeared in print, that the anisotropy of elastic scattering should become apparent at energies of the incident particles on the order of 600 Mev. In the region of high energies, according to our interpretation, the scattering anisotropy should be even greater than at energies of $\sim 10^9$ ev.

It is worth emphasizing that the "average" characteristics of the elementary process of collision of primary particles with light nuclei deduced by us are in good agreement with the altitude dependence of the high energy nucleonic component of cosmic radiation: it has long been known that the intensity of the nucleonic component decreases with the atmospheric depth according to the exponential law: $e^{-\frac{P}{L_{abs.}}}$ where $L_{abs.} = 120$ g/cm^2 is the absorption free path, which

has been measured with an accuracy to within a few percent. If for our calculations we take a value of 60 g/cm^2 for the collision free path and the experimentally observed energy loss of 30% (the remaining energy being retained by one nucleon) we arrive at a value of 116-118 g/cm^2 (depending on the form of the generating function used) for the mean absorption free path of the nucleonic component of the global flux. On the other hand, if it is assumed that the average energy loss going for the production mesons amounts to 50%, the computed value for the absorption free path comes out to be 85-90 g/cm^2 which is in conflict with the experimental data.

The ratio of the free path for absorption to that for collision is determined by the form of the energy spectrum and the generating function W(U), characterizing the probability that the nucleon will retain, after collision, a fraction U of the energy of the incident particle.

In the case of a spectrum represented by a power function

$$\frac{L_{in}}{L_{abs}} = 1 - \int W(U) U^{\gamma-1} dU$$

where γ is the exponent of the differential energy spectrum of the particle, U is the fraction of the energy carried off by the nucleon, L_{in} is the mean free path for interaction, and L_{abs} is the path for absorption (see Fig. 7).

Inasmuch as γ is close to 2, the value of L_{abs} depends primarily on the mean value of U rather than on the specific form of the function W(U). Taking advantage of this circumstance we can elucidate the characteristics of the interaction of 10^{10}-10^{12} ev primary protons with light nuclei.

The interaction free path for particles of 10^{10} ev energy has been measured experimentally. In air it is 60-70 g/cm^2. Hence for 10^{10} ev particles, $L_{in}/L_{abs} \approx 0.5$. The few measurements of the free path for absorption of particles in the 10^{11}-10^{12} ev interval made to date yield a value of L_{abs} = 110-120 g/cm^2. If we assume that the nuclear interaction cross section does not decrease with increasing particle energy, we obtain $L_{in}/L_{abs} \approx 0.5$ for the 10^{11}-10^{12} ev energy range. However, as was already noted, this ratio is determined primarily by the fraction of energy lost (expended on meson formation). Hence at energies of 10^{11} and 10^{12} ev the incident particles lose an average of about 30% of their energy incident to collision with light nuclei. An average loss of say 50% would lead to an absorption free path value of 85-90 g/cm^2, clearly incompatible with the experimental data.

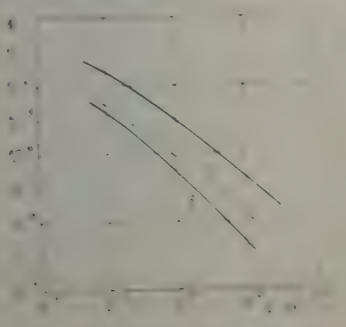

Fig. 8. Integral energy of primary particles (1) and energy spectra of pi mesons (2) and mu mesons (3) at sea level. N = particles cm^{-2} sec^{-1} sterad^{-1}.

It can easily be shown that in the 10^{12} ev energy region, too, the major portion of the unexpended energy of the primary particle is not carried off by pi mesons. To this end we need only compare the spectrum of primary particles with the spectrum of the generated pi mesons. The pi-meson spectrum in the region of high energies can readily be reconstituted from the spectrum of mu mesons of great energy, observed in experiments underground. (It is assumed that the interaction cross section for high-energy pi mesons is not greater than the geometric cross section of the nuclei and that as a result of interaction with a nucleus the pi meson loses all its energy. This assumption, if incorrect, can only lead to an over-estimated value of the calculated flux of pi mesons of the given energy.)

Fig. 8 shows the integral spectrum of primary

particles (curve 1) and the pi-meson spectrum (curve 2) as re-established from data on the spectrum of mu mesons at sealevel and underground. It will be seen that for each proton of a given energy there are formed in the entire atmosphere but 0.05 pi mesons of the same energy. It can readily be deduced from the curves that the probability of the concentration of over 70% of the energy of a primary particle on one pi meson is less than 0.1. Hence there is good reason to expect the interaction of 10^{12} ev particles with light nuclei will not differ markedly from the interaction process involving 10^{10} ev particles, i.e., that only a small portion - under 50% of the available energy will be expended on the formation of mesons. The "unexpended" remainder of the energy will, in most cases, be carried off by one particle which will be neither a pi meson nor any other, heavy meson disintegrating into a small number of pi or mu mesons. Barring the hypothetical existence of some as yet unknown particles, we can safely postulate that the unexpended part of the energy is carried off by nucleons (or in some cases by hyperons).

Thus the summarized experimental data indicates that the interaction of nucleons with light nuclei has the same general characteristics over the entire range of primary particle energies from 3 to 1000 Bev: about 30% of the energy is lost on the formation of mesons, while most of the remaining 70% is carried off by a single nucleon.

Thus we are in the right to speak of the primary nucleon as an individual, segregated particle. This leads us to the concept of the "transparency" of atomic nuclei to high-energy nucleons: on the one hand in encountering a nucleus the nucleon undergoes, with a probability approaching 100%, an inelastic collision accompanied by the formation of mesons; on the other hand, in passing through the nucleus the nucleon loses only about 30% of its energy. Although the cited data on the low energy loss pertain to nucleon-nucleus collisions, there is no reason to expect that in the case of nucleon-nucleon collisions there will be a greater meson-formation energy loss or greater fractioning of the energy among a larger number of secondary nucleons.

To explain the aforementioned effects we assume that in the collision of nucleons there may be an independent interaction of parts of the nucleons with each other or, in the extreme case, meson-meson interaction.* Ideas along this line have been put forward by Heisenberg, Feinberg and Charnavski and by Baba.

If we assume an internal structure for nucleons, at least in the sense that separate parts of the meson field of one nucleon can interact independently with separate parts of the meson field of another nucleon, the degree of inelasticity of nucleon-nucleon collisions will be determined by the character of the meson field and the impact parameter. Inasmuch as most of the collisions are necessarily peripheral - i.e., occur with large impact parameters - only the small amount of energy bracketed in the overlapping volumes of the meson fields is released for meson formation.

It must be noted that the above-cited experimental data (retention of the greater fraction of its initial energy by the incident nucleon, the independence of this fraction of the energy of the primary nucleon as well as the low value and independence of the primary energy of the momentum of the recoil nucleon) are simply consequences of the relativistic transformation if it be assumed that, in a non-central collision of two nucleons, the striking-nucleon forces acting on the nucleon at rest are 1) independent of the energy of the former (at relativistic velocities) and 2) small in absolute magnitude.

---

*If this hypothesis is correct, we may expect a difference between collisions of mesons with nucleons and of two nucleons with each other. In the first case the inelasticity of the collisions should be appreciably greater.

We assume that interaction forces between the nucleons come into being and correspondingly greater energy losses occur only when the centers of the nucleons approach to within a range less than $r_0 = \hbar/c\mu$. This situation may be a consequence of the existence in nucleons of a separate, distinctive central region, a "kernel" serving as the carrier of the so-called kernel charge.

The suggested nucleon interaction mechanism would lead us to expect that even at very high energies of the incident particles - say of the order of 10^{14} ev - we should expect a small average energy loss for meson formation and retention after collision of the major portion of the energy by a single nucleon.

The latest experimental data[12] on investigations of extensive air showers show that even at ultra-high energies the greater portion of the energy of the primary particle is concentrated on one particle or, in any case, on a very small number of particles.

If the above suppositions that the interaction may occur between separate parts of the meson fields of colliding nucleons correspond to reality, studies of the energy losses incident to collisions of high-energy nucleons with other nucleons and atomic nuclei may offer a promising approach to the problem of clarifying the structure of nucleons.

"Lebedev" Physical Institute of the
Academy of Sciences of the USSR
and
"Lomonosov" Moscow State University

References

1. S.N.Vernov, A.E.Chudakov & A.E.Charakhch'ian, Izv. AN SSSR, Ser. Fiz., 17, 13, (1953); N.L.Grigorov & V.S.Murzin, Izv. AN SSSR, Ser.Fiz., 17,21 (1953).
2. A.N.Charakhch'ian, Thesis, Moscow 1952.
3. S.I.Brikker, S.N.Vernov, N.L.Grigorov, I.M.Evreinova & T.N.Charakhch'ian, Doklady AN SSSR, 61, 629 (1948).
4. S.N.Vernov, N.L.Grigorov & A.N.Charakhch'ian, Vestnik MGU (Moscow State University Review), 11, 71 (1949); N.L.Grigorov, I.M.Evreinova & S.P.Sokolov, Doklady AN SSSR, 81, 379 (1951).
5. S.N.Vernov, Zhur. eksp. i teor. fiz., 19, 621 (1949).
6. S.A.Azimov, N.A.Dobrotin, A.L.Liubimov & K.P.Ryzhkova, Izv. AN SSSR, Ser. fiz., 17, 80 (1953); W.D.Walker, J.P.Walker & K.Greisen, Phys. Rev., 80, 546 (1950); J.G.Ashworth & K.Sitte, Phys. Rev., 97, 159 (1955).
7. N.L.Grigorov, Doklady AN SSSR, 94, 835 (1954).
8. N.L.Grigorov, Thesis, Moscow State University, 1954.
9. N.L.Grigorov, I.D.Rapoport & G.I.Shipulo, Doklady AN SSSR, 91, 471 (1953); I.D.Rapoport, Izv. AN SSSR, Ser. Fiz., 19 (1955) (Present issue of the Bulletin).
10. T.N.Charakhch'ian, Thesis, Moscow State University, 1955.
11. G.T.Zatsepin, Doklady AN SSSR, 99, 959 (1954).
12. N.A.Dobrotin, G.T.Zatsepin, S.I.Nikol'skii, L.I.Sarycheva & G.B.Christiansen, Izv. AN SSSR, Ser. fiz. 19 (1955)(See next issue of the Bulletin).

INTERACTION OF COSMIC RAY PROTONS WITH LIGHT NUCLEI ACCORDING TO WILSON CLOUD CHAMBER MEASUREMENTS AT 9 km ALTITUDE

- L.T.Baradzei, V.I.Rubtsov, Iu.A.Smorodin, M.V.Solov'ev, B.V.Tolkachev & Z.I.Tulinova

Particularly favorable conditions for investigating the interaction of cosmic ray protons with nuclei obtain at high altitudes by virtue of the high intensity of the proton flux and the trifling content of pi mesons in the N-component.

According to Adams and Anderson[1] the intensity of protons having energies over 400 Mev at 9-10 km altitude is about 15% relative to the penetrating component of cosmic radiation. On the other hand, due to the decay of mesons in the higher, low-density layers of the atmosphere, the proportion of pi mesons in the nucleo-active component does not exceed a few percent of the number of protons.

In the present investigation the interaction of protons with Be^9 nuclei was studied by means of a Wilson chamber, 200 mm in diameter and having a 50 mm deep illuminated region. The chamber was operated in a magnetic field of about 9000 oersteds. The beryllium plate, 5.3 g/cm^2 thick, was mounted so as to permit measurement of the steric angles between the shower particles and the track of the primary particle. The error in measuring the steric angles was about 1°. The "false curvature" of the particle paths in the chamber corresponded to a momentum of $2 \cdot 10^9$ ev/c.

In our experiments we employed the two systems for controlling the chamber illustrated in Fig. 1. With arrangement A the chamber was actuated by the passage of even one charged particle through all five rows of the telescope counters, three of which were located above the chamber and two, with a 9 cm thick lead absorber between them, below the chamber. This method of control permitted recording all nuclear events produced by charged particles, the products of which comprised at least one penetrating particle. With control arrangement B all protons of energies exceeding 150 Mev passing through the apparatus were recorded.

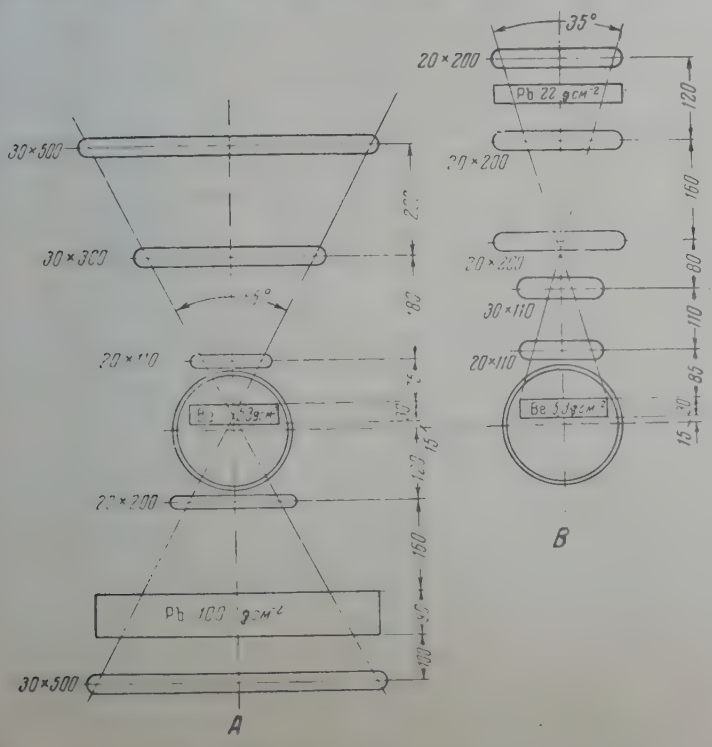

Fig. 1. Cloud chamber location and counter control systems used in the experiments.

According to the data of Ref. 2, effective generation of mesons through interaction with heavy nuclei begins at proton energies of about $3 \cdot 10^9$ ev. Charakhch'ian[3] arrives at about the same value from an analysis of the latitude dependence of the number of showers from lead; it follows from Charakhch'ian's data that the intensity of shower-producing protons at altitudes of 9-10 km is only approximately 0.25 particles

cm^{-2} min^{-1} $sterad^{-1}$, i.e., equal to around 1% of the intensity of penetrating particles at these altitudes.

In order to evaluate the energy of shower-producing protons we ran a control experiment in which the penetrating showers from an 8 cm thick lead plate were photographed. It was found that penetrating showers were generated in 5% of the cases of the passage of penetrating particles through the apparatus. Assuming that the free path for interaction with nuclei in lead is 160 g/cm^2, we can readily deduce that protons of energies $> 3 \cdot 10^9$ ev amount to 8–10% of the number of penetrating particles at the given altitude. The mean energy of the shower-producing protons is found to be approximately $6 \cdot 10^9$ ev.

We obtained 4108 photographs of the cloud chamber in the magnetic field at 9000 meters altitude. Of these, 2818 were taken with control system A and 1290 with control system B. The number of interactions in which generation of mesons occurred was virtually the same with both control systems and amounted to 0.88±0.20% of the total number of triggering particles. In addition we recorded about 1% cases of scattering through angles of 3° to 20°, which were also cases of nuclear interaction but involving protons of lower energies.

With the control system B in use, in addition to shower cases the apparatus recorded cases of disintegration of the beryllium nuclei not accompanied by generation of mesons. Such disintegrations comprised about 25% of the number of electronic-nuclear showers from the beryllium. About half these interactions resulted in pairs of particles with scattering angles of around 80°. From the values of the momenta and steric angles these events may be interpreted as cases of scattering of a proton from a proton having a momentum of $\sim 10^8$ ev/c in the nucleus.

The total number of observed electronic-nuclear showers from beryllium as compared with the number from lead yields an interaction free path in beryllium of 50 g/cm^2, as computed on the basis of the geometric cross section of the beryllium nucleus. This means that the protons producing showers in beryllium must have a mean energy close to that of the protons giving rise to interactions in lead.

The observed showers from beryllium had the following distribution as regards number of particles:

Number of particles	2	3	4	5	6	11	12
Number of showers	16	7	1	4	1	1	1

An idea of the angular distribution and the momenta of the particles comprising these showers may be gained from an examination of Fig. 2, in which the sections of these showers in the plane normal to the path of the primary particle are also shown.

Showers of three particles are cases of generation of one or two charged mesons. In 7 of the 16 observed two-particle showers, one of the particles can be identified as a meson from the polarity of the charge or the momentum and ionization. In shower No. 6321 both the observed particles are oppositely charged mesons. The other two-particle showers must also be cases of meson production since the observed angles between the particles could not be realized in elastic collisions. Thus one or two charged mesons are formed in 75% of the cases of meson generating interactions of cosmic rays with beryllium nuclei. An analogous situation must obtain incident to the generation of mesons in the atmosphere as a result of the interactions of protons with the nuclei of nitrogen and oxygen.

It may be noted that the ratios between the numbers of showers with different particle-multiplicities obtained by us agree within the limits of the considerable experimental error with the data obtained by means of nuclear

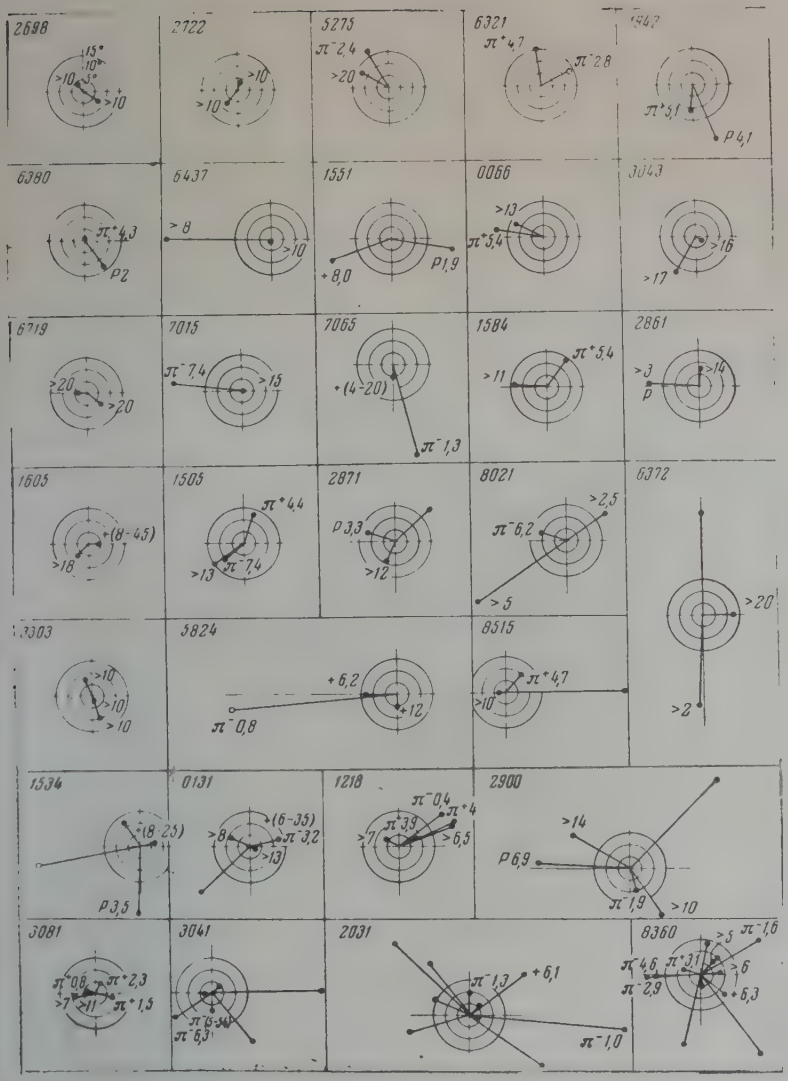

Fig. 2. Sections of the 31 observed showers from beryllium in a plane normal to the path of the primary particle. The distance from the point representing the shower particle is proportional to the angle between the direction of ejection of the particle and the direction of the primary particle. • - particles emerging into the upper hemisphere; o - particles scattered into the lower hemisphere. The figures near the points are the momenta in 10^8 ev/c units. In cases where the mass of the particle could be determined from momentum and ionization measurements, the particles are identified accordingly.

emulsions,[2] even though in emulsions the interactions in most cases occur with nuclei whose atomic weight is close to 100.

Camerini at al[4] note that at one and same energy of the primary particles the number of mesons produced may vary in a wide range. It is difficult to explain the frequency of interactions accompanied by the formation of a large number of mesons by their dependence on the energy, particularly in view of the slow increase in the multiplicity of the mesons with increasing energy of the primaries discovered by Charakhch'ian[3] in experiments at different latitudes. The value of the zenith angles in cases Nos. 8360 and 2031 also indicates that the energy of the primary particle involved is several times 10^{10} ev. Thus it would appear that appreciable variations of the number of generated mesons also obtain in interactions with light nuclei and are, apparently, connected with the character of the elementary interaction.

Differences between the electronic-nuclear showers produced in interactions with the nuclei of atoms present in photographic emulsions and those of beryllium become apparent when we compare the angular distributions of the shower

particles. Whereas the magnitude of the mean steric angle between the shower particles and the primary particle in the showers observed by us is 23 ± 3° for showers of 2-3 particles and 17 ± 3° for showers comprising 4 or more particles, the corresponding mean values for interactions in emulsions are about 50° and 40°.

Comparison of data on the energy distribution of the shower particles is difficult because of the impossibility of separating the mesons and protons from among the shower particles. The momentum distribution of shower particles shows that in showers from beryllium about 50% of the particles have momenta exceeding 10^9 ev/c. The corresponding value obtained from the pi-meson spectrum for showers produced in photographic emulsions is 18%.[4] At the same time an appreciably smaller number of recoil protons having energies of several Mev are generated in the interaction of primary particles with light nuclei than are produced in interaction with the nuclei of the elements contained in photographic emulsions. From observation of the specific ionization of the shower particles it proved feasible to identify protons where their energy did not exceed 180 Mev. Such slow protons - one in each shower - were detected in seven cases of interaction. In no case were two or more such slow protons observed in the same shower.

The average number of 40 to 150 Mev protons per electronic-nuclear shower from beryllium is about one fifth the number found in interactions in nuclear emulsions. It may also be noted that protons of such energies emerge after interaction with a beryllium nucleus at a much smaller angle relative to the direction of the primary particle than in interactions with photographic emulsion nuclei: the average scattering angle in our experiments was 25 - 10° whereas the corresponding angle for emulsions exceeds 60°.[2]

In view of the foregoing it may be assumed that most cases of interaction of protons with a beryllium nucleus may be regarded as the interaction of two nucleons and analyzed accordingly.

Let us consider the partition of energy between the two colliding nucleons in the case when one or two mesons are produced. We recorded 24 such cases. In six of these cases one slow proton with an energy not exceeding 120 Mev was recorded (Nos. 6380, 1551, 1942, 2861, 2871 and 1534). In addition there are four cases in which one of the nucleons is not apparent, although both nucleons should be charged: these are the pairs with negative mesons (Nos. 7015, 7065, 5275 and 6321). Production of a negative meson can occur according to any one of the following interactions:

$$p + n \rightarrow p + p + \pi^-,$$

$$p + p \rightarrow p + p + \pi^+ + \pi^-,$$

$$p + n \rightarrow p + n + \pi^+ + \pi^-.$$

None of these reactions can lead to the appearance of a shower of two charged particles. The energy of the not recorded proton, on the basis of its range in the beryllium plate, should not be greater than 50 Mev. However, the proton energy may be as high as 200 Mev if we take account of the fact that the proton may interact with other nucleons of the beryllium nucleus. Thus regarding at least 10 of the 24 interactions under discussion we can safely assert that the proton has an energy not exceeding 200 Mev.

Invoking the laws of the conservation of energy and momentum, we can deduce the following relationship for nucleon-nucleon interactions:

$$\sqrt{(\sum p)^2 + M^2} + M = \sum E,$$

From this it will be seen that the sum of the total energies ΣE_i of all the particles after the interaction must exceed the sum of the longitudinal momenta p_i (in energy units) by a value close to the equivalent of the mass M of the nucleon. This relationship may obtain when the shower comprises either slow nucleons, characterized by a great difference between the energy and momentum, or particles scattered at large angles to the direction of the primary particle with a great difference between the value of the momentum and its longitudinal component.

Thus, for example, in the case of shower No. 1505, consisting of three particles having momenta of $4 \cdot 10^8$, $8 \cdot 10^8$ and $13 \cdot 10^8$ ev/c and scattered at angles of 13, 11 and 15° relative to the direction of the primary, the sum of the total energies is $28.3 \cdot 10^8$ ev, while $\sqrt{(\Sigma p_i)^2 + M^2} + M = 35.4 \cdot 10^8$ ev. Thus to satisfy the laws of the conservation of energy and momentum a nucleon with a momentum not exceeding $5 \cdot 10^8$ ev/c must be ejected. The conservation laws can also be satisfied by the ejection at a large angle of a neutral particle of high energy, characterized by a difference of 10^9 ev between its energy and total momentum in energy units. However the absence of similar charged particles in showers precludes this possibility.

Analogous results are obtained from like analyses of the other showers of two-three particles in which slow nucleons are not apparent.

The possibility of the emergence of two high-energy nucleons cannot be excluded in the case of showers Nos. 8021 and 6372, where both nucleons might be protons with minimal ionization, and showers Nos. 5824 and 9515, where the ejected nucleons may be a proton and a neutron.

Thus in most cases of interaction leading to the generation of one-two pi mesons, one of the nucleons is ejected with a relatively low energy. It follows, if we take into account symmetry in the center of inertia system of the colliding nucleons, that the other nucleon must carry off most of the energy of the primary particle.

Studies of the generation of pi mesons in n-p collisions at energies of $1\text{-}2 \cdot 10^9$ ev, carried out on the cosmotron,[5] disclose an anisotropy of the scattering of the nucleons in their center of inertia system, leading to the indicated tendency in the partition of energy between the nucleons, i.e., the cosmotron experiments also indicate that one of the nucleons carries off most of the energy.

Our data favor the assumption that as the energy of interactions, leading to the generation of one-two mesons increases, the asymmetry of the partition of energy between the product nucleons becomes greater.

"P.N.Lebedev" Physical Institute of the
Academy of Sciences of the USSR and the
"M.V.Lomonosov" Moscow State University

References

1. R.V.Adams & C.D.Anderson, Rev. Mod. Phys., 20, 334 (1948).
2. Wilson, editor, Physics of Cosmic Rays, Russian Trans., M. 1954.
3. S.N.Vernov & A.N.Charakhchi'ian, Doklady AN SSSR, 91, 487 (1953).
4. U.Camerini, J.H.Davies et al., Phil. Mag., 42, 1260 (1951).
5. W.B.Fowler, R.P.Shutt et al., Phys. Rev., 95, 1026 (1954).

SPECTRA OF THE GENESIS OF PI MESONS AND PROTONS IN GRAPHITE

- N.M.Kocharian, G.S.Saakian, M.T.Aivazian,
Z.A.Kirakosian and A.S.Aleksanian

1. Description of apparatus

The measurements with which this report will be concerned were effected by means of the magnetic spectrometer pictured in Fig. 1. The working section of the field produced by the electromagnet had the following dimensions: 10 cm in the directions perpendicular to the lines of force, 69 cm in the vertical direction (height of the pole pieces) and 18 cm along the horizontal (width of the pole pieces). The field strength was maintained rigorously constant at 7100 oersteds. The lead absorber A_0, having a thickness of 32 g/cm^2, was mounted 64 cm from the upper edge of the pole pieces of the electromagnet. It more than covered the full solid entry angle of the apparatus and served to eliminate the electron background. The paths of the particles in the field were determined by means of the coordinate counter rows K_1, K_2 and K_4. Each row comprised 55 counters 4.6 mm in diameter, arranged in two layers (for details see Ref. 1). The counters of row K_3 served for controlling the reliability of the path determinations; in this row the counters were also arranged in two layers but were 8 mm in diameter. In order to minimize multiple scattering in the counter walls the last counters in rows K_2 and K_3 were equipped with aluminum cathodes. The graphite absorber G_1, 7.3 g/cm^2 in thickness, was located 4 cm above the coordinate counter row K_1. Immediately above this absorber there was a double layer of counters, 1 cm in diameter and 45 cm in length. Above this was the second absorber G_2 with a surface density of 32.8 g/cm. Absorber G_2 was surrounded by counters: single layers on the sides and a triple layer on top. Thus we could distinguish between and investigate separately the charged particles produced by neutrons

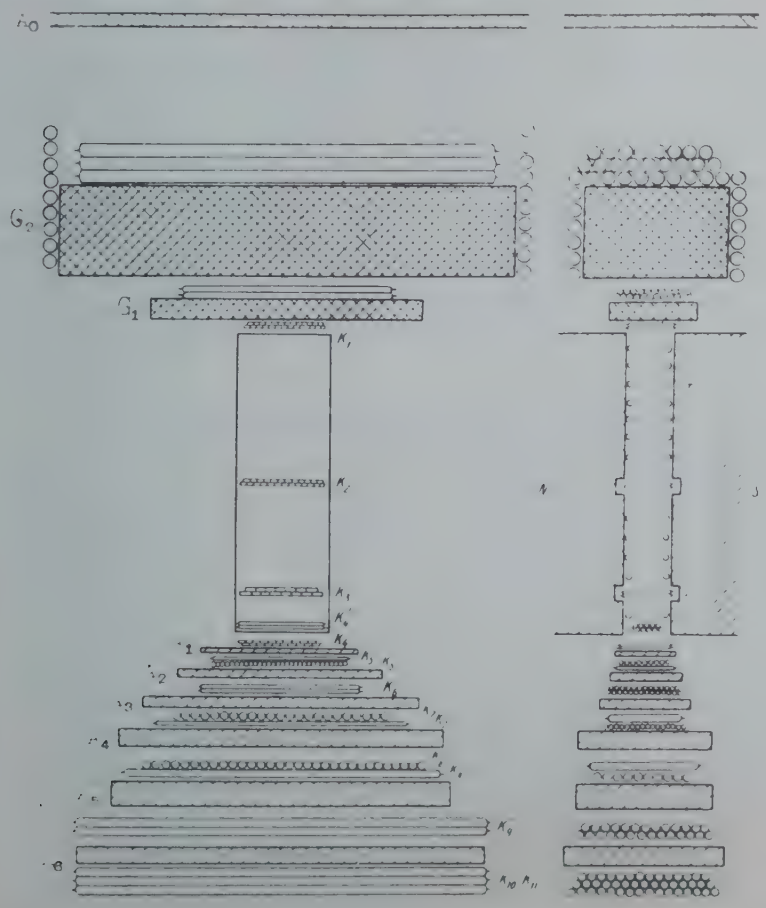

Fig. 1. Diagram of magnetic spectrometer. Two mutually perpendicular sections. N and S) pole pieces of electromagnet; A_0) lead absorber, A_1 - A_6) copper absorbers, G_1 and G_2) graphite absorbers, K_1 - K_4) coordinate rows of counters, K'_4- K'_{11}, K_5, K_7 and K_8) rows of counters between absorbers, T) pole-face counters.

in the thick absorber G_2 and in the thin absorber G_1.

Six copper absorbers A_1 - A_6 were mounted under the magnet gap; these had superficial densities of 10.6, 18.3, 23.1, 36.4, 52.9 and 35.6 g/cm^2, respectively. Taking the counters into account the total thickness of material under the magnet gap was 178 g/cm^2. Two-layer trays of counters were located between the absorbers, as shown in the figure.

The method of processing the experimental data, developed by Kaitmazov,[2] allows finding the value of δ, the quantity inversely proportional to the radius of curvature of the particle path. For our apparatus the momentum p of the particle, in Bev/c, is related to δ by the expression

$$p = \frac{6{,}36}{\delta}. \qquad (1)$$

The root square error in determining the momentum of the particle is given by (see Ref. 1):

$$\sqrt{(\Delta p)^2} = p\sqrt{K^2p^2 + \frac{b^2}{\beta^2}}, \qquad (2)$$

where K = 0.045 c/(Bev), b = 0.017 and β is the velocity of the particle (expressed as a fraction of the speed of light).

The term Kp gives the error in measuring the momentum due to the finite dimensions of the counters, while b/β is the error due to multiple coulombic scattering of the particles in the walls of counters K_2 and K_3. The errors involved in measurements of momenta of 0.5, 1, 2, 5 and 10 Bev/c amounted to 4, 5, 10, 23 and 45%, respectively.

2. Spectrum of the genesis of π mesons

In the present report we shall give the data relating to the generation of pi mesons and protons by neutrons in the thin graphite absorber G_1. The data relating to the production of particles in the thick absorber G_2 are still being processed and will be published in the near future.

During the period of measurement ($2.82 \cdot 10^6$ sec) there were recorded 308 negative pi mesons, having an energy $E > 0.21$ Bev, generated by neutrons in the absorber with a total thickness of 7.3 g/cm^2 graphite and 0.5 g/cm^2 copper (half the thickness of the counters located under and over the graphite absorber).

The experimental data are summarized in Table 1. The last column lists the ordinates of the differential spectrum of the genesis of negative pi mesons, calculated for a superficial density of 1 g/cm^2 of graphite. These figures were obtained by dividing the observed number of pi mesons (ΔN, Col. 3) by $S\omega\sigma x f \Delta E$, where S is the area of the lowest row of coordinate counters, ω is the solid angle of the apparatus, t is the period of measurement, σ is the transmission factor of the apparatus, x = 7.8 g/cm^2 - the superficial density of the absorber, f is

Table 1

Energy distribution of the 308 observed π mesons

Intervals of deviat. δ (relative units)	Energy intervals, Bev	Number of π mesons observed, ΔN	Mean energy $\bar{E}$, Bev	Transm. factor σ	Ordinates of differential spectrum, 10^{-7} sec^{-1} ster^{-1} g^{-1} (Bev)$^{-1}$
40 : 28	0,212 : 0,267	45	0,240	0,55	130
28÷21	0,267÷0,334	55	0,300	0,73	97,5
21÷16	0,334÷0,412	53	0,373	0,82	72,4
16 : 12	0,412 : 0,539	40	0,480	0,885	28,9
12 : 8	0,539 : 0,807	39	0,678	0,93	14,1
8 : 5	0,807 : 1,28	29	1,04	0,965	5,52
5 : 3	1,28÷2,12	14	1,65	1,0	1,46
3 : 1	2,12÷6,36	22	4,24	1,0	0,453
1 : 0	6,36 : ∞	11	—	1,0	—

the recording efficiency and ΔE is the breadth of the given energy interval of the particles.

The product $S\omega t = 1.78 \cdot 10^7$ cm^2 sec sterad. The transmission factor of the apparatus was computed according to the data of Refs. 3 and 4. The recording efficiency f is determined by misses in the coordinate row counters, cases of simultaneous tripping of several counters in two or more coordinate rows (showers) and the dead time of the installation. The relative number of misses was about 0.06. Shower data were, in general, processed; however, in some cases processing was impossible. Here one must distinguish clearly nuclear showers from other cases of multiple triggering of the counters in the coordinate rows, presumably caused by non-nuclear events. In some cases of multiple triggering of the counters in rows K_1 and K_2 (and sometimes even in K_3 and K_4 - see Fig. 1) we could not uniquely determine the trajectory of the particle. The relative fraction of such "ambiguous" cases was about 0.05. There were also cases where one counter in the first row and then several counters in K_2 and/or K_3 were activated. These effects were caused by δ-electrons ejected by relativistic particles from the walls of the counters in rows K_2 and K_3, narrow air showers accompanying the recorded particle, and, in a few cases, accidental coincidences. The relative fraction of all such cases was about 0.06.

After each actuation of the system, about one second was required for the system to return to the operating state. The apparatus recorded about 70 particles per hour; hence the equipment was blocked (dead) about 0.02 of the time.

On the basis of the above figures we arrive at a recording efficiency of approximately 0.82.

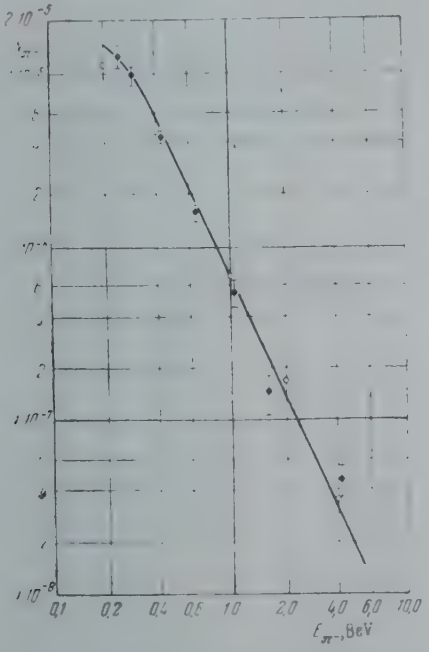

Fig. 2. Energy spectrum of mesons generated in the graphite absorber G_1. Ordinates: number of π mesons in sec^{-1} sterad^{-1} g^{-1} (Bev)$^{-1}$ units. Solid dots - our points; circles - point based on the data of Garibian & Gol'dman (Ref.5).

In contrast to our procedure in earlier investigations, in the present experiments we took into account the cases when the particles traversing the magnetic field were accompanied by showers, i.e., when several counters were triggered in coordinate row K_1.

The paths of all the negative pi mesons were subjected to careful processing with the aid of special templets. These templets were drawn to the scale of the apparatus and made it possible to check and verify the particle trajectories. The cases when the particle was accompanied by showers in one or more of the counter rows were scrutinized with particular care. Despite this it proved impossible to process a number of showers. As noted above the number of such showers amounted to about 5% of the total number of observed particles.

Analysis of the shape of the pi-meson energy spectrum in the 0.212 to 6.36 Bev energy interval leads to the expression

$$n_\pi(E)\,dE = \frac{a\,dE}{(E_0 + E)^\gamma}, \qquad (3)$$

where E is the total energy in Bev, $\gamma = 2.2$, $E_0 = 0.03$ Bev, $a = 0.69 \cdot 10^{-6}$ sec^{-1} sterad^{-1} g^{-1} (Bev)$^{\gamma-1}$. Thus $n_\pi(E)\,dE$ represents the vertical flux of negative pi mesons produced by neutrons in a layer of graphite having a superficial density of 1 g/cm^2. The shape of the spectrum is pictured in Fig. 2. The

deviations shown are root mean square errors. The circle points represent the spectrum for pi mesons generated in air, based on the computations of Garibian & Gol'dman.[5] To permit comparison with our data, the ordinates of the spectrum given by Garibian and Gol'dman were divided by

$$1 + \frac{N_p(E)}{N_n(E)}\left(1 + \frac{N_{\pi^+}(E)}{N_{\pi^-}(E)}\right)\rho(h)\,e^{\Delta h/\lambda},$$

where $N_p(E)$ and $N_n(E)$ are, respectively, the number of protons and neutrons capable of producing π^- mesons of energy $E > 0.2$ Bev; $N_{\pi^+}(E)$ and $N_{\pi^-}(E)$, respectively, are the number of positive and negative pi mesons of energy E, generated by the neutrons, $\rho(h)$ is the density of air at an atmospheric depth $h = 670$ g/cm^2 (in Ref. 5 the spectrum was computed for $h = 670$ g/cm^2 and the ordinates represent the number of mesons produced in 1 cm^3 of air, whereas in ours they represent the number generated in a 1 g/cm^2 thickness of graphite); λ is the absorption path for the nucleonic component in air, assumed to be equal to 120 g/cm^2 and Δh is the difference in depths. Our experiments were carried out at a depth corresponding to 700 g/cm^2 of air + 30 g/cm^2 of graphite (thickness of absorber G_2); consequently, $\Delta h = 60$ g/cm^2. We assumed $N_p(E)/N_n(E)$ to be equal to unity.

The ratio of the number of negative to positive pi mesons was determined from our experimental results. It was found that with $E < 1$ Bev, $N_{\pi^-}/N_{\pi^+} \approx 1.10 \pm 0.08$.

3. Proton spectrum

During the same observation period, concurrently with the pi mesons, we recorded 1089 protons with $E > 0.05$ Bev, generated by neutrons in the layer of matter having a total superficial density of 7.3 g/cm^2 of graphite + 0.54 g/cm^2 of copper (counter walls). The experimental results are listed in Table 2.

The arrangement of absorbers (superficial density 178 g/cm^2 Cu), located under the magnet gap, made it possible to separate the fluxes of the generated protons and π^+ mesons with momenta $p \leqslant 1$ Bev/c. The ratio between the numbers of negative and positive pi mesons was determined in this momentum region. For a more accurate determination of this ratio we utilized the flux of pi mesons generated in the thin graphite absorber G_1. We found that for $p < 1$ Bev/c the ratio equals 1.10 ± 0.08; as the momentum increases the ratio slowly decreases, approaching unity

Table 2

Distribution of 1089 observed protons according to energy and momenta

Deviation δ intervals (relative units)	Momentum interval Bev/c	Energy interval, Bev	Number of observed protons ΔN	Transmission factor σ	Ordinates of differential energy spectrum, 10^{-7} sec^{-1} ster^{-1} g^{-1} (Bev)$^{-1}$	Ordinates of differential distribution in momentum, 10^{-7} sec^{-1} ster^{-1} g^{-1} (Bev/c)$^{-1}$
20÷17	0,318÷0,376	0,052÷0,073	109	0,82	574	200
17÷14	0,376÷0,455	0,073÷0,105	194	0,87	591	246
14—13	0,455÷0,490	0,105÷0,120	84	0,90	510	233
13—12	0,490÷0,530	0,12 ÷0,14	95	0,91	456	228
12—11	0,530÷0,579	0,140÷0,164	98	0,92	420	190
11—10	0,579÷0,636	0,164÷0,193	83	0,93	269	137
10—9	0,636÷0,707	0,193÷0,237	81	0,94	171	106
9—8	0,707÷0,795	0,237÷0,29	82	0,95	142	85,2
8—7	0,795÷0,91	0,29 ÷0,37	78	0,96	89	51,7
7—6	0,91 ÷1,06	0,37 ÷0,47	45	0,97	40	25,0
6—5	1,06 ÷1,27	0,47 ÷0,64	55	0,98	30,5	21,0
5—4	1,27 ÷1,59	0,64 ÷0,91	42	0,99	13,6	11,5
4—3	1,59÷2,12	0,91 ÷1,38	27	1,0	5,0	4,45
3—1	2,12÷6,36	1,38 ÷5,49	13	1,0	0,276	0,258

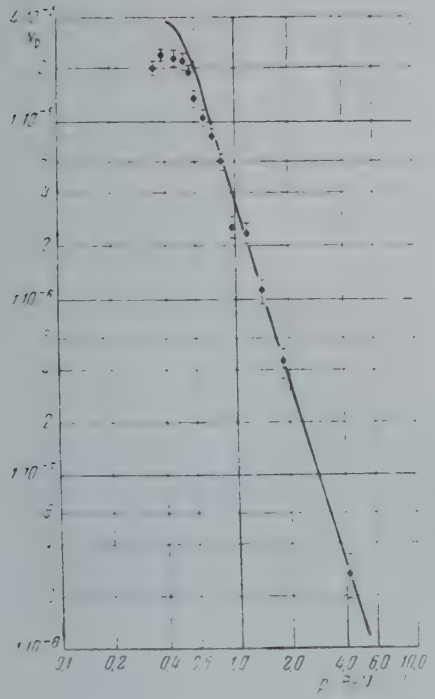

Fig. 3. Momentum distribution of protons generated in graphite absorber G_1. N_p = = protons sec^{-1} $sterad^{-1}$ $g^{-1}(Bev/c)^{-1}$.

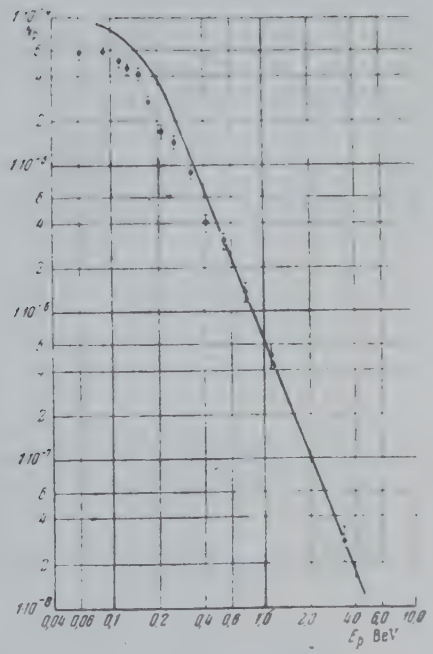

Fig. 4. Energy spectrum of protons generated in graphite absorber G_1. N_p = protons $sec^{-1}sterad^{-1}$ g^{-1} Bev^{-1}.

for mesons with $p \sim 1$ Bev/c. In separating the proton flux in the $p > 1$ Bev/c region, it was assumed that in this region ratio of negative to positive mesons was unity (i.e., that the number of positive mesons equalled the number of negative pi mesons; hence the number of negative mesons with the corresponding momenta was subtracted from the total number of positive particles in the given momentum interval.

Inasmuch as absorber G_1 was relatively thin, secondary nuclear processes could be disregarded. The ionization energy loss for protons with $p \leqslant 0.8$ Bev/c ($E \leqslant 0.3$ Bev), however, is appreciable, so that to obtain the true proton spectrum the ionization loss must be taken into account. The appropriate corrections were computed on the assumption that on the average the particles were generated at the center of the absorber plate.

The momentum spectrum of the generated protons is shown in Fig. 3. The indicated deviations are root mean square errors. The smooth curve in the $p < 0.08$ Bev/c region was drawn taking the ionization losses into account.

It should be noted that there must be a certain number of deuterons included in the recorded flux of particles.[6] However, in our experiments we were not able to evaluate the proportion of deuterons accompanying the protons.

The energy spectrum of the generation of these particles, on the assumption that they are all protons, is shown in Fig. 4. This spectrum in the region where $E > 0.2$ Bev can be approximated by the power law:

$$n_p(E)\,dE = \frac{b}{E^{\gamma}}\,dE, \qquad (4)$$

where $b = 0.71 \cdot 10^{-6}$ sec^{-1} $sterad^{-1}$ g^{-1} $(Bev)^{\gamma-1}$ and $\gamma = 2.6$; $n_p(E)\,dE$ is the number of protons generated in a graphite layer having a superficial density

of 1 g/cm^2.

It is of interest to compare the number of shower pi mesons (i.e., mesons with a total energy $E \geqslant 0.22$ Bev) with the number of protons having $E > 0.5$ Bev. The number of negative pi mesons, according to (3), equals $3.08 \cdot 10^{-6}$ particles per (g sec sterad). According to our experimental data the number of positive mesons should be approximately equal to the number of negative mesons. Hence with our method of separating the particles the number of protons amounts to about 18% of the total number of shower particles.

The authors wish to thank S.N.Vernov and N.L.Grigorov for discussion of the experimental data.

Physical Institute of the
Academy of Sciences of the Armenian SSR

References

1. N.M.Kocharian, Doklady AN SSSR 98, 369 (1954).
2. S.D.Kaitmazov, Doklady (Reports) AN Armenian SSR, 14, 129 (1951).
3. N.M.Kocharian & S.D.Kaitmazov, Izv. AN Armenian SSR, 7, 43, (1954).
4. G.S.Saakian, Izv. AN Armenian SSR 7, 54 (1954).
5. G.M.Garibian & I.I.Gol'dman, Zhur. eksp. i teor. fiz., 26, 257 (1954).
6. U.Camerini, P.H.Fowler, W.O.Lock & H. Muirhead, Phil. Mag., 41, 413 (1950).

* * * * * * * * * * *

ENERGY SPECTRUM OF PROTONS AT 3200 METERS ABOVE SEA LEVEL

– N.M.Kocharian, G.S.Saakian, M.T.Aivazian,
Z.A.Kirakosian & A.S.Aleksanian

1. Probability of stopping protons

In the preceding experiments in our laboratory the proton spectrum was obtained for the momentum region to 2 Bev/c. At greater momenta the copper absorbers located under the magnet gap do not permit of effecting direct separation of the proton and mu-meson fluxes. However the fluxes can be distinguished indirectly if we investigate the nuclear interactions of the particles in the absorber, since mu mesons do not interact with nuclei, whereas protons do interact.

In the present experiments there were six copper absorbers with a total thickness of 178 g/cm^2 below the magnet gap. Mu mesons stopped in these absorbers had momenta up to about 0.4 Bev/c. Protons having momenta $p \leqslant 1.1$ Bev/c could also be stopped due to ionization losses, while the stopping of protons having higher momenta could occur only as a result of nuclear interactions. Here "stopping" is understood to apply to cases of nuclear interactions when not only the primary proton but also all the secondary products of the nuclear encounter disappear in the absorber assembly. Thus, knowing the probability $W(E)$ of a proton being stopped as a function of the proton energy, we could readily calculate the true number of protons traversing the solid angle of the spectrometer from the number of stopped particles of momenta $p > 1.1$ Bev/c.

In order to determine the probability $W(E)$ it is necessary to have a proton flux through the magnetic spectrometer and to measure the ratio of the number of protons stopped in the absorbers to the number traversing them as a function of the energy. We obtained such a flux when the two absorbers G_1 and G_2 were in place over the counters in our apparatus (see Ref. 1: preceding

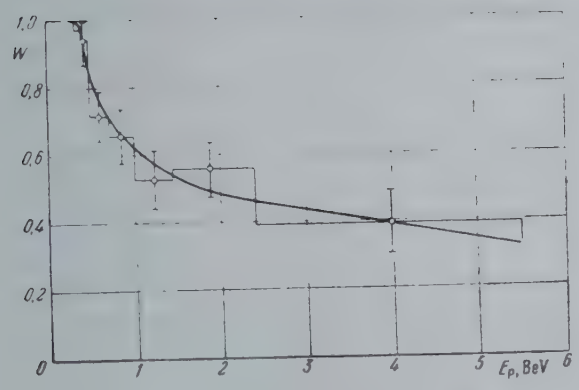

Fig. 1. Probability of stopping of protons in graphite absorbers. Proton energies in Bev; vertical scale is laid off in ratios of number of protons stopped to total number of protons traversing the magnetic spectrometer. Deviations are root mean square errors.

article, Fig. 1) and investigated the spectra of the protons and pi mesons generated in the graphite absorbers by neutrons. The apparatus recorded all the particles, both those stopped and those passing through the absorbers. The generated negative particles could only be π^- mesons, while the positive particles were both protons and π^+ mesons.

In the case of particles having momenta ≤ 1.1 Bev/c, the absorber arrangement permitted direct separation of the proton flux from the π^+ meson flux. For proton–meson separation in the region of higher momenta we determined the ratio between positive and negative mesons. As was pointed out in Ref. 1 (preceding article) the ratio of negative to positive pi mesons with momenta under 1 Bev/c was 1.1 ± 0.08; with increasing momentum the ratio decreases slowly and apparently tends to unity. We assumed, therefore, that at momenta exceeding 1 Bev/c this ratio is equal to unity. Hence in determining the number of protons with $p > 1$ Bev/c we subtracted the number of negative pi mesons (with the given momentum) from the total number of particles. The distribution of protons by energies obtained in this manner is shown in Table 1. Fig. 1 gives the curve for the variation of the probability of the proton being stopped in the absorber with the energy.

Table 1

Distribution of protons by energies and momenta

Deviation intervals (relative units).	Momenta intervals, Bev/c	Energy intervals, Bev	No. of protons: Total	No. of protons: Stopped	Probability of stopping W(E)
8—7	0,795÷0,91	0,29÷0,37	316	309	0,98
7—6	0,91÷1,06	0,37÷0,47	255	243	0,95
6—5	1,06÷1,27	0,47÷0,64	256	185	0,72
5—4	1,27÷1,59	0,64÷0,91	197	128	0,65
4—3	1,59÷2,12	0,91÷1,38	122	65	0,53
3—2	2,12÷3,18	1,38÷2,38	55	31	0,56
2—1	3,18÷6,36	2,38÷5,49	43	17	0,39

2. Spectrum of protons in air

We also carried out measurements aimed at determining the proton spectrum in air by means of the same apparatus. For these measurements the graphite absorbers G_1 and G_2 (Ref. 1: preceding article, Fig. 1) were removed so that only the 32 g/cm^2 lead absorber remained over the magnet gap.

In the course of the measurement period ($1.77 \cdot 10^4$ sec) we recorded 6852 >0.03 Bev protons stopped in the absorbers. All the data pertinent to the proton spectrum are listed in Table 2.

To compute the proton flux in a given momentum (or energy) interval, the observed number of particles – listed in the fourth column of Table 2 – was divided by

$$S\omega\tau\sigma fW = 5.9 \cdot 10^6 \sigma W, \qquad (5)$$

Table 2

Distribution in energy and momentum of protons stopped in the absorbers

Interval of deviation δ (relative units).	Momentum intervals, Bev/c	Energy intervals, Bev	Number of observed particles Δ N	Transmission factor σ	Probability of stopping W(E)	Ordinates of differential distribution in momentum 10^{-5} cm^{-2} sec^{-1} ster^{-1} (BeV c^{-1})$^{-1}$	Ordinates of differential energy spectrums 10^{-5} cm^{-2} sec^{-1} ster^{-1} (Bev)$^{-1}$
26÷21	0,245÷0,303	0,031÷0,048	105	0,732	1	42	150
21÷17	0,303÷0,376	0,048÷0,073	228	0,815	1	65,4	193
17÷14	0,376÷0,455	0,073÷0,105	369	0,875	1	93,2	221
14÷12	0,455÷0,531	0,105÷0,14	436	0,905	1	108	234
12—11	0,531÷0,579	0,14÷0,164	284	0,92	1	110	220
11—10	0,579÷0,636	0,164÷0,193	398	0,93	1	128	252
10—9	0,636÷0,707	0,193÷0,237	506	0,94	1	129	208
9—8	0,707÷0,795	0,237÷0,29	617	0,95	1	126	209
8—7	0,795÷0,91	0,29÷0,37	731	0,96	1	113	162
7—6	0,91÷1,06	0,37÷0,47	827	0,97	0,99	98	147
6—5	1,06÷1,27	0,47÷0,64	772	0,98	0,79	81,5	101
5—4	1,27÷1,59	0,64÷0,91	562	0,99	0,65	47,3	56,1
4—3	1,59÷2,12	0,91÷1,38	503	1,0	0,56	29,2	33,0
3—2	2,12÷3,18	1,38÷2,38	386	1,0	0,5	12,4	13,2
2—1	3,18÷6,36	2,38÷5,49	108	1,0	0,4	1,45	1,48
1—0	6,36÷∞	5,49÷∞	13	1,0	—	—	—

where $t = 1.77 \cdot 10^6$ sec is the duration of measurement, S is the area of the lowest row of coordinate counters (row K_1, Fig. 1 of preceding article), ω is the solid angle of the apparatus, σ is the transmission factor, f is the recording efficiency and W is the probability of the protons being stopped in the absorbers located below the magnet gap.

The values of W used in the calculations are taken from the curve of Fig. 1. The efficiency of recording f in the proton measurements was 0.78. In these measurements the end counters T, located on the pole pieces of the electromagnet were connected in anticoincidence; consequently the effective length of the coordinate row counters was 8 cm and hence $S\omega$ equalled 4.26 cm^2 sterad.

The proton energy spectrum derived in this manner is shown in Fig. 2. At energies over 2 Bev the slope of the curve $\gamma \approx 2.8$. The indicated deviations are root mean square errors for the number of observed protons computed without taking into account statistical errors in the determination of the stopping probability W. If we assume that in the $E > 5.5$ Bev region the proton spectrum is described by the equation $aE^{-2.8}dE$ we find $W = 0.09$.

Let us compare this spectrum with the proton spectrum given by Kocharian.[2] In doing so we must first take into account that in our measurements there was an absorber A_0 having a thickness of 32 g/cm^2 of lead over the apparatus, whereas Kocharian gives an absorption coefficient of 1/315 for protons having momenta $p > 1$ Bev/c. Hence for purposes of comparison the ordinates of Fig. 2 must be multiplied by $e^{32/315} = 1.11$. After making this correction the proton intensity based on our experiments comes out to be about 10% less than in Ref. 2.

Let us compare the intensity of nucleons in the atmosphere at a depth of 705 g/cm^2 with the intensity of the primary radiation at the boundary of the atmosphere. According to Ref. 3, the intensity values for nucleons with kinetic energies greater than 1, 2, 4 and 6 Bev are 0.168, 0.134, 0.0947 and 0.067 nucleons cm^{-2} sec^{-1} sterad^{-1}, respectively. From the spectrum given in the same work we find that the intensities of protons of the same energies are $3.39 \cdot 10^{-4}$, $1.23 \cdot 10^{-4}$, $0.41 \cdot 10^{-4}$ and $0.228 \cdot 10^{-4}$ protons cm^{-2} sec^{-1} sterad^{-1}, respectively.

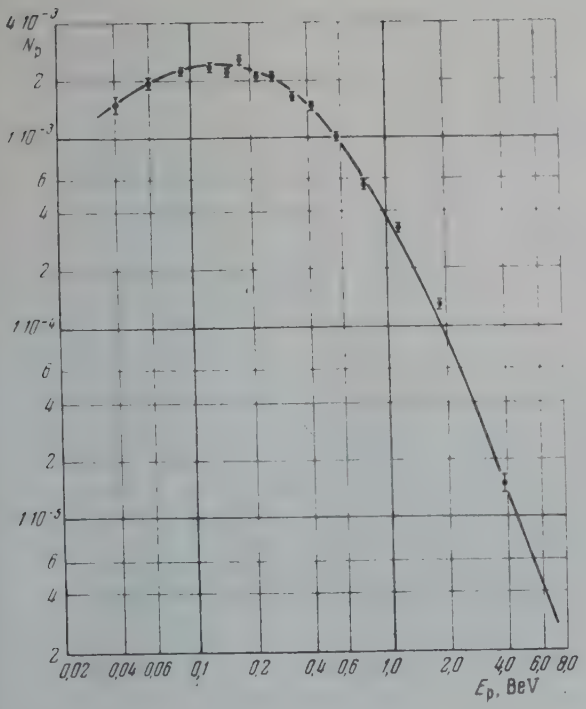

Fig. 2. Energy spectrum of protons at 3200 meters altitude. Number of protons in cm^{-2} sec^{-1} $sterad^{-1}$ $(Bev)^{-1}$. Deviations are root mean square errors.

In calculating the proton intensities we allowed for the influence of the 32 g/cm^2 thick lead absorber located above the apparatus (the intensities taken from the spectrum shown in Fig. 2 were increased by 10%). To obtain the total number of nucleons, the final proton figures were multiplied by 2 since it was assumed that at the energies in question the number of neutrons is equal to the number of protons. Comparing the nucleon intensity so determined with the intensity of primary nucleons we find the absorption coefficients for protons with energies exceeding 1, 2, 4 and 6 Bev are 1/127, 1/112, 1/100 and 1/97, respectively.

Physical Institute of the Academy of Sciences of the Armenian SSR

References

1. N.M.Kocharian, G.S.Saakian, M.T.Mivezian, et al. The present issue of the Bulletin.
2. N.M.Kocharian, Zhur. eksp. i teor. fiz., 28, 160 (1955).
3. W. Heisenberg, Kosmische Strahlung, Berlin, 1953.

* * * * * * *

IONIZATION SPECTRA OF COSMIC RADIATION PARTICLES IN THE STRATOSPHERE

- I.D.Rapoport

The investigations of the intensity of cosmic radiation based on measurements of the number of charged particles and the ionization produced by them, reported in Refs. 1-3, indicated that there is an appreciable flux of strongly ionizing particles in the stratosphere, whose contribution amounts to over 1/3 the total ionization. In connection with this it appeared of interest to determine the ionization spectrum of these particles (with a view to identifying the nature of these ionizing particles). The experiments to this end were carried out in 1951-1953 at the latitude of Moscow.

The experiments comprised two parallel series of measurements. In the first the vertical flux of particles having ranges equal to or greater than 1.7 g/cm^2 of Al was recorded. In the second, the particles were recorded re-

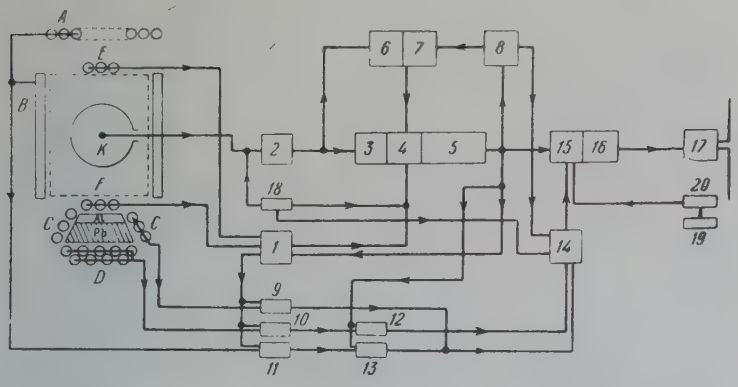

Fig. 1. Diagram of the equipment: K) pulse ionization chamber, E,F) telescope counters, A, B, C & D) groups of hodoscopic counters. 1) coincidence circuit controlling gate 4 in amplifier channel 2 & 3, 5) signal converter at output of amplifiers, 6) supplementary amplification stage, 7) threshold circuit controlled by auto-generator 8, 9-11) circuits receiving and selecting signals from the hodoscope, 12 & 13) delay circuits, 14) generator of markers of types 1 and 4 shown in Fig. 2, 15 & 16) modulators, 17) transmitter, 18) calibrating circuit, 19) barograph, 20) barograph signal generator.

gardless of their range or direction with a registration threshold on the order of 0.4 the mean pulse produced by relativistic particles. Both series were realized simultaneously on the same apparatus, the design of which incorporated a small spherical ionization chamber of aluminum, having a gas (spectrally pure argon) volume of about 8 liters and an electronic component collection time of about $5 \cdot 10^{-5}$ sec.

The chamber K (see Fig. 1) was located between the two trays of telescope counters E and F, which served to separate out the vertical flux (within a solid angle of about 0.12 sterad). The minimal range of particles recorded by the telescope was 1.7 g/cm^2. Counter D, located under 5 cm of lead and 2 cm of aluminum, recorded particles of the hard component that had traversed the telescope. The other groups of counters, covering the chamber to 77% of the solid acceptance angle, recorded cases of accompanying showers (counters A and B), and shower formation in the lead plate (counter C) and, in the measurements of the second series, permitted separating the part of the radiation consisting of particles with a range inferior to 1.7 g/cm^2 of Al (counters A and B).

The radio equipment designed by us provided for fairly reliable operational (i.e., with the apparatus balloon borne) detection and reception of ionization pulses in a wide range of ionizations: from minimum ionizations corresponding to relativistic particles to ionizations of about 70 times the minimum.

The ionization pulses were recorded in the following manner. The chamber pulses entering the main amplifier group 2-5 (Fig. 1) were blocked by the gate circuit 4 which passed the signal only

a) when the coincidence circuit 1 was actuated (passage of a particle through the telescope), or

b) if the pulse from the chamber after going through the amplifier 6 was of sufficient height to trigger the threshold circuit 7 and was not immediately preceded by a signal, permitting recording, from the trigger auto-generator 8; thus the last limited the load on the recording channel to the allowable level.

The chamber pulses (having passed through the gate 4 and converter 5) modulated (in circuits 15 and 16) the oscillations of the transmitter so that the duration of the radiated signal train would correspond uniquely to the height of the pulse. In addition pulses from the hodoscopic counters A, B, C and D were applied to the transmitting channel via the selecting (9-11), delay (12 & 13) and coding (14) circuits.

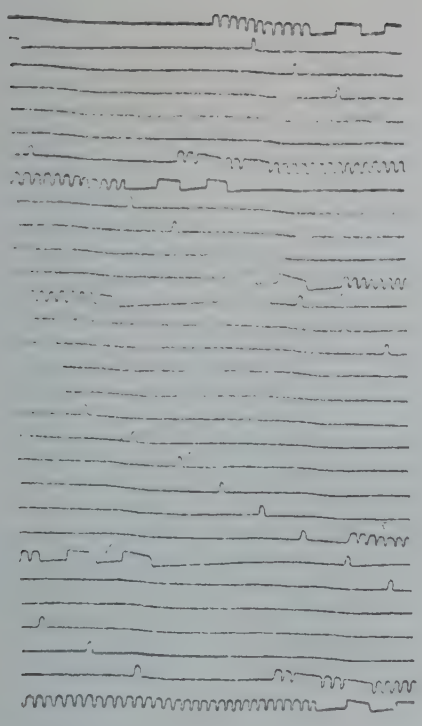

Fig. 2. Sample oscillogram showing record of signals received from the balloon-borne equipment at 23 km altitude: 1) pulse from trigger generator, allowing recording of pulse 2 from the ionization chamber, exceeding the set threshold value; 3) pulse from ionization chamber due to the passage of the particle thru the telescope, 4) marker indicating that pulse 3 is caused by a particle of the hard component, 5) calibrating control signals, 6) barograph signals, 7) pulse from counters surrounding the ionization chamber.

The instrumentation also included the barograph circuits 19 & 20 and the calibrating circuit 18, which served to control the amplification factor and the noise level in the amplifiers in flight. An interlocking arrangement prevented superposition of the different signals in the transmission channel.

The transmitted signal was recorded by the receiving equipment on the ground. By way of illustration a sample of the record of signals transmitted from an altitude of 23 km is reproduced in Fig. 2. Pulse 1 is the characteristic signal of the trigger generator which at instant t_o brings the system into operation, permitting recording of the following pulses provided they exceed the set registration threshold. The wide rectangular signal 7 at the end of signal 2 (recorded at t_1) indicates that the particle passed through the counters surrounding the chamber. The duration of the signal $2(t_2 - t_1)$ here equals $16 \cdot 10^{-3}$ sec, which corresponds to an ionization pulse height of 1.6 times the value for the most probable ionization in the hard component spectrum at sea level. The interval $(t_1 - t_o)$, averaged over many pulses, yields an indication of the intensity of the flux of the recorded particles. Pulse 3, which arrived second after the starting signal 1, is due to a particle that passed through the telescope. The next marker 4 indicates that the given particle traversed the lead plate.

The measurements in the stratosphere followed calibration of the transmission equipment to an accuracy of within 3% and control measurements of the ionization spectra of hard and soft component particles at sea level. The ionization spectrum for particles of the hard component so obtained was found to be in satisfactory agreement with the curve for the distribution of the fluctuation of ionization losses, computed according to Landau[4] taking account of the energy spectrum of mesons at sea level.[5] According to these measurements, the most probable ionization of a hard component particle is 53 ± 2 ion pairs/cm, while the mean specific ionization is 68 ± 1 ion pairs/cm; the mean specific ionization for particles of the soft component is 81 ± 2 ion pairs/cm (here only the statistical errors of measurement are given).

Measurements at different levels in the stratosphere up to 26 km above sea level were then made with the described equipment.

We turn first to the spectra of the particles recorded by the telescope. Histograms of the ionization pulses of hard component particles at sea level and at 8.8–12 km altitude are shown in Fig. 3. The smooth curve, plotted for purposes of comparison in histogram b, repeats the distribution curve for sea level (shown in histogram a) but is adjusted to take into account the change in the noise level in the amplifiers in flight. The ionization values are plotted in units of the most probable ionization of a particle of

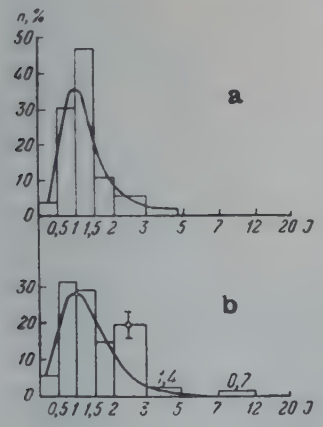

Fig. 3. Histograms of the ionization pulses due to particles of the hard component at sea level (a) and at 8.8–12 km altitude (b). The ionization J is scaled in relative units, the ionization unit being the most probable ionization in the spectrum of the hard component at sea level. The smooth curve in b is the distribution curve pertaining to sea level (shown in a), redrawn taking account of the change in the noise level in flight.

the hard component at sea level. A salient feature of the histograms is the "excess" at altitudes above 8 km (as compared with sea level measurements) of particles of the hard component in the 1.5–3 ionization units interval; it amounts to approximately 10%. A similar "excess" but of about 5–6% is apparent in the soft component spectrum in the 3–10 ionization units interval (see Fig. 5). The presence of a high energy cut-off in the detection of the excess particles in the region of three-fold ionization permits identifying these as protons; this is substantiated by the data of Adams, Anderson et al[6] on the proton spectrum at 9 km, which make it reasonable to expect the presence of the noted excess of strongly ionizing particles in the aforementioned respective ionization

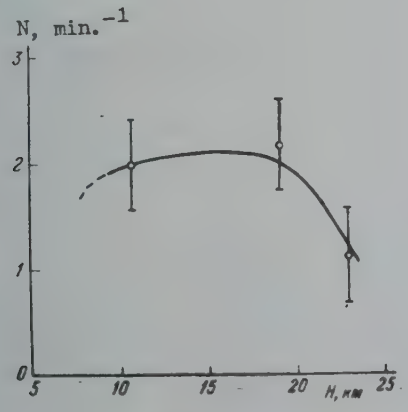

Fig. 4

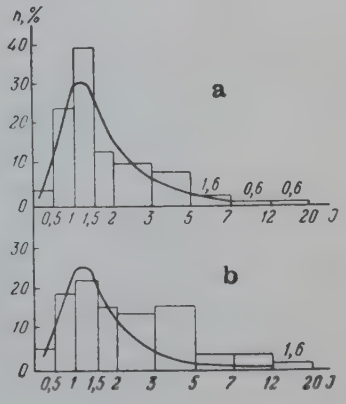

Fig. 5

Fig. 4. Variation of the intensity of secondary protons, characterized by 1.5–3-fold unit ionization, with altitude.

Fig. 5. Histograms of the ionization pulses of the soft component particles at 8.8–12 km (a) and 22.6–23.6 km (b). Ionization scaled in the same relative units as in Fig. 3. The distribution curves, obtained at sea level and adjusted for the change in noise level in flight, are plotted for comparison.

intervals. The flux of strongly ionizing protons attains an appreciable level at 8-9 km, remains fairly constant up to approximately 19 km and then, beginning at this depth (about 65 g/cm^2) falls off towards the outer boundary of the atmosphere, thus confirming the secondary nature of the particles (Fig. 4).

Beginning at shallow depths on the order of 35-40 g/cm^2, strongly ionizing particles, having a four-fold ionization (i.e. in the 3-5 ionization units interval) become increasingly dominant in the spectra as the boundary of the atmosphere is approached (see Fig. 5). Their mean range, as determined from the variation of the flux with altitude, is approximately 40 g/cm^2. The value of the flux of these particles, which may be identified as primary α-particles, extrapolated to the boundary of the atmosphere amounts to 20% of the total primary radiation flux. This is in good agreement with the data on the flux of primary α-particles obtained by means of nuclear emulsions.[7] The maximum ionization pulses recorded incident to the passage of single particles through the chamber correspond to the ionization produced by oxygen nuclei. The appreciable increase with altitude of the mean specific ionization of the particles, recorded by the telescope, must be attributed to the multiply charged particles in primary radiation (Fig. 6, Curve 1). A certain increase in the ionizing power at medium altitudes (from 71 ± ion pairs/cm at sea level to 85 ± 5 ion pairs/cm at 10-19 km) is undoubtedly due to the flux of secondary, strongly ionizing protons.

The results obtained in measurements with the telescope are juxtaposed in Fig. 6 with the data based on measurements of the global intensity of cosmic radiation (number of particles and ionization) made by Grigorov et al.[3] According to these authors the specific ionization at 16 km should be 130 ion pairs/cm, which is about 1½ times the value obtained by us. The difference between curves 1 and 2 (Fig. 6) appreciably exceeds the possible experimental errors and must be ascribed to the effect of short-range, strongly ionizing particles not detected by the telescope. An analysis of the ionization spectra obtained in the second series of measurements (without limitation of the range of the recorded particles) leads to the same conclusion. After taking account of the small contribution (about 8% of the total ionization) of peripheral particles traversing the chamber along short chords and remaining under the detection threshold (about 15% of the total flux), averaging of these spectra leads to values in good agreement with the results of Ref. 3 (see Fig. 6). Comparison of the spectra and the records of the counters surrounding the chamber make it possible to separate the particles not recorded by the telescope and to determine their ionizing power. A certain portion of these particles - small in number (about 1.5% of the total flux of charged particles) but substantial as regards the contribution to ionization (about 30% of the total "excess" ionization)-is comprised by short-range, strongly ionizing particles — mainly protons; these particles give up an appreciable energy in the chamber: as much as is liberated in the passage of seven or more relativistic particles. The nature of these particles and their genetic connection with nuclear

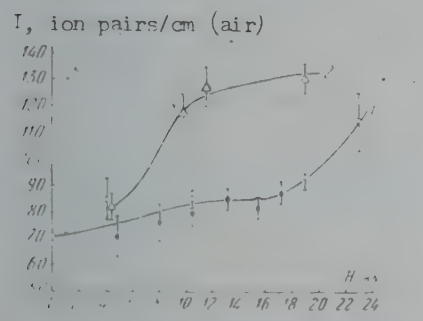

Fig. 6. Variation of the mean specific ionization of cosmic ray particles with altitude. Solid dots and circles (curve 1) - results of measurements with pulse ionization chamber and vertical telescope; triangles — measurements with ionization chamber without telescope. Curve 2 is drawn on the basis of measurements with an integral chamber and a single counter (Ref. 3).

disintegrations have been established in a number of investigations of ionizing collisions in chambers flown into the stratosphere.[3 & 8] A considerable portion of these particles, having ranges under 1.7 g/cm^2 of Al and comprising about 20% of the global flux in the stratosphere, cannot be identified as protons or slow mesons. The component generating these particles must be neutral (as follows directly from the indications of the hodoscopic counters), but only a minor fraction of these particles can be recoil nuclei, produced by the neutron flux. It is probable that these particles are mainly electrons with an upper energy bound of about 7 Mev. Their high ionizing power (double that of a relativistic particle) may be explained by multiple scattering of these particles. Experimental data on the multiple absorption in light matter of monoenergetic electrons in the energy interval in question[9-11], as well as the calculations made by Solov'ev[8] for the equilibrium electron spectrum in the stratosphere, tend to confirm this assumption. Particles characterized by a relativistic ionization constitute about 70% of the global flux in the stratosphere.

The data on the spectrum of strongly ionizing particles in the stratosphere obtained as a result of our experiments are summarized in the accompanying table.

Spectrum of strongly ionizing particles in the stratosphere (at 18-20 km)

Ionization intervals*	Mean ionization in the interval	Range	% of particles in given interval	Nature of particles
1,2÷1	1,7	> 57 g/cm² Pb + 7g/cm² Al	4±1	Secondary protons
2÷5,5	3	> 1,7 g/cm² Al < 57 g/cm² Pb + 7 g/cm² Al	3±1	Secondary protons
1,2÷5,5	2,1	< 1,7 g/cm² Al	20±3	Electrons
>5,5	11	≥ 1,7 g/cm² Al	3±0,5	Mainly protons

*Unit of ionization = mean ionization produced by a relativistic particle.

The author wishes to express his deep gratitude to S.N.Vernov and N.L. Grigorov for their sympathetic interest in the work and helpful discussions.
"M.V.Lomonosov" Moscow State University.

References

1. S.N.Vernov, N.L.Grigorov & F.D.Savin, Doklady AN SSSR 57, 137 (1947).
2. S.I.Brikker, S.N.Vernov, I.M.Evreinova, S.P.Sokolov, et al Doklady AN SSSR 57, 141 (1947).
3. N.L.Grigorov, I.M.Evreinova & S.P.Sokolov, Doklady AN SSSR 81, 379 (1951).
4. L.D.Landau, J. Phys. USSR, 8, 204 (1944).
5. B.Rossi, Rev. Mod. Phys. 20, 384 (1948).
6. R.V.Adams, C.D.Anderson, P.E.Lloyd, R.R.Rau et al, Rev. Mod. Phys., 20, 334 (1948).
7. H.L.Bradt, B. Peters, Phys. Rev., 77, 54 (1950).
8. A.D.Solov'ev, Thesis MGU, 1953.
9. K.D.Sinel'nikov, A.K.Val'ter, A.Ia.Taranov, A.V.Ivanov et al, Zhur. eksp. i teor. fiz. 9, 127 (1939).
10. F.L.Hereford, C.P.Swann, Phys. Rev., 78, 727 (1950).
11. J.G.Trump, K.A.Wright, A.M.Clarke, J. Appl. Phys., 21, 345 (1950).

INVESTIGATION OF THE IONIZING POWER OF COSMIC RADIATION AT 3200 METERS BY MEANS OF PROPORTIONAL SCINTILLATION COUNTERS

- L.P.Kotenko

We used stilbene and naphthalene crystals, measuring 17 x 24 x 24 mm and 14 x 11 x 21 mm respectively, to determine the ionization of cosmic ray particles at 3200 meters altitude. The arrangement of the telescope, crystal, photomultiplier and absorbers is shown in Fig. 1. The six Geiger counter telescope T discriminated the particles traversing the crystal K at small angles to the vertical. The flashes in the crystal were amplified by the photomultiplier and then by a linear amplifier. The output pulses from the amplifier were applied to the vertical deflection plates of a cathode-ray tube. At the instant of passage of a particle, the electron beam went on and the deflection of the beam was photographed. At the same time the camera recorded the array of neon lamps connected with the rows of counters between the absorbers as well as the neon lamps connected to the "shower" counters (Л in Fig. 1). Thus the neon lamps indicated the range of the particles and any accompanying showers. The installation was controlled by appropriate radio circuits. The linearity of the amplifier was checked by means of a special generator. The amplitude proportionality of the photomultiplier response to short light flashes was verified with the aid of a spark generator by varying the spark-to-photocathode distance. By increasing the potential between the plate and the last dynode we succeeded in obtaining linear amplitude amplification up to 8 v with light flashes of 10^{-9}-10^{-8} sec duration.

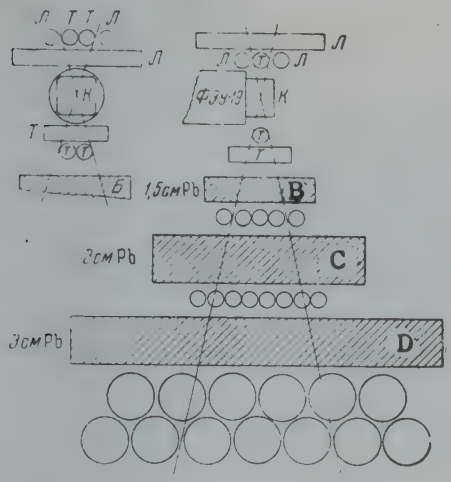

Fig. 1. Arrangement of telescope, crystal, photomultiplier and absorbers. Л - shower counters; T - telescope; K - crystal, ФЭУ-19 - photomultiplier, B, C & D - lead absorbers with trays of filter counters located under them.

Fig. 2 shows the differential ionization spectra of cosmic radiation particles as measured by means of the stilbene crystal in experiments with 22 cm of lead over the apparatus. The horizontal scale is laid off in relative units of light output from the crystal; the vertical scale gives the number of particles per the given light output interval. Spectrum A pertains to particles which traversed 7.5 cm lead, i.e., all three of the absorbers under the crystal. Spectra B, C and D pertain respectively to particles stopped in absorbers B, C and D (see Fig. 1). Cases of showers are not included in these distributions. Obviously these spectra consist mainly of mu mesons inasmuch as the soft component must have been wholly absorbed by the 22 cm thickness of lead above the apparatus. The ionizing power of mu mesons with a range of 7.5 cm Pb is already minimal. In consequence of the "density effect"* no logarithmic growth of the ionization loss after the ionization minimum was observed and consequently all the mu mesons in the spectrum A must have the same minimum ionization. In view of this the histogram A can be regarded as the fluctuation curve of our measure-

*Below we give experimental proof of the existence of the "density effect" for stilbene and naphthalene crystals.

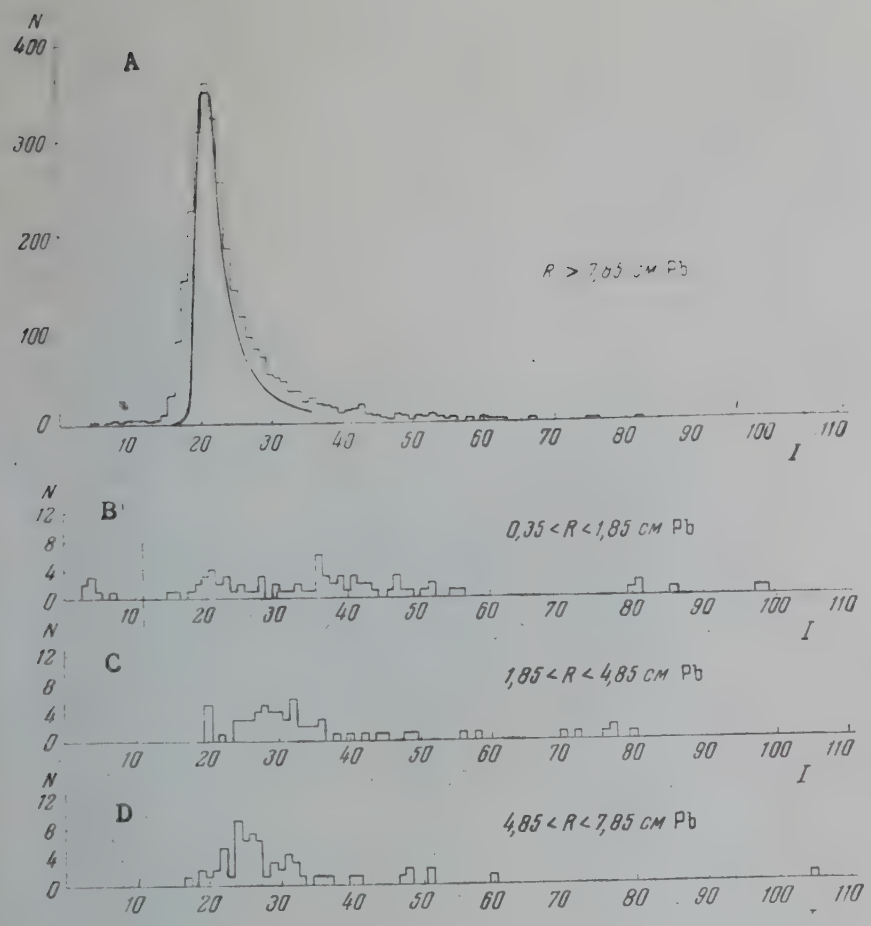

Fig. 2. Differential spectra of the ionization of cosmic ray particles. 22 cm thickness of lead above the apparatus. Spectrum A corresponds to particles traversing all three absorbers below the crystal; spectra B, C & D pertain to particles stopped in absorbers B, C & D, respectively (see Fig. 1). The numbers of particles on which the plots of A, B, C & D are based are 2885, 76, 65 and 66. The number of particles with ionization I > 100 amounts to 1 particle for spectrum A and 3 particles for spectrum B.

ments. The fluctuation curve must coincide with the fluctuation curve of Landau[1] if the scattering of the results of the ionization measurements is determined only by the fluctuation of the ionization losses.* The curve after Landau is represented by the smooth curve in Fig. 2 A. The half-width of Landau's fluctuation curve is 20%; the experimental curve is 1½ times wider. This difference is apparently connected with statistical straggling of the number of electrons ejected from the photomultiplier cathode by photons from the scintillator.

Histograms B, C & D in Fig. 2 pertain to mu mesons stopped in the respective absorbers under the crystal. The most likely ionizations, computed according to Landau's equation[1] taking the corrections for the density effect into account should be 2 I_{min}, 1.35 I_{min} and 1.2 I_{min}, respectively. The maxima in histograms C and D are accordingly actually displaced some 35 and 20% relative to the minimum ionization, i.e., with respect to the maximum of histogram A. However, the first spectrum (particles stopped in B), in addition to particles whose ionization is close to double the minimum value (i.e., mu mesons), comprises a group of particles whose ionization is close to the minimal. These particles are presumably relativistic electrons since these are the only known particles that can have minimum ionization and a range equivalent to

*The corrections of Brunck & Leisegang[2] to the theory of Landau[1] do not apply to the present measurements since they take into account the influence of the inner electrons on the ionization loss, while the light output of scintillation crystals is due to the electrons of the outer shells.

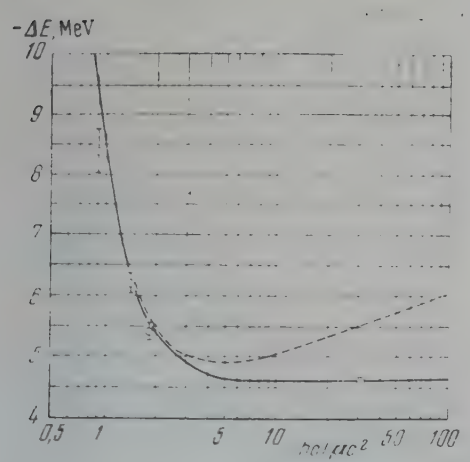

Fig. 3. Dependence of the most likely ionization loss ($-\Delta E$) in a stilbene crystal (taking the density effect correction into account) on the value of the ratio $pc/\mu c^2$ (p is the momentum and μ the rest mass of the particle). Solid line - curve taking density effect into account; dash line - disregarding the density effect correction. Experimental points - the most likely values of the light output of the stilbene crystal as a function of the momentum of the mu mesons. The point corresponding to hard mu mesons was normalized.

the thickness of the first absorber. These electrons are of secondary origin and are apparently δ-electrons, formed in the lowest layer of the absorber above the apparatus by the hard component of cosmic radiation. According to the measurements the number of electrons under the top 22 cm of lead, absorbed in the 1.5 cm thick lead filter, is approximately equal to the number of mu mesons stopped in the same 1.5 cm filter. The appearance of a small group of particles with an ionization close to zero in this spectrum is presumably due to showers of low density. A low density shower can produce the fourth coincidence and yet only graze the crystal.

In Fig. 3 the solid curve represents the variation of the most probable energy losses in the stilbene crystal with the value of the ratio $pc/\mu c^2$ (p - momentum; μ - rest mass of the particle), computed according to the equation of Landau[1] taking into account the correction for the density effect according to Sternheimer.[3] The dash-line curve is plotted without making correction for the density effect. The experimental points represent the most likely values of the light output of the stilbene crystal, depending on the momenta of the mu mesons stopped in the first, second and third absorbers as well as of hard mu mesons traversing all three absorbers. The average momenta of the soft mu mesons were determined from the average range, allowing for the extension in range due to coulombic scattering.[4] The mean momentum of the hard mu mesons was found from the distribution in momentum of mu mesons at mountain altitudes, taking into account the cut-off of the spectrum by the absorbers. The point corresponding to the hard mu mesons was normalized.

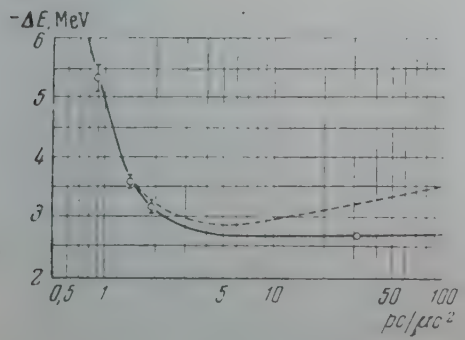

Fig. 4. Same as Fig. 3 but for the naphthalene crystal.

The most likely values of the light output according to the histograms of Fig.2 were determined by the "method of maximum likelihood".[5-7] The most probable values for the measurements were evaluated by a more simple method, based on cutting off the histograms to the right of the maximum in the region of the greatest deviations of the ionization from its most likely value (see Appendix).

The uncertainties of the experimental points in Fig. 3 correspond to the 60-70% reliability limits. The error for the point pertaining to hard mu mesons is $\pm 0.5\%$, which corresponds approximately to the thickness

of the ionization loss curve in the figure.

It will be seen from Fig. 3 that in the interval from minimal to twice minimal ionization the light output is proportional to the energy loss due to ionization. At double the minimal ionization, however, a deviation (amounting to about 10%) to the side of lower light output efficiencies becomes apparent. Further it will be seen that the experimental points fit the theoretical ionization loss curve, calculated by taking the density effect into account and fall far from the curve computed disregarding the density effect correction. Thus if we put the point for hard mu mesons on the latter (dash-line) curve, the points for $pc/\mu c^2$ equal to 1.4 and 1.8 will fall at a distance of about five mean square deviations from the curve. Thus we have shown that the density effect does exist in stilbene crystals and that it is correctly predicted by the theory of the effect.

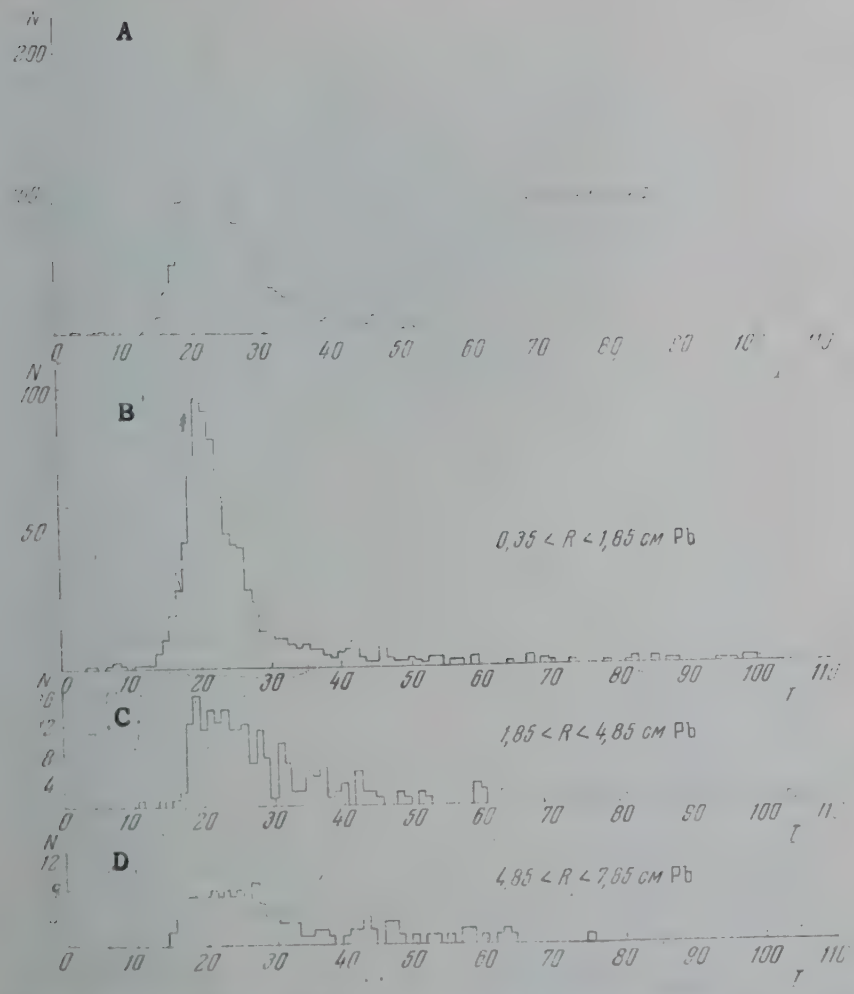

Fig. 5. Differential spectra of the ionization of cosmic ray particles at 3200 meters. In these measurements there was only a layer of light matter having a superficial density of 30 g/cm^2 over the apparatus. For identification of the spectra see Fig. 2. The numbers of particles on which spectra A, B, C & D are based are 1889, 885, 218 and 141, respectively. The number of particles with $I > 110$ is 2 for spectrum A, 8 for B and 2 for D.

The results of analogous measurements made with the naphthalene crystal are shown in Fig. 4. Here, too, it will be seen that the light output of the crystal is proportional to the energy loss due to ionization, but in this case the deviation from proportionality, noted for the stilbene crystal, is not observed. The satisfactory fit of the experimental points to the theoretical energy loss curve, calculated allowing for the density effect, and the impossibility of making them fit the curve computed without taking the effect into account, indicate that the density effect does obtain in naphthalene crystals as well and is dependably predicted by theory.

Fig. 5 shows the differential ionization spectrum of

cosmic ray particles obtained at 3200 meters with no special absorber above the apparatus. That is, the shielding over the apparatus consisted only of a 30 g/cm^2 thickness of light material. Here spectrum A pertains to hard particles (particles penetrating 7.5 cm lead) - mainly mu mesons. Spectra B, C and D represent the soft component and, hence, comprise primarily electrons. The purest electron spectrum is B, since the shower fraction of the electrons is cut off by the first (1.5 cm lead) absorber and the number of mu mesons and strongly ionizing particles stopped in this absorber amounts to only a few percent of the number of electrons. In spectrum C we have a mixture of electrons, mesons and strongly ionizing particles or protons. Spectrum D is also due to a mixture of electrons, mesons and protons.

It will be seen from spectra A and B that the most probable ionization of relativistic electrons, according to calculations taking the density effect into account, is identical with the minimum ionization. Accurate determinations of the most likely ionization of relativistic mesons and electrons, based on three series of measurements (the results of the other two series are not reproduced here), yield a value within 1.5% of the minimal. In particular, this indicates that the light output of the crystal at relativistic energies depends (to within 1.5%) only on the ionization density and not on the nature of the particles. For non-relativistic energies the light output is also dependent upon the nature of the particles (see Taylor, Jentschke et al[8] and Frey, Grim et al[9]).

Lastly, from the spectra of Fig. 5 we can evaluate the number of strongly ionizing particles, or protons, stopped in 7.5 cm of lead as a result of ionization losses. Calculations show that the hardest protons - i.e., the protons stopped in absorber D - must produce an ionization equal to 2.6 I_{min}, while the softest mesons - the mesons vanishing in the first absorber B - produce an ionization of about 2 I_{min}. Obviously one can make a rough evaluation of the number of protons comprised in the soft spectra by counting the particles with an ionization exceeding 2.3 I_{min}. Such an evaluation, made on the basis of the three series of measurements, indicated that the protons account for 4.8% of the total hard component. However, this percentage is clearly an over-estimate since, in addition to protons, the strongly ionizing particles comprise a certain number of electrons and mesons. Subtracting the number of electrons and mesons (as estimated from electron and meson distribution data) reduces the percentage of protons to 3.5%. Thus the number of strongly ionizing particles, or protons, stopping in 7.5 cm of lead at 3200 meters altitude and under a 30 g/cm^2 thickness of light matter amounts to 3.5 $\pm$ 1% relative to the hard component; this corresponds to a vertical flux of protons with a momentum of 0.8 Bev/c equal to $(2.1 \pm 0.6)\cdot 10$ (Bev/c)$^{-1}$ cm^{-2} sec^{-1} sterad^{-1}.

In their investigation Kocharian et al[10] obtained the distribution of protons in momentum at 3200 meters. On the basis of their curves, the number of protons having a momentum of 0.8 Bev/c, comes out to be $2.3\cdot 10^{-3}$ (Bev/c)$^{-1}$ cm^{-2} sec^{-1} sterad^{-1}, i.e., a value in agreement with ours within the limits of the experimental errors. Nor are our values inconsistent with the data of Miller et al[11] who investigated the proton-meson component at 3400 meters with the aid of a cloud chamber. These authors give a value of $1.1\cdot 10^{-3}$ (Bev/c)$^{-1}$ cm^{-2} sec^{-1} sterad^{-1} for the flux of protons with a momentum of 1 Bev/c. This is about half our value; if we take into account the shape of the incident proton spectrum (exponent 2.6-2.8 — Refs. 10 & 12), we must expect a reduction of exactly this amount in going from 0.8 Bev/c to 1 Bev/c.

APPENDIX: Determination of the Most Probable Ionization Loss

It is known that if the mean ionization of particles is determined on the basis of measurements with a proportional counter, at relativistic energies the resultant value will not agree with the mean ionization defined by the Bethe-Bloch equation. Hence for comparing experiment with theory it is the usual practice to determine the most probable value of the ionization, i.e., the value corresponding to the maximum in the distribution curve. The method of determining the parameters for any given distribution law and, in particular, the most likely value of a number of measurements was first proposed by Fisher (see Cramer[5]), who called it the "method of maximum likelihood." Practical procedures for applying the method are also described by Becker et al[6] and Eliseev et al[7]. However the processing of data by this method is time consuming and we, therefore, attempted to find a simpler method.

The difference between the mean and the most probable value of the ionization loss as a function of the energy stems from the rapid increase in the number of δ-electrons with energy. In the present experiments, i.e., for the mesons energy interval in question, the difference in losses amounts to about 10%. The method of determining the most likely value that we employed is based on cutting off the histograms in the region of high ionizations (see Fig. 2), that is, on excluding the high-energy δ-electrons. Thus, if one computes the mean ionization from the cut-off histograms, its variation with energy should coincide with that of the most probable value of the ionization. It is essential, however, to find the "equivalent" cut-off points for all the histograms. We proceeded in the following manner. First, we chose a cut-off boundary for one of the spectra (specifically, histogram A of Fig. 2) in the region of 1½-2-fold minimal ionization and then computed the ratio of the mean value of the ionization for the cut-off spectrum to the ionization at the boundary. Then we guessed at a likely cut-off point for the next spectrum and computed the same ratio for it. If the latter ratio proved larger than the former, the cut-off boundary was shifted to the right (if smaller, to the left) and the ratio computed anew. Two or three successive approximations were generally sufficient to establish the "equivalent" cut-off boundary. The cut-off points for the other two spectra were determined in a like manner. The mean values of the cut-off spectra must be proportional to the corresponding most probable values of the histograms. Hence by dividing all the mean values for the cut-off spectra by the mean value for the hard spectrum (histogram A of Fig. 2) we obtain the most probable ionizations of the particles minimum ionization units.

Some of the data shown in Fig. 2 were processed both by the method of maximum likelihood and by the above-mentioned cut-off method: the most likely ionization calculated by the two methods agreed within 1%. The measurement errors (on the order of 2.5%), corresponding to the 60-70% reliability limits (root mean square for the cut-off spectra), also proved to be virtually identical. Checks showed that the selection of the initial cut-off boundary, provided it is in the 1½-2 time minimum ionization interval, is not critical: computations starting with different initial points in the said region lead to identical values of the most likely ionization. As evidence of the time-saving afforded by the cut-off method, we need only point out that whereas processing of the histograms of Fig. 2 by the method of maximum likelihood would have required over a month, these histograms were processed by the cut-off method in a few hours.

In general, if there is an experimental histogram with a large number of measurements relatively distant from the peak and the theoretical shape of the distribution curve is known (a necessary condition for application of the method of maximum likelihood), the most probable value of the quantity in question

can readily be evaluated by establishing an appropriate cut-off boundary on the distribution curve (drawn to any suitable scale) and operating as described above; to go over from the mean value for the cut-off histogram to the most probable value for the entire series of measurements the said mean value must be multiplied by the ratio of the most likely value of the distribution curve to the mean value for the cut-off curve. Selection of the cut-off boundary so that the mean for the cut-off curve will be equal to the most probable value will be expedient only if in the process not too many measurements are excluded, for otherwise the statistical error will be unduly increased.

"P.N.Lebedev" Physical Institute of the
Academy of Sciences of the USSR

References

1. L.D.Landau, Journ. Phys. USSR, 8, 201, (1944).
2. O.Blunck & S.Leisegang, ZS. Phys., 128, 500 (1950).
3. R.M.Sternheimer, Phys. Rev. 88, 851 (1952).
4. I.Ia.Pomeranchuk, Zhur. eksp i teor. fiz., 18, 759, (1948).
5. H.Cramer, Mathematical Methods of Statistics (in Rus. Trans.) M. 1948.
6. J.Becker, P.Chanson, E.Nageotte, P.Treille et al, Proc. Phys. Soc., A65, 437 (1952).
7. G.P.Eliseev, V.K.Kosmachevskii & V.A.Liubimov, Doklady AN SSSR 90, 755 (1953).
8. C.J.Taylor, W.K.Jentschke, M.E.Remley, F.S.Eby et al, Phys.Rev.84,1034 (1951).
9. H.B.Frey, J.M.Grim, W.M.Priston & T.S.Gray, Phys.Rev., 82,372 (1951).
10. N.M.Kocharian, M.T.Aivazian, Z.A.Kirakosian & S.D.Kaitmazov, Doklady, AN Armenian SSR, 17, 33 (1953).
11. C.E.Miller, J.E.Henderson, D.S.Potter & J.Todd, Jr. Phys.Rev.,85, 981 (1951).
12. M.G.Mylrol & J.G.Wilson, Proc.Phys.Soc., A64,404 (1951).

* * * * * * * * * *

INVESTIGATION OF THE ORIGIN OF THE SOFT COMPONENT OF COSMIC RAYS IN THE STRATOSPHERE AT GEOMAGNETIC LATITUDE 51° NORTH

– P.N.Ageshin, A.N.Charakhch'ian & T.N.Charakhch'ian

In their experiments Vernov and his coworkers[1] established that the intense generation of the electronic-photonic component observed in the stratosphere could not be explained solely by the formation of electrons incident to the decay of mu mesons. Shortly after the discovery of neutral pi mesons in accelerator experiments, the Bristol group[2] detected the presence of neutral pi mesons — generated in nuclear emulsion stars — in the stratosphere as well. In view of the relatively high probability of the generation of neutral pi mesons in stars with their subsequent decay ($\pi^0 \rightarrow 2\gamma$) it is commonly assumed that the excess of the electronic-photonic component in the stratosphere is a consequence of the genesis of π^0 mesons. On the basis of the now available data on spectrum of the generation of π^0 and π^+ mesons in the stratosphere and their decay schemes, one can "plot" the passage of the electronic-photonic component through the atmosphere and compute, for example, the electron energy spectrum at different altitudes. Although rigorous calculations of this sort have not yet been made, it is of interest to obtain experimental data on the range distribution of charged particles in the stratosphere, if only for the purpose of comparing such data with the results deduced from theoretical considerations.

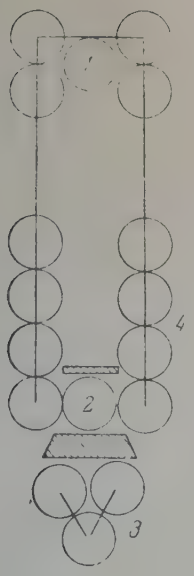

Fig. 1. Arrangement of counters. Absorbers shown are for measurement of particles with ranges from 2 to 6.6 g/cm^2. Counters 1 & 2 form the telescope; hodoscopic counters 4 serve for exclusion of lateral showers; counters 3 served to limit the range interval of the recorded particles from above.

We measured the altitude dependence of the number of particles of the soft component in the range intervals 0.4-0.9, 1.2-2.0, 2.0-6.6 and 6.6-11.3 g/cm^2 glass or aluminum at latitude 51°N. The numbers of particles in these range intervals were measured simultaneously (during the same flight) by means of an array of four counter telescopes. For control purposes two independent series of measurements were carried out; the resultant data agree within the limits of the statistical errors.

The arrangement of counters for one of the telescopes is shown in Fig. 1. In order to eliminate the influence of lateral showers the telescopes, consisting of counters 1 and 2, were surrounded by groups of side counters 4, as shown in the figure. The results of measurements showed that an appreciable portion -- some 15-20% relative to the number of single particles traversing the telescope -- of the coincidences in the telescope were due to particles of lateral showers. It should be of interest to elucidate the nature and origin of these lateral showers, which are characterized by a high intensity under the conditions of the experiment (in the stratosphere); this will be the subject of future investigations.

The parallel connected counters 3 covered the solid angle of the telescope 1 & 2. The record of the coincidences of 1 and 2, not accompanied by discharges of counters 3 and lateral shower counters 4, provides a measure of the number of particles in the given range interval.

The results of our measurements are presented in Fig. 2. The vertical scale gives the number of particles (cm^{-2} min^{-1} sterad^{-1}) observed for the given range interval, the horizontal scale shows the depth in g/cm^2 equivalent. It will be seen that the curves for all four range intervals exhibit maxima in the stratosphere. The altitude dependence and the actual number of particles in the 0.4-0.9 and 1.2-2.0 g/cm^2 intervals are virtually identical. The altitude dependences

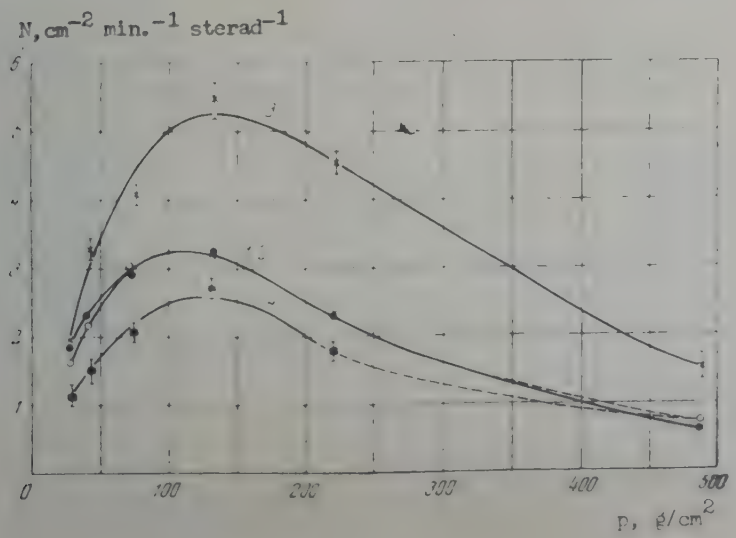

Fig.2. Variation of the number of soft component particles with atmospheric depth in different range intervals: 1) 0.4 - 0.9 g/cm^2, 2) 1.2-2.0 g/cm^2, 3) 2.0-6.6 g/cm^2, 4) 6.6-11.0 g/cm^2 (aluminum).

for the 2.0-6.6 and 6.6-11.3 g/cm^2 intervals are also close, but the numbers of particles in the two intervals differ by a factor of two.

From the data of Fig. 2 we can readily deduce the differential range spectra of the charged particles of the soft component at the depths from 30 to 500 g/cm^2. The spectra for different depths are plotted in Fig. 3; the plots have been adjusted to coincide at the point corresponding to the 2.0-6.6 g/cm^2 range interval.

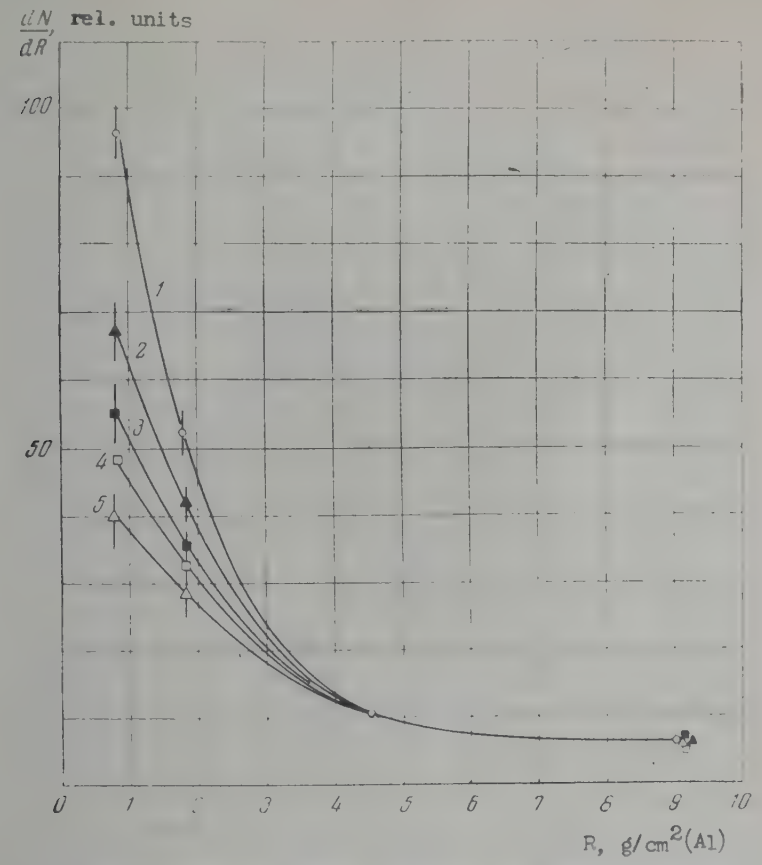

Fig. 3. Differential range spectra of particles of the soft component at different atmospheric depths: 1) 30, 2) 77, 3) 136, 4) 222 and 5) 490 g/cm^2.

Let us clarify the nature of the recorded short-range particles. At 24 km the total number of short range particles, having ranges inferior to 11.3 g/cm^2 of aluminum, according to our results, equals 30% of the total number of charged particles at this altitude and about 70% of the total number of soft component particles. It is natural to assume that there are virtually no mu mesons among the recorded short-range particles, since mu mesons not only lose their energy in the process of ionization but also disintegrate in the stratosphere. An evaluation of the effect of slow protons where our measurements are concerned is somewhat more difficult. To this end we can profitably make use of the data on excess ionization in the stratosphere, obtained by Grigorov and Rapoport.[3] If the excess ionization is ascribed to the action of protons, the ranges of which fall into only the first two range intervals of our measurements, the number of such protons would amount to about 10% of the number of particles recorded for the said intervals. Consequently it may reasonably be assumed that the range spectra of charged particles of the soft component, shown in Fig. 3, represent the range spectra of electrons at practically all depths. Where electrons are concerned the first two range intervals of our experiments correspond to effective energies of about 1.5 to 6 Mev, while the second pair of intervals corresponds to 6 to 40 Mev.

As may be seen the range spectrum of the soft component particles - electrons - becomes increasingly softer with decreasing depth. This effect is hard to explain from the point of view of electromagnetic cascade processes. Thus let us suppose that the electrons with ranges in the first two intervals, observed, for example, at the smallest depth (30 g/cm^2), originate not directly

but through electromagnetic cascade processes. Then from the view point of theory one should expect an increase in the proportion of these particles with depth, rather than the observed decrease.

In 1951, using counter telescopes, we measured the number of particles, having ranges under 1 cm of lead, in the stratosphere at latitudes 31 and 51°N. The results of these measurements (which will be published separately) showed that the magnitude of the latitude effect for such particles in the stratosphere is close to that of the latitude effect for primary particles (between the same latitudes) and greatly exceeds the latitude effect for mu mesons and for electrons with longer ranges. This, too, stands in the way of attributing the origin of the predominant number short-range electrons recorded at 51° N latitude to cascade multiplication of the electronic-photonic component in the upper layers of the stratosphere.

Thus, in order to explain the observed phenomena -- 1) the presence of a large number of low-energy electrons at small atmospheric depths, 2) the continuous softening of the range spectrum of the electrons with decreasing depth and 3) the great latitude effect for electrons of low energies -- we must, apparently, hypothesize a new mechanism for the generation of the low-energy electronic-photonic component in the stratosphere.

In conclusion the authors wish to thank S.N.Vernov for his interest in the investigation and discussion of the results.

"M.V.Lomonosov" Moscow State University
and
"P.N.Lebedev" Physical Institute of the
Academy of Sciences of the USSR

References

1. S.N.Vernov, Zhur. eksp. i teor. fiz. 19, 621 (1949).
2. A.G.Carlson, J.E.Hooper & D.F.King, Phil.Mag., 41, 701 (1950).
3. N.L.Grigorov, I.D.Rapoport & G.T.Shipulo, Doklady AN SSSR, 91,491 (1953).

* * * * * * *

NARROW AIR SHOWERS IN THE STRATOSPHERE

- P.N.Ageshin, A.N.Charakhch'ian & T.N.Charakhch'ian

Our initial measurements in the stratosphere showed that with no absorber in the counter telescope an appreciable number of the coincidences recorded was due to secondary shower particles. The number of counter activations caused by accidental coincidences was small. The ratio of the total number of coincidences from secondary showers to the expected (calculated) number of accidental coincidences depended on the experimental conditions and varied from 2 to 10 in different experiments. In addition we were able to record directly the coincidences caused by secondary showers by means of a hodoscopic system of counters, appropriately located in relation to the telescope counters (see Ref. 1). The ratio of the number of coincidences in the telescope due to secondary showers to the number of single particles passing through the counters varied between 0.05 and 0.25, depending on the conditions of the experiment.

Further observations showed that the installation of a thin absorber in the telescope reduced the number of coincidences arising from secondary showers.

It follows that among the particles comprising secondary showers there are some with short ranges. It was also noted that with lead plates set near the hodoscope counters the pulse frequency ofthese counters was higher than when the counters were at a greater distance from the lead plates. This indicated the presence of photons in the secondary showers.

The data thus obtained on secondary showers in the stratosphere did not allow of drawing any definite deductions regarding their origin. To this end it was essential to establish whether the initiation of these showers was localized in the apparatus (generation of stars in various parts of the equipment, electronic-nuclear showers, showers from electrons, etc.) or whether part of these showers originated in the air above the apparatus. In the latter case study of these showers in the stratosphere would be worthwhile. Below we give the results of measurements from which it follows that an appreciable part of the secondary showers may be considered to be narrow air showers in the stratosphere.

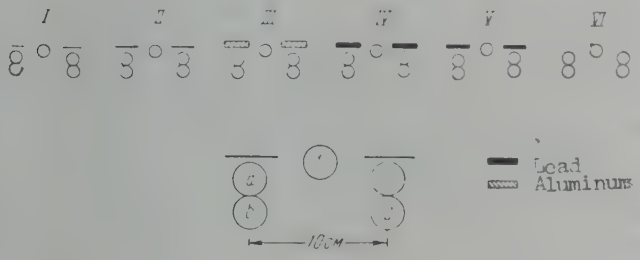

Fig. 1. Arrangement of the six counter groups in the apparatus for measuring the number of air showers. The arrangement of counters is identical in all groups. One group is pictured to an enlarged scale in the lower part of the figure. The absorber thickness in groups I, II, IV and V was 1, 2, 8 and 4 mm of lead, respectively; the plate over group III was 10 mm thick aluminum.

Our measurements were accomplished by means of equipment in which the counters were arranged as shown in Fig. 1. The counter groups differed in that different absorber plates were mounted over the counters a and c. Lead plates having a thickness of 1, 2, 8 and 4 mm, respectively, were mounted over counters a and c of groups I, II, IV and V; the counters of group III were decked with 10 mm thick aluminum plates; there were no absorber plates over the counters of group VI. All plates measured 20 cm along the length of the counters and 4 cm at right angles thereto. The effective dimensions of the counters were: length - 20 cm; diameter - 2 cm.

The length of the box in which the six counter groups were housed was 140 cm; the width, 40 cm; the depth, 7 cm. The top cover (0.3 mm thick aluminum sheet) of the box was 1.2 cm distant from the counters. In addition to the counters the box housed the counter circuits consisting of one miniature vacuum tube, two neon tubes and associated components (one circuit for each counter). The counters comprised the major portion of the weight of this part of the equipment (not counting the weight of the plates). The housing box was mounted on four posts one meter in height; the lower ends of these posts were attached to another container holding the heavier components of the apparatus.

The electronic circuit and other equipment provided for the transmission of radio signals corresponding to coincidences of pulses in the following counters: abc, abc+2, abc+1 and abc+2+1. The coincidences were recorded independently for each of the six groups.

Coincidences abc (for each group) could be due to 1) accidental coincidences, 2) δ-electrons ejected from the walls of counters a or b by the passage of single particles through counters a and c or b and c. Inasmuch as all six counter groups were identical the numbers of accidental coincidences and δ-showers could not differ appreciably from group to group. Furthermore the number of coincidences stemming from these trivial causes can be readily calculated.

The circumstances under which the different kinds of coincidences occur differ, depending on whether the coincidences are produced by particles of secondary showers (particles of showers generated in various parts of the apparatus and of air showers) or particles of showers originating in the plates over the counters a and c of the given group. As indicated in Fig. 1, counter 1 is located between counters a and c, between the two absorber plates. Accordingly, for coincidences arising from the generation of charged particles in either of the two absorber plates, the probability of a pulse in counter 1 will be close to 100% (for uncharged particles emerging from the plates the likelihood of activation of counter 1, as of counters a and c, will be small). In the case of secondary showers inducing coincidences, the probability of a discharge of counter 1 will be small if the number of particles in the shower is not large. Therefore the cases in which counter 1 is not activated may be associated with secondary showers, while the number of cases in which it is activated may be viewed as the upper bound of the number of coincidences produced by the shower particles generated in the absorber plates of a given counter group. Hence, it is expedient to examine, for each group of counters separately, the cases in which counter 1 is not activated and the cases in which a discharge is observed, to wit:

1) abc and abc + 2;
2) abc + 1 and abc + 2 + 1.

The variation of the number of coincidences with altitude for the first set of these coincidences is shown in Fig. 2, while that for the second is given in Fig. 3.

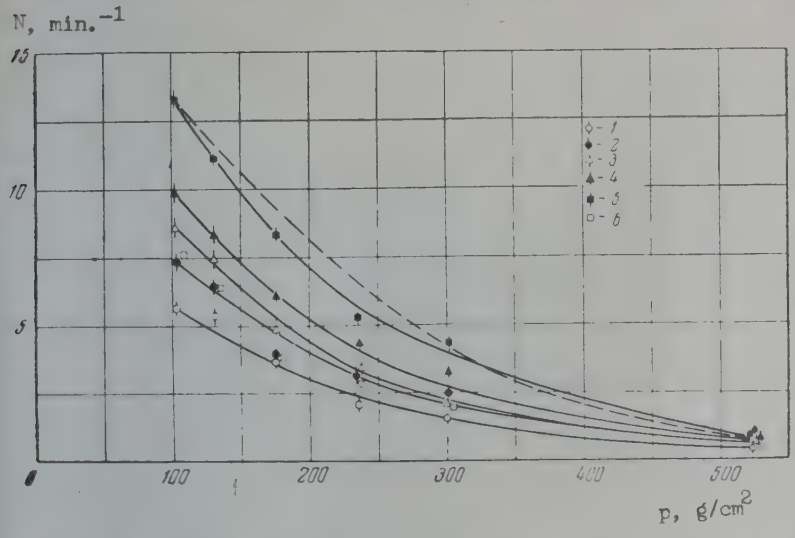

Fig. 2. Variation of N, the total number of coincidences in counter sets abc and abc+2 with the depth of atmosphere p, for absorbers of different thickness: 1) no absorber; 2) 1 mm thick lead absorber; 3) 2 mm lead; 4) 4 mm lead; 5) 8 mm lead; 6) aluminum 10 mm thick.

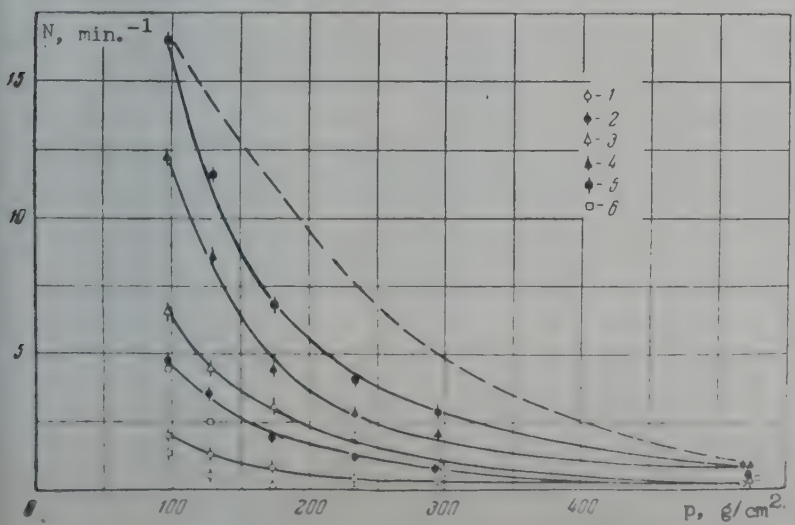

Fig. 3. Same as Fig. 2, but for coincidences in counter sets abc+2+1 and abc+1.

The increase in the number of coincidences for counter combinations abc and abc+2 with increased thickness of the absorber plates (see Fig. 2) indicates that the secondary showers causing these coincidences comprise photons. It is important to establish whether these photons originate in the apparatus or in the air. The lead plates located over

the counters are mounted in contact with the top cover of the box. Thus there is virtually no high density material above these plates. Accordingly photons generated in the material of the apparatus must be propagated in the direction counter-to-plate.

In view of this, it is difficult to see how the effect described by the curves of Fig. 2 could be due to photons from the material. It may be concluded, therefore, that the observed transition effect in the number of showers pertains to photons incident on the apparatus from above, i.e., to photons of narrow atmospheric showers. Hence it would appear desirable to make further detailed experimental studies of the characteristics of narrow atmospheric showers in the stratosphere.

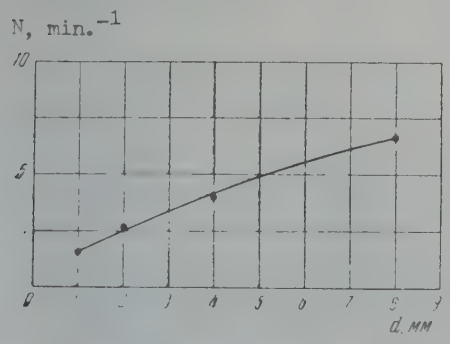

Fig. 4 The dependence of N, the total number of coincidences for counter combinations abc and abc+2 on the thickness of the lead plates over the counters, after subtraction of the corresponding number of coincidences in group VI. The data were obtained from measurements at an atmospheric depth of 107 gm/cm^2.

If we take the number of single particles which pass through the two counters a and b as our unit, the number of air showers recorded with a 8 mm lead filter at a depth of 100 gm/cm^2 is about 0.5%. Some information regarding the energy of photons in narrow air showers can be deduced from the data on the variation in the number of recorded showers. The variation of the number of recorded showers with the thickness of the absorber plates (after subtraction of the number of showers recorded by the group of counters without absorbers) is shown in Fig. 4. However, our conclusions regarding the photon energies will be entirely different depending on whether we assume that the coincidences in counters abc and abc+2 are due solely to photons or to combinations of a charged particle (electron) and a photon. Our latest preliminary results suggest that a significant number of coincidences in counters abc and abc+2 are produced solely by photons.

The results given above do not fully exhaust the various aspects of the phenomena studied. Hence it is not yet feasible to draw definite conclusions about the nature and origin of narrow air showers in the stratosphere. However, from the point of view of experimental technique, it appears possible to investigate the various aspects of the effect in detail and to elucidate the various questions raised by the results of our observations.

The authors express deep appreciation to S.N.Vernov for his interest in the work and for discussions of the results.

"Lomonosov" State University of Moscow
and
"Lebedev" Physical Institute of the
Academy of Sciences of the USSR

Reference

1. A.N.Charakhch'ian, Thesis, FIAN, Moscow 1952.

* * * * * * *

SOME RESULTS OF AN INVESTIGATION OF NUCLEAR DISINTEGRATIONS IN TUNGSTEN, COPPER AND ALUMINUM PRODUCED BY COSMIC RAYS

- Zh.S.Takibaev

1. Procedure

A prolonged search[1] for an effective method of investigating nuclear disintegrations in diverse pure elements by means of thick-emulsion photographic plates led us to select the following procedure.

The pure element in which nuclear disintegrations are to be studied is prepared in the form of fine wires 50-200 μ thick. In our experiments we used tungsten, copper and aluminum wires. The wires were arranged in parallel rows and clamped between photographic plates, set with the emulsions face to face. If the emulsions are moistened beforehand and the plates clamped with sufficient force, the wires are pressed into the emulsion, i.e., are so to say immersed in the emulsion medium (in many cases the wires were clamped between emulsion films rather than between photographic plates). In our experiments with plates the thickness of the emulsion layer attained 1200-1500 μ, while the total thickness of the stack reached 5 cm. After exposure of the plates or emulsion films to cosmic rays at the mountain laboratory or in the stratosphere, the wires immersed in the emulsion were removed and the plates or films developed in the prescribed manner. The developed emulsions were scanned along the impression left by the withdrawn wires. The tracks of particles of interest to us could easily be traced from one pair of emulsions to the next in the stack by virtue of the special markers formed on the wires in the process of fabrication.

Each star formed in the wires (see figure) is recorded on both emulsions of the facing pair. The corresponding halves of the star could be accurately matched on the basis of the imprints left in the emulsion by the markers on the wires. In analyzing the individual disintegration events satisfactory results are obtained by subdividing the field of view under the microscope into appropriately oriented quadrants; this facilitates distinguishing true nuclear disintegrations with a small number of rays from accidentally intersecting or overlapping particle tracks in the vicinity of the impressions left by the wires.

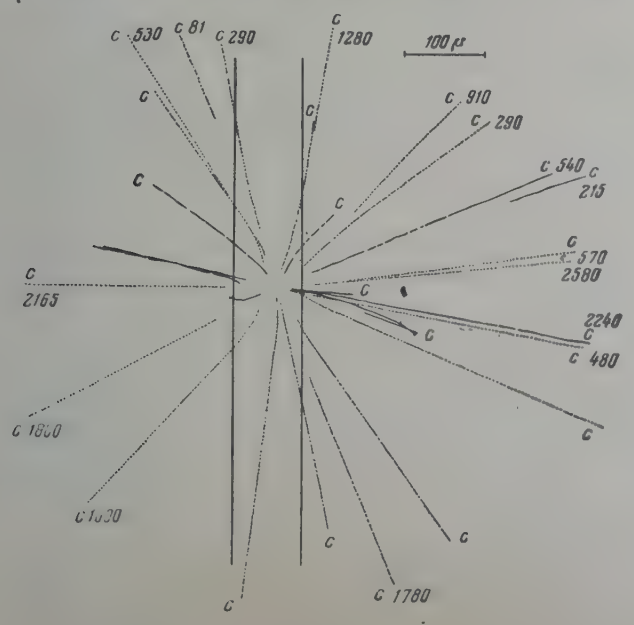

Photograph of star formed in tungsten wire (the wire boundaries are indicated by two vertical lines). The letters C indicate the ends of tracks directed towards the glass of the plates; the figures give the path in microns.

Experiments show that the speed of the emulsion is not impaired by impressing the wires; there is, however, an appreciable distortion of the tracks in the depressed areas. These distortions were taken into account in measuring the multiple scattering angles by the interference method.[2]

In a series of experiments the wires were clamped between two emulsion films; these

pairs were also assembled into a stack, forming a sort of "emulsion chamber". However, processing of such "emulsion chambers" presented considerable difficulties. Hence, for the most part we used stacks consisting of alternating emulsion films and photographic plates coated with emulsion on both sides. Thus the plate, film and wire assembly resembled a sort of multi-layer cake.

2. Experimental Results

Stacks of emulsions and plates incorporating wires of different pure elements, assembled as described above, were exposed at an altitude of 4375 meters (Mt. Komsomol) in the vicinity of Alma-Alta for a period of forty days. It was initially assumed that the photographic emulsions would record all charged particles having relativistic velocities, but our checks showed that our emulsions were not sensitive enough to do this in all cases.

We recorded a total of 179 stars in tungsten and 109 stars in copper. The distribution of these stars with different numbers of grey tracks (N_g) according to the total number of rays (N_h) is shown in Table 1. It follows from this distribution that in nuclear disintegration of heavy elements there are many "weak" stars with 3-6 rays. Also, the relative number of grey tracks in the stars formed in tungsten is somewhat higher than in the stars produced in copper. This is evidence of the relatively higher intensity of formation of grey tracks in heavy nuclei; the effect is apparently connected with the development of intra-nuclear cascade processes.

Table 1

Distribution of stars with different numbers of grey tracks (N_g) formed in tungsten and copper as a function of the total number of rays (N_h) according to measurements made at 4375 meters

	N_g \ N_h	2	3	4	5	6	7	8	9	10	11	12	14	15	16	22	32
Tungsten	1		14	13	12	3	1	2	1	—	1	1	—	—	—	—	—
	2		4	12	9	7	2	—	—	3	—	—	—	—	—	—	—
	3		3	6	2	5	1	2	2	1	1	—	1	—	—	—	—
	4		—	1	1	—	1	1	1	—	—	—	1	—	—	2	—
	5		—	—	—	1	1	1	—	—	2	—	—	1	—	—	—
	6		—	—	—	—	—	—	1	—	—	—	—	—	1	—	—
	18		—	—	—	—	—	—	—	—	—	—	—	—	—	—	1
	Total number of stars with N_h rays	1	44	43	35	18	8	7	7	4	4	1	2	1	1	2	1
Copper	1		15	8	6	3	—	—	—	—							
	2		4	5	3	1	3	—	—	—							
	3		—	4	2	3	—	—	1	1							
	4		—	1	1	—	1	—	—	—							
	5		—	—	1	—	—	1	—	—							
	6		—	—	—	—	—	—	1	1							
	Total number of stars with N_h rays		45	28	17	8	4	1	2	2							

We evaluated the relative star formation cross sections for tungsten, copper and the photographic emulsion on the basis of the experimental data. The results throw some light on the relative transparency of these nuclei. Thus, we can write

$$\frac{N_W}{N_{Cu}} = \frac{\sigma_W q_W}{\sigma_{Cu} q_{Cu}},$$

where N_W and N_{Cu} are respectively the numbers of stars formed in tungsten and in copper per 1 cm^3 per sec, q is the number of nuclei per cm^3 and σ is the

Distribution of stars with different numbers of grey tracks (N_g) formed in tungsten, copper and alumunum as a function of the total number of rays (N_h) according to measurements in stratosphere.

	N_g \ N_h	2	3	4	5	6	7	8	9	10	11	12	13	14	15	16	17	18	19	20	21	22	23	24	25	26	29	30	32	35
Tungsten	1		2	6	12	5	4	3	5	—	1	—	—	—	—	—	—	—	—	—	—	—	—	—	—	—	—	—	—
	2		1	6	6	5	3	9	4	8	—	1	2	—	1	1	1	—	—	—	—	—	—	—	—	—	—	—	—	—
	3		—	—	5	2	2	6	8	2	5	—	1	1	3	—	—	—	—	—	—	—	—	—	—	—	—	—	—	—
	4		—	—	2	1	—	3	—	5	2	3	2	1	—	1	1	1	—	—	—	—	—	—	—	—	—	—	—	—
	5		—	—	—	—	—	1	1	2	2	2	2	—	—	1	—	1	—											
	6		—	—	—	—	—	—	—	1	1	2	—	3	2	—	1	—	—											
	7		—	—	—	—	—	—	1	1	—	—	1	2	—	1	3	—	2	1	—	—	2							
	8		—	—	—	—	—	—	—	—	—	—	1	—	—	—	—	—	—	—	—	—	—	—	—	—	—	—	—	—
	9		—	—	—	—	—	—	—	—	—	—	—	—	1	—	—	—	—	1	3	—	—	—	—	—	1	—	—	—
	10		—	—	—	—	—	—	—	—	—	—	—	—	—	—	1	1	—	—	—	—	1	—	—	—	—	—	1
	11		—	—	—	—	—	—	—	—	—	—	—	—	—	—	—	—	—	—	—	—	—	—	1	—	—	1	—	—
	12		—	—	—	—	—	—	—	—	—	—	—	—	—	—	—	—	—	—	—	—	—	—	1	—	—	—	—	—
	14		—	—	—	—	—	—	—	—	—	—	—	—	—	—	—	—	—	—	—	—	—	—	—	—	—	—	—	—
	16		—	—	—	—	—	—	—	—	—	—	—	—	—	—	—	—	—	—	—	—	—	—	—	1	—	—	—	—
	18		—	—	—	—	—	—	—	—	—	—	—	—	—	—	—	—	—	—	—	—	—	—	—	—	—	1	—	—
	Total number of stars with N_h rays		18	31	36	16	11	23	19	20	11	8	9	8	8	4	7	2	3	2	4	—	4	1	2	1	1	2	—	1
Copper	1		13	13	6	8	3	—	—	1	—	—	—	—	—	—	—	—	—	—	—	—	—	—	—	—	—	—	—
	2		2	7	3	2	2	—	—	—	—	1	—	—	1	—	—	—	—	—	—	—	—	—	—	—	—	—	—
	3		1	3	4	—	1	1	—	—		—	—	—	—	—	—	—	—	—	—	—	—	—	—	—	—	—	—
	4		—	—	—	1	—	1	—			—	—	—	—	—	—	—	—	1	—	—	—	—	—	—	—	—	—
	7		—	—	—	—	—	—	—	—	—	—	—	—	—	—	—	—	—	—	—	1	—	—	—	—	—	—	—	—
	18		—	—	—	—	—	—	—	—	—	—	—	—	—	—	—	—	—	—	—	—	—	—	—	—	—	1	—	—
	Total number of stars with N_h rays	1	42	37	18	13	6	2	—	1	—	1	—	—	1	—	—	—	—	1	—	1	—	—	—	—	—	1	—
Aluminum	1		7	9	5	2	3	1	—	—	—	—	—																
	2		1	6	3	1	3	1	—	—	1	—	—																
	3		—	—	—	1	1	1	1	1	—	1	—																
	4		—	1	1	2	—	1	—	—	—	—	—																
	5		—	—	—	—	1	1	—	—	—	—	—																
	6		—	—	—	—	—	1	—	—	—	—	—																
	7		—	—	—	—	—	—	—	—	—	—	1																
	Total number of stars with N_h rays	1	22	26	12	8	8	6	2	1	1	1	1																

star formation cross section. Consequently,

$$\frac{\sigma_W}{\sigma_{Cu}} = \frac{N_W \rho_{Cu} A_W}{N_{Cu} \rho_W A_{Cu}},$$

where ρ is the density of the material and A is its atomic weight.

The experimental data yield a value of about 3 for σ_W/σ_{Cu}, while the ratio of the geometric cross sections $(\sigma_W/\sigma_{Cu})_{geom} \simeq 2$. Whence it follows, if we set $\sigma_W \approx \sigma_{geom}$, that $\sigma_{Cu} \simeq 0.75\,\sigma_{geom}$.

The experimental data obtained as a result of a series of sonde balloon flights into the stratosphere are presented in Table 2. The tracks in 466 stars formed in tungsten, copper and aluminum were analyzed and classified as black, grey or "fine". The distribution of stars with different numbers of grey tracks (N_g) as a function of the total number of rays (N_h) is given in Table 2. Comparison of the distribution of the stars formed in the different elements at 4375 meters (Table 1) with the corresponding distribution of stars in the same elements in the stratosphere (Table 2) leads us to conclude that the number of fast protons emitted incident to star formation will increase with increasing atomic number of the struck nucleus and with the energy of the striking particle. This again is evidence that cascade processes occur in nuclei, particularly in heavy nuclei at stratospheric altitudes.

Among the nuclear events we found a number of complete disintegrations of copper and aluminum nuclei into the component nucleons (for example the 32 ray star in Cu); no cases of complete disintegration were observed in tungsten.

We feel it would be premature to give here the results relative to the "fine" tracks of stars formed in the investigated elements inasmuch as the statistical data so far available are insufficient for drawing definitive conclusions. However, it may tentatively be noted that the average multiplicity $(\bar{n}_s)$ in the interval $10 > n_s \geqslant 6$ is apparently independent of the atomic number of the disintegrated nucleus while the frequency with which stars with $6 \geqslant n_s \geqslant 2$ appear is markedly dependent on the atomic number. These data pertain to the experiments in the stratosphere. So far the above deductions do not follow from the results obtained at 4375 meters.

In addition to analyzing the character of the nuclear disintegrations, we investigated in detail the nature of the particles (protons, α-particles, etc.) emitted by the various nuclei when disintegrated by cosmic ray particles. Analyses of the tracks were carried out by different methods, in particular by the method of measuring the depth of curvature, which does not depend on the degree of regression (some degree of regression is unavoidable in exposing nuclear emulsions under mountain conditions).

In conclusion the author wishes to thank S.N.Vernov, N.A.Dobrotin and N.L. Grigorov for their interest in the investigation and M.G.Antonova and T.P. Diogenova for their expert assistance in processing the films and plates.

Physical-Technical Institute of the
Academy of Sciences of the Kazakh SSR

References

1. Zh.S.Takibaev, Zhur. eksp. i teor. fiz., 24, 229, 233 (1953).
2. Zh.S.Takibaev, Vestnik (Review) AN Kazakh SSR. 9, 101 (1954); Zh.S.Takibaev & V.N.Shakhvorostov, Zhur. eksp. i teor. fiz., 26, 507 (1954).

* * * * * * *

INTERACTION OF 10^{10}–10^{11} EV COSMIC RAY PARTICLES WITH LIGHT NUCLEI ACCORDING TO MEASUREMENTS AT AN ALTITUDE OF ABOUT 4 KM

- N.G.Birger, V.V.Guseva, G.B.Zhdanov, S.A.Slavatinski & G.M.Stashkov

In the fall and winter of 1953–54, working over a period of 2000 hours, we obtained about 5000 photographs of a Wilson cloud chamber operated in a magnetic field. The work was done in our laboratory at 3860 meters elevation. The cloud chamber contained a beryllium plate having a thickness of 9.8 g/cm^2. The chamber was controlled by a system of counters, designed to separate electronic-nuclear showers produced either in the lead covering the entire apparatus or in the beryllium plate inside the chamber. Formation of electronic-nuclear showers in the plate was observed on 50 photographs. The steric angles and the momenta of the shower particles were carefully measured in processing these photographs. The greatest measured momentum was $3.5 \cdot 10^9$ ev/c. About 60% of the observed showers consisted of four or more charged particles. The averaged angular distribution of the shower particles in the center of mass system of the two colliding nucleons (it is assumed that the observed events were all nucleon-nucleon interactions) is symmetrical and nearly isotropic.

In the $5 \cdot 10^8$–$3 \cdot 10^9$ ev/c momentum interval we also obtained the distribution in momentum of the shower particles (mesons), formed in light matter.

* * * * * * *

THE AIR-LEAD TRANSITION CURVE AND ANGULAR DISTRIBUTION OF SINGLE COSMIC RAY PARTICLES

- A.P.Zhdanov & P.I.Fedotov

In order to determine the shape of the air-lead transition curve and the angular distribution of single cosmic ray particles, we carried out an experiment in which K-2521 photographic plates exposed to cosmic radiation at an altitude of 5000 meters were examined. In all, about 5000 tracks were measured and analyzed. The results of the analyses may be summarized as follows:

1) There is a definite transition effect evidenced in the transition of particles from air to lead; the magnitude of the transition effect (under 1.4 cm lead) attains 30%.

2) The value of the mean free path for primaries in lead as determined from the air-lead transition curve is 282 ± 20 g/cm^2.

3) The mean free path in lead for secondary component particles as deduced from the same transition curve is 13.3 ± 3 g/cm^2.

4) A qualitative examination of the interactions of the different particles comprising the primary component with lead nuclei shows that the observed transition effect may be due primarily to protons and charged pi mesons.

5) Comparison of the angular distributions of single particles under lead plates of different thicknesses indicates that the increase in the number of particles under lead plates is attributable to "knock-on" secondary particles.

6) The angular distribution of singular particles is distinctly anisotropic.

* * * * * * *

INVESTIGATION OF PROTON-PROTON INTERACTION AT HIGH ENERGIES

– M. G. Meshcheriakov, N. P. Bogachev and B. S. Neganov

1. Introduction

In this article we shall report on some of the results of our investigation of collisions of protons with protons in the 460-660 Mev region, in which p-p interactions include elastic scattering and formation of mesons by the following reactions:

$$\text{I. } p + p \rightarrow d + \pi^+,$$
$$\text{II. } p + p \rightarrow p + n + \pi^+,$$
$$\text{III. } p + p \rightarrow p + p + \pi^0.$$

In addition to these reactions, in single p-p collisions at energies from 600 Mev the generation of two pi mesons is also energetically possible.

The experiments were carried out in 1951-1954 on the synchrocyclotron of the Institute of Nuclear Problems of the USSR Academy of Sciences.[1-5]

2. Experimental Procedure

Proton beam

The non-polarized beam of protons brought out from the synchrocyclotron was collimated to the requisite dimensions in passing through the aperture in a 3.6 meter long steel block built into the four meter thick concrete shielding wall. In most experiments the diameter of the beam at the target was approximately 2 cm. The energy of the primary protons was determined by measuring the Čerenkov radiation angle: in the 1951-52 experiments the energy was 460.0 ± 0.9 Mev, while in the 1953-54 experiments the energy was 657 ± 2 Mev. The straggling in momentum did not exceed 1%. The density of the proton flux in the beam was 10^6 protons cm^{-2} sec^{-1} (on the average). The intensity of the beam was monitored by means of an argon-filled ionization chamber, which was calibrated by determining the absolute value of the charge collected by a large proton trap. Appropriate account was taken of the loss of charge due to leakage of secondary particles (the correction amounted to about 2%). Analysis of proton tracks in emulsions sensitive to particles of minimum ionization made it possible to evaluate the current rise in the chamber, due to entry into the beam of particles undergoing multiple scattering in the collimator walls. The corresponding correction was less than 1%.

Method of conjugate telescopes

Elastic p-p scattering and reaction (I) were separated from the other processes by recording both secondary particles by means of conjugate telescopes, each of which consisted of three scintillation counters (Fig. 1). The photomultipliers with diphenyl acetylene or anthracene crystals were located in a steel box to shield them from the fringe magnetic field of the synchrocyclotron. The secondary particles were recorded in the solid angle subtended by the face of

the first (nearest the target) crystal in the defining telescope. In both telescopes the distance between the first and second crystals was 6 cm, while the distance between the second and third was 18 cm. In order to minimize the effect of multiple scattering, the crystals, which usually had a thickness of about 1 cm, were selected so that their dimensions increased with the distance from the telescope window. Special care was taken to select crystals having a uniform sensitivity to the detected particles over the entire surface.

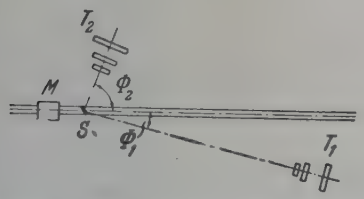

Fig. 1. Diagram of the experiment: T_1) defining telescope; T_2) conjugate telescope; M) monitor; S) target.

The electronic circuits permitted simultaneous recording of both coincidences from the telescopes and triple or double (in any desired combination) of the individual telescope counters. The resolving time of the triple coincidence circuit of each telescope was $3 \cdot 10^{-8}$ sec; the resolving time of the circuit handling the pulse coincidences from the two telescopes was $5 \cdot 10^{-8}$ sec. The curve of the number of triple coincidences vs the voltage on the photo multipliers had a plateau of approximately 300 volts. In the region of the plateau the proton recording efficiency of the three-counter telescope remained constant at 0.94 ± 0.02 in the energy interval from 50 to 615 Mev. The telescopes were mounted on a goniometer stand by means of which the angle between the optical axes of the telescopes and the beam could be measured to within 0.1°. In adjusting the equipment particular attention was given to insuring coplanarity of the optical axes of the telescopes and the axis of the proton beam.

The particles were identified by measuring their ranges in absorbers mounted in the telescopes in front of the last crystals or from the height of the counter output pulses. The nature of the nuclear process, culminating in the ejection of two charged particles, was established from the angles of scattering of the secondary particles; in practice, this amounts to determining the variation of the coincidence rate with the angle between the telescopes. Fig. 2 shows the results of such measurements for p-p scattering at 460 Mev obtained in the case when one of the telescopes was set at an angle of 42° relative to the beam, while the other was swung from 36 to 48° to the other side of the beam. Calculations show that under the conditions of this experiment the deviation due to relativism from the 90° angle between the paths of a scattered proton and a recoil proton should amount to 6.26°; the experimentally determined value was 6.2° ± 0.2°. This quantitative agreement indicates that at 460 Mev proton-proton collisions, not involving the formation of a meson, are rigorously elastic. Observations at 657 Mev lead to an analogous conclusion.

As may be seen from Fig. 2, the coincidence count dropped to zero at angles above 86°. This indicated that there were virtually no low-energy protons in the primary beam. The coincidences vanished completely when an absorber, completely stopping all elastically scattered protons, was installed in one of the telescopes. When the paraffin target was replaced by a graphite one the coincidence rate fell off by a factor of about 40.

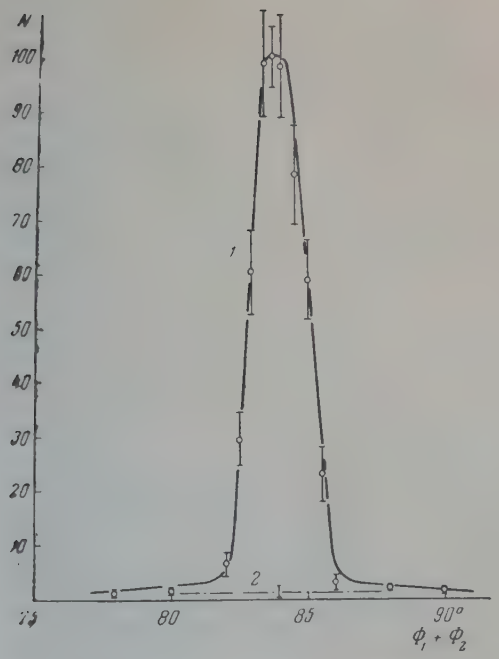

Fig. 2. Variation of number N of coincidences with scattering angle $\Phi_1 + \Phi_2$: 1) effect from hydrogen; 2) background from C.

Target

The yield of elastically scattered protons and positive pi mesons in the p-p scattering experiments was determined from the difference in the number of counts obtained with a paraffin ($CH_{2.083}$) target and with a graphite target, both targets containing an equal number of carbon atoms per unit area. The surface density of the targets used in most cases lay between 500 and 900 mg/cm^2. The differential cross section values obtained with targets of different surface densities agree within the limits of the experimental error.

3. Elastic Proton-Proton Scattering

Proton-proton scattering at 460 Mev

In the $55 \leqslant \theta \leqslant 90^\circ$ (center of mass) angular interval, the elastic p-p scattering was observed by the method of conjugate telescopes. In addition, the scattering of protons in the $20 \leqslant \theta \leqslant 90^\circ$ interval was also observed by a single telescope. Appropriate corrections were introduced to allow for accidental coincidences and misses, as well as absorption and multiple scattering of the protons in the target and scintillation counters. The effect due to the presence of positive pi mesons among the secondary protons was subtracted from the results obtained by means of the single telescope. We also carried out control experiments to establish that the passage of an elastically scattered proton through the telescope defining the solid angle ω, inside which the p-p scattering was observed, is always accompanied by the passage of a recoil proton through the conjugate telescope. Under typical experimental conditions $\omega = (1.01\ 0.01) \cdot 10^{-3}$ sterad.

The differential cross section $\frac{d\sigma}{d\omega}$ for p-p scattering at the given angle θ (c.m. system) was determined according to the relationship

$$\frac{d\sigma}{d\omega} = \frac{[1 + (E/2Mc^2)\sin^2\Phi]^2}{1 + E/2Mc^2} \cdot \frac{1}{4\cos\Phi} \cdot \frac{Q(\Phi)}{\eta(\Phi)} \cdot \frac{1}{Nn\omega}, \qquad (1)$$

where E is the kinetic energy of the proton, Mc^2 is the proton rest energy, N is the number of hydrogen atoms per unit area of the target in the direction of the beam, n is the number of protons striking the target per unit time and $Q(\Phi)$ and $\eta(\Phi)$ are, respectively, the counting rate and the recording efficiency for protons scattered within the solid angle ω at the angle with the direction of the

primary beam. The angle of scattering θ (c.m. system) is related to the corresponding scattering angle Φ (laboratory system) by the relationship

$$\operatorname{tg}\frac{\theta}{2} = (1 + E/2Mc^2)^{\frac{1}{2}} \operatorname{tg}\Phi. \qquad (2)$$

The resultant values of the differential scattering cross section are shown in Fig. 3: points 1 represent results obtained with the single telescope; points 2 the results obtained by the method of conjugate telescopes. The indicated uncertainties are root mean square errors due only to statistical straggling of the counts. An evaluation of the other sources of error indicates that the overall uncertainty in the absolute values of the cross section amounts to about 10%.

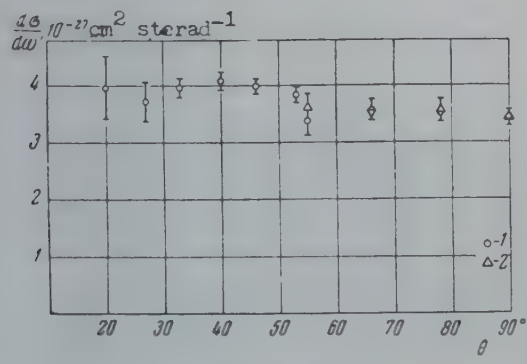

Fig. 3. Differential p-p scattering cross sections at 460 Mev: 1) single telescope measurements, 2) method of conjugate telescopes.

As may be seen from Fig. 3, the differential cross section at 460 Mev increases slowly with decreasing angle. A further indication that p-p scattering is not entirely isotropic was given by experiments in which the relative yield of protons scattered at 90 and 30° was measured by means of a single telescope. It was found that the ratio

$$\left(\frac{d\sigma}{d\omega}\right)_{30^\circ} \Big/ \left(\frac{d\sigma}{d\omega}\right)_{90^\circ} = 1.14 \pm 0.06.*$$

For 90° $\frac{d\sigma}{d\omega} = (3.50 \pm 0.20) \cdot 10^{-27}$ cm² sterad⁻¹.

Linear extrapolation of the differential cross section values into the region of low angles leads to a value of $(22 \pm 2) \cdot 10^{-27}$ cm² for the total cross section for elastic p-p scattering.

Proton-proton scattering at 657 Mev

The differential p-p cross section scattering at 657 Mev was measured in an angular range from 30 to 90° by the method of conjugate telescopes. The results, showing the corresponding statistical errors, are shown in Fig. 4 from which it will be seen that at 657 Mev the differential cross section increases rapidly with decreasing angle. The ratio of the differential cross sections at 30 and 90° equals 2.7 ± 0.2. At 90° the value of the differential cross section is $(2.1 \pm 0.2) \cdot 10^{-27}$ cm² sterad⁻¹. The total elastic p-p scattering cross section at 657 Mev, as determined by linear extrapolation of the differential cross section into the region of small angles, equals $(23 \pm 2) \cdot 10^{-27}$ cm².

---

* This result was obtained in 1952.[1] Data on p-p scattering at energies to 340 Mev were available at that time;[6] from these it was apparent that for large angles the scattering is independent of the energy and angle within the limits of the experimental errors (10-15%). Recently, it has been found[7,8] that at 435 and and 428 Mev the scattering cross section increases (about 20%) with decreasing angle.

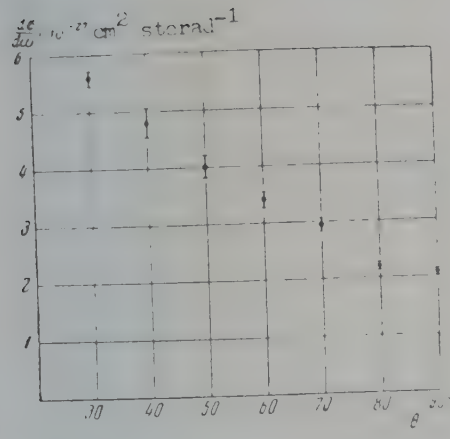

Fig. 4. Differential p-p scattering cross section at 657 Mev, as measured by the method of conjugate telescopes.

Determination of differential p-p scattering cross sections in the 460-657 Mev region

From results of the two above-described experiments, we can conclude that as the proton energy is increased from 460 to 657 Mev, the p-p scattering becomes increasingly anisotropic. The next stage in determining the attributes of p-p scattering in the 460-657 Mev region consisted of experiments in which the energy dependence of the differential cross sections at 30 and 90° (c.m. system) was determined by the method of conjugate telescopes. To obtain protons of the requisite intermediate energies suitable paraffin absorbers were set in the path of the beam in front of the collimator. The differential cross sections measurements were carried out under rigorously identical conditions over the entire energy range, except that it was necessary to adjust the angles Φ_1 and Φ_2 of the telescopes to either side of the beam as the primary energy proton was increased. These angles were found from the relation $\mathrm{ctg}\Phi_1 \cdot \mathrm{ctg}\Phi_2 = 1 + E/2Mc^2$. The probable statistical error of measurement at 90° was less than 3%. Analysis of all the other sources of error indicates that the absolute values of the differential cross sections were determined within about 5% at 90° and about 8% at 30°.

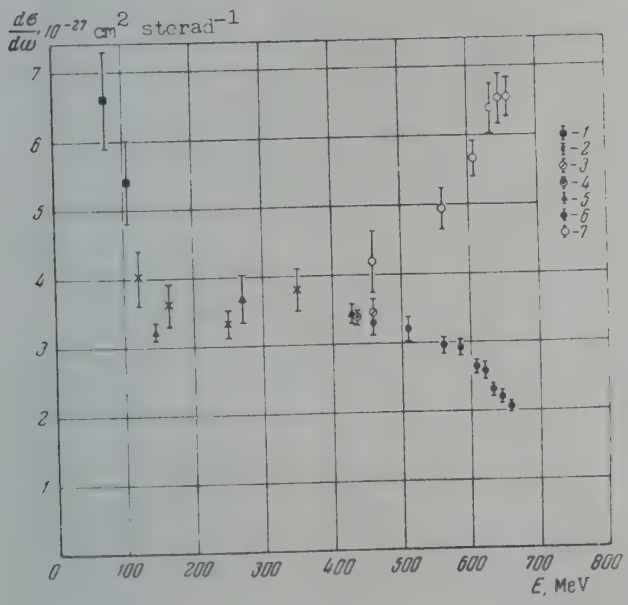

Fig. 5. Energy dependence of the differential scattering cross section at 30 and 90°. All measurements, except 7 were made at 90°; 7, at 30°. 1) Data from Ref. 9; 2) Ref. 6; 3) Ref. 1; 4) Ref. 7; 5) Ref. 10; 6 and 7) Ref. 4.

The results of these experiments are shown in Fig. 5, together with the results obtained in other investigations (Refs. 1, 6, 7, 9, and 10) for a scattering angle of 90° and energies in the 75-437 Mev interval. It will be seen that the differential cross section value at 90° remains nearly constant from 140 to 460 Mev and then begins to fall off slowly as the energy is increased to 560 Mev. As the energy is further increased the decrease becomes more rapid. Thus, going from 610 to 657 Mev, the differential cross section at 90° goes down from $(2.63 \pm 0.10) \cdot 10^{-27}$ to $(2.05 \pm 0.07) \cdot 10^{-27}$ cm^2 sterad^{-1}. As for $\left(\frac{d\sigma}{d\omega}\right)_{30°}$, it increases about 1.6 times

as the energy is increased from 460 to 657 Mev. The values of the ratio of the differential cross sections at 30 and 90°, which are listed in Table 1, also indicate that the departure of p-p scattering from isotropism is most rapid in the 560-657 Mev interval.

Table 1

Values of the ratio $\left(\frac{d\sigma}{d\omega}\right)_{30°} / \left(\frac{d\sigma}{d\omega}\right)_{90°}$ for p-p scattering in the 460-657 Mev interval

E, MeV.....	460	562	610	634	645	657
$\left(\frac{d\sigma}{d\omega}\right)_{30°} / \left(\frac{d\sigma}{d\omega}\right)_{90°}$	1,26±0,15	1,67±0,15	2,16±0,15	2,77±0,20	2,97±0,25	3,20±0,20

Discussion of experimental results on p-p scattering

In the case of collisions of identical nucleons only the $^1S_0$ and $^3P_0$ states can give isotropic scattering. The maximum contribution of these states to the cross section is $2\lambda^2$ cm^2 sterad^{-1} (λ is the nucleon wavelength in the c.m. system). At 460 Mev this equals about $3.5 \cdot 10^{-27}$ cm^2 sterad^{-1}. Thus, the experimental value of the differential cross section for p-p scattering through large angles can be qualitatively explained if we assume that the scattering is due primarily to interaction in the $^1S_0$ and $^3P_0$ states with the phase shift of the corresponding waves differing little from 90°. The assumption, made by some investigators that the phase shift of the $^3P_0$ wave differs appreciably from the phase shift of the $^3P_1$ and $^3P_2$ waves is equivalent to the assumption of strong spin-orbit coupling. The purpose of our further analysis of the attributes of p-p interaction is qualitative interpretation of such effects as the deviation from isotropism of the scattering observed in the present experiments and the polarization of protons in p-p collisions, reported by De Carvallo et al.[11] Both these effects definitely indicate that in the energy region in question other states in addition to the $^1S_0$ and $^3P_0$ participate in the p-p scattering and contribute to the asymmetry of the cross section.

The results obtained at 657 Mev indicate that the differential cross section is strongly dependent on the scattering angle. Obviously in this case in addition to states making an isotropic contribution to the cross section, a significant role is played by other states characterized by total angular momentum differing from zero. A noteworthy feature of the effect under consideration is that in going from 460 to 657 Mev the attenuation of scattering at large angles is roughly compensated for by the increase in scattering through angles under 50°, so that the total elastic p-p scattering cross section remains almost constant (within the limits of the experimental error) at $23 \cdot 10^{-27}$ cm^2.

In view of the fact that inelastic processes are always accompanied by elastic scattering forward one might attempt to explain the sharp increase in the frequency of p-p scattering to small angles by the great increase in the cross sections for reactions (I, II and III) in the given energy region. Actually, as will be shown below, the contribution of inelastic processes to the total p-p interaction cross section increases from about 18% at 460 Mev to about 45% at 657 Mev (see Table 2).

We shall be able to judge of the validity of a similar explanation for the fact that the rapid increase in the cross section for meson formation of processes is associated with the appearance of strong angular dependence of p-p scattering only when a theory, describing elastic nucleon-nucleon scattering and the production of mesons in nucleonic collisions from a unified viewpoint, is developed. Here we can only note that repeated attempts to describe interactions between nucleons at high energies with the aid of different potentials have so far been unsuccessful.

It is worth emphasizing that the change in the character of p-p scattering is most pronounced precisely in the 560-660 Mev interval of incident proton energies, i.e., at energies on the order of 260-300 Mev in the c.m. system. It is known that at these energies the cross sections for scattering of pi mesons by nucleons and for photomeson production increase rapidly and pass through a resonance type maximum. This similarity of all three processes is undoubtedly a reflection of properties common to the interaction of nucleon and meson fields.

One of the possible explanations of the non-monotonic variation of the scattering and photomeson production cross sections is based on the assumption of the existence of an excited nucleon state characterized by an isobaric spin 3/2, ordinary spin 3/2 and an excitation energy of 300 Mev. In the light of this assumption it is natural to think of a nucleon-nucleon collision as a "two-stage" process: first the particles are excited and then the excited nucleons decay with the emission of a meson. In conformity with this concept the rapid change in the properties of p-p scattering in the 560-660 Mev region might be interpreted as an indication that in this energy interval p-p interaction begins to proceed without intermediate formation of an excited proton state.

4. Production of Mesons in p-p Collisions

The $p + p \rightarrow d + \pi^+$ reaction at 460 Mev

Reaction (I) was identified in our experiments by recording the coincidences between pi mesons and deuterons by means of the conjugate telescopes. The yield of pi mesons was measured in the interval of angles from 17 to 55° (30 to 90° in the c.m. system), measured from the direction of the narrowly collimated proton beam. Under the conditions of the experiment the height of the pulses, due to deuterons, was about twice the height of the pulses produced by the primary protons. In order to reduce the accidental coincidences background, due to the heavy loading of the deuteron-detecting telescope by protons scattered from carbon nuclei in the target, the deuteron pulses were separated from the pulses produced by elastically scattered protons by means of a suitable discriminator in the deuteron telescope. In the course of control experiments it was found 1) that the presence of an absorber stopping all deuterons in the deuteron telescope always caused the effect from reaction (I) to vanish and 2) that under conditions where the telescopes were set relative to each other at angles not corresponding to the kinetics of reaction (I) no coincidences between pi mesons and deuterons were recorded. In the same series of experiments it was established that the observed effect receives no contribution from reaction (II). Taking into account the efficiency of the electronic circuits in recording triple coincidences between the scintillation counters in

the telescopes and double coincidences between the telescopes, the absorption and scattering of pi mesons and deuterons in the target and the crystals, as well as the decay of pi mesons in flight, we estimate the efficiency of recording cases of reaction (I) in the present experiments to be 0.73 ± 0.04.

In converting from the differential cross section $\left(\frac{d\sigma}{d\omega}\right)_{\Phi_\pi}$ for reaction (I) measured at angle Φ_π in the laboratory system to the corresponding differential cross section $\left(\frac{d\sigma}{d\omega}\right)_{\theta_\pi}$ in the center of mass system we used the following equation

$$\left(\frac{d\sigma}{d\omega}\right)_{\theta_\pi} = \left[\frac{1-\beta_c^2\cos^2\Phi_\pi}{\sqrt{1-\beta_c^2}\left(\gamma\cos\Phi_\pi + \sqrt{1-\frac{\gamma^2-\beta_c^2}{1-\beta_c^2}\sin^2\Phi_\pi}\right)}\right]^2 \times \sqrt{1-\frac{\gamma^2-\beta_c^2}{1-\beta_c^2}\sin^2\Phi_\pi}\left(\frac{d\sigma}{d\omega}\right)_{\Phi_\pi},$$

where $\gamma = \frac{\beta_c}{\beta'_\pi}$, β_c is the velocity of the center of mass system relative to the laboratory system and β'_π is the velocity of the meson in the center of mass system. The angles Φ_π and θ_π are related by the expression

$$\operatorname{tg}\Phi_\pi = \sqrt{1-\beta_c^2}\cdot\frac{\sin\theta_\pi}{\cos\theta_\pi + \beta_c/\beta'_\pi}.$$

The results of determination of the angular distribution of pi mesons from reaction (I) at 460 Mev are shown in Fig. 6. The variation of the differential cross section for reaction (I) with the angle of ejection of the pi meson in the c.m. system is described by

$$\frac{d\sigma}{d\omega} = (2{,}13 \pm 0{,}20)\,[(0{,}24 \pm 0{,}03) + \cos^2\theta]\cdot 10^{-28}\ \text{cm}^2\ \text{sterad}^{-1}$$

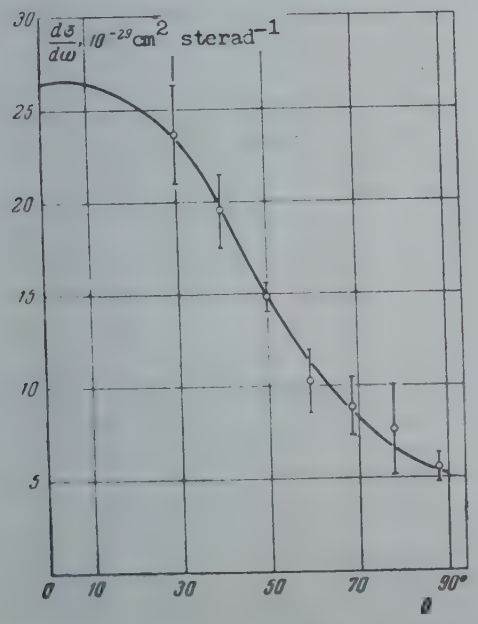

Fig. 6. Angular distribution of π^+ mesons from the p + p → d + π^+ reaction at 460 Mev.

The numerical factors in this expression were determined by the method of least squares. Assuming that the angular distribution of pi mesons is described by this expression in the region of small angles as well, and integrating $d\sigma/d\omega$ over the solid angle, we obtain for total cross section for reaction (I): σ(I) = (15.4 ± 1.6)·10^{-28} cm^2. The ratio of the differential cross sections at 0 and 90°

$$\left(\frac{d\sigma}{d\omega}\right)_{0^\circ} \Big/ \left(\frac{d\sigma}{d\omega}\right)_{90^\circ} = 5{,}1 \pm 0{,}8.$$

In the case when the pseudoscalar π^+ mesons are created only in the s- and p-states, transitions to the $^3S_1$ state of the final n-p system are allowed from the $^1S_0$, $^3P_1$ and $^1D_2$ states of the initial p-p system; the $^1S_0 \longrightarrow {}^3S_1$ and $^3P_1 \longrightarrow {}^3S_1$ transitions lead to an isotropic meson distribution while the $^1D_2 \longrightarrow {}^3S_1$ leads

to a distribution of the form $1/3 + \cos^2\theta$. Inasmuch as near the threshold of meson production the amplitudes of the $^1S_0 \rightarrow {}^3S_1$ and $^1D_2 \rightarrow {}^3S_1$ transitions (corresponding to the emission of mesons in the p-state) must be proportional to the momentum of the meson, while the amplitude of the $^3P_1 \rightarrow {}^3S_1$ transition (associated with emission of mesons in the s-state) is constant, we can expect the emission of mesons in the s-state to make a noticeable contribution to the cross section for reaction (I) only at relatively low meson energies.

The angular distribution found in the present investigation corresponds to the production of mesons primarily (if not exclusively) in the p-state. Even if there is some formation of mesons in the d-state at 460 Mev, the contribution to the cross section of the corresponding transitions certainly does not exceed 10%. The departure of the experimentally determined angular distribution from $1/3 + \cos^2\theta$ is apparently due to interference of transitions from the $^1S_0$ and $^1D_2$ states of the p-p system. In this case, as calculations given in Refs. 12 and 13 show, the angular distribution of mesons can be represented as

$$F(\theta) \sim \frac{1 + \frac{\varepsilon^2}{2} + \sqrt{2}\,\varepsilon\cos\sigma}{3\left(\frac{\varepsilon^2}{2} - \sqrt{2}\,\varepsilon\cos\sigma\right)} + \cos^2\theta,$$

where $\eta = \varepsilon e^{i\sigma}$ is a parameter entering into the linear combination of the spherical vector functions, corresponding to the $^1S_0 \rightarrow {}^3S_1$ and $^1D_2 \rightarrow {}^3S_1$ transitions in the wave function of the final state. The relative contribution of these transitions to the partial cross section for the production of mesons in the p-state depends upon the value of the parameter ε^2. In the general case it is impossible to establish unambiguously the ratio between the intensities of the $^1S_0 \rightarrow {}^3S_1$ and $^1D_2 \rightarrow {}^3S_1$ transitions from the shape of the angular distribution without recourse to additional experimental data: for example, information on the polarization of deuterons in reaction (I). For the angular distribution found in the present experiment a possible, but not unique, choice of ε and σ is one where $7 < \varepsilon^2 < 280$ when the phase σ varies from 0 to 72° (or from 180 to 108°). If we accept that this selection of the values of ε and σ is correct, we can conclude that at 460 Mev the production of mesons in reaction (I) is due mainly to the $^1D_2 \rightarrow {}^3S_1$ transition, corresponding to non-central interaction in the p-p system. This would mean that mesons are produced in reaction (I) and absorbed in the reaction

$$\text{IV. } \pi^+ + d \rightarrow p + p$$

mainly in the state where their orbital momenta are parallel to the spins of the deuterons. Thus the angular distribution of mesons in reaction (I) is consistent with the hypothesis that meson-nucleon interaction is strong for the states with an angular momentum of 3/2.

The $p + p \rightarrow d + \pi^+$ in the 510-657 Mev proton energy region

The procedure followed in observing reaction (I) in the 510-657 Mev region was the same as in the preceding experiment, except that in this case the telescope for recording deuterons consisted of five scintillation counters; of these the last two, operating in coincidence with each other, were connected in anticoincidence with the three first counters. An absorber thick enough to stop all deuterons, but passing protons elastically scattered in the target

from carbon nuclei, was installed in front of the last two counters. The use of this absorber sharply reduced the accidental coincidences background in registering deuterons scattered at small angles to the primary beam without sacrifice of the efficiency of recording mesons from reaction (I). An experimentally determined correction, taking into account the contribution of reaction (II) to the number of pi meson-deuteron coincidences, was introduced in processing the experimental results. This correction is essential because in this energy region reaction (II) is appreciably more intense than reaction (I).

The experimentally determined distribution of pi mesons from reaction (I) at 657 Mev is shown in Fig. 7. The variation of the differential cross section for reaction (I) with the angle of ejection of the meson is characterized by

$$\frac{d\sigma}{d\omega} = (4{,}35 \pm 0{,}25)\,[(0{,}23 \pm 0{,}03) + \cos^2\theta] \cdot 10^{-28} \text{ см}^2 \text{ sterad}^{-1}$$

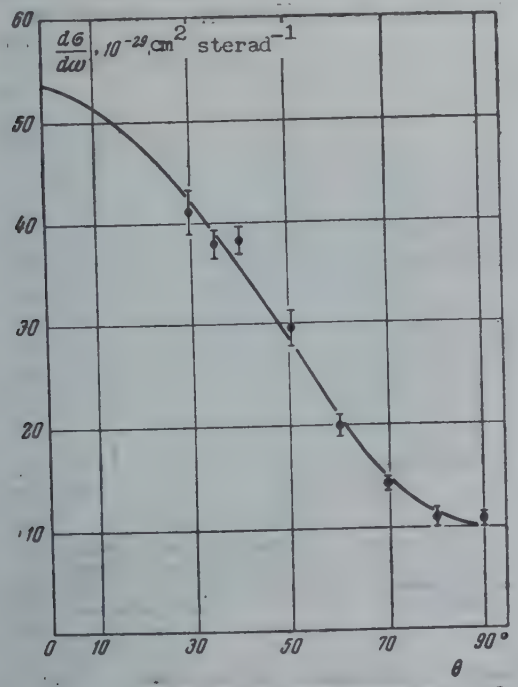

Fig. 7. Angular distribution of π^+ mesons from the $p + p \rightarrow d + \pi^+$ reaction at 657 Mev.

Extrapolation into the region of small angles and integration over the solid angle yield the following value for the total cross section for reaction (I):

$$\sigma(\text{I}) = (3.1 \pm 0.2) \cdot 10^{-27} \text{ cm}^2.$$

Taking advantage of the fact that the angular distribution of mesons from reaction (I) in the region of large angles increases little as the proton energy is increased from 460 to 657 Mev (the corresponding increase in the pi meson energy in the c.m. system is from 72 to 150 Mev) we were able to determine the total cross section for intermediate energies from the values of the differential cross section found for a given angle. The most convenient values for these calculations proved to be the results obtained for mesons scattered at 50° in the c.m. system.

The values of σ(I) determined in this manner together with the results of the preceding experiment and the values obtained by other investigators[14-18] at lower energies are shown as a function of the pi meson energy in Fig. 8.

As may be seen from Fig. 8, in the interval where the data overlap our results are in satisfactory agreement with those of other investigators. It should be noted that the total cross sections for reaction (I) at 25, 40, 53, 76 and 94 Mev were found from the reverse reaction (IV) with the aid of the principle of detailed equilibrium, on the assumption that the spin of the π^+ meson is zero.

We found the excitation curve for reaction (IV) by means of the relationship $\sigma(\text{IV}) = \frac{2}{3}\frac{k^2}{q^2}\sigma(\text{I})$, where q is the momentum of the meson and k the momentum of the proton in the c.m. system. It turned out

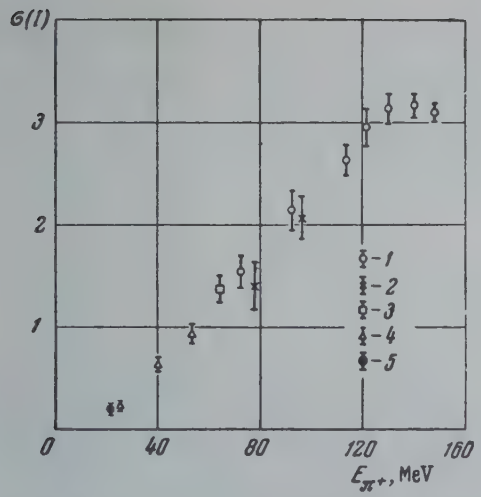

Fig. 8. Variation of the total cross section for the p + p $\rightarrow$ d + π^+ reaction with the π^+ energy according to the data of different investigators: 1) Refs. 2 and 5; 2) Ref. 14; 3) Ref. 15; 4) Ref. 16; 5) averaged results from Refs. 17 and 18.

that the cross section for reaction (IV) passes through a maximum at a pi-meson energy of about 130 Mev (c.m.). The cross sections for meson-nucleon scattering and photomeson production reach maximum values at about the same value of the pi-meson energy. The fact that the cross section for reaction (I), like the cross sections for meson-nucleon scattering and photomeson production processes, varies non-monotonically with the energy suggests that all three processes are due to the same meson-nucleon interaction mechanism, a mechanism possibly connected with the existence of an excited state of the nucleon.

At 657 Mev (just as at 460 Mev) the angular distribution corresponds to emission of mesons primarily in the p-state. This result taken in conjunction with the fact that meson-nucleon interaction (as apparently follows from experiments on meson scatterings in hydrogen) is strongest for states having an isobaric spin of 3/2 and an angular momentum of 3/2 leads us to conclude that in the energy interval under consideration the principal contribution to the non-monotonically varying cross section for reaction (I) is made by the $^1D_2$ state of the p-p system.

Further deductions regarding the properties of reaction (I) must await measurements of the total cross section at even higher energies and elucidation of the angular distribution of mesons in the region of angles under 30° where the effect due to generation of mesons in the d-state should become noticeable.

Remarks concerning the relationship between elastic scattering and meson production processes in p-p encounters

The data regarding the total cross sections for elastic p-p scattering and meson formation in reaction (I) at 460 and 657 Mev, obtained in our experiments, are summarized in Table 2. The total cross sections for p-p interaction at the same energies were evaluated by interpolation of the data obtained at proton energies of 410, 535, 615, and 830 Mev by Shapiro et al.[19] The total cross sections for reaction (III) were measured by Kozodaev et al[20] at 480 and 670 Mev. In converting from these energies to 460 and 657 Mev, we assumed that in the vicinity of 500 Mev $\sigma(\text{III}) \sim q^6$, while in the 600-680 Mev interval $\sigma(\text{III}) \sim q^{4.5}$ (here q is the maximum momentum of the pi meson in the c.m. system).

Outstanding features of proton-proton collision in the energy interval in question are the stable value of the elastic scattering cross section and the rapid rise with energy of the cross section for meson production processes. Because of this at 657 Mev the contribution of inelastic processes to the total p-p interaction cross section proves to be only slightly smaller than the contribution due to elastic scattering. At this energy reaction (I) makes a

Table 2

Total cross sections for p-p interaction and meson production processes in p-p collisions (in 10^{-27} cm^2)

Energy Mev	Total p-p interaction	Elastic p-p interaction	Inelastic processes	$p+p \to d+\pi^+$	$p+p \to p+p+\pi^0$	$p+p \to p+n+\pi^+$
460	28±2	22±2	~6	1,5±0,2	0,4±0,2	~ 4
657	41±2	23±2	~18	3,1±0,2	3,4±0,7	~11,5

relatively small contribution to the total pi-meson production cross section. The rapid increase in this cross section for reaction (II) with energy may be due both to the increase in the intensity of the $^1D_2 \to {}^3S_1$ and $^1S_0 \to {}^3S_1$ transitions, proceeding in this case without intermediate formation of a deuteron, and to the augmented importance of other transitions, primarily transitions from odd triplet states of the p-p system. In this connection it should be noted that the considerable departure from isotropism of p-p scattering as the energy is increased from 460 to 657 Mev also points to the appearance in p-p interactions of a state with a total angular momentum differing from zero.

The above evaluation of the cross section for reaction (II) at 657 Mev was arrived at on the assumption that the production of two mesons in a single p-p collision makes a relatively small contribution to the total interaction cross section. At present we have no direct data on the magnitude of the cross section for this process near its threshold.

Institute of Nuclear Problems of the
Academy of Sciences of the USSR

Note added in proof. The data obtained in the investigations of elastic p-p scattering of the Refs. 21 and 22, published after presentation of our original report at the Conference, substantiates our results. Some of the values given in Table 2 should be revised in the light of further post-Conference experiments carried out at the Institute of Nuclear Problems. The total p-p interaction cross sections as determined by Dzhelepov, Moskalev and Medved'[23] by direct measurements at 460 and 660 Mev equal 27.6 ± 0.4 and 41.4 ± 0.6 millibarns. By interpolation of the data of these investigators relating to 540 and 580 Mev we find that the total p-p interaction cross section at 560 Mev equals 34 ± 0.5 mb. The total elastic p-p scattering cross sections at 460, 560 and 660 Mev as refined on the basis of measurements of the differential elastic p-p scattering cross section in the region of small angles made by Bogachev are respectively 24.0 ± 0.6, 25.2 ± 0.8 and 24.7 ± 1.0 mb. Evaluations of the total cross sections for the $p + p \to p + n + \pi^+$ reaction at 460, 560 and 660 Mev yield values of 1.7 + 0.8, 4.7 + 1.1 and 10.2 ± 1.4, respectively.

References

1. M.G.Meshcheriakov, N.P.Bogachev, B.S.Neganov et al, IIaP AN SSSR (Institute of Nuclear Problems of the USSR Academy) Report (1952); B.S.Neganov, IIaP AN SSSR Report (1954; Doklady AN SSSR, 99, 955, (1954).
2. M.G.Meshcheriakov, B.S.Neganov, N.P.Bogachev et al, IIaP AN SSSR (1952); Doklady AN SSSR 100, 673 (1955).
3. N.P.Bogachev, I.K.Vzorov, IIaP AN SSSR Report April 1954; Doklady AN SSSR 99, 931 (1954).
4. M.G.Meshcheriakov, B.S.Neganov, L.M.Soroko & I.K.Vzorov, Doklady AN SSSR 99, 959 (1954).
5. M.G.Meshcheriakov, B.S.Neganov,Doklady AN SSSR 100, 677 (1955).
6. O. Chamberlain, E.Segre, & C.Wiegand, Phys.Rev. 83, 923 (1951).
7. W.E.Mott, R.B.Sutton, J.G.Fox & J.A.Kane, Phys. Rev., 90, 712 (1953).
8. A.J.Hartzler, R.T.Siegel, Phys. Rev., 95, 185 (1954).
9. R.Birge, V.Cruse & N.Ramsay, Phys.Rev., 83,274 (1951).
10. J.Marshall, L.Marshall & V.Nedzel, Phys.Rev., 92,834 (1953).
11. H.G.DeCarvallo, E.Heiberg, J.Marshall et al, Phys.Rev., 94, 1796 (1954).
12. K.Watson, C.Richman, Phys. Rev., 83, 1256 (1954).
13. V.B.Berestetski, Doklady AN SSSR, 94, 421 (1954).
14. H.L.Stadler, Phys. Rev., 96, 496 (1954).
15. H.T.Fields, J.G.Fox, J.A.Kane et al, Phys.Rev., 95, 638 (1954).
16. R.Durbin, H.Loar & J.Steinberger, Phys.Rev., 84,581 (1951).
17. D.L.Clark, A.Roberts & R. Wilson, Phys. Rev., 83,649 (1951).
18. W.F.Cartwright, C.Richman, M.N.Whitehead et al, Phys. Rev., 91,677 (1953).
19. A.M.Shapiro, C.P.Leavitt & F.F.Chen, Bull. Am. Phys.Soc., 29; 4, 75 (1954).
20. A.A.Tiapkin, M.S.Kozodaev & Iu.D.Prokoshkin, Doklady AN SSSR 100,689 (1955).
21. Ia.M.Selektor, M.S.Nikitin, E.G.Pogomolov & S.M.Zombkovski, Doklady AN SSSR 99, 967 (1954).
22. L.J.Smith, A.N.McReynolds & G. Snow, Phys.Rev., 97, 1186 (1955).
23. V.P.Dzhelepov, V.I.Moskalev & S.V.Medved', Doklady AN SSSR 104,380 (1955).

SCATTERING OF 460-660 MEV PROTONS BY PROTONS

- S. Ia. Nikitin, Ia. M. Selektor,
E. G. Bogomolov and S. M. Zombkovski

1. Introduction

In recent years there have been a number of investigations of proton-proton scattering in the 100-435 Mev energy interval.[1-8] It has been established that in this interval the scattering is isotropic in the center of mass system and that the absolute value of the scattering cross section is virtually independent of the energy and equals about 3.7 mb/sterad. It must be noted that the absolute value of the cross section found in the latest investigations[1,2] is some 20-30% smaller than the value determined earlier by Oxley and Shamberger[5] and Towler[3] but agrees with the cross section reported by Chamberlain, Segré and Wiegand[4]. This appreciable difference should presumably be attributed to the fact that in the earlier investigations the intensity of the proton beam was determined from the $C^{12}(p, pn)\,C^{11}$ reaction, the cross section for which is not accurately known.

At a proton energy close to 430 Mev there appears to be some departure from isotropism; however, the results of different investigations carried out at this energy are clearly in conflict. Thus, according to Marshall, Marshall and Nedzel[6] at 429 Mev the scattering cross section equals 3.42 mb at 90° (c.m. system) and falls to 2.86 mb at 28° (c.m. system), whereas according to Mott, Sutton, Fox and Kane[7] the scattering cross section at 435 Mev equals 3.39 mb at 90° and increases to 4.49 mb at 25.2° (c.m.). Sutton et al[8] recently published a report on their scattering experiments at 437 Mev: they discovered that at this energy the differential scattering cross section increases somewhat in the region of small angles ($\sigma_{16.6°}/\sigma_{90°} = 1.19$), which is in conflict with the results of Marshall et al[6] and, at best, in poor agreement with the measurements of Mott et al[7] at 435 Mev.

In the present investigation we studied proton-proton scattering at 460, 560 and 660 Mev (the experiments at 460 were carried out in 1952). The measurements were made on the synchrocyclotron of the Institute of Nuclear Problems of the USSR Academy of Sciences. The 460 and 660 Mev beams were obtained directly from the accelerator; the 560 Mev protons were obtained by slowing down the 660 Mev particles in graphite absorbers.

2. Experimental Procedure

Fig. 1 shows a diagram of the apparatus used in measuring proton scattering at 460 Mev. The proton beam from the synchrocyclotron was thoroughly collimated and directed at the paraffin target P. The protons scattered in the target were recorded by the telescope A, consisting of four proportional counters, while the recoil protons were recorded by counter B.* The number of p-p scattering events was determined by the differential method on the basis of alternate measurements with a paraffin and a graphite target. In the case of scattering through angles under 45°, when the energy of

---

* Strictly speaking, both protons participating in the scattering process are identical. The distinction between scattered protons and recoil protons is made purely for convenience of exposition.

the recoil protons is small and simultaneous recording of the scattered and the recoil proton becomes difficult, only the scattered protons were recorded by means of telescope A. In this case a tungsten absorber, having a surface density of 125 g/cm^2, was installed between the third and fourth counters of the telescope in order to exclude slow protons and pi mesons.

The experimental arrangement used in the measurements at proton energies of 560 and 660 Mev is pictured in Fig. 2. In these experiments both scattered and recoil electrons were recorded

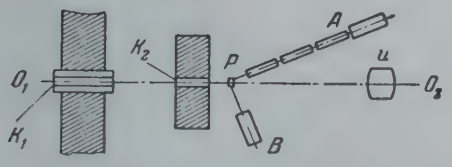

Fig. 1. Diagram of apparatus used in proton scattering measurements at 460 Mev: A) telescope of four proportional counters, B) recoil proton counter, u) ionization chamber, P) target, K_1 and K_2) collimators, O_1 and O_2) proton beam.

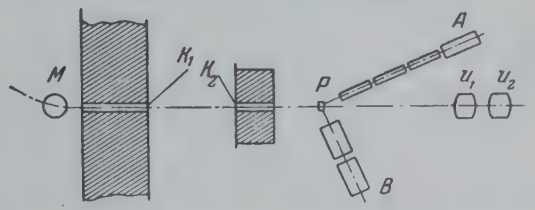

Fig. 2. Diagram of apparatus used at 560 and 660 Mev: A) telescope of four proportional counters recording scattered protons, B) telescope of two counters recording recoil protons, P) target, u_1 and u_2) ionization chambers, K_1 and K_2) collimators, M) magnet.

simultaneously by means of telescope A, consisting of four proportional counters, and telescope B, made up of two proportional counters. The relative intensity of the proton beam was determined by means of the ionization chambers u_1 and u_2, located behind the target. The indications of the ionization chambers were calibrated against a Faraday cup.

3. Proton Beam

Location of collimators

The proton beam brought out from the synchrocyclotron was collimated by means of a system of collimators. The location of the collimators and monitoring apparatus in the experiments at 460 Mev is shown in Fig. 1. The first collimator K_1 was built into the 1.5 meter thick concrete shielding wall and consisted of a set of close-fitting, concentric brass tubes. The second collimator K_2, built into a 1 meter thick wall, was located at a distance of about four meters from the first. For these experiments the inside diameter of collimator K_1 was 5 cm; that of collimator K_2 was 2-3 cm.

The location of the collimators and monitoring equipment used in investigating scattering at 560 and 660 Mev is shown in Fig. 2. In this case the proton beam was deflected by the bending magnet M and collimated by collimators K_1 and K_2. Collimator K_1 consisted of a steel bar 3.6 meters long with a 5 cm diameter axial aperture, mounted into the 4 meter thick concrete wall. The second collimator K_2 was located at about 6 meters from K_1; it is diagrammed in Fig. 3. Collimator K_2 had provision for installation of graphite absorbers for the purpose of attenuating the energy of the bombarding protons.

After passing through the absorbers the proton beam is further collimated by a brass tube (3 in Fig. 3) having an inside diameter of 19 mm. With the absorbers in place the angular divergence of the beam was markedly increased due to scattering in the graphite. However, only protons scattered through an angle of less than 1° could impinge on the target, mounted at a distance of about 40 cm from the exit aperture of the collimator.

Part of the protons deflected from their initial direction in going through the absorber pass through the walls of tube 3 and missing the target (the diameter of the target used in measuring the angular dependence of the scattering cross section was somewhat smaller than the diameter of the collimator aperture) may still enter the ionization chambers u_1 and u_2. In investigating the angular dependence of scattering this additional flux through the ionization chambers does not introduce any error since in this case we are interested only in the relative intensity of a proton beam. However, in measuring the absolute value of the scattering cross section, this additional flux, if at all appreciable, may result in a considerable error. Hence in the measurements of the absolute cross section at 560 Mev the measuring equipment was moved back to a distance of 1.5 meters from collimator K_2 and an additional collimator was installed in front of the target.

Alignment of the collimators and measuring equipment was checked by the blackening of x-ray film exposed at the collimator entrance and exit.

Measurement of beam intensity

The relative intensity of the proton beam was monitored by means of ionization chambers. In the experiments at 460 Mev one ionization chamber was used; this chamber is pictured in Fig. 4. The chamber was filled with pure argon at a pressure of 2 atmospheres. The ionization chamber current was amplified by a balanced pliotron circuit which was connected to a DC amplifier; the output of the latter was fed to a recording galvanometer having a sensitivity of 5 ma per scale deflection.

The use of the pliotron circuit as the first amplification stage and employment of 100% feedback in the DC amplifier insured a high degree of operating stability. The zero drift per hour of the equipment as a whole was equivalent to a change of 1-2 mv in the voltage at the output of the pliotron circuit; under the same conditions the change in potential on the pliotron output circuit due to the proton beam amounted to 200-300 mv .

In the experiments at 560 and 660 Mev, two ionization chambers were set in the path of the beam. The first, as in the 460 Mev case, was connected to a DC amplifier and recording galvanometer as described above; the second chamber was connected to a current integrator. The ionization chambers were calibrated against a Faraday cup, especially designed for the present investigation. For purposes of calibration the Faraday cup was set up behind the ionization chambers and the indications of the chamber instruments compared with the charging current of the Faraday cup.

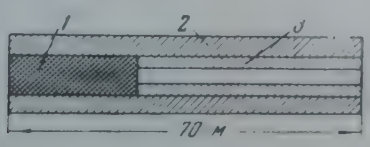

Fig. 3 Collimator K_2 (see Fig. 2): 1)Graphite absorber, 2) Steel bar, 3)brass tube.

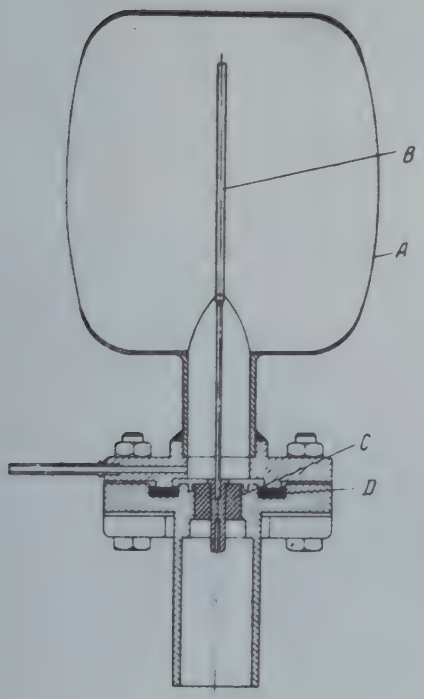

Fig. 4. Diagram of ionization: A) housing, B) collecting electrode, C) amber insulator, D) rubber gasket.

4. Geometry of the Experiment and Design of the Counters.

The angle between the directions of the scattered and the recoil protons was defined by the relationship

$$\operatorname{tg}(\theta_L + \varphi_L) = \left(1 + \frac{2Mc^2}{E}\right)\operatorname{tg}\theta_L + \frac{2Mc^2}{E}\operatorname{ctg}\theta_L, \quad (1)$$

where M is the rest mass and E is the kinetic energy of the incident proton and θ_L and φ_L are, respectively, the angles of ejection of the scattered and recoil protons in the laboratory system.

In quasi-elastic scattering of protons from carbon nuclei such rigorous correlation is virtually absent, so that with simultaneous recording of the scattered and recoil protons the scattering from the carbon nuclei makes only an insignificant contribution to the total number of recorded scattering events in the paraffin target. In the present experiment the solid angle was defined by the dimensions of the counters of telescope A; telescope B recorded recoil protons. In order to record all the recoil protons, corresponding to the protons scattered in the direction of telescope A, rather large counters must be used in telescope B.

In the scattering measurements at 560 and 660 Mev two counters 8 cm in diameter and 14 cm in length were used in telescope B; these recorded all the recoil protons corresponding to the scattered protons traversing telescope A. The distance from the target to the back face of the last counter in telescope B was 50 cm in most cases. The first three counters in telescope A were 2 cm in diameter and 14.5 cm long; for convenience of adjustment they were mounted in a common glass flask. The fourth counter was 4 cm in diameter and 15 cm long. The distance between the target and the third counter (the one defining the solid angle) of telescope A was approximately 90 cm in most of the experiments. The distance between the third and fourth counters of telescope A was 7.5 cm.

In some cases in the experiments at 460 Mev, when the angular distribution was being measured, the counters used in telescope B were 4 cm in diameter and 15 cm long. These did not record all the recoil protons; this made it necessary to introduce a correction taking into account the dependence of the effective solid angle on the angle of scattering. In measuring the absolute value of the cross sections the smaller counters in telescope B were replaced by larger ones (different sizes were used) which recorded all the recoil protons. Counters of the same size and design were used in telescope A at all energies.

All counters were filled with a mixture of argon and methane (100 mm Hg A and 300 mm Hg CH_4). The argon was the spectrally pure product; the methane was carefully purified by fractional distillation

and repeated passing over a pulverized barium getter to remove all traces of oxygen. The operating voltage on counters of telescope A was 2000-2400 v; that on the counters of telescope B was 2500-2800 v. The pulses on the counters were amplified by preamplifiers and carried to the coincidence circuit by suitable high-frequency cables. The overall gain in each channel was $1.5 \cdot 10^4$. The resolving time of the coincidence circuit equalled $2 \cdot 10^{-7}$ sec. Both the number of coincidences between telescopes A and B and the number of coincidences in telescope A were recorded simultaneously.

5. Scatterers

The hydrogenous scatterers were targets of paraffin. All targets were cylindrical and were suspended in a holder having provision for rotation about a vertical axis. In the angular distribution measurements the dimensions of the targets were such that the entire target was within the beam (diameter of target 15-20 mm, thickness 1.0-1.5 g/cm^2 paraffin; diameter of beam 20-30 mm). For the absolute cross section measurements the diameter of the target (30 mm) was greater than that of the beam (20 mm). The thickness of the paraffin targets was such that there were $1.190 \cdot 10^{23}$ hydrogen atoms per cm^2.

The background due to accidental coincidences and scattering of protons from the carbon nuclei in the paraffin was measured by means of graphite targets, equivalent to the paraffin ones as regards the number of carbon atoms per cm^2 and of the same diameter as the corresponding paraffin targets.

The proton-proton scattering effect (i.e., the effect due to hydrogen) was determined as the difference between the number of coincidences with the paraffin and with the corresponding graphite target. There was virtually no admixture of accidental coincidences in the number of p-p scattering events determined in this manner. This is confirmed by the fact that the p-p scattering effect varied linearly (statistical accuracy 3%) as the beam intensity was increased up to 2.5 times.

In the experiments at 460 Mev the recoil protons, corresponding to the protons scattered to 45° (c.m. system) underwent appreciable multiple scattering in the target. An appropriate correction, amounting to about 4.5%, was introduced in processing the experimental results.

6. Control Measurements

We ran a number of control experiments to check the operation of the apparatus. One of the important indices characterizing proper and stable operation of the equipment is independence of the count (effect from hydrogen) of the potential on the counters (i.e., existence of a voltage plateau). The presence of an effective voltage plateau was verified prior to each series of measurements both by simultaneous measurement of the voltage on all counters and by reading the voltage on one of the counters with a steady potential on the others. A typical curve for the last case is shown in Fig. 5. It will be seen from the curve that beginning with a voltage of about 2000 v the number of coincidences measured (within the limits of counting statistics) remains constant over a considerable voltage interval. Inasmuch as the pulse height from the proportional counters depends on the proton energy, the voltage plateau check was made with the telescopes A and B in the locations corresponding to the upper and lower limits of the angular scattering interval investigated.

The presence of a voltage plateau indicates that the amplified voltage pulses are appreciably greater than the response threshold of the coincidence circuit and are properly standardized in the last amplifier stages. In this case the number of coincidences registered is independent of variations of the gas amplification of the counters and the gain of the amplifier. In all experiments, the voltage on the counters was set some 100-150 v above the beginning of the plateau.

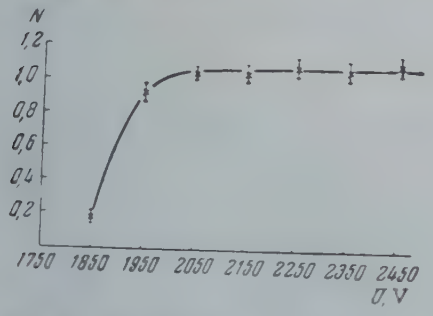

Fig. 5. Variation of number N of coincidences between telescopes A and B with the voltage on the first counter of telescope A with a constant potential on the other counters.

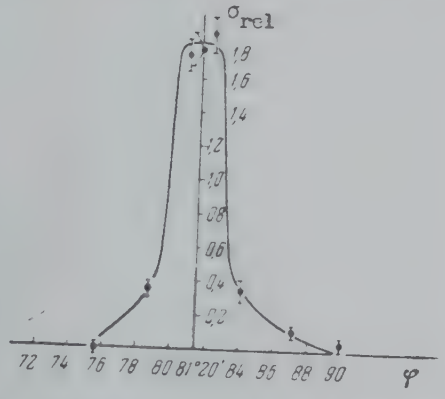

Fig. 6. Number of coincidences between telescopes A and B (see eq. (1) as a function of the angle φ between them. E_p = 660 Mev; θ_L = 40° 40'.

The presence of slow protons in the beam can give rise to appreciable errors in measurements of both the angular distribution of the scattered protons and the absolute value of the cross sections. The absence of protons of low energy was verified in the following manner: as follows from equation (1), the angle between the protons emerging from the target in the case of slow protons (non-relativistic) equals 90° while for protons of energies above 450 Mev this angle is less than 84° (with $\theta_{c.m.}$ = 90°). Thus measurements of the number of coincidences as a function of the angle between the telescopes serves as an indication of the proportion of slow protons in the beam. Appropriate measurements were carried out at proton energies of 460 and 660 Mev; the results obtained at 660 Mev are shown in Fig. 6. The appreciable width of the curve is due to the large size of the counters installed in telescope B. In order to enhance the angular resolution, telescope B, in the course of these measurements was moved back to 120 cm from the target (distance from back face of second counter to target). As may be seen from the curve the number of coincidences between the telescopes at an angle of 90° between them fell virtually to zero, indicating that there were few low-energy protons in the beam. At 560 Mev we did not record the entire dependence curve but only checked for the absence of coincidences at 90°.

As has been noted, fairly large proportional counters were used in the experiments (up to 8 cm in diameter). In view of this the migration time of the electrons from point of formation to the filament was comparable to the resolving time of the coincidence circuit. In order to make sure that the coincidence circuit did not miss any of the pulses the resolving time was varied from 0.2 to 0.6 μsec: the number of coincidences due to p-p scattering remained virtually constant.

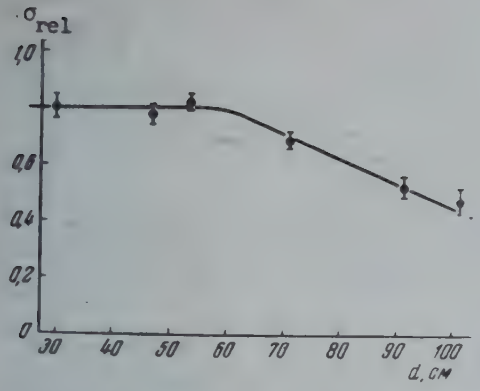

Fig. 7. Variation of the number of coincidences between telescopes A and B with the distance d of the back face of the last counter in B from the target. (Some of the measurements were made with only one counter in B, in this case d is the distance from the back face of this counter to the target.)

In the experiments at 560 and 660 Mev all the recoil protons, corresponding to the scattered protons traversing telescope A, were recorded in telescope B. To make sure that this was actually so we measured the number of coincidences between telescopes A and B as a function of the distance of B from the target. These verification measurements were carried out at scattering angles of 12° 57' and 17° 21' (corresponding to 30 and 40° in the c.m. system at 660 Mev). The results of the measurements at 17° 21' are shown in Fig. 7. It will be seen that when the distance from the back face of telescope B to the target is less than 70 cm the number of coincidences is independent of this distance and hence in this case all the recoil protons are recorded. An analogous curve was obtained for θ_L = 12° 57'. It follows from the shape of the curves that the number of coincidences recorded is not affected to any appreciable extent by multiple Rutherford scattering of the recoil protons in the target.

7. Measurement of Angular Dependence of the p-p Scattering Cross Section

In this investigation we first measured the angular distribution of the scattered protons (in relative units). Then we determined the differential scattering cross section in absolute units at one or more scattering angles and used these values to normalize the curve for the angular dependence of the p-p scattering cross section. Such separation of the absolute measurements is expedient in view of the fact that they require a whole series of control experiments, which should be made immediately preceding the absolute determination.

The scattering cross section in relative units was determined as

$$\sigma_{rel} = \frac{N_p}{I_p} - \frac{N_g}{I_g} \qquad (2)$$

where N_p is the number of coincidences between telescopes A and B with the paraffin target, N_g is the number of coincidences with the graphite target and I_p and I_g are the corresponding integral intensities in relative units (number of counts recorded by the mechanical register of the integration chamber current integrator or the area under the curve recorded by the galvanometer.)

In the experiments we simultaneously recorded the scattered and recoil protons in the interval of angles from 45 to 90° at 460 Mev, 40 to 90° at 560 Mev and 30 to 90° at 660 Mev. As was noted

above, at 460 Mev not all the recoil protons, corresponding to scattered protons recorded by telescope A, were detected by counter B. In this case an appropriate correction, taking account of the dependence of the solid angle on the angle of observation of the scattered protons, was introduced. The dependence of the effective solid angle on the angle of scattering is shown in Fig. 8. The calculated values were verified experimentally: the ratio of the differential cross sections at 45 and 90° was measured by replacing the usual counter in B by a larger one, capable of recording all the recoil protons. The resultant measurements were in good agreement with the other data. Only individual scattered protons were recorded at 460 Mev in the angular interval from 30 to 45°. In order to exclude all slow protons and pi mesons produced by the $p + p \rightarrow \pi^+ + d$ and $p + p \rightarrow \pi^+ + p + n$ reactions a tungsten absorber, having a surface density of 125 g/cm^2, was inserted between the third and fourth counters of telescope A. The results obtained in this case were adjusted to coincide at the point with the curve obtained as the result of simultaneous recording of the scattered and recoil protons.

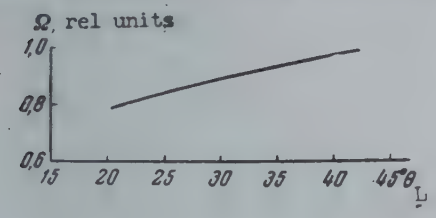

Fig. 8. Dependence of effective solid angle defined by telescopes A and B on scattering angle (E_p = 460 Mev).

In the case when both protons participating in the scattering were recorded, the background, as measured with the graphite target, amounted to 8-14% at 460 and 660 Mev and did not exceed 25% at 560 Mev. In the cases when only the scattered protons were recorded the ratio of the number of coincidences with the paraffin target to the number with the graphite target equalled 1.2-1.3.

We carried out several series of measurements of the angular dependence of the p-p scattering cross section at each of the proton beam energies. The results of the individual series are in good agreement within the limits of the statistical error.

In order to avoid possible errors connected with changes in the sensitivity of the monitors during the period between experiments (up to two months) in averaging the individual curves, the curves were brought to the same scale in the following manner: the curve characterized by the highest statistical accuracy of the measurements was selected and the ratio of the ordinates in it and in some one other curve was computed for each scattering angle. The ratio of the scale to the two curves was then determined as the average of the ordinate ratios. The total number of pulses measured for each of the two curves is thus utilized in computing the average ordinate ratio and consequently the error in converting the curves to the same scale is less than the statistical error of the individual measurements. After being brought to the same scale in this way the curves were averaged in the conventional manner.

8. Measurement of the Absolute Differential p-p Scattering Cross Section

The absolute value of the differential p-p scattering cross section was measured at 460 Mev for 41° 49' and 27° 19', at 560 Mev for an angle of 26° 52' and at 660 Mev for 17° 21' and 26° 22'. The ionization chambers were recalibrated against the Faraday cup

before each series of measurements. The absolute value of the cross section was computed as

$$\sigma_L(\theta_L) = \frac{\frac{N_p}{I_p} - \frac{N_g}{I_g}}{n\Omega}$$

where n is the number of hydrogen atoms per cm^2 in the paraffin target, Ω is the effective solid angle and I_p and I_g are the respective intensities of the proton beam in the measurements with the paraffin and graphite targets.

The greatest errors in these measurements are connected with determining the effective solid angle. To determine Ω we measured the number of coincidences in telescope A at two different distances of the telescope from the scatterer. The solid angle defined by telescope A was computed according to the equation

$$\Omega = \frac{S}{a^2}\left(\sqrt{\frac{N_1 I_2}{N_2 I_1}} - 1\right)^2,$$

where S is the area of the third counter, a is the distance between the two locations of the telescope, N_1 and N_2 are the numbers of coincidences for the first and second positions of the telescope and I_1 and I_2 are the corresponding integral intensities of the proton beam. The described method makes it possible to find the value of the solid angle to within 3.5-4.5%. The value of the solid angle was redetermined immediately prior to each absolute scattering cross section measurement. Paraffin having a known chemical composition — $CH_{2.07}$ — was used in preparing the targets. The error in determining the value of n did not exceed 0.5%.

The error in measuring the integral intensity of the proton beam is comprised of the errors involved in measuring the relative intensity and the errors connected with calibrating the ionization chamber against the Faraday cup. The errors in measuring the relative intensity of the beam are, in turn, made up of the errors in reading the record of the galvanometer (0.7-1.0%), the errors due to non-linearity of the characteristics of the electronic equipment (under 0.5%), and the errors connected with the zero drift of the electrometric system during the measurement period (not over 0.6-0.7%). Hence, the mean error in determining the relative intensity of the beam does not exceed 1.3-1.4%. The error associated with calibration of the chamber with reference to the Faraday cup is comprised of the errors in determining the capacitance of the Faraday cup (under 0.8%), the error in determining the correction for residual gas in the cup housing (1-1.2%) and the errors connected with the zero drift of the electrometric system (under 0.5%). In addition, in comparing the indications of the chamber and cup, one should take into account errors connected with the human factor (errors in determining the instant when the indicator pointer passes over a graduation, etc.); we evaluate this as being 1%. Thus the overall mean error in determining the intensity of the proton beam is 1.8-2%.

The absolute p-p scattering cross sections in the laboratory system obtained as a result of our measurements are listed in Table 1. In these measurements we used a paraffin target with $1.190 \cdot 10^{23}$ hydrogen atoms per cm^2. The initial measurements of the absolute cross section at 460 Mev led to a value of $1.28 \cdot 10^{-26}$ cm^2 $sterad^{-1}$ at $\theta_L = 41^\circ 41'$. However, since the accuracy of these first measurements was not particularly high we carried out a series of supple-

Table 1

Absolute values of the differential p-p scattering cross section

Energy Mev	Scattering Angle, θ_L	$\Omega\ 10^{-4}$ sterad	$\sigma_L, 10^{-26}$ cm^{2}ster^{-1}
460	41°41′	3,74±0,22	1,10±0,09
460	27°19′		1,55±0,11
560	26°52′	4,39±0,15	1,51±0,13
660	17°21′	4,30±0,16	2,32±0,12
660	26°22′	4,50±0,16	1,46±0,07

mentary experiments in which the 460 Mev beam was obtained by slowing down 660 Mev protons in graphite absorbers set in the entry section of collimator K_1 (see Fig. 2). In these experiments the scattered protons were recorded by telescope A consisting of four proportional counters and all the recoil protons were recorded by telescope B consisting of two large proportional counters. These experiments resulted in the absolute values of the cross section at 460 Mev shown in Table 1.

Results

The results of our determinations of the angular dependence of the scattering cross section were normalized in absolute units to the data of Table 1 and converted to the center of mass system by means of the following equation

$$\sigma_{c.m}(\theta_{c.m}) = \frac{\sigma_L(\theta_L)}{4\cos\theta_L} \cdot \frac{\left(1+\frac{E}{2Mc^2}\sin^2\theta_L\right)^{\frac{3}{2}}}{1+\frac{E}{2Mc^2}},$$

where E is the kinetic energy of the protons in the beam, M is the proton mass, $\sigma_{c.m.}(\theta_{c.m.})$ is the scattering section in the center of mass system and $\sigma_L(\theta_L)$ is the cross section in the laboratory system. The final results in the center of mass system are listed in Table 2 and shown in Fig. 9.

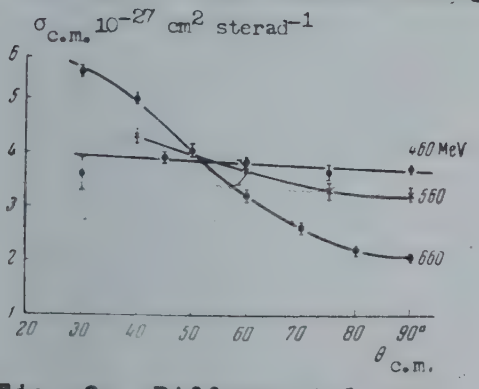

Fig. 9. Differential p-p scattering cross sections at 460, 560 and 660 Mev.

The uncertainties indicated in Fig. 9 and Table 2 pertain only to statistical errors of measurement. The overall errors in determining the absolute cross section amount to 7% at 460 Mev, 10% at 560 Mev and 5% at 660 Mev.

9. Discussion of Data

The most interesting result of the present investigation is perhaps the detection of a noticeable anisotropy in the scattering cross section at energies in the 560-660 Mev interval. As is known the scattering cross section remains fully isotropic in the center of mass system up to about 400 Mev. In the 415–435 Mev region, the data obtained by different investigators are in conflict. However, it can be assumed that in this energy interval the scattering cross section increases somewhat with decreasing angle. At 460 Mev, according to our data the ratio of the cross sections at 45 and 90° equals 1.06, i.e., the

anisotropy is neglible. These data are in agreement with the results of Sutton et al[8] ($\sigma_{16.6^\circ}/\sigma_{90^\circ}$ = 1.19 at 437 Mev) but in conflict with the results of Marshall et al[6] ($\sigma_{28^\circ}/\sigma_{90^\circ}$ = 0.84 at 429 Mev) and Mott et al[7] ($\sigma_{25.2^\circ}/\sigma_{90^\circ}$ = 1.32 at 435 Mev).

Table 2

Dependence of differential p-p scattering cross section on scattering angle at different proton energies

Scattering Angle (c.m)	σ, 10^{-27} cm^2 sterad^{-1}		
	E_p = 460 MeV	E_p = 560 MeV	E_p = 660 MeV
90°	3,68±0,09	3,22±0,13	2,06±0,08
80°	—	—	2,19±0,11
75°	3,60±0,12	3,28±0,14	—
70°	—	—	2,59±0,10
60°	3,82±0,09	3,66±0,19	3,20±0,12
50°	—	—	4,03±0,12
45°	3,89±0,09	—	—
40°	—	4,32±0,14	4,97±0,10
30°	3,57±0,31	—	5,47±0,12

The results of our experiments indicate that the cross section is very weakly dependent on the angle at energies under 460 Mev. At 560 Mev we observe a noticeable anisotropy in the character of the angular distribution of the scattered protons ($\sigma_{40^\circ}/\sigma_{90^\circ}$ = 1.34). Finally, at 660 Mev the scattering cross section is markedly anisotropic ($\sigma_{30^\circ}/\sigma_{90^\circ}$ = 2.66). The appearance of anisotropy at 560-660 Mev, which can be attributed to the presence of terms with $j > 0$ (j is the total angular momentum) in the scattered wave, is not particularly surprising; what is surprising rather is the absence of anisotropy at proton energies of 100 to 400 Mev.

It will be seen from Fig. 9 that at $\theta_{c.m.} = 90^\circ$ the scattering cross section diminishes rapidly with increasing energy. The opposite obtains at small scattering angles, where the cross section increases rapidly with energy. At angles on the order of 50-55° the cross section remains virtually constant in the interval from 460 to 660 Mev and agrees with the values determined at 260-400 Mev.

At 460 Mev the cross section at 90° equals $3.68 \cdot 10^{-27}$ cm^2 sterad^{-1} which is appreciably greater than the maximum possible value of the cross section for pure S-scattering. The large value of the cross section and the virtually isotropic distribution of the scattered protons is readily explained if we assume that at this energy scattering is due principally to interaction of protons in the $^1S_0$ and $^3P_0$ states.

It is impossible to compare the experimental results with theory since at present we have no reasonably rigorous theory of nuclear forces. For the same reason we cannot at present carry out an unambiguous phase analysis of the experimental data.

Measurements of proton-proton scattering in the 460-660 Mev interval have also been made by Meshcheriakov and his co-workers[9-11]; their data are in good agreement with the results of our experiments within the limits of the experimental error.

In conclusion we wish to express our profound gratitude to A. I. Alikhanov and A. G. Meshkovski for discussion of the results and aid in the investigation. We also wish to thank M. G. Meshcheriakov for making the present investigation possible and the entire operating personnel of the synchrocyclotron for their efficient work.

References

1. D. Fischer & G.Goldhaber, Phys. Rev., 95, 1350 (1954).
2. O.Chamberlain & J.D.Garrison, Phys. Rev., 95, 1349 (1954).
3. O.A.Towler, Phys. Rev., 85, 1024 (1952).
4. O.Chamberlain, E.Segré & C.Wiegand, Phys. Rev., 83, 923 (1951).
5. C.L.Oxley & R.D.Shamberger, Phys. Rev., 85, 416 (1952).
6. J. Marshall, L.Marshall & V.A.Nedzel, Phys. Rev., 92, 834 (1953).
7. W.E.Mott, R.B.Sutton, J.G.Fox & J.A.Kane Phys. Rev., 90, 712 (1953).
8. R.B.Sutton, T.H.Fields, J.G.Fox, J.A.Kane et al, Bull. Am. Phys. Soc., 29, 4, 75 (1954).
9. M.G.Meshcheriakov, N.P.Bogachev, B.S.Neganov & E.V.Piskarev, Doklady AN SSSR, 99, 955 (1954).
10. N.P.Bogachev & I.K.Vzorov, Doklady AN SSSR, 99, 931 (1954).
11. M.G.Meshcheriakov, B.S.Neganov, L.M.Soroko & I.K.Vzorov, Doklady AN SSSR, 99, 959 (1954).

* * * * * * * * * * * * * * * *

EXPERIMENTAL INVESTIGATION OF THE INTERACTION OF NEUTRONS WITH NUCLEONS AND DEUTERONS AT ENERGIES IN THE 380-590 MEV REGION

- V. P. Dzhelepov, Iu. M. Kazarinov, B. M. Golovin V. B. Fliagin and V. I. Satarov

Introduction

Experimental data on the scattering of identical nucleons yield information on nuclear interaction of particles in antisymmetric states. The interaction of high-energy nucleons in symmetric states can be investigated only by observing the scattering of neutrons by protons.

The present report is devoted to a description of the major part of the investigations carried out by the authors in 1950-1952 on the synchrocyclotron of the Institute of Nuclear Problems of the USSR Academy of Sciences. The experiments comprise investigation of elastic scattering of neutrons by protons and neutrons as well as a study of exchange scattering of neutrons by deuterons, carried out for the purpose of clarifying the spin-dependence of exchange forces.[1-5] We shall also discuss part of the data obtained in our 1954 experiments with neutrons of 500 and 590 Mev mean energy.[6-8]

1. Neutron Beam

The high energy neutrons were obtained as a result of the interaction of protons, accelerated in thesynchrocyclotron, with the neutrons of a beryllium target. To this end the beryllium target, 2.5 or 4 cm thick, was mounted inside the vacuum tank of the accelerator and bombarded with 480 or 680 Mev protons. A neutron beam, 2 or 5 cm in diameter was separated from the high energy neutron beam by means of a brass collimator built into the 5 meter thick concrete shielding wall. (In the experiments with 500 and 590 Mev neutrons the shielding wall had a thickness equivalent to

8.5 meters of conventional concrete.) The experimental arrangement is shown in Fig. 1. The angular divergence of the neutrons in the collimated beam did not exceed 0.3°.

All the experiments were made with non-polarized neutron beams since the collimator defined neutrons emitted only in the direction of motion of the protons at the point of incidence on the target. The intensity of the neutron beam at energies above 300 Mev amounted to about $2 \cdot 10^4$ neutrons cm^{-2} sec^{-1} (as determined by the method of n-p scattering) at the location of the measuring instruments.

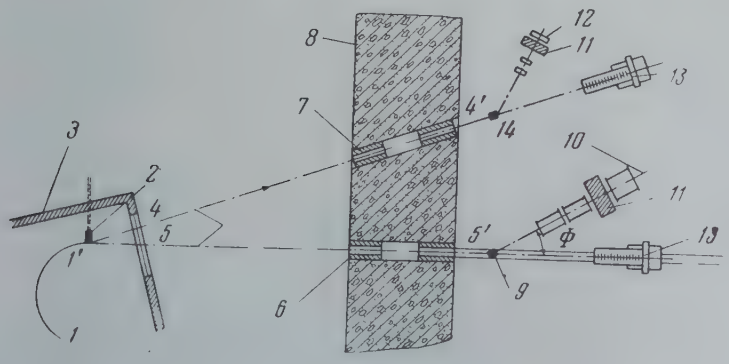

Fig. 1. General diagram of the experiments: 1-1') proton path in synchrocyclotron, 2) target, 3) wall of vacuum tank, 4-4' and 5-5') direction of motion of neutrons, 6) main collimator, 7) auxiliary collimator, 8) concrete shielding wall, 9) scatterer (paraffin and carbon or heavy and ordinary water), 10) telescope of proportional or scintillation counters, 11) copper absorber, 12) monitor telescope, 13) bismuth chamber, 14) scatterer (paraffin), Φ) angle of ejection of recoil protons from scatterer.

The distribution of neutrons in energy was determined with reference to the energy spectrum of recoil protons from n-p collisions, measured by two independent methods[3] for a recoil angle of 20°; in one series of experiments the neutron spectrum was determined from the absorption curve for the recoil protons in copper; in the other series of experiments the detector successively measured the number of recoil protons in the given energy interval E_p-(E_p + ΔE_p). The results obtained with both methods were in satisfactory agreement. The distributions found for two values of the proton energy (480 and 680 Mev) are shown in Fig. 2. The maximum in the neutron energy spectrum occurs at 395 ± 10 Mev in the first case and at 610 ± 10 Mev in the second.

2. General Characteristics of Apparatus and Procedure

The principal method of measuring employed in the present experiments was that of counting the recoil protons produced in n-p collisions in hydrogenous scatterers mounted in the collimated neutron beams.

The main difference between the individual experiments lay in the use of different detectors for recording the recoil protons. In experiments for determining the n-p elastic scattering cross sections and measuring the spectrum of the neutrons produced by 480 Mev protons (Fig. 2) the recoil protons were recorded by means of telescopes comprised of proportional counters (three per telescope) connected in coincidence. The counters were filled with 90% argon and 10% carbon dioxide at a total pressure of 760 mm Hg. The operating voltage was 2-2.5 kv. The resolving time of the counter coincidence circuit was $4 \cdot 10^{-7}$ sec; this resolving time proved adequate given the pulse frequency of the accelerator.

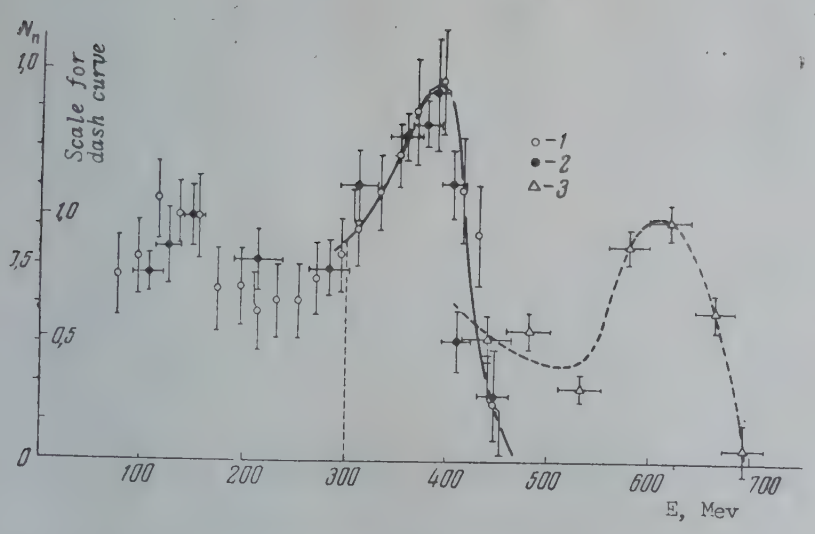

Fig. 2. Distribution of neutrons, produced by protons, in energy at E_p = 480 Mev (solid curve and points 1 and 2) and E_p = 680 Mev (dash curve and points 3). 1) results of measurements by means of absorption curve; 2 and 3) results obtained by the differential method.

The use of proportional counters in these experiments proved convenient because in this case the telescope can readily be converted to operate as a differential detector (for determining the neutron spectrum). The conversion was effected by reducing the voltage on the last counter; the gas amplification in the counter was thereby reduced and the electronic detector circuit was triggered only by pulses produced in the counter by protons of 20-30 Mev energy. The energy of the recoil protons was brought down to the requisite value by means of absorbers installed between the counters.

The experiments on determining the differential cross section for exchange n-d scattering and the n-n scattering cross section necessitated the use of detectors having a higher resolving power for recording the recoil protons. Hence in these experiments we used telescopes composed of scintillation counters which were also connected in coincidence. In these telescopes we used FEU-19 type photomultipliers and naphthalene crystals with an admixture of 2% anthracene (1952) or crystals of diphenyl acetylene (1954). The resolving time of the coincidence circuit in this case was $5 \cdot 10^{-8}$ sec. The counter plateau under typical conditions measured about 200 v and was carefully verified before each series of experiments. Scintillation counter telescopes were also used in determining the spectrum of neutrons produced by the 680 Mev protons (Fig. 2) and for measuring the total n-p and n-d interaction cross sections.

In order to record the scattering of only high energy neutrons and eliminate recording of recoil protons produced by slower neutrons in the beam, the energy threshold of the telescope (detector - 10 in Fig. 1) was artificially raised. This was done by installing a copper or tungsten absorber 11 between the second and third counters; the thickness of this absorber was varied depending on the angle of ejection of the protons so that only recoil protons produced by neutrons of over a certain energy could pass through the absorber. The last counter in the telescopes was always of appreciably greater diameter than the first two (in case of the proportional counters for example the first two counters were 2 cm in diameter, the last 4 cm). This was done expressly in order to reduce to a minimum the proton count loss due to multiple coulombic and diffraction scattering in the absorbers. Under our experimental conditions this scattering loss did not exceed 5-10%.

The intensity of the neutron beam during the experiments was monitored by a similar telescope and a multilayer ionization chamber 13 with bismuth coated electrodes. These monitoring instruments were usually located in a neutron beam separated by means of an auxiliary collimator (7 in Fig. 1).

The entire equipment was mounted on two metal stands equipped with adjusting screws for regulating the position of the telescopes in a vertical plane and graduated circles with reference to which the angles between the telescope axes and the neutron beam could be read off to within 0.2°.

3. Elastic Neutron-Proton Scattering at 380 Mev Neutron Energy

For the purpose of determining the relative differential cross sections for scattering of neutrons of the given energy by protons we measured[1,2] the angular distribution of the recoil protons ejected by the neutrons from a hydrogenous target, i.e. determined the function $N_p(\Phi) = k_1 \sigma_{np}(\Phi)$, where Φ is the angle of ejection of the recoil proton from the scatterer (in the laboratory system; see Fig. 1), $\sigma_{np}(\Phi)$ is the sought n-p scattering cross section and k_1 is a constant coefficient.

The neutron scatterers employed were discs of pure paraffin ($CH_{2.08}$) and graphite (C) having the same slowing-down power for protons. The effect of neutron scattering by free protons was determined as the difference of the effects due to the aforementioned scatterers taking into account the difference in the number of carbon atoms contained therein. The paraffin scatterer had a surface density of 3 g/cm^2 in the measurements in the $0° \leqslant \Phi \leqslant 50°$ interval and 1.5 g/cm^2 in the $50 \leqslant \Phi \leqslant 70°$ angular interval. The mean proton energy loss in the scatterers varied from 4-8 to 5-10 Mev, respectively. The curve for $N_p(\Phi)$ was determined in the range of recoil angles from 0 to 70° with an angular resolution of 2.5-3°.

The experimental data were corrected to allow for proton losses due to nuclear absorption and multiple scattering in the absorbers. These corrections were determined experimentally with fair accuracy for the telescope detector in a series of special experiments, carried out with an external proton beam from the synchrocyclotron. The maximum correction at $\Phi = 0°$ amounted to 40% of the uncorrected value of $N_p(\Phi)$.

Analysis showed that under the given experimental conditions any charged pi mesons, formed in the n-p encounters, were stopped in the copper absorbers and, therefore, not recorded by the proton detector. Hence it was not necessary to make any correction in the curve to take into account the effect of mesons.

The absolute differential elastic n-p scattering cross sections were determined, as usual, by normalizing the $\sigma_{np}(\Phi)$ curve to the total elastic n-p scattering cross section $\sigma_{np}^{t.e}$ according to the equality

$$\sigma_{np}^{t.e} = 2\pi \int_0^{\pi/2} \sigma_{np}(\Phi) \sin\Phi \, d\Phi. \qquad (1)$$

We determined the total n-p interaction cross section for neutrons of the same mean energy in a series of separate experiments by the method of knocking out neutrons under conditions of "good" geometry (see Section 4 below). According to these measurements the total interaction cross section $\sigma_{np}^{total} = (34 \pm 2) \cdot 10^{-27}$ cm^2 at 380 Mev. (Here and below we give total cross section data which have been revised and refined relative to our 1954 values - Ref. 1).

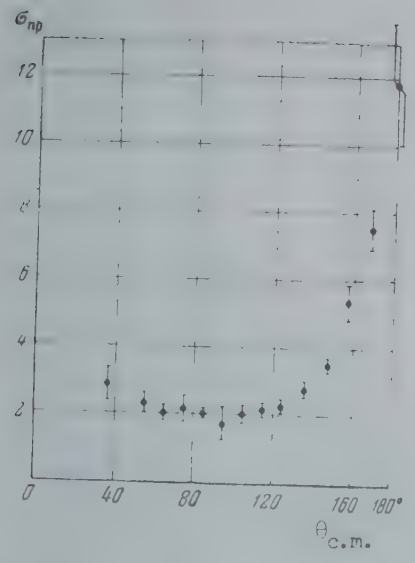

Fig. 3. Differential n-p scattering cross section at 380 Mev mean neutron energy. $\theta_{c.m.}$) neutron scattering angle in center mass system; σ_{np}) elastic n-p scattering cross section in 10^{-27} cm^2 sterad^{-1}.

Since the total cross section for the formation of neutral and charged mesons in n-p encounters, according to the data in the literature (see, for example, Ref. 9), at this energy equals about $1 \cdot 10^{-27}$ cm^2, the total cross section for elastic n-p scattering $\sigma_{np}^{t.e} = (33 \pm 2) \cdot 10^{-27}$ cm^2.

Fig. 3 shows the final values for the differential elastic n-p scattering cross section obtained after normalization (1) to $33 \cdot 10^{-27}$ cm^2 and conversion to the center of mass system of the colliding nucleons. In computing the values shown in Fig. 3 we took account of the small variation of the differential cross section in the region of angles under 40° (c.m. system) found in investigation of Ref. 10 for neutrons of 400 ± 25 Mev. The uncertainties in the figure pertain to counting statistics only. We evaluate the overall error in the differential cross section values, allowing for the small ambiguity in extrapolating the $N_p(\Phi)$ curve in the Φ = 70-90° interval, as about 15%.

4. Determination of the Total n-p and n-d Interaction Cross Sections at 380, 500 and 590 Mev

In the experiments devoted to determining the total cross section for n-p and n-d interaction, samples of the investigated materials were placed in the neutron beam in front of the main collimator 6 (Fig. 1), some 50 cm from the entrance aperture. The neutrons passing through the sample and collimator were detected by the telescope that recorded recoil protons ejected at an angle of 20° from the polyethylene scatterer permanently mounted in the neutron beam. The energy threshold of the detector in the experiments with the neutrons whose spectrum is shown in Fig. 2 was 300 Mev. The cross sections measured with this cut-off energy pertain to neutrons having a mean effective energy of 380 Mev. The cross sections for 500 and 590 Mev neutrons (dash-line spectrum in Fig. 2) were determined under conditions where the detector did not respond to neutrons of energies under 320 and 470 Mev, respectively. The geometry of the experiment was such that neutrons scattered in the sample through angles greater than 15' were not recorded by the telescope.

The total cross sections were computed from

$$\sigma^{total} = \frac{1}{\eta x} \ln \frac{N_0}{N_n} \qquad (2)$$

where N_n and N_o are the relative intensities (background subtracted) of the neutrons of equivalent effective energies, measured with and without the sample in the beam, η is the number of nuclei per cm^3 of the sample and x is the thickness of the sample in cm.

The neutron-proton interaction cross section was determined as the difference between the total cross sections for paraffin ($CH_{2.08}$) and graphite (C) or polyethylene $(CH_2)_n$ and graphite. The total neutron-deuteron interaction cross section was found from measurements with heavy (99.8% concentration) and ordinary water. As shown by careful qualitative analysis, the investigated materials were of high purity (content of heavy admixtures less than one tenth of 1%).

Table 1

Total n-p and n-d interaction cross sections (in 10^{-27} cm^2)

Cross section	Neutron energy, Mev		
	380	500	590
σ_{np}^{total}	34±2	35±2	36±2
σ_{nd}^{total}	57±2,0	65±2,5	72±2,5

The results of the determinations of the total cross sections for n-p and n-d interaction at the three effective values of the neutron energy are listed in Table 1. Comparison of these cross sections with the values found in the literature for lower energies (Fig. 4) shows that the total n-p interaction cross section remains almost constant over the entire range from 250 to 500 Mev. The lowest value is observed at E_n = 350-450 Mev. The total n-d interaction cross section has a minimum value in the vicinity of 250-350 Mev and then increases noticeably with increasing energy; thus the variation of the total n-d interaction cross section with energy from 200 to 600 Mev is rather similar to the variation of the total p-p interaction cross section in the same energy interval.*

5. Discussion of the Results on Neutron-Proton Scattering

The first and obvious deduction we can make on the basis of our experimental data (see Fig. 3) is that at 380 Mev the contribution to n-p interaction made by exchange forces is nearly equal to the contribution due to ordinary forces.**

The differential elastic n-p scattering cross sections vary little with angle in a wide range of angles (55-125°) and are fairly large (close to $2 \cdot 10^{-27}$ cm^2 $sterad^{-1}$) much as was found for 180 Mev

---

* The total p-p scattering cross sections up to 345 Mev shown in Fig. 4 were not derived by direct measurement; they were obtained in Ref. 11 by integration of the differential cross section curves. The cross sections for 460 and 660 Mev were deduced in the same manner in Refs. 12 and 13.

** The data obtained in investigation of Ref. 10, in which the n-p scattering cross sections at E_n = 400 ± 25 Mev were also determined in the region of small scattering angles, are indicative of a certain asymmetry of the $\sigma_{np}(\theta)$ curve relative to 90°; the cross sections in the $13 < \theta < 30°$ region prove to be considerably smaller than the cross sections at angles between 150 and 170°. In view of the fact that the contribution made by scattering through small angles to the integral n-p interaction cross section is small, our conclusion regarding the near equality of the contributions made by ordinary and exchange forces to nucleonic interaction at ~400 Mev remains valid even if the above-mentioned asymmetry is taken into account.

and 260 Mev neutrons by other investigators.[16,17] In conformity with this the total n-p scattering cross section also exhibits a relatively small decrease with energy in the 200-400 Mev interval.

These results of our experiments are in clear conflict with the predictions of perturbation theory and, as Dzhelepov[2] has shown, cannot be interpreted in the framework of phenomenological theory operating with static potentials. Under these conditions and in connection with the lack of a precise theory, there may be some value in the approach to phenomenological investigation of nucleon-nucleon interaction, utilizing the charge independence of nuclear forces concept. This hypothesis is substantiated in the region of low nucleon energies (i.e., by the equality of n-p and p-p interactions in the $^1S_0$ state, the similarity of levels in mirror nuclei, etc.). If we turn to the experimental facts, so far available, on the scattering of high-energy nucleons by nucleons (including the results of the experiments described herein) we must say that the present data at least do not contradict the charge independence of nuclear forces hypothesis. A consequence of this hypothesis, the relationship between the differential cross sections for elastic n-p and p-p scattering characterized by

$$2\left[\sigma_{np}(\theta)+\sigma_{np}(\pi-\theta)\right]-\sigma_{pp}(\theta)>0, \qquad (3)$$

is realized in a wide range of energies extending up to 400 Mev. In fact acceptance of this hypothesis allows us to move forward to some extent in analyzing the results of nucleon-nucleon scattering experiments. It must be noted that the assumption of charge independence, as Smorodinski[18] has shown, makes it feasible to determine separately - from experimental results on n-p and p-p scattering - the contributions to the cross section for the interaction in a system of two nucleons made by states with different values of the isobaric spin, T = 0 and T = 1. It is found in the analysis that the angular dependences of the cross sections for scattering of nucleons in states with different values of T are markedly different: whereas $\sigma_{T=1}(0)$, which, according to the charge invariance hypothesis, is equal to $\sigma_{pp}(0)$, in the 150-400 Mev neutron energy interval is independent of the angle and determined principally by interaction in the $^1S_0$ and $^3P_0$ states, the phases of which are close to $\pi/2$, the cross section for scattering of neutrons by protons in states with T = 0, $\sigma_{T=0}$, defined by the left part of inequality (3), is described by a curve reminiscent of the one obtained from perturbation theory. Evidence of the strong angular dependence of the cross section for scattering in the state with T = 0 is furnished by the figures in the fifth and sixth columns of Table 2, listing the average values of these cross sections at different neutron energies, as computed by us on the basis of the available experimental data on n-p and p-p scattering.

The pronounced anisotropy of scattering in the case of nucleons with T = 0 indicates that an appreciable number of symmetric states, such as $^3S_1$, $^1P_1$, ^3D, etc., whose phases are appreciably less than $\pi/2$, participate in n-p interactions. Apparently one consequence of the participation in n-p interactions (in a group of states with T = 0) of an appreciable number of states with such phases is the experimentally observed weaker polarization of neutron beams produced in n-p scattering, as compared with the polarization of proton beams obtained through proton scattering by protons of high energies.

Further evidence of the difference in the nature of the interaction of nucleons in states with different isobaric spins is furnished by the difference in the character of the energy dependences of the

Table 2

Averaged values of the total and differential cross sections for scattering of nucleons by nucleons in states with different values of isobaric spin

E_n, MeV	$\sigma^{t.e}_{T=0}$ *	$\sigma^{t.e}_{T=1} = \sigma^{t.e}_{pp}$	$\sigma^{t.e}_{np}$	$\sigma_{T=0}(90°)$	$\sigma_{T=0}(0°)$	$\sigma_{T=1}(90°)$
	10^{-27} cm^2			10^{-27} cm^2 sterad^{-1}		
100	110	32	71	10,8	54	5
150	69	27	48	5,0	40	4,3
200	59	23	41	4,2	36	3,7
300	47	23	35	3,6	32	3,7
400	43	23	33	3,0	31	3,7

* $\sigma^{t.e}_{T=0} = 2\sigma^{t.e}_{np} - \sigma^{t.e}_{pp}$. (t.e = total elastic)

total scattering cross sections for the nucleons in these states. Thus it can be seen from Table 2, $\sigma^{t.e}_{T=0}$ varies by a factor of one and a half in the 150-400 Mev interval, whereas $\sigma^{t.e}_{T=1}$ remains virtually constant.

In this connection a new fact, which comes to light as we go to still higher neutron energies is of interest. For 590 Mev neutrons, as follows from our data on the total n-p interaction cross section (see Table 1) and on the cross section for the formation of pi-mesons on hydrogen nuclei* by 590 Mev neutrons the total elastic n-p scattering cross section amounts to only $(26-28)\cdot10^{-27}$ cm^2 instead of $33\cdot10^{-27}$ cm^2 as observed at 380 Mev. Since, on the other hand, the total elastic p-p scattering cross section, characterizing the interaction of nucleons in the state with T = 1, remains constant over the entire energy range from 150 to 660 Mev (see Fig. 4), it follows that the noted decrease of the elastic n-p scattering cross section as the energy is increased from 400 to 600 Mev must be due to further weakening of the interaction between nuc-

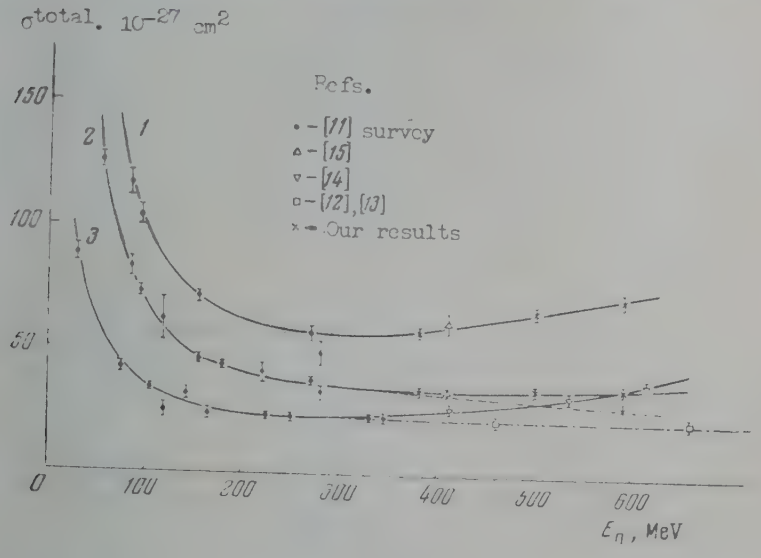

Fig. 4. Energy dependence of the total cross sections for n-d, n-p and p-p interactions: 1, 2 and 3) total n-d, n-p and p-p interaction cross sections, respectively: dash-line sections — elastic scattering cross sections for the corresponding nucleons.

---

* According to Ref. 7 the total cross section for the formation of neutral pi mesons in n-p collisions at 590 Mev equals $6\cdot10^{-27}$ cm^2, while according to Ref. 8 $\sigma(n + p \rightarrow \pi^{\pm} + \ldots) \approx (3-4)\cdot10^{-27}$ cm^2.

leons in states with isobaric spin zero.

Apparently a consequence of the different energy dependences of the interaction cross sections for nucleons with different isobaric spins is that the total cross section for elastic n-p scattering in the 100-590 Mev interval is roughly described by an empirical equation of the form

$$\sigma_{np}^{t.e} = A + \frac{B}{E_n} \qquad (4)$$

where A and B are constants.

In the light of the charge independence of nuclear forces hypothesis, the symmetry of the n-p scattering curve relative to the 90° angle experimentally observed at energies on the order of 400 Mev may be regarded as a consequence of the interference of interactions of nucleons in states with different isobaric spins.

6. Exchange Scattering of 380 Mev Neutrons from Deuterons

The results of n-p scattering experiments, carried out with high-energy neutrons, clearly show how large a contribution is made by exchange forces to the interaction between a neutron and a proton. However, we can draw no definite conclusions regarding the spin dependence of exchange forces on the basis of the results of such experiments alone. It was assumed that to clarify this important aspect of nuclear interaction it would be necessary to perform experiments with polarized nucleon beams and polarized targets.

In 1951 Pomeranchuk[19] suggested a different approach for obtaining information on the dependence of exchange forces on the spin. This consists of investigating the angular distribution of fast protons from exchange collisions of high-energy neutrons with deuterons, i.e., protons from the reaction

$$n + d \rightarrow p + (n + n) \qquad (5)$$

(here the notation (n + n) is used to indicate that the two neutrons from the encounter are characterized by a low relative velocity) and comparing the results of these experiments with the data on the scattering of neutrons by free protons. Pomeranchuk calls attention to the fact that, in view of the parallelism of the spins of the particles comprising the deuteron, under conditions when the momentum of the fast proton after the collision is nearly equal to the momentum of the striking neutron, the probability of exchange n-d scattering accompanied at the same time by an exchange of spins between the nucleons is sharply reduced. This means that protons having an energy close to the energy of the incident neutrons can be produced in reaction (5) only as a result of exchange collisions occurring without exchange of spins. (Chew[20] reaches a similar conclusion in his investigation.) According to the theory developed by Pomeranchuk, one can deduce from a comparison of n-d and n-p scattering results the ratio between the amplitude of spin-exchange scattering and the amplitude of spin-nonexchange scattering: $\bar{b}/\bar{a}$.

In the experiments of Refs. 2 and 4 a scintillation counter telescope was used to measure the difference $N_p'(\Phi)$ between the numbers of recoil protons ejected at a given angle Φ (in the laboratory system) to the neutron beam from scatterers with ordinary water and with heavy water, containing equal numbers of atoms of hydrogen and

deuterium. The neutron beam was 2 cm in diameter; the geometry of the detector permitted measuring the differential cross sections with an angular resolution of 0.75°. The energy threshold of the proton detector was about (300 Mev)·$\cos^2\Phi$. (With this threshold the elastically scattered deuterons were not recorded by the detector and hence did not distort the experimental results.)

The value of $N'_p(\Phi)$ (in relative units), proportional to the difference between the cross sections for exchange n-p and n-d collisions, for a given angle is defined by

$$N'_p(\Phi) = k_2[\sigma_{np}(\Phi) - \sigma_{nd}^{exc}(\Phi)]. \qquad (6)$$

The absolute values of the exchange cross section $\sigma_{nd}^{exc}(\Phi)$ can be found by dividing the numbers $N'_p(\Phi)$, determined as described above, by the numbers of recoil protons $N''_p(\Phi) = k_2\sigma_{np}(\Phi)$, recorded by the detector under similar conditions (as regards the intensity of the neutron beam, geometry of the detector and number of protons in the scatterer) from n-p collisions. The values of $N''_p(\Phi)$ were measured as usual as the difference of the effects due to paraffin and to graphite. From the ratios

$$\frac{N'_p(\Phi)}{N''_p(\Phi)} = 1 - \frac{\sigma_{nd}^{exc}(\Phi)}{\sigma_{np}(\Phi)}, \qquad (7)$$

determined in this manner it was possible to compute the values of $\sigma_{nd}^{exc}(\Phi)/\sigma_{np}(\Phi)$ for angles from 0 to 40° with satisfactory accuracy and then (using the previously found n-p scattering cross sections) to determine the absolute exchange cross sections for the same mean neutron energy (380 Mev).

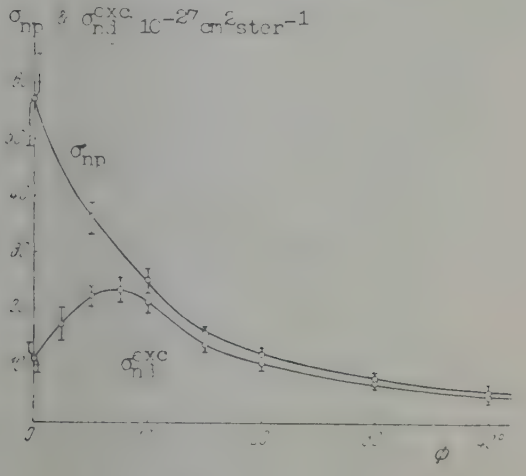

Fig. 5. Differential cross sections for exchange n-d and n-p scattering at 380 Mev.

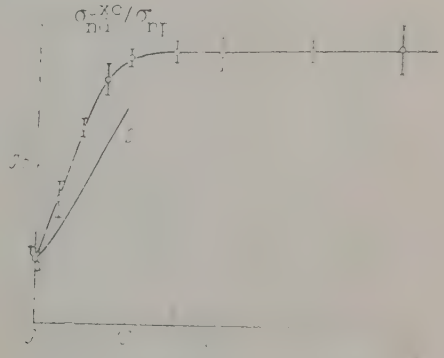

Fig. 6. Ratio of cross sections for exchange n-d and n-p scattering at 380 Mev. 1) experimental curve, 2) theoretical curve.

The results of the determinations are shown in Figs. 5 and 6. The earlier measured values of $\sigma_{np}(\Phi)$ (see Sec. 3 above) are also plotted in Fig. 5. A particularly sharp drop in the proton yield from exchange n-d collisions as compared with the yield from n-p collisions is manifest in the region of angles close to 0°. A 10-15% lower proton yield from n-d collisions is also observed in the 15-40°

interval of recoil angles. This is qualitatively in agreement with the results obtained in experiments with 90 Mev[21] and 270 Mev[22] neutrons; according to these experiments the cross section for the yield of fast protons in the region of angles $\vartheta > 10^\circ$ amounts to about 70-80% relative to $\sigma_{np}(\vartheta)$. The decrease in the value of the ratio $\sigma_{nd}^{exp}(\vartheta)/\sigma_{np}(\vartheta)$ with decreasing energy in a region of large recoil angles may be partly due to the effect of the Pauli exclusion principle. The indicated decrease may also be a consequence of the fact that at lower energies of the incident nucleons a large proportion of the recoil protons from n-d collisions is imparted an energy below the response threshold of the detector as a result of internal motion of the nucleons in the deuteron.

Fig. 6 also shows a theoretical curve computed for angles under 5° by means of equations (35) and (39) given by Pomeranchuk in Ref. 19. As may be seen, this curve shows qualitative agreement with the experimental data. However, the quantitative difference between the curves is considerable. The principal reason for the divergence is apparently the fact that non-central interaction between the nucleons is not taken into account in Ref. 19.

Using the relationship of Ref. 19 we can evaluate roughly the limits of the variation of the ratio of the spin-nonexchange and the spin-exchange scattering amplitudes on the basis of the experimentally determined value — 0.2 ± 0.035 — for $\sigma_{nd}^{exc}(0^\circ)/\sigma_{np}(0^\circ)$. It would appear that the ratio lies between the limits

$$0.5 \leqslant \frac{|\bar{a}|}{|\bar{b}|} \leqslant 1.2 \qquad (8)$$

On the basis of (8) we can make a new and original deduction regarding the nature of n-p interaction at high energies: the inequality shows that there is a high probability of a simultaneous exchange of spins in exchange n-p collisions. This means that the contributions made to exchange n-p interaction by spin-exchange and spin-nonexchange forces are of the same order of magnitude.

In the light of this deduction and of what we know regarding exchange, central and tensor forces we can, presumably, draw the general conclusion that a characteristic of nuclear interaction of nucleons is that all components of this interaction are comparable in order of magnitude.

7. Elastic Neutron-Neutron Scattering at 300 Mev

In experiments described below (also see Refs. 2 and 5), the cross section for elastic scattering of neutrons by neutrons of 300 Mev effective energy was determined on the basis of a comparison of the angular distributions of neutrons scattered by deuterons and by free protons, as measured under identical conditions. The possibility of using n-d scattering data for obtaining information on elastic n-n scattering is based on the fact that, according to present day concepts, at a sufficiently high energy of the incident nucleons, in most cases these interact intensively with only one of the nucleons forming the deuteron.

Calculations of the total cross section for n-d scattering to a given angle (carried out by one of the present authors in the momentum approximation[23]) showed that at scattering angles (in the laboratory system) under $50\text{-}60^\circ$ the n-d scattering cross section is described by

$$\sigma_{nd}(\theta_L) = [\sigma_{nn}(\theta_L) + \sigma_{np}(\theta_L)]\alpha + \sigma_{int}(\theta_L) \qquad (9)$$

where $\sigma_{nn}(\theta_L)$ and $\sigma_{np}(\theta_L)$ are, respectively, the cross sections for scattering of neutrons through the angle θ_L by free neutrons and by protons, $\sigma_{int}(\theta_L)$ is the "interference cross section" due to superposition of the neutron waves scattered by the neutron and proton of the deuteron and α is a computed theoretical function of θ_L.

The dependences of α and $\sigma_{int}(\theta_L)$ on the scattering angle found in Ref. 23 indicate that at 300-400 Mev the coefficient α for $\theta_L \leq 50\text{-}60^\circ$ is virtually equal to unity while σ_{int} in the $20 \leq \theta \leq 50\text{-}60^\circ$ interval at the maximum does not exceed 15% of the n-p scattering cross section measured at the same angle. In going to greater angles (in the indicated angular interval) and higher energies, $\sigma_{int}(\theta_L)$ decreased rapidly. In view of this we can assume that under the indicated conditions the cross section for n-n scattering is described with satisfactory accuracy by

$$\sigma_{nn}(\theta_L) \approx \sigma_{nd}(\theta_L) - \sigma_{np}(\theta_L) \qquad (10)$$

It follows from expression (10) that in order to find the elastic n-n scattering cross section it is sufficient to determine the values of the flux of neutrons scattered to the same angle by hydrogen and deuterium. In view of the low intensity of the neutron beam produced by the accelerator in such experiments and of the low efficiency of the currently available methods of recording fast neutrons, the procedure used in the first experiments was based on the utilization of thick scatterers and neutron detectors subtending relatively large solid angles. In these experiments the neutron beam was 3 cm in diameter; the scatterers were thin-wall cylindrical vessels, 6 cm in diameter and up to 80 cm in length filled with heavy water (99.8% concentration) or ordinary water. The neutron detector was a fission chamber with bismuth coated annular electrodes (outer 52 cm dia., inner 12 cm dia.). The basic experimental data for determining relative values of the differential n-n scattering cross sections were the relative counting rates ($\nu_1(x)$ and $\nu_2(x)$) of the detector with the scatterers of D_2O and H_2O, containing an equal number of nuclei, placed alternately in the neutron beam at the same distance x from the electrode (Fig. 7).* The solid angle of incidence of the scattered neutrons on the detector obviously changes as the distance x is varied; this makes it possible to investigate the requisite interval of scattering angles.

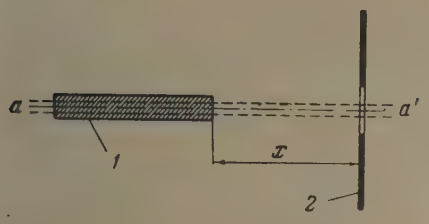

Fig. 7. Diagram of experiments with annular fission chamber: aa') neutron beam, 1) scatterer (D_2O or H_2O), 2) annular electrode coated with bismuth.

The mathematical formulation of the method utilized was given by Tambovtsev.[24] He derived equations expressing the relationship between the experimentally determined values of $\nu_1(x)$ and $\nu_2(x)$ and the values of the function

---

* Analysis showed that under the experimental conditions obtaining it was unnecessary to make any correction, connected with recording of elastically scattered deuterons by the detector, in the experimental value of $\nu_1(x)$.

$$S(\theta_{c.m}) = k_3\left[\sigma_{nn}(\theta_{c.m}) + \sigma_{int}(\theta_{c.m})\right] \qquad (11)$$

in relative units; here k_3 is a constant coefficient.

Table 3

Values of the function S(θ) and the interference cross section for different n-scattering angles

$\theta^{\circ}_{c.m}$	$S(\theta_{cm})_{rel}$	$S'(\theta_{cm})$	$S''(\theta_{cm})$	$\sigma^{max}_{int}(\theta_{cm})$	$\overline{S(\theta_{c.m})}$
		10^{-27} cm^2 ster^{-1}			
12	2,1±0,4	7,7±1,5	8,4±2,3	—	7,9±1,5
16	1,6±0,3	5,8±1,2	6,4±1,7	—	6,0±1,0
20	1,3±0,2	4,7±0,8	5,2±1,6	—	4,8±0,7
30	0,85±0,2	3,1±0,8	3,4±1,2	—	3,2±0,6
40	0,85±0,2	3,1±0,8	3,4±1,2	0,6	3,2±0,6
50	0,94±0,2	3,4±0,8	3,8±1,3	0,36	3,5±0,8
60	1,03±0,2	3,7±0,8	4,1±1,3	0,20	3,8±0,6
70	1,00±0,2	3,6±0,8	4,0±1,1	0,10	3,75±0,6
80	1,00±0,2	3,6±0,8	4,0±1,1	0,09	3,75±0,6
90	0,97±0,25	3,5±1,0	3,9±1,4	0,04	3,6±0,8

$\sigma_{nn}(\theta_{c.m})$

In the computations due account was taken of the absorption of neutrons in the scatterer, the distribution in energy of the incident neutrons and the efficiency of the fission chamber in detecting neutrons of different energies; the latter was found on the basis of our earlier measurements[3] of the fission cross section for bismuth at 120 and 380 Mev, as well as on the basis of experiments on the fission of bismuth, induced by high-energy protons.

The numerical values of the function $S(\theta_{c.m})$ in relative units found in Ref. 24 are listed in the second column of Table 3. According to calculations* the effective energy to which the listed values and the function pertain is 300 Mev.

In the present investigation we used two independent methods for determining the values of $S(\theta_{c.m})$ in absolute units. In the first of these, the integral of $S(\theta_{c.m})$ taken over all the scattering angles was equated to the difference between the total cross sections for n-d and n-p scattering:

$$\int S(\theta_{c.m})\,d\Omega = \sigma^{total}_{nd} - \sigma^{total}_{np} \qquad (12)$$

In view of the weak energy dependence of these cross sections, in normalizing the values, we used the value of this difference (appropriately corrected for the effect of meson production) found from measurements with neutrons of 380 Mev mean effective energy, i.e., $(22 \pm 1.5)\cdot 10^{-27}$ cm^2. The values of the function normalized in this manner are listed in the third column of Table 3.

The second method of normalizing $S(\theta_{c.m})$ is based on a procedure, developed by us, for determining the absolute n-n scattering cross sections by means of comparing these cross sections with those for n-p scattering.

In later experiments we used a new instrument, which is now called a "neutron telescope."** In these experiments we utilized the principle of recording high energy neutrons from n-p or n-n collisions by

---

* The calculations were carried out by E. P. Tambovtsev in the laboratory of N. P. Bogoliubov; the authors of the present report take this occasion to thank both of them.

** A similar instrument was later independently designed and used by Hill et al[25] for measuring the total n-p and n-n interaction cross sections at 1.4 ± 0.2 Bev.

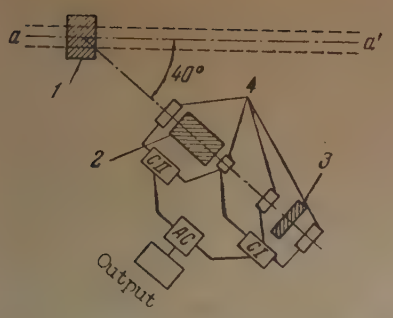

Fig. 8. Diagram of neutron telescope: aa') neutron beam, 1) scatterer, 2) converter, 3) absorber, 4) scintillation counter; CI) triple coincidence circuit, CII) double coincidence circuit, AC) anticoincidence circuit.

counting the "recharge" protons formed in a converter of light matter, located in the path of the neutrons (Fig. 8). The protons were counted by a telescope set at an angle of 40° to the neutron beam and consisting of three scintillation counters connected for coincidence (circuit CI in Fig. 8). In order to obviate the recording of charged particles emanating from the scatterer we made use of a coincidence circuit designed to record pulses from two counters located immediately in front and behind the converter (circuit CII) and connected in anti-coincidence with circuit CI. The recording threshold for neutrons (cut-off energy) is determined as usual by the thickness of a copper absorber mounted in the path of the protons between the second and third counters of circuit CI.

As a result of the experiments made with the neutron telescope and small scatterers of D_2O and H_2O, as well as of CH_2 and C, and with the aid of the data on $\sigma_{np}(\theta_{c.m})$, it was found that for neutrons of 380 Mev mean energy and $\theta_{c.m} = 85^\circ$

$$S(85^\circ) = (4.0 \pm 1.1)\cdot 10^{-27}\ \text{cm}^2\ \text{sterad}^{-1} \qquad (13)$$

The absolute values of the function $S(\theta_{c.m})$, deduced by means of (13), are listed in the fourth column of Table 3. The sixth column of the table shows the values of $\overline{S(\theta_{c.m})}$, computed by averaging the results obtained with the two methods of normalizing. Inasmuch as at angles $\theta_{c.m} \geqslant 50^\circ$ the values of $\sigma_{int}(\theta_{c.m})$ constitute only a small correction, the cross sections for $\theta_{c.m} \geqslant 50^\circ$, listed in the sixth column represent the differential cross sections for neutron scattering by free neutrons. In the average

$$\sigma_{nn}(\theta_{c.m}) = (3.7 \pm 0.6)\cdot 10^{-27}\ \text{cm}^2\ \text{sterad}^{-1} \qquad (14)$$

It will be seen that in the investigated angular range ($50 \leqslant \theta_{c.m} \leqslant 90^\circ$) the cross section $\sigma_{nn}(\theta_{c.m})$ agrees, within the limits of the experimental error, with the cross section $\sigma_{pp}(\theta_{c.m})$, measured at the same angle, and, apparently is also weakly dependent on the scattering angle. In view of this it is reasonable to assume that at 300 Mev the n-n scattering cross section is determined primarily by the interaction of neutrons in the $^1S_0$ and $^3P_0$ states, i.e., the states which also play a predominant role in p-p scattering.

Further evidence in favor of the equality of nuclear n-n and p-p interactions at high energies and, consequently, in favor of charge symmetry of nuclear forces is furnished by the experimentally established equality (within the limits of experimental error) of the total n-d and p-d interaction cross sections at the same incident-nucleon energy: according to our measurements (see Table 2) $\sigma_{nd}^{total} = (57 \pm 2)\cdot 10^{-27}$ cm^2 at $E_n = 380$ Mev, while according to the data of Ref. 26, $\sigma_{pd}^{total} = (55.6 \pm 2.2)\cdot 10^{-27}$ cm^2 at $E_p = 408 \pm 10$ Mev.

The equality of the n-n and p-p interactions and the circumstance that the difference $\sigma_{nd}^{total} - \sigma_{pd}^{total}$ in the 200-600 Mev region is close

to the value of the total p-p interaction cross section measured at the same energies (see Fig. 4) lead us to conclude that at these energies interference effects make only a small contribution to the total cross section for n-d interaction. The noted rapid increase in the cross section difference at energies above 300 Mev is apparently due to the great increase in the probability of meson production in n-n collisions, very much as in the case of p-p collisions.

Juxtaposition of the determined differential n-n scattering cross sections with the corresponding cross sections for n-p scattering shows that the following inequality obtains

$$\sigma_{np}(90^\circ) \geqslant \frac{1}{4}\sigma_{nn}(90^\circ)$$

and that, consequently, the results of the n-n scattering experiments are also not in conflict with the charge independence of nuclear forces hypothesis.

Conclusions

The following conclusions may be drawn from the discussion of the experimental data cited above.

1. At 380 Mev neutron energy the contributions made by exchange and ordinary forces to the interaction between neutrons and protons are nearly equal; spin-exchange and spin-nonexchange forces participate in the exchange interaction of nucleons with intensities of the same order of magnitude.

2. The differential and total elastic n-p scattering cross sections change little with energy from 260 to 380 Mev.

3. The interaction of 380 Mev neutrons with protons is primarily elastic in character. The meson production cross section at 380 Mev amounts to only 3% of the total n-p interaction cross section. The contribution of inelastic processes (meson formation) increases rapidly with increasing energy and at 590 Mev already accounts for about 25% of the total interaction cross section.

4. The data obtained in investigating the interaction of neutrons in the 300-600 Mev interval with neutrons and deuterons are evidence in favor of charge symmetry of nuclear forces in this energy region.

5. The results of the experiments on scattering of 300-380 Mev neutrons by nucleons do not conflict with the charge independence of nuclear forces hypothesis. Qualitative analysis of experimental data shows that the interaction of nucleons in states with different isobaric spins differs markedly; the intensity of interaction of states with isobaric spin zero decreases substantially with increasing energy up to 590 Mev.

6. The next stage of investigation (in line with utilizing the concept of charge independence of nuclear forces), concurrently with refining the present data on scattering by non-polarized neutron beams, should be separate determination of the interaction between nucleons in different spin states with a given value of isobaric spin by means of experiments with polarized beams.

In conclusion the authors desire to express their gratitude to M. G. Meshcheriakov, I. Ia. Pomeranchuk, Ia. A. Smorodinski and L. I. Lapidus for their interest in the work and valuable discussions. We thank the entire operating crew, headed by A. V. Chestnyi, of the synchrocyclotron of the Institute of Nuclear Problems of the USSR Academy of Sciences for their efficient and helpful work.

Institute of Nuclear Problems of the
Academy of Sciences of the USSR

References

1. V.P.Dzhelepov, Iu. M.Kazarinov, IIaP AN SSSR (Institute of Nuclear Problems of the USSR Academy) Report (June 1951); Doklady AN SSSR 99, 939 (1954).
2. V.P.Dzhelepov, Thesis, IIaP AN SSSR , 1954.
3. V.P.Dzhelepov, Iu.M.Kazarinov, B.M.Golovin & V.B.Fliagin, Report IIaP AN SSSR (1953); V.B.Fliagin, Report IIaP AN SSSR (1954).
4. V.P.Dzhelepov, Iu.M.Kazarinov & V.B.Fliagin, Report IIaP AN SSSR (1952); Doklady AN SSSR, 100, 655 (1955).
5. V.P.Dzhelepov, B.M.Golovin & V.I.Satarov, Report IIaP AN SSSR (1953); Doklady AN SSSR 99, 943 (1954).
6. V.P.Dzhelepov, V.I.Satarov & B.M.Golovin, Report IIaP AN SSSR (1954).
7. V.P.Dzhelepov, V.B.Fliagin & K.O.Oganesian, Report IIaP AN SSSR (1954).
8. Iu.M.Kazarinov, Iu.N.Simonov, Report IIaP AN SSSR (1954).
9. H.Rosenfeld, Phys. Rev., 96, 139 (1954).
10. A.Hartzler, R.Siegel & W.Opitz, Phys. Rev., 95, 591 (1954).
11. V.I.Gol'danskii, A.L.Liubimov & B.V.Medvedev, USP fiz. nauk. 48, 531 (1952); 49, 3 (1953).
12. M.G.Meshcheriakov, N.P.Bogachev, B.S.Neganov & E.V.Piskarev, Doklady AN SSSR 99, 955 (1954).
13. N.P.Bogachev & I.K.Vzorov, Doklady AN SSSR 99, 931 (1954).
14. A. Shapiro, C. Leavit & F. Chew, Bull. Am. Phys. Soc., 29, 4, 75 (1954).
15. V.Nedzel, Phys. Rev., 94, 174 (1954).
16. G. Gurnsey, R. Mott & B. Nelson, Phys. Rev., 88, 15 (1952).
17. E. Kelly, C. Leith, E. Segré & C. Wiegand, Phys. Rev., 79, 96 (1950).
18. Ia.A.Smorodinskii, Report AN SSSR (1953); Problemy sovremennoi fiziki (Problems of modern physics) Issue 7, p.7, M., 1954.
19. I.Ia.Pomeranchuk, Doklady AN SSSR, 78, 249 (1951); Zhur. eksp. i teor. fiz., 21, 1113 (1951).
20. F.Chew, Phys. Rev., 84, 710 (1951).
21. W.Powell, The results of his investigation are cited in Ref. 20.
22. J. Cladis, I. Hadley & W.Hess, Phys. Rev., 86, 110 (1952).
23. B.M.Golovin, Report IIaP AN SSSR (1954).
24. E.P.Tambovtsev, Report IIaP AN SSSR 1952 & 1954.
25. D.Hill, T.Coor, W.Hornyak, L.Smith & G.Snow, Bull.Am.Phys.Soc., 29, 1, 54 (1954).
26. J.Marshall, L.Marshall & V.Nedzel, Phys.Rev., 91, 717 (1953).

PRODUCTION OF NEUTRAL MESONS BY HIGH-ENERGY NUCLEONS

- M. S. Kozodaev, A. A. Tiapkin, Iu. D. Baiukov, A. A. Markov and Iu. D. Prokoshkin

The existence of showers comprising high-energy photons and electrons in addition to hard penetrating particles has been demonstrated in numerous investigations of cosmic rays made with the aid of cloud chambers,[1-7] ionization chambers and counters,[8-10] and thick nuclear emulsions.[11] It has been established in a number of these investigations that heavy particles, electrons and photons are produced in a single high-energy nuclear interaction event. Oppenheimer[12] in 1947 first advanced the hypotheses that charged and neutral mesons may be formed in commensurate quantities in collisions of high-energy nucleons and that neutral mesons may disintegrate into two photons.

However, there was at that time no experimental data offering convincing proof of the existence of neutral mesons.

The first real experimental confirmation of the existence of neutral pi mesons was obtained by Bjorklund, Crandall, Moyer and York[13] in an investigation of the high-energy γ-radiation from targets of various substances (Be, C, Cu and Ta) bombarded with 340 Mev protons. The γ-spectra in this investigation were measured by means of a two-channel pair spectrometer. Investigation of the photon energy spectra, measured at 0, 47, 133 and 180° to the direction of the incident protons, showed that a plausible explanation of the regularities observed in the spectra is predicted on assuming that the γ-quanta are obtained as a result of the decay of neutral particles having a mass of about 300 m_e, produced in collisions of the protons with the nuclei of the target. Analysis of the variation of the γ-radiation intensity with the proton energy further substantiated the assumption that the hard quanta are created as the result of the decay of neutral pi mesons, since it was found that the threshold for the formation of the γ-quanta lies in the 170-200 Mev region. Below the threshold energy only a few radiation loss photons were recorded.

Shortly after the aforementioned investigation, Steinberger, Panofsky, and Steller[14] demonstrated conclusively that neutral pi mesons are also formed when C and Be nuclei are irradiated with 330 Mev gamma-quanta. In this investigation the high-energy γ-quanta were recorded with two scintillation-counter telescopes connected for coincidence. The procedure used made it possible to prove experimentally that neutral pi mesons break-up into two γ-quanta. Finally, Carlson, Hooper and King,[15] using thick nuclear emulsions exposed to cosmic rays at 21 km above sea level, showed that π^0 mesons are also formed in the stars produced by the high-energy particles; they also estimated the lifetime of these π^0 mesons.

The mass of the neutral pi meson was evaluated from the data of the above investigations and was found to lie between 280 and 300 electron masses. From the fact that the π^0 meson disintegrates into two gamma-quanta it was deduced that the spin of the π^0 meson is zero spin. Since the lifetime of neutral mesons is short (on the order of $5 \cdot 10^{-15}$ sec) and they can travel only a few microns before decaying, π^0 mesons can be studied only by the γ-quanta, resulting from their disintegration. For the same reason, the nuclear interactions of the π^0 mesons can be studied only by investigating the nucleons of the nucleus in which they are created.

The present report is devoted to a series of investigations of the production of neutral mesons by high-energy nucleons, carried out by the authors in 1950-1954, on the accelerator of the Institute of Nuclear Problems of the USSR Academy of Sciences.

An investigation by M. S. Kozodaev and A. A. Markov[16] made in the first half of 1950 showed that hard γ-quanta are emitted when a copper target is bombarded with 560 Mev α-particles. The hard γ-radiation was studied in the 30-100 Mev interval by means of a 12-channel hodoscopic pair spectrometer. In spite of the considerable background present during these measurements, a maximum was observed in the gamma spectrum in the 70-80 Mev region. It was concluded from the character of the energy spectrum and the measured yield of hard quanta that a substantial portion of the observed hard γ-radiation cannot be attributed to the excitation of the nuclei and to Bremsstrahlung of the α-particles.

In 1951-2 two studies of the production of pi mesons by 470 Mev protons were made. Equipment was built for a detailed study of the energy spectra and the angular distribution of the hard γ-quanta. To

this end, Baiukov, Kozodaev, Markov, Sinaev, and Tiapkin[30] substantially improved the 12-channel pair spectrometer used in the above-mentioned 1950 investigation, more than doubling the energy measurement range (the range of γ-quantum energy), enhancing the recording efficiency and improving the selection and registration systems.

The spectrometer was capable of measuring γ-quantum energies in the 20 to 460 Mev range. Polepieces with a spread of 60° were used for measurements in this range. The gap between polepieces was 3 cm. Varying the magnetic field intensity in the gap changed the range of the energies recorded. The maximum magnetic field intensity was 16,000 oersteds.

Tantalum converters, measuring 2 x 2.5 cm, from 0.02 to 0.035 cm thick, depending on the range of energies measured, were employed. Since thin converters had to be used for the measurements at low energies, the efficiency of the spectrometer was relatively low; polepieces set at an angle of 180° were used in measuring the spectra in the 20-110 Mev range. The gap between polepieces in this case was 4 cm; the tantalum converters used measured 3 x 6 cm.

Rows of coordinate proportional counters, recording positrons and conversion electrons, were located along the sides of the polepieces. Each row comprised six groups of counters (channels). Two rows of selection counters were placed behind the coordinate counters. The proportional counters were filled with pure methylal ($CH_2(OCH_3)_2$). The copper cathode of each counter was 8 mm in diameter.

Pulses from each group of coordinate counters and from each row of selection counters were amplified and shaped. The shaped pulses from the selection counters were fed to a quadruple-coincidence network. The quadruple-coincidence pulses were in turn applied to a triple-coincidence circuit together with the coincidence pulses from the electron and positron recording coordinate counters. This resulted in a sextuple-coincidence system, which produced the control pulse. The resolving time of the coincidence circuits was $5 \cdot 10^{-7}$ sec. In the presence of a control signal, the amplified pulses from the coordinate counters actuated a system of six-contact relays. The contacts of these relays were connected to operate 11 electromechanical registers, each energized by the closing of a different pair of relay contacts, corresponding to the recording of γ-quanta in a specific energy interval. The number of pairs in the activation of which each coordinate counter participated, was also recorded by an appropriate electromechanical counter. The readings of these 12 counters allowed of evaluating the relative efficiency of the coordinate counters.

In their investigation of gamma-energy spectra, Baiukov, Kozodaev, Markov, and Tiapkin[17] mounted targets of Be, C, Cu, Pb in the internal proton beam of the accelerator. In their experiments, the gamma spectrometer 2 (see Fig. 1) was placed in housing 1, made of concrete slabs, 11 meters distant from target 3 along line 4, tangent to the circular orbit of the protons. The γ-quanta spectra were measured at angles of 0 and 180° to the direction of motion of the protons. The intensity of the γ-quanta flux was gaged by monitor 5, which recorded the number of γ-quanta from the Čerenkov radiation of the electrons produced by the quanta. This counter effectively recorded all γ-quanta of energies above 10 Mev. In determining the cross section for the production of the π^0 mesons, the activation of polystyrol films was used as a measure of the proton flux through the beryllium target.

The energy spectra of the γ-quanta formed in the beryllium target are shown in Figs. 2 and 3 for the 0 and 180° observation angles. Some

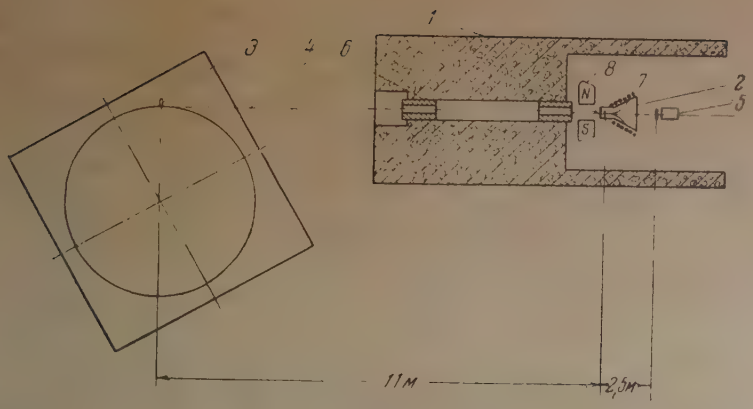

Fig. 1. Diagram of experiment: 1) concrete housing, 2) γ-spectrometer, 3) target, 4) photon beam, 5) monitor, 6) collimator, 7) coordinate counters, 8) magnet.

60,000 electron-positron pairs were counted in determining the spectrum in the 0° direction. The spectrum for 180° is plotted on the basis of 5,000 pairs.

The ratio of the γ-quanta yields at 0 and 180° was measured with a telescope containing a Čerenkov-radiation counter. The relative values of the proton flux through the beryllium target were determined in these measurements

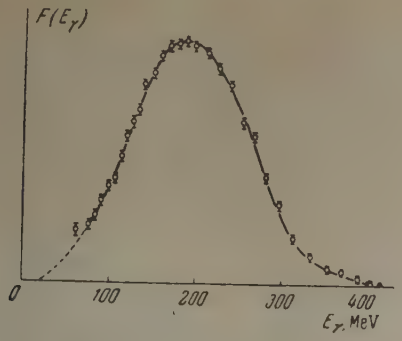

Fig. 2. Energy spectrum of γ-quanta produced on Be nuclei by 470 Mev protons, recorded at 0° to direction of protons.

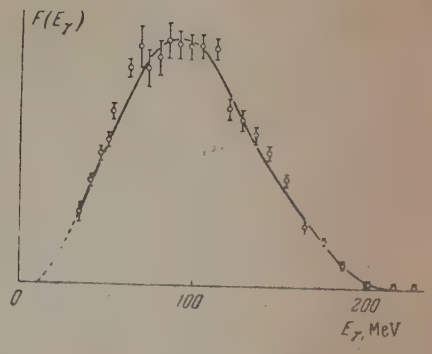

Fig. 3. Same as Fig. 2, but at 180°.

from the level of radioactivity induced in copper foils. The ratio of the numbers of electron-positron pairs recorded by the detector for the same value of proton flux at 0 and at 180° was 6.4 ± 0.4. Since the mean efficiencies of recording the γ-quanta were not identical at 0 and at 180°, owing to the energy difference, the ratio of the differential cross section for photon production after appropriate correction for the difference in efficiencies proved to be

$$\frac{d\sigma^{\gamma}(0°)}{d\omega}\Big/\frac{d\sigma^{\gamma}(180°)}{d\omega} = 5{,}3 \pm 0{,}5.$$

When transformed to the center of mass system, the spectra obtained at 0° and 180° differ little from each other. It follows, therefore, that the π° mesons are produced as a result of collisions of the protons with individual nucleons rather than with the nucleus as a whole. The minor difference between the transformed spectra may be due to the effect of intra-nuclear motion of the nucleons. Because the protons collide with nucleons in different energy states within the nucleus there is no unique center of mass system, transformation to which would yield fully identical spectra. The effective velocity of the center of mass system for which the best coincidence

of the spectra is obtained is $\overline{\beta}_c \sim 0.4$. Measurement of the energies corresponding to end points of the spectra make it possible to determine the value of β_c corresponding to the maximum nucleon collision energy. The value of β_c found in this manner turned out to be 0.36, whence it follows that the maximum kinetic energy of the nucleons in the nucleus, manifested in the collisions in question, is approximately 20 Mev.

Analysis of the spectra shows that the angular distribution of the created neutral mesons in the colliding-nucleon center of mass-system is anisotropic. If the π° meson distribution were isotropic, the maximum of the γ-spectrum, measured at 0° to the direction of the proton beam, should be located in the vicinity of 105 Mev and the position of this maximum should be independent of the character of the energy distribution of the mesons. Actually, the spectrum measured by us has a maximum at approximately 190 Mev. The considerable shift of the γ-spectrum maxima into the region of higher energies indicates that the neutral mesons are generated mainly not in the S state. To explain the observed shift of the maximum of the spectrum one must assume that the neutral mesons, formed in nucleon collisions are ejected (in the c.m. system) predominantly at small angles to the direction of motion of the colliding nucleons. Whitehead and Richman[18] established that the angular distribution of the positive pi mesons, formed in p-p collisions, is satisfactorily described by the $\cos^2\theta$ law. A study of the $p + p \rightarrow \pi^+ + d$ reaction at 460 Mev, carried out at the Institute of Nuclear Problems by Mescheriakov, Neganov, Bogachev and Sidorov[19] showed that the angular distribution of the mesons is characterized by $(0.24 + \cos^2\theta)$. According to the calculations of Watson and Bruckner[20] such an angular distribution can be obtained by using the pseudo-scalar variant of meson theory with pseudo-vector coupling. If a considerable portion of the π° mesons formed in collisions of protons with beryllium nuclei is also distributed according to the $\cos^2\theta$ law, the peak of the γ-spectrum will be shifted to the side of higher energies.

We must note here that when neutral pi mesons are produced by protons on beryllium nuclei, their angular distribution will not necessarily obey the $\cos^2\theta$ law, because in this case the pi mesons are formed in collisions of protons with nucleons which are bound in the beryllium nucleus, and which are in various energy states at the instant of collision. Scattering and absorption of π° mesons by the nuclei in which they are formed must also influence their angular distribution. The scattering should tend to equalize the angular distribution: make it more isotropic in the laboratory system. In order to study the effect of scattering of π° mesons on their angular distribution, we measured the γ-ray spectra obtained with targets of both light elements (Be and C) and heavy elements (Cu and Pb). If the scattering of π° mesons really does affect the angular distribution substantially, then in the case of heavy elements the maximum of the γ-spectrum should be shifted toward 70 Mev, i.e., toward the position of the maximum for isotropic distribution. Our measurements showed that, within the limits of the experimental error, the γ-ray spectra have virtually equal end points in the case of both light (Be, C) and heavy (Cu, Pb) elements (Figs. 2 and 4). If the peaks of the spectra for the heavy elements are shifted at all into the region of lower energies, the shift certainly does not exceed 20 Mev. This leads to the conclusion that the scattering of π° mesons in nuclear matter is weak; this is, apparently to be explained by the predominance of absorption of mesons.

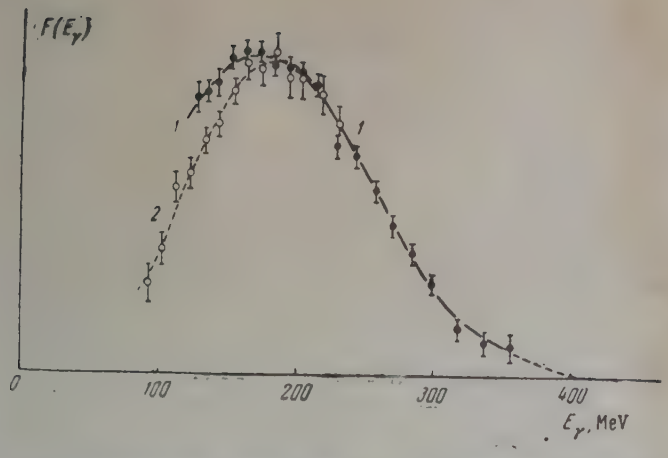

Fig. 4. Energy spectra of γ-quanta formed in bombarding copper (1) and lead (2) targets with 470 Mev protons, recorded at 0°.

et al[22] give the energy spectra of γ-quanta of beryllium targets with 430 Mev protons. These spectra are in agreement with our results.

Crandall and Moyer,[21] in a report published late in 1953, give the spectra of γ-quanta from the decay of neutral mesons, produced by bombardment of a carbon target with 340 Mev protons. This report confirms our conclusion that the angular distribution of the neutral mesons is anisotropic, even when they are formed on complex nuclei, for the maximum of the spectrum, as measured by Crandall and Moyer, also occurs at a much higher energy than would correspond to an isotropic angular distribution. Marshall produced in the bombardment

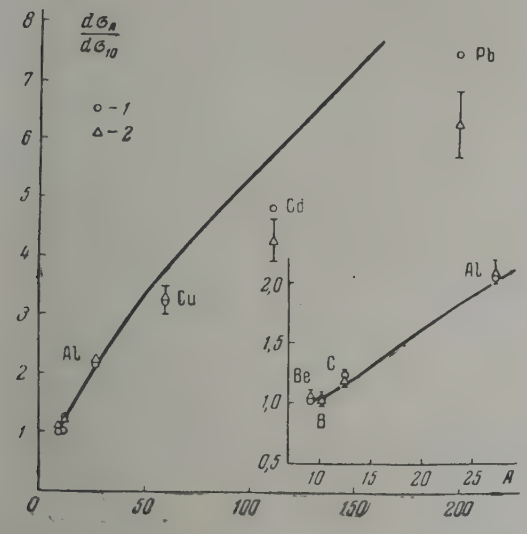

Fig. 5. Relative cross sections for the production of γ-quanta at 0° by 470 Mev protons on the nuclei of different elements: 1) Data based on Čerenkov radiation counter measurements; 2) data based on γ-spectrometer measurements. The curve represents a dependence of the form

$$0{,}16\left(A-\frac{2}{3}Z\right)A^{-1/3}$$

In addition to investigating the spectra and the character of the angular distribution of the γ-quanta, Kozodaev, Tiapkin, Baiukov, Vanetsian, and Markov,[17,23] in 1951-1952, measured the cross sections for the production of neutral mesons by 470 Mev protons on various elements. In these experiments the photon flux was measured with two different instruments: a 12-channel pair spectrometer and a telescope containing a Čerenkov radiation counter. The values of the proton flux through the target were determined from the activation of polystyrol films and from the gamma-activity induced in copper foils calibrated by the calorimetric method. The positron activity of the polystyrol films was measured by means of a set up recording γ-γ coincidences. Fig. 5 shows the results of measurement of relative yields of γ-quanta at 0°, obtained with the nuclei of various elements (the yield of γ-quanta at A = 10 was taken as the reference unit). The values of the relative outputs of the γ-quanta, measured with the spectrometer and with the Čerenkov-radiation counter telescope agree,

within the limits of the statistical error, in the case of Be, B, C, Al and Cu. In the case of heavier elements (Cd, Pb) the yields recorded with the Čerenkov counter were somewhat higher than the values obtained with the γ-spectrometer. This discrepancy is due to the missed counts due to overloading of the telescope counters (the telescope consisted of two rows of proportional counters and a Čerenkov counter).

As can be seen from the curve of Fig. 5, the cross section for the production of γ-quanta on complex nuclei increases more slowly than the number of nucleons in the nucleus. This is indicative of strong absorption of π^0 mesons in nuclear matter.

If we assume that the mesons are formed on all the nucleons of the nucleus, the total cross section for the production of π^0 mesons on a nucleus of mass number A can be represented in the following form

$$\sigma_A = f_A [\bar{\sigma}_{pn}(A - Z) + \bar{\sigma}_{pp} Z],$$

where $\bar{\sigma}_{pn}$ and $\bar{\sigma}_{pp}$ are the mean values of the cross section for the production of π^0 mesons on the intra-nuclear neutrons and protons and the factor f_A takes into account the absorption of mesons in the nucleus. According to calculations of Bruckner et al,[24] made for the case when the meson absorption cross section is much greater than the scattering cross section, the factor f_A is given by the following function:

$$f_A = 3\left[\frac{1}{2x} - \frac{1}{x^3} + \frac{1}{x^3}(1 + x)e^{-x}\right],$$

where $x = \frac{r_0 \cdot A^{1/3}}{\lambda_\pi}$, and λ_π is the mean free path of the π^0 mesons in the nuclear matter. From the γ-quanta yield, obtained experimentally for Be, C, and Al, we calculate, using this expression for f_A, the upper limit of the mean free path of the neutral mesons for absorption in the nucleus: $\lambda_\pi \leqslant 1{,}5 r_0$, where $r_0 = 1.3 \cdot 10^{-13}$ cm. From experiments described below, it follows that $\frac{\sigma_{pp}}{\sigma_{pn}} = \frac{1}{3}$.

If mesons are formed only on the surface nucleons ($x \ll 1$), the total cross section for the production of π^0 mesons on a complex nucleus should be proportional to $\left(A - \frac{2}{3} Z\right) A^{-1/3}$. As can be seen from Fig. 5, in the region of heavy nuclei the differential cross section for the formation of γ-quanta increases at a much slower rate than called for by the law corresponding to strong absorption of mesons ($\lambda_\pi \sim 0$). This indicates that there are other processes affecting the production of π^0 mesons on complex nuclei. We shall return to this problem below in connection with our discussion of the results of the 1954 experiments.

The absolute differential cross section for the production of γ-quanta on carbon was determined with the γ-spectrometer and the telescope with a Čerenkov radiation counter. The differential cross section for 0^0, in 10^{-27} cm^2 sterad^{-1} units equals 6.7 ± 2 as measured with the spectrometer and 5.8 ± 2 as measured with the telescope. The average value of the cross section is $(6.2 \pm 1.6) \cdot 10^{-27}$ cm^2 sterad^{-1}.

We used the differential method in determining the differential cross section for p-p collisions; i.e., we subtracted the γ-quanta yield from carbon from the yield from a polyethylene target. It was found that the differential cross section for the production of

γ-quanta in p-p collisions at 470 Mev (at $\theta = 0^\circ$) equals

$$\left(\frac{d\sigma^\gamma}{d\omega}\right)^{0^\circ}_{pp} = (0{,}26 \pm 0{,}17)\cdot 10^{-27} \text{ см}^2 \text{ sterad}^{-1}$$

as measured with the telescope and

$$\left(\frac{d\sigma^\gamma}{d\omega}\right)^{0^\circ}_{pp} = (0{,}30 \pm 0{,}20)\cdot 10^{-27} \text{ см}^2 \text{ sterad}^{-1}$$

as measured with the γ-spectrometer.

The average value of the differential cross section from the two series of measurements is $(0.28 \pm 0.18)\cdot 10^{-27}$ cm^2 sterad^{-1}.

The differential cross sections obtained for the formation of γ-quanta make it possible to determine the total cross section for the production of neutral mesons. For this purpose it is necessary to know the angular and energy distributions of the mesons in the center of mass system or the angular distribution of the γ-quanta in the laboratory system. The total cross section for the production of neutral mesons is related to the differential cross section by

$$\sigma_{\pi^0} = \frac{1}{2}\,\alpha\cdot\Omega\cdot\left(\frac{d\sigma^\gamma}{d\omega}\right)_{0^\circ},$$

where $\alpha = \frac{1-\beta_c}{1+\beta_c}$ is a coefficient which takes into account the transformation of the solid angles for gamma rays and Ω is a coefficient, dependent on the angular and energy distributions of the π^0 mesons. In case of collisions of 470 Mev protons with hydrogen nuclei α = 0.38. Evaluations, using the momentum approximation, showed that for complex nuclei the most reliable value under the conditions of our experiments is $\bar{\alpha}$ = 0.42, corresponding to β_c = 0.41. The evaluation was made on the assumption that distribution in momentum of the nucleons in the nucleus is Gaussian, with the root mean square momentum being 120 Mev/c (the corresponding energy is $\sim$8 Mev), and that the cross sections for the $p + p \to \pi^0 + 2p$ and $p + n \to \pi^0 + (p + n)$ reactions are described by the functions $\sigma_{pp} \sim p^6_{max}$ and $\sigma_{pn} \sim p^3_{max}$ where p_{max} is the maximum possible momentum of the meson; the ratio of the p-p and p-n cross sections at a 470 Mev was assumed to be 1/3.

The coefficient Ω can have different values depending on the energy and angular distributions of the π^0 mesons in the c.m. system; in the case of isotropic distribution, it equals 4 . The value of this coefficient was found according to the following equation:

$$\Omega = \frac{2\pi\int_0^\pi \varphi(\theta)\sin\theta\cdot d\theta}{\int_0^\infty f(\varepsilon)\cdot W(\varepsilon)\,d\varepsilon}.$$

Here $\varphi(\theta)$ is the angular distribution of the mesons in the center of mass system, ε is the total energy of the mesons in mc^2 units, $W(\varepsilon)$ is the energy spectrum of the mesons, and

$$f(\varepsilon) = \int_{\varepsilon_{\gamma min}}^{\varepsilon_{\gamma max}} F(\varepsilon_\gamma, \varepsilon)\,d\varepsilon_\gamma,$$

where $F(\varepsilon_\gamma, \varepsilon)$ is the energy spectrum of the γ-quanta, corresponding to a given angular distribution of π^0 mesons having an energy ε. In case of a $\cos^2\theta$ law angular distribution we have

$$f(\varepsilon)=\frac{\varepsilon^2+1}{\varepsilon^2-1}-\frac{\varepsilon}{(\varepsilon^2-1)^{3/2}}\ln\frac{\varepsilon+\sqrt{\varepsilon^2-1}}{\varepsilon-\sqrt{\varepsilon^2-1}}.$$

The energy spectrum $W(\varepsilon)$ was approximated from the measured γ-spectrum; on the assumption that the angular distribution is proportional to $\cos^2\theta$ we found $\Omega = 2.5$. In the case of neutral meson production, it is actually better to approximate the angular distribution of the mesons by the expression $a + \cos^2\theta$, and, therefore, the coefficient Ω should be somewhat greater than 2.5π. A precise value of the factor $a\Omega$ can be found by measuring the angular distribution of the γ-quanta in the laboratory system.

Using the average value of the differential cross section for carbon - $(6.2 \pm 1.6)\cdot 10^{-27}$ cm^2 sterad^{-1} - we obtain (assuming the angular meson distribution to be proportional to $\cos^2\theta$) that the total cross section for the production of pi mesons by 470 Mev protons on carbon is

$$\sigma_C = (10{,}2 \pm 2{,}6)\cdot 10^{-27}\ \text{см}^2.$$

Using the average value of the differential cross section

$$\left(\frac{d\sigma^\gamma}{d\omega}\right)^{0^\circ}_{pp} = (0{,}28 \pm 0{,}18)\cdot 10^{-27}\ \text{см}^2\ \text{sterad}^{-1}$$

we obtain for the total cross section for the production of π° mesons in p-p collisions

$$\sigma_{pp} = (0{,}67 \pm 0{,}43)\cdot 10^{-27}\ \text{см}^2$$

in case of an isotropic meson distribution and

$$\sigma_{pp} = (0{,}42 \pm 0{,}27)\cdot 10^{-27}\ \text{см}^2$$

in case of an angular meson distribution proportional to $\cos^2\theta$. This result agrees with the data obtained in the investigation of Ref. 25.

In 1954 A. A. Tiapkin, M. S. Kozodaev and Iu. D. Prokoshkin[26] investigated the processes of π° meson production in collisions of 670 Mev protons with the nuclei of various elements. To measure the flux of hard γ-quanta they developed a high-efficiency telescope consisting of a scintillation counter and a Čerenkov radiation counter. The spectral response of this telescope was determined experimentally, and this enabled them to make certain conclusions concerning the character of the γ-ray spectrum. By increasing the distance between the telescope components and placing absorbers between them it was possible to increase its energy threshold; this also allowed of making a rough analysis of the spectra. The proton flux through the target was determined calorimetrically by measuring the temperature difference at the ends of a calibrated heat conductor, which also served as the target holder.

The telescope was used to measure the relative γ-quanta yields from the decay of π° mesons produced in the bombardment of H, D, Li, Be, B, C, Al, Cu, Cd, Sn and Pb nuclei with 670 Mev protons. The γ-quanta fluxes were measured at 0° and 180° to the direction of motion of the protons. The results of the measurements are given in Fig. 6. It will be seen that the yield of γ-quanta at 0° increases appreciably more slowly than according to the $A^{2/3}$ law. This agrees with the results of our measurements with 470 Mev protons. However, their measurements at 670 Mev of the γ-flux at 180° showed that the dependence of the γ-quanta yield on the atomic weight is in good

agreement with the $A^{2/3}$ law. The observed small systematic departure from this law can be explained by the difference in the π^0 meson production cross sections for p-p and p-n collisions. If this difference is taken into account, the γ-quanta yield at 180° from the decay of the mesons produced on the surface of the nucleus, should be proportional to $\left[\left(\frac{A-Z}{A}\right)\bar{\sigma}_{pn}+\frac{Z}{A}\bar{\sigma}_{pp}\right]A^{2/3}$. The best agreement with the experimental results obtains if we take

$$\frac{\bar{\sigma}_{pn}}{\bar{\sigma}_{pp}}=2{,}0\pm0{,}5.$$

If we attribute the observed variation in the values of the differential cross sections for the production of γ-quanta at 180° on the nuclei of different elements to the strong absorption of the mesons created throughout the nucleus, we must assume $\lambda_\pi \leqslant 0{,}5\, r_0$. This value of the absorption mean free path for neutral mesons in nuclear matter is substantially less than the value of λ_π obtained for charged mesons by direct measurements. This means that, in addition to absorption, there must be other effects that substantially lower the probability of meson formation on the nucleons inside the nucleus.

We measured the ratio of the γ-quanta yields at 0 and 180°:

$$\eta_A=\frac{d\sigma^\gamma(0°)}{d\omega}\Big/\frac{d\sigma^\gamma(180°)}{d\omega}.$$

As can be seen from Fig. 7, where the results of our measurements are given, a rapid decrease in the value of η_A is already observed for light-nuclei. The reduction in the ratio may be due to a number of causes: partial opaqueness of the nucleus to the bombarding protons in the presence of strong meson absorption, scattering and absorption of mesons in the nucleus, etc. The fact that the gamma yield at 0° deviates from the $A^{2/3}$ law can be readily explained for the heavy elements by recourse to the partly opaque nucleus model. The greater portion of the recorded γ-radiation is produced by the decay of π^0 mesons moving from the target to the telescope (this is connected with the transformation of the solid angles). In measurements at 180°, the major portion of such mesons is liberated from the surface of the nucleus, which is freely attained by protons; and hence one can naturally expect the $A^{2/3}$ law to be fulfilled here, if we assume that

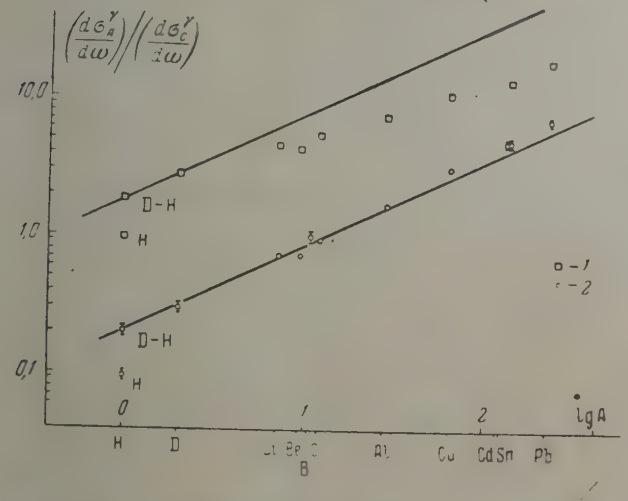

Fig. 6. Gamma-quanta yield from bombardment of different elements with 670 Mev protons: vertical scale laid off in terms of the ratio of the yield at 0 and 180° from elements of mass number A to the yield from carbon at 180°. 1) points for yield at 0° from the investigated elements; 2) same for yield at 180°. The straight lines represent a $A^{2/3}$ variation.

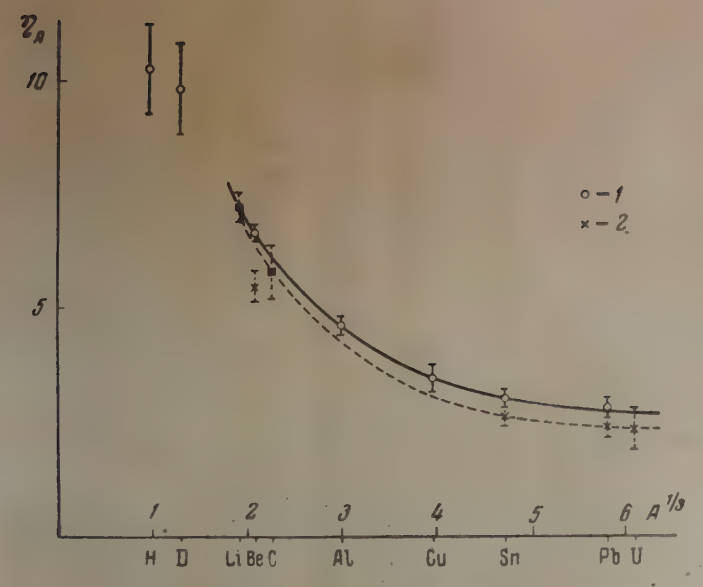

Fig. 7. Variation of γ-quanta yield ratios at 0 and 180° with mass number A: 1) according to measurements of total flux; 2) according to measurements of hard portion of flux only.

the mesons are formed principally on the surface of nuclear nucleons. On the other hand, in measurements at 0°, the surface of the nucleus, emitting most of the recorded pi mesons, is shielded from the bombarding protons by the nucleons of the target. As the mass number A increases, the shielding effect increases and consequently the ratio η_A falls off.

This shielding effect and the absorption of mesons in the nuclei, which alter the angular distribution of the γ-quanta, should also lead to softening of the γ-spectrum as a whole with increasing atomic weight. To check this we measured the γ-quanta yields and the ratio η_A for various elements using a detector with a high energy threshold (dotted curve in Fig. 7). Only the hard γ-quanta, comprising approximately 1/5 of the total γ-flux[26] were recorded in this experiment.

The accompanying table gives the values of ratios M(A)/M(12) for 0° and 180°; M(A) is the ratio of the number of hard γ-quanta to the total gamma flux for various elements.

The data show that the spectrum of the γ-quanta due to hydrogen is considerably softer than the γ-quanta spectra produced on complex nuclei.

TABLE

Elements:	H	D	Li	Be
$\left[\frac{M(A)}{M(12)}\right]_{0°}$	0,5±0,2	0,8±0,2	1,00±0,05	0,8±0,1
$\left[\frac{M(A)}{M(12)}\right]_{180°}$	0,5±0,3	0,9±0,2	1,00±0,1	1,00±0,03
Elements:	**C**	**Sn**	**Pb**	**U**
$\left[\frac{M(A)}{M(12)}\right]_{0°}$	1,00±0,04	0,92±0,5	0,95±0,04	0,92±0,04
$\left[\frac{M(A)}{M(12)}\right]_{180°}$	1,00±0,03	—	—	—

In measurements at 0°, only a small difference between the spectra for the light and heavy elements is observed. This will, apparently, be difficult to reconcile with the marked asymmetry of the angular distribution of gamma-quanta produced on heavy elements found in our experiments.

If the process of formation of π^0 mesons is symmetrical in the "forward and backward" directions in the c.m. system (and this is true for p-p collisions in view of the fact that the ejected particles are indistinguishable), the

ratio η_H is determined only by the Doppler effect and equals 9.6 at 670 Mev proton energy. According to calculations made using the momentum approximation, this ratio is reduced somewhat owing to intranuclear motion of the nucleons in a complex nucleus. Thus, if we take $\sigma_{pp} \sim p^6_{max}$, $\sigma_{pn} \sim p^3_{max}$, σ_{pp}/σ_{pn} (at 670 Mev) = 1/2, we obtain $\bar{\eta}$ = 9.0, if we assume a Gaussian law distribution of the nucleons in momentum with a root mean square momentum of 120 Mev/c, cut off at p_{max} = 200 Mev/c. On the other hand, if we assume a Fermi distribution in momentum with an end point energy of 22 Mev, we obtain $\bar{\eta}$ = 8.2.

The differential cross sections for the production of γ-quanta on hydrogen were measured, at 0 and 180°, by the differential method, i.e., by alternately bombarding graphite and polyethylene targets. Since the targets employed were virtually free of heavy impurities, we monitored the proton flux by measuring the activity of the annihilation radiation from the targets themselves. This method, though similar to the calorimetric one, has several advantages and permits excluding the influence of the shape and density of the target. The values of the cross sections (as percentages of the cross section for carbon) were 18 ± 1% at 0° and 9.5 ± 0.8% at 180°. Thus η_H = 11 ± 2. The value of η_H was also measured by the differential method with LiH and Li and was found to be 10 ± 1. The experimentally obtained values of η_H agree, within the limits of experimental error, with the theoretical value of 9.6. This is additional proof that the value η_C = 5.8 ± 0.2 obtained by us is reliable and that the ratio η_A is considerably smaller than $\bar{\eta}$ even in the region of the lightest nuclei (Li, Be, and C).

In determining the absolute cross sections for the production of π^0 mesons we took into account the absorption of the γ-quanta in both the target and air. Special experiments were run to determine the correction for taking account of the low-energy cutoff of the telescope. The efficiency of the telescope was evaluated experimentally by successively disconnecting the individual multipliers.

The differential cross section for the production of γ-quanta in p-p collisions at 0° (or 180°) in the center of mass system was determined to be

$$\left(\frac{d\sigma^\gamma}{d\omega}\right)_{pp} = (0{,}59 \pm 0{,}13) \cdot 10^{-27} \text{ см}^2 \text{ sterad}^{-1}$$

Assuming the distribution of the π^0 mesons to be isotropic, we obtain for the total meson production cross section at 670 Mev:

$$\sigma_{pp} = (3{,}7 \pm 0{,}8) \cdot 10^{-27} \text{ см}^2.$$

The differential cross section for the production of γ-quanta on deuterium was measured by the differential method (LiD - Li) and was found to be

$$\left(\frac{d\sigma^\gamma}{d\omega}\right)^{0°}_{pd} = (1{,}8 \pm 0{,}3) \cdot 10^{-27} \text{ см}^2 \text{ sterad}^{-1}$$

From this we obtain the total cross section for π^0-meson production in p-n collisions (neglecting the coupling of the nucleons in the deuterium nucleus):

$$\sigma_{pn} = (7{,}8 \pm 1{,}6) \cdot 10^{-27} \text{ см}^2.$$

An important characteristic of the meson production process is the dependence of the cross section on the collision energy of the

nucleons. Some information regarding this can also be obtained by investigating meson production on complex nuclei. However, in this case it is impossible to interpret the results rigorously, for it becomes necessary to make a number of assumptions concerning the momentum distribution of the nucleons in the nucleus, the effect of the Pauli exclusion principle, etc.

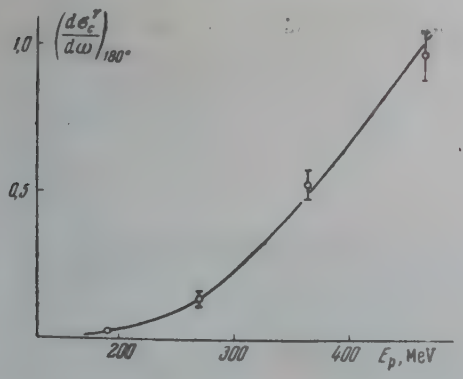

Fig. 8. Variation of the γ-quanta yield from carbon at 180° with the proton energy.

We measured[26] the cross sections for the formation of neutral mesons on carbon by 190, 270, 370, and 460 Mev protons. In these experiments the proton energy was varied by locating the carbon target inside the vacuum tank of the accelerator at different distances from the center of the proton orbits. The γ-quanta were observed at an angle of 180°. The results are shown in Fig. 8. These results are not in conflict with the energy dependence of the cross section for the production of π^0 mesons in collisions of free nucleons, as determined from other experiments.

If we compare the total cross section values obtained by us at 670 and 470 Mev — $\sigma_{pp}(670) = (3.7 \pm 0.8)\cdot 10^{-27}$ cm^2 and $\sigma_{pp}(470) = (0.5 \pm 0.3)\cdot 10^{-27}$ cm^2 — with the results of Mather and Martinelli[27] — $\sigma_{pp}(340) = (0.010 + 0.003)\cdot 10^{-27}$ cm^2 — we conclude that the rate of increase in the cross section σ_{pp} diminishes as the collision energy of the protons increases. In going from 340 to 470 Mev, the cross section increases 36 times, corresponding to the relationship $\sigma_{pp} \sim p_{max}^{6\pm1}$, where p_{max} is the maximum momentum of the π^0 mesons in the proton center of mass system. Such a dependence of the cross section on the momentum is due to the fact that maximum-intensity transitions to the final S_N-state for nucleons and p_π-state for mesons are forbidden. On the other hand, transistions to other end states (for example P_N and P_π) are responsible for the dependence of the cross section on a high power of the momentum (p_{max}^6 or p_{max}^8) and the low value of the cross section near the threshold. From our measurements at 470 and 670 Mev, we find that the dependence of the cross section on p_{max} in the 470-670 Mev region can be represented as

$$\sigma_{pp} \sim p_{max}^{4,5\pm0,5}.$$

Comparison of the p-n cross section at 670 Mev, obtained by us, with the value of this cross section at 340 Mev,[27,28]

$$\sigma_{pn}(340) = (0{,}23 \pm 0{,}08)\cdot 10^{-27} \text{ см}^2,$$

shows that the cross section varies in the following manner:

$$\frac{\sigma_{pn}(670)}{\sigma_{pn}(340)} = \left[\frac{p_{max}(670)}{p_{max}(340)}\right]^{3,2\pm0,4}$$

(The cross section $\sigma_{pn}(340)$ given here was computed as the difference $\sigma_{pd} - \sigma_{pp}$.

This does not conflict with the fact that in the above reaction the π^0 meson is created in the P state while the nucleons remain in the S state. Measuring the relative cross sections we obtained

$$\frac{\sigma_{pd}}{\sigma_{pp}} = 3{,}1 \pm 0{,}3.$$

Neglecting the coupling of the nucleons in the deuteron, at 670 Mev, we have

$$\frac{\sigma_{pn}}{\sigma_{pp}} = 2{,}1 \pm 0{,}3.$$

The last value is in good agreement with the results of Ref. 29.

Conclusions

The results obtained by us in the investigations described in this report lead to the following conclusions concerning the mechanism of π^0-meson production by high-energy nucleons.

1. Neutral pi mesons are formed on complex nuclei in collisions of the bombarding protons with the individual nucleons of the nucleus rather than with the nucleus as a whole.

2. At 470 Mev, the π^0 mesons produced on a complex nucleus usually emerge at small angles to the direction of motion of the nucleons. A term proportional to $\cos^2 \theta$ appears to be predominant in the expression characterizing the angular distribution of the π^0 mesons.

3. As the proton energy is increased to 670 Mev, the rate of increase of the cross section for the production of π^0 mesons in p-p collisions falls well below the rate observed at energies under 470 Mev.

4. When complex nuclei are bombarded with 670 Mev protons, mesons are produced primarily on the surface of the nuclei. At this energy the effect cannot be attributed wholly to the absorption of mesons in the nucleus.

5. The angular distribution of the γ-quanta, formed in the decay of the π^0 mesons, is highly dependent on the mass number of the bombarded nucleus: at higher mass numbers the angular distribution of the γ-quanta becomes increasingly isotropic in the laboratory system.

6. It follows from the observed dependence of the γ-quanta angular distribution on the mass number that the energy spectra of γ-quanta from the decay of π^0 mesons produced on light and heavy elements should differ substantially in the region of low gamma energies. This difference in spectra was apparently not detected in earlier investigation, owing to the inadequate accuracy of the measurements in the low energy region.

We wish to thank A. N. Sinaev and M. M. Kuliukin for their aid in developing the experimental equipment.

Institute of Nuclear Problems of the
Academy of Sciences of the USSR

References

1. J.Daudin, Ann. de physique, 19, 10 (1944).
2. G.Rochester, Proc. Rov. Soc., A187, 464 (1946).
3. N.G.Birger, Doklady AN SSSR, 61, 245 (1948).
4. S.Azimov, N.Birger & A.Gorbunov, Doklady AN SSSR, 65, 625 (1949)
5. W.Fretter, Phys. Rev., 73, 41 (1948); Phys.Rev., 76, 511 (1949).
6. G.Chao, Phys. Rev., 75, 581 (1949).
7. B.Gregory, B.Rossi & J.Tinlot, Phys. Rev. 77, 299 (1950).

8. H.Bridge, B.Rossi & R.Williams, Phys.Rev., 72, 257 (1947).
9. S.Kuchai & I.Rozental', Doklady AN SSSR, 60, 1523 (1948).
10. L.Korablev, &. Liubimov & A.Miller, Doklady AN SSSR, 61, 633 (1948).
11. M.Kaplon, B.Peters & H.Bradt, Phys. Rev., 76, 1735 (1949).
12. New York Meeting of American Physical Society, Jan.1947; H.Lewis, J.Oppenheimer & S.Wouthuysen, Phys. Rev., 73, 127 (1948).
13. R.Bjorklund, W.Crandall, B.Moyer & H.York, Phys. Rev., 77, 213 (1950).
14. J.Steinberger, W.Panofsky & J.Steller, Phys. Rev., 78, 802 (1950).
15. A.Carlson, T.Hooper & D.King, Phil. Mag., 41, 701 (1950).
16. M.Kozodaev & A.Markov, General Report, IIaP AN SSSR (Institute of Nuclear Problems of the USSR Academy) for the first half of 1950.
17. M.Kozodaev, A. Tiapkin, A.Markov & Iu.Baiukov, Report IIaP AN SSSR (1952).
18. M.Whitehead & C. Richman, Phys. Rev., 83, 855 (1951).
19. M.Meshcheriakov, B.Neganov, N.Bogachev & V.Sidorov, Report IIaP AN SSSR (1952).
20. K.Watson & K.Bruckner, Phys. Rev., 83, 1, (1951).
21. W.Crandall & B.Moyer, Phys. Rev., 92, 749 (1953).
22. J.Marshall, L.Marshall, V.Nedzel & P.Warshaw, Phys. Rev. 88,632 (1952).
23. M.Kozodaev, A.Tiapkin & R.Vanetsian, Report, IIaP AN SSSR (1952).
24. K.Bruckner, R.Serber & K.Watson, Phys. Rev., 84, 258 (1951).
25. B.Pontekorvo, G.Selivanov & V.Zhukov, Report, IIaP AN SSSR (1952).
26. A.Tiapkin, M.Kozodaev & Iu.Prokoshkin, Report, IIaP AN SSSR (1954).
27. J.Mather & E.Martinelli, Phys. Rev., 92, 780 (1953).
28. R.Hales, B.Moyer, Phys. Rev., 89, 1047 (1953).
29. B.Pontekorvo & G.Selivanov, Communication presented at IIaP AN SSSR.
30. Iu.Baiukov, M.Kozodaev, A.Markov, A.Sinaev & A.Tiapkin, Report IIaP AN SSSR (1955).

ISOTOPIC INVARIANCE OF THE PI-MESON FIELD

- A. M. Baldin

The present paper constitutes a theoretical introduction to the following report by Belousov, Kutsenko and Tamm. Its principal purpose is to show that a direct confirmation of the hypothesis of the isotopic invariance of the pi-meson field is furnished by investigations of elastic photomeson production reactions (non-catastrophic) such as $\gamma + d \to d + \pi^0$; $\gamma + He^4 \to He^4 + \pi^0$; $\gamma + C^{12} \to C^{12} + \pi^0$, **etc.**

The isotopic invariance hypothesis is already widely accepted in view of the numerous indications following from experiments on the interaction of mesons with nucleons and nuclei. Furthermore, various experiments have been proposed and partly realized to verify the very important assumption that π^+, π^-, **and** π^0 **mesons form an isotropic triplet. Typical of these experiments is the comparison of the angular distributions for the following reactions:**[1]

$$p + p \longrightarrow \pi + d$$
$$n + p \longrightarrow \pi + d$$

The results of these experiments are in good agreement with deductions drawn on the basis of the isotopic invariance hypothesis. However, experiments of this type are merely a verification of one of the numerous consequences of the hypothesis. They only show that the investigated effect in particular does not contradict the isotopic invariance hypothesis. To prove the isotopic invariance hypothesis, it is necessary to show that the wave function of the π^0 meson field transforms as the third component of a vector in isotopic space and that all other possible types of symmetry of the π meson field in the isotopic space are contrary to experiment. Investigation of the reactions mentioned above allows of checking the hypothesis in this manner.

Omitting non-essential factors let us write the Hamiltonian for the interaction of nucleons with a neutral-meson field

$$H = g_p \frac{1+\tau_3}{2} \varphi + g_n \frac{1-\tau_3}{2} \varphi. \qquad (1)$$

The first term corresponds to the interaction of the neutral meson field with a proton while the second corresponds to the interaction with a neutron (φ is the wave function describing the neutral meson field). This rather general interaction Hamiltonian can be written as follows (introducing new constants):

$$H = g_0 \varphi + g_3 \tau_3 \varphi. \qquad (2)$$

Let us impose the condition that this Hamiltonian meet the requirements of symmetry with respect to a 180° rotation about the X axis in isotopic space. The existence of such a type of symmetry, as is known, can be considered proven. It is what is termed charge symmetry.

It can be seen from eq. (2) that two types of invariance are possible: 1) a 180° rotation in the isotopic space may leave the sign of φ unchanged (φ is a scalar), or 2) the 180° rotation does change the sign of φ (φ is the third component of a vector). In a case of the first type $g_p = g_n$, while in the second $g_p = -g_n$.

Theoretical analyses of the aforementioned reactions, carried out by the author jointly with V. V. Mikhailov,[2-4] showed that the cross sections for these reactions depend greatly on which of the above symmetry variants is selected. It was shown that if the first type of invariance were realized in nature, the cross section for elastic photoproduction would be much smaller than the cross section for inelastic photoproduction (with destruction of the nucleus).

On the other hand with the second variant, the cross sections for photomeson production on d, He^4, C^{12} and other nuclei with and without destruction of the nucleus should be of the same order of magnitude. This result was rigorously derived without recourse to nuclear models, specific field theories or dubious computation schemes.

An experimental study of the effect in question in the case of deuterium is described in the following report. This study, in our opinion, leads to an unambiguous conclusion regarding the sign of the coupling constants associated with the interaction of the π^0-meson field with a proton or a neutron or (what is equivalent) concerning the transformation properties of the wave function of the π^0-meson field.

We note that the cross section for elastic photoproduction of

mesons on He^4 was recently measured.[5] The results of these experiments also directly confirm the validity of the isotopic invariance hypothesis.

"P. N. Lebedev" Physics Institute of the
Academy of Sciences of the USSR

References

1. P.H.Hildebrand, Phys. Rev., 89, 1090 (1953).
2. V.V.Mikhailov & A.M.Baldin, Doklady AN SSSR, 84, 47 (1952).
3. A.M.Baldin & V.V.Mikhailov, Doklady AN SSSR, 91, 497 (1953).
4. A.M.Baldin, Doklady AN SSSR, 94, 949 (1954).
5. E.K.Goldwasser, H.J.Koester & F.E.Mills, Phys. Rev., 95, 1692 (1954).

* * * * *

ABSTRACTS

PHOTOPRODUCTION OF NEUTRAL PI MESONS ON DEUTERONS

- A. S. Belousov, A. V. Kutsenko and E. I. Tamm

1. The confirmations of the isotopic invariance hypothesis available at the present time are based only on verifications of the consequences of this hypothesis, i. e. proofs of the less general type of symmetry, namely, invariance with respect to a 180° rotation in the XY plane and with respect to the replacement of all neutrons by protons, protons by neutrons, and π^+ and π^- mesons by π^- and π^+ mesons.

2. All that is needed to exclude a type of symmetry that is less general (than the isotopic invariance) is to investigate the character of the wave function describing the neutral meson field. According to the isotopic invariance hypothesis, the wave function of the π^0-meson field should be described by the third component of a vector in isotopic space; a consequence of this is that the neutron-meson field and proton-meson field coupling constants must be opposite in sign, i.e., that $g_n = -g_p$. In the case when the π^0-meson field wave function is a scalar g_n and g_p have the same sign.

3. The relative signs can be determined by investigating the photoproduction of π^0 mesons on deuterons:

$$\gamma + d \to \begin{cases} d + \pi^0 & \text{I} \\ p + n + \pi^0. & \text{II} \end{cases}$$

A. M. Baldin and V. V. Mikhailov have shown, on the basis of general quantum-mechanical considerations, that the cross section for reaction I is strongly dependent on the relative signs of g_n and g_p, viz:

$$\frac{\sigma_I(g_n = -g_p)}{\sigma_I(g_n = g_p)} \approx 40, \quad \sigma_{II} \approx \sigma_I \quad (g_p = -g_n).$$

4. The cross sections for reactions I and II were measured, using synchrotron produced γ-rays with a maximum energy of 250 Mev.

We identified the deuterons and the recoil protons from the difference in the time of flight of these particles in a semi-circular trajectory in a magnetic field. We recorded the delayed coincidences between one of the γ-quanta from the decay of the π^0 meson and the recoil product; here the length of the delay characterizes the mass of the recoil particle, i.e. identifies it as being proton or deuteron.

5. The results of the measurements indicate that the cross sections for reactions I and II are identical. Consequently, the coupling constants associated with neutron and proton interaction with the π^0 meson field have opposite signs which substantiates the isotopic invariance hypothesis and excludes the less general type of symmetry.

* * * *

PHOTOPRODUCTION OF CHARGED PI MESONS ON HYDROGEN AND DEUTERIUM

- M. I. Adamovich, G. V. Kuz'micheva, V. G. Larionova and S. P. Kharlamov

The production of π mesons by photons on nucleons is a process of primary interest in the study of the properties of mesons and their interactions with nucleons. It has been shown in many experimental investigations of photoproduction of π^+ mesons on hydrogen that electric-dipole absorption of photons by the proton predominates near the photoproduction threshold.

We investigated the photoproduction of π^--mesons on deuterium using thick nuclear emulsions filled with deuterium (saturated with heavy water). We investigated the angular and energy distributions of the π^- mesons and the dependence of the cross section for the $\gamma + d \rightarrow p + p + \pi^-$ reaction on the photon energy. The experiments were carried out on the Physics Institute of the Academy of Sciences synchrotron at a maximum gamma energy of 250 Mev.

The results indicate that electric dipole absorption of the photons is apparently the predominant process near the threshold of photomeson production. Juxtaposition of our results with available data on the photoproduction of π^+ mesons on hydrogen shows that the formation of π^- mesons on deuterium is identical with that on free neutrons, within the limits of the measuring statistics.

The experimental results also indicate the presence of spin interaction leading to a change in the spin of the nucleonic system incident to photoproduction of π^- mesons on deuterons. The lower limit for the probability of a change in spin of the nucleonic system near the π-meson production threshold is 40%.

INVESTIGATION OF THE (γ, p) REACTION AT ENERGIES UNDER 30 MEV

- E. M. Leikin, P. M. Osokina, and B. S. Ratner

Photonuclear reactions offer a means of investigating the interaction of electromagnetic radiation with nuclei. For interpreting the results obtained in the 10-30 Mev photon energy region, investigators have turned to the concept of a collective mechanism of photon absorption and a model in which the photons are assumed to interact with the individual nucleons of the nucleus ("direct photo-effect"). Published data do not permit of drawing any definitive conclusions regarding the mechanism of photon absorption by medium and heavy nuclei.

In view of this we undertook a more detailed investigation of the angular and energy distributions of photoprotons ejected from a number of different elements. The experiments were carried out on the synchrotron of the Physical Institute of the Academy of Sciences at photon energies up to 30 Mev. The collimated γ-ray beam was intercepted by a target located in the vacuum tank. The protons were recorded by means of thick nuclear emulsions, exposed at different angles to the γ-ray beam. The yield of protons from copper was measured at maximum γ-ray energies of 19, 24, 28 and 30.5 Mev; the yield from nickel at 21.5, 25.5 and 28.0 Mev. Preliminary data have also been obtained for aluminum and lead.

Comparison of the experimental results with statistical theory indicates that the direct interaction mechanism plays a substantial role. It was found that when the maximum incident γ-ray energy is increased from 24 Mev to 28 and 30.5 Mev, a radical change occurs in the angular distribution, the energy spectrum and the yield of fast photoprotons from copper.

The results can be interpreted as being due to the influence of nuclear shell structure. The results obtained with nickel substantiate this interpretation.

YIELD AND ANGULAR DISTRIBUTION OF HIGH-ENERGY PHOTONEUTRONS*

- P.S. Baronov and V.I. Gol'danski

1. We investigated the yield and angular distribution of high-energy photoneutrons from Li, Be, C, Al, Fe, Cu and Pb by means of a high threshold neutron detector, utilizing the $C^{12}(n, 2n)C^{11}$ reaction in inorganic phosphors having a high concentration of carbon. Positrons from the decay of the C^{11} were recorded by means of photomultipliers connected in a double coincidence circuit. The efficiency of recording the activity of the C^{11} isotope was established by comparison of the indications with standardized carbon detectors; this made it possible to determine the absolute values of the photoneutron flux. The sensitivity of the neutron detector used in the experiments was high enough to warrant its use as a high-energy neutron dosimeter.

---

* For the full report see Zhur. eksp. i teor. fiz., 28, 621, 746 (1955). Translation in JETP (Soviet Physics), Vol. 1, p. 576, 613 (1955).

2. The most detailed data were obtained for carbon. The angular distribution of neutrons having energies above ~30 Mev, ejected from carbon irradiated by bremsstrahlung photons of 250 and 200 Mev maximum energy (produced by the synchrotron of the Physics Institute of the USSR Academy of Sciences), exhibits a sharp peak at an angle of 45° relative to the incident photon beam. The differential angular cross sections for 45° at 250 and 200 Mev photon energy are, respectively, $(3.1 \pm 0.12)\cdot 10^{-28}$ and $(1.7 \pm 0.13)\cdot 10^{-28}$ cm^2 sterad^{-1} per effective quantum. The angular distribution at 250 Mev is characterized in relative units by

30°	45°	60°	75°	90°	120°	135°	150°
0,71±0,10	1,00	0,76±0,07	0,59±0,11	0,45±0,05	0,41±0,07	0,39±0,09	0,33±0,09

3. Comparison of the absolute values of the differential cross section and the data on the energy dependence of the yield of fast photoneutrons from carbon with the analogous data for photodisintegration of deuterium and the formation of photostars shows that high energy neutrons are formed primarily through two processes: photodisintegration of "quasi-deuterons" and the formation of photostars. The pronounced forward bunching observed in the angular distribution of fast photoneutrons is due to that fraction of the photoneutrons which is formed in the stars, apparently, in connection with the production of mesons on the nucleons of the nucleus.

4. The distribution of fast photoneutrons from Be, Al and Pb at 250 Mev maximum photon energy approximates the angular distribution of photoneutrons from C nuclei and, also, exhibits a peak at 45°. This peak is less pronounced for Pb (and particularly for Be) than for C. The neutron yield from C, Al, Fe, Cu and Pb is characterized by $\sigma \sim A^{1.4}$. The yield from Be is approximately 1.5 times greater than might be expected from extrapolation of the data for the other nuclei.

5. The cross section for the direct photoeffect $C^{12}(\gamma, n)C^{11}$ is observed to increase by about 10^{-28} cm^2 per effective quantum in the 50-250 Mev photon energy interval.

ERRATUM

In REPORT No. 8. RAMAN SPECTRA OF CERTAIN AROMATIC HYDORCARBONS (Vol. 19, page 206 of the translation, page 225 of the original) under the data on 1,3,5-TRIMETHYL-2-ALLYBENZENE (p. 211 of translation) the value for t_{freeze} should read — 2.1° (instead of 2.1°).

BULLETIN of the Academy of Sciences of the USSR - Physical Series
Vol.19, No. 5, 1955 - Conference on the Physics of Cosmic Rays (15-23 Dec.1954)

TABLE OF CONTENTS

	Page Orig.	Trans.
Transactions of the Third All-Union Conference on the Physics of Cosmic Rays (Publication note)	490	442
Opening address - S.N. Vernov	491	443
Investigation of the interaction of nucleons with light nuclei at energies of 10^9-10^{12} ev - S.N.Vernov, N.L.Grigorov, G.T.Zatsepin and A.E.Chudakov	493	445
Interaction of cosmic ray protons with light nuclei according to Wilson cloud chamber measurements at 9 km alt. - L.T.Baradzei, V.I.Rubtsov,Iu.A.Smorodin,M.V.Solov'ev,B.V.Tolkachev & Z.I.Tulinova	502	453
Spectra of the genesis of pi mesons and protons in graphite - N.M.Kocharian, G.S.Saakian, M.T.Aivazian, Z.A.Kirakosian and A.S.Aleksanian	508	458
Energy spectrum of protons at 3200 meters above sea level - N.M.Kocharian, G.S.Saakian, M.T.Aivazian, Z.A.Kirakosian and A.S.Aleksanian	515	463
Ionization spectra of cosmic radiation particles in the stratosphere - I.D.Rapoport	519	466
Investigation of the ionizing power of cosmic radiation at 3200 meters by means of proportional scintillation counters - L.P.Kotenko	525	472
Investigation of the origin of the soft component of cosmic rays in the stratosphere at geomagnetic latitude 51° North - P.N.Ageshin, A.N.Charakhch'ian & T.N.Charakhch'ian	533	478
Narrow air showers in the stratosphere - P.N.Ageshin, A.N.Charakhch'ian & T.N.Charakhch'ian	537	481
Some results of an investigation of nuclear disintegrations in W, Cu and Al produced by cosmic rays - Zh.S.Takibaev	541	485
Interaction of 10^{10}-10^{11} ev cosmic ray particles with light nuclei according to measurements at an altitude of about 4 km - N.G.Birger, V.V.Guseva, G.B.Zhdanov, S.A.Slavatinski and G.M.Stashkov	546	489
The air-lead transition curve and angular distribution of single cosmic ray particles - A.P.Zhdanov & P.I.Fedotov	547	489
Investigation of proton-proton interaction at high energies - M.G.Meshcheriakov, N.P.Bogachev & B.S.Neganov	548	490
Scattering of 460-660 Mev protons by protons - S.Ia.Nikitin, Ia.M.Selektor, E.G.Bogomolov & S.M.Zombkovski	561	503

	Page Orig.	Trans.
Experimental investigation of the interaction of neutrons with nucleons & deuterons at energies in the 380-590 Mev region - V.P.Dzhelepov, Iu.M.Kazarinov, B.M.Golovin, V.B.Fliagin and V.I.Satarov	573	514
Production of neutral mesons by high-energy nucleons - M.S.Kozodaev,A.A.Tiapkin, Iu.D.Baiukov, A.A.Markov and Iu.D.Prokoshkin	589	529
Isotopic invariance of the pi-meson field - A.M. Baldin	604	543

ABSTRACTS

Photoproduction of neutral pi mesons on deuterons - A.S.Belousov, A.V.Kutsenko and E. I. Tamm	605	545
Photoproduction of charged pi mesons on hydrogen and deuterium - M.I.Adamovich, G.V.Kuz'micheva, V.G.Larionova & S.P.Kharlamov	606	546
Investigation of the (γ, p) reaction at energies under 30 Mev - E.M.Leikin, R.M.Osokina and B.S.Ratner	607	547
Yield and angular distribution of high-energy photoneutrons - P.S. Baranov and V.I. Gol'danski	607	547

Translated in 1956 by
Columbia Technical Translations
5 Vermont Ave., White Plains,N.Y.

Price: $20.00 per copy.
Individual articles at $1.00 per page.

ON THE THEORY OF THE MULTIPLE PRODUCTION OF PARTICLES

- S. Z. Belen'ki

Apparently the statistical theory of the multiple production of particles, originated by Fermi[1], leads to better agreement with experiment than do other theories in the region of high energies. It should be mentioned that Fermi's initial hypothesis has undergone a series of substantial changes. A number of weaknesses and inconsistencies were shown to exist in the theory. Landau[2] carried out calculations on multiple production processes using relativistic hydrodynamics. Various aspects of the process of multiple production were also investigated by Pomeranchuk[3] and Feinberg and Chernavski.[4] As a result of these investigations, and particularly because of Landau's work, many consequences of the present form of the statistical theory of multiple production of particles are substantially different from those following from the theory as originally formulated by Fermi. In this report we shall consider a number of problems relating to the multiple production of particles.

First, we want to examine the question of how many particles of different masses are involved in a multiple production process. If strong interaction obtains between nuclei and particles having a mass different from that of the pi meson, such particles must be produced in "stars." Generally speaking, one may similarly expect the formation of nucleons and heavier particles. According to Fermi's theory the number of particles in a star is determined during the first stages of the collision process while the "temperature" of the system significantly exceeds the rest energy of the nucleons. In this case the relative number of particles of the various sorts is determined by the number of possible states of such particles. For example, the number of possible states for nucleons is 8 (four types of nucleons and two spin orientations) while for pi-mesons this number is equal to 3.

Considering this circumstance, as well as the differences in the statistics applicable to nucleons and to pi mesons, the ratio of the number of nucleons to the number of pi mesons turns out to be approximately two. According to Fermi the number of heavy mesons produced should be approximately equal to the number of pi mesons. As far as the energy per particle is concerned, at high disintegration temperatures, all particles are equivalent in this regard and each obtains approximately the same energy regardless of its nature.

However, Fermi's considerations are inconsistent since the system disintegrates into individual particles not at the initial instant of collision but appreciably later (see Ref. 3). While hydrodynamic disintegration is under way the number of particles is indeterminate. It is determined at some temperature T_k of the system, characterized by

$$T_к \sim m_\pi c^2, \qquad (1)$$

where m_π is the pi meson mass and T_k is measured in energy units. At this temperature the range of the particle becomes equal to the linear dimensions of the system. Since the rest energy of heavy mesons exceeds T_k, it has been suggested that the number of heavy mesons must be quite small. This deduction is based on the following equation for the particle density, valid in the non-relativistic approximation:

$$n \sim \exp\left(-\frac{m_\pi c^2}{T_к}\right). \qquad (2)$$

In this equation the mass enters into the exponent and hence the density is very sensitive to variation of the mass. However, equation (2) is only approximate and is valid only when $m_\pi c^2 > T_к$. Moreover, the critical temperature T_k is a parameter of the theory and is not known in advance. When $T_к = m_\pi c^2$ equation (2) is no longer valid. Accordingly, in Ref. 5 we made a more accurate calculation of the number of particles of various masses as a function of the disintegration temperature; in these calculations we assumed that during the disintegration particles do not interact and that relativistic formulae apply to the temperature dependence of the density. The ratio of the number of heavy particles to the number of pi mesons proved to be dependent on $\frac{m_K c^2}{T_к}$ and $\frac{m_\pi c^2}{T_к}$ (where m_K in the mass of the heavy mesons) as well as on the heavy meson spin. We also computed the ratio of the mean energies of the heavy and pi mesons. It should be noted that this ratio is independent of the coordinate system in which the calculations are carried out. The results of the calculations are given in the tables of Ref. 5. It can be seen from these tables that in the neighborhood of $T_к \sim m_\pi c^2$ the number of heavy mesons need not be small but may actually be comparable to the number of pi mesons. These particles carry off a considerable part of the energy. The larger proportion of heavy particles present in this case is associated with the fact that at $T_к \sim m_\pi c^2$ the particles already have a rather large mean energy. For example, at $T_к \sim 1{,}5\, m_\pi c^2$ the mean kinetic energy of the pi mesons equals $3\, m_\pi c^2$.

Let us now turn to an evaluation of the disintegration temperature T_k. In order that disintegration of the system at T_k be possible, the mean free path l of the particles must be shorter than the characteristic dimensions L of the system. The characteristic dimensions of the system $L \sim \frac{\hbar}{m_\pi c}$. Strictly speaking this quantity is weakly dependent on the energy of the system and, according to Landau's calculations, can be approximated by $L = \frac{\hbar}{m_\pi c}\left(\frac{E}{Mc^2}\right)^{1/12}$, where M and E are, respectively, the mass and energy of the initial nucleon. The path length $l \approx 1/n\sigma$. It is not difficult to calculate the ratio l/L if we assume $\sigma = \pi\left(\frac{\hbar}{m_\pi c}\right)^2$, and take for n the meson density at the disintegration temperature T_k. The results of the calculations are given in the table.

It will be seen that the disintegration temperature lies between 0.7 and 1.5 $m_\pi c^2$. Actually when $l/L \ll 1$ disintegration cannot occur since the path length is too short, while when $l/L \gg 1$ the system cannot exist because of the smallness of its dimensions. It should be noted that the ambiguity of our estimate (due to the fact that σ and L are known only as to order of magnitude) does not permit a theoretical determination of the disintegration temperature T_k. When $T_к = 1{,}2\, m_\pi c^2$ the equilibrium number of mesons of mass 970 m_e (on the assumption that their isobaric spin is 1) is 32% of the number of pi mesons, while the number of mesons of mass 1300 m_e constitutes 16%

of the number of pi mesons. Daniel et al[6] report that heavy mesons are found in stars in numbers comparable to the number of pi mesons. However, Powell[7] expresses doubts regarding these results. The small number of heavy particles produced could serve as an indication of the low disintegration temperature of the system. On the other hand, it is conceivable that some of the heavy particles interact only weakly with nucleons and are therefore not formed in stars. This is also suggested by the relatively long life time of all heavy particles, which it is difficult to reconcile with the assumption of strong nuclear interactions unless we also assume that heavy particles are produced in pairs. In the last case strong nuclear interaction is entirely possible, but our calculations must then be appropriately modified.

Let us now go on to the question of the number and energy of nucleons participating in collisions and produced therein. In the interaction of a nucleon with a nucleus a simultaneous collision with several nucleons in the nucleus is involved. All experimental data currently available fully substantiate the fact that nuclear charge is conserved in all nuclear processes. This must be borne in mind in making calculations. It is necessary to introduce the Gibbs (chemical) potential μ, which in calculations involving heavy mesons could be neglected or equated to zero, into the distribution function for the number of nucleons.

The magnitude of μ is determined by the condition that the difference between the number of nucleons and anti-nucleons (if they are formed) in the system must equal the number of initial nucleons. The appropriate calculations were carried out in Ref. 8, where the following result is obtained:

$$\frac{N_н}{N_\pi} = \sqrt{\left(\frac{N_{н0}}{N_{\pi 0}}\right)^2 + \left(\frac{N_0}{N_\pi}\right)^2}, \qquad (3)$$

where $\frac{N_н}{N_\pi}$ is the ratio of the sum of the numbers of nucleons and anti-nucleons to the number of pi mesons, $\frac{N_0}{N_\pi}$ is the ratio of the number of initial nucleons to the number of pi mesons, $\frac{N_{н0}}{N_{\pi 0}}$ is the ratio of the number of nucleons and anti-nucleons to the number of pi mesons when $N_0 = 0$.

Let us see how conservation of nuclear charge affects the formation of anti-nucleons. If, for example, $T_к = 1{,}5\, m_\pi c^2$, we have $\frac{N_{н0}}{N_{\pi 0}} = 0.27$ and the number of anti-nucleons equals 0.135. Let us assume that $\frac{N_0}{N_\pi} = 0.15$ (this corresponds, for example, to 3 nucleons and 20 mesons). Whence $\frac{N_н}{N_\pi} = 0.3$. Then the number of all nucleons formed is 0.15 and of anti-nucleons 0.075. Thus, in taking into account the number of initial nucleons the number of anti-nucleons in this example is reduced by a factor of almost two.

Let us now turn to the energy of nucleons and pi mesons. It is not hard to see that the energy available per nucleon depends only on the disintegration temperature and is independent of the Gibbs potential (see Ref. 8). This follows if we employ the relativistic Maxwell distribution rather than the Fermi distribution, which we are fully justified in doing.

In order to obtain a quantity independent of the reference system, we must take the ratio of the energy acquired by a nucleon to the energy acquired by a pi meson. This quantity depends only on the disintegration temperature and its experimental determination would, apparently, be the best means of evaluating the disintegration temperature. The table of values of this quantity, α is given in Ref. 8.

With $\frac{T_к}{m_\pi c^2} \ll 1$, $\alpha = 6.8$; at $\frac{T_к}{m_\pi c^2} = 0.5$, $\alpha = 3.76$; at $\frac{T_к}{m_\pi c^2} = 1.5$, $\alpha = 2.16$. From this it is clear that, in cases of not very high disintegration temperatures, the energy acquired by a single nucleon is several times larger than the energy acquired by a single pi meson. By way of example let us consider the case when the energy of the initial nucleon is 10^{11} ev. If this nucleon collides, on the average, with two nucleons, seven mesons will be formed in the encounters. If we assume that $\frac{T_к}{m_\pi c^2} \approx 0.5$, the ratio of the energy carried off all the nucleons to the total energy turns out to be 0.64. It should be noted, however, that at such energies deductions from the theory have only a qualitative significance.

The genesis of heavy particles (Λ particles), also possessing nuclear charge, is possible in nuclear collisions. Such collisions can be included in our discussion (see Ref. 8). Calculations show that at $T_k = 1.2\, m_\pi c^2$ and with $N_o = 0$, the number of anti-nucleons produced in stars is 2.3 times larger than the number of lambda hyperons. On the other hand already at $N_o/N_\pi = 0.15$ the number of hyperons produced is two times larger than the number of anti-nucleons. With a decrease in the critical temperature T_k, the relative role of the hyperons will be even greater.

Present day theory of multiple production of particles considers only nucleon-nucleon collisions and virtually neglects collisions of nucleons with nuclei, which are very important from the experimental point of view. We note that the theoretical analysis of nucleon-nucleon collisions carried out by Landau[2] can be divided into two parts: in the first part he examines the dependence of the total number of particles produced on the energy of the initial particle; in the second, the angular and energy distributions of the particles. The total number of particles is computed rather simply on the basis of general thermodynamic considerations; the second part of the analysis involves the use of relativistic hydrodynamics. It may be noted that the results obtained for the total number of particles are very much more accurate than those for the distributions in angle and energy.

The first part of Landau's calculations for nucleon collisions is based on the following considerations. Since the process of hydrodynamic expansion occurs adiabatically and since shock waves are absent, the entropy of the system remains constant during the expansion; the entropy changes only at the initial instant of collision, that is, during the period of compression. Furthermore, the number of particles remains indeterminate during the entire duration of the process and is determined only at a temperature equal to the temperature T_k of disintegration of the system. It can be shown that the total number of particles produced is proportional to the change in entropy at the beginning of the process:

Dependence of the ratio l/L on the critical temperature for two values of the nucleon energy

$\frac{T_к}{m_\pi c^2}$	$E = Mc^2$	$E = 10^3\ Mc^2$
0,5	16	9
0,7	5	3
1,0	1,2	0,7
1,5	0,36	0,21
2	0,12	0,07

$$N = \text{const. } S, \qquad (4)$$

where N is the total number of particles and S is the total change in entropy. Because the change in entropy is determined at the initial instant of collision it can readily be calculated by virtue of the symmetry of the system.

Let us now consider encounters of a nucleon with a nucleus (or collisions of two nuclei of different atomic weights). It is not hard to see that in this case even the computation of the total number of produced particles, the first and relatively simple part of the analysis, becomes fairly complex. Since the distance between particles in the nucleus is of the order of the range of nuclear forces and each elementary collision results in the production of several particles, the nuclear encounter must lead to the formation of particles throughout the entire nuclear region traversed by nucleon. In its passage through the nucleus, the nucleon will interact not with the entire nucleus but only with a part of it. This matter will be considered below. To begin with let us note that in the presence of initial nucleons it is necessary to re-examine the relation (4) which was proved on the condition that initial nucleons are absent. Using the relations of statistical physics we can deduce the following relation for this case (Ref. 9):

$$\frac{N}{N_0} = \varphi\left(T_к, \frac{N^*}{N_0}\right), \qquad (5)$$

where N is the total number of created particles and nucleons participating in the collision, N_0 is the number of initial nucleons, N* is the number of particles in the case when $N_0 = 0$, and T_k is the system disintegration temperature.

It can readily be seen that the value of N* is proportional to the change in entropy. The function φ was computed for different temperatures beginning with $T_k = 0.5\, m_\pi c^2$. It turned out that equation (4) is applicable when $N^*/N_0 > 2$, provided N is understood to be the sum of the number of particles produced in the collision plus the number of initial nucleons participating in the collision. For $N^*/N_0 < 2$, the number of created particles decreases, while for $N^*/N_0 \ll 1$, $N/N_0 \to 1$.

The next problem is that of computing the entropy, which in the case of collisions of a nucleon with a nucleus is considerably more difficult than for nucleon-nucleon collisions.

Let us extend our picture of nuclear matter as a continuous medium to the first stage of the collision, i.e. to the compression stage. We must emphasize that under these conditions we speak of the propagation of "shock waves" and "travelling waves" through a nucleon only in a conditional sense, and the corresponding calculations are carried through only for heuristic purposes. Let us select a reference system in which the nucleon and nucleus have equal but opposite velocities. Due to the Lorentz contraction, in this reference system the nucleon and nucleus constitute two very thin disks. As a consequence the problem may be viewed as a one-dimensional one. The collision of a nucleon with a nucleus can thus be treated as a collision of a

Dependence of the ratio l/L on the critical temperature for two values of the nucleon energy

$\frac{T_к}{m_\pi c^2}$	$E = Mc^2$	$E = 10^2\ Mc^2$
0,5	16	9
0,7	5	3
1,0	1,2	0,7
1,5	0,36	0,21
2	0,12	0,07

$$N = \text{const. } S, \qquad (4)$$

where N is the total number of particles and S is the total change in entropy. Because the change in entropy is determined at the initial instant of collision it can readily be calculated by virtue of the symmetry of the system.

Let us now consider encounters of a nucleon with a nucleus (or collisions of two nuclei of different atomic weights). It is not hard to see that in this case even the computation of the total number of produced particles, the first and relatively simple part of the analysis, becomes fairly complex. Since the distance between particles in the nucleus is of the order of the range of nuclear forces and each elementary collision results in the production of several particles, the nuclear encounter must lead to the formation of particles throughout the entire nuclear region traversed by nucleon. In its passage through the nucleus, the nucleon will interact not with the entire nucleus but only with a part of it. This matter will be considered below. To begin with let us note that in the presence of initial nucleons it is necessary to re-examine the relation (4) which was proved on the condition that initial nucleons are absent. Using the relations of statistical physics we can deduce the following relation for this case (Ref. 9):

$$\frac{N}{N_0} = \varphi\left(T_к, \frac{N^*}{N_0}\right), \qquad (5)$$

where N is the total number of created particles and nucleons participating in the collision, N_0 is the number of initial nucleons, N* is the number of particles in the case when $N_0 = 0$, and T_k is the system disintegration temperature.

It can readily be seen that the value of N* is proportional to the change in entropy. The function φ was computed for different temperatures beginning with $T_k = 0.5\, m_\pi c^2$. It turned out that equation (4) is applicable when $N^*/N_0 > 2$, provided N is understood to be the sum of the number of particles produced in the collision plus the number of initial nucleons participating in the collision. For $N^*/N_0 \leq 2$, the number of created particles decreases, while for $N^*/N_0 \leq 1$, $N/N_0 \to 1$.

The next problem is that of computing the entropy, which in the case of collisions of a nucleon with a nucleus is considerably more difficult than for nucleon-nucleon collisions.

Let us extend our picture of nuclear matter as a continuous medium to the first stage of the collision, i.e. to the compression stage. We must emphasize that under these conditions we speak of the propagation of "shock waves" and "travelling waves" through a nucleon only in a conditional sense, and the corresponding calculations are carried through only for heuristic purposes. Let us select a reference system in which the nucleon and nucleus have equal but opposite velocities. Due to the Lorentz contraction, in this reference system the nucleon and nucleus constitute two very thin disks. As a consequence the problem may be viewed as a one-dimensional one. The collision of a nucleon with a nucleus can thus be treated as a collision of a

nucleon with a "tube" cut out of the nucleus. When the nucleon and tube approach, shock waves are propagated in both directions in the material of the nucleon and nucleus. In the chosen reference system the matter contained between the shock waves will be in a state of rest. The shock wave propagated in the nucleon will reach the boundary before the shock wave propagated in the tube. When the wave reaches the boundary the material will begin to escape. A decompression wave will travel through the nuclear matter with the speed of sound in the medium. At the same time the shock wave which has not yet reached the boundary will continue to be propagated in the same direction. The calculation of the entropy will be different, depending on whether or not the travelling wave overtakes the shock wave before the latter reaches the boundary. Taking into account that the equation of state of the compressed nuclear material is $p = \varepsilon/3$ (here p is pressure, and ε is the energy density) we obtain that the speed of sound $c_0 = c/\sqrt{3}$, while the speed of the shock wave $D = c/3$, where c is the velocity of light. It is obvious that the travelling wave will overtake the shock wave if the length of the tube $l = 3.7\,d$, where d is the "length" of the nucleon. For shorter tube lengths the change in entropy can easily be computed. We obtain the equation

$$\frac{S}{S_0} = \frac{1}{2}\left(\frac{l}{d} + 1\right), \qquad (6)$$

where S_0 is the change in entropy incident to a nucleon-nucleon collision. The uncertainty as regards the shape of the nucleon leads to inexactness of equation (6). In the case of a collision of a light nucleus with a heavy one the equation becomes more exact; d in this case represents the "length" of the light nucleus. For tube lengths exceeding $3.7\,d$ the solution becomes more complicated. The travelling wave in this case will catch up with the shock wave. However, it will not go through the shock wave but will be reflected from it. In this case we will have a region bounded by the shock and travelling waves. To describe the motion of the medium in this case it is necessary to use the equation for arbitrary one-dimensional motion of a compressible gas, derived, for the relativistic case, by Khalatnikov.[10] The change in entropy of the system caused by the passage of the shock wave can be computed, although the calculations involved are rather cumbersome (see Ref. 9).

For the change in entropy in the case when $l \geqslant 3{,}7\,d$ we obtain the expression

$$\frac{S}{S_0} = 0{,}92\left(\frac{l}{d} - \frac{1}{4}\right)^{3/4}. \qquad (7)$$

If we average equations (6) and (7) over all possible collisions in the nucleus from head-on collisions to extreme peripheral ones, we get the expression

$$\frac{S}{S_0} = A^{0{,}19}, \qquad (8)$$

which is accurate to within 5% (where A is the atomic weight). Equations (4) and (8) jointly give the dependence of the multiplicity on the atomic weight. This dependence turns out to be weak (also see Ref. 11). Thus the multiplicity for lead (A = 207) differs from that for nitrogen (A = 14) by a factor of only 1.7.

The angular and energy distributions resulting from collisions of nucleons with nuclei require a special analysis which is currently underway.

"P. N. Lebedev" Physical Institute of
the Academy of Sciences of the USSR

References

1. E. Fermi, Progr. Theor. Phys., 5, 570 (1950).
2. L.D.Landau, Izv. AN SSSR, Ser. fiz. 17, 51 (1953).
3. I.Ia.Pomeranchuk, Doklady AN SSSR, 78, 889 (1951).
4. E.L.Feinberg & D.S.Chernavski, Doklady AN SSSR, 81, 795 (1951); Doklady AN SSR, 91, 511 (1953).
5. S.Z.Belen'ki, Doklady AN SSSR, 99, 523 (1954).
6. R.Daniel, J.H.Davies, J.H.Mulvey & D.H.Perkins, Phyl. Mag., 43, 753 (1952).
7. C.F.Powell, Nuovo Cim., 11, Suppl. No.2,165 (1954).
8. S.Z.Belen'ki, Zhur. eksp. i teor. fiz., 28, 111 (1955).
9. S.Z.Belen'ki & G.A.Milekhin, Zhur. eksp. i teor. fiz., 29, 20 (1955).
10. I.M.Khalatnikov, Zhur. eksp. i teor. fiz., 27, 529 (1954).
11. I.L.Rosental' & D.S.Chernavski, Usp. fiz. nauk, 52, 185 (1954).

* * * *

STATISTICAL MECHANICS OF SYSTEMS WITH CONSERVATION OF CHARGE AND ITS APPLICATION TO THE THEORY OF MULTIPLE PRODUCTION OF PARTICLES

- V. B. Magalinski and Ia. P. Terletski

1. Introduction

In the statistical treatment of the multiple production of particles at high energies, as initially proposed by Fermi,[1] both the average number of particles and the ratios of the particles of different types are calculated in the "thermodynamic" approximation by the usual equations of quantum statistics for an ideal Bose or Fermi gas with a variable number of particles; these equations are derived without taking into account the conservation of charge (electric, nuclear, etc.). For processes with a low multiplicity, however, when the total charge of the system (i.e., the number of primary particles, all of the same charge) is comparable to the number of particles formed, it would be more correct to use statistical formulas derived taking the law of charge conservation into account. Thus a more detailed investigation of multiple particle production in the frame of the "thermodynamic" approximation is possible only when the usual quantum statistics are generalized to include the case of a system in which charge is conserved.

In the present article we effect this generalization, use it to deduce new, more exact equations for the average number of particles and the mean energy in the approximation of Boltzmann statistics and establish the relationship between these equations and those of conventional statistical mechanics.

The results so obtained are used to clarify several questions related to the theory of multiple production of particles. Specifically, we examine several particular cases of meson production incident to nucleon-nucleon collisions.

2. Calculation of the sum-over-states, the average number of particles and the mean energy of a system with charge conservation

Let us consider an ideal gas composed of neutral, positively charged, and negatively charged particles. The total number of particles of each type can change as a result of the formation of neutral particles and charged pairs; the difference, however, between the number of positive particles n^+ and the number of negative ones n^- (that is, the total charge of the system) must, in view of charge conservation, remain constant and equal to the original number ν of particles of the same type and having same charge,* or in other words

$$n^+ - n^- = \nu = \text{const.} \tag{1}$$

Let the system have the nondegenerate energy levels ε_k. Then, designating the corresponding occupation numbers by n_k^0, n_k^+, and n_k^- the sum-over-states can be written in the following form:

$$Z = \sum_{\substack{n_1^0\, n_2^0 \\ n_1^+\, n_2^+ \\ n_1^-\, n_2^-}} \sum \ldots \prod \left(q_k^{(0)}\right)^{n_k^0} \left(q_k^{(1)}\right)^{n_k^+ + n_k^-} \delta\left[\nu_1, \sum_k (n_k^+ - n_k^-)\right]. \tag{2}$$

Here

$$q_k^{(0)} = q_k e^{\mu_0/\theta}, \quad q_k^{(1)} = q_k e^{\mu_1/\theta}, \quad q_k = e^{-\varepsilon_k/\theta},$$

θ is the absolute temperature expressed in energy units, μ_0 and μ_1 are the Gibbs potentials of the neutral and charged particles, respectively, and $\delta[a, b]$ is the Kronecker delta:

$$\delta[a, b] = \begin{cases} 1, & \text{when } a = b, \\ 0, & \text{when } a \neq b \end{cases}$$

(a and b are integers).

The multiplications $\prod_k$ and the sums $\sum_k$ are taken from one to infinity; the sums over n_k^0, n_k^+ and n_k^- are taken from zero to infinity in the case of Bose statistics, and from zero to one in the case of Fermi statistics.

Making use of the integral representation of the Kronecker delta

$$\delta[a, b] = \frac{1}{2\pi} \int_0^{2\pi} e^{-i(a-b)x} dx, \tag{3}$$

we can write the sum-over-states (2) in the following form (see, for instance, Ref. 2):

$$Z = \frac{1}{2\pi} \int_0^{2\pi} e^{-i\nu x} \sum_{n_k^0, n_k^+, n_k^-} \prod_k \left(q_k^{(0)}\right)^{n_k^0} \left(q_k^{(1)}\right)^{n_k^+ + n_k^-} e^{i(n_k^+ - n_k^-)x} dx =$$

$$= \frac{1}{2\pi} \int_0^{2\pi} e^{-i\nu x} \prod_k \sum_{n_k^0, n_k^+, n_k^-} \left(q_k^{(0)}\right)^{n_k^0} \left(q_k^{(1)}\right)^{n_k^+ + n_k^-} e^{i(n_k^+ - n_k^-)x} dx. \tag{4}$$

The sums under the integral sign are simple to evaluate both in the case of Bose statistics and in that of Fermi statistics. In fact,

---

* In the initial state the system is assumed to contain charged particles of only one polarity.

$$\sum_{n_k^0, n_k^+, n_k^-} (q_k^{(0)})^{n_k^0} (q_k^{(1)})^{n_k^+ + n_k^-} e^{i(n_k^+ - n_k^-)x} = \sum_{n_k^0} (q_k^{(0)})^{n_k^0} \sum_{n_k^+} (e^{ix} q_k^{(1)})^{n_k^+} \sum_{n_k^-} (e^{-ix} q_k^{(1)})^{n_k^-} =$$

$$= (1 \pm q_k^{(0)})^{\pm 1} (1 \pm e^{ix} q_k^{(1)})^{\pm 1} (1 \pm e^{-ix} q_k^{(1)})^{\pm 1}. \tag{5}$$

Here the upper symbol refers to Fermi statistics; the lower one to Bose statistics. From (5) the sum-over-states (4) can be written

$$Z = \frac{1}{2\pi} \int_0^{2\pi} e^{-i\nu x + \Phi(x)} dx, \tag{6}$$

where

$$\Phi(x) = \pm \sum_k \ln (1 \pm q_k^{(0)}) \pm \sum_k \ln (1 \pm e^{ix} q_k^{(1)}) \pm \sum_k \ln (1 \pm e^{-ix} q_k^{(1)}). \tag{6'}$$

Let us calculate Z in the Boltzmann approximation, when $q_k \ll 1$. In this case

$$\Phi(x) \approx q_0 + 2q_1 \cos x, \tag{7}$$

where

$$q_0 = q e^{\mu_0/\theta}, \quad q_1 = q e^{\mu_1/\theta}, \quad q = \sum_k q_k. \tag{7'}$$

Inserting (7) in (6), we find immediately that

$$Z = Z_0 Z_1, \tag{8}$$

where

$$Z_0 = e^{q_0}, \quad Z_1 = I_\nu(2q_1), \tag{8'}$$

($I_\nu(y)$ is the Bessel function of the imaginary argument y).

For the free energy $\Psi = -\theta \ln Z$, we obtain

$$\Psi = \Psi_0 + \Psi_1, \tag{9}$$

where

$$\Psi_0 = -\theta \ln Z_0, \quad \Psi_1 = -\theta \ln Z_1, \tag{9'}$$

that is, the free energy of the total system is simply equal to the sum of the free energies of the neutral and charged particles. It is possible to find all the pertinent characteristics of the system from expressions (8), (9'), (9), and (9'), namely:
the average occupation numbers

$$\bar{n}_k^{(0)} = \left(q_k^{(0)} \frac{\partial}{\partial q_k^{(0)}} \ln Z_0 \right)_{\mu_0 = 0}, \tag{10}$$

$$\bar{n}_k^{(1)} = \left(q_k^{(1)} \frac{\partial}{\partial q_k^{(1)}} \ln Z_1 \right)_{\mu_1 = 0}, \tag{11}$$

the average numbers of particles

$$\bar{N}_0 = -\left(\frac{\partial \Psi_0}{\partial \mu_0} \right)_{\mu_0 = 0}, \tag{12}$$

$$\bar{N}_1 = -\left(\frac{\partial \Psi_1}{\partial \mu_1} \right)_{\mu_1 = 0}, \tag{13}$$

and, finally, the mean energy of the system

$$\bar{E} = \left(\psi - \theta \frac{\partial \Psi}{\partial \theta} \right)_{\mu_0, \mu_1 = 0} = \bar{E}_0 + \bar{E}_1. \tag{14}$$

Since the difference between the kind of statistics we are considering and the statistics with a fixed number ν of particles is significant only in the region of energies sufficiently high for particle production, we can limit ourselves to consideration of an ultra-relativistic gas. Transforming the sum in expression (7') for q to an integral, in the usual way, we obtain

$$q = \frac{b\Omega\theta^3}{\pi^2 c^3 \hbar^3}, \tag{15}$$

where Ω is the volume in which the gas is confined and b is the number of possible states with different polarizations. In this case expressions (10), (12), and (14) give the usual formulas of black body radiation for a gas of neutral particles:

$$\bar{n}_0(\varepsilon) = e^{-\varepsilon/\theta}, \qquad \bar{N}_0 = q, \quad \bar{E}_0 = 3\theta q = 3\theta \bar{N}_0. \tag{16}$$

It is, however, of greater interest to consider the equations describing a gas of charged particles. They are different from the corresponding ones for the neutral gas and, as is easy to show with the aid of (11) and (13)-(15), are of the following form:

$$\bar{n}_1(\varepsilon) = 2\frac{I'_\nu(\rho)}{I_\nu(\rho)} e^{-\varepsilon/\theta}, \tag{17}$$

$$\bar{N}_1 = \rho\frac{I'_\nu(\rho)}{I_\nu(\rho)}, \tag{18}$$

$$\bar{E}_1 = 3\theta\bar{N}_1, \tag{19}$$

where $\rho = 2q$.

Let us agree to call these expressions, which describe an ideal gas consisting of oppositely charged particles, the equations of charge statistics.

3. Analysis of the equations of charge statistics

The dimensionless parameter ρ that appears in (17) and (18) has a simple physical meaning. It can be seen from expression (16) that, to within a factor close to unity, ρ is identical with the average number of particles in an ultra-relativistic ideal gas having 2b internal degrees of freedom, as calculated by the usual quantum statistics for systems with a variable number of particles. It is therefore convenient to take ρ as a parameter for comparing our equations (17) and (18) of charge statistics with the corresponding expressions (16) of the usual quantum statistics.

Let us transform equations (17) and (18) to a more descriptive form by invoking the well-known relation from the theory of Bessel functions:

$$\rho I'_\nu(\rho) - \nu I_\nu(\rho) = \rho I_{\nu+1}(\rho). \tag{20}$$

The final equations assume the following form:

$$\bar{n}_1(\varepsilon) = 2e^{-(\varepsilon-\beta)/\theta}, \tag{21}$$

$$\bar{N}_1 = \nu + \bar{N}_d, \tag{22}$$

where

$$\beta = \theta \ln\frac{\bar{N}_1}{\rho},$$

$$\bar{N}_d = \rho\lambda_\nu(\rho),$$

$$\lambda_\nu(\rho) = \frac{I_{\nu+1}(\rho)}{I_\nu(\rho)}.$$

The quantity $\lambda_\nu(\rho)$ characterizes the ratio of the number of particles formed as calculated by charge statistics to the number of such particles as calculated by the usual statistics; it may be approximated with good accuracy (especially accurately for small values of ρ) by the expression

$$\lambda_\nu(\rho) = \frac{I_{\nu+1}(\rho)}{I_\nu(\rho)} \approx 1 - e^{-\rho/2(\nu+1)}. \qquad (23)$$

Equation (23) actually determines the degree to which charge statistics depart from the usual quantum statistics for systems with a total charge ν at a given temperature θ; i.e., it determines the limits of applicability of charge statistics. It can be seen from (23) that the equations of charge statistics are significantly different from the usual ones in the region where

$$\frac{\rho}{\nu+1} \sim 1.$$

We can draw the following deductions on the basis of equations (21) and (22):

1. When charge conservation is taken into account, a certain effective potential β appears in equation (21) for the mean occupation numbers. This quantity β vanishes for $\rho \gg \nu$, which corresponds to transition to the usual statistics with a variable number of particles. On the other hand, if $\rho \ll \nu$, then β becomes the Gibbs potential of a system with a constant number ν of particles; that is, charge statistics goes over into the usual statistics of a system with a fixed number of particles.

2. The total number of charged particles $\bar{N}_1$ is comprised of two parts: the minimum number ν of particles for the given system, which is equal to the initial number of charged particles, and the mean number of particles produced in the form of pairs $\bar{N}_d = \rho\lambda_\nu(\rho)$.

It follows from (23) that the number of pairs formed at a given temperature (i.e., at a given ρ) decreases rapidly as the charge increases; in other words, the charge, so to say, plays the role of an "anticatalyst" in the process of pair creation. For $\rho \gg \nu$, we have $\bar{N}_d = \rho$, which is in agreement with the result derived from the theory of black body radiation; at sufficiently large values of ν (so that $\nu \gg \rho$), virtually no particles are produced, and the mean number of particles remains constant and equal to ν.

The case $\nu = 0$ is of particular interest. It is easy to see from (23) that a difference between charge statistics and the usual one statistics persists in this case as well, particularly at relatively moderate temperatures ($\rho \ll 1$), when

$$\lambda_0(\rho) = 1 - e^{-\rho/2} \approx \rho/2. \qquad (24)$$

In general in the range of relativistic not-too-high temperatures ($\theta \sim mc^2$), the average number of pairs formed is proportional to ρ^2 whereas the average number of neutral particles created is proportional to ρ. As follows from (16) and (19), this leads to different temperature dependences of the mean radiation energy for a neutral gas ($\bar{E} \sim \theta^4$) and for a gas of charged particles ($\bar{E}_1 \sim \theta^7$).

4. Some additions to the Fermi theory of multiple creation of mesons and nucleon-antinucleon pairs.

According to Fermi's hypothesis[1], pi-mesons and nucleon-antinucleon pairs are produced in a certain small volume as a result of

nucleon-nucleon encounters and the average number of these is defined by equations that are valid for systems in thermodynamic equilibrium. In the calculations, however, use is made of the equations of the usual quantum statistics, rather than those of charge statistics, which, as we have shown above, give substantially different results in cases of low multiplicities of created particles. Inasmuch as at very high energies, when ν is small in comparison with the number of particles produced, the equations of charge statistics coincide with those of the usual statistics, the application in this energy region of charge statistics within the framework of the Fermi hypothesis can lead to no new results. Essentially new results are obtained by the application of charge statistics in the region of lower energies, when the average number of particles created is comparable to ν, i.e., to the number of primary charged particles. In the present article, charge statistics is applied to those reactions that take place without a change in the charge of the primary (initial) nucleons and in which charged mesons are produced only in pairs.

In calculating the average number of charged pi mesons in Fermi theory, the same equations are used as in computing of the number of neutral pi mesons. Charged pi mesons, however, as opposed to the neutral ones, obey the laws of charge statistics, and hence for finding the average number of particles it is necessary to use equations (22) and (23) rather than the conventional expressions for black body radiation (16), which are applicable only to the case of a gas of neutral particles.

Equations (16), (22) and (23) immediately give the ratio of the number of neutral pi mesons to the number of charged pi mesons (for $\nu = 0$), namely,

$$\alpha \equiv \frac{\overline{N_0}}{\overline{N_d}} = \frac{1}{2\,(1-e^{-\rho/2})}. \qquad (25)$$

The above relationship coincides with that derived from the Fermi theory only for very large values of ρ. As the multiplicity of the process decreases, i.e., as the value of ρ falls off, α increases. Furthermore, since meson production occurs primarily without charge exchange, the results obtained are in agreement with experimental data.[3,4]

To calculate the number of nucleon-antinucleon pairs created in the process of nucleon-nucleon collisions, it is again necessary, in view of the law of conservation of nuclear charge,[5] to utilize the equations of charge statistics. Thus, for example, in the collision of two nucleons ($\nu = 2$), the number of nucleon-antinucleon pairs formed must be computed by means of the equation

$$\overline{N}_d = \rho(1 - e^{-\rho/6}), \qquad (26)$$

rather than by the equation $\overline{N}_d = \rho$, which is used in Ref. 1. Equation (26) yields a much smaller number of nucleon-antinucleon pairs than the black body radiation expression. This number becomes even smaller if Fermi's hypothesis is applied to the collision of nucleons with nuclei and the energy liberated is assumed to be redistributed among several of the nucleons of the nucleus. Not taking into account the creation of particles in subsequent nucleon-nucleon and meson-nucleon collisions, the number of nucleon-antinucleon pairs produced is defined by

$$\overline{N}_d = \rho[1 - e^{-\rho/2\,(A+2)}], \qquad (27)$$

where A is the number of nuclear nucleons participating in the collision.

If $A \gg 1$, then the ratio of the number of nucleon-antinucleon pairs to the number of mesons is given by

$$\delta = \frac{8}{3}\left[1 - e^{-\rho/2(A+2)}\right], \tag{28}$$

where ρ is taken for the nucleon-antinucleon gas ($b = 4$), i.e., the polarization states of both the neutrons and protons are taken into account). For high energies and small values of A, this ratio, as may have been expected, becomes equal to the Fermi theory one:

$$\delta = \frac{8}{3};$$

however, for energies that are not too high and at large values of A it is substantially lower.

In conclusion, let us determine the dependence of the average number $\overline{N}_1$ of charged mesons, formed in the process of nucleon-nucleon collision without charge exchange, on the primary energy. Let us denote the total energy of the initial nucleon in the center of mass system, expressed in units of the nucleon rest energy, through γ; the same energy in the laboratory system through $\gamma_0 = 2\gamma^2 - 1$, and finally, through γ_k, the energy per nucleon, in the c.m. system, corresponding to the meson production threshold. The region of medium energies, when $\gamma_0 < 10$ and $\gamma < 2.4$ is of interest where charge statistics are concerned. In this case the probability of nucleon-antinucleon pair production is negligible and we shall, therefore, not take it into account.

Making use of formulas (16) and (21)-(23) for $\gamma = 0$, and setting

$$E = \overline{E}_0 + \overline{E}_1 = 2(\gamma - \gamma_k)$$

and

$$\theta = 0{,}1\,\gamma^{1/3}\rho^{1/3}$$

(see also (15) and (19)), we obtain

$$\rho^{4/3}\left[\lambda_0(\rho) + \frac{1}{2}\right] = 6{,}7\,\frac{\gamma - \gamma_k}{\gamma^{1/3}} \tag{29}$$

and

$$\overline{N}_1 = \rho\lambda_0(\rho). \tag{30}$$

Eliminating ρ by simultaneous graphical solution of (29) and (30), we obtain the dependence of the average number of charged mesons on the initial energy. In the energy region under consideration this dependence can be written in the form

$$\overline{N}_1 = k(\gamma - \gamma_k), \tag{31}$$

where $k \approx 2.67$; i.e., the average number of charged mesons varies linearly with the primary energy, which is in agreement with experiment (see, for instance, Ref. 6).

"M. V. Lomonosov" Moscow State University

References

1. E.Fermi, Elementary Particles (Russian trans.) M., 1953.
2. M.A.Leontovich, Statisticheskaia fizika (Statistical Physics)M.-L.1944.

3. A. G. Carlson, J.E.Hooper & D.T.King, Phil. Mag., 41, 701 (1950).
4. U.Camerini, P.H.Fowler, W.O.Lock & H.Muirhead, Phil.Mag.,41,413 (1950).
5. E.P.Wigner, Proc. Nat. Acad. Sci., 38, 449 (1952).
6. Physics of Cosmic Rays, Wilson, editor (Russian trans.) Vol. 1 M. 1954.

* * * * *

CASCADE CURVES FOR ELECTRONS AND PHOTONS IN LIGHT AND HEAVY ELEMENTS

- I. P. Ivanenko

The equations of electromagnetic cascade shower theory are commonly solved by the method of functional transforms (Laplace-Mellin transform with respect to the energy E and Mellin transform with respect to the depth t (the depth is measured in cascade units)). This method is applicable because the asymptotic [completely screened] expressions for the pair-production and bremsstralung cross sections employed in the theory are homogeneous functions of the energy. However, this method is not applicable in the following cases:

1) When the energy E_o of the primary particles is close to the critical energy β.

2) In analyzing cascade processes in heavy elements inasmuch as a) the total absorption coefficient for photons changes greatly with the energy (for example, in lead it drops from 0.773 at high energies to 0.25 at the critical energy) and b) the scattering of the shower particles is very great. It is known that in the region of the cascade maximum about 80% of the particles have an energy less than the critical. For example, for lead, β = 6.4 Mev; for particles of this energy the mean square angle of multiple scattering

$$\bar{\vartheta}^2 = \left(\frac{E_к}{E}\right)^2 \gg 1,$$

where E_k = 21 Mev.

A number of attempts have been made to overcome these difficulties.

Bernstein[1] developed a complicated and cumbersome method of successive approximations to correct for the deviation of the photon absorption coefficient from the asymptotic value [i.e., the correction to the solution obtained by using completely screened cross sections]. However, Bernstein's method is applicable only in the case of small deviations of the coefficient, i.e., only in the case of light elements and high incident energies ($\ln (E_o/\beta) > 1$).

Dallaporta et al[3] solved the equations of the theory, using an approximation for the energy dependence of the photon absorption coefficient. Their calculation procedure is complicated and the resultant curves are unsatisfactory inasmuch as the area under them is not equal to E_o/β. Moreover, the electron energy spectra at the cascade maximum for air and lead differ from each other and from the equilibrium spectrum.*

---

* It is proved in cascade shower theory that in the region of the cascade maximum the electron energy spectrum is close to the "equilibrium" spectrum for any energy dependence of the photon absorption coefficient.

Heisenberg[3] gives an approximate expression for $N(E_0,E,t)$, the number of particles of energy greater than E at depth t, formed by a primary particle of energy E_0 on condition that $\ln E_0/\beta > 1$. The curves given in Heisenberg's book differ by more than 30% from Snyder's exact curves and yield an incorrect number of particles at the cascade maximum for both light and heavy elements as well as distorted particle energy spectra. Furthermore, they do not take scattering of cascade electrons into account.

Wilson,[4] using the Monte Carlo method, calculated the cascade curves in lead for certain particular cases. However, Wilson fails to take correct account of cascade-electron scattering and successively computes the number of electrons produced by photons of energies under 10 Mev!

One can approach the solution of the basic equations of cascade theory in a different way, namely, one can determine the function $N(E_0,0,t)$ from its moments:

$$\bar{t}^n(E_0,0)=\int_0^\infty N(E_0,0,t)\,t^n\,dt\Big/\int_0^\infty N(E_0,0,t)\,dt. \qquad (1)$$

Knowing all the moments $\bar{t}^n$, one can, in principle, find the function itself. Belen'ki[5] obtained a recurrence equation permitting successive calculation at all the moments taking into account the dependence of the photon absorption coefficient on the energy and scattering of the shower electrons

$$\overline{[t_p^n(E_0,0)]_p}=\frac{n}{E_0}\int_0^{E_0}\{P_{p,0,n}(E_0,E)\,[\overline{t_p^{n-1}}(E,0)]_p+\Gamma_{p,0,n}(E_0,E)\,[\overline{t_p^{n-1}}(E,0)]_\Gamma\}\,EdE, \qquad (2)$$

where

$$P_{p,0,n}(E_0,E)=\int_0^\infty\int_{(\omega)}P_p(t,E_0,E,\vartheta)\cos^n\vartheta\,d\omega\,dt,$$

and $P_p(t,E_0,E,\vartheta)$ is the number of electrons in the energy interval E to E + dE at the depth t to t + dt, moving in the solid angle ϑ to $\vartheta+d\vartheta$, produced by the primary electron of energy E_0; the photon distribution functions are denoted through Γ. Thus, in order to find the moments $\bar{t}^n$ one must know the "equilibrium" spectra, integrated over the thickness, of the electrons $P_{p,0,0}(E_0,E)$ and photons $\Gamma_{p,0,0}(E_0,E)$, analytic expressions for which were first found by Tamm and Belen'ki[6] as a result of an approximate solution of the integrated basic equations of cascade theory. The mathematical approximations made in solving these equations can be evaluated by the method of successive approximation developed by Rossi.[7] The correction to the solution of Tamm and Belen'ki does not exceed 4.5%.

The error introduced into the "equilibrium" spectrum by the simplifying initial assumptions (i.e., by the use of asymptotic expressions for the cross sections for pair production and bremsstrahlung, the approximate manner of taking account of the Compton effect and the neglect of recoil electrons of high energy) can be evaluated only by comparing the results obtained in this manner with the results of calculations dispensing with these simplifying assumptions.

Rossi and Klapman[8] integrated the averaged-over-the-thickness equations by numerical methods, accurately taking into account all the processes of interaction of radiation with matter (air) and obtained $N_p(E_0,E)$ for a constant value of $E = 10^7$ ev as a function of E_0 (with $E_0 \geq 10^7$ ev). The spectrum of Tamm and Belen'ki differs by less than 4% from the spectrum calculated by Rossi and Klapman. Thus it may be assumed that for $E \geqslant 10^7$ ev the "equilibrium" spectrum in light matter differs from the exact spectrum by not more than 4%.

Hence, using equation (2) one can, in principle, compute all the moments $\bar{t}^n$ with adequate accuracy. In practice, however, only the first two or three moments can be evaluated.

Zatsepin[10] was the first to compute the cascade curves from the values of their first two moments. The approximate expression for the cascade curve used in Ref. 10 is valid when $\ln (E_0/\beta > 1$ and for $t > \bar{t}_{max}$. In order to find the cascade curve it is necessary to solve a system of three transcendental equations, which greatly complicates the computations. If, using the method of Ref. 10, it is desired to utilize the third moment in constructing the curve, it is necessary to seek a different form of the approximation dependence.

We propose a method of constructing the cascade curves based on utilizing a system of polynomials, orthogonal over the interval from 0 to ∞. We approximate the cascade curve by means of the sum over Lager's polynomials:

$$N(t, E_0, 0) = (\gamma t)^i e^{-\gamma t} \sum_{n=0}^{k} A_n L_n^i(\gamma t). \tag{3}$$

The coefficients A_n are determined from the condition of orthogonality of the polynomials $L_n^i(x)$ by the following equality

$$A_n = \frac{\gamma n!}{\Gamma(n+i+1)} \int_0^\infty N(E_0, 0, t) L_n^i(\gamma t)\, dt. \tag{4}$$

The coefficients are directly related to the moments of the curve: for example, with $i = 1$

$$A_0 = \gamma \frac{E_0}{\beta}, \quad A_1 = \frac{\gamma}{2} \cdot \frac{E_0}{\beta} [2 - \gamma \bar{t}(E_0, 0)],$$

$$A_2 = \frac{\gamma}{3} \cdot \frac{E_0}{\beta} [3 - 3\gamma \bar{t}(E_0, 0) + \frac{\gamma^2}{2} \bar{t}^2(E_0, 0)] \quad \text{and so on.} \tag{5}$$

We assume the coefficient γ to be equal to the absorption coefficient for the most penetrating part of the radiation, i.e., the photons.

It was found that the polynomials $L_n^0(x)$ and $L_n^1(x)$ allow of the most accurate calculation of the cascade curves from the minimal number of moments: for $\ln(E_0/\beta) > 1$ the approximate curves differ from the exact ones by less than 5%. Curves constructed on the basis of two moments ($k = 2$ in (3)) differ from the curves plotted on the basis of three moments by only 10-15%. We computed the first three moments for primary electrons and photons with $0.1 < E_0/\beta < 5$ for light elements. For lead we calculated (taking into account the dependence of the photon adsorption coefficient on the energy, scattering and ionization loss) the first two moments with $0.5 < E_0/\beta < 60$, also, for the primary electrons and photons. The cascade curves for the primary photon were approximated by means of the sum (3) of the polynomials $L_n^1(x)$. The cascade curves for the primary electrons were approximated by means of the sum over the polynomials $L_n^0(x)$.

Equation (3) does not exactly satisfy the boundary condition

$$N(t, 0, E_0)|_{t=0} = 1. \tag{6}$$

Since we desire to compute the cascade curves at energy $E_0/\beta \sim 1$, where the number of particles at the cascade maximum is close to unity, it is important to have the approximation curve satisfy the boundary condition (6) exactly. We approximate the cascade curves for the primary electron by the expression

$$[N_p(E_0, 0, t)]_p = e^{-\gamma t} \left[\sum_{n=0}^{k} A_n L_n^0(\gamma t) + C L_{k+1}^0(\gamma t) \right]. \tag{7}$$

The constant C is determined from condition (6).

From the known moments for the primary electron and photon, evaluated taking into account scattering and ionization loss, we can compute the moments for the primary particles by means of the arbitrary spectrum

$$[\bar{t}_p^n(E_0, 0)]_{\Phi(E_0, E)\Gamma} = \int_0^{E_0} \Phi_\Gamma(E_0, E)\,[\bar{t}_p^n(E, 0)]_\Gamma \int_0^{E} P_{\Gamma,0,0}(E, E')\,dE'dE \Big/ \int_0^{E_0} P_{\Phi\Gamma 0,0}(E_0, E)\,dE. \quad (8)$$

We carried out numerical computations for a primary photon spectrum of the form

$$\Phi_\Gamma(E_0, E) = \begin{cases} 1/E & \text{for } E < 330\ \text{MeV}, \\ 0 & \text{for } E > 330\ \text{MeV}. \end{cases} \quad (9)$$

The corresponding values of $\{\bar{t}_p^n(E_0, 0)\}_{\Phi\Gamma(E_0, E)}$ were determined from the experimental data of Ref. 9. The following results were obtained:

$\bar{t}_{theo}$	$\bar{t}_{exp}$	$\overline{t^2}_{theo}$	$\overline{t^2}_{exp}$
5.89 ± 0.12	5.9 ± 0.2	53.4 ± 2	55 ± 4

The theoretical and experimental values of $\bar{t}$ differ by 1%; the values of $\overline{t^2}$ by 4% (the difference is still within the limits of the experimental and computational errors), whereas when scattering is not taken into account t_{theo} with $\sigma = \sigma_0$ is 33% smaller than t_{exp}, while with $\sigma = \sigma(E)$, t_{theo} is about 10% greater than t_{exp}.

Thus, if scattering is taken into account with maximum possible accuracy, cascade shower theory satisfactorily agrees with experiment for heavy elements.

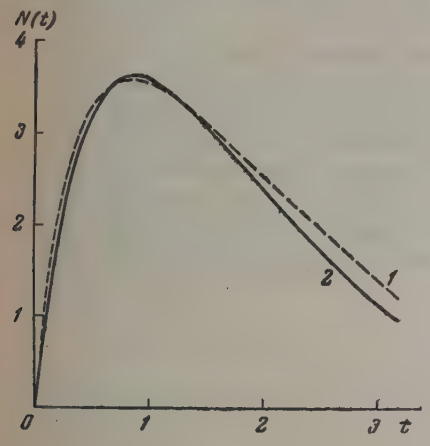

Fig. 1. Comparison of calculated cascade curve with experimental data: 1) experimental curve from Ref. 9 obtained for photons with spectrum ~1/E in carbon, 2) curve obtained by averaging (3) over photon spectrum (9).

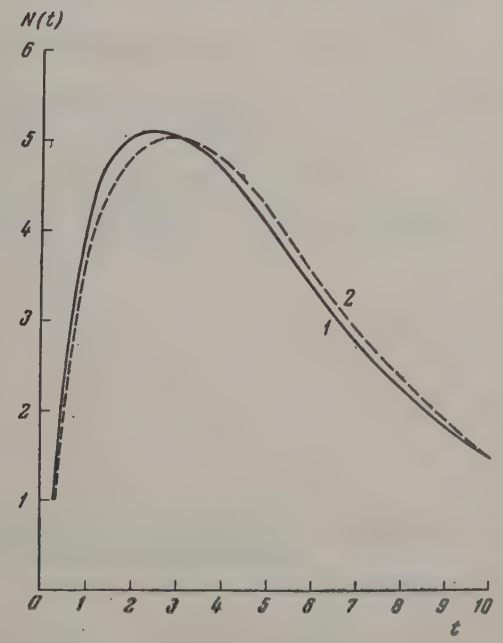

Fig. 2. Same as Fig. 1 but for Pb.

We constructed cascade curves on the basis of equations (3) and (7). The cascade curves for primary photons in carbon and lead were averaged over the spectrum (9). Experimental cascade curves for photons with spectrum (9) in carbon and lead have been determined by Blocker et al.[9] The curves for carbon are juxtaposed in Fig. 1:

curve 1 is taken from Ref. 9; curve 2 was obtained as a result of our calculations. The normalization point is t = 0.1. It will be seen that up to t = 2 the curves differ by less than 5% while at greater values of t the difference attains 20%. This may be explained by the fact that in the calculations the coefficient γ was assumed equal to the asymptotic value of the photon absorption coefficient (0.773), whereas in the energy region in question the photon absorption coefficient is some 10-15% smaller, which leads to a greater penetrating power of the shower.

Analogous data for lead are given in Fig. 2. Curve 1 is taken from Ref. 9; curve 2 is the calculated curve. The normalization point is t = 0.5. The curves differ from each other by less than 5% over the entire range; this is within the limits of the experimental and computational errors.

Thus, it will be seen that by means of the method of moments and using only the first two moments it is possible to construct the cascade curves in light and heavy elements for primary particles in the energy range E_0 = 0.1-100β (or greater) with an accuracy of within 5-10%.

Moscow State University

References

1. I.B.Bernstein, Phys. Rev., 80, 995 (1950).
2. N.Dallaporta & E.Clementel, Nuovo Cim., 3, 235 (1946); N.Dallaporta & G.Polani, Nuovo Cim., 4. 1 (1947); E.Clementel, & L.Fabbrichesi, Nuovo Cim. 5, 78 (1948).
3. W.Heisenberg, Kosmische Strahlung - Springer, Berlin, 1953.
4. R.Wilson, Phys. Rev., 86, 261 (1952).
5. S.Z.Belen'ki & B.I.Maksimov, Zhur. eksp. i teor. fiz., 22, 102 (1952).
6. I.E.Tamm & S.Z.Belen'ki, J. Phys. USSR, 1, 177 (1939).
7. B.Rossi, High Energy Particles (Russian trans.), M.-L., 1955
8. B.Rossi & S.J.Klapman, Phys. Rev., 61, 414 (1942).
9. W.Blocker, R.W.Kenney & W.K.H.Panofsky, Phys. Rev., 79, 414 (1950).
10. G.T.Zatsepin , Doklady AN SSSR, 63, 243 (1948).

* * * * *

APPLICATION OF THE RANDOM TRIALS [MONTE CARLO] METHOD TO CALCULATION OF INTRANUCLEAR CASCADES

- V. V. Chavchanidze

The method of random trials is a new, comparatively little known, method of calculating complex statistical phenomena. In the foreign literature this method is known under the name of the Monte Carlo method.* The idea of the method in its simplest form was first advanced by Ulam and Von Neumann.[1]

---

* Translator's Note: For the sake of simplicity it will hereinafter be referred to as the Monte Carlo method or M.C.M.

The method was applied to calculations of intranuclear cascades by Goldberger[2], as well as by Bernardini, Booth and Lindenbaum.[3] These authors examined the case where the star-producing particle has a comparatively low energy. Wilson[4] calculated electron and photon initiated showers in layers of lead of different thicknesses. Puppi, De Sabbata and Manaresi[5] used the Monte Carlo method to investigate the mechanism of pi-meson absorption by nuclei. It was shown in all these studies that the method yields excellent results.

The Monte Carlo method is applicable to problems of a stochastic character and can be used for the calculation of stochastic effects of any complexity. In using this method it is essential to know the probabilities of the elementary events that are the "links" of the "chain" constituting the investigated effect or process.

The application of the M.C.M. to the solution of any stochastic problem consists of sequential theoretical reproduction of the effect under conditions close to those under which it occurs in nature.

The essence of the Monte Carlo method may be described as follows. A complex stochastic process is regarded as a sequence of a finite number of elementary stochastic processes. Assuming that the probability distribution laws for the elementary processes are known, the expected results of trials are divided into equal probability groups. Then the outcome pertaining to one of these groups, taken at random, is considered to be the actual result of an experiment. This outcome is then taken as the point of departure for finding a "random" result for the elementary event which is to be its iterative successor, etc. In this fashion the stochastic uncertainty of the expected outcome of a future trial is replaced, step by step, by the concrete numerical result of a trial which consists of selecting "by chance" one of equally probable events. Having reached the n-th event, defining the final stage of the effect or process, everything is started all over again from the beginning, introducing into the process a new factor or object (for example, a new particle). Having "introduced" in this fashion 100-200 particles, there is obtained a distribution of the objects (particles) in the final state. In principle, if the laws determining the elementary events were exactly known, then the results obtained by the M.C.M. would be similar to those determined experimentally. In this sense the Monte Carlo method may be termed a "theoretical experiment."[6,7]

The Monte Carlo method can be used to solve such problems as the following: 1) calculation of multiple and single scattering of charged particles in matter, 2) calculation of the energy losses of particles in matter, 3) calculation of electronic-photonic cascades, 4) calculation of extranuclear cascades, 5) calculation of intranuclear cascades, accompanied or not accompanied by pi-meson production, as well as many other statistical problems encountered in modern physics.

Obviously the problems solvable by the M.C.M. can also be solved by other stochastic methods which are fundamentally reducible to analytic determination of the distribution function of the final states, but such other approaches are often barred by insuperable mathematical difficulties that force abandonment of efforts to solve the problem.

Among the advantages of the M.C.M. over others, the following may be mentioned.

1. While for other stochastic methods (such as the method of differential equations, the method of integral equations, the method of characteristic equations, the method of moments, the methods of mathematical statistics, Markov's method and the like), it is

necessary to have analytical expressions for the a priori probabilities, or the differential cross sections for the elementary events, for the M.C.M. a graphical specification of these is sufficient, i.e., it is sufficient to know the experimental values of the differential or integral cross sections for the elementary processes. This means that the M.C.M. can be applied for the calculation of a complex stochastic chain immediately upon determining the experimental values of the cross sections for the elementary events, without waiting for the formulation of a theory of these events and without recourse to simplified empirical expressions for the differential cross sections.

2. Actually none of the other known mathematical methods can effectively solve a problem of the probability law for the distribution of final states where the probable result of a subsequent event is stochastically related to the results of the preceding events. On the other hand, problems of this kind are readily solved by the M.C.M.

3. M.C.M. is characterized by exceptional clarity: Any involved complex of statistically linked events is reduced to a chain of elementary events.

4. After the preliminary preparation of curves and development of the scheme of calculation, the actual computations can be carried out by lower-caliber mathematical personnel.

5. The method allows of a fairly simple evaluation of the influence of errors on the initial (basic) parameters on the final distribution.

6. The method allows of "reproduction" of events with whatever statistics are necessary. This permits "reproduction" of an effect with fluctuations characteristic of the actual case. If the number of repetitions of the random process (spins of the wheel of chance) is made sufficiently great the resultant curves will be identical with the actual distribution curves for the final states of the effect.

Work was carried out in our department on the utilization and improvement of the M.C.M. (Refs. 6-8).*

The method in its original form consisted of the following. Let us assume that we have some process characterized by the differential spectrum $f(x)dx$, giving the probability that x lies in the interval $(x, x+dx)$. For example, let $f(\varepsilon)d\varepsilon$ be the value of the energy loss per collision event (say the energy radiated in the form of a photon). In this case $f(\varepsilon')$ represents the energy-loss "density" in the neighborhood of ε'.

Next let us imagine that we have a circle on which we have laid off arcs proportional to the probabilities that the loss is equal to 1 ev, 2 ev, 3 ev, etc. Let the 0-1 ev arc be proportional to the value of $f(\varepsilon)$ at the 1 ev point, the 1-2 ev arc be proportional to at 2 ev, etc. Thus the divisions will not be uniform, and the frequency of finding this or that division in arcs of equal length will generate the probability law $f(\varepsilon)$ for the quantity ε.

Now let us attach our graduated circle to a disk mounted on the shaft of a motor and equipped with a suitable brake; the disk is free to rotate when the motor is started and is brought to a stop when the motor is switched off and the brake applied. We start the motor and then apply the brake at random. The probability of any given energy

---

* The following graduate students in the Physics Department of "I. V. Stalin" Tbilisi State University participated in the development of the M.C.M.: A. M. Morozov, V. A. Kumsishvili, Iu. A. Shuander, R. L. Skhirtladze, O. Ia. Gelman, A. V. Tagviashvili, L. A. Sarkisian, N. I. Gelashvili.

loss interval stopping opposite a stationary pointer will obviously be proportional to the length of the arc occupied by this interval on our graduated circle. Actually, any equal sector of the circle will stop in front of the pointer with equal probability, but since the designations of the sectors are distributed non-uniformly, an interval bearing a given designation will "come out" with a probability proportional to the corresponding ordinate of the differential distribution curve.

Let us examine the case when the probability of occurrence of some stochastic quantity x depends on some parameter α. Let us consider, for example, the slowing down of a charged particle by ionization in matter. In this case the energy loss probability is given by the

$$f(\varepsilon, v_0)\,d\varepsilon = \frac{A\,d\varepsilon}{v_0^2\varepsilon^2}, \qquad (1)$$

where A is the normalization constant, v_0 is the velocity of the particle prior to collision and ε is the energy loss. Assuming v_0 to be known, we can plot the curve for $f(\varepsilon, v_0)$ on the circle. Then if we "play" the process of energy loss, i.e., perform the operation of spinning and randomly stopping the circle, we will obtain a specific "realized" energy loss, for example, ε' (ε' is a concrete number). If ε' is large, the energy loss may affect the velocity of the particle, in this case before the next "spin" it will be necessary to take into account that the value of v_0 in (1) has changed. This means, in practice, that we must plot a new distribution of the divisions on the circle. After this redistribution, we can "spin" for the energy loss in the second collision, etc. Obviously, the operation of repeatedly plotting new divisions on the circle is very onerous and difficult.

It would obviously be desirable, therefore, to modify the method so as to do away with the circle that has to have its subdivisions changed after every spin.[4] This can be accomplished in the following manner.

We take a sheet of drawing paper and scale x and $F(x, \alpha) = \int f(x', \alpha)\,dx'$, (where α is a parameter) along its edges, i.e., prepared a graph. For example, in the case of ionization losses $F(\varepsilon, v_0) = \int f(\varepsilon', v_0)\,d\varepsilon'$, where $F(\varepsilon, v_0)$ is the probability that the energy loss will take on a value between 0 and ε when the parameter v_0 has a particular value. When $\varepsilon = \infty$ we will have $F(\infty, v_0) = 1$. It is clear that the curve $F(\varepsilon, v_0)$ will be a monotonic curve, and that no two curves $F(\varepsilon, v_0)$ and $F(\varepsilon, v_0')$ will intersect. Knowing in advance the interval bounding the variation of the parameter v_0, we can readily plot on our sheet the curves for $F(\varepsilon, v_0)$, $F(\varepsilon, v_0')$, $F(\varepsilon, v_0'')$, ..., $F(\varepsilon, v_0^n)$, where the number of curves in the family is determined by the accuracy required. No curve will intersect any other curve in the same family. Thus with the aid of such a family of integral curves, we can make successive "spins" for random values of ε in the entire interval of the possible values of ε and v_0.

Let us now imagine that this plot is rolled onto a cylinder around an axis parallel to the axis of ε, and that the cylinder is mounted on a drum having arrangements for being rotated and quickly braked and a stationary pointer or index (see figure) on the side. Obviously, after being spun, the cylinder can stop with equal probability with any section of the ordinates opposite the index, which permits finding the corresponding ε. It can easily be shown that operations of spinning the circle with the differential curve and spinning the cylinder with the integral curves are equivalent.[6-8] The operation of the machine, i.e., its randomness, is most readily checked using Kolmogorov's criterion (see Ref. 9).

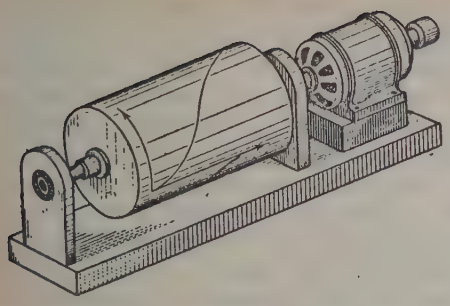

Simplest model of a Monte Carlo machine.

A group of graduate students, under the supervision of the author, prepared tables of random numbers by means of the machine.[6-8] Later, in connection with certain statistical calculations, we started to use the table of random numbers prepared in 1936 by M. Kadyrov.[10] It appeared, however, that several pages of Kadyrov's tables do not satisfy Kolmogorov's criterion. Accordingly, it was necessary to correct some of the pages. The corrections were made by the M.C.M. (we discarded numbers by the law of chance, knowing the excess of numbers larger than 0.5, compared with those smaller than 0.5).

Having a table of random numbers (T.R.N.) it is possible to carry on any stochastic calculation using different columns of the tables. The primary rule in use of a T.R.N. consists in choosing the first number entirely at random and then taking the others from the column in accord with some set, invariable rule.[6,7] The violation of this rule will, of course, result in subjective selection of the random numbers and, therefore, invalidate the procedure.

Employment of the T.R.N. showed that they can completely replace a Monte Carlo machine.[6,7] However, to make this clearly evident it is necessary to show that the equivalent of "spinning" for any stochastic values can be accomplished by "drawing" numbers from a T.R.N.

Let us examine a typical example: assume we have a high-energy positron moving through matter. The positron may participate in any of the following processes: 1) an ionizing collision with cross section σ_i, 2) a bremsstrahlung process with cross section σ_r, or 3) an annihilation process with cross section σ_a. Assume that we know that some one of these processes has occurred. It is necessary to decide which specific process it was. We know only the a priori probabilities of the processes

$$\tau_i = \frac{\sigma_i}{\sigma}, \quad \tau_r = \frac{\sigma_r}{\sigma}, \quad \tau_a = \frac{\sigma_a}{\sigma},$$

where $\sigma = \sigma_i + \sigma_r + \sigma_a$. From the conventional point of view it is simplest to assume that of N_0 positrons $\tau_i N_0$ undergo an ionizing collision, $\tau_r N_0$ undergo radiative slowing down and $\tau_a N_0$ experience annihilation. However, we know that in reality the laws of probability will be manifest and greater or smaller fluctuations will occur. The M.C.M. permits us to reproduce such natural flucturations. Let us construct the curves for "spinning" for the process type. On our cylinder chart let us lay off values of τ_i and $\tau_i + \tau_r$ along the vertical axis, as functions of the positron energy. In this case it is clear that the constructed curves will divide the plot into three regions: ionization, bremsstralung and annihilation. For example, let the energy of the particle be E_0 = 10 Mev, and let the a priori probabilities of the three processes be, respectively, 0.212, 0.295, 0.493. If the random number resulting from "spinning" for the process type turned out to be 0.412, then it is clear that the radiative loss process has "won" or come out.

This is the situation that obtains in "spinning" for the type of process, when we are dealing with discrete random values depending on a continuous parameter (in our example, E_0 is the parameter). Since in this case the ordinate varies from 0 to 1, it is possible

to use a table of random numbers to "draw" the random number. In an analogous fashion one can "spin" or "draw" for the type of atom with which the particle collides while moving through air, a photographic emulsion, etc. In a similar way it is possible to "draw" for the probabilities of formation of any particular number of particles in nucleon-nucleon collisions. Up to this point we have assumed that the particles initiating reactions are monoenergetic. Many actual problems, however, involve cases where the incident particles have a definite energy spectrum. We can show that fluctuations in the energy distribution of incident particles may be taken into account by the M.C.M. if we make use of either the experimental or the theoretical differential energy spectrum of the incident particles.[6,7]

Let the differential energy spectrum be given in the form

$$P(E)\,dE = \frac{A\,dE}{E^{\gamma}} \quad (E_a \leqslant E \leqslant E_b).$$

Then it is easy to see the function

$$\tau(E)\,dE = \frac{(1-\gamma)\,E^{-\gamma}dE}{(E_b^{-\gamma+1} - E_a^{-\gamma+1})}$$

will be the normalized function giving the probability density of the appearance in the general flux of a particle having an energy in the interval from E to E + dE. Then as usual we can construct the integral distribution function $T(E)\,dE = \int_{E_a}^{E} \tau(E')\,dE'$ and "spin" or "draw" for the particle energy, i.e., determine its value with the aid of the T.R.N. It is clear that the process of "drawing" for the energy of the "initiating" particle must precede "drawing" for all other characteristics of the event being studied.

Thus we have shown that the M.C.M. does not at all require the use of a Monte Carlo machine. The availability of T.R.N. makes such machines wholly unnecessary. The lack of understanding of this point has, until now, impeded the widespread use of this convenient and powerful method of calculating complex statistical phenomena.

In order to make clear the features of the method let us outline the detailed scheme for calculating internuclear cascades not accompanied by the formation of pi mesons. The process will be a typical chain or serial process. It may be noted that in an analogous fashion one can construct the calculation schemes for such other serial processes as extranuclear cascades, internuclear cascades involving the formation of pi mesons, electron-nuclear cascades, etc.

A typical M.C.M. calculation scheme for an intranuclear cascade initiated by a nucleon of medium energy (under 500 Mev), if we utilize the model of Bernardini et al described in Ref. 3, will comprise the following steps.

1. We "draw" for the energy of the incident nucleon. To this end we construct a chart for $F_1(E)$, where

$$F_1(E) = \frac{\int_{E_{min}}^{E} f_1(E')\,dE'}{\int_{E_{min}}^{\infty} f_1(E')\,dE'};$$

$f_1(E)$ defines the differential energy spectrum of the incident nucleons (this may be done separately for protons and neutrons, if their energy spectra differ). As a consequence of the "drawing" we obtain a specific numerical value for $E = E_0'$. That is, we assume that the initial

kinetic energy of the striking nucleon is E_0'.

2. We "draw" for the nucleon-nucleus impact parameter with the aid of a graph for $F_2(r)$, where

$$F_2(r) = \frac{r^2}{R^2}$$

(here R is the nuclear radius, while r is the impact parameter). As a result, we obtain the specific value $r = r'$.

3. We "draw" for the azimuth angle of collision, using a graph for $F_3(\varphi)$, where

$$F_3(\varphi) = \frac{\varphi}{2\pi}$$

(φ is the azimuth angle measured from a fixed reference plane).

4. We "draw" for the free path of the nucleon in heterogeneous nuclear matter to its first collision with the nucleons of a nucleus. To this end we construct a graph for $F_4(y)$, where

$$F_4(y) = 1 - e^{-y},$$

and $y = \sigma \int_0^x N(x')\,dx'$. Here $\sigma = \sum_{i=1}^{p} \sigma_i$ is the sum of the total cross sections of all the processes which may occur as a result of a collision at the given energy of the incident nucleon and $N(x)$ is the density of nucleons in the nuclear matter at point x. The "drawing" gives us the specific value $y = y'$, from which we can readily find the specific value of x, if we have a graph for the dependence of y on x. In practice it is convenient to join this graph to the "drawing" chart for y along the x-axis, with the latter oriented vertically. Using this dual construction we find the specific value of x directly (from the random number). In the case when the nucleus is homogeneous $y = \sigma N x = x/l$, where l is the mean free path. If our "drawing" yields a value of y' for which the associated value of $x > 2L_{r'} = 2\sqrt{R^2 - (r')^2}$, this will signify that the nucleon emerged from the nucleus without undergoing a collision. The convenience of the suggested procedure lies in the fact that one can very simply "draw" for the path of the nucleon which has undergone its penultimate collision inside the nucleus.

Assume that the next-to-the-last collision took place at the distance l' from the surface of the nucleus, with an impact parameter $r = r'$. There upon the particle started moving in a certain direction with an impact parameter $r = r''$. Since the curves for $y_r = \int_0^x N_r(x')\,dx'$ can be constructed in advance for 10-30 different values of the impact parameter, knowing that $r = r''$, it is possible to "make a drawing" with subsequent graphical determination of x on the basis of the curve $y_{r''} = \int_l^x N_{r''}(x')\,dx'$. Since in "drawing" for the path lengths, we will encounter diverse values of l, it is rather difficult to plot in advance the function $y_r = \int N_r(x')\,dx'$ for the different possible path values.

In this case it is convenient to use the following procedure: plot the $y_r = \int_0^x N_r(x')\,dx'$ curves in advance with y_r being laid off along the horizontal axis and x along the vertical axis downward. Then to "draw" the path length for the particle which has undergone its

penultimate collision with $x = l'$ and moving with the impact parameter $r = r''$, we shift the point of the $y_{r''}$ curve, corresponding to the point $x = l'$, to the origin of coordinates and then "draw" in the ordinary manner, determining x on the displaced curve. Again if we "draw" a random number for which $x > 2\sqrt{R^2 - (r'')^2} - l'$, this will indicate that the particle has emerged from the nucleus without undergoing collision. With this method of following the motion of a nucleon in a nucleus we can dispense with referring to the rectangular or spherical coordinates of the nucleus.

5. We "draw" for the target, i.e., the type of particle with which the nucleon collides. If $\rho_p(r)$ and $\rho_n(r)$ are, respectively, the proton and neutron densities, then the "drawing" can be made with aid of a plot typical for the "drawing" of discrete random values. For the a priori probabilities with the given r, we choose

$$\tau_n(r) = \frac{\rho_n(r)}{\rho_n(r) + \rho_p(r)} = \frac{\rho_n(r)}{\rho(r)}, \quad \tau_p(r) = \frac{\rho_p(r)}{\rho_n(r) + \rho_p(r)} = \frac{\rho_p(r)}{\rho(r)}.$$

Having constructed the plot for $\tau_n(r)$ as a function of r (here r is the radius vector of the point of collision of the nucleons), we can readily "draw" for the target particle at any value of r, invoking the fact that $\tau_n(r) + \tau_p(r) = 1$. If the nucleus is homogeneous,

$$\tau_p = \frac{Z}{N+Z} = \frac{Z}{A} \quad \text{and} \quad \tau_n = \frac{N}{N+Z} = \frac{N}{A}$$

(N is the number of neutrons and Z the number of protons in the nucleus). When we know with which particle the incident particle collided, we must determine the momentum of the nucleon experiencing the collision (at very high energies of the incident particle this "drawing" may be dispensed with).

6. We "draw" for the momentum of the struck nucleon. Here we must make some assumption regarding the nucleon momentum distribution in the nucleus. For example, if we assume that $4\pi f(p) p^2 dp$ is the probability that the momentum of the nucleon lies inside a spherical layer of thickness dp, the "drawing" is made according to a graph for $F_6(p)$, where

$$F_6(p) = \frac{\int_0^p f(p) p^2 dp}{\int_0^\infty f(p) p^2 dp}.$$

If it is assumed that the distribution in momentum of the nucleons is described by Fermi's law for a degenerate gas, then instead of the foregoing we have

$$F_6(P) = \begin{cases} \left(\frac{p}{p_0}\right)^3 & p \leqslant p_0, \\ 0 & p > p_0, \end{cases}$$

where p_0 is the limiting value of the momentum.

7. We "draw" for the polar angle of the momentum of the nucleon with which the collision took place. The "drawing" is made with the aid of a plot of $F_6(\vartheta)$, where

$$F_6(\vartheta) = \frac{1 - \cos\vartheta}{2}.$$

The "drawing" for the azimuth angle of the nucleon's momentum is made with the aid of a chart for

$$F_7(\Phi) = \frac{\Phi}{2\pi}.$$

Having determined the values of p, ϑ and Φ, we have fully established the momentum vector p of the nuclear nucleon.

8. We pass over to the center of mass system of the colliding nucleons, using the usual mathematical procedure.

9. We "draw" for the type of process. For this it is necessary to know all the partial cross sections as functions of the initial energy of the colliding particle (in the laboratory or in the c.m. system). If the $\sigma_i(E_0)$ are given, it is simple to find $\tau_i(E_0) = \frac{\sigma_i(E_0)}{\sigma(E_0)}$, where $\sigma(E_0) = \sum_{i=1}^{n} \sigma_i(E_0)$. As a result of the "drawing" we will know which process occurred in the collision. For example, suppose we determined the process to have been elastic scattering of neutron from a nuclear proton; in this case the subsequent calculation is performed as follows:

10. We "draw" for the scattering angle of the incident nucleon with the aid of the integral distribution function

$$F_8(\theta) = \frac{1}{\sigma_s}\int_0^{\theta}\left(\frac{d\sigma}{d\theta'}\right)_s d\theta',$$

where σ_s is the total elastic scattering cross section.

11. We determine the direction of motion of the recoil nucleon.

12. We find the momenta and energies of the colliding particles in the initial system.

After this we "follow" both nucleons, repeating the above procedure beginning with step 3 (since the impact parameter is determined by the direction of motion of the secondary nucleon). We "follow" the particles until they emerge from the nucleus; in this way we take strict account of the geometry of the nucleus. In the new "drawing," instead of elastic scattering, inelastic nucleon-nucleon scattering may be "drawn." In this case the procedure for "drawing" the scattering angle for one of the nucleons becomes more complex. Let the inelastic scattering be accompanied by the formation of one π meson. In such a case we must know the differential cross section $\frac{d^2\sigma}{d\theta dk}$, where k is the momentum of the generated meson. Then the "drawing" is made in two stages. First we "draw" for the momentum of the π meson with the aid of the integral distribution function

$$F_9(k) = \frac{\int_0^{k}\left(\frac{d\sigma}{dk'}\right)dk'}{\int_0^{\infty}\left(\frac{d\sigma}{dk'}\right)dk'} = \frac{\int_0^{k} dk' \int_0^{\pi}\left(\frac{d^2\sigma}{d\theta dk'}\right)d\theta}{\sigma}.$$

then after determination of a concrete $k = \bar{k}$, we "draw" for the angle of scattering with reference to the curve of the $F(\theta, k)$ family for which $k = \bar{k}$:

$$F_{10}(\theta, \bar{k}) = \frac{\int_0^{\theta}\left(\frac{d^2\sigma}{d\theta' dk}\right)_{\bar{k}} d\theta'}{\int_0^{\pi}\left(\frac{d^2\sigma}{d\theta' dk}\right)_{\bar{k}} d\theta'}.$$

Practically, the $F(\theta,k)$ curves are constructed for different values

of k in advance, and then the "drawing" is made using the curve, appropriate to the result obtained in the foregoing "drawing."

After we have followed all the nucleons of the nuclear cascade, we start the process of "drawing" all over again, that is, we start a new cascade-initiating particle. By "introducing" some 200-300 particles in this way, it is possible to construct the functions for the distribution of the emerging particles in momentum (energy) and angle. It is possible to construct a correlation curve between the angles of ejection and the energy of the emerging particles. It is important to note that by this means it is possible to obtain full information regarding the nature of nuclear cascades if correct assumptions are made concerning the probabilities of elementary processes. If there are two competing hypotheses, we can make "drawings" on the basis of both and then, using experimental results for comparison, choosebetween them. For the "drawing" it is not at all necessary to have analytic expressions for the probabilities of the elementary processes; it is sufficient to have a graphic representation of the differential cross sections as, for example, in the case of elastic n-p scattering. Then by means of graphical integration it is easy to construct a normalized integral distribution function which can as readily be used for the "drawing" as a curve plotted on the basis of an analytic expression.

Experience showed that the "drawing" operation is the least time consuming part of the calculations and that most time is taken up by ordinary algebraic operations such as are involved in passing from one coordinate system to another, etc.

It is essential to point out that with an unlimited increase in number of trial particles, the results obtained with the M.C.M. will approach the limiting distribution laws for the given parameters of the ejected particles. However, in nuclear physics experiments and cosmic ray work, it is a characteristic fact that the number of particles initiating nuclear cascades is limited (as, for example, in the case of stars in nuclear emulsions). Therefore, it is desirable to supplement an actual experiment by a "theoretical experiment," i.e., by enhancing the actual statistics through an increase in the number of particles "introduced."

Having found in this way the limiting distribution law (the number of particles "introduced" is significantly larger than the number of cascade-initiating particles), we can readily determine the possible fluctuations that may be encountered in observing a limited number of cascade-initiating particles (i.e., for example, the limited number of stars observed in photographic emulsions).

It seems to us that for practical M.C.M. calculations Kadyrov's tables can be used (with due care), particularly since more extensive random number tables constructed especially for the M.C.M. and meeting today's rigorous criteria, do not exist.

We think that the M.C.M., in the form in which it has been described here, can serve as a working instrument in the hands of experimental and theoretical physicists for calculations of statistical phenomena. It seems to us, further, that there is no foundation for the skeptical attitude often displayed toward the M.C.M., since it has been shown that no special Monte Carlo machine is necessary and that tables of random numbers can be employed in calculating by this method with almost the same ease as tables of logarithms are used in ordinary calculations.

Physical Institute of the
Academy of Sciences of the Georgian S.S.R.

References

1. S.Ulam & J.VonNeumann, Bull. Am. Math. Soc., 53, 1120 (1947).
2. M.L.Goldberger, Phys. Rev., 74, 1269 (1948).
3. G.Bernardini, E.T.Booth & S.J.Lindenbaum, Phys. Rev., 88, 1017 (1952); Symposium, "Iadernye reaktsii pri bol'shikh energiiakh", (Nuclear reactions at high energies) Vol.II M., 1954.
4. R.R.Wilson, Phys. Rev., 86, 261 (1952).
5. G.Puppi, V.DeSabbata & E.Manaresi, Nuovo Cim., 9, 726 (1952).
6. V.A.Kumsishvili, Thesis, Tbilisi State Univ., 1954.
7. Iu.A.Shuander, Thesis, Tbilisi State Univ., 1954.
8. A.M.Morozov, Thesis, Tbilisi State Univ., 1954.
9. B.V.Gnedenko, "Kurs teorii veroiatnostei",(Course in the theory of probability), M.-L., 1950.
10. M.Kadyrov, "Tablitsy sluchainykh chisel." (Tables of random numbers). Tashkent, 1936

ELEMENTS OF RELATIVISTIC MAGNETO-AERODYNAMICS

- K. P. Staniukovich

The motion of a gas in strong magnetic fields when the energy density is high or the velocity is close to that of light can be of considerable interest. In the present article we shall consider the basic relations of relativistic magneto-aerodynamics, and shall take up in some detail the one-dimensional motion of a gas in a magnetic field; we shall also show that for one-dimensional motion we may look for exact solutions even in the case of arbitrary fields or forces acting on the particles of the moving gas. We shall also consider the elements of the theory of shock waves both in relativistic magneto-aerodynamics and in the case of arbitrary fields.

In order to derive the basic equations of relativistic magneto-aerodynamics, let us consider the energy-momentum tensors of the electromagnetic field and of the gas moving in this field. We shall here consider a pure field without charges.

The energy-momentum tensor of the electromagnetic field in the reference system in which a given volume element of the gas is at rest is of the form[1]

$$\overset{*}{T}_{ik} = \frac{1}{4\pi}\left[F_{il}F_{kl} - \frac{1}{4}F_{lm}^2\delta_{ik}\right], \tag{1}$$

where the F_{ik} are the components of the field. If the components are expressed in terms of the electric and magnetic field, we have

$$\left.\begin{aligned} \overset{*}{T}_{\alpha\beta} &= \frac{1}{4\pi}\left[-E_\alpha E_\beta - H_\alpha H_\beta + \frac{E^2+H^2}{2}\delta_{\alpha\beta}\right], \\ \overset{*}{T}_{4\alpha} &= \frac{iS_\alpha}{c} = \frac{i}{4\pi}[\mathbf{EH}]_\alpha, \quad -\overset{*}{T}_{44} = \overline{W} = \frac{1}{8\pi}(E^2+H^2). \end{aligned}\right\} \tag{2}$$

Here E and H are the electric and magnetic field strengths, S_α are components of the Poynting vector S, and W is the energy density of the field.

In an arbitrary reference system, the components of the tensor T^*_{ik} are of the form

$$T^*_{11} = \frac{1}{\theta^2}\left[\overline{T}^*_{11} + 2\frac{a}{c^2}\overline{S}_1 + \frac{a^2}{c^2}\overline{W}\right], \quad T^*_{12} = \frac{1}{\theta}\left(\overline{T}^*_{12} + \frac{a}{c^2}\overline{S}_2\right),$$
$$T^*_{13} = \frac{1}{\theta}\left[\overline{T}^*_{13} + \frac{a}{c^2}\overline{S}_3\right], \quad -icT^*_{41} = S_1 = \frac{1}{\theta^2}\left[\overline{S}_1\left(1+\frac{a^2}{c^2}\right) + a\left(\overline{W} + \overline{T}^*_{11}\right)\right],$$
$$T^*_{22} = \overline{T}^*_{22}, \quad T^*_{23} = \overline{T}^*_{23}, \quad -icT^*_{42} = S_2 = \frac{1}{\theta}\left(\overline{S}_2 + a\overline{T}^*_{12}\right),$$
$$T^*_{33} = \overline{T}^*_{33}, \quad -icT^*_{43} = S_3 = \frac{1}{\theta}\left[\overline{S}_3 + a\overline{T}^*_{13}\right],$$
$$-T^*_{44} = W = \frac{1}{\theta^2}\left[\overline{W} + \frac{2a}{c^2}\overline{S}_1 + \frac{a^2}{c^2}\overline{T}^*_{11}\right].$$

Here

$$\theta = \sqrt{1 - \frac{a^2}{c^2}},$$

where a is the velocity of the reference system.

The tensors $\overline{T}^*_{ik}$ and T^*_{ik} are symmetric, and, therefore,

$$T^*_{\alpha\beta} = T^*_{\beta\alpha}, \quad T^*_{4\alpha} = T^*_{\alpha 4}. \tag{3}$$

The energy-momentum tensor of the gas (for macroscopic bodies) in an arbitrary system of reference is of the form

$$T_{ik} = (p + \rho c^2) U_i U_k + \delta_{ik} p, \tag{4}$$

or

$$T_{\alpha\beta} = \frac{(p+\rho c^2) u_\alpha u_\beta}{c^2\theta^2} + \delta_{\alpha\beta} p, \quad T_{4\alpha} = \frac{i(p+\rho c^2) u_\alpha}{c\theta^2}, \quad T_{44} = -\frac{\left(\rho c^2 + p\frac{a^2}{c^2}\right)}{\theta}, \tag{5}$$

where U_i and U_k are the four-velocity components, u_α and u_β are the usual three-dimensional components of the velocity; this tensor is symmetric, and therefore

$$T_{\alpha\beta} = T_{\beta\alpha}, \quad T_{4\alpha} = T_{\alpha 4}.$$

The quantity $\rho c^2 = \varepsilon$ is the energy density in the reference system in which the given volume element is at rest.

We find the equation of motion of the gas and the equation of energy conservation as the gas moves in the field together with the equation of the field without charges by setting

$$\frac{\partial\left(T^*_{ik} + T_{ik}\right)}{\partial x_k} = 0. \tag{6}$$

From this we obtain

$$\left.\begin{aligned} \frac{1}{ic}\cdot\frac{\partial}{\partial t}\left[T^*_{44} + T_{44}\right] + \frac{\partial}{\partial x_\alpha}\left[T^*_{4\alpha} + T_{4\alpha}\right] = 0, \\ \frac{1}{ic}\cdot\frac{\partial}{\partial t}\left[T^*_{\alpha 4} + T_{\alpha 4}\right] + \frac{\partial}{\partial x_\beta}\left[T^*_{\alpha\beta} + T_{\alpha\beta}\right] = 0. \end{aligned}\right\} \tag{7}$$

The calculation of the derivatives presents no difficulty. The first equation gives the law of conservation of energy, and the second gives the three equations of motion. In addition to these equations, it is necessary, when there is a field present, to take into account Maxwell's equations and, on going from the stationary to an arbitrary system of coordinates, to take into account the Lorentz transformation.

In cosmic space the electric conductivity is extremely large,

and we may therefore set the electric field equal to zero in the stationary system of reference (E = 0); then, denoting the field strengths in the moving system of reference by $\mathbf{E}^*$ and $\mathbf{H}^*$, we have

$$\operatorname{rot}\mathbf{E}^* = -\frac{1}{c}\cdot\frac{\partial \mathbf{H}^*}{\partial t}. \tag{8}$$

Let us assume that $\mathbf{E}^*$, $\mathbf{H}^*$ and $\mathbf{H}$ are related by the Lorentz transformations:

$$E_x^* = 0, \quad E_y^* = \frac{a}{c\theta}H_z, \quad E_z^* = -\frac{a}{c\theta}H_y, \quad H_x^* = H_x, \quad H_y^* = \frac{H_y}{\theta}, \quad H_z^* = \frac{H_z}{\theta}. \tag{9}$$

From (8) and (9) we have

$$\left.\begin{aligned} &\frac{\partial H_x}{\partial t} - \left[\frac{\partial}{\partial y}\left(\frac{aH_y}{\theta}\right) + \frac{\partial}{\partial z}\left(\frac{aH_z}{\theta}\right)\right] = 0, \\ &\frac{\partial\left(\frac{H_y}{\theta}\right)}{\partial t} + \frac{\partial}{\partial x}\left(\frac{aH_y}{\theta}\right) = 0, \\ &\frac{\partial\left(\frac{H_z}{\theta}\right)}{\partial t} + \frac{\partial}{\partial x}\frac{(aH_z)}{\theta} = 0. \end{aligned}\right\} \tag{10}$$

In addition we must take account of the fact that

$$\operatorname{div}\mathbf{H} = 0. \tag{11}$$

The field components in the moving system of reference are simplified because all the $\overline{S}_x = 0$.

$$\left.\begin{aligned} &T_{11}^* = \frac{1}{\theta^2}\left[\overline{T}_{11}^* + \frac{a^2}{c^2}\overline{W}\right], \quad T_{12}^* = \frac{\overline{T}_{12}^*}{\theta}, \quad T_{13}^* = \frac{\overline{T}_{13}^*}{\theta}, \\ &S_1 = \frac{a}{\theta^2}[\overline{W} + \overline{T}_{11}^*], \quad S_2 = \frac{a}{\theta}\overline{T}^*, \quad S_3 = \frac{a}{\theta}\overline{T}_{13}^*, \\ &W = \frac{1}{\theta^2}\left[\overline{W} + \frac{a^2}{c^2}\overline{T}_{11}^*\right]. \end{aligned}\right\} \tag{12}$$

Thus the problem of finding the equations of relativistic magnetoaerodynamics for the case E = 0 can be considerably simplified and the final equation can be written in the three-dimensional vector form.

Let us now consider the problem one-dimensional motion of the medium, which is of particular interest. First let us examine the case in which the vector H is parallel to the velocity (we shall take $u_1 = a$ and $u_2 = u_3 = 0$, where u_1, u_2, u_3 are the components of the velocity along the X, Y, Z axes, respectively): $H = H_x$ and $H_y = H_z = 0$. In this case

$$\overline{T}_{11}^* = -\frac{H^2}{8\pi}, \quad \overline{T}_{22}^* = \frac{H^2}{8\pi}, \quad \overline{T}_{33}^* = \frac{H^2}{8\pi}, \quad \overline{T}_{44}^* = -\frac{H^2}{8\pi} = -\overline{W}. \tag{13}$$

The remaining components of the tensor $\overline{T}_{ik}^*$ are all zero. Further, we find that

$$T_{11}^* = -\frac{H^2}{8\pi}, \quad T_{22}^* = \frac{H^2}{8\pi}, \quad T_{33}^* = \frac{H^2}{8\pi}, \quad T_{44}^* = -\frac{H^2}{8\pi} = -W \tag{14}$$

The remaining components of the tensor T_{ik}^* are all zero.

Since $[\mathbf{aH}] = 0$ and $H_0 = H = H_x$, equation (10) gives $\frac{\partial H}{\partial t} = 0$. Furthermore, since $\operatorname{div}\mathbf{H} = 0$ (in the present case this gives $\frac{\partial H}{\partial x} = 0$), we note that

$$H = \text{const.} \tag{15}$$

This case is trivial and is of no practical interest. The motion of the gas in a constant magnetic field does not differ from the motion in the absence of a field.

Let us now consider the case in which the vector H is normal to the direction of motion, and remains oriented in the same direction.

Let $u = a$ and $u_2 = u_3 = 0$, then

$$H = H_z, \quad H_x = H_y = 0; \tag{16}$$

which gives

$$\overline{T}^*_{11} = \frac{H^2}{8\pi}, \quad \overline{T}^*_{22} = \frac{H^2}{8\pi}, \quad \overline{T}^*_{33} = -\frac{H^2}{8\pi}, \quad -\overline{T}^*_{44} = \frac{H^2}{8\pi} = \overline{W}. \tag{17}$$

The remaining components of the tensor $\overline{T}^*_{ik}$ are zero. It is easy to see that

$$T^*_{11} = \frac{1+\frac{u_1^2}{\theta^2}}{c^2}\cdot\frac{H^2}{8\pi}, \quad T^*_{22} = \frac{H^2}{8\pi}, \quad T^*_{33} = -\frac{H^2}{8\pi},$$

$$T^*_{44} = \frac{-\left(1+\frac{u_1^2}{\theta^2}\right)}{c^2}\cdot\frac{H^2}{8\pi} = -W, \quad T^*_{14} = T^*_{41} = \frac{iu_1}{c\theta^2}\cdot\frac{H^2}{4\pi} = \frac{iS_1}{c}. \tag{18}$$

The remaining components of the tensor T^*_{ik} vanish.

Since

$$H_0 = \frac{H}{\theta}, \quad E_0 = \frac{u_1 H}{c\theta}, \quad \operatorname{rot}\left[\frac{u_1 H}{\theta}\right] = \frac{\partial\left(\frac{u_1 H}{\theta}\right)}{\partial x}, \tag{19}$$

equation (10) gives

$$\frac{\partial\frac{H}{\theta}}{\partial t} + \frac{\partial\left(\frac{u_1 H}{\theta}\right)}{\partial x} = 0. \tag{20}$$

The equation $\operatorname{div} H = 0$ is then identically satisfied, since

$$H_z = H = H(x). \tag{21}$$

The components of the macroscopic tensor T_{ik} for one-dimensional motion are of the form

$$T_{11} = \frac{(p+\rho c^2)u_1^2}{c^2\theta} + p = \frac{p+\rho u_1^2}{\theta^2}, \quad T_{22} = p, \quad T_{33} = p, \quad T_{41} = \frac{i(p+\rho c^2)u_1}{c\theta^2}, \quad T_{44} = -\frac{\rho c^2 + \frac{u_1^2}{c^2}p}{\theta^2}. \tag{22}$$

Equations (7) for the above type of motion of the gas in a magnetic field are of the form

$$\left.\begin{aligned} &\frac{\partial}{\partial t}\left[\frac{\rho c^2 + p\frac{u_1^2}{c^2}}{\theta^2} + \frac{H^2}{8\pi}\cdot\frac{1+\frac{u_1^2}{c^2}}{\theta^2}\right] + \frac{\partial}{\partial x}\left[\frac{(p+\rho c^2)u_1}{\theta^2} + \frac{u_1}{\theta^2}\cdot\frac{H^2}{4\pi}\right] = 0, \\ &\frac{\partial}{\partial t}\left[\frac{(p+\rho c^2)u_1}{c^2\theta^2} + \frac{u_1}{c^2\theta^2}\frac{H^2}{4\pi}\right] + \frac{\partial}{\partial x}\left[\frac{\rho u_1^2 + p}{\theta^2} + \frac{1+\frac{u_1^2}{c^2}}{\theta^2}\cdot\frac{H^2}{8\pi}\right] = 0. \end{aligned}\right\} \tag{23}$$

We can arrive at this system of equations by writing the tensor T_{ik} in the form

$$T_{ik} = \left(p + \rho c^2 + \frac{H^2}{4\pi}\right)U_i U_k + \delta_{ik}\left(p + \frac{H^2}{8\pi}\right), \tag{24}$$

contemplating its further transformation only for one-dimensional motion. This tensor can be also written in the form

$$T_{ik} = (p' + \rho' c^2) U_i U_k + \delta_{ik} p', \tag{25}$$

where

$$p' = p + \frac{H^2}{8\pi}, \quad \rho' c^2 = \rho c^2 + \frac{H^2}{8\pi}, \tag{26}$$

i.e., we have added the magnetic pressure and magnetic energy density to the pressure and energy density.

We can immediately consider the generalized case, when

$$p' = p + p^*, \quad \varepsilon' = \varepsilon + \varepsilon^*, \tag{27}$$

where

$$\varepsilon' = \rho' c^2, \quad \varepsilon = \rho c^2,$$

and p^* and ε^* are, respectively, the additional pressure and energy due to the field.

From the condition $\frac{\partial T_{ik}}{\partial x_k} = 0$ and equation (25), it is easy to obtain the following differential equations:

$$\frac{d\varepsilon'}{ds} + (p' + \varepsilon') \frac{\partial U_k}{\partial x_k} = 0, \quad \frac{dU_i}{ds} + \frac{1}{p' + \varepsilon'} \left[\frac{\partial p'}{\partial x_i} + U_i \frac{dp}{ds} \right] = 0, \tag{28}$$

where $ds = c\theta\, dt$. Since

$$d(\varepsilon' v) = T d\sigma - p' dv + \lambda dv, \tag{29}$$

where σ is the entropy, v is the specific volume, and λ is a function of p' and ε' (for $p' = 0$ and $\varepsilon' = 0$, we have $\lambda = 0$), it follows from the first of equations (28) that

$$\frac{T}{v} \frac{d\sigma}{ds} + (p' + \varepsilon') v \frac{\partial \frac{U_k}{v}}{\partial x_k} + \frac{\lambda}{v} \frac{dv}{ds} = 0. \tag{30}$$

For adiabatic motion, when $d\sigma = 0$, we have

$$\frac{\partial \frac{U_k}{v}}{\partial x_k} + \frac{\lambda}{v} \frac{dv}{ds} \cdot \frac{1}{(p' + \varepsilon') v} = 0, \tag{31}$$

and, by comparing equation (31) with the first of equations (28) we find that

$$\frac{d\varepsilon'}{p' + \varepsilon'} = -\frac{dv}{v} + \frac{\lambda\, dv}{(p' + \varepsilon') v}.$$

But the field variables should not enter into the continuity equation and it should always be of the form

$$\frac{\partial \frac{U_k}{v}}{\partial x_k} = 0. \tag{32}$$

Therefore $\lambda \equiv 0$ and the thermodynamic identity (29) must be written in the form

$$d(\varepsilon' v) = T d\sigma - p' dv, \tag{33}$$

and the relation between p', ε' and v is of the form

$$\frac{d\varepsilon'}{p' + \varepsilon'} = -\frac{dv}{v}. \tag{34}$$

The second of equations (28) for the case of one-dimensional motion can be brought into the form

$$\frac{1}{\theta^2}\left(\frac{\partial u_1}{\partial t}+u_1\frac{\partial u_1}{\partial x}\right)+\frac{c^2}{p'+\varepsilon'}\left(\frac{\partial p'}{\partial x}+\frac{u_1}{c^2}\cdot\frac{\partial p'}{\partial t}\right)=0. \tag{35}$$

The continuity equation (32) then becomes

$$\frac{\partial \ln v}{\partial t}+u_1\frac{\partial \ln v}{\partial x}-\frac{1}{\theta^2}\left(\frac{\partial u_1}{\partial x}+\frac{u_1}{c^2}\cdot\frac{\partial u_1}{\partial t}\right)=0. \tag{36}$$

If it is written in the form

$$\frac{\partial \frac{v}{\theta}}{\partial t}+\frac{\partial\left(\frac{u_1 v}{\theta}\right)}{\partial x}=0, \tag{37}$$

then by comparing this with equation (20) for the case of gas motion in a field in which the magnetic field vector is normal to the direction of motion we find directly that for the adiabatic case

$$H=\frac{b(\sigma)}{v}, \tag{38}$$

where $b(\sigma)=b$ is a function of the entropy. For isentropic motion

$$H=\frac{b}{v}, \tag{38a}$$

where b = const.

Let us consider the thermodynamic identity (29) in greater detail. Since we must have

$$d(\varepsilon v)=T d\sigma-p\,dv, \tag{39}$$

then by subtracting (39) from (29) we arrive at the expression

$$d(\varepsilon^* v)=-p^* dv+\lambda\,dv.$$

Since the additional pressure p^* should create an additional energy

$$\varepsilon^* v=-\int p^* dv, \tag{40}$$

we get the result that $\lambda\equiv 0$, which substantiates the result we obtained previously.

In the particular case being investigated, we have

$$\varepsilon^*=\frac{H^2}{8\pi} \quad \text{and} \quad p^*=\frac{H^2}{8\pi}$$

and therefore

$$d(H^2 v)=-H^2 dv \quad \text{or} \quad v\,dH+H\,dv=0.$$

Whence, we have $Hv=b$, i.e., we obtain relation (38a), wherein b may be either a function of the entropy or a constant.

It is now clear that equation (34) is equivalent to

$$\frac{d\varepsilon}{p+\varepsilon}=-\frac{dv}{v}. \tag{41}$$

If we write the adiabatic equation in the form

$$p=Av^{-k}, \tag{42}$$

then (since $\varepsilon=\rho c^2$) we obtain the equation

$$\frac{d\rho}{dv}=-\left(\frac{\rho}{v}+\frac{Av^{-(k+1)}}{c^2}\right).$$

Whence

$$\rho v = 1 + \frac{Av^{-(k-1)}}{(k-1)c^2} = 1 + \frac{pv}{(k-1)c^2} \tag{43}$$

or more generally, without the form of the adiabatic equation being assumed,

$$\rho v = 1 + \frac{-\int p dv}{c^2}. \tag{44}$$

This equation shows that an energy density $\frac{-\int p dv}{c^2}$ due to the pressure is added to the rest energy density.

Let us now transform equations (35) and (36). First we introduce the new quantity

$$dq = \frac{du_1}{\theta^2} = \frac{du_1}{1 - \frac{u_1^2}{c^2}} = \frac{c}{2} d \ln \frac{c + u_1}{c - u_1}. \tag{45}$$

We then introduce the velocity of sound

$$\omega = c\sqrt{\frac{dp}{d\varepsilon}} = \sqrt{\frac{dp}{d\rho}}. \tag{46}$$

We replace $\frac{c^2 dp'}{p' + \varepsilon'}$ by the quantity $\omega\varphi\, d\Omega$, where

$$d\Omega = -\varphi\omega\, d \ln v, \tag{47}$$

$$\varphi^2 = -\frac{c^2 dp'}{(p' + \varepsilon')\omega^2 d \ln v} = \frac{dp'}{dp} \cdot \frac{d\varepsilon}{d\varepsilon'}; \tag{48}$$

and thus

$$d\Omega = -c\sqrt{\frac{-dp' d \ln v}{p' + \varepsilon'}}. \tag{49}$$

Equations (35) and (36) then take on the form

$$\left.\begin{aligned} \frac{\partial q}{\partial t} + u_1 \frac{\partial q}{\partial x} + \omega\varphi\left(\frac{\partial \Omega}{\partial x} + \frac{u_1}{c^2} \cdot \frac{\partial \Omega}{\partial t}\right) = 0, \\ \frac{\partial \Omega}{\partial t} + u_1 \frac{\partial \Omega}{\partial x} + \omega\varphi\left(\frac{\partial q}{\partial x} + \frac{u_1}{c^2} \cdot \frac{\partial q}{\partial t}\right) = 0. \end{aligned}\right\} \tag{50}$$

It is clear that the quantity $\omega\varphi$ plays the role of the effective velocity of sound; let us denote it by ω^*.

$$\omega^* = \omega\varphi = c\sqrt{\frac{-dp'}{(p' + \varepsilon') d \ln v}} = c\sqrt{\frac{dp'}{d\varepsilon'}}. \tag{51}$$

We have also

$$d\Omega = -\omega^* d \ln v \quad \text{and} \quad \varphi = \frac{\omega^*}{\omega}. \tag{52}$$

Then equations (50) become

$$\left.\begin{aligned} \frac{\partial q}{\partial t} + u_1 \frac{\partial q}{\partial x} + \omega^*\left(\frac{\partial \Omega}{\partial x} + \frac{u_1}{c^2} \cdot \frac{\partial \Omega}{\partial t}\right) = 0, \\ \frac{\partial \Omega}{\partial t} + u_1 \frac{\partial \Omega}{\partial x} + \omega^*\left(\frac{\partial q}{\partial x} + \frac{u_1}{c^2} \cdot \frac{\partial q}{\partial t}\right) = 0. \end{aligned}\right\} \tag{53}$$

Adding the two equations and taking their difference, we obtain

$$\frac{\partial (q \pm \Omega)}{\partial t} + \frac{u_1 \pm \omega^*}{1 \pm \frac{u_1 \omega^*}{c^2}} \cdot \frac{\partial (q \pm \Omega)}{\partial x} = 0. \tag{54}$$

This gives two families of characteristics: along the lines

$$\frac{dx}{dt} = \frac{u_1 \pm \omega^*}{1 \pm \frac{u_1 \omega^*}{c^2}} \tag{55}$$

the conditions

$$q \pm \Omega = \text{const}. \tag{56}$$

are satisfied. It is simple also to find the particular solutions of the system of equations (53):

$$x = \left(\frac{u_1 \pm \omega^*}{1 \pm \frac{u_1 \omega^*}{c^2}} \right) t + F(u_1), \quad q = \pm \Omega + \text{const}. \tag{57}$$

If the particular solutions or the equations of the characteristics are known, equations (54) can be reduced to a single canonical equation, which is readily solved either by a method due to Riemann or by the method of characteristics. The procedure is generally known and we do not propose to describe it here.

Let us calculate ω^* and Ω for the particular case under consideration. Since

$$p' = p + \frac{H^2}{8\pi}, \quad \varepsilon' = \rho c^2 + \frac{H^2}{8\pi},$$

and

$$p = Av^{-k}, \quad \rho = \frac{1}{v} + \frac{Av^{-k}}{(k-1)\, c^2}, \quad H = \frac{b}{v},$$

we will have

$$p' = Av^{-k} + \frac{b^2}{8\pi v^2}, \quad \varepsilon' = \frac{c^2}{v} + \frac{Av^{-k}}{(k-1)} + \frac{b^2}{8\pi v^2}. \tag{58}$$

Whence, we obtain

$$\frac{\omega^{*2}}{c^2} = \frac{dp'}{d\varepsilon'} = \frac{kAv^{1-k} + \frac{b^2}{4\pi v}}{c^2 + \frac{k}{k-1} Av^{1-k} + \frac{b^2}{4\pi v}} = \frac{kpv + \frac{H^2 v}{8\pi}}{c^2 + \frac{kpv}{k-1} + \frac{H^2 v}{4\pi}}. \tag{59}$$

We now determine

$$d\Omega = -\omega^* d \ln v = -c \sqrt{\frac{kAv^{1-k} + \frac{b^2}{4\pi v}}{c^2 + \frac{k}{k-1} Av^{1-k} + \frac{b^2}{4\pi v}}} \cdot \frac{dv}{v}. \tag{60}$$

From this, the particular solutions can be written as

$$\ln \frac{1 + \frac{u_1}{c}}{1 - \frac{u_1}{c}} \pm 2 \int \sqrt{\frac{kAv^{1-k} + \frac{b^2}{4\pi v}}{c^2 + \frac{k}{k-1} Av^{1-k} + \frac{b^2}{4\pi v}}} \cdot \frac{dv}{v} = \text{const}, \tag{61}$$

and

$$x = \frac{\frac{u_1}{c} \pm \sqrt{\frac{kAv^{1-k} + \frac{b^2}{4\pi v}}{c^2 + \frac{k}{k-1}Av^{1-k} + \frac{b^2}{4\pi v}}}}{1 \pm \frac{u_1}{c}\sqrt{\frac{kAv^{1-k} + \frac{b^2}{4\pi v}}{c^2 + \frac{k}{k-1}Av^{1-k} + \frac{b^2}{4\pi v}}}} ct + F(u_1). \tag{61}$$

If

$$p = (k-1)\rho c^2, \tag{62}$$

where k is an arbitrary parameter (it determines the limiting relation between p and ρ), then

$$\rho = \frac{Av^{-k}}{(k-1)c^2} \tag{63}$$

and

$$p = Av^{-k}, \quad p' = Av^{-k} + \frac{b^2}{8\pi v^2}, \quad \varepsilon' = \frac{A}{k-1}v^{-k} + \frac{b^2}{8\pi v^2}, \tag{64}$$

i.e., we arrive at the relationships just obtained without the term c^2/v. At the limit $k = 4/3$. Let us investigate this limiting case. For it, we have

$$\frac{d\Omega}{c} = -\sqrt{\frac{\frac{4}{3}Av^{\frac{2}{3}} + \frac{b^2}{4\pi}}{4Av^{\frac{2}{3}} + \frac{b^2}{4\pi}}} \cdot \frac{dv}{v}. \tag{65}$$

Let us set $\frac{4}{3}A\frac{4\pi}{b^2}v^{\frac{2}{3}} = z$, then

$$\frac{\Omega}{c} = -\frac{3}{2}\int\sqrt{\frac{z+1}{3z+1}} \cdot \frac{dz}{z} = \ln\left[\sqrt{3z+1} + \sqrt{3(z+1)}\right]^{\sqrt{3}}\left[\frac{\sqrt{3z+1}+\sqrt{z+1}}{\sqrt{z}}\right]^{-3};$$

whence

$$\frac{\Omega}{c} = \ln\left[\sqrt{3\left(\frac{4}{3}Av^{\frac{2}{3}} + \frac{b^2}{4\pi}\right)} + \sqrt{4Av^{\frac{2}{3}} + \frac{b^2}{4\pi}}\right]^{\sqrt{3}}\left[\sqrt{4Av^{\frac{2}{3}} + \frac{b^2}{4\pi}} + \sqrt{\frac{4}{3}Av^{\frac{2}{3}} + \frac{b^2}{4\pi}}\right]^{-3} v + \text{const}. \tag{66}$$

Thus

$$\left(\frac{1 - \frac{u_1}{c}}{1 + \frac{u_1}{c}}\right)^{\pm 1} = \text{const} \cdot v\left(\sqrt{4Av^{\frac{2}{3}} + \frac{3}{4}\cdot\frac{b^2}{\pi}} + \sqrt{4Av^{\frac{2}{3}} + \frac{b^2}{4\pi}}\right)^{\sqrt{3}}\left(\sqrt{4Av^{\frac{2}{3}} + \frac{b^2}{4\pi}} + \sqrt{\frac{4}{3}Av^{\frac{2}{3}} + \frac{b^2}{4\pi}}\right)^{-3}. \tag{67}$$

The plus sign gives a compression wave; the minus sign, a rarefaction wave (for gas motion to the right). In addition,

$$x = \frac{\frac{u_1}{c} \pm \sqrt{\frac{\frac{4}{3}Av^{\frac{2}{3}} + \frac{b^2}{4\pi}}{4Av^{\frac{2}{3}} + \frac{b^2}{4\pi}}}}{1 \pm \frac{u_1}{c}\sqrt{\frac{\frac{4}{3}Av^{\frac{2}{3}} + \frac{b^2}{4\pi}}{4Av^{\frac{2}{3}} + \frac{b^2}{4\pi}}}} \cdot ct + F(u_1). \tag{68}$$

For a rarefaction wave and expansion into vacuum $(v \to \infty)\, u_1 \to c$.

A similar result is also obtained in the absence of a magnetic field. In the presence of a magnetic field and for a given expansion $v \longrightarrow v_0$, where v_0 is sufficiently large) u_1/c is closer to unity than without the field, which follows from equation (67).

Let us now consider the fundamentals of the theory of a plane shock wave. Since for one-dimensional motion the components of the energy-momentum tensor are given by

$$\left.\begin{aligned} T_{11} &= \frac{\left(p+\rho c^2+\frac{H^2}{4\pi}\right)u_1^2}{c^2\theta^2}+p+\frac{H^2}{8\pi}=\frac{p+\rho u_1^2+\left(1+\frac{u_1^2}{c^2}\right)\frac{H^2}{8\pi}}{\theta^2}, \\ T_{14} &= \frac{i\left(p+\rho c^2+\frac{H^2}{4\pi}\right)u_1}{c\theta^2}, \end{aligned}\right\} \tag{69}$$

in passing through the discontinuity (the shock wavefront) these quantities must be conserved:

$$\left.\begin{aligned} \frac{p+\rho u_1^2+\left(1+\frac{u_1^2}{c^2}\right)\frac{H^2}{8\pi}}{1-\frac{u_1^2}{c^2}} &= \frac{p_0+\rho_0 u_{10}^2+\left(1+\frac{u_{10}^2}{c^2}\right)\frac{H_0^2}{8\pi}}{1-\frac{u_{10}^2}{c^2}}, \\ \frac{\left(p+\rho c^2+\frac{H^2}{4\pi}\right)u_1}{1-\frac{u_1^2}{c^2}} &= \frac{\left(p_0+\rho_0 c^2+\frac{H_0^2}{4\pi}\right)u_{10}}{1-\frac{u_{10}^2}{c^2}}. \end{aligned}\right\} \tag{70}$$

Here the index $_0$ is used to indicate the parameters ahead of the wavefront; the parameters without this subscript are those at the wavefront. Let us rewrite the last equation in the form

$$\frac{\left(pv+\rho vc^2+\frac{H^2 v}{4\pi}\right)}{\sqrt{1-\frac{u_1^2}{c^2}}}\cdot\frac{u_1}{v\sqrt{1-\frac{u_1^2}{c^2}}}=\frac{\left(p_0v_0+\rho_0v_0c^2+\frac{H_0v_0}{4\pi}\right)}{\sqrt{1-\frac{u_{10}^2}{c^2}}}\cdot\frac{u_{10}}{v_0\sqrt{1-\frac{u_{10}^2}{c_0^2}}}.$$

The quantities

$$pv+\rho vc^2+\frac{H^2v}{4\pi}=I \tag{71}$$

and

$$\frac{u_1}{v\sqrt{1-\frac{u_1^2}{c^2}}}=j \tag{72}$$

are the heat content and mass flux. These quantities are conserved independently of one another in the case of stationary flow (see, for example, equation (37)). Hence, the totality of the quantities that are conserved in passing through the shock wave front is

$$\left.\begin{aligned} \frac{p+\rho u_1^2+\left(1+\frac{u_1^2}{c^2}\right)\frac{H^2}{8\pi}}{1-\frac{u_1^2}{c^2}} &= \frac{p_0+\rho_0 u_{10}^2+\left(1+\frac{u_{10}^2}{c^2}\right)\frac{H_0^2}{8\pi}}{1-\frac{u_{10}^2}{c^2}}, \\ \frac{I}{\sqrt{1-\frac{u_1^2}{c^2}}} &= \frac{I_0}{\sqrt{1-\frac{u_{10}^2}{c^2}}}, \quad \frac{u_1}{v\sqrt{1-\frac{u_1^2}{c^2}}}=\frac{u_{10}}{v_0\sqrt{1-\frac{u_{10}^2}{c^2}}}, \end{aligned}\right\} \tag{73}$$

where the first equation gives conservation of the momentum flux density; the second, of the energy density flux and the third is the continuity equation.

Making use of the equations of state (isentropes) before and after the wavefront,

$$p = Av^{-k}, \quad p_0 = A_0 v_0^{-k}, \tag{74}$$

where $A_0 < A$, since the entropy increases behind the front, we can determine the relation of ρ, p and v. Let us also put down the relation between H and v (for the case in which the vector H is perpendicular to velocity and maintains its orientation on both sides of the front):

$$H = \frac{b}{v}, \quad H_0 = \frac{b_0}{v_0}. \tag{75}$$

Then the system of equations (73) becomes

$$\frac{p + \frac{u_1^2}{v} + \frac{pu_1^2}{(k-1)c^2} + \left(1 + \frac{u_1^2}{c^2}\right)\frac{b^2}{8\pi v^2}}{1 - \frac{u_1^2}{c^2}} = B_1,$$

$$\frac{c^2 + \frac{kpv}{k-1} + \frac{b^2}{4\pi v}}{\sqrt{1 - \frac{u_1^2}{c^2}}} = B_2, \quad \frac{u_1}{v\sqrt{1 - \frac{u_1^2}{c^2}}} = B_3. \tag{76}$$

If v_0, A_0, b_0, and u_{10} are known, then B_1, B_2 and B_3 are known constants.

Eliminating u_1 and u_{10} from these equations we obtain the equation for the Hugoniot adiabatic curve, relating p and v with p_0 and v_0. The second equation of (76) is the Bernoulli equation. Equations (76) uniquely determine the parameters p, v and u_1 behind the shock wave.

If we go over to the reference system in which the gas in front of the shock wave is stationary, then

$$-u_{10} = D_y \tag{77}$$

determines the velocity of the shock wave. The gas velocity behind the front will be

$$\bar{u}_1 = \frac{D_y + u_1}{1 + \frac{u_1 D_y}{c^2}}. \tag{78}$$

It is easy to generalize the above equations to include the case of arbitrary fields; here the components of the energy-momentum tensor will be

$$T_{11} = \frac{p + \rho u_1^2 + p' + \varepsilon' \frac{u_1^2}{c^2}}{\theta^2}, \quad T_{14} = \frac{iu_1(p + p' + \rho c^2 + \varepsilon')}{c\theta^2}. \tag{79}$$

The basic equations of shock wave theory will become

$$\left.\begin{aligned} \frac{p + \rho u_1^2 + p' + \varepsilon' \frac{u_1^2}{c^2}}{1 - \frac{u_1^2}{c^2}} &= \frac{p_0 + \rho_0 u_{10}^2 + p_0' + \varepsilon_0' \frac{u_{10}^2}{c^2}}{1 - \frac{u_{10}^2}{c^2}}, \\ \frac{I}{\sqrt{1 - \frac{u_1^2}{c^2}}} = \frac{I_0}{\sqrt{1 - \frac{u_{10}^2}{c^2}}}, \quad \frac{u_1}{v\sqrt{1 - \frac{u_1^2}{c^2}}} &= \frac{u_{10}}{v_0\sqrt{1 - \frac{u_{10}^2}{c^2}}}, \end{aligned}\right\} \tag{80}$$

where

$$I = pv + \rho v c^2 + p'v + \varepsilon' v, \quad I_0 = p_0 v_0 + \rho_0 v_0 c^2 + p_0' v_0 + \varepsilon_0' v_0, \tag{81}$$

and

$$d\varepsilon' = -p' dv.$$

Such "arbitrary" fields can arise incident to collisions of relatively complex particles such as nuclei and nucleons, in the process of disruption and disintegration of nuclei into "smaller" and less "complex" particles such as nucleons and the creation of new particles such as mesons.

If no less than ten such particles are created in the process the macroscopic equations derived in the present article are entirely applicable both to macroscopic description of the processes of collision and fractioning of particles, when shock waves are formed, and to analysis of the process of the rapid dispersion of a "gas" that has been compressed by passing shock waves. It is possible that this approach may be of interest in the study of the nature of cosmic rays.

We have shown (in Ref. 2) that in the collision of particles and the subsequent dispersion of the quasi-relativistic gas, formed in the collision, almost all of the energy goes into the leading (frontal) particles. In this case the following relation holds:

$$\frac{1}{2}\left(1-\frac{u_{1M}}{c}\right)=\left(\frac{1-\frac{u_{10}}{c}}{8}\right)^{\sqrt{3}}, \qquad (82)$$

where u_{1M} is the maximum dispersion (scattering) velocity and u_{10} is the velocity of each of the colliding particles.

If we assume the fields (equivalent to external fields) created in this type of process to be "repulsive," then the above-mentioned energy redistribution will be even more noticeable (it may be increased several-fold); if, however, the fields tend to "contract" the relativistic gas, then the redistribution effect will be reduced, possibly to zero. Quantitative calculations for cases involving known fields can be carried out on the basis of the outlined theory. The presence of fields may alter the velocity (energy) distribution of the particles, which can also be calculated if these fields are known.

"N. E. Bauman" Moscow Higher Technical School

References

1. L.Landau & E.Lifshits, Teoriia polia, M.-L. 1948. (Translated into English under the title "Classical Theory of Fields", Addison-Wesley 1951.

2. K.Staniukovich, Trudy 3-go soveshchaniia po voprosam kosmogonii (Transactions of the Third Conference on Problems of Cosmogony), M.-L. 1954.

* * * *

ON AN IONIZATION EFFECT RELATED TO THE OBSERVATION OF ELECTRON-POSITRON PAIRS AT VERY HIGH ENERGIES

- A. E. Chudakov

At present a large number of collisions involving particles of very high energies (10^{12} to 10^{13} ev) have been recorded by means of nuclear emulsions exposed in the stratosphere. In a number of cases it was possible to observe electron-positron pairs created by photons having an energy an order of magnitude lower than that of the colliding particles. These photons are apparently formed in the decay of π mesons generated in the collision.

It may be assumed that with the further accumulation of data and of experimental techniques it will be possible to observe the creation, in emulsions, of pairs having energies of 10^{12} to 10^{13} eV. Accordingly it is useful to inquire about the probable characteristics and appearance of such pair tracks in photographic emulsions.

The particular characteristics of interest are related to the small angle of divergence between the components of the pair. The divergence (relative scattering angle) is inversely proportional to the energy and, already at 10^{11} eV, it is so small that no separation is discernible over a distance of one centimeter. Evidently such pairs will appear as single tracks with double the relativistic ionization. This precludes determining the energy of the pair from the angle of divergence. However, with further increases in the energy above 10^{12} eV one may expect a specific ionization effect which should make determination of the pair energy possible and should present a certain intrinsic interest. The expected effect consists of a decrease in the ionization (compared to the double relativistic value) along those parts of the path where the distance between the positron and the electron is less than the range of their interaction with the electrons of the medium. This decrease in ionization is associated with the fact that the field of a pair of opposite charges drops off at long ranges much more rapidly than the field of a single charge.

In order to obtain the dependence of the increase in ionization on the motion of the pair it is necessary to compute the energy transfer by two parallel-moving charges to an electron in the medium. The calculation can be readily carried out on the assumption that the mean energy transferred to the electrons of the medium, at a given impact parameter, can be calculated classically.

In Fig. 1 are shown the relative positions of the electron and positron of the pair and of an electron of the medium, located at the point 0. The pair is moving along a normal to the plane of the drawing.

The momenta transferred to the electron at 0 by the pair components are, respectively,

$$p_1 = \frac{2e^2}{r_1 c} \quad \text{and} \quad p_2 = \frac{2e^2}{r_2 c}. \tag{1}$$

The energy transferred to the electron at 0, is

$$\varepsilon = \frac{p_1^2 + p_2^2 - 2p_1 p_2 \cos\varphi}{2m} = A\left(\frac{1}{r_1^2} + \frac{1}{r_2^2} - 2\frac{\cos\varphi}{r_1 r_2}\right), \tag{2}$$

where $A = 2e^4/mc^2$.

Expressing φ and r_2 in terms of α and l (l' is the distance between the components of the pair), we will get

$$\varepsilon = \frac{A}{r_1^2} \cdot \frac{A}{1 + \frac{r_1^2}{l^2} - 2\frac{r_1}{l}\cos\alpha}. \tag{3}$$

The relation obtained must be averaged over α, and integrated over the impact parameter r_1. The averaging over α gives

$$\overline{\varepsilon} = \frac{A}{r_1^2}\frac{1}{\pi}\int_0^{\pi} \frac{d\alpha}{1 + \frac{r_1^2}{l^2} - \frac{2r_1}{l}\cos\alpha} = \frac{A}{r_1^2} \cdot \frac{1}{\left|1 - \frac{r_1^2}{l^2}\right|}. \tag{4}$$

The integration over the impact parameter r_1 must be carried out from r_{min} to r_{max}, but excluding the singular point for $r_1 = l$; this singularity arises through the fact that in the averaging over α, when $r_1 = l$, the second particle of the pair (in Fig. 1, this is the

positron) appears at the point 0. Yet we must impose the condition that at short ranges the energy losses must be small for both the electron and the positron. This can be accomplished, without changing the method of calculation, by introducing appropriate integration limits:

$$T = \int_{r_{min}}^{l-\rho} 2\pi r_1 dr_1 \bar{\varepsilon}(r_1) + \int_{l+\rho}^{r_{max}} 2\pi r_1 dr_1 \bar{\varepsilon}(r_1). \tag{5}$$

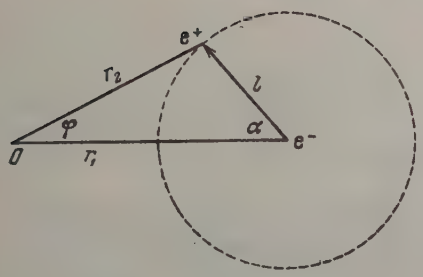

Fig. 1. Relative locations of the electron and positron of the pair at the instant of passing near the electron located in the medium at 0.

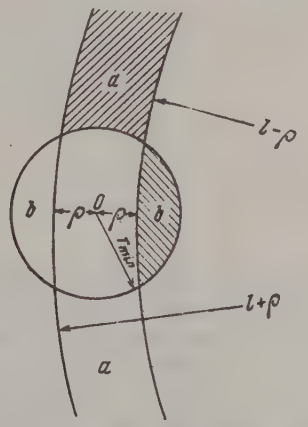

Fig. 2. Diagram illustrating selection of the value of parameter ρ, determining the width of the annular region omitted from the integration. With $\rho = r_{min}/2$, exclusion of this region is equivalent to the exclusion of a circle with radius r_{min} and center at 0.

The total loss of energy through ionization per unit path length of the components of the pair is determined as T_n, where n is the electron density in the medium.

In the above we are assuming that

$$r_{min} \ll l \tag{6}$$

and

$$r_{max} \gg l \tag{7}$$

The selection of ρ is illustrated in Fig. 2.

In formula (5) no account is taken of the cases in which the positron gets into region a; on the other hand, the cases in which it gets into region b are included, although these should not be considered. Obviously, the correct value for T will be obtained in the case when the energy transferred to the electron at the point 0 will be the same regardless of whether the positron gets into region a or b.

Computing this energy under the assumption (6) for both cases and equating the calculated values, we get

$$\int_{r_{min}}^{\infty} \frac{dr}{r} \arcsin\frac{\rho}{r} = \int_{\rho}^{r_{min}} \frac{dr}{r} \arccos\frac{\rho}{r} \tag{8}$$

from which, after substituting $\arccos\frac{\rho}{r} = \frac{\pi}{2} - \arcsin\frac{\rho}{r}$ and integrating, we find

$$\frac{\pi}{2}\ln\frac{r_{min}}{\rho}=\int_0^1\frac{d\xi}{\xi}\arcsin\xi=\frac{\pi}{2}\ln 2$$

and, consequently

$$\rho=\frac{r_{min}}{2} \tag{9}$$

Inserting this value of ρ in eq. (5), and invoking expression (4), we find

$$T=2\pi A\left[\int_{r_{min}}^{l-\frac{r_{min}}{2}}\frac{dr}{r\left(1-\frac{r^2}{l^2}\right)}+\int_{l+\frac{r_{min}}{2}}^{r_{max}}\frac{dr}{r\left(\frac{r^2}{l^2}-1\right)}\right], \tag{10}$$

which in view of condition (6) gives:

$$T\approx 2\pi A\left(2\ln\frac{l}{r_{min}}+\frac{1}{2}\ln\frac{r_{max}^2-l^2}{r_{max}^2}\right). \tag{11}$$

Equation (11) is valid provided both condition (6) and condition (7) are fulfilled. To clarify the limits of applicability of (11) in the $l \leqslant r_{max}$ region, let us make more precise our understanding of r_{max}: The momentum communicated to the electron of the medium is given by expression (1) if the particle passes at a range less than r_{max}, and is equal to zero in case this distance is greater than r_{max}. In view of this definition of r_{max}, equation (11) is not valid when $l \leqslant r_{max}$ for two reasons: 1) with $r_{max} - l < r_1 < r_{max}$ (see Fig. 1) our calculation took into account the influence of the positron when $r_2 > r_{max}$; 2) the calculations did not comprise the impact parameters $r_1 > r_{max}$. Yet, with $r_{max} < r_1 < r_{max} + l$ we can have $r_2 < r_{max}$. It can readily be shown that ignoring these marginal effects leads to a decrease in the value of T, compared with its exact value.

Both inaccuracies vanish when $r_{max} \to \infty$, but in this case T will be over-valued. Inasmuch as the second term in equation (11) vanishes when $r_{max} \to \infty$, the inequality

$$2\pi A\cdot 2\ln\frac{l}{r_{min}}\geqslant T\geqslant 2\pi A\left(2\ln\frac{l}{r_{min}}+\frac{1}{2}\ln\frac{r_{max}^2-l^2}{r_{max}^2}\right)$$

is valid.

Thus the maximum inaccuracy in T is determined by the second term in (11), which can be neglected when $l \leqslant 0.6\ r_{max}$ (the resultant error will be $<1\%$).

When $l > 2r_{max}$, T should correspond simply to the double ionization; this will be the case when $T = 2\pi A\cdot 2\ln(r_{max}/r_{min})$. As a result

$$T=2\pi A\cdot 2\ln\frac{s}{r_{min}},\qquad \text{where}\begin{cases} s=l & \text{with } l\leqslant 0{,}6\,r_{max},\\ s=r_{max} & \text{with } l>2r_{max}.\end{cases}$$

If the angle of divergence of the pair is ϑ, then at a distance x from the point of formation of the pair, the ionization will be

$$I=2I_0\frac{\ln\frac{s}{r_{min}}}{\ln\frac{r_{max}}{r_{min}}},\quad \text{where}\begin{cases} s=\vartheta x & \text{with } \vartheta x\leqslant 0{,}6\,r_{max}\\ s=r_{max} & \text{with } \vartheta x>2\,r_{max}\end{cases}, \tag{12}$$

and I_o is the ionization produced by a single particle.

Now we must determine r_{min} and r_{max}. For the minimum value of the impact parameter we can take the Compton wave-length $\lambda \simeq 4 \cdot 10^{-11}$ cm.

The choice of r_{max} in our case is determined by the screening effect owing to polarization of the medium; the electrons of the medium can be assumed to be free. In this case it is necessary to take $r_{max} \sim c/\nu$, where $\nu^2 = 4\pi ne^2/m$ (see Ref. 5) (n is the electron density; in emulsions $n \sim 10^{24}$ cm^{-3}, which gives $r_{max} \sim 5 \cdot 10^{-7}$ cm). Of course, the idea that the polarization of the medium is ineffective at ranges under r_{max} and, on the other hand, leads to complete cessation of interaction at long ranges is only a tentative assumption. However, since the result depends logarithmically on r_{max}, this idealization cannot lead to any great distortion.

The classical method of computing the ionization loss by the method of impact parameters, which we have employed above, cannot pretend to complete exactness. In the first place this applies to the case of small impact parameters which cannot be treated classically.

However, if we are interested only in energy losses by small decrements, which determine ionization along the track of a particle over a short distance, the role played by "near" collisions is not particularly important. The fact that the ionization arising from "near" collisions is nevertheless taken into account fairly accurately follows from the fact that the value of $\ln (r_{max}/r_{min})$ with the chosen value of r_{min} agrees well in the region of minimal losses with the numerical value of the corresponding logarithm in Bloch's formula.

Fundamentally, the effect of ionization weakening, under consideration, is determined by large impact parameter ("far") collisions which, as is known, can be considered classically. When computing the mean energy transfer in this case, the electrons of the medium may be regarded as free, since the collision time is short compared to the periods of the atomic oscillators. Actually, the collisions determining the effect have durations on the order of $\Delta t \leqslant r_{max}/c\gamma$, where $\gamma = 1/\sqrt{1 - \beta^2}$. For $\gamma \sim 10^5$, we have $\Delta t \leqslant 10^{-23}$ sec, which is some eight orders of magnitude smaller than the periods of atomic oscillators. The non-simultaneity of the interactions of the electron and positron of the pair is of the same order of magnitude, due to thedifference in their respective velocities. Thus, the difference in the times of flight of the electron and positron over a distance x is $\Delta t' = \frac{x}{v_1} - \frac{x}{v_2} \approx \frac{x}{c\gamma^2}$ (v_1 and v_2 being the respective velocities of the particles). For $x = r_{max}/\vartheta$ and $\vartheta \approx 1/\gamma$, this gives $\Delta t' \sim r_{max}/c\gamma$. There is no reason to suppose, therefore, that quantum-mechanical treatment will substantially alter the obtained result.

Fig. 3 shows the variation of the ionization with the path length of the pair in a nuclear emulsion, computed according to equation (12) for different values of the angle ϑ. The section of the curve where I is not determined by (12) is indicated by a dash-line.

As is known, the relationship between the angle ϑ and the energy of the photon is not single-valued. The corresponding angular distribution is given by a universal function of the ratio ϑ/ϑ_0, where $\vartheta_0 = E_0 mc^2/E_+ E_-$, where E_0, E_+ and E_- are the energies of the photon, the positron and the electron, respectively. This function has a pronounced maximum at $\vartheta/\vartheta_0 = 1$. From this it is clear that the angle ϑ is largely determined by the particle which carries away a smaller part of the energy than the photon. A sharp falling off of the cosmic ray energy

spectrum leads to the result that the actual angle ϑ will, in most cases, correspond to the maximum of the distribution curve and an equal partition of the energy between two components of the pair. This gives $\vartheta \sim 4\pi mc^2/E_0$. Whence we obtain, for example, for $\vartheta = 10^{-6}$ a photon energy $E_0 \sim 2 \cdot 10^{12}$ eV. Turning to Fig. 3 and taking into account the accuracy of measurement of the relativistic ionization in photoemulsions, we find that the effect should be detectable, at $E_0 \sim 10^{12}$ eV. (With sufficiently high statistics it should be detectable even with $E_0 \sim 10^{11}$ eV.)

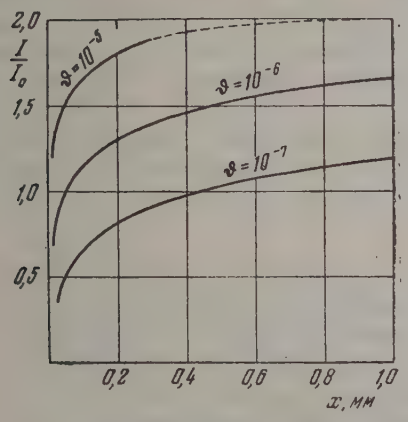

Fig. 3. Dependence of the ionization produced by an electron-positron pair on the distance from the point of creation of the pair for different scattering (divergence) angles ϑ.

In the deriving expression (12), it was assumed that the distance between the components of the pair is determined only by the angle of divergence ϑ (i.e., $\sim \vartheta x$). Actually, however, the separation of the pair will also be affected by multiple scattering. Inasmuch as the multiple scattering separation is proportional to $x^{3/2}$, it will become the determining factor at sufficiently large values of x. Assuming that the length of the t-unit in the emulsion equals 3 cm and that the most probable angle of divergence is ϑ_0, we can readily evaluate the mean separation taking multiple scattering into account:

$$\sqrt{\overline{l^2}} \approx \vartheta x \sqrt{1 + 15x}.$$

It will be seen that the relative effect of the scattering is determined not by the energy but solely by the path length x. Over a path length of 1 cm the separation is increased by a factor of four due to multiple scattering. For a path length under 1 mm the effect of scattering is small and leads only to an insignificant modification of the curves of Fig. 3 (a few percent).

An effect, analogous to the above, must be observable also during the separation of identically charged particles, except that in this case the ionization will decrease as the particles diverge from $I_0(z_1 + z_2)^2$ to $I_0(z_1^2 + z_2^2)$, where z_1 and z_2 are the charges on these particles. Equation (12) in this case is replaced by the following expression:

$$I = I_0 \left[(z_1 + z_2)^2 - 2z_1 z_2 \frac{\ln \frac{s}{r_{min}}}{\ln \frac{r_{max}}{r_{min}}} \right].$$

Identically charged pairs with small angles of divergence are produced, for example, in the case where complex nuclei of primary cosmic rays undergo only a small perturbation in the collision. If it is assumed that the kinetic energy of the nuclear fragments in the center of mass system in such collisions is of the order of 10 MeV, the effect should be observable when the energy of the primary nucleus is of the order of 10^{13} eV per nucleon. From an experimental point of view, such occurrences, apparently, are more difficult to detect than electron-positron creation at energies of 10^{12} eV.

In conclusion it may be noted that in the case of electron-positron pairs of sufficiently high energy there should probably be a decrease not only of the ionization loss but also of the radiation loss. However, this effect is of less practical interest since it is several orders of magnitude smaller than the decrease in radiation loss due to a process described by Landau and Pomeranchuk in Ref. 7.

"P. N. Lebedev" Physical Institute of the
Academy of Sciences of the USSR

References

1. J.J.Lord, J.Fainberg & M.Shein, Phys. Rev., 80, 970 (1950).
2. M.F.Kaplon & D.M.Ritson, Phys. Rev., 88, 386 (1952).
3. D.Lal, Y.Pal, B.Peters & M.S.Swami, Proc. Indian Acad. Sci.,36,75 (1952).
4. J.H.Molvey, Proc. Roy. Soc., A221, 367 (1954).
5. N.Bohr, Passage of atomic particles through matter (Russian trans.)M. 1950.
6. A.Borsellino, Phys. Rev., 89, 1023 (1953).
7. L.D.Landau & I.Ia.Pomeranchuk, Doklady AN SSSR., 92, 735 (1953).

* * * * *

THE RADIATION AND SCATTERING OF FAST PARTICLES IN A MEDIUM

- M. L. Ter-Mikaelian

Emission by fast particles in cases of coulomb interaction has been the subject of numerous investigations. We want to call attention to the fact that, at relativistic speeds, the radiation incident to collisions of fast particles with individual atoms depends to a considerable extent on the index of refraction of the medium.* This influence is important not only in emission at atomic frequencies (as, for instance, is the case in the Čerenkov effect) but, with increasing initial electron energy, in the radiation of hard quanta for which the index of refraction is very nearly equal to unity. The reason for the influence can readily be understood in view of the following considerations. The field potentials of a rapidly moving particle are given by the expressions

$$\varphi = \frac{e}{R - \frac{vR}{c}} \quad \text{and} \quad A = \frac{v}{c}\varphi,$$

where R is the distance from the charge to the point of observation and v is the velocity of the particle. The potentials A and φ increase (and this means that the radiation, also, increases) as $v \to c$ only for those directions for which $\theta \approx mc^2/E$, where θ is the angle between the direction of radiation and the velocity of the particle. If the emission occurs in a medium, the velocity c must be replaced by $c' = c/\sqrt{\varepsilon}$. Let us consider radiation of frequencies greater than the atomic. Then

$$\sqrt{\varepsilon} = 1 - \frac{2\pi NZe^2}{m\omega^2},$$

---

* This should also be taken into account in calculating radiative corrections to electromagnetic processes.

where N is the number of atoms per cm^3. The denominator in the expressions for the potentials reduces to

$$1-\frac{vR}{Rc}\sqrt{\varepsilon}\approx 1-\frac{v}{c}+\frac{\theta^2}{2}+\frac{2\pi NZe^2}{m\omega^2}.$$

It will be seen that for frequencies $\omega<\sqrt{\frac{4\pi NZe^2}{m}}\cdot\frac{E}{mc^2}$ it is essential to take into account the effect of the medium. In particular, it can be seen that with $v\to c$ and $\theta\approx mc^2/E$ the potentials no longer increase and radiation must, consequently, be less effective. Thus in calculating the radiation intensity it is necessary to use Maxwell's macroscopic equations. The possibility of using them for calculating the emission of quanta of wave-lengths much shorter than atomic dimensions is demonstrated in Ref. 1. Omitting the details of the derivation, we give the expression for the number of emitted quanta per unit path length in the energy interval dE' for the case of complete screening:

$$dN=\frac{1}{L}\cdot\frac{{}^4/_3E^2-{}^4/_3EE'+E'^2}{E^2E'}\cdot\frac{dE'}{1+\frac{4\pi NZe^2h^2}{m^2c^4}\left(\frac{E}{E'}\right)^2}, \qquad (1)$$

where

$$\frac{1}{L}=\frac{4N}{137}\left(\frac{Ze^2}{mc^2}\right)^2\lg 191Z^{-1/3}.$$

Expression (1) remains valid up to energies of the order of E_0, determined by the relation

$$E_0=\left(\frac{mc^2}{E_s}\right)^2\frac{6L}{c}\sqrt{\frac{4\pi NZe^2}{m}}\,mc^2, \qquad (2)$$

where

$$E_s=\sqrt{4\pi\cdot 137}\,mc^2.$$

For dense media, consisting of elements toward the end of the periodic system, $E_0\approx 10^{10}$ eV.

With further increases in the energy, it is essential to take into account, as Landau and Pomeranchuk have shown,[2] the effect of multiple scattering on bremsstrahlung radiation. The theory of this effect, classical as well as quantum-mechanical, has been given by Migdal[3] (we limit ourselves here to exposition of the results for frequencies much lower than the initial energy of the electrons). The results of these investigations indicate that at energies higher than E_0, in the frequency interval

$$\left(\frac{4\pi NZe^2}{m}\right)^{2/3}\left(\frac{6E^2L}{E_s^2c}\right)^{1/3}\ll\omega\ll\frac{E_s^2}{6m^2c^3L}\left(\frac{E}{mc^2}\right) \qquad (3)$$

the intensity of radiation is given by the Landau-Pomeranchuk equation:

$$dI\approx\frac{e^2}{2c}\sqrt{\omega}\,\frac{E_s}{E}\,d\omega\sqrt{\frac{c}{6\pi L}}. \qquad (4)$$

The exact formula was derived by Migdal.

In the region of low frequencies

$$\sqrt{\frac{4\pi NZe^2}{m}}\ll\omega\ll\left(\frac{4\pi NZe^2}{m}\right)^{2/3}\left(\frac{6E^2L}{E_s^2c}\right)^{1/3} \qquad (5)$$

the limiting case of equation (1)

$$dI=\frac{E_s^2m}{12\pi^2LNZ}\cdot\frac{\omega^2d\omega}{E^2} \qquad (6)$$

remains valid. Only for very high frequencies

$$\frac{E_s^2}{6m^2c^3L}\left(\frac{E}{mc^2}\right)^2 \ll \omega \ll \frac{E}{h} \qquad (7)$$

does the usual Bethe-Heitler formula

$$dI = \frac{4}{3}e^2\frac{d\omega}{L}. \qquad (8)$$

remain valid (provided that $\omega \ll E/h$). From the conditions (3) and (7), it will be seen that, with increasing energy, the region of applicability of the Landau-Pomeranchuk equation expands and, for energies of the order of 10^{12}-10^{13} eV in dense media, extends to cover almost the entire interval of frequencies, excepting the very low ones (condition (5)) for which the eq. (6) holds.

From this it follows that at high energies light particles become penetrating, i.e., that the energy loss per t-unit (radiation length) becomes small in comparison with the initial energy (see eq. (4)). Exact formulas for the emission of any quanta, taking into account multiple scattering, have been deduced by Migdal. It is interesting to note that the Bethe-Heitler formula still remains valid for a narrow interval of very hard quanta.[2] However, this does not invalidate the above deduction regarding the increased penetrating power of particles.

Let us now turn to consideration of the scattering of particles in a medium. In scattering on atoms it is necessary to distinguish between elastic scattering and scattering in which the atom is excited. Elastic scattering (collision with nuclei) takes place when the particle moves inside the atom; on the other hand, when the passage is at a distance (large impact parameter) screening by the atomic electrons comes into effect and the scattering cross section falls sharply. It follows that the formulae of elastic scattering will remain valid in a medium since, at such small (atomic) distances, the influence of neighboring atoms may be neglected. (To avoid confusion, let us note that considering bremsstrahlung as a combination of the independent processes of scattering and radiation, we convince ourselves that the influence of the medium is evinced only where the latter process is concerned.)

As for inelastic scattering, the atom may absorb energy in both close collisions and in encounters at ranges much greater than atomic dimensions. In fact, if the atom may be compared to an assembly of oscillators (absorbing quanta, the frequencies of which are close to the natural frequencies of the oscillators), the absorption will be effective in those cases when the collision time is shorter than the oscillator period (T). The collision time (in order of magnitude) is $(p/v)\sqrt{1 - v^2/c^2}$, where v is the velocity of the incident particle and p is the collision parameter. If this time is $<T$, then the atom will absorb energy. With $v \to c$ this will occur at very great distances and it may be assumed that in such cases the influence of neighboring atoms (the Tamm-Frank-Fermi effect) must be taken into account. Hence, in calculating the ionization loss (with large impact parameters) it is essential to use Maxwell's macroscopic equations

$$\Delta A - \frac{\varepsilon}{c^2}\cdot\frac{\partial^2 A}{\partial t^2} = -\frac{4\pi}{c}\,j$$

and

$$\Delta\varphi - \frac{\varepsilon}{c^2}\cdot\frac{\partial^2\varphi}{\partial t^2} = -\frac{4\pi}{c}\,\rho,$$

where ρ is the charge density and j migration current.

The remainder of the calculation reduces to an ordinary quantum-mechanical problem solvable in the Born approximation. Naturally, in this way, we arrive at the results of Tamm-Frank and the results of Fermi.

This method of calculation allows investigation of certain details not susceptible to classical consideration of the problem. On the other hand, it leads (in the same approximation as the classical) to the expression for losses in "far" collisions, i.e., for collisions with transfer of a momentum less than $K_{\rho max}$:

$$-\frac{dE}{dx}=\frac{2e^2c}{\pi v^2}\int_0^{K_{\rho max}} K_\rho dK_\rho \int_0^\infty d\omega \frac{\sigma(\omega)}{|\varepsilon(\omega)|^2}\cdot\frac{\frac{\omega^2}{v}\left|\frac{v^2}{c^2}\varepsilon-1\right|+K_\rho^2}{\left|\left(\frac{v^2}{c^2}\varepsilon-1\right)\frac{\omega^2}{v^2}-K_\rho^2\right|^2}, \qquad (9)$$

where $\sigma(\omega)$ is the absorption coefficient.

For "near" collisions (i.e., for collisions in the perpendicular direction of a momentum greater than $K_{\rho max}$ we come to the equations for collisions of free particles. Simple integration of equation (9), with $v \to c$, leads to the expression for losses in "far" (large impact parameter) collisions:

$$-\frac{dE}{dx}=\frac{2\pi NZe^4}{mv^2}\ln\frac{K_{\rho max}^2\cdot mc^2}{4\pi NZe^2}.$$

Matching this with the expression for losses in free collisions we arrive at the equation for ionization losses. The detailed paper concerned with ionization losses will be published later.

Physical Institute of the
Academy of Sciences of the USSR

References

1. M.L.Ter-Mikaelian, Doklady AN SSSR., 94, 1033 (1954).
2. L.D.Landau & I.Ia.Pomeranchuk, Doklady AN SSSR., 92, 535, 735 (1953).
3. A.B.Migdal, Present issue of the Bulletin.

CONTRIBUTION TO THE THEORY OF ANTIPROTON FORMATION

- L. M. Afrikian

In spite of the fact that at the present time it is not possible to investigate the problems of antinucleons with any degree of consistency, estimation of the cross-sections for antiproton formation is not without interest in connection with the possibility of producing antiprotons in the new powerful accelerators. We investigated, within the framework of the charge-invariance pseudo-scalar meson theory, the following reactions for antiproton formation ($\tilde{p}$):

1. $\pi^- + p \to n + p + \tilde{p}$,
2. $\pi^+ + n \to p + p + \tilde{p}$,
3. $\pi^- + n \to n + n + \tilde{p}$,
4. $p + p \to p + p + p + \tilde{p}$,
5. $n + p \to n + p + p + \tilde{p}$,
6. $n + n \to n + n + p + \tilde{p}$.

The cross sections were calculated in the first non-vanishing approximation of perturbation theory, which corresponds to the third order approximation of the theory for processes (1, 2, 3), and to the fourth order approximation for (4, 5, 6). In this approximation no account is taken of the inverse reaction of the nucleon's own meson field. Hence, the approximation can be expected to ba valid only at the threshold of the processes, at energies of the produced nucleons (and antiprotons) considerably lower than the excitation energy of the first isobaric state $\Delta \approx 250$ ev, i.e., at $E - E_0 \ll 2$, where E_0 is the threshold energy of the process of antiproton formation in the laboratory system.

For the processes (1, 2, 3) (formation of antiprotons by π mesons on nucleons),

$$E_0 = 4M - \frac{\mu^2}{2M}$$

which corresponds to a kinetic energy of the incident π meson of

$$T_0 = 4M - \mu\left(1 + \frac{\mu}{2M}\right) = 3.45 \text{ Bev}$$

where M is the mass of the nucleon, and μ is the π-meson mass.

For the processes (4, 5, 6) (formation of antiprotons in collisions of nucleons)

$$E_0 = 7M,$$

which corresponds to a kinetic energy of the incident nucleon of

$$T_0 = 6M = 5.6 \text{ Bev}.$$

It should be noted that π mesons with energies $T_0 \gtrsim 3.45$ Bev begin to be emitted in nucleon collisions when the kinetic energy of the incident nucleon (in the system where the second nucleon is stationary) attains

$$T_{min} = 4.15 \text{ Bev}.$$

Hence the production of antiprotons in nucleon collisions may proceed through the formation of real π mesons with energies $T_0 \gtrsim 3.45$ Bev,

already at nucleon energies which are significantly lower than the threshold of antiproton production in nucleon collisions.

Recently antiproton production in nucleon collisions near the threshold was examined by Fox[1] and Thorn[2]. In these studies the cross sections were calculated without taking into account the interaction of the product particles. In view of this, their result can be assumed, at best, to pertain only to a narrow energy interval at the upper bound of the threshold region; moreover, Fox and Thorn omitted from consideration the extremely important processes (in the given energy interval), leading to the formation of particles in bound states (such as deuterons[3]). Thus for the case of pseudoscalar coupling, Thorn[2] obtained the expression

$$\Phi(n, p) = 5{,}4 \cdot 10^{-29} \left(\frac{f^2}{4\pi}\right)^4 \left(\frac{E - 2M}{M}\right)^{1/2} \text{см}^2;$$

for the cross section for process (5) (in the c.m. system). Taking into account the interaction of the particles in the final state leads to the following expression for the cross section for the same process

$$\Phi'(n, p) = 1{,}5 \cdot 10^{-29} \left(\frac{f^2}{4\pi}\right)^4 \left(\frac{E - 2M}{M}\right)^{1/2} \text{см}^2.$$

Finally, the immediate proximity of the threshold, there may occur processes ending in the formation of deuterons according to the scheme*

$$n + p \to d^+ + p + \tilde{p},$$

and also the possibility of the antiproton capture in deuteron-like "orbits" of the nucleons is not precluded, for example,

$$n + p \to d^- + p + p.$$

The last possibility is due to the fact that the sign of the interaction constant is the same for nucleons and antinucleons in pseudoscalar fields; it may, therefore, be assumed that at relatively large distances on the order of the range of π-meson forces nucleon-antinucleon interactions are analogous to nucleon-nucleon interactions. In this case the cross section for the formation in the final state of a nucleon pair of the deuteron type will be

$$\Phi_1(n, p) = 6{,}5 \cdot 10^{-31} \left(\frac{f^2}{4\pi}\right)^4 \left(\frac{E - 2M}{M}\right)^2 \text{см}^2,$$

while for the process

$$n + p \to d^+ + d^0$$

we have, analogously,

$$\Phi_2(n, p) = 4 \cdot 10^{-33} \left(\frac{f^2}{4\pi}\right)^4 \left(\frac{E - 2M}{M}\right)^{1/2} \text{см}^2.$$

Here it must be noted that the lifetime of the antiproton in the bound state of the deuteron type is $\sim 10^{-21}$ sec.

Thus, taking account of the interaction of the product particles

---

* The following designations are employed in the present paper: d^+ - ordinary deuteron, d^- - deuteron-like system consisting of a neutron and an antiproton, d^0 - deuteron-like system of a proton and an antiproton.

is important in evaluating the absolute value and the energy dependence of cross sections in the threshold region. A special article in the JETP will be devoted to the detailed investigation of the effects (1-3), (4) and (6).

This investigation was carried out under the direction of V. L. Ginzburg, whom the author wishes to thank. The author is also indebted to M. A. Markov for constant interest in the work and helpful discussions.

"P. N. Lebedev" Institute of the
Academy of Sciences of the USSR
and
Physical Institute of the
Academy of Sciences of the Armenian SSR

References

1. D. Fox, Phys. Rev., 94, 499 (1954).
2. R. N. Thorn, Phys. Rev., 94, 501 (1954).

* * * * *

Abstracts

THE INFLUENCE OF MULTIPLE SCATTERING ON BREMSSTRAHLUNG AND PAIR PRODUCTION

(Abstract: Full report in Doklady AN SSSR, 96, 49 (1954).)

- A. B. Migdal

1. In bremsstrahlung and pair production, the behavior of the electron at macroscopic distances from the nucleus is relevant. For this reason, as was shown by Landau and Pomeranchuk, in dense media pair production and bremsstrahlung are affected by multiple scattering. Landau and Pomeranchuk evaluated of the cross section for these processes at ultra-high energies.

2. With the aid of the classical kinetic equation we have obtained a quantitative solution of the problem of bremsstrahlung emission of soft quanta, taking into account multiple scattering.

3. We deduced a quantum kinetic equation for multiple scattering which allows quantitative solution of problems dealing with bremsstrahlung emission of any quanta and pair production in a dense medium at any arbitrary energies.

In the case of media of sufficiently low density, the results obtained go over into the Bethe-Heitler formula.

Academy of Sciences of the USSR.

ANALYSIS OF HIGH-ENERGY STARS

(Abstract)

- D. S. Chernavski

The report is devoted to an analysis of the stars formed in collision of very high energy (10^{12} ev) nucleons with nuclei, described in the publications of Kaplan.

The importance of this analysis stems from the fact that the angular distribution of the number of particles evinced in these stars permits of direct comparison with the theory of the multiple production of particles, developed by Landau. In extensive air showers (the other source of our information on nuclear processes at high energy) the distribution in angle of the particle energies plays an important part; this Landau's theory does not predict nearly as well.

The analysis is based on Landau's theory, supplemented by the assumption that the collision of a nucleon with a nucleus is equivalent to the collision of a nucleon with a "tube" of nuclear matter and that in a certain system of coordinates the distribution of the number of particles is symmetrical. As a result of the analysis it is shown that in cases when the nucleon collides with a short "tube", equivalent to not more than 3-4 nucleons the angular distribution in the stars is in good agreement with Landau's theory. Cases of collision with a long "tube", consisting of a large number of nucleons, require further theoretical investigation.

"P. N. Lebedev" Physical Institute of the
Academy of Sciences of the USSR.

* * * * *

ON FLUCTUATIONS IN THE INTERACTION OF HIGH-ENERGY PARTICLES

(Abstract: Full report in Zhur. eksp. i teor. fiz. - JETP - 29, 296 (1955).

- M.I.Podgoretski, I.L.Rozental'
and D.S.Chernavski

The influence of the thermal motion in multiple production of particles processes is examined in the report. The investigation is carried out in the framework of the theories of Fermi and Landau. It is shown that taking thermal motion into account leads to an increase in the probability that one particular particle will carry off a large fraction of the energy of the primary particle.

"P. N. Lebedev" Physical Institute of the
Academy of Sciences of the USSR.

* * * * *

DIFFRACTIONAL DISINTEGRATION OF DEUTERONS

(Abstract: Full report in Zhur. eksp. i teor. fiz. - JETP - 29,115 (1955)

- E. L. Feinberg

1. It is shown that fast deuterons involved in collisions with nuclei can undergo not only processes accompanied by destruction of the target nucleus and

"disruption" processes involving splitting of the deuteron in the electric field of the nucleus, but also a distinctive disintegration process (independent of the electric field), in which the nucleus experiences only a small recoil. This process is a consequence of the fact that all the other processes leading to attenuation of the primary deuteron beam, give rise to diffraction of the deuterons. Acquiring an additional momentum in the diffraction, the deuteron may undergo disintegration.

2. It follows from general considerations (conservation laws, the uncertainty principle, etc.) that this process can occur on any type of nuclei in the case of deuterons having an energy exceeding a few Mev.

3. Specific calculations of the cross section are carried out on the assumption that the nucleus is absolutely opaque to nucleons (the deuteron energy must, therefore, be not higher than 150-200 Mev) and that the Coulomb field of the nucleus can be neglected (the deuteron energy accordingly must not be less than some tens of Mev).

4. The exact nature of the process cross section depends on the form of the wave function characterizing the internal motion in the deuteron. Hence numerical calculations were made only for the part of the process that is connected with relatively large impact parameters when it is necessary to use only the wave function of the deuteron at distances exceeding the effective range of nuclear forces, where this function is known.

5. Calculations, carried out in collaboration with A. I. Aliev, showed that the total cross section for this part of the process is the same as for the "disruption" process and is independent of the deuteron energy. The products of the disintegration are ejected with approximately the same distributions in angle and energy as in the "disruption" processes. Hence in practice the process can be detected only in experiments in which the ejection of the proton and the neutron are observed simultaneously. In the observations of "disruption" made so far the products of diffractional disintegration cannot be separated from the products of the "disruption". The influence of the diffractional disintegration may explain the observed excess experimental value of the "disruption" cross section over the theoretically deduced cross section.

"P. N. Lebedev" Physical Institute of the
Academy of Sciences of the USSR.

* * * * *

GENERAL RELATIONSHIPS IN THE DECAY OF HEAVY MESONS

(AAstract: Full report in Zhur. eksp. i teor. fiz. - JEPT - 27, 257 (1954))

I. S. Shapiro

1. The selection rules imposed by parity and angular momentum considerations are briefly formulated for the case of decay to 2-3 bosons with zero spins.

2. The decay schemes of $\tau^{\pm}$ mesons and θ^{o} particles are analyzed in the light of the formulated selection rules for the purpose of establishing the necessary conditions under which the particles form isotopic triplets. It is shown that the formation of a triplet can occur only when the spins of the particles are $\geqslant 1$.

3. On the assumption that both the isotopic and ordinary spins are equal to unity, the theoretically conceivable modes of $\tau^{\pm}$-meson and θ^{o}-particle decay, that might compete with those now known to exist, are analyzed.

4. In the light of the deductions the question of the possible identity of theta, kappa and chi mesons is examined.

"M. V. Lomonosov" Moscow State University.

ON THE QUESTION OF THE EXISTENCE OF ANTINUCLEONS

(Abstract: Full report in Doklady AN SSSR, 99, 737 (1954).

- Iu. M. Shirokov

It is commonly assumed that present day theory inescapably predicts the existence of antinucleons. This prediction, however, is founded on unnecessarily rigorous (sufficient but not necessary) conditions of relativistic invariance.

If we make use of the necessary and sufficient conditions of relativistic invariance it turns out that for particles with spin $\frac{1}{2}$, in addition to the Dirac equation there exists yet another equation with a two-component wave function. For particles described by this equation the existence of antiparticles is not obligatory. Consequently, from the point of view of theory the question of the existence of antinucleons remains open.

"M. V. Lomonsov " Moscow State University.

* * * * *

ON THE STOPPING OF HEAVY PARTICLES

(Abstract)

- I. I. Gol'dman & S. A. Kheifets

1. Unstable negative particles may either be captured by the nuclei of the absorber material or undergo disintegration. To determine the relative probabilities of the two processes, it is essential to know the slowing-down time. An appreciable fraction of the slowing-down time is spent in an interval of velocities much lower than those of valence electrons, i. e., in the region where the usual Bethe-Bloch ionization loss formula is inapplicable. To find the slowing-down time of a particle, we investigated the mechanisms of energy loss in the low-speed region.

2. The motion of a heavy meson, because of its large mass, turns out to be classical in a wide energy interval. Therefore, classical concepts of trajectory, impact parameter, etc., are applicable to meson motion over the entire range of speeds which are of interest.

3. The mechanisms of energy loss by positively and negatively charged particles are completely different. A negative slow meson or hyperon, even when it is moving with a large impact parameter will approach to within a comparatively small distance of the nucleus due to the strong attraction of the latter. In the course of its approach it can acquire considerable speed and this leads to noticeable energy losses. In contrast to this a positive meson does not penetrate into the central region of the atom and loses its energy almost exclusively as the result of elastic collisions with atoms.

4. Different energy loss processes predominate in different energy regions and in materials having different atomic numbers. The energy losses for the following processes were investigated: a) elastic collisions, b) inelastic collisions with atoms and c) scattering. In addition, the problem of negative particle capture on an atomic shell was studied.

Physics Institute of the
Academy of Sciences, Armenian SSR.

INVESTIGATION OF INTERACTIONS OF PARTICLES OF HIGH AND ULTRAHIGH ENERGIES WITH NUCLEI AND NUCLEONS

- N. A. Dobrotin, G. T. Zatsepin, S. I. Nicol'ski, L. I. Sarycheva, and G. B. Khristiansen

Investigations of the interactions of high and ultra-high energy particles with nuclei and nucleons have led to a series of important discoveries and in particular to the proof of the existence of multiple production of particles, nuclear cascades and a number of other phenomena. One may expect the parameters characterizing the internal attributes of nucleons and other "elementary" particles to be most clearly revealed in this high energy region.

Since the terminology for the different energy regions met in cosmic ray research is not definitively established, we believe it useful to introduce the following definitions: hereinafter we will call energies up to $3 \cdot 10^{10}$ ev low; the predominant processes for N-component particles in this energy interval are energy losses due to star production (disintegrations) and ionization of the atoms of the medium; we classify as moderate energies in the $3 \cdot 10^{9}$ - $2 \cdot 10^{10}$ ev interval; i.e., the energy interval which can be studied by the deflecting effect on charged particles of the earth's magnetic field; it is convenient to assign energies in the $2 \cdot 10^{10}$ - 10^{13} ev interval to the high energy region, in which the elementary events can be studied by means of emulsion techniques and, partly, with the aid of cloud chambers; and, finally, we shall call energies above 10^{13} ev ultra-high energies; our principal source of information on particle interactions in this region is still observation of extensive air showers.

In studies of phenomena induced by high energy particles of especial interest is investigation of so-called "jets"; these are showers observed in photographic emulsions, which comprise a comparatively large number of relativistic particles (up to 40) concentrated in a very narrow cone (which is indicative of the high energy of the primary particle) and a small number of strongly ionizing particles (from 0 to 5).

An important question is involved in the study of "jets": are they formed in the interaction of a nucleon with a nucleon, or of a nucleon with a whole column of nucleons lying in the nucleus along the path of the incident nucleon (with a "tube"), or even with the entire nucleus? A whole series of papers published recently (1953-1954, Refs. 1 through 9) is devoted to the study and interpretation of "jets."

In most of these papers jets are interpreted to be the result of interactions of the initial nucleon with a peripheral nucleon or with a nucleus of hydrogen, the authors' conclusions being based on the small number of strongly ionizing particles in the jet. Starting with this premise one can deduce such fundamental characteristics of an elementary interaction event as the dependence of the number of secondary particles on the energy of the primary particle, the distributions in angle and energy of the secondary particles and their constitution. Some authors[5,6] suggest that the jets are formed in the interaction of a primary nucleon not with a single nuclear nucleon but, rather, with a whole group of nucleons concentrated in a "tube" cut through the nucleus by the incident nucleon. In this hypothesis it is assumed (to certain extent the assumption is supported by the results of calculations) that the transverse momentum transferred by the incident nucleon to the nucleus is small and that the

nucleus is, therefore, relatively weakly excited; there occurs an internal rearrangement in the nucleus, leading to the ejection of a small number of highly ionizing particles.

The question of whether it is possible to consider the interaction of a nucleon with a nuclear nucleon as a series of successive independent collisions, or whether it is more correct toregard the collision as one of a nucleon with a system of nucleons distributed along its path, i.e., as a simultaneous interaction of the nucleon with a "tube" of nuclear material, was thoroughly investigated by Rosenthal and Chernavski[10]. Their analysis shows that at moderate energies one cannot exclude the possibility of a collision event being split up into a series of distinct successive interactions of the incident nucleon with the nucleons of the nucleus. At high energies the second alternative (simultaneous interaction with a tube) appears to be more in accord with reality.

In general the available experimental data on the dependence of the number of shower particles on the atomic number of the target nuclei support this conclusion. The most detailed results have been obtained by Kaplon's group[11]. In these experiments thick emulsions, separated by thin metal plates, were employed. The dependence of the number N_s of secondary relativistic particles (produced at a given energy of the primary particle) on the atomic weight A of the struck nucleus, was determined. According to the findings of Kaplon et al, when the primary particle energy is of the order of $5 \cdot 10^{12}$ ev, the mean number of secondary relativistic particles formed on the nuclei equals 24 for lead, 18 for brass, 14 for silver and bromine and 14 for the light elements (N, O, C). The experimentally obtained weak dependence of the number of secondary particles on the atomic number of the target nucleus agrees better with the picture of a nucleon interaction with a column of nuclear material, than with the concept of an intranuclear cascade, since in the interaction with a column, N_s will be proportional to $A^{0.2}$ (Ref. 12), while in successive interactions with individual nucleons $N_a \sim 2A^{1/3}$ (Ref. 10).

Investigation of the dependence of the number N_s of secondary shower particles on the energy E_o of the primary particle is of great interest since such results enable us to choose between the various theories of the elementary event of secondary particle formation (according to the theory of Oppenheimer-Lewis $N_s \sim E^{1/3}$; according to Heisenberg's theory $N_s \sim E_o^{1/2}$; according to Fermi-Landau $N_s \sim E_o^{1/4}$).

For the high energy region results obtained with the aid of photographic plates show that at one and the same energy for the generating nucleon, there are formed jets containing different numbers of particles (the number of particles in different jets can vary by a factor of seven).

In view of this it becomes difficult to determine the exact dependence $N_s(E_o)$. It should be noted that this broad spread in itself does not contradict the Fermi-Landau theory since, in forming jets, the incident nucleons can interact with the nuclear matter contained in "tubes" of various lengths. It is also necessary to take into account the possibility of fluctuations in interactions with the nuclear material in a "tube" of given length in the case of distant peripheral collisions, investigated by Feinberg and Chernavski[13].

Some authors[1,3,7] believe it possible to divide the observed jets into two classes, one of which is satisfactorily described by $N_s \sim E_o^n$ with $n = 1/4$, the other by the same relation but with $n = 1/2$. However, this conclusion is still far from definitive.

Of extreme importance to clarification of the character of interactions of high and ultra high energy particles are the investigation of the angular distribution of particles in the c.m. system and the determination of the correlation between scattering angle and the energy of the particles. The angular distribution of the secondary particle flux in the c.m. system can be obtained from photographic plate data on the assumption that the scattering distribution is symmetrical with respect to the equatorial plane of the collision.

Nevertheless this problem has not yet been unambiguously solved. In a number of investigations of collisions at energies on the order of 10^{13} ev a noticeable anisotropy in the c.m. system has been observed.[14] However, in other investigations carried out in the high-energy region with the aid of photographic plates, it is concluded that the angular distribution of secondary particles in the c.m. system is isotropic or quasi-isotropic.[7] It is quite probable that these divergences are due to the fact that collisions at different energies are involved. Investigation by the method of emulsions of the angular distribution in energy of the flux of secondary particles in jets is, as yet, not feasible because of the difficulties in determining the energy of ultra-relativistic particles from their scattering.

Let us turn now to an examination of the characteristics of particle interactions at high and ultra-high energies deduced from the data on extensive air showers. The ample experimental material accumulated in recent years (1944-1954) leaves no doubt that extensive air showers cannot be interpreted simply as gigantic electronic-photonic showers initiated in the atmosphere by primary particles of ultra-high energy. The basic characteristics of an extensive shower (its development in depth and laterally) differ from the analogous characteristics of electronic-photonic cascades. Thus, the absorption of shower particles in the atmosphere, according to electromagnetic cascade theory, occurs according to the $e^{-\lambda(s)t}$ law, where s is a function of the total energy E_o of the shower. For example, according to theory particle fluxes in showers with energies $E_o \sim 3 \cdot 10^{14}$ ev and $E_o \sim 6 \cdot 10^{15}$ ev should be attenuated in the atmosphere between mountain altitudes and sea level by factors of 14 and 5.5, respectively. According to the experimental data, however, their absorption is about the same.

The spatial distribution function for shower particles at large distances from the shower core is also anomalous: the spatial distribution of particles is wider than for pure electronic-photonic cascades.

A significant part in the picture of shower development is played by anomalies related to the presence in showers of large numbers of penetrating particles other than electrons and photons. Experiments carried out in our laboratory,[15,16] show that the fraction of penetrating particles increases with increasing distance from the shower core and attains 40-60% at the peripheries of the shower. On the whole, at sea-level, penetrating particles constitute up to 10% of the total number of shower particles[16]. Inasmuch as their mean energy is at least an order of magnitude higher than the mean energy of the electronic-photonic component, the total energy carried by the penetrating particles exceeds the total energy of the electronic-photonic component of the shower.

In the light of these contradictions between experimental results and the deductions from cascade theory and an analysis of the properties of electron-nuclear showers one of the authors[17] advanced a new

nuclear-cascade scheme of shower development in 1948. In this scheme, in view of the decisive part played by nuclear processes in the development of extensive showers, the shower is regarded as consisting of two parts: a cascade of N-active particles, forming what might be termed the skeleton of the shower, and an electronic-photonic cascade, drawing energy (through π^0 mesons) from the N-component throughout the air shower. The nuclear-cascade picture of the development of extensive air showers is,currently, the basic guiding idea in our researches.

The role of the nuclear-cascade process could be different at different stages of the shower development, depending on the nature of the elementary event initiating the shower and on the effective "threshold" for production of electronic-nuclear showers. However, direct experimental investigation of the composition of the penetrating component of extensive air showers at sea-level shows that even at the last stages of shower development, the fraction of N-component particles (i.e., of penetrating particles producing electronic-nuclear showers) does not decrease at any rate and that, therefore, the nuclear-cascade process is the dominant and decisive one at all stages of shower development.

Experimental techniques now permit quantitative study of the nuclear-cascade process. Hence there is need for a theoretical method of calculation of the nuclear cascade process under various assumptions regarding the nature of the elementary cascade-initiating event. Comparison of the experimental and theoretical characteristics of the nuclear cascade process would then make it possible to choose between the possible various models of the elementary event. Such a general method of theoretical calculation of the nuclear cascade process has been recently developed independently by several authors[18] ("generalized method of successive generations"). The results of applications of this method will be examined below.

The most accurate method for experimental investigation of extensive air showers is "the method of correlated hodoscopes" which has seen rapid development in recent years. The basic idea of this method was first put into practice in 1950 by the Pamir expedition.[15] The essence of the method in its latest version consists in reproducing the actual distribution of the flux densities, practically continuously, over a large area of the shower cross section, including the shower core. The name, "the method of correlated hodoscopes", stems from the fact that the particle flux densities are indicated by a group of counters, connected to a hodoscope assembly and triggered simultaneously at the instant of passage of an extensive air shower.

It is evident that by means of this method it is possible to identify each recorded shower, i.e., to determine the location of the core and the number of particles in the shower, since both of these characteristics are easily determined through direct examination of the observed flux density distribution. It is worth noting that the method of correlated hodoscopes permits investigating the shower structure at distances varying from tens of centimeters to a kilometer from the axis, even though the number of particles in these showers may differ by several orders of magnitude.

Employing the correlated hodoscope method we carried out, during 1950-1953, a detailed investigation of the structure of extensive air showers through a study of the spatial distribution of the flux densities of particles of various kinds. These investigations were made in the atmosphere at the altitude of Pamir (about 4000 meters) and of Moscow (150 meters above sea level).

The arrangement of counters in the 1952 Pamir assembly is shown in Fig. 1 (also see Ref. 19). The assembly comprised more than 1500 hodoscopic counters, divided into 22 groups. Most of the groups consisted of 48 counters. The counter area within a group varied. The density of shower particles in a given point was determined with an accuracy of within 30% from the number of counters activated in a given group. The error in determining the location of the shower core, based on a picture of the passage through all counter groups, was about one meter. Fig. 2 shows a typical spatial particle distribution in an individual shower.

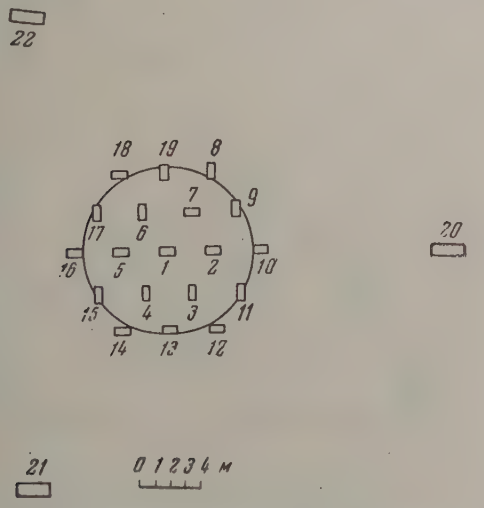

Fig. 1. Arrangement of hodoscopic counter groups.

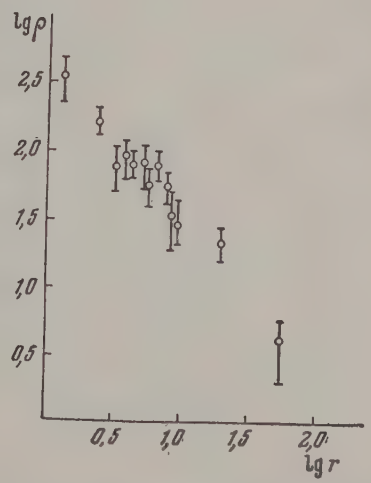

Fig. 2. The spatial distribution of the particle flux densities $\rho(r)$ in an individual shower.

According to our results[19,15] the spatial distribution $\rho(r)$ of the flux densities of all shower particles at mountain altitudes is described by $1/\sqrt{r}$ at distances r from 20 to 100 cm from the shower axis; in the interval $2 < r < 100$ meters the law characterizing the distribution becomes $(1/r)e^{-r/80}$ while with $r > 160$ the law becomes $1/r^3$. It also turned out that the spatial distribution, at least at distances $2 < r < 100$ meters, is not sensitive to changes in the energy of the primary particle initiating the shower. Thus, within a ten to one range of energies, the spatial distribution in this distance interval is described by the law $1/r^{0.65 \pm 0.05}$ regardless of the shower energy. The results shown on Fig. 3, which we obtained for the spatial distribution of particles in showers initiated by primary particles of different energies, all fit a single common curve. The triangles pertain to showers with a total number of particles $N = 2 \cdot 10^4$ ($E_o \sim 5 \cdot 10^{13}$ ev), the dots to showers with $N = 7 \cdot 10^4$ ($E_o \sim 1\text{-}2 \cdot 10^{14}$ ev) and the crosses to showers with $N = 6 \cdot 10^5$ ($E_o \sim 10^{15}$ ev). The data have been normalized to the point corresponding to $r = 9$ meters.

At sea level the spatial distribution of all shower particles is described by the law $1/r$ at distances of the order of meters, and by $(1/r)e^{-r/55}$ at distances of the order of tens of meters;[20] the law goes over to $1/r^{2.6}$ when r is of the order of hundreds of meters.[21] Here, too, the distribution is insensitive to changes in the shower

energy. It can readily be seen that the spatial distribution in the central region of showers at mountain altitudes, as well as at sea level, will be characterized by the same law if for our unit of distance we choose the t-unit (cascade length), employed in the electromagnetic cascade theory.

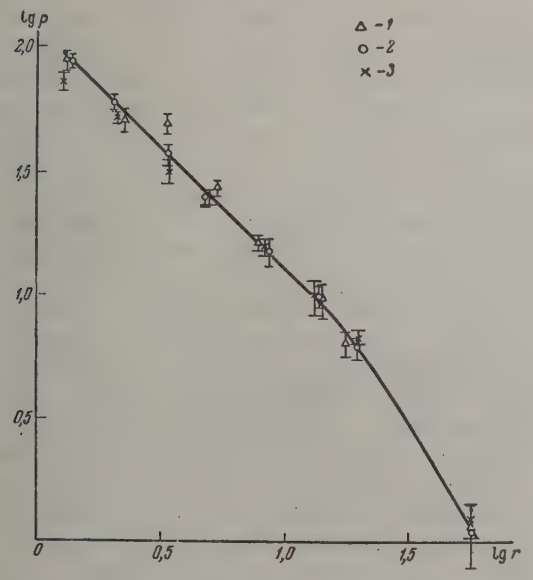

Fig. 3. Spatial distribution of the flux densities of particles in showers initiated by primary particles of different energies: (1) $E_0 \approx 5 \cdot 10^{13}$ ev; (2) $E_0 \approx 1\text{-}2 \cdot 10^{14}$ ev; (3) $E_0 \approx 10^{15}$ ev.

Furthermore, we investigated the spatial distribution of penetrating particles (separately for the N-active and passive particles) in the central regions of extensive air shower, as well as at their peripheries, i.e., at distances of the order of hundreds of meters from the core. The flux density of N-active particles is distributed according to the 1/r law at distances from 2 to 20 meters both at mountain altitudes and at sea level[20,22]. The curve characterizing the energy flux distribution of the N-active particles, according to our qualitative results appears to be even steeper. The sharp peak observed in the spatial distribution of the N-component indicates that, even at sea level, there is an appreciable flux of high energy N-active particles in the shower core and that their number relative to the total number of particles, remains constant at all altitudes.

The cited experimental data on the structure of extensive air showers allows us to draw a number of important conclusions regarding the characteristics of the elementary interaction events at high and ultra-high energies. First, let us examine the angular distribution of particles formed in an elementary event in the light of the observed distribution of the electronic-photonic component of showers. The energy spectrum of the electronic-photonic component of extensive air showers at mountain altitudes (in all cases including that of the nuclear-cascade mechanism) must correspond to the spectrum of the electronic-photonic cascade just past its maximum development ($s \geqslant 1$). According to the experimental results, the distribution of electrons in the shower is approximately characterized by 1/r when $2 < r < 10$ meters. Such a spatial distribution of the particles in an electronic-photonic shower, near the maximum development of the shower, can be fully explained only through multiple scattering of the electrons.

Thus, the divergence of the particles, due to nuclear processes, is not manifest in the spatial distribution of electrons in a shower. It follows that the angles between the particles produced in nuclear collisions are small. If it is assumed that the number of particles in the shower is proportional to the energy of the shower-initiating particle, then from the above-cited particle density distribution data we can conclude that the energy flux density of the particles originating in the first interaction of the proton, initiating the

shower, falls off faster than as $1/\theta$, where the angle $\theta > \delta$ ($\delta = r_\delta/H$, where r_δ is the minimum distance beginning with which the $1/r$ law becomes valid, and H is the path length of the secondary particles from the locus of their formation to the level of observation). Assuming (on the basis of the experiments described above) that $r_\delta = 2$ meters, and taking $H = 1.5 \cdot 10^4$ meters for our conditions, we find $\delta \leqslant 1.7 \cdot 10^4$ [$1.3 \cdot 10^{-4}$?].

If we assume that the energy of the primary nucleon $E_o = 10^{14}$ ev and that the mass M of the stationary "particle" is equal to the mass of the column of nucleons in the nucleus of the air atom encountered by the primary proton, we get $\delta_{c.m.} = 2.2^o$. On the other hand assuming that M equals the mass of a single nucleon, we find $\delta_{c.m.} = 4^o$. Therefore, for the secondary particles produced by a primary particle of 10^{14} ev energy or higher, the density of the energy flux falls off with increasing scattering angle (starting with $\delta_{c.m.} \leqslant 4^o$) faster than as $1/\theta$. This dependence is indicative of a pronounced asymmetry in the scattering of the secondary particles in the c.m. system. This deduction is in direct contradiction with Fermi's theory.[23] Head-on collisions, investigated by Fermi, result in an isotropic distribution of particles in the c.m. system. Taking into account collisions with a finite impact parameter results in some preponderance in the "forward-backward" direction. However, as Rosental' and Chernavski[10] showed, the decrease in the energy flux density to angles corresponding approximately to $r \approx 9$ meters, according to Fermi's theory, is slower than as $1/\theta$. Thus, even if non-central collisions are taken into account, Fermi's theory contradicts experiment. According to Landau's theory,[24] in the c.m. system there must be a marked concentration of the energy flux density near the collision axis. The energy flux density must increase with decreasing angle between the direction of ejection and the collision axis (down to very small angles of the order $\delta_{c.m.} = (2/\gamma_{c.m.})^{0.8}$, faster than as $1/\theta$ (the range of angles within which the energy flux density is constant is approximately inversely proportional to the energy of the colliding nucleons in the c.m. system). For a shower produced by a primary particle of energy 10^{14} ev in the c.m. system, beginning with $\delta_{c.m.} = 1.3^o$, the decrease in the density of the energy flux proceeds faster than as $1/\theta_{c.m.}$ while beginning with the angle $\theta_{c.m.} = 4.5^o$, the decrease is faster than as $1/\theta^2_{c.m.}$.

The experimental data available at present are still insufficient to make a quantitative comparison of the deductions of Landau's theory regarding the angular distribution of particles with experiment. However, from what has been said above, it is clearly in much better agreement with the realities of the elementary interaction event at ultra-high energies than is Fermi's theory.

In addition, analysis of our results obtained on extensive air showers allows of drawing definite conclusions concerning the character of energy partition among the particles participating in an elementary interaction event. In the region of moderate energies this problem has been solved, in the first approximation, by the thorough researches of Grigorov.[25] Grigorov analyzed in detail data he obtained at various latitudes on the transition effect for the soft component in the stratosphere and on "impacts" in ionization chambers. His analysis shows, convincingly, that 10^{10} ev primary protons transfer only about 30% of their energy to the mesons and slow secondary nucleons formed in a single nuclear interaction. The major part of the energy of the primary particle (about 70%) is retained by a single nucleon (which may undergo charge exchange in the interaction event).

Significant information on the distribution of energy in elementary interactions at high energies (approximately to 10^{12} ev) may be obtained from the altitude variation of the N-component of such energies; this had already been done for the region of moderate energies.[26] Experiments aimed at investigating the absorption of the flux of N-component particles with energies of the order of 10^{12} ev were made in 1952.[27] In determining the altitude dependence the experimenters selected showers which could be ascribed to initiating particles having energies in the vicinity of 10^{12} ev. It turned out that the absorption range for such particles* $1/\mu = 112 \pm 11$ grams/cm^2.

The range for absorption of N-component particles of lower energies (10^{10} - 10^{11} ev), determined using the same apparatus as in Ref. 27, was $1/\mu = 131 \pm 3$ g/cm^2, which is in agreement with many measurements of this quantity made by other investigators.

To obtain information about the elementary event at these high energies, the experimental values for the range for absorption must be compared with the range for interaction for the same N-component particles in substances having an atomic number close to the average atomic number of air.**

As is well known, the absorption coefficient μ and the interaction coefficient μ_0 are related by the following equation:

$$\mu = \mu_0 [1 - \Delta(E)]$$

Where the N-component spectrum is described by a power function, Δ, as can be shown,[30] is determined by the following expression:

$$\Delta(E) = \int_0^1 U^\gamma f_E(U)\,dU,$$

where $f_E(U)dU$ is the probability of the formation of a secondary particle with an energy E, amounting to a fraction U of the energy of the primary particle; γ is the exponent of the N-component energy spectrum curve. It will be seen from the cited experimental results that the quantity Δ is very weakly dependent on the energy of the primary particle: at $E \sim 10^{10}$ ev, $\Delta = 0.5 \pm 0.05$ and at $E \sim 10^{12}$ ev, $\Delta = 0.4 \pm 0.06$. As has already been noted,[31] in interactions of nucleons with light atomic nuclei in the 10^{10} ev region, 2/3 of the energy of the primary particle is carried away by a single nucleon. In view of the fact that Δ remains virtually constant in going from $E \sim 10^{10}$ ev to $E \sim 10^{12}$ ev, we may conclude that in the neighborhood energies of the order of 10^{12} ev, too, the major part of the energy of the primary particle is carried off by one nucleon.

As we noted before, extensive air showers are the source of information on the distribution of energy in elementary interactions at ultra-high energies. If we know the total energy of the shower E_0 and the maximum energy E of the N-component particles at the level of observation, then denoting through α the fraction of the energy carried off by one of the nucleons involved in the elementary interaction, we get

---

* The result for 10^{12} ev particles obtained in Ref. 28 by the emulsion chamber method ($1/\mu = 120$ gm/cm^2) in the stratosphere does not at any rate contradict these values.

** Such a substance, for example, is carbon for which, according to Ref. 29, $1/\mu_0 = (70 \pm 5)$ gm/cm^2.

$$\alpha^{l} = \frac{E}{E_0} \qquad (1)$$

where l is the number of ranges for interaction from the boundary of the atmosphere to the level of observation.

An estimate of the maximum energy of the N-component particles in an extensive air shower near sea level can be obtained from the spatial distribution of shower particles near the axis of the shower. It follows from our results, given above, that the flux density of shower particles at sea level increases in accordance with the $1/r$ law up to distances of the order of 1 meter. The fact that the rate of increase in density of the particle flux does not fall off up to about 1 meter from the axis indicates that as a result of nuclear interactions near sea level there are produced (through the agency of π^0 mesons and photons) electrons having an energy of up to approximately $5 \cdot 10^9$ ev*. From this we deduce that the energy of the N-component particles that generate the electronic component in the central region of the shower must be in excess of 10^{11} ev.

As has been mentioned above, a spatial distribution at sea level for showers with energies $E \sim 10^{14}$ ev is described by the $1/r$ law up to $r \sim 1$. Therefore, inserting $E \sim 10^{11}$ ev, $E_0 \sim 10^{14}$ ev and $l \sim 15$ in equation (1) we get $\alpha = 0.6$.

The high degree of energy concentration on a single secondary particle and the data on the angular distribution cannot be reconciled with the basic deductions from Fermi's theory. According to Fermi's theory, the colliding particles form a single system in which statistical equilibrium is established. The formation of secondary particles due to the disintegration of this system is determined by the statistical weights of the possible states. Even without further analysis, it is clear that such a mechanism of the elementary event cannot yield a high concentration of energy on a single particle or energy independence of the absorption coefficient for the particles. A somewhat different situation prevails in the hydrodynamic theory of particle interactions at ultra-high energies developed by Landau. The examination of the hydrodynamic picture of the collision of two nucleons, carried out by Landau, shows that a considerable fraction of the energy of the primary particle will be concentrated on a small number of secondary particles. It is necessary to point out, however, that the present equations of the theory become inapplicable when the energy of the secondary particles approaches that of the primary particle.

For this reason, in our calculations we made a smooth extrapolation of the energy spectrum into the region of the highest secondary particle energies. The energy spectrum curves obtained in this way were used for calculating the variation with altitude of the N-component with $E > 10^{12}$ ev by the method of "successive generations." It turned out that the results of the calculation did not agree with the experimental data. Thus, for an atmospheric depth corresponding to 100 g/cm^2, the theoretical value of the absorption range $1/\mu$ is 83 gm/cm^2, while for a depth corresponding to 800 gm/cm^2, $1/\mu = 74$ gm/cm^2. In contrast to this, from the above-cited data of Ref. 27

---

* Electrons of such energy, according to the theory of multiple scattering, are predominant at distances about 1 meter from the axis of the shower.

(as well as the results of Kaplon et al) it appears that $1/\mu = 115$-120 g/cm^2. The theoretical value of Δ in equation $\mu = \mu_0(1 - \Delta)$ does not exceed 0.25 and decreases rapidly with increasing atmospheric depth. Actually, as we have seen above, Δ depends weakly on the altitude of the observations and remains almost constant at 0.5-0.4.

For the theoretical value of the absorption coefficient to coincide with the experimental value, it is necessary to assign an even higher concentration of energy on a small number of particles than we did in our calculations based on Landau's theory. However, it is possible that this lack of agreement is due not to inadequacies of the theory, but to inaccuracies in calculating the energy spectra according to Landau.

Summing up, it may be said that our investigations permit establishing the following characteristics of elementary interactions of particles at high and ultra-high energies: 1) the angular distribution of secondary particles in the center of mass system is markedly anisotropic; 2) a major fraction of the energy of the primary particle is concentrated on one nucleon or on an extremely small number of nucleons, not only at moderate energies but at energies at least up to 10^{12} ev.

In conclusion, it is necessary to make a number of remarks about the direction of further investigations. The experimental results given above on extensive air showers indicate that the structure of the central regions of these showers not only at sea level, but even at mountain altitudes, is largely determined by interaction processes at energies of the order of $10^{11} - 10^{12}$ ev (and not by processes in the region of ultra-high energies).

Therefore, manifestation in the atmosphere of the processes characteristic of ultra-high energies must be sought at earlier stages of shower development, i.e., at greater altitudes.

On the other hand, in studying these processes it may be helpful to investigate high-energy N-component particles and μ mesons in showers. For example, study of the energy distribution of N-component particles in the shower core should enable us to draw certain specific deductions regarding the characteristics of processes at energies above $10^{11} - 10^{12}$ ev.

It should be noted, also, that study of the flux of N-component particles in shower cores at different altitudes appears to be the only possibility for checking Landau's theory in the region where it is known to be applicable ($E > 10^{12}$ ev). At the same time, further investigation of the details of the pattern of interactions at high energies by more direct methods must be stressed. Since an important part in the development of extensive air showers is played by interactions at high energies, further detailed data regarding them, obtained by any other methods, would naturally facilitate the investigation of processes in the region of ultra-high energies.

"P. N. Lebedev" Physical Institute of the
Academy of Sciences of the USSR
and
"M. V. Lomonosov" Moscow State University

References

1. G.Bertolino, A.Debenedetti, G.Lovera & M.Vigone, Nuovo Cim. 10, 991 (1953).
2. C.C.Dilworth, S.J.Goldsack, T.F.Hoang & L.Scarsi, Nuovo Cim.,10,1261(1953).
3. T.F.Hoang, Jour. de Phys., 14, 395 (1953).
4. C.Dilworth, S.J.Goldsack, T.F.Hoang, & L.Scarsi, C.R., 236, 1551 (1953).
5. W.Heitler & C.Terreaux, Proc. Phys. Soc., A66, 929 (1953).
6. C.B.A.McCusker & F.C.Roesler, Nuovo Cim., 11, 98 (1954).
7. T.F.Hoang, Journ. de Phys., 15, 337 (1954).
8. C.C.Dilworth, J.Goldsack, T.Hoang & L.Scarsi, Nuovo Cim., 11, 424 (1954).
9. G.Bertolino & D.Pescetti, Nuovo Cim., 12, 630 (1955).
10. L.L.Rozental' & D.S.Chernavski, Usp fiz. nauk., 52, 185 (1954).
11. M.F.Kaplon, D.M.Ritxon & W.D.Walker, Phys. Rev., 90, 716 (1953).
12. S.Z.Belen'ki & G.A.Milekhin, Zhur. eksp. i teor.fiz., 29, 20 (1955.)
13. E.L.Feinberg & D.S.Chernavski, Doklady AN SSSR, 91, 511 (1953).
14. M.F.Kaplon & D.M.Ritson, Phys. Rev., 83, 386 (1952).
15. G.B.Khristiansen, Thesis, Phys. Inst. Academy of Sciences, M. 1953.
16. L.Kh.Zidus, M.I.Adamovich, M.A.Ivanovskaia et al, Zhur. eksp. i teor. fiz., 22, 440 (1952).
17. G.T.Zatsepin, Doklady AN USSR, 67, 993 (1949).
18. G.T.Zatsepin, I.L.Rozental', Doklady AN SSSR, 99, 369 (1954); N.L.Grigorov, Thesis, Moscow State Univ., 1954.
19. Iu.N.Vavilov, S.I.Nikol'ski & E.I.Tukish, Doklady AN SSSR, 93, 223 (1953); O.I.Dovzhenko & S.I.Nikol'ski, Doklady AN SSSR, 102, 241 (1955).
20. A.T.Abrosimov, A.A.Bedniakov, V.I.Zatsepin, Iu.A.Nechin et al, Zhur. eksp. i teor. fiz., 30, 1 (1956).
21. L.Kh.Zidus, N.M.Blinova, V.G.Videnski & L.D.Suvorov, Doklady, AN SSSR, 74, 477 (1950).
22. Iu.N.Vavilov, S.I.Nikol'ski & V.P.Sarantsev, Zhur. eksp. i teor. fiz., 28, 505 (1955).
23. E.Fermi, Progr. Theor. Phys., 5, 570 (1950); Phys. Rev., 81, 683 (1951).
24. L.D.Landau, Izv. AN SSSR, Ser. fiz., 17, 51 (1953).
25. N.L.Grigorov & V.S.Murzin, Izv. AN SSSR, Ser. Fiz., 17, 21 (1953).
26. G.T.Zatsepin, Zhur. eksp. i teor. fiz., 19, 1104 (1949).
27. K.P.Ryzhkova & L.I.Sarytseva, Zhur. eksp. i teor. fiz., 28, 618 (1955).
28. M.Kaplon, J.Klose, D.Ritson & W.Walker, Phys. Rev., 91, 1573 (1953).
29. S.A.Azimov, N.A.Dobrotin, A.L.Liubimov & K.P.Ryzhkova, Izv. AN SSSR Ser. fiz., 17, 80 (1953).
30. G.T.Zatsepin, Thesis,Phys. Inst. ofthe USSR Academy of Sciences,M. 1954.
31. S.N.Vernov,N.L,Grigorov, G.T.Zatsepin & A.E.Chudakov, Izv. AN SSSR Ser. fiz., 19, 493 (1955); Translation in Bulletin Vol. 19, No. 5, p. 445).

STRUCTURE OF EXTENSIVE AIR SHOWERS AT SEA LEVEL

- A.T.Abrosimov, V.I.Zatsepin, V.I.Solov'eva, G.B.Khristiansen & P.S.Chikin.

In the fall of 1953 we carried out an investigation of the structure of extensive air showers at sea level by determining the spatial distribution of the flux densities of shower particles of different kinds in the vicinity of the cores. The investigation was carried out by the method of correlated hodoscopes,[1] which in principle permits analyzing each recorded shower individually. The installation consisted of over 1600 GM counters connected into a hodoscope installation of the type described by Korablev.[2]

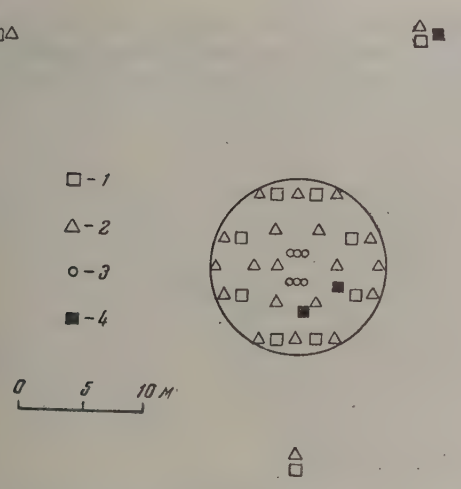

Fig. 1. Diagram of hodoscope installation used for studying the structure of extensive air showers: 1) group of 24 hodoscopic counters of 330 cm^2 area each; 2) group of 48 hodoscopic counters, 24 each 100 cm^2 and 24 each 24 cm^2; 3) counter group connected into control circuit (4 counters of 330 cm^2 area each in this group were connected in parallel; 4) N-particle detectors.

Part of the counters, arranged in groups of 24, served for determining the flux densities of all shower particles (mainly electrons). The use of counters of different areas made it possible to record particle fluxes of densities ranging from 1 to 1000 particles per square meter. Other counters located under lead and iron absorbers served for recording penetrating N-component particles.

Fig. 1 shows a diagram of the installation. Forty-seven density indicators were distributed uniformly in a circle 14 meters in diameter; nine indicators were mounted at distances of 15, 20 and 30 meters from the center of the installation. The four penetrating particle detectors were distributed in the following manner: two in the central region of the installation, one 20 and one 30 meters from the center. This hodoscopic system permitted effective study of showers of 10^{14}–10^{15} ev energy whose cores passed through the central circle, containing the concentration of density indicators.

The installation recorded showers producing coincidences in the six groups of control counters (group area 0.132 m^2 — see 3 in Fig. 1) located at the center of the central circle. Thus, in this investigation, we employed the simplest method of distinguishing showers according to the particle flux densities; this method introduces no discrimination due to variations in structure.

Over a period of approximately a month we recorded about 600 showers with cores traversing the area of the central circle. The hodoscopic system gave a clear picture of the distribution density of the particle flux in the vicinity of the core for each of the recorded showers.

The flux density ρ was determined directly from the data on the number of triggered (m) and not discharged (n - m) counters in each group by means of the equation $\rho = \frac{1}{\sigma} \log \frac{n}{n-m}$, where σ is the area of each counter. Inasmuch as this equation is predicated on a Poisson distribution of the shower particle paths, it can be used for determining the densities only for the indicators

which were removed from the axis core by a distance exceeding their linear dimensions. If for no other reason, therefore, the spatial distribution of the particle flux can be investigated by means of this type of installation only for distances from the shower core exceeding 1 meter.

The penetrating particle detectors did not, of course, give a picture of the density distribution of penetrating particles in each shower but only recorded whether or not such particles struck the detectors. However, by separating showers with an equal total number of particles, one can determine the flux density of the penetrating N-component particles by means of the equation

$$\rho = \frac{1}{S(1-e^{-\mu d})} \ln \frac{n_0}{n_0 - m_0},$$

where n_0 is the total number of showers, m_0 is the number of showers in which penetrating particles are recorded by the detector, S is the area occupied by the detector counters, d is the thickness of the absorbers and $1/\mu$ is the range for interaction of the N-component particles.

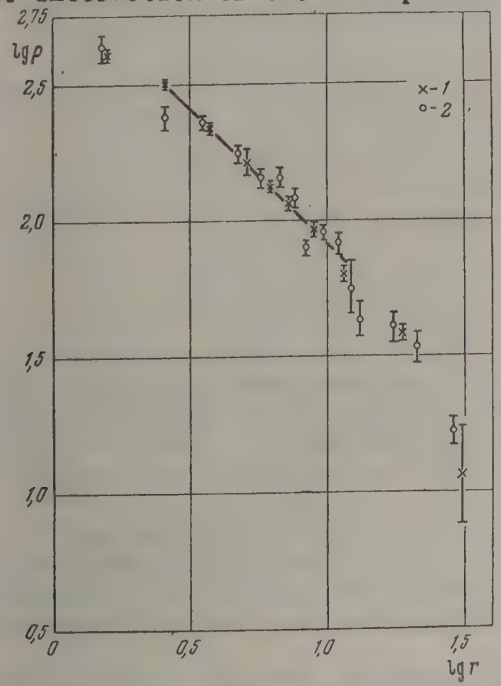

Fig. 2. Spatial distribution of the density of the electronic component in the central region of air showers. Experimental points: 1) for showers with $N = 4 \cdot 10^4$; 2) for showers with $N = 4 \cdot 10^5$. Solid curve - from Ref. 3.

The location of the shower core and the number of particles therein were found by direct comparison of the indications of the flux density indicators for the given shower. On the basis of data obtained we plotted the spatial distributions of the densities ρ of the electron and N-component particle fluxes in the radial range from 2 to 30 meters from the shower axis. The spatial distribution of electrons was obtained by averaging the distributions found for showers with approximately the same number of particles N. The averaging was carried out for two groups of showers with mean values of N differing by a factor of 10. The spatial distributions curves for the showers with $N = 4 \cdot 10^4$ and $N = 4 \cdot 10^5$ are shown in Fig. 2. The distribution for the first group in the $2 < r < 10$ meter radial interval is characterized by $1/r^n$ with $n = 1.00 \pm 0.05$; that for the second group by the same law, but with $n = 0.95 \pm 0.08$. The spatial distribution of the N-component can be characterized by the same $1/r^n$ law but with $n = 1.1 \pm 0.2$; this pertains to showers for which $N = 8 \cdot 10^4$. A like sharp increase in the N-component flux density was also observed for showers with $N \sim 10^4$. The proportion of N-component particles in relation to the electronic component in the 2-10 meter radial range interval is approximately 1%.

The data indicate, for one thing, that at sea level extensive air showers do have a definite, pronounced core. The existence of the core follows from the observed spatial distribution of both the electronic and the N-components. It is noteworthy that the existence of a core was observed even in a case of showers with a minimum number of particles $N \sim 10^4$.

Our data on the structure of extensive air showers at sea level are compared

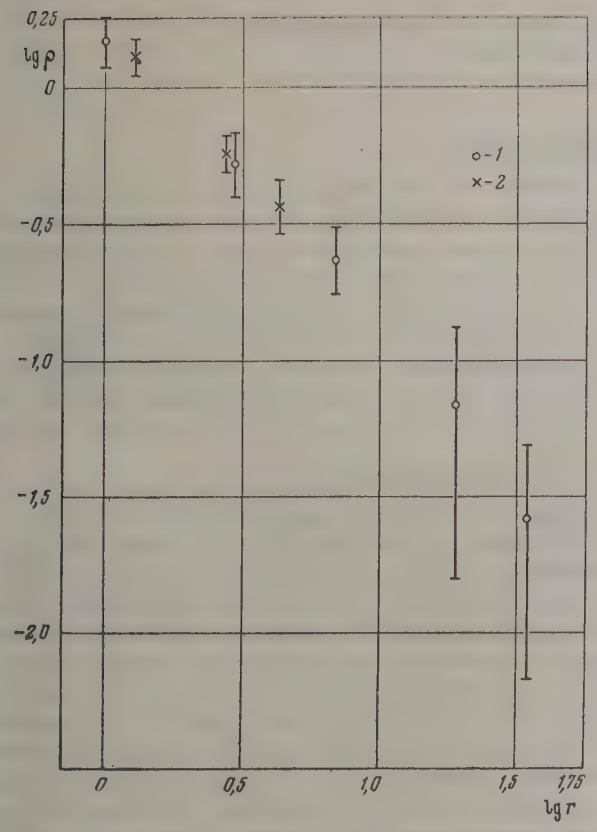

Fig. 3. Spatial distribution of the density of the N-component particles in the central region of showers. Experimental points: 1) present investigation and 2) Ref. 4.

with the corresponding data obtained at mountain altitudes by Vavilov et al[3,4] in Figs. 2 and 3, where the differences in air density have been allowed for.

The experimental data indicate that the structures of the central regions of extensive air showers are virtually identical at the two stages of their development. The ratios between the number of N particles and electrons are also almost equal.

From this it may be concluded that there is some process that leads to a continuous "renewal" or "regeneration" of the structure of the investigated shower regions. This "renewal" must occur at the expense of the high-energy N-component particles, moving in the core and transferring part of their energy to the electrons and N-particles of the neighboring, central shower region as a result of interactions with the nuclei of air atoms. (It has been shown in Ref. 1 that the electronic component in the central shower region is effectively regenerated by neutral pi mesons generated in nuclear collisions of N-component particles of 10^{11}–10^{12} ev energy.)

Apparently, there is established, in the lower layers of the atmosphere, an approximate equilibrium between the electronic-photonic and penetrating-particle components in the central region of a shower, on the one hand, and the N-component particles of the shower core, on the other hand.

"P.N.Lebedev" Physical Institute of the
Academy of Sciences of the USSR
and
"M.V.Lomonosov" Moscow State University

References

1. N.A.Dobrotin G.T.Zatsepin, S.I.Nikol'ski, L.I.Sarytseva & G.B.Khristiansen, Present issue of the Bulletin.
2. L.N.Korablev, Doklady AN SSSR, 62, 215 (1948).
3. Iu.N.Vavilov, S.I.Nikol'ski & E.I.Tukish, Doklady AN SSSR,63, 233 (1953).
4. Iu.N.Vavilov, S.I.Nikol'ski & V.P.Sarantsev, Zhur. eksp. i teor. fiz. 28, 505 (1955).

INVESTIGATION OF COSMIC RAYS UNDERGROUND

- E.L. Andronikashvili, M.F. Bibilashvili, I.V. Sakvarelidze and G.R. Khutsishvili

Introduction

Underground investigations of cosmic rays are of interest in that they help throw light on the properties of high-energy mu mesons. Underground investigations of the penetrating particles contained in extensive air showers are of particular interest for they permit drawing a number of deductions regarding elementary events occurring at energies of 10^4–10^5 Bev.

Before describing the experimental investigations of the penetrating component of extensive showers, performed by us during 1953-4 at the Physics Institute of the Academy of Sciences of the Georgian SSR, let us review briefly the results obtained by Cocconi and Greisen.[1]

1. The Cocconi-Greisen Experiments

The Cocconi-Greisen apparatus comprised four groups of counters, located 60 meters apart on the surface of the earth and serving as a shower-selection system, and one underground group, situated at a depth of about 1,600 meters water equivalent (m.w.e.). To permit determining the angles at which the penetrating particles struck the underground group, the latter was comprised of several layers of hodoscopic counters. Cocconi and Greisen determined the correlation of the mu mesons penetrating to this depth (the minimum energy corresponding to a depth of 1,600 m.w.e. is approximately 600 Bev) with extensive air showers. In addition, they used two underground counter groups to plot the variation of the number of coincidences between these two groups (number of penetrating particles) with the distance between them (the "separation curve"). Cocconi and Greisen found that $F(M)$ is proportional to $M^{-3.4}$, where $F(M)dM$ is the number of extensive air showers having a mu-meson multiplicity in the interval $(M, M + dM)$.

According to Cocconi and Greisen, the average number of mu mesons having an energy in excess of 600 Bev in a shower is proportional to $N^{0.6}$, where N is the number of electrons in the shower. In other words, the fraction of penetrating particles in showers varies approximately as $N^{0.4}$. They also found that the average number of mu mesons having energies over 600 Bev in the recorded showers is approximately proportional to $E_0^{3/4}$ (E_0 is the energy of the primary particle.).

If all the mu mesons were produced by the decay of pi or chi particles, formed in the first nuclear cascade event, the Fermi and Landau theories would call for the above exponent to be 1/4. The faster rise in the number of penetrating particles with energy is attributed by Cocconi and Greisen to the fact that the number of nuclear cascade events increases with the energy of the primary particle.

2. Distribution in Energy of Penetrating Particles in Extensive Showers

The apparatus used in our study to determine the energy spectrum of the penetrating component of extensive air showers consisted of three surface counter groups, each having an effective area of one square meter, located at the vertices of an isosceles right triangle, 30 meters on the side, and an underground group comprising two trays of counters, each tray extending over the full 1 m^2 area. An 8 cm thick layer of lead was placed between trays to prevent the underground group from being activated by the equilibrium soft component and other background radiation. The trays of the underground group were connected for coincidence, thereby virtually eliminating all chance coincidence background from the entire set-up.

The electronic circuits recorded separately triple coincidences among the surface groups and quadruple coincidences including the underground group. The resolving time of circuits was $2.5 \cdot 10^{-6}$ sec.

The underground group was located at different depths: 2.5, 5.6, 27.0, 65.5 and 148.0 m.w.e. The number of quadruple coincidences was determined as a function of the effective depth of the underground group.

Table 1

Number of triple and quadruple coincidences recorded with the underground group at different depths

Depth of underground counter group, m.w.e.	Duration of measurements, hours	No. of triple coincidences	No. of quadruple coincidences	No. of triple coincidences per hour	No. of quadruple coincidences per hour
2,5	97	1360	107	13,9±0,7	1,1 ±0,1
5,6	118	1615	108	13,5±0,6	0,85±0,07
27,0	416	5720	120	13,6±0,4	0,29±0,03
65,5	554	7625	105	13,7±0,3	0,19±0,02
148	852	11180	106	13,9±0,2	0,13±0,01

It was essential to record the triple coincidences in order to control the geometry of the three surface groups and monitor the operation of the counters as well as to determine the proportion of mu mesons in the showers.

The results of our measurements at the different depths are given in Table 1. The effect of the lead absorber inserted between the trays of the fourth counter group is taken into account in the data of the first two series of measurements.

Let us denote by $K_4(h)$ the number of quadruple coincidences obtained with the underground counter group at a depth h, and by $\alpha(h)$ the fraction of penetrating particles in the shower, having a range greater than h*. In general, α depends not only on h but also on the shower density.

Assuming the shower density to be virtually uniform over the lateral dimensions of the recording system, we obtain the following equation for $K_4(h)$:

$$K_4(h) = \int_0^\infty \frac{A}{\rho^{\varkappa+1}} d\rho \,(1 - e^{-\rho\sigma})^3 (1 - e^{-\alpha\rho\sigma}), \qquad (1)$$

where σ is the effective area of each row of counters and $\frac{A}{\sigma^{\varkappa+1}} d\rho$ is the number of showers having a density in the interval $(\rho, \rho + d\rho)$. Analogously for the number of triple coincidences we have

$$K_3 = \int_0^\infty \frac{A}{\rho^{\varkappa+1}} d\rho \,(1 - e^{-\rho\sigma})^3. \qquad (2)$$

Considering that our measurements show $K_3 = 13.7$ coincidences per hour and $\varkappa = 1.4$ (according to measurements made at sea level by many investigators), we obtain after simple mathematical manipulations:

$$K_4(\lambda) = 2{,}9 A \sigma^{1,4} \alpha\,[1 - 0{,}62\,\alpha^{0,4}] \qquad (3)$$

We note that in the integration we assumed α to be independent of ρ; more accurately speaking, we chose values of α corresponding to the value of ρ

*The quantity h represents the thickness of dense absorber above the underground group. Including the atmosphere, i.e., measuring h from the top of the atmosphere, would have the effect of raising the initial section of the energy spectrum given below.

predominant in integral (1).

Using equation (3) and our experimental data, we determined the fraction of penetrating particles with a range greater than h contained in extensive showers. Proceeding in this manner we evaluated the function $\alpha(h)$* in extensive showers.

The values of α determined on the basis of equation (3) and the data in Table 1 are listed in Table 2.

Table 2

Fraction of penetrating particles with ranges greater than h as determined at different depths

Absorber thickness, m.w.e.	2,5	5,6	27,0	65,5	148
$\alpha(h)$, %	4,5	3,4	1,1	0,7	0,47

The quantity $\alpha(h)$ gives the fraction of penetrating particles with ranges greater than h contained in extensive showers. On the other hand, the range h is related to the minimum energy,** E = 0.2 h Bev, which gives us the dependence of α on E. In other words $\alpha(E)$ represents a quantity $M(>E)/N$ averaged over all showers (N is the number of electrons in a given shower and $M(>E)$ is the number of mu mesons having an energy greater than E in the same shower). The variation of α with E is given in the accompanying figure.

In the 0.5--30 Bev energy interval the dependence of α on E is given by

$$\alpha(E) = \text{const} \cdot E^{-(0,58 \pm 0,05)}. \qquad (4)$$

The deductions above are approximately arrived at in view of the following:

1. We did not take into account the variation in shower density over distances commensurate with the lateral dimensions of our recording system. Since these dimensions are on the order of 30 meters, the actual variation in ρ may be considerable. Analysis of the ratio K_4/K_3 shows that if the variation in density is not allowed for, the deviation from proportionality between K_4 and α is small. It may be assumed that this deviation from proportionality will also be small under the conditions of our experiments.

2. We calculated K_3 and K_4 by subdividing the integration region into two or three intervals and substituting an approximate (constant) value for the expression under the integral for each interval. The resultant errors, however, are small.

3. We did not take into consideration the fact that the effective solid angle subtended by the underground group diminishes with increasing depth. However, even at the greatest depth (55 meters underground) the solid angle is so large, that practically all the mu mesons remain within it. Hence allowing for the angular effect would reduce the exponent in equation (4) by an insignificant amount.

*The correction term $0.6\ \alpha^{0.4}$ in equation (3) is considerably smaller than unity, nevertheless it was taken into account in determining α.

**The relationship between the energy and the range in lead differs from that given above because in lead the losses per 1 m.w.e. are 0.13 Bev rather than 0.2 Bev as in soil.

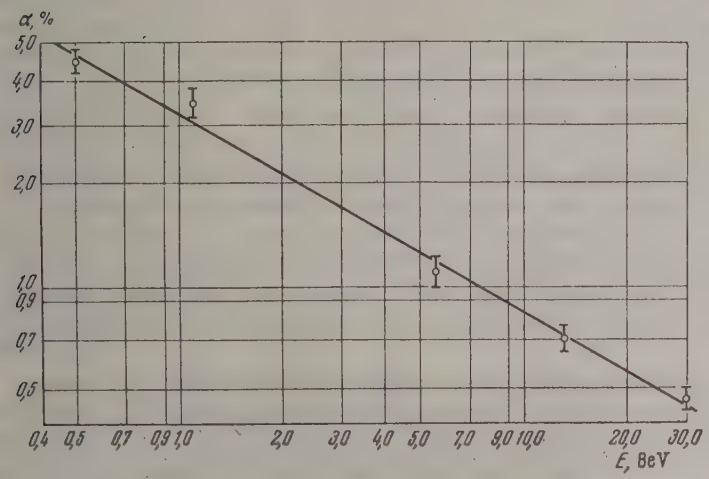

Distribution in energy of the penetrating component of extensive air showers: $\alpha(E) = \text{const} \cdot E^{-(0.58 \pm 0.05)}$. Horizontal scale: energy determined on the basis of the range measured from the surface of the ground.

4. We assumed that α depends only on h. Actually α is also a function of ρ. In computing K_4 at any given depth it is essential to use a value of ρ close to a certain optimum value $\bar{\rho}$. Hence in the case of great depths we obtain from our experimental data values of α for showers of greater density. In other words, as the depth is increased the factor $1 - e^{\alpha \rho \sigma}$ decreases due to the reduction in α (for the same value of ρ) and hence the system becomes more sensitive to denser showers.

Little is known at present regarding the dependence of α on ρ (for mu mesons of higher energies). We only know that α decreases with increasing shower density. Hence actually α will fall off more slowly with increasing energy E for showers with a given ρ than is indicated by the data of Table 2. However, a detailed study shows that the effect is small in our experiments.

It follows from our experimental data that the integral spectrum of mu mesons in showers having densities in the interval from 2 to 5 particles per m^2 is reasonably closely approximated by the curve in the accompanying figure. (Calculations showed that our apparatus recorded primarily showers characterized by a mean density in this interval.)

We thus have for mu mesons in the 0.5–30 Bev energy interval:

$$M(>E) = \text{const} \cdot E^{-\gamma} \qquad (5)$$

where $\gamma = 0.58 \pm 0.05$. Naturally, for very large values of E the spectrum should be steeper (fall off faster than 1/E; otherwise the energy of the mu meson component would diverge). Let us note that approximately the same value for γ was obtained by George, who matched his data to those of Greisen and McMaster. However, in view of the substantial difference in the measurement procedures employed in these three experiments, such matching can only be regarded as a doubtful procedure.

Finally we must emphasize that the spectrum of shower mu mesons falls off with the energy at a considerably slower rate than the spectrum of single mu mesons. This suggests that the energy of the mu-meson component constitutes a considerable portion of the total energy of showers.

3. Spatial Distribution of Penetrating Particles of Extensive Showers

This investigation covered the distribution of penetrating particles having energies in excess of 13 Bev.

We employed the core selector method[3] for determining the location of the shower axes. The principle of operation of the selector is based on separating

the shower region containing high-energy electrons (1-6 Bev). Inasmuch as the distance of these electrons from the core, according to cascade theory, is about 2-3 meters at sea level, locating the high-energy electron region automatically determines the position of the shower core. However, in view of the fact that in reality fluctuations in the distance may considerably exceed the theoretical value, there may be a sizeable error in determining the location of the core. The accuracy in determining the core positions may be evaluated by plotting a "separation curve" for two similar set-ups.

We determined experimentally that our selectors separated a central region some 15 meters in diameter with an accuracy to within 10%. In order to increase the number of showers recorded we employed three core selectors. The electronic equipment recorded separately the coincidences between each of these selectors and the underground group. The resolving time of the electronic circuit was $5 \cdot 10^{-6}$ sec.

As in the distribution-in-energy experiments, the underground counter group consisted of two counter trays, each 1 m^2 in area. The trays were located one above the other with an 8 cm thick layer of lead between them. The resolving time of the circuit recording double coincidences in the underground group was also $5 \cdot 10^{-6}$ sec.

We made three series of experiments. In the first the core selectors were located immediately over the underground group. We shall arbitrarily call this the 0 m distance from the core. The arbitrariness is due, on the one hand, to the uncertainty in determining the position of the core by the selectors themselves and, on the other, to the fact that shower axes may form an appreciable angle with the vertical. In the second and third series of measurements the core selectors were set up at 20 and 30 meters, respectively, from the underground group.

The measurements showed that the number of penetrating particles diminishes rather slowly with the distance from the core, i.e., that there is a "plateau". The number of coincidences between the core selector and underground group with the selector in the 0 m and 30 m positions differs by only 30%. The number of coincidences drops off sharply at 60 meters.

Cocconi et al[3] carried out analogous investigations on penetrating particles having energies of 0.3-0.8 Bev. The density "plateau" for particles of such energies attained 90 m. The fact that the number of penetrating particles in extensive air showers hardly diminishes to a distance on the order of 30 m from the core indicates that the mean energy of the penetrating particles exceeds 10 Bev not only in the core portion, but also at a considerable distance from it. This again is proof of the substantial contribution made by such particles to the total shower energy.

It must be noted, however, that the results of our experiments on the spatial distributions are still tentative.

Conclusions

Underground investigations of the penetrating component of extensive air showers are important if only because they make it possible to determine the fraction of mu mesons formed by the decay of pi and chi mesons, generated in primary events at ultra-high energies. As was shown in 1954 by Greisen, the problem can be solved through systematic observation of the temperature dependence of the intensity of the hard component at great depths. This results from the fact that as the temperature rises the atmosphere expands and the importance of the decay effect increases accordingly. At mu-meson energies above 10 Bev the predominant role is played not by the decay of mu mesons as such but the

decay of heavier mesons resulting in the creation of mu mesons. Greisen showed that there should, consequently, be observed a positive correlation between the density of the atmosphere and the number of coincidences at great depths underground. Unfortunately, attempts to effect the appropriate measurements, undertaken by Coccini and others, have so far been unsuccessful owing to large experimental errors.

Nor can the question of the distribution in mass of the penetrating particles be regarded as definitely clarified, particularly at great depths, where the contribution of single mu mesons of the vertical component no longer predominates over the contribution made by the penetrating particles of extensive air showers.

The solution of these very important problems is related to further investigation of the energy spectrum of penetrating shower particles at the usual depths of from 20 to 150 m.w.e., as well as new studies at great depths of the energy spectrum up to 500-1000 Bev.

Of no less interest would be experiments aimed at determining the detailed spatial distribution at various depths and the angular distribution of the penetrating particles and cores of extensive air showers.

Investigations which should contribute to the solution of the outlined problems are now being undertaken at the Physics Institute of the Academy of Sciences of the Georgian SSR.

In conclusion the authors desire to thank S.N.Vernov for valuable discussions.

Physics Institute of the
Academy of Sciences of the Georgian SSR

References

1. P.H.Barrett, L.M.Bollinger, G.Cocconi et al, Rev.Mod.Phys., 24,133 (1952).
2. E.P.Georgec, J.W.MacAnuff & J.W.Sturgess, Proc.Phys.Soc.,A66,346 (1953).
3. G.Cocconi, V.Cocconi-Tongiorgi & K.Greisen, Phys.Rev., 76,1020 (1949).

* * * * * * *

USE OF THE RESIDUAL RANGE-SCATTERING METHOD FOR THE DETERMINATION OF THE MASS OF PARTICLES IN A CLOUD CHAMBER WITH ABSORBER PLATES

- M.I.Daion

Cloud chambers containing a large number of metal plates are widely used at present for cosmic-ray research. The determination of the mass of charged particles in such chambers is a rather complicated task. In some cases a rough estimate of the mass can be made, for example, from the residual range and the ionization.

In 1953 Annis, Bridge and Olbert[1] derived equations by means of which the masses of particles coming to rest in the chamber can be computed statistically from the scattering angles and the corresponding residual ranges. In their calculations they introduced a quantity $\eta_i = \varphi_i R_i^{\alpha}$ (where φ_i is the projection of the scattering angle of the particle, R_i is the corresponding residual range and $\alpha = 0.55$) and obtained, in the so-called "normal" approximation (see Ref. 1),

the following expression for the mean square value of η_i:

$$\rho = \left(\frac{1}{n}\sum_1^n \eta_i^2\right)^2 = A\left(\frac{m_e}{m}\right)^{-\alpha}, \qquad (1)$$

where m is the mass of the scattered particle, m_e is the electron mass, n the number of observed scattering angles of the particle in the chamber plates, and A a constant, dependent virtually only on the properties of the scattering matter.

We note that usually the number of plates in a cloud chamber and, consequently, the number of observed scattering angles per particle does not exceed 10-15. Hence owing to the fluctuations in φ_i the accuracy with which the mean value of the mass of a single particle is determined is quite low. However, it is sometimes possible to group particles of the same kind (mass) by certain features (for example, by type of decay) and thus increase considerably the statistical accuracy with which the mean value of the mass is determined. This method was used by Rossi et al[2] in 1953 to determine the mass of S-particles. It is of interest to check expression (1) against particles whose mass is accurately known, for example, protons or mesons. We made such a check in the investigation of Ref. 3, carried out using an Alikhanian-Alikhanov magnetic mass spectrometer in conjunction with a large Wilson cloud chamber*: the mass of mesons and protons, identified by their momentum and range, was determined independently from their scattering and residual range in the cloud chamber.

We wish to call attention here to the fact that in using equation (1) two factors must be taken into account.

1. The projection of the scattering angle φ_i' usually observed on the photographs, differs from the angle φ_i used in equation (1) and equal to the projection of the scattering angle on a plane passing through the initial trajectory (prior to scattering in the given brass plate). Only under certain experimental conditions (for example, when the photographic camera is sufficiently remote from the chamber and the trajectories of the particles form not too large an angle with the plane parallel to the plane of the front window of the chamber, through which the photographs are taken) is it possible to use φ_i', in computing the mass according to (1), since $\Sigma\varphi_i'^2$ exceeds $\Sigma\varphi_i^2$ by only a few percent.

2. Equation (1) takes only coulombic scattering of the particles into account. It can be seen that this equation is highly sensitive to large scattering angles, yet there is a high probability of scattering to large angles due to nuclear scattering and sometimes a large scattering angle may be simulated by experimental errors. Even such rare cases of anomalously large angles greatly reduce the mass value computed according to equation (1).

Under our experimental conditions the "geometry" for the proton trajectories was such that the error in determining the mass introduced by the use of φ_i' instead of φ_i should not amount to over a few percent. However, the proton mass as computed by means of equation (1) turned out to be 1,000 ± 1.50 m_e (on the basis of measurements of 100 angles of scattering in the 0.5 cm thick brass plates) and 1,300 ± 170 m_e (on the basis of measurements of 138 angles of scattering in the 0.2 cm brass plates).** So great an underestimate of the mass is apparently due to anomalously large scattering angles associated with nuclear interaction. According to calculations the maximum number of anomalous angles, corresponding to the geometric cross section for the interaction of the protons with copper nuclei should be approximately 4 (in the 0.5 cm plates) and about 2.5 (in the 0.2 cm plates).

*The chamber contained seven brass plates, two 0.5 cm thick and five 0.2 cm thick.

**The statistical uncertainties in the determined values of the mass here and below are calculated using the following equation: $\Delta m/m = 2.22\,\Delta\Pi/\Pi$ where $\Delta\Pi/\Pi$ is given by equation (30) of Ref. 1.

To eliminate the influence of large scattering angles it is possible to modify equation (1), namely, to calculate the theoretical mean square value of η (left side of expression (1) by means of a distribution function for η_i cut off at a certain value $\eta = \eta_0$ and, accordingly, to eliminate from consideration all experimental values $\eta_i > \eta_0$ from the calculation of the experimental value of $\left(\frac{1}{n}\Sigma\eta_i^2\right)^{\frac{1}{2}}$

We note that the coefficient A in equation (1) changes little if the distribution function is cut off at different points wherever $\eta > 3\rho_T$, where ρ_T is the root mean square value of η calculated for protons according to equation (1). The term with which the distribution function is terminated is arbitrary and only comparison with experiment can indicate the most advantageous cut-off point.

It turned out that cutting off the distribution function at $\eta = 3\rho_T$ results in the following values for the proton mass: 1,600 ± 240 m_e from the scattering in the 0.5 cm plates and 1800 ± 235 m_e from the scattering in the 0.2 cm plates. In both cases we discarded four experimental values of η_i, this being approximately the expected maximum number of cases of anomalous nuclear scattering.

The author wishes to thank A.I.Alikhanian for his interest in the work, and also A.A.Ter-Saakov, F.R.Arutiunian and M.L.Ter-Mikaelian for aid in processing the data.

References

1. M.Annis, H.S.Bridge & S.Olbert, Phys. Rev., 89, 1216 (1953).
2. H.S.Bridge, C.Peyron, B.Rossi & R.Safford, Phys. Rev. 90, 921 (1953).
3. M.I.Daion, Doklady AN SSSR, 100, 453 (1955).

* * * * * * *

DISTRIBUTION IN MOMENTUM OF PI MESONS AT 3200 METERS ABOVE SEA LEVEL

-A.I.Alikhanian & V.Sh.Kamalian

The investigation discussed herein was carried out in 1953-4 for the purpose of measuring the distribution in momentum of pi mesons produced in collisions of cosmic ray neutrons with lead nuclei. It is known that in encounters of nucleons of moderate energies with nuclei pi mesons are produced much more frequently than heavy mesons; hence in the first approximation the distribution of mesons generated in such encounters is represented by the pi-meson distribution.

Until recently the available information on the pi-meson spectrum in cosmic radiation was limited to the data obtained by Camerini at stratospheric altitudes by the method of nuclear plates. Yet for the solution of a number of problems it is essential to know the pi-meson distribution at sea level and mountain altitudes. It is particularly important to know the pi-meson spectrum in determining the distribution in mass of cosmic ray particles inasmuch as in many cases the stopping of pi mesons as a result of nuclear collisions may simulate heavy mesons.

Our determinations of the momentum distribution of pi mesons were made at 3200 meters above sea level (Mt. Aragats) by means of a magnetic mass spectrometer (field intensity 6850 oersted). The mass spectrometer was equipped with a hodoscopic counter array, comprising six bays, housing lead plates 3-8 cm thick, completely surrounded by counters. The measurements were made with total lead

thicknesses of 10, 13, 15 and 18 cm. The hodoscopic array was located immediately above the spectrometer; it served to detect cases of the generation of charged particles by the neutral component of cosmic radiation.

The charged particles produced in any one of the lead plates were further investigated in the magnetic spectrometer in the usual manner: the momentum and polarity of the particles were determined and, in the case of particles stopped in the absorbing filters, the mass was evaluated. The root mean square error in determining the momentum did not exceed 3% for momenta of $2 \cdot 10^8$ ev/c and 10% for 10^9 ev/c. The recording system was activated regardless of whether the generated particle was stopped in one of the absorbers or traversed all of them.

Selection of trajectories

We selected for analysis only those particles whose trajectories in the plane of magnetic deflection comprised not less than four points closely fitting a circular arc and were represented by a straight line, clearing the pole pieces of the magnet, in the plane perpendicular to the deflection plane.

Further, in plotting the spectrum we used only the four-point arc trajectories of particles which did not trigger counters at least in the row decking the lead plates and two rows of the hodoscopic counter array. Particles with such trajectories were assumed to have been generated in the lead by the neutral component. In such cases there were sometimes observed brief flashes in some rows of the hodoscopic array, due to multiple-prong stars generated by high energy neutrons.

For the most part single particles were recorded in the magnetic spectrometer, although in some cases the components of stars extended to the first row of the mass spectrometer counters and produced additional flashes.

In plotting the distribution in momentum we utilized both the trajectories of single particles and the trajectories of particles producing the "additional flashes" in the tubes connected with the counters in the first row. The absorbing filters were comprised of graphite plates having a total thickness of 32 g/cm^2 and copper plates having a thickness of about 130 g/cm^2.

Results

It is known that a larger fraction of charged particles generated in lead by cosmic ray neutrons is comprised of protons; the smaller fraction, of mesons. At high energies identification of the particle is fraught with difficulties which in the case of the nuclear emulsion method make it altogether impossible to separate protons from mesons. The magnetic spectrometer, on the other hand, permits distinguishing mesons from protons by the polarity of the charge even at very high energies. In the present investigation, in order to exclude protons fully we utilized generated negative particles. In the $(2\text{-}17) \cdot 10^8$ ev/c momentum interval we recorded a total of 793 negative particles satisfying the indicated selection rules.

The differential momentum distribution of these particles (both those stopped in the absorber assembly and those traversing it) is shown in the accompanying figure. It will be seen that the number of particles falls off rapidly with increasing momentum. Of the 798 particles, 85 had momenta in the 1-1.7 Bev/c interval, while the number of particles with a momentum above 1.7 Bev/c equalled only 34. Thus particles with a momentum in excess of 1 Bev/c comprise only 14% of the generated negative particles.

The pi-meson distribution is satisfactorily described by a power function of the form

$$N(p)dp = N_0 p^{-\gamma} dp$$

where p is the momentum and $\gamma = 2.8 \pm 0.2$.

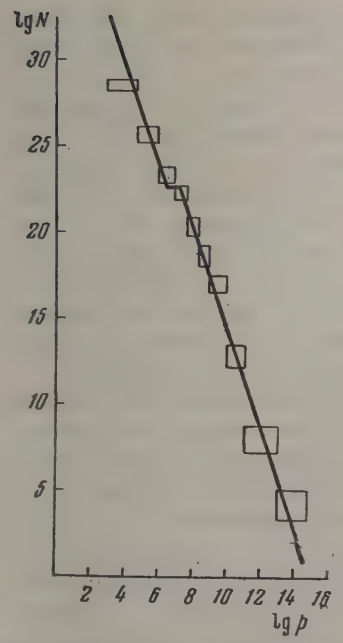

Distribution in momentum of pi mesons generated in lead by the neutral component of cosmic radiation.

A salient feature of the distribution curve is the "irregularity" at $4\text{-}5\cdot10^8$ ev/c; below this point the curve has approximately the same slope as above it (i.e., in the region of small momenta). A similar irregularity is apparent at 500–700 Mev in the energy spectrum given by Camerini. The irregularity may be due to the fact that in addition to π mesons the particles generated in the lead include a certain proportion of heavier mesons. Further investigations by means of an ionization chamber are needed to clarify the anomalous shape of the distribution curve; appropriate investigations are planned for the near future.

Comparing our distribution curve with the spectrum given by Camerini, we note a marked difference in the slope of the curves: Camerini's spectrum for π mesons produced in stars, recorded in nuclear emulsions in the stratosphere, is also described by a power function but with an exponent of only 1.5. Our value of the exponent γ equal 2.8 ± 0.2 is minimal since it pertains to the spectrum of mesons emerging from a thick block of lead. The true spectrum can be deduced from our experimental one by introducing the appropriate corrections associated with the ionization losses of the mesons in the lead plates. Thus making ionization loss corrections on the assumption that nuclear absorption of π mesons in lead is virtually independent of the energy, we obtain a corrected spectrum described by a power function with $\gamma = 3 \pm 0.2$. It may be noted that the distribution of protons generated by neutrons in lead at the same altitudes, according to the measurements of Dadaian and Merzon[1], is also described by a power function with the same exponent.

Our data permit of drawing certain deductions regarding nuclear interactions of π mesons in the stopping absorbers used in our experiments. In particular they permit of establishing the number of cases of stopping of the π mesons in the absorbers due to nuclear collisions. It is important to know the number of such cases of "non-ionization" stopping in determining the distribution in mass of cosmic ray particles by the range-momentum method. Let us review the data on all the particles which came to rest or underwent interaction (star formation and scattering) in the absorbers having a total thickness of 6 cm graphite as well as on the particles which traversed the graphite absorbers without experiencing interaction.

Data on the interaction of pi mesons in 6 cm thickness of graphite absorbers for different momentum intervals.

p, 10^9 eV/c	Number of particles traversing apparatus	Number of cases of interaction: Expected (geom. sect.)	Observed	Expected for $\sigma = 0.76\sigma_{geom.}$
2,35 ÷ 4,7	108	19	35	
4,7 ÷ 8,0	129	25	16	16
4,7 ÷ 17,0	214	38	21	26

The data for different momentum intervals are listed in the accompanying table. The first interval (235–470 Mev/c) corresponds to particles of 500–1200 m_e, coming to rest in the 6 cm graphite absorber due to ionization losses. In this interval the number of particles traversing the apparatus without detectable interaction equalled 108. Assuming

that the cross section for the interaction of π mesons with carbon nuclei is equal to the geometric cross section we find that with this graphite thickness (6 cm) 19 of the total number of 143 particles should undergo nuclear encounters. Actually the number observed was 35, i.e., approximately twice the expected number. In the second momentum interval (470–800 Mev/c) 129 particles traversed the graphite plate without interaction; on the basis of the above assumption 25 cases of interaction should have been expected, but only 16 were observed.

It is known from experiments with accelerators that the cross section for the interaction of π mesons having a momentum of 550 Mev/c with graphite nuclei equals about 0.7 the geometric cross section. Assuming this value of a cross section to be valid in the 470–800 Mev/c interval the number of expected interactions comes out to be 16, which is in agreement with the experimental data.

It follows from the above that in the 235–470 Mev/c interval at least half the particles cannot be due to the encounters of the π mesons with nuclei. Hence it may be assumed that the "excess" cases of stopping are associated with heavy mesons having masses of 500–1200 m_e.

Analogous conclusions were reached earlier in investigations carried out by means of a magnetic spectrometer with a proportional counter. According to the data of Kharitonov,[2] not more than 35% of the cases of generation of particles with a mass of about 1000 m_e can be ascribed to collisions of pi mesons with nuclei. A similar result was obtained in experiments made with a magnetic spectrometer operated in conjunction with a cloud chamber by Alikhanian, Shostakovich, Fedorov and Merzon.

Conclusions

1. In the present investigation we determined the distribution in momentum of π mesons generated by cosmic radiation in lead. This distribution is described by a power function with an exponent $\gamma = 3 \pm 0.2$.

2. In the 235–470 Mev/c interval at least half the cases of stopping of π mesons are not due to nuclear interactions.

Physical Institute of the
Academy of Sciences
of the Armenian SSR

References

1. A.T.Dadaian & G.I.Merzon, Izv. AN SSSR, Ser. fiz., 17, 72 (1953).
2. V.M.Kharitonov, Thesis, Physical Institute of the Academy of Sciences of the Armenian SSR, Erevan, 1955.

THE TRANSITION EFFECT FOR STARS AND ITS CONNECTION WITH CASCADE MULTIPLICATION OF PARTICLES OF THE NUCLEONIC COMPONENT

-Zh.S.Takibaev

In general, it is rather difficult to determine the location of the maximum of the transition curve for stars and find the dependence of this maximum on the atomic number of the absorber material and on the altitude of the experiment. The difficulties are due, first, to the ambiguity of the expression for the interaction cross section and second to the impossibility of taking into account the entire diversity of secondary star-initiating particles (both charged and neutral) in view of the fact that some of these have as yet been little studied (hyperons, K, τ and other particles), to say nothing of the fact some may still be unknown. In addition, there are purely mathematical difficulties, which can always be overcome and which, therefore, are not fundamental in nature, although they are very serious in the energy range from one hundred to several thousands Mev. In fact, as is well known, if the star-initiating particles have very high energies ($E > 3$Bev) it is possible to neglect their ionization losses, their spatial distribution (using the linear case for the first approximation) and the variation of their nuclear cross-section with energy (i.e. to assume this cross section to be equal to the geometrical cross section.

At low energies ($1 \cdot 10^2$–$3 \cdot 10^3$ Mev) one cannot neglect these factors in a rigorous calculation of the intensity of all particles (protons, neutrons and pi mesons) although in some cases (for example in the case of interest to us here), some of them can legitimately be disregarded.

Even though, in view of the difficulties indicated above, a general analysis may seem premature, we shall attempt below to present a scheme for solving the problem, based on the concept of cascade multiplication of star-producing particles. It must be noted that the concept advanced by Messel: of the successive interaction of an incident nucleon with the individual nucleons of a nucleus is not applicable at very high energies, where it is apparently impossible[2] to consider the individual interactions as wholly independent. Nevertheless, the model of successive interactions can reasonably be employed in the analysis of transition curves since in this case we deal primarily with processes occurring in the region of medium energies. The analysis of the problem presented in this article is general in character and is not predicated on any specific cross-section function, although in the numerical calculations we use the form of the cross section employed by Heitler, Janossy, and Messel.[1] Before proceeding to a theoretical interpretation of the experimental facts, some of which have already been published,[3] we shall describe briefly the experiments performed and the results obtained. This sequence will facilitate the discussion and, in addition, will be of help in comparing the experimental results with the deductions from theory.

The results presented below are based on data obtained in approximately 30 pilot balloon ascents into the stratosphere, made in 1951–4. It must be noted that during the first years we employed low-sensitivity (slow) emulsions; this is one of the major shortcomings of this phase of the work. In later flights we tried to supplement the early results with new data obtained with fast, sensitive emulsions. However, inasmuch as the transition effects for stars and slow pi mesons are studied principally by comparing the total numbers of stars and pi mesons, the use of fast emulsions does not introduce any qualitative corrections to the previous results.

1. To determine whether a transition effect is present in absorbers having a considerably lower atomic number than lead,[3] we employed an absorber assembled of paraffin and graphite plates. The principal purpose of the experiment was to determine the change in the intensity of the flux of star-initiating particles

in the stratosphere incident to the transition from air to a paraffin or graphite absorber. For comparison lead absorbers were also used in the experiments simultaneously with the paraffin and graphite ones. The arrangement of the photographic plates and absorbers is shown in Fig. 1. The lead absorbers consisted of small plates measuring 3 x 4.5 x 0.4 cm. All the photographic plates, identified in the figure by Roman numerals, were mounted horizontally. During the flight a graphite absorber was located 6 meters above the framework, holding the other absorbers. One stack of photographic plates was exposed separately approximately 3 meters above the apparatus (under the parachute); the data obtained with these plates are marked "Air" in Table 1. Curve 1 of Fig. 2 shows the variation with time of the altitude of the plate and absorber assembly pictured in Fig. 1.

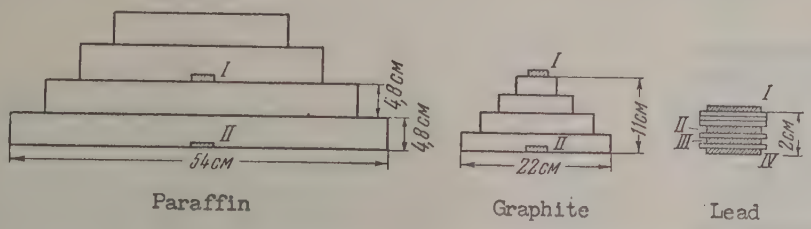

Fig. 1. Arrangement of photographic plates and absorbers (paraffin, graphite and lead). Photographic plates mounted horizontally under absorbers of different thickness are identified by Roman numerals.

Table 1

Results of the investigation of the variation of star-production in emulsions with the material and thickness of the absorber according to measurements at 17–21 km.

Absorber & plate number*	Number of events per 1 cm^2		
	$N \geqslant 3$	N_p	$(N \geqslant 3) + N_p$
"Air"	8	10,4	18,4
Lead			
I	8,2	10,6	18,8
II	8,1	10,6	18,7
III	8	11,4	19,4
IV	9	11,6	20,6
Paraffin			
I	6,2	13,4	19,6
II	8	12,1	20,1
Graphite			
I	7,8	11,5	19,3
II	7,9	10,5	18,4

*See Fig. 2 and text for relative location of plates and absorbers. N_p = N radioactivity

Table 1 gives the results of a thorough examination of the photographic plates, exposed at 17–21 km under absorbers of different thicknesses: The $N \geqslant 3$ column shows the number of stars, having three or more prongs, produced by cosmic ray particles per cm^2 of emulsion; under N_p is the corresponding number of small stars, attributed to radio-active contamination of the emulsion. Since the photographic emulsions employed in the experiment were far from fresh, the number of radioactivity stars was considerable.

It follows from the data of Table 1 that the intensity of the flux of star-producing particles hardly changes incident to the transition from air to paraffin, graphite and lead. Comparison of these data with the results of Ref. 3 leads to the conclusion that the considerable transition effect we observed in that investigation was due to the fact that the altitude of the apparatus and the effective thickness of the absorber were considerably greater than in the present experiments (the absorber thickness was over 2 cm greater). We conclude, therefore, that the transition effect for stars is observed in the case of lead absorbers only at altitudes exceeding 20 km. Nor was any transition effect observed in the present experiment for paraffin and graphite absorbers, 25 and 11 cm

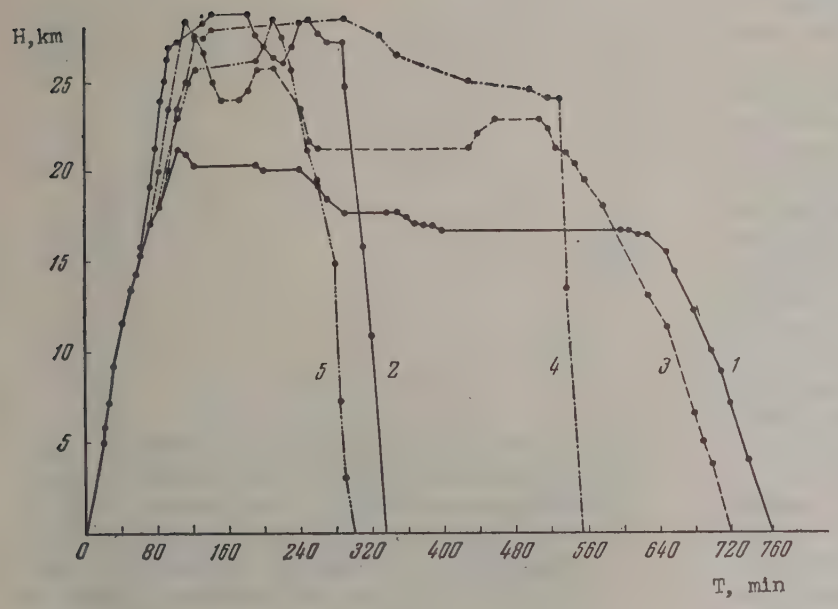

Fig. 2. Variation of altitude with time for some of the ascents with photographic plates. 1 & 2 - records of ascents with arrangements of plates and rectangular absorbers pictured in Fig. 1; 3 - record of ascent with arrangement of plates & rectangular absorbers shown in Fig. 3, a; 4 - record for arrangement of plates & hemispherical absorbers in Fig. 3 b.

thick, respectively. On the other hand, at an altitude of about 27 km (the record for this flight is given by Curve 2 of Fig. 2) the number of stars under 11 cm graphite increased by only 10-15%. It follows that the role of unstable particles was insignificant in the transition effect.

2. In the further experiments we employed photographic plates sensitive to relativistic charged particles. In addition, we made a number of changes in the arrangement of the photographic plates and absorbers and developed a ballast device which helped the apparatus attain high altitudes and insured flights of much longer duration than in the preceding experiments.

Below we summarize some of our experimental results. The arrangement of photographic plates and absorbers used is shown in Fig. 3, a. Plate stacks I and II were exposed at 5 and 2.5 m above the apparatus, while the remaining stacks were placed inside the set-up, surrounded by lead blocks of different thicknesses. Only the parachute and the envelopes of the pilot balloons were above stacks I and II. All other accessories of the apparatus were located below the absorbers. Photographic plates IV and V were placed between lead absorbers in the form of rectangular plates.

A specially designed ballast releasing device was used to maintain

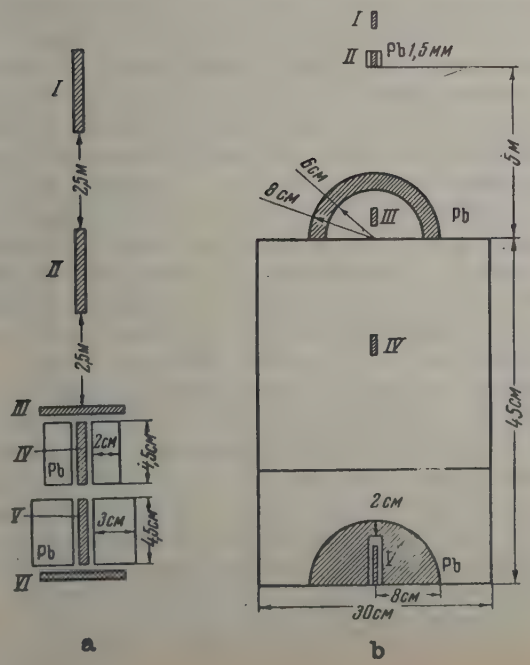

Fig. 3. Arrangement of photographic plates under lead absorbers of different thickness. Photographic plates designated by Roman numerals. Rectangular covering plates were used in arrangement a; hemispherical lead covers in arrangement b.

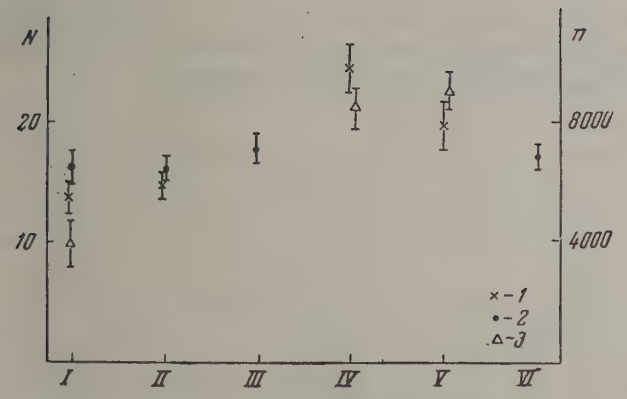

Fig. 4. Transition effect for stars and single tracks of strongly ionizing particles. Abscissae - photographic plate numbers as per Fig. 3, a; ordinates - number of stars (at left) and number of single tracks (at right). 1) & 2) stars in the two different types of emulsions, 3) single tracks. The flight record is shown by curve 3 in Fig. 2.

the apparatus at the desired high altitude for a prolonged period: upon reaching a certain altitude one of the ballast weights was released automatically; then the remaining weights were released at preset time intervals. Thus the total weight of the load was reduced as the lifting power of the pilot balloons diminished, thereby keeping the apparatus at high altitude for a long time. It can be seen from the record shown in Fig. 2 (curve 3) that the apparatus remained aloft at 20 to 25 km for approximately 7 hours (average altitude 24 km).

Two types of photographic plates were used in these experiments. Stacks I and II included one plate of each type; stacks IV and V consisted of plates of only one type; stacks III and VI were wholly of the other type. The emulsion in stacks III and VI proved to be more sensitive than that in IV and V. The experimental results are plotted in Fig. 4, where the plate stack numbers (as per Fig. 3, a) are laid off on the horizontal scale and the ordinates represent the number of stars (left) and the number of individual tracks (right). It can be seen that at the measurement altitude (approximately 24 km average) the transition effect for stars amounted to 1.64 ± 0.30, i.e., approximately 60%, while the generation effect, i.e., the ratio of the actually observed value of the flux to the value of the flux without taking generation into account, amounted in this case to approximately 70% for a thickness on the order of 3 cm (the indicated uncertainty was computed in differential form; the root mean square error is considerably smaller). The number of stars with more than 6 prongs hardly varies with the thickness of the absorber, indicating that the star-initiating particles generated in the absorber are primarily particles of low energy. It would appear from the graph that the maximum number of stars corresponds to an effective absorber thickness of about 3 cm; it must be noted, however, that the number of stars under 3 cm absorber does not greatly exceed the number under a thickness of 4 cm. Actually, in this case the transition effect amounts to only 1.34 ± 0.27, so that it is almost impossible to determine the true position of the maximum from these data.

3. As noted above, the lead absorbers used in the earlier flights were in the form of rectangular plates. Hence we had to speak in terms of the thickness of the plate or of the effective thickness of the absorber relative to the star-initiating component assumed to have an isotropic angular distribution in the atmosphere. In view of this ambiguity, in a later experiment we employed lead absorbers in the shape of hemispheres. The form and arrangement of absorbers in this variant is pictured in Fig. 3, b. With such hemispherical absorbers N-component particles, arriving from any direction above the horizontal, traverse an equal absorber thickness prior to reaching the emulsions of stack III. Consequently in this case we can speak of a specific absorber thickness and attempt to determine the position of the transition curve maximum in a more accurate manner.

Table 2

Results of the investigation of the variation of star-production in emulsions with the location of the photographic plates relative to the hemispherical absorbers, according to measurements at 25-28 km altitude

Type of event *	Number of plate stack					Control plate data
	I	II	III	IV	V**	
$N \geq 2$	48,6	45,1	60,2	45,7	53,8 63,9	5,9
$N \geq 3$	28,6	28,9	39,8	36,3	36,9 34,2	3,9
N_p	33,1	23,5	34,9	22,7	34,9 36,2	23,6
$(N \geq 2) + N_p$	81,7	68,6	95,1	68,4	88,7 100,1	29,5
$(N \geq 3) + N_p$	61,7	52,4	74,7	59,0	71,8 70,4	27,5
$n \geq 3$ $n \geq 7$	2491 ± 273 720 ± 147	2485 ± 184 547 ± 88	3215 ± 208 888 ± 109	2954 ± 199 967 ± 114	3016 ± 220 629 ± 101	351 ± 101 29 ± 29

*N - number of stars per 1 cm^2 emulsion; n - number of stars per 1 cm^3 of emulsion. Figures at right of N and n indicate the number of prongs. N_p - number of small stars ascribed to radioactive contamination of the emulsion.

**The second row of figures in this column pertains to a re-examination of the photographic plates.

The variation in altitude with time of the apparatus with the hemispherical absorber is shown in Fig. 2 (curve 4). As may be seen, the plates were exposed primarily at 25-28 km (average 27 km). The results of a careful examination of the plates are given in Table 2. We can conclude from this table that at these altitudes the transition effect for stars under a hemispherical lead absorber 2 cm thick is not more than 30 %. Actually, the ratio of the number of stars with 3 or more prongs in the emulsion exposed under the lead hemisphere (stack III) to the number of such stars in the emulsion exposed in air (above the apparatus - stack I) amounts to 1.29 ± 0.22. Approximately the same number of stars are produced under a lead hemisphere 8 cm thick as are produced under a 2 cm hemisphere. The number of stars having more than 7 prongs hardly changes in the transition from air to absorber. Consequently, the transition effect is due to stars having a small number of prongs (3-7). In other words, primarily low-energy (50-500 Mev) star-producing particles are generated in the absorber, as a result of which the flux of star-initiating particles under the absorbers is increased by about 30%. The results of this experiment also failed to give a definite solution to the problem of the position of the transition curve maximum. Nevertheless, one can assert that generation of star-initiating particles predominates over their absorption under a lead hemisphere 8 cm thick. In fact, were there no generation of star-producing particles in the absorber, we would have under an 8-cm layer of lead $J = J_0 \exp(-x/L_a) \approx 0.75\, J_0$, where, according to Ref. 4, $L_a = 320$ g/cm^2 is the absorption range. Whereas in our experiments we obtained $J = J_0$ (1.29 ± 0.22). This shows that particles generated in the

absorber play an important part in star production. The generation effect thus amounts to 1,72 ± 0.29.

4. We turn now to a brief description of the results of another experiment, also aimed at investigating the transition effect for stars. The flight record in this case is shown by curve 5 in Fig. 2. In this flight the apparatus was at an altitude exceeding 25 km.

The density of stars having three or more prongs in the photographic plates exposed in air in this experiment amounted to about 22 per cm^2. In the emulsions exposed under a lead cover over 3 cm thick (the diagram of the apparatus is not shown here), the density of the three or more prong stars was was 28.4 per cm^2. It follows that the increase in the number of stars in this experiment was also about 30% and the generation effect about 45–50%. From the distribution of the number N* of stars as a function of their multiplicity (number of prongs N_h), it follows that the transition effect is due mainly to small stars (3–6 prongs). This directly substantiates the earlier obtained indication that the star-producing particles generated in the absorber have energies, for the most part, in the 50 to 500 Mev range.

We have reported above only some of the results obtained in some 30 balloon flights. Many interesting details (the altitude dependence of the number of stars produced, the generation of slow pi mesons and information on the transition effects at different altitudes) have necessarily been omitted. Below we list some of the deductions arrived at as a result of all these experiments.

The transition effect for stars with $N_h \geq 3$ and for π mesons is strongly dependent on the atomic number of the absorber material and on the altitude of the observations.

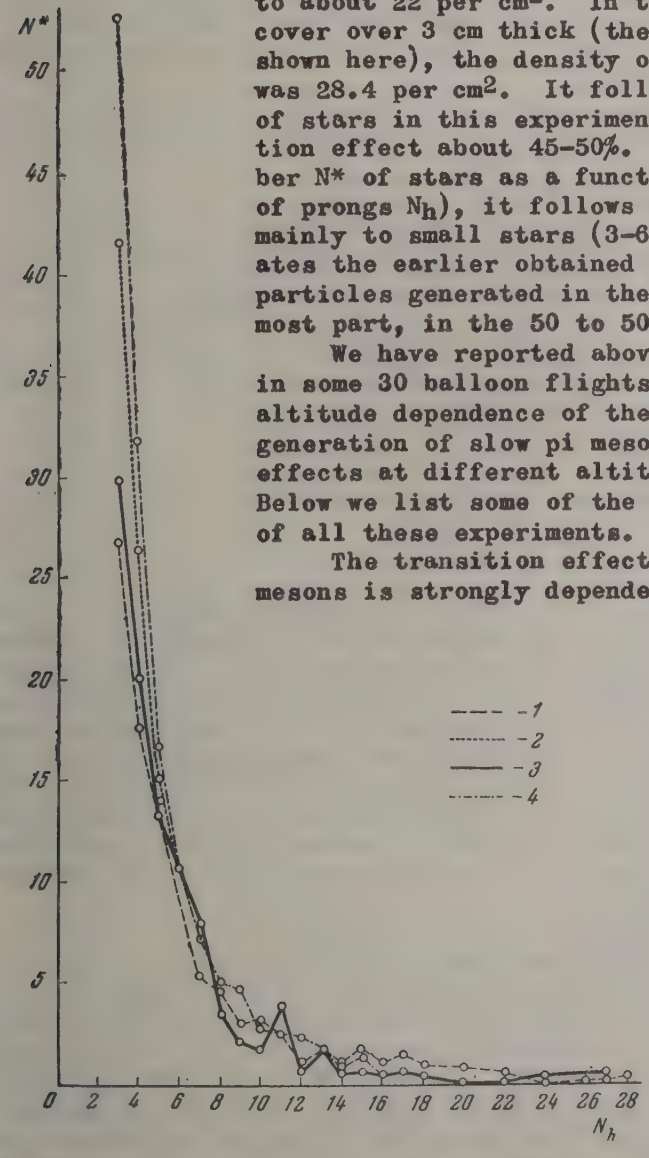

Fig. 5. Distribution of the number N* of stars as a function of their "size", i.e., the number of prongs N_h.

In all our experiments at altitudes from 22 to 29 km we observed an increase of 20–50% in the number of stars produced in photographic plates under lead absorbers over the number of stars formed in photographic plates without absorbers, the actual percentage depending on the altitude of observation and the thickness of the lead blocks surrounding the emulsions. As can clearly be seen from Tables 1 and 2 and Fig. 4, the effect is greatest (near 50%) at altitudes of 28–30 km, while at 20–23 km, the effect is so weak that it can be detected only by examining many plates with a minimal background. The effect was not discerned at all in the experiments carried out at altitudes below 20 km (see Table 1 and flight-record curve 1 in Fig. 2). Inasmuch as experiments[4] performed at mountain altitudes (3,865, 4,000 and 4,375 meters) also failed to show a noticeable increase in

the number of stars under lead, we assume that at altitudes below 20 km no increase in the number of stars should be observed under an absorber. This conclusion is also confirmed by our experiments at 9 km, the results of which are not listed in this article.

In the case of light-element absorbers (graphite and paraffin) no increase in the number of stars in emulsions exposed under an absorber over the number in photographic emulsions exposed in air (no absorber) is noticeable up to 24 km altitude. Only at about 27-29 km do we find an increase of as much as 10-20% under 30 cm of graphite.

It has been established (see Fig. 5) that the transition effects for stars both in heavy-element (lead) and light-element (graphite and paraffin) absorbers are associated primarily with stars with 3-6 prongs. This indicates that star-producing particles of relatively low energy are generated in the absorbers.

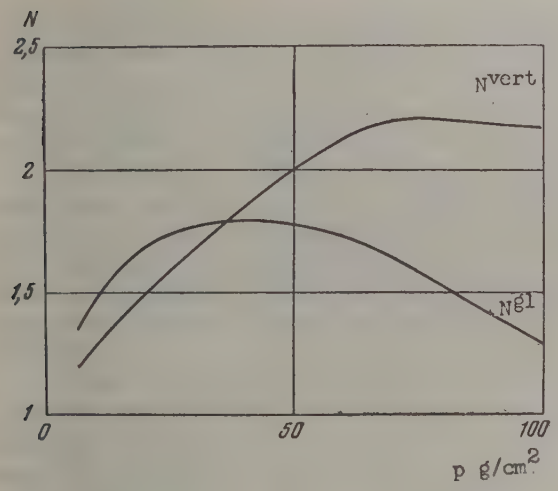

Fig. 6. Altitude dependence of the number N of stars in the stratosphere, taking account of the contribution of the primary component α-particles to star production. N^{vert} - the number of stars produced by the vertical flux; N^{gl} - the number of stars produced by the global flux of star-initiating particles, with the number of stars outside the atmosphere normalized to unity.

We also determined the altitude dependence of the number of stars in the 20 to 27-29 km altitude interval. We found that the number of stars at 22 km is some 10-20% greater than at 27-29 km. This result is only in qualitative agreement with the data of Ref. 5, but is in good agreement with our calculated curve (Fig 6); we, therefore, do not list the experimental data herein.

Lastly, we determined the number of slow π mesons on the basis of the number of π-μ-decays and σ-stars and established that the number of slow mesons increases appreciably when even a thin absorber of lead, copper, graphite or lead is mounted above the photographic plates.

Below we suggest an interpretation of the experimental results obtained for star production in the stratosphere on the basis of general concepts regarding the passage of the nucleonic component of cosmic radiation through matter.

Let us assume that the transition effect for stars is investigated at a certain depth θ_B of the atmosphere. Our problem is to determine the total number N of particles of energy $>E$, capable of initiating star-type nuclear disintegrations at a depth θ_A in the given absorber. We assume, in line with the accepted concepts, that the star-producing particles are primarily neutrons, protons and π mesons of sufficiently high energy. Consequently, any one of these particles in penetrating the absorber to the depth θ_A can generate a certain number of neutrons, protons and π mesons by cascade multiplication. Let us denote through $N_n(E_n, E, \theta_A)$, $N_p(E_n, E, \theta_A)$ and $N_\pi(E_n, E, \theta_A)$ respectively, the number of neutrons, protons and π mesons of energy $>E$ at the depth θ_A, generated by one neutron of energy E_n entering the absorber from the air. Then the total number of such particles produced by the neutrons, protons and π mesons of energies greater than E_n, E_p and E_π will be given by

$$.(N E, \theta_A, E_n, E_p, E_\pi, \theta_B) = \sum_{i,k} \int_{E_k=E}^{\infty} N_i(E'_k, E, \theta_A) K(E'_k, E_c, \theta_B) dE'_k,$$

where the indices i and k assume three separate values, corresponding to neutrons, protons and π mesons, $K(E'_k, E_c, \theta_B) dE'_k$ is the differential spectrum of these particles in the atmosphere and E_c is the geomagnetic cut-off energy. We can locate the position of the transition curve maximum from the condition

$$\frac{\partial N(\theta_A, E, E_c, \theta_B)}{\partial \theta_A} = 0.$$

If we assume that star-production is feasible at $E \geqslant 50$ Mev and that $E_c = 2 \cdot 10^3$ Mev (the mean energy threshold at medium latitudes) and if we evaluate the parameters in the numerical expressions according to Messel,[1] we obtain $\theta_{Pb} = 0.578 - 0.414\ \theta_B$, where θ_B is measured in units of 65 g/cm^2 and θ_{Pb} in units of 160 g/cm^2. Only nucleons were taken into account in the numerical calculations.

As mentioned above, in none of the experiments did we succeed in obtaining the exact position of the transition curve maximum in terms of the absorber thickness. Any experimental determination of the exact location of the maximum at a specific altitude is out of the question since the maximum is rather diffuse and furthermore both the position of the maximum and its height depend on the altitude of observation which necessarily varies somewhat during a balloon flight.

The aforementioned calculations explain the altitude dependence of the transition effect for stars as well as the dependence of the location of the maximum of the transition curve on the altitude of measurement, but they do not explain the magnitude of the transition effect in lead. To explain the appreciable transition effect for stars observed in the case of lead absorbers it is necessary to take into account the ionization loss of protons and the excess of neutrons in the nuclei of heavy elements such as lead.

Clarification of the altitude dependence of the number of stars produced at altitudes above 20 km is essential for an understanding of the transition curve. If we allow for the presence of about 20% α-particles in the primary component, the altitude dependence of stars can be represented in the form of the curve shown in Fig. 6. In plotting the curve we assumed that in interacting with nuclei of the air α-particles produce, on the average, 2-2.5 star-initiating particles (mainly nucleons resulting from the decay of the α-particles themselves), which subsequently multiply exactly as primary protons.

In conclusion I wish to thank S.N.Vernov, N.A.Dobrotin and N.L.Grigorov for their interest in the investigations. I must also express my gratitude to the personnel of the Central Aerological Observatory for their assistance in carrying out the ascents.

Physical-Technical Institute of the
Academy of Sciences of the Kazakh SSR

References

1. H.Messel, Progress in Cosmic Ray Physics, Vol. II p. 135 - Amsterdam, 1954.
2. I.L.Rozental' & D.S.Chernavski, Usp fiz. nauk., 52, 185 (1954).
3. Zh.S.Takibaev, Zhur. eksp. i teor. fiz., 23, 543 (1952).
4. Zh.S.Takibaev, M.P.Ostiakov & D.Kaipov, Zhur. eksp. i teor. fiz., 23, 456 (1952).
5. P.Freier, E.Ney & F.Oppenheimer, Phys. Rev., 75, 1451 (1949).

INVESTIGATION OF THE PRODUCTS OF NUCLEAR DISINTEGRATIONS INITIATED BY FAST NEUTRONS IN LEAD

-A.V.Khrimian

In 1949 Alikhanian, Daion and Kharitonov[1] showed that at 3250 meters altitude there is an intense flux of high energy neutrons capable of generating protons in matter. Subsequently the nature and spectra of the particles produced by the fast neutrons were investigated in the same laboratory by means of mass spectrometers.[2,3] In these investigations, however, only single particles traversing the spectrometer were studied. Thus the products generated in multiple-prong stars were, at least in part, excluded.

The nature of all fast particles comprising such stars has not yet been fully established. We have virtually no direct data on the composition of the secondary particles having momenta exceeding 1 Bev/c and little information on the ratio of π^- to π^+ mesons among the fast particles comprising nuclear disruption stars. The available data on the N_{π^-}/N_{π^+} ratio pertain only to slow mesons (<40 Mev) and the values reported by different investigators[4-6] are in sharp conflict. The results of studies of shower particles by means of cloud chambers[7-9] and nuclear plates[10] are as yet inadequate for drawing definitive conclusions.

In 1954 we showed that the mass spectrometer of Alikhanian and Alikhanov can be used for investigating the particles comprising stars and determining their nature.[11] The possibility of determining the charge polarity and the high accuracy of momentum measurements afforded by this method make it feasible to analyze fast particles comprising stars, i.e., to extend the investigation into the region of very high energies where the nuclear emulsion method is no longer applicable. By means of the mass spectrometer method we succeeded in obtaining data on the composition of nuclear particles having momenta in excess of 1 Bev/c.[11]

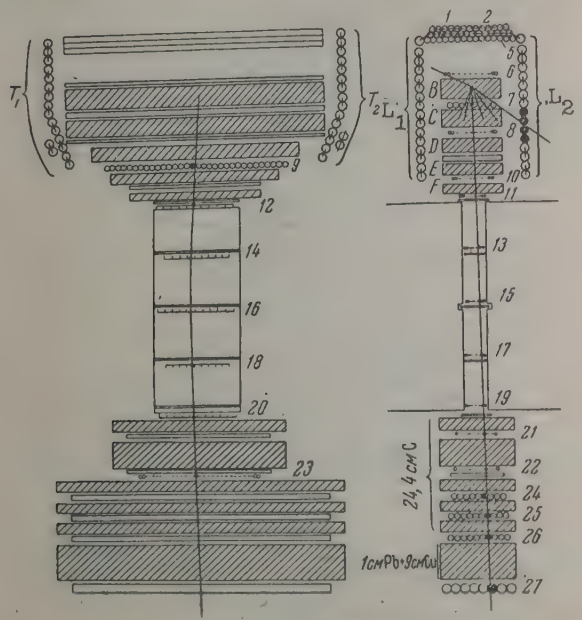

Fig. 1. Diagram of mass spectrometer (mutually perpendicular vertical sections). The upper and lower parts of the apparatus contain arrays of hodoscopic counters with absorbers, serving for determining the nature of both primary and secondary particles.

In the present report we give data on the ratio between the number of positive and negative fast π mesons created in stars. On the basis of this data we evaluate the number of π mesons among shower particles, having momenta greater than 1 Bev/c.

We carried out the investigation by means of the Alikhanian and Alikhanov mass spectrometer at an altitude of 3250 meters above sea level (Mt. Aragats). The apparatus is diagrammed in Fig. 1. It consisted of a mass spectrometer (magnetic field intensity 6850 oersted) and a supplementary hodoscopic counter array, mounted under the spectrometer. The design of the apparatus permitted observation of particles entering into the composition of single prong as well as multiple

prong stars, produced by neutral particles in the lead absorbers B,C,D,E and F located in the hodoscope assembly. The particle trajectories in the plane of magnetic deflection were determined by means of the coordinate counter rows 9, 12, 14, 16, 18, 20 and 23; the trajectories in the plane perpendicular to the plane of deflection were recorded by rows 5, 6, 7, 8, 10, 11, 13, 15, 17, 19, 21, 22, 24, 25, 26 and 27. Rows 6, 8, 10, 24, 25, 26 and 27 were comprised of two layers; the counters covering the slits between the coordinate counters were connected in parallel. A star was assumed to be created in lead plates B, C, D, E or F by a neutral particle if no charge particle was recorded in the counters of rows 1 through 6. The probability of a simultaneous miss in rows 3-6 is less than 10^{-3}. The lateral rows L_1 and L_2 and the end rows T_1 and T_2 served to separate particles entering the hodoscopic array from the side and to record particles ejected laterally. The trajectories of every particle ejected by a star were analyzed by means of a special templet. We selected only those events in which the spatial pattern of the particle's passage through the apparatus could be determined unambiguously. The trajectories of the particles traversing the magnetic field were established by no less than four coordinates in both the mutually perpendicular planes.

The root mean square error in determining momenta was 10% for momenta of 1 Bev/c and 50% for 5 Bev/c.

Ratio of negative to positive pi mesons.

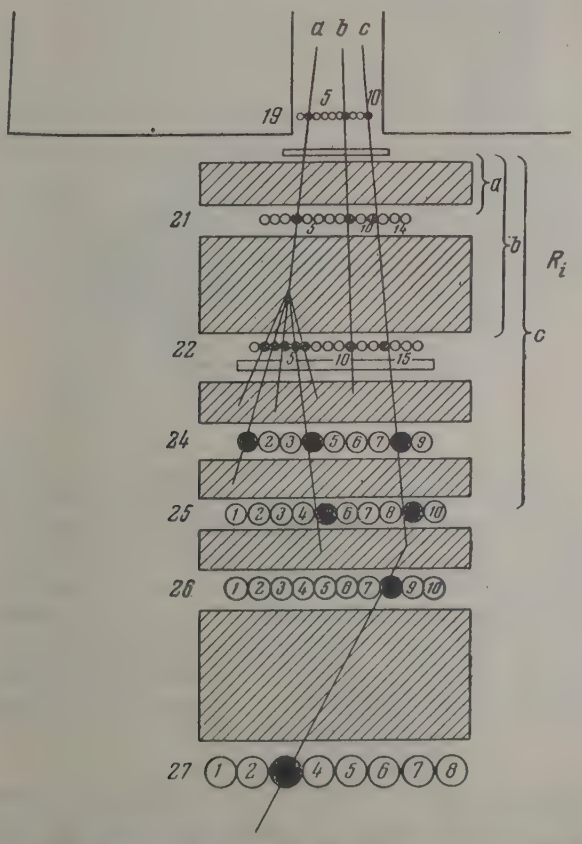

Fig. 2. Determination of observational ionization range R_i from the path length of the particle to the first nuclear interaction event (cases a and c) or to point of stopping due to ionization loss (case b).

In order to determine N_{π^-}/N_{π^+}, it was necessary to separate the K^+ and π^+ mesons from the protons. To this end we determined the upper limit of the particle mass on the basis of the momentum and the observed ionization range R_i, i.e., the range to the first observed nuclear interaction event or to the point at which the particle came to rest in the absorbers due to ionization loss (Fig. 2). In this way we separated all positive particles having a mass under 1400 m_e; this criterion was sufficient for dependable discrimination between positive mesons and protons. In determining the $N_{\pi^-, K^-}/N_{\pi^+, K^+}$ ratio we used an analogous method for separating the negative particles.

As Daniel et al[12] showed most of the mesons in ordinary stars are pi mesons. According to the evaluations of Kamalian and Alikhanian[13] K-mesons amount to only 10-15% of the number of π mesons in the investigated momentum interval. Consequently the magnitude of the $N_{\pi^-, K^-}/N_{\pi^+, K^+}$ ratio is determined primarily by the ratio of π^- to π^+ mesons.

For fast N-component particles the observational range is actually

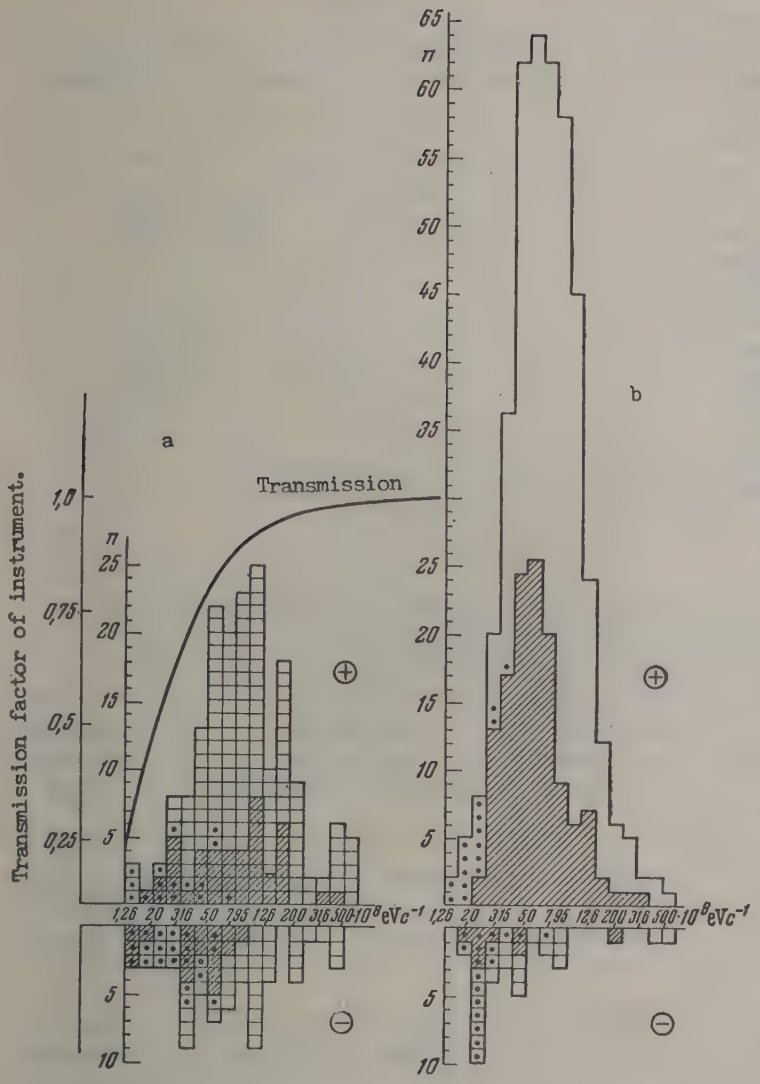

Fig. 3. Distribution in momentum of secondary particles generated by neutral radiation in lead: a) distribution for particles obviously originating in multi-prong stars ($n > 2$); b) distribution for particles observed without accompanying showers ($n = 1$). Hatching designates momentum distributions of particles created in plates E and F (see Fig. 1). Dots identify particles of mass $\leq 1400\ m_e$ as determined from momentum and range measurements.

determined not by the "ionization" range but by the range to nuclear interaction.* Hence correct determination of the ratio $f = N_{\pi^-}/N_{\pi^+}$ by the given method is possible only on condition that the total cross sections for nuclear interaction of positive and negative mesons are equal in the absorber used. In our experiment this condition is fulfilled inasmuch as the basic data for determining the charge ratio were obtained by means of graphite absorbers (in 90% of the cases, the observed range proved to be not in excess of 39 g/cm^2 C), for which the two cross sections are equal to within 10%, at least at 130 Mev/c. (Ref. 14 and 15).

The momentum distributions of the secondary particles generated in the lead absorbers by neutral radiation are shown in Fig. 3. Histogram a pertains to cases when the particle clearly originated in a multi-prong (>2) star.* Histogram b includes particles observed without accompanying showers ($n = 1$); part of them presumably pertain to type $n > 2$ stars, whose other components were either not recorded by the hodoscopic array or, being short range particles, were immediately absorbed in the first lead plate. In this respect the spectra of the particles originating in plates E and F (hatched in histogram) were appreciably "purer", since the relative thinness in these plates and the fact that they were surrounded by small diameter counters greatly facilitated detection of small stars. On the basis of momentum and range measurements we separated 32 positive and 40 negative particles of mass $\leq 1400\ m_e$. In Fig. 3 they

*In practice this limits the application of the given method (and of the "range-momentum" method in general) in the region of large momenta.

Table 1

Distribution in mass of secondary particles of mass $\leq 1400\ m_e$ in the observed stars.

Type of star	Meson charge	Upper limit of particle mass (in m_e)			
		≤ 1400	≤ 1000	≤ 600	≤ 500
$n \geq 2$	+	16	15	5	3
$n \geq 2$	−	22	19	9	4
$n = 1$	+	16	13	10	6
$n = 1$	−	18	13	7	4
$n \geq 1$	+	32	28	15	9
$n \geq 1$	−	40	32	16	8

are identified by dots and more detailed data pertaining to them are listed in Table 1. The solid line in Fig. 3, a indicates the transmission factor of the apparatus, i.e., the dependence of the recording efficiency on the momentum. In the absorbers used in our measurements pi mesons having momenta from 120 to 230 Mev/c were stopped due to ionization losses. The recording efficiency of our apparatus for particles of such momenta is small and consequently the number of pi mesons stopped as a result of ionization losses, appearing in our data, is also small. (see Table 1).

Table 2

Comparison of our results with the data of other investigators on the products of nuclear disintegration

Method, altitude & Ref.	Nature of particles		Momentum intervals, Mev/c	Ratio	Results	
	Primary	Secondary			Refs. 16, 8 & 9	Our data (f = 125)*
Emulsion; 50 mm Hg press. alt. (16)	Charged and neutral	mesons	140–580	$\frac{N_\pi}{N_p}$	1.34	$\frac{77}{53} = 1.45$
		protons	660–1230			
Cloud chamber w. mag. field 3410 m. (8)	Charged (partly neutral)	Shower particles	125	$\frac{N^+}{N^-}$	1.83	$\frac{107}{59} = 1.81$
Cloud chamber; 2840 m. (9)	Charged and neutral	Shower particles	740(p)	$\frac{N_p}{N_\pi}$	0.77	$\frac{78}{108} = 0.73$
			115( )			

*If f differs appreciably from 1.2 ± 0.4 the results diverge (see Table 3).

It follows from the cited data that approximately equal numbers of π^- and π^+mesons having momenta in the 125–600 Mev/c interval are produced in both large ($n > 2$) and small ($n = 1$) stars generated in lead by neutral radiation. (It is assumed that the total cross sections for nuclear interaction of π^+ and π^-mesons in lead are equal.)

We compared our results with data of other investigators on the assumption that, at momenta greater than 600 Mev/c, f is also approximately equal to unity (Table 2). For the comparison, the particle groups and momentum intervals were selected taking into account the experimental conditions of the investigations described in the references. The general agreement of the data indicates that at momenta above 600 Mev/c, too, approximately equal numbers of π^+ and π^- mesons are produced in stars, regardless of the nature of the primary particles.

Composition of secondary particles having momenta 10^9 ev/c

The number of π mesons among the shower particles having momenta above 1 Bev/c was determined on the basis of the spectra of negative and positive particles having momenta in this region and the ratio $f = N_{\pi^-}/N_{\pi^+}$. These data are given for both multi-prong ($n > 2$) and $n = 1$ type stars in Fig. 2 and Tables 1-3.

Table 3

Dependence of f according to our data on the ratio between the numbers of different particles

Investigated ratio	Ref. giving comp. data	f					
		0,8	1	1,5	2	5	10
N_π/N_p	[16]	2,86	1,76	1,30	1,08	0,81	0,71
N^+/N^-	[8]	2,09	1,93	1,73	1,63	1,44	1,39
N_p/N_π	[9]	0,49	0,61	0,82	0,97	1,32	1,47

The following conclusions can be drawn on the basis of the data.

1. In stars generated by neutrons in lead, approximately equal numbers of π^- and π^+ mesons ($f = 1.2 \pm 0.4$) are produced in the 125-600 Mev/c momentum interval (assuming equal nuclear interaction cross sections for π^- and π^+ mesons). The charge ratio does not change appreciably in the region of momenta exceeding 600 Mev/c (at any rate up to 2 Bev/c) and is apparently weakly dependent (in Pb) on the nature of the primary particles.

2. Pi mesons comprise 40-50% of the number of shower particles having momenta greater than 1 Bev/c.

3. The distribution in momentum of "single" pi mesons produced in lead 13-25 cm thick (Fig. 3, b) differs noticeably from the distribution of pi mesons accompanied by showers (Fig. 3, a) observed under identical conditions: specifically, the ratio $n_a/(n_a + n_b)$ amounts to about 0.6 in the region of momenta under 1 Bev/c and to about 0.9 in the region above 1 Bev/c. Approximately 40% of the pi mesons observed in stars have momenta ≥ 1 Bev/c.

4. Single pi mesons comprise only 15% of all the "single" particles generated in the momentum region under 1 Bev/c and 5% in the region above 1 Bev/c. About 90% of all the pi mesons have momenta under 1 Bev/c.

In conclusion I wish to thank A.I.Alikhanian for his interest in the work and his valuable suggestions, T.L.Asatiani, G.V.Khrimian, V.Sh.Kamalian and A.M.Gal'per for their assistance in the investigation and I.I.Gol'dman, M.L. Ter-Mikaelian and G.P.Eliseev for discussion of the results.

Physical Institute of the
Academy of Sciences
of the Armenian SSR

References

1. A.I.Alikhanian, M.I.Daion & V.M.Kharitonov, Zhur. eksp. i teor. fiz., 19 739 (1949).
2. A.V.Khrimian, Doklady AN SSSR, 85, 75 (1952).
3. A.Dadaian & G.Merzon, Doklady AN SSSR, 86, 259 (1952).
4. I.Barbour, Phys. Rev. 78, 518 (1950).
5. H.Yagoda, Phys. Rev. 85, 891 (1952); 95, 648 (1954).
6. J.Y.Mei, E.Pickup, Can. J. Phys., 30, 430 (1952).
7. K.H.Barker, & C.C.Butler, Proc. Phys. Soc., A64, 4, (1951).
8. N.R.Whetten, R.S.Preston, R.V.Adams, R.M.Walker et al, Phys. Rev., 93, 1356 (1954).
9. I.Kita & O.Minakawa, J. Phys. Soc., Japan, 9, 6 (1954).
10. U.Camerini, J.H.Davies, P.H.Fowler, C.Franzinetti, et al, Phil. Mag., 42 1241 (1951).
11. A.V.Khrimian, Doklady AN SSSR, 96, 1155 (1954).
12. R.R.Daniel, J.H.Davies, J.H.Mulvey, D.H.Perkins, Phil. Mag., 43, 753 (1952)
13. V.Sh.Kamalian & A.I.Alikhanian, Doklady AN SSSR, 97, 425 (1954).
14. H.L.Anderson, E.Fermi, D.E.Nagle & G.B.Yold, Phys. Rev., 86, 413 (1952).
15. M.W.Aarons, J.F.Ashkin & F.Feiner, Phys. Rev., 90, 342 (1953)..
16. Progress in Cosmic Ray Physics, v. 1, p. 24, fig. 10 - Amsterdam, 1952.

* * * * * * *

DETERMINATION OF THE MASS OF COSMIC RAY PARTICLES BY MEANS OF A WILSON CLOUD CHAMBER*

- M.S.Kozodaev & A.I.Filoppov

Studies of the composition of cosmic radiation led a number of investigators to postulate the existence of heavy mesons, having a mass greater than that of a π meson. However, in 1950 there were still few data on these heavy particles. Our experiments of 1950-2, carried out at 3250 meters above sea level (Mt. Aragats) by means of a cloud chamber, were devoted to measuring the mass and investigating the properties of heavy mesons, generated by cosmic ray particles in a block of lead mounted above the apparatus. The masses were determined from the momentum and range of the particles. The momenta were evaluated from the curvature of the particle tracks in a cylindrical cloud chamber operated in a magnetic field of 4500 oersteds.

In the measurements of 1950-1 (Experiment 1) absorbers were employed to determine the range. The particles traversing the chamber and coming to rest in the absorber were recorded by means of three trays of counters connected in coincidence and a fourth tray connected in anticoincidence. Only one absorber plate was mounted under the chamber; with this arrangement the equipment recorded particles having ranges between 10.4 and 22.4 g/cm^2 (air equivalent). Since the actual range could, with equal probability, have any value in this interval, below we give two values of the masses, one corresponding to the minimum thickness of the absorber, the other to the maximum. In reality the uncertainty in determining the mass is still greater owing to multiple scattering in the gas

*A description of the equipment used in the experiments will be published in the journal "Pribory i metody eksperimental'noi fiziki" (Apparatus and methods of experimental physics).

of the chamber, statistical fluctuations, etc. These additional errors in determining the mass were evaluated taking into account the possible errors in measuring the momentum and range. In order to check the computed values we made measurements of the curvature of the tracks of stopped particles with the magnetic field turned off. This experimental verification showed that the computed values of the error in determining the mass were correct.

The values of the momentum for particles of different mass recorded by our apparatus are given in Table 1.

Table 1

Values of momentum for particles of different mass

Mass of particles, m_c	1836	1000	600	276	209
Momentum, Mev-c	470÷590	305÷395	215÷285	125÷175	105÷145

Over 1500 photographs were obtained in the 1950-1 experiments. Only the photographs in which the tracks were in the central region of the chamber and free of distortion were used for mass determinations. As a result of this selection it proved possible to evaluate the mass of 120 particles that came to rest in the absorber. The results showed that, among these, 81 particles could be classified as protons and 33 as π and μ mesons. The remaining 6 particles had a mass greater than that of a π meson. The data on these particles are listed in Table 2.

Table 2

Data on particles with a mass exceeding that of a π meson, recorded in 1950-1951

Mass, m_e		charge
from	to	
945—130	1300+185	+
770—110	1055+150	+
725—100	995+140	+
725—100	995+140	+
690—85	955+130	—
620—75	870+115	—

In determining the masses we proceeded on the assumption that the range in the absorber is determined solely by the ionization loss. However, due to the fact that π mesons are also subject to non-ionization losses, it is possible that the mass values are over-estimated. Without further experimental investigation it is difficult to determine how many of the particles were "erroneously" classified as heavy mesons because of non-ionization slowing down. However, the distribution in momentum of all the recorded cases of stopping indicates an appreciable increase in the density of the particles in the region of momenta corresponding to heavy mesons.

In the measurements of 1952 (Experiment 2) we used improved equipment which allowed of observing the character of the stopping and more accurate determination of the range of the particles. This apparatus is pictured in the accompanying figure. The cylindrical cloud chamber (I), 200 mm in diameter, was employed to measure the momenta (field intensity 4500 oersted), while for observing the stopping and measuring the range we used the rectangular chamber (II), measuring 400 x 250 x 130 mm and containing five transverse brass plates, each 4 mm thick. The equipment was capable of recording particles having ranges between 8.4 and 21.4 g/cm^2 (air equivalent). A lead plate having a thickness of 8 cm was mounted over the apparatus.

The four trays of counters and associated electronic equipment were arranged to record only particles which traversed the top (cylindrical) chamber and came to rest in the lower one. The apparatus recorded particles of different masses

having approximately the same momentum as in Experiment 1.

We obtained 2100 photographs over a period of 350 hours of effective operation. The mass of the recorded particles was determined only when the following conditions were satisfied: 1) the tracks in the two chambers showed geometric continuity, 2) the track was located in the central region of the cylindrical chamber, 3) the track in the cylindrical chamber was free of distortion and 4) the particle stopped in the rectangular chamber due to ionization loss.

Table 3

Data on particles with a mass exceeding that of a π meson, recorded in 1952

Mass, m_e		charge
from	to	
940—130	1045+145	+
925—130	1005+140	+
1215—170	1325+180	+
1065—145	1135+155	+
1065—145	1135+155	+

After discarding the data failing to meet the above requirements, we found it possible to determine the masses of 99 particles. The determinations showed that 63 particles could be identified as protons, 23 as π mesons and 8 as μ mesons. The values of the mass of the remaining five particles are listed in Table 3.

In view of the fact that all the recorded particles stopped as a result of ionization losses, errors due to nuclear interaction are obviated. On the basis of evaluations of the apparatus errors we computed the probability of obtaining momentum values corresponding to particles of mass 500–1000 m_e in determining the momenta of protons and pi mesons. This probability was found to be less than 0.1%, while the mathematical expectation of recording a proton or meson as a particle having a mass of 500–1000 m_e was found to equal 0.1 particle. Thus we can safely assert that there do exist heavy mesons with a mass of about 1000 m_e. This result substantiates the findings of our 1950-1 experiment in which we observed a small group of particles having masses in the vicinity of 1000 m_e.

Among the recorded cases of stopping of heavy mesons only one is accompanied by a visible secondary particle. The secondary particle is observed to pass through two brass plates in the chamber without a noticeable increase in ionization. From the ionization range and scattering this particle cannot be either a proton or positron but must be identified as either a π or μ meson having a kinetic energy in excess of 40 Mev. In the other cases of stopping of heavy mesons no discernible secondary particles were observed probably because the energy of these was insufficient for them to emerge from the plate. Analysis of the photographs shows that in approximately 50% of the cases of stopping of positive π and μ mesons in the plates decay positrons are observed. Calculations show

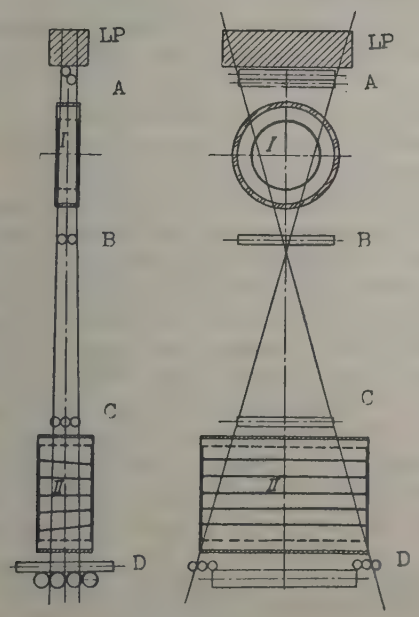

Apparatus used in Experiment 2:
I) cylindrical cloud chamber, II) rectangular cloud chamber with brass plates. A, B and C) counter trays connected in coincidence; D) counter tray connected in anti-coincidence, LP) lead plate 8 cm thick. Distance between centers of chambers I & II = 700 mm.

that approximately this number of decay positrons should emerge from the plates used and that consequently we could effectively observe secondary particles if their range were long enough.

In our experiment we did not record any cases of stopping of particles that could be unambiguously identified as τ mesons. This may be taken to mean that either there are very few τ mesons among the K-mesons formed in lead or that the lifetime of the τ mesons is appreciably shorter than the lifetime of the recorded heavy mesons. However according to data in the literature[4] the lifetime of τ mesons is longer than $5 \cdot 10^{-9}$ sec and in this case they should be recorded in the experiments. Hence it must be assumed that the first supposition is the correct one (i.e., that few τ mesons are produced).

It may be of interest to evaluate the percentage of heavy mesons with respect to the number of π mesons produced under our experimental conditions. Taking the transmission factor of the apparatus into account this comes out to be $6 \pm 4\%$. However it must be noted that this is evaluation made on the basis of the upper limit of the transmission factor so that the indicated percentage may be an over-estimate. In relation to the number of protons the percentage of heavy mesons is $12 \pm 7\%$. In this case the uncertainty due to errors in evaluating the transmission factor is smaller.

We also observed a positive particle having a mass between 525^{-60} and 570^{+65} m_e. We assigned this particle to the group of π mesons, despite the relatively great deviation from the nominal mass value. At the point where this particle came to rest there is observed a secondary particle which, from the scattering and ionization, we identified as a positron.

From Tables 2 and 3 it will be seen that all the heavy mesons recorded in Experiment 2 were positive, while of the six particles assigned to this group in Experiment 1 four are also positive. The preponderance of positive particles cannot be ascribed to statistical fluctuations. The following explanations are suggested for the appreciable excess of positive heavy mesons under the conditions of our experiment:

1. For the most part only positive mesons are created.
2. Negative mesons have a very short lifetime and decay before reaching the recording part of the apparatus; this is in agreement with the data obtained by the photographic plate method which permits recording particles with a very short life.
3. Negative mesons interact strongly with matter and therefore do not reach the recording part of the apparatus.

The existence of a large excess of positive heavy mesons having a mass of about 1000 m_e is also reported by Gregory et al.[5 & 6] Since the group of heavy mesons recorded in Experiment 1 may include lighter mesons stopped as a result of non-ionization losses, it is entirely possible that all the heavy mesons of mass 1000 m_e actually observed in the experiment are positively charged particles. On the basis of the geometry of the experiment and the velocities of the particles it may be assumed that the lifetime of the recorded K-mesons must be greater than $5 \cdot 10^{-9}$ sec. There are indications in the literature that K-mesons with a lifetime greater than $5 \cdot 10^{-9}$ sec do exist.[6&7]

We take this occasion to express our gratitude to I.V.Kurchatov and A.I. Alikhanian for making the present investigation possible and to V.M.Fedorov for his help in the 1950-1 measurements. We also want to thank A.A.Markov and A.N. Sinaev for their help in the work.

Institute of Nuclear Problems of the
Academy of Sciences of the USSR

References

1. A.Alikhanian, A.Alikhanov, V.Morozov, G.Muskhelishvili et al, Doklady AN SSSR, 58, 1321 (1947).
2. R.Brown, U.Camerini, P.Fowler, H.Muirhead et al, Nature,163,82 (1949).
3. A.Alikhanian, I.Gurevich, D.Samoilovich & Kh.Babaian, Zhur. eksp. i teor. fiz., 19, 667 (1949).
4. E.Amaldi, E.Fabri, T.Hoang, W.O.Lock et al, Nuovo Cim., 12, Suppl. No.2 419 (1954).
5. B.Gregory, A.Lagarrigue, L.Leprince-Ringuet et al, Nuovo Cim., 11, 292 (1954).
6. R.Armenteros, B.Gregory, A.Lagarrigue et al, Nuovo Cim.12, Suppl. No. 2, 324 (1954).
7. L.Mezzetti, J.W.Keuffel, Nuovo Cim., 12, Suppl. No. 2, 245 (1954).

* * * * * * *

MEASUREMENTS OF THE LIFETIME OF POSITIVE PI MESONS

-M.S.Kozodaev, A.A.Markov & A.A.Tiapkin

The lifetime of π mesons in cosmic radiation was first measured by Camerini and his co-workers in 1948.[1] Recording the inverse flux of μ mesons by means of photographic plates they determined the mean lifetime of π mesons as $(6 \pm 3)\cdot 10^{-9}$ sec. In the same year Richardson[2], measuring the attenuation of a meson beam in a magnetic channel by means of photographic plates determined the lifetime of π^- mesons produced on an accelerator. The value of the mean life obtained in these measurements was $(1.11^{+0.31}_{-0.22})\cdot 10^{-8}$ sec. Martinelli and Panofsky[3], using the same method in 1950, obtained a value of $(1.97^{+0.17}_{-0.14})\cdot 10^{-8}$ sec for the mean life of π^+ mesons.

In 1950 Kraushaar et al[4] were the first to use an electronic (scintillation crystal) method for measuring the life of π mesons. They obtained a value of $(1.65 \pm 0.33)\cdot 10^{-8}$ sec for the mean life of π^+ mesons. However, Chamberlain et al[5], using an analogous method found the mean life of π^+ mesons from an accelerator to be equal to $(2.65 \pm 0.12)\cdot 10^{-8}$ sec.

Thus the results of measurements carried out in 1948-1950 by different investigators are in disagreement far beyond the limits of the experimental error indicated by the reporting investigators. The greatest divergence obtains for the lifetimes of cosmic ray π mesons. In view of this we undertook to measure the lifetime of π^+ mesons in 1955 at 3250 m altitude (Mt. Aragats). In the work we used an electronic system capable of measuring time intervals on the order of 10^{-8} sec with an accuracy to within 10^{-9} sec. However, the self-quenching counter with a 5.6 mm diameter cathode used for the time measurements had a mean discharge delay time of $2.4\cdot 10^{-8}$ sec. Chance delays due to fluctuations of the leading edge of the pulses were virtually eliminated inasmuch as the counters operated in the region of high surpotentials, while the counter pulses were amplified and standardized by means of an appropriate electronic circuit. The fluctuations of the counter pulse delays made it impossible to utilize cases of decay occurring within an interval of less than $4\cdot 10^{-8}$ sec for determining the lifetime of π mesons. However, the main difficulty encountered in using self-quenching counters is connected with the low efficiency in recording $\pi \rightarrow \mu$-decay events, owing to the short range of secondary μ mesons. Under these

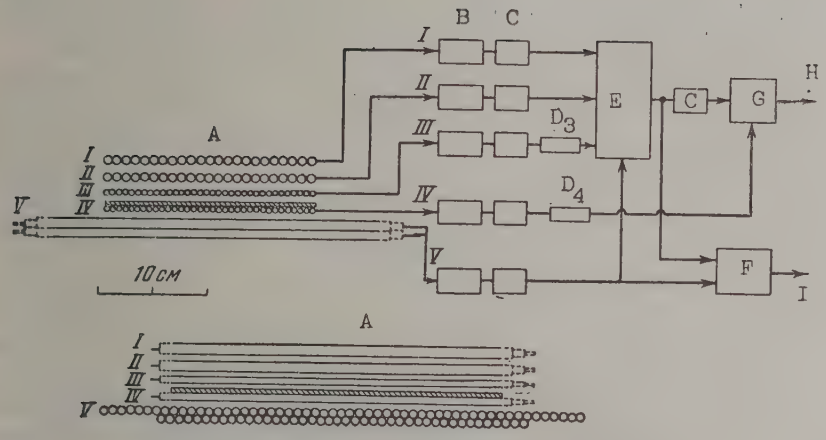

Fig. 1. Block diagram of apparatus: A) five layers of counters (insert: side view of counters), B) amplifier, C) level setter, D_3 & D_4) delay lines in channels III and IV (delay times - $9 \cdot 10^{-8}$ & $17.5 \cdot 10^{-8}$ sec, respect.), E) circuit operated by coincidences in channels I, II & III and anticoincidences in V, F) coincidence circuit for pulses from output of E and delayed pulses from V, G) measuring unit, H) line to oscillograph, I) to oscillograph shutter.

conditions it was necessary to effect a rigid selection of the pulses, permitting of dependable separation of the comparatively rare $\pi \to \mu$-decay events. In order to separate these events the control system was adjusted to record cases of stopping of μ mesons on the basis of the delayed decay positrons. In addition the geometric location of individual counter groups, connected in coincidence and anticoincidence, was chosen so as to insure maximum efficiency in recording secondary particles and reduced to a minimum the possibility of recording a time interval not connected with the decay of a π meson.

A block diagram of the apparatus is pictured in Fig. 1. Counter groups I, II and III, connected for coincidences, and group V, connected in anticoincidence with the above three groups, served to separate cases when the particle came to rest in the apparatus. A pulse, corresponding to a case of stopping of the particle (events I + II + III - V), from the output of the coincidence-anticoincidence circuit E was applied to the measuring unit G, where prior to the arrival of the pulse from channel IV it charged the measuring capacitor. The voltage appearing on the measuring capacitor was proportional to the time between the pulse from circuit E and the pulse in channel IV leading from the counters of row IV.

In the described apparatus the channel of the pulse initiating the time measurement actuates the triple coincidence circuit, while the section of the circuit cutting off the charging of the measuring capacitor does not contribute to the selection of pulses but only effects the necessary electronic conversions of the counter pulses. As calculations and tests showed such systems have an unfavorable distribution of delay times, characterized by a higher probability of long delays of the coincidence pulse due to a primary particle. In order to eliminate this asymmetry in the statistical distribution of the delayed pulses, delay line D_3 with a delay time of $9 \cdot 10^{-8}$ sec was introduced into channel III. The introduction of this delay line also made it feasible to use large diameter (8 mm) counters in channels I and II. In addition the incorporation of a delay line in channel III enhanced the operation of the anticoincidence circuit, so that discharges in counters of group V blocked triple coincidences even in the case of pulse delays of up to $12.5 \cdot 10^{-8}$ sec. In order also to measure the delay of pulses in the counters of row III relative to pulses in row IV, the delay line D_4, having a delay time of $17.5 \cdot 10^{-8}$ sec, was connected into channel IV.

Pulses formed simultaneously on the outputs of channels III and IV produced a finite change in the voltage on the measuring capacitor.

The voltage pulses formed on the measuring capacitor, appropriately amplified and shaped, were fed to a type MPO-1 electromagnetic oscillograph. Thus the oscillograph film recorded deflections of the scope beam, proportional to the measured time intervals. To facilitate converting the magnitude of the deflections to time intervals, we recorded calibration pulses (markers) corresponding to known intervals. Voltage pulses on the measuring capacitor and, hence, on the oscillograph appeared each time the combination of events I + II + + III − V occurred. To permit making control measurements, the apparatus had provision for installing a 2.8 g/cm^2 thick lead absorber between the counters of rows III and IV. By determining the number of pulses at the output of circuit E with and without the absorber in place, we established that in the predominant number of cases the pulses on the output were due not to particles stopping in the apparatus but to particles traversing the apparatus, but not recorded by the counters of group V (or recorded with a great delay). Thus, for 1560 ± 20 particles passing through the apparatus per minute, only about three pulses appeared on the output of circuit D; this indicated that the efficiency of the anticoincidence system was about 99.8%. This high efficiency was attained with the counters of group V arranged in two layers, which eliminated the inefficiency connected with the presence of spaces between the counters and substantially lowered the probability of a great delay of the pulses in channel V.

If the discharges in the counters of rows III and IV were not subject to accidental delays, the pulses on the measuring capacitor due to particles traversing the apparatus would be equal in value, corresponding to a zero time interval. Inasmuch as the lifetime of π mesons is commensurate with the time of accidental delays in the discharge of the counters, it was necessary to avoid recording a large number of short time intervals, corresponding to the passage of particles through the apparatus. This problem was solved by having the shutter of the oscillograph controlled by a displaced-coincidence circuit. A voltage pulse was formed on the output of this circuit only when there was a pulse in the counters of group V lagging $(0.5\text{–}5.0)\cdot10^{-6}$ sec behind the triple coincidence pulse. This pulse opened the shutter of the loop oscillograph so that only intervals accompanied by the decay of μ mesons in the apparatus were recorded on the photographic film of the oscillograph.

Thus a "time pulse" on the measuring capacitor was recorded on the film every time there was coincidence of the discharges in the counters of the upper three groups in the absence of discharges in the counters of group V within $12.5\cdot10^{-8}$ sec but followed by a discharge in these counters, delayed by $(0.5\text{–}5.0)\cdot10^{-6}$ sec. Actually two electromagnetic oscillographs were employed to record these selected pulses: the film of one recorded deflections corresponding to short time intervals (under $12.5\cdot10^{-8}$ sec), while that of the other registered beam deflections corresponding to intervals greater than $0.5\cdot10^{-6}$ sec.

In cases when a μ meson, coming to rest between counter rows III and IV, decayed within $(0.5\text{–}5.0)\cdot10^{-6}$ sec and produced a positive or negative electron that passed through the counters of rows IV and V, the film of the second oscillograph recorded a pulse corresponding to a $\mu\rightarrow$e-decay. If, on the other hand, the μ meson decayed in a time longer than $12.5\cdot10^{-8}$ sec but shorter than $0.5\cdot10^{-6}$ sec, the pulse formed on the measuring capacitor was not recorded, inasmuch as in this case the shutter of the oscillograph remained closed. In the case of decay of μ mesons stopped in the apparatus in a time shorter than $12.5\cdot10^{-8}$ sec there was also no record made since not only did the oscillograph shutter remain closed, but in general there was usually no pulse formed on the measuring capacitor.

The counters used in the experiments had copper walls 100 μ thick; consequently a positron, passing through the counters of row IV, entered the counters connected in anticoincidence. Thus, by virtue of the high efficiency of the counter group V and the use of the delayed coincidence circuit, that opened the shutters of the oscillographs in the case of a μ meson decay within an interval shorter than $12.5 \cdot 10^{-8}$ sec, the corresponding short time intervals were not recorded. The brief interval could be recorded only in the relatively rare cases when the μ mesons, formed by the decay of π^+ mesons stopped in the counter walls, entered one of the counters of row IV and, decaying, yielded positrons that passed through the counters of group V. Thus the purpose of the present investigation was determination of the statistical distribution of the time intervals connected with the decay of π mesons.

The low background of chance coincidences in these measurements was attained by enhancing the efficiency of the counters of group V and by locating them immediately behind the counters of group IV. For example, for any time interval of the order of 10^{-8} sec, due to purely chance events, to be recorded there had to be a full coincidence of the following three independent events: 1) passage of a particle not detected by the counters of groups IV and V through the telescope formed by the first three counter groups, 2) a subsequent passage (with a delay on the order of 10^{-8} sec) through the counters of group IV of a particle not detected by the counters of group V and 3) the passage through the counters of group V of a particle delayed $(0.5\text{–}5.0) \cdot 10^{-6}$ sec in time. The frequency of the first and second events is determined largely by the efficiency and relative location of the counters comprising group V. These two factors also play an important part in reducing the effect of other possible coincidences.

In general false measurements were due mainly to μ mesons that passed through the first four counter rows and lodged in the apparatus between counter rows IV and V. In such cases the first oscillograph should theoretically record a pulse corresponding to a zero time interval. Actually, however, due to chance delays in the discharge of the counters of group IV, instead of zero intervals, time intervals in excess of $4 \cdot 10^{-8}$ could be recorded on the film. In order to be able to separate the recorded intervals corresponding to actual cases of $\pi \rightarrow \mu$-decay from cases connected with the rare prolonged delays in the discharge of the counters in group IV, it was necessary to know accurately the statistical distribution of the counter discharge delays. The curve for the distribution of discharges due to the passage of particles through the apparatus was carefully plotted and studied prior to starting the π-meson lifetime measurement and was re-determined after every 100 hours of operation. In these control measurements, the oscillograph shutter was opened directly by the pulse formed on the measuring capacitor and, to reduce the anticoincidence effectiveness, the upper counter layer of group V was disconnected. The determined distribution of the discharge delays in the counter rows III and IV showed no deviation from symmetry, i.e., the relative delay of the pulses from the counters of row IV was duplicated by the delay pattern for the pulses from row III.

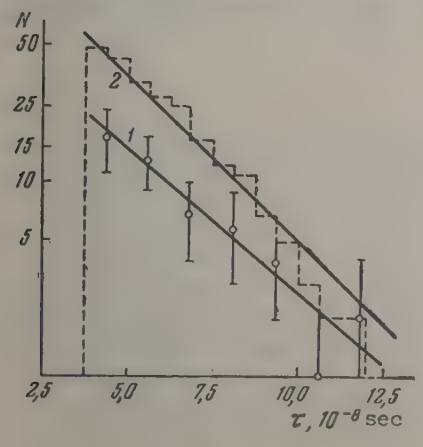

Fig. 2. Differential (1) and integral (2) distributions of time delay intervals.

In measuring the lifetimes of π mesons we recorded the time intervals corresponding both to the relative delay of the pulses from the counters of row IV and the delay of the pulses

from the counters of row III. From the number of time intervals exceeding $4 \cdot 10^{-8}$ sec, corresponding to the delay of pulses in the counters of row III we determined the number of intervals exceeding $4 \cdot 10^{-8}$ sec, corresponding to the delay of pulses in the counters of row IV but not associated with the decay of pi mesons. In the course of the measurements we recorded 135 time intervals exceeding $4 \cdot 10^{-8}$ sec. Of these 92 corresponded to a relative delay in the pulse from the counters of row IV, while the remaining 43 intervals corresponded to a relative delay of the pulses in the counters of row III. After subtracting the latter 43 time intervals, the statistical distribution of which was taken in accord with the curve characterizing the delays in the discharges in the counters, we obtained the distribution of the remaining 49 time intervals. This time interval distribution is plotted to a logarithmic scale in Fig. 2. The mean life of π^+ mesons, as determined from the slope of the straight line drawn through the experimental points by the method of least squares, taking into account the statistical weight of the individual measurements, proved to be $(2.9 \pm 0.7) \cdot 10^{-8}$ sec. The integral distribution of the recorded time intervals (number of intervals greater than each of the horizontal scale values) is also plotted in Fig. 2. The mean life of π^+ mesons evaluated according to this integral data equals $(2.7 \pm 0.7) \cdot 10^{-8}$ sec. The relatively large measurement error is due both to the small number of recorded time intervals and to the presence of a background from μ mesons, in the determination of which an appreciable statistical error is also involved.

The mean life of μ mesons, as determined on the basis of the statistical distribution of the time intervals between the limits of 0.5 and $5.0 \cdot 10^{-6}$ sec, was found to be $(1.9 \pm 0.3) \cdot 10^{-6}$ sec. The results of this investigation have been described in Ref. 6. Despite the low statistical accuracy of the measurements it can be asserted that the determined mean life of π^+ mesons is in conflict with the results of early determinations (Refs. 1-4) and in agreement with the data of more recent measurements (Refs. 5, 7-10).

In conclusion we wish to thank I.V.Kurchatov and A.I.Alikhanian for their attention and assistance in carrying out the present investigation and Iu.A. Prokof'ev, who participated actively in the initial and preparatory stages of the investigation.

Institute of Nuclear Problems of the
Academy of Sciences of the USSR

References

1. U.Camerini, H.Muirhead et al, Nature 162, 433 (1948).
2. J.R.Richardson, Phys. Rev., 74, 1720 (1948).
3. E.A.Martinelli & W.K.H.Panofsky, Phys. Rev., 77, 465 (1950).
4. W.L.Kraushaar et al, Phys. Rev., 78, 486 (1950).
5. O.Chamberlain, F.R.Mozley et al, Phys. Rev., 79, 394 (1950).
6. M.S.Kozodaev, A.A.Markov & A.A.Tiapkin, Report, IIaP AN SSSR (Institute of Nuclear Problems of the USSR Academy), 1950.
7. M.Jakobson, A.Schulz et al, Phys. Rev., 81, 894 (1951).
8. C.Wiegand, Phys. Rev., 83, 1085 (1951
9. W.L.Kraushaar, Phys. Rev., 86, 513 (1952).
10. L.M.Lederman, E.T.Booth et al, Phys. Rev., 83, 685 (1951).

INVESTIGATION OF COSMIC RADIATION AT SEA LEVEL WITH THE AID OF A MASS SPECTROMETER BY MEASURING THE MOMENTA AND IONIZATION OF INDIVIDUAL PARTICLES.

-V.A.Liubimov, G.P.Eliseev & V.K.Kosmachevski

In the present investigation we effected an improvement in the mass spectrometer method of investigating cosmic ray particles, which consisted of combining the mass spectrometer with a system permitting more accurate measurement of the ionizing power of individual particles (by means of a multiple-layer proportional counter). Measurement of the ionizing power notably expanded the experimental potentialities in that it made it possible to extend the investigation of cosmic ray particle spectra into the region of non-ionization stopping of N-component particles in a wide interval of momenta.

Determination of mass spectra on the basis of the momentum and ionization of cosmic ray particles

Determination of the mass of particles on the basis of momentum and range measurements by means of a magnetic mass spectrometer has a serious shortcoming stemming from the fact that in many cases the particles come to rest due to non-ionization losses: on the one hand N-component particles interact with each other and, on the other hand, electrons, which are present in appreciable quantities in cosmic radiation, are stopped due to bremsstralung. In such cases the mass evaluated from the measured momentum and range may differ appreciably from its true value. Obviously this circumstance has greatly complicated the interpretation of individual cases, particularly those of particles having mass values, based on the observed momentum and range, intermediate between the pi-meson and proton masses.

Confirmation that a charged particle came to rest due to purely ionization losses could be obtained from measurement of the ionization produced by the particle. Measurements of the ionizing power of particles by means of a mass spectrometer were attempted in the investigations of Refs. 1 & 2 (by means of a ten-layer, low efficiency counter and a proportional counter) and in the laboratory of Alikhanian[3] (by means of two proportional counters). However, the procedures used in these investigations proved to be too rough to permit identification of individual particles from the ionization produced by them and were found suitable only for determining the ionizing power of large groups of particles having the same velocity.

A considerable improvement in the accuracy of ionization measurements was necessary to permit identification of individual particles from their ionization and momentum. The requisite improvement proved realizable after development of an effective method of processing the experimental results. In Ref. 2 we showed that it is possible, by means of a "universal" method of processing, to determine the most probable value of the ionization to an accuracy of within 10% from four measurements of the ionizing power of monoenergetic particles, made by a proportional counter with an accuracy on the order of 30%.

For the purpose of measuring the ionization we prepared a special four-layer proportional counter which permits obtaining four independent measurements of ionization produced by an individual particle. The ionization of the particle is then determined by the "universal" method from the four measured values. The actual accuracy with which the four-layer counter allows of determining the ionizing power of individual particles was found experimentally by measuring the ionization produced by electrons. The ionization produced by electrons capable of traversing the magnetic field of a mass spectrometer lies on the plateau of the ionization curve and is, consequently, independent of the particle's momentum. In this respect electrons are highly suitable particles for checking

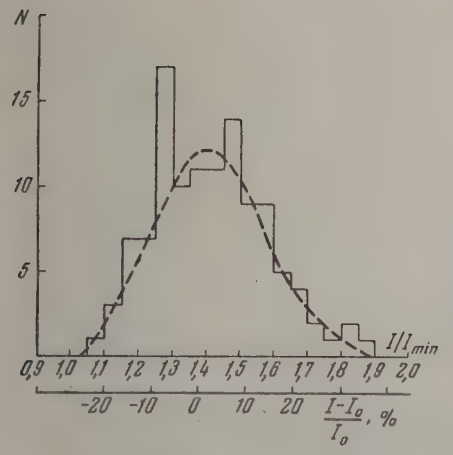

Fig. 1. Distribution of values of ionization produced by fast electrons, according to measurements with a four-layer proportional counter; $I_0 = 1.38\ I_{min}$ = the most probable ionization by a fast electron. Relative error of measurement of ionizing power of a single particle, $\sqrt{\overline{\sigma^2}} = 12\%$.

Table 1

Variation of the error in determining the mass of a charged particle from its momentum and ionization with the magnitude of the ionization.

$\frac{I}{I_{min}}$	8	4	1,9	1,2
$\frac{pc}{\mu c^2}$	0,345	0,570	1,0	1,72
$\frac{1+(pc/\mu c^2)^2}{2}$	0,5	0,66	1,0	2,0
$\frac{\Delta I}{I}$, %	±11,4	±11,4	±11,4	±11,4
$\frac{\Delta M}{M}$, %	±5,7	±7,5	±11,4	±22,8

the operation of the counter. The values of the ionization obtained with the four-layer counter for 115 electrons are shown in the form of a histogram in Fig. 1; the criterion for selection of electrons was the formation of showers in lead absorbers. It was found from these experimental data that the error in determining the ionization of an individual particle by means of the four-layer counter was 10-12%. This accuracy is already sufficient for making mass determinations on the basis of ionization and momentum. Table 1 lists the errors in determining the mass on the basis of the momentum and ionization as a function of the accuracy in measuring the ionization for particles having different ionizing powers. The fourth row lists the average experimental errors obtained in measuring the corresponding ionization of an individual particle by means of the four-layer counter. The errors in determining the mass ensuing from these errors in finding the ionization are listed in row 5. It will be seen that the interval of ionizations in which reasonably accurate mass determination is feasible extends from 1.2 to 10 I_{min}. The latter value represents the upper limit of the ionizations our electronic equipment was capable of measuring.

In order to check this new method of mass determination we undertook an investigation of the mass spectrum of cosmic ray particles at sea level. The study was made on a mass spectrometer permitting measurements of both the momentum and the range of the particles. The four-layer proportional counter was installed in the magnet gap. The mass spectrometer was in general similar to that used in the investigation of Ref. 1, except for certain modifications enhancing the accuracy of measurements of high momenta. We obtained the spectra of particles under 2 and 5 cm Pb, stopping in graphite trapping absorbers under the instrument (ranges — 0.7 to 12 cm C). In addition we studied the spectra under 0.2, 10 and 40 cm Pb* when the particles came to rest in a lead trapping absorber

*Above the lead the apparatus had a cover of only 12 g/cm² of light matter.

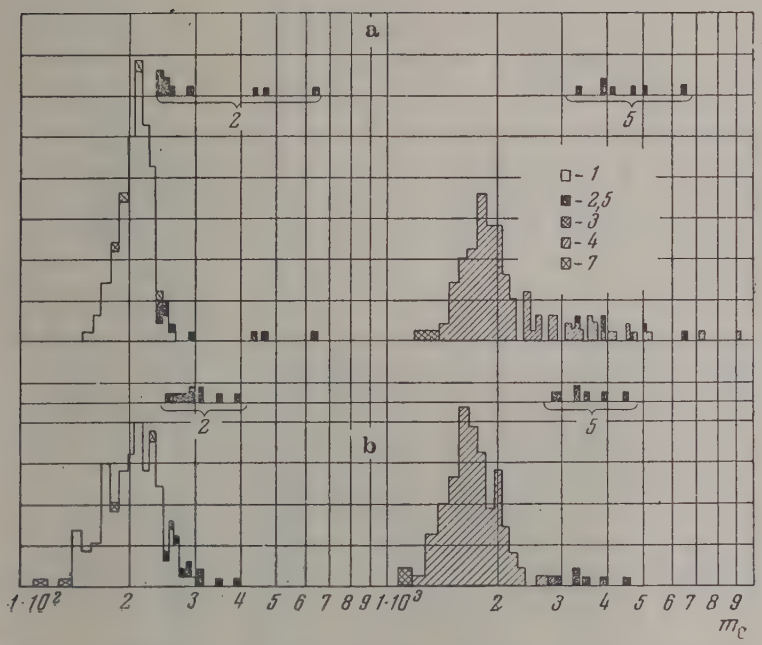

Fig. 2. Mass spectra of particles under 5 cm lead (range interval 0.7–12 cm C). a – Spectrum determined from momentum and range measurements, b – from momentum and ionization measurements; 1) μ mesons, 2) π mesons, 3) particles of about 1000 m_e mass, stopped in graphite absorber due to ionization loss, 4) protons, 5) deuterons, 7) electrons.

(ranges — 0.2 to 6 cm Pb). Measurement of the masses simultaneously by two methods not only permitted comparing the two methods but in most cases also made it possible to identify the particles unambiguously. The mass spectrum obtained under 5 cm Pb of the particles coming to rest in the graphite absorber is shown in Fig. 2. The distribution on the basis of masses determined from range and momentum measurements is shown in the upper part of the figure; in the lower part of the figure we give the distribution of the same particles according to the masses deduced from measurements of the momentum and ionization. It will be seen that the distribution of mesons in mass is close to the Gaussian in both cases. The mean error in determining the mass of an individual μ meson is ± 9% for the momentum–range method and ± 13.8% for the ionization–momentum method.

Particles whose mass is determined by both methods appearing to be greater than 250 m_e were assumed to be π mesons. With this manner of selection, the background of μ mesons among the π mesons was virtually negligible. It will be seen from Fig. 2 that the value of the mass of π mesons determined from the range and momentum is excessively high in a number of cases; this is due to non-ionization slowing down. Thus the π mesons simulate particles of intermediate mass. On the other hand the masses of the same π mesons, as determined from momentum and ionization measurements, form a close group about the average value. The mean error in determining the mass of an individual π meson from the momentum and ionization is about the same as the error in determining the μ meson mass.

The difference in the shape of the distributions characterizing the two methods of mass determination is particularly clear in the case of protons. In the case of determinations on the basis of range and momentum the distribution curve is asymmetric and has an extended "tail" in the region of high mass values, owing to non-ionization stopping. In fact non-ionization stopping makes it virtually impossible to separate protons from deuterons on the basis of momentum and range measurements, whereas in the case of momentum and ionization measurements they are readily separated. The error in determining the mass of individual protons from the momentum and ionization is approximately 14.2%. Four of the particles stopped in the graphite trapping absorber in the experiments under 5 cm lead proved to have masses close to 1000 m_e as determined from the

Table 2

Characterization of particles of intermediate mass obtained in all the experiments.

Trapping filter	Thickness of plate over the apparatus cm Pb	Charge	Momentum, 10^8 ev/c	Ionization, I/I_{min}	Range and behavior	Mass from ionization, m_e	Mass from range, m_e	Probability that the particle is a proton
Graphite, 0.7-12 cm	5*	—	3,87÷4,17	4,7 ±0,52	1,5÷6,7 см C	1400±170	1390÷3160	0
Same	5*	—	1,90÷2,08	8,05±0,9	1,6÷7,3 см C	1130±160	160÷1060	0
Same	5	+	4,17÷4,46	2,79±0,8	9,6÷11,1 см C	1110±100	1285±115	0,0002
Same	5	+	3,87÷4,17	3,5 ±0,35	6,7÷8,2 см C	1250±150	1400±165	0,0004
Same	2	+	4,17÷4,76	2,85±0,2	11,1÷12,6 см C	1190±140	1310±160	0,0001
Lead, 0.2-6 cm	0**	—	3,87	5,7 ±0,62	Star or decay	1740±150	—	0
Same	2*	—	2,50÷2,62	5,45±0,7	Star or decay	1090±120	—	0
Same	10*	+	6,10÷6,55	1,6 ±0,15	4,6÷6,2 см Pb	1075±140	1585±200	0,001
Same	0**	+	1,95÷2,04	2,9 ±0,3	Scattering or decay	575±55	—	—
Same	0**	+	2,82	2,18±0,2	Scattering or decay	565±35	—	—

*Particles generated by the neutral component.
**Apparatus decked only by about 12 g/cm^2 of light matter.

momentum range and ionization. Analogous results were obtained in the other experiments. In the experiments under 2 cm lead a few particles with a mass on the order of 500 m_e came to rest in the graphite absorber; on the basis of ionization these could not be distinguished from electrons, since fast electrons, having an ionization independent of momentum, can "simulate" any mass when this is being determined from the momentum and ionization. The data on particles of intermediate mass obtained in all the experiments, extending over a period of 2297 hours, are summarized in Table 2.

Complete spectra of N-component particles and the ratios between the intensities of different cosmic ray particles at sea level

In making measurements on the basis of momentum and range the masses of particles can be investigated only in a narrow interval of momentum (corresponding to the range interval); moreover inside this interval it is essential to distinguish between cases of ionization and non-ionization stopping. There may obviously be particles impossible to tag by the momentum-range method, i.e., particles whose distribution in momentum starts not from zero momentum but from some value greater than the cut-off momentum corresponding to the given range interval. On the other hand, using the momentum-ionization method we can distinguish between different particles in a virtually unlimited range of momenta. Thus measurement of ionization made it feasible to extend the investigation of particle spectra into the region of non-ionization stopping. Hence identifying the particles from the momentum and ionization and knowing the cross section for the interaction of the particles in the material of the trapping absorber we can readily plot the complete distributions in momentum of the N-component particles. Fig. 3 shows the complete momentum distribution obtained in this manner under 5 cm lead on the mass spectrometer with a graphite trapping absorber. The data on the particles comprised in this spectrum are listed in Table 3. In the first line we list the total number of particles that traversed the apparatus over an operating period of 844 hours; in the second line we show the number of particles that stopped due to ionization loss in the 0.7-12 cm graphite range interval. The third line gives the ratios of the number of different particles to the total number of mu mesons (in %); finally the fourth line shows the ratios of the number of particles coming to rest in the graphite trapping absorbers due to ionization loss to the total number of mu mesons (in %).

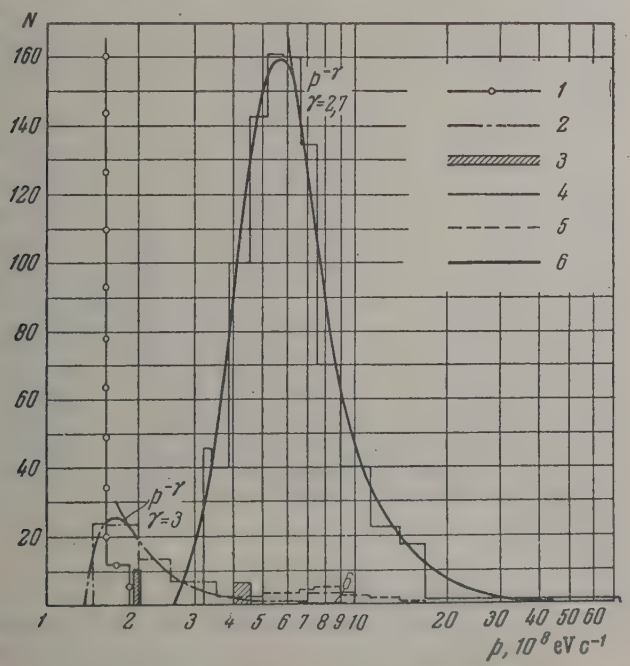

Fig. 3. Distribution in momentum of particles obtained under 5 cm lead (range interval 0.7-12 cm C); 1) μ mesons, 2) π mesons, 3) particles of 1000 m_e mass, 4) protons, 5) deuterons, 6) tritons.

The results of measurements on the mass spectrometer with trapping absorbers of 0.2 to 6 cm Pb under the apparatus obtained under a 10 cm thick layer of lead over

Table 3

Number of particles of different types obtained in experiment under 5 cm lead

Number of particles & ratios	μ mesons	π mesons	K-particles of mass 900 m_e	Particles of mass 1000 m_e	Protons	Deuterons	H^3
Total(N_{tot})	100,000	69	20	4	925	41	2
With range 0.7 R 12 cm C(N_R)	367	10	0	4	388	15	2
$\frac{N_{i\,tot}}{N_{\mu tot}}$, %	100	0.07	0.02	0.004	1	0.04	0.002
$\frac{N_{iR}}{N_{\mu tot}}$, %	0.37	0.01	—	0.004	0.4	0.015	0.002

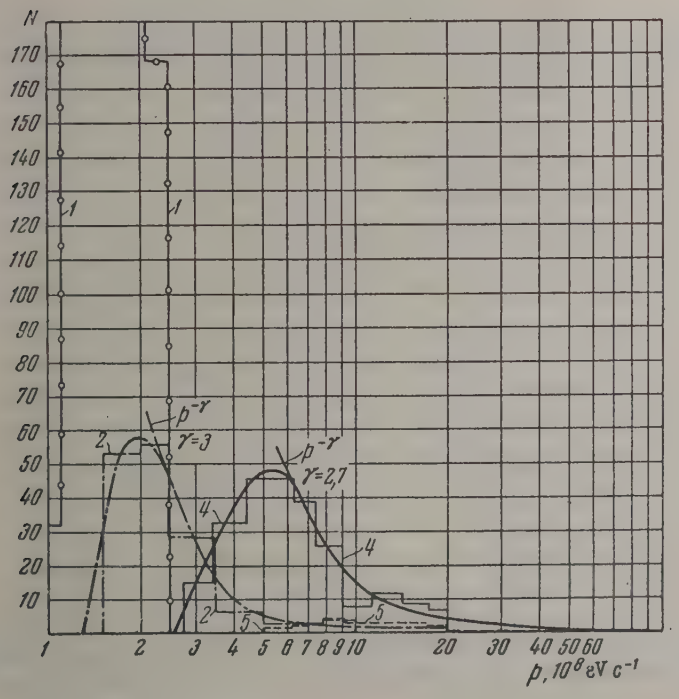

Fig. 4. Distribution in momentum of particles under 10 cm of lead (range interval 0.2–6 cm Pb). Designations same as in Fig.,3.

an effective period of 379 hours are shown in the form of curves in Fig. 4, with the data on the particles summarized, as in the preceding case, in Table 4. The steep slope of the distribution in momentum of pi mesons in the region of small momenta is reflected by the change in the ratios of the number of π and μ mesons stopping due to ionization loss in the lead trapping absorbers as compared with the ratios found with the graphite absorbers (Tables 3 and 4). These results explain why a greater number of pi mesons were found in earlier experiments[4] on a mass spectrometer with lead trapping absorbers as compared with the number determined in our experiments[1] with graphite absorbers.

The intensities of protons, deuterons, pi mesons and electrons obtained in experiments under 0, 2, 5, 10 and 40 cm of lead are shown in Fig. 5.

Table 4

Number of particles of different types obtained in experiment under 10 cm Pb

Number of particles	μ mesons	π mesons	K-particles of mass M_K 900 m_e	Particles of mass M 1000 m_e	Protons	Deuterons	H^3
Total(N_{tot})	45,000	105	16	1	305	34	—
With range 0.2 R 6 cm Pb(N_R)	597	58	—	1	164	10	—
$\frac{N_{i\ tot}}{N_{\mu tot}}$, %	100	0.23	0.03	0.002	0.68	0.075	—
$\frac{N_{iR}}{N_{\mu tot}}$, %	1.3	0.13	—	0.002	0.36	0.022	—

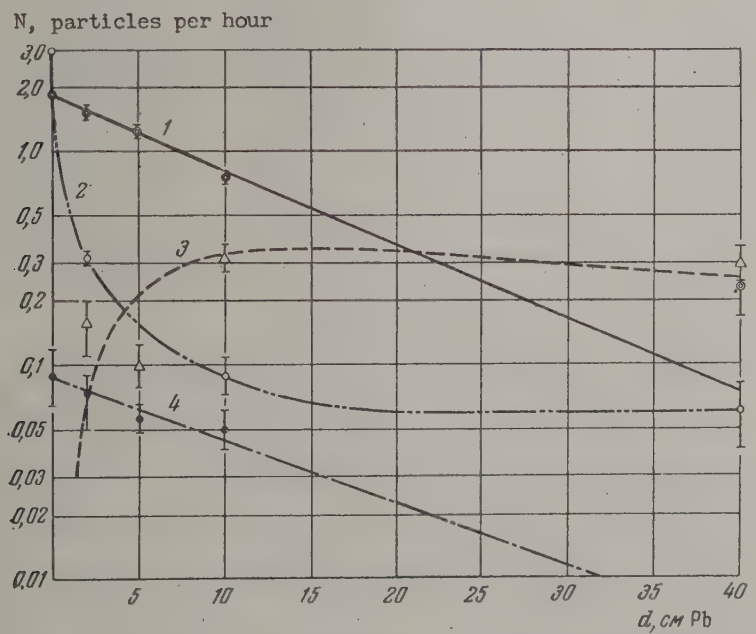

Fig. 5. Intensities of cosmic ray particles observed under lead absorbers of different thickness: 1) protons, 2) electrons (& positrons) 3) π mesons and 4) deuterons.

Pi-meson spectra

In studying the spectra of the N-component particles, the total spectrum of π mesons presents the greatest interest. In general investigations of this spectrum is difficult due to the low intensity of π mesons in cosmic radiation. The spectrum of π mesons in the stratosphere was obtained by means of photographic plates by Camerini et al.[5] The spectrum of π mesons generated by the neutral component was determined at mountain altitudes by Kamalian & Alikhanian.[6]

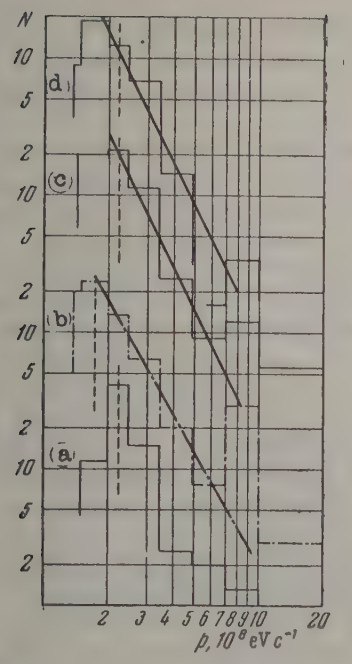

Fig. 6. Pi-meson spectrum under various thicknesses of lead: a) 2 cm, b) 5 cm, c) 10 cm, d) 40 cm; a,c and d obtained with trapping absorbers of lead (0.2-6 cm Pb), b obtained with graphite trapping absorbers (0.7-12 cm C).

In order to distinguish the π mesons from protons these investigators selected only particles with a negative charge. Although the intensity of mesons at sea level is much lower than at mountain altitudes, we were able to plot their spectrum since measurement of the ionization made it possible to utilize all the particles coming to rest in the trapping absorber. All the π mesons could be distinguished from μ mesons on the basis of the ionization, range and momentum, up to the cut-off momentum corresponding to the maximum ionization range in the trapping absorber; hence the deduced spectrum is the complete spectrum of π mesons having momenta under the cut-off value. In the case of particles having momenta exceeding the cut-off value, stopping in the trapping absorbers will occur only as a result of nuclear interactions and, consequently, in plotting the complete spectrum it is necessary to multiply the number of cases of non-ionization stopping by a coefficient, dependent upon the thickness of the trapping absorbers and the cross section for the interaction of π mesons with the material of the absorbers. Up to momenta of 10^9 ev/c, π mesons (and other N-component particles) are easily distinguished from protons by the ionization; on the other hand, μ mesons having such momenta cannot come to rest in the trapping absorbers in view of their nuclear inactivity. In the region of momenta $> 10^9$ ev/c, where the ionization produced by protons is weak, it was necessary to use only particles of negative charge. The complete π-meson spectra under 2, 5, 10 and 40 cm lead are plotted in Fig. 6. The total spectrum of π mesons under 5 cm lead (spectrum b) was obtained with graphite trapping absorbers (0.7-12 cm C) in experiments extending over a period of 844 hours. The sharp decrease in the region of small momenta can be explained by the fact that in apparatus having an appreciable length and a small solid angle (i.e., a mass spectrometer) primarily particles originating in stars with a narrow angular divergence cone are recorded, while most of the soft π mesons which are ejected from stars at large angles escape detection. The maximum of the spectrum lies in the region of particles stopped as a result of non-ionization losses and corresponds to a momentum of about $1.9 \cdot 10^8$ ev/c. Up to $7 \cdot 10^8$ ev/c the spectrum is satisfactorily described by a power function and when plotted in logarithmic scale fits a straight line corresponding to an exponent $\gamma = 3$. This exponent for our π-meson spectrum is in agreement with the exponent for the spectrum of π mesons generated by the neutral component, found by Kamalian and Alikhanian.[6] In our spectrum there is an anomalous increase in the number of particles in the $(7-12) \cdot 10^8$ ev/c momentum interval, which appreciably exceeds the statistical error. In this momentum interval we observed seven particles: 2 negative and 5 positive. It is noteworthy that the ionization of these particles on the average equals $(1.14 \pm 0.06)\ I_{min}$, while the ionization of π mesons should be on the order of $1.02\ I_{min}$. The ionization of protons in this momentum interval is still fairly large (about $2-2.5\ I_{min}$) and the part of the anomaly in the meson spectrum, due to positive particles, can be attributed to protons exhibiting ionization straggling. Nor can the anomaly be attributed to electrons, in-

asmuch as the ionization of electrons is somewhat higher (1.4 I_{min}), while the number of electrons in this momentum interval is virtually negligible. The mass of the particles responsible for this anomaly in the π-meson spectrum, as computed from the momentum and ionization proved to be 880 ± 80 m_e. The ionization curve in the 1-1.4 ionization interval is two-valued, hence formally we can ascribe a second mass value to these particles, namely, 100 ± 50 m_e. We shall hereinafter designate these particles, responsible for the anomaly in the pi-meson spectrum, as K-particles.

The spectra under 2, 10 and 40 cm lead were obtained with the set-up in which the graphite trapping absorber was replaced by lead (0.2-6 cm Pb). On the one hand this increased the probability of cases of non-ionization stopping and, on the other, enhanced the identification of electrons on the basis of shower formation in the lead. The cut-off values of the momentum, corresponding to the maximum ionization range of π mesons in the trapping absorbers are indicated by the vertical dash-lines in Fig. 6. The spectra obtained under 10 and 40 cm lead (spectra c and d) approximately duplicate the shape of the π-meson spectrum obtained under 5 cm lead with the graphite trapping absorber. It is interesting to note that the peaks of the spectra coincide, although in the experiment under 5 cm lead with graphite absorbers this maximum is dependent on non-ionization stopping, whereas in the experiments with the lead trapping absorbers the peaks lie below the momentum cut-off corresponding to the maximum range. The spectrum obtained under 2 cm lead differs markedly from the spectra under greater thicknesses of lead and, presumably, reflects transition effects.

Of particular interest is the fact that an anomaly in the number of particles is also discernible in the $(7\text{-}12)\cdot 10^8$ ev/c momentum interval in the π-meson spectra obtained under 10 cm lead. These particles, too, are characterized by a higher average ionization than that of π mesons. Seven such particles were recorded over a period of 379 hours of measurement under 10 cm lead.

K-particles

Let us review the experimental data characterizing the properties of the particles forming the anomalies in the π-meson spectra and observed in the experiments under 5 cm lead (trapping absorber 0.7-12 cm C) and under 10 cm lead (trapping absorber 0.2-6 cm Pb). In all we detected 14 such particles: 8 positive and 6 negative.

1. The ionization averaged over the anomaly-producing particles in the $(7\text{-}12)\cdot 10^8$ ev/c momentum interval proved to be $I_K = (1.14 \pm 0.04)\ I_{min}$ [$I_+ = (1.15 \pm 0.06)\ I_{min}$; $I_- = (1.13 \pm 0.06)\ I_{min}$], whereas the ionization of pi mesons in this interval should be $I = 1.02\ I_{min}$. In order to verify our calibration, we computed the ionization for π mesons in the neighboring $(3.5\text{-}6)\cdot 10^8$ ev/c momentum interval, which happens to correspond to the minimal ionization of π mesons. The value computed on the basis of 12 particles proved to be in excellent agreement with the expected $I_\pi = (1.00 \pm 0.03) I_{min}$. Thus there can be no doubt that the ionization of the particles forming the anomaly is significantly higher than of π mesons.

2. The average mass of a K-particle, computed on the basis of the momentum and ionization for the entire group of these particles, proved to be $(880 \pm 40)\ m_e$.

It must be noted that this value may be an under-estimate since the $(7\text{-}12)\cdot 10^8$ ev/c momentum interval in which all the particles were taken may comprise a number of π mesons with unit ionization; in all probability there are few such π mesons however.

3. All the K-particles came to rest in the trapping absorbers as a result of non-ionization losses, which serves as experimental evidence of their ability to interact "in flight" with nuclei of the absorber materials with a cross section commensurate with the geometric.

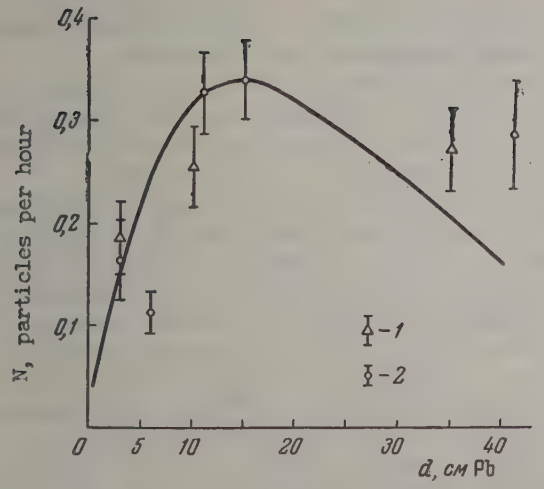

Fig. 7. Transition curve for π mesons: 1) experimental points from Ref. 10, 2) our experimental points. Curve taken from Ref. 11.

4. All the K-particles entered the apparatus almost vertically. The angular divergence of the K-particles did not exceed ±6° whereas the solid angle of the apparatus is much greater (± 18-20°). This is direct evidence that the K-particles originate in stars produced by particles of very high energy.

5. Of the 14 K-particles observed in our experiments, only one occurred in a star initiated by a neutral component particle. This serves to explain why no anomaly in the number of particles was observed in the (7-12)·10^8 ev/c momentum region in the spectrum of π mesons generated by the neutral component, obtained in the experiments of Kamalian and Alikhanian.[6]

6. As may be seen from the spectrum, the number of K-particles is several times greater than the number of π mesons in the momentum interval in which the K-particles appear. The number of K-particles in relation to the total number of π mesons amounts to about 20%. We note that Daniel et al,[7] using photographic plates, observed the yield of K-mesons and π mesons from stars initiated by protons of different energies. According to their data, in the case of stars formed by 10-50 Bev protons, the number of K-mesons relative to the number of π mesons also amounts to 20%; the percentage falls off rapidly for stars initiated by particles of lower energies. These data also indicate that there exists a K-meson production threshold and are in full agreement with the results of our experiments.

Transition effect for pi mesons

The total number of π mesons as a function of the thickness of absorber above the apparatus is shown in the form of a transition curve in Fig. 7. It will be seen that there appears to be a maximum in the region corresponding to a 2-3 cm thickness of lead over the apparatus; such maxima have already been noted by Shapiro et al[8] and Schopper et al[9]. There may be a connection between the unusual shape of the π meson spectrum under 2 cm lead and the existence of a maximum in the transition curve in the same region. The main maximum of the transition curve corresponds to an absorber thickness of 10-15 cm lead which is in agreement with experimental results obtained by Kamalian.[10] Beyond this point the curve falls off, but apparently more slowly than follows from theory.[11]

Conclusions

Let us summarize the conclusions that may be drawn from analysis of the experimental data obtained in all the mass spectrometer experiments involving the measurements of ionization of individual particles.

1. Measurement of the ionization together with the momentum and range of the particles made it possible to separate π mesons from μ mesons coming to rest as a result of ionization losses and thereby substantiate the results of previous investigations,[1, 4] in which only the momenta and ranges were measured.

2. Measurement of ionization made it possible to distinguish protons,

deuterons and tritons, which was impossible on the basis of only momentum and range determinations owing to the non-ionization stopping of the protons.

3. Ionization measurements confirmed the existence and the quantitative data (obtained in the investigation of Ref. 1 on the basis of momentum and range measurements) regarding particles of about 1000 m_e mass coming to rest in the trapping absorbers due to ionization losses.

4. Measurement of ionization appreciably extended the experimental potentialities inasmuch as it made it possible to investigate cases of non-ionization stopping of N-component particles. Hence on the basis of cases of ionization and non-ionization stopping we were able to plot the complete spectra of such N-component particles as protons, deuterons and tritons and establish quantitative relationships between the numbers of cosmic ray particles at sea level under lead absorbers of different thicknesses.

5. Measurement of ionization made it possible to study the complete π-meson spectra and plot the transition curve for π mesons.

6. The results of ionization measurements helped explain the anomaly observed in the π-meson spectrum. It is apparently due to the presence of a group of N-component particles having a mass on the order of 900 m_e, coming to rest in the absorbers as the result of non-ionization losses.

In conclusion the authors wish to express their gratitude to A.I.Alikhanov who guided the investigation and to thank V.P.Kanavets and Z.F.Garapov who participated in processing the results.

Academy of Sciences of the USSR

References

1. A.I.Alikhanov & G.P.Eliseev, Zhur. eksp. i teor. fiz., 25, 368 (1953).
2. G.P.Eliseev, V.K.Kosmachevski & V.A.Liubimov, Doklady AN SSSR, 90, 995 (1953).
3. A.I.Alikhanian & V.M.Kharitonov, Doklady AN SSSR, 85, 295 (1952); 92, 1125 (1953).
4. A.I.Alikhanov & G.P.Eliseev, Zhur. eksp. i teor. fiz., 21, 1009 (1951).
5. U.Camerini, P.H.Fowler, W.O.Lock & H.Muirhead, Phil.Mag., 41, 413 (1950).
6. V.Sh.Kamalian & A.I.Alikhanian, Doklady AN SSSR, 97, 425 (1945).
7. R.R.Daniel, J.H.Davies, J.H.Mulvey & D.H.Perkins, Phil.Mag., 43, 753 (1952)
8. M.M.Shapiro, B.Stiller, M.Birnbaum & F.W.O'Dell, Phys.Rev.,83, 455 (1951).
9. E.Schopper, K.H.Hocker & G.Kuhn, Phys.Rev., 82, 444 (1951).
10. V.Sh.Kamalian, Doklady AN SSSR, 95, 1169 (1954).
11. G.Saakian, Izv. AN Armenian SSR, 6, 65 (1953).

* * * * * * *

ANOMALOUS SCATTERING OF MU MESONS IN GRAPHITE

-A.I.Alikhanov & G.P.Eliseev

In studying the mass spectrum of cosmic ray particles at sea level we encountered the effect of abnormally great scattering of μ mesons in the graphite trapping absorbers of the mass spectrometer; this scattering is appreciably greater than might be expected on the basis of coulombic interaction of μ mesons with nuclei. Similar anomalies in the scattering of μ mesons have been observed by a number of investigators in lead and in photographic emulsions.

Let us review the results obtained by different observers.

In their experiments Whittemore and Shutt[1] used two cloud chambers with a magnetic field applied in the gap between the two chambers. A lead plate 5 cm thick was mounted horizontally in the center of the lower chamber. The apparatus recorded cases of scattering of μ mesons in the 0.3-3.1 Bev/c interval. It was found that 0.15% of the mesons were scattered in accordance with the scattering theory of Olbert[2] (on a nucleus of finite dimensions). The total number of cases of scattering, however, amounted to 2.65 % relative to the primary flux; thus an additional 2.5% of the μ mesons, over and above the number predicted by theory, were scattered in the absorber. No assymetry connected with charge polarity was observed.

George, Redding and Trent[3] used a cloud chamber underground at a depth corresponding to 60 m.w.e. The chamber contained two lead plates each 2 cm thick. The observers determined the scattering of μ mesons in these plates. In two series of experiments, additional lead absorbers decked with counters were installed above and below the chamber. The absorbers under the chamber permitted separating the softer component from the general μ-meson flux. In comparing the number of observed cases of μ-meson scattering to different angles with the theory for scattering from a point nucleus it was found that beginning with an angle of 6^0 there was an appreciable excess of the actually scattered mesons over the theoretical value. This excess was particularly great at angles over 15^0. The anomalous scattering cross section (i.e., the cross section corresponding to the excess scatterings as compared to theory) averaged over the entire spectrum was found to be $2 \cdot 10^{-28}$ cm^2/nucleon.

In the 100-300 Mev interval, where the intensity of the flux amounted to 5% of the total flux intensity, the anomalous scattering cross section attained a value of $4 \cdot 10^{-27}$ cm^2/nucleon. Under the experimental conditions the number of π mesons and protons comprised less than 0.05% of the total number of particles traversing the apparatus. Taking account of the nuclear interactions of this minor admixture of π mesons and protons would reduce the effect by approximately 2% of its observed value. The absence of multiplication and cases of scattering to very large engles indicated that there were virtually no electrons among the scattered particles.

The experiments of Leontic and Wolfendale were carried out at sea level.[4] They separated the μ mesons by means of a counter telescope with a 1 m thickness of lead between the counter trays. A cloud chamber containing six 2 cm thick (each) lead plates was located under the telescope. Cases of scattering of μ mesons having momenta from 285 Mev/c were recorded. Comparison of experimental results with the theory for scattering on a nucleus of finite dimensions yielded a value of $(1.5 \pm 0.7) \cdot 10^{-28}$ cm^2/nucleon for the cross section for anomalous scattering to angles over 10^0. With the minimum scattering angle increased to 20^0 the anomalous scattering cross section fell off by about one order of magnitude.

McDiarmid[5] worked with a cloud chamber underground at a depth of 26 m.w.e. There was a 10 cm thick layer of lead above the chamber; in the chamber were six 2 cm thick lead plates. Measuring the small coulomb scattering angles and determining the momenta therefrom McDiarmid sub-divided the total meson flux into three energy groups. In addition to the small angles appreciably greater angles were observed in each group. The investigator found that in the first group (momenta 200-600 Mev/c) the scattering is in agreement with the theory of scattering from a point nucleus (the theoretical distribution of Molière[6]). The theoretical scattering curve after Olbert (on a nucleus on finite dimensions) for the given group almost coincides with the Molière distribution curve. In the second group (500-1700 Mev/c) the experimental points fit Molière's curve which falls appreciably higher than the curve for a nucleus of finite dimensions

(Olbert). In the third group (meson momenta above 1000 Mev/c) the experimental points at scattering angles of 4-5° fall on the Molière curve, while at angles near 7° they fall below the Molière curve but still appreciably above the curve for scattering on a nucleus of finite dimensions. McDiarmid comes to the conclusion that at energies corresponding to momenta of 200-600 Mev/c the anomalous scattering effect is absent but is apparent at higher energies. His results are in general agreement with the results of Whittemore & Shutt and Leontic & Wolfendale. McDiarmid concludes that further experiments, particularly at high energies, are necessary. In view of the absence of a precise nuclear model, McDiarmid, unlike most other investigators, feels it premature to attempt explaining the anomaly in the scattering of μ mesons by recourse non-electric short-range forces.

Kannangara and Shrikantia[7] investigated the scattering of μ mesons in G-5 nuclear emulsions under 60 m.w.e. of ground. The scattering was observed on individual emulsion grains and the effect of multiple scattering thereby excluded. In all they recorded seven cases of scattering to angles greater than 7°. The number of such deflections to be expected on the basis of the point nucleus model is 10; the number based on the finite dimensions model is 3.7. In the 100-600 Mev/c range in which about 1/15th of the total number of mesons recorded in the plates is comprised, the investigators obtained a cross section for scattering to angles over 7° of $(3.4 \pm 1.5) \cdot 10^{-27}$ cm^2/nucleon, while their cross section for anomalous scattering is $(1.5 \pm 1) \cdot 10^{-27}$ cm^2/nucleon. The last named authors also cite unpublished data of Walker on the scattering of μ mesons in graphite. Walker beamed mesons of over 1.5 Bev through a 1 inch thick graphite plate and among 21,500 particles traversing the plate found one case of scattering through an angle greater than 5°. From this he concluded that the anomalous scattering cross section in carbon for 1.5 Bev μ mesons is less than $2 \cdot 10^{-29}$ cm^2/nucleon.

Rochester and Wolfendale[8] reviewed and revised the data obtained by Kannangara and Shrikantia[7] on the basis of later findings on the spectrum of μ mesons underground. They found that the correction to the spectrum, based on a more accurate nuclear model, went far to compensate the anomalous scattering effect at low energies. However the anomaly in μ-meson scattering for the entire spectrum turned out to be somewhat greater. Rochester and Wolfendale conclude that in view of the shortcomings of theory and the lack of accurate computations there is as yet no sufficient justification for attributing the anomalous scattering to the influence to non-electric short range interaction of μ mesons with nuclei. It may be noted however that none of the authors mentioned doubts the actual existence of the anomaly.

Investigation of μ-meson scattering in graphite

We now turn to a description of our experiments on the scattering of μ mesons in graphite.

Measuring the mass of cosmic ray particles by means of a mass spectrometer, we separated a large group of μ mesons and measured the angles through which they are scattered in passing through the graphite plates of a trapping absorber. We carried out two series of measurements: for soft μ mesons (i.e., the mesons coming to rest in the trapping absorber) and for hard μ mesons (i.e., the mesons passing through the absorber). In each case the maximum and the minimum angles were measured. In our calculations we used the minimum angle for the most part; in a few cases we used the appropriately averaged angular values.

Series I

In 790 cases of the passage of μ mesons through the absorber we recorded 78 cases of scattering through plane angles in the 10-32° interval. From among these we selected only the cases when the meson traversing the telescope and

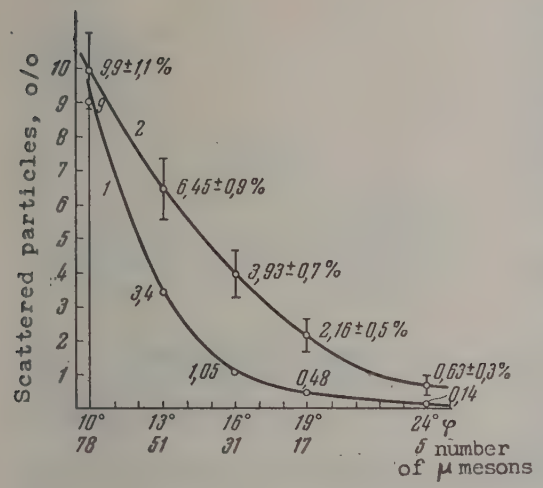

Fig. 1. Anomalous scattering of μ mesons in graphite. Curve 1 is drawn through computed values; curve 2 through experimental ones.

entering the trapping absorber (consisting of graphite plates inter-layered with thin-wall aluminum counters) exhibited a break in its path recorded by at least two rows of counters. A further condition was that after the stopping and decay of the meson there would be a clearly discernible trace of the decay electron; in cases when the decay electron moved downward, the decay event was additionally recorded by the electronic circuit according to the delay in the discharge of the counters in the lower rows.

We computed the probability of meson-scattering due to coulombic interaction with carbon nuclei. The expected (calculated) and actually recorded numbers of cases of scattering are shown in Fig. 1. Of the 78 scattered mesons 45 were positive and 33 negative. The decay of 24 mesons was recorded by the electronic circuit as described above; in the remaining 54 cases there was a clearly discernible decay electron track. The ratio 24/78 = 31% is the usual value determined by the geometry of our trapping absorber assembly. For plane scattering angles over 16° the anomalous scattering cross section (background subtracted) $\sigma_{an} = 6.65 \cdot 10^{-26}$ cm^2/nucleus = $(5.5 \pm 1.4) \cdot 10^{-27}$ cm^2/nucleon. The mean kinetic energy at which the scattering took place was 47 Mev; the mean momentum $1.1 \cdot 10^8$ ev/c.

Identification of particles. Electrons and all particles heavier than μ mesons were wholly excluded. The small number of π mesons, that might be comprised in the investigated μ meson mass interval, could not yield a contribution to the μ-meson scattering (due to nuclear interaction) in excess of 0.1 case per the 78 recorded.

Series II

The scattering of high energy μ mesons was investigated in experiments with a 50 cm thick layer of lead above the apparatus. The investigated μ mesons were divided into three energy groups. The first group comprised μ mesons having momenta in the $(1.95\text{–}3) \cdot 10^8$ ev/c interval; the mean kinetic energy of the particles in this group equalled $1.7 \cdot 10^8$ ev. The second group comprised μ mesons with momenta $(3\text{–}4.5) \cdot 10^8$ ev/c and a mean energy $2.8 \cdot 10^8$ ev. Mu mesons with momenta $(4.5\text{–}8.2) \cdot 10^8$ ev/c characterized by a mean energy of $5.4 \cdot 10^8$ ev were classed in the third group.

Identification of particles. There were virtually no electrons in any of the three μ-meson groups. According to our experimental data π mesons having momenta over $2 \cdot 10^8$ ev/c have an intensity under 0.1% relative to the μ-meson flux under 50 cm of lead. Hence there were approximately 3 π mesons among the 3192 investigated μ mesons. Allowing for the probability of nuclear scattering of π mesons in the trapping absorber we find that the contribution of π mesons could at most amount to 0.2 cases of the 24 recorded cases of scattering. Protons with momenta under $5.5 \cdot 10^8$ ev/c were wholly excluded (stopped in the lead absorber). Protons in the $(5.5\text{–}8.2) \cdot 10^8$ ev/c momentum interval (partially overlapping the third meson group interval) could be present in the amount of about 7; taking account of the probability of nuclear scattering of protons in the trapping absorbers we find that the contribution of protons to scattering could

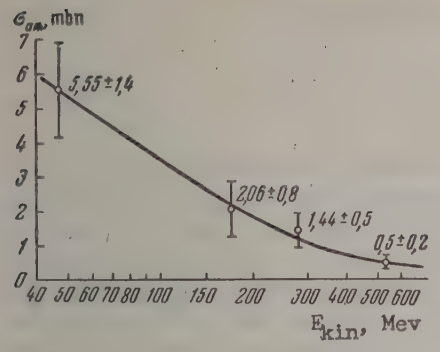

Fig. 2. Energy dependence of cross section for anomalous μ-meson scattering.

amount to not more than 0.5 cases per 8. In addition the ionization of the particles entering the telescope was measured by means of a 10 layer, low efficiency counter. On the basis of the indications of this counter one positive particle with $I/I_{min} > 1.7$ was excluded from the cases of scattering in the third group.

The cross sections for anomalous μ-meson scattering in all the investigated energy intervals are shown in Fig. 2.

For the first μ meson group the computed number of cases of scattering due to coulombic interaction (background) amounted to 0.41% relative to the total number of mesons traversing the apparatus, while the number of observed cases of scattering amounted to 1.36%; whence the anomalous scattering cross section

$$\sigma_{an} = (2.1 \pm 0.8) \cdot 10^{-27} \text{ cm}^2/\text{nucleon}.$$

In the second group the background amounted to 0.40%; the observed effect 1.12%. Hence

$$\sigma_{an} = (1.44 \pm 0.5) \cdot 10^{-27} \text{ cm}^2/\text{nucleon}.$$

In the third group the background amounted to 0.14%, the observed effect 0.44%. Hence

$$\sigma_{an} = (0.5 \pm 0.2) \cdot 10^{-27} \text{ cm}^2/\text{nucleon}.$$

It follows from the above data that there is a definite anomaly in the scattering of μ mesons. It should be noted however that these data were obtained as a by-product of experiments concerned with the determination of mass spectra, rather than from experiments designed primarily for investigating scattering. Further experimental and theoretical investigations are necessary in order to elucidate the nature of the anomaly and determine whether it is due to non-electric interaction of μ mesons with nuclei or can be explained through better theoretical interpretation of coulombic interaction.

Academy of Sciences of the USSR.

References

1. W.L.Whittemore, & R.P.Shutt, Phys. Rev., 88, 1312, (1952).
2. S.Olbert, Phys. Rev., 87, 319 (1952).
3. E.P.George, J.L.Redding, & P.T.Trent, Proc. Phys. Soc., A66, 533 (1953).
4. B.Leontic, A.W.Wolfendale, Phil. Mag., 44, 1101 (1953).
5. J.B.McDiarmid, Phil. Mag., 45, 933 (1954).
6. G.Moliere, ZS. Naturforsch., 2a, 133 (1947); 3a, 78 (1948).
7. M.L.T.Kannangara & G.S.Shrikantia, Phil. Mag., 44, 1091 (1953).
8. G.D.Rochester & A.W.Wolfendale, Phil. Mag., 45, 980 (1954).

SCATTERING OF SLOW MU MESONS IN COPPER

- A.I.Alikhanian and V.G.Kirillov-Ugriumov

1. Introduction

It is known that μ mesons that have fallen into atomic orbits may remain in the field of nuclear forces for a prolonged period without interacting with nucleons. This indicates the absence of noticeable non-coulomb forces between very slow μ mesons and nucleons. On the other hand, investigations of scattering of μ mesons with momenta above 100 Mev/c, as reported by many authors, do not agree with the angular distribution to be expected if the interactions between μ mesons and nuclei are assumed to be purely coulombic. The difference between the observed angular distribution of μ mesons and the theoretical distribution for coulomb scattering from a finite nucleus is now termed anomalous scattering. Considerable experimental difficulties have so far proved an obstacle to determining the actual magnitude of anomalous scattering.

Kannangara[1], Leontic[2], McDiarmid[3] and others think that at energies in the region of several hundred Mev the observed angular distribution corresponds to the theoretical curves for the case of coulomb scattering from a nucleus whose charge is concentrated at a point or, more exactly, in a volume significantly smaller than the volume of a sphere of radius $R = 1.2 \cdot 10^{-13} A^{1/3}$cm, where A is the mass number. George, Reading and Trent[4] investigated the scattering of 100-300 Mev μ mesons. Their distribution curve in the region of large scattering angles lies higher than for the expected distribution for scattering from a point nucleus.

Attempts have been made to estimate the contribution to anomalous scattering made by incoherent scattering and the interaction of the magnetic moments of the nucleons and the μ mesons, and to evaluate the angular distributions deriving from various models of the charge distribution in the nucleus.[5, 6 & 9] These estimates yielded values smaller than the observed magnitude of the anomalous scattering. In spite of these results a number of authors continue to hold the view that anomalous scattering can be successfully explained with the aid of a better nuclear model and more refined experimental data on μ-meson scattering. Other authors (George, Leontic, Kannangara) are inclined to ascribe forces of non-coulombic character to fast μ mesons.

We studied the scattering of μ mesons in the $(0.8\text{-}1.3) \cdot 10^8$ ev/c momentum interval in thin layers of copper. This momentum interval corresponds to the lower bound of the momentum range in which anomalous scattering has been observed. The use of thin copper plates reduces background from coulomb scattering to large angles.

2. Apparatus

Our investigation of μ-meson scattering was carried out on Mt. Aragats (3200 meters above sea level) with the aid of a magnetic mass spectrometer and a cloud chamber.[7] The apparatus is shown in Fig. 1. A hodoscopic system of 10 rows of counters was arranged in a uniform magnetic field of 6500 oersted. Each of the counters was connected through an electronic circuit to a neon tube on the signal board. From the lighting-up of the neon tubes it was possible to establish up to five points defining the projections of the particle trajectories in both the plane parallel and the plane perpendicular to the magnetic field. The multiple plate cloud chamber was mounted flush against the pole pieces of the magnet. A row of counters, connected in anticoincidence with three trays of the telescope counters, was located under the cloud chamber. The chamber was rectangular in shape and had a volume of 36 liters and expansion cylinders at both ends. Inside the chamber were two 5 mm and seven 2 mm thick copper plates.

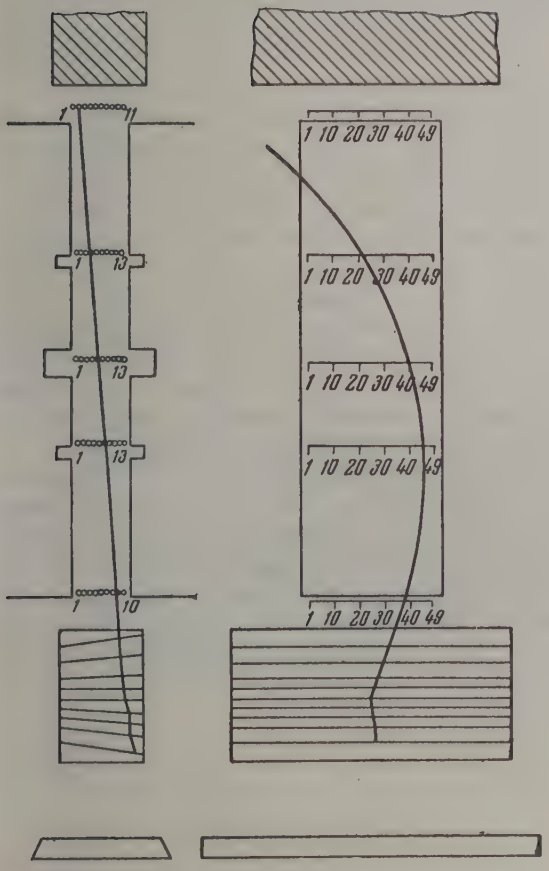

Fig. 1. Diagram of the apparatus. Only 5 of the 10 rows of counters are shown in each view.

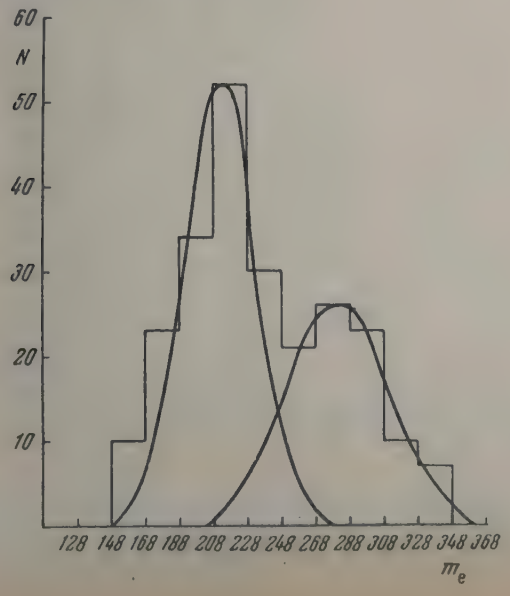

Fig. 2. Mass spectrum of particles stopped in the base of the chamber.

For analysis of μ-meson scattering we also used the results of measurements made during 1952-1953 in which the same mass-spectrometer was employed in conjunction with a smaller (250 x 400 x 100 mm) cloud chamber, equipped with 3 mm thick copper plates. Accordingly, in this paper we include data on μ-meson scattering in copper plates of 5, 3 and 2 mm thickness. Over the entire apparatus there was a layer of lead 6 cm thick, which shielded the mass-spectrometer from electrons.

3. Identification of particles and momentum and angle measurements

The particle mass determinations in the mass-spectrometer were made on the basis of momentum and range. The momentum was evaluated from the curvature of the trajectory in the magnetic field, while the range was determined by the number of plates in the chamber the particle traversed. Gross errors in determining the mass were obviated by strict adherence to the following three conditions:

1) All counters triggered incident to the passage of a given particle had to be on the circular arc of the trajectory projection perpendicular to the magnetic field and on a straight line in the plane normal to the field.

2) The two sections of the trajectory in the telescope and in the cloud chamber had to match (the location of the trajectory in the chamber was determined stereoscopically).

3) Where a particle stopped in the chamber there had to be a discernible thickening of the track near the end of its path.

Exact determinations of mass, on the basis of which the mass spectrum was constructed, were made only for particles that came to rest inside the Wilson chamber. For our purposes it was also possible to use those cases in which the particle stopped in the base of the chamber, for in such cases non-ionization stopping could not ef-

fect accuracy of the μ-meson mass determinations, while the somewhat greater uncertainty in the determined range still allowed not only separation of mesons from protons and particles of intermediate energies, but of π and μ mesons from each other.

The experimentally obtained mass distribution in the 150 to 400 m_e region for the particles stopped in the base of the chamber is closely approximated by two Gaussian curves with a half-width corresponding to a root mean square error of 11%. If we assume that all particles for which the measured value of the mass falls below 240 m_e are μ mesons, while those whose mass value is larger are π mesons, then the mean value for the particles of the μ-meson group is 207 m_e, while that of the π-meson group comes to 294 m_e. The spectrum of the particles that stopped in the base of the chamber is shown in Fig. 2. Analysis of this spectrum shows that no more than 15% of the π mesons should fall into the μ-meson group. Fig. 3 shows the mass spectrum pertaining to the cases of stopping inside the chamber, where the admixture is even less. Both spectra (Figs. 2 and 3) are given without correction for the transmission factor of the apparatus.

For comparing the observed angle of meson scattering with its expected value for coulombic interaction, it is necessary to know the momentum of the meson at the point of scattering. If the mass of the particle is known, this momentum can be determined from the residual range (after scattering). The accuracy in measuring the residual momentum depends on the accuracy in determining the residual range. In plotting the angular distribution we used only the angles of μ-meson scattering obtaining in cases of scattering that occurred in a plate at least two plates ahead of the point of stopping.

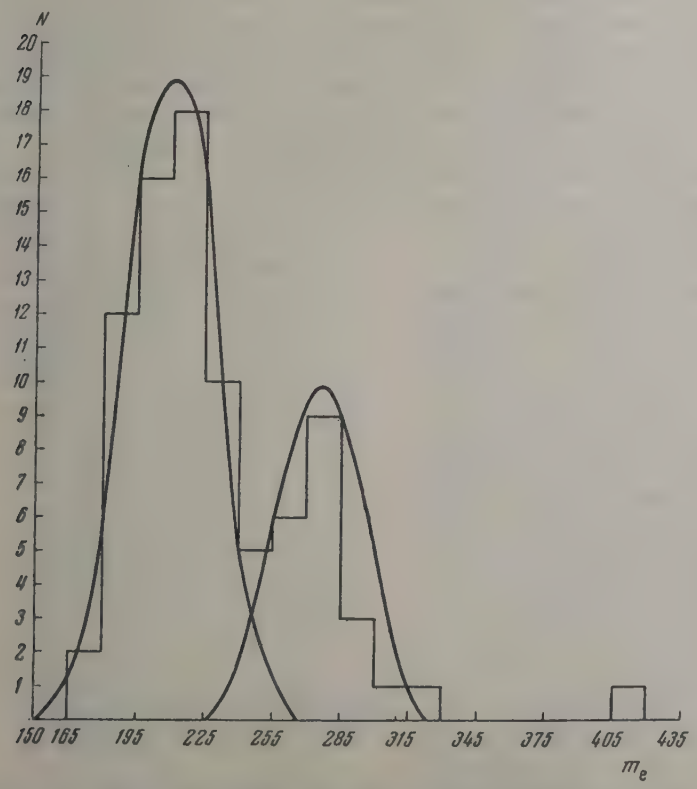

Fig. 3. Mass spectrum of the particles stopping in the plates inside the cloud chamber.

Evaluation of the residual range of particles that came to rest in the thin plates inside the cloud chamber differed from that outlined above only in that the particle was assumed to have stopped at the center of the plate at which the track ended. This makes it possible to determine the residual range with an error of less than 12%.

The procedure for determining the momentum of particles stopping in the base of the cloud chamber was the following. The value of the mass for each particle that fell into the μ-meson group was taken equal to 207 m_e. It was assumed that the deviation of the measured value of the mass from the true mass was due to inaccuracy in measurement of the range (the thickness of the chamber base was 12 mm of copper). Then, from the initial momentum measured in the mass spectrometer and the assumed "true" mass, we computed the

"true" range. In the overwhelming number of cases the "true" range ended in the base of the chamber. The residual range was computed from the center of the plate where the scattering took place to the "true" stopping point of the particle, taking into account the angle of the trajectory relative to the surface of the plate. The difference between the measured and the "true" range, associated with the "by-pass factor", was evaluated by means of Pomeranchuk's equation, and turned out to be about 3.5%.

Accuracy in angle measurements was limited mainly by the usual distortions associated with operation of a cloud chamber (diffuseness of tracks, turbulences, etc.). Since the distances between the plates were relatively small (22 mm), the probable error in measuring the angles due to the aforementioned factors is estimated to be $\pm 0.8^\circ$. It is important to note that since the error is virtually constant over the entire angular range, the relative error decreases with increasing angle.

4. Results of measurements

Altogether 1100 cases of μ-meson scattering were studied in the three series of experiments with 2, 3 and 5 mm thick copper plates. The total range in copper of the μ mesons in the $(0.8\text{–}1.3)\cdot 10^8$ ev/c momentum interval was about 3.5 meters. The number of expected cases of μ-meson scattering to a given angle due to coulomb interactions is strongly dependent on the meson momentum. To permit a better comparison of the experimental and theoretical data, the investigated momentum interval was divided into two parts: $(0.8\text{–}1.03)\cdot 10^8$ ev/c and $(1.04\text{–}1.3)\cdot 10^8$ ev/c. In the individual series of experiments the width of the investigated momentum interval varied somewhat one way or the other. For each momentum subinterval, we plotted the integral angular distributions of the μ mesons for the corresponding plate thickness. The experimental distributions were compared with the theoretical curve calculated by using Bethe's[8] equations for evaluating the angular distribution of particles singly scattered from a point nucleus; these equations were deduced on the basis of Molière's theory.

In Fig. 4 are given the integral curves of the angular distribution of mesons scattered in copper plates of 2 mm thickness. The theoretical curves were plotted for the averaged value of the momentum of all the particles in the given momentum subinterval. There is satisfactory agreement in both subintervals between the experimental and theoretical data in the region of small angles. In the region of angles whose projection is greater than 15%, the observed number of cases of scatterings in the $(0.8\text{–}1.03)\cdot 10^8$ ev/c interval exceeds the number expected from Molière's theory. A similar picture is observed in the case of measurements with plates 5 mm in thickness. In the 3 mm thick plates the number of observed cases of scattering to large angles exceeds the theoretical value not only in the $(0.8\text{–}1.03)\cdot 10^8$ ev/c angle but in the $(1.04\text{–}1.3)\cdot 10^8$ ev/c interval as well.

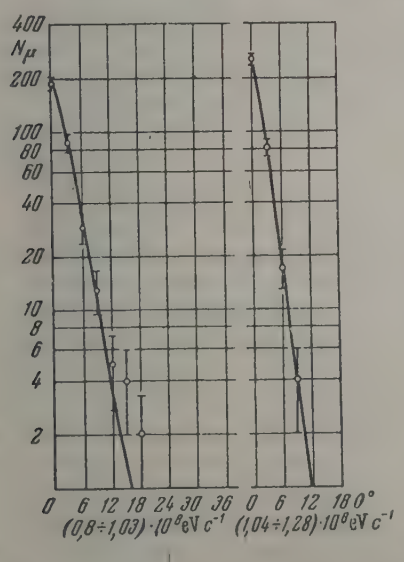

Fig. 4. Integral angular distributions of μ mesons scattered in 2 mm thick copper plates for two momentum intervals.

It is of interest to examine more closely the angular region where theory and experiment diverge.

The data on μ-meson scattering to angles whose projections exceed different angles α, averaged for all three series of measurements, are summarized in the accompanying table. As noted by M.I. Daion, one cannot, in general, compare the results based directly on measurements of the scattering angles on photographs of the chamber with the

Table

Scattering of μ mesons to angles greater than α

α°	Observed number of cases mu meson scattering	Expected number of cases*	W	σ_{an}, 10^{-27} cm^2/ nucleon
10	74	68,48		
15	23	15,67	0,025	3,5
17	17	10,3	0,02	4,2
20	8	5,03	0,085	1,4

* Expected number of cases of scattering due to coulomb scattering and scattering of π mesons

theoretically predicted distribution described above. Variations of the inclination of the primary track relative to the plane of the film, non-orthogonality of the projections and optical distortion can lead to systematic errors. In view of the strong dependence of coulomb scattering on the magnitude of the angle, we made special measurements to determine the requisite corrections to the observed angles. A goniometer, capable of being swung through a wide range of angles, was mounted in a volume bounded by the same kind of glass plates as those enclosing the working volume of the cloud chamber. Pictures were taken of the goniometer in different parts of the chamber and oriented at different angles to the plane of the photographic film, using the same geometry and a camera identical with the one employed in photographing the chamber. We found that in the central portions of the chamber the systematic error did not exceed 4% even when the primary track was inclined at 15% to the plane of the film. Towards the sides of the chamber the error attained 12% under the more unfavorable conditions. The results given in the second column of the table were obtained after making the appropriate correction for the systematic error in the measured angle for each case of scattering. The inclination of the initial trajectory was determined by a stereo-comparator, while the magnitude of the correction was determined from the described control measurements corresponding to the given trajectory angle and point of scattering in the chamber. For the overwhelming majority of trajectories the systematic error turned out to be less than 3%. In the third column of the table is given the expected number of cases of scattering to an angle with a projection greater than α on the assumption that the scattering takes place with a coulomb interaction on a point nucleus. Appropriate corrections for admixtures of π mesons have been made in the tabulated values.

As mentioned previously, the maximum number of π mesons counted as μ mesons is not greater than 15% of the number of true μ mesons stopped in the base of the chamber. Assuming that all cases of nuclear scattering of mesons fall into the 10–40° angular interval, we find that for angles greater than 17° the "background" due to π-meson scattering by nuclei is smaller by at least a factor of eight than the "background" resulting from coulomb scattering of μ mesons. It follows from this that π-meson scattering by nuclei can be neglected in determining the "background" in the given experimental intervals of angles and momenta. However, the admixture of π mesons may become important for the following reason. For trajectories of particles stopped in the base of the chamber the calculation of the residual range, made above, depends on the particle mass. If the particle assumed to be a μ meson turns out, actually, to be a π meson, then its true residual range will be smaller than the calculated "μ meson" residual range. The quantity $p\beta$, which determines the probability of coulomb scattering, may turn out to be smaller for a certain part of these π mesons than the corresponding value for μ mesons.

Analysis of all particle trajectories which terminated in the base of the

chamber showed that of the maximum possible 15% admixture of π mesons, according to the measured momentum, only 6.3% could reach the base of the chamber as such. Actually only part of these 6.3% of the particles reaching the chamber could be π mesons. Assuming that the admixture of π mesons represents only 4% (this value is doubtless the upper limit), we could determine the residual range of the π mesons and evaluate their coulomb scattering, thus arriving at the requisite correction.

From the table it is clear that the observed number of cases of μ-meson scattering to angles exceeding 15, 17 and 20° is larger than the expected number of cases of scattering (with the "background" due to π mesons subtracted). It is possible to argue that the difference between the second and third columns of the table is due to chance fluctuations. The probability of such fluctuations calculated by Poisson's formula is shown in the fourth column, while in the fifth column we give the values of the cross section for anomalous scattering if the entire difference between the experimental and theoretical results is attributed to this effect.

The results given in the table incorporate all the data obtained for each narrow momentum sub-interval and for every series of measurements with plates of the corresponding thickness. A shortcoming of the data processed in this way is that the background from coulomb scattering in a given angular interval, in the 5 mm thick plates, being greater than in the 2 mm plates, may mask a possible effect not related to coulomb interaction. The same thing has to be said about adding the results obtained for various momentum intervals, corresponding to faster and slower mesons.

Bethe determined the probability of coulomb scattering to angles larger than a given one as a function of a dimensionless parameter φ, equal to

$$\varphi = \frac{\theta}{\chi B^{1/2}},$$

where Θ is the measured angle of scattering, while

$$\chi^2 = \frac{4\pi N t e^4 Z (Z+1) z^2}{(pv)^2}$$

Here N is the number of atoms per cm^3, Z is the charge of the nucleus, z is the charge of the particle, t is the thickness of the plate, p is the momentum of the particle, v is the speed of the particle and B is a slowly varying function of the plate thickness and the particle momentum, which, under our experimental conditions, may be regarded as constant for all the measurements. In this way, without any particular limitations on the magnitude of the angles, momenta or thicknesses, it is possible to calculate the quantity φ, and then the probability of coulomb scattering.

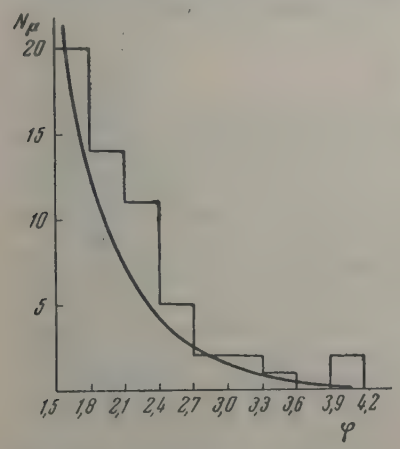

Fig. 5. Differential angular distribution of μ-meson scattering.

The differential curve for the angular distribution of cases of scattering in φ units is shown in Fig. 5; the expected distribution is represented by the solid curve in the figure. It will be seen that in the neighborhood of 2.1 there is some excess in the experimental data above the theoretical. It should be noted that the theoretical curve is plotted on the assumption that all the particles are μ mesons and that they all undergo purely coulomb scattering. Apparently even full allowance for the admixture of π mesons

cannot fully explain the observed difference.

Typical examples of the cases of meson scattering to large angles are shown in Figs. 6 and 7. In the measurements with the 3 mm Cu plates, a lead plate of 13 mm thickness was also placed in the cloud chamber. It is characteristic that none of the observed cases of passage of particles through this plate is accompanied by cascade-production events.

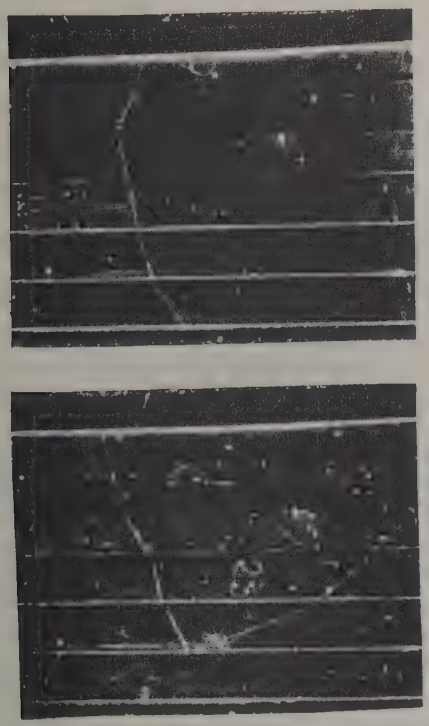

Fig. 6. Examples of stopping of μ-meson scattering to large angles in the 3 mm thick copper plates.

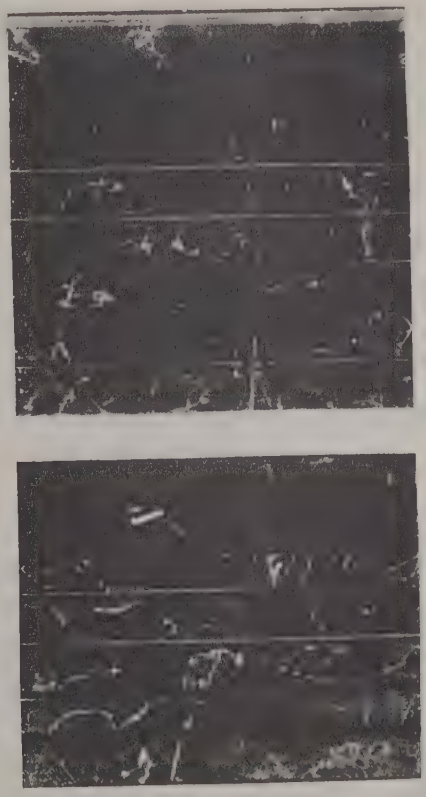

Fig. 7. Examples of μ-meson scattering to large angles in the 2 and 5 mm thick copper plates.

5. Discussion of the results

From the preceding section it is clear that our measurements agree with theoretical results in the region of small angles. At the same time there is observed some excess in the number of cases of scattering to large angles over the predictions of Molière's theory.

The divergence between the observed and theoretical results may be attributed to the following causes:

1) The presence of an excessively large number of π mesons in the flux of particles assumed to consist of μ mesons; if so, the cases of scattering to large angles may be attributed to π mesons;

2) Contamination of the μ-meson flux by electrons.

3) The fact that the number of cases of anomalous scattering includes cases of $\mu \rightarrow e$-decay;

4) The fact that the equation for calculating the expected coulomb scattering effect is invalid because some important effects or factors are neglected.

To analyze the effect which might be produced by the π mesons, we studied

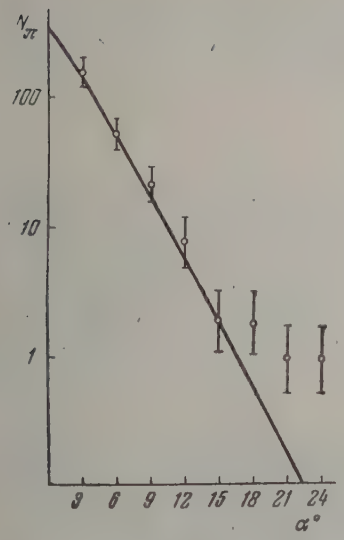

Fig. 8. Integral angular distribution of π mesons scattered in the 5 mm thick Cu plates.

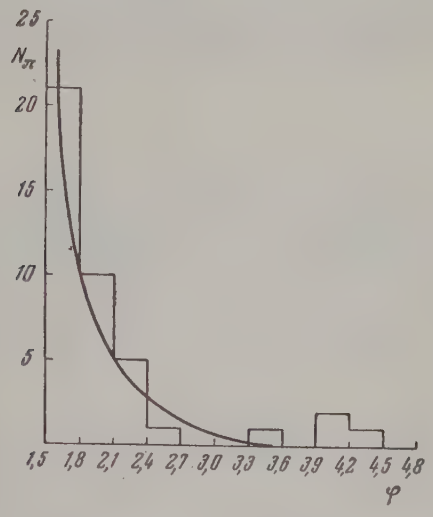

Fig. 9. Differential angular distribution of π-meson scattering.

the scattered particles with measured masses between 240 and 400 m_e. These particles were identified as π mesons*. The data on the scattering of this group of particles were taken from the same experiments as that on μ mesons and, accordingly, the experimental conditions in both cases were identical. Fig. 8 shows the angular distribution of π mesons which incurred scattering in the 5 mm thick copper plates; Fig. 9 gives the π meson distribution as a function of the parameter φ. From these distributions it is clear that there is no reason for assuming the existence of significant experimental errors that would lead to an excess of cases of μ-meson scattering to large angles. The excess of π mesons scattered to angles with a parameter $\varphi > 3$, should evidently be attributed to nuclear scattering. The cross section for such scattering amounts to about 0.15 of the geometrical cross section of Cu nuclei. This value probably corresponds to diffraction scattering of π mesons. It should be noted that in the observed scattering, the π mesons lose virtually no energy since, otherwise, the measured value of the mass would be larger than that actually observed.

It is very doubtful that cases of scattering to larger angles can be $\mu \rightarrow e$-decay events. The cloud chamber operated under conditions such that a triple ionization could always be distinguished from a single one. Moreoever, in this case there should be observed a preponderance of positive particles among those undergoing anomalous scattering. However, the ratio between the negative and the positive particles scattered to angles larger than 17° was 0.66, while in the overall flux of the recorded μ mesons, this ratio was equal to 0.72 ± 0.08.

In Molière's theory, coulomb scattering is regarded as occurring on a point nucleus. The assumption of nuclear charge concentration at a point is in conflict with other well established evidence concerning nuclear structure. However, any nuclear model postulating finite dimensions of the nucleus leads only to a decrease in the expected number of cases of scattering to large angles and, therefore, to an increase in the anomalous effect. It must be noted, however,

*These data were obtained and processed by F.Arutiunian of the Physical Institute of the Academy of Sciences of the Armenian S.S.R.

that the difference between scattering on a point nucleus and scattering on a nucleus of finite size is small in the range of angles and μ-meson momenta investigated. The difference becomes significant in the region of angles larger than

$$\theta_{cr} \sim \frac{\lambda}{R} ,$$

where λ is the DeBroglie wavelength, and R is the radius of the nucleus. Under our conditions the mean projection of θ_{cr} equalled about 17°. For this angular region the theoretical curve, calculated on the assumption of a uniform distribution of charge in a sphere of radius $R = 1.4 \cdot 10^{-13} A^{1/3}$ cm, differs from the curve for single scattering on a point nucleus by not more than 10%. If the effect associated with finite nuclear dimensions is taken into account, then the expected background due to coulomb scattering will be decreased by only a few percent.

Precise measurement of the momenta is of extreme importance in conducting experiments on the scattering of slow μmesons. From this point of view, results obtained for the scattering of μ mesons in the region of several hundred Mev, using relatively crude methods for evaluating the momenta, appear to us unconvincing and, therefore, the coulomb scattering background so obtained — uncertain.

Conclusions

The measurements described above showed that:

1) Molière's theory, in the form in which it has been used by Bethe, gives a distribution of cases of scattering of π and μ mesons in good agreement with experiment in the region of small angles.

2) In the momentum interval from 80 to 139 Mev/c there is an excess of cases of μ-meson scattering to angles with a projection greater than 15°, which corresponds to a scattering cross section of the order of 10^{-27} cm^2/nucleon.

3) The observed excess of cases of scattering to large angles indicates the existence of anomalous scattering of μ mesons in the 80-130 Mev/c momentum interval. However, the small number of cases of scattering observed does not allow of a definitive conclusion regarding the character of the anomalous scattering of μ-mesons in this momentum region. Further accumulation of experimental data is essential.

The authors are grateful to M.L.Ter-Mikaelian for assistance in the investigation and discussion of the results, as well as to M.E.Daion, N.V.Shostakovich, G.I.Merzon, B.N.Deriagin, V.I.Nicolaev and Ia.G.Potapov, student of MIFI, for assistance in making the measurements and processing the data.

"P.N.Lebedev" Physical Institute of the
Academy of Sciences of the USSR

References

1. M.Kannangara & G.Shrikantia, Phil. Mag., 44, 1091 (1953).
2. B.Leontic & A.Wolfendale, Phil. Mag. 44, 1101 (1953).
3. J.B.McDiarmid, Phil. Mag., 45, 933 (1954).
4. E.George, J.Redding & P.Trent, Proc. Phys. Soc., A66, 533 (1954).
5. G.Rochester & A.Wolfendale, Phil. Mag., 45, 980 (1954).
6. D.Tidman, Proc. Phys. Soc., A67, 559 (1954).
7. A.Alikhanian, V.Kirillov-Ugriumov, N.Shostakovich & V.Fedorov, Doklady AN SSSR, 92, 255 (1953).
8. H.Bethe, Phys. Rev., 89, 1256 (1953).
9. E.Amaldi, C.Fidecaro & F.Mariani, Nuovo Cim., 7, 553 (1950).

ON THE SPATIAL DISTRIBUTION OF CHARGED PARTICLES IN THE VICINITY OF THE CORE OF AN EXTENSIVE AIR SHOWER

- S.I.Nikol'ski

(Abstract)

1. In the present investigation the distribution of charged particles in the range from 0.2 to 5 meters from the axis of an extensive air shower was studied by means of a large number of hodoscopic counters concentrated in a small area. The spatial distribution is characterized by $1/r$ for distances of 2-10 meters and by $1/r^2$ for distances under 1 meter.

2. This distribution is evidence of the formation of an electronic-photonic component in the depth of the atmosphere by N-component particles, whose energy may be evaluated as 10^{12} ev and higher.

"P.N.Lebedev" Physical Institute of the
Academy of Sciences USSR

* * * * * * *

ČERENKOV RADIATION IN EXTENSIVE AIR SHOWERS

-V.I.Gol'danski, G.B.Zhdanov, N.M.Nesterova &
A.E.Chudakov

(Abstract)

1. The total yield of Čerenkov radiation from cosmic radiation has been evaluated as $1.8 \cdot 10^{-8}$ erg cm^{-2} sec^{-1} $sterad^{-1}$ (about 5000 quanta cm^{-2} sec^{-1} $sterad^{-2}$ in the optical region of the spectrum) which amounts to not over 0.1% of the constant component of the continuous spectrum of the night sky that is not connected with stellar and zodiacal light.

2. The distribution in altitude of the Čerenkov radiation due to different components of cosmic rays is given. The greatest contribution to the total yield is due to the radiation generated at altitudes of 10-15 km. More than 92% of the radiation is due to electrons, over 7% to mu mesons and only about 0.3% to protons.

3. An equation is deduced for determining the height of the light pulse produced in the light receiver with a given radius incident to the passage of a single particle in a vertical direction at a certain distance from the center of the receiver. Light flashes due to individual particles can be discerned against the glow of the night sky with a light receiver having a radius of not over 10 cm and an effective collecting angle of 0.1 sterad, provided the response threshold corresponds to the simultaneous entry of about 100 quanta and the resolving time of the apparatus is about 10^{-8} sec; the counting rate for flashes due to Čerenkov radiation must be about 1 flash per minute.

4. Čerenkov radiation associated with the occurrence of extensive air showers was investigated. The showers were considered to be downward-expanding cones with a vertical axis and an angle of divergence determined by Rutherford scattering of the shower particles. In the calculations, account was taken of both the diffuse luminescence (connected with the excess of the mean angle of the Rutherford scattering over the angle of emission of the Čerenkov radiation) and the directional Čerenkov radiation (at very small mean Rutherford scattering

---

*For full account see V.I.Gol'danski & G.B.Zhdanov, Zhur. eksp i teor. fiz. 26, 405 (1954) and N.M.Nesterova & A.E.Chudakov, Zhur. eksp i teor. fiz 28, 384 (1955).

angles). The calculations gave the form of the distribution in height of the Čerenkov radiation, produced by the particles of extensive atmospheric showers for different distances between the shower axis and the center of the light receiver as well as the variation of the amplitude of the light flash and the probability of its being recorded on the distance between the shower axis and receiver center. By way of example, numerical calculations are made for the frequency of recording of light flashes for apparatus with a light receiver of 500 cm^2 area, a light collecting angle of 0.15 sterad, a response threshold of $\sim$ 1300 photons and a resolving time of $3 \cdot 10^{-8}$ sec (the characteristics of the apparatus used by the English physicists Golbreit & Jelley). The calculations give 70 pulses per hour which is in good agreement with the experimental result (60 pulses per hour).

5. The possibility of utilizing observations of Čerenkov radiation for studying the energy spectrum and the spatial structure of extensive air showers is indicated.

6. Preliminary experiments on studying the radiation of extensive air showers were carried out with an apparatus consisting of a parabolic mirror 30 cm in diameter, a photomultiplier and an appropriate electronic circuit (the collection angle equalled approximately 0.1 sterad; the resolving time about $5 \cdot 10^{-8}$ sec). The function characterizing the pulse distribution in height (over a 1 to 10 height range) proved to be close to a power function with an exponent of 1.5, in agreement with the shape of the density spectrum of extensive air showers. In recording coincidences between light flashes and the indications of hodoscopes detecting showers within a radius of 50 meters, it was found that only about 4% of the light flashes are accompanied by hodoscope indications. This substantiated the calculations of the dependence of the probability of recording light flashes on the distance between the shower axis and the light receiver, according to which the Čerenkov radiation in extensive showers is concentrated within a radial range of under 250 meters from the shower core. The experiments confirm the feasibility of observing Čerenkov radiation in extensive air showers having energies of the order of 10^{14} ev.

"P.N.Lebedev" Physical Institute of the
Academy of Sciences of the USSR.

* * * * * * *

DISTRIBUTION IN MOMENTUM OF CHARGED PARTICLES IN ELECTRONIC-NUCLEAR SHOWERS

-L.D.Gedevanishvili, Z.Sh.Mandzhavidze, N.N.Roinishvili,
Z.I.Tsagareli, A.I.Tsintsabadze & G.E.Chikovani

(Abstract)

The distribution in momentum of charged particles in electronic-nuclear showers was investigated by means of a counter controlled cloud chamber mounted in a magnetic field. A lead plate 30 mm thick was located under the chamber. The first row of counters was mounted between this plate and a decking lead absorber serving to exclude the soft component. The second and third rows of counters, located under the chamber were separated by a 50 mm thick layer of lead. The chamber expansion was triggered by six-fold coincidences: simultaneous discharges in one of the counters of the first row, three of the counters in the second row and two of the counters in the third row. The showers were generated in the layer of lead immediately above the chamber. The observations

were made at an altitude of 3900 meters above sea level in the laboratory of the El'brus Expedition sponsored by the "I.V.Stalin" Tbilisi State University and the Physical Institute of the Georgian SSR Academy of Sciences.

The integral distribution in momentum of charged particles of both polarities in the range from 40 to 2000 Mev, plotted on the basis of measurements of the track curvature, is characterized by a power function with an exponent of 0.5.

Subsequently the distribution in momentum was again determined using the same cloud chamber, but with a 10 mm thick lead plate, in which the showers were generated. This excluded the multiplication of electrons which could occur in the thick generator plate mounted above the chamber and which could lead to degradation of the initial spectrum. This second series of observations was carried out at 2000 meters above sea level. The integral distribution in momentum of charged particles of both polarities was found to be the same, within the limits of the experimental error, as in the measurements at 3900 meters.

Institute of Physics of the
Academy of Sciences of the Georgian SSR
and
"I.V.Stalin" Tbilisi State University

* * * * * * *

ON THE USE OF PHOTOMETRY FOR EVALUATING THE IONIZATION OF PARTICLES IN A CLOUD CHAMBER

- V.M.Fedorov, G.I.Merzon & M.I.Daion

In processing photographs of tracks in a Wilson cloud chamber it is often necessary to evaluate roughly the mass of stopped particles. This can be done for example, from the ionization (by the method of counting droplets) and the residual range. However, in many cases the experimental conditions do not allow of obtaining photographs of the track in the form of an agglomeration of droplets, i.e., the image of the track obtained is virtually structureless. Photographs of this sort are obtained, for example, in a cloud chamber operated in conjunction with a magnetic mass spectrometer.[1 & 2] In such cases, due to appreciable reduction (1/20), the width of the track image is only 0.1-0.2 mm so that it is impossible to distinguish individual droplets. Examination of the tracks of relativistic particles and those of mesons and protons coming to rest in the absorber plates intersecting the chamber shows that they differ noticeably as regards both the absolute degree of blackening and the density gradient.

We tried to find a method for objective evaluation of the difference and to relate the density of the track images with the ionizing power of the particles for the purposes of exploring the possibility of evaluating particle masses from the ionization at different residual ranges. For the initial measurements we selected photographs of tracks of protons and mesons whose mass had been determined with high accuracy on the basis of momentum and range in mass spectrometer experiments. The blackening was evaluated by photometry of these photographs on an MF-2 microphotometer [microdensitometer]. By way of a standard, corresponding to minimal ionization, we took photographs of the tracks of hard particles and high-energy particles, initiating nuclear disintegrations in the absorber plates of a cloud chamber. We selected positive particles having momenta above $2.4 \cdot 10^8$ ev/c and negative particles with momenta over $4 \cdot 10^8$ ev/c.

At these values of the momentum, the ionization produced by protons and light mesons differs from the minimum ionization by 10 and 5% respectively.

The microdensitometer recorded the value of the photocurrent from the instrument's photoelectric tube, illuminated by light beamed through the photometered section of the film and limited by a special slit. The dimensions of the slit could be varied over a wide range. In our measurements we used a slit width equal to 1/10-1/15 the width of the track of a relativistic particle and a slit length equal to about 1/3 the distance between adjacent track images. The slit was oriented parallel to the track and displaced in a direction perpendicular to it. With each displacement of the slit by a distance equal to its width the densitometer recorded the current characterizing the degree of blackening (density) of the viewed section. The sum of the measured current values (background subtracted), therefore, characterized the total blackening of the track image.

In this manner we measured the successive sections of the tracks of 41 hard particles having an ionization close to the minimal: 18 protons and 11 mesons. Investigation of the blackening of the tracks of hard particles passing through different parts of the chamber showed that in a chamber with "back-lighting" the illuminating conditions are not uniform. Hence for further investigations we selected only particles passing through the central uniformly illuminated region of the chamber. Investigation of the tracks of hard particles also showed that they produced an approximately equal track density (mean deviation about 25%) in the different inter-plate sections of the chamber.

The integral curves for the dependence of the density (blackening in relative units) on the residual range are shown in the accompanying figure. Curve 1 pertains to protons; curve 2, to mesons. For purposes of comparison, we also give the curve for hard particles. (For these the blackening was integrated successively over all the inter-plate sections of the chamber, starting from the lowest one). It will be seen that there is clear grouping of the data in accord with the particle masses. Thus the method permits separating mesons from protons with certainty.

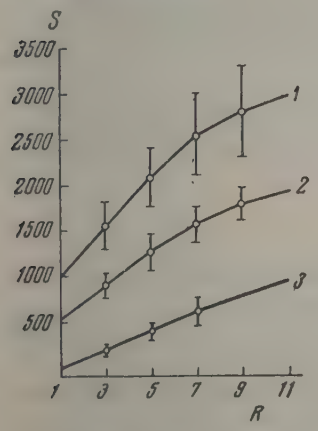

Integral curves for the variation of blackening S (in relative units) with the residual range R (in mm Pb). Curve 1 - proton tracks, 2 - meson tracks, 3 - tracks of hard particles.

Comparison of the relative blackening with the ionization (see Table), computed for the corresponding values of the residual range, shows only very approximate agreement. A better quantitative comparison can be made if instead of blackening we use the intensity of the light producing the blackening and assume that the intensity of the light scattered by the track is proportional to the ionization

Comparison of the relative blackening of the photographs of tracks with the relative ionization produced by the particles

Residual range, mm, Pb	Mean value of blackening		Calculated relative ionization	
	for mesons	for protons	for mesons	for protons
0÷2	3,71	6,5	Over 3,3	—
2÷4	2,5	5,0	3,3÷2,3	Over 6,9
4÷6	2,35	3,62	2,3÷2,0	6,9÷5,6
6÷8	1,75	2,95	2,0÷1,8	5,6÷4,6

produced by the particle. In the "normal exposure" region of the emulsion the blackening is a linear function of the logarithm of the light intensity. However, the angular coefficient of this dependence, i.e., the gamma, may vary not only from one film to another but also from one section of a given film to another. The value of gamma is greatly dependent on the type of emulsion, the period of storage, conditions of development and so on. The difficulties associated with the variation in gamma can be circumvented by imposing suitable calibration marks on the film by means of a step-weakener, as is the practice in spectrum analysis.

In the present investigation we were unable to determine the gamma and hence cannot correlate the light intensity with the ionization. However, imposition of calibration marks by photographing a step-weakener on each frame should present no particular difficulties and would make such correlation a simple matter.

There is appreciable scattering of the density values of the tracks of particles of the same kind as measured on different photographs. The reason for this is that the cases of stopping selected for comparison were photographed at different times over a period of several months during which the operating conditions of the chamber (temperature, pressure and composition of the gas) obviously changed somewhat. This variation could readily be allowed for if, in addition to the investigated particles, a few particles with minimal ionization were photographed on each plate; density comparisons could then be made for each photograph separately with reference to the minimal ionization tracks.

We feel that it would be best to investigate the blackening by means of a recording microdensitometer designed to record a continuous density curve.

There is reason to hope that the method of evaluating ionization by means of photometry, if properly developed, can be used to distinguish between particles even closer in mass than mesons and protons, particularly in analyzing photographs made in chambers with uniform lighting.

In conclusion the authors wish to thank A.I.Alikhanian for his interest in the work.

Note added in proof. Subsequent to presentation of this report at the Conference two descriptions of similar application of the photometry method have appeared in the literature (Refs. 4 & 5).

"P.N.Lebedev" Physical Institute of the
Academy of Sciences of the USSR

References

1. M.Daion & V.Fedorov, Zhur. tekh. fiz., 25, 771 (1955).
2. A.I.Alikhanian, V.Kirillov-Ugriumov, N.Shostakovich & V.Fedorov, Doklady AN SSSR, 92, 255 (1953).
3. S.L.Mal'del'shtam, Vvedenie v spektral'nyi analiz. - (Introduction to spectrum analysis) M.-L. 1946.
4. J.Butterworth, Phil. Mag. 46, 884 (1955).
5. F.K.Bjornerud, R.S.J., 26, 836 (1955).

DEPENDENCE OF THE PROBABLE IONIZATION DUE TO MU MESONS ON THEIR MOMENTUM

- V.A.Liubimov, G.P.Eliseev, V.K.Kosmachevski & A.V.Kovda

In order to determine the mass of charged particles from the values of the momentum and the most probable ionization, it is necessary to know the dependence of the probable ionization of the medium on the particle velocity. In the case of slow particles this dependence has been thoroughly studied, but this cannot be said of relativistic particles which fall within the region of the logarithmic increase of ionization. Only within recent years have there begun to appear experimental reports dealing with the velocity dependence of the ionization produced by relativistic particles.

The present investigation was undertaken for the purpose of making a quantitative comparison of the experimentally determined relation between the ionization of the gas in a proportional counter and particle velocity with the relation calculated from theory.

The theory of total energy losses experienced by charged relativistic particles during their passage through matter was worked out by Fermi and has been extended by Week, Halpern and Hall and others[1]. This theory predicts that the total energy loss by relativistic particles at speeds approaching that of light increase logarithmically as the particle velocity increases. This increase of losses in a gas occurs despite a polarization effect in the medium and is consequent upon the increase in the maximum energy that the particle can transfer to atomic electrons. The polarization effect merely results in a reduction of the slope of the logarithmic branch of the ionization curve in comparison with the slope of the curve plotted without taking the effect into account.

If the collisions are divided into "far" and "near" (according to the distance between the particle trajectory and the atom), then it is obvious that in the case of the "far" collisions the polarization effect will cause the logarithmically increasing energy loss to reach a saturation value at some particle velocity, i.e., will lead to a "plateau" in the energy loss curve. We shall show that the most probable ionization loss (the quantity measured in proportional counters) coincides numerically with the average energy loss in "far" collisions. Consequently, it becomes possible to apply the formulas for the average loss in "far" collisions to determining the dependence of the probable ionization of the medium on the particle velocity. With this purpose in mind, let us consider the distribution of fluctuations in ionization losses. The curve for these fluctuations is asymmetrical and is described by the function (see Ref. 2):

$$\varphi\left(\frac{\Delta-\Delta_0}{\xi}\right)\frac{1}{\xi},$$

where $\xi = 1{,}54\cdot 10^5 \mu \frac{\Sigma Z}{\Sigma A}\cdot\frac{1}{\beta^2}$, μ is the quantity of the substance in g/cm^2 in the layer under observation and the function φ denotes the probability of an energy loss , where the most probable loss is Δ_0. The middle section of the distribution $\varphi\frac{1}{\xi}$ is determined by the energy loss in "far" collisions, while the distribution in the region of large values of Δ is determined by the knock-on (δ) electrons formed in "near" collisions. The most probable energy loss is determined on the curve by the coordinate of the distribution maximum and is found from the condition

$$\left[\varphi\frac{1}{\xi}\right]'_{\Delta}=0,$$

whence $\Delta_{prob} = \Delta_0$.

The average, or median, loss is determined by the coordinate of the "centroid" of the distribution and is found from the relation

$$\overline{\Delta} = \int_0^{\Delta_0+W_{max}} \Delta\cdot\varphi\left(\frac{\Delta-\Delta_0}{\xi}\right)\frac{1}{\xi}\,d\Delta,$$

where W_{max} is the maximum energy which can be transferred to an electron in a collision. On account of the asymmetry of the distribution, the average loss is not identical with the most probable one. In order to get the average loss to coincide with the probable one, it is necessary to cut off the maximum transferred energy at a certain value $W_{max} = W_0$. With the section of the distribution curve in the region of large energy losses truncated, the distribution becomes more symmetrical. The value of W_0 is determined precisely from the condition that

$$\overline{\Delta} = \int_0^{\Delta_0 + W_0} \Delta \cdot \varphi\left(\frac{\Delta - \Delta_0}{\xi}\right)\frac{1}{\xi}\, d\Delta = \Delta_0.$$

For the Landau distribution, $W_0 \approx 1.6$

Thus, if the average loss is sought only for the "far" collisions wherein the energy transferred is $\sim 1.6\,\xi$, we find that this average loss numerically coincides with the most probable loss in the given layer of matter. Consequently if, in the Bethe-Bloch formula for average energy losses, the value $1.6\,\xi$ is substituted for W_{max}, we obtain with sufficient accuracy Landau's formula for the most probable losses:[2]

$$\overline{\Delta} = \xi\left[\ln\frac{2mv^2 W_{max}}{I^2(1-\beta^2)} - \beta^2\right] = \xi\left[\ln\frac{2mv^2\,1{,}6\xi}{I^2(1-\beta^2)} - \beta^2\right] = \xi\left[\ln\frac{2mv^2\xi}{I^2(1-\beta^2)} + 0{,}47 - \beta^2\right] \approx \Delta_0$$

(Landau has 0.37 instead of 0.47).

It is not difficult to show that in cases where the experimentally observed distribution of fluctuations is wider than Landau's a value must be substituted for W_0 in the Bethe-Bloch formula for which $\overline{\Delta}_{exp} = \Delta_{0\,exp}$. In our case W_0 proved to be equal to 5ξ, i.e.,

$$\Delta_0 = \xi\left[\ln\frac{2mv^2\cdot 5\xi}{I^2(1-\beta^2)} - \beta^2\right].$$

Thus we have obtained a formula for the dependence of probable ionization on the particle velocity for those cases where we have a distribution different in form from that of Landau. Now if we introduce into this formula a correction for the density effect after Boudini[1] and write the expression for a mixture of gases, we obtain the final formula, which is the one we used in comparing theory with our experimental data:

$$\Delta_0 = \sum_i \xi_i \left[\ln\frac{2mv^2\cdot 5\xi_i}{I_i^2\left(1-\beta^2+\frac{\alpha}{\bar{\omega}_0^2}\beta^2\right)} - \beta^2\right],$$

where the summation is carried out over all the components of the gas mixture. Here

$$\alpha = \frac{4\pi Ne^2}{m},\quad \bar{\omega}_0 = \frac{\bar{I}}{\hbar}.$$

In the present investigation the ionization curve for μ mesons was determined over a wide momentum range, encompassing both the region of minimum ionization and the region of the Fermi "plateau". Particle momenta were measured on an improved mass spectrometer over a wide range of values: in the $0.46\cdot 10^8$–$7.5\cdot 10^9$ ev/c interval in the first and third measurement series, when the first and fifth trays of the counters were placed directly over and under the pole pieces of the magnet and in the $2.2\cdot 10^8$–$4.2\cdot 10^{10}$ ev/c interval in the second measurement series, when the first and fifth trays were separated and located at a distance of 77 cm above and below the pole pieces, respectively.

The ionization was measured by means of a four-layer proportional counter (filled with Ar at 85 mm Hg and C_3H_8 at 365 mm Hg col). The design of the counter made it possible to obtain four independent readings for each ionizing

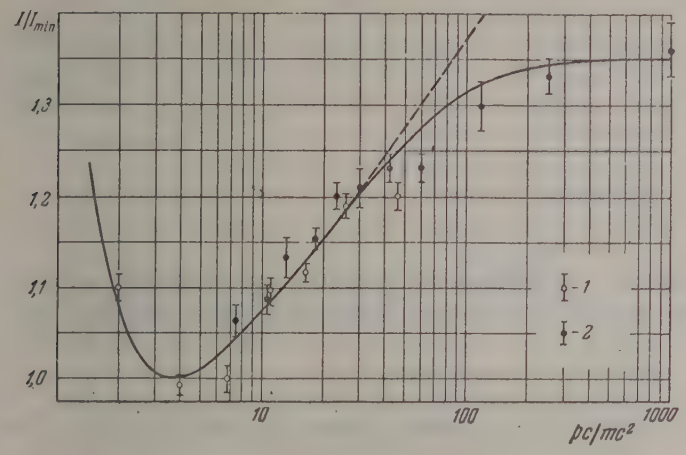

Fig. 1. Variation of probable ionization due to μ mesons with velocity. Abscissae: ratio of the momentum pc to the μ-meson mass mc^2. Experimental points: 1) "constricted" position (with the counters next to the polepieces of the magnet); 2) "extended" position (with counters at a distance of 77 centimeters from the polepieces). Curves: calculated dependence of ionization on momentum; solid line: curve when the density effect is taken into account; dash-line: when the density effect is neglected.

particle passing through the apparatus. This made it feasible to attain a high accuracy of determination with relatively few observed particles. The most probable values of the ionization due to μ mesons were calculated within each momentum interval by the universal method, which, for the case of a Landau distribution, gives from 2 to 3 times higher accuracy than calculation by the method of mean-arithmetical evaluation.

Fig. 1 shows a comparison of the experimental points with the theoretical curve for the probable ionization due to μ mesons plotted according to the improved formula given above. Points 1 were obtained in the "constricted" position (counter trays at polepieces) which took in the region of minimum ionization. Points 2 were obtained in the "extended" position, which made it possible to take in the region of the Fermi ionization plateau. The momentum of the last point could not be measured directly; it was determined by averaging over the μ-meson spectrum and proved equal to $1.2 \cdot 10^{11}$ ev/c. In the $2 \cdot 10^9$–$1.5 \cdot 10^{10}$ ev/c interval the ionization was calculated for negatively charged particles only, inasmuch as a possible admixture of protons, having a minimum ionizing power in this momentum range, could distort the measurements of the ionization due to μ mesons. In our investigation (described in Ref. 3) we succeeded in measuring the logarithmic increase in the ionization loss up to $p = 3 \cdot 10^{10}$ ev/c.

The results of the present investigation show:

1) the presence of a logarithmic increase in the ionization produced in the counter gas by μ mesons in the momentum range from $4 \cdot 10^8$ to $2 \cdot 10^{10}$ ev/c (in agreement with the results of Becker,[4] Kharitonov,[5] and our earlier experiments[3]);

2) the existence of a polarization effect in the counter gas (in agreement with Refs 6, 7 & 8);

3) momentum independence of the probable ionization due to μ mesons having momenta exceeding $3 \cdot 10^{10}$ ev/c; in this investigation the curve showing the independence was carried to $1.2 \cdot 10^{11}$ ev/c;

4) agreement of the experimental results with the Fermi-Boudini theory of ionization losses by relativistic μ mesons.

The possibility of representing the most probable ionization loss as the average loss of energy due to "far" collisions, where the maximum transferred energy is cut off at a certain value W_0, yields a simple and yet precise method for calculating the most probable ionization from a few ionization values (the truncation method). Let the n measured ionization values $\Delta_1, \Delta_2, \ldots, \Delta_n$ correspond

to the distribution function $\varphi\left(\frac{\Delta_i - \Delta_0}{\xi}\right)\frac{1}{\xi}$. Let the area under the symmetrical distribution curve obtained by cutting off the distribution curve in the region of greatest losses be related to the total area under the entire distribution curve as

$$\alpha = \frac{\int_0^{\Delta_0+W_0} \varphi\frac{1}{\xi}\,d\Delta}{\int_0^{\Delta_0+W_{max}} \varphi\frac{1}{\xi}\,d\Delta}.$$

Then we discard $(1-\alpha)n$ of the maximum values from among the measured values and find the most probable ionization value as the average of the remaining values:

$$\Delta_0 = \overline{\Delta}_{cut} = \frac{\Delta_i + \Delta_k + \dots}{\alpha n}.$$

Further, if σ is the mean square error of the Gaussian distribution equivalent to the distribution $\varphi\frac{1}{\xi}$ with the greatest loss region cut off (i.e., equal to it in area and height), then the error in the determined value Δ_0 is given by

$$\delta\Delta_0 = \frac{\sigma}{\sqrt{\alpha n}}.$$

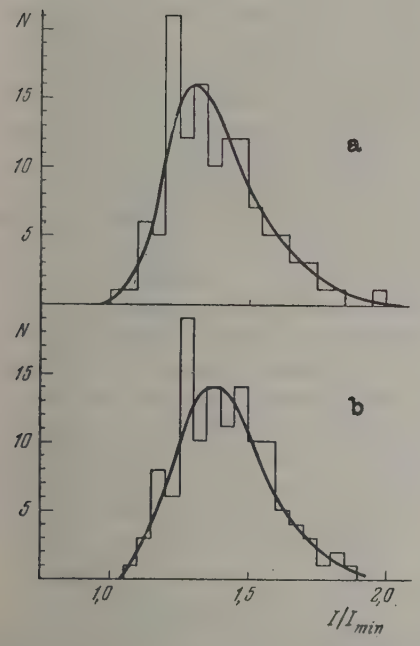

Fig. 2. Ionization distributions characterizing the accuracy of determining the ionization produced by a single particle with a four-layer counter, where the experimental data are processed:
a) by the truncation method $\left[\left(\sqrt{\overline{\sigma^2}}\right)_{25\%} = \pm 10{,}9\%\right]$,
b) by the "universal" method $\left[\left(\sqrt{\overline{\sigma^2}}\right)_{uni} = \pm 11{,}3\%\right]$

For the experimental ionization distribution obtained with our counter it proved necessary to discard about 25% of the maximum values; i.e., where there were four ionization values per particle, to discard the one maximum value and average the remaining three.

To check the truncation method, the results of measuring the ionization of 122 electrons were processed. Their ionization lies on the Fermi plateau in the ionization curve. The distribution obtained is shown in Fig. 2a. For the sake of comparison the same data processed by the "universal" method[3] are shown in Fig. 2b. It is evident that the truncation method, although much simpler, is no less accurate than the "universal" one.

It must be admitted that the "universal" method must still be used where it is necessary to plot an error curve for the probability calculations.

In conclusion the authors express their deep gratitude to A.I.Alikhanov, who directed the investigation, and L.D.Landau for reviewing the results.

Academy of Sciences of the USSR

References

1. "Problemy sovremennoi fiziki", (Problems of modern physics), Ser. 5,No.7, M., 1953.
2. L.D.Landau, Journ. of Phys. USSR, 8, 201 (1944).
3. G.P.Eliseev, V.K.Kosmachevski & V.A.Liubimov, Doklady AN SSSR, 90, 995 (1953).
4. J.Becker, P.Chanson, E.Nageotte, P.Treille, et al, Proc. Phys. Soc., A65, 437 (1952).
5. V.M.Kharitonov, Doklady AN SSSR, 86, 285 (1952).
6. S.Ghoch, D.B.Jones & J.G.Wilson, Proc., Phys. Soc., A67, 331 (1953).
7. V.M.Kharitonov & A.Barski, Doklady AN SSSR, 93, 645 (1953).
8. J.K.Parry, H.D.Rathgeber & J.L.Rouse, Proc. Phys. Soc., A66, 541 (1953).

* * * * * * *

LIQUID BUBBLE CHAMBERS FOR INVESTIGATING IONIZING PARTICLES

- G.A.Blinov, Iu.S.Krestnikov & I.I.Pershin

It is generally known that pure liquids can be superheated, i.e., heated without visible boiling to a temperature well above the boiling point of the liquid at the given pressure. The liquid may be obtained in the superheated state either by raising its temperature at constant pressure or by reducing the pressure at constant temperature. In the first case the transition to the superheated state is slow; by using the second procedure one can effect a rapid transition to the superheated state. This is the procedure used in working with liquid bubble chambers. The time during which the superheated liquid remains quiescent, i.e., does not erupt, depends on the number of chance factors but the mean time - "the time delay to eruption"-decreases rapidly with increasing temperature. At low temperatures a sufficiently pure liquid may remain in the quiescent superheated state for many minutes.

In 1952 Glaser[1] showed that the delay to eruption of diethyl ether at 140°C is very sensitive to ionizing radiation: the liquid erupts without delay if a γ-ray source is brought near the container. In subsequent communications,[2-4] Glaser reported that photographs of ionizing particle tracks can be obtained in superheated ether and isopentane and published two photographs of cosmic ray particles in an ether chamber. It must be noted that these photographs were not of particularly high quality. In 1954 Hildebrand & Nagle[5] and Wood[6] published reports on similar experiments with isopentane, liquid nitrogen and liquid hydrogen.

At the suggestion of Alikhanov, we undertook the development of liquid bubble chambers with ether and propane, suitable for investigating high-energy particles. The experiments with ether confirmed in general the results reported by Glaser. We, too, obtained photographs of cosmic ray particle tracks. The experiments with propane (C_3H_8) showed that this is a superior liquid for use in bubble chambers and made it possible to obtain several hundred high quality stereo-photographs working with proton and neutron beams brought out from the synchrocyclotron of the Institute of Nuclear Problems of the USSR Academy of Sciences. The results appear in Ref. 7. From our work we can draw a number of conclusions regarding the possibilities of using bubble chambers in research and the optimum operating conditions for such chambers.

There are two main reasons for the difficulties encountered in photographing cosmic ray particle tracks in liquid bubble chambers operating on the

pressure release principle. The first is connected with the rather short sensitivity time of the chamber. This time is determined primarily by the conditions of the generation and growth of the bubbles. Adsorption on the walls of the container, contamination of the liquid and any background due to the presence of extraneous ionizing particles lead to the appearance of minute bubbles and thereby reduce the effective utilization time for photographing the tracks of cosmic ray particles. The rapid growth of the minute bubbles (a matter of a few microseconds under the conditions employed by Glaser and of a few tenths of a microsecond under our conditions) results in the chamber filling with large bubbles, making photography of tracks impossible.

The second reason for the difficulties encountered in using liquid chambers for photographing cosmic ray tracks is connected with the fact that up to the instant of opening of the pressure relief valve the liquid is not in a superheated state and it is not known whether the liquid can "remember" the passage of the ionizing particle for the interval necessary to attain the reduction in pressure. The method used by Glaser[2-4] and ourselves for controlling the light flashes by means of a coincidence circuit incorporating counters is inadequate in view of the short delay time to eruption.

In working with accelerators the short sensitivity time of the bubble chamber is not a shortcoming, since the operation of the chamber can readily be synchronized with that of the accelerator. Furthermore, the particle tracks are not noticeably distorted during the short time necessary for the growth of bubbles. This explains the faultless tracks illustrated in our photographs (Figs. 1 & 2). The number of bubbles attains 100-120 per 1 cm path, while their diameter is less than 0.1 mm. It may be concluded from our photographs that particles with different ionizing powers exhibit different bubble densities along their tracks. By appropriately varying the temperature one can determine the range of the observed ionizations. Furthermore the rate of growth of the bubbles can be controlled, without changing the sensitivity of the chamber to ionization, by varying the pressure relief differential and the temperature of the

Fig. 1. Particle tracks in propane bubble chamber, irradiated with 600 Mev neutrons during two successive pulses of an intensity corresponding to the pulsed operating regime of the synchocyclotron. The sensitivity time of the propane chamber was over 0.01 sec.

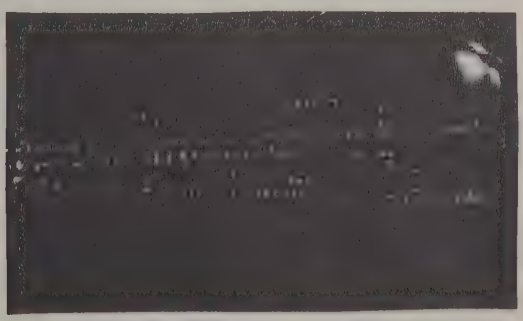

Fig. 2. Tracks produced in bubble chamber by 650 Mev protons.

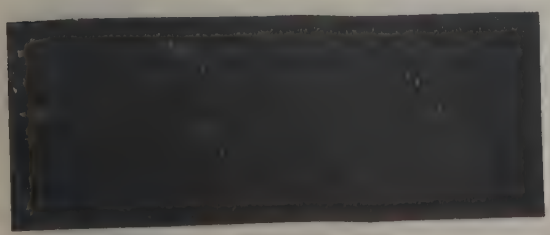

Fig. 3. Nuclear disintegrations in carbon (stars), produced by 600 Mev neutrons. The different prongs have different numbers of bubbles per unit track length.

liquid. Thus by slowing the rate of growth one can extend the effective sensitivity time of the chamber.

In view of the large amount of material contained in bubble chambers they constitute a very efficient instrument for detecting nuclear interactions of high-energy particles. As regards density of the medium, liquid bubble chambers occupy an intermediate position between nuclear emulsions (density 4 g/cm^3) and high pressure cloud chambers (the density in a chamber filled with argon at 100 atmospheres is 0.18 g/cm^3). The density of propane in a liquid chamber operated at 50-70° C is about 0.3-0.4 g/cm^3. At this temperature a unit volume of propane contains as many hydrogen nuclei as gaseous hydrogen at 800 atmospheres pressure (disregarding the compressibility of hydrogen).

The very first photographs showed the possibilities inherent in bubble chambers where the investigation of nuclear reactions induced by high-energy particles is concerned. We photographed stars (Fig. 3), associated with the disintegration of hydrogen nuclei by neutrons of 600 Mev maximum energy. We also want to call attention to the exceptional potentialities of bubble chambers for the identification of π^+ and π^- mesons coming to rest in the chamber. In the case of π^+ mesons one can observe the entire sequence of the $\pi \rightarrow \mu \rightarrow$ e decay: a 4.1 Mev μ^+ meson, appearing as a result of the decay of the stopped π^+ meson, leaves a 4-5 mm long track in the propane and then decays, yielding a clearly distinguishable positron track. Even with a chamber having an effective volume of only 10 cm^3 we soon succeeded in photographing a case of the generation of a π^- meson, produced by a fast neutron on a carbon nucleus. Slow π^- mesons can be unambiguously identified inasmuch as they leave at the end of their track a clearly distinguishable star produced in the capture of the π^- meson by a carbon nucleus.

When the nature of the particles participating in a process is known, one can in many cases separate the reactions on carbon from those on hydrogen by means of a propane chamber. The separation may be based on the difference of the scattering angles between the products of the nuclear reactions on carbon and hydrogen.

The possibility of measuring momenta in a propane chamber is determined principally by the influence of multiple scattering. It is known that the effect of the material, in which the reaction is observed, on the extent of multiple scattering is characterized by the unit radiation length in the material. Straightforward calculations show that the radiation length for liquid propane is approximately equal to the radiation length in argon at 100 atmospheres. Thus multiple scattering in propane is appreciable and gives rise to a large error in measuring momenta by means of ordinary magnetic fields in the case of a chamber of small dimensions. However, by using sufficiently large chambers one can measure momenta with fairly high accuracy in an extensive range. The measurement procedure can be analogous to that used in high pressure, argon-filled cloud chambers, but the accuracy of momentum determination (for equal apparatus dimensions and magnetic field intensities) will be higher in a propane chamber owing to the absence of distortion and the narrowness of the tracks. One can readily obtain tracks only 0.05 mm wide in propane.

Our experiments showed that there are no serious obstacles to making large liquid bubble chambers and we are at present engaged in the design of such a chamber.

It may be noted that a number of other liquids can be used for filling bubble chambers. The composition of the liquid selected will be dictated primarily by the nature of the physical problems involved. Different liquids can also be used to extend the possibilities of measuring the physical attributes of the particles whose tracks are photographed in the chamber. Thus, for example, by selecting a liquid containing a component with a large atomic number

we can make use of the multiple scattering effect for determining momenta, as is done in using nuclear emulsions. On the other hand by using hydrogen to fill the chamber we obtain an apparatus characterized by a minimal multiple scattering and permitting of accurate measurement of particle momenta in the wide range of values at the magnetic field intensities commonly employed in working with Wilson cloud chambers. The absence of distortion of the tracks in bubble chambers makes it possible to measure the angles between tracks with high accuracy.

We can safely assert that the liquid bubble chamber will prove to be a highly effective tool in the investigation of nuclear interactions and the properties of particles at high energies.

We wish to thank A.I.Alikhanov for a series of valuable suggestions, utilized to advantage in the present investigation.

Academy of Sciences of the USSR

References

1. D.A.Glaser, Phys. Rev., 87, 665 (1952).
2. D.A.Glaser, Bull. Am. Phys. Soc., 28, 72 (1953).
3. D.A.Glaser, Phys. Rev., 91, 762 (1953).
4. D.A.Glaser, Nuovo Cim., 11, Suppl. No. 2, 361 (1954).
5. R.M.Hildebrand & D.E.Nagle, Phys. Rev., 92, 517 (1953).
6. J.G.Wood, Phys. Rev., 94, 731 (1954).
7. G.A.Blinov, Iu.S.Krestnikov & I.I.Pershin, Doklady AN SSSR, 99, 929 (1954).

* * * * * * *

Publication note: Starting with the next volume (Vol. 20) the frequency of the Bulletin is increased to twelve issues per annum.

BULLETIN of the Academy of Sciences of the USSR - Physical Series
Vol. 19, No. 6, 1955 - Conference on the Physics of Cosmic Rays (15-23 Dec.1954)
(Continued from Vol. 19, No. 5)

TABLE OF CONTENTS

	Page Orig.	Trans.
On the theory of the multiple production of particles - S.Z.Belen'ki	611	551
Statistical mechanics of systems with conservation of charge and its application to the theory of multiple production of particles - V. B. Magalinski and Ia. P. Terletski	617	557
Cascade curves for electrons and photons in light and heavy elements - I. P. Ivanenko	624	564
Application of the random trials [Monte Carlo] method to calculation of intranuclear cascades - V. V. Chavchanidze	629	568
Elements of relativistic magneto-aerodynamics - K. P. Staniukovich	639	578
On an ionization effect related to the observation of electron-positron pairs at very high energies - A. E. Chudakov	651	589
The radiation and scattering of fast particles in a medium - M. L. Ter-Mikaelian	657	595
Contribution to the theory of antiproton formation - L.M.Afrikian	661	599
The influence of multiple scattering on bremsstrahlung and pair production - A. B. Migdal (Abstract)	665	601
Analysis of high energy stars - D. S. Chernavski (Abstract)	663	602
On fluctuations in the interaction of high-energy particles - M. I. Podgoretski, I. L. Rozental' and D. S. Chernavski (Abstract)	663	602
Diffractional disintegration of deuterons - E. L. Feinberg (Abstract)	663	602
General relationships in the decay of heavy mesons - I. S. Shapiro	664	603
On the question of the existence of antinucleons - Iu. M. Shirokov	664	604
On the stopping of heavy particles - I. I. Gol'dman & S. A. Kheifets	665	604
Investigation of interactions of particles of high and ultrahigh energies with nuclei and nucleons - N. A. Dobrotin, G. T. Zatsepin, S. I. Nicol'ski, L. I. Sarycheva and G. B. Khristiansen	666	605
Structure of extensive air showers at sea level - A. T. Abrosimov, V. I. Zatsepin, V. I. Solov'eva, G. B. Khristiansen & P. S. Chikin	677	616
Investigation of cosmic rays underground - E. L. Andronikashvili, M. F. Bibilashvili, I. V. Sakvarelidze & G. R. Khutsishvili	681	619
Use of the residual range scattering method for the determination of the mass of particles in a cloud chamber with absorber plates - M. I. Daion	697	624

	Page Orig.	Trans.
Distribution in momentum of pi mesons at 3200 meters above sea level - A. I. Alikhanian and V. Sh. Kamalian	707	626
The transition effect for stars and its connection with cascade multiplication of particles of the nucleonic component - Zh. S. Takibaev	687	630
Investigation of the products of nuclear disintegrations initiated by fast neutrons in lead - A. V. Khrimian	700	638
Determination of the mass of cosmic ray particles by means of a Wilson cloud chamber - M. S. Kozodaev & A. I. Filoppov	711	643
Measurements of the lifetime of positive pi mesons - M. S. Kozodaev, A. A. Markov & A. A. Tiapkin	715	647
Investigation of cosmic radiation at sea level with the aid of a mass spectrometer by measuring the momenta and ionization or individual particles - V. A. Liubimov, G. P. Eliseev & V. K. Kosmachevski	720	652
Anomalous scattering of mu mesons in graphite - A. I. Alikhanov & G. P. Eliseev	732	662
Scattering of slow mu mesons in copper - A. I. Alikhanian & V. G. Kirillov-Ugriumov	737	667
On the spatial distribution of charged particles in the vicinity of the core of an extensive air shower - S. I. Nikol'ski (Abstract)	747	676
Čerenkov radiation in extensive air showers - V. I. Gol'danski, G. B. Zhdanov, N. M. Nesterova & A. E. Chudakov (Abstract)	747	676
Distribution in momentum of charged particles in electronic-nuclear showers - L. D. Gedevanishvili, Z. Sh. Mandzhavidze, N.N.Roinishvili, Z. I. Tsagareli, A. I. Tsintsabadze & G. E. Chikovani (Abstract)	748	677
On the use of photometry for evaluating the ionization of particles in a cloud chamber - V. M. Fedorov, G. I. Merzon & M. I. Daion	750	678
Dependence of the probable ionization due to mu mesons on their momentum - V. A. Liubimov, G. P. Eliseev, V. K. Kosmachevski & A. V. Kovda	753	681
Liquid bubble chambers for investigating ionizing particles - G. A. Blinov, Iu. S. Krestnikov & I. I. Pershin	758	685

Translated in 1956 by
Columbia Technical Translations
5 Vermont Ave., White Plains, N. Y.